

Oil-Field Chemistry

ACS SYMPOSIUM SERIES **396**

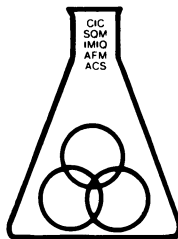
Oil-Field Chemistry

Enhanced Recovery and Production Stimulation

John K. Borchardt, EDITOR
Shell Development Co.

Teh Fu Yen, EDITOR
University of Southern California

Developed from a symposium sponsored
by the Division of Petroleum Chemistry, Inc.,
and the Division of Geochemistry
of the American Chemical Society
at the Third Chemical Congress of North America
(195th National Meeting of the American Chemical Society),
Toronto, Ontario, Canada,
June 5-11, 1988



American Chemical Society, Washington, DC 1989



Library of Congress Cataloging-in-Publication Data

Oil field chemistry: enhanced recovery and production stimulation
John K. Borchardt, editor, Teh Fu Yen, editor.

Developed from a symposium sponsored by the Division of Petroleum Chemistry, Inc., and the Division of Geochemistry of the American Chemical Society at the Third Chemical Congress of North America (195th Meeting of the American Chemical Society), Toronto, Ontario, Canada, June 5–11, 1988.

p. cm.—(ACS Symposium Series, 0097–6156; 396).
Bibliography: p.

Includes index.

ISBN 0–8412–1630–4

1. Oil fields—Production methods—Congresses.

I. Borchardt, John K., 1946– . II. Yen, Teh Fu, 1927– . III. American Chemical Society. Division of Petroleum Chemistry. IV. American Chemical Society. Division of Geochemistry. V. American Chemical Society. Meeting (195th: 1988: Toronto, Ont.) VI. Series: ACS symposium series; 396

TN870.C51245 1988
622'.33827—dc20

89–6829
CIP

Copyright © 1989

American Chemical Society

All Rights Reserved. The appearance of the code at the bottom of the first page of each chapter in this volume indicates the copyright owner's consent that reprographic copies of the chapter may be made for personal or internal use or for the personal or internal use of specific clients. This consent is given on the condition, however, that the copier pay the stated per-copy fee through the Copyright Clearance Center, Inc., 27 Congress Street, Salem, MA 01970, for copying beyond that permitted by Sections 107 or 108 of the U.S. Copyright Law. This consent does not extend to copying or transmission by any means—graphic or electronic—for any other purpose, such as for general distribution, for advertising or promotional purposes, for creating a new collective work, for resale, or for information storage and retrieval systems. The copying fee for each chapter is indicated in the code at the bottom of the first page of the chapter.

The citation of trade names and/or names of manufacturers in this publication is not to be construed as an endorsement or as approval by ACS of the commercial products or services referenced herein; nor should the mere reference herein to any drawing, specification, chemical process, or other data be regarded as a license or as a conveyance of any right or permission to the holder, reader, or any other person or corporation, to manufacture, reproduce, use, or sell any patented invention or copyrighted work that may in any way be related thereto. Registered names, trademarks, etc., used in this publication, even without specific indication thereof, are not to be considered unprotected by law.

PRINTED IN THE UNITED STATES OF AMERICA

American Chemical Society
Library
1155 16th St., N.W.
Washington, D.C. 20036

ACS Symposium Series

M. Joan Comstock, *Series Editor*

1989 ACS Books Advisory Board

Paul S. Anderson
Merck Sharp & Dohme Research
Laboratories

Alexis T. Bell
University of California—Berkeley

Harvey W. Blanch
University of California—Berkeley

Malcolm H. Chisholm
Indiana University

Alan Elzerman
Clemson University

John W. Finley
Nabisco Brands, Inc.

Natalie Foster
Lehigh University

Marye Anne Fox
The University of Texas—Austin

G. Wayne Ivie
U.S. Department of Agriculture,
Agricultural Research Service

Mary A. Kaiser
E. I. du Pont de Nemours and
Company

Michael R. Ladisch
Purdue University

John L. Massingill
Dow Chemical Company

Daniel M. Quinn
University of Iowa

James C. Randall
Exxon Chemical Company

Elsa Reichmanis
AT&T Bell Laboratories

C. M. Roland
U.S. Naval Research Laboratory

Stephen A. Szabo
Conoco Inc.

Wendy A. Warr
Imperial Chemical Industries

Robert A. Weiss
University of Connecticut

Foreword

The ACS SYMPOSIUM SERIES was founded in 1974 to provide a medium for publishing symposia quickly in book form. The format of the Series parallels that of the continuing ADVANCES IN CHEMISTRY SERIES except that, in order to save time, the papers are not typeset but are reproduced as they are submitted by the authors in camera-ready form. Papers are reviewed under the supervision of the Editors with the assistance of the Series Advisory Board and are selected to maintain the integrity of the symposia; however, verbatim reproductions of previously published papers are not accepted. Both reviews and reports of research are acceptable, because symposia may embrace both types of presentation.

Preface

THE VARIOUS FIELDS OF CHEMISTRY play an important role in the discovery and exploitation of oil and gas reserves. Improved drilling and well completion fluids, cement slurries, hydraulic fracturing and acidizing fluids to improve well productivity, various chemical additives to be used in these fluids, and chemicals for enhanced oil recovery are essential to the improvement of production economics and to an increase in recoverable hydrocarbon reserves. Chemistry will become increasingly important in future hydrocarbon production with the decreased likelihood of major onshore discoveries, increased discovery and production costs associated with deep offshore wells and Arctic frontier provinces, and the decline in drilling since early 1982.

The multidisciplinary nature of oil-field chemistry includes the development of surfactants and polymers for enhanced oil recovery, drilling and completion fluids, and stimulation fluids. Study of relevant inorganic and organometallic chemistry has resulted in the development of improved polysaccharide cross-linking agents, corrosion inhibitors, improved cement slurry additives, and completion fluids. Polymer chemistry has resulted in improved cement slurry additives to control cement set time, fluid loss, compressive strength, and formation damage characteristics. Contributions of organic chemistry include development of improved antioxidants and more cost-effective monomer syntheses for the production of oil-field polymers.

The study of foam behavior in porous media; interfacial phenomena, especially the aggregation and arrangement of surfactants in oil–aqueous systems; aqueous fluid–rock mineral interactions, particularly that of strong acids with siliceous minerals; the interaction of polymers and organic chemicals with rock; and the rheological behavior of polymer solutions and gels are all important physical chemistry and engineering research areas. Biology also plays an important role. Bacterial growth in wellbores and within formations has long been recognized as a serious problem. It causes hydrogen sulfide formation and corrosion problems that require careful operating practices and the use of bactericides. One of the most exciting recent research areas has involved the promotion and utilization of the growth of bacteria within formations to improve oil recovery.

Oil-field chemistry has undergone major changes since the publication of earlier books on this subject. Enhanced oil recovery research has shifted from processes in which surfactants and polymers are the primary promoters of increased oil production to processes in which surfactants are additives to improve the incremental oil recovery provided by steam and miscible gas injection fluids. Improved and more cost-effective cross-linked polymer systems have resulted from a better understanding of chemical cross-links in polysaccharides and of the rheological behavior of cross-linked fluids. The thrust of completion and hydraulic fracturing chemical research has shifted somewhat from systems designed for ever deeper, hotter formations to chemicals, particularly polymers, that exhibit improved cost effectiveness at more moderate reservoir conditions.

Although opinions on the timing of the next oil shortage differ, oil is a finite resource and the current oil-production surplus is definitely a temporary phenomenon. Despite some cutbacks, major oil companies, some chemical companies, and various academic groups and research institutes are all maintaining oil-field chemistry research and development programs. The long lead time required for much oil-field chemistry research, particularly enhanced oil recovery, requires that basic research, laboratory product development, and field testing all be maintained. This will enable the industry to respond when the current oil surplus vanishes and to develop chemicals and processes that will be economical, even at current oil prices.

The symposium on which this book is largely based was held with the temporary nature of the current oil-production surplus in mind. The Division of Geochemistry, Inc., provided part of the cost of printing color photographs within the text. The views and conclusions expressed herein are those of the authors.

The editors thank the authors for their contributions and the referees, the unsung heroes of science, for their diligent and timely manuscript reviews. Last, but certainly not least, we thank Cheryl Shanks of the ACS Books Department, without whose patience, help, and encouragement this volume would not be possible.

JOHN K. BORCHARDT
Shell Development Company
P.O. Box 1380
Houston, TX 77251-1380

TEH FU YEN
School of Engineering
University of Southern California
Los Angeles, CA 90089-0231

March 23, 1989

Chapter 1

Chemicals Used in Oil-Field Operations

John K. Borchardt

Westhollow Research Center, Shell Development Company, Houston,
TX 77251-1380

Chemicals of various types are used in every stage of drilling, completing, and producing oil and gas wells. This review describes these chemicals, why they are used, and recent developments. These chemicals include common inorganic salts, transition metal compounds, common organic chemicals and solvents, water-soluble and oil-soluble polymers, and surfactants. As existing fields become depleted, use of chemistry to maintain production via well stimulation, more efficient secondary recovery operations, and enhanced oil recovery become ever more important.

The modern chemical industry is highly dependent on crude oil and natural gas feedstocks. Conversely, chemicals, the science of chemistry and chemical engineering join petroleum engineering to play an important roll in the production of oil and gas. The discovery rate of of major new oil fields is declining, particularly in the United States. As the petroleum industry becomes more dependent on increasing production from existing fields, the use of chemicals to more efficiently drill and operate oil and gas wells and enhance productivity from these fields will grow. Environmental considerations will probably be an increasingly important in the choice of chemicals used in well treatment fluids particularly in offshore locations. While geochemistry plays a role in the discovery of oil and gas and production chemicals are used to break produced oil-water emulsions and as friction reducers in pipelines, this review will be restricted to the chemistry and chemicals involved in drilling, completing, stimulating, and operating production and injection wells and in enhanced oil recovery.

Drilling Fluids

Drilling fluids (1-3) are often called drilling muds because of their appearance. This is due to the dispersed clays added to most

0097-6156/89/0396-0003\$13.95/0

© 1989 American Chemical Society

drilling fluids. The drilling fluid is circulated down the drill pipe, around the drill bit, and up the wellbore while drilling is in progress. The purpose of the drilling fluid is to cool and lubricate the drill bit, suspend formation cuttings and lift them to the surface, and control formation pressure reducing pressure surges up the wellbore (thereby reducing the possibility of blowouts). By cooling the drill bit and removing the cuttings from the bottom of the well bore, the rate of drilling can be increased. The drilling fluid is designed to be thixotropic *i.e.*, have high viscosity under low shear conditions when moving up the wellbore carrying suspended solids and have low viscosity under the high shear conditions near the drill bit where rapid fluid movement is necessary to cool the drill bit.

Drilling fluids usually contain water as the primary component. However, oil-based muds may be used for high temperature operations and for drilling highly water-sensitive formations. Oil-based muds are of two types, oil-external emulsions containing as much as 50% water in the internal phase or an oil-based fluid containing little if any water.

A great many additives can be used to impart desired properties to the drilling fluid. In general, the deeper and hotter the well, the more chemical additives are needed to obtain the desired fluid properties. These additives can be classified into different types by function. These include: Weighting materials which are used to adjust fluid density and thus hydrostatic pressure exerted on the formation by the wellbore fluid. The objective is to prevent sudden pressure surges or blowouts during drilling while simultaneously avoiding excessive fluid leak-off into formations being penetrated by the well bore. Barium sulfate (barite) is the most commonly used weighting agent. Other insoluble minerals used include hematite, siderite, and lead sulfide. Salts may be dissolved in the base water to increase fluid viscosity. The use of high density calcium chloride, sodium and calcium bromides, and zinc bromide solutions and blends thereof has become common in the U.S. Gulf Coast region (4-6). These fluids are somewhat corrosive (7) and the use of corrosion inhibitors such as thiocyanate ion has been recommended. However, these fluids have excellent formation damage characteristics; fluid leakoff from the wellbore into the formation has little adverse effect on rock permeability (8,9). Fluid loss additives such as solid particles and water-thickening polymers may be added to the drilling mud to reduce fluid loss from the well bore to the formation. Insoluble and partially soluble fluid loss additives include bentonite and other clays, starch from various sources, crushed walnut hulls, lignite treated with caustic or amines, resins of various types, gilsonite, benzoic acid flakes, and carefully sized particles of calcium borate, sodium borate, and mica. Soluble fluid loss additives include carboxymethyl cellulose (CMC), low molecular weight hydroxyethyl cellulose (HEC), carboxymethylhydroxyethyl cellulose (CMHEC), and sodium acrylate. A large number of water-soluble vinyl copolymers and terpolymers have been described as fluid loss additives for drilling and completion fluids in the patent literature. However, relatively few appear to be used in field operations.

Controlling fluid loss is particularly important in the case of the expensive high density brine completion fluids. While copolymers and terpolymers of vinyl monomers such as sodium poly(2-acrylamido-2-methylpropanesulfonate-co-N,N-dimethylacrylamide-co-acrylic acid) has been used (10), hydroxyethyl cellulose is the most commonly used fluid loss additive (11). It is difficult to get most polymers to hydrate in these brines (which may contain less than 50% wt. water). The treatment of HEC particle surfaces with aldehydes such as glyoxal can delay hydration until the HEC particles are well dispersed (12). Slurries in low viscosity oils (13) and alcohols have been used to disperse HEC particles prior to their addition to high density brines. This and the use of hot brines has been found to aid HEC dissolution. Wetting agents such as sulfosuccinate diesters have been found to result in increased permeability in cores invaded by high density brines (14).

Foaming agents provide another way to reduce fluid loss in the drilling fluids. Mist or foam drilling is used in relatively shallow formations; commonly used foaming agents include C₁₄₋₁₆ alpha-olefin sulfonates and alcohol ethoxysulfates. While these drilling fluids have not been used extensively in recent years, the development of improved foaming agents and systems containing water thickening polymer to stabilize the foam has been reported (15). Defoamers are used to reduce undesirable foaming which often occurs when saline drilling fluids exit the well bore. Tributylphosphate, low molecular weight aliphatic alcohols, polyglycols, fatty alcohol glycol ethers, acetylenic glycols, aluminum stearate, potassium chloride, silicone-based defoamers, and sodium alkylaromatic sulfonates have been used.

Lost circulation chemical treatments are necessary when the drill bit penetrates a "thief" zone and very large amounts of drilling fluid are lost to the formation. In this situation, the addition of water thickeners or solid particles may not be sufficient. The face of the formation can be plugged using a rapidly setting cement slurry or a process involving the in-situ gelation/precipitation of sodium silicate, treatment with Portland cement, and in less serious cases by plugging the formation face with shredded cellophane, crushed walnut and almond hulls, cedar and cane fibers, and carefully sized sodium chloride and calcium carbonate particles. Viscosifiers are used as rheology modifiers to aid in suspending rock cuttings as they are carried to the surface. Many of the fluid loss additives described above are used in this application. Clays such as bentonite (montmorillonite) are the most commonly used rheology modifiers. The main organic polymers that are used, polysaccharides and acrylamide and acrylate polymers, often have limited temperature stability or exhibit excessive temperature thinning in deep hot wells. At concentrations below 2.8 g/L, xanthan gum is a more effective solids suspending agent than HEC, CMC, and partially hydrolyzed polyacrylamide (16).

While starches are commonly used, they are relatively poor viscosifiers. Acids and bacterial enzymes readily attack the acetal linkages resulting in facile depolymerization. Both formaldehyde and isothiazolones have been used as starch biocides (17). Development of improved high temperature water viscosifiers for drilling and other oil field applications is underway. For the

present, oil-based drilling fluids offer the best alternative for elevated temperature applications despite their relatively high cost.

Stabilizing agents are used to maintain drilling fluid rheological properties at highly elevated downhole temperatures. Chromium and chromium-free lignosulfonates, polyglycol ethers, sodium poly(styrene sulfonate-co-maleic anhydride), and a melanin polymer have been used in this application. Additives such as sodium diethylthiocarbamate have been used to stabilize aqueous polysaccharides such as xanthan gum (18).

Flocculants cause colloidal clay particles to coagulate thus promoting separation from the drilling fluid which has been circulated down the wellbore and returned to the surface. The treated fluid may then be pumped back down the well bore. Sodium chloride, hydrated lime, gypsum, sodium tetraphosphate, polyacrylamide, poly(acrylamide-co-acrylic acid), cationic polyacrylamides, and poly(ethylene oxide) have been used commercially.

Thinners and dispersants are used to prevent excessive flocculation of clay particles and maintain pumpability of the fluid. Tannins, various lignosulfonate salts, sodium tetraphosphate and other phosphates, and synthetic polymers such as sodium poly(styrene sulfonate-co-maleic anhydride) have been used.

Friction reducers such as partially hydrolyzed polyacrylamide may also be used in drilling fluids (19). They allow fluid to be circulated through the well bore more easily thereby reducing horsepower requirements for the circulating pumps and thus decreasing well treatment costs.

Lubricants offer a means of reducing torque and increasing the effective horsepower to the drillbit by reducing friction. Various vegetable oils, graphite powder, soaps, asphalt blends, air-blown asphalt colloids, diesel oil, and fatty acid esters have been used.

Pipe-freeing agents are used to reduce friction and increase lubricity in areas of expected drill pipe sticking such as angles in deviated wellbores. Soaps, surfactants, oils, soda lime, glass beads, and cationic polyacrylamide have been used.

Corrosion inhibitors are used to reduce the corrosion of surface equipment, surface casing, and the drill string by drilling and well treatment fluids. Many different corrosion inhibitors have been used. These include amine salts such as ammonium sulfite-bisulfite blends, zinc carbonate, zinc chromate, hydrated lime, fatty amine salts of alkylphosphates, cationic polar amines, ethoxylated amines, and tertiary cyclic amines. Commercial products are usually proprietary blends of chemicals.

Bactericides are used to control bacterial growth which can cause corrosion, plugging of the formation face, and alteration of drilling fluid rheological properties. Paraformaldehyde, glutaraldehyde, sodium hydroxide, lime derivatives, dithiocarbamates, isothiazolones, and diethylamine have all been used.

pH control aids in reducing corrosion and scaling and in controlling interaction of the drilling fluid with formation minerals. Sodium hydroxide, calcium carbonate, sodium bicarbonate, sodium carbonate, potassium hydroxide, magnesium oxide, calcium oxide, fumaric acid, and formic acid have all been used commercially in this application.

Formation damage control chemicals are added to reduce the permeability damage that occurs when drilling fluid enters the formation. This also aids in preventing erosion of the formation into the wellbore. Maintaining the cylindrical geometry and uniform diameter of the wellbore aids in subsequent cementing operations. Potassium chloride, ammonium chloride, sodium chloride, gypsum, sodium silicate, partially hydrolyzed polyacrylamide and poly(acrylamide-co-acrylic acid), certain polymers having quaternary ammonium groups in the repeat unit (see Chapter 10), and lignosulfonate derivatives have all been used to reduce formation damage.

Scale inhibitors are used to prevent the formation of insoluble calcium salts when the drilling fluid contacts formation minerals and saline formation waters. Commonly used scale inhibitors include sodium hydroxide, sodium carbonate, sodium bicarbonate, polyacrylates, polyphosphates, and phosphonates.

Emulsifiers have been used to prepare oil-external emulsion drilling fluids. Surfactants used as emulsifiers include fatty acid salts, fatty acid amides, petroleum sulfonates, and lignosulfonates.

Because of the relatively low cost of many of the chemicals used in drilling fluids, development of more cost effective additives is a major challenge. However, improved high temperature polymers, surfactants, and corrosion inhibitors are under development in many laboratories.

Cementing Fluids (20,21)

After completion of the drilling operation, steel casing is lowered down the well bore and into the drilling fluid. A spacer fluid is then pumped down the well bore to remove the drilling fluid and prevent contact of the drilling mud with the cement slurry. Efficient displacement of the drilling mud also promotes bonding of the cement slurry to rock surfaces.

Intermixing of the spacer and the drilling fluid should not produce solids or a high viscosity phase. Most spacers are aqueous and contain polymers to increase fluid viscosity. Spacer density is usually intermediate between that of the drilling fluid and the cement slurry (22). Salts may be added to control fluid density and pH. Surfactants are used to aid removal of drilling mud from formation surfaces. Water-wetting surfactants also aid in making the casing and exposed rock surfaces water-wet to promote good cement bonding (23). This is particularly important when using oil-based drilling fluids.

Turbulent flow at reasonable pump rates aids in removal of drilling mud from surfaces (24). Downhole devices called scrapers can be installed on the casing to scrape drilling mud residues from formation surfaces. Other devices called centralizers may be attached to the casing to center it in the wellbore.

With increased development work from offshore platforms, more non-vertical (deviated) wells are being drilled. Settling of mud solids to the low side of the well bore can result in a continuous channel of undisplaced drilling mud solids in the casing annulus

that reduce the effectiveness of cement bonding (25,26). Conversely, cement solids can settle from the slurry before it sets resulting in a channel of water in the high side of the casing annulus. Proper design of both the drilling fluid (particularly through use of surfactants as dispersants) and the cement slurry (including good control over cement set time) are necessary to prevent this.

The cement slurry is pumped down the casing and up the annular space between the casing and the formation. The spacer and drilling fluid are thus displaced by the cement slurry. A compatible fluid (one that does not substantially alter the set time of the cement slurry) is pumped into the wellbore to displace nearly all the cement slurry into the annular space between the casing and the formation. The well is then shut in to allow the cement to set. This bonds the casing to the formation and isolates oil- and gas-bearing formations from aquifers and brine-containing formations. Fluid communication between formations can adversely affect production operations or lead to contamination of potable water aquifers.

Incomplete displacement of fluid from the annular space can result in gaps in the cement sheath through which fluids from different formations can intermingle. In this situation, a "squeeze cementing" treatment is required to plug these gaps. Portland cement or rapidly setting sodium silicate slurries can be used in this operation.

When cementing high pressure gas formations, the gas can penetrate the cement slurry before it sets greatly weakening the set cement (27). Various solutions to this problem have been proposed including the use of cement slurry formulations which expand as they harden thereby resisting gas invasion (28). Foamed cement slurries have been used to provide a low density cement slurry to reduce permeability damage to highly sensitive formations through reduced fluid loss (29). Glass microspheres have also been used to substantially reduce cement slurry density (30, 31). Other additives which reduce cement slurry density to a lesser extent include bentonite, fly ash, silicates, perlite, gilsonite, diatomaceous earth, and oil emulsions (see citations in reference 29).

Corrosion-resistant cements have been developed for use in wells used to inject supercritical carbon dioxide for enhanced oil recovery (32). These are based on Portland cement and high levels (as much as 40% wt.) of additives such as fly ash. Epoxy resins have been successfully used as cements in corrosive environments (33).

Lignosulfonates and lignosulfonate derivatives are used extensively as cement set time retarders (20, 21). Many of the same additives used in drilling muds are used in cement slurries and spacer fluids for similar purposes.

Completion Fluids and Operations (1,20,34)

After cementing the well, communication must be established with the productive formation. This is done in an operation called perforating. The wellbore is filled with a non-damaging fluid of

the proper density to control pressure surges while not exhibiting excessive fluid loss to the formation. A perforating tool or "gun" is lowered into the well bore and placed opposite the productive formation. The gun fires projectiles or powerful jets of gas generated in small explosions to penetrate the casing and cement sheath. Perforations are generated in a controlled pattern and spacing chosen after considering the formation properties and productive capacity. A small amount of acid may be used to wash the perforations to remove pulverized debris which reduces the fluid carrying capacity of the perforations and adjacent formation. Production tubing is then lowered into the hole and the productive portion(s) of the well isolated using sealing tools called packers (21). This is done to produce from more than one formation simultaneously and to minimize the volume of oil and gas in the wellbore during production.

Fluid loss from the wellbore to the formation may be reduced using the less permeability damaging drilling fluid loss additives described above. In saturated brines, carefully sized sodium chloride particles have been used to temporarily plug the formation face (35). The particles may be dissolved by pumping a less saline fluid down the wellbore.

Sand production from poorly consolidation formations is a significant problem in important oil producing areas such as the U.S. Gulf Coast; Kern County, California; Venezuela; Alberta; Nigeria; and Indonesia. The most commonly used technique for sand control is called gravel packing. A slurry of as much as 1.8 kg of carefully-sized sand particles per liter of aqueous fluid is pumped downhole. The sand particle size is chosen based on size analyses of the formation sand (19,36). The sand-carrying capacity of the water is enhanced by increasing its viscosity using 20-80 lb polysaccharide per 1000 gallon. The most commonly used polysaccharide is hydroxyethyl cellulose because its low content of insoluble solids minimizes permeability damage to the formation (37).

Carboxymethyl cellulose and derivitized guar are occasionally used in this application (1). Methods of stabilizing polysaccharides originally developed for hydraulic fracturing applications (see below) hold promise for increasing the range of temperatures at which polysaccharide polymers can be used in gravel packing applications.

Certain mixtures of polymers have been shown to form complexes which exhibit substantially higher than expected solution viscosity under low shear conditions. Xanthan gum blends with guar gum (38, 39), sodium poly(styrene sulfonate) (40), polyacrylamide (41), sulfonated guar gum (38), sodium poly(vinylsulfonate) (40), hydrolyzed sodium poly(styrene sulfonate-co-maleic anhydride) (38), and poly(ethylene oxide) (41) and blends of xanthan gum and locust bean gum have exhibited substantially higher than expected solution viscosity (42, 43).

An enzyme, acid, or oxidative "breaker" is added to effect a controlled depolymerization and thus a programmed loss of fluid viscosity. This depolymerization is timed to occur when the sand-laden fluid is opposite the productive formation. The sand then drops out of suspension and is packed against the formation. The sand creates a high permeability fluid pathway from the formation

into the wellbore while substantially preventing the migration of formation particles. Downhole tools such as wire-wrapped screens or liners are used in conjunction with gravel packing. These devices serve to hold the sand in place.

Since formation damage is a critical factor in successful gravel pack treatments, continuing efforts are being made to improve the formation damage characteristics of polysaccharide fluids both before and after depolymerization (37). Recently, grades of hydroxyethyl cellulose having improved formation damage characteristics were introduced into the market place.

Injecting epoxy, furan, or furan-formaldehyde resins into poorly consolidated formations to consolidate them was a common sand control practice for thin highly productive formations (44-46). Organic solvents (46) and silane coupling agents (47) are used to promote adhesion of the resin to the rock surface. Excess resin is flushed deeper into the formation to minimize resin hardening in the flow channels since this would reduce formation permeability.

While effective, the relatively high cost of this sand control method as compared to gravel packing has restricted its use. The use of aqueous slurries of epoxy resins can reduce solvent costs (44). Surfactants, particularly fluorochemicals, may hold promise for increasing epoxy resin fluidity (49). The *in situ* crosslinking of polybutadiene has been proposed as a method of reducing resin costs (50). The gravel packing technique could be used to place resin-coated sand against a poorly consolidated formation (51-53). The resin is then cured resulting in a hard, but permeable mass holding formation sand grains in place. Silica dissolution in high temperature steam injection wells can destroy the integrity of a gravel pack and lead to sand production when the well is placed back on production (54). Use of a resin-coated sand could aid in maintaining gravel pack stability and effectiveness.

Another method of sand control is use of a silicon halide which reacts with water at the surface of sand grains forms SiO_2 which can bond the grains together (55). Reducing the cost of sand consolidation could be very useful since the applicability of gravel packing methods is limited by the bottom hole circulating temperature and the limited temperature stability of polysaccharide polymers.

Hydraulic Fracturing (20,56)

Since hydraulic fracturing is reviewed in a subsequent chapter, this important production stimulation technique will be only briefly discussed. Hydraulic fracturing is a process whereby the permeability of a formation is increased by generating high permeability cracks in the rock. Particulate suspensions (usually sand slurries) are injected at sufficiently high rates (which require high injection pressures) to generate fractures in the rock which are held open by the suspended proppant in the fracturing fluid. The majority of hydraulic fracturing treatments are performed using water-based fluids; foams (with nitrogen or carbon dioxide as the gas phase) have been used extensively in recent years to reduce formation damage. Oil-external emulsions have also been used for

the same purpose. Ingredients used in hydraulic fracturing are chosen from the following:

A viscosifier, usually a polysaccharide, is used to suspend the proppant during pumping and placement in the rock fracture. Generally 2-7g of guar per liter of fracturing fluid is used. Hydrolytic depolymerization beings at 79.6°C (34). The degradation rate in alkaline media, acid, and in the presence of cellulase and hemicellulase enzymes has been determined (1). Most fracturing treatments employ a crosslinked polymer.

A disadvantage of guar is the relatively high level of insoluble materials normally left in the product after processing, 10-14% wt. (57). Alkaline refining can reduce the insoluble materials level substantially, to ca. 3.9% wt. (58). Guar derivatives such as HPG and carboxymethylhydroxypropyl guar (CMHPG) contain fewer insolubles, <2% wt. (59,60). HPG also exhibits better high temperature stability and resistance to hydrolytic decomposition as compared to guar (1). Locust bean gum, karaya gum, and gum traganth have been used to a limited extent as viscosifiers and fluid loss additives (61-63).

Hydroxyethyl cellulose has been used in fracturing fluids not requiring the increased viscosity and longer break times provided by crosslinking. Until recently, it has been difficult to crosslink HEC (64). This has limited its use in hydraulic fracturing applications despite its excellent formation damage characteristics. Hydroxyethyl celluloses containing vicinal hydroxy groups are more easily crosslinked (65) and exhibit better shear stability (66). Zr(IV) has been used to crosslink HEC (64). Crosslinked CMHEC tends to show more shear degradation on passing through pumps and small orifices in downhole tools than crosslinked HPG fluids (67).

Other viscosifiers described in the literature include acrylate copolymers such as poly(acrylamide-co-dodecylmethacrylate) (68) and poly(vinyl alcohol) (69). The driving force behind using synthetic polymers is presumably better high temperature stability.

The use of ionomers such as lightly sulfonated polystyrene as an oil-based fracturing fluid viscosifier has been studied (70). The most commonly used oil-based viscosifiers are phosphate esters of various types (56,71,72).

Fluid loss additives are used are used to reduce the rate of fluid loss from the fracture to the formation and to naturally occurring macro- and micro-fractures within the formation. Silica flour (73,74), oil-soluble resins (75), diesel oil emulsions (5% by volume) (74) have also been used.

Proppants are solid particles used to hold open the fracture after conclusion of the well treatment. Criteria to choose the economically most effective proppant for a given set of formation conditions have been discussed (76). While sand is the most commonly used proppant because of its low cost, resin-coated sand, sintered bauxite, and Al₂O₃ particles have also been used because of their greater compressive strength and resistance to dissolution at high temperature and pH (55). While epoxy resins are most commonly used, the use of other resins such as phenol-formaldehyde has been described.

Sand has been treated with oil-soluble organosilicon compounds to form a hydrophobic proppant (77). A double layer resin coating has also been developed. The inner layer coating the sand particle is a cured gamma-aminopropyltriethoxysilane - hexamethylenetetramine. The outer layer is an uncured mixture of the same two chemicals which cures within the fracture to form a consolidated permeable mass holding the fracture open (78).

Crosslinking agents are used to increase solution viscosity and thus solids suspending properties of fluids at $T > 150^{\circ}\text{F}$. The most commonly used crosslinking agents are organotitanates, borates, and zirconium compounds. Organozirconates are the preferred crosslinkers for hydroxyethyl cellulose (79-81). Antimonates and aluminum compounds have also been used as polysaccharide crosslinkers. Encapsulation of crosslinkers and the use of ligands to complex with the transition metal atom have been used to delay crosslinking (82). Delayed crosslinking which occurs within the formation under lower shear conditions can provide higher and more predictable crosslinked fluid viscosity (83). Polyamines such as tetramethylenediamine can be used to accelerate crosslinking reactions (84).

A breaker: an enzyme (at $T < 140^{\circ}\text{F}$), strong oxidizing agent, or an acid, is used to depolymerize polysaccharides and break crosslinks such that viscosity declines at a controlled rate so that the proppant may be deposited in the fracture. Too rapid proppant dropout would cause a premature "sand-out" which prevents future extension of the fracture. Peroxydisulfates are the most frequently used breakers. Less reactive organic peroxides may be preferred for high temperature formations (85).

Chemical stabilizers have been used to reduce the rate of oxygen-promoted degradation of polysaccharides at $T > 225^{\circ}\text{F}$. Methanol and sodium thiosulfate are the most commonly used (86). Sodium dithiocarbamate, alkanolamines, and thiol derivatives of imidazolines, thiazolines, and other heterocyclic compounds have also been tested for this application. Calcined dolomite (87) and Cu(I) and Cu(II) salts (88) have been reported to increase the thermal stability of HEC.

Biocides are used to prevent aerobic bacterial degradation of fracturing fluids in surface mixing and storage tanks. Anaerobic bacterial growth in the wellbore and within the formation has to be controlled to prevent introduction and/or growth of these bacteria within the formation during the fracturing treatment and subsequent generation and production of hydrogen sulfide. Glutaraldehyde, chlorophenates, quaternary amines, and isothiazoline derivatives have been used (89,90). The biocide is best added to the base fluid before addition of the polysaccharide viscosifier.

pH buffers are added to the base fluid to keep the pH basic. This promotes rapid polymer particle dispersion and controls polysaccharide hydration rate to avoid formation of large, partially hydrated particles.

Other techniques to promote complete polymer hydration include vigorous mixing and slow addition of the polysaccharide. Specially designed mixing devices have been used to promote rapid particle dispersion (91). Adding already prepared dispersions of guar, HPG, and HEC in nonaqueous media is another means of promoting rapid

polymer particle dispersion and complete hydration (81,92). Wetting polymer surfaces with ethylene glycol (92) or isopropanol (93) has also been used as a means of promoting rapid polymer dispersion prior to the onset of hydration.

Various particle surface treatments have been used to delay polymer hydration until polymer particles have been thoroughly dispersed. These include guar treatment with borax (2,94) and HEC treatment with glyoxal (95).

Buffers also are used to maintain the proper pH for the cross-linking reaction to occur at an optimum rate. Sodium bicarbonate and sodium carbonate are used to attain basic pH while weak acids: acetic, fumaric, formic, and adipic, are generally used to obtain acidic pH values.

Formation damage control additives are added to reduce permeability damage caused by clay swelling and consequent fine particle migration (which can also occur in the absence of clay swelling). Potassium chloride, ammonium chloride, sodium chloride, and, for longer term treatment effectiveness, organic polymers containing quaternary ammonium groups in the repeat unit have been used for this application. While avoiding permeability damage to the formation adjacent to the propped fracture is critical in determining initial hydrocarbon production rate, fluid conductivity in the propped fracture is the primary determinant of long-term productivity (96).

Surfactants are used to stabilize water-in-oil emulsions and to promote rapid return of injected fluids and a faster return of the well to hydrocarbon production. Although they are expensive, water-soluble fluorochemicals have been shown to be effective in this application (97,98).

Foams have become widely used to limit the fluid lost to the formation and thus reduce formation damage. Foam cell size plays a major role in determining fluid rheology (99). Guar, HPG, and xanthan gum stabilize the foam bubbles by increasing the viscosity of the surrounding aqueous fluid. Both nitrogen and carbon dioxide have been used as the internal phase of the foam (100-102) and foams based on each exhibit similar rheological behavior in laminar flow (102) and similar fluid loss behavior (103,104). The carbon dioxide is pumped as a supercritical fluid which changes to a gas downhole (105).

Acidizing Chemicals (20,106)

Acid treatments fall into three general types:

Acid washing is used to dissolve acid-soluble scales from the well bore and to open gravel packs and perforations plugged by such scales.

Matrix acidizing is the injection of acids into the formation at a pressure below the formation parting pressure (the pressure at which natural fractures are forced open by injected fluids). Properly designed, the injected acid enters the flow channels of the formation and flows radially outward from the wellbore dissolving mineral fine particles in the flow channels. Minerals forming the flow channel walls also react with the acids. These processes increase formation permeability near the wellbore. The end result

is to increase well productivity without increasing the produced water:oil or gas:oil ratios.

So-called "wormholes" can be formed when the injected acid primarily enters the largest diameter flow channels in carbonate rock further widening them (107). Acid only invades the small flow channels a short distance greatly reducing treatment effectiveness. High fluid loss rates, low injection rates, and reduced rates of acid-rock reactions decrease the wormhole length.

In the third type of acidizing, fracture acidizing, acid is injected above the parting or fracture pressure of the formation. The acid reacts with the minerals on the exposed fracture face in a process called etching. With sufficient etching, the fracture does not reseal when normal well production or injection operations are resumed.

Acids can sometimes break emulsions within the formation either by reducing the pH or by dissolving fine particles which can stabilize emulsions. Breaking the emulsion reduces fluid viscosity thus increases the fluid carrying capacity of the flow channel. Acids may be used as breakers to reduce the viscosity of acid-sensitive fracturing gels.

Acids are sometimes used ahead of fracturing fluids to dissolve mineral fine particles and allow more rapid injection of the fracturing fluid. When used as the initial stage of a squeeze cementing treatment, the acid-promoted mineral and drilling mud particle dissolution can result in increased entry of the cement slurry into the desired portions of the formation.

Acids are selected based on the nature of the well treatment and the mineralogy of the formation. The critical chemical factors in properly selecting an acid are: stoichiometry (how much formation material is dissolved by a given amount of acid), the equilibrium constant (complete reaction of the acid is desired), and reaction rate between the acid and the formation material (106).

Mineral acids include hydrochloric acid and blends of hydrochloric and hydrofluoric acid (usually 12% HCl/3% HF). Hydrochloric acid is used to acidize carbonate formations. Its advantages are relatively low cost, high carbonate mineral dissolving power, and the formation of soluble reaction products (which minimizes formation damage). The primary disadvantage of hydrochloric acid is its corrosive nature.

Hydrofluoric acid may be prepared by dilution of a concentrated aqueous solution or by reaction of enough ammonium bifluoride with aqueous 15% HCl to prepare a 12% HCl/3% HF solution. Hydrochloric - hydrofluoric acid blends have the major advantage of dissolving siliceous mineral including clays and silica fine particles. HCl/HF blends are quite corrosive.

Earlier corrosion inhibitors limited the maximum strength of the acid to 15% by weight. Improved corrosion inhibitors (see below) have made the use of higher acid concentrations, such as 28% HCl more common. More dilute solutions may initially be injected in sandstone acidizing to reduce the formation of insoluble sodium and potassium fluorosilicates by displacing saline formation water before injection of hydrochloric acid.

Organic acids used in carbonate rock acidizing include formic, acetic, sulfamic, and chloroacetic acids. These have the advantage of being less corrosive than the mineral acids. This permits use in applications requiring a long contact time with pipe (as perforating fluids) or with aluminum- or chrome- plated pump parts. It is also easier to retard (inhibit) reaction of organic acids with carbonates at elevated temperatures. This permits deeper penetration of the acid treatment fluid into the formation. Organic acids are used to a much smaller extent than mineral acids due to their higher cost and incomplete reaction with many carbonate minerals. Sulfamic and chloroacetic acids are seldom used except in situations such as remote well locations where their solid form (100% activity) makes transportation costs a critical consideration. The 180°F decomposition temperature limits the use of sulfamic acid to temperatures below ca. 160°F.

Mixed acid systems are blends of mineral acids and organic acids. Combinations that have been used in carbonate acidizing include acetic acid/HCl and formic acid/HCl. While these are less corrosive than hydrochloric acid alone, the organic acid may not react completely with the rock. Blends of formic acid and hydrofluoric acid have been used in high temperature sandstone acidizing and are less corrosive than HCl/HF blends.

High fluid injection rates are often required. For this reason, friction reducers are often used in acid fracturing. These include polyacrylamide and acrylamide copolymers, guar gum, hydroxyethyl cellulose, and karaya gum (108)

In many cases, it is desirable to retard the rate of acid - rock reactions to permit deeper penetration of the treatment fluid into the formation. Four techniques have been used to accomplish this: using retarded acids which generate HF in situ, chemically retarding the acid by placing an organic film on rock surfaces, using polymers to increase acid viscosity (use of so-called "gelled" acids), and foaming or emulsifying the acid to increase the apparent viscosity.

Retarded acids are primarily applicable to sandstone acidizing. Fluoroboric acid slowly hydrolyzes to form the more reactive hydrofluoric acid (109,110). The time required for this hydrolysis process may enable deeper penetration of the HF into the formation although one report contradicts these findings (111). Na_2TiF_6 and similar salts also slowly generate HF in acid media (112). Phosphorous acid addition to hydrochloric acid has been used to reduce the HCl reaction rate with limestone (113).

Organic polymers have been used to increase the viscosity of acids. The primary application is in fracture acidizing. Binary and ternary acrylamide copolymers are the most commonly used chemicals for this application. Many of these polymers degrade rapidly in strong acids at temperatures $\geq 130^\circ\text{F}$; development of more stable polymers suitable for high temperatures is desirable. Recently developed polymers for this application include acrylamide copolymers with:

- methacryloyltrimethylammonium chloride (114)
- 2-acrylamido-2-methylpropanesulfonic acid (115)
- methacryloyloxyethyltrimethylammonium methosulfate (116).
- N-vinyl lactam (117)

Other polymers used in this application include:

poly(vinylpyrrolidinone) (118,119)

sodium poly(vinylsulfonate-co-vinylamide) (120)

sodium poly(acrylamide-co-N-vinyl lactam-co-vinyl sulfonate) (119)

and mixtures of sodium

poly(2-acrylamido-2-methylpropanesulfonate-co-N-vinylacetamide) and

poly(acrylic acid-co-vinylformamide-co-vinylpyrrolidinone) (120).

Despite its limited stability in acid (1), guar gum has been used to thicken 3-15% hydrochloric acid (121). An allyl ether - guar gum adduct has been proposed for use as an acid viscosifier (122). Zr(IV) crosslinked CMHEC has been used to thicken hydrochloric acid (81).

Low viscosity oil-external retarded hydrochloric acid micro-emulsions exhibiting quite low acid diffusion rates (ca. 1% of that of aqueous HCl) have been developed (123,124). Foaming (125) or emulsifying acid (106) also has the effect of limiting the contact of the acid with formation surfaces and increasing acid viscosity thereby reducing the rate of acid-rock chemical reactions. The foaming agents are generally nonionic surfactants and the gas phase is usually nitrogen. The acid is usually the internal phase of emulsified acids and the fluid contains 10-30% of a low viscosity hydrocarbon as the external phase. Polyacrylamide has been used to thicken the aqueous phase of hydrochloric acid emulsions (126) while nonionic surfactants have been used as the emulsifiers (127). Overall, emulsified acids appear to be the most suitable for high temperature formations.

By adding an oil-wetting surfactant to an acid, one can promote the temporary formation of a film on formation surfaces thus reducing the rate of rock dissolution. Acids containing these surfactants are known as chemically retarded acids.

Surfactants are also used to break low mobility oil emulsions. Organic amines and quaternary ammonium salts (128), alkylphenol ethoxylates (128), poly(ethylene oxide-co-propylene oxide-co-propylene glycol) (129) and alkyl- or alkylaryl polyoxyalkylene phosphate esters (130) are among the surfactants that have been used.

Mutual solvents have been used to reduce surfactant adsorption on formation minerals, particularly oil-wetting surfactants (131). Ethylene glycol monobutyl ether is the most commonly used mutual solvent.

Formation permeability damage caused by precipitation of dissolved minerals such as colloidal silica, aluminum hydroxide, and aluminum fluoride can reduce the benefits of acidizing (132-134). Careful treatment design, particularly in the concentration and amount of HF used is needed to minimize this problem. Hydrofluoric acid initially reacts with clays and feldspars to form silicon and aluminum fluorides. These species can react with additional clays and feldspars depositing hydrated silica in rock flow channels (106). This usually occurs before the spent acid can be recovered from the formation. However, some workers have concluded that permeability damage due to silica precipitation is much less than previously thought (135).

Precipitation of Fe(III) compounds from acid solutions as the pH increases above 2.2 is a particular problem. Complexing agents that have been used include 5-sulfosalicylic acid and citric acid (136); dihydroxymaleic acid (137); ethylenediaminetetraacetic acid (138); lactic acid (138); blends of hydroxylamine hydrochloride, citric acid, and glucono- δ -lactone (139); nitriloacetic acid; blends of citric acid and acetic acid; lactic acid; and gluconic acid (140).

Diverting agents assist in distributing acid more uniformly through the perforated formation interval (141). These are usually oil-soluble hydrocarbon resin particles. They may be dissolved by post-acid injection of xylene or similar solvents. Oil-soluble waxes, naphthalene, and solid organic acids such as benzoic acid have also been used (142). Best results are obtained using a broad range of particle sizes.

Blends of sodium hypochlorite with 15% HCl and with 12% HCl/3% HF have been used to stimulate aqueous fluid injection wells (143). Waterflood injection wells have also been stimulated by injecting linear alcohol propoxyethoxysulfate salts in the absence of any acid (144). The oil near the well bore is mobilized thus increasing the relative permeability of the rock to water (145). Temperature effects on interfacial tension and on surfactant solubility can be a critical factor in surfactant selection for this application (146).

Corrosion inhibition is primarily associated with acidizing. Buffered hydrofluoric acid compositions have been shown to be less corrosive (147). Corrosion inhibitors are designed to reduce the rate of reaction of fluid with metal surfaces, generally by forming films on the surfaces. Acetylenic alcohols and amines are frequently components of corrosion inhibitor blends. Other compounds that have been used include nitrogen heterocyclics, substituted thioureas, thiophenols, and α -aminoalkyl thioethers (148).

Arsenic compounds can be very effective corrosion inhibitors but their toxicity, ineffectiveness in hydrochloric acids above 17% active and in the presence of H_2S , and their ability to poison refinery catalysts has limited their use (148). Epoxy resins have been coated onto metal surfaces and cured with a polyamine to reduce corrosion (149).

High density brine completion fluids also often require the use of corrosion inhibitors (8,9). Blends of thioglycolates and thiourea; alkyl, alkenyl, or alkynyl phosphonium salts; thiocyanate salts; mercaptoacetic acid and its salts; and the reaction products of pyridine or pyrazine derivatives with dicarboxylic acid monoanhydrides have been used as high density brine corrosion inhibitors.

Hydrogen sulfide promoted corrosion can be a serious problem (150); the best solution is prevention. Corrosion problems can be minimized by choice of the proper grades of steel or corrosion resistant alloys, usually containing chromium or nickel (150, 151) and avoiding generation of H_2S by sulfate reducing bacteria in situations where H_2S is not initially present. Cathodic protection of casing is often effective for wells less than 10,000 feet deep (150).

Scale inhibitors may also be used in acidizing. These include alcohol ethoxysulfonic acids (152). Scale inhibitors are also used in water and enhanced oil recovery injection wells and include low molecular weight poly(vinylsulfonate), poly(methylmethacrylate-co-ethylenediamine) (153), bis(phosphonomethylene)aminomethylene carboxylic acid, and poly(acrylic acid-co-3-acrylamido-3-methylbutanoic acid). Ethylenediaminetetraacetic acid and similar complexing agents have been used to remove scale from formation surfaces near wellbores.

Formation Damage Control Chemicals

The fluid flow capacity of rock, particularly the rock adjacent to an oil or gas well is critical in determining well productivity. The region near the wellbore acts as a choke for the entire formation; because the flow is radial more and more fluid is flowing through a given volume of rock as the fluid approaches the well bore. The reduction of the rock fluid carrying capacity is referred to as formation damage.

Formation damage may be due to invasion of rock capillaries by solid particles in wellbore fluids (drilling and completion fluids) and plugging of rock capillaries adjacent to fractures by fine solid particles in fracturing fluids. These fines may be generated when sand-laden fracturing fluid passes through small orifices such as choke valves at high flow rates and pressures (67) or by proppant crushing within the fracture. They may also be due to the use of solid fluid loss additives. This type of formation damage may be reduced by filtration of fluids before their entry into the well bore and by proper choice and sizing of solid particles used in drilling, gravel packing, and fracturing fluids. Acidizing the rock immediately adjacent to the wellbore can dissolve clays, silica particles, and precipitates plugging rock flow channels. However, precipitation of hydrated silica, fluoroaluminates, and iron compounds (above pH 2.2) in acidizing can cause formation damage reducing well treatment effectiveness (see above).

Reduced injectivity due to formation damage can be a significant problem in injection wells. Precipitate formation due to ions present in the injection water contacting counterions in formation fluids, solids initially present in the injection fluid (scaling), bacterial corrosion products, and corrosion products from metal surfaces in the injection system can all reduce permeability near the wellbore (153). The consequent reduced injection rate can result in a lower rate of oil production at offset wells. Dealing with corrosion and bacterial problems, compatibility of ions in the injection water and formation fluids, and filtration can all alleviate formation damage.

Formation damage can also be caused by chemical and physical interactions of fluid and rock. Low salinity fluids can cause swelling of water-expandable clays. The resulting larger clay dimensions can reduce the fluid carrying capacity of rock flow channels. The expanded clay particles are more susceptible to the shear forces of flowing fluids. In addition, clays act as the cementing medium in many sandstone formations. Swelling weakens this cementation and can cause the release of mineral fine

particles. Fines migration in Berea sandstone occurs when the salinity of the flowing phase drops below a critical salt concentration (CSC) (155,156). The CSC varies for different monovalent cations in solution and decreases with increasing ion exchange affinity of the clay for the cation. The CSC of multivalent cations is very low (157). Flowing fluids can carry these fine particles to constrictions in the flow channels where they form a plug.

Inorganic salts: KCl, NH_4Cl , CaCl_2 , or high concentrations of NaCl have been used in wellbore fluids, fracturing fluids, and injection fluids to temporarily reduce formation damage by converting the more water-expandable smectite and mixed layer clays to less swelling forms through ion exchange processes. However, the potassium, ammonium, or calcium ions on the clays are themselves subject to ion exchange processes and the clays may later be converted back to the more water-expandable sodium form. Once clay swelling has occurred, injection of salts will not reverse formation damage. An acidizing treatment to partially dissolve the clays is required for this.

The addition of potassium hydroxide to injection waters has been used to stabilize clays and maintain injectivity (158). Some degree of permanence appears to result from this treatment since injectivity appeared to be substantially maintained during subsequent injection of low salinity water.

More permanent stabilization of water-swelling clays may be achieved by bonding the clay surface cation exchange sites together so that simultaneous ion exchange at a large number of sites is required for desorption of the clay stabilizer. This may be accomplished by injection of hydroxyaluminum, zirconyl chloride, or certain quaternary ammonium salt polymers. A 6-12 hour well shut-in period is required to allow polymerization of hydroxyaluminum on formation surfaces to occur (159). Because hydroxyaluminum is removed from mineral surfaces by fluids at pH3, it cannot be used in conjunction with acidizing treatments. However, treated clays are stable to high temperatures and hydroxyaluminum can be used in 500°F steam injection wells.

Zirconyl chloride can be used to stabilize swelling clays in both acidic environments and in the presence of 600°F steam (160). No well shut-in time is required for polymerization to occur so zirconyl chloride may be used in conjunction with hydraulic fracturing treatments (161).

Quaternary ammonium salt polymers are more versatile and have been used in drilling fluids, completion fluids, acidizing treatments, and hydraulic fracturing. No well shut-in period is required. Care in choosing the particular polymer to be employed in a fracturing treatment is needed because some polymers can interfere with the function of the crosslinker. Some of these polymers are also stable to high temperature steam and have been successfully used to treat high temperature steam injection wells. Recent developments in organic polymer formation damage control polymers are discussed in chapter 10 of this book.

Fine particle migration can occur in the absence of water-swelling clays. Migrating fines can include the migrating clays kaolinite, illite, chlorite, and some mixed layer clays and fine silica particles (162,163). Fine particle migration is promoted when the

flowing phase is the rock wetting phase (162), is affected by flowing fluid salinity (155-157) and pH (164), and is accelerated by rapid flow rates (165). A critical flow velocity exists below which fines migration is greatly reduced (166).

Conventional inorganic and cationic organic polymer clay stabilizers have been shown to be effective in substantially preventing permeability damage due to clay swelling and consequent fines migration (see Table 1, Chapter 10). However, most of these polymers are much less effective at preventing fines migration in the substantial absence of swelling clays. Recently developed quaternary ammonium salt polymers have been shown to be effective in reducing migration of a variety of mineral fine particles in the absence of swelling clays (see Chapter 10).

Adsorption of corrosion inhibitors or cationic surfactants can reduce sandstone formation permeability. Alcohols can be used to remove corrosion inhibitors from rock surfaces. Oil-soluble corrosion inhibitors may be dissolved by organic solvents such as xylene or toluene containing a mutual solvent, most often ethylene glycol monobutyl ether, EGMBE (167). Aqueous fluids containing 5-10% EGMBE can be used to dissolve cationic surfactants.

Paraffin deposits adjacent to production wells can greatly reduce productivity by plugging fluid flow channels. Deposition of these waxy crude oil deposits can also occur in perforations and production tubing. Scraping has been used to remove deposits from production tubing. Hot oil washes have been used to dissolve paraffins above the perforations. Washing with organic solvents such as xylene or toluene has been used to remove paraffins from perforations and the formation (167). Addition of amines to these solvents can aid in solubilizing asphaltene deposits (167).

Emulsion blocks within the formation can form as a result of various well treatments and are more easily prevented (by using surfactants in conjunction with well treatments, see above) than removed. Aromatic solvents can be used to reduce the viscosity and mobilize oil-external emulsions (167). Low molecular weight urea-formaldehyde resins have been claimed to function in a similar manner in steam and water injection wells (168,169). Water-external emulsion blocks can be mobilized by injection of water to reduce emulsion viscosity.

Gypsum scaling (calcium sulfate precipitation) can occur as aqueous formation fluids cool and experience pressure drops near and in the production wellbore. In wells producing from more than one oil-bearing formation, mixing of different formation waters can also give rise to this scaling problem. The most common solution is washing the wellbore with basic solutions of potassium acetate, potassium glycolate, potassium citrate or potassium hydroxide. Scale deposits are converted to dispersed particles which can be circulated out of the wellbore. A chelating agent such as ethylenediamine tetraacetic acid can aid in dissolving calcium sulfate deposits. Hydrochloric acid following the basic treatment can also be used to dissolve calcium sulfate (167).

Injectivity can be reduced by bacterial slime which can grow on polysaccharides and other polymer deposits left in the wellbore and adjacent rock. Strong oxidizing agents such as hydrogen

peroxide, sodium perborate, and occasionally sodium hypochlorite can be used to remove these bacterial deposits (143,170,171).

Rock Wettability

Wettability is defined as "the tendency of one fluid to spread on or adhere to a solid surface in the presence of other immiscible fluids" (145). Rock wettability can strongly affect its relative permeability to water and oil (145,172). Wettability can affect the initial distribution of fluids in a formation and their subsequent flow behavior. When rock is water-wet, water occupies most of the small flow channels and is in contact with most of the rock surfaces. The converse is true in oil-wet rock. When the rock surface does not have a strong preference for either water or oil, it is termed to be of intermediate or neutral wettability. Inadvertent alteration of rock wettability can strongly alter its behavior in laboratory core floods (172).

In water-wet reservoirs being waterflooded, oil is displaced ahead of the water. The injection water tends to invade the small and medium-sized flow channels (or pores). As the water front passes, the remaining oil is left in the form of spherical, unconnected droplets in the center of pores or globules of oil extended through interconnected rock pores but completely surrounded by water. This oil is immobile and there is little oil production after injection water breakthrough at the production well (145).

In a strongly oil-wet rock, water will tend to invade the larger pores as oil is found in the smaller pores or as a film on rock surfaces. Because the water preferentially flows through the larger pores, flow channels to the producing well develop and water only slowly invades the smaller flow channels. This results in a higher produced water:oil ratio and a lower oil production rate than in the water-wet case.

Care must be taken in all well treatment and injection operations not to alter rock wettability in an undesired manner. Use of carefully selected surfactants in well treatment fluids is a way to accomplish this. Rock wettability can be altered by adsorption of polar materials such as surfactants and corrosion inhibitors, or by the deposition of polar crude oil components (173). Pressure appears to have little influence on rock wettability (174). The two techniques used to study wettability, contact and relative permeability measurements, show qualitative agreement (175-177). Deposition of polar asphaltenes can be particularly significant in carbon dioxide enhanced oil recovery.

Primary and Secondary Oil Recovery

Primary oil recovery is the production of oil driven to wellbores by the energy of fluids under pressure in the reservoir. As reservoir pressure is reduced by oil production, additional recovery mechanisms may operate. One is natural water drive as water from an adjacent more highly pressured formation is forced into the oil-bearing formation by the pressure differential between the formations. Gas drive, expansion of a gas cap above the oil as

oil pressure declines can also drive additional oil to the wellbore. Additional oil may be produced by compaction of the reservoir rock as this pressure is reduced by oil production. Generally the additional oil produced by reservoir compaction is small. As the natural pressures in the reservoir decrease, oil production declines. The oil well may then be placed "on pump" to maintain production at economic levels; the pump is used to draw oil to the surface and keep the production well relatively free of fluid. (The pressure of a column of fluid can decrease the rate of fluid entry into the wellbore.)

Primary production typically recovers 10-25% of the oil originally in place in the reservoir. The efficiency of primary production is related to oil properties, reservoir properties, geometric placement of oil wells, and the drilling and completion technology used to drill the wells and prepare them for production. Waterflooding or secondary oil recovery is a means of adding energy to the reservoir. Water injection through some wells results in a pressure differential across a reservoir resulting in the movement of oil and injected water to offset production wells. The geographic arrangement of production and injection wells is critical to maximizing oil recovery and can be related to the geology of the reservoir (145). Salinity of the available injection water can have an important effect on the efficiency of oil recovery. Scaling, the formation of insoluble precipitates when the saline injection water contacts a formation brine, is a particularly common problem and many scale inhibitors have been developed to reduce precipitation near the injection wells where permeability reduction can greatly reduce injection rate (see above).

Injection rate can have a major effect on the economics of secondary oil recovery. Acidizing or carefully designed hydraulic fracturing treatments can be used to increase injection rates. More recently well treatments that do not interrupt normal water injection operations have increased in frequency. Addition of surfactant to the injection water (144,146) can displace the oil remaining near the production well. The lower oil saturation results in an increase in the water relative permeability (145). Consequently a greater water injection rate may be maintained at a given injection pressure or a lower injection pressure. Thus smaller and cheaper injection pumps may be used to maintain a given injection rate. While the concentration of surfactant in the injection water is relatively high, the total amount of surfactant used is not great since it is necessary only to displace the oil from a 6-10 foot radius around the injection well.

Extensive waterflooding began in the 1940's. Currently waterflooding accounts for about 40% of domestic oil production. Waterflooding typically recovers 15-25% of the oil originally in place.

Organic and inorganic polymers have been used to improve the results obtained in waterflooding. Crosslinked polymers (see below) have been used to reduce the permeability of fractures and high permeability streaks so that injected water flows through a larger fraction of the reservoir volume. The polymer is injected with a crosslinker or the crosslinker may be injected after the

polymer. In either case, crosslinking occurs in situ. Sodium silicate gelation has also been used in this application (178,179). The use of organic polymers in injection wells is discussed below. Both in situ crosslinking of partially hydrolyzed polyacrylamides (180) and quaternary ammonium salt polymers with long sidechains (181) have been used to reduce the permeability of water producing zones adjacent to production wells and decrease the produced water:oil ratio.

Enhanced Oil Recovery

Primary and secondary oil recovery together recovery only 25-50% of the oil originally in place in a reservoir. Cumulative U.S. production of 133 billion barrels of oil and remaining reserves of 27.5 billion barrels account for only 33% of the 488 billion barrels of oil discovery to date (182). In a more recent reference (183), recoverable reserves as of Jan. 1, 1989 were estimated to be 26.5 billion barrels. The increasing cost of discovering major new oil reserves in the U.S. (which most likely exist in frontier regions of Alaska and deep water offshore) make unrecovered oil in known fields an attractive target. Its location is known and much of the infrastructure: wells, storage tanks, pipelines, roads, etc. are already in place.

Major disincentives to enhanced oil recovery are the lack of tax incentives and a substantial decline in the price of oil since the end of 1981. All the investment in new wells and surface facilities and injectants must take place before any incremental oil is produced.

This decline in the price of oil has resulted in major changes in the types of enhanced oil recovery (EOR) being studied in the laboratory and field tested. Steam injection and injection of miscible gases, primarily CO₂, remain of great interest due to the relatively low cost of the injectants (although they are quite expensive as compared to water). More expensive injectants such as used in micellar polymer flooding can often efficiently recover oil. However, the large concentration of surfactant (often as much as 2-5% wt plus the additional cost of the polymer used to provide mobility control (see below), usually used in concentrations of 100-1000ppm, have made these fluids prohibitively expensive.

Recent research and field tests have focused on the use of relatively low concentrations or volumes of chemicals as additives to other oil recovery processes. Of particular interest is the use of surfactants as CO₂ (184) and steam mobility control agents (foam). Also combinations of older EOR processes such as surfactant enhanced alkaline flooding and alkaline-surfactant-polymer flooding have been the subjects of recent interest. Older technologies: polymer flooding (185,186) and micellar flooding (187-189) have been the subject of recent reviews. In 1988 84 commercial products: polymers, surfactants, and other additives, were listed as being marketed by 19 companies for various enhanced oil recovery applications (190).

Other important issues influencing the economics of oil recovery include methods of determining fluid movement and behavior within the reservoir (191); the effect of oil composition on oil

recovery, particularly in miscible flooding (192); and corrosion control (193). Seismic, geotomographic, controlled-source audio magnetotelluric, and pressure analyses as well as tracer chemical injection and analyses are all used to understand fluid movement within the reservoir and monitor EOR processes (191).

Oil Recovery Mechanisms

The amount of oil recovery promoted by an injected fluid is related to its ability to displace the oil it contacts in the reservoir, termed the oil displacement efficiency (ODE), and to the relative amount of the reservoir invaded by the injected fluid, termed the volumetric sweep efficiency (VSE). Total oil recovery may be expressed as:

$$\text{Oil Recovery} = \text{VSE} \times \text{ODE}$$

For example, consider a reservoir which has produced 40% of the oil originally in place. If an injection fluid contacts 70% of the reservoir and has an oil displacement efficiency of 70% of the remaining oil (42% of the oil originally in place) then the maximum enhanced oil recovery is 49% of the oil remaining in place or 29% of the oil originally present in the reservoir. (Trapping and other oil loss mechanisms are neglected in this simplified treatment.) Total oil recovery has increased to 69%.

This example illustrates the importance of using chemicals to improve both the volumetric sweep efficiency and the oil displacement efficiency. Although the greatest attention has been given to increasing the oil displacement efficiency, primarily through the use of surfactants, a government study indicated that volumetric sweep efficiency is the greatest obstacle to increasing oil recovery (194).

Improving Volumetric Sweep Efficiency

Volumetric sweep efficiency is determined by the permeability and wettability distribution in the reservoir and by the properties of injected fluids. Waterflooding characteristically exhibits poor volumetric sweep efficiency. The more expensive the injection fluid, the more important it is to have a high volumetric sweep efficiency so that the injected fluid contacts and thus mobilizes a larger volume of oil. High permeability streaks or layers (thief zones) and natural or induced rock fractures can channel the injected fluid through a small portion of the reservoir resulting in a low volumetric sweep efficiency.

Crosslinked polymers have been widely used to substantially seal these thief zones and fractures thus directing subsequently injected fluids to different parts of the reservoir increasing VSE in waterflooding and chemical flooding. The most commonly used polymers are partially hydrolyzed polyacrylamides (195) although field applications of crosslinked xanthan gum have also been reported (196). These are generally injected at concentrations of 1000-5000 ppm and crosslinked in situ. Treatments are restricted to the near-wellbore region due to the kinetics of the crosslinking

process. The most commonly used crosslinkers are Al(III) (196-198) and Cr(III) compounds(199). The injected fluid preferentially enters the thief zone. The well is shut in to allow crosslinking to occur. After 1-7 days depending on the treatment, normal injection operations are resumed.

Aluminum (III) citrate and sodium aluminate have been used as crosslinkers. The polymer and crosslinker solutions are injected as alternate slugs. A layer of adsorbed polymer is built up which is then crosslinked to subsequently injected polymer (200). Cationic polyacrylamide may be used in the initial treatment stages to promote rapid polymer adsorption (201). Adjustment of the pH may allow deeper penetration of the fluids in an aluminate crosslinking system prior to gelation (202). A process involving injection of alternate slugs of stoichiometrically equivalent amounts of partially hydrolyzed polyacrylamide and $Al_2(SO_4)_3$ has been evaluated in the laboratory; permeability of sand packs were reduced by more than 96% (203). Mixtures of Al(III) and Zr(IV) have also been evaluated as partially hydrolyzed polyacrylamide crosslinkers (204).

Sodium bisulfite and thiourea have been used to reduce injected Cr(VI) to the reactive Cr(III) species that promotes crosslinking (205,206). Kinetic studies suggest that the crosslink structure includes two chromium atoms bridged by oxygen (205). Gradual dissolution of colloidal $Cr(OH)_3$ has been used to delay crosslinking to permit deeper polymer penetration in the formation prior to crosslinking (207) as has the use of Cr(III) propionate (208). Injection of unhydrolyzed polyacrylamide followed by *in situ* hydrolysis delays Cr(III) crosslinking (209). The rate of the hydrolysis reaction is dependent on temperature but not on injection and formation water salinity (210). Studies suggest that 5-10% hydrolysis is the optimum to produce a crosslinked polyacrylamide (211).

Occasionally it may be desirable to have a rapid crosslinking take place. Blends of chromium triacetate and hydrochloric acid have been used in this situation (212). Gelation time decreases substantially as applied shear increases (213,214). Thus, static laboratory gelation time experiments should not be used to predict gelation time in actual well treatments.

Organic crosslinkers have also been used. These include glyoxal (215) and formaldehyde. Use of hypohalite salts (216,217) and epichlorohydrin (218,219) have been found to increase gel stability.

Copolymers of sodium acrylate with sodium 2-acrylamido-2-methylpropane sulfonate (220) or N,N-dimethylacrylamide (221) have been found useful for preparing crosslinked systems that must function at high temperatures and relatively high salinity. Chromium crosslinked gels prepared from a 3:1 blend of partially hydrolyzed polyacrylamide and guar gum have been found to have a higher strength and stability than gels prepared from the partially hydrolyzed polyacrylamide alone (222).

Crosslinked xanthan gums have also been used to reduce the permeability of thief zones. Trivalent chromium and aluminum have been used as crosslinkers (223,224). While crosslinker effectiveness is reduced at high salinity, Cr(III) has been used in the field at

salinities as great as 166,000 ppm total dissolved solids (224). Xanthan gum can be precipitated by quite high concentrations of divalent metal ions to plug thief zones (225). Xanthan gum plus a partially methylated melamine-formaldehyde resin has been used to form a gel (226).

Carboxymethylhydroxyethyl cellulose has been gelled by hydrated lime (227). Succinoglycan has been crosslinked by Cr(III), Al(III), Zr(IV), Ti(IV), and other trivalent metal ions (228,229).

Careful sizing of the treatment and choice of injection rates is required to prevent inadvertent overtreatment *i.e.*, excessive treatment of oil-containing rock. The post-treatment fluid injection rate is usually significantly less than that prior to treatment. While successful applications of this technology in waterfloods and in surfactant polymer floods have been reported, temperature and pH stability limitations of the polymer and the crosslinking chemistry result in few if any applications in steam and CO₂ injection wells.

Reactive monomers such as acrylamide in concentrations of 2-5%w and various additives including a free radical polymerization initiator may be used to form polymers in situ (230-232). An optional reactive difunctional monomer such as N,N'-methylenebis(acrylamide) can be added to the formulation to form a cross-linked polymer in the high permeability zone. The low viscosity aqueous fluid may be injected at relatively high rates and preferentially enters the high permeability zones to a greater extent than do non-Newtonian polymer solutions (233). Polymerization takes place forming a high permeability mass that greatly reduces rock permeability. If no difunctional monomer is used, this mass may be slowly dissolved by injection water. This process increases injection water viscosity (see below).

If the two functional groups of the difunctional monomer differ substantially in reactivity, the difunctional monomer may be injected without any comonomer. An example is 2-hydroxyethylacrylate which can polymerize rapidly through the carbon-carbon double bond and form crosslinks more slowly through hydrogen atom abstraction from the hydroxyl group. Less reactive monomers such as 2-hydroxyethyl acrylate and the use of less reactive polymerization initiators permit the use of this technology in somewhat higher temperature formations.

Lignosulfonates may be crosslinked in situ using Cr(III) (234,235) or an acidic gas such as CO₂ (227) to promote crosslinking. Crosslinked lignosulfonate has been reported to be quite effective at high formation temperatures. Lignosulfonate concentration is usually 2-3% by weight. This gelation technology has been evaluated in field tests in both waterflood and steam injection wells. An advantage of this technology appears to be the ability of this system to crosslink at long distances from the injection well bore. Chemical reactivity at formation temperatures and in situ dilution effects can limit the effective treatment radius of the crosslinked polymer systems described above. Blends of lignosulfonate and sodium silicate have also been evaluated in the field (236).

Phenol-formaldehyde resins (237, 238), urea-formaldehyde resins (239,240), melamine-formaldehyde resins (241), furfuryl

alcohol resins (242) and resins of formaldehyde plus sulfonated tannin extract (243) or alkali Kraft lignin (244) have been evaluated to seal thief zones near water and steam injection wells. Polymer gels formed in situ from polyvinyl alcohol and aldehydes (245) and by Cr(III) crosslinking of alkylene oxide - styrene block copolymers (246) have also been evaluated.

Surfactant precipitation may be used for in-depth permeability reduction of thief zones (247). This process is based on the sequential injection of a slowly propagating ionic surfactant followed by an aqueous spacer containing no surfactant, and then a more rapidly propagating ionic surfactant of the opposite charge type. In a sandstone reservoir, one would initially inject a cationic surfactant and then an anionic surfactant. The oppositely charged surfactants gradually mix in the high permeability portions of the reservoir resulting in the formation of precipitates. These precipitates plug flow channels and the cumulative effect is to reduce permeability in the most flooded portions of the reservoir diverting injectant to rock zones containing higher oil saturations. The economically limiting factors in the use of this process would probably be the cost and propagation rate of the cationic surfactant.

The use of polyethylene glycol ethers in a process in which a high viscosity emulsion is formed on contact with residual crude oil has also been tested as a means of plugging thief zones using surfactants (248-250). Precipitation of sodium pectate when fresh water solutions contact brine has been proposed as a method of plugging high permeability zones (251).

Polymer Flooding (186,187,252)

Even in the absence of fractures and thief zones, the volumetric sweep efficiency of injected fluids can be quite low. The poor volumetric sweep efficiency exhibited in waterfloods is related to the mobility ratio, M . This is defined as the mobility of the injected water in the highly flooded (watered-out) low oil saturation zone, m_w , divided by the mobility of the oil in oil-bearing portions of the reservoir, m_o , (253,254). The mobility ratio is related to the rock permeability to oil and injected water and to the viscosity of these fluids by the following formula:

$$M = m_w/m_o = (k_{rw}/\mu_w)/(k_{ro}/\mu_o)$$

wherein k_{rw} and k_{ro} represent the relative permeability to water and oil respectively and μ_w and μ_o represent the viscosity of the aqueous and oil phases respectively.

The displacing fluid may be steam, supercritical carbon dioxide, hydrocarbon miscible gases, nitrogen or solutions of surfactants or polymers instead of water. The VSE increases with lower mobility ratio values (253). A mobility ratio of 1.0 is considered optimum. The mobility of water is usually high relative to that of oil. Steam and oil-miscible gases such as supercritical carbon dioxide also exhibit even higher mobility ratios and consequent low volumetric sweep efficiencies.

The first mobility control agents were partially hydrolyzed polyacrylamides having molecular weights of $1-5 \times 10^6$ (254-259) and xanthan gum (biopolymer) (1,34,260). Virtually all field projects have used polymers from one of these two classes although variations in polymer molecular weight and structure have been made to improve performance properties (see below). Relatively low polymer concentrations (down to ca. 100ppm) can significantly increase injected water viscosity. The increase in apparent viscosity in porous media was often significantly greater than that exhibited in conventional laboratory viscosity measurements (259). Another benefit of both polyacrylamides and xanthan gum is a long-lasting decrease in rock permeability to aqueous fluids that persists even during long periods of water injection. This residual resistance effect has been observed in laboratory tests and some field trials. After termination of polymer injection, the North Stanley Field and North Burbank Unit 29 polymer field tests exhibited injected water permeability reductions attributed to residual resistance effects that lasted for more than three years and more than seven years respectively (261,262).

Each polymer type has important advantages and significant disadvantages. These are summarized in Table I and discussed below for polymers representative of those presently used.

Table I. Properties of Polyacrylamide and Xanthan Gum EOR Polymers

Property	Polyacrylamide	Xanthan Gum
Brine tolerance	very limited, esp. to Ca^{+2} , Mg^{+2}	good tolerance to mono- and divalent cations
Transition metal cations	easily crosslinked	easily crosslinked
Shear stability	undergoes irreversible shear degradation	reversible shear thinning.
Thermal stability	maximum use T 225° - 250° F	maximum use T 160 - 170° F
Hydrolytic stability	hydrolysis promoted by acid or base. Partially hydrolyzed product more sensitive to Ca^{+2} , Mg^{+2}	hydrolytic depolymerization promoted by acid or base esp. at high T
Oxidative stability	susceptible	particularly susceptible esp. at high T
Microbial degradation	susceptible to attack by yeasts, fungi, bacteria	very susceptible in aerobic conditions

Compared to partially hydrolyzed polyacrylamide, xanthan gum is more expensive, more susceptible to bacterial degradation, and less stable at elevated temperatures (1). However, xanthan gum is more soluble in saline waters, particularly those containing divalent metal ions; generally adsorbs less on rock surfaces; and is substantially more resistant to shear degradation (1,34). The extensional viscosity of the semi-rigid xanthan molecule is less than that of the flexible polyacrylamide (263).

In addition to the normal problems of completely dissolving particles of water-thickening polymers, xanthan gum contains insoluble residues the cumulative effect of which is to decrease polymer injectivity. Fermentation broths containing 8-15% by weight xanthan can be used to prepare solutions which contain no undissolved polymer particles (264). Flash drying of polymer broths can produce a solid product which dissolves more readily in injection waters (264). Other means of improving xanthan solution injectivity include brief (30 sec) ultrasonic treatment at 60-80 MHz (265), solid polymer hydration in solutions of metal complexing agents such as sodium citrate (266) or low concentrations of boron species (266), heat treatment (267,268), bentonite treatment followed by filtration through diatomaceous earth (266,269), passing xanthan solutions through a colloid mill (270), treatment with methylenebis(isocyanate) (271), cellulase enzymes (272,273), proteases (272,273), polysaccharide hydrolases (274), or caustic agents plus an enzyme (274). Flow channels adjacent to the well-bore which have been plugged with solid xanthan residues may be reopened by treatment with oxidizing agents such as hydrogen peroxide.

Use of oxygen scavengers (275,276,277) and bactericides (278) is common practice in field operations. Among the oxidation stabilizers used are thiourea (279), sodium dithionite (280), guanidine acetate (281), and a blend of sodium sulfite, thiourea, and 2-propanol (282). Among the other chemicals studied as xanthan gum and polyacrylamide stabilizers are: sodium bisulfite, sodium 2-mercaptobenzothiazole and benzoimidizol (283), 2-thioimidazolidone (284), 1-tolylbiguanide (285), 2-thiazoline-2-thiolate (286), dithiocarbamates (287), methionine (288), thiosulfuric acid (289), and phosphonic acid esters (290), and mixtures of isobutanol, sodium 2,4,6-trichlorophenate, and sodium diethylenetriaminepentaacetic acid (291).

When dissolved in more saline waters, xanthan gum produces a higher apparent viscosity than the same concentration of polyacrylamide (292). Prehydration of xanthan in fresh water followed by dilution in the saline injection water has been reported to provide higher viscosity than direct polymer dissolution in the same injection water. Optical rotation and intrinsic viscosity dependence on temperature indicate xanthan exists in a more ordered conformation in brine than in fresh water (293).

Although high concentrations of pyruvate ring-opened polymers exhibit increased tolerance to divalent metal ions in high density completion fluids (294), at low polymer concentrations, xanthan containing the intact pyruvate ring exhibits higher brine solution viscosity and better filterability than its ring-opened analog (295). A xanthan gum containing pyruvate rings in most of the

polymer repeat units has been produced by a proprietary strain of Xanthamonas campestris (296) and evaluated for polymer flooding applications (295).

Other microbial polysaccharides have also been evaluated for use in enhanced oil recovery. These include scleroglucan (299-300) which is thought to exist in solution in a rigid helical conformation, polymers produced by the bacterium Pseudomonas methanica (301), by Leuconostoc mesenteroides (302), by Aerobacterium NC1B11883 (303), the alga Porphyridium aeruginium (304), and nonionic glucose homopolysaccharides produced by fungi (305). Xanthamonas bacteria have also been used to produce a polysaccharide comprising glucose and mannose units in a 2:1 ratio. This polymer has been claimed to be a better water viscosifier than xanthan gum (306). Saccharide polymers may be prepared by the polymerization of 3-O-methacryloyl-D-glucose (307).

Most polyacrylamides used as mobility control agents are actually partially hydrolyzed or are acrylamide - acrylic acid (or sodium acrylate) copolymers produced by emulsion copolymerization (308). Emulsion polymers are used to avoid the high shear degradation and undissolved solid particle problems often associated with solid polyacrylamide dissolution. Another method of avoiding problems associated with hydration of solid polymer particles is acrylamide solution polymerization at the wellhead. The polymerization can be designed to proceed at adequate rates and in saline injection waters to provide polymers of adequate viscosity characteristics (309). Polyacrylamide is usually hydrolyzed in base to produce a random distribution of acrylate groups. This random distribution is similar to that obtained in a copolymer having the same acrylate group content (310). Acid hydrolysis results in a more block-like distribution of acrylate units (311). ⁶⁰Co irradiation has been used to initiate polymerization and prepare particularly high molecular weight polyacrylamides (312).

Electrostatic repulsion of the anionic carboxylate groups elongates the polymer chain of partially hydrolyzed polyacrylamides increasing the hydrodynamic volume and solution viscosity. The extensional viscosity is responsible for increased resistance to flow at rapid flow rates in high permeability zones (313). The screen factor is primarily a measure of the extensional (elongational) viscosity (314). The solution properties of polyacrylamides have been studied as a function of NaCl concentration and the parameters of the Mark-Houwink-Sakaruda equation calculated (315). Maximum freshwater viscosity occurs at ca. 35% hydrolysis (316) while maximum viscosity in a Ca^{+2} -containing brine occurs at 10-15% hydrolysis. Metal ions interact with carboxylate groups reducing their mutual repulsion and thus decreasing hydrodynamic volume and solution viscosity. Divalent metal ions reduce viscosity more than monovalent ones (317). Above 33-35% hydrolysis, interaction with Ca^{+2} causes polyacrylamide precipitation (318). The major mode of polyacrylamide decomposition at elevated temperature (in the absence of oxygen) is hydrolysis (319,320). Thus, the concentration of divalent metal ions has an effect on viscosity retention at high temperature. Chelating and sequestering agents have been used to reduce the adverse effect of

divalent (316) and multivalent metal ions on polyacrylamide solution viscosity (321,322).

Proper well completion, particularly perforation design, can reduce polyacrylamide shear degradation during entry into the formation (313).

Acrylamide copolymers designed to reduce undesired amide group hydrolysis, increase thermal stability, and improve solubility in saline media have been synthesized and studied for EOR applications. These polymers still tend to be shear sensitive. Acrylamide comonomers that have been used include 2-acrylamido-2-methylpropane sulfonate, abbreviated AMPS, (1,321-324), 2-sulfoethylmethacrylate (325,326), diacetone acrylamide (324, 326), and vinylpyrrolidinone (327,328). Acrylamide terpolymers include those with sodium acrylate and acrylamido-N-dodecyl-N-butyl sulfonate (329), with AMPS and N,N-dimethylacrylamide (330), with AMPS and N-vinylpyrrolidinone (331), and with sodium acrylate and sodium methacrylate (332). While most copolymers tested have been random copolymers, block copolymers of acrylamide and AMPS also have utility in this application (333).

Acrylamide terpolymers having a heterocyclic ring in the polymer backbone have been shown to exhibit improved viscosity and shear degradation properties (334,335). A disadvantage of acrylamide copolymers is their greater cost as compared to partially hydrolyzed polyacrylamides. Acrylamide graft copolymers have been studied in an effort to reduce copolymer costs. These include acrylamide graft copolymers with starch (336), dextran (337), and lignin (338).

Polymer association complexes (38-43, see above) including those which form micelle structures by association of hydrophobic groups such as nonylphenoxy polyethylene glycol acrylates (339), acrylamide terpolymers containing hydrophobic alkylacrylamides (340-343), and poly(styrene-co-maleic anhydride) vinylbenzylpolyglycol ethers (344) substantially increase water viscosity at quite low polymer concentrations. Similar hydrophobically modified polysaccharides such as hexadecyloxyhydroxyethyl cellulose (345) may be suitable for use in enhanced oil recovery. These polymer association complexes exhibit much higher solution viscosity than equal concentrations of conventional polymers.

The substantial decrease of polyacrylamide solution viscosity in mildly saline waters can be utilized to increase injection rates by adding a quaternary ammonium salt polymer to the polyacrylamide mixing water (346,347). If the cationic charge is in the polymer backbone and substantially shielded from the polyacrylamide by steric hindrance, formation of an insoluble interpolymer complex can be delayed long enough for polymer injection. Upon contacting formation surfaces, the quaternary ammonium salt polymer is adsorbed reducing solution salinity and thus increasing viscosity away from the wellbore where it will not adversely affect injectivity. By using a clay stabilizing quaternary ammonium salt polymer, formation damage associated with low salinity polyacrylamide solvents can be reduced (348).

Propagation of enhanced oil recovery chemicals through rock is critical to the success of an EOR project. Polymer retention in permeable media has been the subject of considerable study (349)

and mechanical entrapment as well as adsorption has been identified as a cause of polymer loss (350,351). Sacrificial adsorption agents may be used to reduce the adsorption of expensive polymers and surfactants. Lignosulfonates and their derivatives have been extensively evaluated for this application (34,352-356). Other chemicals tested for this application include poly(vinyl alcohol) (357), sulfonated poly(vinyl alcohol) (358), sulfonated poly(vinylpyrrolidinone) (358), low molecular weight polyacrylates (359), and sodium carbonate (360).

Surfactants for Mobility Control

Despite its relatively high mobility, water has been used to decrease the mobility of even higher mobility gases and supercritical CO₂ used in miscible flooding (361). While water mobility can be up to ten times that of oil, the mobility of gases can be 50 times that of oil (362). The following formula is used to calculate gas:oil mobility ratios (363):

$$M = \left[\left(\frac{k_g}{\mu_s} \right) + \left(\frac{k_w}{\mu_w} \right) \right] \bigg/ \left[\left(\frac{k_o}{\mu_o} \right) + \left(\frac{k_w}{\mu_w} \right) \right]$$

wherein k refers to permeability, μ to viscosity, and g , s , o , and w to gas, miscible solvent, oil, and water respectively. The water may be injected simultaneously with the gas or in alternate slugs with the gas (WAG process). X-ray computerized tomography of core floods has demonstrated the increased volumetric sweep efficiency attained in the WAG process (364).

The WAG process has been used extensively in the field, particularly in connection with supercritical CO₂ injection and some success have been reported (365-367). However, it would be desirable to develop a method to further reduce the viscosity of injected gas, particularly CO₂, the most commonly used gas (actually injected as a supercritical fluid) in the U.S.. While limited studies on increasing the viscosity of CO₂ through the use of supercritical CO₂-soluble polymers and other additives have been reported (368, see also Chapter 29 and references therein), the major direction of research has been the use of surfactants to form low mobility foams or supercritical CO₂ dispersions within the formation.

The behavior of foam in porous media has been the subject of extensive study and recently a collection of papers on this subject (369), a review of foam rheology (370), and an extensive bibliography (371) have been published. X-ray computerized tomographic analysis of core floods indicated that addition of 500 ppm of an alcohol ethoxycerylsulfonate increased volumetric sweep efficiency substantially over that obtained in a WAG process (364).

The role of various surfactant association structures such as micelles and lyotropic liquid crystals (372), adsorption-desorption kinetics at liquid-gas interfaces (373) and interfacial rheology (373) and capillary pressure (374) on foam lamellae stability has been studied. Microvisual studies in model porous media indicate

that the predominant mechanisms of in situ foam generation are snap-off at pore constrictions (375,376), lamellae leave-behind (375), and lamellae division (375).

The reason for wide-spread interest in the use of surfactants as gas mobility control agents (369) is their effectiveness at concentrations of 0.1%wt (377) or less (364). This low chemical requirement can significantly improve process economics.

Another advantage is the wide range of surfactant classes and chemical structure variations within each class of surfactant which can be screened to optimize surfactant performance for a given set of reservoir conditions. Any change in surfactant structure should increase the propagation rate and the displacement efficiency. It has been noted that this is possible only by decreasing surface viscosity (378). Among the classes of surfactants studied for this application are alcohol ethoxylates and their sulfate and sulfonate (364,379-384), and carboxylate (385) derivatives, alkylphenol ethoxylates (382), alpha-olefin sulfonates (383), and alkylated diphenylether disulfonates (386). Increased linear hydrophobe carbon chain length, decreased hydrophobe branching, and increased ethoxy group chain length was found to increase foam stability (380). When using mixtures of surfactants or surfactants plus an alcohol, foam stability, injected breakthrough time at the core outlet, and oil recovery were maximized when the two surfactants or the surfactant and the alcohol had the same carbon chain length (387,388). Addition of a water-thickening polymer to the aqueous phase will stabilize the foam (389-391).

In addition to the mobility control characteristics of the surfactants, critical issues in gas mobility control processes are surfactant salinity tolerance, hydrolytic stability under reservoir conditions, and surfactant propagation. Lignosulfonate has been reported to increase foam stability and function as a sacrificial adsorption agent (392). The addition of sodium carbonate or sodium bicarbonate to the surfactant solution reduces surfactant adsorption by increasing the aqueous phase pH (393).

Alcohol ethoxysulfates have been used in field tests as foaming agents for nitrogen (394) and carbon dioxide (395). Application of alcohol ethoxysulfates is restricted due to its limited hydrolytic stability at low pH and elevated temperature (396).

High temperature steam has also been used in enhanced oil recovery, for the recovery of highly viscous crude oils (397). In heavy oil fields, water flooding is often omitted and steam injection begun immediately after primary production. Steam injection temperature, usually 350-450^oF in California oil fields, can reach 600^oF in Canadian and Venezuelan projects. Heat is transferred from the steam to the rock and crude oil reducing oil viscosity. This increases oil mobility thereby enhancing oil production.

Gravity override is the migration of the steam to the upper portion of the formation and is caused by the low steam density. This results in channeling of the steam through the upper portion of the reservoir and a low volumetric sweep efficiency. Surfactants have been used as steam mobility control agents in both laboratory and field tests to prevent this gravity override thereby increasing volumetric sweep efficiency. Surfactants that have been

used in field tests include C₁₆₋₁₈ alpha-olefin sulfonates, alkyltoluene sulfonates, and neutralized dimerized alpha-olefin sulfonic acid.

Careful screening procedures are required to evaluate surfactants as steam foaming agents (398,399). Increasing the hydrophobe carbon number in alpha-olefin sulfonates from 14-16 to 16-18 to >25 has been reported to improve foam strength (400,401). In alkylaromatic sulfonates, longer linear alkyl groups (402) or dialkyl substitution (403) seem to have the same effect. Other alkylaromatic sulfonates containing benzene, toluene, or xylene rings (402, 404); two fused aromatic groups (405); and the diarylether group (406) have been favorably evaluated as steam foaming agents. The neutralized dimer of an alpha-olefin sulfonate has also been used (407).

The high temperature steam will cool and eventually condense as it propagates through the oil reservoir. In order to maintain foam strength as the steam cools, a noncondensable gas, most often nitrogen or methane, is usually added to the injectant composition (408). A method of calculating the optimum amount of noncondensable gas to use has been reported (409).

Critical parameters affecting surfactant performance are surfactant propagation rate and surfactant stability at steam temperatures that can reach more than 600°F. Surfactant propagation rate can be reduced by adsorption, precipitation, and partitioning into the oil phase. Adsorption increases with increasing salinity and decreases with increasing temperature (410). A numerical model of foaming agent transport has been developed which uses the surface excess variable in describing surfactant adsorption (411).

Surfactant propagation can be improved by the use of additives. Both surfactant partitioning and precipitation tend to increase with increasing calcium ion concentration (412) so minimizing divalent metal ion concentration in the surfactant solution is desirable. Injection of a surfactant preslug containing NaCl will convert clays to their sodium form reducing, later ion exchange processes that result in the presence of Ca²⁺ ions in the surfactant solution (413,414). The use of a hydrotrope such as sodium xylene sulfonate has been reported to increase oil recovery in laboratory steam foam floods of sandpicks (415). The hydrotropes may function as sacrificial adsorption agents or interact with the foaming agent to stabilize lamellae and increase foam strength. Thermal stability of the foaming agent in the presence of high temperature steam is essential. While alkylaromatic sulfonates possess superior chemical stability at elevated temperatures (416-419), alpha-olefin sulfonates possess sufficient chemical stability to justify their use at steam temperatures characteristic of most U.S. steamflood operations. Decomposition is a desulfonation process which is first order in both surfactant and acid concentrations (417). Since acid is generated in the decomposition, the process is autocatalytic. However, reservoir rock has a substantial buffering effect. The addition of high pH agents such as sodium hydroxide to the surfactant solution has been reported to increase foam strength and stability (420). The sodium hydroxide may function by precipitating with calcium ions to improve surfactant propagation (421). This is also the mechanism

by which sodium carbonate and trona ($\text{Na}_2\text{CO}_3/\text{NaHCO}_3$) function when used as steam foam additives (422). These additives can also maintain the pH at a high enough value to reduce the rate of surfactant decomposition. In addition, the added base may interact with petroleum soaps naturally found in the crude oil to more efficiently displace oil (420); the consequent lower oil saturation can result in a more stable foam.

High sulfur content heavy crude oil may be recovered more efficiently using transition metal ions such as Ti or V and optionally carbon monoxide as steam additives (423).

Improving Oil Displacement Efficiency

The use of relatively large concentrations of surfactants, usually 2-5%w, to substantially increase oil displacement efficiency has been the subject of very extensive study (188-190,424-426). This complex process usually involves the injection of a brine preflush to adjust reservoir salinity followed by injection of a micellar slug comprising the surfactant, a "cosurfactant" (usually a C_{4-6} alcohol) and a hydrocarbon. A polymer solution is usually injected after the micellar slug to reduce viscous fingering of the drive fluid into and through the micellar slug. This viscous fingering causes dilution of the surfactant, less contact of the micellar slug with the crude oil, and trapping of some of the micellar slug in the reservoir. Process effectiveness depends on maintaining an ultralow interfacial tension (<0.01 dynes/cm) between the injected surfactant slug and the crude oil (427). The surfactant-rich microstructures involved in oil recovery include vesicles as well as micelles (428). Interfacial tension behavior is sensitive to the presence of air and is both temperature and pressure dependent, it can be different for stock tank oil and live (containing dissolved gases under pressure) reservoir crude oil (174). Therefore interfacial tension, phase behavior, and core flood tests should be carefully designed.

By about 1980, the emphasis of research had shifted from inexpensive surfactants such as petroleum sulfonates to more expensive but more effective surfactants tailored to reservoir and crude oil properties. Critical issues are: surfactant performance in saline injection waters, surfactant adsorption on reservoir rock, surfactant partitioning into the crude oil, surfactant chemical stability in the reservoir, surfactant interactions with the mobility control polymer, and production problems caused by produced emulsions. Reservoir heterogeneity can also greatly reduce process effectiveness. The decline in oil prices dating from the end of 1981 halted much of this research due to the relatively high cost of micellar processes (also called surfactant polymer flooding). Since 1982 the number of field projects in progress evaluating this technology has dropped from 20 to 9 (429). Only one field test since 1982 has been successful enough that expansion of the project has been considered (430).

The thrust of surfactant flooding work has been to develop surfactants which provide low interfacial tensions in saline media, require less cosurfactant, are effective at low concentrations, and exhibit less adsorption. The optimal salinity concept and the

salinity requirement diagram (431,432) are extremely useful when screening surfactants. When comparing the performance of different surfactants, it is important that the comparison be made at the optimal salinity of each surfactant or, if it is not possible to adjust injection water salinity, in the actual injection water to be used in a given field project.

While nonionic surfactants such as alcohol ethoxylates, alkylphenol ethoxylates (433) and propoxylates (434) and alcohol propoxylates (434) have been studied, most recent work has been on anionic surfactants: alcohol propoxysulfates (434), alkylphenol propoxysulfates (434), alcohol alkoxyalkylsulfonates (435), alkylphenol alkoxyalkylsulfonates (435), secondary alkane sulfonates (436), alpha-olefin sulfonates (436), calcium or magnesium salts of alpha-olefin sulfonates (437), internal olefin sulfonates (438), blends of alpha- and internal olefin sulfonates (439), blends of branched olefin sulfonates and polyoxyalkylene alkylphenyl ether sulfates (440) or alkylaryl alkoxy sulfate (441), sulfonated Friedel-Crafts alkylation products of benzene, toluene, and xylene with alpha-olefins (442), alkylalkoxyphenol sulfonates (sulfonate group on the benzene ring) (443), styrylaryloxy ether ethylsulfonates (ethylsulfonate group at end of the alkoxy chain) (444), the ethoxyethylsulfonate salt of dicyclopentadiene (445), carboxymethylated linear alcohol ethoxylates (445-448), carboxymethylated alkylphenol ethoxylates (448), carboxypropylated alcohol ethoxylates and alkylphenol ethoxylates (449), and branched (twin-tail) carboxymethylated alcohol ethoxylates (450). Increasing the length of an ethoxy chain reduces the critical micelle concentration (380, 451). Cosurfactant requirements can be minimized using a surfactant having a short branched hydrophobe or branched (vs. linear) alkyl substituent on an aromatic group (452,453) and a long ethoxy group chain (453).

Blends of surfactants optimized for seawater or reservoir brine salinity include linear alkylxylene sulfonate/alcohol ether sulfate mixtures (454,455). Alkyl- and alkylarylalkoxymethylene phosphonates (456), and amphoteric surfactants (457,458) have also been evaluated for use in surfactant flooding.

High concentrations (1-10%) of lignosulfonate have sufficient interfacial activity to increase oil recovery from unconsolidated sands (459) and have been shown to interact synergistically with petroleum sulfonates to produce an ultralow interfacial tension (460) and substantially increase oil recovery (461). Paper industry spent sulfite liquors function in a similar manner if they are not in the Ca^{+2} or Mg^{+2} forms which precipitate the petroleum sulfonates (462). Low molecular weight ethoxylated, sulfated, or sulfonated lignin phenols have been used alone in surfactant floods and found to recover more than 75% of the oil remaining after waterflood (463). The use of alkylated oxidized lignins has also been studied (464).

Of these surfactants, two classes are worthy of further note. The alpha-olefin sulfonates have been found to possess good salt tolerance, chemical stability at elevated temperatures, and appear to exhibit good oil solubilization and low interfacial tension over a wide range of temperatures (438,465). While being less salt tolerant, alkylaromatic sulfonates exhibit excellent chemical

stability. The nature of the alkyl group, the aryl group, and the ring isomer distribution produced in the Friedel-Crafts alkylation of the aromatic compound (452,466) can all be adjusted to optimize surfactant performance under a given set of reservoir conditions.

The effect of temperature, pressure, and oil composition have all been the subjects of intensive study and only a leading reference (467) will be cited. Surfactant propagation is a critical factor in determining the economics of an oil recovery process and has been the subject of many investigations (468). Recently liquid flow microcalorimetry has been used to study surfactant adsorption and determine the adsorption isotherm and entropy of adsorption (469,470). The use of high pressure liquid chromatography to analyze low surfactant concentration core flood effluents has aided in determining which components of commercially produced surfactants most rapidly propagate through rock (471). Commercial surfactant synthesis synthesis can then be modified to maximize the content of these rapidly propagating components. Mass spectral analysis could also be applied to this problem to identify chromatographic elution peaks and reduce the need to synthesize model compounds. Surfactant retention due to partitioning into residual crude oil can be significant relative to adsorption and reduce surfactant propagation rate appreciably (472).

The use of sacrificial agents to increase the surfactant propagation rate through reservoir rock has been proposed. Lignosulfonates and chemically modified lignosulfonates (34,352-356) and sodium saccharite wastes from wood pulping (473) have been evaluated as sacrificial adsorption agents. Injection of solutions containing K^+ , NH_4^+ , and zirconium ions prior to surfactant injection has been found to decrease surfactant adsorption (474). This is believed to occur by clay stabilization which reduces later swelling and fines migration (processes which increase the surface area exposed to the surfactant solution). Alkaline chemicals (422,423), particularly sodium silicate (475), which precipitate in the presence of divalent metal ions can increase the surfactant propagation rate.

Intermixing of the polymer mobility control fluid with the surfactant slug can result in surfactant - polymer interactions which have a significant effect on oil recovery (476). Of course, oil - surfactant interactions have a major effect on interfacial behavior and oil displacement efficiency. The effect of petroleum composition on oil solubilization by surfactants has been the subject of extensive study (477).

Caustic flooding involves the injection of high pH agents such as sodium hydroxide, sodium carbonate or sodium silicate to generate surfactants in situ by interaction with organic acids present in crude oil (478,479). The crude oil acid number (the number of grams of KOH required to neutralize one gram of crude oil) should be >0.5 . A number of different oil recovery mechanisms are thought to be operative: lowering of the capillary number (the ratio of viscous to capillary forces) through interfacial tension reduction, altering rock wettability (usually from oil-wet to water-wet), oil emulsification and entrapment of oil which results in a lower water mobility (in turn resulting in a greater injected water volumetric sweep efficiency), oil emulsification and entrainment in the

flowing aqueous phase, and possibly the solubilization of rigid films that may form at the oil-water interface.

While the injected chemicals are relatively inexpensive, large quantities must be injected due to reaction of the high pH agents with reservoir clays (480) and by precipitation by divalent metal ions present in formation waters. (This precipitation has been used to reduce adverse surfactant and polymer interactions with divalent metal ions by injecting a caustic preflush prior to a micellar polymer flood (481)). The presence of a lignosulfonate (482) or a polyacrylate (483) in the alkaline injectant has been reported to reduce this precipitation. Ion exchange processes promoting solubilization of divalent metal ions (484) limit the effectiveness of preflushes injected prior to the caustic solution. Which is the best of the three major alkaline agents used in this process: sodium hydroxide, sodium carbonate, and sodium orthosilicate, is the subject of some dispute. At equivalent Na_2O levels, the three alkaline agents gave equivalent recovery of each of nine different crude oils was obtained in laboratory core floods (485). The inclusion of surfactant in the caustic formulation (surfactant enhanced alkaline flooding) can increase optimal salinity of the saline (NaOH is a salt) alkaline formulation thereby reducing interfacial tension and increasing oil recovery (481,486,487). Both nonionic and anionic surfactants have been evaluated in this application (488,489) including internal olefin sulfonates (487,490), linear alkylxylene sulfonates (490), petroleum sulfonates (491), alcohol ethoxysulfates (487,489,492). Ethoxylated alcohols have been added to some anionic surfactant formulations to improve interfacial properties (486). The use of water thickening polymers, either xanthan or polyacrylamide to reduce injected fluid mobility mobility has been proposed for both alkaline flooding (493) and surfactant enhanced alkaline flooding (492). Crosslinked polymers have been used to increase volumetric sweep efficiency of surfactant - polymer - alkaline agent formulations (493).

While this technology appears quite promising and a field project is in progress (494), field pilot results are unavailable as yet.

Miscible gas flooding is currently the preferred technology to increase oil displacement efficiency. Supercritical CO_2 (361,495,496) and various hydrocarbon injectants (361,497,498) undergo complicated physical interactions with crude oil that result in stripping out of the low molecular weight components (which increases oil production). In addition, the rapid or gradual development of miscibility with the remaining crude oil constituents results in mobilization of at least some of the oil. Either partial or complete miscibility with the oil may be developed depending on the nature of the injectant, crude oil properties, and reservoir conditions, particularly temperature. In addition, the interaction of the injectant with the crude oil can result in changes in rock wettability which can affect oil recovery and reduce injectivity. As noted previously, both surfactants and polymers may be used to reduce the mobility of these low viscosity injectants. Steam flooding (397,499,500) can greatly increase the recovery of high viscosity crude oils through heat thinning processes. As noted previously, surfactants can be used to reduce the mobility of

the high temperature steam. Interfacial tension reduction promoted by steam foaming agents can also increase oil recovery (see Chapter 18). Since heavy crude oils have relatively high acid numbers, it is not surprising that addition of alkaline agents to high temperature steam can increase recovery of these oils (501,502). The in situ combustion method of enhanced oil recovery through air injection (397,503,504) is an exceeding complex process chemically. However, because little work has been done on the effect of chemical additives to oil recovery efficiency, this process will not be discussed herein.

Summary and Conclusions

Current and projected oil prices have resulted in oil recovery processes based on organic chemicals as the primary oil recovery agent being uneconomic. As a result, both R&D and commercial activities have been redirected to the use of relatively low quantities of chemicals to increase the effectiveness of waterflooding, supercritical CO₂ and gas injection EOR, and steam flooding. The recent emphasis has been on the use of chemicals to increase the volumetric sweep efficiency of these EOR processes. While a number of crosslinked polymer systems have been shown to be effective in substantially reducing the permeability of thief zones, methods for achieving greater treatment radii (from the injection well) are desirable. Experience with surfactant foams or dispersions as mobility control agents is more limited so the potential of this technology in economically improving volumetric sweep efficiency is less clear. Additional field tests are needed.

Literature Cited

1. Chatterji, J.; Borchardt, J.K. *J. Pet. Technol.*, 1981, 32 2042-2056.
2. Chilingarian, G.V.; Vorabutr, P. Drilling and Drilling Fluids, Elsevier Science Publishing Co., Inc. New York, 1981.
3. Clark, R.K.; Nahm, J.J. in Kirk-Othmer Encyclopedia of Chemical Technology, M. Grayson, Ed.; John Wiley & Sons, New York, 1982, 3rd Edit., Vol. 17, pp. 143-167.
4. Saunders, G.C. West German Patent 2 949 741, 1980.
5. Bruton, J.R. World Oil, 1979, 189 (7), 71-4.
6. Poole, G. Oil Gas J., 1981, 79 (28), 159, 161.
7. Ezzat, A.M.; Augsburger, J.J.; Tillis, W.J. *J. Pet. Technol.*, 1988, 40, 491-8.
8. Doty, P.A. SPE Drilling Eng., 1986, 1, 17-30.
9. Morgenthaler, L.M. SPE Production Eng., 1986, 1, 432-436.
10. Borchardt, J.K.; Rao, S.P. U.S. Patent 4 554 081, 1985.
11. House, R.F.; Hoover, L.D. French Patent 2 488 325, 1982.
12. Socha, G.E. U.S. Patent 4 373 959, 1983.
13. Pelezo, J.A.; Corbett, Jr., G.E. French Patent 2 578 549, 1986.
14. Walker, T.E.; Strassner, J.E. West German Patent 3 521 309, 1985.
15. Miura, M.; Harada, E.; Domon, F. Japan Patent 62 153 382, 1987.

16. Salamone, J.C.; Clough, S.B.; Salamone, A.B.; Reid, K.I.G.; Jamison, D.E. Soc. Pet. Eng. J., 1982, 22, 555 (1982).
17. Haack, T.; Shaw, D.A.; Greenley, D.E. Oil Gas J., 1986, 84 (1), 82.
18. Vio, L.; Meunier, G. French Patent 2 552 441, 1985.
19. Meltzer, Y.L. Water-soluble Polymers: Technology and Applications, Chem. Process Rev., Noyes Data Corp., Park Ridge, N.J., 1972, pp. 17-19.
20. Allan, T.O.; Roberts, A.P. Production Operations, 2nd edit., Oil & Gas Consultants, Inc., Tulsa, 1982, Volumes 1 and 2.
21. Smith, D.K. Cementing, Society of Petroleum Engineers, Dallas, 1974, Monograph No. 4
22. Smith, R.C. Oil Gas J., Nov. 1, 1982, 72-5.
23. Carter, L.G.; Evans, G.W. J. Pet. Technol., 1964, 16, 157-60.
24. Brice, Jr., J.W.; Holmes, B.C. J. Pet. Technol., 1964, 16, 503-8.
25. Keller, S.R.; Crook, R.J.; Haut, R.C.; Kulakofsky, D.S. J. Pet. Technol., 1987, 39, 955-60.
26. Crook, R.J.; Keller, J.; Wilson, M.A. J. Pet. Technol., 1987, 39, 961-6.
27. Cheung, P.R.; Beirute, R.M. J. Pet. Technol., 1985, 37 (6), 1041-1048.
28. Griffin, T.J.; Spangle, L.B.; Nelson, E.B. Oil Gas J., June 25, 1979, 143-151.
29. Harms, W.M.; Febus, J.S. J. Pet. Technol., 1985, 37 (6), 1049-1057.
30. Smith, R.C.; Powers, C.A.; Dobkins, C.A. J. Pet. Technol., 1980, 32, 1438-44.
31. Harms, W.M.; Lingenfelter, J.T. Oil Gas J., Feb. 2, 1981, 59-66.
32. Bruckdorfer, R.A.; Coleman, S.E. U.S. Patent 4 635 724, 1987.
33. Cole, R.C.; Borchardt, J.K. Drilling, 1985 (4), 44.
34. Borchardt, J.K. Encyclopedia of Science and Engineering, John Wiley & Sons, New York, 1987, Volume 10, 328-369.
35. Mondshine, T.C. U.S. Patent 4 175 042, 1979.
36. Saucier, R.J. J. Pet. Technol., 1974, 26, 205-12.
37. Pober, K.W.; Huff, H.M.; Darlington, R.K. J. Pet. Technol., 1983, 35, 2185.
38. Borchardt, J.K. U.S. Patent 4 524 003, 1985.
39. Norton, C.J.; Falk, D.D. U.S. Patent 3 919 092, 1975.
40. Borchardt, J.K. U.S. Patent 4 508 629, 1985.
41. Knight, R.K. U.S. Patent 4 039 028, 1977.
42. Kovacs, P. Food Technol., 1973, 27, 26.
43. Rocks, J.K., Food Technol., 1971, 25, 22.
44. Hong, K.C.; Milhone, R.S. J. Pet. Technol., 1977, 29, 1657.
45. Muecke, T.W. J. Pet. Technol., 1974, 26, 157.
46. Rensvold, R.F. Soc. Pet. Eng. J., 1983, 23, 238.
47. Penberthy, Jr., W.L.; Shaughnessy, C.M.; Gruesbeck, C.; Salathiel, W.M. J. Pet. Technol., 1978, 30, 845.
48. Young, B.M.; Totty, K.D. U.S. Patent 3 404 735, 1968.
49. Yano, A.; Yasue, T. Japan Kokai Tokkyo Koho 63 23 922, 1988; Chem. Abs., 1988, 109, 232346p.
50. Burger, J.; Gadelle, C.; De Chou, J.S. French Patent 2 575 500, 1986.

51. Suman, G.O. World Oil, Nov. 1974, 179, 63.
52. Murphey, J.R. U.S. Patent 4 259 205, 1981.
53. Underdown, D.R.; Das, K. J. Pet. Technol., 1985, 37, 2006-12.
54. Watkins, D.R.; Kalfayan, L.J.; Watanabe, D.J.; Holm, J.A. SPE Production Eng., 1986, 1, 471-477.
55. Davies, D.R.; Richardson, E.A.; Van Zanten, M. Eur. Pat. Appl. 30 753, 1981.
56. Economides, M.J.; Nolte, K.G., Eds. Reservoir Stimulation, Schlumberger Educational Services, Houston, 1987.
57. Githens, C.J.; Burnham, J.W. Soc. Pet. Eng. J., 1977, 17, 5.
58. Wu, S.N. Eur. Pat. Appl. 163 271, 1984.
59. Clark, P.E.; Underwood, J.S.; Steiner, T.M. Canadian Patent 1 090 112, 1977.
60. N.R. Morrow and J.P. Heller in Developments in Petroleum Science; Donaldson, E.C.; Chilingarian, G.V.; Yen, T.F. Eds., Elsevier, Amsterdam, 1985, Volume 17A, pp. 47-74.
61. Barker, S.A.; Stacey, M.; Zweifel, G. Chem. Ind. London, 1957, 330.
62. Dill, W.R. U.S. Patent 4 466 893, 1984.
63. Stauffer, K.B. in Handbook of Water-Soluble Gums and Resins; Davidson, R.L., Ed.; McGraw-Hill, New York, 1980, pp. 11/1-11/31.
64. Nierode, D.E.; Kehn, D.M.; Kruk, K.F. U.S. Patent 3 934 651, 1976.
65. Almond, S.W.; Conway, M.W. U.S. Patent 4 553 601, 1985.
66. Brode, G.L.; Stanley, J.P.; Partain, III, E.M. U.S. Patent 4 579 942, 1986.
67. Roll, D.L.; Himes, R.; Ewert, R.; Doerksen, J. SPE Production Eng., 1987, 2, 291-6.
68. Constein, V.G.; King, M.T. U.S. Patent 4 541 935, 1985.
69. Prikryl, J.; Oliva, L.; Kubat, V. Czech. Patent 235 624, 1986.
70. Lundberg, R.D.; Peiffer, D.G.; Sedillo, L.P.; Newlove, J.C. U.S. Patent 4 579 671, 1986.
71. Burnham, J.W.; Tiner, R.L. U.S. Patent 4 200 539 (1980).
72. Griffin, Jr., T.J. U.S. Patent 4 174 283, 1979.
73. Zigrye, J.L.; Whitfill, D.L.; Sievert, J.A. J. Pet. Technol., 1985, 37, 315.
74. Penny, G.S.; Conway, M.W.; Lee, W. J. Pet. Technol., 1985, 37, 1071.
75. Gulbis, J. in reference 56, p. 4-11.
76. Anderson, R.W.; Phillips, A.M. J. Pet. Technol., 1988, 40, 223-8.
77. Needham, R.B.; Thomas, C.P.; Wier, D.R. U.S. Patent 4 231 428, 1980.
78. Graham, J.W.; Sinclair, R.A. U.S. Patent 4 585 064, 1986.
79. Runmo, G.J. Eur. Pat. Appl. 92 756, 1983.
80. Kucera, C.H. British Patent 2 108 112, 1983.
81. Harris, L.E. U.S. Patent 4 324 668, 1982.
82. Reference 75, pp. 4-5, 4-6.
83. Gregory, G.J. Oil Gas J., 1982, 83 (37), 80.
84. Payne, K.L. U.S. Patent 4 579 670, 1986.
85. Misak, M.D. U.S. Patent 3 922 173, 1975.
86. Reference 75, p. 4-9.
87. Malone, T.R.; Foster, J., T.D.; Executrix, S.T. U.S. Patent 4 290 899, 1981.

88. Rygg, R.H. British Patent 2 090 308, 1982.
89. Reference 75, p. 4-9 and references therein.
90. Millar, S.W. U.S. Patent 4 552 591, 1985.
91. Sortwell, E.T.; Solovinski, M.; Mikkelsen, A.R. U.S. Patent 4 507 450, 1985.
92. Hoover, L.D.; House, R.F. British Patent 2 070 611, 1981.
93. House, R.F.; Hoover, L.D. French Patent 2 488 325, 1982.
94. Bayerlein, F.; Habereeder, P.P.; Keramaris, N.; Kottmair, N.; Kuhn, M. French Patent 2 513 265, 1983.
95. Mosier, B.; McCrary, J.L.; Guilbeau, K.G. U.S. Patent 4 530 601, 1982.
96. Reference 75, p. 4-10.
97. Clark, H.B.; Pike, M.T.; Rengel, G.L. J. Pet. Technol., 1982, 34, 1565-9.
98. Penny, G.S.; et. al. U.S. Patent 4 425 242, 1984.
99. Hirt, D.E.; Prud'homme, R.K.; Rebenfeld, L. J. Dispersion Sci. Technol., 1987, 8, 55-73.
100. Reference 75, pp. 4-7, 4-8 and references therein.
101. Black, H.N.; Langsford, R.W. J. Pet. Technol., 1982, 34, 135-40.
102. Reidenbach, V.G.; Harris, P.C.; Lee, Y.N.; Lord, D.L. SPE Production Eng., 1986, 1, 31-41.
103. Harris, P.C. SPE Production Eng., 1987, 2, 89-94.
104. Ward, V.L. SPE Production Eng., 1986, 1, 275-8.
105. Garbis, S.J.; Taylor III, J.L. SPE Production Eng., 1986, 1, 351-358.
106. Williams, R.B.; Gidley, J.L.; Schechter, R.S. Acidizing Fundamentals, Society of Petroleum Engineers, Dallas, SPE Monograph No. 6, 1979.
107. Hung, K.M.; Hill, A.D.; Sepehrnoori, K. J. Pet. Technol., 1989, 41, 65-6.
108. Reference 106, p. 97.
109. Thomas, R.L. U.S. Patent 4 151 878, 1979.
110. Thomas, R.L.; Suby, F.A. U.S. Patent 4 160 483, 1979.
111. Kunze, K.R.; Shaughnessy, C.A. Soc. Pet. Eng. J., 1983, 23, 65-72.
112. Blumer, D.J. U.S. Patent 4 703 803, 1987.
113. Dill, W.R. West German Patent 2 925 748, 1980.
114. Nehmer, W.L. British Patent Appl. 2 163 790, 1986.
115. Norman, L.R.; Conway, M.W.; Wilson, J.M. J. Pet. Technol., 1984, 36, 2011.
116. Roper, L.E.; Swanson, B.L. U.S. Patent 4 205 424, 1980.
117. Burns, L.D.; Stahl, G.A. U.S. Patent 4 690 219, 1987.
118. Haltmar, W.C.; Lacey, E.S. U.S. Patent 4 207 946, 1980.
119. Engelhardt, F.; Schmitz, H.; Hax, J.; Gulden, W. European Patent 44 508, 1982.
120. Engelhardt, F.; Piesch, S.; Balzer, J.; Dawson, J.C. PCT Internat. Patent Appl. 82 02 252 (1982).
121. Swanson, B.L. Eur. Patent Appl. 7 012, 1980.
122. Costanza, J.R.; DeMartino, R.N.; Goldstein, A.M. U.S. Patent 4 057 509, 1977.
123. Hoefner, M.L.; Fogler, H.S.; Stenius, P.; Sjoblom, J. J. Pet. Technol., 1987, 39, 203-8.

124. Hoefner, M.L., Fogler, H.S. Chem. Eng. Prog., 1985, 40.
125. Ford, W.G.F. J. Pet. Technol., 1981, 33, 1203-1210.
126. Khasaev, A.M.; Sadykhov, M.G.; Kurbanova, Kh. G. Azerb. Neft. Khoz., 1978, 32.
127. Jones, W.L. British Patent 2 141 731, 1987.
128. Reference 106, p. 97.
129. Crema, S.C. U.S. Patent 4 676 916, 1987.
130. Walton, W.B. U.S. Patent 4 541 483, 1985.
131. Hall, B.E. J. Pet. Technol., 1975, 27, 1439-42.
132. Walsh, M.P.; Lake, L.W., Schechter, R.S. J. Pet. Technol., 1982, 34, 2097-2112.
133. Dria, M.A.; Schechter, R.S.; Lake, L.W. SPE Production Eng., 1988, 3, 52-62.
134. Labrid, J.C. Soc. Pet. Eng. J., 1975, 15, 117-28.
135. Crowe, C.W. J. Pet. Technol., 1986, 38, 1234-40.
136. Street, Jr., E.H. U.S. Patent 4 167 214, 1979.
137. Dill, W.R.; Walker, M.L.; Ford, W.G.F. U.S. Patent 4 679 631, 1987.
138. Nehmer, W.H.; Coffey, M.D. British Patent Appl. 2 158 487, 1985.
139. Walker, M.L.; Ford, W.G.F.; Dill, W.R.; Gdanski, R.D. U.S. Patent 4 683 954, 1987.
140. Reference 106, pp. 101-102.
141. Brannon, D.H.; Netters, C.K.; Grimmer, P.J. J. Pet. Technol., 1987, 39, 931-42.
142. Reference 106, p. 100.
143. Clementz, D.M.; Patterson, D.E.; Aseltine, R.J.; Young, R.E. J. Pet. Technol., 1982, 34, 2087-96.
144. Taggart, D.L.; Heffern, E.W. U.S. Patent 4 690 217, 1987.
145. Craig, Jr., F.F. The Reservoir Engineering Aspects of Water Flooding, Society of Petroleum Engineers, Dallas, Monograph No.3, 1971, pp. 19-22.
146. Dymond, P.F.; Spurr, P.R. SPE Reservoir Eng., 1988, 3, 165-74.
147. Scheurman, R.F. SPE Production Eng., 1988, 3, 15-21.
148. Reference 106, pp. 92-95.
149. Wu, Y. British Patent Appl. 2 082 589, 1982.
150. Tuttle, R.N. J. Pet. Technol., 1987, 39, 756-62.
151. Wilhelm, S.M.; Kane, R.D. J. Pet. Technol., 1986, 38, 1051-61.
152. Tate, J.F.; Maddox, Jr., J.; Shupe, R.D. Canadian Patent 1 051 649, 1979.
153. Redmore, D.; Outlaw, B.T. U.S. Patent 4 315 087, 1982.
154. Patton, C.C. J. Pet. Technol., 1988, 40, 1123-6.
155. Khilar, K.C.; Fogler, H.S. Soc. Pet. Eng. J., 1983, 23, 55-64.
156. Khilar, K.C.; Fogler, H.S. J. Colloid Interface Sci., 1984, 101 (1), 214-24.
157. Kia, S.F.; Fogler, H.S.; Reed, M.G.; Vaidya, R.N. SPE Production Eng., 1987, 2, 277-83.
158. Sydansk, R.D. J. Pet. Technol., 1984, 36, 1366-74.
159. Reed, M.G. J. Pet. Technol., 1972, 24, 860-64.
160. Veeley, C.D. J. Pet. Technol., 1969, 21, 1111-18.
161. Peters, F.W.; Stout, C.M. J. Pet. Technol., 1977, 29, 187-94.

162. Muecke, T.W. J. Pet. Technol., 1979, 31, 144-150.
163. Gruesbeck, C.; Collins, R.E. Soc. Pet. Eng. J., 1982, 22, 847-856.
164. Kia, S.F.; Fogler, H.S.; Reed, M.G. J. Colloid Interface Sci., 1987, 118, 158-68.
165. Reference 20, Volume 2, p. 99.
166. Leone, J.A.; Scott, E.M. SPE Reservoir Eng., 1988, 3, 1279-86.
167. Broaddus, G. J. Pet. Technol., 1988, 40, 685-7.
168. Blair, Jr., C.M. U.S. Patent 4 337 828, 1982.
169. Blair, Jr., C.M.; Stout, C.A. Oil Gas J., May 20, 1985, 83 (55). 133.
170. Cusack, F.; Lappin-Scott, H.M.; Costerton, J.W. Oil Gas J., Nov. 9, 1987, 85, 87.
171. Hensel, Jr., W.N.; Sullivan, R.L.; Stallings, R.H. Pet. Eng. Int., 1981(5), 155.
172. Anderson, W.G., J. Pet. Technol., 1987, 39, 1453-67.
173. Anderson, W.G., J. Pet. Technol., 1986, 38, 1125-44. 173. Reference 144, pp. 19-21.
174. Hjelmeland, O.S.; Larrondo, L.E. SPE Reservoir Engr., 1986, 1, 321-8.
175. Owens, W.W.; Archer, D.L. J. Pet. Technol., 1971, 23, 873-8.
176. Morrow, N.R.; Mungan, N. Rev. Inst. Franc. Petrole, 1971, 629-50.
177. Treiber, L.E.; Archer, D.L.; Owens, W.W. Soc. Pet. Eng. J., 1972, 12, 531-40.
178. Elphinstone, E.A.; McLaughlin; H.C.; Smith, C.W. Canadian Patent 1 070 936, 1980.
179. Downs, S.L.; Gohel, M.G. J. Pet. Technol., 1974, 26, 557-70.
180. Peddycoart, L.R. Oil Gas J., Feb. 4, 1980, 78, 52.
181. Weaver, J.D.; Harris, L.E.; Harms, W.M. U.S. Patent 4 460 627, 1984.
182. Geosciences Research for Oil and Gas Discovery and Recovery, U.S. Dept. of Energy, Washington, D.C., March, 1987.
183. Oil Gas J., December 26, 1988, 86 (52), 49.
184. Smith, D.H. Surfactant-Based Mobility Control - Progress in Miscible-Flood Enhanced Oil Recovery, ACS Symposium Series No. 373, American Chemical Society, Washington, D.C., 1988.
185. Neale, R.R.; Doe, P.H. J. Pet. Technol., 1987, 39, 1503-7.
186. Kessel, D.G.; Volz, H.; Maitin, B. Proc. World Pet. Congr., 1977, 12th (Vol. 3), 355-64.
187. Ling, T.F.; Lee, H.K.; Shah, D.O. Spec. Publ. - R. Soc. Chem., 1987, 59 (Ind. Appl. Surfactants), 126-78.
188. Miller, C.A.; Qutubuddin, S. Surfactant Sci. Ser., 1987, 21 (Interfacial Phenom. Apolar Media), 117085.
189. Tomich, J.F.; Laplante, D.L.; Snow, T.M. Proc. World Pet. Congr., 1977, 12th (Vol. 3), 337-46.
190. Pet. Eng. Int., May, 1988. 79-81.
191. Leighton, A.J.; Wayland, J.R. J. Pet. Technol., 1987, 39, 129-36.
192. Holm, L.W.; Josendal, V.A. Soc. Pet. Eng. J., 1982, 22, 87-98.
193. Martin, R.L.; Braga, T.G. Mater. Perform., 1987, 26, 16-22.
194. Technical Constraints Limiting Application of Enhanced Oil

- Recovery Techniques to Petroleum Production in the United States, U.S. Dept. of Energy, DOE/BETC/RI-83/9 (DEB4003910), Jan., 1984.
195. Reference 34, pp. 350-351.
 196. Reference 34, p. 344.
 197. Norton, C.J.; Fak, D.O. U.S. Patent 4 343 363, 1982.
 198. Sandiford, B.B.; Dovan, H.T.; Hutchins, R.D. U.S. Patent 4 413 680, 1983.
 199. Prud'homme, R.K.; Uhl, J.T.; Poinsette, J.P.; Halverson, F. Soc. Pet. Eng. J., 1983, 23, 804.
 200. Willhite, G.P.; Jordan, D.J. Polym. Prepr. Am. Chem. Soc. Div. Polym. Chem., 1981, 22 (2), 53.
 201. Sloat, B. Pet. Eng. Int., 1977, 20.
 202. Dovan, H.T.; Hutchins, R.D. SPE Res. Eng., 1987, 2, 177-188.
 203. Norton, C.J. Canadian Patent 1 217 629, 1987.
 204. Hanlon, D.J.; Almond, S.W. European Patent Appl. 161 858, 1985.
 205. Prud'homme, R.K.; Uhl, J.T. Proc. Fourth Joint Symposium on Enhanced Oil Recovery, Tulsa, Okla., Apr. 15-18, 1984, Paper No. SPE/DOE 12640 .
 206. Jordan, D.J.; Green, D.W.; Terry, R.E.; Willhite, G.P. Soc. Pet. Eng. J., 1982, 22, 463.
 207. Routson, W.G. U.S. Patent 3 687 200, 1972.
 208. Mumallah, N.A. SPE Reservoir Eng., 1988, 3, 243.
 209. Sydansk, R.D. U.S. Patent 4 744 418, 1988.
 210. Moradi-Araghi, A.; Doe, P.H. SPE Reservoir Eng., 1987, 2, 189-93.
 211. Nanda, S.K.; Kumar, R.; Sindhvani, K.L.; Goyl, K.L. ONGC Bull., 1986, 23, 175-85.
 212. Sydansk, R.D. U.S. Patent 4 723 605, 1988.
 213. Aslam, S.; Vossoughi, S.; Whillhite, G.P. Chem. Eng. Commun., 1986, 48, 287-301.
 214. Hyang, C-G.; Green, D.W.; Willhite, G.P. SPE Reservoir Engr., 1986, 1, 583-592.
 215. Vio, L. U.S. Patent 4 155 405, 1979.
 216. Sullivan, E.J.; Jones, G.D. U.S. Patent 4 125 478, 1978.
 217. Pliny, R.J.; Regulski, T.W. European Patent 5 835, 1979.
 218. Sidorov, I.A.; et. al. USSR Patent 1 040 118, 1983.
 219. Ech. E.; Lees, R.D. U.S. Patent 4 579 667, 1986.
 220. Ryles, R.G.; Robustelli, A.G.; Cicchiello, J.V. European Patent Appl. 200 062, 1986.
 221. Ryles, R.G.; et. al. European Patent Appl. 273 210, 1988.
 222. Falk, D.O. U.S. Patent 4 688 639, 1987.
 223. Hessert, J.E.; Johnston, Jr., CC. U.S. Patent 4 110 230, 1978.
 224. Abdo, M.K. U.S. Patent 4 574 887, 1986.
 225. Hurd, B.G. U.S. Patent 3 581 824, 1971.
 226. Colegrove, G.T. U.S. Patent 4 157 322, 1979.
 227. Clear, E.E. U.S. Patent 4 321 968, 1982.
 228. Dasinger, B.L.; McArthur, H.A.I. European Patent Appl. 251 638, 1988.
 229. Sampath, K. U.S. Patent 4 640 358, 1987.
 230. McLaughlin, H.C. U.S. Patent 3 334 689, 1967.
 231. Borchardt, J.K. U.S. Patent 4 439 334, 1984.

232. Argabright, P.A.; Rhudy, J.S. U.S. Patent 4 503 909, 1985.
233. Seright, R.S. Proc. 1989 SPE International Symposium on Oilfield Chemistry, Society of Petroleum Engineers, Dallas, 1989, pp. 389-402.
234. Felber, B.J.; Dauben, D.L. Soc. Pet. Eng. J., 1977, 17, 391.
235. Felber, B.J.; Christopher, C.A. U.S. Patent 4 428 429, 1984.
236. Lawrence, D.D.; Felber, B.J. U.S. Patent 4 275 789, 1981.
237. Whitworth, A.J.; Tung, S.Y.S.; Hajto, E.A. U.S. 3 686 372, 1972.
238. Allan, B.W. U.S. Patent 4 299 690, 1981.
239. Soreau, M.; Siegel, D. French Patent 2 551 451, 1985.
240. Navritil, M.; Batycky, J.P.; Sovak, M.; Mitchell, M.S. Canada Patent 1 187 404, 1985.
241. Balitskaya, Z.A.; et. al. U.S.S.R. Patent 878 904, 1981.
242. Hess, P.M. J. Pet. Technol., 1980, 32, 1834-42.
243. Navritil, M.; Mitchell, M.S.; Sovak, M. U.S. Patent 4 663 367, 1987.
244. Navritil, M.; Mitchell, M.S.; Sovak, M. Canada Patent 1 217 932, 1987.
245. Marocco, M.L. U.S. Patent 4 664 194, 1987.
246. Chung, H.S.; Sampath, K.; Schwab, F.C. U.S. Patent 4 653 585, 1987.
247. Harwell, J.H.; Scamehorn, J.F. U.S. Patent 4 745 976, 1988.
248. Schievelbein, V.H.; Kudchadker, M.V.; Varnon, J.E.; Whittington, L.E. U.S. Patent 4 161 982, 1979.
249. Schievelbein, V.H. U.S. Patent 4 161 983, 1979.
250. Varnon, J.E.; Schievelbein, V.H.; Kudchadker, M.V.; Whittington, L.E. U.S. Patent 4 161 218, 1979.
251. Schievelbein, V.H.; Park, J.H. U.S. Patent 4 160 480, 1979.
252. Stahl, G.A.; Schulz, D.N.; Eds. Water Soluble Polymers for Petroleum Recovery, Plenum, New York, 1988.
253. Crafts, B.C.; Hawkins, M.F. Applied Petroleum Reservoir Engineering, Prentice-Hall, New York, 1959.
254. Reference 145, pp. 45-7.
255. Sandiford, B.B.; Keller, Jr., H.F. U.S. Patent 2 827 964, 1958.
256. Sandiford, B.B.; Keller, Jr., H.F. U.S. Patent 3 116 791, 1964.
257. Sandiford, B.B. U.S. Patent 3 308 885, 1967.
258. Sandiford, B.B. J. Pet. Technol., 1964, 16, 917.
259. Pye, D.J. J. Pet. Technol., 1964, 16, 911.
260. Chang, H.I. J. Pet. Technol., 1978, 30, 1113-1128.
261. Smith, R.V.; Burtch, F.W. Oil Gas J., Nov. 24, 1980, 78, 127.
262. Lorenz, P.B.; Trantham, J.C.; Zornes, P.R.; Dodd, C.G. SPE Reservoir Eng., 1986, 1, 341-53.
263. Jones, D.M.; Walters, K.; Williams, P.R. Rheological Acta, 1986, 26, 20.
264. Cahalan, P.T.; Peterson, J.A.; Arndt, D.A. U.S. Patent 4 053 699, 1977.
265. Carter, W.H.; Christopher, C.A.; Jefferson, T. West German Patent 2 809 136, 1979.
266. Sandford, P.A.; Laskin, A. Eds; Extracellular Microbial Polysaccharides, ACS Symposium Series No. 45; American Chemical Society: Washington, D.C., 1977.

267. Abdo, M.K., U.S. Patent 3 771 462, 1973.
268. Rhone-Poulenc Specialties Chimique, Japan Kokai Tokkyo Koho 62 39 643, 1987; Chem. Abstr., 1987, 107, 42858u.
269. Casad, B.M.; Conley, D.; Ferrell, H.H.; Stokke, O.M. U.S. Patent 4 212 748, 1980.
270. Bragg, J.R. British Patent Application 2 115 430, 1983.
271. Rinaudo, M.; Milas, M. Int. J. Biol. Macromol., 1980, 2, 45.
272. Holding, T.J.; Pace, J.W. British Patent 2 065 689, 1981.
273. Kohler, N.; Longchamp, D.; They, M. J. Pet. Technol., 1987, 39, 835-43.
274. Stokke, O.M. U.S. Patent 4 165 257, 1979.
275. Knight, B.L.; Jones, S.C.; Parsons, R.W. Soc. Pet. Eng. J., 1974, 14, 643.
276. Grollman, U.; Schnable, W., Polymer Degradation and Stability, Applied Science Publishers, London, 1982, pp. 353-362..
277. Wellington, S.L. Soc. Pet. Eng. J., 1983, 23, 901-12.
278. Cadmus, M.C.; et. al. Appl. Environ. Microbiol., Aug. 1982, 5.
279. Lee, S.L. West German Patent 2 715 026, 1977.
280. Philips, C.J. European Patent 106 666, 1984.
281. F. Dawans, Binet, D.; Kohler, N.; Quang, D.V. U.S. Patent 4 454 620, 1984.
282. Wellington, S.L. Canadian Patent 1 070 492, 1980.
283. Kanda, S.; Kawamura, G. U.S. Patent 4 481 316, 1985.
284. Kanda, S.; Kawamura, G. Japan Kokai Tokkyo Koho 61 275 337, 1986.
285. Niita, A.; Arai, T.; Funato, R.; Sato, T. Japan Kokai Tokkyo Koho 62 184 048, 1987.
286. Niita, A.; Arai, T.; Funato, R.; Sato, T. Japan Kokai Tokkyo Koho 62 184 047, 1987.
287. Niita, A.; Arai, T.; Funato, R.; Sato, T. Japan Kokai Tokkyo Koho 62 177 052, 1987.
288. Nakanishi, Y. Japan Kokai Tokkyo Koho 62 277 407, 1987.
289. Judson, C.P. European Patent Application 196 199, 1986.
290. Nitta, A.; Ito, Y.; Nitta, A. Japan Kokai Tokkyo Koho 61 136 545, 1986.
291. Contat, F.; Boutin, J. European Patent Application 241 340, 1987.
292. Chen, C.S.H.; Sheppard, E.W. J. Macromol. Sci. Chem. Part A, 1979, 239.
293. Chen, C.S.H.; Sheppard, E.W. Polym. Prepr. Am. Chem. Soc., Div. Polym. Chem., 1978, 19 (1), 424-9.
294. Wernau, W.C. West German Patent 2 848 984, 1979.
295. Holzwarth, G.M. European Patent 103 483, 1984.
296. Phillips, J.C.; Miller, J.W.; Wernau, W.C.; Tate, B.E.; Auerbach, M.H. Soc. Pet. Eng. J., 1985, 25, 594.
297. Donche, A.F. World Biotech Rep., 1985, 1, 429-36.
298. Meldrum, I.G. Comm. Eur. Communities, {Rep.} EUR, 1985, Vol. 2, 776-83.
299. Doster, M.S.; Nute, A.J.; Christopher, C.A. U.S. Patent 4 457 372, 1984.
300. Rinaudo, M.; Vincendon, M. Carbohydr. Polym., 1982, 2, 135.
301. Hitzman, G.O. U.S. Patent 4 096 073, 1978.
302. Linton, J.D.; Evans, M.W.; Godley, A.R. European Patent 135 953, 1985.

303. Thompson, B.G.; Jack, T.R. U.S. Patent 4 561 500, 1985.
304. Savins, J.G. U.S. Patent 4 079 544, 1978.
305. Lindoerfu, R.; et. al. West German Patent 3 643 467, 1988.
306. Vanderslice, R.W.; Shanon, P. European Patent Application 211 288, 1987.
307. Graaflund, T. European Patent Application 237 132, 1987.
308. Frank, S.; Coscia, A.T.; Schmitt, J.M. U.S. Patent 4 439 332, 1984.
309. Borchardt, J.K. U.S. Patent 4 439 334, 1984.
310. Klein, J.; Heitzman, R. Makromol. Chem., 1978, 179, 1895.
311. Halverson, F.H.; Lancaster, J.E. Macromolecules, 1985, 18, 1139.
312. Boutin, J.; Contat, F. French Patent 2 495 217, 1982.
313. Southwick, J.G.; Manke, C.W. SPE Reservoir Eng., 1988, 3, 1193-1201.
314. Prud'homme, R.K. SPE Reservoir Eng., 1986, 1, 272-6.
315. Munk, P.; Aminabhavi, T.M.; Williams, P.; Hoffman, D.E.; Chmelir, M. Macromolecules, 1980, 13, 871-5.
316. Muller, G.; Laine, J.P.; Fenyó, J.C. J. Polym. Sci. Polym. Chem. Ed., 1979, 17, 659.
317. Ward, J.S.; Martin, F.D. Soc. Pet. Eng. J., 1981, 21, 623.
318. Chen, G.S.; Neidlinger, H.H.; McCormick, C.L. Prepr. Pap. Nat. Meet. Div. Pet. Chem. Am. Chem. Soc., 1984, 29 (4), 1147.
319. Ryles, R.G. SPE Reservoir Eng., 1988, 3, 23-34.
320. Moradi-Araghi, A.; Doe, P.H. SPE Reservoir Eng., 1987, 2, 189-98.
321. Szabo, M. J. Pet. Technol., 1979, 31, 553.
322. Szabo, M. J. Pet. Technol., 1979, 31, 561.
323. McCormick, C.L.; Johnson, C.B. Biotechnol. Mar. Polysaccharides, Proc. Annu. MIT Sea Grant Coll. Program Lect. Semin., 3rd, 1984 (Pub. 1985), 213-48.
324. McCormick, C.L. J. Macromol. Sci. Chem. Part A. 1985, 22, 955.
325. McCormick, C.L., Hester, R.D.; Neidlinger, H.H.; Wildman, G.C. BETC Prog. Rev., 1979, 20, 61.
326. McCormick, C.L., Blackmon, K.R.; Elliott, D.L. Prepr. Pap. Nat. Meet. Div. Pet. Chem. Am. Chem. Soc., 1984, 29 (4), 1159.
327. Stahl, G.A. U.S. Patent 4 644 020, 1987.
328. Doe, P.H.; Moradi-Araghi, A.; Shaw, J.E.; Stahl, G.A. SPE Res. Eng., 1987, 2, 461.
329. Ching, T.Y. West German Patent 3 627 456, 1987.
330. Ryles, R.G. European Patent Application 233 533, 1987.
331. Engelhardt, P.; Greiner, U.; Schmitz, H.; Gulden, W.; von Halasz, S.P. West German Patent 3 220 503, 1983.
332. Ito, Y.; Niuta, A.; Sudo, Y.; Hayashi, K. Japan Kokai Tokkyo Koho 62 15 279, 1987.
333. Wu, M.M.; Ball, L.E. U.S. Patent 4 540 498, 1985.
334. Martin, F.D.; Hatch, M.J.; Abouelezz, M.; Oxley, J.C. Polym. Mater. Sci. Eng., 1984, 51, 688.
335. Ball, L.E.; Griffin, L.M.; Antloger, K.M.; Nemacek, A.L. U.S. Patent 4 653 584, 1987.
336. Pledger, Jr., H.; Meister, J.J.; Hogen-Esch, T.E.; Butler, G.B. Polym. Prepr. Am. Chem. Soc. Div. Polym. Chem., 1981, 22 (2), 72.

337. Neidlinger, H.H.; McCormick, C.L. Polym. Prepr. Am. Chem. Soc. Div. Polym. Chem., 1979, 20 (1), 901.
338. Meister, J.J.; et. al. Polym. Prepr. Am. Chem. Soc. Div. Polym. Chem., 1984, 25 (1), 266.
339. Schulz, D.N.; Kaladas, D.A.; Maurer, J.J.; Bock, J.; Pace, S.J.; Schulz, W.W. Polymer, 1987, 28, 2110-15.
340. Bock, J.; Siano, D.B.; Turner, R. U.S. Patent 4 694 046, 1987.
341. Bock, J.; Valint, P.L. U.S. Patent 4 730 028, 1988.
342. Bock, J.; Valint, P.L.; Pace, S.J. U.S. Patent 4 702 314, 1987.
343. Bock, J.; Pace, S.J.; Schulz, D.N. U.S. Patent 4 709 759, 1987.
344. Evani, S.; Rose, G.D. Polym. Mat. Sci. Eng., 1987, 57, 477-81.
345. Landoll, L.M. Netherlands Patent 80 03 241, 1980.
346. Borchardt, J.K.; Brown, D.L. U.S. Patent 4 409 110, 1983.
347. Borchardt, J.K.; Brown, D.L. Oil Gas J., Sept. 10, 1984, 89, pp. 150,152,154,156.
348. Shuler, P.J.; Kuehne, D.L.; Uhl, J.T.; Walkup, Jr., G.W. SPE Reservoir Engr., 1987, 2, 271-80.
349. Willhite, G.P.; Dominguez, J.G. in Improved Oil Recovery by Surfactant and Polymer Flooding, Academic Press, Washington, D.C., 1977, pp. 511-553.
350. Friedmann, F. SPE Reservoir Eng., 1986, 1, 261-271.
351. Cohen, Y.; Christ, F.R. SPE Reservoir Eng., 1986, 1, 113-18.
352. Hong, S.A.; Bae, J.H. SPE Reservoir Eng., 1987, 2, 17-27.
353. Kalfoglou, G. U.S. Patent 4 627 494, 1986.
354. Howard, J.; Stirling, M. U.S. Patent 4 713 185, 1987.
355. Bansal, B.B.; Hornof, V.; Neale, G. Can. J. Chem. Eng., 1979, 57, 203.
356. Novosad, J. Can. J. Pet. Technol., 1984, 23, 24.
357. Chen, C.S.H.; Sheppard, E.W. U.S. Patent 4 284 517, 1981.
358. Clint, J.H.; Hodgson, P.K.G.; Tinley, E.J. British Patent 2 148 356, 1985.
359. Horton, R.L. U.S. Patent 4 574 885, 1986.
360. Arf, T.G.; et. al. SPE Reservoir Eng., 1987, 2, 166-76.
361. Stalkup, Jr., F.I. Miscible Displacement, Monograph Volume 8, Society of Petroleum Engineers, Dallas, 1983, pp. 62-67.
362. Caudle, B.H.; Dye, A.B. Trans. AIME, 1958, 213, 281.
363. Reference 361, p. 32.
364. Wellington, S.L.; Vinegar, H.J. J. Petroleum Technol., 1987, 39, 885-98.
365. Reference 361, pp. 147-158.
366. Stalkup, Jr., F.I. J. Pet. Technol., 1984, 36, 815-826.
367. Desch, J.B.; et. al. J. Pet. Technol., 1984, 36, 1592-1602.
368. Heller, J.P.; Dandge, D.K.; Card, R.J.; Donaruma, L.G. Soc. Pet. Eng. J., 1985, 25, 679-86.
369. Smith, D.H. Surfactant-Based Mobility Control - Progress in Miscible-Flood Enhanced Oil Recovery, ACS Symposium Series No. 373, American Chemical Society, Washington, D.C., 1988.
370. Heller, J.P.; Kuntamukkula, M.S. Ind. Eng. Chem. Res., 1987, 26, 318.

371. Ali, S.M. Farouq; Selby, R.J. Oil Gas J., 1986, 84 (5), 57, 60-3.
372. Friberg, S.E.; Solans, C. Langmuir, 1986, 2, 121-6.
373. Malhotra, A.K.; Wasan, D.T. Chem. Eng. Commun., 1987, 55, 95-128.
374. Khatib, Z.I.; Hirasaki, G.J.; Falls, A.H. SPE Reservoir Eng., 1988, 3, 919-26.
375. Ransohoff, T.C.; Radke, C.J. SPE Reservoir Eng., 1988, 3, 573-85.
376. Owete, O.S.; Brigham, W.E. SPE Reservoir Eng., 1987, 2, 315-23.
377. Craig, Jr., F.F.; Lummus, J.L. U.S. Patent 3 185 634, 1965.
378. Hahn, P.S.; Ramamohan, T.R.; Slattey, J.C. AIChE J, 1985, 31, 1029-35.
379. Borchardt, J.K.; Bright, D.B.; Dickson, M.K.; Wellington, S.L. in Reference 338, pp. 163-80.
380. Borchardt, J.K. in Reference 369, pp. 181-204.
381. Holm, L.W. U.S. Patent 4 706 752, 1987.
382. Wellington, S.L. U.S. Patent 4 380 266, 1983.
383. Buckles, J.J. U.S. Patent 4 706 750, 1987.
384. Wellington, S.L.; Resiberg, J.; Lutz, E.F.; Bright, D.B. U.S. Patent 4 502 538, 1985.
385. Borchardt, J.K. U.S. Patent 4 799 547, 1989.
386. Settlemyer, L.A.; McCoy, M.J. U.S. Patent 4 739 831, 1988.
387. Sharma, M.K.; Shiao, S.Y.; Bansal, V.K.; Shah, D.O. in Macro- and Microemulsions, ACS Symposium Series No. 272, American Chemical Society, Washington, D.C., 1985, pp. 87-103.
388. Sharma, M.K.; Shah, D.O.; Brigham, W.E. SPE Reservoir Eng., 1986, 1, 253-60.
389. Mitchell, T.O. U.S. Patent 4 676 316, 1987.
390. Zhukov, I.N.; Polozova, T.L.; Shatova, O.S. Kolloidn. Zh., 1987, 49, 758-62; Chem. Abstr., 1987, 108, 63029a.
391. Hutchins, R.D.; Dovan, H.T. European Patent Application 212 671, 1987.
392. Djabbarah, N.F. Canadian Patent 1 221 305, 1987.
393. Falls, A.H. U.S. Patent 4 733 727, 1988.
394. Holm, L.W. J. Pet. Technol., 1970, 32, 1499-1506.
395. Holm, L.W.; Garrison, W.H. SPE Reservoir Eng., 1988, 3, 112-118.
396. Talley, L.D. SPE Reservoir Eng., 1988, 3, 235-243.
397. Prats, M. Thermal Recovery, Monograph Volume 7, Society of Petroleum Engineers, Dallas, 1982.
398. Castanier, L.M.; Brigham, W.E. Chem. Eng. Prog., 1985, 81, 37-40.
399. Strycker, A.R.; Madden, M.P.; Sarathi, P. SPE Reservoir Eng., 1987, 2, 543-8.
400. Isaacs, E.E.; McCarthy, F.C.; Maunder, J.D. SPE Reservoir Eng., 1988, 3, 565-72.
401. Muijs, H.M.; Keijzer, P.P.M. U.S. Patent 4 693 311, 1987.
402. Janssen van Rosmalen, R.; Muijs, H.M.; Keijzer, P.P.M. West German Patent 3 510 765, 1985.
403. Muijs, H.M.; Keijzer, P.P.M., West German Patent 3 734 075, 1988.
404. Huang, W.S.; Gassmann, Z.Z.; Hawkins, J.T.; Schievelbein, V.H.; Hall, W.L. West German Patent 3 503 532, 1985.

405. Angstadt, H.P. U.S. Patent 4 699 214, 1987.
406. Lim, T. PCT International Patent Application 85 05 146, 1985; Chem. Abstr., 1985, 104, 171228a.
407. Duerksen, J.H.; Wall, R.G.; Knight, J.D. U.S. Patent 4 576 232, 1986.
408. Falls, A.H.; Lawson, J.B., Hirasaki, G.J. J. Pet. Technol., 1988, 40, 95-104.
409. Falls, A.H.; Lawson, J.B.; Hirasaki, G.J. U.S. Patent 4 570 711, 1986.
410. Novosad, J.; Maini, B.B.; Huang, A. J. Can. Pet. Technol., 1986, 25, 42-6.
411. Huang, A.Y.; Novosad, J. Proc. Eng. Found. Conf. Fundam. Adsorpt., 2nd, 1986 (Pub. 1987), 265-75.
412. Lau, H.C.; O'Brien, S.M. SPE Reservoir Eng., 1988, 2, 1177-1185.
413. Dilgren, R.E.; Lau, H.C.; Hirasaki, G.J. U.S. Patent 4 597 442, 1986.
414. Lau, H.C. U.S. Patent 4 617 996, 1986.
415. Angstadt, H.P.; Rugen, D.F.; Cayias, J.L. French Patent 2 557 198, 1985.
416. Maini, B.B.; Ma, V. J. Can. Pet. Technol., 1986, 25, 65-9.
417. Angstadt, H.P.; Tsao, H. SPE Reservoir Eng., 1987, 2, 613-8.
418. Isaacs, E.D.; Prowse, D.R. U.S. Patent 4 458 759, 1984.
419. Duerksen, J.H. SPE Reservoir Eng., 1986, 2, 44-52.
420. Shen, C.W. U.S. Patent 4 702 317, 1987.
421. Lau, H.C. U.S. Patent 4 609 044, 1986.
422. Lau, H.C. U.S. Patent 4 727 938, 1988.
423. Hyne, J.B.; Clark, P.D. U.S. Patent 4 506 733, 1985.
424. Shah, D.O.; Schechter, R.S., Eds. Improved Oil Recovery by Surfactant and Polymer Flooding, Academic Press, New York, 1977.
425. Poettmann, F.H. in Improved Oil Recovery, Interstate Oil Compact Commission, Oklahoma City, Okla., 1983, pp. 173-250.
426. van Poolen, H.K. Fundamentals of Enhanced Oil Recovery, pp. 114-151.
427. Morgan, J.C.; Schechter, R.S.; Wade, W.H. in Proc. Sect. 52nd Colloid Surf. Sci. Symp.; Mittal, K.L., Ed.; Plenum Press, New York, 1979, Vol. 2, 749-75.
428. Puig, J.R.; Scriven, L.E.; Davis, H.T.; Miller, W.G. Chem. Eng. Commun., 1988, 65, 169-85.
429. Aalund, L.R. Oil Gas J., 1988, 86, 33-73.
430. B. Cox and J. Schubert, Eds. 1986 EOR Project Source Book, Pasha Publications, Arlington, Va., 1986.
431. Nelson, R.C. Soc. Pet. Eng. J., 1982, 22, 259-70.
432. Puerto, M.C.; Gale, W.W. Soc. Pet. Eng. J., 1977, 17, 193-200.
433. Graciaa, A.; Fortney, L.M.; Schechter, R.S.; Wade, W.H.; Yiv, S. Soc. Pet. Eng. J., 1982, 20, 743-9.
434. Puerto, M.C. West German Patent 3 542 063, 1986.
435. Cardenas, R.L.; Harnsberger, B.G.; Maddox, Jr., J. U.S. Patent 4 270 607, 1981.
436. Barakat, Y.; et. al., Soc. Pet. Eng. J., 1983, 23, 913-18.
437. Morita, H.; Kawada, Y.; Yamada, J.; Ukigai, T. U.S. Patent 4 512 404, 1985.

438. Morita, H.; Kawada, Y.; Yamada, J.; Ukigai, T. U.S. Patent 4 555 351, 1982.
439. Okada, T.; Morita, H.; Hagiwara, M. Japan Kokai Tokkyo Koho 60 152 794, 1985.
440. Thaver, R. British Patent Application 2 160 242, 1985.
441. Thaver, R. British Patent Application 2 184 763, 1987.
442. Aldrich, H.S.; Ashcraft, T.L.; Puerto, M.C.; Reed, R.L. West German Patent 3 303 894, 1983.
443. Greif, N.; Oppenlaender, K.; Sewe, K.U. West German Patent 3 422 613, 1984.
444. Schmidt, R.; Rupp, W.; Schneider, G.; Kohn, E.M. European Patent Application 264 867, 1988.
445. McCoy, D.R.; Gipson, R.M.; Naylor, C.G. U.S. Patent 4 426 302, 1984.
446. Chiu, Y.C.; Hwang, H.J. Colloids Surf., 1987, 28, 53-65.
447. Balzer, D. West German Patent 3 523 355, 1987.
448. Shaw, J.E. J. Am. Oil Chem. Soc., 1984, 61, 1395-9.
449. Liu, K.C. U.S. Patent 4 692 551, 1987.
450. Abe, M.; Schechter, R.S.; Selliah, R.D.; Sheikh, B.; Wade, W.H. J. Dispersion Sci. Technol., 1987, 8, 157-72.
451. Abe, M.; Schechter, D.; Schechter, R.S.; Wade, W.H.; Weerasooriya, U.; Yiv, S. J. Coll. Interface Sci., 1984, 114, 342.
452. Puerto, M.C.; Reed, R.L. Soc. Pet. Eng. J., 1983, 23, 669-82.
453. Lalanne-Cassou, C.; et. al. J. Dispersion Sci. Technol., 1987, 8, 137-56.
454. Fernley, G.W. West German Patent 3 535 371, 1984.
455. Bolsman, T.A.B.M.; Daane, G.J.R. SPE Reservoir Eng., 1986, 1, 53-60.
456. Heiss, L.; Schneider, G.; Trost, A. West German Patent 3 407 565, 1985.
457. Baviere, M.; Durif-Varambon, B.; Salle, R. French Patent 2 547 860, 1984.
458. Kalpacki, B.; Chan, K.S. U.S. Patent 4 554 974, 1985.
459. Bansal, B.B.; Hornof, V.; Neale, G. Can. J. Chem. Eng., 1979, 57, 203.
460. Manasrah, K., Neale, G.H.; Hornof, V. Cellul. Chem. Technol., 1985, 19, 291.
461. Kalfoglou, G. West German Patent 2 918 197, 1980.
462. Babu, D.B.; Neale, G.; Hornof, V. Cellul. Chem. Technol., 1986, 20, 663-72.
463. Nase, D.G.; Whittington, L.E.; Ledoux, W.A.; Debons, F.E. U.S. Patent 4 739 040, 1988.
464. Morrow, L.R.; Dague, M.G.; Whittington, L.E. U.S. Patent 4 739 041, 1986.
465. Baviere, M.; Bazin, B.; Noil, C. SPE Reservoir Eng., 1988, 3, 597-603.
466. Aldrich, H.S.; Puerto, M.C.; Reed, R.L. French Patent 2 589 858, 1987.
467. Hjelmeland, O.S.; Larrondo, L.E. SPE Reservoir Eng., 1986, 1, 321-8.
468. Somasundaran, P.; Shafick, H.H. Soc. Pet. Eng. J., 1985, 25, 343-50 and references therein.

469. Van Os, N.M.; Haandrikman, G. Langmuir, 1987, 3, 1051-6.
470. Noll, L.A. Colloids Surf., 1987, 26, 43-54.
471. Hofman, Y.L.; Angstadt, H.P. Chromatographia, 1987, 24, 666-70.
472. Lorenz, P.B.; Trantham, J.C.; Zornes, D.R.; Dodd, C.G. SPE Reservoir Engr., 1986, 1, 341-53.
473. Hohnson, J.S.; Jones, R.R.M. Ann. Chim. (Rome), 1987, 77, 229-44.
474. Doleschall, S.; et. al. Hungarian Patent 42 575, 1987.
475. Krumrine, P.H.; Ailin-Pyzik, I.B.; Falcone, Jr., J.S. Prepr. Am. Chem. Soc., Div. Pet. Chem., 1981, 26 (1), 195-8.
476. Methemitis, C.; Morcellet, M.; Sabbadin, J.; Francois, Eur. Polym. J., 1986, 22, 619-27 and references therein..
477. Bourrrel, M.; Verzaro, F.; Chambu, C. SPE Res. Eng., 1987, 2, 41-53.
478. Reference 426, pp. 104-111.
479. Neil, J.D.; Chang, H.L.; and Gefferm, T.M. in Improved Oil Recovery, Interstate Oil Compact Commission, Oklahoma City, 1983, pp. 52-66.
480. Mohnot, S.M.; Bae, J.H.; Foley, W.L. SPE Reservoir Eng., 1987, 2, 653-63.
481. Holm, L.W.; Robertson, S.D. J. Pet. Technol., 1981, 33, 161-72.
482. Chan, K.S.; Majoros, S.J. U.S. Patent 4 466 892, 1984.
483. Mohnot, S.M.; Chakrabarti, P.M. U.S. Patent 4 714 113, 1987.
484. Bunge, A.L.; Radke, C.J. Soc. Pet. Eng. J., 1983, 23, 657-68.
485. Burk, J.K. SPE Reservoir Eng., 1987, 2, 9-16.
486. Shuler, P.J.; Kuehne, D.L.; Lerner, R.M. J. Pet. Technol., 1989, 41, 80-88 and references therein.
487. Nelson, R.C.; Lawson, J.B.; Thigpen, D.R.; Stegemeier, G.L. Proc. 1984 SPE Enhanced Oil Recovery Symposium, Society of Petroleum Engineers, Dallas, 1984, pp. 417-424.
488. Saleem, S.M.; Faber, M.J. Rev. Tec. INTEVEP, 1986, 6, 133-42; Chem. Abstr., 1986, 106, 159007m.
489. Saleem, S.M.; Hernandez, A. J. Surf. Sci. Technol., 1987, 3, 1-10.
490. Pitts, M.J. Prepr. Am. Chem. Soc., Div. Pet. Chem., 1988, 33 (1), 169-72.
491. Peru, D.A. Report, 1986, NIPER 212; Chem. Abstr., 1986, 104, 140693k.
492. Lawson, J.D.; Thigpen, D.R. U.S. Patent 4 502 541, 1985.
493. Neale, G.H.; Khulbe, K.C.; Hornof, V. Can. J. Chem. Eng., 1987, 65, 700-3.
493. Lin, F.F.J.; Besserer, G.J.; Pitts, M.J. J. Can. Pet. Technol., 1987, 26, 54-65.
494. Enhanced Recovery Week, June 16, 1984, pp. 1,4.
495. Mungan, N. in Improved Oil Recovery, Interstate Oil Compact Commission, Oklahoma City, 1983, pp. 113-72.
496. Reference 426, pp. 132-145.
497. Johansen, R.T. in Improved Oil Recovery, Interstate Oil Compact Commission, Oklahoma City, 1983, pp. 91-112.
498. Reference 426, pp. 114-131.
499. Reference 426, pp. 3-40.
500. Ali, S.M. Farouq; Meldau, R.F. in Improved Oil Recovery,

- Interstate Oil Compact Commission, Oklahoma City, 1983, pp. 311-350.
501. Tiab, D.; Okoya, C.U.; Osman, M.M. J. Pet. Technol., 1982, 34, 1817-27.
 502. Babu, D.M.; Hornof, V.; Neale, G. Can. J. Chem. Eng., 1984, 62, 156-9.
 503. Crawford, P.B.; Cju, C. in Improved Oil Recovery, Interstate Oil Compact Commission, Oklahoma City, 1983, pp. 251-309.
 504. Reference 426, pp. 41-55.

RECEIVED February 21, 1989

Chapter 2

Application of Chemistry in Oil and Gas Well Fracturing

Weldon M. Harms

Halliburton Services, P.O. Drawer 11431, Duncan, OK 73536-0428

Hydraulic pressure stimulation (fracturing) of oil and gas wells has now accumulated 40 years of history and experience. The actual practice and application of this technique supports a multi-billion dollar service industry which annually utilizes in excess of 130 million pounds of chemical additives. This chapter will describe the fracturing fluids that are used and some of the additives, their purpose, and the principles that make their use effective as well as necessary. Information presented will update a body of review literature that covers the prior years of fracturing(1). Chemicals are added for specific purposes which are identifiable by their descriptive title. Veatch(2) has compiled a thorough general list of the additives added to fracturing fluids.

Typical Functions or Types of Additives Available For Fracturing Fluid Systems

- Antifoaming agents
- Bacteria control agents
- Breakers for reducing viscosity
- Buffers
- Clay stabilizing agents
- Crosslinking or chelating agents (activators)
- Demulsifying agents
- Dispersing agents
- Emulsifying agents
- Flow diverting or flow blocking agents
- Fluid-loss control agents
- Foaming agents
- Friction reducing agents
- Gypsum inhibitors
- pH control agents
- Scale inhibitors
- Sludge inhibitors
- Surfactants
- Temperature stabilizing agents
- Water-blockage control agents

To better understand the need for chemical additives we first

0097-6156/89/0396-0055\$12.50/0

© 1989 American Chemical Society

must become familiar with the physical and engineering aspects of fracturing. The process is ordinarily conducted with viscous fluids that are prepared by introducing gelling agents or viscosifiers to the fracturing fluid. Fracturing of gas and oil wells is performed for one primary reason: to increase the rate of production of fluids held by a localized zone beneath the earth's surface. Generally the zones that require treatment to attain acceptable flow rates consist of hard, consolidated rock. Rock does contain pores and some rock has cracks along layers (natural fractures). Rock also possesses interconnective channels (permeability) through which fluid can flow under pressure. If permeability is low and flow is not substantial then fracturing must be considered. Low flow rates usually mean a well is not profitable.

Fluids, both liquids and gas, readily transmit pressure. By pressuring up fluids (called frac fluids) on the surface with high pressure pumps and discharging them into the wellbore of a well at high rates, the parting pressure of a rock zone can be exceeded and a crack (a fracture) created. After the well is drilled, wellbores usually are lined with high pressure-resistant steel pipe which is cemented into place to protect and isolate sensitive formations, water zones, or strata of little interest. The entry point of the pressurized fluid is controlled by perforating the steel pipe lining opposite the zone of interest, usually with explosive shape charges or by high pressure jetting(3). Perforating creates small holes that penetrate through the steel casing. The holes generally are 0.25-0.5 inches (6-13mm) in diameter.

These holes (1-4 per foot of pipe) provide access to the earthen formation of interest but also create a restriction to fluid flow and subject the frac fluid to high shear forces. This shear is in addition to laminar or turbulent shear forces experienced in transit through the pipe. Well pipes are generally 0.3-5 miles (0.48-8 Km) in length which requires a fluid transit time of 1-20 minutes at the high rates necessary to fracture a well. Therefore it is important that the chemical additives contained in the pressurized fluid be tolerant of high shear. Intramolecular bonds of polymers can be cleaved by high shear which can drastically alter molecular weight, and subsequently viscosity. Chemical intermolecular bonds (crosslinkages) also can be broken, destroying the fluid colligative properties conferred by crosslinkages; therefore, chemical additive packages must be carefully tested and designed to derive optimal performance under shear. Once the fracturing fluid exits through the perforations and enters the rock, it then encounters much reduced shear in the fracture, except at the very leading edge where the crack is being propagated. After the fluid enters the fracture a new problem other than shear is encountered: fluid leakoff. The rock formation adjacent to the induced fracture is capable of accepting fluid as a result of the permeability and the natural fractures that are present. This loss of fluid can result in insufficient fluid being available to extend the fracture. Fluid loss control agents therefore are added(4).

The formation may also contain minerals that are chemically or physically sensitive to the fluid. For that reason clay stabilizing agents, surfactants(5), etc. are also added to the fluids. Fluids that will be produced from the well may contain problem-causing

contaminants which require the addition of demulsifiers, mineral deposition (scale) inhibitors(6), or paraffin deposition preventives to the fracturing fluid.

Flow in undisturbed rock normally is radial toward a site of lower pressure (the wellbore). The fracture crack created by high pressure injection usually forms perpendicular to the least principle stress that exists in the rock. The induced fracture intersects and disrupts the radial flow pattern such that flow becomes linear and more direct to the well. This phenomenon has been intensively examined and discussed by authors working in the discipline of rock mechanics as applied to hydrocarbon reservoirs. Hydraulic fractures created in oil and gas wells grow mainly vertically, parallel to the wellbore as depicted in Figure 1 and extend on either side of the perforated wellbore as "wings"(7-11). It is common for these wings to exceed 100 ft in height and hundreds of feet in length (Figure 2), but width remains comparatively narrow. At the wellbore it usually is less than 0.25 in. (6 mm) and for the vast majority of the fracture area width never exceeds 0.5 in (13 mm) wide (Figure 3).

The shape and exact dimensions of induced fractures remains a topic of lively interest. Researchers who model fracture behaviors, or their shapes and dimensions, disagree as to which mathematical expressions best predict the job results(12). Other than rate of fluid leakoff, the two most important parameters that a good model should predict are height and fracture width. The growth of fracture height usually determines whether the fracture will stay within the desired zone, or extend down into a water-bearing zone (a costly and undesired occurrence), or upward away from the hydrocarbon saturated layer. Prediction of induced fracture characteristics is important because a single fracturing treatment requires a considerable monetary investment (\$10,000-2,000,000). If the prediction of the induced fracture is inaccurate, the fracture too small or in the wrong place, then hydrocarbon production may remain inadequate; if the fracture is too massive the additional hydrocarbon production may not offset the greater expense of the large-scale treatment. If the model is incorrect then the fracturing treatment may have to be terminated early and additional, expensive, remedial formation and wellbore cleanout steps taken before the well can produce hydrocarbons. It may be necessary to treat the well a second time(13,14).

Width assumes a great importance when one realizes that to maintain conductivity through the induced fracture it is nearly mandatory that the crack be filled with a solid spacing agent (called proppant) which will prevent the crack from closing completely after the hydraulic pressure on the well is released. The fracture must be wide enough to permit entry of proppant to a distance sufficient to stimulate production. Tons of proppant are normally required to fill this void. Therefore the fracturing fluid must suspend the proppant long enough for it to be transported and placed, by flow, throughout the fracture. To preserve the maximum accessible flow area, the proppant should be uniformly suspended inside the entire propped fracture area while the fracture closes. Kaspereit(15), as well as Smith(16), has made the point that fracture conductivity can be a limiting factor. If the

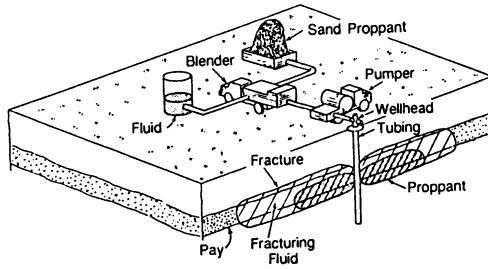


Figure 1. Fracturing process, equipment, and growth of vertical “wings”. (Reproduced with permission from ref. 2. Copyright 1983 Society of Petroleum Engineers.)

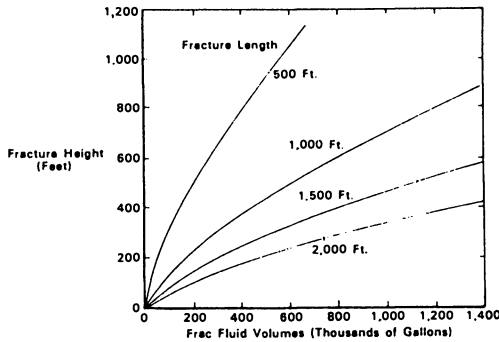


Figure 2. Typical fracture dimensions. (Reproduced with permission from ref. 2. Copyright 1983 Society of Petroleum Engineers.)

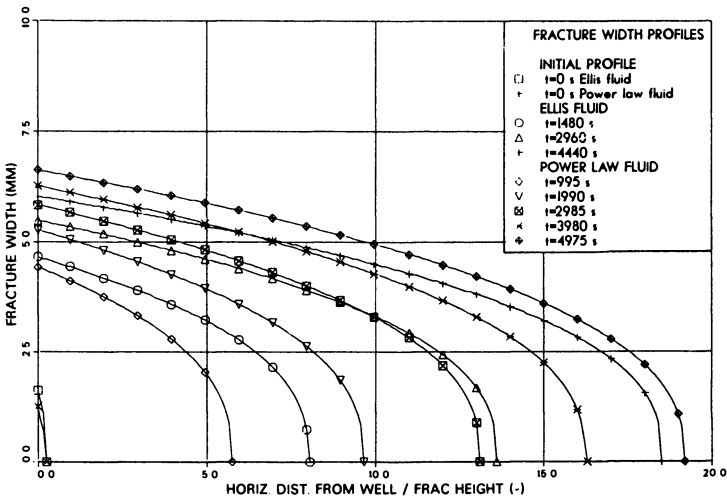


Figure 3. Fracture width vs. length. (Reproduced with permission from ref. 362. Copyright 1983 Society of Petroleum Engineers.)

proppant falls before closure, production increase can be drastically reduced. Simplistically, viscosity controls the width of the fracture and to a large degree the time of proppant settling. Wider fractures result from increased pressure drops within the fracture. More viscous fluids cause greater pressure drops. Width can be increased by increasing fluid viscosity and/or fluid injection rates. These two variables usually work at odds with one another, since viscous fluids often resist high pumping rates.

Chemicals must yield fluids with improved viscosity and flow properties and must provide proppant transport and suspension properties for the many hours required for a well treatment. This may be difficult to achieve since temperatures inside the fracture can range between 60°- 500°F+ according to depth. Without the correct physical fluid properties it is not possible to place much proppant before excessive pressure resistance is generated (typical steel pipe and pumping equipment can operate between 4,000-15,000 psi; special equipment allows treatments to 20,000 psi) and pumping has to be terminated due to well "screen out" or "pressure out." Three years (and 10,500 fracture treatments) after fracturing was introduced, it was clearly recognized by Clark, et al.(9), that successful fracturing treatments demanded effective viscosifiers as well as fluid loss control agents.

Fracturing Fluids

Gelled Oils. The first pressurized fluids used to fracture stimulate wells were hydrocarbon liquids. Credit for conception of well stimulation by hydraulic fracturing generally has been given to Clark(7,9,17,18) or alternately to Farris(19), both of whom worked for Stanolind Oil Co. and filed for patent protection simultaneously on May 28, 1948. Other authors(20) place the conception and use as early as 1925. The first recorded application was conducted by Stanolind Oil (now Amoco Production Co.) in 1947 in Grant County, Kansas in the giant Hugoton gas field(7). One thousand gallons of gasoline without any proppant was used. The treatment design involved multiple stages. Typical results of this type of treatment were later presented by Clark(9). The gasoline was viscosified by use of napalm(21,22). Napalm is a specially precipitated, granular aluminum soap(23) prepared from a mixture of oleic, naphthenic, and coconut fatty acids. Gelled hydrocarbons remained the preferred hydraulic fracturing fluids for about 10 years. These fluids could carry moderate quantities of proppant (1-3 lb/gal) and viscosity could be adjusted by changing the oil used or the gelling agent concentration.

Refinements in napalm chemistry were introduced throughout the industry (1950-1960) using other fatty acid aluminum salts as well as sodium or potassium tall oil mixtures(23-26), which are rosin and fatty acids derived from digested, pulped pine wood. Gelling agent chemicals were selected and formulated to give best performance with different hydrocarbon liquids such as kerosene, diesel No. 1, diesel No. 2, residual oils, "refined oil," and some crude oils according to customer preference and acceptance. Performance can be achieved with these metallic soaps but the very viscous gels created are limited in temperature application ($\leq 150^{\circ}\text{F}$) and most are very

sensitive to moisture contamination. The gels can be intentionally broken by the introduction of chelating agents(27), by acids, or by brine water.

In 1970, Monroe and Rooker(28) claimed the use of aluminum salts of acid orthophosphate esters as viscosity builders for use in fracturing fluids. The application of these materials began a new era of hydrocarbon gelling agents. Monroe(29) later claimed the use of Fe_3O_4 as a metal activator of phosphate esters and in 1971 described several other metals(30) that could be used with amine neutralization agents. Numerous metallic ionic derivatives can be used as effective "activators" or crosslinkers to prepare a gel. Most of these metals exist as several species in equilibrium. Aluminum is ordinarily used. Ryles(31) commented on the properties of aluminum species as has Arnson(32), Lauzon(33), Schecher(34), and Baes and Mesmer(35). The distribution of aluminum species is very sensitive to pH (Figure 4).

Phosphate esters can function as friction pressure additaments(36) as well as viscosity builders in hydrocarbon fracturing liquids. A bothersome feature of pumping fluids in narrow steel pipe at the high rates and pressures necessary to fracture rock is that friction is created and a significant pressure drop in the pipe occurs. Friction pressure drop is proportional to the square root of the fluid velocity. A high enough pressure to cause a fracture to open and elongate must be applied by pumps on the surface at all times during the treatment. Additional rate and subsequently more horsepower is required to overcome pressure losses due to friction. More horsepower increases treatment costs and can be a limiting factor in whether a well can be successfully treated. Therefore "friction reducers" are a very important class of additives routinely added to fracturing fluids to lower costs and improve treatment efficiency.

Aluminum crosslinked orthophosphate esters are still the major hydrocarbon gellants used today. Typically 1% by volume acid phosphate ester (ca. 100 moles) plus the stoichiometric equivalent of 33 moles of sodium aluminate or aluminum chloride in solution are added to 1000 gallons of hydrocarbon. Sufficient alkaline solution (caustic or amine) is then added to neutralize the acid phosphate ester and create a viscous gel. Viscosity development depends on the correct degree of neutralization. Excess acid or alkali will result in much lower viscosities. In large industrial applications such as fracturing chemistry it is usually not economically practical to use isolated, highly purified materials. Instead the phosphate ester product mixtures have been adapted. The esters can be prepared from several routes such as phosphorous pentoxide, phosphorous pentachloride, phosphorous oxychloride, or ester exchange. Different product mixtures are obtained from these routes. Zangen(37), et al. and Moule and Greenfield(38) have commented on some of the complexities of phosphate ester products.

Oil Gel Breakers. Many fracturing gels remain too viscous inside the fracture after placement, thereby preventing flow of hydrocarbons from the well. Fracture fluids should eventually lose their viscosity after the fracture job has been completed. Breakers are chemicals intentionally added to fracturing fluids to decrease or

destroy their viscous properties to permit recovery of fluids after the well has been fractured and propped. Since breakers are preferably added during treatment it is necessary that their action be delayed during the job duration, often 1-8 hours long. Hill(39) described various formate, acetate, benzoate, etc derivatives that are useful to break gelled oils. McKenzie(40) published data on the use of selected acids as gelled oil breakers. Daccord, et al.(41) claimed that addition of a partially neutralized acidic aluminum salt provides a one stage preparation of oil gels which can be broken by the addition of 4-nitro-benzoic acid. Since gelled oils contain little water it takes a period of time before these additives change the "non-aqueous" pH of the oil gel and break it. Numerous improvements(42) in orthophosphate gellants have been reported during the 19 years since their introduction.

Mechanism of Oil Gelation by Orthophosphate Esters

The mechanism of how these viscosifiers alter the properties of hydrocarbon fluids has not been intensively examined but some results and proposals have been published. In 1970 Baker, et al. summarized their findings on the friction reduction properties of metallic soap derivatives(43) and proposed a colloidal association configuration of the molecules in micelles as the operative mechanism. Earlier Rose and Block(44-46) had proposed a bridged associational model between metal and phosphate molecules to explain the high intrinsic viscosity development and low-temperature flexibility imparted by mixed alkyl phosphates with Zn(II) or Co(II) ions. This association structure is thought to be operative in poly(phosphonatoalanes)(47) and aluminum orthophosphate ester gels, as per Burnham, et al.(48) McKenzie(40) proposed a similar, three-dimensional associated structure involved in a dynamic chemical equilibrium (Figure 5) that could assimilate all the modifying agents known to affect these type gels.

Fendler(49) published regarding his pursuit of "surfactant vesicles" as a mimic of biological membranes. These are defined as smectic mesophases of synthetic surfactant bilayers containing entrapped water(50,51). Dihexadecyl phosphate was the surfactant used. This molecule bears a resemblance to the dialkyl phosphate esters used in oil gelation technology. It may be that some of the oil gels used as fracturing fluids consist of micelles having associated hydrophobic layers that surround the water contained in the oil gel. Oil fracturing fluids are never entirely water-free. Humidity contributes significant moisture and the metallic "activator" is usually added as an aqueous solution. It is known that micelles require shear or sonication energy in order to form. Oil gels must be sheared in order to form. Micelles are dynamic species possessing interior viscosities. Micelles can maintain substantial pH gradients between the bulk liquid phase and the entrapped phase. Oil gels are viscous and can maintain stability for hours in the presence of acids or alkalis which are added as breakers. One representation of a vesicle(51) consists of a three-dimensional equilibrium specie -- similar in some respect to the suggestions presented by McKenzie.

Whatever the active mechanism is, from these publications it

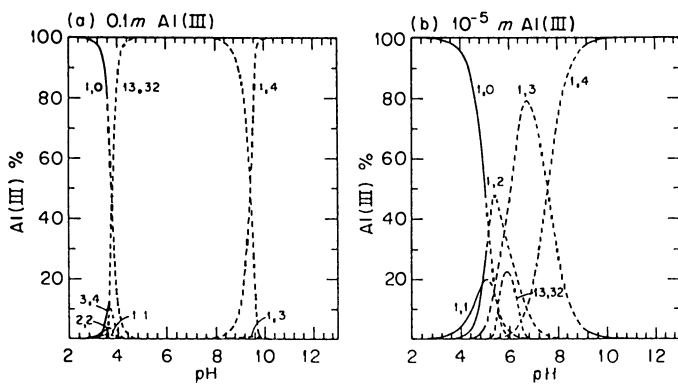


Figure 4. Aluminum cross-linker moiety depends upon pH of gelled fluid. (Reproduced with permission from ref. 35. Copyright 1976 Wiley & Sons.)

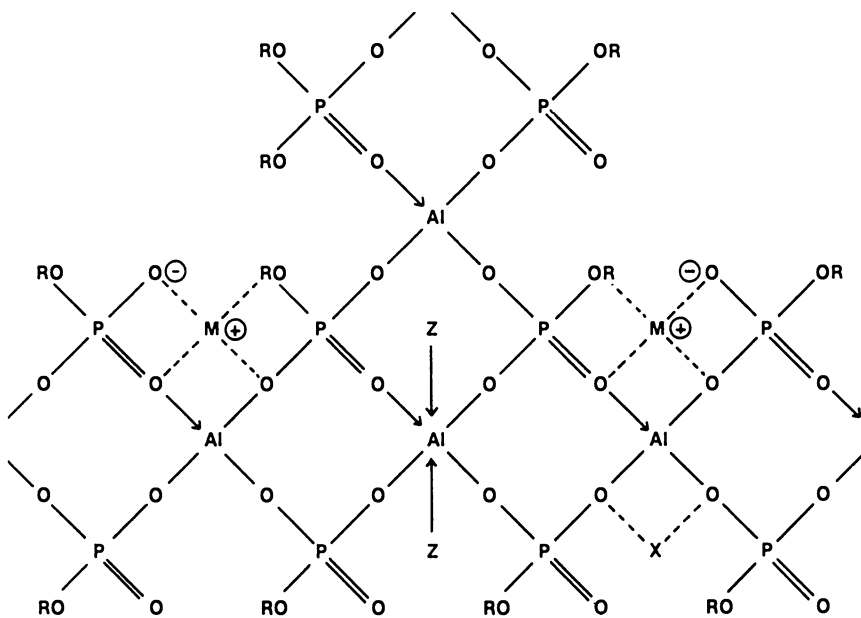


Figure 5. Proposed 3-D associated gel network model. (Reproduced with permission from ref. 40. Copyright 1980 Society of Petroleum Engineers.)

can be concluded that orthophosphate ester gels exist as a dynamic, associated network in equilibrium. Since the network is formed by associative attractions rather than rigid covalent bonds it has the ability to eventually reheal if destroyed by physical shear forces, an attractive property for a fracturing fluid. At the same time equilibrated associative attractions can be altered by numerous polar molecules, much more easily than covalently bonded gels can be altered. Associative oil gels are sensitive to polar contaminants. The gels can be broken by water, alcohols, acids, bases, and surfactants.

Water Gelling Agents

Fracturing effectiveness was quickly proven in 1947 using hydrocarbons as the pressurized fluid(9). Well owners were reluctant to use water as a fluid because of the massive damage to hydrocarbon flow and recovery that can occur when untreated water is contacted with water-sensitive formations(52,53). Certain clays and shales are notorious for sloughing and swelling in fresh waters. Microscopically clays consist of deposited mineral layers which act as ion exchange sites (Figure 6). The tiny clay particles shrink or expand depending on the cation to which they are exposed. Even if the localized swelling at the point of contact doesn't completely close all permeability tiny disturbed clay solids may be released by ionic or mechanical shock and transported by flow as "fines" which can accumulate and plug rock permeability.

Acids were an early exception to the no water rule. It was recognized that aqueous solutions of acids would inhibit swelling of clays and shales as well as dissolve any acid-soluble minerals contained in a formation. By 1933 commercial well stimulation with hydrochloric acid was of great interest. A whole separate methodology and treatment chemistry has since evolved around acidizing and fracture acidizing(54). Water emulsions, mainly emulsified acids, and gelled acids thickened with polymeric additives were applied early in the history of well treatment.

By 1953 gelled water fracture treatments were used to improve injectivity in water injection wells in waterflood projects. Frictional pressures with water or brine fluids generally were lower than with hydrocarbon fracturing fluids and could be lessened further by the addition (0.1 to 0.5% W/W) of natural polysaccharide or synthetic polymers. Flammability problems and cost were minimal with water and viscosity thinning due to increasing temperature often affected water gels to a lesser degree than hydrocarbon gels. Yet interest in fracturing oil and gas wells with water-based gels remained subdued until 1957.

Clay Stabilizers

Perhaps the key development that began to tip the balance in favor of water-base fluids was recognition that formation damage by water could be controlled. Control was first provided by inorganic salts dissolved in the water. Operators knew that native brine solutions (usually 6-37% NaCl) caused little or no damage to the formations they were produced from.

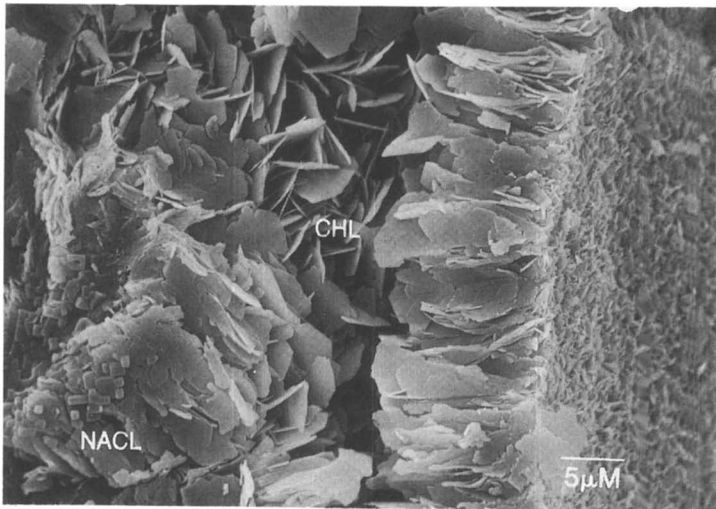
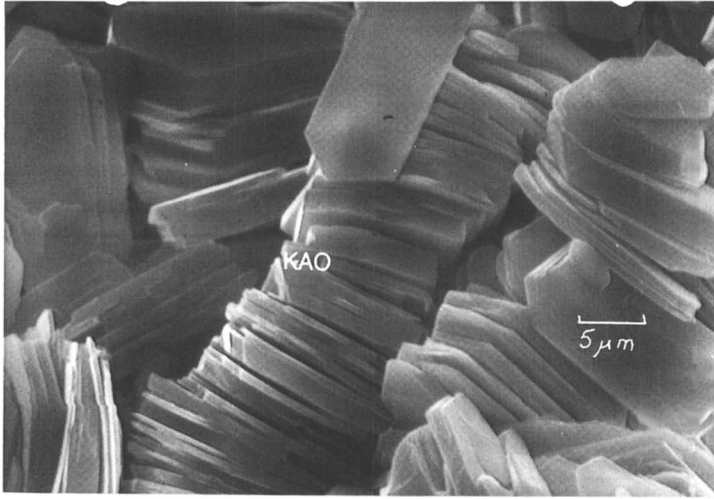


Figure 6. Scanning electron microscope photos of the troublesome clay minerals: kaolinite, chlorite, smectite, and illite. (Reproduced with permission, Halliburton Services.) *Continued on next page.*

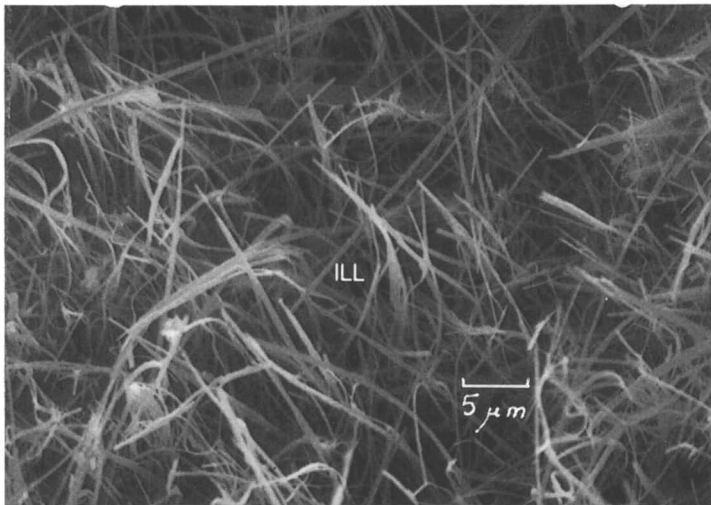
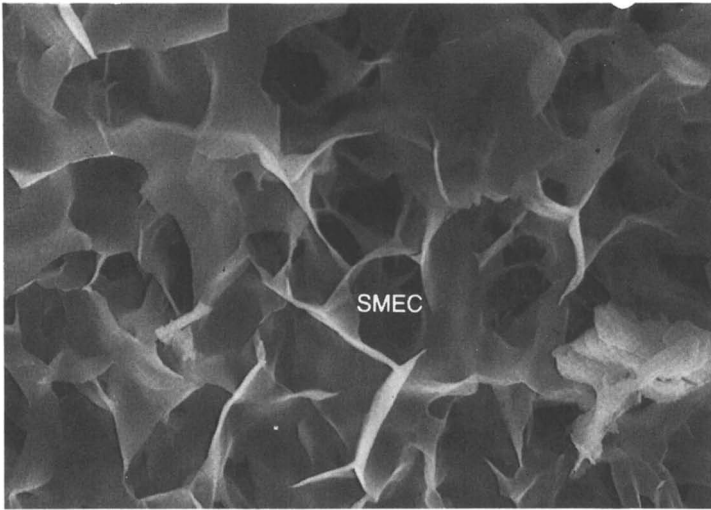


Figure 6. *Continued.*

From 1958 to 1970 inorganic salts such as CaCl_2 (53,55,56), MgCl_2 (57), KCl (55-58), hydroxyaluminum chloride (59-63), and zirconyl chloride (64-67) were introduced and found acceptance as clay protection additives. Each salt has its own peculiar set of advantages and disadvantages. It is now routine to include 2% KCl by weight of water as a clay treatment chemical in nearly all fracture waters.

Each of these cations participates in an ion-exchange reaction with protons on the surface of clay particles. Aluminum and zirconium are said to form polynuclear complexes with multiple positive charge centers that can exchange with more than one proton site and therefore possibly provide more effective protection than can simple monovalent or divalent cations. Multiple bonding is believed to offer some benefit in preventing the migration of fines. All the benefits derived from treating with metal salts can be largely nullified by treating the formation with HCl solutions. This can be a disadvantage since acidization is a common practice employed to economically increase hydrocarbon production from depleted wells.

In 1956 Brown, in a series of patents (68-75), disclosed that clays could be treated with di-, tri-, or tetra-substituted ammonia derivatives. Later, McLaughlin, et al. (76,77), introduced cationic polymers as permanent clay protective chemicals. A series of published results describing laboratory and field applications soon became available (78-81). Structural details of the cationic polymers appeared in patents (82-85). In general the polymers are polyamine derivatives, mostly quaternary in nature. Theng (86,87) has discussed how the multiple cationic centers in these polymers can interact and permanently protect clays. Callaway (88) et al. has noted that cationic polymers may interfere with the performance of crosslinked fracturing fluids.

The effect of pH on both clay swelling and fines production has been widely discussed (89-95). Little consensus is found in this literature. Suggested treatments range from application of fluoboric acid (96) to 15% KOH (92) solutions -- both treatments are believed to create a protective silicate film that inhibits release of fines. Polyacrylate polymers can provide protection against swelling of smectite clays and shales (97-100).

Several articles with informative bibliographies covering formation protection additives have appeared recently (97,101,102). The exact rock formation sample in question, the ionic strength of the treatment fluid, the preventive additives that are present, the pH of the fluid, and the test procedure employed all have significant effects on the test results. However, with careful experimentation using representative materials a preventive additive package can be administered as part of a water-based fracture treatment to allow effective stimulation of most hydrocarbon reservoirs. Because of this, water-based fracturing fluids are used in approximately 90% of all fracture treatments performed today.

Gelling Agents (Viscosifiers)

During the 1950-1965 era, a number of water viscosifying agents were examined and introduced in rapid succession. Anderson and

Baker(103) state that Karaya gum was the first to be used. Synthetic products, e.g., polyethylene oxides(104), polyacrylates, polyacrylamides, and polyetherglycols were in competition with natural polymers like starch, guar, cellulose derivatives, alginates, carrageenan, and locust bean gum. The basic physical and structural properties of the various polysaccharide thickeners have been compiled and reviewed by numerous authors and editors(105-109).

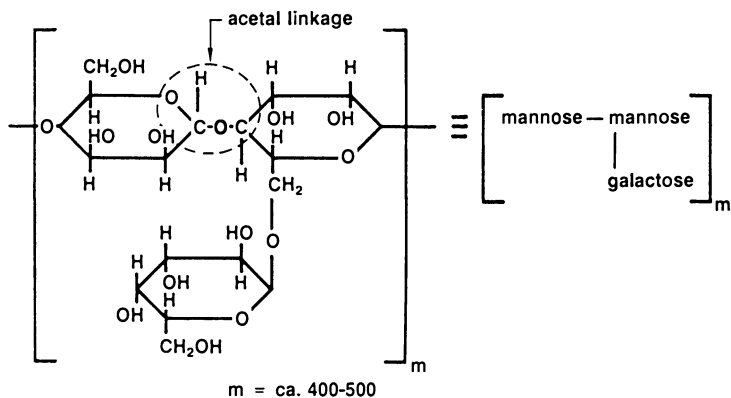
Cost and performance effectiveness of the natural polysaccharide thickeners quickly established these materials as preferred water gelling agents over synthetic polymer viscosifiers. Synthetic polymers were found to be more cost effective as friction reducers(110) and remain in routine use as such. Generally these friction reducers are acrylamide (for cost effectiveness) copolymers that contain up to 40% of a second monomer (for improved performance) to impart anionic or cationic properties; such as acrylamidopropanesulfonate (AMPS), acrylic acid, or dimethylaminoethylmethacrylate (DMAEM), etc. The greater effectiveness of synthetic polymers as friction reducers as compared to polysaccharides is related to high molecular weight as well as the size of the extended, hydrated synthetic polymer chain. Monomer identity and ratio alone do not tell the whole story on effectiveness since other parameters can result in divergent friction reducing performances(111).

Guar Viscosifiers

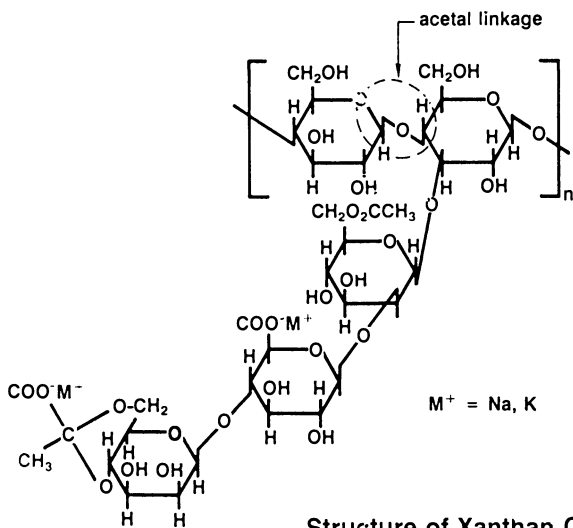
Guar gum, a heteropolysaccharide, introduced in 1953(103), quickly became the most widely used aqueous viscosifier. Its viscosification capability ranks ahead of the other natural gums (Table 1). Guar is a branched galactomannan found in the interior portion of the bean seeds of the guar plant (*Cyamopsis tetragonolobus*). The beans are harvested and then processed by grinding away the outer seed hull (to remove proteins and trash material) to obtain the relatively pure interior endosperm that is practically all water-soluble polygalactomannan. Molecular weight of the polymer has been estimated as 440,000 to 1.6 million(112,113).

Derivatized guar is also in common use. Derivatization usually lowers insoluble residue content, improves rate of viscosity yield, and increases the high temperature stability of the polymer. The most prevalent derivatized guar in use is hydroxypropyl guar (HPG) prepared by caustic treatment of guar with propylene oxide(114). Field introduction of this polymer was described by various authors(115-117). Carboxymethylhydroxypropyl guar (CMHPG) also has found general acceptance(118-120). The presence of a carboxyl group allows access to crosslinking chemistry not available with hydroxyl groups alone. The structures of guar and some other commonly used polysaccharide gelling agents are represented in Figure 7. Chatterji and Borchardt(121) have assembled a chart of the general applications of these materials (Table 2).

Numerous other derivatives of guar have been prepared by attaching modifying molecules to the guar backbone. Illustrative of the modifying molecules are chloroacetic acid(122), acrolein(123), ethylenimine(124), acrylamide(125), aminomethylphosphonic acid(126), and methyl bromide(127). None of these have achieved widespread use

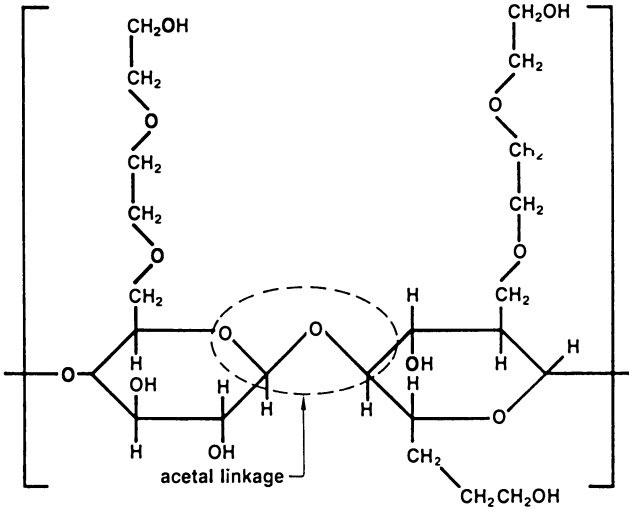


Chemical Structure of Guar Gum

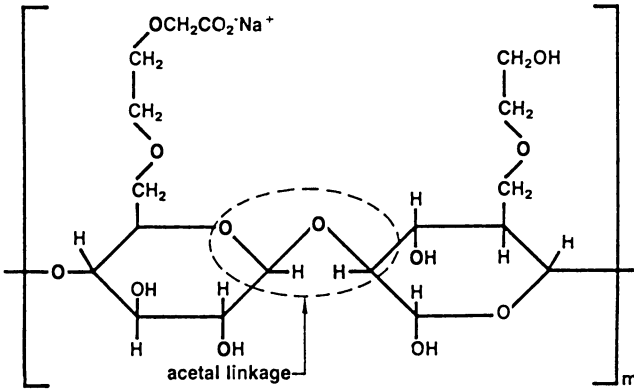


Structure of Xanthan Gum

Figure 7. Structures of several polysaccharide gelling agents. (Reproduced with permission from ref. 121. Copyright 1980 Society of Petroleum Engineers.) *Continued on next page.*



Structure of Hydroxyethyl Cellulose



Idealized Structure of Sodium Carboxymethylhydroxyethyl Cellulose

Figure 7. Continued.

Table 1. Relative Viscosities of Natural Polysaccharide Gelling Agents

Gum	cps
Gum arabic (20% by wt)	50
Locust bean gum	100
Methylcellulose	150
Gum tragacanth	200
Carrageenan	300
High-viscosity sodium carboxymethylcellulose	1200
Gum karaya	1500
Sodium alginate	2000
Guar gum	4200

NOTE: Reproduced with permission from ref. 105. Copyright 1973 Academic Press.

Table 2. General Properties of Common Oil Field Gelling Agents

Polymer	Cost ^b	Viscosity ^c (cps) 40 lb/1000 gal at 300 rpm	Shear ^d Stability	Salt ^e Tolerance	Acid ^f Stability	Enzyme ^g Stability	Residue ^h in Broken Gel	Applications
Guar Gum	1	34	3	C	N.S.	N.S.	R	Drilling fluids, spacers, friction reduction, in stimulation, fracturing and lost circulation (crosslinked guar gum gels), fluid loss additive in drilling, spacer and fracturing fluids
Hydroxypropyl Guar	1	36	3	C	N.S.	N.S.	R	Drilling fluids, spacers, completion and workover fluids, friction reducer in fracturing, fracturing and lost circulation (crosslinked HPG gels), fluid loss additive in drilling spacer and fracturing fluids
CMC	2	55	3	IC	N.S.	N.S.	RF	Drilling fluids
HEC	2	37	3	C	N.S.	N.S.	RF	Fluid loss additive for cementing spacers, completion and workover fluids, fracturing fluids, friction reduction in stimulation, enhanced recovery
CMHEC	2	32	3	C	N.S.	N.S.	RF	Fluid loss additive and retarder for cementing, spacers, gelling weak acids, temporary diverting agents in fracturing (crosslinked gels)
Xanthan Gum	4	34	1	C	M.S.	M.S.	RF	Drilling, completion, fracturing and enhanced oil recovery
Polyacrylamide (Partially Hydrolyzed)	3	34	2	IC	S	S	RF	Fluid loss additive in cementing, drilling fluids, friction reduction in fracturing, enhanced oil recovery, scale inhibitor
Copolymer of Polyacrylamide	3	25	2	MC	S	S	RF	Fluid loss additive in cementing, drilling fluids, friction reduction in fracturing, enhanced oil recovery, water-oil ratio reduction, improvement of injection profile (usually crosslinked)

a - These properties were determined using representative polymers of each class. Changing the specific polymers could substantially alter the properties listed here. This table is meant to be a generalized description and not a rigid list of specifications.

b - The order of cost per pound of polymer, 1 being the cheapest and 4 being the costliest. The cost will vary with the supplier and the amount of order.

c - Viscosity data reflect the numbers obtained with a particular polymer in fresh water. Changing the molecular weight, degree of substitution, moles of substitution or the nature of monomers in the copolymer will drastically alter the viscosity.

d - The order of shear stability, 1 being the least shear stable and 3 being the most. Xanthan gum solution viscosity is not permanently reduced by shear.

e - C = compatible, IC = Incompatible.

f - N.S. = Not Stable, M.S. = Moderately Stable, S = Stable.

g - N.S. = Not Stable, M.S. = Moderately Stable, S = Stable.

h - R = Residue present, RF = Residue Free.

NOTE: Reproduced with permission from ref. 121. Copyright 1980 Society of Petroleum Engineers.

in fracturing fluids. Cationic derivatives are prepared by treating polysaccharides with vinyl monomers such as 3-chloro-2-hydroxypropyl trimethyl ammonium chloride. Cationic guar was used as the gelling agent in one high temperature crosslinked fracture fluid(128,129).

Cellulose Viscosifiers

Cellulose polymer has also been studied extensively as has its derivatives. Cellulose is a linear homopolysaccharide of glucose units linked via $\beta(1-4)$ glycoside bonds. It is highly crystalline in nature and insoluble in water. Derivatization is required to render the polymer water soluble. The most common cellulose derivatives used in fracturing fluids are hydroxyethylcellulose (HEC) prepared by ethoxylation of cellulose, and carboxymethylhydroxyethyl cellulose (CMHEC) prepared by treatment of cellulose with ethylene oxide followed by treatment with chloroacetic acid to provide carboxymethyl substitution on the backbone(130). Similar in many respects to CMHPG, this anionic, doubly-derivatized cellulose gains the valuable properties of the carboxymethyl group (water solubility and complexation ability) while the presence of the hydroxyethyl group improves salt tolerance and acid resistance. These properties make the use of HEC or CMHEC preferred over guar when preparing viscosified acids or brines.

Carboxymethyl cellulose (CMC) is widely used as an additive to prepare drilling fluids and certain specialty fluids but failed to maintain acceptance in fracturing fluids because of its salt sensitivity and narrow temperature application range(131). Cellulose derivatives are widely used as viscosifiers but do not command the volume of usage of guar and guar derivatives. This preference is due in part to the stereochemical and structural difference between guar and cellulose and in part due to the higher cost of cellulose derivatives. Guar has a mannose backbone with numerous branches of galactose sub-units, which contain *cis* 3,4-hydroxyl groups. Cellulose is composed entirely of glucose sub-units, where all adjacent hydroxyl groups are *trans* to each other. Branching provides guar with different characteristics than the more linear cellulose derivatives and the presence of *cis*-hydroxyl groups in the galactose moieties promotes interaction of the guar molecules with many metal cations which do not interact with the *trans*-hydroxyl groups of cellulose derivatives.

Xanthan is a natural, highly-branched polysaccharide produced by the bacterium *Xanthomonas campestris*(132). The backbone consists of a cellulose chain with attached trisaccharidic side chains. The terminal saccharide of the branch is a pyruvic acid derivatized mannose unit (Figure 7). As such this terminal unit provides both a carboxyl group and *cis*-hydroxyl moieties. These groupings provide interactive sites that endow xanthan with special properties in solution as well as providing sites for crosslinker interactions to occur. Xanthan self-associates to form helical structures. For this reason an accurate molecular weight is difficult to determine. Southwick(133) et al. believes the base molecular weight of individual strands to be 2×10^6 . Salamone(134), et al. reviewed the overall uniqueness of xanthan. Most applications of xanthan seek to take advantage of the suspending properties of the polymer or its ability to interact with other polymers(135,136).

Xanthan has several undesirable properties. It ordinarily forms microgel particles that can plug permeability(137), it is expensive relative to other natural polysaccharide gel agents, and it resists degradation by ordinary gel breaker additives. These features have kept xanthan applications in fracturing gels to a minimum. Some literature(138) on xanthan has appeared. Carico(139-140) has published comparative information about the various gelling agents. Xanthan has been adapted to foam fracturing gels. Xanthan gels can be broken by the addition of lithium hypochlorite(141).

Selection of a gelling agent to prepare viscous fluids is determined by many factors. Cost and performance are primary properties to be respected. Secondary properties can change original choices based solely on cost and viscosity performance alone. Factors such as pH stability, interaction with metal crosslinkers, response to brines, rate of hydration, temperature susceptibility, dispersibility, compatibility with other additives, and residue left after break often(142) influence the ultimate selection. Derivatization of polysaccharides is done to enhance certain performance features. Variations in moles of substitution and degree of substitution can cause very pronounced changes in behavior(143). These differences can arise because of crosslinking density as well as changes in the binding sites.

Effective complexation chemistry with metal ion complexing agents is highly desirable and is a most important feature of the majority of fracturing fluids used today. Crosslinking ordinarily increases the viscosity of a polymer solution 5 to 20 fold (Figure 8) and therefore offers a cost effective method of providing highly viscous polymer gels. Complexation by many metal crosslinking ions is a function of multiple interactions with hydroxyl groups and is dependent on hydroxyl spatial orientation. Cis-hydroxyl groupings appear to provide increased crosslinking abilities. Angyal(144,145) attributes complexation effectiveness of polyhydroxy materials to the ability to assume a sequence of axial, equatorial, axial hydroxyl groups. Cis-diol characteristics can be conferred on cellulose polymers by derivatization with appropriate dihydroxy monomers(146,152). Ordinary derivatized cellulose fluids used in gravel packing or fracturing fluids are useful only to about 220°F(149,150). The presence of the cis-dihydroxy grouping increases the operating temperature range of cellulosic polymers beyond 220°F.

Dispersion of Gelling Agents

Dispersion of polymeric viscosifiers is often difficult because the initial contact of the untreated polymer with water results in very rapid hydration of the outer layer of particles which creates a sticky, rubbery exterior layer that prevents the interior particles from contacting water. The net effect is formation of what are referred to as "fish eyes" or "gel balls." These hamper efficiency by lowering the viscosity achieved per pound of gelling agent and by creating insoluble particles that can restrict flow both into the formation and back out of it. The normal remedy for this behavior

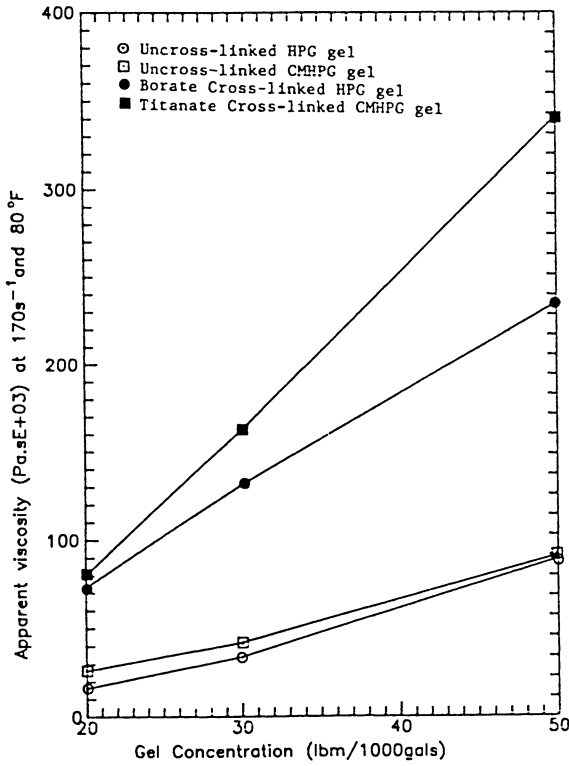


Figure 8. Cross-linking increases gel viscosity. (Reproduced with permission from ref. 330. Copyright 1987 Society of Petroleum Engineers.)

is to control particle size and provide surface treatment modifications to the polymer. One seeks to delay hydration long enough for the individual polymer particles to disperse and become surrounded by water. Then no dry particles are trapped inside a gelled coating. This can be achieved by slightly reacting or coating the polymer with borate salts(155,156), glyoxal(157,158), non-lumping HEC(159), sulfosuccinate(160), metallic soaps(161), surfactants(162), or materials of opposite surface charge to the polymer(163). Polymers have also been dispersed into a water-in-oil emulsion which is then inverted after addition to water(164).

Another recent innovation to improve the efficiency of polymer addition to water and derive the maximum yield from hydrophylic polymers was introduced by Briscoe(165,166). The method involved the preparation of a stabilized polymer slurry (SPS) to be added to water. Briscoe used water as the suspension liquid, usually also containing dissolved KCl as a clay stabilizer, and formulated a package of inhibitors (borate and caustic) to prevent the polymer from hydrating until the pH was lowered. These concentrates remain in routine use today.

Aqueous concentrates can suspend a limited quantity of polymer (ca 0.8 lb/gal) due to the physical swelling and viscosification that occurs in a water-based medium. Higher quantities (up to 5 lb/gal) of solids can be suspended in a diesel fuel carrier fluid. This fact and a desire for greater efficiency of equipment use led to the development of diesel-based SPS concentrates. First used in 1985(167-170), use of these SPS concentrates has spread rapidly(171-173).

Suspension of water soluble solids in oil can be achieved by a variety of chemical additives. Chemical suspension additives that have been suggested include alkyl mercaptophosphonic acids(174), organophylic clay plus hydroxypropyl cellulose(175), polyols(176), aluminum stearate(177), organophylic clay plus surfactant(178-181), aluminum phosphate esters(182), and acrylate copolymers(183-184). The most commonly cited suspending agent employed to prepare oil dispersions is organophylic clay. This material is prepared by treating smectite-type clays with fatty-quaternary amines. Organophylic clays were first described by Hauser(185-188) and Hauser(189,190) and have routinely been used to viscosify oil-based drilling fluids(191). Improvements have been claimed in preparing these materials(192-195). Since organophylic clays are insoluble solids their use in preparing SPS concentrates should be minimized and generally restricted to applications where their presence is not objectionable. The presence of solid residues can lower fracture conductivity and therefore production(142,196). SPS concentrates can be prepared using residue-free synthetic polymers(184) that will not affect fracture conductivity.

Crosslinked Fracture Fluids

Historically, as wells are drilled deeper and operating temperatures increased, new methods are sought to improve fluid properties to suspend proppant at the higher temperatures. The use of very high loading levels of gelling agent soon reaches a practical economical and operational limit. High viscosities developed from large

polymer loadings in the surface mixing equipment leads to poor mixing efficiency of additional polymer solids into an already thickened gel. Also excessive frictional pressure resistances can be encountered during placement.

Distinctly different approaches to avoid these problems and still achieve high viscosities were conceived and applied. The different approaches can be categorized as 1) preparation of emulsions or foams and 2) addition of crosslinkers to the polymer. Two separate processes which utilized crosslinking of polymer gelling agents were pursued. These are the use of secondary (or delayed) gelling agents and the use of metallic crosslinkers added on-site.

All the methods involve preparation of an initial, primary, hydrated, viscous solution referred to as base gel or linear gel. The viscosity of this base gel at surface conditions is between 25-100 centipoise (as measured at 511 sec^{-1} shear rate with a Fann viscometer). Base gel viscosity is then caused to increase even further for performance at higher temperatures. How this viscosity increase is achieved distinguishes the two processes that utilize crosslinking of a gelling agent. Ely(197), employed addition of a second polysaccharide that had been treated (crosslinked) with a difunctional aldehyde or other chemical coating agent to render the polysaccharide very slowly hydratable below 140°F . This crosslinked polysaccharide can be added to the viscous base gel as a secondary gelling agent to be activated by solvation at higher temperature. The use of a secondary gelling agent delays the initial hydration of a major portion of viscosifier and protects it from degradation for a period of time. Eventually it hydrates and provides extended viscosity in the formation. Horton(198) has provided a brief overview of secondary gelling agents compared to a primary crosslinked fluid. Field application data and well treatment results after use of this technique have been reported(199-201). Refinements have been made to improve the characteristics of the secondary agents(202,203). This technique can provide viscosity for long periods of time at high temperatures but suffers from the requirement of large amounts of total polymer (up to 2%), and higher amounts of residue(142).

The second type of crosslinked gelled fluid, the one most widely used today, involves the addition of a metal crosslinking agent to a fully hydrated base gel to create exceptionally viscous fluids. These types of gels were being pursued in other industrial applications(204) besides oilfield. The first use of a crosslinked fluid as a fracturing gel(205-207) was introduced by Holtmyer, et al. in 1969. It took advantage of the ability of antimony(V) to crosslink guar related materials at pH 5. The onset of antimony crosslinking can be somewhat delayed by control of pH(208). Insight into the rheological behavior of antimony crosslinked gels has been provided by Chakrabarti, et al(209). Nearly simultaneously(205-207) with the introduction of antimony crosslinked guar gels a sodium dichromate plus sodium sulfite crosslinked guar gel system employing in situ reduction of Cr(VI) to Cr(III) was also field tested. In response other groups introduced fluids(153,210-213) based on Kern's(214) preparation of viscous borate crosslinked fracturing gels at pH greater than 8.

Boron gels had been known for many years. Boeseken and coworkers(215) in 1913-1933 had examined in detail borate crosslinked gels prepared from polysaccharides that contained cis-diol (galactose) sugar moieties. Deuel and Neukom(216) verified Boeseken's work and proposed a three-dimensional network structure. Roy, et al.(217) reviewed the complexation ability of tellurate, borate, and arsenite ions and found that the complexes formed were decreasingly stable in that order. Slate(218) determined that borate-contaminated fluids could be viscosified by guar gum after treatment of the water with polyols (e.g. sorbitol, mannitol, glycerol, etc) that had superior complexation ability with borates. McIrvine(219) noted that the effect of borate crosslinking could be delayed by addition of MgO as a delayed-action caustic agent. Similarly Chrisp(220) would later suggest this technique for use with transition metal crosslinkers. Conner and Bulgrin(221) published complexation constants for borate and 15 simple polyols and concluded that the capability to delay crosslinking depended on the ease of the polyol to attain coplanarity of hydroxyl carbons and oxygens when entering the complex. This ability was affected by degree of substitution of the carbon atoms. Savins(222) examined the rheological behavior of polyvinylalcohol (PVA) -- borate complexes and commented on several postulated mechanisms to explain the "bizarre rheological properties of shear thickening complexes." He preferred the mechanism proposed by Bourgoin(223) as the source of the rheological effects. Schultz and Myers(224) employed dynamic oscillatory rheometry to examine PVA-borate gels and found that the borate crosslink density dropped with increasing temperature, that the borate bond required 5.8 Kcal/mol to break, and that effective borate crosslinks create a network four-fold the mass of the original polymer. The low activation energy probably explains why borate gels are useful only as relatively low temperature fracturing fluids, generally used at temperature lower than 150°F. Another possible cause is the change in boron species(35) created by increasing temperature (Figure 9).

Gorin and Mazurek(225,226) used ^{13}C -NMR to monitor the effects of borate complexation on carbon atoms of polyols and categorized the cyclic complexes into four types. The type of complex observed was dependent on borate concentration as well as the stereochemical configuration of the hydroxyl groups on the polyol. Nickerson(227) also commented on the mechanism of borate crosslinking. Ochiai et al(228,229). reported ionic strength effects on borate crosslinking density. The sensitivity of borate crosslinking to polyhydroxyl stereochemistry has also been extensively studied by Moore, et al.(230). Maerker and Sinton(231) found borate/PVA gels to be both shear-thickening and shear-thinning fluids. Only mesohydroxyl dyads were capable of complexation with boron and hysteresis studies indicated that shear could change intramolecular and intermolecular bonding. Sinton(232) extended this examination by ^{11}B NMR to conclude that two complexed species may exist and that possibly these represent intrachain and interchain bonds. The gel behavior under shear would reflect elongation of the bonded polymer molecules. Knoll and Prud'homme(233) suggested that crosslink formation was a result of electron sharing through pi-orbital overlap as had been described by Noll(234) in silicon polymers.

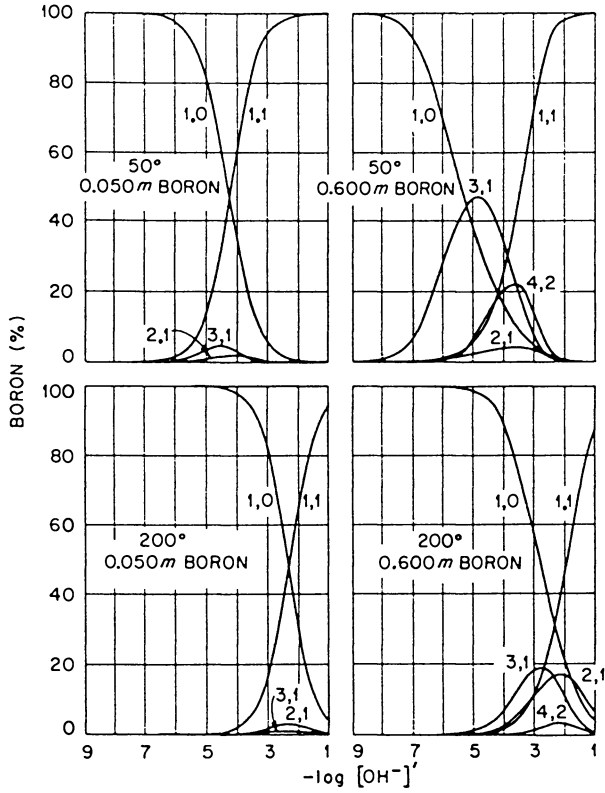


Figure 9. Boron cross-linking moiety depends on pH and temperature. (Reproduced with permission from ref. 35. Copyright 1976 Wiley and Sons.)

In 1971, Rosene and Shumaker(235) described the field application of borate crosslinked fracturing gels. Free(213,236) taught an improved "continuous" application of borate crosslinked fracturing fluids by incorporation of a delayed onset alkaline agent (MgO). During preparation of borate crosslinked fluids, the crosslink occurs very rapidly once the pH and borate concentration becomes high enough(237). The performance of the fracturing gel is dependent upon borate concentration and pH(263). At pH 8 to 10, a vigorous thickening of the polymer gel is noticed. Mondshine(234) has accomplished the design of a delayed onset borate crosslinked fracturing fluid by selecting appropriate buffers and natural borate ores to provide a slowly soluble borate source. Application of this type borate crosslinked fluid allows useful viscosity development even at temperatures as high as 220°F.

Use of boron crosslinked fracturing gels in low temperature applications remains commonplace as they have the reputation of being inexpensive and also can re-heal after being sheared. This re-healing and their high pH nature can also lead to difficulty in obtaining a break in the gel after it has been placed in the fracture. The enzyme breakers normally used to break polysaccharides do not perform very well at elevated pH. If oxidative breakers are applied they provide limited effectiveness since borate gels are used mainly for lower temperature applications where the oxidative breakers have difficulty with thermal initiation, unless special activators are included(239-241). These activators require extra attention to detail to achieve the correct break times.

The use of other crosslinking metals developed simultaneously with the use of antimony, chromium, and boron(borate). Tiner, et al.(242) introduced titanium (IV) crosslinkers in 1975 as ammonium tetralactonate or bis(triethanolamine)bis(isopropyl)titanium(IV). Upon contact with water soluble titanium (IV) derivatives ordinarily form orthotitanic acid, $Ti(OH)_4$, which rapidly forms oligomeric metatitanic acid, $[Ti(OH)_2]_x$ and titanium dioxide. Electron donors such as the hydroxyl groups of polysaccharides, if properly oriented, can participate in the sequence of titania reactions and a crosslinked gel network results. Various titanium metal crosslinkers remain in common use today. More will be said about titanium crosslinked gels later.

McDaniel, et al. in 1975 published(243) a description of the crosslinking chemistry of Cr(III), reduced in situ from Cr(VI), which apparently had developed from the work of Clampitt(244-247). This system, similar in many respects to the previously mentioned Cr(III)-guar gel, used sodium dichromate and sodium hydrosulfite as a redox couple activated by HCl to complex CMC or CMHEC. Davidson(248) has also adapted chromium crosslinked gels. Significant effort has been recently expended to understand the nature of in situ Cr(III) formation with the ultimate goal being to control the time of crosslinking. Willhite and collaborators(249-252) have published (1981-84) a series of findings. Prud'homme, et al.,(249,250) recently examined the rheological behavior of this type crosslinking with polyacrylamide. Interpretation of storage modulus (G') rheology behavior indicated a sequential increase in crosslink sites by an olation mechanism. The

use of chromium crosslinkers in fracturing gels has declined because of environmental concerns.

Aluminum(III) continues to be used in crosslinked aqueous fracturing fluids as well as EOR fluids(255-259). Al(III) is more environmentally acceptable than Cr(III)(259). Crosslinking polymers with aluminum can be achieved at pH up to 4.5 or in the transition region near 9.5(255). Aluminum chemistry is very pH dependent since the distribution of aluminum species changes from solubilized Al(3+) cations at low pH (e.g. aluminum citrate) to insoluble Al(OH)₃ in the neutral regions, to soluble Al(OH)₄ at higher pH regions (Figure 4). The use of partially hydrolyzed polyacrylamides crosslinked by Al(III) in citric acid to prepare viscous fluids was claimed by Gall and Johnston(260). Aluminum crosslinked fracturing gels are normally restricted to temperatures less than 225°F(153,261).

The antimonate, borate, and titanate crosslinked gels as already described have remained in general use. Modifications of buffers, ligands, and accessory additives were made as necessary to improve and regulate performance. By the late 1970 the industry became aware that delay of the crosslinking reaction was a much desired behavior. Fully crosslinked gels can generate significantly more frictional resistance to flow than uncrosslinked base gel. Frictional resistance is costly in injection pump horsepower requirements and represents an undesirable property that needs to be minimized whenever possible. One can lessen frictional resistance if the fluid being pumped does not begin crosslinking until it nears the perforations of the well pipe. Even more undesirable is the fact that crosslinked gels are sensitive to high shear and most do not recover from the destructive effects of shear. To determine shear susceptibility one can run a rheogram, where shear stress vs shear rate is determined as shear is methodically increased and then methodically decreased. Any change in fluid behavior between the increasing shear regime vs decreasing shear response is called hysteresis. Hysteresis is a reflection of the shear sensitivity of a crosslinked fluid. If a fluid has not been altered or damaged by shear it will give identical performance in the downward regime as it did in the upward shear regime. A practical way of minimizing the effects of high shear on a crosslinked fluid during the fracturing treatment is to delay the onset of crosslinking until the fluid reaches a region of lower shear (i.e., beyond the well pipe and inside the fracture). Turbulence in the pipe and shear encountered when the fluid passes through the perforations are the primary sources of high shear. Once the fluid exits the pipe into the formation, shear forces drop to a lower level, usually 10-100x less.

Early methods of delaying the metal crosslinker additive centered on mixing an additional chemical with the crosslinker or in the fracture mixing water to cause a delayed activation. For example, undiluted titanium triethanolamine crosslinks aqueous polymer base gels nearly instantaneously upon addition. The reaction can be delayed by up to 2 minutes by diluting the titanate with water(262). This approach provides a workable system but not an ideal one since the actual length of delay is affected by numerous factors such as temperature, concentration of water, time of contact with water, alcohols, and any chelating agents present(263-269). This type

"delayed" crosslinker also suffers from the lack of long term stability. Titanium triethanolamine water solutions have to be discarded after aging a few hours.

Small quantities of 2,4-pentanedione (acetylacetone) added to the polymer gel solution can regulate the crosslink onset(263-269) from organo-Ti(IV) and organo-Zr(IV) crosslinking agents. Elphinstone and Dees(269) achieved delay from titanium bis acetylacetone enolate dihydroxide by virtue of the presence of the complexing ligand as well as adding the crosslinker as a solid. The use of secondary complexing agents suffers from unpredictable response behaviors because of the same variables that affect the "water-delayed" crosslinkers. Also, increasing the concentration of chelating agents can quickly maximize the delay threshold and completely prevent the metal from creating a crosslinked gel.

In 1980 a new concept in the application of delayed metal crosslinkers appeared--the concept of using a storage-stable, delayed onset crosslinking agent to avoid the undesirable effects of instantaneous or early crosslinking on the surface was introduced. Conway(270,271) prepared these agents by chemically reacting equal volumes of titanium triethanolamine, water, and polyhydroxyl compound (such as glycerol, mannitol, xylitol). The length of delay was regulated by the selection of polyhydroxyl compound. These delaying effects of various polyols upon titanium triethanolamine paralleled the much earlier results of Lagally and Lagally(272), Mills(273), and Russell(274).

Zirconium Crosslinkers. The history of the discovery of new oil and gas reserves shows a clear trend toward deeper drilling, where temperatures are very hot. In order to provide better fluids to withstand these temperatures more effective crosslinkers and gelling agents have gradually been introduced. Thus, antimony and boron complexes gave way to chromium and titanium crosslinked gels. Use of zirconium(IV) crosslinkers for preparation of improved high temperature fracturing gels began about 1981. Rummo reported(263-265) on acetylacetonate delayed titanium(IV) and zirconium(IV) complexes. Baumgartner, et al.(275), compared their Zr(IV) high temperature fracturing gel to a Ti(IV) gel(1983). Additional details were later made available (1985) by LaGrone, et al.(276) and Williams(277,278). This crosslinker apparently is a zirconium(IV) triethanolamine mixture (1:8.9)(277). Kucera(279) claimed the usefulness of a "water-activated" mixture of Zr(IV):triethanolamine chelate (1:3). Field application of this type system was described(280) by Walser (1985). Baranet, et al., taught that these type gels had better temperature stability if the triethanolamine ratio was increased; also the crosslink time became more delayed(281). Payne(282) described techniques whereby control of crosslinking onset of Zr(IV) and Ti(IV) metals could be accelerated by polyamines or delayed by glyoxal or triethanolamine. Horton formulated a "one-bag" gelling mixture(283) that contained guar derivatives along with solid Zr(IV) acetylacetonate and a regulating amount of buffering agent. A similar "one-bag" formulation for acid fracturing gels was developed by Githens(284). Almond (1984) was issued a series of patents claiming Zr(IV) delayed crosslinking agents with α -hydroxyacid ligands which were found

useful to crosslink CO₂-containing fluids(285-287). Applications of these type fluids were described by Almond and Garvin(288), and Sandy, et al.(120) Zhao(289) used ZrOCl₂ to prepare inexpensive crosslinked polyacrylamide or guar gels. He also claimed simple Ti(IV) salts for preparation of fracturing fluids used in the Peoples Republic of China. Hodge(290,291) claimed hydroxyacetic acid mixtures of Zr(IV) for use with CMHPG gelling agents, with or without CO₂ being present. Anderson and Paktinat(199) preferred a mixed metal crosslinker containing Zr(IV) lactate and Al(III) chlorohydrate for use with CMHPG.

Titanium Crosslinkers. Improved Ti(IV) crosslinkers for high temperature application were also introduced during this period. Hollenbeak and Githens(292) prepared delayed Ti(IV) complexors by adding sorbitol or other saccharide agents. Putzig claimed Ti(IV) amine chelates treated with monosaccharide delaying agents could be prepared(293) as solids which were useful for fracturing gel crosslinkers as well as creating thixotropic properties to cementing slurries. Wadhwa found that mixed titanate crosslinkers that contained boric acid(294) could give early crosslinked gel strength as well as provide high temperature performance as the titanate(s) activated. Putzig(295) similarly claimed that mixtures of several Ti(IV) chelates could be used to achieve regulated crosslink onset. Smeltz(296) examined mixed ligand Ti(IV) derivatives by incorporating α -hydroxyacids and polyols.

As more stable crosslinked gels for application at high temperatures have been developed efforts have also been made to find additives that extended the life of gels at high temperatures. The incorporation of alcohols (5-30%) helps but suffers several disadvantages, such as cost, hazardous handling, and behavioral interferences. Thiosulfate and thiourea salts have found routine application(297-299). Use of 0.5% triethanolamine(300) is claimed to provide protection as has been isothiazolones(301), dolomite,(302) borohydride,(303) aminoacetamides,(304) dithiocarbamides,(305) iodates,(306) benzoquinone(307-308), and alcohol plus thiourea(309). Researchers such as Shupe(310), Wellington(311), Thomas(312), Glass(313), Braga(314), and Ryles(31,315) have examined the high temperature stability of polymers.

The level of interest in crosslinked gels continued at an accelerated pace. Conway et al.(316-318) discussed (1980) the instrumentation and evaluation procedures commonly in use at that time and compared crosslinked gel systems at high temperature. They discussed and ranked the performance capabilities of various metal crosslinkers Ti(IV), Sb(V), Cr(III), B(III), Sb(III). A chemical model for crosslinked fracturing gels was proposed (transesterification) and it was mentioned that crosslinked fluid rheology performance was dependent upon early shear history. The model represented a covalent metal ester intramolecular bridge between strands of polymer. Rummo(263) invoked a similar description. Clark(319) introduced the use of a pressure rheometer to examine the behavior of crosslinked fracturing fluids. This instrument employed parallel plate instrumentation to measure fluid viscosity as opposed to a Couette geometry rheometer in general use

throughout the oil field laboratories(320). The use of the parallel plate device in a dynamic oscillatory mode allows one the ability to measure fluid stress response to an applied in-phase shear and an out-of-phase strain. It also allows characterization of viscous fluids at very high shear(321) The in-phase stress measurement provides information about the elasticity of the fracturing gel and is defined as the storage modulus, G' . The stress component that is out-of-phase with the applied strain (but in-phase with the velocity gradient) is designated the loss modulus, G'' . This parameter offers a measure of the viscosity provided by the gel system. Gel performance can thus be tested and expressed as two fundamentally different parameters, elasticity and viscosity. Since viscosity of a gel can be characterized by a variety of methods including determination of G'' most researchers have since focused their attention on the changes observed in the storage modulus G' . An increase in G' indicates formation of a greater gel network with more three-dimensional structure, and hence represents a direct correlation to the extent of crosslinking. Careful analysis of G' and G'' behavior offers clues to the molecular interactions that occur. Prud'homme(322-324) and several collaborators(143,233,253-255,325-329), Acharaya(330), Menjivar(331), and Jiang(332) have probed the mechanism of how crosslinkers interact with polymer gels.

The mechanistic description provided by Conway(317,318) was modified(262,323) after observing the behaviors of three crosslinkers [boron (sodium tetraborate, pH \sim 9), titanium acetylacetonate (1:9 with isopropanol, pH \sim 5) and titanium triethanolamine (1:9 with water, aged 30 min, pH \sim 9)] with two model sugars; methyl- β -D-galactopyranose and methyl- α -D-mannopyranoside. The borate solution interacted with the sugars as expected. Unequivocal ^{13}C NMR shifts attributed to formation of complexes were observed. Neither titanium crosslinker solution caused an observable ^{13}C NMR shift with the model sugars(262). Still it is well known that these crosslinkers cause a dramatic change in the properties of polysaccharide base gels. It was concluded(262,323) that the vast bulk of both of the organotitanate crosslinkers rapidly formed unreactive, colloidal TiO_2 . It was reasoned that this left only a few reactive TiOH sites exposed on the outer surface of the colloidal TiO_2 spheres. These sites were insufficient in number to significantly interact with the model sugars to cause an observable ^{13}C NMR shift; below the level of detection of the instrument, but are effective enough to crosslink polysaccharide polymers. Kramer and Prud'homme concluded(262) that crosslinking of polysaccharide gels by addition of organotitanate complexes is by TiO_2 sols, not by a monomeric Ti(IV) cation.

Dynamic light scattering (DLS) experiments(327) with water aged titanates indicated several important features of these colloidal TiO_2 sols; A) their size is important to their crosslinking behavior, B) their size is regulated by the amount of water added and the length of time aged after mixing with water, C) the colloidal TiO_2 particles are in equilibrium with the organo-titanate precursor, and D) pH affects the equilibrium. Because pH, ionic strength, time-of-aging, and water content are widely variable parameters in a field preparation of polysaccharide

fracturing gels it is not surprising that the final fracturing gel properties can sometimes be difficult to control(268,333,334). Buffering agents are commonly added to regulate pH and 2% KCl is ordinarily added to prevent clay swelling but its presence also provides a more uniform ionic strength. Unfortunately the addition of KCl cannot overcome the undesired effects exerted on crosslinking chemistry by the natural contaminants of many field waters. The effectiveness of buffering agents is more than a pH effect alone. Factors that can affect crosslinking rates and fracturing gel performance include surface temperature, polymer concentration, salt concentrations, fluid loss additives, surfactants, mutual solvents, alcohols, and also the anionic identity of buffering agents. For this reason, quality control procedures have been established and are routinely followed to help ensure optimum fracturing gel performance(335).

Zasadzinski, Chu, and Prud'homme, by use of transmission electron microscopy (TEM) of freeze-fractured samples of gels, observed ionic strength effects on the microscopic physical gel structure(336). Increased salt content resulted in a higher degree of association of polymer molecules, condensation occurred, and the polymer chains appeared much thicker. The presence of salt is believed to strengthen polymer hydrogen bonding at the expense of hydroxyl group water of hydration. The effect makes the polymer more hydrophobic and likely accounts for their observation that the presence of salt made the guar gels more susceptible to mechanical shear degradation. Shearing resulted in the appearance of ruptures in the crosslinked gel network along weak zones. The gel network bounded inside by the rupture lines appeared unaffected. The TEM procedure also showed that the colloidal TiO_2 crosslinks appeared to weld together polymer strands already associated by hydrogen bonding.

Kramer, et al.(262,327) and Knoll(233), on the basis of G' , G'' response concluded that gels kept in continuous motion during the crosslink formation period have completely different 3-D networks than gels allowed to stand in a quiescent state prior to analysis on the rheometer. This observation confirmed the early comments of Conway(317) and has had important implications for fracturing gel research and modeling since crosslinked fracturing gels as applied in the field ordinarily do not experience a quiescent period, yet nearly all test data accumulated prior to 1986 was collected from samples that had experienced at least a momentary quiescent period.

Emulsions. Emulsion fluids and foams came into routine use in competition with crosslinked fluids during 1970-80. Simple, barely stable emulsions had been used early in fracturing. These were mainly emulsified acids that "broke" when the acid spent on the formation surfaces. In the late 1960's Kiel became a proponent of very high viscosity oil fluids as a method to place exceptional (at the time) amounts of proppant(337,338). To avoid the frictional resistance typical of gelled oils he advanced the concept of preparing a very viscous oil-external emulsion with one part fresh water, 0.1% sodium tallate surfactant, and two parts oil. The viscous emulsion had to be pumped simultaneously with a water stream to minimize frictional pressure. This process was clumsy and still

created frictional problems. A better emulsion fluid using a quaternary amine surfactant and brine water was developed. Also the inclusion of a polymer in the aqueous phase caused a significant increase in emulsion viscosity(339-341). These emulsions reportedly had very low fluid loss properties, and the field data published suggested that wells treated with the emulsion cleaned up with greater production than from wells treated with other contemporary fluids. A variety(342) of emulsion fluids (usually 70% water) continue in use today(338) and are preferred by some on the basis of causing minimal damage to conductivity(343-346). Even so, emulsion treatments usually are more costly than crosslinked aqueous fracturing fluids.

Foamed Frac Fluids. Foams have properties very similar to emulsions. Both fluids consist of a dispersed phase carried inside a continuous phase(347). In foams the dispersed phase is a gas. Emulsions are liquid-in-liquid dispersions. Both types of dispersions provide large increases in viscosity when higher percentages of dispersed phase are introduced. This viscosity is useful to create fracture width and suspend proppant. Figure 10 illustrates the viscosity behavior of a typical foam. Operationally foams and emulsions are ordinarily applied with 55-90% internal dispersed phase, where the enhanced viscosity properties are unmistakable. The placement of a pressurized gas into a hydrocarbon bearing formation offers a significant advantage over other fracturing fluids. When pressure is released on the surface the gas expands and rises, carrying liquids, fines, and debris with it. Foams generally are excellent well clean-out fluids. In some instances, foam fluids cause much less conductivity damage to fracture channels than other stimulation fluids. Several recent articles (which include useful bibliography references) on oil-field foam applications are available(348-352).

Chemically, the preparation of a "stable" foam or emulsion requires the use of a surfactant to aid in dispersion of the internal phase and prevent the collapse of the foam (or emulsion) into separate bulk phases. The selection of a surfactant is made on the basis of severity of conditions to be encountered, the gas to be entrained (N₂, CO₂, LPG, CH₄, or air), the continuous phase liquid (water, alcohol, or oil), and half-life of foam stability desired. Foam viscosity and stability can be enhanced viscosifying the continuous phase with thickening agents. These are mostly the same thickening agents used to prepare viscous fracturing base gels. Public information about the specific chemical identity of the surfactants and stabilizers in use is scant(353-355) (Figure 11). Performance of foamed fluids is heavily dependent upon the size and distribution of the individual foam cells that are present, therefore the generator, testing apparatus, pressure and procedures employed are critical parts of the evaluation and the observed results. Contaminants (salts, acids, alkalies, etc) in the liquid phase also can cause drastic changes in foam performance.

Aqueous fracture foams are the least expensive not only because of the low cost of water but also due to the availability of inexpensive surfactants that foam water and brines easily and effectively. Oil and alcohol foams are much more costly due to the

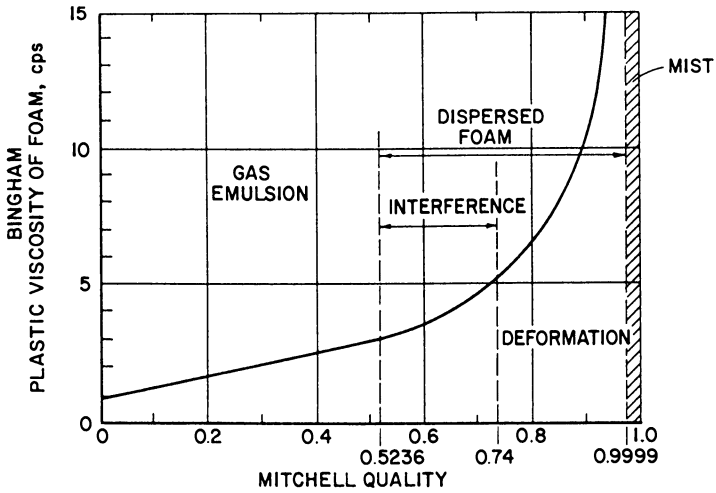


Figure 10. Foam viscosity depends on percent internally dispersed gas (Mitchell quality). (Reproduced from ref. 363. U.S. Patent 3 937 283, 1976.)

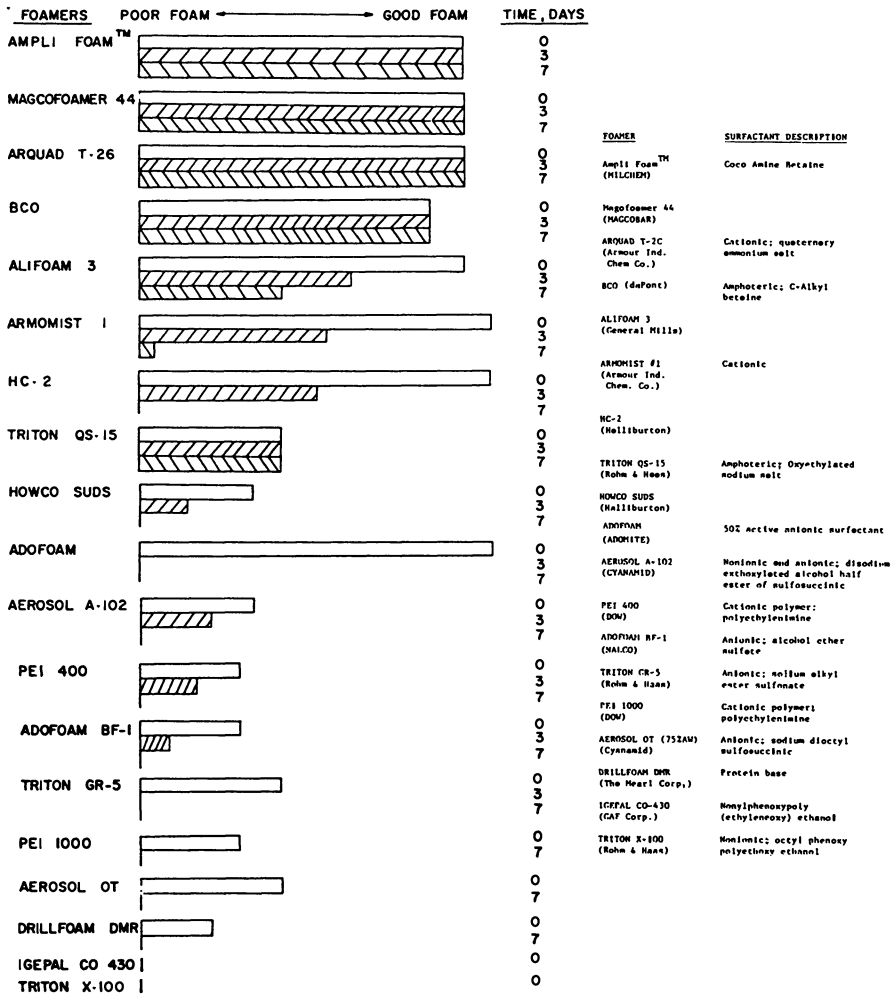


Figure 11. Performance of foaming agents. (Reproduced with permission from ref. 353. Copyright 1978 Society of Petroleum Engineers.)

expense of the hydrocarbon or alcohol and the requirement for high performance (and expensive) surfactants. Fluorinated surfactants are normally required(356-359). These materials are noted for their ability to drastically lower the surface tension between phases which makes them effective foamers for oil or alcohol.

Summary

This chapter has presented an overview of some major areas of fracturing chemistry from a historical, functional, mechanistic, as well as bibliographical viewpoint. Space constraints dictated that other very important fracturing chemistry topics be only lightly addressed. Notably absent is the chemistry of numerous surface active fracturing additives. Surface active chemicals play major roles in antifoaming agents, clay stabilization, de-mulsifying additives, dispersing agents, emulsifying agents, foaming agents, sludge inhibitors, and water-blockage control additives(5,360,361). Some of these have been discussed but many were not. A limited bibliography for de-mulsifying (non-emulsifiers) agents, sludge inhibitors, and water blockage control chemicals is provided in the Appendix(361).

Acknowledgment

I wish to thank Halliburton Services for the opportunity to assemble this manuscript and S. K. McCulloch; only with her assistance was the project completed.

Literature Cited

1. See Appendix Reviews of Oil & Gas Fracturing
2. Veatch, R.W., Jr. J. Pet. Technol. 1983, 35(4) 677-864; *ibid* Part 2 1983, 35(5) 853-864.
3. Cramer, D.D. Oil Gas J. 1987, 85(50), 40-45.
4. See Appendix Fracturing Fluid Leakoff
5. Anderson, W.G.: "Wettability Literature Survey;" Part 1, J. Pet. Technol. 1986, 38(10), 1125-1144; *ibid*, Part 2, 38(11), 1246-1262; *ibid*, Part 3, 38(12), 1371-1378; *ibid*, Part 4, 1987, 39(10), 1283-1300; *ibid*, Part 5, 39(11), 1453-1468; *ibid*, Part 6, 39(12), 1605-1622.
6. Rogers, L.A.; Tomson, M.B.; Matty, J.M.; Durrett, L.R. Oil Gas J. 1985, 83(13), 97-108.
7. Howard, G.C.; Fast, C.R. Hydraulic Fracturing, Monograph Series, Society of Petroleum Engineers of the American Institute of Mining, Metallurgical and Petroleum Engineers: Dallas, TX., 1970, 2.
8. Dickey, P.A.; Andersen, K.H. "The Behavior of Water-Input Wells;" Amer. Pet. Institute, Secondary Recovery of Oil in the United States, 2nd Ed. 1950, 332-40.
9. Clark, J.B.; Fast, C.R.; Howard, G.C. "A Multiple Fracturing Process for Increasing the Productivity of Wells," 1952 Spring Meeting of the Midcontinent District API, Wichita, KS, March 19-21.
10. Scott, P.P., Jr.; Bearden, W.G.; Howard, G.C. "Rock Rupture as Affected by Fluid Properties;" Soc. Pet. Eng. J. 1953, 111-124; *Trans.*, AIME, 198.

11. Hubbert, M.K.; Willis, D.G.: "Mechanics of Hydraulic Fracturing;" Soc. Pet. Eng. J. 1957, 153,166,167; Trans., AIME, 210.
12. See Appendix Modelling of Fracture Behavior
13. Conway, M.W.; McMechan, D.E.; McGowen, J.M.; Brown, D.; Chisholm, P.T.; Venditto, J.J. "Expanding Recoverable Reserves Through Refracturing"; SPE paper 14376, 1985 SPE Annual Technical Conference and Exhibition, Las Vegas, September 22-25.
14. Venditto, J.J.; Chisholm, P.; Wiggins, M.; Conway, M. "Refracturing Completed Wells Can Be Cost Effective", PETROLEUM ENGINEER International August 1986, 26-34.
15. Kaspereit, D.H. "Fracture Design for Suspended Sand Packs"; SPE paper 1843, 1979 SPE Annual Technical Conference and Exhibition, Las Vegas, September 23-26.
16. Smith, J.E. "Effect of Incomplete Fracture Fill-Up at the Wellbore on Productivity Ratio"; Proc. Annu. Southwest. Pet. Short Course, April 1975, 135-144.
17. Clark, J.B. US Patent 2 596 844, 1952.
18. Clark, J.B. US Patent 2 596 845, 1952.
19. Farris, R.F. US Patent 23 733, reissued 1953.
20. Prusick, J.H.; Morgan, Z.V "The Use of Emulsions and Related Techniques in the Treatment of Oil and Gas Wells"; Pet. Engineer (May 1954) B54-B56.
21. Fieser, L.F.; Harris, G.C.; Hershberg, E.B.; Morgana, M.; Novello, F.C.; Putnam, S.T. Ind. Eng. Chem. 1946, 38(8), 768-773.
22. Fieser, L.F. US Patent 2 606 107, 1952.
23. Kirk-Othmer Encyclopedia of Chemical Technology; Wiley:New York, 1978, 3rd Ed, Vol 2, 202 "Aluminum Carboxylates" and Vol 8, 34 "Driers and Metallic Soaps".
24. Self, E.S. US Patent 2 461 483, 1949.
25. Dawson, R.D. US Patent 2 350 154, 1944.
26. Anderson, F.M. US Patent 2 430 039, 1947.
27. Magram, S.J. US Patent 2 774 740, 1956.
28. Monroe, R.F.; Rooker, B.E. US Patent 3 494 949, 1970.
29. Monroe, R.F. US Patent 3 505 374, 1970.
30. Monroe, R.F. US Patent 3 575 859, 1971.
31. Ryles, R.G. "Elevated Temperature Testing of Mobility Control Reagents", SPE paper 12008, 1983 SPE Annual Technical Conference and Exhibition, San Francisco, CA, October 5-8.
32. Arnson, T.R. Tappi, 1982, 65(3), 125-129.
33. Lauzon, R.V. Oil Gas J. 1982, 80(36), 124,126.
34. Schecher, W.D.; Driscoll, C.T. Water Resources Res., 1987, 23(4), 525-534.
35. Baes, C.F. Jr.; Mesmer, R.E. "The Hydrolysis of Cations", Chapur on Boron, Aluminum, Scandium; Wiley:New York, 1976.
36. Crawford, D.L.; Earl, R.B.; Monroe, R.F. US Patent 3 757 864, 1973.
37. Zangen, M.; Marcus, Y.; Bergmann, E.D. Sep. Sci. 1967 2(2), 187-197.
38. Moule, H.A.; Greenfield, S. J. Chromatog. 1963, 11, 77-83.
39. Hill, D.G. US Patent 3 990 978, 1976.

40. McKenzie, L.F. "Hydrocarbon Gels of Alumino Alkyl Acid Orthophosphates", SPE paper 9007, 1980 Fifth International Symposium on Oilfield and Geothermal Chemistry, Stanford May 28-30.
41. Daccord, G.; Lemarczyk, R.; Vercaemer, C. US Patent 4 507 213, 1985.
42. See Appendix Chemistry of Gelled Oils
43. Baker, H.R.; Bolster, R.N.; Leach, P.B.; Little, R.C. Ind. Eng. Chem. Prod. Res. Develop. 1970, 9(4), 541-548.
44. Rose, S.H.; Black, B.P. J. Am. Chem. Soc. 1965, 87(9), 2076-77.
45. Rose, S.H.; Black, B.P. J. Polym. Sci., 1966 4(A-1), 573.
46. Rose, S.H.; Black, B.P. J. Polym. Sci., 1966 4(A-2), 583.
47. Schmidt, D.L.; Flagg, E.E. J. Polym. Sci., 1968, 6(A-1), 3235-3244.
48. Burnham J.W.; Harris, L.E.; McDaniel, B.W. "Developments in Hydrocarbon Fluids for High Temperature Fracturing", SPE paper 7564, 1978 SPE Annual Technical Conference and Exhibition, Houston, October 1-3. See also J. Pet. Technol., 1980, 32(2), 217-220.
49. Fendler, J.H. Acc. Chem. Res., 1976, 9, 153-161.
50. Fendler, J.H. Acc. Chem. Res., 1980, 13, 7-13.
51. Fendler, J.H. J. Phys. Chem., 1980, 84, 1485-1491.
52. Hewitt, C.H. J. Pet. Technol., 1963, 15(8), 813-818.
53. Gray, D.H.; Rex, R.W. "Formation Damage in Sandstones Caused by Clay Dispersion and Migration", 1966 Fourteenth National Conference on Clays and Clay Minerals, 355-366.
54. See Appendix Acidizing, Fracture Acidizing
55. Monaghan, P.H.; Salathiel, R.E.; Morgan, B.E. J. Pet. Technol. 1959, 11, 209-215.
56. Reed, M.G. Production Monthly, 1968, 32, 18.
57. Jones, F.O. Jr. J. Pet. Technol., 1964, 16(4), 441-446.
58. Black, H.N.; Hower, W.F. "Advantageous Use of Potassium Chloride Water for Fracturing Water Sensitive Formations", 1965 Spring Meeting of the Mid-Continent District Division of Production, Wichita, KS, March 31-April 2.
59. Reed, M.G. "Stabilization of Formation Clays with Hydroxy-Aluminum Solutions", SPE paper 3694, 1981 SPE Annual California Regional Meeting, Los Angeles, November 4-5.
60. Reed, M.G.; Coppel, C.P. "Sand Stabilization with Hydroxy Aluminum Solutions," SPE Paper 4168, 1972 SPE Annual California Regional Meeting, Bakersfield, November 8-10.
61. Coppel, C.P.; Jennings, H.Y. Jr.; Reed, M.G. "Field Results from Wells Treated with Hydroxy-Aluminum", SPE paper 3998, 1972 SPE Annual Meeting, San Antonio, October 8-11.
62. Haskin, C.A.; Reed, M.G.; Coppel, C.P. Oil Gas J. 1975, 73(45), 217-220.
63. Haskin, C.A. "A Review of Hydroxy-Aluminum Treatments"; SPE Paper 5692 1976 SPE Symposium for Formation Damage Control Meeting of AIME, Houston, January 29-30.
64. Velej, C.D. "How Hydrolyzable Metal Ions Stabilize Clays to Prevent Permeability Reduction"; SPE paper 2188, 1968 SPE Annual Meeting of AIME, Houston, September 29-October 2.
65. Christenson, R.M.; McBane, B.N. US Patent 3 382 924, 1968.

66. Veley, C.; Casey, G., Jr. "In-Place Clay Stabilization Cuts Formation Sand Entry"; World Oil(June 1973)52-54.
67. Peters, F.W.; Stout, C.M. J. Pet. Technol. 1977, 29(2), 187-194.
68. Brown, W.E. US Patent 2 761 835, 1956.
69. *ibid.* 2 761 836.
70. *ibid.* 2 761 837.
71. *ibid.* 2 761 838.
72. *ibid.* 2 761 839.
73. *ibid.* 2 761 840.
74. *ibid.* 2 761 841.
75. *ibid.* 2 761 842.
76. McLaughlin, H.C.; Elphingstone, E.A.; Hall, B. "Aqueous Polymers for Treating Clays in Oil and Gas producing Formations"; SPE paper 6008, 1976 SPE Annual Technical Conference and Exhibition, New Orleans, October 3-6.
77. McLaughlin, H.O., Sr.; Elphingstone, E.A.; Remington, R.E., II; Coates, S. "Clay Stabilizing Agent Can Correct Formation Damage," World Oil(May 1977) 58-60.
78. Black, H.N.; Ripley, H.E.; Beecroft, W.H.; Pamplin, L.O. "Drilling and Fracturing Fluid Improvements for Low-Permeability Gas Wells in Canada"; SPE paper 7926, 1979 SPE Symposium Low Permeability Gas Reservoirs, Denver, May 20-22.
79. Young, B.M.; McLaughlin, H.C.; and Borchardt, J.K. J. Pet. Technol., 1980, 32(12), 2121-2130.
80. Hall, B.E. Oil Gas J. 1978, 76(30), 68-70.
81. Borchardt, J.K.; Roll, D.L.; Rayne, L.M. "Use of a Mineral Fines Stabilizer in Well Completions"; SPE paper 12757, 1984 SPE California Regional Meeting, Long Beach, April 11-13.
82. McLaughlin, H.C.; Weaver, J.D. US Patent 4 366 071, 1982.
83. *ibid.* 4 366 072.
84. *ibid.* 4 366 073.
85. McLaughlin, H.C.; Weaver, J.D. US Patent 4 374 739, 1983.
86. Theng, B.K.G.: "Clay-Polymer Interactions: Summary and Perspectives", Clays and Clay Minerals, 1982, 30(1), 1-10.
87. *ibid.* "The Chemistry of Clay-Organic Reactions", Wiley:New York, (1974).
88. Callaway, R.E. "Clay Protection Chemicals: A Practical Evaluation and Application Technique for Their Use in Stimulation Fluids", SPE paper 10663, 1982 SPE Formation Damage Control Symposium, Lafayette, March 24-25.
89. Coulter, G.R.; Hower, W. "The Effect of Fluid pH on Clays and Resulting Formation Permeability", Proc. Annu. Southwest Pet. Short Course, April 1975.
90. Simon, D.E.; McDaniel, B.W.; Coon, R.M. "Evaluation of Fluid pH Effects on Low Permeability Sandstones"; SPE paper 6010, 1976 SPE Annual Technical Conference and Exhibition, New Orleans, October 3-6.
91. Sydansk, R.D. "Stabilizing Clays With Potassium Hydroxide", SPE paper 11721, 1983 California Regional Meeting, Ventura, March 23-25.
92. Coulter, A.W., Jr.; Frick, E.K.; Samuelson, M.L. "Effect of Fracturing Fluid pH on Formation Permeability", SPE paper 12150, 1983 SPE Annual Technical Conference and Exhibition, San Francisco, October 5-8.

93. Kia, S.F.; Fogler, H.S.; Reed, M.G. J. Colloid Interface Sci., 1987, 118(1), 158-168.
94. Burk, J.H. "Comparison of Sodium Carbonate, Sodium Hydroxide, and Sodium Orthosilicate for EOR", SPE Reservoir Engineering, February 1987, 10-15.
95. Radenti, G.; Palumbo, S.; Zucca, G. "Potassium Carbonate Fluid Inhibits Highly Reactive Clays", PETROLEUM ENGINEER International, September 1987, 32,34,36,40.
96. Thomas, R.L.; Crowe, C.W. "New Chemical Treatment Provides Stimulation and Clay Control in Sandstone Formations," SPE Paper 7012, 1978 SPE Third Symposium on Formation Damage Control, Lafayette, February 15-16.
97. Clark, R.K. "Polymer Effectiveness in Stabilizing Shales of Various Compositions," Polym. Mater. Sci. Eng. 1984, 51, 1-5.
98. Hawkins, R.R. US Patent 3 122 203, 1964.
99. Chesser, B.G. "Design Considerations for an Inhibitive, Stable Water-Based Mud System", SPE Drilling Engineering, December 1987, 331-336.
100. Wilcox, R.D.; Jarrett, M.A. "Polymer Deflocculants: Chemistry and Application", IADC/SPE paper 17201, 1988 IADC/SPE Drilling Conference, Dallas, February 28-March 2.
101. Krueger, R.F. J. Pet. Technol., 1986, 38(2), 131-152.
102. Leone, J.A.; Scott, E.M. "Characterization and Control of Formation Damage During Waterflooding of a High-Clay-Content Reservoir", SPE paper 16234, 1987 SPE Production Operations Symposium, Oklahoma City, March 8-10.
103. Anderson, R.W.; Baker, J.R. "Use of Guar Gum and Synthetic Cellulose in Oilfield Stimulation Fluids", SPE paper 5005, 1974 SPE Annual Meeting, Houston, October 6-9.
104. Davis, J.A., Jr.; Rhudy, J.S. US Patent 3 747 681, 1973.
105. Whistler, R.L.; BeMiller, J.N., Eds "Industrial Gums; Polysaccharides and Their Derivatives", 2nd Ed, Academic, New York, 1973.
106. Rowell, R.M.; Young, R.A., Eds, "Modified Cellulosics"; Academic, New York, 1978.
107. Davidson, R.L., Ed, "Handbook of Water-Soluble Gums and Resins," McGraw-Hill, Inc, 1980.
108. Carraher, C.E.; Moore, J., Eds, "Modification of Polymers"; Plenum Press, New York, 1983.
109. Glass, J.E. "Water-Soluble Polymers: Beauty with Performance", Advances in Chemistry Series 213, Amer. Chem. Soc., Washington, D.C., 1986.
110. See Appendix Friction and Drag Reducers
111. Malachosky, E.: "Status Report: Oil Field Copolymers," PETROLEUM ENGINEER, International, April 1987, 48-53.
112. Barth, H.G.; Smith, D.A. J. Chromatog., 1981, 205, 410-415.
113. Robinson, G.; Ross-Murphy, S.B.; Morris, E.R. Carbohydr. Res., 1982, 107, 17-31.
114. Jordan, W.A. US Patent 3 483 121, 1969.
115. White, J.L.; Means, J.O. J. Pet. Technol. 1975, 27(9), 1067-1073.
116. Holcomb, D.L.; Smith, M.O. "The Use of a Low-Concentration Crosslinked Hydroxyalkyl Polymer System as a Highly Efficient

- Fracturing Fluid", 1975 Proc. Annu. Southwest. Pet. Short Course, April, 129-134.
117. Githens, C.J.; Burnham, J.W. Society of Petroleum Engineers Journal(February 1977) 5-10.
 118. Nordgren, R.; Jones, D.A.; Wittcoff, H.A. US Patent 3 723 408, 1973.
 119. Anderson, J.L.; Paktinat, J. US Patent 4 635 727, 1987.
 120. Sandy, J.M.; Wiggins, M.; Venditto, J.J. Oil Gas J., 1986 84(35), 52-54.
 121. Chatterji, J.; Borchardt, J.K. J. Pet. Technol., 1980, 32(11), 2042-2056.
 122. Moe, O.A. US Patent 2 520 161, 1950.
 123. Nordgren, R. US Patent 3 225 028, 1965.
 124. Nordgren, R. US Patent 3 303 184, 1967.
 125. Nordgren, R. US Patent 3 346 555, 1967.
 126. Tessler, M.M. US Patent 4 276 414, 1981.
 127. DeMartino, R.N.; Wayne, N.J. US Patent 4 169 798, 1979.
 128. Harms, S.D.; Goss, M.L.; Payne, K.L.: "New Generation Fracturing Fluid for Ultrahigh-Temperature Application", SPE paper 12484, 1984 SPE Formation Damage Control Symposium, Bakersfield, February 13-14.
 129. Payne, K.L. US Patent 4 579 670, 1986.
 130. Chrinsonson, R.M. US Patent 2 618 632, 1968.
 131. Thomas, D.C.: "Thermal Stability of Starch and Carboxymethyl Cellulose Polymers Used in Drilling Fluids," SPE Paper 8463, 1979 SPE Annual Technical Conference and Exhibition, Las Vegas, September 23-26.
 132. Patton, J.T. US Patent 3 729 460, 1970.
 133. Southwick, J.G.; Lee, H.; Jamieson, A.M.; Blackwell, J. Carbohydr. Res., 1980 84, 287-295.
 134. Salamone, J.C.; Clough, S.B.; Salamone, A.B.; Reid, K.I.G.; Jamison, D.E. Soc. Pet. Eng. J., 1982, 22(8), 555-56.
 135. Rees, D.A. Biochem. J., 1972, 126(1), No. 2, 257-273.
 136. Clark, P.E.; Halvaci, M.; Ghaeli, H. "Proppant Transport by Xanthan and Xanthan-Hydroxypropyl Guar Solutions: Alternatives to Crosslinked Fluids," SPE/DOE paper 13907, 1985 SPE/DOE Low Permeability Gas Reservoirs, Denver, May 19-22.
 137. Chauveteau, G.; Kohler, N. "Influence of Microgels in Xanthan Polysaccharide Solutions on Their Flow Through Various Porous Media," SPE paper 9295, 1980 SPE Annual Technical Conference and Exhibition, Dallas, September 21-24.
 138. See Appendix Xanthan Gum
 139. Carico, R.D.; Bagshaw, F.R. "Description and Use of Polymers Used in Drilling, Workovers, and Completions," SPE paper 7747, 1978 SPE of AIME Production Technology Symposium, Hobbs, October 30-31.
 140. Carico, R.D. "Suspension Properties of Polymer Fluids Used in Drilling, Workover, and Completion Operations," SPE paper 5870, 1976 SPE of AIME Annual California Regional Meeting, Long Beach, April 8-9.
 141. Gall, B.L.; Maloney, D.R.; Raible, C.J. "Permeability Damage to Artificially Fractured Cores," NIPER- Final Report, National Institute for Petroleum and Energy Research, Bartlesville, OK, May 1988.

142. See Appendix Frac Gel Residue and Formation Damage
143. Kramer, J.; Prud'homme, R.K.; Norman, L.R.; Sandy, J.M. "Characteristics of Metal-Polymer Interaction in Fracturing Fluid Systems," SPE paper 61914, 1987 SPE Annual Technical Conference and Exhibition, Dallas, September 27-30.
144. Angyal, S.J.; Greeres, D.; Mills, J.A. Aust. J. Chem., 1974 27, 1447-56.
145. Angyal, S.J. Aust. J. Chem., 1972, 25, 1957-66.
146. Engelskirchen, K.; Galinke, J. US Patent 4 001 210, 1977.
147. Engelskirchen, K.; Galinke, J. US Patent 4 013 821, 1977.
148. Reid, A.R. US Patent 4 096 326, 1978.
149. Lukach, C.; Majewicz, G.; Reid, A.R. US Patent 4 523 010, 1985.
150. Almond, S.W.; Himes, R.E. US Patent 4 552 215, 1985.
151. Almond, S.W.; Conway, M.W. US Patent 4 553 601, 1985.
152. Brode, G.L.; Stanley, J.P.; Partain, E.M. III. US Patent 4 579 942, 1984.
153. White, J.L.; Rosene, R.B.; Hendrickson, A.R.: "New Generation of Frac Fluids", 1973 SPE Annual Meeting, Edmonton, May 8-12.
154. Majewicz, T.G. US Patent 4 400 502, 1983.
155. Goldstein, A.M. US Patent 2 868 664, 1959.
156. Shelso, G.J.; Seaman, B. US Patent 3 808 195, 1974.
157. Engelskirchen, K.; Galinke, J. US Patent 3 350 386, 1967.
158. Boudreaux, J.R. US Patent 3 475 334, 1969.
159. Bishop, R.G.; Desmarais, A.J.; Reid, A.R. US Patent 3 455 714, 1969.
160. Whelan, K. US Patent 3 503 895, 1970.
161. McClain, D.M. US Patent 4 148 766, 1979.
162. Majewicz, T.G. US Patent 4 400 502, 1983.
163. Almond, S.W. US Patent 4 487 866, 1984.
164. Anderson, D.R.; Frisque, A.J. US Patent Re. 28 474, 1974.
165. Briscoe, J.E. US Patent 4 336 145, 1982.
166. *ibid.*: US Patent No. 4,466,890(1984).
167. Harris, P.C.; Harms, W.M.; Norman, L.R.: "Study of Continuously Mixed Crosslinked Fracturing Fluids With a Recirculating Flow Loop Viscometer", SPE paper 17044, 1987 SPE Eastern Regional Meeting, Pittsburgh, October 21-23.
168. Harms, W.M.; Yeager, R. Oil Gas J., 1987, 85(44), 37-39.
169. Harms, W.M.; Watts, M.; Venditto, J.J.; Chisholm, P. "Diesel-Based HPG Concentrate is Product of Evolution", PETROLEUM ENGINEER International(April 1988), 51,53.
170. Yeager, R.R.; Bailey, D.E. "Diesel-Based Gel Concentrate Improves Rocky Mountain Region Fracture Treatments", SPE paper 17535, 1988 SPE Rocky Mountain Regional Meeting, Casper, May 11-13.
171. Constien, V.G.; Brannon, H.D.; Bannister, C.E. Oil Gas J., 1988, 86(23), 49-54.
172. Brown, E.; Hoover, M. "An Improved System for Making Predictable, High Quality Fracturing Fluids Under Field Conditions", 1988 Proc. Annu. Southwest. Pet. Short Course, Lubbock, 49-61.
173. Brannon, H.D.: "Fracturing FLuid Slurry Concentrate and Method of Use," Europ. Pat. Appl., 0 280 341 A1, 1988.
174. Fuller, G.; Toombs, A.J.L. US Patent 3 779 723, 1973.

175. Pickens, P.A.; Lindroth, T.A.; Carico, R.D. US Patent 4 312 675, 1982.
176. Dawans, F.; Binet, D.; Kohler, N.; Vu, Q.D. US Patent 4 393 151, 1983.
177. Hoover, L.D. US Patent 4 330 414, 1982.
178. House, R.F. US Patent 4 435 217, 1984.
179. Hatfield, J.C. US Patent 4 566 977, 1986.
180. Pelezo, J.A.; Corbett, G.E., Jr.; Siems, D.R. US Patent 4 615 740, 1986.
181. Burkhalter, J.F.; Weigand, W.A. US Patent 4 687 516, 1987.
182. Watson, K.E.; Sharp, K.W. US Patent 4 622 153, 1986.
183. Dymond, B.; Langley, J.; Howe, M. US Patent 4 670 501, 1987.
184. Harms, W.M.; Norman, L.R. US Patent 4 772 646, 1988.
185. Jordan, J.W. J. Phys. Chem. 1949 53, 294-306.
186. Jordan, J.W.; Hook, B.J.; Finlayson, C.M. J. Phys. Chem. 1950, 54 1196-1208.
187. Jordan, J.W. US Patent 2 966 506, 1960.
188. Jordan, J.W.; Nevins, M.H.; Stearns, R.O.; Cowan, J.C.; Beasley, A.E., Jr. US Patent 3 168 475, 1965.
189. Hauser, E.A. US Patent 2 531 427, 1950.
190. Hauser, E.A. US Patent 2 531 812, 1950.
191. Schmidt, D.D.; Roos, A.F.; Cline, J.T., "Interaction of Water with Organophilic Clay in Base Oils to Build Viscosity," SPE Paper 16683, 1987 SPE Annual Technical Conference and Exhibition, Dallas, 311-326.
192. Finlayson, C.M.; Jordan, J.W. US Patent 4 105 578, 1978.
193. Finlayson, C.M. US Patent 4 081 496, 1978.
194. Goodman, H. US Patent 4 631 019, 1986.
195. Knudson, M.I., Jr.; Jones, T.R. US Patent 4 664 842, 1987.
196. Pye, D.S.; Smith, W.A.: "Fluid Loss Additive Seriously Reduces Fracture Proppant Conductivity and Formation Permeability," 1973 SPE Annual Meeting, Las Vegas, Sept. 30-Oct. 3.
197. Ely, J.W.; Chatterji, J.; Holtmyer, M.D.; Tinsley, J.M. US Patent 3 768 566, 1973.
198. Horton, R.L.: "Fracturing Fluids for High-Temperature Reservoirs", Drilling (December 1982) 72-78.
199. Seidel, W.R.; Stahl, E.J. Jr. J. Pet. Technol. 1972, 24(11), 1385-1390.
200. Hsu, C.H.; Conway, M.W. J. Pet. Technol. 1981, 33(11), 2213-2218.
201. Holditch, S.A.; Ely, J. "Successful Deep Well Stimulation Utilizing High Proppant Concentration", SPE paper 4118, 1972 SPE Annual Meeting, San Antonio, October 8-11.
202. Ely, J.W.; Chatterji, J.; Holtmyer, M.D.; Tinsley, J.M. US Patent 3 898 165, 1975.
203. Ely, J.W.; Tinsley, J.M. US Patent 4 210 206, 1980.
204. See Appendix Crosslinked Gels from Other Industries
205. Holtmyer, M.D.; Githens, C.J. "Field Performance of a New High-Viscosity Water Base Fracturing Fluid", SPE paper 875-24-E, 1970 Spring Meeting of the Rocky Mountain District Division of Production, Denver, April 27-29.
206. Holtmyer, M.D.; Githens, C.J.; Tinsley, J.M. US Patent 4 021 355, 1977.

207. Holtmyer, M.D.; Githens, C.J.; Tinsley, J.M. US Patent 4 033 415, 1977.
208. Harris, W.F., Jr. US Patent 4 568 481, 1986.
209. Chakrabarti, S.; Guillot, D.; Rondelez, F.: "Gelation of Hydroxypropylguar Under Simple Shear", Polymer Preprints 27(1), 247(April, 1986).
210. Alderman, E.N. "Super Thick Fluids Provide New Answers to Old Fracturing Problems"; SPE paper 2852, 1970 SPE Spring Symposium, Fort Worth, March 8-10.
211. Dysart, G.R.; Richardson, D.W.; Kannenberg, B.G. "Second Generation Fracturing Fluids," paper 906-15-H, 1970 Spring Meeting of the Southwestern District Division of Production, Odessa, March 18-20.
212. Holcomb, D.L.; Smith, M.O. "The Use of a Low-Concentration Crosslinked Hydroxyalkyl Polymer System as a Highly Efficient Fracturing Fluid," 1975 Proc. Annu. Southwest. Pet. Short Course, April, 129-134.
213. Free, D.L.; Frederick, A.F.; Thompson, J.E.: "Fracturing with a High-Viscosity, Crosslinked Gel- Continuous Fracturing Technique", J. Pet. Technol. 1978, 30(1), 119-122.
214. Kern, L.R. US Patent 3 058 909, 1962.
215. Boeseken, J., Ber., 46,(1913)2612; Bl., (4), 53(1933)1332.
216. Deuel, von H. and Neukom, H.: "Über die Reaktion von Borsäure und Borax mit Polysacchariden und anderen hochmolekularen Polyoxy-Verbindungen", Nature 1948, 161, 96.
217. Roy, G.L.; Laferriere, A.L.; Edwards, J.O. J. Inorg. Nucl. Chem. 1957, 4, 106-114.
218. Slate, R.L. US Patent 3 096 284, 1963.
219. McIrvine, J.D. US Patent 3 108 917, 1963.
220. Chrisp, J.D. US Patent 3 301 723, 1967.
221. Conner, J.M.; Bulgrin, V.C. J. Inorg. Nucl. Chem. 1967, 29, 1953-1961.
222. Savins, J.G. Rheol. Acta, 1968, 7(1), 87-93.
223. Bourgoin, D. J. Chemie. Phys., 1963, 59, 923.
224. Schultz, R.K.; Myers, R.R. "The Chemorheology of Poly(vinyl Alcohol)-Borate Gels", Macromolecules 1969, 2.
225. Gorin, P.A.J.; Mazurek, M. Can. J. Chem. 1973, 51, 3277-3286.
226. Gorin, P.A.J.; Mazurek, M. Carbohydr. Res. 1973 27, 325-339.
227. Nickerson, R.F. J. Polym Sci. 1971, 15, 111-116.
228. Ochiai, H.; Fujino, Y.; Tadakoro, Y.; Murakami, I. Polymer J. 1982, 14(5), 423-426.
229. Ochiai, H.; Kurita, Y.; Murakami, I. Makromol. Chem. 1984, 185, 167-172.
230. Moore, R.E.; Barchi, J.J., Jr.; Bartolini, G. J. Org. Chem. 1985, 50, 374-379.
231. Maerker, J.M.; Sinton, S.W. J. Rheol. 1986, 30(1), 77-99.
232. Sinton, S.W. Macromolecules, 1987, 20, 2430-2441.
233. Knoll, S.K.; Prud'homme, R.K.: "Interpretation of Dynamic Oscillatory Measurements for Characterization of Well Completion Fluids", SPE paper 16283, 1987 SPE International Symposium on Oilfield Chemistry, San Antonio, February 4-6.
234. Noll, W.: "Chemistry and Technology of Silicons", Academic, 1968, 368.

235. Rosene, R.B.; Shumaker, E.F. "Viscous Fluids Provide Improved Results from Hydraulic Fracturing Treatments," SPE paper 3347, 1971 SPE Rocky Mountain Regional Meeting, Billings, June 2-4.
236. Free, D.L. US Patent 3 974 077, 1976.
237. Shah, S.N.; Harris, P.C.; Tan, H.C. "Rheological Characterization of Borate Crosslinked Fracturing Fluids Employing A Simulated Field Procedure"; SPE Paper 18589, 1988 SPE Production Technology Symposium, Hobbs, N.M.
238. Mondshine, T.C. US Patent 4 619 776, 1986.
239. Chatterji, J. US Patent 4 144 179, 1979.
240. Brown, R.A.; Norris, R.D. US Patent 4 552 675, 1985.
241. Hinkel, J.J. US Patent 4 560 486, 1985.
242. Tiner, R.L.; Holtmyer, M.D.; King, B.J.; Gatlin, R. US Patent 3 888 312, 1975.
243. McDaniel, R.R.; Houx, M.R.; Barringer, D.K. "A New Generation of Solid-Free Fracturing Fluids", SPE paper 5641, 1975 SPE Annual Meeting, Dallas, September 28-October 1.
244. Clampitt, R.L. US Patent 3 727 689, 1973.
245. Clampitt, R.L. US Patent 3 727 688, 1973.
246. Clampitt, R.L.; Hessert, J.E. US Patent 3 727 687, 1973.
247. Clampitt, R.L. "Gelled PROD Fluid for High Temperature Fracturing," 1975 Proc. Annu. Southwest. Pet. Short Course, April, 109-114.
248. Davidson, C.J. Eur Pat Appl 0 142 407, 1984.
249. Southard, M.Z.; Green, D.W.; Willhite, G.P. "Kinetics of the Chromium (VI)/Thiourea Reaction in the Presence of Polyacrylamide", SPE/DOE paper 12715, 1984 SPE/DOE Fourth Symposium on Enhanced Oil Recovery, Tulsa, April 15-18.
250. Aslam, S.; Vossoughi, S.; Willhite, G.P. "Viscometric Measurement of Chromium(III)-Polyacrylamide Gels by Weissenberg Rheogoniometer", SPE/DOE paper 12639, 1984 SPE/DOE Fourth Symposium on Enhanced Oil Recovery, Tulsa, April 15-18.
251. Huang, C-G.; Green, D.W.; Willhite, G.P. "An Experimental Study of the In-Situ Gelation of Chromium(+3)-Polyacrylamide Polymer in Porous Media", SPE/DOE paper 12638, 1984 SPE/DOE Fourth Symposium on Enhanced Oil Recovery, Tulsa, April 15-18.
252. Terry, R.E.; Huang, C.G.; Green, D.W.; Michnick, M.J.; Willhite, G.P. Soc. Pet. Eng. J. 1981, 22(4), 229-235.
253. Prud'homme, R.K.; Uhl, J.T. "Kinetics of Polymer/Metal-Ion Gelation", SPE/DOE paper 12640, 1984 SPE/DOE Fourth Symposium on Enhanced Oil Recovery, Tulsa, April 15-18.
254. Prud'homme, R.K.; Uhl, J.T.; Poinsette, J.P.; Halverson, F. Soc. Pet. Eng. J., 1983, 24(10), 804-808.
255. Ghazali, H.A.; Willhite, G.P. "Permeability Modification Using Aluminum Citrate/Polymer Treatments: Mechanisms of Permeability Reduction in Sandpacks," SPE Paper 13583, International Symposium on Oilfield and Geothermal Chemistry, Phoenix, April 9-11.
256. Green, P.C.; Block, J.C. US Patent 4 486 318, 1984.
257. Abdo, M.K.; Chung, H.S.; Phelps, C.H.; Klaric, T.M. "Field Experience with Floodwater Diversion by Complexed Biopolymers"; SPE/DOE paper 12642, 1984 SPE/DOE Symposium on Enhanced Oil Recovery, Tulsa, April 15-18.
258. Abdo, M.K. US Patent 4 141 842, 1979.

259. Dovan, H.T.; Hutchins, R.D.: "Development of a New Aluminum-Polymer Gel System for Permeability Adjustment," SPE/DOE Paper 12641, 1984 SPE/DOE Fourth Symposium on Enhanced Oil Recovery, Tulsa, April 15-18.
260. Gall, J.W.; Johnston, E.L. US Patent 4 018 286, 1977.
261. Majewicz, T.G. US Patent 4 486 335, 1984.
262. Kramer, J.; Prud'homme, R.K.; Wiltzius, P.; Miran, P.; Knoxll, S. Colloid & Polymer Science, 1988 266:1-11.
263. Rummo, G.J. Oil Gas J., 1982, 80(37), 84,89.
264. Chemical Abstracts 102(18):141960h
265. Chemical Abstracts 100(8):54290w
266. Conway, M.W. US Patent 4 470 915, 1984.
267. Crowe, C.W. US Patent 4 317 735, 1982.
268. Payne, K.L.; Harms, S.D. "Recent Developments in Polymer Fracture Fluid Technology"; 1984 AIChE National Meeting, Anaheim, May 20-24.
269. Elphinstone, E.A.; Dees, J.M. US Patent 4 369 124, 1983.
270. Conway, M.W. US Patent 4 462 917, 1984.
271. *ibid.* 4 502 967.
272. Lagally, P.; Lagally, H. TAPPI, 1956, 39(11), 747-754.
273. Mills, J.A. Biochem Biophys Res Commun, 1961/62, 6(6), 418-421.
274. Russell, C.A. US Patent 2 894 966, 1959.
275. Baumgartner, S.A.; Parker, C.D.; Williams, D.A.; Woodruff, R.A., Jr. "High Efficiency Fracturing Fluids for High-Temperature, Low-Permeability Reservoirs", SPE/DOE paper 11615, 1983 SPE/DOE Symposium on Low Permeability, Denver, March 14-16.
276. LaGrone, C.C.; Baumgartner, S.A.; Woodroof, R.A., Jr. Soc. Pet. Eng. J. 1985, 25(9), 623-628.
277. Williams, D.A. US Patent 4 534 870, 1985.
278. Williams, D.A.; Woodroof, R.A., Jr.; Box, P.C. Oil Gas J., 1982, 80(13), 141-145.
279. Kucera, C.H. US Patent 4 683 068, 1987.
280. Walser, D.W. "Field Study of a New High-Temperature Fracturing Fluid in South Texas", SPE Production Engineering(May 1988) 187-191.
281. Baranet, S.E.; Hodge, R.M.; Kucera, C.H. US Patent 4 686 052, 1987.
282. Payne, K.L. US Patent 4 579 670, 1986.
283. Horton, R.L. US Patent 4 505 826, 1985.
284. Githens, C.J. US Patent 4 566 979, 1986.
285. Almond, S.W. US Patent 4 448 975, 1984.
286. Almond, S.W. US Patent 4 477 360, 1984.
287. Hanlon, D.J.; Almond, S.W. US Patent 4 460 751, 1984.
288. Almond, S.W. and Garvin, T.R.: "High Efficiency Fracturing Fluids for Low-Temperature Reservoirs," 1984 Proc. Ann. Southwest Pet. Short Course, 76-80.
289. Zhao, F. Chemical Abstract 106(24); 199015A, Chemical Abstract 105(12), 100219h.
290. Hodge, R.M. US Patent 4 657 080, 1987.
291. Hodge, R.M. US Patent 4 657 081, 1987.
292. Hollenbeak, K.H.; Githens, C.J. US Patent 4 464 270, 1984.

293. Putzig, D.E. Eur Pat Appl 0 138 522 A2, 1984. Chemical Abstracts 103(6):39588t.
294. Wadhwa, S.K. US Patent 4 514 309, 1985.
295. Putzig, D.E. Eur Pat Appl 0 195 531 A2, 1986. Chemical Abstracts 106(2):7301q
296. Smeltz, K.C. US Patent 4 609 479, 1986.
297. Goldstein, A.M. US Patent 3 146 200, 1964.
298. Jordan, W.A. US Patent 3 084 057, 1963.
299. Elbel, J.L.; Thomas, R.L.: "The Use of Viscosity Stabilizers in High Temperature Fracturing," SPE Paper 9036, 1980 SPE Rocky Mountain Regional Meeting, Casper, May 14-16.
300. Chemical Abstracts 102(10):81253j and Chemical Abstracts 101(24):213581f
301. Haack, T.K.; Shaw, D.A.; Greenley, D.E. Oil Gas J. 1986, 84(1), 81-83.
302. Malone, T.R.; Foster, T.D., Jr.; Foster, S.T. US Patent 4 290 899, 1981.
303. Phillips, J.C.; Tate, B.E. US Patent 4 458 753, 1984.
304. Lai, J.T. US Patent 4 310 429, 1982.
305. Vio, L.; Meunier, G. US Patent 4 599 180, 1986.
306. Sandell, L.S. US Patent 4 486 317, 1984.
307. Podlas, T.J. US Patent 4 183 765, 1980.
308. Kohn, R.S. US Patent 4 452 639, 1984.
309. Wellington, S.L. US Patent 4 218 327, 1980.
310. Shupe, R.D. J. Pet. Technol., 1981, 33(8), 1513-1529.
311. Wellington, S.L. Soc. Pet. Eng. J., 1983, 23(12), 901-912.
312. Thomas, D.C. Soc. Pet. Eng. J., 1982, 22(4), 171-180.
313. Glass, J.E.; Soules, D.A.; Ahmed, H. "Viscosity Stability of Aqueous Polysaccharide Solutions", SPE paper 11691, 1983 California Regional Meeting, Ventura, March 23-25.
314. Braga, T.G. "Effects of Commonly Used Oilfield Chemicals on the Rate of Oxygen Scavenging by Sulfite/Bisulfite," SPE Production Engineering, May 1987, 137-142.
315. Ryles, R.G. "Chemical Stability Limits of Water-Soluble Polymers Used in Oil Recovery Processes," SPE Paper 13585, 1985 International Symposium on Oilfield and Geothermal Chemistry, Phoenix, April 9-11.
316. Conway, M.W.; Pauls, R.W.; Harris, L.E.: "Evaluation of Procedures and Instrumentation Available for Time-Temperature Stability Studies of Crosslinked Fluids," SPE paper 9333, 1980 SPE Annual Technical Conference and Exhibition, Dallas, September 21-24.
317. Conway, M.W.; Almond, S.W.; Briscoe, J.E.; Harris, L.E.: "Chemical Model for the Rheological Behavior of Crosslinked Fluid Systems," SPE Paper 9334, 1980 SPE Annual Technical Conference and Exhibition, Dallas, September 21-24.
318. Conway, M.W.; Almond, S.W.; Shah, S.N. Polym Mater Science Eng 1984, 51, 7-12.
319. Clark, P.E. "Stimulation Fluid Rheology - A New Approach," SPE Paper 8300, 1979 SPE Annual Technical Conference and Exhibition, Las Vegas, September 23-26.
320. Cameron, J.R.; Gardner, P.C.; Veatch, R.W., Jr. "New Insights on the Rheological Behavior of Delayed Crosslinked Fracturing Fluids", SPE paper 18209, 1988 SPE Annual Technical Conference and Exhibition, Houston, October 2-5.

321. Kramer, J.; Uhl, J.T.; Prud'homme, R.K. Polym Eng Sci, 1987, 27(8), 598-602.
322. Prud'homme, R.K. "Rheological Characterization of Fracturing Fluids," Final Report API PRAC Project 84-45, American Petroleum Institute, Dallas, TX (1985).
323. Prud'homme, R.K. "Rheological Characterization of Fracturing Fluids," Final Report API PRAC Project 85-45, American Petroleum Institute, Dallas, TX (1986).
326. Prud'homme, R.K. Polym Mat Sci Eng, 1986, 55, 798.
327. Kramer, J.; Prud'homme, R.K.; Wiltzius, P. J. Colloid and Interface Sci., 1987.
328. Yoshimura, A.S.; Prud'homme, R.K.: "Viscosity Measurements in the Presence of Wall Slip in Capillary, Couette, and Parallel-Disk Geometries," SPE Reservoir Engineering, May 1988, 735-742.
329. Prud'homme, R.K.; Ellis, S.; Constien, V.G. "Reproducible Rheological Measurements on Crosslinked Fracturing Fluids," SPE paper 18210, 1988 SPE Annual Technical Conference and Exhibition, Houston, October 2-5.
330. Acharya, A.; Deysarkar, A.K. "Rheology of Fracturing Fluids at Low-Shear Conditions," SPE paper 16917, 1987 SPE Annual Technical Conference and Exhibition, Dallas, September 27-30.
331. Menjivar, J.A.: "On the Use of Gelation Theory to Characterize Metal Crosslinked Polymer Gels," Chapter 13, Advances in Chemistry Series 213, American Chemical Society, Washington, DC 1986.
332. Jiang, T.Q., Young, A.C., and Metzner, A.B. "The Rheological Characterization of HPG Gels: Measurement of Slip Velocities in Capillary Tubes," Rheol Acta 25:397-404 (1986).
333. Freck, J.;Gottschling, J. "A Field and Laboratory Study of Polysaccharides in Fracturing Treatments," 1984 Proc. Annu. Southwest. Pet. Short Course, April, 141-156.
334. Hodge, R.M.; Baranet, S.E. "Evaluation of Field Methods to Determine Crosslink Times of Fracturing Fluids," SPE paper 16249, 1987 SPE International Symposium on Oilfield Chemistry, San Antonio, February 4-6.
335. See Appendix Quality Control of Fracturing Fluids
336. Zasadzinski, J.A.N.; Chu, A.; Prud'homme, R.K. Macromolecules, 1986, 19 2960.
337. Matthews, T.M. "Field Use of 'Superfrac' - A New Hydraulic Fracturing Technique," SPE paper 2625, 1969 SPE Annual Meeting of AIME, Denver, September 28-October 1.
338. Kiel, O.M. J. Pet. Technol. 1970 22(1), 89-96.
339. Kiel, O.M. US Patent 3 710 865, 1973.
340. Sinclair, A.R. J. Pet. Technol. 1970, 22(6), 711-719.
341. Sinclair, A.R.; Terry, W.M.; Kiel, O.M. J. Pet. Technol. 1974, 26(7), 731-738.
342. See Appendix Emulsion Frac Fluids
343. Gidley, J.L.; Mutti, D.H.; Nierode, D.E.; Kehn, D.M.; Muecke, T.W. J. Pet. Technol. 1979, 31(4), 525-531.
344. Roodhart, L.; Kuiper, T.O.; Davies, D.R. "Proppant Rock Impairment During Hydraulic Fracturing," SPE paper 15629, 1986 SPE Annual Technical Conference and Exhibition, New Orleans, October 5-8.

345. Roodhart, L.P.; Davies, D.R. "Polymer Emulsion: The Revival of a Fracturing Fluid", SPE/DOE paper 16413, 1987 SPE/DOE Low Permeability Reservoirs Symposium, Denver, May 18-19.
346. Davies, D.R.; Kulper, T.O.H. J. Pet. Technol. 1988, 40(5), 550-552.
347. Schwartz, L.W.; Princen, H.M. J. Colloid Interfacial Sci. 1987 118(1), 201-211.
348. King, G.E. "Foam and Nitrified Fluid Treatments - Stimulation Techniques and More", SPE paper 14477, Distinguished Lecturer Program, 1985-86.
349. Ali, S.M.F.; Selby, R.J. Oil Gas J. 1986, 84(5), 57-63.
350. Ely, J.: "Recent Mechanical and Chemical Improvements in Foam Fracturing", 1985 Proc. Annu. Southwest. Pet. Short Course, April 23-25.
351. Reidenbach, V.G.; Harris, P.C.; Lee, Y.N.; Lord, D.L. "Rheological Study of Foam Fracturing Fluids Using Nitrogen and Carbon Dioxide", SPE paper 12026, 1983 SPE Annual Technical Conference and Exhibition, San Francisco, October 5-8.
352. Grundmann, S.R.; Lord, D.L. J. Pet. Technol., 1983, 35(3), 597-601.
353. Elson, T.D.; Marsden, S.S., Jr. "The Effectiveness of Foaming Agents at Elevated Temperatures Over Extended Periods of Time", SPE paper 7116, 1978 SPE California Regional Meeting of AIME, San Francisco, April 12-14.
354. Eakin, J.L.; Taliaferro, R.W. Oil Gas J., 1962, 60(49), 131-134.
355. Harms, S.D.; Payne, K.L. "Factors Affecting the Selection of Foaming Agents for Foam Stimulation", 1983 Proc. Annu. Southwest. Pet. Short Course, November.
356. Holcomb, D.L.; Callaway, R.E.; Curry, L.L. "Foamed Hydrocarbon Stimulation Water Sensitive Formations", SPE paper 9033, 1980 SPE Rocky Mountain Regional Meeting, Casper, May 14-16.
357. Crema, S.C.; Alm, R.R. "Foaming of Anhydrous Methanol for Well Stimulation", SPE paper 13565, 1985 International Symposium on Oilfield and Geothermal Chemistry, Phoenix, April 9-11.
358. Crema, S.C. US Patent 4 609 477, 1986.
359. Clark, H.B. J. Petro. Technol. 1980, 32(10), 1695-1697.
360. Hall, B.E. "Workover Fluids. Part I - Surfactants have differing chemical properties that should be understood to ensure proper application," World Oil(May 1986) 111-114; *ibid* "Part 2 - How the various types of surfactants are used to improve well productivity," World Oil(June 1986) 64-67; *ibid* "Part 3 - Use of alcohols and mutual solvents in oil and gas wells," World Oil(July 1986) 65-67; *ibid* "Part 4 - Use of Clays and fines stabilizers and treaters," World Oil(October 1986) 61-63; *ibid* "Part 5 - How certain chemicals react to stabilize clays and fines in the formation," World Oil(December 1986), 49,50.
361. See Appendix Non-Emulsifiers, Water Blockage Additives
362. Guillot, D; Dunand, A. "Rheological Characterization of Fracturing Fluids Using Laser Anemometry" SPE paper 12030, 1983 58th Annual Technical Conference and Exhibition, San Francisco, October 5-8.
363. Blauer, R.E.; Durborow, C.J. US Patent 3 937 283, 1976.

RECEIVED February 21, 1989

Chapter 3

Effect of Anionic Comonomers on the Hydrolytic Stability of Polyacrylamides at High Temperatures in Alkaline Solution

R. W. Dexter and R. G. Ryles

American Cyanamid Company, Chemical Research Division, Stamford,
CT 06904-0060

Hydrolysis of amide groups to carboxylate is a major cause of instability in acrylamide-based polymers, especially at alkaline pH and high temperatures. The performance of oil-recovery polymers may be adversely affected by excessive hydrolysis, which can promote precipitation from sea water solution. This work has studied the effects of the sodium salts of acrylic acid and AMPS*, 2-acrylamido-2-methylpropanesulfonic acid, as comonomers, on the rate of hydrolysis of polyacrylamides in alkaline solution at high temperatures. Copolymers were prepared containing from 0-53 mole % of the anionic comonomers, and hydrolyzed in aqueous solution at pH 8.5 at 90°C, 108°C and 120°C. The extent of hydrolysis was measured by a conductometric method, analyzing for the total carboxylate content. It was found that the rate of hydrolysis decreased as the mole ratio of the anionic comonomers increased, and that AMPS was more effective in preventing hydrolysis at all of the temperatures studied.

Polymers designed for the enhancement of oil recovery must remain in solution throughout the predicted life of the flood to provide the required viscosity for oil displacement. During polymer flooding using brines or sea water as solvents, the hydrolysis of amide groups present in polyacrylamides to form carboxylates limits the useful lifetime of the polymer due to the formation of complexes with magnesium and calcium ions [2,3]. These may be precipitates or gels. The objective of this work was to investigate copolymers of acrylamide having greater resistance to hydrolysis at high temperatures, and with a lower tendency to form insoluble precipitates in sea water.

AMPS* is a registered trademark of the Lubrizol Corporation

The hydrolysis of polyacrylamide and acrylamide/sodium acrylate copolymers has been extensively studied [1,2,3,5,6,7,8,-9,10], in relatively strongly alkaline conditions, above pH 12. These studies demonstrated that the hydrolysis of the amide groups is hydroxide-catalyzed and that neighboring ionized carboxyl groups in the polymer inhibit the hydrolysis by electrostatic repulsion of the hydroxide ions. Senju et al. [6] showed that at temperatures up to 100°C, there is an apparent limit to the extent of hydrolysis of polyacrylamide when approximately 60% of the amide groups are hydrolyzed.

The hydrolysis of acrylamide copolymers in dilute alkaline conditions for long periods at high temperatures up to 120°C, as found in harsh reservoirs, has not been extensively studied. Metzner et al. [1] have considered the chemical stability of acrylamide copolymers with various proportions of sodium acrylate in sea water at 90°C. They showed that precipitation of the polymers occurred when approximately 40% of the polymer was in the carboxylate form, and attributed this to the formation of magnesium and calcium complexes. Nonionic polyacrylamides are unsatisfactory in polymer floods because of their low viscosity and high adsorption. Anionic polyacrylamides containing 20–30% acrylic acid can be obtained with higher viscosity and lower adsorption, and are generally quite effective. However, even moderate increases in the hydrolysis of these polymers raises the carboxylate content to a level at which precipitation of calcium and magnesium complexes occurs, thereby shortening the effective lifetime of the polymer. (The separate and independent instability due to chain scission of polyacrylamides by oxidation has been shown to be minimal in reservoirs in the absence of molecular oxygen [4]).

EXPERIMENTAL

Materials. Monomers used in the preparation of the copolymers were as follows: acrylamide as a 50% solution in water, stabilized with cupric ion, supplied by American Cyanamid Company; acrylic acid supplied by BASF; and AMPS*, 2-acrylamido-2-methylpropanesulfonic acid, (recrystallized grade) obtained from Lubrizol. The sodium salts of acrylic acid and AMPS were prepared by gradual neutralization of the monomers with sodium hydroxide solution, maintaining a temperature of 0 to 5°C, to give a final concentration of 50%.

All copolymers were prepared by solution polymerization, under adiabatic conditions, giving at least 99.9% conversions. The polymer gels were granulated and then dried at 90°C to a residual water content of 10 to 12%. The active polymer content of each sample was calculated from the initial weight of the comonomers and the weight of the dried gel. Hydrolysis of the polymers was determined by conductometric titration to be less than 0.2% of the acrylamide charge. The molecular weight of the polymers was 8–10 million as determined by intrinsic viscosity measurements.

The composition and concentration of polymers in the test solutions for hydrolysis are shown in Table 1. The concentration of the sodium acrylate and sodium AMPS copolymers with acrylamide were calculated to provide 0.025 molar solutions of amide units, to simplify the kinetics.

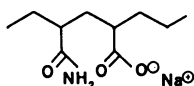
Table 1. Composition and Concentration of Polymers

<u>Mole % Anionic Comonomer in Copolymers</u>	<u>% w/w Active Polymer in Solution</u>	
	<u>Sodium acrylate Copolymers</u>	<u>Sodium AMPS Copolymers</u>
0.00	0.178	0.178
7.70	0.197	0.226
15.40	0.222	0.286
22.40	0.254	0.349
33.50	0.296	0.467
43.00	0.355	0.609
53.30	0.444	0.803

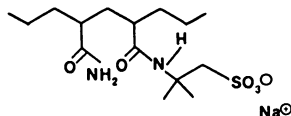
Solutions of each copolymer were prepared by dissolving the appropriate amount of copolymer in deionized water and rolling the solutions for 16 hours.

ANIONIC ACRYLAMIDE COPOLYMERS

SODIUM ACRYLATE



SODIUM AMPS*



HYDROLYSIS EXPERIMENTS

Conditions for hydrolysis experiments were selected to simulate harsh reservoir environments. Moderately alkaline (pH 8.5) solutions, high temperatures, and long reaction times up to 120 days were used. The pH of the solutions remained at 8.5 or slightly higher, ensuring that all anionic groups were fully ionized.

A portion of each solution was retained for analysis of carboxylate content at zero time. Samples of the polymer solutions were weighed into glass jars, the pH adjusted to 8.5 and the jars were sealed with tightly fitting screw caps. The jars were placed in thermostatted ovens at 90°, 108°, and 120°C. After the appropriate time, the jars were removed, cooled and weighed to ensure no loss of contents, prior to analysis for hydrolysis.

The extent of hydrolysis of the copolymers was determined by conductometric titration. The increase in carboxylate content was determined by difference, before and after hydrolysis. (The AMPS content of the polymers, where measured, was determined by colloid titration with poly [diallyl dimethyl ammonium chloride].)

KINETICS

The rate of hydrolysis of acrylamide is assumed to be equal to the rate of formation of carboxylate groups in the early stages of reaction, for both sodium acrylate and AMPS copolymers.

$$\frac{d[\text{COO}^-]}{dt} = - \frac{d[\text{AMD}]}{dt} = K'[\text{AMD}][\text{OH}^-]$$

$$\frac{d[\text{COO}^-]}{dt} = K[\text{AMD}] \quad \text{at zero time and constant pH}$$

$$K = \frac{d[\text{COO}^-]}{dt} \quad [\text{AMD}] = 0.025 \text{ at zero time}$$

$$\frac{0.025}{0.025}$$

Plots of the concentration of carboxylate formed vs. time were drawn for each copolymer, and the initial rates of hydrolysis were determined by measurement of the slope of the tangent to the curve at zero time. The pseudo-unimolecular rate constant (K) is given by:

$$K = \frac{\text{initial slope}}{0.025}$$

Confirmatory values of K were obtained from plots of $\log \frac{0.025}{0.025 - [\text{COO}^-]}$ vs. time in the early stages of the reaction,

although deviations from a straight line occurred in later stages.

RESULTS

The rate of hydrolysis of acrylamide in copolymers with sodium acrylate or AMPS, 2-acrylamido-2-methylpropanesulfonic acid, decreased as the proportion of the anionic comonomers was increased. This effect was much more marked with AMPS than with sodium acrylate, and occurred at 90°, 108°, and 120°C. Typical results at 108°C [Figs. 1 and 2] show the increase in carboxylate content of acrylamide copolymers containing sodium acrylate and AMPS respectively.

The calculated pseudo-unimolecular rate constants (k) for the hydrolysis reaction [Fig. 3], clearly show the inhibiting effect of AMPS, relative to sodium acrylate at all three temperatures.

The total carboxylate content in a range of sodium acrylate copolymers is shown in Fig. 4, calculated as the sum of the initial carboxylate and carboxylate formed during hydrolysis. These values may be compared with the total carboxylate content in AMPS copolymers [Fig. 2].

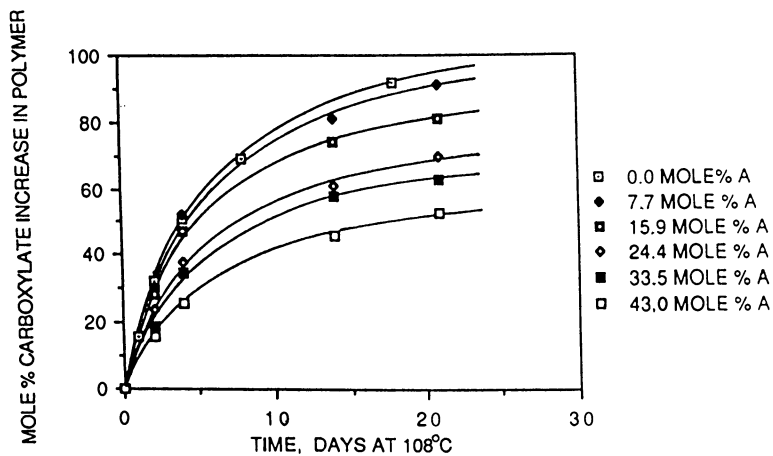


Figure 1. Hydrolysis of amide in sodium acrylate (A) copolymers at 108 °C, pH 8.5, 0.025 M amide.

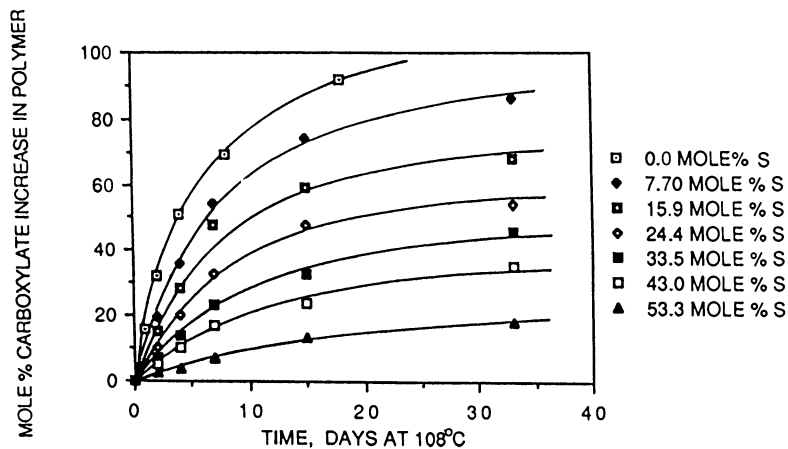


Figure 2. Hydrolysis of amide in AMPS (S) copolymers at 108 °C, pH 8.5, 0.025 M amide.

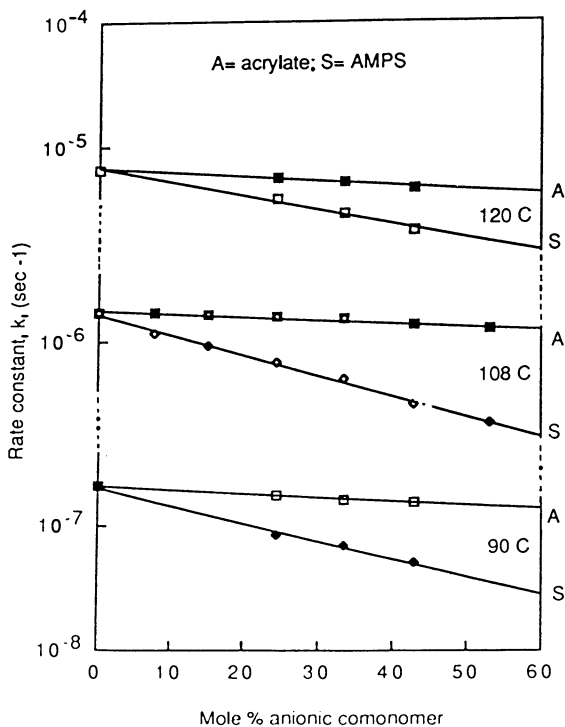


Figure 3. Initial rate constants for hydrolysis of acrylamide copolymers at 90, 108, and 120 °C.

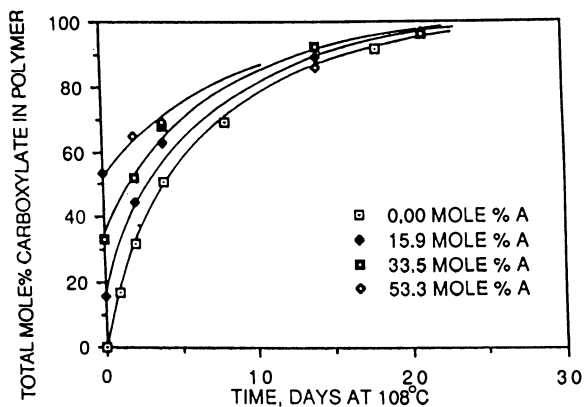


Figure 4. Total mole percent carboxylate in sodium acrylate (A) copolymers at 108 °C, pH 8.5, 0.025 M amide.

DISCUSSION

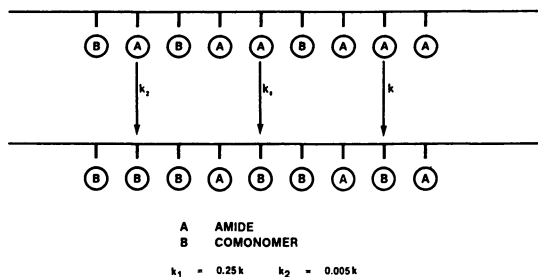
The mechanism of base catalyzed hydrolysis of either homopolyacrylamide or of copolymers of acrylamide and acrylic acid has been studied extensively. It is well known that the rate of hydrolysis of amide groups in such copolymers decreases significantly as the charge on the polymer is increased [2,3,5,7]. This phenomenon has been mainly attributed to electrostatic effects, repulsion between charges on the macroion and on the approaching hydroxide anion. It is generally believed that specific neighboring group effects, inhibition by adjacent pendant carboxyl groups, dominate [7]. However, Morowetz [5] has proposed that the total charge on the polymer does play an important role.

The data presented here confirms the work of these previous authors showing that the rate of amide group hydrolysis decreases as the level of anionicity is increased. This was found to be true for both carboxylated and sulfonated copolymers. However, the rate of amide group hydrolysis in the AMPS copolymers was found to be further inhibited for any given level of anionicity, e.g., at 30 mole % anionicity the rate of hydrolysis of amide groups in the AMPS copolymers was found to be ca. 1/2 that of the corresponding acrylate copolymer at all of the temperatures studied. Since the total charge on these copolymers was the same and all groups were fully ionized under these reaction conditions, this difference cannot be attributed to a macroion charge effect.

As far as neighboring group inhibition is concerned, sequence distribution can play an important role, e.g. Morowetz [5] showed that partially hydrolyzed polyacrylamide hydrolyzes more slowly than an acrylic acid copolymer of the same charge. The former has a more even distribution of groups leading to a greater proportion of the least reactive BAB triad (where A are the acrylamide and B are the acrylic acid moieties).

Also, Higuchi and Senju [7] have proposed that the overall rate constant is composed of three distinct rate constants corresponding to the hydrolysis of the three possible triad configurations, AAA, AAB, and BAB, and have found that the relative reactivity is 1:0.25:0.005. Thus, the overall rate is determined by the relative proportions of these configurations and a relative composite rate constant K can be derived as follows:

KINETIC SCHEME FOR THE HYDROLYSIS OF ACRYLAMIDE COPOLYMERS



$$K = \frac{k [AAA] + 0.25 k [AAB] + 0.005 k [BAB]}{[AAA] + [AAB] + [BAB]}$$

where k is the rate for AAA hydrolysis

The relative proportions of triads is determined by the synthetic conditions chosen as described above for acrylic acid copolymers of acrylamide derived by either direct copolymerization or by hydrolysis. Also, the polymerization pH has a considerable effect on the reactivity in acrylamide/acrylic acid copolymerization. Table 2 shows the triad distribution, integrated to full conversion, for 30 mole % anionic copolymers of acrylamide using the reactivity ratios taken from Ponratnam [11] for acrylic acid and from McCormick [12] for AMPS. From these data (the acrylamide/acrylic acid copolymer prepared at pH = 4 is shown for comparison) composite relative rate constants K were obtained assuming equal reactivity for the acrylic and AMPS based triads of the same sequence. These data show that K for the sodium acrylate copolymer should be ca. 17% lower than for the sodium AMPS copolymer. Since our experimental data show a significant reduction, ca. 50%, for the sodium AMPS copolymer, we can only conclude that sequence distribution effects on neighboring group inhibition cannot be the dominant controlling factor in the hydrolysis of these copolymers. However, the pendant group of the AMPS monomer does possess a geminal dimethyl group which may associate more strongly with the hydrophobic polymer backbone. Such a configurational arrangement may place the negatively charged sulfonate group in very close proximity to any neighboring amide group resulting in increased repulsion of hydroxide anion. The carboxyl groups in acrylic acid copolymers are bonded directly to the polymer chain and are therefore, unlikely to form associations over several bond lengths.

Table 2. Triad Distributions and Composite Rate Constants (K) for 30 Mole % Anionic Acrylamide Copolymers

Monomer B	Polym. pH	r_B	r_A	Triad Distribution						K
				AAA	AAB	BAB	ABA	ABB	BBB	
Acrylic Acid	4.0	0.57	0.32	0.30	0.28	0.12	0.22	0.07	0.01	0.53k
Sodium Acrylate	8.0	0.12	0.63	0.25	0.34	0.11	0.27	0.03	0	0.47k
AMPS Na	9.0	0.49	0.98	0.31	0.31	0.08	0.18	0.10	0.02	0.55k

LITERATURE CITED

1. P. Davidson and E. Mentzer, SPE 9300, presented at the 55th Annual Technical Conference, Dallas, TX, 1980.
2. R.G. Ryles, SPE 13585, presented at the International Symposium on Oilfield and Geothermal Chemistry, Phoenix, AZ, April, 1985.
3. A. Moradi-Araghi and P.H. Doe, SPE 13033, presented at the 59th Annual Technical Conference, Houston, TX, Sept. 1984.

4. R.G. Ryles, SPE 12008, presented at the 58th Annual Technical Conference, San Francisco, CA, 1983.
5. S. Sawant and H. Morowetz, Macromolecules, 17, 2427, (1984).
6. K. Nagase and K. Sakaguchi, J. Polym. Sci. (A), 3, 2475, (1965).
7. M. Higuchi and R. Senju, J. Polym. Sci., (3), 3, 370, (1972).
8. G. Smets and A.M. Hesbain, J. Polym. Sci., 40, 217, (1959).
9. J. Moens and G. Smets, J. Polym. Sci., 23, 931 (1957).
10. S. Mukhopadhyay, B. Ch. Mitra, and S.R. Pailt, Indian J. Chem., 7, 903 (1963).
11. S. Ponratnam and S.L. Kapur, Makromol. Chem., 178, 1029, (1977).
12. C.L. McCormick and G.S. Chen, J. Polym. Sci., 20, 817, (1982).

RECEIVED September 7, 1988

Chapter 4

Predictions of the Evolution with Time of the Viscosity of Acrylamine–Acrylic Acid Copolymer Solutions

Houchang Kheradmand and Jeanne François

Institut Charles Sadron, CRM–EAHP, CNRS–ULP, 6 rue Roussingault,
67083 Strasbourg-Cedex, France

This work deals with an attempt to predict the evolution at long term of the thickening properties of acrylamide-acrylic acid copolymer solutions, from their hydrolysis and degradation kinetics. A Monte-Carlo method is proposed to simulate hydrolysis process. By introducing at each step of this calculation the molecular weight deduced from degradation equations and using semi-empirical laws for the molecular weight and charge density dependences of the intrinsic viscosity, we have obtained some tendencies for the variations of the thickening power with time, under various conditions of temperature, pH and salinity.

One of the main problem encountered when hydrosoluble polymers are used in chemical tertiary process of oil recovery is the prediction of the evolution of the thickening properties of their solutions.

In the case of acrylamide-acrylic acid copolymers, such a prediction requires a good knowledge and understanding on the three following aspects:

i) the hydrolysis of amide groups which leads to the enhancing of the polyelectrolyte character of the polymer. Different experimental works have dealt with the dependence of this kinetics on pH, temperature and initial polymer composition(1-6). More recently a Monte-Carlo simulation method has been proposed in order to predict the variation of the hydrolysis degree under different conditions(7-8).

ii) the chemical degradation of the chain which can be due to various mechanisms according to the pureness of the samples, the method used for its synthesis, the nature of the ions present in the brine (oxidizing or reducing ions), the oxygen content of the brine and the temperature.

iii) these two chemical processes leading to changes in the polymer charge and molecular weight respectively are expected to strongly modify the solution viscosity. Then the relation between viscosity and these two parameters must be known for the given conditions of application.

In recent works, we have studied the kinetics of both hydrolysis and degradation of a acrylamide-acrylic acid copolymer containing 17% of acrylate groups. The purpose of this paper is to give some predictions of the thickening properties evolution based upon semi-empirical viscosity laws.

Hydrolysis kinetics

It is well known that the base hydrolysis of polyacrylamide is catalyzed by OH^- ions (first order reaction) and obeys autoretarded kinetics due to the electrostatic repulsion between the anionic reagent and the polymeric substrate(3-5). In the range of slightly acid pH ($3 < \text{pH} < 5$), Smets and Hesbain(6) have demonstrated a mechanism of intramolecular catalysis by undissociated neighbouring carboxylate groups analogous to that observed in low molecular weight compounds such as phthalimic acid(10). By assuming that Hydrolysis simply results from these two mechanisms no reaction was expected in the range of pH near neutrality. However, Muller(2) has shown that the modification of already partially hydrolyzed polyacrylamide cannot be neglected if one considers reaction times of several months. A more recent systematical study(7,8) of the reaction at different pH, temperatures and initial carboxylate contents led us to propose the simple following model, for $3 < \text{pH} < 9$. We have considered two types of reacting monomer units:

- the units which have an undissociated neighbouring group which catalyses the reaction with a rate constant k_n independent on pH (units X)

- the other units (units Y) whose hydrolysis rate k_a is not simply proportional to (OH^-) concentration (as in the range of high pH) but varies with pH according to an empirical rule:

$$\log k_a = \log k_{a0} + \text{pH} (C_A - C_B \alpha \tau - C_C (\alpha \tau)^2) \quad (1)$$

where τ is the fraction of carboxylate groups in the polymer, α is their ionization degree and C_A, C_B, C_C are constants. This expression corresponds to the following experimental observations:

i) for the unhydrolyzed polyacrylamide, only units of type Y must be considered in the initial step of the reaction and intramolecular catalysis has not to be taken into account. In relation (1), we have obtained a rate constant k_a varying as :

$$\log k_a = \log k_{a0} + C_A \text{pH} \quad (2)$$

This shows that pH increase favors hydrolysis reaction of Y units.

ii) for partially hydrolyzed polymers (or polyacrylamide in a second step), the increase of k_a with pH is lowered when the charge density ($\alpha \tau$) increases (see fig.10 of ref.8). This retardating effect is expressed by the terms $(C_B \alpha \tau)$ and $(C_C (\alpha \tau)^2)$.

At each reaction time , and for a given polymerization degree N , the number of units X is:

$$N_x = N_{AB} (1 - \alpha) \quad (3)$$

where N_{AB} is the number of diades AB (acrylamide :A; acrylic acid :B). The number of Y units is $N - N_x$.

Then the modelization of the hydrolysis kinetics requires at each time the knowledge of α and N_{AB} . α can be calculated by writing the different relations of dissociation equilibria of water, polyacid and NH_3 (produced by the hydrolysis reaction). We have proposed to determine N_{AB} at each reaction step and simulate the whole kinetics by using a Monte-Carlo method .(see ref.8).

In Figure 1 we compare the calculated and measured variations of τ for a copolymer of initial $\tau = 17\%$. Let us remark that in these experiments, the pH has not been adjusted at a constant value and the hydrolysis process induces a change of pH in the solution. We have taken into account this effect in our calculations. In fig.2, we give the predicted hydrolysis kinetics for the same polymer sample but in the case where pH remains constant.

Degradation kinetics

We have previously performed a systematical study of the degradation of a acrylamide-acrylic acid copolymer called sample C(of acrylate content $\tau = 17\%$ and molecular weight $M_w = 6 \cdot 10^6$) prepared by photocopolymerization by using benzyl methyl ketal as catalyst(11). The observed behaviors have been compared with those of a sample obtained by base hydrolysis of polyacrylamide called sample H (approximately same M_w and $\tau = 30\%$), in some particular cases.

In the practical application, the chemical stability of these polymers at high temperature will essentially depend on the content of oxygen and ions of transition metals in the brine. It is the reason why we have investigated their behaviors for several months (at least 3) ,at $80^\circ C$ and under three main conditions (see fig.3).

-without oxygen and salts of transition metals

Under such conditions , sample C is not degraded , M_w measured by light scattering remaining constant for 6 months. A slight increase of reduced viscosity (η_{red}) will be later explained by the hydrolysis of amide groups.

- in the presence of oxygen and without salts of transition metals

After 3 months of ageing, η_{red} is reduced by a factor 6 while M_w is 10 times lower than initial $M_{w(0)}$. We have observed that the degradation follows a random process of link breaking since the linear expression^(12,13):

$$\ln (1 - M_{w(0)}) - \ln (1 - M_{w(t)}) = k t \quad (4)$$

has been obtained. Moreover, the degradation leads to the formation of shorter linear chains and at each time the intrinsic viscosity (η) can be obtained from relation (4) and the classical Mark-Houwink law:

$$(\eta) = K M_w^a \quad (5)$$

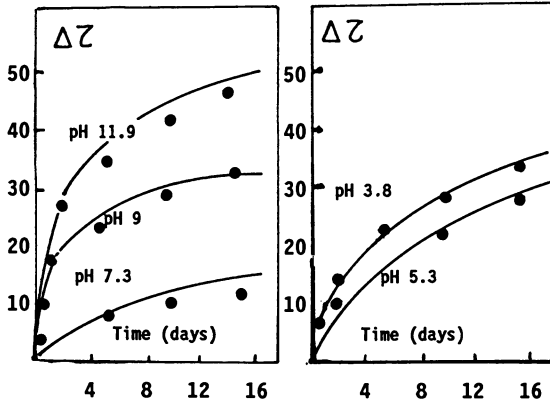


Figure 1. Calculated and experimental (●) hydrolysis kinetics Copolymer C, T=80°C, different initial pH

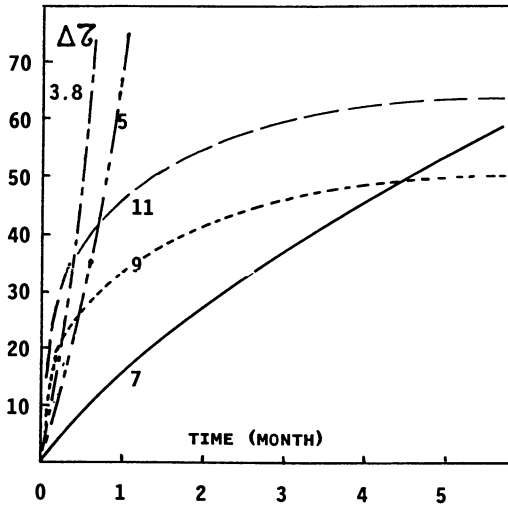


Figure 2. Calculated hydrolysis kinetics for Copolymer C at 80°C at different constant pH

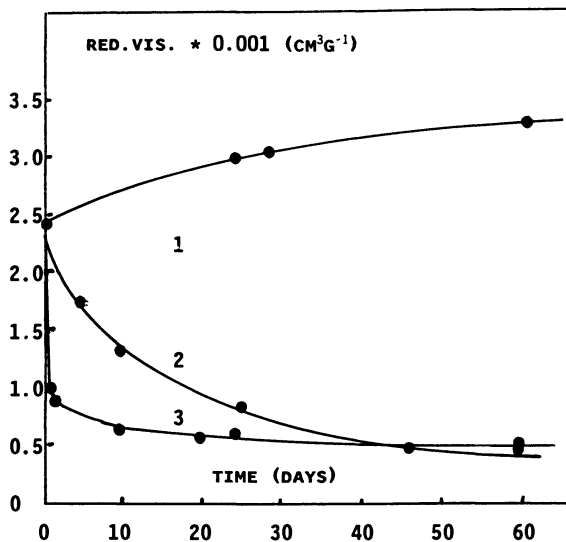


Figure 3. Degradation kinetics of Copolymer C at 80°C
1: without oxygen ; 2 : with oxygen ;
3: without oxygen and with 5 ppm of Fe²⁺

Under these conditions, the degradation kinetics of sample H is similar, with a different value of k in relation (4). However, the origin of the phenomenon is different: for sample H, the degradation is due to the decomposition of chain hydroperoxides by traces of Fe^{III} . The sample C does not contain peroxides nor Fe^{III} and we have explained its instability by the presence of catalyst residues.

The purification by precipitation in methanol of both samples allows to obtain a very good stability for 6 months.

- in absence of oxygen and with salts of transition metals

In fig. 3, we compare the evolutions of η_{red} of free oxygen solutions of copolymer C with and without 5 ppm of Fe^{II} . As confirmed by light scattering measurements, the presence of ferrous ions induce a quasi instantaneous degradation of this polymer followed by a much slower reaction.

The purified sample C is not degraded under such conditions while degradation is measured before and after purification of sample H. This results confirms the difference of degradation mechanism according to the method of preparation of the polymer.

Oxidizing ions (Cu^{II} or Fe^{III}) as well as reductants ions (Cu^{I} or Fe^{II}) induce the degradation of these polymers.

Dependence of the viscosity on molecular weight and charge density of the polymer

If the polymer concentration c_p is lower than c_p^* , the critical concentration of chain overlapping, one can express the viscosity η of the solution by:

$$\eta = \eta_0 + \eta_0 (\eta) c_p + K' \eta_0 (\eta)^2 c_p^2 \quad (6)$$

where η_0 is the solvent viscosity

K' is the Huggins constant which varies with the thermodynamical quality of the solvent (salinity and temperature)

For the calculation of η of a solution of copolymer of given τ , α and M_w under given conditions of salinity and temperature, one must know the variation laws of (η) and K' with these parameters.

- intrinsic viscosity (η)

In the classical theories of polyelectrolytes, the chain expansion is characterized by the electrostatic excluded volume parameter, z_{e1} with:

$$z_{e1} = i^2 M_w^{1/2} / c_s \quad (7)$$

where i is the ionization degree and c_s the concentration of added electrolyte (14). A dependence of the intrinsic viscosity with $1/C_s$ is then predicted while experiments show that (η) varies as $1/c_s^{1/2}$. Fixmann et Al. (15) have proposed an expression which gives a better account for experimental data ($(\alpha^3 - 1)$ varying as $1/c_s^{1/2}$, α' being the chain expansion). Nevertheless, in spite of the numerous expressions proposed, they generally do not take into account the strong interactions between counter ions and polyions for the high values of the charge parameter ξ

$$\xi = e^2 / D k T b \quad (8)$$

where e is the proton charge, D the dielectric constant, k the Boltzmann constant, T the absolute temperature and b the average

distance between two charged groups along the chain, varying as $1/\alpha r$.

The Manning theory(16,17) predicts a critical value ξ_c above which counterions are condensated on polyion. In the case of monovalent ions, $\xi_c = 1$ and for $\xi > \xi_c$, the chain expansion predicted by the classical theories is overestimated if the ionization i is not corrected by a fixation term. Koblansky et Al have shown(18) that ion condensation occurs for values of ξ much lower than ξ_c in the case of partially hydrolyzed polyacrylamide. They have found for Na^+ that the activity coefficient γ does not vary with ξ as predicted by the Manning theory (16,17) but according to a empirical law:

$$\gamma = 0.96 - 0.42 \xi^{1/2} \quad (9)$$

in the absence of simple electrolytes.

Kowblansky et Al (19) have also measured the intrinsic viscosity of hydrolyzed polyacrylamide of a given molecular weight as a function of r for $\alpha = 1$ and their results can be fitted by the expression:

$$(\eta) = (\eta)_0 + k_s * \xi * \gamma * M_w \quad (10)$$

where $(\eta)_0$ is the intrinsic viscosity of the uncharged polymer

$$(\eta)_{0(25)} = 9.3 * 10^{-3} * M_w^{0.75} \text{ (cm}^3 \text{g}^{-1}) \text{ at } 25^\circ\text{C} \quad (11)$$

and k_s is a coefficient which depends on the salinity:

$$k_s = 4.7 * 10^{-4} / c_s^{1/2} - 1.33 * 10^{-4} \quad (12)$$

c_s is the molar concentration of monovalent salt (NaCl)

Such empirical expressions have been also verified by Kulkarni et Al.(21) and Kheradmand(7) but they have been established for room temperature. In fact, we have to know the temperature dependence of the two terms of relation (10):

-For the first non electrostatic term, such a dependence can be calculated from the classical Flory theory and the value of the theta temperature of unhydrolyzed polyacrylamide ($\theta = 265^\circ\text{K}$ (22))

$$(\eta)_{0(T)} = (\eta)_{0(25)} * (1-\theta/T)/(1-\theta/298)^{3/5} \quad (13)$$

-For the electrostatic term, there is a lack of reliable data and predictions dealing with the variation of the ions -polyion interactions with temperature. If one considers the relation (8), the product $D * T$ is a decreasing function of temperature but the term $\xi * \gamma$ decreases for the high values of ξ and increases for the low values of ξ . Nevertheless, these variations are negligible and we have considered, in a first approximation, that the electrostatic term remains constant for $20 < T < 80^\circ\text{C}$.

The final expression for (η) is:

$$(\eta) = 9.33 \cdot 10^{-3} \cdot M^{0.75} \cdot ((1 - 265/T)/0.11)^{3/5} + (4.7 \cdot 10^{-4} / c_s^{1/2} - 1.3 \cdot 10^{-4}) \cdot \xi \cdot \gamma \cdot M_w \quad (14)$$

($\text{cm}^3/\text{g}^{-1}$) (see examples of results in Figure 4)

- Huggins constant K'

Let us remark that relation (6) is given for polymer concentration c lower than the critical overlapping concentration c^* above which higher terms in c must be considered. In fact, the concentration practically used (around 10^{-3} g/cm^3) corresponds to the semi-dilute regim for which the behavior is not well known in the case of polyelectrolytes. We have however kept relation (6) by introducing for K' a mean apparent value determined from our experiments ($K' = 1$)

By combining expressions (6) and (14), one can obtain an approximative value of the solution viscosity if only monovalent ions are present in the solution.

In the presence of alkalno-earth cations, one must take into account not only viscosity decrease due to electrostatic screening and condensation which theoretically occurs at lower values of ξ ($\xi = 0.5$) but also phase separation (23-25). We will take the case of Ca^{2+} as example.

- Kowblansky et Al.(26) have obtained for activity coefficient of Ca^{2+} :

$$\gamma = 0.43 - 0.26 \xi^{1/2} \quad (15)$$

We have recently performed systematical measurements of the intrinsic viscosity of acrylamide-acrylic acid copolymers for large ranges of τ and α , in the presence of CaCl_2 (26). Our results show that the empirical relation (14) can be extended to the case of divalent cations by using the value of γ given in relation (15). It should then possible to predict the variation of intrinsic viscosity at infinite dilution ,but at finite concentration the formation of aggregates makes difficult the determination of the Huggins constant.

- It is now well known that the addition of Ca^{2+} in aqueous solutions of these copolymers induces phase separation with precipitation of a phase constituted by a polymer-Ca complex. From turbidity measurements, it is possible to define a critical concentration c_a^* above which this phenomenon occurs(23-25).

c_a^* decreases with c_p for $c_p < c_p^*$ and increases for $c_p > c_p^*$

c_a^* is an decreasing function of temperature ,the demixing is obtained by heating

c_a^* increases by addition of NaCl

c_a^* decreases by increasing τ for $\tau < 50\%$

Some aspects of this behavior are given in Figure 5 and more details can be found in ref. 24 and 25;

Viscosity evolution

- in absence of degradation

We have seen that such polymers are not degraded in absence of oxygen. On an other hand, it is possible to avoid degradation

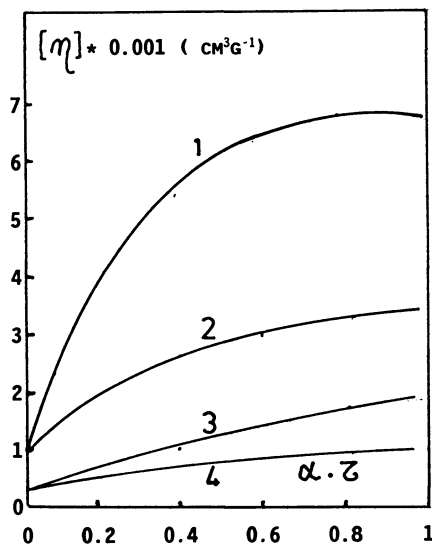


Figure 4. Calculated variations of (η) as a function of $\alpha * \tau$
 1 and 2 : $M_w = 5 \cdot 10^6$ $c_s = 0.1$ and $0.5N$; 3 and 4 : $M_w = 10^6$
 same c_s

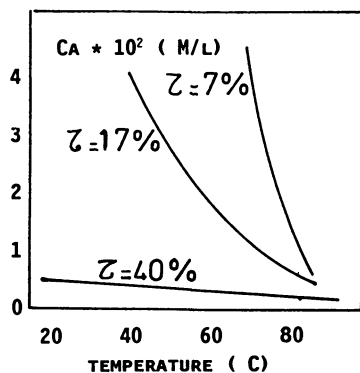


Figure 5. Solubility limit of different copolymers (1000 ppm)
 in the presence of Ca^{2+} as a function of temperature

either by purification or by addition of stabilizing compounds (7,9,27) under all the practical conditions. We have then calculated the variations of viscosity with time by combining the hydrolysis kinetics and viscosity expressions (at constant M_w) under different conditions of constant pH and salinity.

The Figure 6 corresponds to the predictions for the copolymer C of 17% of acrylic content at 80°C. For $\text{pH} > 7$, an increase of viscosity can be expected but the form of the curves changes with pH: at high pH, the initial hydrolysis rate is higher than at pH 7 and this leads to a higher initial increase of viscosity. But in the second step of the hydrolysis, the kinetics is strongly autoretarded at $\text{pH} > 9$ and the slow variation of τ corresponds to a slight increase of viscosity while at pH 7, complete hydrolysis can be reached and a higher viscosity is expected for a long aging time.

For $\text{pH} < 7$, the hydrolysis is very fast (see figure 2) and a limiting value of viscosity can be reached after 1 month but the polymer is slightly ionized : the product $\alpha\tau$ passes through a maximum which also induces a maximum in the viscosity curves.

Finally, all these variations are strongly reduced by increasing salt concentration.

We have reported in Figure 7 the expected variations of viscosity at five temperatures for the same polymer in the presence of 0.1NaCl at pH 7. Two opposite effects explain these curves: the initial viscosity is a decreasing function of T while the hydrolysis rate increases with increasing T.

Some remarks can be made about the evolutions in the presence of Ca^{2+} , although it is difficult to think that some brine could contain only this type of cations without monovalent cations. Before any aging, a copolymer of 17% of acrylate content begins to demix for $\text{CaCl}_2 > 2.5 \cdot 10^{-2}$ M/l and this limit is lower for higher initial values of τ . If $\text{CaCl}_2 < 5 \cdot 10^{-3}$ M/l, no precipitation will occur even if τ reaches the value 1. For an intermediate concentration of CaCl_2 , for instance 10^{-2} M/l, phase separation can be expected after 20 months and 3.5 months at 60°C and 80°C respectively.

-when degradation occurs

i) in the presence of oxygen

In this case, we must take into account the variation of M_w through relation (4). An example of results is given in Figure 8. It is obvious that the degradation is the main phenomenon and a high loss of viscosity can be predicted. Since hydrolysis has an increasing effect on the viscosity, it was interesting to determine the M_w variation which could lead to a constant value of viscosity (see Figure 5b). We can observe that M_w must remain higher than $3.7 \cdot 10^6$

ii) in absence of oxygen and with ions of transition metals

In this case, the very fast degradation induces the high initial loss of viscosity as already measured and predictions for a long time do not present interest.

Conclusion

In this work, we propose a method based on different combined semi-empirical laws to predict the evolution of the viscosity of a solution of acrylamide - acrylic acid copolymer. In fact, it appears

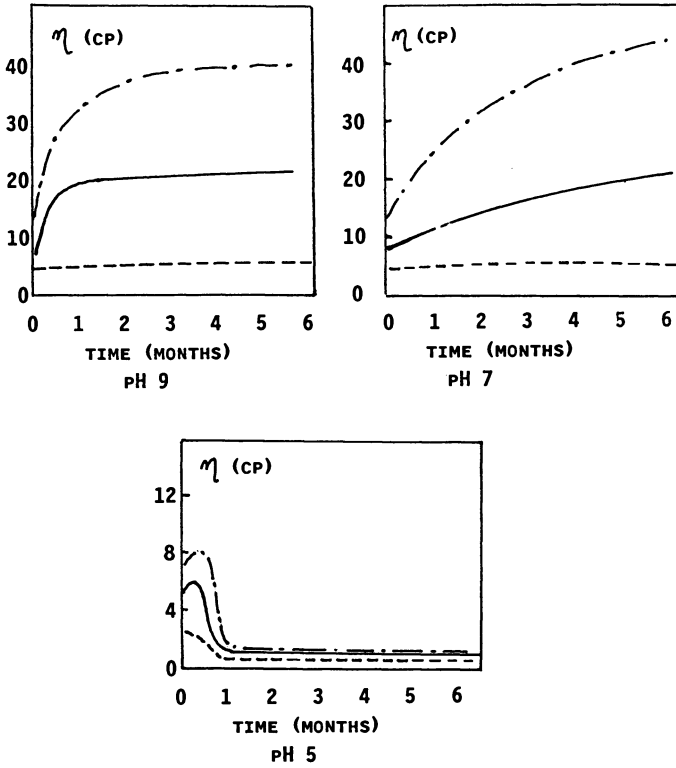


Figure 6. Predictions of viscosity evolution for Copolymer C without degradation at 80°C and different pH; (---) $c_s = 0N$; (—) $c_s = 0.1N$; (- - - -) $c_s = 0.5N$

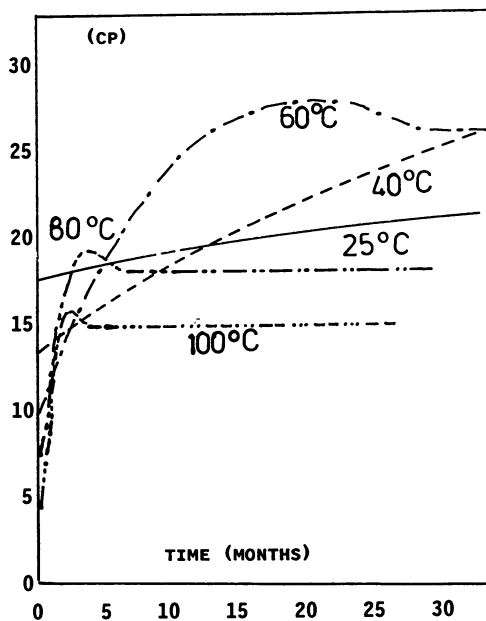


Figure 7. Predictions of viscosity evolution for copolymer C at pH 7, 0.1 NACL at different temperatures

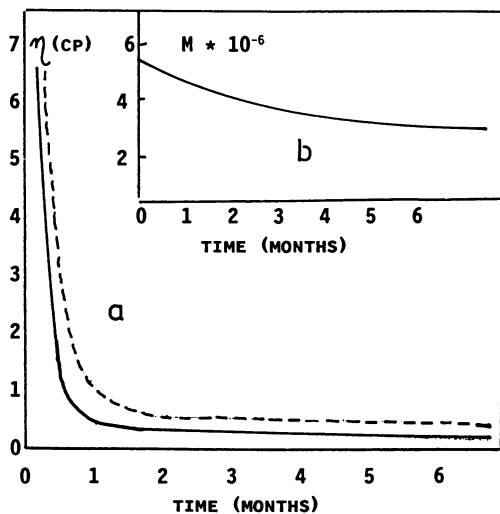


Figure 8. a: Predictions of viscosity evolution for Copolymer C with degradation in the presence of oxygen at 80°C and pH7 ; (-----) $c_s = 0.05N$; (————) $c_s = 0.1N$
 b : calculated decrease of M_w able to compensate hydrolysis effect

that in absence of degradation, the behaviors must be rather independent on the origin of the polymer and only depend on its initial properties and on the pH, salinity and temperature of the brine. When degradation occurs, it is generally due to impurities, then the kinetics is not universal and must be the object of a specific study for each sample.

This work has benefited from grants from Compagnie Française des Pétroles. The authors are indebted for fruitful discussions to Doctor V. Plazanet.

Literature Cited

1. Muller G.; Fenyo J.C.; Selegny E.J. J. Appl. Polym. Sci. 1980, 25, 627
2. Muller G. Polymer Bulletin 1981, 5, 31
3. Higuchi M.; Senju R. Polymer 1972, 3, 370
4. Sawant S.; Morawetz H. Macromolecules, 1984, 17, 2427
5. Truong N.D.; Galin J.C.; François J.; Pham Q.T. Polymer, 1986, 27, 459
6. Smets G.; Hesbain A.M., J. Polym. Sci. 1959, 23, 217
7. Kheradmand H. thesis L. Pasteur University Strasbourg 1987
8. Kheradmand H.; François J.; Plazanet V. Polymer 1988, 29, 860
9. Kheradmand H.; François J.; Plazanet V. J. Appl. Polym. Sci under press
10. Bender M.L.; Chow Y.L.; Chloupek F. J. Amer. Chem. Soc. 1958, 80, 5380
11. Boutin J.; Contat S. French Patent N 249 217 issued to Rhone Poulenc Ind.
12. Jellinek H.H.G.; Degradation of Vinyl Polymers Academic press, New-york 1955
13. Vink H. Makromol. Chem. 1963, 67, 105
14. Yamakawa H. Modern theory of Polymer Solutions Harper and Row New-York 1971
15. Fixman M.; Solnick J. Macromolecules, 1978, 11, 863
16. Manning G. J. Chem. Phys. 1969, 51, 924
17. Manning G. Acc. Chem. Res. 1979, 12, 442
18. Kowblansky M.; Zema P. Macromolecules, 1981, 14, 166
19. Kowblansky M.; Zema P. Macromolecules, 1981, 14, 1451
20. François J.; Sarazin D.; Schwartz T.; Weill G. Polymer, 1979 20, 969
21. Kulkarni R.A.; Gundiah S. Makromol. Chem., 1984, 185, 957
22. Kanda A.; Sarazin D.; Duval M.; François J. Polymer, 26, 406
23. Ikegami A.; Imai N. J. Polym. Sci., 1962, 56, 133
24. Truong N.D.; Galin J.C.; François J.; Pham Q.T. Polymer Communications, 1984, 25, 208
25. Truong D.N.; François J. in Solid-Liquid Interactions in Porous Media, Ed. Technip, Paris, 1982, p.251
26. Medjadhdi G.; Sarazin D.; François J. Unpublished results
27. Muller G.; Kohler N. in 2nd European Symposium on Enhanced Oil Recovery, Ed. Technip, Paris, 1982 p. 87

RECEIVED February 2, 1989

Chapter 5

Interactions Between Acrylamide–Acrylic Acid Copolymers and Aluminum Ions in Aqueous Solutions

Ramine Rahbari, Dominique Sarazin, and Jeanne François

Institut Charles Sadron, CRM–EAHP, CNRS–ULP, 6 rue Boussingault,
67083 Strasbourg-Cedex, France

Phase separation, gelation and viscosity of acrylamide-acrylic acid copolymer solutions containing aluminium chloride have been studied as a function of pH, salinity and composition of the polymer. In the range of polymer concentration investigated, the most common behavior is phase separation with loss of viscosity and formation of large aggregates. At pH 5 gelation phenomenon can occur due to the presence of polynuclear ions of aluminium and the conditions of gel formation are studied as a function of salinity. At pH 7, phase separation is due to flocculation of $\text{Al}(\text{OH})_3$ particles by polymer bridges. These behaviors are discussed from ^{27}Al NMR data giving the fraction of Al ions bound on the polymer and from of a model of electrostatic interactions.

The strong interaction of polyvalent cations with polyions is well known to strongly alter the rheological properties of hydrolyzed polyacrylamide used in the tertiary oil recovery process (1-4). The influence of divalent cations have already been studied (5-7) but the rôle played by the presence of small quantities of aluminium ions has never been investigated.

In a first part of this paper, we will discuss results of a ^{27}Al NMR study of the binding of Al ions on acrylamide-acrylic acid copolymers as a function of pH, at the light of a simple electrostatic model. The second part deals with the phase diagrams, physical gelation and precipitation phenomenon, for different copolymer compositions and under various conditions of concentrations, pH and salinity.

Experimental

in this study AD10, AD17, AD27 and AD37 (Rhône Poulenc Industries) (8) of acrylate content τ (mole %) equal to 1.5, 7, 17 and 27, and

of weight average molecular weight M_w approximately $5 \cdot 10^6$. An other sample (PAMNH) ($\tau=0.3\%$ and $M_w=10^6$) has been prepared in our laboratory by photopolymerization.

The details concerning the experimental methods used in this work can be found in ref. 9 and 10.

Solutions of Aluminium Chloride

The pure $AlCl_3$ solutions neutralized by NaOH contain ions of general formula $Al_i(OH)_p^{(3i-p)+}$, which can be mononuclear (Al^{+++} , $Al(OH)^{++}$, $Al(OH)_2^+$ and $Al(OH)_3$) or polynuclear ($Al_2(OH)_4^{4+}$ and $Al_{13}(OH)_p^{(39-p)+}$) and also non ionic species ($Al(OH)_3$). Their amounts depend on the neutralization ratio R ($R = (NaOH/AlCl_3)$) according to six different equilibrium laws of constants $K_{i,p}$

$$(Al_i(OH)_p)^{(3i-p)+} = \frac{(Al^{+++}) * K_{i,p} * f_{i,p}}{f_{i,p} * (H^+)^i} \quad (1)$$

where $f_{i,p}$ is the activity coefficient of $Al_i(OH)_p^{(3i-p)+}$ which can be obtained from Debye-Huckel expression (11-13). The solubility of Al^{+++} is limited by:

$$(Al^{+++}) * (OH^-)^3 < K_s \quad (2)$$

By using a set of $K_{i,p}$ and $f_{i,p}$ values found in literature, we have calculated the compositions of $AlCl_3$ solutions (without polymer) at two different concentrations (see figure 1).

If one considers the pH range of major interest in application ($4.5 < pH < 8$), it appears:

- around pH = 5, for the low $AlCl_3$ concentrations only mononuclear species are present while at higher concentrations, polynuclear ions and non ionic species are preponderant. The time is also an important parameter since polyions (Al_{13}^{3+}) progressively disappear and after 6 months aging, only non ionic species are in equilibrium with monovalent ions $Al(OH)_2^+$. 15 days aged solutions have been used in this study; The composition of the solutions given in Figure 1 have been confirmed by NMR and correspond to this aging time (9,11-12).

- around pH = 7, $Al(OH)_3$ is present at more than 90% and it has been shown that the size of aggregates depend on concentration and aging time. We have recently shown (14) by electrophoresis measurements that the $Al(OH)_3$ particles are positively charged and become neutral only after a long time (6 months) of heating at 80°C. Elastic and quasi-elastic light scattering measurements have revealed that their size scales as $C^{1.3}$: at 1 ppm of Al (or $3 \cdot 10^{-5}$ M/l), the radius of gyration R_{ga} is 500 Å while at 12 ppm $R_{ga} = 15000$ Å. Moreover these particles have a form of plaquets as already described (15,16)

Model of electrostatic interactions

It is well known that the concentration of ionized groups COO^- on the polymer chain obeys the classical law:

$$pK_a = (COO^-) * (H^+) / (C_{ip} - COO^-) \quad (3)$$

where C_{ip} is the molar concentration of carboxylic groups.

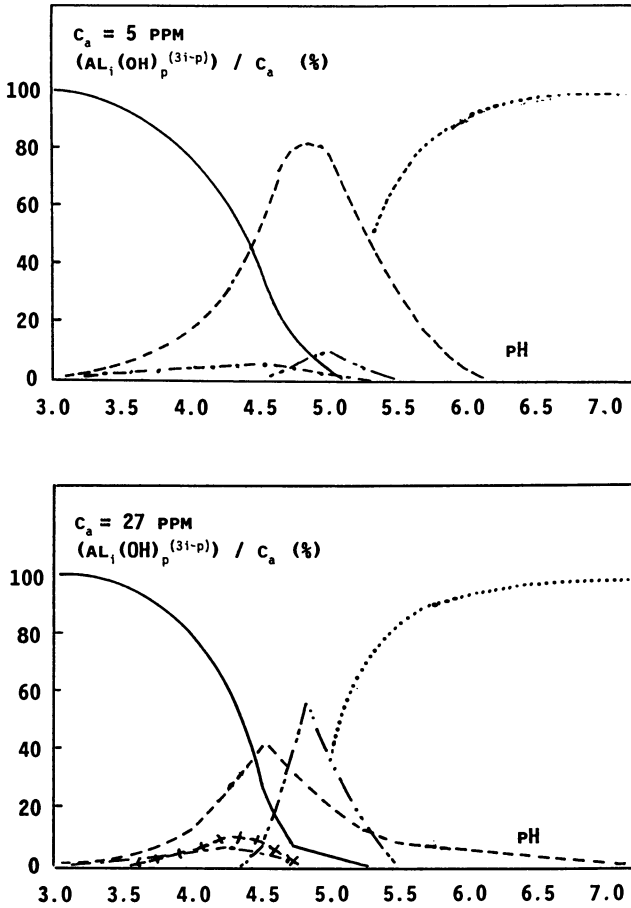
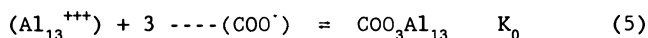
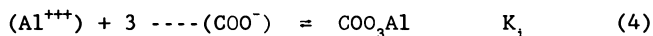


Figure 1 : AlCl₃ solutions : Calculated fractions of Al⁺⁺⁺ (—), Al(OH)₂⁺ (-·-·-), Al(OH)₂⁺ (- - - -), Al₂(OH)₂⁴⁺ (+ + + +) Al₁₃(OH)₂₇³⁺ (-·-·-) and Al(OH)₃ (·····)

In order to obtain a rough evaluation of the fraction of aluminium bound on polymer, we have assumed in a first approach:

i) the polyelectrolyte effects due to the polymer are negligible and the distribution of ionic species in the bulk can be considered as uniform. Such an assumption can be considered as correct if the polymer concentration c_p is higher than c_p^* , the critical concentration of chain overlapping.

ii) among the different possible interactions between polymer and aluminium species, the most important are the electrostatic interactions between carboxylate groups COO^- and the Al trivalent ions which are oppositively charged. Then we have taken into account the equations corresponding to the following equilibria, with constants K_1 and K_0 :



By using the expressions (1) to (5), it is possible to calculate the concentrations of the different ionic ($\text{Al}_i(\text{OH})^{(3i-p)+}$ and COO^-) and non ionic ($\text{Al}(\text{OH})_3$, COOH , COO_3Al and $\text{COO}_3\text{Al}_{13}$) species in the mixed AlCl_3 - polymer solutions as a function of pH and composition.

As shown in Figures 2 and 3, we have found two maxima in the amount of the "bound" monomeric ions or more precisely the difference between the total monomeric ions concentration in absence and presence of polymer (NMR experiments give this quantity): for pH = 4 and pH = 4.6. Comparison with figure 1 indicates that these maxima correspond to the formation of COO_3Al and $\text{COO}_3\text{Al}_{13}$ respectively. For very aged or very dilute AlCl_3 solutions where polynuclear ionic species are absent, only one maximum is found, around pH = 4.5.

²⁷Al NMR
Bottero et Al.(11,12) have shown that ²⁷Al NMR allows to distinguish the mononuclear from the polynuclear species of Aluminium ions in AlCl_3 solutions. We have performed the same type of studies by adding different amounts of copolymers and we have measured the decrease of monomeric Al ions concentration by increasing the polymer content. Figures 2 and 3 give some examples of results; "Al bound" as measured by NMR is plotted as a function of pH, for two different systems and can be compared with the values calculated for $K_1=10^{14}$ and $K_0=10^{16}$.

As expected from the model, we observe:

i) Two reproducible maxima at pH slightly shifted with respect to predictions, ii) the amount of Al ions bound onto polymer increases by increasing τ and the same couple of K_1 and K_0 values gives a rather good account of experimental results for $1.5\% < \tau < 30\%$. This result shows that is reasonable to neglect other type of interactions between aluminium ions and the polymer: for instance coordination binding with amide groups.

This first study is very important: the good agreement between calculation and experiments justifies the previous

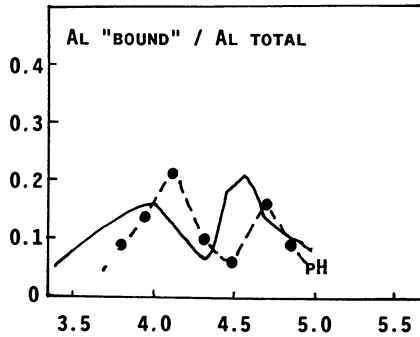


Figure 2 : Interactions polymer-aluminium : concentration of bound aluminium ions for AlCl_3 (27 ppm) and AD27 (0.25 g/l) Full line : Calculated curve ; Dotted line :NMR results

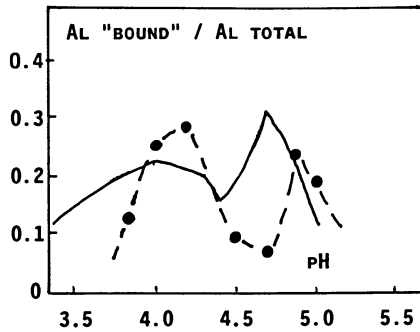


Figure 3: Interactions polymer-aluminium : concentration of bound aluminium ions for AlCl_3 (27 ppm) and AD37 (0.25 g/l) Full line : calculated curve; dotted line :NMR results

hypothesis. Moreover it clearly demonstrates that polynuclear ions of Al strongly interact with polymers and will play an important role in their stability, particularly around pH 5. However, we must point out that, by hypothesis, the interactions between non ionic species of aluminium ($\text{Al}(\text{OH})_3$) are not taken into account in our calculation and in NMR studies these Al species do not give any signal. Thus, our model is rather good for $\text{pH} < 6$ where non ionic species are negligible and is predicted to fail for $\text{pH} > 6$.

Phase diagrams and viscosity

This part deals with the stability of the polymer in the presence of the different species of aluminium. For strongly charged polyelectrolytes such as polyphosphate or sodium polyacrylate in the presence of divalent cations ($\text{Ca}^{++}, \text{Ba}^{++}, \dots$), it has been shown that precipitation occurs when a given fraction of charged groups is "neutralized" by the binding of the cations and this situation is realized for a molar concentration of cations of the same order of magnitude than that of charged groups (17,18). In the case of acrylamide-acrylic acid copolymers, the problem becomes more complex since the distance between the charged groups is much higher depending on τ . Truong (5,7) has recently shown that the relative probability to form intra or inter molecular bridges must be taken into account. If intramolecular fixation is preponderant, precipitation can be expected while in the case where the intermolecular bridgings are favoured physical gelation should occur with or without syneresis effects.

From these qualitative considerations and taking into account only electrostatic interactions according to our model, we could expect the following features for the behavior of acrylamide-acrylic acid copolymer in the presence of aluminium:

- no interaction with unhydrolyzed polymer (PAMNH) since only electrostatic interactions are considered in the model
- for $\tau > 0$, the maximum of instability should be observed at the pH values where the interaction with ionic Al species has found to be maximum in NMR experiments and no effect is expected at pH 7 if really only uncharged species of Aluminum are present. Moreover, the high valency and great size of Al_{13} ions could lead to gelation.

We will summarize the results of a systematical study of these systems by phase titration, turbidimetry and viscosimetry. The concentration ranges were $0 < c_a < 20 \text{ ppm}$ for Al and $0 < c_p < 1000 \text{ ppm}$ for the polymer, pH being ranging between 4 and 7.

Phase titration

In a first series of experiments, we have studied the phase separation of a same composition (C_a and c_p constant), for varying pH. The fraction of precipitated polymer was determined by potentiometric titration of the supernatant phase and from the ratio of its viscosity η with the viscosity η_0 of free aluminium polymer solution. An example of results is given in Figure 4 for a copolymer with $\tau = 17\%$, $c_a = 5 \text{ ppm}$, $c_p = 500 \text{ ppm}$. The experiments show that instability is maximum at pH 4.7. The calculated fraction of carboxylate groups neutralized by the formation of a specie $\text{Al}(\text{COO})_3$ has also a maximum around the same pH. In fact, the good agreement between calculation and experiment is limited to low Al concentration, as we will see later.

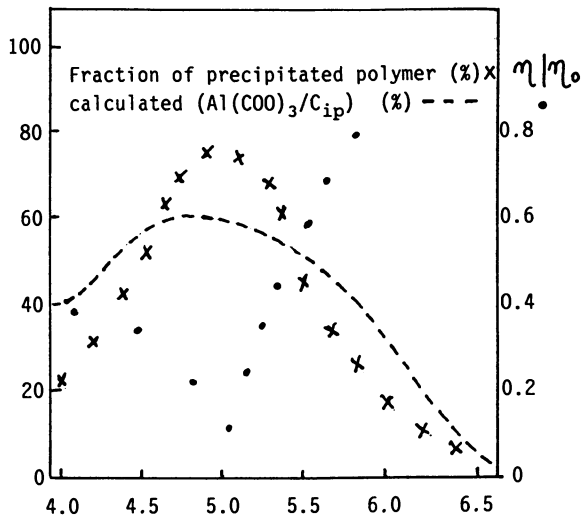


Figure 4: Phase titration of system AD27 (5 g/l) - Al (5 ppm)
(see test)

Turbidimetry and viscosimetry

In a second series of experiments, we have maintained the pH at two values 5 and 7 and changed the concentrations of Al and polymer.

i) "Unhydrolyzed" polyacrylamide ($\tau=0.3\%$)

No turbidity has been detected in the concentration ranges investigated. However the reduced viscosity η_{red} is a decreasing function of C_a at pH 5 and pH 7. This result shows that this polymer interacts with aluminium although no phase separation has been observed.

In fact this "unhydrolyzed" polyacrylamide sample is slightly charged and its low polyelectrolyte character is confirmed by a slight difference of η_{red} values at pH 7 and 5, for salt free solutions. A really neutral polymer should be necessary to differentiate low effects of electrostatic interactions from non ionic interactions, coordination binding at low pH and hydrogen bonds at pH 7. Nevertheless, at this pH, the adsorption of the chain on $Al(OH)_3$ aggregates can probably be considered as the main origin of the loss of viscosity.

ii) Copolymer of low acrylate content : AD10

The behaviors are quite different at pH 7 and pH 5

pH 5: we have observed the phase diagram represented in Figure 5 where three domains must be distinguished:

- domain A for $c_a < 7 * c_{ip}$: transparent solutions (both concentrations expressed in Mole/l)
- domain B for $c_p > c_p^*$ (c_p^* being the critical polymer concentration of chain overlapping) and $7 * c_{ip} < c_a < 10 * c_{ip}$: transparent gels
- domain C for $c_a > 10 * c_{ip}$: phase separation with dense microgels in equilibrium with solution.

In the domain A, η_{red} increases by increasing c_a and in the domain B the gel formation has been confirmed by measurements of elastic modulus. This phenomenon is due to the predominant presence of polynuclear ions of Al (see Figure 1). The pH range where gelation occurs is very narrow and at pH 4 and 6 only phase separations are observed.

Gelation does not occur for high content of NaCl (20 g/l): only phase precipitation occurs at higher values of c_a and can be attributed to the interactions with the $Al(OH)_3$ species.

pH 7: the turbidity of the solutions increases for aluminium concentrations higher than a limit c_a^* , indicating phase separation and this limit slightly increases with c_p . In the range of homogeneous solutions η_{red} decreases by increasing c_a . This polymer is then less stable than PAMNH with respect to $Al(OH)_3$ particles and this phase separation was not predicted by our electrostatic model.

iii) copolymers of $\tau > 7\%$ **pH 5 in pure water**

In the absence of added salts (NaCl) and in the whole ranges of pH and composition investigated, gelation has never been observed with copolymers of $\tau > 7\%$.

There is simply a domain ($c_a < c_a^*$) of transparent solutions and a domain ($c_a > c_a^*$) of phase separation. As shown in Figure 6 c_a^*

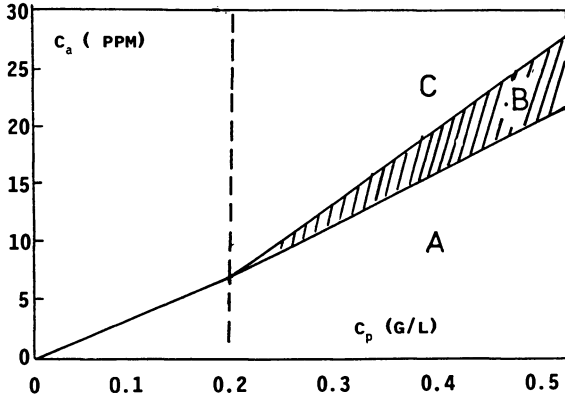


Figure 5 : Phase diagram of AD10- $ALCl_3$ at pH 5 in pure water

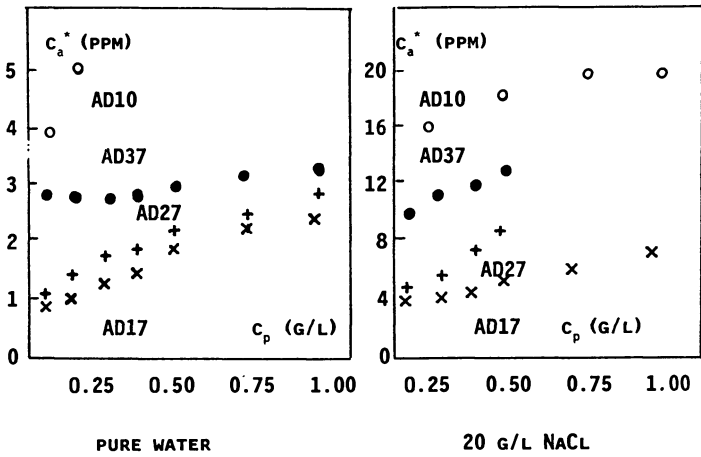


Figure 6 : Variations of c_a^n as a function of c_p at pH 5

slightly increases with c_p and also depend on τ . The polymer which appears to be the less stable is AD17. The values of c_a^* are very low ($< 3\text{ppm}$) and the phase separation is clearly due to the interactions with mononuclear trivalent ions Al^{3+} because they are preponderant at this Al concentration range.

Our calculation made for $c_a = c_a^*$ shows that phase separation begins when only 20 to 30% of the totality of carboxylate groups are neutralized but one can deduce from phase titration that, at c_a^* , only a low fraction of polymer is precipitated containing the major part of Al. These different observations reveal for the stability with respect to Al features very different from that defined with alkalino-earth cations. For instance, in the presence of Ca^{2+} , the order of stability is inverse: $\text{AD17} > \text{AD27} > \text{AD37} > \text{AD60}$ and the values of c_a^* are much higher(7).

The solution viscosity decreases in the presence of very low number of aluminium species (see examples on Figure 7). This decrease is observed even for $c_a < c_a^*$ when the solutions are still transparent and for all the values of c_p . The variation of η_{red} is found to be faster for the lower polymer concentrations.

pH-5 with added NaCl

The phase diagrams of AD17, AD27 and AD37 have been studied in the presence of 20g/l of NaCl. The same behavior as in pure water was found again for AD17, with higher values of c_a^* (see Figure 6). On the contrary, AD27 and AD37 are able to form gels for $c_p > c_p^*$ with phase diagrams quite identical to that presented in Figure 5 for AD10 in pure water. The gel domain corresponds to the same Al concentration range and gelation must also be attributed to polyions Al_{13}^{3+} .

In the case of AD17, only decrease of viscosity is observed while for $c_p > c_p^*$, the viscosity of AD27 and AD37 solutions measured at the newtonian plateau is an increasing function of c_a .

pH 7 in pure water

The stability of these copolymers is slightly better at pH 7 than at pH 5 (see Figure 8). For instance for AD37, at $c_p > 0.5$ g/l, separation begins for $c_a = 7$ ppm to be compared with 3 ppm at pH 5. Nevertheless, they are less stable than PAMNH and AD10 and the same order of stability is found: $\text{AD17} < \text{AD27} < \text{AD37}$. This confirms the role played by the electrostatic interactions.

Phase titrations have well confirmed that the precipitated phase contains polymer, then the turbidity cannot be due to a flocculation of $\text{Al}(\text{OH})_3$ particles without polymer adsorption.

pH 7 with added NaCl

As expected from electrostatic screening hypothesis, the addition of NaCl has an increasing effect on the stability (see Figure 8). Moreover, while c_a^* increases with c_p , in pure water, the reverse is observed at 20g/l of NaCl.

Discussion

pH 5

The comparison between phase diagrams and composition of AlCl_3 solutions shows that gelation occurs:

- if $c_p > c_p^*$
- when Al_{13}^{3+} polyions are present. It seems that the size of these ions (diameter 20 Å) favors intermolecular bridges: for the same

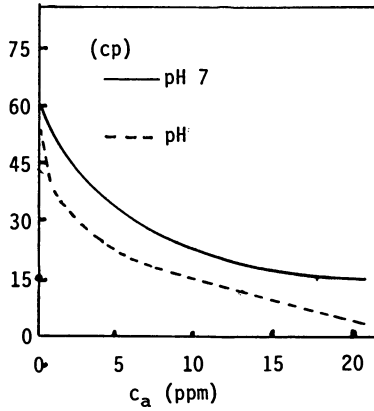


Figure 7 : Variations of the viscosity of the AD27 solution (0.5 g/l) as a function of c_a

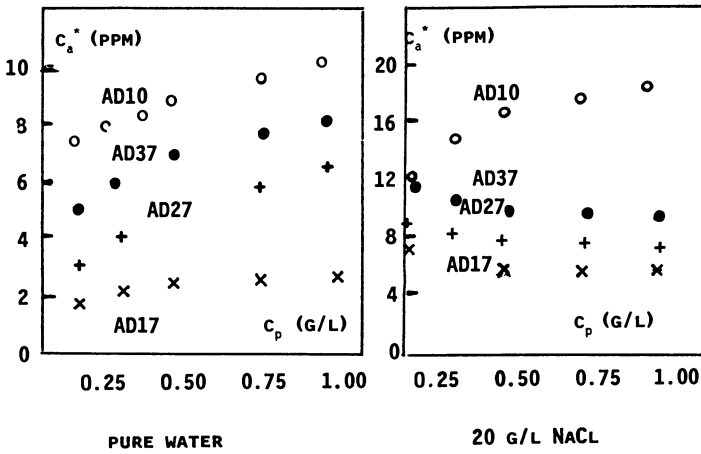


Figure 8 : Variations of c_a^* as a function of c_p at pH 7

calculated fraction of neutralized carboxylate groups, at lower pH, only phase separation is observed with mononuclear ions Al^{3+} .

-for a narrow range of hydrolysis degree depending on the ionic strength

-if the carboxylate groups are completely neutralized (results of our calculation and of electrophoresis measurements)(14)

We can then deduce that gelation requires well defined conditions corresponding to suitable respective probabilities of intra and intermolecular bridges:

-for $c_p < c_p^*$, in all cases only intramolecular bridges can be expected and then phase separation occurs when a fraction of carboxylate groups is neutralized at an Al concentration increasing with increasing salinity and effects of screening out of the electrostatic counter ions-polymer interactions. The same phenomenon was observed with Ca^{2+} cations(7).

-for $c_p < c_p^*$, the formation of intermolecular bridges becomes possible but it can lead to a tridimensional network only if the probability of intramolecular bridges remains lower than that of intermolecular ones: this is the case for $\tau > (1.5 + x)\%$, in pure water or $(7 + x)\% < \tau < (27 + x)\%$ for 20 g/l of NaCl (our studies do not allow us to precise the values of x and the exact limits). This means that the average distance between the dissociated carboxylate groups inside a chain must be of the same order of magnitude as the average intermolecular distance. This is realized only for slightly charged polymers in pure water, where all carboxylate groups are effective for fixation (case of AD10). This become possible in large excess of salt which acts by decreasing the number of groups able to bind AL counter ions : then gelation occurs for polymers of higher hydrolysis degree but disappears for AD10 because the binding is too weak and the number of bridges too low.

On the other hand ,a stable gel can only be formed if all the polymer charges are neutralized so that electrostatic repulsions of polymer segments between reticulation points are weak enough.
pH 7

The problem is slightly different since the size of $Al(OH)_3$ particles are much higher than that of Al_{13}^{3+} polyions. This is a problem of flocculation of charged particles by polymer of opposite charge. Nevertheless, it is well known that hydrogen bonds can be formed between hydroxyl groups of $Al(OH)_3$ and amide groups of the polymer(19).

If only electrostatic effects are responsible for polymer adsorption and flocculation, our results can be explained according to the same scheme as that used by Furusawa et Al.(20) to interpret the destabilization of negatively charged latex by a cationic polymer. In a first step, the adsorption of the polymer leads to the neutralization of the particles which are no more stabilized by electrostatic repulsions and there is flocculation (we have not studied this step since in our experiments polymer was always in large excess with respect to $Al(OH)_3$). In a second step the adsorption inverses the charge and (we have indeed measured by

electrophoresis a negative charge of the aggregates) the electrostatic repulsion is established again leading to the restabilization (c_a increases with c_p in pure water but there is screening out of this repulsion at high ionic strength). This could qualitatively explain the variations of c_a^* with c_p, τ and ionic strength.

In a second hypothesis, one can consider that the adsorption is mainly due to hydrogen bonds and that electrostatic attraction between polymer and particles only brings them together. In such case, the influence of c_p and τ on the stability should be related to the number of amide groups available for hydrogen bonds and the increase of salinity should lead to the collapse of the chain and reduce the probability of interparticles bridging. Only measurements of adsorption isotherms and determination of the conformation of the adsorbed chains could help the interpretation. One could indeed expect large loops in the first hypothesis and more flattened conformation if hydrogen bonds are predominant.

This work has benefited from grants from Institut Français du Pétrole and we thank Dr. J. Lecourtier and Dr. G. Chauveteau for fruitful discussions

Literature Cited

1. Mungan N. Soc. Pet. Eng. J. 1972 , 469
2. Nouri H.H.; Root, P.J. Paper SPE 3523 ,1971, SPE 46th Meeting
3. Martin F.D.; Sherwood N.S. Paper SPE 5339,1975, SPE Meeting
4. Muller G.; Lainé J.P.; Fenyo J.C. J. Polymer. Sc. 1979, 17,659
5. Truong N. Thésis 1984 University Louis Pasteur Strasbourg
6. Schwartz T.; François, J. Makromol. Chem., 1981, 182,2757
7. Truong N.; François, J. in "Solid-Liquid Interactions in Porous Media" Ed Technip Nancy 1984 p.251
8. Boutin J.; Contat S. French Patent,1980 n°249 217
9. Rabhari R.; François J. Polymer, 1988, 29, 845
10. Rabhari R.; François J. Polymer, 1988 , 29, 851
11. Bottero J.Y.; Cases J.M.; Fiessinger F. J. Phys. Chem., 1980, 84, 2933
12. Bottero J.Y.; Marchal J.P.; Cases J.M.; Poirier J.E. Bull. Soc. Chim. de France, 1982, 11,1439
13. Akitt J.W.; Farthing A. J. of Magn. Res., 1978, 32,345
14. R. Rabhari Thesis 1988 University Louis Pasteur Strasbourg
15. Bottero J.Y.; Tchoubar D.; Cases J.M.; Fiessinger F. J. Phys. Chem. 1984, 86,3667
16. Bale M.D.; Schmidt P.W. J. Phys. Chem., 1958, 11,1179
17. Strauss U.P.; Siegel A. J. Phys. Chem. 1963, 67,2663
18. Ikegami A.; Imai, N. J. Polym. Sci., 1962 , 56, 133
19. Pefferkorn E.; Nabzar L.; Carroy A. J. Coll. Interface. Sci., 1985, 106,96
20. Furusawa K., ; Kanesawa M.; Yamashita S. J. Coll. Interface. Sci., 1984, 99,341

RECEIVED February 2, 1989

Chapter 6

Gelation Mechanism of Chromium(III)

Paul Shu

Mobil Research and Development Corporation, Central Research
Laboratory, Princeton, NJ 08540

The chromium(III) ion is a common crosslinker of many polymer gels used in reservoir permeability profile control. It has been generally recognized that olated chromium(III) species are involved in the crosslinking, but the detailed mechanism is not fully understood. Also, Cr(III) salts and redox generated Cr(III) species do not always yield the olates. Furthermore, Cr(III) olates can vary greatly in their crosslinking reactivity and therefore result in gels of different properties. After studying the gelation of xanthan gum with various Cr(III) species ranging from simple salts to Cr olates of varying degrees of hydrolysis, we propose that the formation of Cr olates is the rate-determining step in a gelation reaction and the simple binuclear Cr olate is the most reactive species for crosslinking.

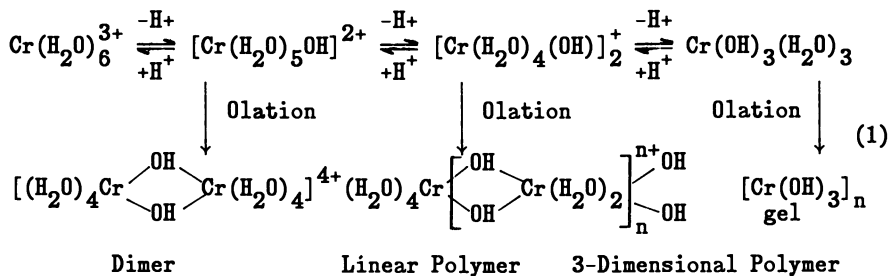
Chromium(III) is a commonly-used crosslinker for preparing profile control gels with polymers having carboxylate and amide functionalities (1a,b). Cr(III) is applied in many forms. For example, it can be used in the form of simple chromic salts of chloride and sulfate, or as complexed Cr(III) used in leather tanning (2), or as *in situ* generated Cr(III) from the redox reaction of dichromate and bisulfite or thiourea. The gelation rate and gel quality depend on which form of Cr(III) is used.

We have found that the Cr olates produced by hydrolysis of Cr(III) ions are the reactive crosslinking species. The different gelation rates are due to the different degrees of olation. Furthermore, by controlling the degree of hydrolysis, Cr(III) derived from various sources mentioned above can exhibit the same gelation rate.

Hydrolysis of Cr(III)

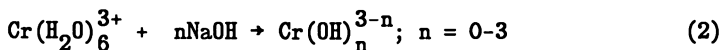
Due to the high charge-to-radius ratio, a hexaaqua Cr(III) cation loses protons to form olates (3a,b) in this hydrolysis process. One, two and three protons can be lost from Cr-coordinated H_2O to yield the mono-, di- and tri- hydroxides of hydrous Cr species,

respectively. These hydroxides then dimerize or polymerize to form Cr olates (Equation 1) through OH or "ol" bridges. Isolation and identification of dimer, trimer, and tetramer were reported by Stunzi and Marty (4a) and higher oligomers by Marty and Spiccia (4b).



The hydrolysis reaction is very slow at ambient temperatures and is accelerated by boiling chromium salt solutions (5). The hydrolysis reaction is characterized by the transformation of the deep blue colored $\text{Cr(H}_2\text{O)}_6^{3+}$ to green colored hydrolyzed olates. Another indication is that an aged or boiled Cr(III) salt solution has a higher neutralization equivalent than a fresh one due to the hydrolytically produced protons. One way to establish hydrolytic equilibria quickly is to add appropriate equivalents of bases such as NaOH to Cr(III) salt solutions.

Olated Cr(III) reagents were prepared according to Equation 2 by reacting $\text{Cr(NO}_3)_3$ with a calculated equivalent of NaOH. Chromic nitrate was used because the freshly prepared solution affords the hexaaqua Cr(III) cations.



The pH and UV-VIS spectral data are listed in Table I. For $n=3$, the product Cr(OH)_3 is a precipitate. Therefore, the UV-VIS spectrum of Cr(OH)_3 was not obtained.

Table I. UV-VIS of Olated Cr(III)*



	λ_1	A1	λ_2	A2	pH
n=0	406	1.367	574	1.159	2.48
1/3	410	1.551	576	1.256	2.66
2/3	414	1.811	578	1.372	2.78
1	418	2.080	580	1.498	2.87
2	420	2.75	584	1.837	3.25
3	NA	NA	NA	NA	4.89

*0.088M

A gradual shift of absorption maxima to longer wavelength and an increased absorbance were observed when Cr^{3+} reacted with more and more NaOH. The shift of peak position and the change in absorbance were also found by Ardon and Stein (6). The spectra of olated Cr prepared by us agree with the literature.

As increasing amounts of NaOH are added to the $\text{Cr}(\text{NO}_3)_3$ solution, the hydrolyzed Cr forms dimeric, polymeric and three-dimensional species. Gelled, amorphous and colloidal $\text{Cr}(\text{OH})_3$ is eventually formed. E. Matijevic reported the preparation of a monodispersed $\text{Cr}(\text{OH})_3$ sol by forced hydrolysis of Cr(III) salt at 90°C (7). Because of the differences in structural features, each olated species ($n=1,2,3$) should react differently with polymers and form gels of different properties.

Gelation Mechanism and Rate of Cr(III) Olates

The gel time of a 2000 ppm Flocon 4800 (a Pfizer xanthan polymer) in 2% NaCl solution was measured with various Cr(III) crosslinkers at room temperature (Table II). In this series of experiments Cr(III) concentration was 90 ppm. The most reactive Cr(III) species were olates derived from $\text{Cr}(\text{NO}_3)_3$ with one and two equivalents of NaOH. Gels formed within 5 minutes and the reaction rate appeared to be diffusion-controlled. $\text{Cr}(\text{NO}_3)_3$ without NaOH required 48 hours to gel the polymer solution. This reflects the time needed to hydrolyze $\text{Cr}(\text{NO}_3)_3$ in Equation 3.

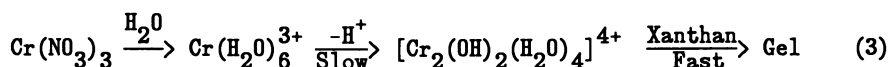


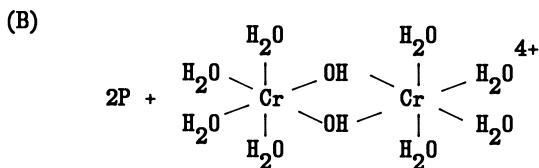
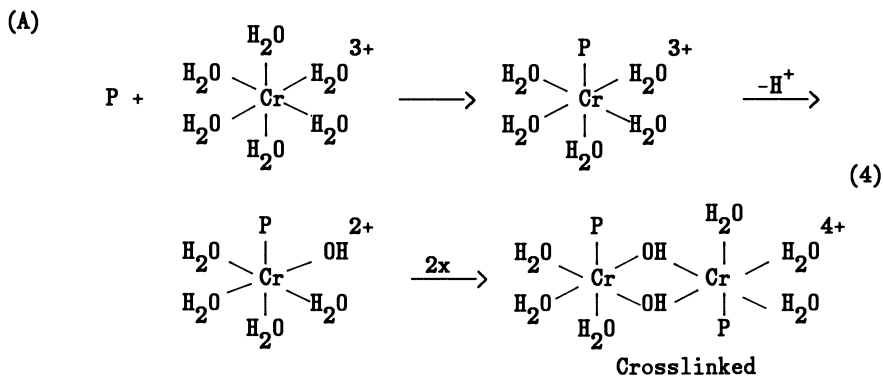
Table II. Variation of Gelation Time by Different Cr(III) Sources

Polymer = 2000 ppm Pfizer Flocon 4800 in 2% NaCl Cr = 90 ppm	
Cr Source	Gel Time
Simple Cr olate	
$\text{OH}^-/\text{Cr} = 1,2$	<5 Minutes
Cr(III) salts*	24-48 Hours
Redox Cr, $\text{Cr}_2\text{O}_7^{=}$ + $\text{S}_2\text{O}_5^{=*}$	1-2 Weeks
Hydrous $\text{Cr}(\text{OH})_3$ colloid	3 Weeks

*Without pH control.

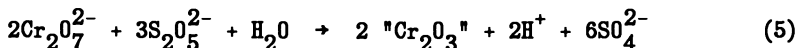
Since low pH suppresses this hydrolysis process, xanthan/NaCl mixtures with a pH lower than 3 did not gel at room temperatures for over a month. The $\text{Cr}(\text{OH})_3$ colloid formed by forced hydrolysis at 90°C (7) takes 3 weeks to gel the xanthan solution. This could be due to the slow dissolution of three dimensional networks of $\text{Cr}(\text{OH})_3$ by polymer ligands. These results strongly suggest that olates are the reactive crosslinking species and the hexaaqua Cr(III) is not. The crosslinking reactivities are about the same for the olates of various degrees of oligomerization. Because the rate of gelation decreases due to heterogeneous reactions and to the reduction of effective Cr concentration at higher degrees of polymerization, the dimeric olate should be the most effective crosslinker.

Prud'homme observed a second-order rate dependency of Cr in the gelation of polyacrylamide and redox-produced Cr(III) (9). He suggested that the binuclear Cr olate is involved in the crosslinking reactions. It was not determined whether the olation reaction of Cr occurred before or after the polymer ligands attached to Cr ions (Equations 4A and 4B). To determine this, we used $\text{Cr}(\text{NO}_3)_3$ and NaOH in 1:1 molar ratio to gel Flocon polymer with different mixing sequences. The mixing sequence markedly affected gel time. Based on the following observations, we strongly favor the "B" gelation scheme. Adding 90 ppm Cr olate prepared by pre-mixing $\text{Cr}(\text{NO}_3)_3$ and NaOH to 2000 ppm Flocon in 2% NaCl led to rapid gelation (<5 min). Adding $\text{Cr}(\text{NO}_3)_3$ to the polymer solution first and followed by adding an equivalent amount of NaOH resulted in a much slower gel time of 6 hours. Adding an equivalent amount of NaOH to the polymer solution and then $\text{Cr}(\text{NO}_3)_3$ resulted in a gel time of 1 hour. These results suggest that the reaction between the polymer ligand and Cr olate is much faster than that of forming Cr olate. Therefore the rate determining step is the formation of olate which involves deprotonation and dimerization. Since the gelation time of $\text{Cr}(\text{NO}_3)_3$ + polymer without NaOH is the longest (1-2 days) among the reaction schemes, the critical step of olation must be the deprotonation.



P = Polymer

Gelation Reaction of Redox Generated Cr(III)

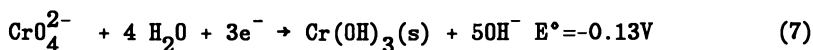
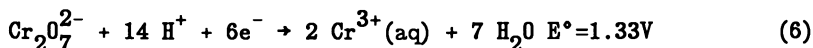


Gelation time of a 2000 ppm Flocon 2% NaCl solution with 90 ppm Cr(III) according to Equation 5 was 2 weeks (Table II), which is in the range of the Cr colloid gelation discussed earlier. Based on the earlier discussion, the gelation reaction of redox generated Cr(III) can also be accounted for with the olation mechanism. However it is

very important to have a better understanding of Cr(VI) \rightarrow Cr(III) reduction, since the reaction rate and the reaction product are highly dependent on the amount of acid present in the redox reaction.

The pH Dependence of Cr(VI) Reduction and Its Products

Chromate is a strong oxidizing agent in acidic media and produces Cr(III) ions in the hydrate form, Equation 6. In neutral and basic media, chromate is a rather weak oxidizer, as evidenced by its negative oxidation potential (Equation 7), and the product is chromic hydroxide (8).

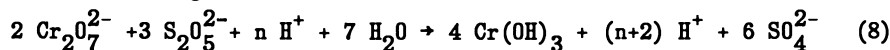


None of the Cr(III) products from Equations 6 or 7 are effective crosslinkers since a chromic aqua ion must be hydrolyzed first to form solated Cr to become reactive. Colloidal and solid chromium hydroxides react very slowly with ligands. In many gelation studies, this critical condition was not controlled. Therefore, both slow gelation times and low Cr(VI) \rightarrow Cr(III) conversion at high chromate and reductant concentrations were reported (9,10).

By adjusting the reaction pH, one can achieve a thermodynamically favorable redox reaction and produce reactive Cr olates in the dimeric or linear polymer forms for crosslinking.

Gelation Reactions by Acidity-Controlled Redox Reactions

The approach is based on proper control of the acidity of the redox reaction mentioned earlier. A general equation of the dichromate-disulfite reaction as a function of acidity is expressed in Equation 8 where Cr(OH)₃ and H⁺ are the hypothetical products.



The reaction of Cr(OH)₃ and H⁺ is the reverse of the hydrolysis of Cr(H₂O)₆³⁺ (Equation 1).³ Therefore by adjusting the acidity of the redox reaction (Equation 8), Cr olates of all oligomerizations can be prepared.

At HCl stoichiometries of n=0, 2, 6 and 10 (Equation 8), the reduction product showed wide variations in gelation reactivity (Table III). At n=2 and 6, the reaction products were very effective in gelling a 2000 ppm Flocon 4800 xanthan polymer because dimeric and linear polymeric Cr olates are formed. On the other hand, at n=0 and 10, gelation was very slow, because highly hydrolyzed material similar to Cr(OH)₃ is the product when n=0, and aqua ion of Cr(III) with blue color is the product when n=10. Furthermore, in the n=10 case, where no gelation occurred after 24 hrs, a gel formed in one hour after enough NaOH was added to yield the suggested dimeric Cr olate. All the above results have shown the importance of acidity in determining the reactivity of Cr(III) produced in a redox reaction.

Table III. Gelation by Acidity-Adjusted Redox Reactions

Polymer = Flocon 2000 ppm in 2% NaCl ; Cr(III) = 90 ppm

$$2\text{Cr}_2\text{O}_7^{2-} + 3\text{S}_2\text{O}_5^{2-} + n\text{H}^+ + 7\text{H}_2\text{O} \rightarrow 4\text{Cr}(\text{OH})_3 + (n+2)\text{H}^+ + 6\text{SO}_4^{2-}$$

nH ⁺	Cr (III) Product	Degree of Cr Polymerization	Gelation Time
0	Cr(OH) ₃	3-d Polymer	No gel in 2 weeks
2	Cr(OH) ₂ ⁺	2-d Polymer	5 Minutes
6	Cr(OH) ²⁺	Dimer	30 Minutes
10	Cr(H ₂ O) ₆ ³⁺	Monomer	2-3 Days

Similar species are formed from both the acid-adjusted redox and the Cr(III) salt - NaOH reactions. A comparison is given in Table IV. The pH of each corresponding pair at the same Cr concentration is very close, further supporting this theory. The UV absorption at ~400 nm of the redox products shifted to shorter wavelength when the starting redox mixture was made more acidic, suggesting that less hydrolyzed Cr was formed at higher acidity. This trend was observed in the preparation of Cr olates by the nNaOH + Cr(NO₃)₃ reaction (Table I).

Table IV. Similar Cr Olates Derived From Redox and From Cr(NO₃)₃ + xNaOH
Cr conc: 90 ppm

Redox Reaction		Cr(III) Product	Cr(NO ₃) ₃ + xNaOH	
nH ⁺	pH		pH	xNaOH
0	5.5	Cr(OH) ₃	4.9	3
2	3.6	Cr(OH) ₂ ⁺	3.3	2
6	2.8	Cr(OH) ²⁺	2.9	1
10	1.5	Cr(H ₂ O) ₆ ³⁺	2.5	0

Further Evidence on Acidity Influence of the Cr Redox Reaction

We noticed that the gelation of polymers by the redox method is promoted if 2-3 times the calculated molar ratio of thiosulfite is used (see half Equation 9 below). The gelation rate was very slow when x=1 or x=4 (Table V).

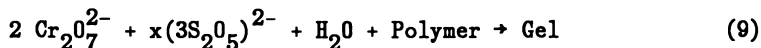
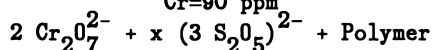


Table V. Gelation Rate as a Function of $S_2O_5^{2-}$ Concentration

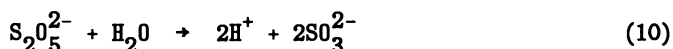
Polymer = 1500 ppm Flocon in 2% NaCl

Cr=90 ppm



x	Gel Time, hr.	Color of Reaction Mixture
1	No gel in 2 weeks	Yellow
2	4	Green
3	2	Green
4	24	Blue

Here, disulfite is functioning as a latent acid, releasing protons and bisulfite upon hydrolysis (Equation 10). At the proper proton concentrations, (x=2, 3), rapid Cr(VI) reduction and fast gelation take place. Therefore at x=2 to 3, the redox reaction should be the same as if acid were added at n=2 to 6 (Equation 9). The gelation reactivity of the two are comparable under these conditions.



At x=1, the redox reaction was very slow and the UV-VIS absorption showed no change with time. The orange - yellowish color persisted for weeks, indicating that there was little or no reduction (i.e., poor conversion) of Cr(VI). At x=4 or more, development of blue color occurred instantly, which is evidence of $Cr(H_2O)_6^{3+}$ production via the acidic redox mechanism. At x=2 to 3, the green color of olated Cr(III) developed in minutes, followed by gelation of the polymer.

Conclusions

- The reactive Cr(III) species in polymer crosslinking are the olates derived from the hydrolysis of hydrated Cr(III) cations.
- The rate-determining step is the deprotonation in the hydrolysis of the Cr^{3+} hydrate.
- In the presence of NaOH or other basic materials, dimerization to form olates becomes the rate-determining step.
- Various Cr(III) olates can be generated from the reduction of Cr(VI) by controlling the amount of the acid.
- The gelation mechanism of redox-Cr(III) follows the same pathway as Cr(III) salt gelation.

Acknowledgments

The author wishes to thank the management of Mobil Research and Development Corporation for permission to present this work. The diligent work of Marie J. Wszolek is greatly appreciated.

Literature Cited

1. (a) Abdo, M. K.; Chung, H. S.; Phelps, C.H.; Klaric, T.M. SPE/DOE Paper 12642, 1984.
(b) Hessert, J. E.; Fleming, P. D. 1979 Tertiary Oil Recovery Conf., Wichita, KS, Apr. 25-26, 1979; p 58-63.
2. Udy, M. J. Chemistry of Chromium and Its Compounds; Vol. 1, ACS Monograph Series No. 132, 1956; p 302.
3. (a) Bailar, J. C., Jr., Ed. The Chemistry of Coordination Compounds; Reinhold Publishing Co.: New York, 1986; Chapter 13, p 448-471.
(b) Colton, R. Coordination Chemistry Reviews 1985, 62, p 85-130.
4. (a) Stunzi H.; Marty, W. Inorg. Chem. 1983, 22, p 2145.
(b) Spiccia, L.; Marty, W. Inorg. Chem. 1986, 25, p 266.
5. Hall, H. T.; Eyring, H. J. Am. Chem. Soc. 1950, 72, p 782.
6. Ardon, M.; Stein, G. J. Chem. Soc. 1956 78, p 2095.
7. Popey, C. G.; Matijevic, E.; Patel, R. C. J. Colloid and Interface Science 1981, 80, No. 1, p 74.
8. Cotton, F. A.; Wilkinson, G. F.R.S., Advanced Inorganic Chemistry, Interscience Publishers, 1972; 3rd Edition, p 841.
9. Prud'homme, R. K.; Uhl, J. T.; Poinsette, J. P.; Halverson, F. Soc. Pet. Eng. J. 1983, p 804.
10. Southard, M. Z.; Green, D. W.,; Willhite, G. P. Paper 12638 SPE/DOE 4th Symposium on Enhanced Oil Recovery, Apr. 16-18, 1984, Tulsa, OK.

RECEIVED January 27, 1989

Chapter 7

Electron Microscopy of Xanthan

Topology and Strandedness of the Ordered and Disordered Conformation

Bjørn T. Stokke, Arnljot Elgsaeter, and Olav Smidsrød

Division of Biophysics and Division of Biotechnology, Norwegian Institute
of Technology, University of Trondheim, N-7034 Trondheim, Norway

Xanthan is a polyelectrolytic exopolysaccharide of potential interest for polymer flooding in high salinity and high temperature reservoirs. Optical rotation dispersion measurements reveal that xanthan undergoes a temperature- or salt-driven cooperative order-disorder conformational transition. Here we present electron micrographs of vacuum-dried and heavy-metal replicated dilute aqueous xanthan solutions. In the ordered conformation xanthan appears as highly elongated molecules with uniform thickness. Observed weight average contour length combined with experimentally determined molecular weight yield a mass per unit length of (1900 ± 200) Dalton/nm for xanthan from several different sources. This finding is consistent with xanthan being double-stranded in the ordered conformation. Electron micrographs of xanthan under disordering conditions show a mixture of species ranging from purely single- and perfectly matched double-stranded species, to double-stranded chains branching into their two subchains as well as different degrees of mismatched chains.

The usefulness of xanthan in polymer flooding for enhanced oil recovery is based on its ability to yield large increase in viscosity at low polymer concentrations under high-temperature and high salinity conditions. This important property of xanthan is determined both by its molecular weight and by the conformation adopted in solution (1).

Xanthan is reported to undergo a chiroptically detected temperature or salt-driven conformational change from an ordered conformation at high salt and low temperature to a disordered conformation either associated with lowering the salt concentration, or with increasing the temperature (2-5). The primary structure of xanthan has been known for about a decade (6,7), but different structures have been suggested both for the ordered and disordered conformation. Some workers (8-13) conclude that the ordered conformation is double-stranded or double-helix, whereas others (14-17) claim that a single stranded description can account for the observed data under

conditions where the ordered conformation is prevailing. For highly purified, low molecular weight xanthan ($M_w = 2 \cdot 10^5$ Dalton), it is reported using light scattering and intrinsic viscosity, that there are no major changes neither in M_w nor in hydrodynamic volume on going through the conformational transition in aqueous solution (18-20). For higher molecular weight species, the radius of gyration decreased while M_w remained essentially constant on passing through the conformational transition (19). Use of cadoxen as solvent yields disordering conditions reported (11,21) to give complete strand separation into single strands.

In this study we use electron microscopy (EM) to study xanthan strandedness and topology both in the ordered and disordered conformation. Correlation of data obtained from electron micrographs to physical properties of dilute aqueous solution on the same sample will be used to provide a working hypothesis of the solution configuration of xanthan. Electron micrographs obtained from xanthan of different origins will be compared to assess similarities and differences in secondary structure at the level of resolution in the used EM technique.

Materials and methods.

Xanthans from several different sources were used in this study: Xanthan samples A, B and C were kindly provided as freeze dried powder of ultrasonic degraded xanthan by Dr. B. Tinland, CERMAV, Grenoble, France. The molecular weights of these samples were determined experimentally in dilute solution by Dr. B. Tinland. Xanthan D was kindly provided as pasteurized, ultrafiltrated fermentation broth by Dr. G. Chauveteau, Institut Francais du Petrole, France. Xanthan E was kindly provided as a freeze dried sample from Dr. I. W. Sutherland, Edinburgh, Scotland. Xanthan F was obtained as a commercial, powdered material (Kelzan, Kelco Inc., a Division of Merck, San Diego CA.). Xanthan G was obtained as a commercial concentrated suspension (Flocon 4800, Pfizer, New York, NY)

Preparation for electron microscopy was carried out by first vacuum-drying dilute glycerol containing aqueous xanthan solutions. A volatile buffer, ammonium acetate, was used as supporting electrolyte to keep xanthan in the desired conformation and to avoid major changes in salt concentration during the vacuum-drying step. The dried preparations were then rotary replicated with Platinum at an angle of 6° . The contours of the visualized molecules in the electron micrographs were digitized and analyzed as described earlier (22,23).

Results

Ordered conformation. Figure 1. shows representative electron micrographs of samples A, B, C, and D vacuum dried from xanthan solutions under ordering conditions as specified in the legend. Xanthan samples A -D appear as unbranched, uniformly thick, convoluted chains. The contour length varies from molecule to molecule as expected for a polydisperse polymer. The electron micrographic

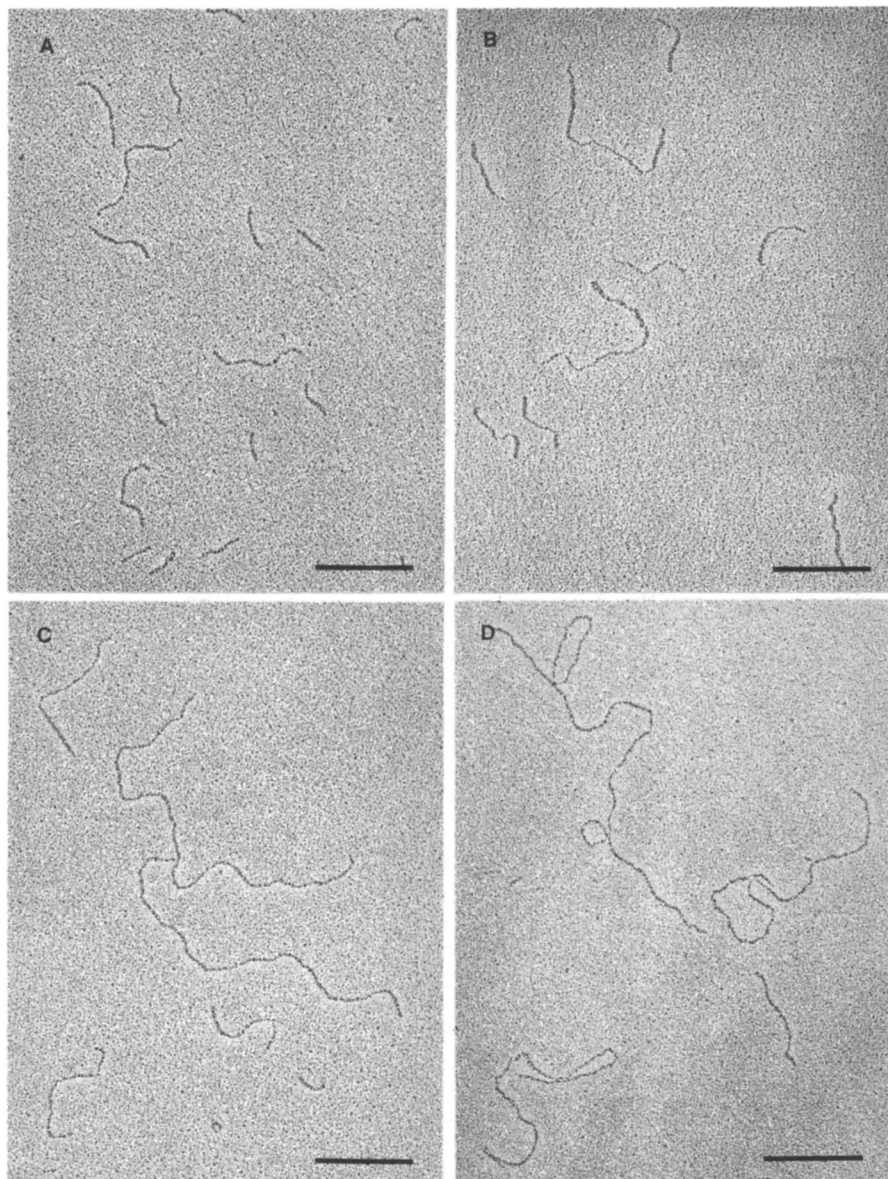


Figure 1. Electron micrographs of xanthan sample A (A), sample B (B) sample C (C) and sample D (D). The electron micrographs were obtained from replicas of vacuum dried solutions containing 100 mM NH_4Ac , 50% glycerol and 3 -10 $\mu\text{g}/\text{ml}$ polymer. Scale bar = 200 nm.

"snapshot" of the molecules reveals a curvature that varies along each polymer chain and is different from chain to chain. This is as expected for random-coil and worm-like polymers undergoing internal thermal fluctuations. Quantitative analysis of these electron micrographs show that the contour length distribution depends on weight average molecular weight determined by light scattering in dilute aqueous solution. Figure 2 shows the contour length distributions for samples A -D. Each contour length distribution is shifted on the ordinate according to its weight average molecular weight determined in dilute aqueous solution. Figure 2 indicates that the contour length distribution can roughly be described as a log-normal distribution. There is no indication of a bimodal distribution. The weight average molecular weight determined by light scattering divided by the weight average contour lengths yields estimates of the mass per unit length in the range 1750 - 2100 Dalton /nm (Table I) for all three xanthan samples (A-C). The estimated ML for the three samples are in the same range as observed for xanthan of other origins (Table II) using the same approach.

Table I. Molecular weights, contour lengths, and linear mass densities

Sample	Mw/10 ⁵	Ln (nm)	Lw (nm)	n	M _L = Mw/Lw (D/nm)	I _p = Lw/Ln
A	2.6	118	150	197	1730	1.3
B	6.5	235	337	184	1930	1.4
C	11.	352	558	160	1971	1.6

Mw is the experimentally determined weight average molecular weight in dilute aqueous solution.

Ln is the number average contour length from the EM data

Lw is the weight average contour length from the EM data

n is the number of molecules in the distribution

M_L is the apparent linear mass density

I_p is the polydispersity index.

Figure 3 shows an electron micrograph of a representative replica region of "native" xanthan E. This native xanthan (Fig. 3) contain a large number of aggregates, whereas after exposure to 80 °C for 2 months in synthetic brine (27) this sample reveals the general features of a polydisperse, uniformly thick worm-like polymer.

Figure 4 shows average end-to-end distance $\langle r^2 \rangle^{1/2}$ versus contour distance L for xanthan D, F and G obtained by quantitative analysis of electron micrographs. Electron micrographs of xanthan samples F and G are reported previously (22,25). The limiting slopes α , $\log (\langle r^2 \rangle^{1/2}) \sim \alpha \log L$ for $L > 300.0$ nm are observed to $\alpha = 0.69$ for xanthan D, $\alpha = 0.57$ for xanthan F, and $\alpha = 0.73$ for xanthan G.

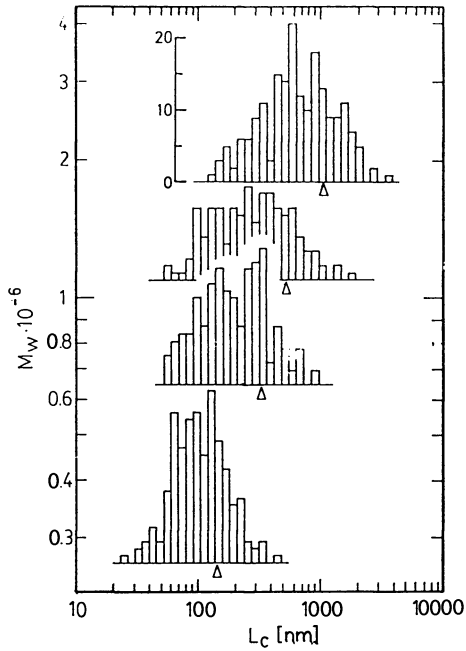


Figure 2. Contour length distributions obtained from electron micrographs of samples A, B, C and D (Fig. 1). The displacement along the y-axis of the contour length distributions corresponds to the reported M_w for each sample. The weight average contour length for each distribution is marked with an arrow.



Figure 3. Electron micrographs of native xanthan sample E. The electron micrographs were obtained from replicas prepared as described in Figure 1. Scale bar = 200 nm.

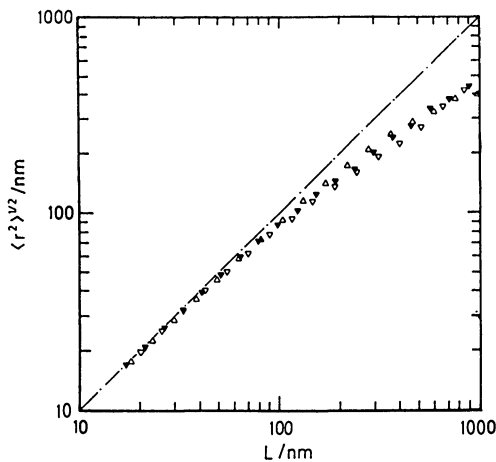


Figure 4. Average end-to-end distance $\langle r^2 \rangle^{1/2}$ versus contour distance L for xanthan from samples D (∇), F (\triangle) and G (\blacktriangledown) calculated from electron micrographs obtained as described in Figure 1. $\langle r^2 \rangle$ was averaged over a total contour distance of 123 μm , 162 μm , and 124 μm for samples D, F and G respectively.

Table II. Molecular weights, contour lengths, and linear mass densities of xanthan reported elsewhere

Sample	Mw/10 ⁵	Ln (nm)	Lw (nm)	M _L = Mw/Lw (D/nm)
D	18.	732	1050	1714
(ref. 26)	21.	671	1079	1946
(ref. 24)	20.3	578	1017	2000
(ref. 24)	5.7	157	238	2390
(ref. 24)	3.1	98.6	165	1880

Disordered conformation. Figure 5 shows electron micrographs of xanthan D and F obtained from xanthan vacuum-dried from solutions yielding the disordered conformation. The various molecular assemblies are assigned as follow: I = single -stranded, II = perfectly matched double stranded, III = branched from double - to single stranded. This assignment will be discussed below.

Discussion

Ordered conformation. The picture emerging from the electron micrographs of xanthan A, B, C and D is that of a highly elongated, uniformly thick, polydisperse polymer. The relation between solution configuration and the model proposed for xanthan D has been discussed in detail elsewhere (26). The electron micrographs further suggest a much higher degree of association in xanthan E before exposure to 80 °C than after (27). The electron micrographs cannot alone be used to determine whether xanthan of samples A, B, and C is double-stranded or single stranded because of potential decoration effects. However, contour length data from electron micrographs in combination with molecular weight of the same samples in solution yields estimated mass per unit contour length, ML, which for xanthan A - D range from 1700 Dalton/nm to 1970 Dalton/nm (Table I). X-ray fiber diffraction (28) yields axial translation of 0.94 nm per pentasaccharide repeat unit for xanthan corresponding to 950 Dalton/nm for a single- stranded molecule, slightly dependent on acetyl and pyruvyl substitution. The obtained ML therefore suggests a double-stranded configuration for xanthans A - D under ordering conditions. We use the notation double-strand rather than double-helix merely to point out that the resolution in the electron micrographs using the present preparation procedure can not distinguish between these two possibilities. Our working hypothesis that xanthans A, B and C are double-stranded is contrary to earlier interpretations of solution data of parallel preparations (29).

The native sample E (Fig. 3) contains a relatively large amount of aggregated structures. Most of them appear to rearrange into perfectly matched double-stranded chains after incubation at 80 °C for 2 months (27). This rearrangement is reported to result in a fivefold increase in the apparent viscosity at a shear rate of 1 s⁻¹ (27). A similar rearrangement of xanthan assemblies is also observed in a unpasteurized fermentation broth after exposure of the sample

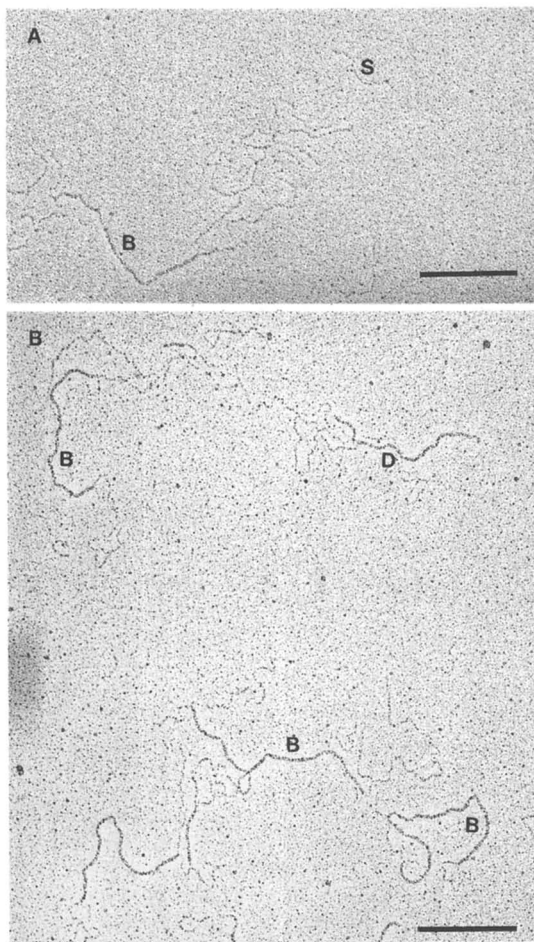


Figure 5. Electron micrographs of xanthan sample F (A), and D (B) obtained from replicas of xanthan vacuum dried from solutions containing 0.1 mM ammonium acetate, 50 % glycerol and 3 - 10 $\mu\text{g}/\text{ml}$ polymer. Specie designation: I = single-stranded, II = perfectly matched doublestranded, III = branching from double- to single-stranded. Scale bar = 200 nm.

to disordering conditions (10⁻⁵ M NaCl, T = 30 °C) at a low polymer concentration (26). The association of xanthan single-chains may result in a double-stranded configuration, or even higher molecular weight aggregates as exemplified in Fig. 3. There might be several factors affecting what structure will be the preferred one: polymer concentration, concentration of divalent ions, and kinetics in the order - disorder conformational transition. Based on model calculations, it can be shown that the perfectly matched double-stranded configuration corresponds to the lowest free energy (30). The aggregates observed in the native material can therefore at the low polymer concentration used in the preparation for electron microscopy be regarded as metastable state, kinetically trapped from the perfectly matched double-stranded configuration.

There appears to be close similarity between the observed scaling behavior of xanthans D, F and G (Fig. 4) indicating that the adsorption of all these xanthan types results in a comparable dimensionality change. However, some atypical chains with highly convoluted segments are occasionally observed in xanthan G. Because of difficulties in unique assignment of a polymer contour to these highly convoluted chains they were excluded from the quantitative analysis. The exclusion of the relative small number of atypical chains affects the scaling behavior of $\langle r^2 \rangle^{1/2}$ versus L only to a minor degree. Xanthan G did not appear to be as densely aggregated as xanthan E possibly because xanthan G was supplied as a concentrated fermentation broth and not as a dried material where more intermolecular association could have occurred.

Disordered conformation. The difference between Fig. 1 and Fig. 5 indicates that during the last stage of the vacuum drying from 10⁻⁴ M NH₄Ac there is not enough time for xanthan to rearrange to the state observed in Fig. 1. Although we use a volatile buffer, an increase in the salt concentration may occur during the vacuum-drying process resulting in a shift towards the ordered condition from the starting solution which corresponds to disordering conditions. The presence of glycerol slows down any tendency to conformational ordering because of increased solution viscosity. It is therefore likely that Fig. 5 reflects some aspects of the disordered state of xanthan, and below we will discuss molecular models suggested by the electron micrographs of the disordered form.

The electron micrographs in Fig. 5 reveal a mixture of molecular assemblies. These assemblies are assigned with a letter based on their thickness and on the following interpretation: Because the configuration under ordering conditions is shown to be double stranded, the observed branching into two thinner strands most likely corresponds to the two single-stranded subchains. The electron micrographs also show that the thin strands are more flexible than the thick ones. The thick strands have close similarity to those observed in electron micrographs prepared from solutions where xanthan is under ordering conditions. This is true both with respect to thickness and apparent tortuosity. Correlation between observed solution properties and the molecular models suggested by this type of electron micrographs is detailed elsewhere (26). Note that similar branching behavior is observed in the disordered conformation (Fig. 5) for xanthan D and G although xanthan D have been reported to be single-stranded (16) whereas

xanthan of the same origin as sample G has been reported to be double-stranded (9). The similar behavior of xanthan D and G in the disordered conformation is also consistent with xanthan D and G having similar ordered conformation.

Similarities and differences between xanthan of different origins. The linear mass densities of the xanthan samples A-C (Table I) are comparable with those obtained using the same method, for xanthan of two alternative sources (Table II). For these three origins, the linear mass densities of highly purified samples are all within experimental uncertainty of that of a double-stranded structure. Thus, the EM method in combination with a molecular weight moment (i.e. Mn from osmometry or Mw from light scattering) yields consistent results as far as the linear mass density concerns irrespective of the origin for these xanthans. This is contrary to interpretations of data obtained from solution properties, in which xanthans of origins A - C and D have been suggested to adopt a single-stranded conformation in the ordered state (16,28). The estimates of ML from the EM method is based on the ratio between a experimentally determined molecular weight average and the corresponding contour length average. Although the number of molecules are at least 10 orders of magnitude smaller in the data from the electron micrographs than the data from dilute aqueous solution, it is in principle possible to estimate contour length averages to be used in combination with any molecular weight average because the distribution is obtained.

In conclusion, we observe only minor differences in configurational properties of highly purified and post-fermentation processed xanthans from various sources. However, other workers have reported differences in physical properties among products of various origins (16,31). Our electron micrograph data on the native material and the observed effect of exposing native xanthan samples to high temperature suggest that differences among various products may reside in differences in post-fermentation processing rather than basic configurational features of xanthan. The forces stabilizing a double-stranded structure could well result in formation of more aggregated structures on double-strand formation at sufficiently high polymer concentration. At temperatures well below the transition temperature such aggregated structures would not dissolve when diluted. Increasing the temperature towards the transition temperature would lower the kinetic barriers needed to overcome to reach the most stable (double-stranded) conformation. The observation of aggregate hydration as a result of high temperature exposure is also supported by the work of Holzwarth and coworkers (33), who patented a method for improving filterability based on temperature treatment. This improved filterability probably arise from dissolution from aggregated molecules to dispersed ones under the temperature treatment.

Acknowledgments

Xanthan samples A, B and C was kindly provided by Dr. B. Tinland, Grenoble, France. Xanthan D was kindly provided Dr. G. Chauveteau,

Paris, France, Xanthan E was kindly provided by Dr. I. W. Sutherland, Edinburgh, Scotland. This work was partly supported by grant V6617 from The Norwegian Academy of Science and Letters.

Literature cited

1. Holzwarth, G.; *Dev. Ind. Microbiol.* 1985, 26, 271.
2. Rees, D.A.; *Biochem. J.* 1972, 126, 257.
3. Holzwarth, G.; *Biochemistry* 1976, 15, 4333.
4. Morris, E.R.; Rees, D.A.; Young, G.; Walkinshaw, M.D.; Darke, A.; *J.Mol. Biol.* 1977, 110, 1.
5. Norton, I.T.; Goodall, D.M.; Frangou, S.A.; Morris, E.R.; Rees, D.A.; *J. Mol. Biol.* 1984, 175, 371.
6. Jansson, P.E.; Kenne, L.; Lindberg, B.; *Carbohydr. Res.* 1975, 45, 275.
7. Melton, L.D.; Mindt, L.; Rees, D.A.; Sanderson, G.R.; *Carbohydr. Res.* 1975, 45, 245.
8. Holzwarth, G.; *Carbohydr. Res.* 1978, 66, 173.
9. Paradossi, G.; Brant, D.A.; *Macromolecules* 1982, 15, 874.
10. Sato, T.; Norisyue, T.; Fujita, H.; *Polymer J.* 1984, 16, 341.
11. Sato, T.; Kojima, S.; Norsiyue, T.; Fujita, H.; *Polymer J.* 1984, 16, 423.
12. Sato, T.; Norisyue, T.; Fujita, H.; *Macromolecules* 1984, 17, 2696.
13. Coviello, T.; Kajiwara, K.; Burchard, W.; Dentini, M.; Crescenzi, V.; *Macromolecules*, 1986, 19, 2826.
14. Muller, G.; Lecourtier, J.; Chauveteau, G.; Allain, C.; *Makromol. Chem., Rapid Commun.*, 1984, 5, 203.
15. Lambert, F.; Milas, M.; Rinaudo, M.; *Int. J. Biol. Macromol.* 1985, 7, 49.
16. Muller, G.; Anhourrache, M.; Lecourtier, J.; Chauveteau, G.; *Int. J. Biol. Macromol.* 1986, 8, 167.
17. Lecourtier, J.; Chauveteau, G.; Muller, G.; *Int. J. Biol. Macromol.* 1986, 8, 306.
18. Liu, W.; Sato, T.; Norisyue, T.; Fujita, H.; *Carbohydr. Res.*, 1987, 160, 267.
19. Hacche, L.S.; Washington, G.E.; Brant, D.A.; *Macromolecules*, 1987, 20, 2179.
20. Liu, W.; Norisyue, T.; *Int. J. Biol. Macromol.*, 1988, 10, 44.
21. Kitagawa, H.; Sato, T.; Norisyue, T.; Fujita, H.; *Carbohydr. Polymers*, 1985, 5, 407.
22. Stokke, B.T.; Elgsaeter, A.; Smidsrød, O.; *Int. J. Biol. Macromol.*, 1986, 8, 217.
23. Stokke, B.T.; Brant, D.A.; in preparation.
24. Kitamura, S.; Kuge, T.; Stokke, B.T.; in preparation.
25. Stokke, B.T.; Smidsrød, O.; Marthinsen, A.B.L.; Elgsaeter, A.; In *Water-Soluble Polymers for Petroleum Recovery*, Stahl, G.A., Schulz, D.N., Eds.; Plenum Press, New York, 1988; p. 243.
26. Stokke, B.T.; Smidsrød, O.; Elgsaeter, A.; *Biopolymers* 1988 (in press)
27. Stokke, B.T.; Kierulf, C.; Foss, P.; Christensen, B.E.; Sutherland, I.W.; in preparation.

28. Moorhouse, R.; Walkinshaw, M.D.; Arnott, S.; *Am. Chem. Soc. Symp. Series* 1977, 45, 90.
29. Milas, M.; Rinaudo, M.; Tinland, B.; *Carbohydr. Polymers*, 1986, 6, 95.
30. Washington, G.E.; Brant, D.A.; personal communication.
31. Morris, V.J.; Franklin, D.; l'Anson, K.; *Carbohydr. Res.* 1983, 121, 13.
32. Lange, E.A.; In *Water-Soluble Polymers for Petroleum Recovery*, Stahl, G.A., Schulz, D.N., Eds.; Plenum Press, New York, 1988; p. 231.
33. Holzwarth, G.M.; Naslund, L.A.; Sandvik, E.I.; U. S. Patent 4 425 246, 1984.

RECEIVED December 12, 1988

Chapter 8

Succinoglycan

A New Biopolymer for the Oil Field

Anthony J. Clarke-Sturman,¹ Dirk den Ottelander, and Phillip L. Sturla

Shell Research Ltd., Sittingbourne Research Centre, Sittingbourne, Kent,
ME9 8AG, United Kingdom

Succinoglycan, a microbially produced polysaccharide with an eight sugar repeating unit, has similar properties to xanthan, and has been successfully used in well completion fluids in the North Sea, where an apparently unique property -- partially reversible viscosity collapse, at a temperature, T_m , determined by the brine composition, was considered^m advantageous. This viscosity collapse is associated with a structural order-disorder transition, which in sea water occurs at around 75°C. (A similar transition, normally at a higher temperature, occurs in xanthan.) In calcium bromide brines, the T_m values of both succinoglycan and xanthan fall, leading to viscosity loss as both biopolymers are more readily degraded in the disordered state. Stability of both biopolymers can be improved by using brines based on potassium formate rather than calcium halides.

The oil price rises in the 1970s stimulated interest in Enhanced Oil Recovery (EOR), and fairly rapidly the biopolymer xanthan, the extracellular polysaccharide from the bacterium Xanthomonas campestris, an organism which normally resides on cabbage leaves, was identified as a leading contender as a viscosifier for polymer enhanced water flooding.

Xanthan, used in EOR trials in the USA, and still being considered elsewhere, has found a niche in drilling fluids, which, together with other oilfield uses, accounts for some 2000 tons per year. Xanthan solutions have several useful properties; they display a highly pseudoplastic rheology, are tolerant to salt, and have good thermal stability. There was we felt, however, some scope for improvement.

¹Current address: Shell International Petroleum Company, PAC/31, Shell Centre, London, SE1 7NA, United Kingdom

"Shell" and Biotechnology. Xanthan is manufactured by fermentation, a biotechnological process. How could "Shell", an oil company, be interested in such processes? The Royal Dutch/Shell Group is, however, no newcomer to biotechnology. The Milstead Laboratory of Chemical Enzymology was set up in 1962 and was headed by Professor John Cornforth, who went on to win the 1975 Nobel prize for Chemistry shortly after he retired. In 1970 a fermentation laboratory was built on the same site.

The first large scale process studied was the conversion of natural gas to 'single cell protein' for animal feed. Although technically successful, the project was finally defeated by a combination of high oil, (and gas), prices and cheap soya beans. It did, however, leave us with a strong background in fermentation technology and microbial physiology.

Work on the fermentation of microbial polysaccharides started in the mid 1970's, with the aim of producing improved polymers. Many thousands of samples were screened for microorganisms which produced viscous polymers. Out of over 2000 such 'slime producing' organisms isolated, only one, identified as a Pseudomonas species, now NCIB 11592, seemed to produce a polymer with interesting new properties.

Succinoglycan. Initially identified advantages of this polymer, succinoglycan, were that aqueous solutions of it were more viscous than solutions containing an equal concentrations of xanthan, and that the polymer tolerated higher concentrations of salt, in the sense that solutions passed more readily through microporous filters. These properties made the polymer of potential interest for EOR.

An interesting characteristic, however, was that at a particular temperature, often around 70°C in sea water for example, the viscosity would collapse, to be partially recovered on cooling.

Experimental

Polysaccharides. Many strains of bacteria produce succinoglycan (1). The Rhizobia, particularly, grow very slowly, and the rate of polymer production is low. Much effort was spent obtaining a strain which produced succinoglycan at a high rate and of good quality (2,3). An organism was selected and a fermentation process developed at laboratory scale. The process has been scaled up successfully and operated at 220 cubic metre scale.

Succinoglycan is now available commercially, in Europe, under the trademark Shellflo-S and as it is a concentrated solution rather than a powder, it readily disperses in brines commonly used in the oilfield.

Shellflo-XA, a proprietary grade of xanthan and cellobond X-100 a hydroxyethylcellulose (HEC) were used for comparative purposes.

Chemical analysis. Succinoglycan, purified by micro-filtration and dialysis, was hydrolysed in 0.5M sulphuric acid at a concentration of approximately 5mg/ml for 16 hours at 95°C. Sugars and acids were determined by HPLC using Biorad HPX-87 columns. No pretreatment was required for acids analysis - detection was by measurement of UV

absorption at 206nm. Sugars analysis required the neutralization of the solution with barium carbonate - detection was by refractive index measurement. Typically over 95% of the carbon in the original sample, which was determined by microanalysis, was recovered in the sugars and acids.

Hakomori methylation analysis, and preparation and GLC of the PAAN derivatives (4), were used to determine the linkages. ¹³C NMR of partially hydrolysed samples confirmed the octasaccharide repeat unit, the beta linkages and the presence of the carboxylic acids.

Rheological measurements. Routine viscosity measurements were made with a Wells-Brookfield micro-cone and plate viscometer, or a Brookfield LVT(D) viscometer with UL adapter. Viscosity-temperature profiles were obtained using the latter coupled via an insulated heating jacket to a Haake F3C circulator and PG100 temperature programmer or microcomputer and suitable interface. Signals from the viscometer and a suitably placed thermocouple were recorded on an X-Y recorder, or captured directly by an HP laboratory data system.

A number of other viscometers were also used, including Haake CV100 and RV3 models. The latter was coupled with a D40/300 measuring head and oil bath circulator for measurements above 100°C. Back pressures up to 4 bar were used and measurements made up to about 160°C.

Hydrolysis rate measurements. Hydrolysis rates were examined by mixing polymer solutions with hydrochloric acid, in apparatus previously described (5). Solutions of polymer and acid are mixed rapidly, and the torque on a rotating PTFE coated fork, attached to a Brookfield LVTD viscometer, recorded as a function of time. Decreases in viscosity were approximated to first-order, and half-lives for viscosity loss calculated.

Results and Discussion

Composition and Structure. Chemical analysis of the polymer from our first strain (NCIB 11592) indicated that it was a polysaccharide containing the sugars, glucose and galactose, and the carboxylic acids -- succinic and pyruvic -- in the approximate ratios 7:1:1:1. A similar polymer had been discovered some years earlier by Harada and his coworkers in Japan (6), produced by an organism which grew on ethylene glycol as sole carbon source. Almost simultaneous with our discoveries (2), the structure of succinoglycan, as the polymer was called, was published (7) (Figure 1).

Like all polymers, succinoglycan, is not a single polymer but a family. Succinoglycan is the extracellular water-soluble polysaccharide produced by a number of *Agrobacterium*, *Rhizobium*, and related species of soil bacteria. All have octasaccharide repeating units (Figure 1) with tetra-glucose units in side chains attached to tetrasaccharide main-chain repeating units, each containing a single galactose sugar. Pyruvic acid is bound as pyruvate ketal on the terminus of each side chain, and succinic acid is bound as mono-ester, at an unknown position or positions, as are acetate groups which are found in some strains.

We have examined succinoglycans from a number of bacteria. The polymers from different organisms have different proportions of acid substituents (Table 1). They also have slightly different physical properties, particularly viscosity (Figure 2). In some cases it may be useful to select a polymer with particular characteristics.

Rheology. The viscosity of dilute solutions rises rapidly with concentration (Figure 3). The rheology is, of course, pseudoplastic: the apparent viscosity falls with increasing shear rate. The viscosity of concentrated solutions, the commercial product for example, is, however, lower than might be expected from extrapolation of low concentration data. This is because, in common with many stiff or rigid molecules such as surfactants, a liquid crystalline phase is present. In succinoglycan the mesophase appears at concentrations greater than about 0.5 per cent w/v.

Comparison of Xanthan and Succinoglycan. The physical properties of succinoglycan and its solutions are similar to those of xanthan. Both polysaccharide molecules are relatively stiff, stiffer even than simple cellulosics such as HEC, and have a molecular masses in excess of two million. Recent work by Rinaudo and coworkers (Personal communication) and Crecenzi and colleagues (Int. J. Biol. Macromol., submitted) has shown that succinoglycan molecules are also stiffer than those of xanthan.

This greater stiffness is one reason why solutions of succinoglycan are more viscous than xanthan solutions of equal concentration. The stiffer the molecule, for a given molecular length, the larger the volume of solution that is swept out as the molecules rotate, and the greater the interaction with neighbouring polymer molecules. Such interactions begin to occur at quite low concentrations, much less than 1 g/l. If the interactions are 'sticky', that is, there is a long contact time, entanglement can occur leading to higher viscosities and ultimately a gel.

Entanglement and weak gel formation are characteristic of some oilfield polysaccharides such as guar and starch, but are present only weakly, if at all, in both xanthan and succinoglycan solutions. Solutions of xanthan and succinoglycan are thus able to pass through porous media such as rock, while guar and starch cannot because of their gel-like nature. Hence the different uses of these polymers in the oilfield.

Order-disorder Transition. In common with xanthan, succinoglycan exhibits an order-disorder transition, which in xanthan has been characterized by a number of techniques, including optical rotation and birefringence measurements (8). Viscosity measurements, as a function of temperature, can show the transition in xanthan (9), although the viscosity change is often small as the xanthan backbone is cellulose and still quite stiff. In contrast, however, the viscosity change in succinoglycan solutions is dramatic (Figure 4).

Effect of Temperature. The fall in viscosity usually occurs over a small temperature range, and to a level close to that of the solvent itself. The recovery of viscosity on cooling is partial (Figure 5)

Table 1. Composition of Succinoglycan from Different Strains

	Glucose	Galactose	Pyruvate	Acetate	Succinate
<i>Pseudomonas sp. NCIB 11592</i>	7	1.02	0.96	<0.3	1.08
<i>Pseudomonas sp. NCIB 11264</i>	7	0.94	0.91	<0.3	0.67
<i>Rhizobium meliloti K24</i>	7	1.00	1.00	1.20	1.65
<i>Rhizobium meliloti DSM 30136</i>	7	1.05	1.02	1.07	1.98
<i>Agrobacterium radiobacter NCIB 8149</i>	7	1.05	0.98	0.35	0.74
<i>Agrobacterium radiobacter NCIB 9042</i>	7	0.94	1.00	<0.3	0.57
<i>Agrobacterium tumefaciens DSM 3020B</i>	7	0.97	0.89	<0.3	0.51

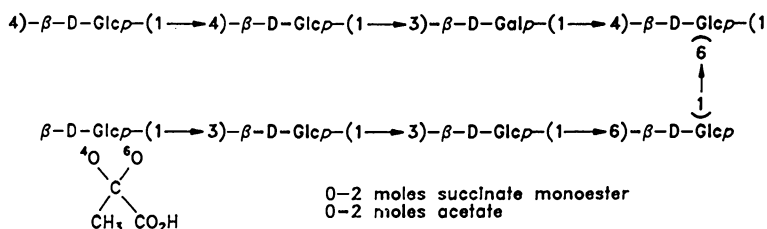


Figure 1. Structure of succinoglycan.

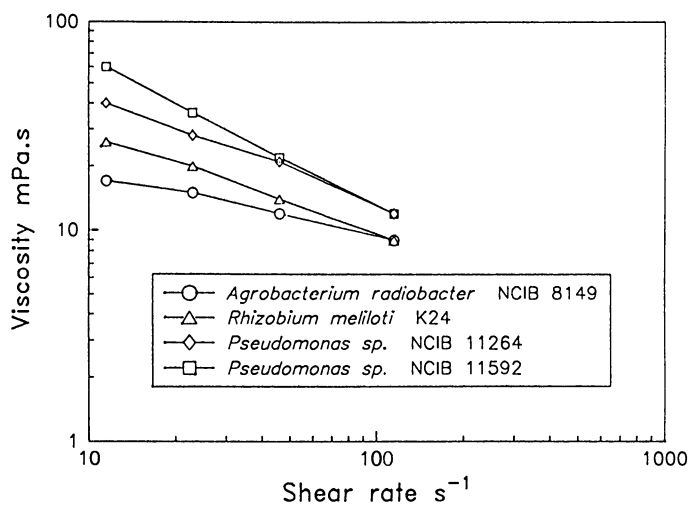


Figure 2. Viscosities of some succinoglycans.

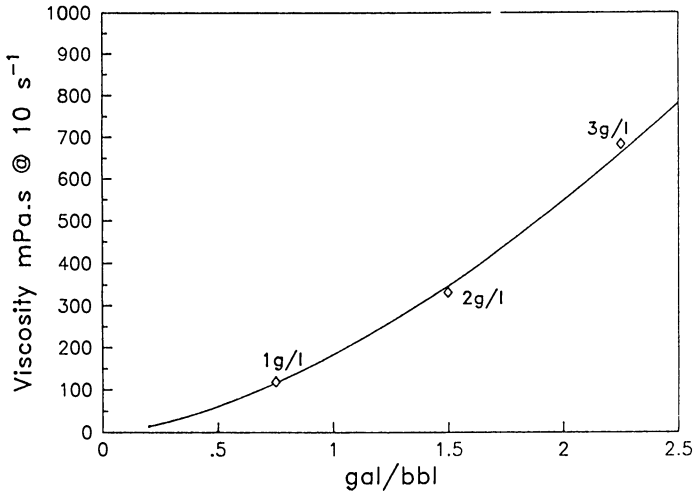


Figure 3. Viscosity as a function of concentration.

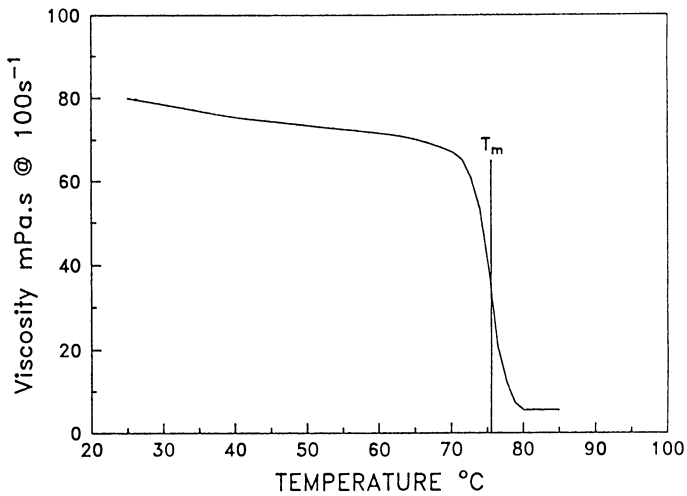


Figure 4. Viscosity of succinoglycan as a function of temperature.

and depends on the structure of the succinoglycan and the nature of the environment.

Transition Temperature. The order-disorder transition temperature mid-point T_m is also determined both by the environment - salinity, pH value, and the nature of the ions in solution, and the structure of the polymer - charge, pyruvate, succinate and acetate content. Most published work describes the low salinity behaviour of such polymers, and has shown that for xanthan, the transition temperature exceeds 100°C as the salinity exceeds about 1 per cent sodium chloride (10).

Salt Effects. In the low salinity region, the charge on the polymer determines the slope (Figure 6), and the acetate content changes the T_m by about 15°C per mole/repeat unit. We have obtained data for solutions of higher salinity. Not only have we looked at sodium chloride, but also salts such as calcium chloride and bromide which are used in heavy brines for drilling and workover operations.

The results (Figure 7), in this case for succinoglycan, are rather surprising. The transition temperature does not always increase or decrease as a function of the salt concentration, but rather, in some brines, a maximum value is reached after which the transition temperature falls with increasing salinity. This is particularly apparent for the two calcium salts, calcium bromide and chloride, both of which are used extensively in heavy brine drilling fluids.

One line, however, that of compound 'X', does increase steadily. It is significant, and we will return to it later.

We have examined a number of different salts and have shown that the transition temperature can almost be altered at will (12), in many cases in line with the Hofmeister or lyotropic series (13-15), a relationship found for many other aqueous systems such as hydrocarbon solubility and protein stability.

The viscosity of xanthan solutions in calcium bromide brines was also measured as a function of temperature. We found that the transition temperature fell rapidly as the concentration of salt was increased, so much so that above 2 molar it fell below that of succinoglycan.

Significance. What is the significance of these observations? For succinoglycan solutions the answer is obvious, above the transition temperature they have little or no viscosity, which may be undesirable. Such polymers are usually used as viscosifiers or for particle suspension. On the other hand, a drop in viscosity may be an advantage if fluid penetrates a formation hotter than the well as there could be little or no subsequent formation damage.

Degradation. There is, however, a second, more important, feature. Above the transition temperature we have shown that both xanthan and succinoglycan are more susceptible to degradation (5). This may be because the polymer side chains become dissociated from the main chain, in a similar manner to the unfolding of proteins. Viscosity changes, however, indicate that main chain linkages have become more

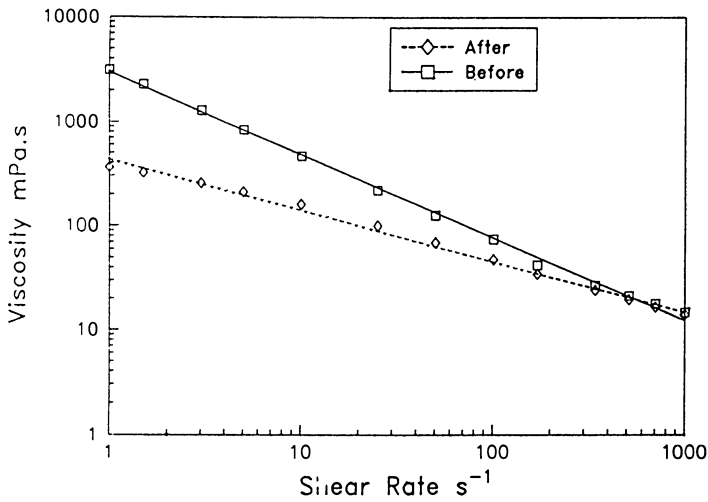


Figure 5. Viscosity of succinoglycan before and after heating.

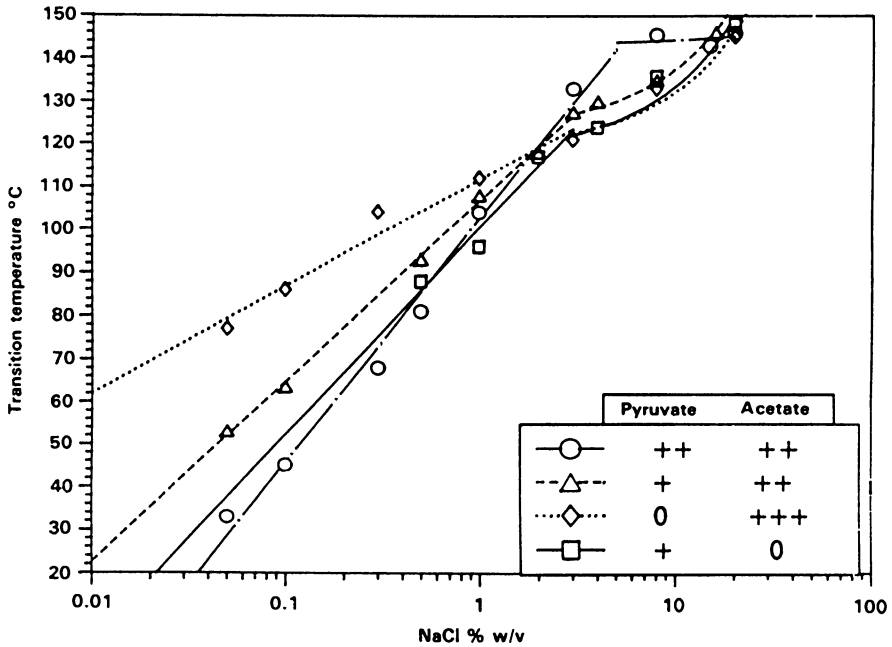


Figure 6. Transition temperature/salinity profile for a number of different xanthans.

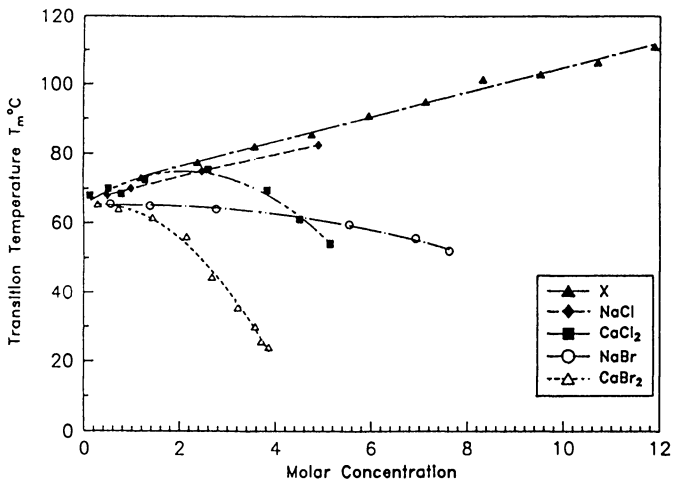


Figure 7. Transition temperature of succinoglycan in different brines.

mobile, perhaps leading to a lower activation energy for hydrolysis, and hence decreased stability. The main chain linkages also become more exposed.

Under many conditions, the viscosity of HEC solutions falls about 100 times faster than that of xanthan solutions. The rate of viscosity loss of Shellflo-S solutions, on the other hand is comparable with that of xanthan solutions at temperatures below the transition temperature, and comparable with that of HEC solutions above.

The relative stabilities of xanthan and Shellflo-S can be reversed. We have made measurements in a number of brines, including calcium bromide (5), and found that xanthan solutions were less stable than those of succinoglycan above about 400g/l (c. 2M).

Transition temperature and stability are, therefore, closely linked. The rate of viscosity loss of both xanthan and succinoglycan solutions increases about 100 fold as the molecules become disordered above T_m . This may be a problem, as some users of xanthan in heavy brines have discovered, but it can be used to advantage.

Well Completion. In well completions it is essential that clean fluids are used, otherwise the production zone can become blocked and oil and gas flows reduced. This is particularly important if the structure is tight. It is also important that the polymer degrades rapidly and leaves little or no residue.

The Troll field, in the Norwegian sector of the North Sea, is the tenth largest gas field in the world, and the biggest offshore in Europe. During the 1985 and 1986 drilling seasons, a formulation containing Shellflo-S was used in some 20 well completion operations. Mixing in the polymer was straightforward and the results were extremely favourable.

It seems probable that in this case the conditions were ideal for Shellflo-S. The water depth is in excess of 300 metres and the reservoir relatively shallow, with a bottom hole temperature of around 70°C, close to the transition temperature.

This combination of long riser and relatively shallow hole probably favours a polymer with a high pseudoplastic index - high viscosity at the low shear rate in the slow-moving fluid in the riser - and rapid, clean breaking at the well bottom temperature.

Such favourable conditions may not occur in many, or any other places. So, is the polymer a one field wonder? Probably not. It was mentioned earlier that it is possible to manipulate the transition temperatures of both Shellflo-S and xanthan by altering the brine. By this means the breaking of the polymer could be adjusted to the required value. The problem is that conventional heavy brines, such as calcium chloride and bromide, decrease the stability of these polymers, when just the reverse is often required, as heavy brines are generally used in deeper, hotter wells.

Increased Stability. Returning to Figure 7, we see that compound 'X' is able to increase the transition temperature substantially. This compound is potassium formate, which can be used at specific gravities up to 1.6. It is possible that, by using a brine based on formate, or perhaps some other salt, biopolymers such as Shellflo-S

and xanthan might be used more widely. We have recently shown (12) that most of the viscosity of a xanthan solution can be retained for up to 40 hours at 153°C in a formate based brine which has the same density as a calcium chloride brine in which xanthan is unstable.

Conclusions

Shellflo-S, succinoglycan is an interesting new polymer for use in the oilfield, in many ways complementary to xanthan. It is particularly appropriate for use in well completion fluids at moderate temperatures, where a more pseudoplastic rheology than that provided by HEC, and a more rapidly breaking polymer than xanthan is required.

The order-disorder transition temperature is a crucial parameter for biopolymers like Shellflo-S and xanthan, as it controls both rheology and breaking sensitivity.

Brine composition and polymer type should be considered together, and could lead to improved control of the viscosity of polysaccharide based drilling fluids.

Shellflo-S. In one area at least, biotechnology has something to offer the oil industry. Many of the polymers used in drilling fluids are based on natural products. They can be cheap like starch or guar or offer performance no synthetic can match, such as xanthan or succinoglycan. Shellflo-S is for use now in such areas as well completion, but more widespread use could follow if its particular range of properties are seen to be useful, and the cost of production is reduced.

Literature Cited

1. Zevenhuizen, L. P. T. M. In Industrial Polysaccharides; Stivala, S. S.; Crecenzi, V.; Dea, I. C. M., Eds.; Gordon and Breach: New York, 1987; pp 45-68.
2. Cripps, R. E.; Ruffell, R. N.; Sturman, A.J. European Patent 40 445 B, 1981.
3. Linton, J. D.; Evans, M. W.; Godley, A.R. European Patent 138 255 A, 1985.
4. Seymour, F. R.; Chen, E. C. M.; Bishop, S. H. Carbohydr. Res. 1979, 73, 19.
5. Clarke-Sturman, A. J.; Pedley, J.B.; Sturla, P.L. Int. J. Biol. Macromol. 1986, 8, 355.
6. Harada, T. Arch. Biochem. Biophys. 1965, 112, 65.
7. Harada, T.; Amemura, A.; Jansson, P. E.; Lindberg, B. Carbohydr. Res. 1979, 77, 285.
8. Milas, M.; Rinaudo, M. Carbohydr. Res. 1979, 76, 186.
9. Morris, E.R.; Rees, D.A.; Young, G.; Walkinshaw, M. D.; Darke, A. J. Mol. Biol. 1977, 110, 1.
10. Holzwarth, G. Biochemistry 1976, 15, 4333.
11. Holzwarth, G.; Ogletree, J. Carbohydr. Res. 1979, 76, 277.
12. Clarke-Sturman, A. J.; Sturla, P. L. European Patent 259 939 A, 1988.
13. Hofmeister, F. Arch. Exp. Path. Pharmacol. 1888, 24, 247.

14. von Hippel, P. H.; Schleich, T. In Structure and Stability of Biological Macromolecules; Timasheff, S. N.; Fasman, G. D. Eds.; Dekker: New York, 1969; Chapter 6, p 417.
15. Friedman, H. L.; Krishnan, C. V. In Water: a comprehensive treatise; Franks, F. Ed.; Plenum: New York and London, 1973; Vol. 3, p 1.

RECEIVED January 18, 1989

Chapter 9

Complex Copolymers for Mobility Control, Water Purification, and Surface Activity

John J. Meister and Chin Tia Li

Department of Chemistry, University of Detroit, Detroit, MI 48221-9987

Complex polymers containing different functional groups and structures with sharply different chemical and physical properties are needed to meet the varied and multifaceted demands of resource recovery. Simultaneously, the supply of oil on our planet is dwindling while the cost of this increasingly scarce resource must eventually go up. The price to use oil to recover oil will then become economically unjustified and additives or process chemicals that are produced from renewable resources will be the materials of choice. The polymers that can be converted to industrial process chemicals are described here and the chemistry that can convert two of these natural products, starch and lignin, to such chemicals is detailed. Synthesis, characterization, and testing of nonionic and anionic graft copolymers of starch show the products to be viscosifiers, drag reducing agents, and surface active agents. Synthesis, characterization, and testing of nonionic, cationic, and anionic graft copolymers of lignin show the products to be viscosifiers, thinning agents, drilling mud additives, and surface active agents.

Most polymers used in oil field operations and resource recovery are synthetic. The man-made materials in common use are: poly(1-amidoethylene) (= polyacrylamide), poly(1-amidoethylene-r-(sodium 1-carboxylatoethylene) (= partially hydrolyzed polyacrylamide), poly(1-amidoethylene-r-(sodium 1-(2-methylprop-1N-yl-1-sulfonate)amidoethylene) (AMPS-acrylamide copolymer), and xanthan gum. Xanthan gum is a synthetic because no one finds a pool or river contaminated with *Xanthomonas compestris* that experiences the right sequence of solute to naturally produce the exocellular gum polymer. A fermenter is a man made object, a tree is not.

The natural polymers in common use are: cellulose, lignin, chitin, starch and guar gum. The natural products had complete

control of the polymer market prior to 1930 but the greater effectiveness of synthetics produced at low cost from petroleum have sharply cut the market share of the natural polymers. This market shift can not be permanent since the growing scarcity of oil will sooner or later affect the price of petroleum-derived chemicals. While oil prices have dropped from 1982 to 1988, this has not added one drop of oil to the world's oil reserves. The price of all petrochemicals must rise in the future and, at that time, we must be ready to make greater use of the renewable sources of carbon that nature provides.

Energy, entropy, and economic considerations make it obvious that the easiest way to replace a synthetic polymer is to start with a natural polymer. The five natural polymers listed above can be used in one of four ways. These are:

1. Use the polymer directly;
2. Decompose the natural polymers into constituent chemicals and react these constituent chemicals into solvents, reagents, and monomers;
3. React the natural polymer to add small substituents to it, thereby forming a useful derivative; and
4. Form a graft, block, or interpenetrating network polymer from the natural polymer.

While the decomposition process of utilization method 2 will become more common in the future, most applications of natural polymers will be based on methods 1, 3, and 4 to make use of the chemical energy and physical structure stored in the molecule by the plant or animal. Current utilization, problems in utilization, and prospects or methods for the future use of the above, five natural products can be assessed on the basis of current technology. After discussing the nature, benefits, and features of all five natural polymers, this analysis will focus on developments in the formation of complex polymers from starch and lignin.

NATURAL POLYMERS.

CELLULOSE AND CELLULOSE DERIVATIVES. Cellulose is the most abundant of all the natural polymers and comprises at least 30 weight percent of the dry mass of all the vegetable matter in the world. The larger plants contain higher fractions of cellulose, so, on a dry basis, wood contains 40 to 50% cellulose(1). This is one of the few natural products that is currently being degraded into chemicals and feed-stocks (method 2). Cellulose is a linear molecule formed by the polymerization of a simple sugar, glucose. Due to very strong intermolecular and intramolecular hydrogen bonding, cellulose is insoluble in water. Water is unable to break these hydrogen bonds and enter into association with cellulose to dissolve it. Thus, to utilize cellulose in resource recovery, water-soluble cellulose derivatives are required. The water-soluble cellulose derivatives available are: sodium carboxymethyl cellulose (CMC,2), hydroxyethyl cellulose (HEC), and sodium carboxymethylhydroxyethyl cellulose (CMHEC) (1,2).

STARCH. Starches are used as components and/or processing aids in the production of resources such as aluminum, paper, copper, water, and oil. The use of this natural polymeric material is based on its

thickening, gelling, adhesive, and film-forming properties, as well as its low cost, controlled quality, and ready availability.

The characteristics of a starch can be modified by chemical, physical, and/or enzyme treatment to enhance or repress its intrinsic properties, or to impart new ones. This capability for modification has been a necessary factor in developing new uses for starch and in maintaining old markets.

There are five prime factors that determine the properties of starches: 1. starch is a polymer of glucose (dextrose); 2. the starch polymer is of two types: linear and branched; 3. the linear polymeric molecules can associate with each other giving insolubility in water; 4. the polymeric molecules are organized and packed into granules which are insoluble in water; and 5. disruption of the granule structure is required to render the starch polymer dispersible in water. The modification of starch takes into account these factors.

Starch is widely distributed as the reserve carbohydrate in the leaves, stems, roots, and fruits of most land plants. It is currently used directly after being separated from the plant as a thickener and dispersant (method 1). It is also used after being phosphorilated or digested (method 3) with several uses under investigation for graft copolymers of starch (method 4). The commercial sources are the seeds of cereal grains (corn, sorghum, wheat, rice), certain roots (potato, tapioca or cassava, arrowroot), and the pith of the sago palm. Since the growth conditions are different in each plant, the starch from each plant source will vary somewhat in appearance, composition, and properties. Consequently, the starch is described by its plant source as corn starch, potato starch, tapioca starch, rice starch, wheat starch, etc(3).

Chemical Composition. Starch is composed of carbon, hydrogen, and oxygen in the ratio of 6:10:5 ($C_6H_{10}O_5$), placing it in the class of carbohydrate organic compounds. It can be considered to be a condensation polymer of glucose and yields glucose when subjected to hydrolysis by acids and/or certain enzymes. The glucose units in the starch polymer are present as anhydroglucose units, the linkage between the glucose units being formed as if a molecule of water is removed during a condensation polymerization. Since the starch is formed in the plant by a biosynthetic process, the polymerization process is a complex one involving enzymes. The glucose units are connected through an oxygen atom attaching carbon atom 1 of one glucose unit to carbon atom 4 of the next glucose unit, forming a long chain or polymer of interconnected glucose units.

Molecular Structure. Most starches consist of a mixture of two polysaccharide types: amylose, an essentially linear polymer, and amylopectin, a highly branched polymer. The relative amounts of these starch fractions in a particular starch are a major factor in determining the properties of that starch.

Amylose. This linear polymer consists of a chain of glucose units connected to each other by 1-4 linkages. The glucose units are in the "alpha-D-glucopyranose" form. This means that the glucose is arranged in the form of a six-membered ring in such a way that the hydroxyl group on carbon atom 1 is on the same side of the ring as the hydroxyl group on carbon atom 2 . This spatial configuration of the alpha-glucose units in amylose differs from that of beta-glucose

units in cellulose where the beta configuration indicates that the hydroxyl group on carbon atom 1 is on the opposite side of the glucopyranose ring from the hydroxyl group on carbon atom 2. Thus, the link connecting the glucosidic oxygen atom to carbon atom 1 of the anhydroglucose units in the amylose chain has a different spatial relationship to the glucopyranose ring than the analogous link in cellulose.

Amylopectin. Amylopectin has a highly branched structure consisting of short linear amylose chains, with a segment chain length ranging from 12 to 50 anhydroglucose units and an average chain length of about 20 anhydroglucose units, connected to each other by alpha-1,6-linkages. These alpha-1,6-linked, anhydroglucose units make up about 4 to 5% of the total repeat units in amylopectin and are the branch points of the molecule. There is no single definite structure for amylopectin. The structure is therefore described in the statistical picture of its structural features and details(4-7).

LIGNIN. Lignin [8068-00-6] is a natural product produced by all woody plants. It is second only to cellulose in mass of polymer formed per annum(8). Lignin constitutes between 15 and 40 percent of the dry weight of wood with variation in lignin content being caused by growing conditions, species type, the parts of the plant tested, and numerous other factors(9). Plants use lignin to 1. control fluid flow, 2. add strength, and 3. protect against attack by microorganisms(10). Each cell of the plant grows its own lignin. The cell undergoes "lignification" in response to an internally-orchestrated series of reactions which take place all during cell differentiation (10). Lignin appears first in the primary (exterior) wall of the cell "corners". As the cell grows, lignin deposits throughout the primary wall and then appears in the secondary, interior wall of the cell. During this growth period, lignin deposits develop in the intercellular region, also. Lignin appears to be attached to the crystalline microfibrils of cellulose by phenylpropane linkages to carboxyl groups. Such a bond structure would be a uronic acid ester linkage (10).

Recent work by Atalla(11) supports the idea that lignin is at least a semi-ordered substance in wood with the plane of the aromatic ring parallel to the cell wall surface. Woody plants synthesize lignin from trans-coniferyl alcohol 1 (pines), trans-sinapyl alcohol 2 (deciduous), and trans-4-coumaryl alcohol 3 by free radical crosslinking initiated by enzymatic dehydrogenation(12). Structures of these alcohols are given in Figure 1.

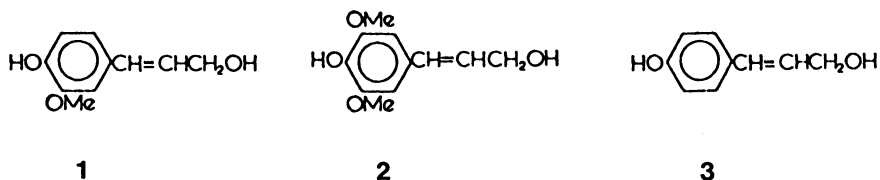


Figure 1. Structure of alcohols 1, 2, and 3.

Different ratios of these alcohols are used by different species of plants to form lignin, with the result that lignins from different sources will have different elemental and functional-group compositions. This alone would give lignin an extensive chemical diversity. Lignin recovery processes which extract lignin from wood, change the chemical composition of lignin and make this material extremely heterogeneous.

Methods for recovering lignin are the alkali process, the sulfite process, ball milling, enzymatic release, hydrochloric acid digestion, and organic solvent extraction. Alkali lignins are produced by the kraft and soda methods for wood pulping. They have low sulfur content (< 1.6 wt. %), sulfur contamination present as thioether linkages, and are water-insoluble, nonionic polymers of low (2,000 to 15,000) molecular weight. Approximately 20 million tons of kraft lignin are produced in the United States each year.

Recovery Methods. The sulfite process for separating lignin from plant biomass produces a class of lignin derivatives called lignosulfonates. Lignosulfonates contain approximately 6.5 weight percent sulfur present as ionic sulfonate groups. These materials have molecular weights up to 150,000 and are very water-soluble. Lignosulfonates are used in resource recovery as cement grouting agents, sacrificial agents in EOR, and thinning agents in drilling muds. The material is therefore directly utilized in energy recovery (method 1).

Milled wood lignin (MWL) is produced by grinding wood in a rotary or vibratory ball mill. Lignin can be extracted from the resulting powder using solvents such as methylbenzene or 1,4-dioxacyclohexane(13). Milling only releases 60 weight percent or less of the lignin in wood, disrupts the morphology of lignin in wood, and may cause the formation of some functional groups on the produced lignin(14). Despite these limitations, milling appears to be an effective way of recovering lignin from plants with only slight alteration. Enzymes which hydrolyze polysaccharides can be used to digest plant fiber and release lignin. After digestion, the lignin is solubilized in ethanol(15). Extensive analytical studies support the idea that enzymatically produced lignin has undergone no major modification in removal from plant material(16-20). Milling and enzyme release are not commercial methods to recover lignin at present but the commercialization of ethanol from biomass processes may make enzyme lignin available in large quantities.

Acid hydrolysis of the polysaccharide portion of wood will release lignin but also causes major condensation reactions in the product(21). These reactions can be minimized by using 41 wt. percent hydrochloric acid in place of other mineral acids but some condensation reactions still occur(22). This is not an effective method by which to obtain unaltered lignin. On the other hand, lignin can be solvent extracted from wood at temperature of 175°C using solvent mixtures such as 50/50 by volume water/1,4-dioxacyclohexane(23). Changes in lignin under these conditions appear to be minor.

Once lignin is separated from other plant products, it is not now widely used in resource recovery. Extensive studies on the modification of lignin have been made(24) because of the enormous mass of kraft lignin produced each year by the pulp and paper

industry. A major method of forming derivatives in the formation of graft copolymers of lignin, molecules in which a sidechain of synthetic polymer has been grown off of a lignin molecule. Graft copolymerization sharply changes the properties of lignin and allows useful products to be made from this waste biomass(25.)

CHITIN. Chitin is the exoskeletal polymer used by most anthropods for structural and protective body parts. It is available in large quantities but is difficult to use. The limited solubility of chitin in all but a few very special solvents and the very limited chemistry and technology available to alter chitin into useful materials has hindered the application of this material to articles of commerce.

GUAR GUM AND ITS DERIVATIVES. (26,27) This polymer is currently utilized by methods one (directly) and three (adding small functional groups to make a derivative) and this will most likely continue to be the case. Guar gum is derived from the seed of the guar plant, *Cyanopsis tetragonolobus* L. Grinding the endosperm of the guar bean produces relatively pure guar gum. The structure of guar gum is that of a branched polymer with the backbone of the polymer composed of mannose units and every other mannose unit having a galactose branch bonded to it. The two monomers - mannose and galactose - are simple sugars, and guar gum is termed a "polysaccharide" or, more specifically, a "galactomannan." There are no ions present in the polymer structure; thus, the polymer is termed "nonionic."

Treatment of guar with ethylene oxide, propylene oxide, and 2-chloroethanoic acid in alkaline medium results in formation of hydroxyethyl guar, hydroxypropyl guar, and carboxymethyl guar, respectively(26). Sequential treatment of guar with two of these chemical reagents can result in the formation of a "double derivative" such as carboxymethyl-hydroxypropyl guar.

Hydroxypropyl guar is the most widely available guar derivative. By controlling the moles of propylene oxide substitution per polymer chain, significant improvement of guar gum properties are observed. Broken hydroxypropyl guar gels contain no more than 2% insoluble residue(28). Hydroxypropyl guar hydrates more rapidly than guar gum in cold water and is more soluble in water-miscible solvents such as methanol, ethanol, and ethylene glycol. Hydroxypropyl guar has a somewhat greater high-temperature stability than guar and is more resistant to enzymatic degradation.

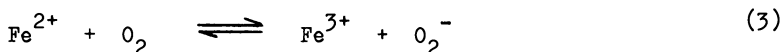
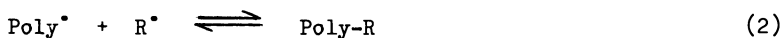
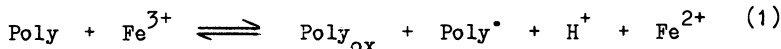
APPLICATIONS TO RESOURCE RECOVERY

Many processes that are basic to the extraction of natural resources are facilitated by addition of polymers. To be useful, the polymers must meet an interrelated list of chemical and physical properties as well as economic criteria. The chemical and physical properties demanded of the polymers are:

Solubility. Solubility in the primary process solvent is a mandatory criteria which is easily met in most extraction processes conducted in water.

Rheology. Polymers are often added to change solvent or process flow properties. The addition of polymers almost always causes nonnewtonian flow behavior in the resulting fluid.

Stability. Polymers must be chemically stable, mechanically stable, and thermally stable for long-term applications. Chemical stability to polymer chain scission can be built into the molecule by 1. increasing backbone bond strength, 2. attaching sterically hindering groups to the backbone to protect it, and 3. making a "ladder-backbone" polymer such as is shown in Figure 2. Typical reactions with the polymer which must be inhibited are illustrated by the redox degradation of a polymer by an iron/oxygen couple (29).



Stability of the polymer to mechanical forces is required because extension and shear forces exerted on the polymer tend to be concentrated, by slippage of the polymer chain, in the center of the molecule(30).

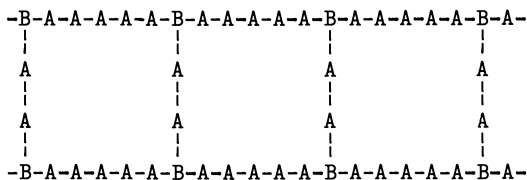


Figure 2. Ladder backbone copolymer.

A requirement that the polymer be thermally stable over a given range of temperature is actually just a demand for chemical stability as a function of temperature. As temperature increases, there is an exponential increase in the rate of any reaction. The reaction-specific temperature (T) at which a given reaction increases sharply in rate is given by

$$T = \frac{\Delta E_a}{R}$$

where ΔE_a is the energy of activation of the reaction and R is the gas constant (26,27).

Surface Behavior. Most extraction processes deal with several phases. At the boundaries between these phases, an interface exists which can be populated with or depopulated of polymer. Situations in which the polymer should accumulate at the surface of one phase are 1. the flocculation of clays and fines or 2. the formation of foams, while situations in which the polymer should depopulate the surface of the phase boundary are 3. minimizing adsorption in mineral acid leaching or 4. minimizing surface tension with surfactants in oil recovery by miscible flooding.

Methods of controlling surface behavior are to: 1. create polar and nonpolar regions in the molecule thus producing a hydrophilic-lipophilic balance in the molecule, 2. charge the

molecule by introducing ionic sites with the same or opposite charge as the boundary, or 3. introduce or remove functional groups in the molecule which produce binding reactions, such as a. hydrogen bond creation or b. nitrogen lone-pair donation, with the surface.

This multitude of properties the polymer must possess dictate that better polymer performance will be obtained from materials with complicated structures. Such polymers are complex polymers: 1) random copolymers, 2) block copolymers, 3) graft copolymers, 4) micellizing copolymers, and 5) network copolymers. There has been a dramatic increase in the past decade in the number and complexity of these copolymers and a sizable number of these new products have been made from natural products. The synthesis, analysis, and testing of lignin and starch, natural product copolymers, with particular emphasis on graft copolymers designed for enhanced oil recovery, will be presented.

COMPLEX POLYMERS FOR RESOURCE RECOVERY

Early applications of polymers to extraction processes were based on the ability of polymers to alter solution rheology. Pye(31) and Sandiford(32) showed that fluid mobility could be effectively reduced by the addition of small amounts of polymer to the solvent. Similarly, Thompson(33) showed that the addition of trace quantities of high molecular weight polymer to solvent reduced friction loss during turbulent flow of the solution. As knowledge of the characteristics needed to do more than change solution rheology grew, complex polymers were prepared and applied.

GRAFT COPOLYMERS. Goggarty was one of the first applications specialists to propose, in 1978, that graft copolymers be used for resource recovery(34). A number of such graft copolymers have now been made and tested and the knowledge gained about products based on lignin and starch will be summarized below.

STARCH GRAFT COPOLYMERS.

Several groups have conducted graft copolymerizations on starch or its purified components, amylose and amylopectin. The syntheses are based on attack of the anhydroglucose unit of starch by cerium (+4) ion. The free radical produced from this attack is then immersed in a monomer solution polymerizable by free radical, chain polymerization and a graft copolymer is formed. This reaction apparently occurs by the formation of a chelate between the cerium (+4) ion and the hydroxyl groups on the number 2 and 3 carbon atoms of the anhydroglucose ring(35-40). This mechanism is not completely confirmed for starch because the investigations on cerium (+4)-polysaccharide reactions were done on cellulose, not starch. Cellulose has an axial-equatorial positioning of the hydroxyl groups on the number 2 and 3 carbon atoms of the repeat unit while starch has these hydroxyl groups both equatorial. These structures are shown in Figure 3. This means that it is possible that the space between the two hydroxyl groups in starch and cellulose may differ enough to cause a different initiation mechanism in the two products. If the same chemistry applies to both molecules, the complexed cerium (+4)

ion executes an oxidation-reduction reaction to convert one hydroxyl group to a carbonyl group and break the 2-3 carbon-carbon bond. This is shown in Figure 4. The free radical may then react with monomer or engage in termination of crosslinking reactions.

Synthesis. Graft copolymer was formed in aqueous solution by ceric-ion-initiated, radical polymerization of monomer on starch. Polymerization was conducted in an inert, N₂ atmosphere. Details of the synthesis procedure may be found in references 41 to 43. In recovering the polymer product, freeze drying was used with care since freeze drying produces a more dissolvable and useful product but can degrade polymers with molecular weights of 1 million or more. Poly(starch-g-(1-amidoethylene)) Poly(starch-g-(1-amidoethylene)) copolymers can be made by ceric-ion-initiated, free radical polymerization of 2-propenamide on starch(41-43). At monomer concentrations in the synthesis mixture of 1.5 m or more, this reaction produces a water-soluble viscosifier with thickening capacity above that of poly(1-amidoethylene), the homopolymer of 2-propenamide. This graft copolymer is readily made. Yields of product are 90 wt % or above(44) and high-molecular-weight samples are made by using molal concentrations of 1.5 or above to insure gelling of the sample during polymerization. The copolymers are good drag reducing agents for promoting pipeline flow(45). Data demonstrating drag reduction by parts-per-million concentrations of these polymers is given in Table 1. Drag reduction tests were run by connecting a 50 mL buret to 2 meters of 0.318 cm o.d. nylon tubing and flowing water by gravity pressure from the vertically held buret through the horizontally held tubing. Passage time measured in this experiment was the time taken for 20 mL of fluid to pass from the buret to the tubing as measured by the movement of the fluid meniscus between the 1 mL and 21 mL marks on the buret. Passage time measurements were then used to calculate percent drag reduction from the equation

$$\% \text{ Drag Reduction} = 100*(t_w - t_p)/t_w \quad (4)$$

where t_w = average efflux time for water, and t_p = average efflux time for polymer solution. Drag reductions of more than 17 percent were achieved with concentrations of polymer of 3 to 4 ppm by weight. Some unpublished work has been performed in industrial laboratories to determine if these copolymers are effective beneficiating agents for bauxite ore.

TABLE 1. Reduction of Drag in the Flow of Water Caused by the Addition of Starch-1-amidoethylene copolymer

Sample Number	Fluid	Graft Copolymer Concentration (wppm)	Passage Time ¹ (second)	Percent of Drag Reduction (%)
32	water	0	35.63 ± 1.11	0
33	Copolymer Solution	3.72	29.3 ± 0.49	17.75
34	Copolymer Solution	6.10	33.5 ± 3.35	6.02

¹Passage times given are the means of 4 determinations.

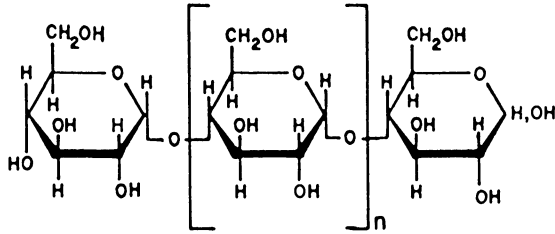


Figure 3. Positioning of hydroxyl groups.

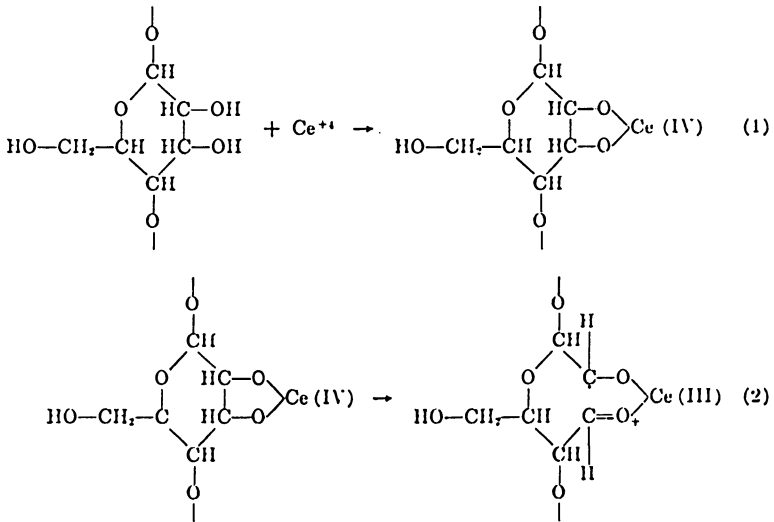


Figure 4. Initiation mechanisms in starch and cellulose.

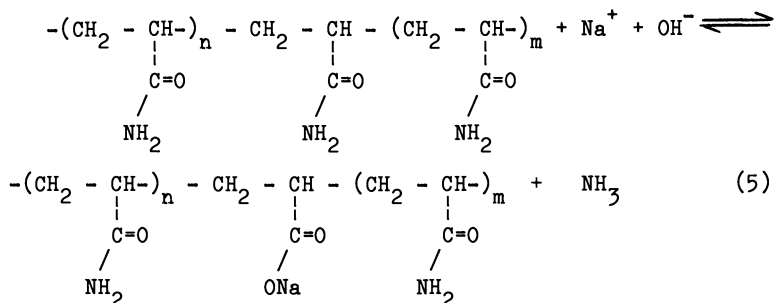
Poly(starch-g-((1-amidoethylene)-co-(sodium 1-carboxylatoethylene))). Poly(1-amidoethylene) is, however, rarely used as a viscosifier. Instead, the homopolymer is reacted with base (hydrolyzed with NaOH) to convert some of the amide units of the polymer to carboxylic acid units. The acid units on the hydrolyzed polymer dissociate in water and produce a polyanionic polymer. This polyelectrolyte expands in water because of ion-ion repulsion and, as an enlarged molecule, is a better viscosifier.

Poly(starch-g-(1-amidoethylene)) copolymer is not a polyelectrolyte and will be a smaller molecule in water than an equal molecular weight, partially hydrolyzed poly(1-amidoethylene). Polyelectrolyte effect should, however, cause the graft copolymer to expand in solution in the same way it causes poly(1-amidoethylene) to expand, so a series of hydrolyzed graft copolymers were prepared from poly(starch-g-(1-amidoethylene))(41-43) and these derivatives were tested to determine the effect of hydrolysis on copolymer properties in solution.

In the following sections, synthesis of the anionic polymers, copolymer molecular weight, limiting viscosity number, electrolyte effects, solution shear thinning, screen factor, polymer radius of gyration, and solution aging will be discussed and data on the copolymers presented.

Materials. Deionized-distilled water was used for all syntheses and distilled water was used in all solutions. All salts were reagent grade and were used as received. Dialysis membrane was Spectrapor no. 2, 12,000 upper molecular-weight-cutoff membrane from Spectrum Medical Industries, Los Angeles, CA.

Hydrolysis. The starting material for the hydrolysis reaction is a 2.0 g sample of previously prepared, graft copolymer(41,42). The copolymer is hydrolyzed in a basic, saline, aqueous solution under anaerobic conditions. Sufficient copolymer is dissolved in sufficient sodium chloride brine to form a combined, final reaction mixture of 2 g/dL copolymer in 1.0 M sodium chloride. Sufficient sodium hydroxide is dissolved in water to yield a final concentration in the combined reaction mixture of 0.5 M. The solutions are saturated with nitrogen, warmed to 40°C, combined, and allowed to react with stirring for 10 minutes under a nitrogen blanket.



The reaction vessel is then packed in ice and the reaction mixture is neutralized to pH 6.5 to 7.0 with aqueous hydrochloric acid. The neutral solution was dialyzed against nitrogen-saturated, distilled water for two days. The polymer solution is precipitated in a 5- to

10-fold excess of vigorously stirred 2-propanone. The precipitated copolymer is filtered from the 2-propanone, slurried in 2-propanone, filtered, and vacuum dried to constant weight. Alternatively, the dialysis solution can be freeze dried to constant weight. Freeze drying produces a more dissolvable and useful product but can degrade polymers with molecular weights of 1 million or more(46). During hydrolysis, exposure of the copolymer to oxygen or acid will result in immediate cleavage of the polyglucoside backbone.

Assays. Nitrogen assays to determine 1-amidoethylene unit content were done by Kjeldahl method. Limiting viscosity numbers were determined from 4 or more viscosity measurements made on a Cannon-Fenske capillary viscometer at 30°C. Data was extrapolated to 0 g/dL polymer concentration using the Huggins equation(44) for nonionic polymers and the Fuoss equation(45) for polyelectrolytes. **Equipment.** Viscosities were measured using Cannon-Fenske capillary viscometers and a Brookfield LV Microvis, cone and plate viscometer with a CP-40, 0.8° cone. Capillary viscometers received 10 mL of a sample for testing while the cone and plate viscometer received 0.50 mL.

Results and Discussion. Of the 12 samples of starch graft copolymer synthesized, half were hydrolyzed to anionic polyelectrolytes. Synthesis data on these 6 samples are given in Table 2. These particular samples were chosen for hydrolysis because the samples can be intercompared to see the effect of synthesis variables on ultimate product properties. Samples 5, 8, and 11 have the same mole ratio of cerium ion to starch backbone, N_{ce} , in their reaction mixture. Samples 7, 8, and 9 all have the same reactable mass per starch molecule, M_{gal} , in their reaction mixtures. In general, as the mass fraction of hydrolyzable sidechain in the graft copolymer increases, the degree of hydrolysis produced by treatment with base increases. Sample 11 is an exception to this rule.

TABLE 2. Hydrolysis of Graft Copolymers to Anionic Terpolymers

Sample Number	Nitrogen Content (wt.%)		Degree of Hydrolysis (number %)	1-amidoethylene Repeat Units (wt. %)
	Before Hydrolysis	After Hydrolysis		
5*	12.24	11.10	9.31	62.04
7	14.82	12.82	13.50	75.11
8	14.85	12.93	12.93	75.27
9*	14.24	12.20	14.33	72.17
10*	15.17	9.64	36.45	76.89
11	14.71	14.14	3.87	74.56

a) Sample numbers are identical to those in previous publications on these compounds (41,42,43,48).

*Hydrolysis data determined from repeated hydrolysis reaction.

Limiting Viscosity Number. Limiting viscosity numbers for the polymers in distilled water are given in Table 3. Limiting viscosity number increases with increasing copolymer molecular weight. Further, after 12 to 14 percent hydrolysis, limiting viscosity number of the derived, partially-hydrolyzed copolymer is 3 to 10 times larger than that of its nonionic precursor. The ratio of $[\eta]$ after

hydrolysis to $[\eta]$ before hydrolysis decreases with increasing weight percent sidechain in the copolymer. Limiting viscosity number ratio is not clearly correlated with molecular weight or degree of hydrolysis, however.

TABLE 3. Limiting Viscosity Numbers for Complex Copolymers in Water and Electrolyte Solution

Sample Number	Limiting Viscosity Number in Distilled Water			Limiting Viscosity Number in 1.0 Molar Sodium Nitrate	
	$[\eta]$ Graft Copolymer	$[\eta]$ Hydrolyzed Graft Copolymer	Weigh Avg. Molecular Weight $M_w \cdot 10^{-6}$	$[\eta]$ Graft Copolymer	$[\eta]$ Hydrolyzed Graft Copolymer
5	3.99	39.48	0.701	3.17	5.00
7	4.12	27.00	2.06	3.32	6.85
8	5.84	25.96	1.19	4.69	6.08
9	6.95	23.29	1.74	5.68	5.58 ^a
10	11.83	48.98	1.00	9.94	7.90 ^a
11	12.18	28.64	3.71	10.03	3.69 ^a

^aPartially degraded during hydrolysis.

Screen Factor. Screen Factor, the ratio of passage time of a solution to that of a solvent in a screen viscometer(45),

$$\text{Screen Factor} = \frac{(\text{Solution Passage Time})}{(\text{Solvent Passage Time})} \quad (6)$$

measures the relaxation time, ϕ , and viscosity, η , of the solution. A screen viscometer produces a flow controlled by the viscoelastic properties of the fluid. The following equation,

$$[f_1(\rho, S, \phi) + f_2(\eta, \phi)] * (dh/dt)^2 + f_3(S, \phi) * (dh/dt) + h = 0 \quad (7)$$

where $f_i(x)$ and constants are defined in reference 43, shows the influence of each fluid property on the change of height with respect to time (t). The derivative, (dh/dt), is the differential of the fluid passage time. Since the quadratic term dominates this equation, the screen factor allows fluids to be compared on the basis of relaxation time.

The screen factors for solutions of the hydrolyzed copolymers (terpolymers) are given in Figure 5. These data show that solution relaxation time increases with increasing polymer concentration and increasing molecular weight. Thus, viscoelastic nature of the solution and polymer entanglements increase with increasing hydrolyzed copolymer concentration and increasing molecular weight. Comparison of screen factor data for equal molecular weight co- and terpolymers at equal concentration shows the terpolymers give more viscoelastic solutions.

Electrolyte Effect on Polymer Solution Rheology. As salt concentration in an aqueous poly(1-amidoethylene) solution increases, the resulting brine becomes a more Theta-solvent for the polymer and the polymer coil compresses(47). This effect is particularly pronounced for partially hydrolyzed poly(1-amidoethylene). The

effect of salt on solution rheology was tested in two ways. First, limiting viscosity numbers in 1.0 molar sodium nitrate were determined. These data are given in Table 3. Second, a series of 0.15 g/dL polymer solutions were made in solutions containing between 0 and 0.35 molar sodium chloride or between 0 and 2.5×10^{-2} molar calcium chloride. Solution viscosity at a shear rate of 45 s^{-1} for these solutions is given in Figures 6, 7, and 8.

Comparison of the limiting viscosity numbers determined in deionized water with those determined in 1 molar sodium nitrate shows a 20 per cent decrease in copolymer intrinsic viscosity in the saline solution. These results are consistent with previous studies using aqueous saline solutions as theta solvents for 2-propenamide polymers(47). Degree of hydrolysis controls the value of limiting viscosity number for the hydrolyzed copolymers in distilled water.

Limiting viscosity numbers of the hydrolyzed graft copolymers in 1.0 molar sodium nitrate are proximate to the values for the unhydrolyzed copolymer in the same solvent. This shows the increase in $[\eta]$ in distilled water upon hydrolysis was due to ion-ion repulsion in the hydrolyzed side chains. Lower values of $[\eta]$ in 1.0 molar sodium nitrate after hydrolysis for the two highest molecular weight copolymers hydrolyzed, numbers 10 and 11, show that the starch backbone of these polymers was partially destroyed during the hydrolysis reaction. This backbone scission is probably due to small amounts of oxygen in the hydrolysis solution. Limiting viscosity number data in Table 3 shows that, in the absence of oxygen, this hydrolysis process sharply increases the size of the polymer in solution without degrading the molecule(48). These graft copolymers possess all the same benefits and blemishes as simple carboxylic-acid containing polymers when applied to resource recovery. The copolymers will 1. adsorb less on negatively charge surfaces, 2. adsorb more on positively charged surfaces, 3. produce higher viscosity at a given concentration in aqueous solution, 4. lose solution viscosity when electrolyte concentration increases, 5. precipitate in the presence of di- or tri-valent cations, and 6. gel in the presence of low solubility, di- or tri-valent cations, more than the nonionic precursor.

Solutions containing 0.15 g/dL polymer and between 0 and 0.342 molar sodium chloride or between 0 and 2.49×10^{-2} molar calcium chloride show declines in viscosity as salt content increases. Solution viscosity of nonionic copolymers declines, at most, 3 percent in the range of electrolyte concentrations tested. Solutions of hydrolyzed copolymer lose viscosity exponentially as electrolyte concentration in the solution increases.

The data show that calcium chloride is 20 times more effective on a concentration basis in compacting hydrolyzed copolymers than is sodium chloride. Radii of gyration shown in Table 4 are calculated with the Flory equation,

$$[\eta] = \frac{\phi < \frac{2}{s} >^{3/2}}{\bar{M}} \quad (8)$$

where the value for ϕ , the Flory constant, is that appropriate for a broad- molecular-weight distribution in the polymer, 3.09×10^{22} /mole when limiting viscosity number is expressed in g/dL. These data show that the copolymers are high radius of gyration viscosifiers which

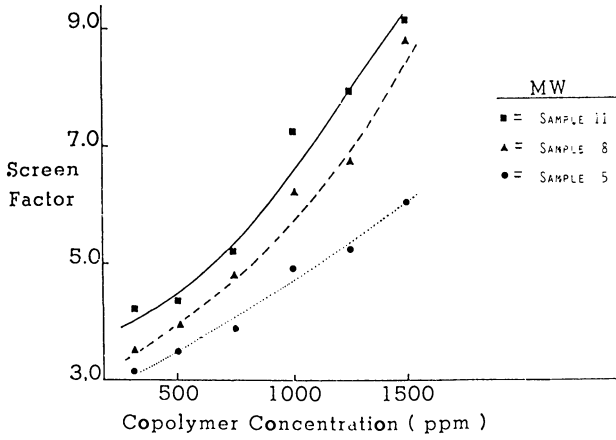


Figure 5. Screen factor of solutions of hydrolyzed poly(starch-g-(2-propenamide)) copolymer.

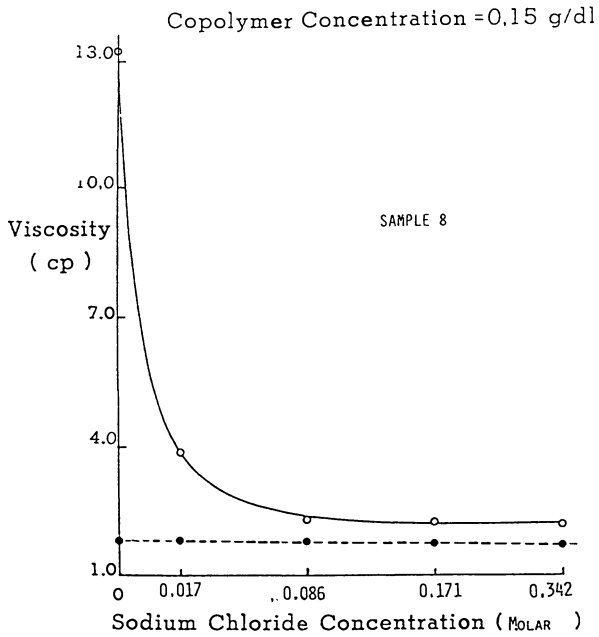


Figure 6. Viscosity of poly(starch-g-(2-propenamide)) in sodium chloride brine.

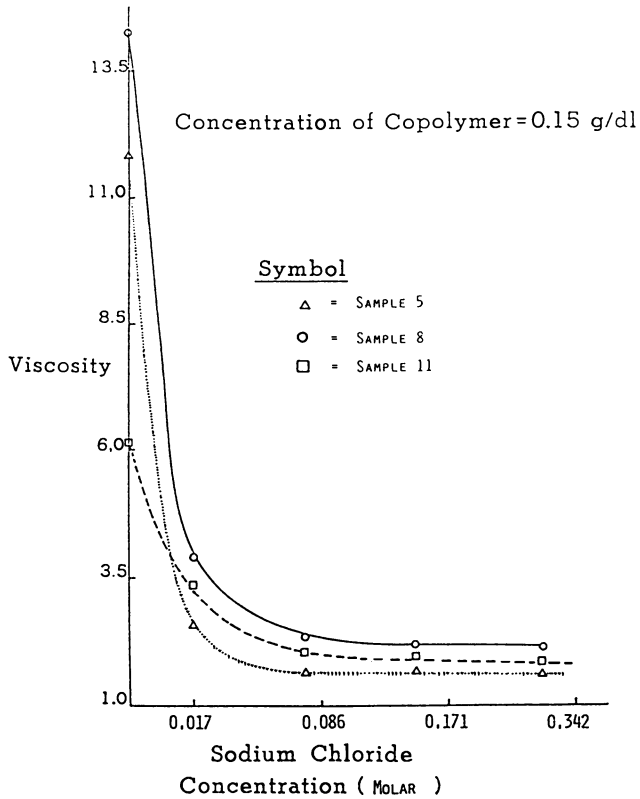


Figure 7. Effect of sodium chloride concentration on the viscosity of hydrolyzed poly(starch-*g*-(2-propenamamide)) copolymer solutions.

significantly expand in size in aqueous solution when hydrolyzed. These data further show that addition of 2- propenamide to starch produces a larger molecule than would be obtained by homopolymerization of the 2-propenamide (see reference 49). The radius of gyration in microns of poly(1-amidoethylene) is

$$\langle \bar{s}^2 \rangle^{1/2} = [1.286 \times 10^{-2} (\bar{M}_w \times 10^{-6})^{1.8}]^{1/3}$$

TABLE 4. Radius of Gyration in Microns, $\langle \bar{s}^2 \rangle^{1/2}$

Copolymer Number	Copolymer (unhydrolyzed)		Hydrolyzed Copolymer		$\langle \bar{s}^2 \rangle^{1/2}$ for an equal Molecular Wt Poly(1-amidoethylene) ^a
	H ₂ O	1 M HNO ₃	H ₂ O	1 M HNO ₃	
5	.208	.193	4.47	.225	.189
7	.302	.281	.564	.357	.361
8	.282	.262	.464	.286	.260
9	.339	.317	.508	.315	.327
10	.337	.317	b	b	.234
11	.527	1.06	b	b	.514

a) This radius of gyration calculated from the Mark-Houwink equation, $[\eta] = 6.31 \times 10^{-5} (\bar{M}_w)^{0.8}$, for poly(1-amidoethylene)(50).

b) $\langle \bar{s}^2 \rangle^{1/2}$ can not be calculated for these degraded polymers.

Viscosity Loss With Time. Poly(1-amidoethylene) solutions lose viscosity with time(51). Several authors have attributed this viscosity loss to oxygen or radical degradation of the polymer(51), but Francois(52) has shown that changes in viscosity only occur in solutions made from broad-molecular-weight-distribution poly(1-amidoethylene). Since very narrow-molecular-weight-distribution poly(1-amidoethylene) produces a stable solution viscosity and since Markis(53) has shown that the original solution viscosity can be obtained by precipitating and redissolving the polymer, it would appear that solution viscosity loss is caused by slow disentangling of a broad- molecular-weight polymer mixture.

To determine if poly(starch-g-(1-amidoethylene)) also exhibited this artifact, a series of polymer solutions were prepared and aged for 2 months. Representative data are presented in Figure 9. These data show that graft copolymers also age and, hence, the copolymers and hydrolyzed copolymers slowly disentangle in solution. This behavior is consistent with the broad molecular weight distribution found for these compounds in reference 2. The data in Figure 9 also show that the lowest molecular weight hydrolyzed copolymer, polymer 5, is biodegraded in solution. Hydrolyzed copolymer 5 showed behavior similar to that of hydrolyzed copolymer 8 and 11 when 1% methanal (formaldehyde) was added to the solution.

Pseudoplasticity. Low-concentration solutions of water viscosifiers are usually nonnewtonian fluids(54) and therefore fail to follow the pressure and flow behavior predicted by newtonian models of flow. To

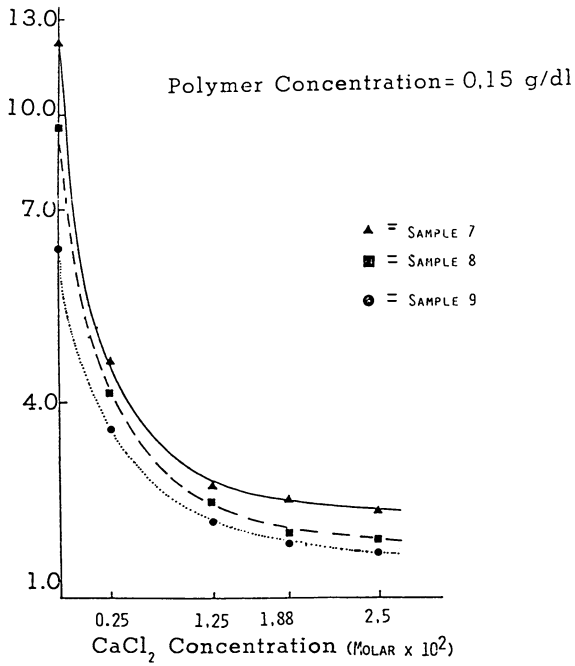


Figure 8. Solution viscosity as a function of calcium chloride concentration for hydrolyzed poly(starch-g-(2-propenamide)) terpolymer.

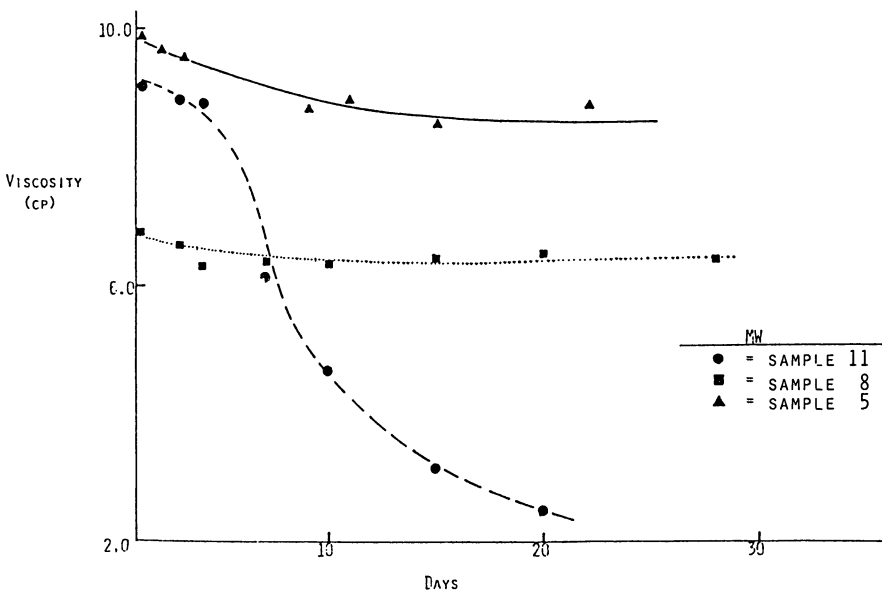


Figure 9. Change with time of viscosity of solutions of hydrolyzed poly(starch-g-(2-propenamide)) copolymer.

determine if the newtonian diffusivity equation or the non-newtonian Iroku equation(55) is needed to predict response to shear of a graft terpolymer solution, the effective viscosity at 5 shear rates was determined for a series of copolymer and hydrolyzed copolymer solutions and the Ostwald-DeWaele exponent, n , was obtained from a match of equation 10 to the data.

$$\eta_e = H \dot{\gamma}^{n-1} \quad (10)$$

In equation 10, H is consistency, η_e is effective viscosity, and $\dot{\gamma}$ is shear rate. Viscosity as a function of concentration in distilled water and shear rate for hydrolyzed copolymers 5, 8 and 11 are shown in Figures 10, 11, and 12, respectively. The Ostwald-DeWaele exponent from the data of Figure 11 is plotted in Figure 13. Data of Figures 10 through 13 show that graft terpolymer solutions are pseudoplastic and become more so (decreasing n) with increasing concentration.

Figure 14 gives limiting viscosity numbers for hydrolyzed copolymer 11 as a function of shear rate. Since limiting viscosity number is a function of molecular size, these data show that solution pseudoplasticity occurs because of compaction of the solvated polymer with increasing shear.

Effective viscosity as a function of shear rate for 0.15 g/dL of copolymer 5 in distilled water is given in Figure 15. The Ostwald-DeWaele exponent for copolymer solutions is greater than that of matching hydrolyzed copolymer solutions at a given concentration. Thus, copolymer molecules are less compactable in solution than are their hydrolyzed derivatives, and pseudoplasticity of polymer solutions increases upon hydrolysis.

Poly(starch-*g*-((1-amidoethylene)-*co*-(sodium 1-(2-methylprop-2N-yl-1-sulfonate)amidoethylene))).

Strongly anionic, highly water-soluble, graft copolymers of starch can be made by adding 2-propenamide and sodium 2,2-dimethyl-3-imino-4-oxohex-5-ene-1-sulfonate (Na DMIH) to the polymerization reactions. See references 43 and 56 for a discussion of these polymers.

LIGNIN GRAFT COPOLYMERS

Lignin [8068-00-6] is a natural product produced by all woody plants. It is second only to cellulose in mass of polymer formed per annum(57). Approximately 20 million tons of kraft lignin are produced in the United States each year(58). This enormous production of cheap biomass has induced a significant effort, stretching over 40 years, to alter lignin into industrial or commercial products. A series of lignin graft(59,60) copolymers have been made which function effectively as drilling mud additives, flocculating agents, and thickening agents. Free radical, graft copolymerization of water-soluble monomers onto kraft or other lignin produces a natural backbone, graft copolymer which functions as a thickening or dispersing agent in water-based, bentonite drilling muds. The complex polymers formed by reacting lignin, calcium chloride, a hydroperoxide, and ethene monomers in anaerobic solvent have the

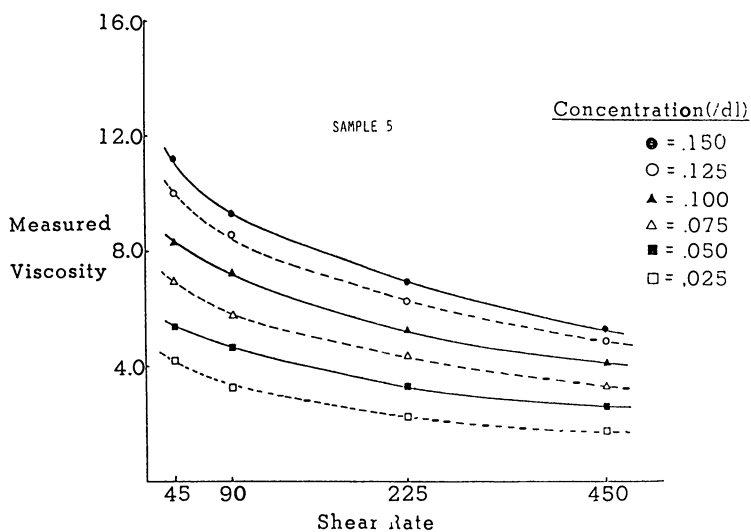


Figure 10. Viscosity as a function of concentration in distilled water and shear rate for hydrolyzed poly(starch-g-(2-propenamide)) copolymer, sample 5.

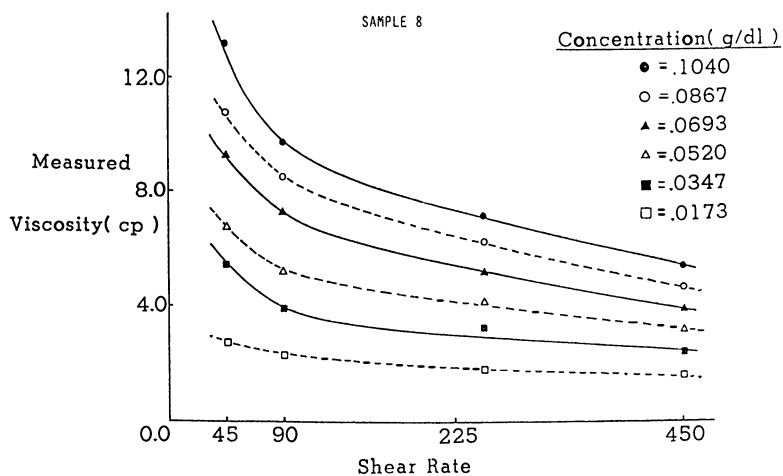


Figure 11. Viscosity as a function of concentration in distilled water and shear rate for hydrolyzed poly(starch-g-(2-propenamide)) copolymer, sample 8.

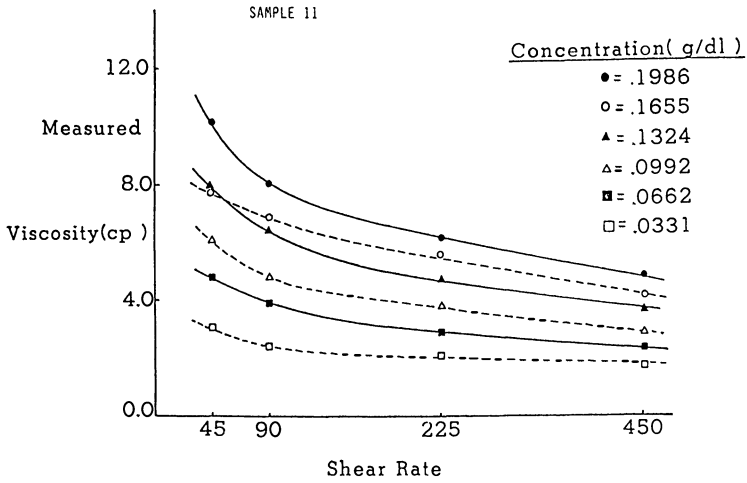


Figure 12. Viscosity as a function of concentration in distilled water and shear rate for hydrolyzed poly(starch-*g*-(2-propenamide)) copolymer, sample 11.

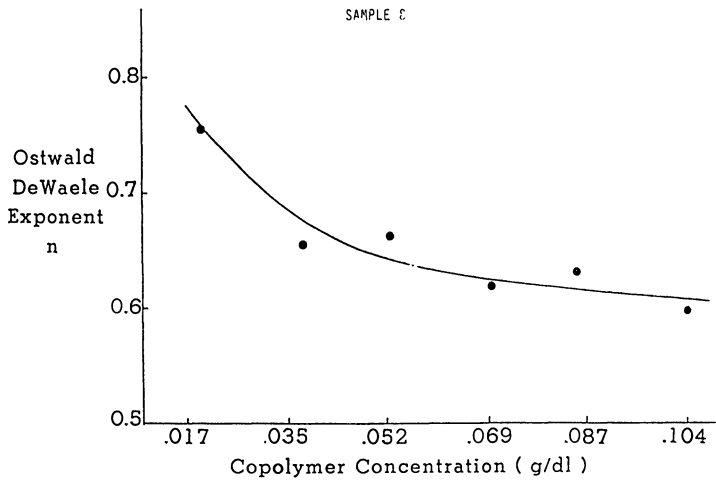


Figure 13. Plot of the Ostwald-DeWaele exponent, sample 8.

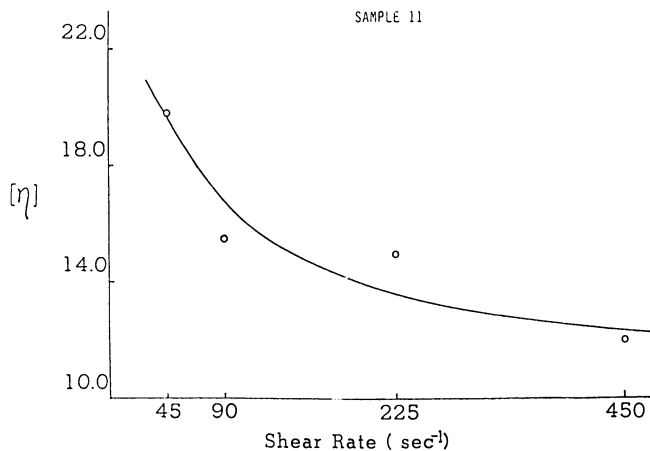


Figure 14. Limiting viscosity numbers for hydrolyzed poly(starch-*g*-(2-propenamide)), sample 11.

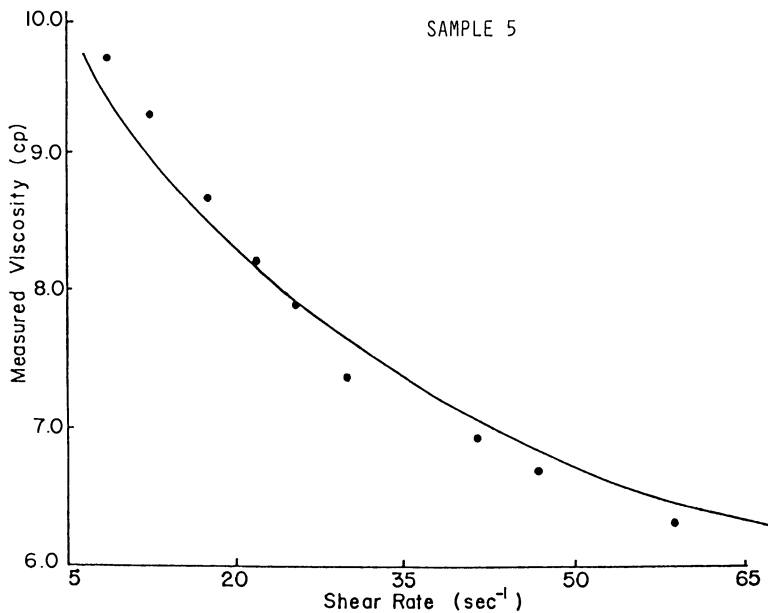


Figure 15. Effective viscosity as a function of shear rate for hydrolyzed poly(starch-*g*-(2-propenamide)), sample 5.

structures given in Figure 16. Synthesis methods, possible synthesis mechanism insights, characterization, properties, and drilling mud tests for these samples are presented below.

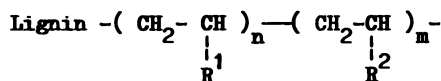


Figure 16. Structure of lignin polymer formed in anaerobic solvent.

SYNTHESIS: The polymerization can be run in any one of several solvents, including dimethylsulfoxide, 1,4-dioxacyclohexane, dimethylformamide, and dimethylacetamide. Dimethylsulfoxide or mixtures based on dimethylsulfoxide have been used as the solvent for all reactions reported here. In other solvents, the product often precipitates as the reaction proceeds. This reaction can be successfully run with mole ratios of the reactants in the following ranges: 1. hydroperoxide to calcium chloride: 0.25 to 32, and 2. hydroperoxide to lignin (M_n): 21 to 113.

Procedure: To a dry Erlenmeyer flask of appropriate size, add one half of the reaction solvent. All reactants, including the dry mass of the hydroperoxide, should not constitute more than 23 weight percent of the reaction mixture or an insoluble product may be produced. Add dry lignin and dry calcium chloride to the reaction vessel and cap with a septum or rubber stopper. In a separate vessel, dissolve 2-propenamide in about one quarter of the DMSO solvent and, in a third vessel, dissolve the sulfonated monomer in the final one quarter of the solvent. Saturate both monomer solutions with N_2 by bubbling with the gas for 10 minutes. Saturate the lignin solution with N_2 for 10 minutes. Add the hydroperoxide to the mixture, bubble with N_2 for 5 minutes, cap, and stir for 10 minutes. While stirring the lignin reaction solution, further saturate the monomer solutions with N_2 . Add the 2-propenamide solution to the lignin solution with stirring and under an N_2 blanket. Wait 1 minute. Add the second monomer solution to the reaction vessel in the same way. Place the reaction vessel in a 30°C bath for 48 hr. The reaction is terminated with a small volume of aqueous, 1% hydroquinone solution and a volume of water equal to $1/3$ of the reaction solution volume is added to the product.

This solution is added to 10 times its volume of 2-propanone and the polymer is recovered by filtration. The solids are redissolved in water. To remove calcium ion from the product, an amount of $\text{Na}_2\text{C}_2\text{O}_4$ equal to the moles of CaCl_2 added to the reaction is placed in the solution. The CaC_2O_4 precipitate is removed by filtration. The filtrate is dialyzed against distilled water for 3 to 5 days using #6 Spectrapor dialysis tubing. The dilute, aqueous solution is then freeze dried to recover the product.

POLY(LIGNIN-G-(1-AMIDOETHYLENE)). Data for a series of graft copolymers made using 2-propenamide are given in Table 5 for copolymers synthesized in dimethylsulfoxide. These data show that maximum yield is obtained when chloride ion to lignin* mole ratio is 492. These nonionic molecules are small in size, readily adsorbed on silica surfaces, and prone to complex di- and tri-valent metal ions

TABLE 5: Lignin-co-(1-amidoethylene) samples. DMSO Data^a

Sample Number	2-propen- amide(g)		Reaction Contents		NO ₂ ^b (g)	Ce(IV) (mL, 0.05N)	Yield ^c (g)	wt.-%	[η] (dl./g)	Product Composition (wt.-%)		
	Lignin (g)	CaCl ₂ (g)	Lignin (g)	CaCl ₂ (g)						N	1-amido	Lignin
1	3.20	0.50	0.50	0.50	0.40/3532	0.15	4.71/2.799	75.68	0.322	15.21	6.50	2.789
2	3.20	0.50	0.50	0.10	0.40/3532	0.15	3.30*/2.56	69.32	0.56	13.34	67.38	5.38 0.73
3	3.20	0.50	0.0503	0.50	0.40/3532	0.15	2.72/2.14	57.85	0.69	13.45	67.91	4.94 0.415
4	3.20	0.50	0.0102	0.50	0.40/3532	0.15	3.16/2.58	70.07	0.77	15.05	76.04	4.60 0.157
5	3.20	0.50	0.25/2208	0.50	0.25/2208	0.15	4.31/3.306	89.36	0.35	13.28	66.95	7.00 2.89
6	3.20	0.50	0.50	0.50	0.152/1342	0.15	4.40/3.34	90.35	0.44	13.03	65.79	6.03 2.86
7@	3.20	0.50	0.50	0.50	0.80/7064	0.15	4.73/3.283	88.75	0.306	12.37	62.31	7.21 2.48
@	3.20	0.50	0.50	0.50	0.416	0.15						
@	3.20	0.50	0.50	0.50	0.416	0.15						
@	3.20	0.50	0.50	0.50	0.15/1325	0.15	4.07/3.307	89.37	0.615	13.55	68.41	5.48 0.757
8	3.20	0.50	0.1	0.50	0.15/1325	0.15	3.90/3.128	84.53	0.666	13.641	68.89	4.94 0.395
9	3.20	0.50	0.0515	0.50	0.15/1325	0.15	3.46/2.863	77.38	0.801	13.734	69.42	4.16 0.0949
10	3.20	0.50	0.010	0.50	0.15/1325	0.15	3.10/2.119	84.77	0.372	11.74	59.12	6.88 3.54
11	2.00	0.50	0.50	0.50	0.15/1325	0.15	3.04/2.091	83.64	0.395	11.67	58.81	6.26 1.007
12	2.00	0.50	0.10	0.50	0.15/1325	0.15	2.68/2.109	84.36	0.478	13.197	66.43	8.15 0.558
13	2.00	0.50	0.0516	0.50	0.15/1325	0.15	1.84/1.44	57.58	0.565	14.162	71.43	6.54 0.33
14	2.00	0.50	0.0107	0.50	0.15/1325	0.15	2.14/1.105	73.64	0.192	7.950	39.53	12.24 5.45
15	1.00	0.50	0.50	0.50	0.15/1325	0.15	1.12/1.063	70.87	0.288	11.515	57.52	13.74 1.65
16	1.00	0.50	0.10	0.50	0.15/1325	0.15	1.49/1.857	57.14	0.275	10.63	52.95	14.95 0.88
17	1.00	0.50	0.0512	0.50	0.15/1325	0.15	1.25/1.919	61.29	0.276	11.516	57.41	15.52 0.325
18	1.00	0.50	0.0113	0.50	0.15/1325	0.15	3.27/	88.38	0.523	15.802	79.43	11.41 0.2
19	3.20	0.50	0.5	0.5	0.4/3532	0.15	4.08/2.896	78.26	0.56	14.062	70.98	5.62 0.679
20	3.20	0.50	0.1	0.15	0.15	0.15						

^a All reactions run in 20.0 mL of dimethylsulfoxide save for the 4 marked samples (@) run in 1,4-dioxacyclohexane.

^b The results given as #1/#2 are #1-g of crude 2-hydroperoxy-1,4-dioxacyclohexane added to the reaction and #2-g of pure peroxide added to the reaction.

^c The yields listed, #1/#2, are: #1 = crude product recovered and #2 = pure product recovered. Weight percent yield is based on pure product recovered.

^f 1-amido = 1-amidoethylene repeat units in the polymer. * = Some product lost during recovery.

from aqueous solution(61,62). Synthesis results for several samples of poly(lignin-g-(1-amidoethylene)) are given in Table 6.

Table 6. Yield and Limiting Viscosity Number for Lignin-(2-propenamido) Reactions^a

sample no.	anhyd CaCl ₂ in reaction mixture, wt %	yield g/wt%	limiting ² viscos no., dL/g	wt %		
				lignin	polymerized 2-propen- amide	Ca after ashing
1	4.0	3.36/90.8	0.59	7.5	67.6	4.91
2	2.0	3.64/98.4	0.46	6.95	73.4	2.25
3 ^c	2.2	1.5/100.0	0.21	12.4	48.3	6.94

^aAll reaction mixtures contain 20.0 mL of oxygen-bubbled, irradiated dioxane, 0.5 g of lignin, and 0.15 mL of ceric sulfate solution. Reactions run in a Pyrex flask and contained 1,4-dioxane irradiated for 3 h and 0.045 mol (3.2 g) of 2-propenamido.

^bDetermined in distilled water at 30°C.

^cReaction run with 0.014 mol (1.0 g) of 2-propenamido.

Other lignins can be reacted with this chemistry. Table 7 shows synthesis data for the preparation of poly(lignin-g-(1-amidoethylene)) from several different lignins. Sample 1 is a kraft pine lignin grafted in a reaction coinitiated with sodium chloride. Lignin used in these studies is a commercial product. The material is a kraft pine lignin prepared in "free acid" form with a number-average molecular weight of 9,600, a weight-average molecular weight of 22,000, and a polydispersity index of 2.29. Ash content of the lignin is 1.0 weight percent or less. The material was used as received. Elemental analysis is C=61.66, N=0.89, H=5.73, S=1.57, Ca=0.08, and Fe= 0.014 weight percent.

Table 7. Poly(lignin-g-(1-amidoethylene)) formed from Various Lignins and Coinitiators

Sample	Lignin	Composition of Reaction(g)			Yield (g/wt %)	
		2-Propen amide	Chloride Salt ^(a)	Hydroper oxide		
1	0.50	3.21	0.68	0.482 mL	21.28	3.46/93.3
2	0.50	3.20	0.62	0.482 mL	21.28	3.48/94.05
3	0.51	3.21	0.62	0.482 mL	21.30	2.48/66.67
4	0.50	3.20	0.62	0.482 mL	21.33	3.50/86.48
5	0.50	3.27	0.64	0.482 mL	21.39	3.20/84.88
6	0.50	3.22	0.63	0.482 mL	21.29	3.26/87.63

a. The same number of moles of chloride ion is used in sample 1 and samples 2 to 4. Sample 1 received sodium chloride while samples 2 to 4 received calcium chloride.

Sample 2 is run with a steam-exploded, solvent-extracted, aspen lignin. This backbone, provide by the Solar Energy Research Institute of Golden, Colorado as DJLX13, is an I-0-TECH process,

wood extract. After steam decompression to disrupt the wood fiber, the wood was extracted with tetrachloromethane at approximately room temperature and reduced pressure. The wood was then extracted with methanol at 60°C and reduced pressure. The lignin sample used was recovered as the methanol extract. Samples 3 and 4 are results on a yellow poplar lignin. The material was produced by BioRegional Energy Associates of Floyd, Virginia. It is produced by steam exploding the wood, washing with water, extracting with alkali, and precipitating with mineral acid. The lignin has a high carboxylic acid content and a high level of phenolic hydroxyl groups. Molecular weight of the product is 1,000 to 1,200.

To see if the phenol hydroxyl group is involved in the grafting reaction, a series of model reactions were run. In these reactions, lignin was replaced by phenol derivatives. The concentration of lignin model compound in each reaction was chosen so that concentration of equal structures in the model reaction and lignin-containing reaction were the same(63). Results from reactions run with phenol, 1-(hydroxymethyl)benzene, 1-(hydroxymethyl)-phen-4-ol, and 3-(4-hydroxyphenyl)-propan-1-ol are given in Table 8. Phenol worked well as a lignin model and allowed 50 percent conversion of monomer to polymer. The two (hydroxymethyl)benzene compounds worked poorly and 3-(4-hydroxyphenyl)-propan-1-ol didn't work at all as a lignin model. These results imply that hydroxyl groups are a probable site for grafting initiation, but that structure controls the capacity of the hydroxyl group to initiate this polymerization.

TABLE 8. Results of Reactions Containing Lignin Models ^a

Lignin Test Compound	g of Model Used	Yield	
		g	%
phenol	0.085	1.64	49.9
1-(hydroxymethyl)benzene	0.088	0.49	14.9
1-(hydroxymethyl)phen-4-ol	0.1023	0.76	23.0
3-(4-hydroxyphenyl)-propan-1-ol	.1254	0	0

^aAll reactions were run using 0.5 g of calcium chloride, 0.15 mL of 0.05 M Ce(+4) solution, and 3.2 g of 2-propenamide in 20 mL of dioxane that had been photolyzed for 3 hr.

POLY(LIGNIN-G-((1-AMIDOETHYLENE)-CO-(SODIUM 1-CARBOXYLATOETHYLENE)))

The copolymer just described can be converted to an anionic polyelectrolyte by hydrolysis of the amide units with strong base. Synthesis data for a sample of poly(lignin-g-(1-amidoethylene)) hydrolyzed to a polyanion are given in Table 9. Hydrolyzed samples are prepared from aqueous solutions containing between 1.0 and 2.5 g/dL of reaction product. A stoichiometric amount of sodium hydroxide that will produce the desired percent hydrolysis is added to the solution, the solution is heated to 50°C with stirring, and is maintained there for 1 hr. Product is recovered by 1. precipitation and drying or 2. dialysis and freeze drying(64). Data from the sample of Table 9, hydrolyzed to four different degrees of hydrolysis, are given in Table 10.

TABLE 9. Synthesis Data on Graft Copolymers

batch no.		2
reaction mixture composition		
1,4-dioxane, mL	20.0	irradiation time after oxygen purge = 3.0 hr.
lignin, g	0.50	
2-propenamides, g	1.00	
0.05 M $\text{Ca}(\text{SO}_4)_2$ solution, mL	0.15	
CaCl_2 , g	0.50	
yield		
grams	1.50	limiting viscosity number in water at 30 °C = 0.21 dL/g
weight percent	100.	
product composition wt %		
lignin	12.44	
1-amidoethylene repeat units	48.3	% hydrolysis = 0

^aThese values are averages for four repetitions of the reaction.

Proof of copolymerization is obtained by real time spectra acquisition of absorbance for size exclusion chromatography effluent(65).

TABLE 10. Elemental Assay, Percent Hydrolysis, and Limiting Viscosity Number for Partially Hydrolyzed Lignin Copolymer-

Sample	elemental assay, wt %					Na	degree of hydrolysis from ^a assay	limiting viscosity number (dL/g)
	C	H	N	S	O			
Batch 2								
e	48.49	7.51	12.76	0.43	28.40	0.02	0	0.13
f	45.69	6.07	8.63	0.57	33.04	7.85	26.6	1.31
g	43.17	5.60	7.14	0.67	33.33	9.72	38.0	4.09
h	46.05	5.94	5.69	0.28	31.47	10.13	50.4	3.84

^aBased on nitrogen loss from sample e.

Hydrolysis increases the terpolymer limiting viscosity number in water by a factor of up to 45. Other previously published data(66-68) show that these terpolymers are nonnewtonian viscosifiers, metal-ion complexing agents, and effective flocculators. These materials are still "small" molecules in aqueous solution, however, and do not function as effectively when used 1. as nonnewtonian viscosifiers or 2. drag reducing agents as do poly(1-amidoethylene-co-(sodium 1-carboxylatoethylene)) copolymers.

APPLICATIONS TO DRILLING MUDS.

In drilling fluids, water-soluble polymers can perform many functions, some of which are:

- Fluid loss control
- Increasing viscosity
- Decreasing viscosity
- Controlling shale hydration
- Flocculating drill solids
- Reducing friction and torque

Use of polymers of simpler structure has already been reviewed(69). The potential for application of complex polymers to the rheological, interfacial, and suspending job demanded in drilling muds is very large. To determine if the lignin graft copolymers made above would function as drilling mud additives, several nonionic and anionic copolymers were tested in a water based mud. Data for the sample prepared for drilling mud tests are given in Table 9. Batch 2 was broken into parts and hydrolyzed with sodium hydroxide to make samples of differing degrees of hydrolysis. Data on these batch fractions are given in Table 10. Mud test data for mud samples containing the lower molecular size samples of batch 2, Table 9, are given in Table 11. These data show that the reaction product produces the desirable effect of lowering yield point, lowering gel strength, and lowering API filtrate volume as degree of hydrolysis of the reaction product increases. After hot-rolling, the reductions in the above three variables are only significant for the reaction product that is 50% hydrolyzed, sample 2h of Table 10.

Though the data are limited, batch 2 samples, which probably have lower molecular weights, appear to give greater yield point lowering and lower gel strength than do samples synthesized with more 2-propanamide in the reaction mixture.

**TABLE 11. Properties of Test Muds Before and After Hot Rolling.
Sample: Batch 2, Table 9**

property	base mud		reaction product							
	bef.	aft.	e		f		g		h	
	bef.	aft.	bef.	aft.	bef.	aft.	bef.	aft.	bef.	aft.
viscosity in cP										
at a shear rate of										
1020 s ⁻¹	79	80	76	103	78	75	67	68	67	63
510 s ⁻¹	58	50	57	77	52	46	44	41	43	38
340 s ⁻¹	50	38.5	48	66	42	35	35	32	33	28
170 s ⁻¹	39	24.5	38	51	29	22	23	19	22	18
gel strength in lb/100 ft ² after mud has set for										
10 s	18	4	9	20	7	4	5	3	3	3
10 min	38	6	44	70	35	5	25	4	12	4
apparent viscosity, cP	40	40	38	52	39	38	34	34	34	32
plastic viscosity, cP	21	30	19	36	26	29	23	27	24	25
yield point, lb/100 ft ²	37	20	38	41	26	17	21	14	19	13
API filtrate vol, mL	12.4	8.0	12.8	12.6	10.0	10.4	10.0	10.0	9.2	9.7

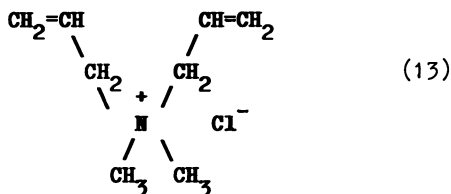
The data from these first two batch tests indicated that poly(lignin-g-(1-amidoethylene)) has properties which make it a potentially effective drilling mud additive. The tests show that poly(lignin-g-(1-amidoethylene)) and its hydrolyzed derivatives act as a high temperature thinner and as a filtrate control agent. The

tests also show (batch 2, Table 11) that reaction products prepared from reactions containing less 2-propenamamide acts as thinners for the base mud. Products from low 2-propenamamide content reactions have smaller molecular size, as shown by their smaller limiting viscosity number (Table 9), and should have lower molecular weights than the products from other reactions.

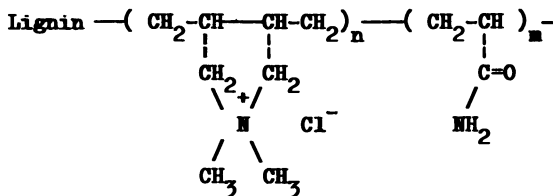
Poly(lignin-g-((1-amidoethylene)-co-(sodium 1-(2-methylprop-2N-yl-1-sulfonate)amidoethylene))).

A strongly anionic, polyelectrolyte can be made from lignin by conducting a graft polymerization in the presence of 2-propenamamide and 2,2-dimethyl-3-imino-4-oxohex-5-ene-1-sulfonic acid or its salts.

Poly(lignin-g-((1-amidoethylene)-co-(methylene 1N,1N-dimethyl-1-ammoniumcyclopenta-3,4-diyl chloride methylene))). A Cationic Graft Copolymer of Lignin. The applications of the anionic graft copolymers described above are many but the negative charge on the polymer or the behavior of the anionic polymer under application conditions often limit the utility of these materials. One solution to this problem is to create new copolymers of lignin which have the appropriate functional groups to perform effectively in a given environment. One such class of new materials with the right parts to function where anionics fail is the class of cationic polymers. Data from such a copolymer will now be presented. This copolymer was made from 4N,4N-dimethyl-4-ammoniumhept-1,6-diene chloride. This cationic monomer was prepared according to the method of Negi, et. al. (70).



Lignin has been reacted with 4N,4N - dimethyl-4-ammoniumhept-1,6-diene chloride monomer to make a cationic graft copolymer. The structure of the copolymer is illustrated by the formula:



The composition, reaction conditions, and yield of copolymer-1 (24-37 series) are shown in Table 12. The content of 4N,4N-dimethyl-4-ammoniumhept-1,6-diene chloride in the reaction ranges from 0 to 30 molar percent of total monomer content. The concentration of lignin, calcium chloride, and monomer in the

Table 12: Synthesis data of cationic lignin-graft copolymer
(lignin-g-2-propenamide-DMDAC)

sample number	Reactant		Reaction parameter				Yield %						
	lignin	CaCl ₂	A	B	DMSO	EDTA		E	Cl mmole	molar ratio	Cl/g	Cl/L	Cl/H
weight in gram		volume in ml											
24-37-1	0.66	0.33	2.35	1.03	29.28	1.30	0.65	12.35	83.8/16/2	0.35	18.7	2.26	68.43
24-37-2	0.65	0.33	2.25	1.25	28.23	1.50	0.65	13.59	80.4/19.6	0.39	20.91	2.49	68.43
24-37-3	0.66	0.33	2.07	1.55	28.82	1.90	0.65	15.69	75.4/24.6	0.43	23.77	2.88	51.37
24-37-4	0.66	0.33	1.93	1.88	33.25	2.30	0.65	17.61	70/30	0.43	26.68	3.23	49.61
24-37-5	0.68	0.34	2.69	-	25.26	-	0.65	6.13	100/0	0.21	9.01	1.12	95.37

- Note: 1. A: 2-propenamide; B: DMDAC
 2. E: 30% hydrogen peroxide (equivalent weight: 8.383 meq/ml)
 3. The concentration of EDTA Na₂ is 200 ppm based on DMDAC
 4. CL/g: Chloride content per unit weight of total reaction mass (mmole/g)
 5. CL/L: Chloride content per unit weight of lignin (mmole/g)
 6. CL/H: Molar ratio of chloride to hydrogen peroxide

reaction are around 1.8, 0.9, and 9.5 percent by weight of total reaction mass respectively, as shown in Table 13. In the reactions listed in Table 12, the ratio of lignin to calcium chloride is 2 to 1 by weight. The yield of reaction ranges from 49.61 to 95.37 weight percent. By comparing yield to reaction chloride ion content, these results indicate that yield of reaction decreases when content of chloride ion (on a molar basis) increases. Simultaneously, however, the yield increases when content of 2-propenamide increases.

Table 13: The composition of Reaction Mixture Used to Make Lignin Graft Copolymers

Sample number	Total mass	(basis: weight percent of total mass)					Yield %
		Lignin Wt%	CaCl ₂ Wt%	Monomer Wt%	Monomer mmole/g		
24-37-1	35.60	1.85	0.93	9.49	1.11	68.43	
24-37-2	34.86	1.86	0.94	10.04	1.13	63.78	
24-37-3	35.98	1.83	0.92	10.06	1.08	51.37	
24-37-4	41.00	1.60	0.80	9.29	0.95	49.61	
24-37-5	29.62	2.30	1.15	9.08	1.28	95.37	

CONCLUSIONS.

Poly(starch-g-(1-amidoethylene)) copolymers can be formed by ceric-ion- initiated, free-radical polymerization of 2-propenamide on starch. Poly(starch- g-[partially hydrolyzed 1-amidoethylene]) can be formed by treatment of an aqueous solution of the copolymer with 0.5 M sodium hydroxide at 40°C under anaerobic conditions. Treatment of the copolymer under these conditions for 10 minutes produces a hydrolyzed copolymer with a degree of hydrolysis between 9.5 and 14.5 percent.

Limiting viscosity numbers of the copolymers increase with increasing molecular weight and upon hydrolysis. At fixed copolymer molecular weight, limiting viscosity number increases with number of grafts per starch molecule. Radii of gyration show the co- and hydrolyzed polymers to be low mass, high- radius-of- gyration viscosifiers. Co- and hydrolyzed polymer solutions are viscoelastic with a relaxation time that increases with increasing polymer concentration in solution or polymer molecular weight. Hydrolyzed copolymers form more viscoelastic solutions than do copolymers.

Viscosity of copolymer solutions decreases by, at most, 3 percent when electrolyte concentration changes from 0 to 0.342 M sodium chloride or 2.45×10^{-2} M calcium chloride. Viscosity of hydrolyzed polymer solutions decreases exponentially with increasing electrolyte concentration in water.

Poly(lignin-g-(1-amidoethylene)), previously made by reacting Kraft, pine lignin, and 2-propenamide in oxygen-bubbled, irradiated dioxane, can be prepared by combining lignin, 2-propenamide, calcium chloride, and a hydroperoxide in such solvents as 1-methyl-2-pyrrolidinone, dimethyl sulfoxide, dimethylacetamide, dimethylformamide, and pyridine. The product, a highly water-soluble, brown solid containing 4 to 7 wt % lignin and 70+ wt % 1-amidoethylene repeat units, is purified by precipitation in 2-propanone and dialysis against water through a 1,000 mol. wt. permeable membrane.

Poly(lignin-g-(1-amidoethylene)) and its hydrolyzed derivative, poly(lignin-g-((1-amidoethylene)-co-(sodium 1-carboxylatoethylene))), lower yield point, lower gel strength, and lower API filtrate volume in a bentonite drilling mud. After hot rolling at 121°C for 16 hr, the graft copolymer outperforms an equal concentration of chrome lignosulfonate when the compounds were tested as thinners or as filtrate control agents.

Products synthesized in reaction mixtures containing 2 g of 2-propenamide/g of lignin acted as thinners in bentonite-based mud.

The performance requirements which must be met by polymers used in resource recovery are job-specific and complex. These requirements have been partially met by creating complex polymers with physical properties which can provide the demanded performance.

While performance of resource recovery processes have been significantly improved in the past two decades, further efforts must be directed to 1. minimize shear degradation, 2. control adsorption, 3. control process rheology, and 4. provide appropriate chemical stability. These are the properties which fundamental and applied research must target during the next decade.

Acknowledgment

This work was partially supported by the National Science Foundation under award number CPE-8260766 and under National Science Foundation grant CBT-8417876. Support of the copolymer testing program by A and R Pipeline Company is gratefully acknowledged.

Keven Anderle, George Merriman, James Z. Lai, Damodar R. Patil, Mu Lan Sha, Nancy Chew, Chin Tia Li, Thomas Buchers, Cesar Augustin, Harvey Channell, and others completed a sizable portion of this work and their aid and effort is greatly appreciated and acknowledged.

LITERATURE CITED.

1. Kirk-Othmer Encyclopedia of Chemical Technology, Vol. 10, Wiley-Interscience, New York, 2nd ED. 1966 pp.741-751.
2. E. Ott, H. M. Spurlin, M. W. Grafflin, High Polymers, Volume V, Cellulose, Wiley-Interscience, New York 1955 Part III.
3. Robert L. Davidson Ed., Handbook of Water-Soluble Gums and Resins Stach and Its Modifications, by M. W. Rutenberg, McGraw-Hill Book Comp, New York, 1980 Chapter 22, ISBN 0-07-015471-6.
4. S. Erlander, D. French, J. Poly. Sci., 1956 20, 7-28.
5. D. French, Chemistry and Biochemistry of Starch, in W. J. Whelan(ed.), Biochemistry of Carbohydrates, Biochemistry Series one, Vol. 5, Universty Park Press, Baltimore, 1975 pp. 267-335,.
6. D. French, Denpun Kagaku, J. Jpn. Soc. Starch Sci., 19, 8-25 (1972).
7. D. French, J. Anim. Sci., 1973 27, 1048-1061.
8. Henry I. Bolker, Natural and Synthetic Polymers, An Introduction, p. 580, Marcel Dekker, New York, 1974 ISBN 0-8247-1060-6.
9. Eero Sjostrom, Wood Chemistry, Fundamentals and Applications, p.69, Academic Press, 1981 ISBN 0-12-647480-X.
10. K. V. Sarkanen, C. H. Ludwig, Lignins' Occurrence, Formation, Structure, and Reactions, p.1, J. Wiley, 1971 ISBN 0-471-75422-6.
11. Joseph Hagen, Chem. Eng. News, (May 6, 1985) 63 (#18), p.33-34.
12. T. Kent Kirk, T. Higuchi, H. Chang, Lignin Biodegradation:

- Microbiology, Chemistry, and Potential Applications, CRC Press, 1980
Vol.1, p. 5, ISBN 0-8493-5459-5.
13. A. Bjorkman, Svensk Papperstidn., 1956 59, 477.
 14. J. C. Pew, Tappi, 1957 40, 553.
 15. F. F. Nord, W. J. Schubert, Holz Froschung, 1951 5, 1.
 16. F. F. Nord, W. J. Schubert, Tappi, 1957 50, 285.
 17. G. de Stevens, F. F. Nord, Fortschr. Chem. Forsch., 1954 3, 70.
 18. G. de Stevens, F. F. Nord, J. Am. Chem. Soc., 1951 73, 4622.
 19. S. F. Kudzin, F. F. Nord, J. Am. Chem. Soc., 1951 73, 690, 4619.
 20. F. F. Nord, G. de Stevens, Naturwissenschaften, 1952 39, 479.
 21. J. C. Pew, J. Am. Chem. Soc., 74, 2850, (1952).
 22. E. Hagglund, Cellulosechemie, 1923 4, 84.
 23. A. Sakakibara, N. Nakayama, J. Jpan, Wood Res. Soc. 1962 8, 153.
 24. David N. S. Hon, Ed., Graft Copolymerization of Lignocellulosic Fibers, ACS Symposium Series #187, Am. Chem. Soc., (1982) ISSN 0097-1656; 187.
 25. Chem. and Eng. News, 1984 62 (#39), 19-20.
 26. R. L. Whistler, Industrial Gums, Academic Press, New York (1973).
 27. F. Smith, R. Montgomery, The Chemistry of Plant Gums and Mucilages, Bk. Reichhold Publishing Corp., New York (1959).
 28. C. J. Githens, J. W. Burnham, Soc. Pet. Eng. J., 1977 17, 5.
 29. H.L. Chang, Polymer Flooding Technology - Yesterday, Today, and Tomorrow, Proceedings of the Soc. Petrol. Eng. Symposium on Improved Oil Recovery, 4/16-19/78, Tulsa, OK. SPE Paper #7043.
 30. F. Bueche, Mechanical Degradation of High Polymers, J. Appl. Polym. Sci., 1960 4, (#10), 101-106.
 31. D.J. Pye, J. Petrol. Tech, 1964 16, (#8), 911.
 32. B.B. Sandiford, J. Petrol. Tech., 1964 16, (#8), 917.
 33. B.A. Toms, Proc. Internat. Rheological Congr., Holland, North-Holland Pub. Co., Amsterdam, 1949 Vol. II, pp 135-141.
 34. W. Barney Gogarty, Micellar/Polymer Flooding - An Overview, Proceedings of The Soc. Petrol. Eng. Symposium on Improved Oil Recovery, SPE Paper #7041, Tulsa, OK, 4/16-19/78.
 35. E.H. Immergut, in Encyclopedia of Polymer Science and Technology, H. F. Mark, N. G. Gaylord, N. M. Bikales, Eds., Interscience, New York, 1965, Vol. 3, p. 242.
 36. G. Mino, S. Kaizerman, E. Rasmussen, J. Am. Chem. Soc., 1959 81, 1494.
 37. G. Mino, S. Kaizerman, E. Rasmussen, J. Polymer Sci., 1959 38, 393.
 38. F. R. Duke, A. A. Forist, J. Am. Chem. Soc., 1949 71, 2790.
 39. F. R. Duke, R. F. Bremer, J. Am. Chem. Soc., 1951 73, 5179.
 40. A. A. Kaitai, U. Kulshrestha, R. H. Marchessault, in Fourth Cellulose Conference (J. Polymer Sci. C, 2), R. H. Marchessault, Ed., Interscience, New York, 1963, P. 403.
 41. J. J. Meister, M. L. Sha, J. Appl. Polym. Sci., 1987 33, 1859-1871.
 42. J. J. Meister, M. L. Sha, J. Appl. Polym. Sci., 1987 33, 1873.
 43. J. J. Meister, D. R. Patil, M. C. Jewell, K. Krohn, J. Appl. Polym. Sci., 1987 33, 1887.
 44. H. Pledger Jr., John J. Meister, T. E. Hogen-Esch, G. B. Butler, Proceedings of the 54th Annual Fall Tech. Confer., Soc. Petrol. Eng., SPE Paper # 8422, Las Vegas, NV, 9/23-26/79

45. G.B. Butler, T.E. Hogen-Esch, J.J. Meister, H. Pledger, Jr., U.S. 4,400,496, 8/23/1983; B. L. Knight, J. Petrol. Tech., 1973 **25**, 618, May.
46. A. A. Berlin, E. A. Penskaya, Dokl. Akad. Nauk SSSR 1956 **110**, 585; H. H. G. Jellinek, S. Y. Fok, Die Makromol. Chem. 1967 **194**, 18.
47. G. Muller, J. P. Lane, J. C. Fenyo, J. Poly. Sci., Poly. Chem. Ed., 1979 **17**, 659-672.
48. John J. Meister, A Review of Synthesis, Characterization, and Properties of Complex Polymers for Use in the Recovery of Petroleum and Other Natural Resources, Chapter 2 in the Book: Water-Soluble Polymers for Petroleum Recovery, Dr.D.N. Schulz, Dr.G.A. Stahl, Editors, Plenum Publishing Corp. 1988 ISBN 0-306-42915-2.
49. J. Francois, D. Sarazin, T. Schwarts, G. Weill, Polymer 1973 **20**, (#8), 106-124.
50. H. Mark, Z. Elektrochem, 1934 **40**, 499; R. Houwink, J. Prakt. Chem., 1940 **157**, 15.
51. D. C. MacWilliams, J. H. Rogers, T. J. West, in Water Soluble Polymers, N. M. Bikales, Editor, Plenum Publishing Company, New York, 1973 106-124.
52. J. Francois, D. Sarazin, T. Schwarts, G. Weill, Polymer 1979 **20**, No. 8, 969-975.
53. N. Narkis, M. Rubhun, Polymer, 1966 **7**, 507-512.
54. Edward T. Severs, Rheology of Polymers, Reinhold Publishing, 1962 92.
55. C. U. Ikoku, Transient Flow of Non-newtonian, Power Law Fluids, Ph.D. Thesis, Petroleum Engineering Department, Stanford University, (1978).
56. John J. Meister, Damodar R. Patil, Margaret C. Jewell, Kyle Krohn, Synthesis, Characterization, and Properties in Aqueous Solution of Poly(Starch-g- [(1-amidoethylene)-co-(sodium 1-(2-methylprop-2N-yl-1-sulfonate)amidoethylene)]), Proceedings of the American Chemical Society Division of Polymeric Materials, 1986 **55**, 380-384.
57. J.J. Meister, D.R. Patil, H. Channell, Proceed. Intern. Symp. on Oilfield and Goetherm. Chem., Soc. Petrol. Eng. Paper #13559, Phoenix, AZ, 4/9-11/85.
58. S. Y. Lin, 1983 In Progress in Biomass Conversion (K. V. Sarkanen, D. A. Tilman, E. C. Jahn, eds.), Vol. 3, pp. 31-78, Academic Press, New York, NY.
59. J.J. Meister, D.R. Patil, Macromolecules, 1985 **18**, 1559-1564.
60. J.J. Meister, Review of the Synthesis, Characterization, and Testing of Graft Copolymers of Lignin, p.305-322 of Renewable-Resource Materials: New Polymer Sources, C.E. Carraher, Jr., L.H. Sperling, Ed., Plenum Press, N.Y. (1985) ISBN 0-306-42271-9.
61. J.J. Meister, D.R. Patil, L.R. Field, J.C. Nicholson, J.Polym.Sci., Poly. Chem. Ed., 1984 **22**, 1963-1980.
62. J.J. Meister, D.R. Patil, H. Channell, J. Appl. Polym. Sci., 1984 **29**, 3457-3477.
63. Goheen, D. W.; Hoyt, C. H. Lignin in the "Kirk-Othmer Encyclopedia of Chemical Technology"; 3rd ed., Wiley-Interscience: New York, 1981; Vol. 14, pp 298-299.
64. J.J. Meister, D.R. Patil, Ind. Eng. Chem. Prod. Res. Devel., 1985 **24**, 306-313.

65. J.C. Nicholson, J.J. Meister, D.R. Patil, L.R. Field, Anal. Chem., 1984 56, 2447-2451.
66. J.J. Meister, D.R. Patil, Macromolecules, 1985 18, 1559-1564.
67. J.J. Meister, Review of the Synthesis, Characterization, and Testing of Graft Copolymers of Lignin, p.305-322 of Renewable-Resource Materials: New Polymer Sources, C.E. Carraher, Jr., L.H. Sperling, Ed., Plenum Press, N.Y. 1985
ISBN 0-306-42271-9.
68. J.J. Meister, J.C. Nicholson, D.R. Patil, L.R. Field, Macromolecules, 1986 19, 803-809.
69. J. Chatterji, J. K. Borchardt, Proceedings of the 55th Annual Fall Technical Conference, Soc Petrol. Eng. Paper 9288, Dallas, Tx, 9/21-24/80
70. Youji Negi, S. Harada, O. Ishizuka, Jo. Applied Poly. Sci., 1967 5, 1951-1985.

RECEIVED January 27, 1989

Chapter 10

Cationic Organic Polymer Formation Damage Control Chemicals

A Review of Basic Chemistry and Field Results

John K. Borchardt

Westhollow Research Center, Shell Development Company, Houston,
TX 77251-1380

Polymers containing quaternary ammonium salt groups in some or all of the polymer repeat units have been evaluated as formation damage control agents in drilling, completion, acidizing, and hydraulic fracturing fluids as well as in enhanced oil recovery. Important chemical structure properties determining effectiveness of formation damage control polymers include polymer molecular weight and location of the quaternary ammonium group in the polymer repeat unit structure. Statistically significant sets of field results indicate two of these polymers are effective formation damage control agents in acidizing oil and gas wells.

Formation damage has become widely recognized as a major contributing factor to rapid productivity decline after well completion or workover. The reduction of formation damage during and after well completion and workover treatments will improve long-term well productivity. The use of certain quaternary ammonium salt polymers to substantially reduce clay swelling and fines migration has become common practice during drilling and well completion and stimulation operations (1).

Gabriel and Inamdar found that quaternary ammonium salt polymers which were highly effective stabilizers of water-swelling clays did not protect test cores from permeability damage caused by fines migration in the substantial absence of water-swelling clays (2). Earlier Reed and Coppel noted similar results when evaluating an effective water-swelling clay stabilizer, hydroxyaluminum, as a silica fines stabilizer (3). Silica fines were stabilized only when the unconsolidated test sand contained at least 2% smectite, a water-expandable clay.

More recently certain quaternary ammonium salt polymers have been claimed to be effective in substantially reducing fine particle migration even in the absence of water-swelling clays (1). However, there is little information readily available concerning

the effect of chemical structure on polymer performance. Therefore, it is worthwhile to review the technical and patent literature on these polymers to determine the effect of polymer molecular weight and repeat unit structure on the performance of these organic polymers as swelling clay and mineral fine particle stabilizers.

Formation Damage. While the causes of formation damage are numerous and may vary from one field to another, they may be grouped into the following general categories:

1. the migration of existing mobile fines within the formation. This is caused by fines entrainment in rapidly flowing fluids. Later fine particle deposition in capillary constrictions causes reduced permeability.

2. generation of mobile fines as a result of acidizing a formation. Fines may also be created by crushing of proppant grains during mixing and pumping of fracturing fluid gels or by the effect of overburden pressure on proppant grains after fracture generation.

3. The creation of mobile fines resulting from low salinity aqueous fluids contacting water-expandable clays. While clay swelling will reduce capillary diameter thus decreasing rock permeability, the major mode of formation damage is thought to be the generation of mobile fine particles. This occurs when the swelling clays act as the primary cementing medium of the formation. Clay expansion increases the mobility of pre-existing fine particles formerly cemented in place. In addition, the expanded clay itself is more likely to undergo disintegration and subsequent migration in the presence of rapidly flowing fluids.

4. fines contained in completion, workover, and stimulation fluids may be introduced into the formation. These fines usually plug flow channels before they penetrate deeply into the formation. Filtration of treatment and injection fluids has become a widespread practice to deal with this problem. Perforating also causes near-wellbore formation damage due to rock crushing and fine particle generation.

Other minerals beside water-swelling clays have been found to undergo fines migration. The permeability damage caused by essentially non-swelling clays such as kaolinite and chlorite is a well-known phenomenon. Silica fines have been identified as a potential source of permeability damage in various poorly consolidated U.S. Gulf Coast formations (1). Other minerals identified as constituents of mobile fine particles include feldspar, calcite, dolomite, and siderite (4,5).

The migration of iron mineral fines, primarily hematite and magnetite, is a common occurrence in portions of the Appalachian Basin. The phenomenon often occurs after well stimulation and can result in the continuing production of iron mineral fines which pose a significant disposal problem. The migration of iron mineral fines through propped fractures can substantially reduce the fracture flow capacity. Many of these iron mineral fines are native to the formation and are not formed by precipitation of acid-soluble iron salts present in injection waters during or after acidi-

zing. (These iron salts can precipitate as the acid spends and the pH increases.)

Organic Polymer Structures

Some of the structures of the organic polymers claimed in the patent literature to be effective swelling clay or mineral fine particle stabilizers are detailed in Table I. Chemical structure considerations for field use include compatibility with fracturing polymer (polysaccharide) crosslinkers and enhanced oil recovery (EOR) chemicals such as anionic surfactants and partially hydrolyzed polyacrylamides and high pH solutions used in caustic flooding. Structures which cause the polymer to increase aqueous fluid viscosity are undesirable. High temperature (500°-600° F) can also be an important consideration for high temperature formations or use in thermal EOR processes such as steam injection.

Organic polymers claimed to be effective swelling clay and mineral fine particle stabilizers in the patent literature can be divided into four classes. The polymers of class 1 have the quaternary nitrogen atom as part of the polymer backbone (6-10). Polymers in this class include poly(dimethylamine-co-epichlorohydrin, abbreviated poly(DMA-co-EPI), and poly(N,N,N',N'-tetramethyl-1,4-1,4-diaminobutane-co-1,4-dichlorobutane), abbreviated poly (TMDAB-co- DCB). These low molecular weights are not surprising since these are condensation polymers. Molecular weights cited range from 800 to 800,000 daltons.

Polymers in which the quaternary nitrogen atom is part of a five- or six-membered ring comprise the second class of polymers. The ring forms part of the polymer backbone as indicated by the second and third polymer repeat units given in Table I. The member of this class cited in several patents is poly(diallyldimethylammonium chloride) abbreviated poly(DMDAAC).

Both five- and six-membered ring structures (see Table I) have been proposed for poly(DADMAC). The most recent work, a ¹³C NMR study, supports a five-membered ring structure for the polymer repeat unit (10). High molecular weight products may be synthesized by free radical polymerization. DADMAC polymers having molecular weights as high as 2.6×10^6 daltons have been evaluated as clay stabilization agents (12).

Both poly(DMA-co-EPI) and poly(DADMAC) have been widely used in the field in acidizing, hydraulic fracturing, sand control, and other well treatments (12).

The third class of polymers contains one or more nitrogen atoms on a pendant sidechain in the polymer repeat unit (13,14). The nitrogen may or may not be quaternary. In addition to being swelling clay stabilizers, these polymers also stabilize non-swelling mineral fine particles. Limited molecular weight data is available but molecular weight values from 50,000 to 1×10^6 daltons have been cited for various polymers.

The final class of polymers are copolymers containing one or more of the repeat units of classes 2 and 3 (15-18). Copolymer effectiveness would presumably be a function of the chemical structures of each comonomer, comonomer sequence distribution, and polymer molecular weight. The comonomer could be a relatively

Table I. Chemical Structures of Clay and Mineral Fines Stabilizers

<u>Polymer Repeat Unit</u>	<u>Reference</u>
	6-9, 12, 13
	6-10, 12, 13
$\text{---} \left(\text{CH}_2 \right)_n \text{N}^+ (\text{CH}_3)_2 \text{---} \right)_n \quad n\text{Cl}^-$	6-9
$\text{---} \left(\text{CH}_2 \right)_6 \text{N}^+ (\text{CH}_3)_2 \text{---} \left(\text{CH}_2 \right)_7 \text{N}^+ (\text{CH}_3)_2 \text{---} \right)_n \quad 2n\text{Cl}^-$	6-9
$\text{---} \left(\text{CH}_2 \text{CH}_2 \text{N}^+ (\text{CH}_3)_2 \right)_n \quad n\text{Cl}^-$	6-9
$\text{---} \left(\text{N}^+ (\text{CH}_3)_2 \text{---} \left(\text{CH}_2 \right)_6 \text{N}^+ (\text{CH}_3)_2 \text{---} \left(\text{CH}_2 \right)_3 \right)_n \quad 2n\text{Br}^-$	12
	12, 14
	15
	17
	16
	18
$A = \left[\text{CH}_2 \text{---} \text{C} \begin{array}{l} \text{CH}_3 \\ \\ \text{CO}_2 \text{H or Na} \end{array} \right]$	

inexpensive chemical as compared to the nitrogen-containing monomer. Only copolymers of class 3 repeat units appear to have been studied.

Laboratory Test Procedures

Swelling Clay Stabilization. The laboratory evaluation test for swelling clay stabilizers is described in detail in reference (18). Briefly, a test column containing a blend of 85% (by weight) 70-170 U.S. mesh sand, 10% silica flour (<325 U.S. mesh), and 5% Wyoming bentonite is prepared. A synthetic brine (see Table II) is injected to establish a standardized flow rate to which subsequent flow rates are compared. The subsequent fluid injection sequence is given in the various data tables. The post-treatment brine flow rate indicates whether the polymer treatment has reduced the test column permeability. Fresh water flow rate determines the effectiveness of the test polymer as a water-swelling clay stabilizer. The fresh water flow rate after aqueous 15% hydrochloric acid injection indicates the durability of the treatment to conditions likely to be encountered in sandstone acidizing.

Mineral Fine Particle Stabilization. Experiments were performed using test columns packed with a well blended mixture of 85% (by weight) 70-170 U.S. mesh sand and 15% mineral fine particles. The size distributions of the mineral fine particles are summarized below:

Table II. Mineral Fine Particle Properties

Mineral	Median Particle Diameter (microns)	Surface Area (meter ² /gram)
silica	22.4	1.200
2:1 silica:kaolinite	0.88 ^a	11.992
calcite	8.9	10.892
hematite	4.4	6.440

a. kaolinite only

A screen with 100 U.S. mesh (149 micrometer) openings was placed at the bottom of the test column to prevent the production of coarse sand particles from the test column. To avoid injection fluid turbulence disturbing the test sand, a 7.5g layer of 20-40 U.S. mesh sand was placed on top of the test sand. All fluids except polymer solutions were filtered prior to injection. Polymer solutions were injected at 5 psia and immediately followed by aqueous fluid at 40 psig. Effluent fluids were collected and filtered through 0.45 micron paper to collect the produced fine particles.

Core floods were performed to determine if treatment polymers would prevent permeability damage caused by fines migration within consolidated rock and whether the adsorbed polymers would themselves reduce core permeability. The tests were performed using Hassler sleeve chambers. With the exception of the polymer

treatment fluid, all injection fluids were passed through a two micron in-line filter prior to injection. There was no shut-in time following polymer treatment of the cores. Flow directions were adjusted to model treatment of both injection and production wells.

Fines production from untreated test sands and permeability damage observed in untreated cores indicated that the laboratory test flow rates were above the critical flow velocity required to initiate fines migration.

Laboratory Test Results - Swelling Clay Stabilizers

The performance properties of two Class 1 polymers, poly(DMA-co-EPI) and poly(TMDAB-co-DCB) as swelling clay stabilizers are summarized in Table III. Results using aqueous 5% hydrochloric acid as the polymer solvent and results noted when flowing aqueous 15% hydrochloric acid through polymer-treated test columns suggest that increasing the polymer molecular weight from 1750 to 7500 daltons may improve poly(DMA-co-EPI) performance in acidizing applications.

Similar molecular weight poly(DMA-co-EPI), 1750 daltons, *ca.* 13 repeat units, and poly(TMDAB-co-DCB), 1500 daltons, *ca.* 11 repeat units were compared. The two condensation polymers appeared to be about equally effective in preventing the swelling of Wyoming bento-nite. Any small differences are probably due to repeat unit chemical structure differences rather than the small variations in polymer molecular weight. The presence of the hydroxyl group and the smaller $N^+ - N^+$ distance in poly(DMA-co-EPI) could affect polymer conformation in solution, geometry of the polymer - clay complex, and surface properties of the polymer - clay complex as compared to poly(TMDAB-co-DCB).

A series of DADMAC polymers was studied using the sample flow test design. The results summarized in Table III suggested that polymer-promoted clay stabilization in neutral media decreased with an increase in molecular weight from 37,000 to 75,000 daltons. However, performance in strongly acidic media such as encountered in acidizing appeared to improve with the same change in polymer molecular weight.

DADMAC polymers were also evaluated as cement slurry additives. The low viscosity polymers had little effect on cement fluid loss rates. The cement filtrate was collected and injected into the test column described above. In the absence of polymer, injection of cement filtrate resulted in rapid plugging of the test column. However, good permeability retention was observed during injection of cement filtrates containing poly(DADMAC). This polymer apparently flocculated fine particles in the cement slurry. This resulted in fewer formation damaging cement fine particles being present in the cement slurry. These particles caused rapid column plugging upon injection of the filtrate which did not contain poly(DADMAC). As before, polymer treated stabilized the test column to fresh water injection (see Table IV). In the absence of poly(DADMAC), fresh water injection would cause rapid column plugging as was observed in the first experiment summarized in Table III.

TABLE III. EFFECTIVENESS OF QUATERNARY AMMONIUM SALT POLYMERS AS SWELLING CLAY STABILIZERS^a

	none	poly(DMA-co-EPI)	poly(DMA-co-EPI)	poly(DMA-co-EPI)	poly(TMDAB-co-DCB)	poly(DADMAC)			
molecular weight	--	1750	7500	1750	7500	1500	37,000	50,000	75,000
polymer concentration % by weight	0	0.37	0.37	0.37	0.37	0.37	2.0	2.0	2.0
polymer solvent	SB	SB	SB	5% HCl	5% HCl	SB	SB	SB	SB
initial SB flow rate, cc/min	14.6	21.2	19.4	26.3	35.3	23.1	14.4	12.8	15.2
post-treatment flow rates, % of initial	100.0	121.2	134.5	85.2	186.2	116.9	102.8	100.0	92.1
fresh water	1.0	159.4	182.0	108.7	124.9	124.2	104.2	100.0	81.6
15% HCl	--	44.8	93.8	10.9	85.5	51.5	73.6	79.6	82.4
fresh water	--	184.0	156.2	117.5	113.1	160.2	91.7	85.9	68.4
diesel oil	--	--	--	139.2	72.2	--	--	--	--
fresh water	--	--	--	24.1	24.2	--	--	--	--
diesel oil	--	--	--	132.1	72.2	--	--	--	--

a. Data taken from references 6-9. The synthetic brine (SB) contained by weight 7.50% NaCl, 0.55% CaCl₂, and 0.20% MgCl₂. Injection volumes of polymer solution, standard brine, fresh water, aqueous 15% HCl, fresh water, and diesel oil were 300cc, 500cc, 500cc, 400cc, 500cc, and 500cc respectively. T = 60°C (140°F).

Table IV. Effectiveness of poly(DADMAC) as a Swelling Clay Stabilizer When Used in Cement Slurries

Fluid Injected	Flow Rate After poly(DADMAC) Treatment poly (DADMAC) Molecular Weight (% of initial brine before filtrate injection)	
	600,000	2,600,000
Standard Brine	47.1	25.6
Fresh Water	56.7	22.3
15% HCl	152.6	75.9
Fresh Water	182.5	78.9

a. The base fluid for the cement slurry was aqueous 5% KCl. Polymer concentration was 6555-6880 ppm.

Results indicated that poly(DADMAC) will reduce damage caused by contact of low salinity fluid lost from the cement slurry with swelling clays present in the formation. An increase in poly (DADMAC) molecular weight from 600,000 to 2.6×10^6 daltons resulted in a decreased polymer effectiveness. The test columns were of relatively high permeability so the thickness of the adsorbed polymer layer, predicted to be greater for the higher molecular weight polymer, would have little effect on the observed flow rates.

Laboratory Test Results - Mineral Fines Stabilizers

While clay swelling and concomitant fine particle migration is a major cause of permeability damage, reduction of permeability caused by fines migration in the absence of swelling clays can also occur. This fines migration is due to a combination of chemical and mechanical forces and is greatest in the near-wellbore region where fluid flow rates are highest. Mineral fine particles which can cause permeability damage include silica, relatively non-swelling clays such as kaolinite, carbonates such as calcite and dolomite, and iron minerals such as hematite, siderite, and magnetite.

A series of U.S. patents (13-17) indicate that polymers containing nitrogen atoms in relative long sidechains are effective in reducing the migration of the various mineral fine particles enumerated above.

Homopolymers. Polymers such as poly(methacrylamido-4,4,8,8-tetramethyl-4,8-diaza-6-hydroxynonamethylene dichloride), abbreviated poly(MDTHD), and a triaza analog, abbreviated poly(MTHHDT), have been shown to be effective stabilizers of silica, calcite, and hematite (14,15) as indicated by the data summarized in Table V.

Results indicated that swelling clay stabilizers such as poly (DMA-co-EPI) which do not possess a quaternary nitrogen atom in a pendant chain may not be very effective at preventing permeability damage due to fines migration in the absence of water-swelling clays.

Table V. Mineral Fines Production From Unconsolidated Test Columns^a

Polymer (N atoms in sidechain)	Mineral Fines Production (% of untreated column), mineral fines used:		
	silica	calcite	hematite
poly(MDTHD) (2)	5.8	28.0	39.5
poly(MTHHDT) (3)	14.3	83.3	66.7
poly(APTMAC) (2)	65.0	49.6	139.5
poly(DMA-co-EPI) (0)	65.0	165.4	139.5

a. The polymer solvent was aqueous 2% NH_4Cl . Polymer concentration was 2% by weight active material. Test temperature was 62.8°C (145°F). Mineral fines production was measured during injection of 27 pore volumes of fresh water.

The methacrylamide backbone of the most effective polymers suggests they are produced by free radical copolymerization. Relatively little molecular weight information on these polymers is available although the molecular weight of a triaza analog of MDTHD has been given as 135,000 daltons (15). Similar polymers having acrylamide backbones such as poly(acrylamido-3-propyltrimethylammonium chloride), abbreviated poly(APTMAC) appear less effective in this application (14) probably due to their greater tendency to increase aqueous fluid viscosity and thus suspend solids (Table V).

Copolymers. Copolymers have also been studied (16-18). While one comonomer contains 1-2 quaternary nitrogen in a flexible pendant chain, the other comonomer was nonionic. Copolymers of the methyl chloride salt of dimethylaminoethyl methacrylate (one quaternary nitrogen atom) and dimethylaminoethyl methacrylate (DMAEMA) and of MDTHD (2 quaternary nitrogen atoms) and DMAEMA, N,N-dimethylacrylamide (NNDMAm) or dimethylaminopropyl methacrylate (DMAPMA) have been studied and the results summarized in Table VI.

Copolymers of MDTHD and DMAPMA appeared to be the most effective silica, calcite, and hematite mineral fines stabilizers. Increasing the copolymer MDTHD content had little effect on polymer performance. Similar results were observed for a series of MDTHD - DMAEMA copolymers and a series of DMAEMA $\cdot\text{CH}_3\text{Cl}$ salt - DMAEMA copolymers (Table VI). In contrast, increasing the MDTHD content of MDTHD - NNDMAm copolymers from 67% to 90% improved copolymer performance as a silica fines and hematite fines stabilizer.

Terpolymers of DMAEMA, the methyl chloride salt of DMAEMA, and a termonomer: the sodium salt of 2-acrylamido-2-methylpropane sulfonic acid (AMPS), methacrylamidopropyltrimethylammonium chloride (MAPTAC), or NNDMAm, were studied (Table VI). For 9% termonomer, AMPS-containing polymers provided the most effective silica fines stabilization. This was somewhat surprising since MAPTAC contains a quaternary ammonium group on a flexible sidechain. Consistent with the relatively poor performance of the 9% MAPTAC terpolymer was the observation that, when the terpolymer MAPTAC content was increased from 9% to 33%, silica fines stabilization was not substantially increased.

TABLE VI. EFFECTIVENESS OF COPOLYMERS AS MINERAL FINES STABILIZERS^a

Copolymer	Treatment Fluid Viscosity (cps)	Mineral Fines Production (% of untreated test column)			
		Silica before 15% HCl injection	Silica after 15% HCl injection	Calcite	Hematite
1:2 MDTHD:NNDMam	1.6	38.1	32.4	77.8	88.9
2:1 MDTHD:NNDMam	1.9	42.3	35.3	---	72.2
2:1 MDTHD:NNDMam	2.2	19.1	20.6	---	---
9:1 MDTHD:NNDMam	---	14.3	26.4	---	---
1:2 MDTHD:DMAEMA	1.7	14.3	23.5	---	94.4
1:1 MDTHD:DMAEMA	2.6	14.3	23.5	---	---
2:1 MDTHD:DMAEMA	---	23.8	23.5	---	100.0
7:3 MDTHD:DMAEMA	---	9.5	---	37.2	57.1
8.75:1.25 MDTHD:DMAEMA	---	19.1	---	---	---
9.0:1.0 MDTHD:DMAEMA	---	9.5	---	---	---
9.5:0.5 MDTHD:DMAEMA	---	9.5	---	---	---
1:9 DMAEMA CH ₂ Cl:DMAEMA	2.7	23.8	29.4	---	---
1:3 DMAEMA CH ₂ Cl:DMAEMA	2.6	23.8	26.5	81.1	77.8
1:1 DMAEMA CH ₂ Cl:DMAEMA	2.6	38.1	29.4	---	---
3:1 DMAEMA CH ₂ Cl:DMAEMA	2.6	28.6	32.4	114.6	100.0
1:1 DMAEMA CHCl ₃ :DMAEMA	5.1	23.8	35.3	---	---
1:2 MDTHD:DMAEMA ^b	---	27.6	---	---	---
1:1 MDTHD:DMAEMA ^b	---	20.7	---	---	---

Continued on page 214

TABLE VI (continued). EFFECTIVENESS OF COPOLYMERS AS MINERAL FINES STABILIZERS^a

Copolymer	Treatment Fluid Viscosity (cps)	Mineral Fines Production (% of untreated test column)			
		Silica before 15% HCl injection	Silica after 15% HCl injection	Calcite	Hematite
DMAEMA (CH ₃) ₂ SO : DMAEMA : AMPS 45.5:45.5:9 1.9		42.9	38.2	----	----
DMAEMA (CH ₃) ₂ SO : DMAEMA : NNDMAM 45.5:45.5:9 2.0		33.3	29.4	----	----
DMAEMA CH ₃ Cl : DMAEMA : MAPTAC 45.5:45.5:9 2.0		23.8	29.4	----	----
DMAEMA CH ₃ Cl : DMAEMA : MAPTAC 33.3:33.3:33.3 1.8		33.3	29.5	----	----

a. See footnote a, Table V for experimental details. Data taken from reference 18.

b. The polymer solvent was aqueous 15% HCl.

The observation that the quaternary ammonium monomer content of MDTHD:DMAEMA and DMAEMA CH_3Cl :DMAEMA copolymers had little effect on their silica fines stabilization properties of prompted an investigation of nonionic polymers as mineral fines stabilizers (17,18). A series of N-vinylpyrrolidinone (NVP) copolymers with DMAEMA have been studied. Results are summarized in Table VII.

Table VII. Reduction of Mineral Fines Production Using NVP Copolymers^a

NVP Comonomer % by weight comonomer	Mineral Fines Production (% of untreated test column)				
	DMAEMA 20	DMAEMA 20	DMAEMA 8	DMAEMA·DMAEMA(CH ₃) ₂ SO ₄ 12	DMAEMA·DMAEMA(CH ₃) ₂ SO ₄ 8
Molecular Weight	1x10 ⁵	1x10 ⁶	1x10 ⁶	1x10 ⁶	1x10 ⁶
<u>Mineral Fines</u>					
Silica					
before 15% HCl	9.5	17.6	9.5		14.3
after 15% HCl	9.5	----	20.6		14.4
Silica/Kaolinite					
before 15% HCl	---	75.6	----		4.4
after 15% HCl	---	52.9	----		5.3
Calcite	---	69.8	----		51.2
Hematite	---	32.4	----		47.6

a. See footnote a, Table V and Laboratory Test Procedures section for experimental details.

Limited silica fines stabilization data indicated that increasing copolymer molecular weight from 100,000 to 1,000,000 daltons had, if anything, a negative effect on silica fines stabilization. At a molecular weight of 1,000,000 daltons, this copolymer appeared to be more effective in stabilizing silica fines than silica/kaolinite, calcite, or hematite fines. However, the results may be due in part to the larger particle size and lower surface area of the silica fines (see Table II).

When the DMAEMA content of NVP - DMAEMA copolymers was reduced from 20% to 8%, the silica fines stabilization effectiveness appeared to improve slightly. When the 80/20 NVP - DMAEMA copolymer was converted to a terpolymer containing 8% DMAEMA $(\text{CH}_3)_2\text{SO}_4$, silica fines stabilization was substantially unaffected. However, stabilization of silica/kaolinite fines was greatly improved. This suggested that the interaction of polymer quaternary nitrogen atoms with anionic sites on mineral surfaces was important for the stabilization of migrating clays but a different interaction was important for the stabilization of silica fines. Calcite fines stabilization improved while hematite fines stabilization effectiveness decreased. This also indicated the nature of the adsorbed polymer - fine particle complex varied for different minerals.

Berea core flood test results (Table VIII) suggested that the presence of DMAEMA $(\text{CH}_3)_2\text{SO}_4$ improved the permeability damage characteristics of 80% NVP copolymers. The kerosene flow rate

TABLE VIII. PERMEABILITY DAMAGE CHARACTERISTICS OF NVP COPOLYMER MINERAL FINES STABILIZERS - BEREA CORE TESTS^a

Injected Fluid	80:20 poly(NVP-co-DMAEMA)		80:12:8 poly(NVP-co-DMAEMA-co-DMAEMA (CH ₃) ₂ SO ₄)	
	Cumulative Volume Injected (cc)	Stabilized Permeability (md)	Cumulative Volume Injected (cc)	Stabilized Permeability (md)
Synthetic Brine	400	104	800	552
Kerosene	800	246	1200	243
Synthetic Brine	1350	27	1600	34
0.25%w polymer ^b	1450	---	1700	---
Synthetic Brine	2560	22	2115	45
Kerosene	2960	185	2515	239

a. See reference 17 for experiment details. T = 60°C (140°F). Polymer molecular weight was 1,000,000 daltons. The Berea sandstone test cores contained 5-10% kaolinite, 2-5% illite, 0-2% chlorite, and 0-5% mixed layer clays.

b. The polymer solvent was aqueous 2% by weight ammonium chloride solution.

after polymer treatment of the core was 98% of the pretreatment flow rate when the polymer contained 8% DMAEMA $(\text{CH}_3)_2\text{SO}_4$ compared to 75% when no DMAEMA $(\text{CH}_3)_2\text{SO}_4$ was present in the polymer.

The results summarized in Table IX indicated that another copolymer which does not contain quaternary nitrogen atoms, poly (DMAEMA - co - methyl acrylate) was also an effective silica fines stabilizer.

Increasing the molecular weight of a copolymer containing 5% methyl acrylate (MA) from 100,000 to 1,000,000 daltons had little effect on silica stabilization effectiveness (see Table IX). Increasing the methyl acrylate content from 5% to 30% had also little effect on silica fines stabilization effectiveness. Acidizing substantially reduced the effectiveness of this class of copolymer. Results for the injection of 10,000 pore volumes of water indicated that silica fines elution from the test column was substantially reduced on a long-term basis.

The effectiveness of nonionic polymers as migrating clay stabilizers and the geometry of the adsorbed polymer - mineral complex may be substantially different for the nonionic polymers and the quaternary ammonium salt polymers. The observation that some quaternary ammonium salt polymers, while effective swelling clay stabilizers, are ineffective mineral fines stabilizers is consistent with a different adsorbed polymer - particle complex geometry on different mineral surfaces.

Monomer reactivity ratios and thus comonomer sequence distributions in copolymers can vary with copolymerization reaction conditions. The comonomer distribution could affect the geometry of the adsorbed polymer - mineral complex and the fines stabilization properties.

Field Test Results

Experiment 1. While there have been a number of reports concerning the effectiveness of quaternary ammonium salt polymers as swelling clay stabilizers in controlling formation damage, the number of wells involved was usually too small for the comparison of results (between well treatments which utilize quaternary ammonium salt polymers and those which do not) to be statistically significant. However, two sets of statistically significant field results for the stimulation of a large number of wells in the Fordache Field (Pointe Coupee Parish, Louisiana) are available (19). The wells were completed in the Wilcox W-8 and Sparta A formations. Average formation permeability was 8.6 and 180 millidarcies respectively. Formation temperatures were 109°C (228°F) and 132°C (270°F) respectively. Swelling and migration of silicate mineral fines were cited as the cause of rapid production declines in these wells.

The stimulation treatments were performed using retarded hydrofluoric acid. A typical retarded hydrofluoric acid treatment consisted of:

1. 100 gal/ft of perforated interval of aqueous 5% HCl
2. 50 gal/ft of perforated interval of aqueous 3%HF/12% HCl
3. 25 gal/ft of perforated interval of 2.8% NH_4F (pH 7-8)
4. 25 gal/ft of perforated interval of aqueous 5% HCl
5. Repetition of steps 3 and 4 five times

TABLE IX. EFFECTIVENESS OF DIMETHYLAMINOETHYLACRYLATE METHYL ACRYLATE COPOLYMERS AS SILICA FINES STABILIZERS^a

weight % DMAEMA	Polymer Molecular Weight	Polymer Concentration (% by weight)	Silica Fines Production (% of untreated column) before 15% HCl	Silica Fines Production after 15% HCl
95	100,000	0.20	23.8	44.1
95	300,000	0.19	9.5	50.0
95	500,000	0.19	14.3	44.1
95	1,000,000	0.19	9.5	47.1
70	200,000	0.40	38.1	41.2
70	>1,000,000	0.45	14.3	50.0
95	1,000,000	0.19	59.5 ^b	-----
70	1,000,000	0.20	55.0 ^c	-----

a. See reference 16 for experimental details. T = 62.8°C (145°F).

b. Total fines production after injection of 10,015 pore volumes fresh water.

c. Total fines production after injection of 10,502 pore volumes fresh water.

6. 100 gal/ft perforated interval of diesel oil or aqueous NH_4Cl
7. the required volume of diesel oil, aqueous NH_4Cl , or nitrogen to displace fluids from the tubing.

Average treatment volume was 600 gallons. All fluids contained 1% (by volume) of water wetting non-emulsifier. The treatments utilizing a cationic organic polymer included the polymer in all aqueous based fluids. The reported polymer concentration of one percent by volume of the aqueous polymer solution as supplied. Active polymer concentration is actually less than this. When the clay stabilization polymer was part of the well treatment, a non-ionic water wetting nonemulsifier was used.

The first set of data is for oil production from 22 wells. A quaternary ammonium salt polymer clay stabilizer was utilized in five of the well treatments. Otherwise the 22 well treatment designs were identical. Use of the clay stabilizer in 5 well treatments resulted in a 131% production increase compared to a 156% increase after stimulation of 17 wells without clay stabilizer. Although the initial overall production response of the five clay stabilizer treated wells was less, the overall production decline rate was 4% per year compared to 16%/yr for the treatments which did not include the clay stabilizing polymer. This decline rate was determined for the period 4 to 24 months after well treatment. It is tempting to speculate that the lower initial production response of the five polymer treated wells was due to the formation of an adsorbed polymer layer which reduced formation permeability (particularly of the Wilcox Formation) significantly.

Gas production from sixteen wells was also analyzed. Twelve retarded hydrofluoric acid treatments did not include the clay stabilization polymer. The overall gas production increase was 116% compared to an overall increase of 200% obtained from four wells for which the clay stabilization polymer was included in the well treatment. With the exception of the use of the clay stabilizer, the sixteen well treatment designs were identical.

Experiment 2. A cationic organic polymer has also been evaluated as a mineral fines stabilizer in a statistically significant number of acidizing treatments utilizing hydrofluoric acid (20). This polymer was reported to remain cationic in both acidic and basic media. Thus the cationic sites appear to be quaternary nitrogen atoms. This study involved twenty offshore Louisiana wells completed in a Miocene sand having a formation temperature of $79^\circ - 82^\circ\text{C}$ ($175^\circ - 180^\circ\text{F}$). Wells in this area had a history of production declines apparently caused by mineral fines migration. A large treatment volume, 18,000 - 28,000 gallons, was used to provide substantial radial penetration of the formation. The treatment design was:

1. 50 gal/ft of formation 15% aqueous HCl containing 5% mutual solvent and 1% water wetting non-emulsifier and 50 lb/1000 gallons citric acid
2. 50 gal/ft of formation aqueous 3% HF/12% HCl
3. 300 gal/ft of formation aqueous retarded HF acid
4. the required volume of fluid required to displace all the acid from the tubing into the formation

A corrosion inhibitor was present in all acid fluids. Eight of the well treatments incorporated a cationic organic polymer mineral fines stabilizer in the first three treatment stages. The active polymer concentration was less than the reported aqueous polymer concentration of one percent (by volume). Again, this was because the polymer was not supplied as a 100% active product.

Production was monitored for 4-6 months after the stimulation treatments. Total oil production from the twelve wells treated without the polymeric mineral fines stabilizer (1100 bbl/day) was decreasing at a rate of 0.13%/day while the produced water:oil ratio remained fairly constant. The eight wells treated using the cationic organic polymer mineral fines stabilizer exhibited a total oil production of 7700 bbl/day which was increasing at a rate of 0.32% per day. The water:oil ratio remained constant.

The twelve wells for which no cationic organic polymer fines stabilizer was used were exhibiting increasing gas production (0.15% per day) four to six months after the well treatments. This increase was due to the performance of one well from which gas production had more than doubled (from 1.46 MM scf/day to 2.14 scf/day). If this well is omitted from consideration, total gas production from the remaining wells was 4.92 MM scf/day and was decreasing at a rate of 0.06%/day. In contrast, total gas production from the eight wells treated using the cationic organic polymer mineral fines stabilizer, 3.39 MM scf/day, was increasing at a rate of 0.49%/day.

Conclusions

Results indicate that the effectiveness of quaternary ammonium salt polymers in stabilizing swelling clays and mineral fine particles is dependent on monomer chemical structure and polymer molecular weight. Long flexible pendant sidechains containing quaternary nitrogen atoms appear to be required for these polymers to function as mineral fine particle stabilizers.

Nonionic copolymers of N-vinylpyrrolidinone also functioned as mineral fine particle stabilizers.

The results of two field experiments involving a statistically significant number of wells indicated that quaternary ammonium salt polymers can function well as swelling clay and mineral fine particle stabilizers under actual field conditions.

Literature Cited

1. Borchardt, J.K.; Roll, D.L.; and Rayne L.M. Proceedings of the 55th Annual California Regional Meeting of the Society of Petroleum Engineers, 1984, pp. 297-310, Paper No. SPE 12757 and references therein.
2. Gabriel, G.A.; Inamdar, G.R. Proceedings of the 56th Annual Fall Technical Conference and Exhibition of the Society of Petroleum Engineers, 1983, Paper No. SPE 12168.
3. Reed, M.G.; Coppel, C.P. Proceedings of the 43rd Annual California Regional Meeting of the Society of Petroleum Engineers, 1972, Paper No. SPE 4186.
4. Muecke, T.W. J. Pet. Technol. 1979, 31, 144.

5. Khilar, K.C.; Fogler, H.S. Soc. Pet. Eng. J., 1983, 23, 55.
6. McLaughlin, H.C.; Weaver, J.D. U.S. Patent 4 366 071, 1982.
7. McLaughlin, H.C.; Weaver, J.D. U.S. Patent 4 366 072, 1982.
8. McLaughlin, H.C.; Weaver, J.D. U.S. Patent 4 366 073, 1982.
9. McLaughlin, H.C.; Weaver, J.D. U.S. Patent 4 366 074, 1982.
10. Anderson, R.W.; Kannenberg, B.G. U.S. Patent 4 158 521 (1979).
11. Lancaster, J.E.; Baccei, L.; Panzer, H.P. J. Polym. Sci. Polym. Lett. Ed., 1976, 14, 549.
12. Smith, C.W.; Borchardt, J.K. U.S. Patent 4 393 939, 1983.
13. Hall, B.E. World Oil December, 1986, 49.
14. Borchardt, J.K.; Young, B.M. U.S. Patent 4 497 596, 1985.
15. Borchardt, J.K.; Young, B.M. U.S. Patent 4 536 305, 1985.
16. Borchardt, J.K.; Young, B.M. U.S. Patent 4 558 741, 1985.
17. Borchardt, J.K. U.S. Patent 4 536 303, 1985.
18. Borchardt, J.K. U.S. Patent 4 563 292, 1986.
19. Holden, III, W.W.; Prihoda, C.H.; Hall, B.E. J. Pet. Technol., 1981, 33, 1485.
20. Presented at the 55th Annual California Regional Meeting of the Society of Petroleum Engineers and available as an addendum to reference 1.

RECEIVED November 28, 1988

Chapter 11

Influence of Calcium on Adsorption Properties of Enhanced Oil Recovery Polymers

L. T. Lee, J. Lecourtier, and G. Chauveteau

Institut Français du Pétrole, B.P. 311, 92506 Rueil-Malmaison, Cedex, France

The influence of calcium on the adsorption of high molecular weight EOR polymers such as flexible polyacrylamides and semi-rigid xanthans on siliceous minerals and kaolinite has been studied in the presence of different sodium concentrations. Three mechanisms explain the increase in polyacrylamide adsorption upon addition of calcium: (i) reduction in electrostatic repulsion by charge screening, (ii) specific interaction of calcium with polymer in solution, decreasing its charge and affinity for solvent, and (iii) fixation of calcium on the mineral surface, reducing surface charge and creating new adsorption sites for the polymer. The intrinsic viscosities of polyacrylamide solutions are significantly lowered in the presence of calcium, and the increase in Huggins constant at high calcium concentrations suggests attractive polymer-polymer interactions. The effects of calcium on polymer-solvent and polymer-surface interactions are dependent on polymer ionicity; a maximum intrinsic viscosity and a minimum adsorption density as a function of polymer ionicity are obtained. For xanthan, on the other hand, no influence of specific polymer-calcium interaction is detected either on solution or on adsorption properties, and the increase in adsorption due to calcium addition is mainly due to reduction in electrostatic repulsion. The maximum adsorption density of xanthan is also found to be independent of the nature of the adsorbent surface, and the value is close to that calculated for a closely-packed monolayer of aligned molecules.

A controlling factor in the success of polymer flooding in enhanced oil recovery (EOR) is the level of polymer adsorption on reservoir rocks. Adsorption depletes polymer from the mobility control slug leading to delayed oil recovery and too high a level of adsorption renders the EOR process uneconomical. Although there has been extensive research in the field of polymer adsorption, a comprehensive study of adsorption of high molecular weight EOR polymers under imposed field conditions has been few (1-10). One of the commonly encountered conditions is the presence of high levels of monovalent and even multivalent ions which can interact with both polymers and solid surfaces, hence complicating further the understanding of the adsorption mechanism. In our previous studies on the

0097-6156/89/0396-0224\$06.00/0

© 1989 American Chemical Society

influence of pH and monovalent ions on adsorption of polyacrylamides and xanthan (9, 10), it has been shown that adsorption of these polymers is mainly governed by a competition of attractive H-bonding and repulsive electrostatic interactions, and that monovalent ions increase adsorption by screening polymer and surface charges and thus reducing electrostatic repulsion.

This study aims at determining the effects of calcium on the adsorption of polyacrylamides and xanthans on siliceous minerals and kaolinite.

Polymers

The polyacrylamides are homopolymer (PAM) and copolymers (HPAM) of acrylamide and acrylate varying from 0 to 50% acrylate content as determined by potentiometric titrations. The average molecular weight for all the samples measured by low angle light scattering is about 8×10^6 daltons. Solutions are prepared by gentle stirring using a magnetic stirrer in de-ionized water containing the required salts and 400 ppm of NaN_3 as stabilizer.

The xanthans (XCPS I, XCPS II) are fully pyruvated samples with mean molecular weights of 1.8×10^6 and 4.2×10^6 daltons respectively (11, 12). Solutions are prepared by diluting a fermentation broth. Any possible existing microgels are removed by a filtration method described elsewhere (13), and low molecular weight impurities are eliminated by ultrafiltration.

Minerals

Siliceous minerals carrying surface silanols (sand and silicon carbide (SiC)) and kaolinite carrying silanols and aluminols are used in this study. The sand is from Entraigues, France. The particle size ranges from 80 to 120 μm and the average specific surface area is $\sim 0.1 \text{ m}^2/\text{g}$. It is washed in 1 M HCl before use. The SiC has a particle size of 18 μm and a specific surface area of $0.4 \text{ m}^2/\text{g}$. The surface of SiC after heat treatment at 300°C and acid washing is oxidized and resembles that of silica (14). The kaolinite is from Charentes (France) and has undergone ion exchange with Na to obtain a homoionic Na-kaolinite. The particle size ranges from 0.2 to 0.8 μm and the total specific surface area is $20 \text{ m}^2/\text{g}$ (15 and $5 \text{ m}^2/\text{g}$ for basal and lateral surface respectively (15)).

Adsorption Measurements

Adsorption is determined by the depletion method using a Dohrmann DC 80 carbon analyzer. The mineral is contacted with the polymer solution and agitated with a mechanical tumbler for 24 hours, a time which has been verified to be sufficient for adsorption to be complete (9). A more detailed description of experimental procedures is given elsewhere (10). All the data reported in this study are taken in the plateau region of the adsorption isotherm.

Polymer Solution Properties

The properties of polymers in solution are investigated in conjunction with adsorption since solution properties are dependent on polymer-solvent interactions

which affect the polymer behavior at the interface. The reduced specific viscosities of HPAM (ionicity = 30%) in 2 g/l NaCl and various concentrations of CaCl₂ are plotted as a function of polymer concentration in Figure 1. For a flexible polyelectrolyte, an increase in salt concentration significantly reduces the intrinsic viscosity, $[\eta]$, due to screening of charged groups on the polymer and thus decreasing the electrostatic persistence length. This is observed upon increasing NaCl from 2g/l (solid line) to 20g/l (dotted line) in the absence of CaCl₂ where $[\eta]$ decreases from 12700 to 4200 cm³/g respectively. For HPAM in the presence of monovalent ions, the $[\eta]$ has been found to be proportional to $c_s^{-1/2}$, where c_s is the monovalent salt concentration (9, 10). In the presence of CaCl₂ (2, 5 and 10 g/l) at 2g/l NaCl, the $[\eta]$ of HPAM decreases even more significantly than expected from ionic strength effect due to specific interactions of the divalent ions with the polymer. Such interactions of HPAM with divalent ions which have also been studied elsewhere (16) using other techniques such as conductivity, densimetry and light scattering alter not only the charge and dimension of the macromolecule but also inter-molecular interactions. The latter is characterized by the Huggins constant, k' (17), which is deduced from the slope of the reduced specific viscosity versus concentration curve. In Figure 2 are $[\eta]$ and k' values (in parentheses) of HPAM (ionicity = 30%) measured in 20g/l NaCl as a function of CaCl₂ concentration. In the absence of Ca²⁺, k' is slightly less than 0.4, a value which corresponds to the theoretical value for free-draining, strictly repulsive non-deformable molecules (17). Upon addition of Ca²⁺, this value increases and reaches 1 at 20g/l CaCl₂, and remains at around the same value at 40g/l CaCl₂. Since the intrinsic viscosities do not decrease significantly in this calcium concentration range and remain at values relatively high compared to θ conditions ($[\eta]_\theta \sim 500$ cm³/g), this high value of k' indicates a tendency for inter-molecular attraction of the macromolecules.

For xanthan (XCPS I), even though its degree of ionicity is higher than that of HPAM, the $[\eta]$ does not appear to be as sensitive to Ca²⁺ (Figure 3). The presence of 2 and 20g/l CaCl₂ produces the same slight effect of reducing the $[\eta]$ from 4300 to 3400 cm³/g, the limiting value at high salinity (11). This is due to the high rigidity of xanthan and thus its large structural persistence length (11, 12) which limits the change in molecular conformation and which renders relatively weak the effects of electrostatic repulsions between charged groups on the polymer chain. The k' in this case remains at 0.4 even up to 20g/l CaCl₂, showing the absence of attractive polymer-polymer interactions.

Polymer Adsorption Properties

Polyacrylamides

Adsorption on Siliceous Minerals. The adsorption of polyacrylamides on siliceous minerals in the presence of monovalent ions has been discussed previously (9, 10). While PAM adsorption is unaffected by monovalent ions since it is not governed by electrostatic factors, HPAM adsorption is increased due to reduction in electrostatic repulsion by charge screening.

In the presence of divalent ions, apart from charge screening, adsorption can be modified due to additional factors arising from specific interactions of the divalent ions with the polymer and the surface. In this case, adsorption of calcium on the SiO₂ surface (15, 18) not only reduces the surface charge but can also

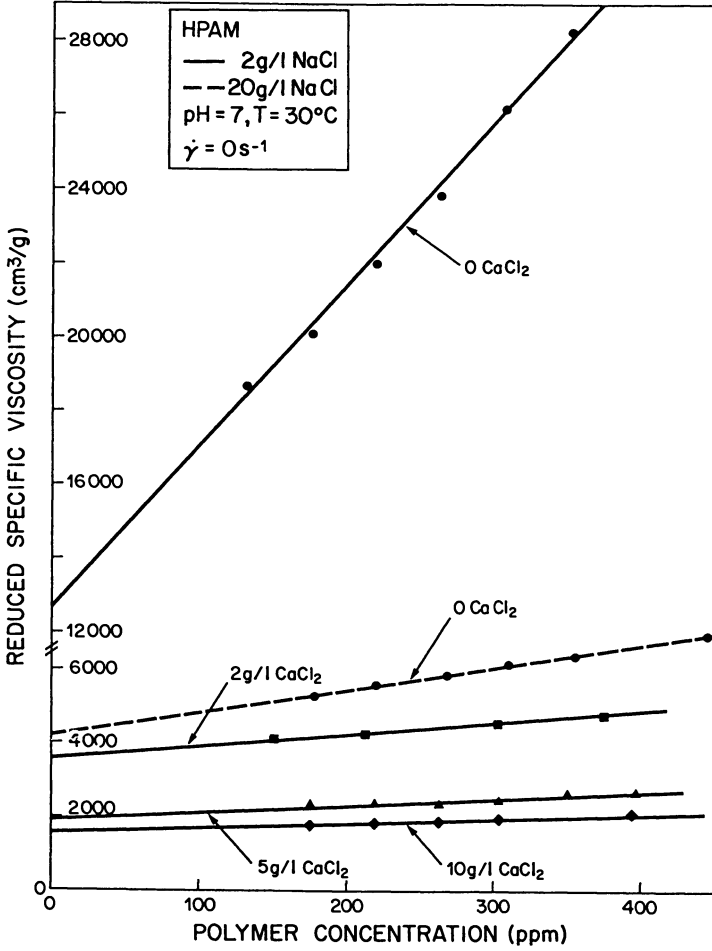


Figure 1. Effect of calcium on zero shear rate reduced specific viscosity of HPAM.

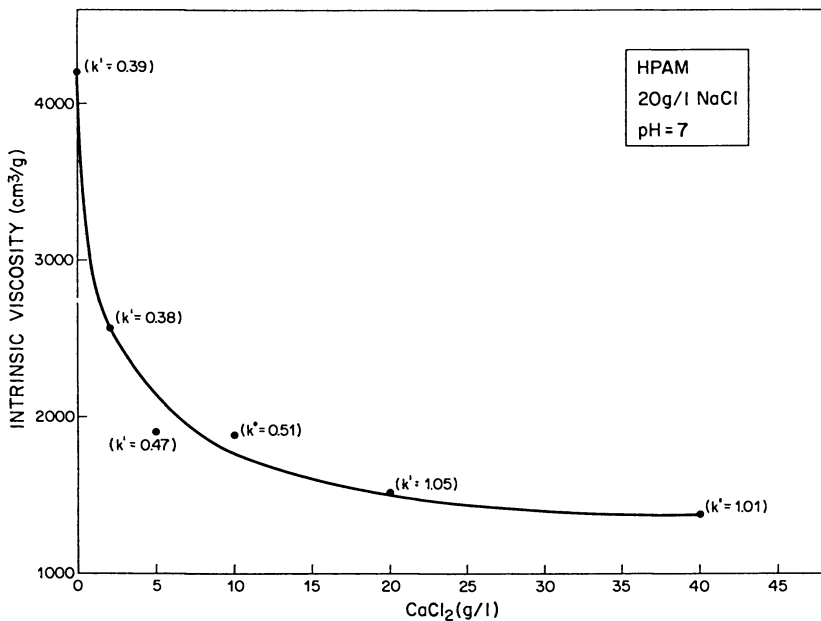


Figure 2. Effect of calcium on intrinsic viscosity and Huggins constant of HPAM.

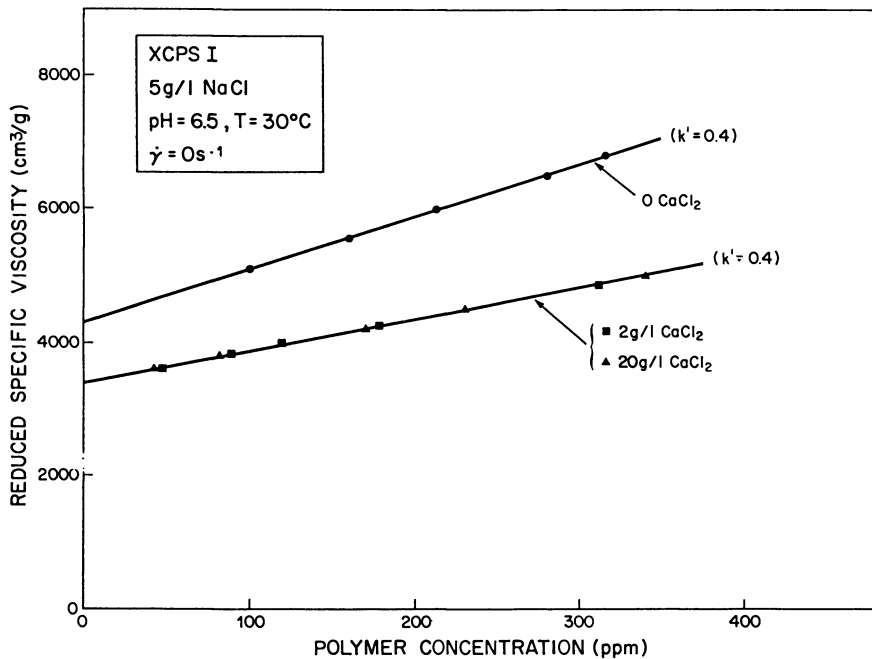


Figure 3. Effect of calcium on zero shear rate reduced specific viscosity of XCPS.

activate polymer adsorption on otherwise non-adsorbent sites (dissociated silanols). The effects of calcium on PAM and HPAM (ionicity = 30%) adsorption at pH 7 in 20g/l NaCl on sand and SiC are shown in Figures 4 and 5 respectively. Although the adsorption of PAM is not governed by electrostatic factors and the $[\eta]$ remains unchanged with Ca^{2+} (see Figure 8) the presence of Ca^{2+} nevertheless provokes a slight but definite increase in its adsorption. This is attributed to the specific interaction of the nonionic polymer with the adsorbed Ca^{2+} . Indeed, weak interaction of Ca^{2+} with PAM has been detected by UV spectroscopy (19). The enhancement in adsorption of PAM by Ca^{2+} is also observed for SiC (Figure 5). Since oxidized SiC surface is similar to SiO_2 surface with a different charge density, Ca^{2+} can be expected to adsorb also on the SiC surface.

The adsorption of HPAM on sand (Figure 4) is not detected below a threshold value of Ca^{2+} due to strong electrostatic repulsion between the polyelectrolyte and the highly charged negative surface. This threshold value, which was also observed in the case of monovalent ions (9), represents the point where the critical adsorption energy is overcome, and once this value is surpassed, adsorption increases sharply. This form of adsorption behavior is in line with predictions of theories on polyelectrolyte adsorption (20).

Mechanistically, calcium increases HPAM adsorption by (i) screening of polymer and surface charges thus reducing electrostatic repulsion, (ii) specific interaction with the polymer in solution decreasing the polymer charge and intrinsic viscosity as shown from the results above, and changing also the polymer affinity for solvent, and, (iii) fixation on the mineral surface serving as a bridge between the negative surface site and polymer. From 1 to 8g/l CaCl_2 , adsorption increases due to the reasons stated above. Between 8 and 15g/l CaCl_2 , adsorption reaches a first plateau where the adsorption density is only about half the value obtained for nonionic PAM; this shows that there is a residual repulsion between the free HPAM and the partially polymer covered sand surface. With further increase in CaCl_2 beyond 15g/l however, adsorption increases until it reaches a second plateau which coincides with the maximum adsorption level for PAM. Interestingly, the region beyond 15g/l CaCl_2 corresponds to the region where the k' increases significantly (see Figure 2). Hence, the additional force of adsorption beyond the first plateau can be related to the occurrence of slight attractive polymer-polymer interactions. An alternative interpretation of the two plateaus observed in the adsorption curve is the existence of two different types of adsorption sites with different reactivities towards the polymer.

Unlike the sand used above, the adsorption of HPAM on SiC at 20g/l NaCl is significant even in the absence of Ca^{2+} (Figure 5). This is mainly due to the lower charge density of SiC, hence the weaker electrostatic repulsion. The higher affinity of HPAM for SiC may also explain the attainment of maximum adsorption at lower Ca^{2+} level, and may also be the reason that the higher interaction of HPAM with Ca^{2+} can induce an adsorption level higher than that of PAM.

Adsorption on Kaolinite. For kaolinite, the polymer adsorption density is strongly dependent on the solid/liquid ratio, S/L , of the clay suspension. As S/L increases, adsorption decreases. This S/L dependence cannot be due totally to auto-coagulation of the clay particles since this dependence is observed even in the absence of Ca^{2+} at pH 7 and at low ionic strength where auto-coagulation as measured by the Bingham yield stress is relatively weak (21). Furthermore, complete dispersion of the particles in solvent by ultra-sonication before addition of

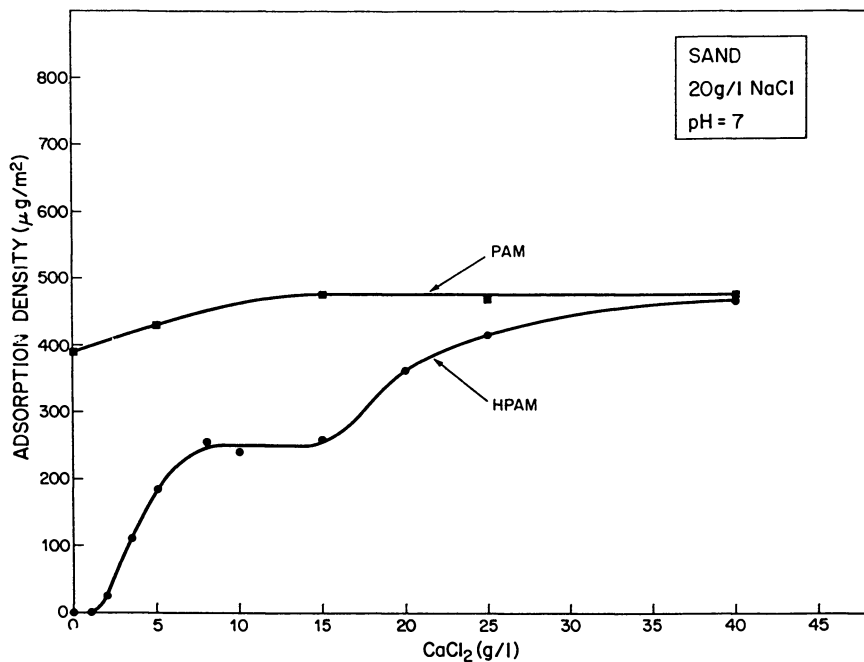


Figure 4. Influence of calcium on adsorption of PAM and HPAM on sand.

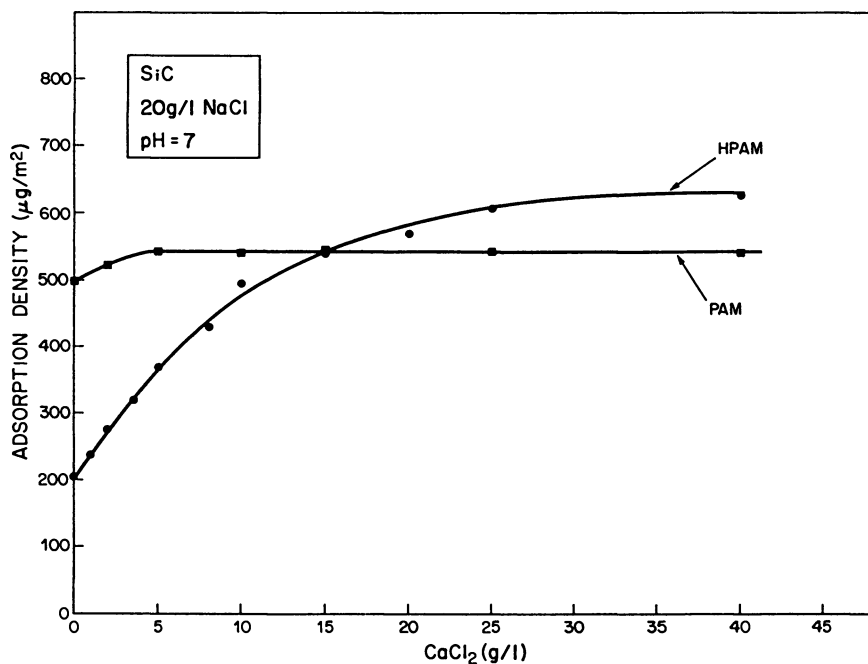


Figure 5. Influence of calcium on adsorption of PAM and HPAM on SiC.

polymer does not eliminate such dependence. The dependence of polymer adsorption on S/L is therefore attributed mainly to the flocculation of clay particles by the adsorbed polymers, a process which is favored at high S/L due to reduced inter-particle distance, and which renders some of the adsorption surface inaccessible. In the presence of calcium however, the effect of coagulation by Ca^{2+} is expected to play an important role. Therefore, in order to obtain a representative level of adsorption density on clay particles, the adsorption of polymers on kaolinite throughout this study is conducted as a function of S/L and the results extrapolated to $\text{S/L}=0$.

In the absence of Ca^{2+} , it has been claimed that adsorption of PAM on kaolinite takes place only on the lateral surface while the basal surface is non-adsorbent (22). However, even though adsorption may take place predominantly on the edge surface due to the presence of the more reactive aluminols, this does not exclude some adsorption on the basal surface. In fact, some recent studies which are in progress have indicated the adsorption of PAM on the kaolinite basal surface (23). For HPAM at low salinities, however, adsorption takes place only on the more reactive aluminols of the edge surface (23).

The adsorption of PAM and HPAM on kaolinite (Figure 6) is increased in the presence of Ca^{2+} due to the reasons stated above for sand and SiC. The fixation of Ca^{2+} on kaolinite is verified experimentally and the results plotted in the same figure.

Effect of Monovalent to Divalent Ratio. The above mentioned interactions of Ca^{2+} with the polyelectrolyte and with the negatively charged surface are electrostatic in nature, which means that an increase in ionic strength by monovalent ions should decrease such interactions. This is shown for the case of SiC at 2 and 20g/l NaCl at pH 7 (Figure 7). In the absence of Ca^{2+} , adsorption of HPAM is lower at 2g/l than at 20 g/l NaCl, but in the presence of Ca^{2+} , the higher interactions of the divalent ion with the negative surface and polyelectrolyte at lower NaCl concentration result in a higher adsorption. Moreover, the adsorption level at high calcium content ($750 \mu\text{g}/\text{m}^2$) is higher than the maximum level obtained in the presence of NaCl alone ($500 \mu\text{g}/\text{m}^2$) (10). This clearly demonstrates that specific interactions of calcium with polymer and surface are significant factors in enhancing HPAM adsorption.

Effect of Polymer Ionicity. The influence of polymer ionicity on solution and adsorption properties is investigated for polyacrylamides varying from 0-50% ionicity in the absence and presence of calcium.

The intrinsic viscosities of the polyacrylamides as a function of polymer ionicity in 2 g/l NaCl and at various levels of Ca^{2+} are shown in Figure 8. In NaCl solution, $[\eta]$ increases continuously with polymer charge due to the increase in electrostatic persistence length of the polymer. In the presence of Ca^{2+} , the $[\eta]$ is reduced for every polymer but at low ionicity and low Ca^{2+} content, the increase in $[\eta]$ with charge is maintained. At higher linear charge density however, a stronger interaction of the polymer with Ca^{2+} significantly reduces the polymer charge and its solubility, resulting in a larger decrease in $[\eta]$ and even precipitation for hydrolysis degrees greater than 30% when more than 2g/l CaCl_2 is added. The $[\eta]$ thus exhibits a maximum as a function of ionicity.

The influence of Ca^{2+} on the variations of adsorption with the degree of ionicity of HPAM on sand at pH 7 in 2 g/l NaCl is given in Figure 9. Without calcium, adsorption decreases with polymer charge because of the increase in

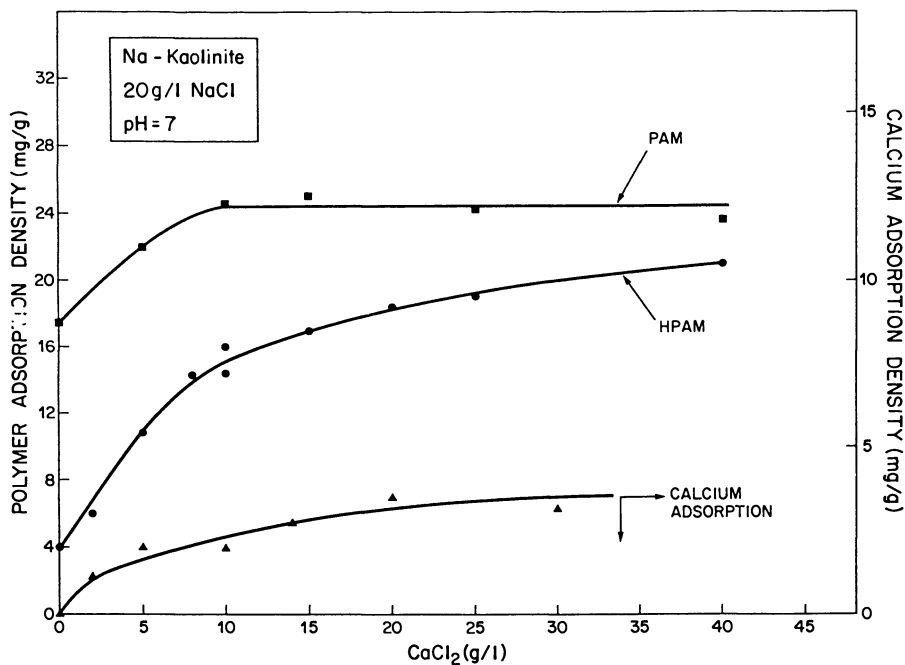


Figure 6. Adsorption of calcium and its influence on adsorption of PAM and HPAM on Na-kaolinite.

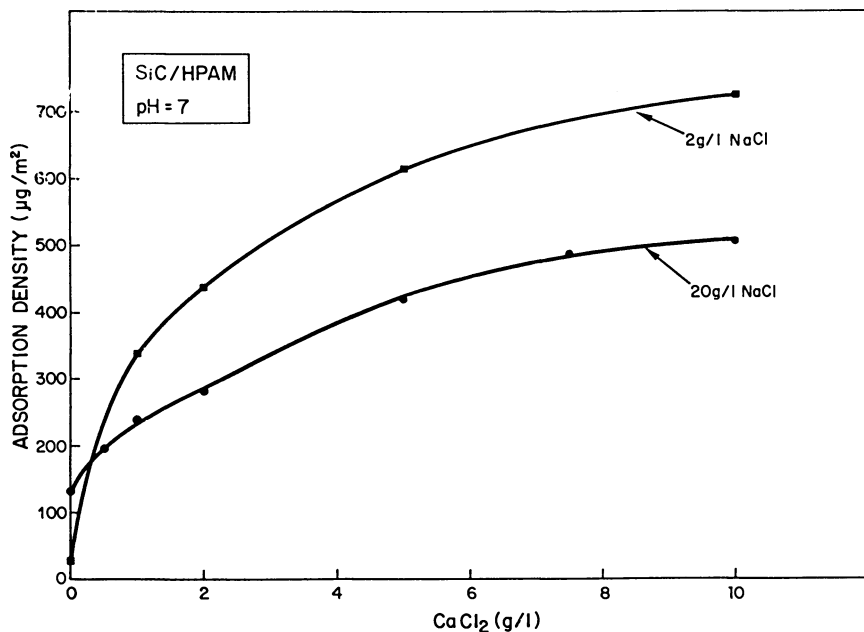


Figure 7. Effect of NaCl on adsorption of HPAM on SiC in the presence of calcium. (Reproduced with permission from ref. 26. Copyright 1988 Institut Français du Pétrole.)

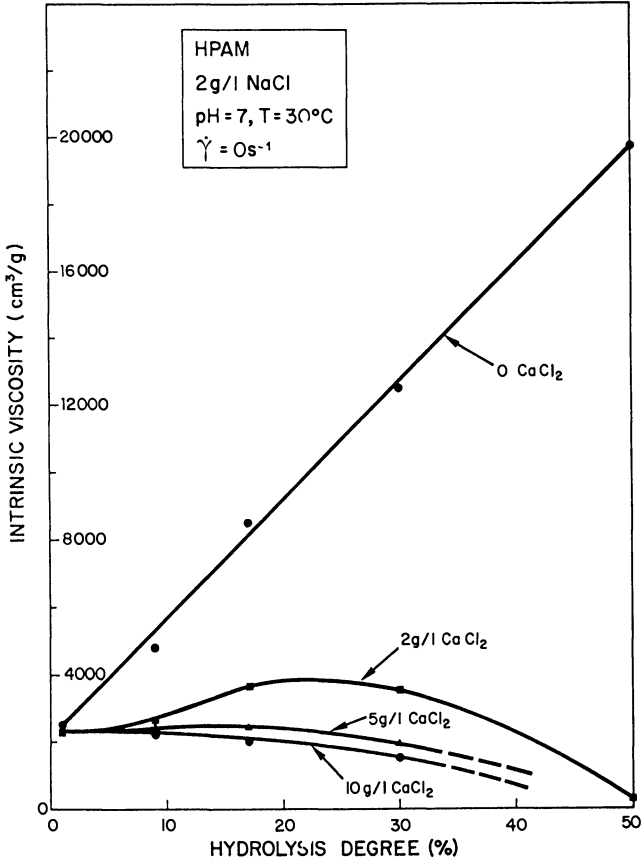


Figure 8. Intrinsic viscosity of HPAM versus ionicity in the presence of calcium. (Reproduced with permission from ref. 26. Copyright 1988 Institut Français du Pétrole.)

electrostatic repulsion between the polymer and the surface. The addition of Ca^{2+} increases the adsorption of each polymer, but the decrease in adsorption with polymer charge is preserved until the degree of ionicity exceeds 30%, at which point the high interaction of polyelectrolyte with divalent ion reduces the solubility of the polymer, and increases its affinity for the surface. Hence, the adsorption of HPAM with ionicity exhibits a minimum. For SiC, on which adsorption is higher, this phenomenon is more pronounced (Figure 10) and a slight adsorption increase is detected even in the absence of Ca^{2+} . This is attributed to a decrease in solubility of the HPAM at high acrylate content (24). Such a minimum is enhanced in the presence of calcium due to the lower solubility of calcium acrylate. As a consequence, the minimum is shifted to a lower value of ionicity.

In the case of kaolinite (Figure 11) where polymer adsorbs strongly and predominantly on the edge surface (see above discussion), the reduction in adsorption with ionicity shows that the overall adsorption is nevertheless governed by the net charge of the clay. Interestingly, an increased adsorption at high ionicity is not observed. A possible explanation is that the nature of interaction of polymer and clay surface is of higher affinity than that of polymer-siliceous surface due to the presence of more reactive aluminols (22). As such, the effect of change in polymer activity due to change in ionicity is suppressed by the more prominent polymer surface interaction.

Xanthans

Adsorption on Siliceous Minerals. All adsorption studies of xanthan (XCPS) in the presence of calcium are conducted at pH 6.5 to avoid precipitation which has been reported at $\text{pH} \geq 7$ for xanthan solutions containing calcium (25).

The adsorption results of both xanthan samples on sand at pH 6.5 in 20g/l NaCl are shown in Figure 12. The presence of calcium is seen to increase the adsorption of both xanthan samples and a maximum in adsorption is reached at high calcium concentrations. These variations are very similar to those observed for XCPS adsorption in the presence of NaCl (26).

Xanthan adsorption is governed by a competition of electrostatic repulsions and attractive H-bonding forces between polymer and surface. For XCPS II, at very low ionic strength, electrostatic repulsion dominates and thus adsorption is detected only after a threshold value of calcium. The maximum adsorption level is attained at a higher Ca^{2+} concentration, and the maximum adsorption of XCPS II exceeds that of XCPS I. This may be an effect of differences in polymer molecular weight and/or structure which can be detected on sand surface due to its heterogeneity in adsorption site density which permits only partial surface coverage by XCPS I. For SiC, which has a more homogeneous adsorption site density, such a difference in maximum adsorption densities for the two samples is insignificant (Figure 13).

In comparison to HPAM where Ca^{2+} increases adsorption by both charge screening and specific interaction with polymer and surface, XCPS adsorption seems to be increased by Ca^{2+} by charge screening only. This is deduced from solution and adsorption properties of the xanthan. Firstly, in solution, even though not much information on the degree of calcium-xanthan interaction can be derived from intrinsic viscosity data due to the structural rigidity of XCPS, studies on XCPS solution stability in the presence of calcium have shown that at $\text{pH} < 7$, no precipitation occurs even at very high calcium concentration (25). Secondly, the maximum adsorption density of XCPS in the presence of calcium does not exceed

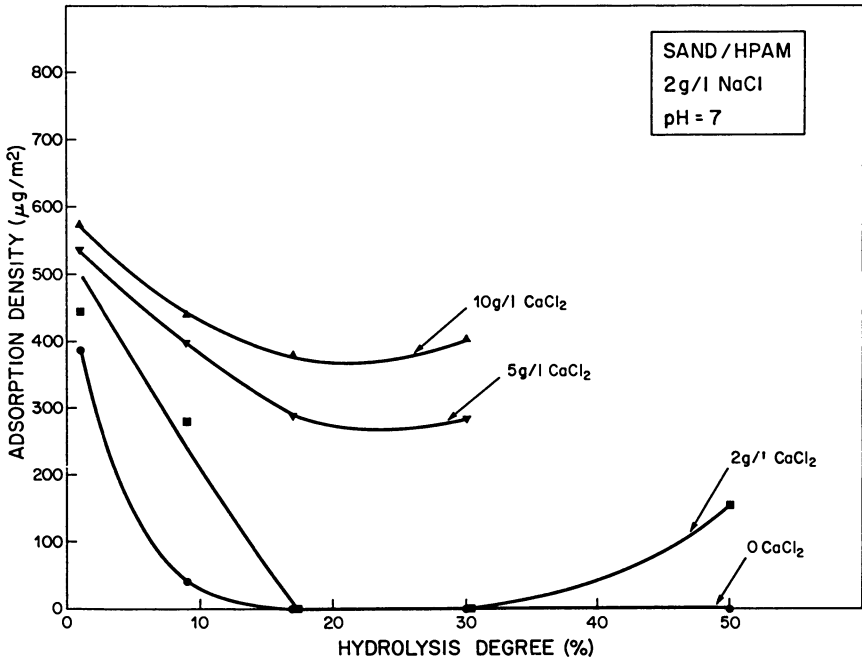


Figure 9. Adsorption of HPAM on sand versus ionicity in the presence of calcium.

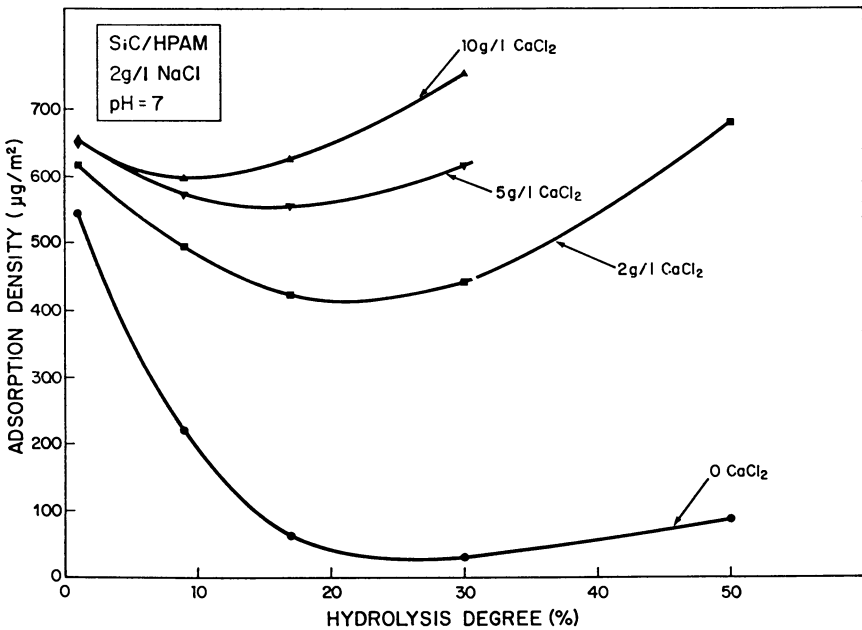


Figure 10. Adsorption of HPAM on SiC versus ionicity in the presence of calcium. (Reproduced with permission from ref. 26. Copyright 1988 Institut Français du Pétrole.)

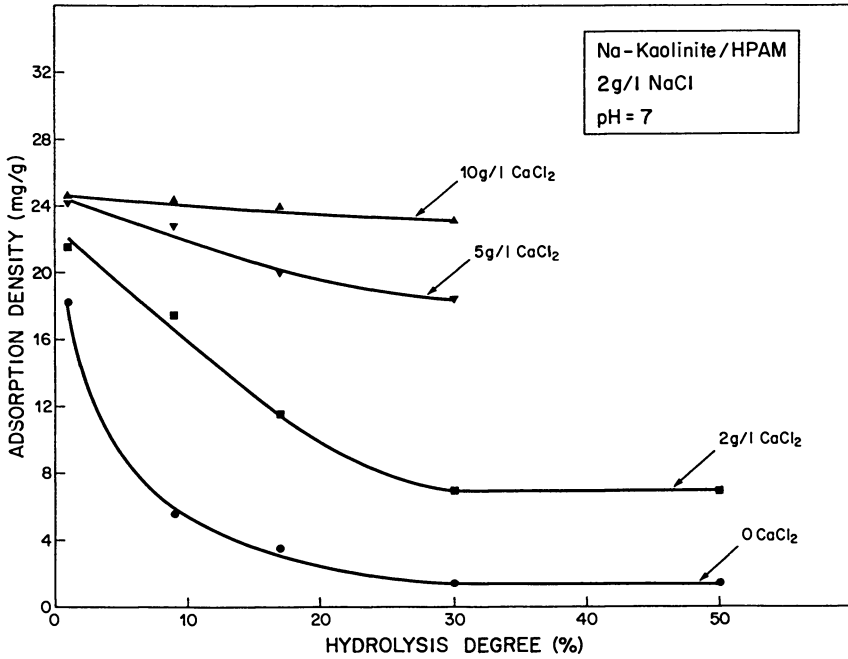


Figure 11. Adsorption of HPAM on Na-kaolinite versus ionicity in the presence of calcium.

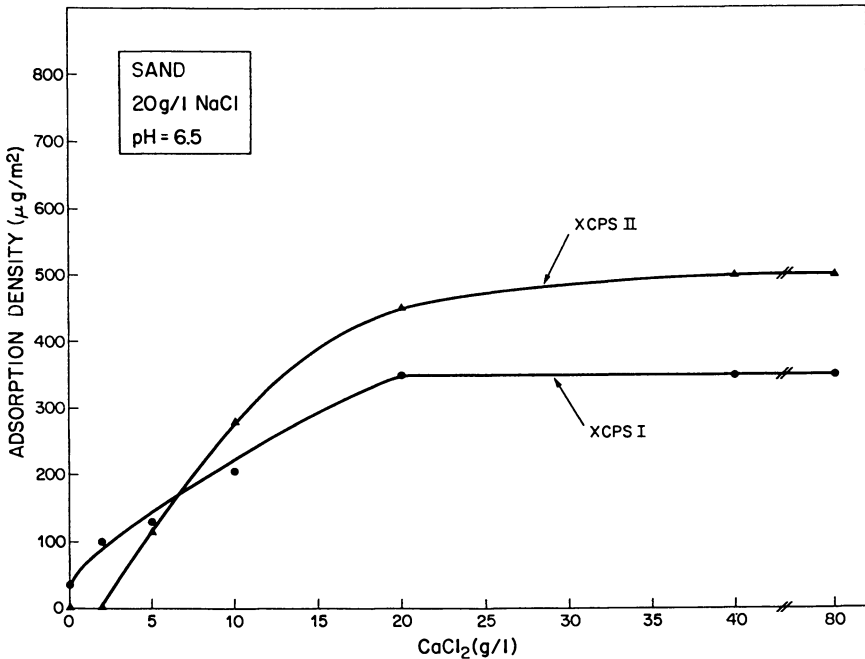


Figure 12. Influence of calcium on adsorption of XPCS on sand.

that obtained at high NaCl concentrations where adsorption is enhanced only by charge screening (26). This is in contrast to the case for HPAM where Ca^{2+} induces an adsorption level which exceeds the maximum adsorption density attained at high monovalent ion concentrations (10).

The charge screening effect of Ca^{2+} in increasing XCPS adsorption is more clearly seen in Figure 13 for the case of SiC where the NaCl content is lower (1g/l). Due to the low initial ionic strength, no adsorption is detected for both XCPS samples at low calcium concentration. The maximum adsorption level in this case is the same as that obtained in the presence of monovalent ions only (26).

Adsorption on Kaolinite. As for polyacrylamides, adsorption of XCPS on kaolinite is conducted as a function of S/L and the results extrapolated to S/L=0. However, the S/L dependence of XCPS adsorption on kaolinite is considerably less than that for HPAM. This is due to the flat conformation of the adsorbed molecules of semi-rigid xanthan (25) compared to the more extended conformation of flexible HPAM (27). The absence of loops and tails in the adsorbed XCPS layer thus diminishes the probability of flocculation of particles by polymer bridging. The slight dependence in adsorption on S/L may therefore be attributed to coagulation of particles induced by Ca^{2+} .

Figure 14 shows the adsorption results of XCPS I on kaolinite at 2 and 20g/l NaCl in the presence of calcium. In this case, the maximum adsorption density (3 mg/g) is significantly less than that of HPAM (~ 21 mg/g). This may be attributed to the rigidity of the xanthan and the relative insensitivity of its adsorption to calcium in comparison to HPAM. The enhancement of XCPS adsorption by the simple effect of charge screening by Ca^{2+} is again evident here from the higher rate of increase in adsorption at higher total ionic strength (in contrast to HPAM - see Figure 7) and the same final adsorption level. Interestingly, applying the fact that adsorption of XCPS takes place on the lateral surface only (23), the total polymer adsorption divided by the lateral surface ($5 \text{ m}^2/\text{g}$) yields an adsorption density of $600 \mu\text{g}/\text{m}^2$. This maximum value of adsorption induced by calcium, as in the case for SiC, corresponds to that obtained in the presence of NaCl only (26), and also to the results of XCPS I and XCPS II on SiC where the maximum adsorption is 550-600 $\mu\text{g}/\text{m}^2$. In addition, it is close to the value calculated ($720 \mu\text{g}/\text{m}^2$) for a close-packing monolayer of aligned XCPS molecules. From the above results, it can be concluded that adsorption of semi-rigid xanthan is not very sensitive to the type of adsorbent surface, and is insensitive to calcium provided that the surface has a homogeneous adsorption site density.

Conclusions

1. The adsorption of anionic polyacrylamides on sand, SiC and kaolinite is significantly increased in the presence of calcium by: (i) reduction of electrostatic repulsion between ionic polymers and surface, (ii) specific interaction of Ca^{2+} with polymers in solution as shown by the significant decrease in intrinsic viscosities and a decrease in affinity of the polymers for solvent, and, (iii) fixation of Ca^{2+} on the negative surface sites acting as a bridge and thus activating polymer adsorption on otherwise non-adsorbent sites. The relative importance of these mechanisms is dependent on polymer ionicity and overall salinity.

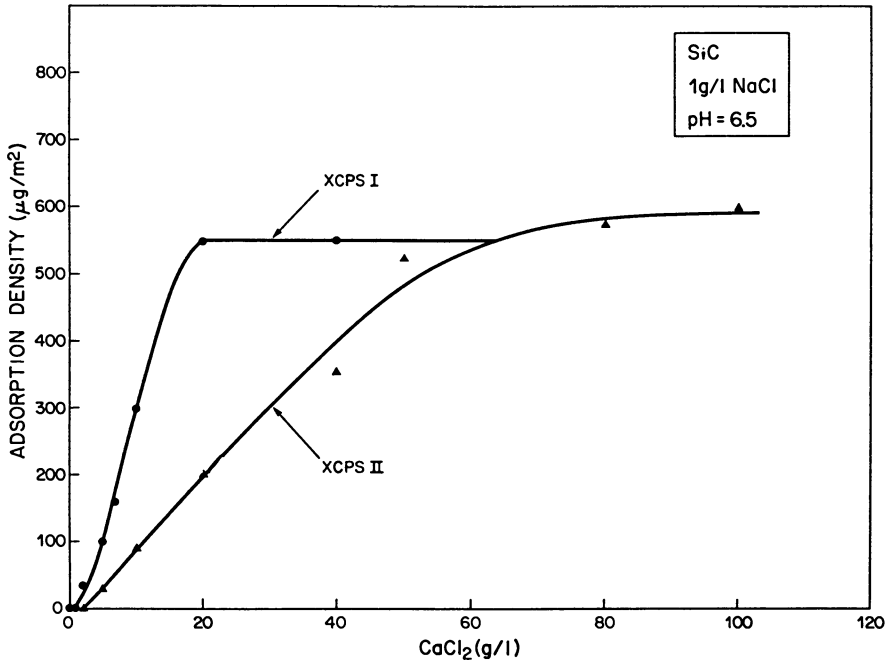


Figure 13. Influence of calcium on adsorption of XCPS on SiC.

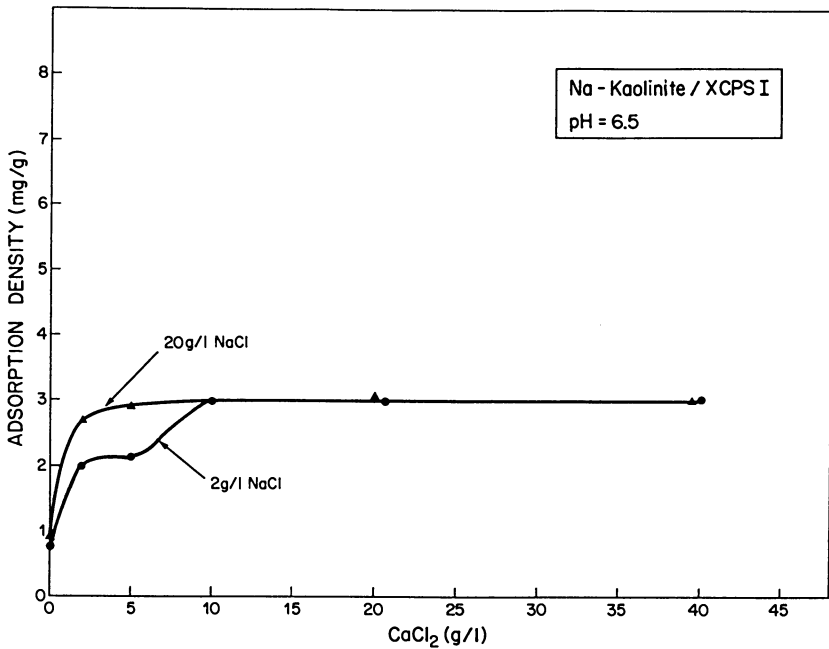


Figure 14. Influence of calcium on adsorption of XCPS on Na-kaolinite.

2. The adsorption of nonionic polyacrylamide is also increased in the presence of calcium, indicating specific interaction of calcium and the polymer.
3. The adsorption of xanthan is increased by calcium but to a less extent than that for HPAM. The increased adsorption seems to be due mainly to the effects of screening of polymer and surface charges by calcium, and the maximum adsorption density is equivalent to that induced by monovalent ions.
4. The maximum adsorption density of semi-rigid xanthan is not very sensitive to the nature of the adsorbent surface provided that the surface has a homogeneous adsorption site density. This maximum level is close to the value calculated for a closely-packed monolayer of xanthan molecules.
5. For polyacrylamides, as a function of polymer ionicity, the presence of calcium induces a maximum in intrinsic viscosity and a minimum in adsorption density on siliceous minerals. This holds important practical implications in EOR since an optimal polymer ionicity can be selected according to field conditions.

Acknowledgments

This work is conducted under the financial support of ARTEP (Association de Recherches sur les Techniques d'Exploitation du Pétrole). The authors would like to thank Ph. Delaplace and M. Nitabah for performing some of the experiments, and Rhone-Poulenc for supplying the polymers.

Literature Cited

1. Willhite, G. P.; Dominguez, J. G. Improved Oil Recovery by Surfactant and Polymer Flooding; Acad. Press Inc.; New York, 1977.
2. Klein, J.; Westerkamp, A. Die Ang. Makr. Chem. 1980, 92, 15.
3. Martin, F. D.; Sherwood, N. S. SPE Paper No. 5339; Rocky Mtn. Mtg., Denver, 1975.
4. Szabo, M. T. SPEJ; 1975, 15, 323.
5. Hollander, A. F.; Somasundaran, P.; Gryte, C. C.; J. Appl. Polym. Sci. 1981, 26, 2123.
6. Shah, S.; Heile, S. A.; Glass, J. E. SPE Paper No. 19561, Phoenix, 1985.
7. Volz, A. V.; ACS Meeting, Annheim, 1986.
8. Chauveteau, G.; Lecourtier, J. The Role of Polymers in Enhanced Oil Recovery; Schulz, D. N. ; Stahl, G. A., Eds., Plenum, 1987.
9. Lecourtier, J.; Chauveteau, G. 3rd. European Symposium on EOR, Rome, April, 1985.

10. Lecourtier, J.; Lee, L. T.; Chauveteau, G. *AIChE Mtg.*, Houston, April, 1987.
11. Muller, G.; Anhourrache, M.; Lecourtier, J.; Chauveteau, G. *Int. J. Bio. Macromol.* 1986, 8, 167.
12. Lecourtier, J.; Chauveteau, G.; Muller, G. *Int. J. Bio. Macromol.* 1987, 8, 306.
13. Chauveteau, G.; Kohler, N. *SPEJ* 1984, 24, 361.
14. Whitman, P. K.; Feke, D. L. *Adv. Ceramic Materials* 1986, 1 (4), 366.
15. Poirier, J. E.; Thesis, Nancy, France, 1984.
16. Schwartz, T.; François, J. *Makromol. Chem.* 1981, 182, 2775.
17. Russel, W. B. J. *Fluid Mech.* 1979, 92, (3), 401.
18. James, R.O.; Healy, T. W. J. *J. Coll. Int. Sci.* 1972, 40, (1), 42.
19. Truong, D. N.; Thesis, Strasbourg, France, 1984.
20. Van der Schee, H. A.; Lyklema, J. *J. Phys. Chem.* 1984, 88, 6661.
21. Rand, B.; Melton, I. E. J. *J. Coll. Int. Sci.* 1977, 60, (2), 308.
22. Nabzar, L.; Carroy, A.; Pefferkorn, E. *Soil Sci.* 1986, 141, (2), 113.
23. Lee, L. T.; Lecourtier, J.; Chauveteau, G.; Unpublished Results, Institut Français du Pétrole.
24. Kulicke, W. M.; Horl, H. H. *Coll. and Polym. Sci.* 1985, 263, 530.
25. Lecourtier, J.; Noik, C.; Barbey, P.; Chauveteau, G. 4th European Symposium on EOR, Hamburg, Oct. 1987.
26. Chauveteau, G.; Lecourtier, J.; Lee, L. T. *Revue de l'Institut Francais du Petrole* 1988, 43, (4).
27. Chauveteau, G.; Tirrell, M.; Omari, A. *J. Coll. Int. Sci.* 1984, 100, (1), 41.

RECEIVED November 28, 1988

Chapter 12

Retention Behavior of Dilute Polymers in Oil Sands

Jitendra Kikani¹ and W. H. Somerton²

¹Department of Petroleum Engineering, Stanford University, Stanford,
CA 94305

²Department of Mechanical Engineering, University of California, Berkeley,
CA 94720

This study investigates the retention behavior of dilute polymer solutions in oil sands. Results indicate that the presence of a large amount of fines and/or a variety of minerals in the sand may result in high adsorption and retention causing excessive loss of polymer and high injection pressures. Injection of a surfactant with the polymer leads to increased oil recoveries because the dilute polymer may selectively adsorb on mineral grain surfaces leaving the surfactant to act at liquid/liquid contacts.

For this study flow (dynamic) and static (batch) tests were carried out on Wilmington oil field unconsolidated sands at reservoir temperatures and flow rates with polyacrylamide (Dow Pusher-500) polymers. Effluent concentration, viscosity, and pH were monitored as a function of time. Extensive characterization studies for the sand were also carried out.

Adequate mobility control between fluid banks is a pertinent factor in the successful application of secondary and tertiary oil recovery processes. During a waterflood, oil viscosities are normally higher than that of the driving aqueous phase and thus there exists an adverse mobility ratio. This causes fingering and/or channeling of the displacing fluid which reduces pattern conformance and results in low sweep efficiencies. In order to improve this situation the mobility of the displacing fluid needs to be reduced. Reduction in the mobility of the displacing fluid can be obtained by increasing the viscosity of the displacing phase or reducing the permeability to the displacing phase(1,2). Polyacrylamide and bio-polymers have proved to be useful for these purposes. These polymers increase the water viscosity substantially at low polymer concentrations. The resulting reduced mobility of the displacing phase suppresses the fingering phenomenon and improves piston-like displacement. In addition to the mobility control provided by viscosity enhancement of water, there is a selective reduction in the permeability to the aqueous phase due to the selective blocking of pores by the polymers(3). Both, viscosity enhancement and permeability reduction to the aqueous phase, act in the direction of decreasing mobility and even for fairly dilute polymer solutions, hold promise that adequate mobility control of fluid banks could be achieved.

As the displacing fluid front advances, the structural complexity of these

0097-6156/89/0396-0241\$06.00/0

© 1989 American Chemical Society

polymers coupled with the complexity of the flow channels in the porous medium cause part of these polymers to be retained in the reservoir. This causes a reduction in the concentration of the polymer solution at the front and consequently a loss of mobility control. In addition to the mechanical filtering of the polymer molecules, adsorption on the grain surfaces reduces the polymer concentration in the displacing fluid. Various retention mechanisms of polymer in porous media are discussed in detail by Willhite and Dominguez(4).

The nature of the polymer controls, to a large extent, the retention behavior in porous media. Partially hydrolyzed polyacrylamide polymer molecules have the capacity of assuming a variety of three dimensional configurations. Also because of competing mechanisms in the polymer formation, there is a wide range of chain lengths. The weight average molecular weight of the polymer used for the present work was 5.89 million (Dow Chemical Co., Personal Communication, 1985). Polyacrylamide polymers used in this study have been studied extensively by a number of researchers(5,6). Susceptibility of these polymers to salinity, pH, shear, temperature, etc. is well documented(7,8). Mechanical entrapment, retention, degradation and adsorption behavior on a number of porous media including fired Berea sandstone(2), bead packs(9) and Ottawa sands(10) have been reported. It is interesting to note here that although numerous studies have been carried out with polyacrylamide polymers, not many studies have been performed on partially oil-saturated reservoir sands. Also, noticeably conflicting results, for polymer retention and adsorption, have been reported in the literature.

The present study investigates the adsorption and trapping of polymer molecules in flow experiments through unconsolidated oil field sands. Static tests on both oil sand and Ottawa sand indicates that mineralogy plays a major role in the observed behavior. Effect of a surfactant slug on polymer-rock interaction is also reported. Corroborative studies have also been conducted to study the anomalous pressure behavior and high tertiary oil recovery in surfactant dilute-polymer systems(11,12).

Experimental

Static(batch) and dynamic(flow) tests were carried out on toluene - extracted and peroxide - treated Wilmington oil field unconsolidated sands with dilute solutions of polyacrylamide (Dow Pusher-500) polymer in 1 wt% NaCl at 50^o C and 1.5 ft./day, simulating reservoir temperature and flow rates. In the static tests, Ottawa sand, with particle size distributions similar to the Wilmington sand, were also used for comparison purposes.

The core - flood apparatus is illustrated in Figure 1. The system consists of two positive displacement pumps with their respective metering controls which are connected through 1/8 inch stainless steel tubing to a cross joint and subsequently to the inlet end of a coreholder 35 cm. long and 4 cm. in diameter. On-line filters of 7 μ m size were used to filter the polymer and brine solutions. A bypass line was used to inject a slug of surfactant solution. Two Validyne pressure transducers with appropriate capacity diaphragms are connected to the system. One of these measured differential pressure between the two pressure taps located about one centimeter from either end of the coreholder, and the other recorded the total pressure drop across the core and was directly connected to the inlet line. A two - channel linear strip chart recorder provided a continuous trace of the pressures. An automatic fraction collector was used to collect the effluent fluids.

Sand and polymer characterization. The oil sands were extracted in a Soxhlet extraction apparatus with toluene as the refluxing liquid. After the extr-

Table I. Mineralogy of Wilmington Oil Sand

Property	Count
Grain Size	
> 210 μm	39.4 %
210 - 74 μm	35.8 %
74 - 43 μm	13.3 %
43 - 2 μm	11.2 %
< 2 μm	0.3 %
Mineral Content	
Quartz	43.0 %
K-Feldspar	21.0 %
Plagioclase	15.0 %
Biotite Mica	10.0 %
Others	11.0 %
Clay Minerals	
Montmorillonite	major
Kaolinite	minor
Illite	trace

-action was complete, the thimbles were dried and the sand poured into a beaker to which distilled water was added just to cover the surface of the sand. The water was brought to a slow boil and a small amount of hydrogen peroxide was added. This was continued at intervals until no more effervescence was observed. This was done because peroxide treatment oxidizes the remaining organics coating the surface of the sand.

Mineralogy of the unconsolidated Wilmington oil sand was obtained by grain size analysis, thin-section study of an impregnated color-stained sample, scanning electron-microscope(SEM), and X-ray diffraction studies. A summary of the results of the study is given in Table I. Surface area of the whole sand sample, the < 2 micron fraction, and the Ottawa sand (quartz) was determined by nitrogen adsorption using helium as the carrier gas in a BET apparatus. The samples were prepared by the freeze - drying technique in a vacuum freeze dryer. In this technique, a suspension of sand sample in deionized water is instantaneously frozen in a liquid nitrogen atmosphere. The sample holder is then attached to the vacuum freeze dryer kept at a temperature of -50° C. This procedure is used to minimize agglomeration of the mineral grains and expose the greatest surface area. The surface areas are reported in Table II. This table also shows the particle size distribution of Ottawa sand used in the static tests.

Table II. Surface Area Measurements

Wilmington Oil Sand, whole rock	0.95 m^2/g
Wilmington Oil Sand, < 2 μ m size	14.9 m^2/g
Ottawa Sand	0.12 m^2/g
composition : > 48 - 65 mesh	40 %
100 - 150 mesh	15 %
150 - 200 mesh	20 %
200 - 325 mesh	15 %
325 - 400 mesh	10 %

Polymer solutions were prepared by standard techniques(13). Viscosities were measured by a Brookfield LVT viscometer with UV adapter. Shear rates of 30 rpm were found to be the most suitable for viscosity measurements up to 400 ppm above which the pseudo-plastic behavior caused significant shear rate dependency on the apparent viscosity. pH of the effluent solutions were measured by a digital pH/ionmeter with combination electrodes. Polymer concentration measurements were performed on a double-beam ratio recording UV-visible spectrophotometer with micro-computer electronics by the use of turbidimetric method presented by Foshee et. al.(13). Wavelength, slit sizes, pH and mixing time were all properly calibrated before use. The calibration curve is shown in figure 2. A detailed description of the procedures and results can be found in reference 14. Figure 2 shows the effect of mixing time on the calibration curve.

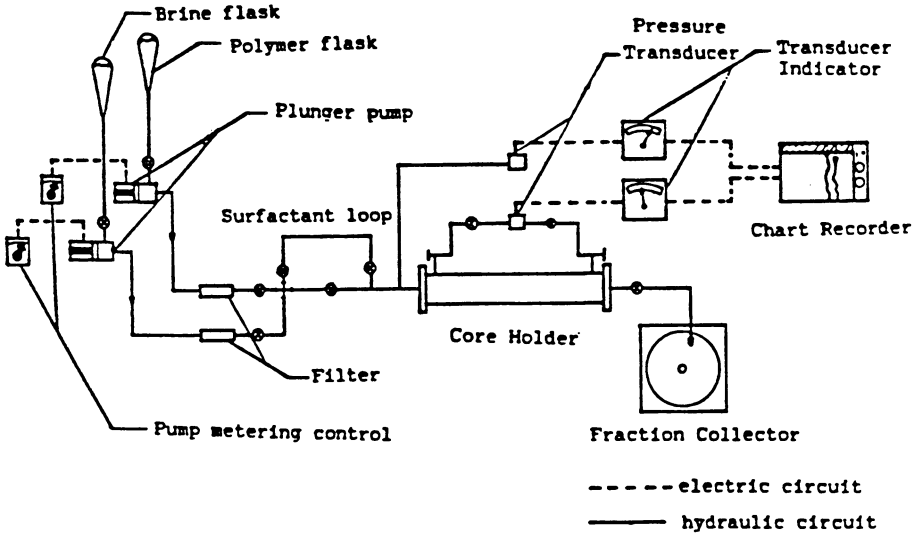


Figure 1. : Schematic of the core flood apparatus

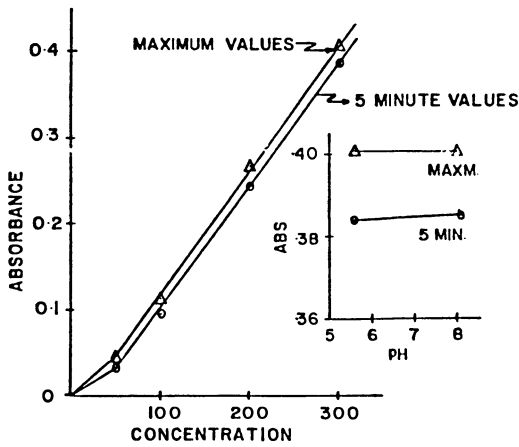


Figure 2. : Effect of pH and time on turbidity measurements for polymer concentration

We note that there is a constant shift in the curve for different mixing times. Experiments were run for various mixing times, and the maximum concentration was observed after about 25 minutes after which concentration started decreasing owing to settling of particles. If we are consistent in the use of either one of the curves the final results are not affected. The inset figure shows the effect of pH on the calibration curve. It is worthwhile noting that, for the range of hydration pH we are interested in, the concentration measurements are independent of the hydration pH.

Flow Tests . One foot long sand packs using Wilmington oil field unconsolidated sand were prepared for each of the flow tests. Porosity and permeability of all the sand packs were within 30-35% and 100-300 md, respectively. All core packs were evacuated to about 1 mm of mercury (Hg) before saturating them under gravity to assure complete water saturation. Table III gives the core and fluid properties for the flow tests. The properties of the cores were chosen so that they are close to the field conditions reported by Krebs(15).

Table III. Core and Fluid Properties

Run No.	Pore Volume cc.	Porosity(ϕ) %	Brine Perm.(k) md	Polymer	
				Conc. ppm	Visc cp
1	129.8	30.6	155.0	300.0	1.13
2	132.5	30.8	120.0	300.0	1.12
3	133.9	31.7	112.0	300.0*	1.20
4	142.5	33.1	323.5	300.0	1.18

* 2.0 % PV slug of surfactant

Brine was flushed through the core at a rate of 1.5 ft/day in a thermostatically controlled temperature bath (at 50⁰ C) until steady state conditions on pressure drop, effluent viscosity and pH were obtained. In Figs. 3 through 6, this is indicated by the steady value of these variables prior to injection of the polymer. This was done for comparison purposes. Prefiltered polymer solution was then injected into the system and the effluent was monitored for concentration of polymer, pH, and viscosity. Pressure drop data were recorded on a strip chart recorder. Positive displacement pumps lined with nitronic alloy were used for displacement experiments. This was done to ensure that ferrous related degradation of polyacrylamides were minimized. In runs carried out with 8.6 cp Ranger zone crude oil (diluted by Chevron 410-H solvent) the core was waterflooded to residual oil saturation before starting polymer injection . A 2.0 percent pore volume slug of 40%(v/w) detergent alkylate sulfonate surfactant was used in one of the runs to evaluate its effect on adsorption and to corroborate earlier observations on residual oil recovery(11).

Static Tests . Static batch tests were carried out in amber colored pyrex bottles cleaned with doubly distilled and deionized water and dried in the oven. Six different samples were prepared for these tests. The significance of each

sample is explained later in this paper. About 200 cm^3 of 300 ppm polymer solution was poured onto 50 grams of sand and kept in the oven for about 24 days. The polymer solutions were monitored for viscosity loss, pH, and concentration periodically to study the adsorption behavior. As the static tests are more diagnostic of adsorption on all the grain surfaces of the sands, results could be compared with the dynamic test results, where polymer solution is not accessible to small pore throats in which the polymer is mechanically obstructed from entry.

Results

Flow Tests. Results of the flow tests are shown in Figures 3 through 6. Figure 3 shows the results of a typical run with a brine saturated sand pack wherein a 300 ppm polymer solution in 1 wt% NaCl was injected at a pH of 8.26. Before this, steady state conditions were established in the core by injecting 1 wt% NaCl. The pH values were stabilized at 8.0 and viscosity at around 1.1 cp. The pressure drop across the core stayed constant up to about 8 PV of polymer injection, the pH stayed in the acidic range, and effluent viscosity was consistently lower than the influent value. At about 8 PV the pressure drop started to build and within 2 PV, increased up to about 100 psi essentially plugging the core. No polymer was eluted until the end of the run.

Since no polymer was detected in the effluent, it is clear that polymer was adsorbed and, when the active adsorption sites were filled, pore throats became smaller and as a result filtering of large molecules occurred causing the large increase in pressure drop due to plugging of the sand pack. It is improbable that low effluent viscosity is caused by scission of polymer chains because of the low shear rates used, however, this could be due to filtering of high molecular weight fractions of the polymer which contribute most to the solution viscosity. Also, random chain-scission resulting from rock-polymer interactions could partly account for low effluent solution viscosities. The lowering of pH while passing through the core may be partly responsible for low solution viscosities(8). Also, plugging of the core cannot be explained by the reformation of microgels due to rehydration of the polymer at a lower pH (16) within the core. This is due to the fact that the actual preparation of the polymer solution was done at a pH ≥ 9.0 and the polymer was stored for a few days before being injected into the core.

In the next run, a core pack was saturated with 8.6 cp (at 50^o C) Rangerzone crude oil and water flooded to residual oil saturation. Polymer flood was then initiated and about 1.2% of the original oil in place (OOIP) was recovered. The results are shown in Figure 4. The pressure profiles show behavior essentially similar to the previous run except that the pressure drop across the core increased to 100 psi within 4 PV of injection of polymer. The steady state values of pH and viscosity were 7.0 and 0.7 cp, respectively. The oil ganglia retained in larger pores resisting displacement probably reduced the amount of polymer adsorbed and reduced the number of pores that the polymer molecules needed to seal off in order to block the core. This could explain the more rapid plugging of the core. Effluent pH and viscosities remained much lower than influent values.

Figure 5 shows the results of the run performed using a surfactant slug. For this purpose, a 0.02 PV slug of 40%(v/w) detergent alkylate sulfonate surfactant(DAS), synthesized by the Morgantown Energy Technology Center of the U.S. DOE and from the waste products of the detergent industry, was injected into a water-flooded core stabilized at an effluent pH of 7.0 and viscosity of 0.7 cp, and the slug was displaced by a 300 ppm polymer solution. Tertiary oil recovery of 4.6% OOIP was obtained which is much higher than the run without the surfactant. This confirms the observations of Williams(11) who obtained higher oil recoveries with dilute polymer solutions in the presence of surfactant but with anomalous pressure behavior. Pressure drop across the core

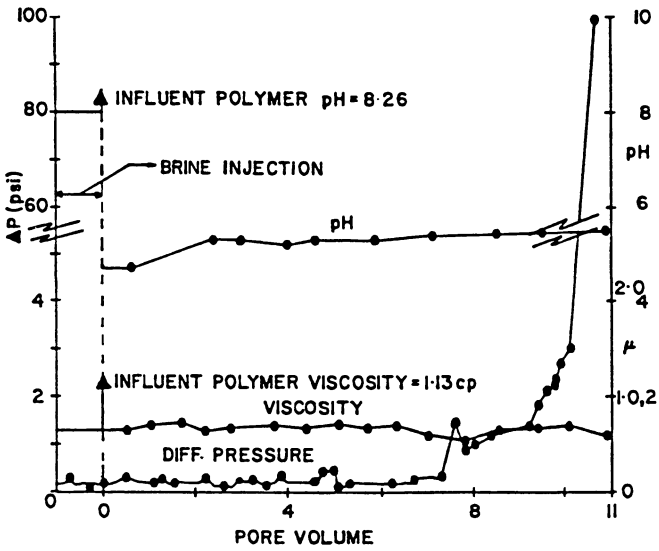


Figure 3. : Effluent Profiles for brine saturated Wilmington sand

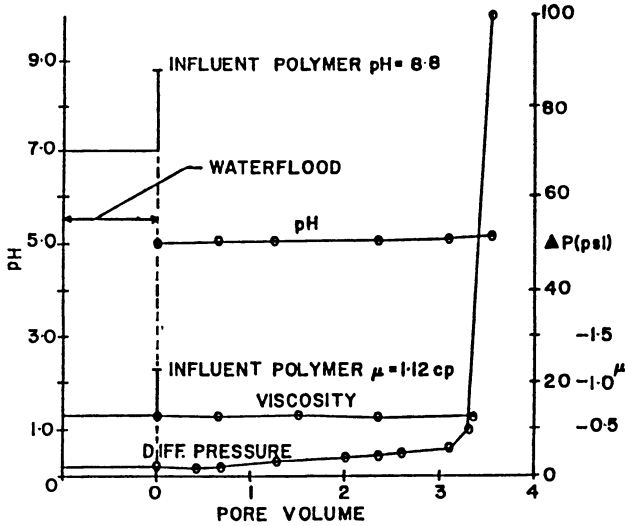


Figure 4. : Effluent Profiles in residual oil-brine saturated Wilmington sand

increased to 148 psi before 2 PV were injected indicating plugging. The pressure behavior in this run is slightly counter-intuitive because one would expect that the breaking up of the oil ganglia by the surfactant should have delayed the pressure increase until plugging by the polymer occurred. This could be explained by rock-polymer-surfactant interactions. The polymer probably acts as a sacrificial agent adsorbing on the grain surfaces and thus, reducing the loss of surfactant. Somasundaran(17,18) has observed such behavior for studies with kaolinites where the surfactant adsorption is considerably reduced in the presence of polymer solution. This would cause the low tension flood to be more effective, yielding higher recoveries. In fact, it is the Capillary number which controls the residual oil saturation. An increase in capillary number reduces the residual oil saturation. The capillary number is directly proportional to the flow velocity and is inversely related to the interfacial tension. Since preferential adsorption of polymer is suspected, the surfactant acts more effectively to reduce the interfacial tension which increases the capillary number. Another way of getting higher capillary numbers is by increasing the flow velocity. Note that, although the pressure drop in the above run was high the velocity was fairly low and was kept constant throughout the run. Thus, the velocity did not contribute to the increase in the capillary number.

In-situ emulsion formation, as proposed by Kamath et al(19), with DAS surfactants may cause higher pressure drops across the core. This is because of the blocking tendency of the emulsion which has lower mobility. This could explain the earlier plugging of the core compared to other runs. Effluent pH and viscosity showed behavior similar to the previous runs. It is worthwhile noting here that such pressure drops were not manifested by face plugging of the core near the entrance. This was confirmed by simultaneously monitoring the pressure at the inlet end of the core as well as the differential pressure across the two pressure taps located about 1 cm. from each end of the core. The inlet end pressure transducer showed reasonably low pressures throughout the run for each experiment.

Low effluent pH, seen consistently in all the flow tests, may be due to Na^+/H^+ exchange which could release hydrogen ions to the flowing fluid and subsequently reduce its pH. This effect has been observed earlier by Somerton, et al(20) in their study of San Joaquin Valley(Kern Front and Midway-Sunset) cores. A reduction in pH may have increased polymer adsorption on clay minerals and may partly account for the high adsorption values observed. This is consistent with the observations of Michaels and Morelos(6) who postulated that the adsorption of polyacrylamide on kaolinite occurs via hydrogen bonding between the un-ionized carboxyl or amide groups on the polymer chains and oxygen atoms on the solid surface. Adsorption is hindered by electrostatic repulsion between the negatively charged clay surfaces and the ionized carboxyl group on the polymer. The adsorption of polymer is thus favored by the reduction in the degree of carboxylate ionization which occurs on reduction of pH.

Expecting a major role particle size distribution and of clay minerals in the anomalous pressure behavior and high adsorption of polymer in the earlier tests, another run (Fig. 6) was carried out without the clay size sand particles (<43 microns) in the core. A 300 ppm polymer solution was injected into the brine saturated core. Polymer broke through after 2.5 PV of polymer was injected, although it never quite achieved the influent concentration. No anomalous pressure behavior was observed; the pressure drop increased from about 0.3 to 1.7 psi across the core which could partly be explained by the greater viscosity of the polymer and perhaps some permeability reduction by selective blocking of the pores. This suggests that the clay-size sand fraction was instrumental in causing plugging in the previous runs. Surface area measurements indicated that

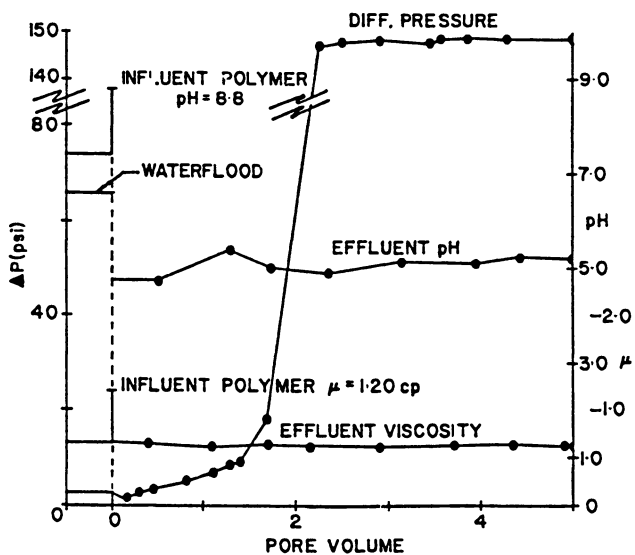


Figure 5. : Effluent profiles for oil-water-surfactant saturated Wilmington sand

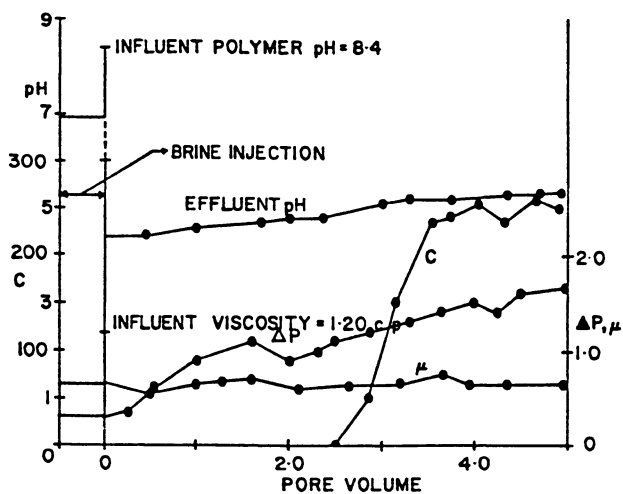


Figure 6. : Effluent profiles in coarse grained fraction of Wilmington sand

although only 11.5% of the sample was clay-size particles, their contribution to the surface area of the whole system was about 70-80%.

Static Tests . Several static tests were carried out to delineate the factors that might have caused the behavior observed in the dynamic tests. Care was taken in these tests to alleviate some of the degradation problems associated with polyacrylamide polymers. Six test samples were prepared. One was a control sample which consisted of polymer solution only, in a pyrex bottle. Measurements made on this control sample should determine whether the environment, i.e., the pyrex bottle, the oxygen the system was being exposed to, or the oven temperature (50^o C), had any effect on the polymer. The second sample consisted of Ottawa sand and polymer solution. This could act as a base case for the study of the effect of mineral content and grain size on adsorption. The third and fourth samples consisted of extracted Wilmington oil sands with polymer solutions hydrated at a pH of 9.4 and 5.05, respectively. The other two samples were prepared from extracted oil sand saturated with Ranger-zone crude oil used in the flow tests, and hydrated at pH values of 9.4 and 5.05. The results of the tests at a pH of 9.4 are shown in Figure 7. The control sample stayed essentially at the original concentration indicating that the environment did not contribute to any polymer degradation or loss. The Ottawa sand showed some adsorption at early times but stabilized thereafter. Extracted sand showed a very sharp drop in concentration at lengths of time, representative of residence times of the polymer in the flow tests. The partially oil-saturated sands showed slightly less stabilized adsorption. Figure 8 depicts the adsorption behavior for the sands hydrated at a pH of 5.05. Comparing Figures 7 and 8 we observe that hydration at a lower pH value showed a greater polymer adsorption. Figure 9 shows the adsorption loss for sand with grain sizes greater than 43 microns. A significantly lower adsorption was observed. The surface area of the fines was 14.9 m²/g compared to the whole sand surface area of 0.95 m²/g. This confirms the observations in the flow tests that the fines had a significant effect on polymer losses.

The amount of polymer retained in the static tests was calculated by a simple material balance. The results of the calculation are shown in Table IV. This table also shows the polymer loss in dynamic tests.

In the static tests the results differ slightly depending on the hydration pH of the polyacrylamide solution(6). The adsorption losses in run 3-S for the Ottawa sand is fairly low compared to the losses with the extracted oil sand. This result was observed in runs 4-S and 5-S too. In run 5-S the < 43 μm grains were removed. This results in lower adsorption but not as low as one would expect, taking into account the reduction in surface area. Willhite and Dominguez(4) documented results from polymer retention tests done by a number of researchers for unconsolidated sandstones and Berea cores. Our static tests showed substantially higher values of adsorption compared to theirs, though they were of comparable values for Ottawa sands. Comparing the adsorption in static tests with the retention in dynamic tests up to the time when the cores were blocked, we note that in the dynamic tests the retention was considerably lower than those in the static tests.

On equating the adsorption with the surface area of the sand and observing the large time constant of decay of adsorption evident from Figs. (7) through (9), it appears that there is a multilayer adsorption process or an inter-layer adsorption within the clay particles which is causing very high polymer losses. Low adsorption on Ottawa sand suggests that there is an effect of the types of minerals present in the sand.

The retention was much higher in the static tests compared to the flow tests. This is partly due to the inaccessibility of the smaller pores by the polymer

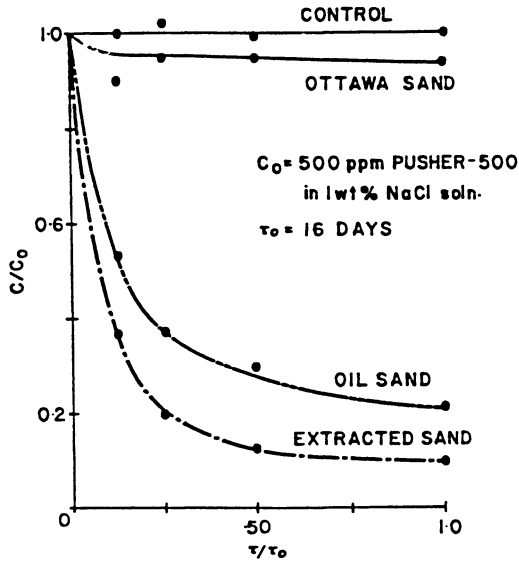


Figure 7. : Static test - Concentration loss

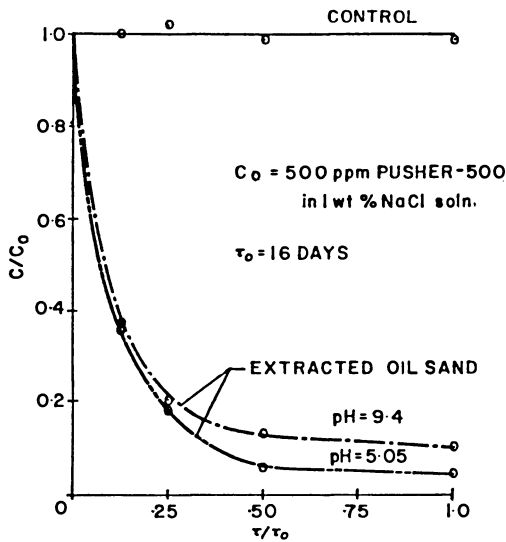


Figure 8. : Effect of rehydration pH on concentration loss in static tests

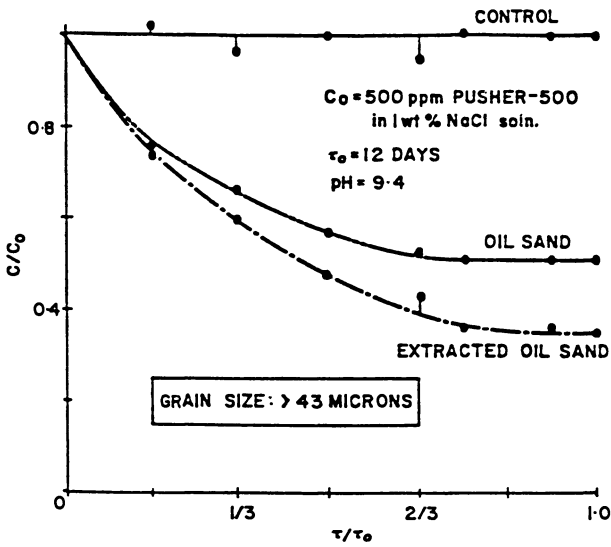


Figure 9. : Static test - Concentration loss (coarse sand)

Table IV. Polymer Loss in Static and Dynamic Tests

Run (Dynamic)	Sand Type	Polymer Loss $\mu\text{g/g}$	Loss Until Polymer Breakthrough $\mu\text{g/g}$
2-D	Extracted Oil Sand	515.3	-
3-D	Oil Sand	180.7	-
4-D	Oil Sand	288.0	-
5-D	Extracted Oil Sand ($>43 \mu\text{m}$)	194.1	141.3
Test (Static)	Sand Type	pH	Polymer Loss $\mu\text{g/g}$
3-S	Ottawa	9.4	45.0
		4.8	45.0
	Extracted Oil Sand	9.4	1170.0
		4.8	1309.5
4-S	Ottawa	9.4	160.0
	Extracted Oil Sand	9.4	1800.0
		5.05	1920.0
	Oil Sand	9.4	1580.0
		5.05	1720.0
5-S	Extracted Oil Sand	9.4	1300.0
	Oil Sand	9.4	980.0

molecules in the flow tests. This is partly offset by trapping of molecules in the pore throats in the case of the flow tests run in low permeability cores having small pore sizes. The second cause for lower retention in the flow tests is the early plugging of the upstream part of the core, preventing polymer from contacting the entire core. As explained earlier, the experiments did not indicate that the retention was confined to an entrance face - plugging effect.

Conclusions

Filtering as well as high adsorption losses of polymers in formations containing substantial amounts of fines may cause a significant loss of mobility control in polymer floods. The mobility control provided by the polymer solutions is also reduced by the decrease in viscosity due to the filtering of the high molecular weight fractions of the polymers. Effect of a variety of minerals present in the oil sands has been observed. High injection pressures could be encountered during polymer injection in oil fields if significant amounts of fines are present. This is caused by pore blockage leading to rapid pressure buildups. Shuler et al(21) report on such problems at West Coyote field single well evaluation program. They attribute the low injectivity and high pressure drops to formation damage caused by the high resistance factor of the polymer used.

High adsorption loss observed in the present work in both dynamic and static tests indicates a possibility of multilayer adsorption. However, the long times required to achieve adsorption equilibrium may indicate interlayer adsorption in the clay minerals.

In the field, such effects as are observed in the laboratory may be mitigated due to the existence of very high shear rates at and near the well bore. Far away from the well bore, the polymer sees a larger flow area and this may preclude agglomeration and blocking of pore channels. Thus, extrapolation to the field has to be done very carefully.

Presence of a DAS surfactant improves tertiary oil recovery although this may cause additional pressure drops across the system.

Acknowledgments

The fellowship support provided by the Jane Lewis Fellowship Committee is appreciated. This research was funded in part by a U.S. Department of Energy grant through Lawrence Berkeley Laboratory.

Literature Cited

1. Pye, David J. *J Pet. Tech.* Aug. 1964, 911-16.
2. Mungan, N.; Smith, F. W. *J Pet. Tech.* Sept. 1966, 1143-50.
3. Sandiford, B. B. *J Pet. Tech.* Aug. 1964, 917-24.
4. Willhite, G.P.; Dominguez, J.G. In *Improved Oil Recovery by Surfactant and Polymer Flooding*, Ed.; Academic Press: New York, 1977, 511-55.
5. Chauveteau, G. *Proc. 56th Ann. Fall Tech. Conf. of SPE*, 1981.
6. Michael, A.S.; Morelos, O. *Ind. and Eng. Chem.*, Sept. 1955, 1801-08.
7. Shupe, R. D. *J Pet. Tech.* Aug. 1981, 1513-28.
8. Mungan, N. *J Can. Pet. Tech.* April-June 1969, 45-50.
9. Jennings, R.R.; Rogers, J.H.; West, T.J. *J Pet. Tech.*, March 1971, 391-401.
10. Maerkar, J. M. *Soc. Pet. Eng. J* Aug. 1976, 172-74.
11. Williams, D. B. M.S. Report, Univ. of California, Berkeley, 1984.
12. Ganapathy, S. M.S. Report, Univ. of California, Berkeley, 1982.

13. Foshee, W.C.; Jennings, R.R.; West, T.J. Proc. 51st Ann. Fall Tech. Conf. of SPE, 1976.
14. Kikani, J. M.S. Report, Univ. of California, Berkeley, 1985.
15. Krebs, H.J. J Pet. Tech., Dec. 1976, 1473-80.
16. Burcik, E.J.; Thakur, G.C. J Pet. Tech., May 1974, 545-48.
17. Somasundaran, P. Annual Report Submitted to NSF and a Consortium of Supporting Industrial Organizations, Columbia University, July 1978.
18. Somasundaran, P. US Dept. of Energy Report # DOE/BC/10082-2.
19. Kamath, K.I. et al, Proc. 51st SPE Calif. Reg. Mtg. Bakersfield, 1981.
20. Somerton, W.H.; Radke, C.J. J Pet. Tech., March 1983, 643-53.
21. Shuler, P.J.; Kuehne, D.L.; Uhl, J.T.; Walkup, G.W. Soc. Pet. Eng. J - Res. Eng., Aug. 1987, 271-80.

RECEIVED November 28, 1988

Chapter 13

Physicochemical Basis of Quantitative Determination of Anionic Surfactant Concentrations by Using an Autotitrator

Robert W. S. Foulser, Stephen G. Goodyear, and Russell J. Sims

Winfrith AEE, Dorchester, Dorset DT2 8DH, England

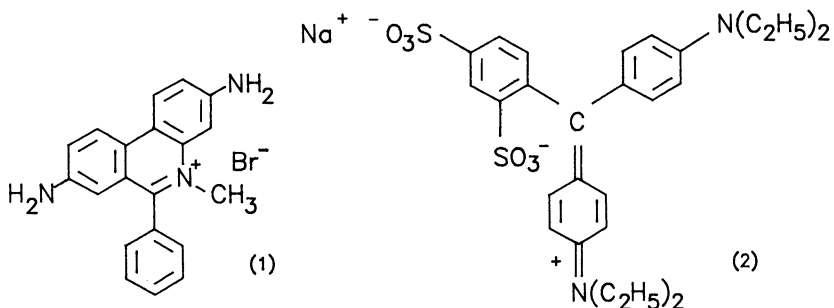
The application of an autotitrator for the determination of surfactant concentrations has been investigated based upon turbidimetric and photometric techniques. The measured titration curves for the two techniques were found to be very similar indicating a common underlying mechanism. Experiments to investigate this mechanism have shown that the light signal measured by the instrument depends on the texture of an emulsion formed by stirring the aqueous and chloroform phases in the titrator cup. Considering the physico-chemical basis of the measurement a rapid, automatic method has been developed and successfully applied to SDBS.

The quantitative determination of surfactant concentration in solution is an essential part of any experimental work on surfactant adsorption or phase behaviour. In the field of experimental enhanced oil recovery the technique employed should be capable of determining surfactant concentrations in sea water, and in the presence of oil and alcohols, the latter being frequently added as a co-surfactant.

As part of the studies undertaken in our laboratory it was necessary to be able to determine quantitatively the surfactant present in large numbers of samples (> 100 per week) arising, for example, from core flooding experiments. The chosen method needed to be rapid to reduce analysis time, and to require little manipulation of the sample to reduce errors. In this paper we report the development of a method for the determination of anionic surfactants based upon autotitration and comment on the physico-chemical basis of the technique.

Numerous methods have been developed for the determination of anionic surfactants and these have been reviewed by Longman (1). The measurement of absorbance of light by a dyestuff-anionic surfactant complex, which has been extracted into an organic solvent is a key feature of many methods, and Sodergren has successfully used segmented flow colorimetry for an automated version of this procedure (2). An alternative is the two phase titration technique, pioneered by Herring (3) which uses dimidium

bromide (1) and disulphine blue (2) as the indicators. This technique, originally introduced by Holness and Stone (4) for qualitative purposes, has been thoroughly investigated by Reid and co-workers (5, 6) and adopted as a standard method (7). More recently potentiometric methods have been employed but these were considered unsuitable because the membrane electrode may fail on prolonged contact with organics as required in this application (8).



EXPERIMENTAL

APPARATUS AND MATERIALS. A Mettler DL40 memotitrator, DK19 Filter Titrator with filters and a DK181 Photrode were purchased from M.S.E. Scientific Instruments, Crawley. Visible spectra were recorded on a Perkin Elmer Lambda 3 spectrophotometer.

Hyamine 1622 (4.0 mmol dm^{-3} solution), disulphine blue, didimidium bromide, sodium chloride (AnalaR grade), sodium hydroxide (AnalaR grade), chloroform (reagent grade) and decane (GPR grade) were purchased from B.D.H. Ltd., Poole. Dodecylbenzenesulphonic acid (98%, remainder sulphuric acid and unsulphonated oil) was purchased from Alpha Chemicals, Coventry. Water (conductivity $18 \text{ M}\Omega^{-1}$) was obtained from a reverse osmosis plant equipped with a MILLI-Q polishing unit. The MILLI-Q polishing unit contained ion exchange and charcoal cartridges, the latter to remove trace organics.

Aqueous solutions of sodium dodecylbenzenesulphonate (SDBS) were prepared by neutralizing dodecylbenzenesulphonic acid solution with sodium hydroxide solution.

PRINCIPLE OF OPERATION OF THE AUTOTITRATOR. The autotitrator operates by detecting the change in light transmission through a stirred solution to which titrant is added, the light intensity is subsequently recorded as a voltage generated by a photocell. The light source (Figure 1) generates high frequency modulated light which passes through a filter, to select the required wavelength, then down the fibre optic cable. The light is split at the probe; one route passing through the solution in the titration vessel, the other through a reference cell. It should be noted that the light collected at the detector cell is the sum of the light transmitted through the solution (reflected back by the concave mirror) and any component which arises by back scattering of light directly from the solution. In the detector the returned light is converted to a signal which represents the change in transmittance of the sample in the titration vessel as the titrant is added.

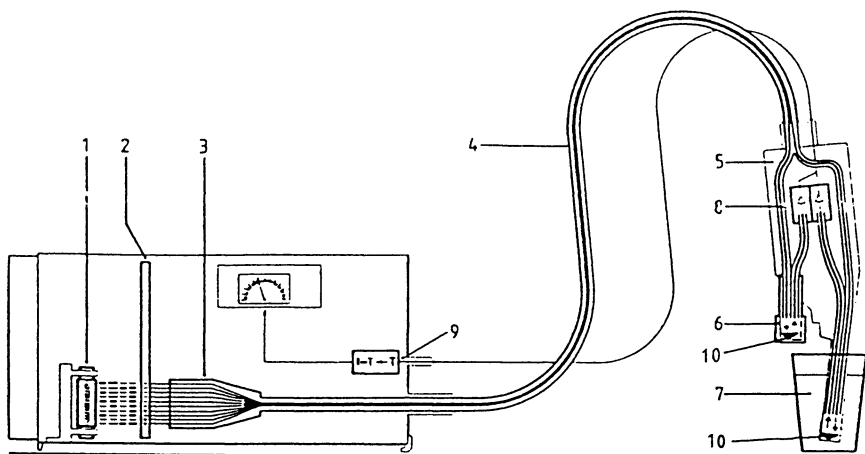


FIGURE 1 Schematic Diagram of Light Source and Probe

- | | |
|---------------------------|--------------------|
| 1 Light Source | 6 Reference |
| 2 Fixed Wavelength Filter | 7 Titration vessel |
| 3 Fibre Optic Converter | 8 Detectors |
| 4 Light conducting cable | 9 Demodulator |
| 5 Probe | 10 Concave mirror |

In a typical titration with the autotitrator a significant fraction of the equivalence volume is added in a single aliquot and allowed to equilibrate before further titrant is added. The end point is detected by comparing changes in the millivolt output of the light source (Figure 1) (9).

After the addition of the initial single aliquot the injection of titrant can proceed in two different modes:

- (i) a drop of titrant (of fixed size) is added if the EMF changes by less than DE (mV) in a specified time interval DT (s).

Unless otherwise stated this mode was used for the titrations reported with DE=1 and DT=1.

- (ii) a drop of titrant is added after a preset time has elapsed from the last drop. This mode of operation has been used in some carefully controlled comparative studies described later.

BASIS OF MANUAL PHOTOMETRIC TITRATION. The determination of anionic surfactants by a photometric titration employs a cationic indicator to form a coloured complex with the surfactant which is insoluble in water but readily soluble in chlorinated solvents (1). The end point of the titration occurs when there is a loss of colour from the organic phase. A considerable improvement in this technique is achieved by the use of a mixture of anionic and cationic dyes (4), for example disulphine blue and dimidium bromide (Herring's indicator (3)). The sequence of colour changes which occurs during the two phase titration of an anionic surfactant (AS) with a cationic titrant (CT) using a mixed indicator consisting of an anionic indicator (AD) and cationic indicator (CD) is summarised in Scheme 1.

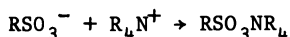
Scheme 1

CD/AS	+	AD + CT	→	AD/CT	+	CT/AS	+	CD
Soluble in CHCl ₃		Soluble in H ₂ O		Soluble in CHCl ₃		Soluble in CHCl ₃		Soluble in H ₂ O
pink colour		green colour		blue colour		colourless		colourless

At the end the cationic indicator (CD) passes into the aqueous phase and a small quantity of the anionic indicator/cationic titrant complex (AD/CT) passes into the organic phase to give a grey/blue tint.

BASIS OF MANUAL TURBIDIMETRIC TITRATION. When a cationic titrant is added to an aqueous anionic surfactant solution a sparingly soluble complex is produced, Scheme 2.

Scheme 2



The quantity of precipitate formed can be controlled by the addition of an organic solvent such as chloroform to the system. The chloroform forms a separate phase in which the complex is soluble and a significant quantity of the complex can be produced

before the solubility limit in the aqueous phase is exceeded. A plot of turbidity versus volume of titrant added would be expected to have a steep fall to the end point followed by a shallow rise as the turbidity of the solution is diluted by excess titrant, ie a "tick" shape.

CHOICE OF FILTER FOR AUTOMATED PHOTOMETRIC TITRATION. At the end of a photometric titration using the above two indicators the colour of the chloroform phase changes from pink to blue. To choose a filter to detect this end point the visible spectra of the separated chloroform layers of surfactant titrations were recorded before, at and beyond the end point, see Figure 2. At 580 nm there was a greater change in absorbance than at 440 nm, thus the 580 nm filter was preferred.

The plot of light transmission versus volume of titrant added would be expected to be a step change, where the equivalence point might reasonably be taken as the position of greatest slope in the titration curve.

EXPERIMENTAL PROCEDURES: AUTOMATED PHOTOMETRIC TITRATION.

Indicator solution (5 cm³) (5) and chloroform (10 cm³) were placed in the titration beaker together with the aqueous surfactant sample and water (30 cm³ less the volume of the surfactant sample). The titration was then carried out with hyamine solution (4.0 mmol dm⁻³) added in 0.05 cm³ increments after the addition of an initial single aliquot.

EXPERIMENTAL PROCEDURES: AUTOMATED TURBIDIMETRIC TITRATION. A method for the automated aqueous turbidimetric titration of surfactants has been published (10) in which anionic surfactants are titrated against N-cetylpyridinium chloride to form a colloidal precipitate near the equivalence point. N-cetylpyridinium halides have a disadvantage in that they have the tendency to crystallise out of solution (5), consequently the strength of the solution may alter slightly without the knowledge of the operator, also the crystals suspended in solution may cause damage to the autotitrator. In view of these drawbacks hyamine was preferred as the titrant.

An aqueous surfactant sample was placed in the titration beaker together with chloroform (10 cm³) and water (30 cm³ less the volume of the surfactant sample). The titration was then carried out using hyamine solution as in the photometric case.

TITRATIONS FOR COMPARISON OF METHODS. The automated photometric and turbidimetric methods were compared using 30 cm³ samples of surfactant solution containing a nominal 20 μmol SDBS to give an equivalence volume of 5 cm³. The effect of salinity on the titrations was studied using samples prepared containing sodium chloride concentrations of 0.0, 0.14, 0.70 and 1.46 wt%. The influence of the choice of filter (580 or 620 nm) was also investigated.

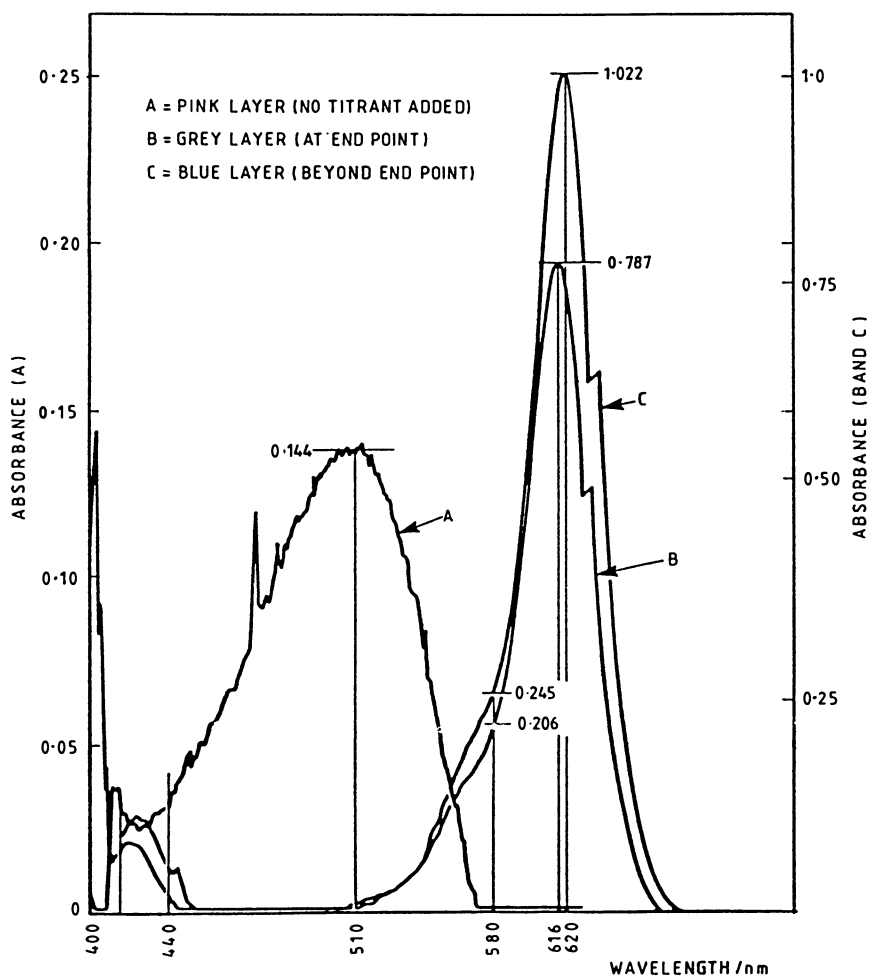


FIGURE 2 Visible spectra of chloroform layers, before, at and beyond the end point of photometric titration

RESULTS AND DISCUSSION

COMPARISON OF METHODS. Both methods were fairly rapid with a typical analysis time of 5 minutes per sample as compared with 30 minutes per sample for the manual method.

A typical photometric titration of SDBS against hyamine at low salinity is shown in Figure 3. It was noted, however, that the titration curve was "V" shaped and not the anticipated step curve. The turbidimetric titration of SDBS against hyamine afforded a curve, Figure 4, very similar to that for the photometric titration.

Photometric and turbidimetric titrations at the same salt level were always similar suggesting that only a turbidimetric signal is seen. Also, there is little difference between the results obtained at 580 and 620 nm wavelength, which further demonstrates the absence of a photometric signal because there is a significant difference in the absorption of the indicator dyes between these wavelengths. Salt concentration, however, has a marked effect on the shape of the titration curve. At low salt concentrations all the curves have a sharp minimum, as shown in Figure 5. As the salt concentration increases this sharp minimum begins to broaden out, until the highest salt level studied (1.46 wt%), causes the curve beyond the titration point to show very little increase, as shown in Figure 6.

EMULSION MECHANISM. The above results show that the indicator was unnecessary because the method is essentially a turbidimetric one. However, the occurrence of a sharp minimum in the titration curve at low salt concentrations, suggests that the formation of a colloidal precipitate is not the underlying mechanism for the turbidity. Consequently, efforts were made to clarify the underlying physico-chemical mechanism of the titration.

During surfactant titrations two observations were made:

- (i) The contents of the reaction vessel were turbid being milky white in appearance, although this was less intense near the endpoint of the titration.
- (ii) If the addition of hyamine and the stirring were stopped two clear phases separated. This occurred significantly faster when the titration was in the region of the endpoint.

It was apparent that when the two immiscible fluids were stirred droplets of chloroform formed in the aqueous phase. It was hypothesised that the response of the phototrode was dominated by light scattered back from the droplets without reaching the mirror and that, as the droplet size decreases, the intensity of the back scattered light increases. This was confirmed in tests by increasing the rate of stirring and so decreasing the droplet size.

This concept allows the shape of the titration curves to be explained by postulating that the chloroform droplet size decreases as the interfacial tension (ift) between the aqueous and chloroform phases is decreased by the presence of active surfactant. As the endpoint in a titration is approached the amount of active SDBS decreases as it complexes with the injected hyamine. The reduction in the amount of active surfactant material results in an increase

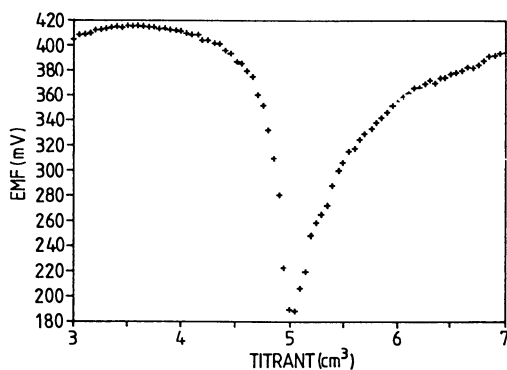


FIGURE 3 Typical photometric titration of SDBS against Hyamine at low salinity

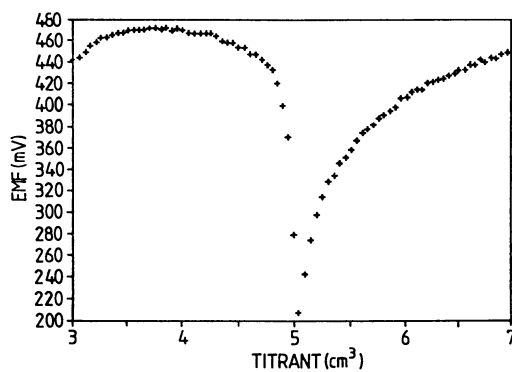


FIGURE 4 Typical turbidimetric titration of SDBS against Hyamine at low salinity

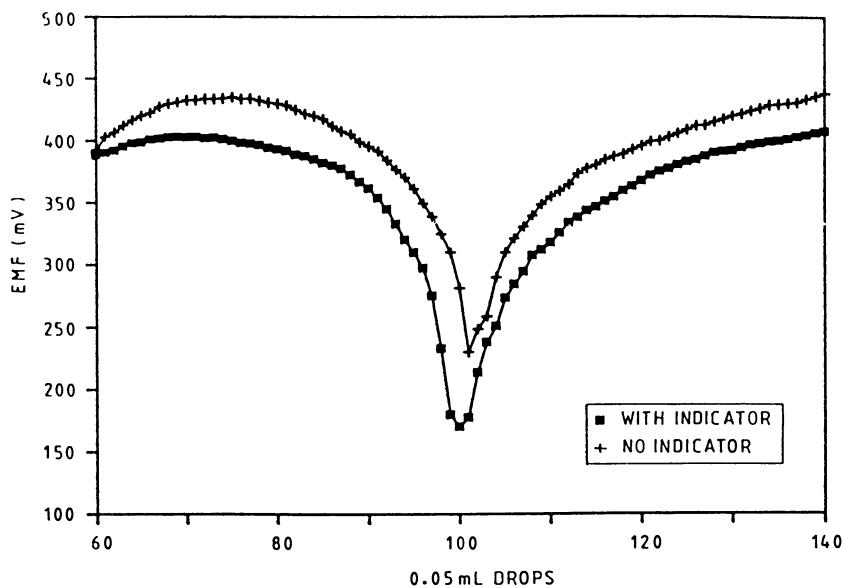


FIGURE 5 Titration curves at 0.0 wt% NaCl using 580 nm light

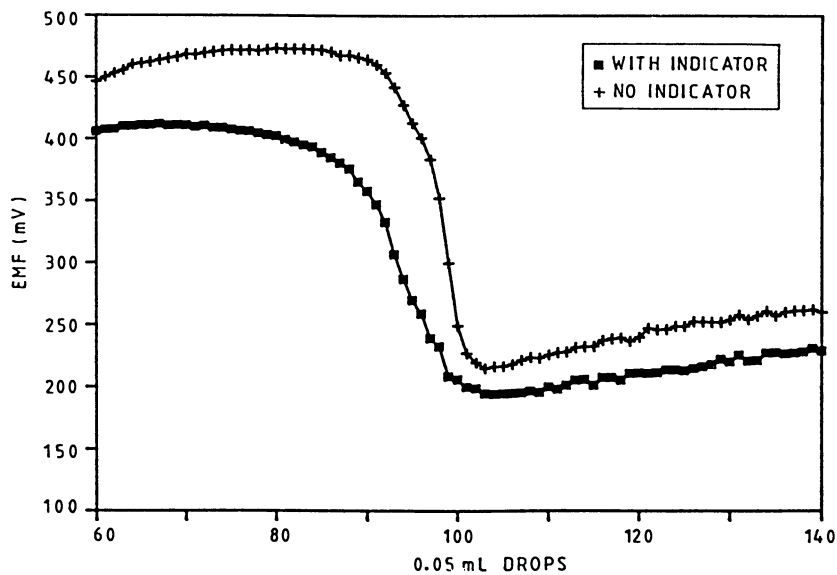


FIGURE 6 Titration curves at 1.46 wt% NaCl using 580 nm light

in droplet size and a corresponding lowering of the transmittance. This process continues to the endpoint where there is no more active surfactant present. At this stage the average droplet size is maximised and, consequently, the transmittance is at a minimum. Further addition of hyamine, which is a cationic surfactant, makes possible the increase in transmittance observed in the titrations (up to 0.70 wt% salt). It is assumed that the presence of salt reduces the ability of the hyamine to lower the ift of chloroform and water (much more so than any reduction for SDBS) and offers an explanation for the variation in the shape of the titration curves with salt level.

TEST OF THE EMULSION MECHANISM. The above hypothesis suggests that at the equivalence point all the SDBS is complexed with hyamine and, effectively, only a brine and chloroform system is present. It also suggests that an excess of either anionic or cationic surfactant causes a change in droplet size and an increase in light scattering. Therefore, it should be possible to mimic the two branches of the titration curve emanating from the equivalence point by starting with pure brine (35 cm³) and chloroform (10 cm³) and using either hyamine or SDBS as titrants. Experiments undertaken to examine this hypothesis are described below.

In order to achieve an initial droplet size distribution in the titration cup the contents were stirred for 230 seconds before injecting any titrant. The mode of operation of the autotitrator was changed to inject 0.05 cm³ of hyamine every 10 seconds to make conditions for each titration exactly the same. The results when hyamine was used as the titrant are shown in Figure 7. This figure shows the expected increase in signal with increasing hyamine concentration and that increasing the salt concentration decreases the slope of the titration curves. The procedure was then repeated using SDBS as the titrant to produce the results plotted in Figure 8. Again the curves show the expected increase in signal with increasing surfactant concentration and the decrease in slope of the titration curve at higher salt levels is consistent with the trend observed in the original tests, although it is less marked than when hyamine is used as the titrant.

These tests established that detection of the chloroform emulsification was the principle underlying action of the autotitrator. However, while there is agreement in the qualitative dependence on the salt level there are differences in the apparent rates of change in signal with aliquot addition. These can be attributed mainly to non-equilibrium effects.

The initial titration aliquots were added automatically on the basis of the rate of change of EMF, mode (i), and the resulting time between aliquot additions was usually shorter than the 10 second equilibration time allowed in the mode (ii) titrations described above. The time differences were especially significant when the transmittance change per 0.05 cm³ aliquot was small, for example when the hyamine was present in excess at high salt concentrations. This means that the mode (i) titrations are more influenced by kinetic effects and so the measured curves are less distinctive as may be seen by comparing the results at 1.46% salt in Figures 6 and 7.

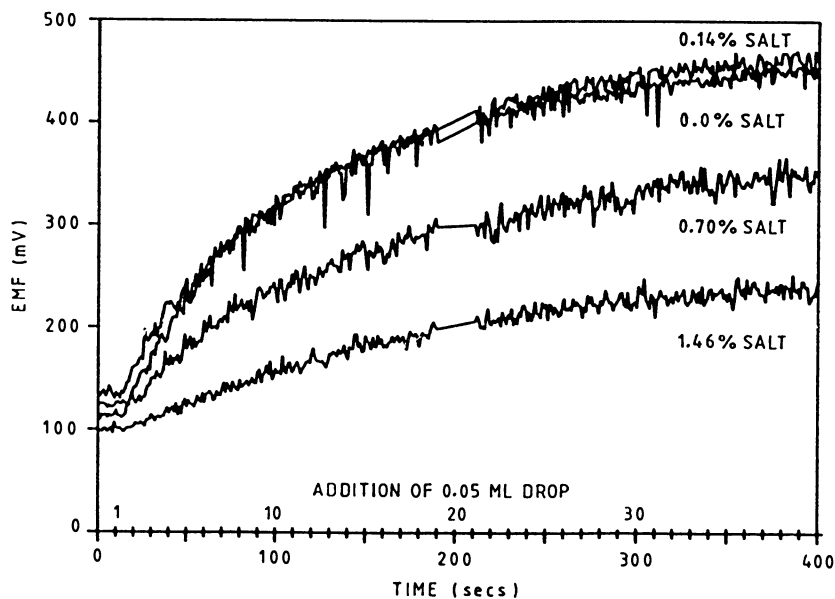


FIGURE 7 Titration of 35 cm³ brine and 10 cm³ chloroform against hyamine. 230 seconds initial equilibration time and 10 seconds between successive titrant additions.

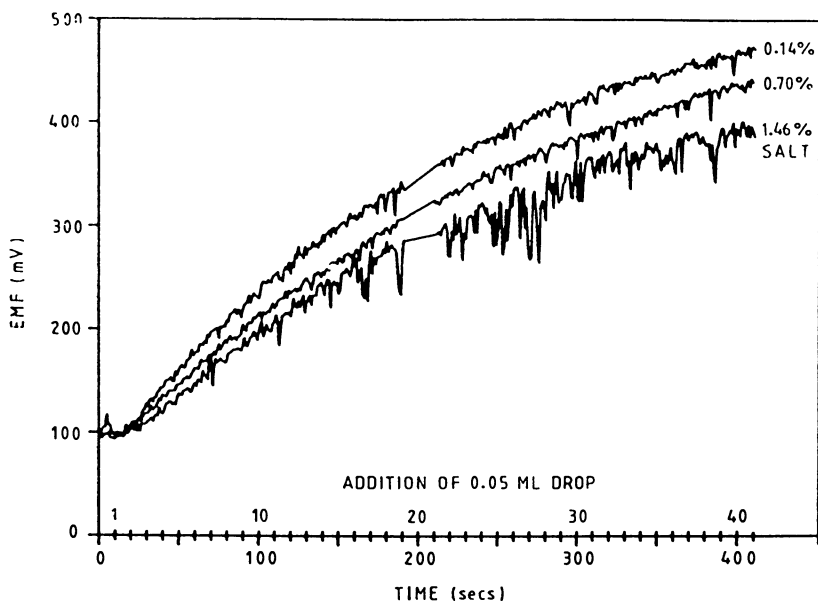


FIGURE 8 Titration of 35 cm³ brine and 10 cm³ chloroform against SDBS. 230 seconds initial equilibration time and 10 seconds between successive titrant additions.

Although the hyamine titrations in Figure 7 are in principle directly comparable with those obtained for titrations (Figures 5 and 6), this is not the case for the SDBS. Firstly, because the volume of water in the reaction vessel is increasing as the concentration of active SDBS increases in Figure 8, while in a real titration it decreases. Secondly, and more importantly, the mechanism by which the equivalence point is reached in a titration is by the aggregation of chloroform droplets as the concentration of active surfactant falls, whereas in Figure 8 the increase in the EMF with increasing SDBS is related to the increase in transmittance as the chloroform droplets break up with stirring. If the rates for these processes are not equal then different curves will be produced unless the reaction vessel contents are allowed to fully equilibrate between aliquots.

An example of these effects is shown in Figure 9 where a mode (ii) surfactant titration has been performed in the absence of salt and allowing a 10 seconds equilibration time between each aliquot. This gives a more clearly defined equivalence point when compared to the mode (i) titration in Figure 5.

A further difference is that the value of the transmittance minima of the titration curves is higher than that found for the water and chloroform system. This is believed to be due to the fact that in a titration the equivalence point will not correspond to an integer number of hyamine aliquots and so, even if the contents of the reaction vessel were allowed to equilibrate fully, there would still be a small amount of uncomplexed surfactant present which will be sufficient to decrease the droplet size and so increase the back-scattered light.

ERROR ANALYSIS. Although the endpoint might be expected to correspond to the steepest point of the curve, the equivalence point has been found to correspond to the minimum of the curve. At low salt levels the use of the steepest point on the titration curve will underestimate the equivalence point by 1% but at higher salt levels the application of this criteria may lead to misleading results with the equivalence point being considerably underestimated. The initial titrations which possess clear minima (i.e. 0 and 0.14 wt% salt) can be analysed using the minimum as the equivalence point with the results shown in Figure 10, where the error bars represent one standard deviation. The results were compared using t-tests. The use of the superfluous indicator gives significantly lower results compared to the purely turbidimetric method, because the mixed indicator has a net cationic dye content which complexes with the SDBS thereby reducing its active concentration. For the turbidimetric method consistent results are obtained at both salinities and with both filters, though the results show less scatter with the 580 nm filter and so its use is preferred.

EFFECT OF OIL. Titrations were performed in which small amounts of decane were added with the surfactant sample. The results were found to be insensitive to the presence of up to 2 cm³ of the decane. This allows the application of the method to both simple aqueous solutions and microemulsions containing significant quantities of decane.

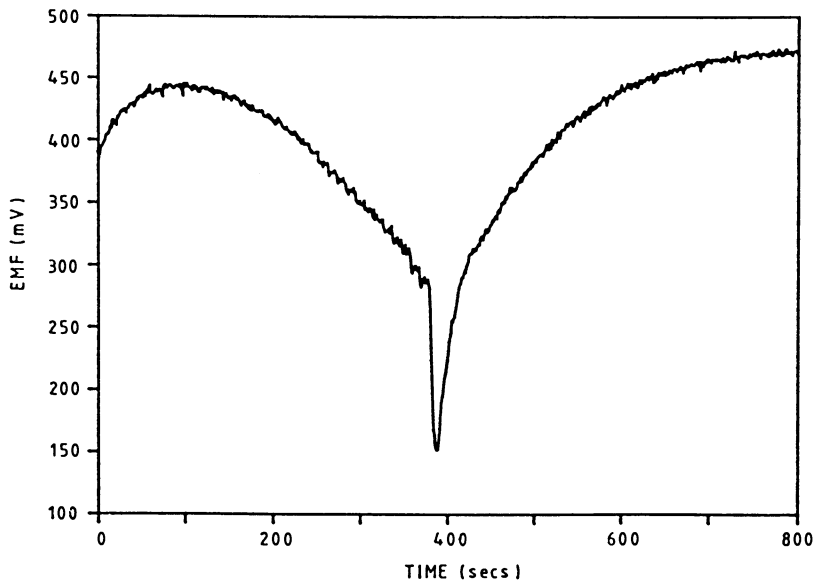


FIGURE 9 Turbidimetric titration SDBS against hyamine. 10 seconds between successive titrant additions.

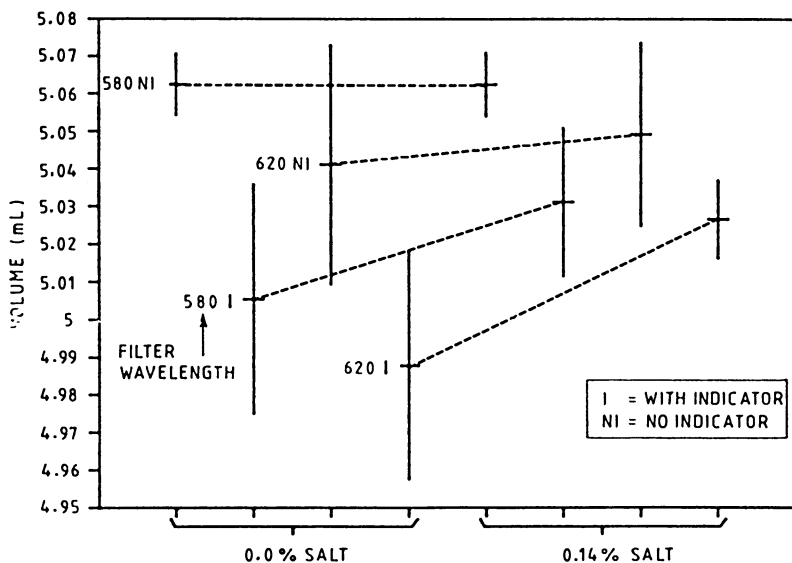


FIGURE 10 Analysis of equivalence volumes from titration curve minima.

CONCLUSIONS

A detailed study of the determination of the anionic surfactant SDBS by automated titration against hyamine using an autotitrator has been undertaken. The following conclusions and observations can be made.

- (i) An automated turbidimetric method using a chloroform phase and hyamine titrant without indicator dyes has been developed for the determination of SDBS concentrations.
- (ii) The mechanism producing the turbidity in the titration cup is postulated to be the formation of chloroform droplets in the aqueous phase under the action of vigorous stirring. Chloroform droplets back-scatter light at an intensity which decreases with drop size and the drop size is determined by the ift between the aqueous and chloroform phases. The ift, and hence the drop size, is decreased by the presence of active uncomplexed surfactant or hyamine.
- (iii) The contents of the titration cup should be stirred at the maximum rate available to enhance the rate of formation of the chloroform droplets.
- (iv) A light source of 580 nm wavelength gave a smaller error than a wavelength of 620 nm.
- (v) The equivalence point should be determined from the minimum in the titration curve which is well defined for salt levels below 0.14% wt% for SDBS. Thus distilled water should be used to dilute surfactant solutions.
- (vi) Sharper minima can be obtained by allowing a longer time interval between titrant additions.
- (vii) This study has been specific to the titration of SDBS against hyamine. However, it will probably apply to other anionic surfactants since the analytical method works by indirectly measuring interfacial tension, and it is a generic property of surfactants to alter ift. Whether or not the method is suitable for a particular surfactant will depend on the detail of the titration curve specific to the surfactant system and the accuracy to which the determination is required. Quantitative results will only be possible when the method possesses a well defined equivalence point determined by the minima of the titration curves. If no such clear definition exists then the method cannot be relied on to give accurate results.

ACKNOWLEDGMENT

This work was carried out for the UK Department of Energy under contract number R5221 as part of its Enhanced Oil Recovery Research.

LITERATURE CITED

1. Longman, G. F.; The Analysis of Detergents and Detergent Products; J. Wiley & Sons, 1978.
2. Södergren, A.; Analyst 1966, 91, 113.
3. Herring, D. E.; Lab Pract. 1962, 11, 113.
4. Holness, H.; Stone, W. R.; Analyst 1957, 82, 166.

5. Reid, V. W.; Longman, G. F.; Heinerth, E.; Tenside 1967, 4, 292.
6. Reid, V. W.; Longman, G. F.; Heinerth, E.; Tenside 1968, 5, 90.
7. Determination of Anionic - Active Matter - Direct Two-phase Titration Procedure, ISO 2771, 1972.
8. Synthetic Anionic Active Matter in Detergents by Potentiometric Titration. ASTM D4251-83.
9. Operating Instructions for the DL4ORC; Mettler Instruments AG, CH-8606 Griefensee, Switzerland.
10. Turbidimetric Titration of Anionic Tensides, Mettler Application No 135; Mettler Instruments AG, CH-8606 Griefensee, Switzerland.

RECEIVED September 23, 1988

Chapter 14

Mixed Micellization and Desorption Effects on Propagation of Surfactants in Porous Media

L. Minssieux

Institut Français du Pétrole, B.P. 311, 92506 Rueil-Malmaison, Cedex,
France

The micellization and adsorption properties of industrial sulfonate/ethoxylated nonionic mixtures have been assessed in solution in contact with kaolinite. The related competitive equilibria were computed with a simple model based on the regular solution theory (RST). Starting from this analysis, the advantage of adding a hydrophilic additive or desorbing agent to reduce the overall adsorption is emphasized. As a test, surfactant slug flow experiments were performed in clayey sandpacks with and without the injection of a desorbent behind the micellar slug. Results show that a substantial decrease in surfactant retention is obtained in calcic environment by such an additive. Likewise, the ethoxylated cosurfactant in the micellar slug can be remobilized simultaneously with sulfonate without any change in its ethylene oxide distribution. The application of the RST to sulfonate/ethoxylated alkylphenol mixtures explains semi-quantitatively the relationship between their properties and composition.

Surfactants are often used for oil production, either for well treatments or in EOR recovery processes such as micellar flooding, controlling the mobility of injected gas by the forming of foam, or huff-and-puff steam injection. Reducing the costs of such operations goes via improving the efficiency of the products injected into the reservoir rock. To achieve this, a good understanding of the properties of surfactants and of their mixtures is required. Considerable fundamental research efforts have been made in this area in recent years, particularly concerning binary mixtures of isomerically pure or purified surfactants (1 - 3) in solution in deionized water or water containing NaCl.

In this paper, we focused on behavior of industrial surfactant mixtures that can be used in calcic saline media, i.e. under conditions often encountered in onshore or offshore fields. The results obtained have been used for the laboratory testing and for interpreting the working mechanisms of a method of reducing losses of products in reservoir rocks and of propagating them more effectively in the formation to be treated.

Surfactants Investigated

Ethoxylated fatty alcohols and alkylphenols were used. The products available on the market make up homologous series containing an average of between 3 and 100 ethylene-oxide groups. They thus have a wide HLB (hydrophilic/lipophilic balance) range. Besides, they are among the least expensive surfactants on the market.

As an anionic surfactant, a synthetic alkylate-base sulfonate containing about 60 % active material (Synacto 476) was used. To make it compatible with the injection water considered (composition in Table I) containing 1500 ppm Ca^{++} and Mg^{++} ions, a nonionic cosurfactant was combined with it, i.e. an unsaturated ethoxylated fatty alcohol with 8 ethylene oxide groups (Genapol). Their main characteristics and properties are listed in Table II.

Micellar Properties of Aqueous Solution of Surfactants

Monomer/Micelle Equilibrium: Mixtures of surfactants, like any surfactant species in an aqueous solution, give rise to monomer or micelle aggregates provided that the concentration reaches a minimum value, called the critical micellar concentration (CMC). The micelles thus formed are mixed, i.e. made up of the different surfactant species in solution.

The corresponding monomer/micelle equilibria can be dealt with by the regular solution theory (RST), as shown in particular by Rubingh in 1979 (1). The application of this theory to numerous binary surfactant systems (2 - 4) has followed and led to a set of coherent results (5).

Without going into this theory in detail, let us reproduce here the equation proposed by Rubingh for the activity factor of surfactant species making up mixed micelles in a binary system :

$$f_1 = e^{\beta_{12} (1 - x_1)^2}$$

$$f_2 = e^{\beta_{12} x_1^2}$$

in which x_1 is the molar fraction of species 1 in the mixed micelles, and β_{12} is the molecular interaction parameter. This parameter takes into consideration the full interaction forces existing between the surfactant moles of a mixed micelle. It is thus entirely characteristic of the surfactant pair considered and of their ionic environment, as shown in the list of values compiled by Nagayaran (5).

Calculating the Characteristic Interaction Parameter of the Micellar Systems

Used: To perform the calculation of β_{12} for the systems examined, i.e. Sulfonate/Genapol/ethoxylated nonylphenol mixtures, the following assumptions were made:

- . Industrial surfactants can be assimilated with a single entity.

TABLE I : Composition of Synthetic Brine

Cations	Conc. (ppm)	Salt concentration (g/l)	
Na ⁺	8,600	NaCl	17.00
K ⁺	65	KCl	0.13
Mg ⁺⁺	290	MgCl ₂ , 6 H ₂ O	2.436
Ca ⁺⁺	1,300	CaCl ₂ , 2 H ₂ O	4.777
Na ⁺	1,918	Na ₂ SO ₄	5.92
		TDS =	30.26

TABLE II : Characteristics of Surfactants Used

Additive	CMC		Ads Plateau		Molecular weight	% active material (A.M.)
	mg/l	M/l	mg/g	μM/g		
<u>Micellar system:</u>						
(Sulf/Gen.)	30		5.20			
as sulf. alone	9	2.33.10 ⁻⁵	1.87	4.86	385	60
Genapol 8 E.O.	30	5.10 ⁻⁵	5.2	8.5	608	>98
<u>Descrbents</u>						
Nonylphenols						
with: 14 E.O.	40	4.78.10 ⁻⁵	0.37	0.44	836	> 98
30 E.O.	160	10.4 "	0.30	0.20	1,540	> 98
50 E.O.	500	20.7 "	0.44	0.18	2,420	> 98
100 E.O.	1,300	28.1 "	0.77	0.17	4,620	97

. There is no molecular interaction between nonionic surfactants with an ethylene-oxide chain, i.e. Genapol and ethoxylated nonylphenols. Indeed, research by Nishikido (6) on polyoxyethylene laurylethers (5 < E.O. number < 49) has shown the ideal behavior ($\beta_{12} = 0$) of their mixtures. Likewise, Xia (7) has found very low β_{12} values for mixtures of ethoxylated fatty alcohols.

. Taking in account the results obtained by Graciaa (8) and Osborne-Lee (9) for alkylbenzene sulfonate and alkylphenols with an increasing degree of ethoxylation, we have considered that the interaction between sulfonate and associated highly ethoxylated nonylphenol (with 30, 50 or 100 E.O.) was predominant in mixed micelles of the mixtures investigated.

. The sulfonate/Genapol pair was assimilated with a pseudo-component, with the cosurfactant acting only as a solubilizer in the brine used.

The mixture of the three additives was then dealt with as a pseudo-binary system to which the RST theory was applied.

Figure 1 gives the measurements of surface tension used for determining the CMCs of sulfonate/Genapol and nonylphenol 30 E.O. mixtures, with the last surfactant being called a desorbent (this term will be justified below). Minimum in surface tension was seen only for a few nonionic solutions (e.g. NP 50 E.O.). In this case, we used dyes that, once solubilized in the micelles, cause the solution to change color, which is another way of measuring the CMC.

The value of the characteristic interaction parameter of these systems (30° C), adjusted from the CMC measurements in Figure 1, was calculated by means of RST and taken equal to -2.5. This value is effectively in the range of the ones found by Graciaa for similar anionic/nonionic mixtures (8).

Limit Concentration of Monomers in Solution: In the calcic environment considered, the CMC values of surfactants are low. For example, sulfonate and Genapol solutions reach their CMC at 30 ppm (Table II). The surfactant solutions injected in practice at concentration of about one or several percent are thus generally used well above their CMC. Under such conditions, the predominant fraction of each surfactant is the micellar form whose composition (x_i) is practically equal to the initial proportion of products (i.e. α_1 for sulfonate). At this concentration level of products, very small proportions of monomer species coexist, the limit concentrations of which are respectively :

$$\text{mono 1 conc} = x_1 f_1 \text{ CMC}_1 = \alpha_1 \text{ CMC}_1 \cdot e^{\beta_{12} (1 - \alpha_1)^2}$$

$$\text{mono 2 conc} = (1 - x_1) f_2 \text{ CMC}_2 = (1 - \alpha_1) \cdot \text{CMC}_2 \cdot e^{\beta_{12} \alpha_1^2}$$

For the pseudo-binary mixture ($\alpha = 0.5$) of sulfonate and nonylphenol with 30 E.O., figure 2 shows how the concentration of each of their monomer calculated by the RST theory (1), varies as a function of the overall surfactant concentration. It can be expected that the asymptotic regime in which monomer concentrations are stabilized will correspond to a plateau of the adsorption isotherm for the surfactant mixtures considered.

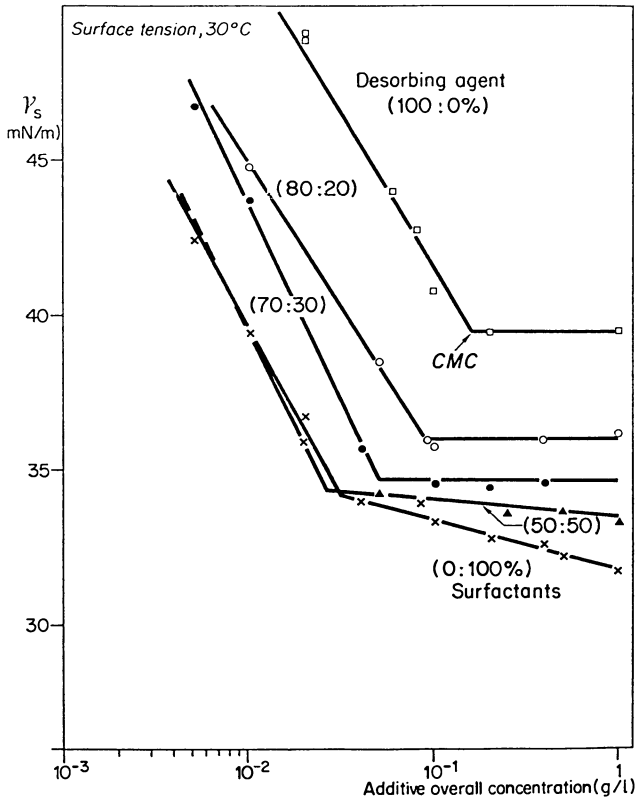


Figure 1. CMC determination of surfactant mixtures. (Reproduced with permission from ref. 16. Copyright 1987 Deutsche Wissenschaftliche Gesellschaft.)

Properties of Surfactant Solutions in Equilibrium with an Adsorbent Solid

Taking Simultaneous Micellization and Adsorption Phenomena into Consideration: In the presence of an adsorbent in contact with the surfactant solution, monomers of each species will be adsorbed at the solid/ liquid interface until the dual monomer/micelle, monomer/adsorbed-phase equilibrium is reached. A simplified model for calculating these equilibria has been built for the pseudo-binary systems investigated, based on the RST theory and the following assumptions :

. Each species is adsorbed individually according to a linear adsorption isotherm until there is an equilibrium concentration in solution equal to the CMC_i of the product considered.

. There are no interactions between species 1 and 2 adsorbed on the solid surface.

. Admicelle formation and associated CAC (Critical admicelle concentration) as proposed by Scamehorn (10) and Harwell (11) were not introduced here for a practical reason : a feasible and fast method of CAC measurement does not seem to exist at the moment. The difficulties related to such delicate determinations appear well from observation of the detailed adsorption isotherms of pure sulfates mixtures published by Roberts et alii (10).

The problem could be even more difficult in the case of industrial anionic/nonionic surfactants, due to their polydispersity and very low CMC in the salty environment considered here. So the corresponding needed CAC data was not available.

. The equilibria are instantaneous.

These assumptions are akin to those taken in account in the mixed adsorption model of Trogus (12). The difference between the two models lies in the relationship linking CMCs of single and mixed surfactants and monomer molar fractions : Trogus used the empirical equation proposed by Mysels and Otter (13); in our model, the application of RST leads to an equation of the same type.

Calculation examples of mixed surfactant adsorption: The solid chosen as the model adsorbent was made up of a natural sand (specific area = $380 \text{ cm}^2/\text{g}$) mixed with 5% clay (Charentes kaolinite with specific area = $26.8 \text{ m}^2/\text{g}$). This material was taken as a model of clayey sandstone reservoirs.

The adsorption plateaus on this solid, determined with each of the surfactants (Table II) and the individual CMC values, were used to calculate the adsorption constants input in the model. Figure 3 compares the total adsorption (sulfonate + NP 30 EO) of the pseudo-binary system investigated as a function of the initial sulfonate fraction of the mixtures under two types of conditions : (1) on the powder solid, batch testing with a solid/liquid ratio, $S/L = 0.25 \text{ g/cc}$ (2) in the porous medium made from the same solid, for which this solid ratio is much higher ($S/L = 4.0 \text{ g/cc}$).

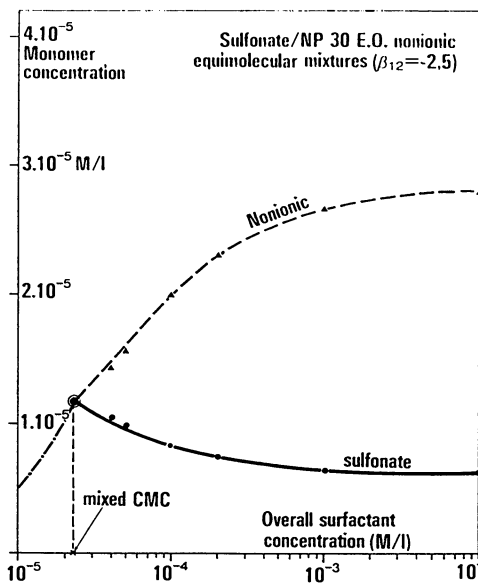


Figure 2. Monomer versus overall surfactant concentrations in micellar solutions.

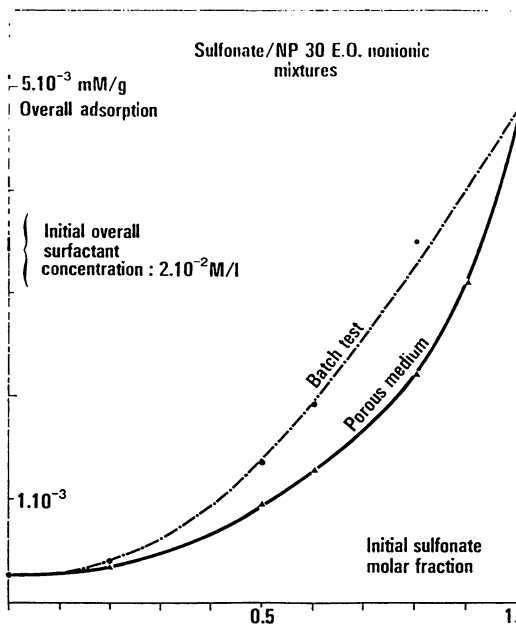


Figure 3. Mixed overall adsorption of pseudobinary systems.

The differences between the two curves can be explained by the sulfonate (the most adsorbed surfactant) monomer concentrations at equilibrium, which were reached in both cases, considering the amounts of surfactants, liquid and solid present. Figure 4 shows a distinct evolution of monomer concentrations for the two solid/liquid ratios considered.

In both cases, overall adsorption and especially that of sulfonate (or "primary" surfactant in the composition of most micellar systems used for EOR) are considerably reduced by simply adding a second product having low adsorption characteristics (NP 30 EO in the above example). This is why we have called this strongly hydrophilic surfactant a desorbent.

Such an idea was patented in 1981 (14). Besides research by Scamehorn and Schechter (15) provided an experimental illustration of this by batch adsorption tests of kaolinite with some purified anionic/nonionic products. Our objective was to enlarge and test this technique under the dynamic flow conditions of industrial surfactant injection in an adsorbent porous medium.

Surfactant Transport in Porous Media: Dynamic Adsorption/Desorption Equilibria

Circulation Test Conditions for Additive Solutions in Porous Media: The sand/kaolinite mixture described above was used to form sandpacks in a Rilsan cell (13 or 30 cm long, 2.5 cm in diameter, 36 % porosity). The corresponding solid/liquid ratio was then 4.72 g/cc.

The surfactant retention tests were performed in the porous medium at 43° C in sandpack ($S_{or} = 0$) saturated with brine (See composition in Table I). The injection flow rate used in these tests (2 cm³/h) corresponds to a front velocity of 30 to 40 cm/day.

A typical sequence followed in this test series consists in injecting : (1) a micellar slug of one pore volume of aqueous solution of 4% of the preceding pseudo-binary system (2% sulfonate/2% Genapol) ; (2) a slug of desorbent solution corresponding to a fixed amount of additive (e.g. equal to 1 PV at a concentration of 0.5 %) ; (3) at least 1.5 PV of brine with no additive.

Reference tests were also performed in the absence of any desorbent (Tests 1 and 2 in Table III). Likewise, the propagation of each desorbent was examined separately, without any prior micellar slug injection. The effluents were sampled for analysis by a fraction collector.

The sulfonate content was determined either by the well-known technique of two-phase titration with hyamine or by liquid chromatography (HPCL). Nonionic surfactants were analyzed by HPLC (16) in the reverse or normal phase mode depending on whether the aim was to determine their content in effluents or to compare their ethylene oxide distribution.

Such products were detected in the UV, using a Waters multiwavelength detector (Model 490 E). The wavelength chosen for the ethylenic nonionic (Genapol), rich

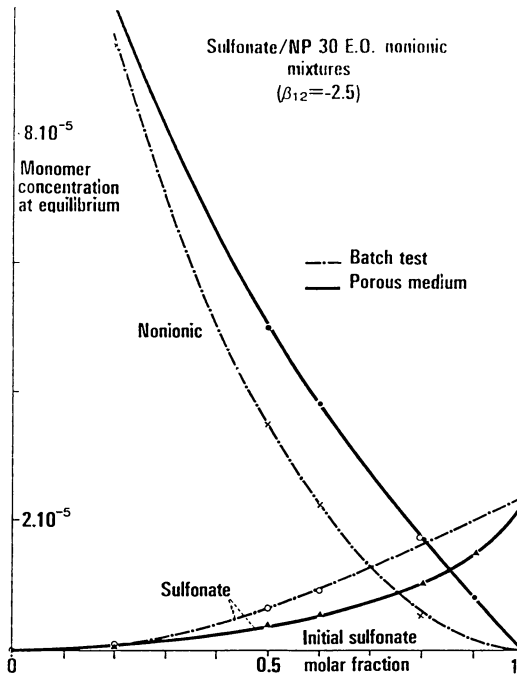


Figure 4. Monomer concentration versus initial sulfonate fraction for two typical solid-liquid ratios.

TABLE III : Adsorption/Description Data From Dynamic Flow Tests

Run n°	Desorbent concentration used		pH effluents	Surfactant retention (mg/g)			Associated concentration in effluents (g/l)		
	g/l	mM/l		sulfonate	ccsurf.	Desorbent mg/g	μM/g	sulfonate cosurf. ratio	Sulfonate
1	0	0	5.0 - 6.0	2.81	4.70			1.67	
2	0	0	5.8	1.85	3.42			1.85	
<u>NP 30 EO</u>									
3	2.7	1.75	6.7 - 7.0	1.22	1.78	0.50	0.32	1.46	1.3 - 1.8
4	5.0	3.25	5.0 - 5.6	1.55	2.60	0.17	0.11	1.68	4.2 - 5.2
5	5.0	3.25	5.8	1.17	2.30	0.46	0.30	1.96	4 - 5
6	5.0	3.25	7.0	1.08	1.92	0.16	0.10	1.78	3.6 - 4.5
<u>NP 50 E.O.</u>									
7	5.0	2.07	6.2	1.08	1.07	0.48	0.20	1	3.5 - 4.5
<u>NP 100 E.O.</u>									
8	5.0	1.08	6.9	1.30	1.90	0.96	0.21	1.46	1.7 - 2.4
									0.7 - 1.3

NOTE: Reproduced with permission from ref. 16. Copyright 1987 Deutsche Wissenschaftliche Gesellschaft.

in double bonds, was 229 nm. 278 nm, wavelenth characteristic of aromatic ring absorption, was taken for the detection of ethoxylated alkylphenols or of the synthetic aromatic sulfonate used.

To mark the displacement front, 150 ppm of sodium iodide was incorporated in the surfactant micellar slug. This tracer can easily be detected in effluents with a UV detector at 229 nm.

Elution of a Surfactant Slug in the Presence of a Desorbent: A mass balance for each of the three additives was used to and results obtained during each test are given in Table III.

The first two tests were performed without any desorbent and used as references, at two distinct levels of equilibrium pH. The performances of three desorbents (NP 30, 50 and 100 E.O.) having an increasing ethoxylation degree were compared at the same mass concentration (0.5%).

Figures 5 and 6 illustrate the surfactant elutions obtained in Tests 4 and 7.

Surfactant Remobilization by Means of Desorbent: It appears from Table III, that, in the presence of a desorbent, 30 to 45% of the sulfonate and 33 to 69% of the Genapol can be remobilized. This assessment is made by comparison with the reference tests performed at the closest pH values.

Figures 5 and 6 show that the concentration of the two surfactants in the effluents increases simultaneously with the production of the desorbent, which confirms the mixed micellization mechanism described above. Figure 5, where the three additives are produced lately, illustrates the phenomenon particularly well. At the lower pH corresponding to strong adsorption conditions for sulfonate (test 4), the one pore-volume micellar slug would have been entirely consumed by the medium in the absence of any desorbent.

Surfactant Transport in an Adsorbent Porous Medium. Chromatographic Aspects: A first observation was made in all the tests in Table III. The breakthrough of both surfactants from the micellar slug always occurs simultaneously without any chromatographic effect (Figures 5 and 6). This stems both from the chemical nature of the two products selected and also from the fact that the injected concentration is much greater than the CMC of their mixtures.

Likewise, in order to evaluate nonionics transport, ethylene-oxide distribution in the cosurfactant (Genapol) was determined by HPLC at two stages of production in test 7 : (1) before breakthrough of the desorbent, i.e. in the presence of sulfonate in the effluent; and (2) after its breakthrough when the three additives coexist in solution in the form of mixed micelles.

Figure 7 shows the quasi identity of the ethylene-oxide distributions of the Genapol samples, analyzed at the outlet of the porous medium. For nonylphenols with 14 and 30 EO, we also checked that the distribution of these nonionic agents (injected in a concentration of 5 g/l) was not appreciably changed after transit via the adsorbent porous medium. Under these conditions, the mixed micelles formed

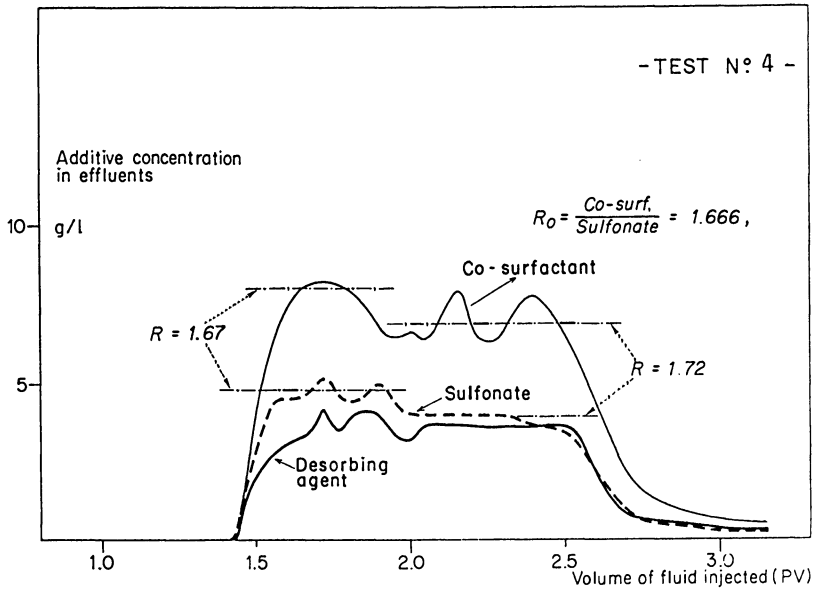


Figure 5. Elution of surfactants by means of desorbent NP 30 E.O. (Reproduced with permission from ref. 16. Copyright 1987 Deutsche Wissenschaftliche Gesellschaft.)

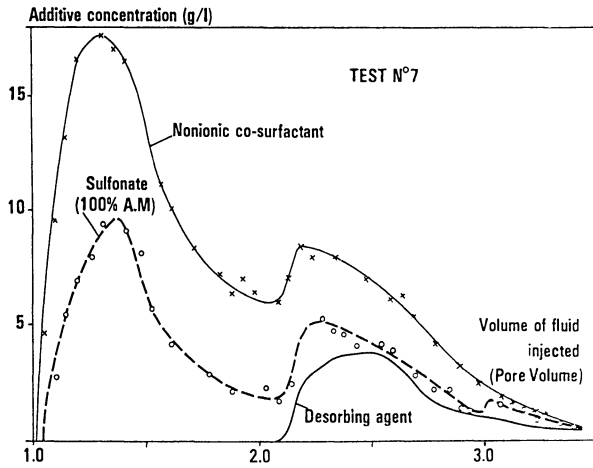


Figure 6. Elution of surfactants by means of desorbent NP 50 E.O.

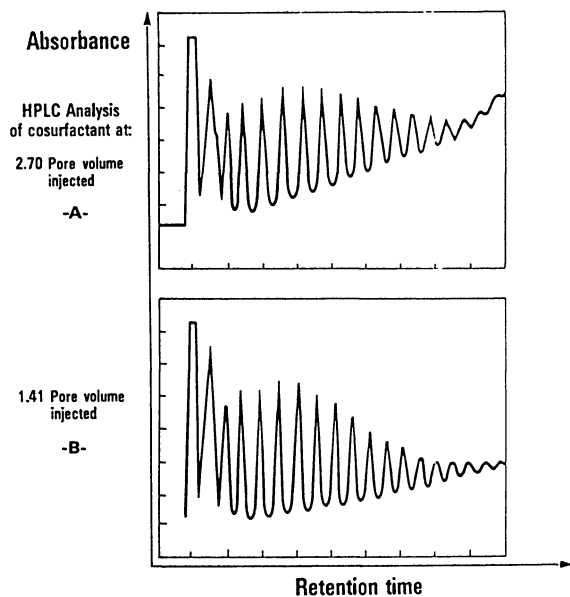


Figure 7. Ethylene oxide distribution of cosurfactant produced before (A) and after (B) desorbent breakthrough. (Reproduced with permission from ref. 16. Copyright 1987 Deutsche Wissenschaftliche Gesellschaft.)

contain all the monomer species of the different constituents of industrial products moving at the same speed. The same analysis remains to be done with the industrial sulfonate used.

It can be mentioned here that we found in another study (17), that these surfactant remobilization mechanisms by mixed micellization also operated in the presence of crude oil in the medium and thus help increase oil recovery.

Comparison of Retention Properties of Three Desorbents with an Increasing Degree of Ethoxylation: The individual behavior of three nonionic desorbents (NP 14, 30 and 100 E.O) is compared in Figure 8. Slug size was 1.16 PV in those tests. The outflow of the tracer indicates the slug front of the additive injected. The concentration used was 5 g/l in all tests. On a weighted basis, it was the NP 30 E.O., that led to the lowest final retention, i.e. 0.30 mg/g of rock (Table II).

Interpretation of Porous Medium Results

As suggested above, the main recovery mechanism of surfactants retained in the rock can be interpreted as a micellization phenomenon inside the pores. Upon contact with micelles from the desorbent agent, the adsorbed surfactants are solubilized in the form of mixed micelles. This also explains the effectiveness of the desorbent still observed at low concentration (0.27% in Test 3 in Table III, concentration much higher than the CMC of NP 30 EO equal to 0.016%).

Comparison: Theoretical Equilibrium Calculations and Results of Circulation Tests in Porous-Media: To make this interpretation more quantitative, the regular solution theory (RST) was applied to sulfonate/desorbent dynamic equilibria reached inside porous media by using the approach described above. In so doing, we assumed that the slugs injected were sufficiently large and that a new equilibrium was reached at the rear of micellar slug in the presence of desorbent.

Calculations were made at the desorbent concentrations used in Tests 3, 6,7 and 8 in Table III. Table IV below gives the respective adsorptions of sulfonate and desorbent as well as their equilibrium concentration. A comparison with the corresponding experimental values in Table III shows good agreement with regard to sulfonate from the micellar slug. On the other hand, losses of desorbent are systematically underestimated. This shows that the assumption of the independent adsorption of both surfactants on the solid is incorrect and that presumably cooperative adsorption of desorbent and sulfonate takes place. Accordingly the model used needs to be improved.

Conclusions

The present study suggests the potential application of a method for reducing surfactant losses in reservoirs, thus, ipso facto increasing their effectiveness. This method consists in incorporating a suitable desorbent in the water used to drive the surfactant slug injected into the formation to be treated.

Such a desorbent may be, for example, a hydrophilic nonionic surfactant, which is among the least expensive on the market and is suitable in calcic environment.

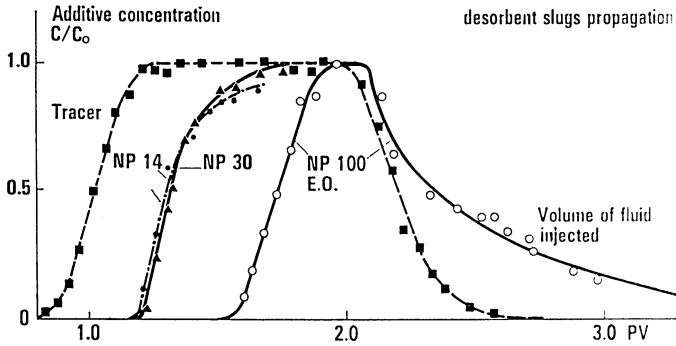


Figure 8. Profiles of additive produced in slug injection runs of three distinct desorbents.

TABLE IV: Computation of Solid/Micellar Solutions Equilibria

Run n°	Desorbent used	Coefft. β_{12}	Sulfonate		Desorbent	
			Loss (mg/g)	Equil. concn. (g/l)	Loss (mg/g)	Equil. concn. (g/l)
3	NP 30 E.O.	- 2.5	1.30	2.40	0.024	2.38
6	NP 30 E.O.	- 2.5	1.14	3.43	0.042	4.80
7	NP 50 E.O.	- 4.45	1.21	3.14	0.006	4.96
8	NP 100 E.O.	- 5.73	1.39	2.26	0.002	4.99

The choice should be optimized as a function of the type of surfactants to be desorbed and the temperature and characteristics of reservoirs.

The critical micellar concentrations of anionic/nonionic surfactant mixtures examined are low in a saline medium, so that, at the concentrations injected in practice, the chromatographic effects resulting from the respective adsorption of monomers are masked. Such surfactants propagate simultaneously in the medium in the form of mixed micelles.

In the same way, after transit through a porous medium, non appreciable change was found in the ethylene oxide distribution of nonionic surfactants used as a cosurfactant or desorbent.

The theory of regular solutions applied to mixtures of aromatic sulfonate and polydispersed ethoxylated alkylphenols provides an understanding of how the adsorption and micellization properties of such systems in equilibrium in a porous medium, evolve as a function of their composition. Improvement of the adjustment with the experimental results presented would make necessary to take also in account the molar interactions of surfactants adsorbed simultaneously onto the solid surface.

Acknowledgments :

This study was partly supported by the European Economic Community.

We wish to express here our appreciation to N. MONIN and G. SYLVESTRE who performed the laboratory tests and analyses.

LITERATURE CITED:

- (1) Rubingh, D. N., Solution Chemistry of Surfactants, K. L. Mittal, ed., vol. 1, 337-354, New York, 1979.
- (2) Holland, P. M. and Rubingh, D. N., "Nonideal Multicomponent Mixed Micelle Model, J. Phys. Chem., vol. 87, 1984-1990, 1983.
- (3) Scamehorn, J.F., Schechter, R.S. and Wade, W. H., J. Disp. Sc. Tech., 3 (3), 261-178, 1982.
- (4) Zhu, B. Y. and Rosen, M. J., J. Coll. Sc., vol. 99 No. 2, June 1984.
- (5) Nagajaran, Microemulsions, Adv. Coll. Int. Sc. November 1986.
- (6) Nishikido, N. et al., Bul. Chem. Soc. Japan, vol 48 (5), 1387-1390, 1975.

- (7) Xia J. et alii, "Effects of Different Distributions of Lyophobic Chain Length on the Interfacial Properties of Nonaethoxylated Fatty Alcohol" in "Phenomena in Mixed Surfactant Systems", J.F. Scamehorn, Ed. 1986, ACS Symposium Series 311, Wash.
- (8) Graciaa A. et alii, "The Partitioning of Nonionic and Anionic Surfactant Mixtures Between Oil/Microemulsion/Water Phases", n° SPE 13 030, Houston, 1984.
- (9) Osborne-Lee I.W. et alii, J. Coll. Int. Sc., Vol. 108, n° 1, Nov. 1985.
- (10) Scamehorn, J.F. Phenomena in Mixed Surfactant Systems; American Chemical Society, Symposium Series : Washington, DC 1986.
- (11) Harwell, J.H. et alii, Aiche J. 1985, 31, 415.
- (12) Trogus, F.J.; Schechter, R.S. ; Pope, G.A.; Wade W.H., J. Petr. Tech. 1979, June, 769.
- (13) Mysels, K.J.; Otter, R.J., J. Coll. Sc. 1961, 16, 474.
- (14) Kudchadker, US Patent 4, 276, 933, July, 1981.
- (15) Scamehorn J.F., Schechter R.S. and Wade WH., "Adsorption of Surfactants on Mineral Oxide Surfaces from Aqueous Solution", J. Coll. Int. Sc., Vol. 85, n° 2, Feb. 1982.
- (16) Minssieux L., "Method for Adsorption Reduction of Mixed Surfactant Systems", Proc. 4th. Eur. EOR Symp., 1987, p. 293.
- (17) Minssieux L., "Surfactant Flood with Hard Water : A Case Study Solved by HLB Gradient", SPE Res. Eng., Vol. 2, N° 4, 605-612, Nov. 1987.

RECEIVED November 28, 1988

Chapter 15

Calorimetric Phase Studies of Model Amphiphilic Petroleum Recovery Systems

Duane H. Smith, G. L. Covatch, and R. O. Dunn¹

Enhanced Oil Recovery Group, U.S. Department of Energy, Morgantown Energy Technology Center, Morgantown, WV 26507-0880

Ways are discussed of measuring both compositions and heats of formation (*i.e.*, excess enthalpies) of two conjugate phases in model amphiphile/water systems by isoperibol titration calorimetry. Calorimetric and phase-volume data are presented for $n\text{-C}_4\text{H}_9\text{OH/water}$ at 30 and 55 °C and for $n\text{-C}_4\text{H}_9\text{OC}_2\text{H}_4\text{OH/water}$ at 55 and 65 °C, and compared to results in the literature. Some considerable practical advantages of calorimetry for the development of oil recovery technologies are pointed out.

Petroleum recovery typically deals with conjugate fluid phases, that is, with two or more fluids that are in thermodynamic equilibrium. Conjugate phases are also encountered when amphiphiles (*e.g.*, surfactants or alcohols) are used in enhanced oil recovery, whether the amphiphiles are added to lower interfacial tensions, or to create dispersions to improve mobility control in miscible flooding (1,2).

Experimental and theoretical studies, as well as computer simulators, all require knowledge of the number and compositions of the conjugate phases, and how these change with temperature, pressure, and/or overall (*i.e.*, system) composition. In short, all forms of enhanced oil recovery that use amphiphiles require a detailed knowledge of phase behavior and phase diagrams.

However, the measurement of phase diagrams is often tedious and time consuming; and the number of variables and combinations of

¹Current address: Northern Regional Research Center, U.S. Department of Energy, Peoria, IL 61604

compounds is very large. Hence, equations-of-state and other thermodynamic models are used to correlate and predict phase behavior. Extensive experience with CO₂/hydrocarbon systems has shown that the correlations are substantially improved when they are based not only on compositions, but on data for other thermodynamic variables as well.

Furthermore, the experimental difficulties of studying phase behavior can be greatly compounded when surfactants are added to a system of oil and/or CO₂ and water, because the surfactant system often forms stable dispersions (emulsions and/or foams). These difficulties may prove to be especially severe in the development of surfactant-based mobility control for miscible flooding, in which the EOR process requires the formation of dispersions, and in which eventually many measurements will have to be made at miscible-flood pressures ($P > 7$ MPa).

For these various reasons one may ask if it is possible to develop automated or semi-automated methods that will simultaneously measure compositions and other thermodynamic parameters at reservoir pressures and temperatures, without waiting for bulk separation of dispersed phases in the apparatus.

In an earlier study calorimetry achieved this objective for the compositional boundaries between two and three phases (3). Such boundaries are encountered both in "middle-phase microemulsion systems" of low tension flooding, and as the "gas, oil, and water" of multi-contact miscible EOR systems (1,2). The three-phase problem presents by far the most severe experimental and interpretational difficulties. Hence, the earlier results have encouraged us to continue the development of calorimetry for the measurement of phase compositions and excess enthalpies of conjugate phases in amphiphilic EOR systems.

This paper considers systems of lesser dimensionality than the previous study, namely, systems of two compounds, which (ignoring the vapor) can form only one or two phases. Specifically, excess enthalpies and phase compositions have been measured (at ambient pressure) by isoperibol calorimetry for n-butanol/water at 30.0 and 55.0 °C and for n-butoxyethanol/water at 55.0 and 65.0 °C. (Butanol, or C4E0, is C₄H₉OH; butoxyethanol, or C4E1, is C₄H₉OC₂H₄OH.) The miscibility gap of each of these systems is shown in Figure 1. For each system, titrations have been performed from the neat compound (water or amphiphile) across the phase boundary (aqueous or amphiphilic conjugate

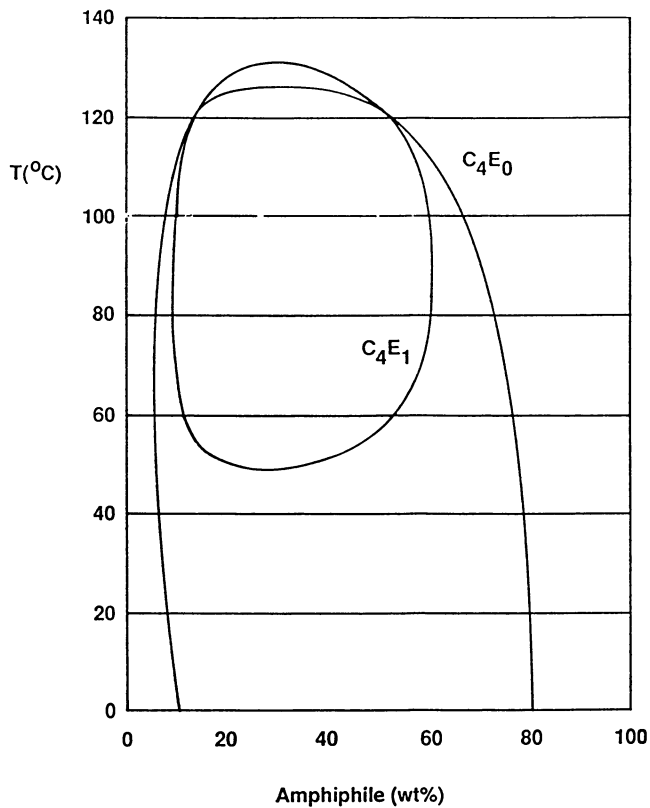


Figure 1. Temperature-composition phase diagrams of n-butanol (C₄E₀) and n-butoxyethanol (C₄E₁), respectively, with water. (redrawn from data in refs. 4 and 5.)

phase) and into the two-phase region. The results are compared (where possible) with previously reported excess enthalpies, or with phase compositions obtained by more conventional phase-diagram methods.

Calorimetry has been successfully used to measure enthalpies and phase boundaries in several CO₂/hydrocarbon systems at reservoir pressures (6). Together, the present and previous studies encompass all of the classes of compounds of the amphiphile/CO₂/hydrocarbon/water systems that are encountered in dispersion-based mobility control for miscible-flood EOR (2).

Experimental

Calorimetric measurements were performed with two Tronac 450 isoperibol calorimeters, and calibrations were made before and after each titration. To calculate heats from changes in thermistor voltage, corrections were made for stirring heat, heat leakage, and change in the energy equivalence ("heat capacity") of the calorimeter and contents due to addition of titrant (7). Titrations of 1.999 cm³/300 s (calibrated at 55 °C) and 1.998 cm³/1200 s (calibrated at 30 °C) were used in the respective calorimeters. Thermistor voltages were recorded at 1 s intervals for the faster titration rate and at 5 s intervals for the slower rate. In a typical measurement sequence two successive 2 cm³ additions of titrant were made to an accurately weighed titer of about 20 cm³. This sequence was then repeated with a different titer composition as many times as necessary to cover the required range of amphiphile/water compositions. An MS-DOS desk-top computer with 640K of random-access memory (RAM) was used to control the calorimeter and to collect thermistor voltages at the fixed time intervals. Spread-sheet macros running on this same computer were used to make various plots, including thermistor voltage vs. time and corrected heat vs. time.

Phase-volume samples were prepared gravimetrically, thermostatted in constant-temperature water baths (± 0.02 °C), and examined visually for the number of phases.

The n-butanol (99.7 mole% stated purity) was from Malinckrodt, and n-butoxyethanol (99+ % stated purity) was from Aldrich. Each was analyzed by gas chromatography for impurities and by Karl Fischer titration for water, and used without further purification. The water was distilled.

Data Treatment and Results

Figure 2 shows measured excess enthalpies for aqueous phases and two-phase mixtures of n-butoxyethanol/water at 55.0 °C. Data from four replicate additions of 2 cm³ of butoxyethanol to water are shown in Figure 2a; Figure 2b shows data from the subsequent addition of an additional 2 cm³ of butoxyethanol to each of the solutions of Figure 2a. (To reduce overlap between the symbols, only every tenth experimental point of each titration has been plotted.) The large discontinuity between successive titrations is caused by the fact that the instrument necessarily takes the enthalpy of the initial composition of each titration to be zero. (The treatment of this discontinuity is discussed below.)

From the phase rule and the compositional path taken in the measurements, one can show that theoretically the system enthalpy (or volume) must be a linear function of composition in the two-phase region (3.8). Hence, one can find the phase boundary (in this case, the composition of the aqueous phase) by fitting a linear regression to experimental points of the two-phase region, and estimating the composition at which the difference between the measurement and the regression exceeds the instrumental noise. We used an iterative spread-sheet computer program that first provided five-point smoothing of the data. Then the program (1) regressed on five points known to be in the two-phase region; (2) checked for collinearity of the next datum; (3) substituted the latter datum for one of the five regression points (1), if collinearity were found; and (4) returned to step (1), continuing until the deviation from linearity was found. As a refinement of this procedure, one may fit a smoothing function to the single-phase enthalpies, and take the point of intersection of the linear and nonlinear smoothing functions as the phase boundary. Unlike the rigor of the linear function of the two-phase region, the choice of smoothing function for the single-phase region is necessarily model-dependent.

The single-phase enthalpies of Figures 2a and 2b are segments of one theoretical curve. Hence, to find the phase boundary with the aid of a smoothing-function fit to single-phase data, one may choose either to fit only the single-phase data of Figure 2b, or to include the data from Figure 2a, as well. Regardless of the choice made for the phase boundary computations, calculation of the enthalpy of formation of the aqueous phase with water as the reference state requires determination of the unknown constant (i.e., the size of the discontinuity) between the data of Figure 2a and the data of Figure 2b.

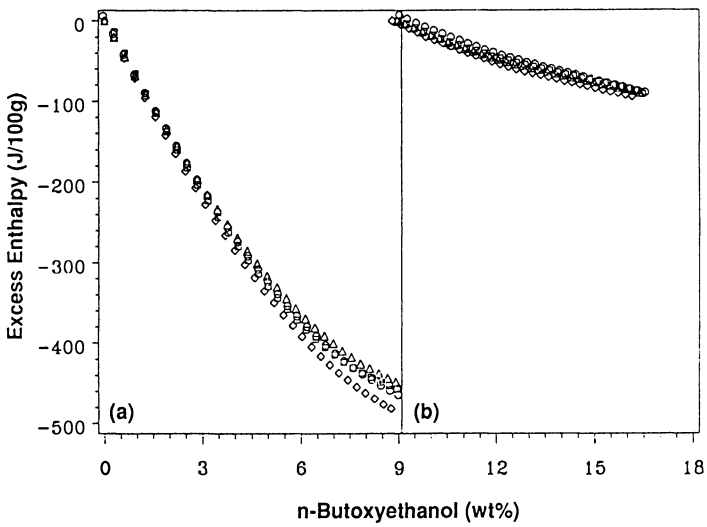


Figure 2. (a) Excess enthalpies of n-butoxyethanol/water at 55.0 °C from four replicate titrations, starting at neat water; (b) continuations of the titrations of (a).

One way to estimate the discontinuity is to simply average the final enthalpies of all of the runs of Figure 2a. However, such a procedure gives undue weight to just a few of the total number of data.

A second procedure is to fit a smoothing function to each group of replicate titrations of a given concentration range; the unknown constant then can be calculated from the different values of the two functions at the concentration that marks the end of the first group of titrations and the beginning of the second group of replicates.

Cubic equations have been used for several alcohol/water systems, and also for the 2-propanol/ CO_2 /water system (as well as for numerous CO_2 /hydrocarbon systems). (6.9,10) Furthermore, although a critical micelle concentration (CMC) has been reported for butoxyethanol and water, and we have calorimetrically measured the CMC of decane-saturated butoxyethanol micelles at 20 °C, there was no evidence of micelle formation at the higher temperatures of the present study (11,12; Smith, D. H., *et al.*, presented at the symposium "Use of Surfactants for Mobility Control in CO_2 and N_2 EOR, Ann Arbor, June 23-24, 1987). These facts suggest fitting simple cubic polynomials

$$\Delta H^E = \sum_{i=0,3} a_i X^i \quad (1)$$

to the measured excess enthalpies, ΔH^E , as a function of the wt% amphiphile, X, to calculate the values of the unknown "discontinuity" parameters a_0 . For heuristic reasons, both of these fitting procedures were tried.

Figure 3 shows the excess enthalpy vs. composition measured for aqueous solutions of n-butanol and water at 30.0 °C; Figure 4 shows corresponding results for the amphiphilic side of the miscibility gap at 55.0 °C. Each Figure shows titration data for compositions inside of the miscibility gap (where the "curve" is linear), as well as enthalpies in a single-phase region. Data from the literature are also shown for comparison with the present results (13-16). Table I shows values of the compositions of the aqueous and amphiphilic phases for n-butanol/water at 30.0 and 55.0 °C and for n-butoxyethanol/water at 55.0 and 65.0 °C. Shown for each composition are the value from calorimetry, as obtained in the present study; the value from phase volume measurements, also obtained in the present study; and a value

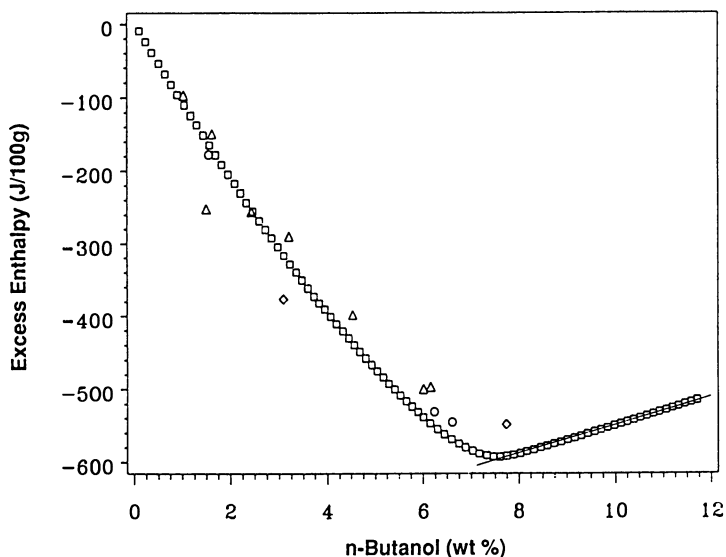


Figure 3. Excess enthalpies of aqueous solutions of n-butanol/ water at 30.0 °C, compared to results from the literature: squares, present results; triangles, ref. 13; circles, ref.14; diamonds, interpolated from ref. 16.

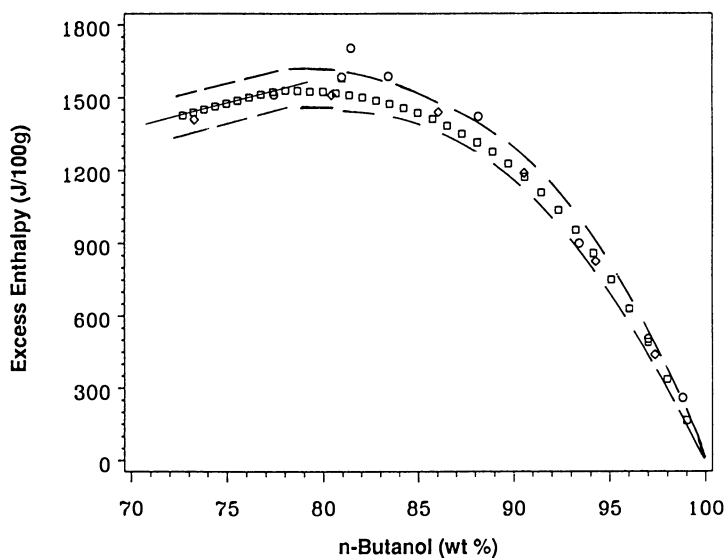


Figure 4. Measured excess enthalpies for the amphiphilic side of the n-butanol/water diagram at 55.0 °C compared to results from the literature.(14,16) (Symbols same as for Fig. 3.)

obtained from the literature. The latter were estimated from a graph of phase-volume measurements for n-butoxyethanol/water, and taken from a table of critically evaluated results for n-butanol/water (4,5). Confidence intervals are also shown.

Table I. Two-Phase Compositions

T (°C)	Aqueous			Amphiphilic		
	Calorimeter	Phase Volume	Liter.	Calorimeter	Phase Volume	Liter.
<i>n-Butanol (wt %)</i>						
30	8.35±.29	6.79±.21	7.05 ^a	78.07±.25	78.88±.13	79.37 ^a
55	5.98±.80	5.75±.25	6.39 ^a	75.79±.79	79.75±.25	76.8 ^a
<i>n-Butoxyethanol (wt %)</i>						
55	13.0±1.3	12.58±.02	13.45 ^b	49.35±.45	50.79±.02	49.4 ^b
65	10.5±.5	10.28±.02	11.08 ^b	56.68±2.0	58.28±.02	57.37 ^b

a - Ref. 4.
b - Ref. 5.

Table II shows the "heats of formation" of the conjugate phases, that is, the excess enthalpies for mixing the appropriate amounts of water and amphiphile (at the same initial temperature and pressure as the final system) to make a unit amount of the conjugate phase. Values labeled "calorimeter" and "phase volume," respectively, are based on the same set of calorimetric titrations. In the former case the phase composition was taken from the calorimetric measurements, and in the latter case the composition was taken from our phase-volume compositions. Literature values for the heats of formation are based on data from references 13-16.

Discussion

Examination of Table I shows that the compositions that we obtained by calorimetry were an average of 0.4 wt% amphiphile lower than the values

Table II. Excess Enthalpies

T (°C)		Aqueous (J/100g)	Amphiphilic (J/100g)
<u><i>n-Butanol:</i></u>			
30	Calorimeter	-573.±13.1	921.6±10.6
	Phase Volume	-582.5 ±11.0	937.3±4.5
	Literature	-546.7±6.9 ^a	736.7±42.4
55	Calorimeter	9.0±.95	1492.5±32.7
	Phase Volume	4.8±.64	1523.0±3.0
	Literature	43.0±67.5 ^a	1524.9±36.4 ^a
<u><i>n-Butoxyethanol:</i></u>			
55	Calorimeter	-518.8±36.8	-705.2±26.4
	Phase Volume	-514.6±36.5	-679.7±26.3
65	Calorimeter	-224.8±24.5	-525.6±29.3
	Phase Volume	-222.3±24.9	-501.2±29.8

a - Ref. 14.

in the literature, whereas the compositions that we obtained from phase volumes were an average of 0.1 wt% amphiphile lower than the literature values. The standard deviations (for the differences between the measurements of this paper and those in the literature) were essentially identical for the calorimetric and phase-volume techniques (0.35 wt%).

Figure 3 shows thirteen previously reported points for the heats of mixing of aqueous solutions of n-butanol and water at 30.0 °C (13,14,16). (Some of these data are obscured by overlap with our results.) The agreement with the previous data appears excellent, although around 7 wt% butanol our enthalpies are somewhat more negative than previously reported values.

In Figure 4 the results from the three different groups are in excellent agreement for butanol concentrations of 90 wt% and greater, although the data from the Russian group scatter somewhat more around our results than do the values interpolated from Westmeier's data.(14,16). At lower amphiphile concentrations the isoperibolic calorimeter measurements are in noticeably better agreement with the data of ref. 16 than with the Russian work (14-16). However, almost all results fall within the 95% confidence interval (dashed lines) for our results.

Although heat capacities have been reported for the butoxyethanol/water system, excess enthalpies that could be compared directly with our results apparently have not been measured (12).

Isoperibol titration calorimetry provides a convenient and rapid way to measure conjugate phase compositions for amphiphile/water systems that have miscibility gaps. When a simple desktop computer is used to control the calorimeter and to record the data, a typical titration takes about one hour to complete, covers a composition range of about 10 wt%, and provides a compositional resolution of 0.03 wt%. (Resolution was limited by the 640K contiguous RAM of our MS-DOS computer; higher resolution would be possible with use of a more sophisticated computer system.) Moreover, the treatment of the data, including determination of the phase compositions, is reduced to simple, documented algorithms, instead of to undocumented judgements that may not be reproducible from one operator to another.

Often the experimentalist will have an approximate idea of the location of a phase boundary from data taken at other temperatures or from measurements on closely related compounds. In such cases, a reasonably accurate guess about the location of the phase boundary may allow one to choose a starting composition that crosses the boundary with only a single titration. This can be considerably more efficient than starting with a neat compound and performing titrations over successive compositional ranges until the phase boundary is found.

However, the titrations must begin with the neat compound, if one desires to measure excess enthalpies referred to a single-compound standard state. In this case the number of experiments and the data

reduction effort are necessarily greater than when it is sufficient to measure only the phase boundary. Much of the extra effort is inherent in titration methods:

The initial and final compositions of a titration experiment are given by

$$X_1^s = W_1^s / (W_1^s + w_2^s) \quad (2a)$$

$$X_1^f = (W_1^s + \delta W_1) / (W_1^s + w_2^s + \delta W_1 + \delta W_2) \quad (2b)$$

where the subscripts refer to the compounds, superscripts *s* and *f* denote starting and final weight fractions (*X*), and δW_i is the weight of component *i* added in the titration. As shown by Equations 2, a titration can cover only a limited range of composition, and the range becomes more limited as X_1^s approaches the value 0.5. Thus the smaller the mutual solubilities of the two components, the greater is the convenience of titration calorimetry for measuring excess enthalpies referenced to neat-compound reference states. One alternative to multi-step titrations is to use flow calorimetry instead. (6).

Sometimes another possibility, which has several advantages of its own, is to use a critical point as the standard state. For example, the lower consolute point is a convenient standard state for the butoxyethanol/ water system, whose lower consolute solution temperature is at about 49 °C. (See Figure 1.) The compositions of the conjugate phase pairs are found at several temperatures from titrations that need only cross the phase boundary. Equations from critical scaling theory, which contain the critical-point composition and/or temperature, are then fit to the compositions. These fits give the critical point, which can also serve as the standard state for the enthalpy data. (Smith, Duane H.; Dunn, R. O. "Excess Enthalpies of Formation of Triconjugate Phases of a Microemulsion System," 43rd Annual Calorimetry Conference, Bartlesville, OK, August 15-19, 1988)

Nonionic and ionic surfactants that contain "ethoxy" (-OC₂H₄-) and "propoxy" (-OC₃H₆-) groups are excellent (i.e., apparently the best available) materials for miscible-flood mobility control and for ultra-low tension flooding. (1, 18-20). However, both ionic and nonionic alkoxylated surfactants commonly exhibit miscibility gaps in water and oilfield brines (18,20-22). (A temperature on the lower part of a

miscibility gap defined by a chosen composition of surfactant, water, and electrolyte is commonly referred to as "the cloud point" of that composition.) To avoid problems of surface handling, injection, and undesired mixing and compositional paths in the formation, it is usually deemed desirable that the miscibility gap of an EOR surfactant/water system be at a sufficiently high temperature that the gap is not encountered in oilfield use. Moreover, important physical properties, such as surfactant adsorption, have been shown to correlate with the distance of the system from the miscibility gap, even when the system remains in the single-phase region (18). Hence amphiphile/water miscibility gaps of the type studied in this paper are of considerable importance in all surfactant-based EOR processes, and the results of this paper show that calorimetry is a useful technique for studying these miscibility gaps. Two further advantages of calorimetric methods are that they require neither that samples transmit light, nor that dispersions cream and break. Since crude oils commonly form stable emulsions and opaque fluids, both of these advantages are of considerable potential value in requisite thermodynamic studies of enhanced oil recovery systems.

Conclusion

Isoperibolic calorimetry measurements on the n-butanol/water and n-butoxyethanol/water systems have demonstrated the accuracy and convenience of this technique for measuring consolute phase compositions in amphiphile/water systems. Additional advantages of calorimetry over conventional phase diagram methods are that (1) calorimetry yields other useful thermodynamic parameters, such as excess enthalpies; (2) calorimetry can be used for dark and opaque samples; and (3) calorimetry does not depend on the bulk separation of conjugate fluids. Together, the present study and studies in the literature encompass all of the classes of compounds of the amphiphile/CO₂/hydrocarbon/water systems that are encountered in dispersion-based mobility control for miscible-CO₂ enhanced oil recovery and in ultra-low tension flooding (1,2,6).

Literature Cited

1. Smith, Duane. H. In Proc. Fifth SPE/DOE Symp. Enhanced Oil Recovery, SPE/DOE 14914, 1986; vol. 1, pp. 441-56.

2. Surfactant-Based Mobility Control: Progress in Miscible-Flood Enhanced Oil Recovery; Smith, Duane H., Ed.; ACS Symposium Series No. 373; American Chemical Society: Washington, D.C., 1988.
3. Smith, Duane H.; Allred, G. C. J. Colloid Interface Science 1988, **124**, 199-208.
4. Alcohols with Water; Barton, A. F. M., Ed.; Pergamon Press: New York, 1984; pp. 32-91.
5. Kahlweit, M.; Strey, R.; Firman, P.; Haase, D. Langmuir 1985, **1**, 281-8.
6. Cordray, D. R.; Christensen, J. J.; Izatt, R. M. Separation Science Technol. 1987, **22**, 1169-81.
7. (a) Eatough, D. J.; Christensen, J. J.; Izatt, R. M. Thermochim. Acta 1972, **3**, 219-232. (b) Christensen, J. J.; Izatt, R. M.; Hansen, L. D.; Partridge, J. A. J. Phys. Chem. 1966, **70**, 2003-2010.
8. Smith, Duane H.; Lane, B. J. J. Dispersion Sci. Technol. 1987, **8**, 217-47.
9. Davis, M. I. Thermochim. Acta 1985, **90**, 313-29.
10. DiAndreth, J. R.; Paulaitis, M. E. In Surfactant-Based Mobility Control: Progress in Miscible-Flood Enhanced Oil Recovery; Smith, Duane H., Ed.; ACS Symposium Series No. 373; American Chemical Society: Washington, D.C., 1988; ch. 4.
11. Mukerjee, P.; Mysels, K. J. Critical Micelle Concentrations of Aqueous Surfactant Systems, U. S. Department of Commerce, NSRDS-NBS **36**, 1971.
12. Roux, G.; Perron, G.; Desnoyers, J.E. J. Solution Chem. 1978, **7**, 639-54.
13. Goodwin, S. R.; Newsham, D. M. T. J. Chem. Thermodyn. 1971, **3**, 325-34; tabulated in ref. 17.
14. Belousov, V. P.; Ponner, V. Vestn. Leningr. Univ., Fiz., Khim. 1970, **10**, 111-15; tabulated in ref. 17.
15. Belousov, V. P.; Panov, M. Yu. Vestn. Leningr. Univ., Fiz., Khim. 1976, **2**, 149-50; tabulated in ref. 17.
16. Westmeier, S. Chemische Techn. 1978, **30**, 354-7.
17. Handbook of Heats of Mixing, Christensen, J. J.; Hanks, R.W.; Izatt, R.M., Eds.; John Wiley and Sons: New York, 1982.
18. Lewis, S. J.; Verkruyse, L. A.; Salter, S. J. In Proc. Fifth SPE/DOE Symp. Enhanced Oil Recovery, SPE/DOE 14910, 1986; vol. I, pp. 389-98.

19. Borchardt, J. K.; Bright, D. B.; Dickson, M. K.; Wellington, S. L. In Surfactant-Based Mobility Control: Progress in Miscible-Flood Enhanced Oil Recovery; Smith, Duane H., Ed.; ACS Symposium Series No. 373; American Chemical Society: Washington, D.C., 1988; ch. 8.
20. Borchardt, J. K. In Surfactant-Based Mobility Control: Progress in Miscible-Flood Enhanced Oil Recovery; Smith, Duane H., Ed.; ACS Symposium Series No. 373; American Chemical Society: Washington, D.C., 1988; ch. 9.
21. Smith, Duane H. J. Colloid Interface Sci. 1985, **108**, 471-83.
22. Smith, Duane H.; Fleming, P. D. III J. Colloid Interface Sci. 1985, **105**, 80-93.

RECEIVED November 28, 1988

Chapter 16

Structure-Performance Characteristics of Surfactants in Contact with Alkanes, Alkyl Benzenes, and Stock Tank Oils

Thomas A. Lawless and John R. Lee-Snape

Winfrith Petroleum Technology Centre, Winfrith AEE, Dorchester, Dorset,
England

The assessment of surfactant structures and optimal mixtures for potential use in tertiary flooding strategies in North Sea fields has been examined from fundamental investigations using pure oils. The present study furthermore addresses the physico-chemical problems associated with reservoir oils and how the phase performance of these systems may be correlated with model oils, including the use of toluene and cyclohexane in stock tank oils to produce synthetic live reservoir crudes. Any dependence of surfactant molecular structure on the observed phase properties of proposed oils of equivalent alkane carbon number (EACN) would render simulated live oils as unrepresentative. Both commercial grade and pure nonionic and anionic surfactants have been evaluated by phase inversion and optimal salinity screening procedures to establish relationships to their molecular structures.

The optimal structure of surfactants for practical and efficient EOR flooding strategies in North Sea oil reservoirs remains largely unresolved. Previous research studies (1-4) have attempted to assess surfactant performance potential using pure synthesised materials. These have been successful in focussing on molecular structural benefits and indentifying some shortcomings associated with differing functional moieties. The present study attempts to probe the relationship between structure and performance of 8 surfactants; 7 of which are commercial in origin.

Cosurfactants have not been employed in the present study. However, surfactants from commercial sources will contain isomers and manufacturing impurities. Nevertheless, a major aim of this study has been to address the performance characteristics of commercial formulations. Wherever appropriate, hydrophobic

structural assemblies were selected that were available in both anionic and nonionic form. Variations in the ethoxylate chain length, the degree of anionic substitution, inorganic salt content and unreacted products will all affect performance behaviour, and therefore demand careful attention. A methodical assessment of all surfactant formulations has been undertaken using the technique of conductivity to determine the temperature or salinity required for phase inversion to occur. Of direct interest is the EACN concept (5) and how pure oils may be related to reservoir crudes. Furthermore the ability of certain aromatics and cyclics to act as separator gas equivalents is also addressed. The influence of ethoxylate inclusion to the surfactant hydrophile and the observed concomitant equivalences, for toluene and cyclohexane have been investigated to follow the applicability of such concepts. These optimal correlations and their inherent sensitivities aid the interpretation of formulation potential for field injection.

Experimental : Materials and Methods

Oils The n-alkane series C₆-C₁₄, toluene and cyclohexane were purchased from BDH, Poole, UK, each with a stated purity of 99%; reagents were used as received. Crude oil samples were obtained from two North Sea fields; one located in the Norwegian sector and the other from the UK sector. Stock tank oil from the Gullfaks field was supplied by Statoil, Norway and the other stock tank oil from an undisclosed source. Both crude oils are derived from sandstone formations with reservoir temperatures of 70° and 101°C respectively.

Brines Analytical grade sodium chloride, purity 99.9% was obtained from BDH and used throughout the study. Water was purified by reverse osmosis, and deionised in a Milli-Q-Reagent system immediately prior to use.

Surfactants Information on the pure and commercial grade surfactants studied with regard to structures, contaminations and activities is detailed in Table I. All surfactants were used as received.

Cloud Point Measurements Cloud points were recorded by the visual observation of aqueous solutions containing 1% W/V surfactant. The measurement defines the temperature at which the system under test shows a characteristic transitional change from a clear solution to an opalescent or cloudy state. All cloud points were recorded in both ascending and descending temperature cycles to ensure data confidence. The influence of salt and/or oils on the cloud point were systematically evaluated.

Phase Inversion The phase inversion of brine/oil/surfactant systems was established routinely by measuring solution conductivity employing a Jenway FWA 1 meter and cell. The process identifies the range over which a large decrease in conductivity occurs as the system under test is converted from an oil in water emulsion to a water in oil emulsion. Phase

TABLE I SURFACTANT SAMPLES UNDER OBSERVATION

TRADE NAME	SUPPLIER	CHEMICAL FORMULA OF MAJOR SYNTHESISED PRODUCT	% SURFACTANT ACTIVITY	NATURE OF SURFACTANT COMPOSITION		INORGANIC SALT CONTENT/%	WATER CONTENT/%
				ANIONIC %	NONIONIC %		
T100	HOECHST W GERMANY	Bu ₃ Ph.(EO) ₁₀ OH	100	-	100	-	-
A7	ICI ENGLAND	C ₁₃₋₁₅ H ₂₇₋₃₁ (EO) ₇ OH	100	-	100	-	-
NP6	ICI ENGLAND	C ₉ H ₁₇ Ph.(EO) ₆ OH	100	-	100	-	-
POE10	SIGMA ENGLAND	CH ₃ (CH ₂) ₇ CH=CH(CH ₂) ₈ (EO) ₁₀ OH	100	-	100	-	-
D3620	HOECHST W GERMANY	Bu ₃ Ph.(EO) ₄ SO ₃ Na	35	~ 26	~ 9	5	60
A3C	ICI ENGLAND	C ₁₃₋₁₅ H ₂₇₋₃₁ (EO) ₃ OCH ₂ CO ₂ Na	85	~ 60	~ 25	7	8
LEONOX I.O.S. (MOL WT = 375)	MITSUBISHI JAPAN	CH ₃ (CH ₂) _m CH=CH(CH ₂) _n SO ₃ Na	35	~ 35	-	4	*53
DIOCTYL SULPHOSUCCINATE	SIGMA ENGLAND	(CH ₃ (CH ₂) ₃ CH(C ₂ H ₅)(CH ₂) ₂ C ₂ O ₄ C ₁₆ H ₃₃ SO ₃ Na	100	~ 100	-	-	-

* 8% unsulphonated oil reported present in this formulation

inversion temperatures were measured in well stirred systems undergoing a temperature change of typically 1 K min^{-1} . Cooling profiles were also recorded and only when the conductivity measurements in the heating and cooling cycles matched were the data recorded. Salinity loadings necessary for phase inversion at a specific temperature were also evaluated. Because of potentially undesirable effects such as gel formation, test temperatures of 40° or 60° C were selected for these experiments. Aqueous solutions containing either 150 or 300 g dm^{-3} NaCl were prepared and used as titrants to promote phase inversion in oil/water/surfactant systems. Care was taken to maintain the water to oil ratio as close to 1 as possible. The surfactant loadings necessary to produce such phase inversions were related to anticipated requirements for all pure oils and stock tank oils. For the purpose of standardisation most tests were performed on systems containing 5% W/V surfactant.

RESULTS

NONIONIC SURFACTANTS

Cloud Points The influence of added NaCl on the observed cloud points of 1% W/V solutions of the four nonionic surfactants under observation are given in Figure 1. Approximately linear correlations were observed as the aqueous NaCl level was increased, with negative coefficients recorded between $0.22 - 0.3 \text{ K.g}^{-1}\text{dm}^3$. Higher loadings of surfactant were found to increase the cloud point. It was observed also that the inclusion of small quantities of oils to surfactant solutions could either elevate or depress the cloud point. The significance of this fact will be developed later.

Phase Inversion Temperatures It was possible to determine the Phase Inversion Temperature (PIT) for the system under study by reference to the conductivity/temperature profile obtained (Figure 2). Rapid declines were indicative of phase preference changes and mid-points were conveniently identified as the inversion point. The alkane series tended to yield PIT values within several degrees of each other but the estimation of the PIT for toluene occasionally proved difficult. Mole fraction mixing rules were employed to assist in the prediction of such PIT values. Toluene/decane blends were evaluated routinely for convenience, as shown in Figure 3. The construction of PIT/EACN profiles has yielded linear relationships, as did the mole fraction oil blends (Figures 4 and 5). The compilation and assessment of all experimental data enabled the significant parameters, attributable to such surfactant formulations, to be tabulated as in Table II.

The PIT dependence profiles generated for the nonionic surfactants in contact with alkanes are given in Figure 6. Their linear correlations allow suitable coefficients to be extracted from these data which may be used in later, derivable inter-relationships. It was observed that variations in the water to oil ratio (WOR) affected the recorded PIT (Figure 7). The

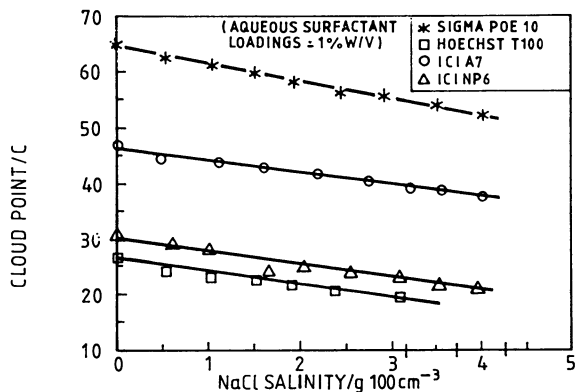


Figure 1. Cloud point variation for different salinities (Aqueous surfactant loadings = 10 g/dm³)

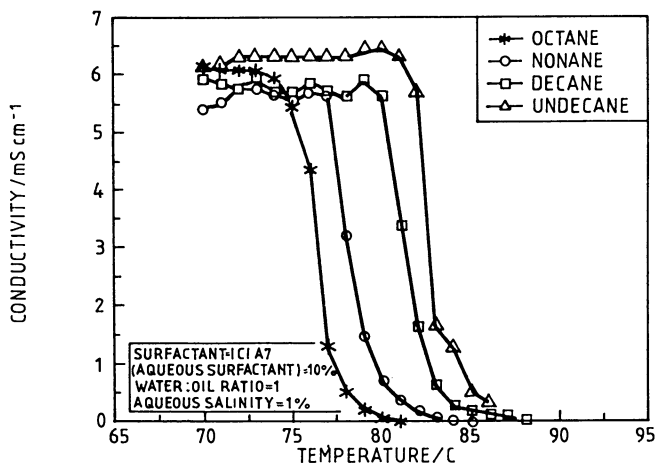


Figure 2. Conductivity/temperature profiles for the alkanes

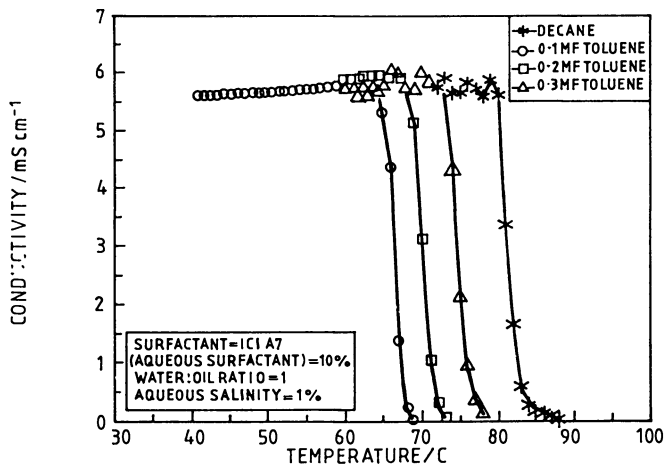


Figure 3. Conductivity/temperature profiles for toluene/decane blends

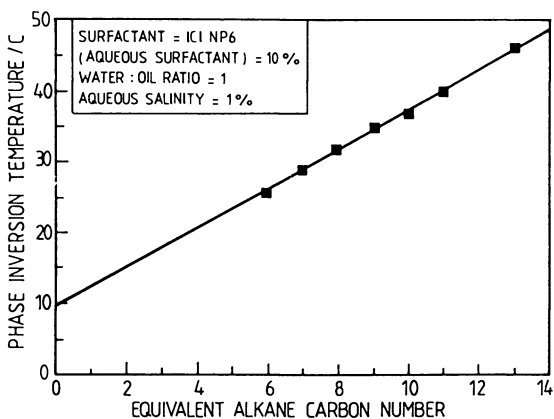


Figure 4. Phase inversion temperature variation for the alkanes

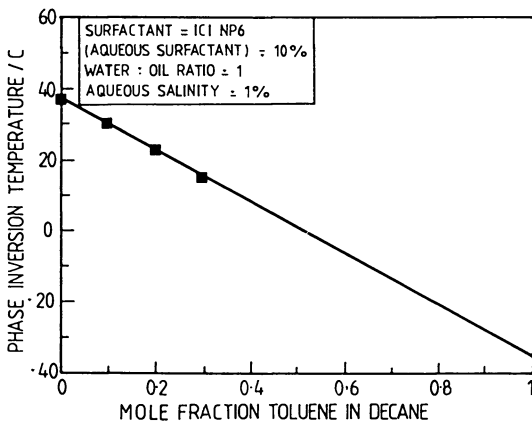


Figure 5. Phase inversion temperature variation for toluene/decane blends

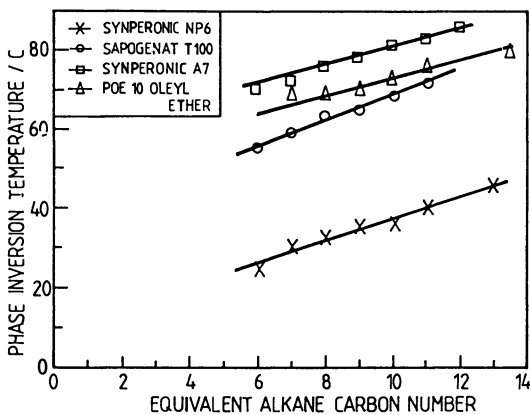


Figure 6. Variation of phase inversion temperature with equivalent alkane carbon number

TABLE II SUMMARY OF PHASE INVERSION TEMPERATURE DATA AND APPROPRIATE DERIVED EQUIVALENTS

SURFACTANT	AQUEOUS PHASE SALINITY /g dm ⁻³	$\frac{d \text{ PIT}}{d \text{ EACH}}$ /K(Unit ACN) ⁻¹	PIT AT EACH=0 /°C	OIL PIT/°C (MEASURED OR EXTRAPOLATED)				OIL EACH FROM PIT			
				TOLUENE	CYCLO- HEXANE	GULLFAKS CRUDE	NINIAN CRUDE	TOLUENE	CYCLO- HEXANE	GULLFAKS CRUDE	NINIAN CRUDE
ICI NP6	10	2.7	10	- 35	-	23	20	- 16	-	4.8	3.7
ICI A7	10	2.2	59	32	-	74	74	- 12	-	6.8	6.8
HOECHST T100	10	3.4	35	9	-	61.5	60.5	- 7.6	-	7.8	7.5
SIGMA POE 10 OLEYL ETHER	50	2.3	50	14	-	65	65	- 16	-	6.5	6.5
ICI A3C	200	5.2	18	- 23	24	*62	*62	- 7.9	1.2	< 8.5	< 8.5

(water to oil ratios were always 1 and the total surfactant loading per system was 5% W/V for all tests except for the ICI A3C system where 2.5% W/V was employed)

* Denotes values recorded on blends composed of 25% by volume crude oil plus 75% by volume decane

recorded PIT values were observed to increase as the WOR declined. No mole fraction blending was available for stock tank oils and percentage volume mixes were adopted for test purposes (Figure 8). All nonionic formulations were capable of phase inverting the two crude oil samples in their native state which permitted a direct EACN value to be assigned to the oils from previously derived standard PIT data shown in Table II. Both reservoir crude oil samples showed somewhat variable EACN values, within the range of 3.7 to 7.8.

Optimal Salinities Because the EACN values ascribed to oil systems are usually derived from salinity scanning, it was considered appropriate to evaluate the salinity tolerance of ICI NP6, and to determine the EACN value for toluene so that a comparison could be made between the two experimental techniques employed in this study. Inspection of Table III reveals an EACN value for toluene of -10.3 which can be compared to the value of -16 determined from PIT data. Such large negative values indicate the importance of the hydrophilic group in determining alkane equivalences and it was desirable to probe how ionic groupings, which also contain oxyethylene linkages as integral parts of their hydrophilic segment, would confer EACN values on toluene and indeed on stock tank oils.

ANIONIC SURFACTANTS

Phase Inversion Temperatures Because of the high solubility and salt tolerance of carboxymethylates it was considered more appropriate to establish PIT values for the alkane series rather than determine extremely high optimal salinities. The estimation of such data permitted the role of temperature to be assessed on an ionic formulation containing oxyethylene groupings. Temperature tolerance was much improved over the native nonionic surfactant hydrophiles (see Figure 9 and Table II) although difficulties were experienced in establishing a PIT value for both stock tank oils. Experimentally, only phase mixtures containing 25% by volume of crude oil in contact with 75% decane were capable of inverting before difficulties arose. Toluene was again determined to have a value less than zero (Figure 10).

Optimal Salinities Phase inversions at optimal salinity were assessed routinely by salt titrations into systems maintained at constant temperature. For the Leonox IOS surfactant system, increasing levels of salinity were necessary to cause the emulsion state to phase invert as the alkane molecular weight increased (Figure 11). The initial conductivity value at the condition where zero salt had been added may in part reflect the salt contamination naturally present within the supplied formulation. The internal olefin sulphonate species again revealed a linear relationship between EACN and optimal salinity as did all ionic formulations under test (see Figures 12 and 13, plus Table III). The estimation of EACN values for both toluene

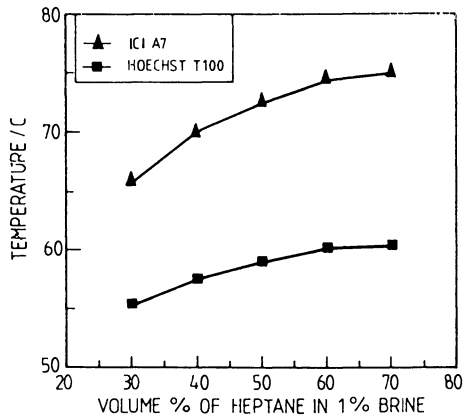


Figure 7. Influence of oil and water volume ratio on the observed PIT

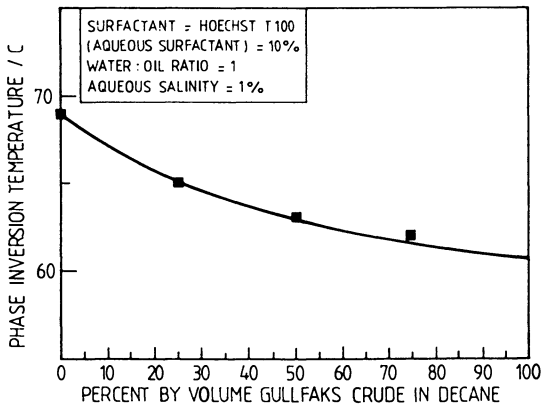


Figure 8. Phase inversion temperature variation for decane/Gullfaks crude blends

TABLE III SUMMARY OF OPTIMAL SALINITY DATA AND APPROPRIATE DERIVED EQUIVALENTS

SURFACTANT	TEST TEMPERATURE /°C	d S* / d EACN /g dm ⁻³ (Unit ACN) ⁻¹	S* AT EACH-O /g dm ⁻³	S* VALUE FOR OILS/g dm ⁻³ (MEASURED OR EXTRAPOLATED)				OIL EACH FROM S*			
				TOLUENE	CYCLO-HEXANE	GULLFAKS CRUDE	NINIAN CRUDE	TOLUENE	CYCLO-HEXANE	GULLFAKS CRUDE	NINIAN CRUDE
LENOX IOS	60	6.1	- 1	- 2	11	*55	*58	- 0.2	2.0	< 9.2	< 9.7
ICI NP6	40	17.8	- 142	- 325	- 153	-	-	- 10.3	- 0.6	-	-
HODCHIST D3620	60	8.0	- 32	- 35	- 9	-	-	- 0.4	2.9	-	-
SIGMA DIOCTYL SULPHOSUCCINATE	40	0.68	0	- 5.2	1.7	**3.5	**3.5	- 7.6	2.5	< 5.2	< 5.2

(Water to oil ratios were all initially 1 prior to titration, and the initial surfactant loading per system was 5% W/V. Salinity values relate exclusively to aqueous phase NaCl solutions).

* Denotes values recorded on blends composed of 25% by volume crude oil plus 75% by volume decane

** Denotes values recorded on blends composed of 50% by volume crude oil plus 50% by volume decane

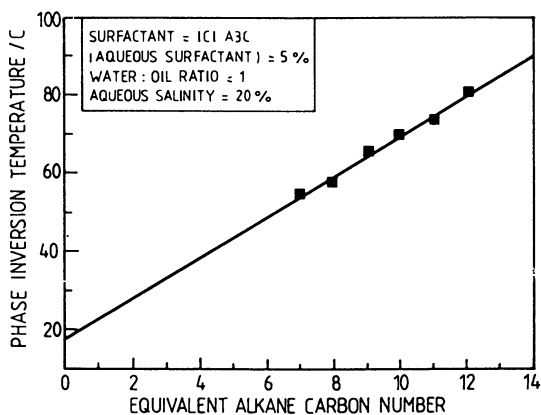


Figure 9. Phase inversion temperature variation for the alkanes

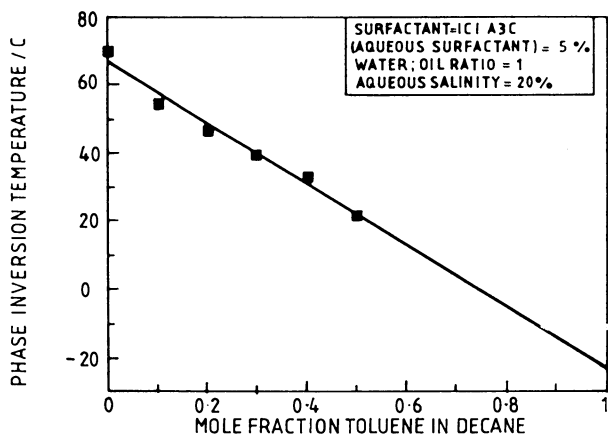


Figure 10. Phase inversion temperature variation for decane/toluene blends

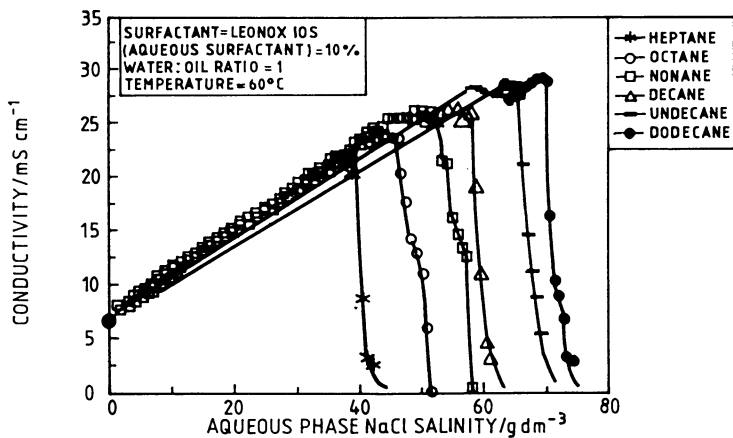


Figure 11. Conductivity titration profiles for the alkanes

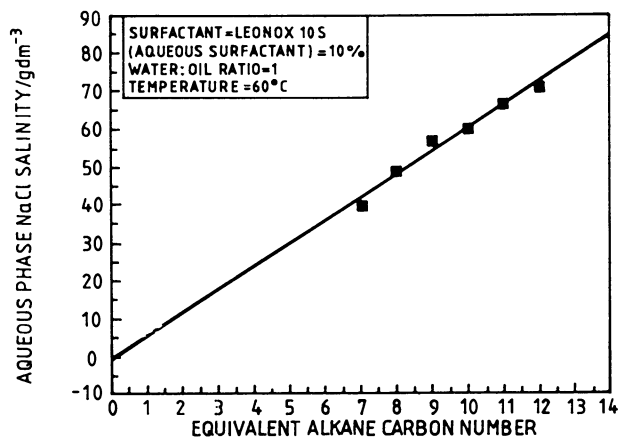


Figure 12. Optimal salinity variation for the alkanes

and cyclohexane (see Figures 14 and 15) was undertaken with all ionics under test. Sulphonate types gave values not too far removed from those proposed by Wade et al (6) whilst other hydrophilic head group surfactants conferred other equivalences. Difficulties were again observed in the production of phase inversion with stock tank oils.

DISCUSSION

Nonionics The selection of nonionic surfactant candidates for test purposes was influenced by a number of requirements which included (a) commercial availability, (b) structural variety, (c) availability of anionic derivatives, and (d) some degree of conformance to the desirable structural requirements proposed by Graciaa et al (7).

Surfactant blends of interest will exhibit clouding phenomena in aqueous solutions undergoing a phase transition from a one phase system to a two phase system at a discrete and characteristic temperature, referred to as the Cloud Point (CP). This value indicates the temperature at which sufficient dehydration of the oxyethylene portion of the surfactant molecule has occurred and this results in its "displacement" from solution. The addition of lyotropic salts will depress the CP, presumably due to the promotion of localised ordering of water molecules near the hydrophilic sheath of the surfactant molecule (8). Furthermore, the addition of different oils to surfactant solutions can induce either an elevation or a depression of the recorded CP and can be used to qualitatively predict the PIT (8,9).

The ability of various oils to be solubilised within micellar interiors or within the palisade layer will undoubtedly influence the conditions for favourable phase behaviour. Any solubilisation that interferes with oxyethylene hydration may cause substantial reductions in the CP. Thus the combined effect of temperature, oil and salinity can control the performance potential of nonionics. It is believed that the alkane series under study in the present work were solubilised into the main interior of the micellar core, but the inclusion of toluene could involve some degree of penetration into the palisade layer. Mole fraction mixing rules were adopted to facilitate the evaluation of the PIT value for toluene and cyclohexane (see Figures 3 and 5) which could then be ascribed EACN values derived from previous alkane/PIT data (Table II). The low negative value recorded for toluene could reflect surfactant hydration interference. Alternatively, deep and effective penetration of toluene into the micellar core could afford such efficient phase transitions by expansion of the average hydrophobe assembly. Reservoir crudes will obviously contain a multiplicity of components, all of which may have either the ability to promote or reduce oxyethylene hydration. The low molecular weight aromatics will induce stronger influences than those observed with their higher alkyl homologues. The PIT values determined for the two reservoir crudes under study yielded EACN values between 3.7-7.8 which may, in part, reflect an equivalent polarity range. No difficulties

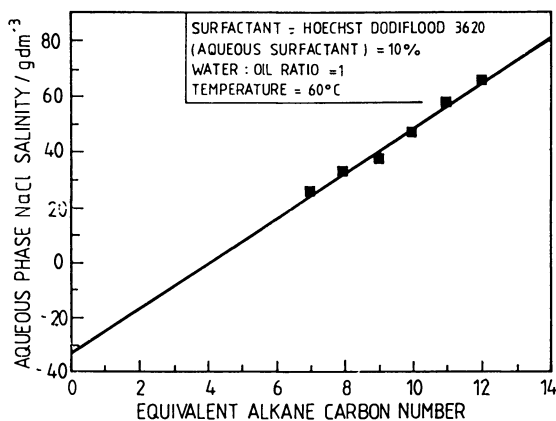


Figure 13. Optimal salinity variation for the alkanes

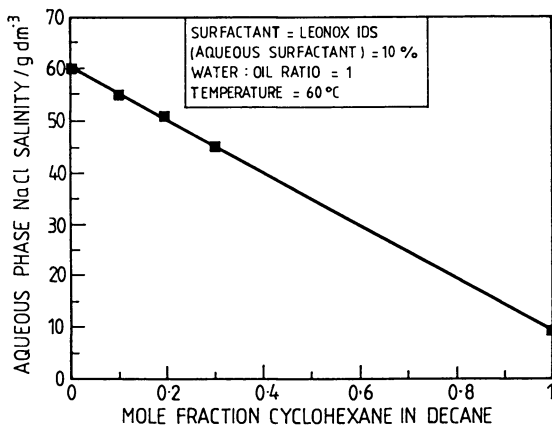


Figure 14. Optimal salinity variation for decane/cyclohexane blends

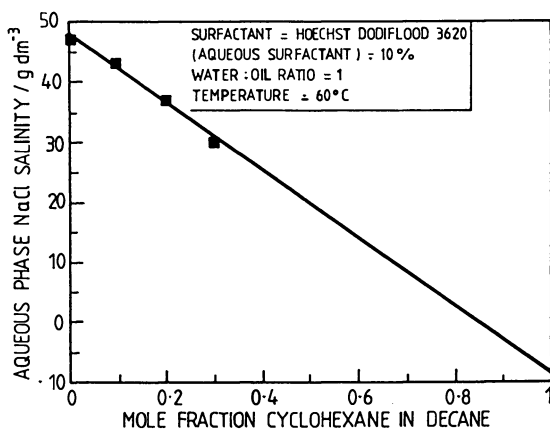


Figure 15. Optimal salinity variation for decane/cyclohexane blends

were experienced in attaining phase inversion conditions with reservoir crudes and adequate solubilisation parameters were available. Variations in the water to oil ratio were shown to affect the recorded PIT (Figure 7). Increased loadings of oleic phase produced increased PIT values over the accessible range of study. Shinoda and Arai (8,10) had previously observed that little variation could be expected for alkanes but that pronounced effects were dominant with aromatics.

Salinity Effects in the Inversion Process It has been shown for anionics that the Salager (11) equation could relate salt and alcohol effects to phase behaviour according to:-

$$\ln S^* = k (\text{ACN}) + f (A) + \dots \quad (1)$$

where S^* = aqueous phase optimal salinity
 k = a constant related to the nature of the hydrophilic group (for sulphonates $k = 0.16$)

and $f (A)$ = function of alcohol type and concentration

In the absence of alcohol the salinity/alkane sensitivity will be dominated by the nature of the surfactant hydrophile. A linear response was observed between optimal salinity and alkane chain length for the ICI NP6 surfactant with a recorded coefficient of $ds^*/d \text{EACN} = 17.8 \text{gdm}^{-3}/\text{unit EACN}$. This high salt tolerance was expected for nonionics and can reflect an equivalence between the ability of both salt and temperature to effect a phase inversion change per unit EACN, via cloud point adjustment. As expected, toluene displayed a remarkable effect on the extrapolated optimal salinity level necessary for phase inversion. The disruption of oxyethylene hydration being far more dominant than any effects derived from limited salt addition. The $[\text{EACN}]_S^*$ value of -10.3 is at variance to that calculated earlier from PIT data and may reflect a non-linear correlation between salt and temperature influences, particularly over the theoretical range necessary here. Cyclohexane was also assessed (see Table III) and ascribed an $[\text{EACN}]_S^*$ value of -0.6. On the basis of these results, the inclusion of such oils as replacements for separator gas components would be inappropriate for pure nonionic systems.

Of interest here is the question relating to the value for the slope coefficient, k , from equation (1), when surfactant structures incorporating both ionic (say sulphonate) and nonionic moieties are included together. The changes in electric double layer effects imparted from salt addition might dominate the packing constraints and therefore the phase inversion process, or perhaps oxyethylene dehydration effects from the presence of toluene could also play a role.

ANIONICS

Phase Inversion Temperature The carboxymethylate surfactant sample available for test purposes exhibited excellent salinity tolerance, in fact too high for practical sea water flooding

requirements. Optimal salinity studies were impracticable but the role of the oxyethylene groups could be established by PIT scanning in the presence of 20% W/V NaCl (see Figures 9 and 10). The dual combination of hydrophilic groups permitted a better temperature tolerance than that usually found for native nonionics (Table II). It is to be expected that changes in salinity loadings will strongly affect charged headgroups while temperature variations will alter oxyethylene hydration. The presence of added toluene was found to strongly reduce the PIT, yielding an $[EACN]_{PIT}$ value of -7.6 which approaches values recorded for nonionic surfactants. Such negative deviations are in general accord with other reported data for this generic class of surfactants (12). Cyclohexane showed an EACN of 1.2 which indicates a less dramatic influence for this saturated cyclic species. Thus oil polarity, oil molar volume and therefore its location within micellar structures will influence hydration, molecular assembly packing and, consequently, the PIT. Difficulties were experienced when stock tank oils were introduced, but this may be a consequence of reduced solubilisation parameter values normally found for reservoir crudes.

Optimal Salinities The phase inversion process may be considered to reflect the balanced nature of the adsorbed surfactant species at the oil/water interface. Simple geometric packing considerations can be used to define the relative areas occupied by hydrophilic and hydrophobic groupings which thereby determine the direction of any preferred curvature. The ability to transform surfactant molecules from one preferred curvature state to another is a necessary requirement for the phase inversion process to occur. Variations in aqueous salinity and temperature, plus the inclusion of various oleic and cosolvent phases, can all induce effective changes in either the hydrophilic or hydrophobic segment and promote phase inversion (13).

Linear responses were evaluated experimentally in optimal salinity/EACN scanning for all ionics under study. Of practical interest is the natural presence of inorganic salts in the commercial grade anionic formulations. For example, concentrates containing 35% W/W surfactant and 5% W/W inorganic salt (along with other components) will yield a 7.1g dm^{-3} salt loading in a prepared 5% W/V surfactant solution. If the inorganic salt is sodium sulphate then the equivalent NaCl level will be 7.1g dm^{-3} simply in ionic strength terms. Thus variations in surfactant loading will naturally induce variable salinity levels and make grid point phase diagrams difficult to unravel. If the inherent salt levels were calculated and some appropriate adjustment invoked to equate sodium sulphate to NaCl, then an approximately parallel plot (of optimal salinity against EACN) to the one recorded here, would be observed. The data recorded herein relates solely to optimal levels derived from added salts. Inspection of Figures 12-15 and Table III reveals sulphonate performance characteristics in contact with alkanes, toluene and cyclohexane. Both sulphonates exhibited some degree of salinity tolerance with the ethoxylated sulphonate being superior. The

inclusion of oxyethylene groups to sulphonate surfactants has been reported to reduce any co-solvent requirements and promote salinity tolerance; but as a consequence solubilisation parameters may be impaired (3). The EACN values determined for toluene (~0) and cyclohexane (between 2 and 3) are in general agreement with values proposed by Wade and co-workers (5). Since the presence or absence of oxyethylene groups appears to have little influence on $[EACN]_S^*$ for toluene and cyclohexane it must be concluded that the ionic sulphonate group dominates the phase evolution process during salt addition. Electric double layer effects may thus control preferred interfacial surfactant curvature, whilst the oil molar volume controls the extent of oil inclusion and micellar hydrophobe expansion. Thus, temperature changes mainly effect the oxyethylene portion of the surfactant. No estimates are available for stock tank oil EACN values, and this may be due to inadequate surfactant loading to facilitate complete solubilisation at the phase inversion condition. All the optimal salinity values recorded in this study were determined by salt titration experiments from an initial condition of WOR = 1. Typically the WOR had shifted to ~1.2 before inversion was recorded; titrations necessitating WOR values 1.4 were never recorded. Dioctyl sulphosuccinate has been reported (14) to be sensitive to the relative volume of oil and water contacted and care was taken therefore to minimise such effects. This surfactant was relatively sensitive to salt loadings and served as the only pure sample under test. The extrapolated EACN values for toluene and cyclohexane were -7.6 and 2.5 respectively, which reveals the importance of the structural nature of surfactants.

CONCLUSIONS

The following conclusions based on the experimental work reported in this paper are :

- Favourable phase inversion conditions, as monitored by conductivity, were established for all surfactant blends in contact with alkanes.
- If favourable crude oil inversion conditions are observed it is possible to calculate alkane equivalences based on either optimal salinity or PIT data.
- Commercial sulphonate formulations behave in a manner qualitatively similar to that expected from pure components during optimal salinity evaluation.
- Optimal salinity values directly influence the nature of the ionic groups, while temperature variations (PIT tests) strongly effect the oxyethylene linkages.
- Inherent salt loadings in commercial grade anionic surfactants will influence observed phase evolution processes.

- The EACN values for toluene were found to vary depending upon the nature of the surfactant molecular structure, but sulphonate systems confirm an EACN equivalence of ~ 0 .

LITERATURE CITED

1. DOE P.H., WADE W.H., SCHECHTER R.S., J.Coll.Int.Sci., 1977, 59, 3, 525-31.
2. DOE P.H., EL-EMARY M., WADE W.H., SCHECHTER R.S., J.Am.Oil Chem.Soc., 1978, 55, 505-12.
3. CARMONA I., SCHECHTER R.S., WADE W.H., WEERASOORIYA U., SPE No 11771, 1985.
4. ABE M., SCHECHTER D., SCHECHTER R.S., WADE W.H., WEERASOORIYA U., YIV S., J.Coll.Int.Sci., 1986, 114, 2,342-56.
5. CAYIAS J.L., SCHECHTER R.S., WADE W.H., J.Coll.Int.Sci., 1977, 59, 1, 31-8.
6. CASH L., CAYIAS J.L., FOURNIER G., MACALLISTER D., SCHARRES T., SCHECHTER R.S., WADE W.H., J. Coll.Int.Sci. 1977, 59, 1, 39-44.
7. GRACIAA A., FORINEY L., SCHECHTER R.S., WADE W.H., YIV S., SPE/DOE NO.9815, 1981.
8. SHINODA K., ARAI H., J. PHYS.CHEM., 1964, 68, 12, 3485-90.
9. AVEYARD R., LAWLESS T.A., J.CHEM.SOC. Farad Trans I., 1986, 82, 2951-63.
10. SHINODA K., ARAI H., J.Coll.Int.Sci., 1967, 25, 429-31.
11. SALAGER J.L., MORGAN J.C., SCHECHTER R.S., WADE W.H., YIV S., J.Coll.Int.Sci., 1982, 89, 1, 217-25.
12. OLSEN D.K., JOSEPHSON C.B., Report for U.S. Department of Energy, July 1987.
13. AVEYARD R., Chem.Ind., 1987, 474-8.
14. AVEYARD R., BINKS B.P., CLARK S., MEAD J., J.Chem.Soc.Farad. Trans.I, 1986, 82, 125-142.

RECEIVED November 28, 1988

Chapter 17

Interfacial Tension of Heavy Oil–Aqueous Systems at Elevated Temperatures

E. Eddy Isaacs, J. Darol Maunder, and Li Jian¹

Alberta Research Council, Oil Sands and Hydrocarbon Recovery
Department, P.O. Box 8330, Postal Station F, Edmonton, Alberta T6H
5X2, Canada

Oil/water interfacial tensions were measured for a number of heavy crude oils at temperatures up to 200°C using the spinning drop technique. The influences of spinning rate, surfactant type and concentration, NaCl and CaCl₂ concentrations, and temperature were studied. The heavy oil type and pH (in the presence of surfactant) had little effect on interfacial tensions. Instead, interfacial tensions depended strongly on the surfactant type, temperature, and NaCl and CaCl₂ concentrations. Low interfacial tensions (<0.1 mN/m) were difficult to achieve at elevated temperatures.

At a given NaCl concentration, an increase in temperature resulted in an increase in interfacial tension. In contrast, for a narrow range of CaCl₂ concentrations, interfacial tensions decreased with increasing temperatures. Changes of the amphiphile at the oil/water interface accounted for some of the experimental observations. Since the extent of oil desaturation is dependent on interfacial tension, the tension data could be used to assess the ability of surfactants to reduce oil saturations in the reservoir for application of surfactants and foams to thermal recovery processes.

The use of surfactants to achieve low (<10⁻¹ mN/m) interfacial tensions between oil and water as a means of enhancing recovery from partially depleted conventional reservoirs is well recognized [1]. In steam injection processes

¹Current address: Research Institute of Petroleum Exploration and Development, P.O. Box 910, Beijing, Peoples Republic of China

for recovering heavy oil from underground deposits, surfactants are used mainly to stabilize the formation of a foam with steam or a non-condensable gas, which acts to divert the steam from depleted zones thereby improving reservoir conformance [2]. A major concern with foam processes is the detrimental effect of residual oil in the swept zone on both foam formation and propagation [3-6]. Reductions in residual saturations over and above that obtained by steam injection are desirable and, in many heavy oil reservoirs, essential to the application of steam-foam processes. However, the extent of heavy oil desaturation is dependent on the reduction in interfacial tension between oil and water [7-9]. Thus, foam-forming surfactants can improve their own cause by reducing interfacial tensions at steam temperatures. Interfacial tension data combined with an understanding of the factors responsible for the interfacial tension behavior at the oil/water interface is, therefore, pertinent to developing rational injection strategies for the application of surfactants and foams to heavy oil recovery.

The interfacial tension behavior of alkane-aqueous NaCl systems containing both pure and commercial surfactant mixtures has been extensively studied. Under narrow ranges of experimental conditions, very low (<0.01 mN/m) interfacial tensions are obtained. Puig et al. [10,11], Franses et al. [12] and Hall [13] have shown that very low tensions are not caused by monolayer adsorption but by a film of a surfactant-rich phase or liquid-crystalline layer at the oleic-water interface. A pictorial representation of some of the microstructures (interpreted from the work of Winsor [14]) that can form in the aqueous, oleic, and interfacial region are shown in Figure 1. Thus, the tension minima are a consequence of changes in microstructures as a function of surfactant concentration, salinity and temperature. However, Chan and Shah [15], Shinoda et al. [16] and, more recently, Aveyard et al. [17] have suggested that very low interfacial tension minima are not necessarily the consequence of a phase change but rather the distribution of surfactant between oil and water and the degree of dissociation of surfactant in the micelle and the oil-water interface.

The interfacial tension behavior between a crude oil (as opposed to pure hydrocarbon) and an aqueous surfactant phase as a function of temperature has not been extensively studied. Burkowsky and Marx [18] observed interfacial tension minima at temperatures between 50 and 80°C for crude oils with some surfactant formulations, whereas interfacial tensions for other formulations were not affected by temperature changes. Handy et al. [19] observed little or no temperature dependence (25-180°C) for interfacial tensions between California crude and aqueous petroleum sulfonate surfactants at various NaCl concentrations. In contrast, for a pure hydrocarbon or mineral oil and the same surfactant systems, an abrupt decrease in interfacial tension was observed at temperatures in excess of 120°C [20]. Nonionic surfactants showed sharp minima of interfacial tension for crude

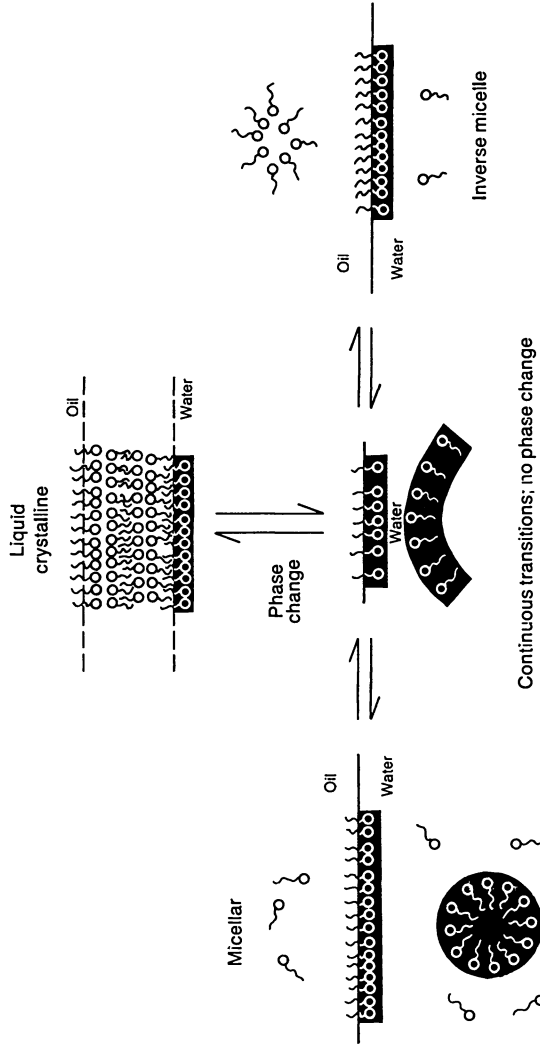


Figure 1: Schematic illustration of possible changes in the microstructure of amphiphiles at the oil/water interface.

oil systems at a temperature corresponding to the cloud point [19].

Isaacs and Smolek [21] observed that low tensions obtained for an Athabasca bitumen/brine-sulfonate surfactant system were likely associated with the formation of a surfactant-rich film lying between the oil and water, which can be hindered by an increase in temperature. Babu et al. [22] obtained little effect of temperature on interfacial tensions; however, values of about 0.02 mN/m were obtained for a light crude (39°API), and were about an order of magnitude lower than those observed for a heavy crude (14°API) with the same aqueous surfactant formulations. For pure hydrocarbon phases and ambient conditions, it is well established that the interfacial tension behavior is dependent on the oleic phase [15,23]. In general, interfacial tension values of crude oil-containing systems are considerably higher than the equivalent values observed with pure hydrocarbons.

In the present paper, interfacial tensions were measured for a number of heavy crude oils at temperatures up to 200°C using the spinning drop technique. However, reliable data cannot be obtained by this or any other drop shape method because of the small density difference between heavy crudes and water which, moreover, tends to decrease as the temperature increases. This problem was overcome by using aqueous D₂O instead of H₂O as has been previously described [5,8,21]. The influence of surfactant type and concentration, mono- and divalent cation concentrations, and pH on the attainment of low interfacial tensions are reported and discussed.

EXPERIMENTAL DESCRIPTION

Materials. Samples of dewatered crude oils were obtained from: the Athabasca oil sands of the McMurray formation by extraction using the commercial hot water process (Suncor Inc.); the Bluesky-Bullhead formation at Peace River, Alberta by solvent extraction of produced fluids; the Clearwater formation at Cold Lake, Alberta by solvent extraction of core material; and the Karamay formation in Xing-Jiang, China. A summary of the physical and chemical properties of the crude oils, including chemical composition, and density-temperature and viscosity-temperature relationships, is given in Table I.

Surfactant mixtures were used as obtained and are listed with their properties in Table II. Sodium chloride and calcium chloride were Fisher reagent grade. Deuterium oxide was Aldrich Gold Label and had a surface tension of 70.4 mN/m at 23°C measured with a Wilhelmy plate tensiometer.

Equipment and Procedures. Crude oil/aqueous interfacial tensions were measured using a spinning drop tensiometer built at the Alberta Research Council and designed for operation at elevated temperatures [21]. The main difficulty in operating at elevated temperatures was the wear on the bearing; improved operation was

Table I: Physical and chemical properties of heavy oils

Measurement	Temperature °C	Athabasca	Peace River	Clearwater	Karamay
Gravity, °API	15	8.9	7.5	10.4	19.7
Density, kg/dm ³	50	0.989	0.994	0.976	0.912
	100	0.958	0.961	0.946	0.876
	150	0.927	0.927	0.916	0.841
	200	0.897	0.899		
Viscosity, mPa.s	50	3350	9136	3172	369
	60	1700	3578	-	-
	100	-	137	133	31
<u>Elemental Analysis</u>					
Carbon		83.3	82.9	84.3	85.6
Hydrogen		10.6	10.7	10.8	12.5
Nitrogen		0.4	0.4	0.4	0.6
Oxygen		-	1.6	1.1	1.2
Sulfur		4.8	5.8	4.4	0.1
<u>Fractional Analysis</u>					
Saturates		24.6	17.0	20.1	48.0
Aromatics		26.2	20.4	11.4	11.5
Polars I		32.5	45.8	16.5	9.2
Polars II		32.5	45.8	7.0	1.2
Polars III		32.5	45.8	23.1	18.9
Asphaltenes		14.7	18.4	16.6	2.0
Acid No. mg of KOH per g		3.6	3.6	1.4	5.0

Table II: Properties of surfactants

Surfactant	Type	Source	% Active	Equivalent Weight
Chaser SD1000	sulfonate dimmer	Chevron	42	-
Enordet C ₁₆ -C ₁₈	α -olefin sulfonate	Shell	30	356
Enordet LTS-18	alkylaryl sulfonate	Shell	12	457
SunTech IV	alkylaryl sulfonate	Sun	15	418
TRS 10-80	petroleum sulfonate	Witco	85	420

achieved by using precision bearings from RHP Canada Inc (No. R8/15) which could be oiled during experiments. Shafts were drilled into the aluminum block used to heat the sample in the spinning drop tube, to allow for oiling of the bearing during operation.

Densities were measured using a Paar DMA 60 meter equipped with DMA 512 and DMA 601 HP external cells. Values in the 50-150°C range were interpolated from measured data (3-5 points); values above 150°C were extrapolated and are less accurate. Interfacial tension measurements at the minimum density difference encountered (0.05 g/cm³) could be in error by as much as 10%, which is within the repeatability of measurements with heavy crude oil samples (see below).

Unless stated otherwise, values of interfacial tension were obtained using D₂O as the aqueous phase. Although the physical properties of H₂O and D₂O are nearly identical, studies have shown that critical micelle concentrations (CMC) of several surfactants [24] and micellar aggregation numbers [25] are higher in D₂O than H₂O. For nonionic surfactants, no significant differences have been observed in the aggregation number [26], but the cloud point is lower in D₂O than H₂O [27]. It has been suggested [26,27] that the greater strength of the O-D...O compared to the O-H...H bond results in differences in intermicellar interactions. For the purpose of the present study, any differences in values measured in D₂O and H₂O have been shown to be small [21]; trends in interfacial tension behavior are expected to be the same.

The aqueous phases were prepared by dispersing surfactant in D₂O or in formation water using magnetic stirring. The solutions were then diluted to the appropriate concentration by the addition of NaCl or CaCl₂, or NaOH or HCl concentrates in D₂O. All concentrations refer to the active surfactant concentration at room temperature.

Oil drops of 2-5 μL were introduced into 0.4 cm i.d. capillary tubes containing the aqueous phase. The more viscous heavy oils were heated for a short period to facilitate this addition. The tubes were then sealed with a tightly fitting silicon-rubber septum. A teflon screw was used to apply pressure on the septum after the capillary tube was inserted into the shaft of the tensiometer. In this manner, temperatures up to 200°C were achieved without loss of liquid.

The 0.4 cm i.d. capillary tubes were used instead of the recommended 0.2 cm i.d. [28] in order to facilitate the addition of highly viscous oils. Figure 2 shows the effect of spinning rate on the interfacial tension of an *n*-butanol/deionized water system using two tube sizes. The dashed line represents the best fit for 15 data points measured using a 0.2 cm i.d. tube, where the mean interfacial tension is 1.76 mN/m (standard deviation of 0.02) with a range of 1.73 to 1.80 mN/m for speeds ranging from

4,050 to 13,460 rev/min. These values agree well with literature [28,29]. Data for the 0.4 cm i.d. tube are in good agreement only below about 8,000 rev/min, increasing gradually thereafter with increasing speed.

It is apparent that with the larger diameter tubes, at high frequencies the drop diameter lags behind the rotational speed of the tube causing an apparent increase in tension. With a more viscous oleic phase as in this study, smaller diameter drops, and lower tension systems, lagging should be more severe and result in higher apparent tensions. As an example, Figure 3 shows that the choice of spinning rate is important in determining the apparent tension for the Clearwater bitumen/surfactant-in-brine system. Generally, for heavy oils and tensions below 1 mN/m, speeds below 6,000 rev/min are preferable. The lower the tension, the lower the preferred speed while still maintaining a length to diameter ratio of about 4. Because of the small density difference between heavy oil and D₂O, the falloff of tensions due to buoyancy effects will occur at a much lower frequency than 4,000 rev/min as reported for *n*-butanol/H₂O and alkane/H₂O systems [28,29].

All measurements were carried out without prior equilibration of the aqueous and hydrocarbon phases. The values reported were obtained at least one hour after steady state had been reached at a given temperature. For calculating the interfacial tensions, the working equations described by Manning et al. [30] were used. Three replicate experiments using an Alberta heavy oil in produced water containing surfactant (LTS-18) as a function of temperature are shown in Figure 4. The same trend was observed for the three experiments with an interfacial tension minimum at 75°C. However, the apparent tension values of one set of measurements varied substantially from the other two, and considerably more than the reproducibility of the method (about 6%). This variation is probably due to the inhomogeneity of the heavy crudes samples because of their colloidal nature and the differences in the chemical species present with each drop of oil selected.

This type of difficulty associated with measurements using chemically ill-defined substrates was also observed during sessile drop measurements carried out on Athabasca bitumen in D₂O [31]. Values in the range of 15-20 mN/m were obtained for measurements with several drops of bitumen, while interfacial tensions for other pure aqueous and oleic systems were accurate to ±0.5 mN/m.

RESULTS AND DISCUSSION

Effect of NaCl Concentration. The presence of surfactant in brine can have a dramatic effect on crude oil-aqueous surfactant tensions even at elevated temperatures [5,21]. Figure 5 shows that the effect of sodium chloride concentration on Athabasca bitumen-D₂O interfacial tensions measured at constant surfactant

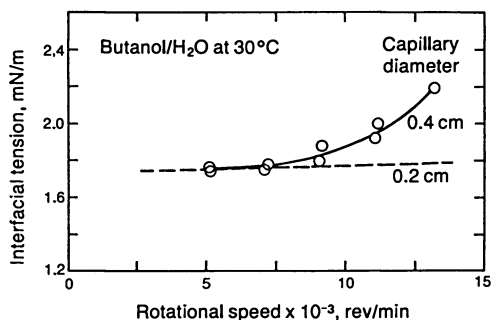


Figure 2: Effect of spinning rate on the interfacial tension of *n*-butanol/water system at 30°C.

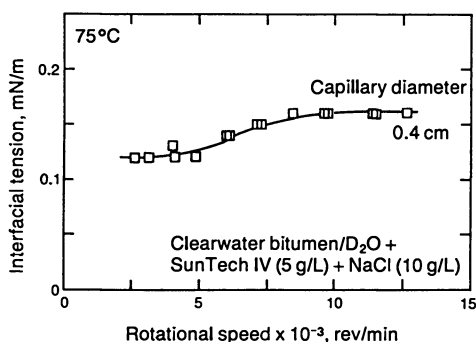


Figure 3: Effect of spinning rate on the interfacial tension of Clearwater bitumen/D₂O, and Sun Tech IV (5 g/L) and NaCl (10 g/L) system at 75°C.

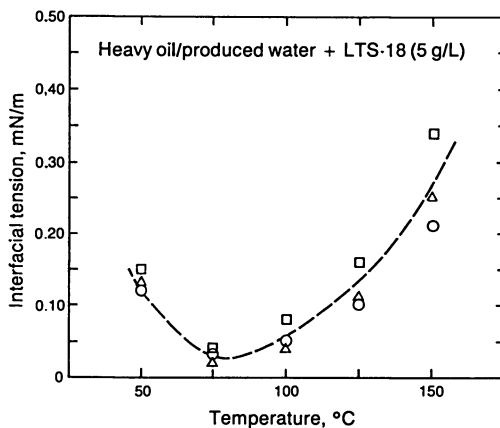


Figure 4: Effect of temperature on the interfacial tension of an Alberta heavy oil in produced water containing LTS-18 surfactant. Data are from three separate replicate experiments conducted under the same conditions.

concentration (2 g/L) and temperature (100°C) depends on the surfactant type. In the case of Enordet C₁₆₋₁₈, interfacial tensions were only slightly affected by salinity, decreasing almost linearly with increasing NaCl concentration. Both the behavior and the range of interfacial tension values were similar to that exhibited [21] by sodium dodecyl sulfate (SDS), a pure association colloid. The decrease in interfacial tension may be due to changes in size, shape and aggregation number of the micelles [14] resulting from changes in the ionic environment (increased NaCl concentration) which do not involve a phase change (see Figure 1).

In contrast to Enordet C₁₆₋₁₈, both TRS 10-80 and Sun Tech IV displayed a tension minimum where the interfacial tension was reduced by 2-3 orders of magnitude (Figure 5). The NaCl concentration at which the tension was at a minimum and the extent of the reduction varied between the two surfactants. At NaCl concentrations much higher than that at which the minimum tension occurred, surfactant precipitation caused non-equilibrium shapes and no measurements were possible. In contrast, Enordet C₁₆₋₁₈ is extremely brine tolerant and data were measured up to 160 g/L NaCl.

In *n*-octane/aqueous systems at 27°C, TRS 10-80 has been shown to form a surfactant-rich third phase, or a thin film of liquid crystals (see Figure 1), with a sharp interfacial tension minimum of about 5×10^{-4} mN/m at 15 g/L NaCl concentration [13]. Similarly, in this study the bitumen/aqueous tension behavior of TRS 10-80 and Sun Tech IV appeared not to be related to monolayer coverage at the interface (as in the case of Enordet C₁₆₋₁₈) but rather was indicative of a surfactant-rich third phase between oil and water. The higher values for minimum interfacial tension observed for a heavy oil compared to a pure *n*-alkane were probably due to natural surfactants in the crude oil which somewhat hindered the formation of the surfactant-rich phase. This hypothesis needs to be tested, but the effect is not unlike that of the addition of SDS (which does not form liquid crystals) in partially solubilizing the third phase formed by TRS 10-80 or Aerosol OT at the alkane/brine interface [11,12].

Effect of Temperature. In the absence of surfactant, interfacial tensions of the Athabasca [21], Karamay [5], and other heavy oils [32] show little or no dependence on temperature. For surfactant-containing systems, Figure 6 shows an example of the effect of temperature (50-200°C) on interfacial tensions for the Athabasca, Clearwater and Peace River bitumens in Sun Tech IV solutions containing 0 and 10 g/L NaCl. The interfacial tension behavior for the three bitumens was very similar. At a given temperature, the presence of brine caused a reduction in interfacial tension by one to two orders of magnitude. The tensions were seen to increase substantially with temperature. For the case of no added NaCl, the values approached those observed [21] in the absence of surfactant.

At first glance, the tension-temperature behavior may be interpreted as that expected for surfactant concentrations at or below the CMC, the concentration at which monolayer coverage is complete. Since the CMC for anionic surfactants increases with temperature [17,33], the surface coverage decreases resulting in a decrease in tension. However, the temperature behavior was very different for Enordet C₁₆₋₁₈ (2 g/L) a surfactant which does not form a surfactant-rich film, and NaCl (0-160 g/L; data given in Table III) solutions. The tensions were not drastically affected by temperature. Moreover, measurements (Table IV) for the Clearwater sample at a higher surfactant concentration (5 g/L) exhibited a trend similar to that observed in Figure 6 with 2 g/L Sun Tech IV. The main difference at the higher concentration was that tension values were 3-5 times lower below 100°C but not significantly different at 150° and 200°C. It thus appears that the interfacial tension-temperature behavior observed for Sun Tech IV and the three bitumens is consistent with a liquid crystalline phase at low temperatures, whose formation is hindered as the temperature increases. As shown previously [5,21], to maintain low interfacial tensions at elevated temperatures required increasing surfactant or electrolyte concentration.

Effect of pH. Interfacial tensions between heavy crude oils and alkaline solutions were measured at temperatures up to 180°C by Mehdizadeh and Handy [34]. They observed that tensions increased with an increase in temperature. However, recovery efficiencies obtained at high temperatures were comparable to those obtained at lower temperatures, apparently because the ease of emulsification at high temperatures counteracted the increase in tension.

To our knowledge, no data on the effect of pH and temperature has been measured in the presence of added surfactant. Figure 7 shows such pH dependence data as measured in this study for Athabasca bitumen in D₂O containing Sun Tech IV (2 g/L) at a constant ionic content of 10⁻² M (adjusted using HCl, NaOH and NaCl) at 50 and 150°C. Data at 100°C (not shown for clarity) fell between those at 50 and 150°C. The dashed curve represents previously reported data [21] at 50°C in the absence of added surfactant, and without maintaining ionic strength. In marked contrast to the no-surfactant case, the interfacial tensions showed essentially no dependence in the 2-12 pH range at 100 and 150°C. The results at 50°C showed no dependence in the 2-9 pH range with a small tension minimum at about pH 11. However, at a given pH, tensions increased with increasing temperature. These results suggest that the surfactant preferentially adsorbs at the oil/water interface and, at high pH, hinders the formation and/or adsorption of natural surfactants at the interface. Further studies are needed to substantiate the results at lower interfacial tension regimes and to investigate the possible implications for a caustic-surfactant process.

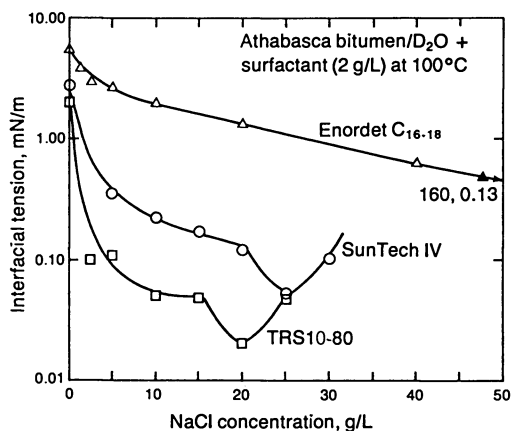


Figure 5: Effect of NaCl concentration on the Athabasca bitumen/D₂O interfacial tension for Enordet C₁₆₋₁₈, Sun Tech IV and TRS 10-80. Closed triangle represents the data measured for Enordet C₁₆₋₁₈ at concentrations up to 160 g/L NaCl.

Table III: Interfacial tension data for the Athabasca bitumen/D₂O and Enordet C₁₆₋₁₈ (2 g/L) system as a function of NaCl concentration and temperature

NaCl Conc., g/L	Interfacial Tension, mN/m		
	50°C	100°C	150°C
0	4.5	6.7	3.5
1.25	2.8	4.0	3.3
2.5	2.1	3.0	3.1
5.0	1.9	2.7	2.7
10.0	1.4	2.0	2.2
20.0	0.66	1.3	1.6
40.0	0.44	6.63	0.86
80.0	0.33	0.42	0.49
100.0	0.21	0.26	0.37
120.0	0.23	0.22	0.22
140.0	0.21	0.21	0.21
160.0	0.17	0.13	0.13

Table IV: Interfacial tension data for the Clearwater bitumen/D₂O and Sun Tech IV system as a function of surfactant and NaCl concentration and temperature

Temperature, °C	NaCl Conc., g/L	Interfacial Tension, mN/m	
		2 g/L Surfactant	5 g/L Surfactant
25	0	-	0.33
50	0	2.1	0.45
75	0	-	0.75
100	0	3.8	0.95
125	0	-	2.6
150	0	5.3	4.3
200	0	5.9	-
25	10	-	0.04
50	10	0.07	0.07
75	10	-	0.10
100	10	0.25	0.14
125	10	-	0.25
150	10	0.44	0.33
200	10	0.28	0.49

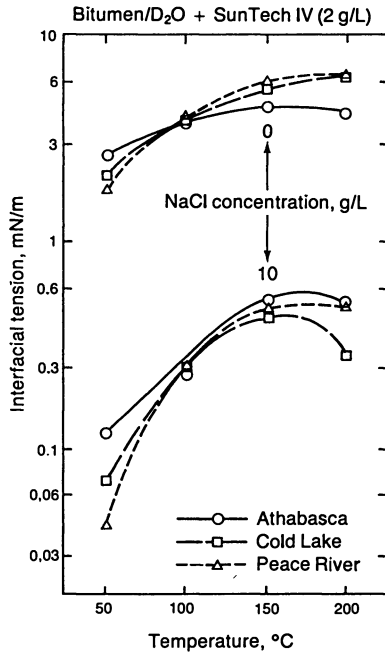


Figure 6: Interfacial tensions for Athabasca, Cold Lake and Peace River bitumen/D₂O systems as a function of temperature and NaCl (0 and 10 g/L) concentration.

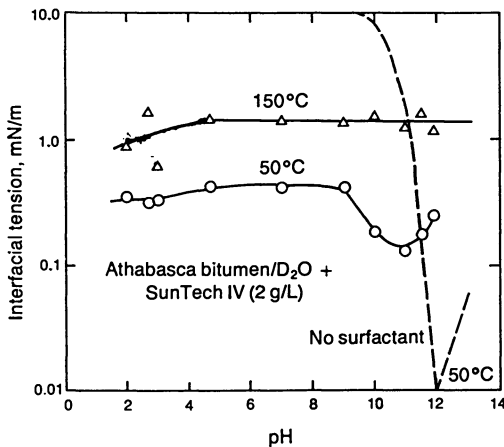


Figure 7: Variation of interfacial tension between Athabasca bitumen and D₂O containing Sun Tech IV (2 g/L) as a function of pH and temperature at constant ionic strength of 10⁻² M. The dashed line represents data from reference [21] at 50°C in the absence of added surfactant or brine.

Effect of Ca^{2+} . In many reservoirs the connate waters contain substantial quantities of divalent ions (mostly Ca^{2+}). In alkaline flooding applications at low temperatures, the presence of divalent ions leads to a drastic increase in tensions [35,36]. Kumar et al. [37] also found that Ca^{2+} and Mg^{2+} ions are detrimental to the interfacial tensions of sulfonate surfactant systems. Detailed studies at elevated temperatures appear to be non-existent.

Figure 8 shows the effect of Ca^{2+} on the interfacial tensions of two oils (Karamay and Clearwater) in Sun Tech IV (5 g/L) and NaCl (10 g/L) solutions at 150°C. The interfacial tension values for the two oils were very similar with as much as an 8-fold reduction, depending on concentration. Interfacial tension minima in the range of 0.06 to 0.1 mN/m were observed at 0.05 and 0.5 g/L CaCl_2 for both oils.

It has been reported by Celik and Somasundaran [38] that the interaction of divalent (and trivalent) cations with sulfonate surfactants causes surfactant precipitation followed by dissolution of the precipitate at higher concentrations. The precipitate redissolution phenomenon is not observed with monovalent ions. Indeed, some surfactant precipitation in the spinning drop tube was observed above concentrations corresponding to the first minimum of Figure 8; it is not known whether redissolution took place at higher concentrations resulting in the second tension minimum.

The interfacial tension-temperature relationships at various CaCl_2 concentrations for Karamay crude in a Sun Tech IV (5 g/L) and NaCl (10 g/L) solution are shown in Figure 9. For 0, 0.025 and 0.1 g/L Ca^{2+} , an increase in interfacial tension with temperature was observed. The interfacial tension values above 150°C were about the same for these concentrations. At temperatures below 100°C, the effect of Ca^{2+} was to increase interfacial tension, probably by hindering the formation of a surfactant-rich phase. This is consistent with the detrimental effect on light oil/brine interfacial tensions (increase from about 10^{-3} to about 10^{-1}) reported by Kumar et al. [37].

For 0.5 g/L Ca^{2+} , the interfacial tension-temperature behavior was reversed compared to that observed at lower concentrations (Figure 9), showing a substantial decrease with temperature. The extent of the reduction was about 3 orders of magnitude compared to the interfacial tension in the absence of surfactant (about 10 mN/m at 180°C). As shown in Figure 10, the same trend was observed for the interfacial tension-temperature behavior of Karamay crude in formation water containing Sun Tech IV. This is not surprising considering that the formation water contained a high amount of divalent (0.25 g/L) and some monovalent (2 g/L) cations. While the mechanism for interfacial tension reduction with increasing temperature remains to be elucidated, this is a positive outcome in terms of reduction in

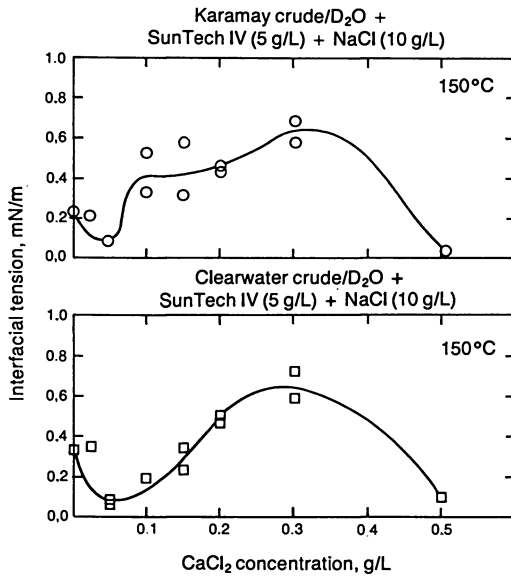


Figure 8: Effect of CaCl₂ concentration on the interfacial tension of oil/D₂O systems containing Sun Tech IV and NaCl for Karamay and Clearwater crudes at 150°C.

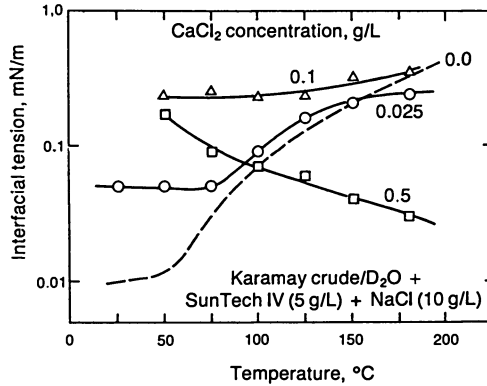


Figure 9: Effect of CaCl_2 concentration and temperature on the interfacial tension of the Karamay crude/ D_2O system containing Sun Tech IV and NaCl. Dashed line represents data in the absence of CaCl_2 (reference [5]).

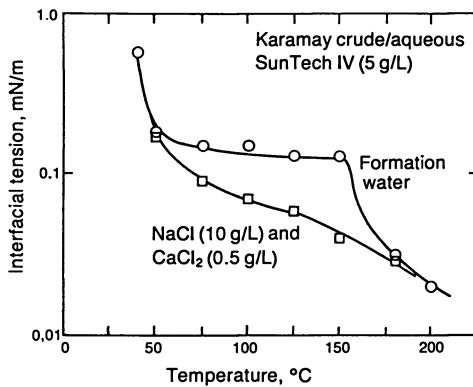


Figure 10: Effect of temperature on the interfacial tension of Karamay crude in reservoir formation water and synthetic brine.

residual saturations which may be crucial for reservoir application of foams at steam temperatures.

SUMMARY AND CONCLUSIONS

The interfacial tension results reported in this paper are part of a study to examine the benefits of using commercial foam-forming surfactants with steam-based processes for obtaining additional oil recovery. Low interfacial tension at elevated temperatures is needed to reduce residual oil saturation and to allow foams to form, or enhance their performance.

Modifications of the conventional spinning drop tensiometer were required for operating at temperatures up to 200°C. Measurements carried out with heavy oil samples required the use of D₂O instead of H₂O to maintain a sufficient density difference between oil and water. For accurate measurements, considerable care must be used to ensure that heavy oil drops do not lag behind the rotation of the capillary tube in the tensiometer. Also, repeatability of measurements conducted with chemically ill-defined substances may be hampered by the inhomogeneity of the oil drops.

In the presence of Sun Tech IV surfactant, the interfacial tension of an Athabasca/brine system showed little or no dependence on pH. However, at a given pH, tension values increased with temperature (50-150°C).

For results where comparisons could be made, the interfacial tension behavior was practically independent of the type of heavy oil used. Interfacial tensions strongly depended on the surfactant type, temperature, and NaCl and CaCl₂ concentrations. Changes in the structure of the amphiphile at the oil/water interface is affected by these variables and accounted for some of the experimental observations.

Low interfacial tensions (<0.1 mN/m) were difficult to maintain at elevated temperatures. At a given NaCl concentration, an increase in temperature (25-200°C) resulted in an increase in interfacial tension. In contrast, in the presence of high amounts of CaCl₂ (0.2 and 0.5 g/L) interfacial tensions decreased with increasing temperatures. Thus, consideration of the range of temperature and water chemistry to be encountered in a given reservoir is important in designing surfactant and foam enhanced recovery processes.

ACKNOWLEDGMENTS

This work was carried out as part of the AOSTRA and Alberta Research Council Core Research Program. Our thanks to Dr. Karel Smolek for assistance with measurements, to Wendy Zwickel for editing, and to Yvonne Mariacci for assistance in typing the manuscript.

LITERATURE CITED

1. Fundamentals of Enhanced Oil Recovery, H.K. van Poolen and Associates Inc., Penn Well Books, Tulsa, 1980.
2. Islam, M.R.; Selby, R.J.; Farouq Ali, S.M. Meeting of the Petroleum Society of CIM, Calgary, June 7-10, 1987 (CIM 87-38-77).
3. Holm, L.W. Soc. Pet. Eng. J., 1968, 359-369.
4. Friedmann, F.; Jensen, J.A. 56th California Regional Meeting of the SPE of AIME, Oakland, April 2-4, 1986 (APE 15087).
5. Isaacs, E.E.; Li, J.; Green, M.K.; McCarthy, F.C.; Maunder, J.D. AOSTRA J. Res., 1988, in press.
6. McPhee, C.A.; Tehrani, A.D.H.; Jolly, R.P.S. SPE/DOE Enhanced Oil Recovery Symposium, Tulsa, April 17-20, 1988 (SPE/DOE 17360).
7. Gopalakrishnan, P.; Bories, S.A.; Combarous, M. Report of the Group d'Etude IFP-IMF, Toulouse, 1978, (SPE 7109).
8. Isaacs, E.E.; McCarthy, F.C.; Smolek, K.F. 2nd European Conference on EOR, Paris, November, 1982.
9. Isaacs, E.E.; Prowse, D.R.; Rankin, J. J. Can. Pet. Tech., 1982, 21, 33.
10. Puig, J.E.; Franses, E.I.; Davis, H.T.; Miller, W.G.; Scriven, L.E. Soc. Pet. Eng. J., 1979, 19, 71.
11. Puig, J.E.; Mares, M.T.; Miller, W.G.; Franses, E.I. Colloids and Surfaces, 1985, 16, 139.
12. Franses, E.I.; Puig, J.E.; Talmon, Y.; Miller, W.G.; Scriven, L.E.; Davis, H.T. J. Phys. Chem., 1980, 84, 1547.
13. Hall, A.C. Colloids and Surfaces, 1980, 1, 209.
14. Winsor, P.A. Chem. Rev., 1968, 68, 1.
15. Chan, K.S.; Shah, D.O. J. Disp. Sci. Technol., 1980, 1, 55.
16. Shinoda, K.; Hanrein, M.; Kunieda, H.; Saito, H. Colloids and Surfaces, 1981, 2, 301.
17. Aveyard, R.; Binks, B.P.; Clark, S.; Mead, J. J. Chem. Soc., Faraday Trans. 1, 1986, 82, 125.
18. Burkowsky, M.; Marx, C. Tenside Deterg., 1978, 15, 247.

19. Handy, L.L.; Amaefule, J.O.; Zeigler, V.M.; Ershaghi, I. 4th Symposium on Oilfield and Geothermal Chemistry, SPE of AIME, Houston, 1979, (APE 7867).
20. Handy, L.L.; El-Gassier, M.; Ershaghi, I. 5th Symposium on Oilfield and Geothermal Chemistry, SPE of AIME, Stanford, 1980, (SPE 9003).
21. Isaacs, E.E.; Smolek, K.F. Can. J. Chem. Eng., 1983, 61, 233.
22. Babu, D.R.; Hornof, V.; Neale, G. Can. J. Chem. Eng., 1984, 62, 156.
23. Cayias, J.L.; Schechter, R.S.; Wade, W.H. J. Colloid Interface Sci., 1977, 59, 31.
24. Emerson, M.F.; Holtzer, A. J. Phys. Chem., 1967, 70, 783.
25. Chang, N.; Kaler, E. J. Phys. Chem., 1985, 89, 2996.
26. Binana-Limbele' W.; Zana, R. J. Colloid Interface Sci., 1988, 121, 81.
27. Pandit, N.K.; Caronia, J. J. Colloid Interface Sci., 1988 122, 100.
28. Manning, C.D.; Scriven, L.E. Rev. Sci. Inst., 1977, 48, 1699.
29. Currie, P.K.; Van Nieuwkoop, J. J. Colloid Interface Sci., 1982, 87, 301.
30. Manning, C.D.; Pesheck, C.V.; Puig, J.E.; Seeto, Y.; Davis, H.T. United States Department of Energy Report, 1983, (DOE/BC/10116-12).
31. Isaacs, E.E.; Morrison, D.N. ADSTRA J. Res., 1985, 2, 113.
32. Flock, D.L.; Le, T.H.; Gibeau, I.P. J. Can. Pet. Tech., 1986, 72.
33. Fennell Evans, D.; Wightman, P.J. J. Colloid Interface Sci., 1982, 82, 515.
34. Mehdizadeh, A.; Handy, L.L. SPE 13072, 59th Annual Technical Conference, SPE of AIME, Houston, 1984, (SPE 13072).
35. Jennings, H.T., Jr.; Johnson, C.E.; McAuiliffe, C.D. J. Pet. Tech., 1974, 26, 1344.
36. Cooke, C.E., Jr.; Williams, R.E.; Kolodzie, P.A. J. Pet. Tech., 1974, 26, 1365.

37. Kumar, A.; Neale, G.; Hornof, V. J. Can. Pet. Tech., 1984, 37.
38. Celik, M.S.; Somasundaran, P. J. of Colloid Interface Sci., 1988, 122, 163.

RECEIVED November 28, 1988

Chapter 18

Oil Recovery with Multiple Micellar Slugs

S. Thomas,¹ S. B. Supon,² and S. M. Farouq Ali¹

¹Department of Mining, Metallurgical and Petroleum Engineering, The University of Alberta, Edmonton, Alberta T6G 2G6, Canada

²Petroleum and Natural Gas Engineering, Pennsylvania State University, University Park, PA 16802

Micellar flooding process has been shown to be an effective tertiary oil recovery technique for watered-out light oil reservoirs, based upon many field tests. However, under the present oil prices it has not been economic in most cases. In other instances, recovery methods such as carbon dioxide flooding may be more attractive. The present research was aimed at improving the efficiency of the micellar flooding process through the use of multiple micellar slugs. The slugs were selected on the basis of the phase behaviour of various ternary systems (crude, water, surfactant). Equilibrium micellar phases chosen from the single phase region or, micellar compositions formed along the dilution path of a suitable micellar slug in the single phase region were used to form the composite slugs. Oil-rich and water-rich slugs were compared for their effectiveness to recover tertiary oil. Multiplicity of slugs on recovery efficiency was examined by injecting portions of oil-rich and water-rich slugs alternately until the desired slug volume was reached. The use of graded composite slugs - starting with an oil-rich slug and ending with a water-rich slug - was successful in improving process efficiency. (Process efficiency, in this work, is defined as the tertiary recovery per unit volume of slug injected). For example, process efficiency increased five fold when a single slug was replaced by a graded composite slug of equivalent size.

The works of various investigators such as Gogarty and Tosch (1), Healy and Reed (2), and Davis and Jones (3), have shown that the micellar flooding process can be used effectively to mobilize residual oil in watered-out light oil reservoirs. Many field tests conducted in the U.S. have further proved its effectiveness. However, the economics of the process remain unattractive for implementing the process for tertiary oil recovery. Recent works by Holm (4), Pope (5), Sayyoun and Farouq Ali (6), Eney and Farouq Ali (7) made significant contributions towards improving the efficiency of the process. The primary objective of this research was to devise a micellar flooding process that is economically as well as technically attractive to the industry, through the use of multiple micellar slugs.

Process Description

Process efficiency, in this study, is defined as the tertiary oil recovery per unit volume of the slug injected. This refers to the efficiency of an oil-rich slug. Economic recovery efficiency varies from slug to slug due to variations in the surfactant content. It should be noted that the micellar slugs were formulated with an effort to keep the cost a minimum.

Basic Process. Hydrocarbon, water/brine and surfactant are the basic components of a micellar solution. A small amount of alcohol is usually added to improve the solution stability, to adjust the viscosity, and to reduce the surfactant loss due to adsorption on the reservoir rock. A suitably formulated micellar slug miscibly displaces the residual oil, leading to a very small final oil saturation. For economic reasons, a small pore volume (2-5%) micellar slug is injected, and it is effectively propagated through the reservoir by the mobility buffer. The mobility buffer protects the slug from dilution by the drive water too early in the process. The efficiency of the process can be augmented by using a suitable composite slug configuration. A composite slug consists of oil-rich and water-rich slugs, injected alternately in two or more steps, until the desired pore volume is reached. The economics of the process can be further enhanced by using a graded composite slug. Such slugs can reduce the surfactant requirement to a minimum, and maximize the tertiary recovery efficiency.

Phase Behaviour Studies and Slug Formulation

The efficiency of a micellar slug to recover tertiary oil is largely dependent on its ability to remain a single phase during the flooding process so that the oil may be displaced "miscibly" and hence, completely. However,

various factors such as slug dilution by reservoir fluids, surfactant loss to the reservoir rock, reservoir salinity etc. influence the phase behaviour adversely. Once slug breakdown occurs, the displacement becomes immiscible and some of the resident oil can be left trapped in the pores. Tertiary recovery can be substantially improved if the slug composition has a minimal multiphase region to prolong the miscible displacement regime, and a low interfacial tension in the multiphase region to enhance the immiscible displacement. Another factor contributing to oil displacement is the relatively larger oleic phase volume at slug breakdown. With these ends in view, a number of phase behaviour studies were made to formulate efficient micellar slugs for the tertiary recovery of three light oils - Bonnie Glen, Provost, and Bradford crudes.

Phase Behaviour Characteristics. Studies of ternary systems, representing crude oil, water/brine and surfactant systems were completed prior to the selection of micellar slugs. The brine used in this study was 2%(wt./vol.) sodium chloride in distilled water. It was found that the phase boundaries depend, to a great extent, on the water/oil ratio in the initial system. Because of the multicomponent nature of the micellar solutions, the phase behaviour of the system is much more complex than a simple three component system. Therefore, a pseudoternary system could only be used to qualitatively correlate the observations on the phase behaviour of the micellar solutions. Due to economic reasons and viscosity requirements, the surfactant and oil concentrations were limited to 5-15% and <50%, respectively. The type and amount of alcohol used were determined by trial and error to obtain adequate viscosity control and solution stability. Having determined the general area of composition for a suitable micellar solution, several solutions were prepared at a given water/oil ratio and varying surfactant concentrations (1-15%). When more than one surfactant were used, they were blended together in a known proportion and treated as a single component in the ternary system. The solutions were prepared by dispersing the surfactant/cosurfactant mixture in the hydrocarbon phase and gradually adding the aqueous phase while maintaining moderate agitation with a magnetic stirrer, until the solution was homogeneous (~5-10 min.). The solutions were allowed to equilibrate in graduated cylinders for 2-4 weeks at the desired temperature. The phase volumes were measured and the type of solution (Type II-, Type II+ or Type III) was determined with the help of IR (infrared) analysis for sulfonate content. The composition points, the tie-lines and the phase envelope showing the multiphase regions were then plotted on the ternary diagram. Micellar solutions were selected

on the basis of their ability to solubilize brine and oil, as well as the compatibility with polymer.

Multiple Micellar Slugs

The efficiency of the displacement process can be further improved by using a multiple micellar slug - a combination of oil-rich and water-rich slugs - instead of a conventional single slug. In this method, a slug that is more compatible with oil (oil-rich) is followed by a slug that is more compatible with water (water-rich). These slugs may be divided into portions and injected alternately in several steps as a 'composite micellar slug'. For example, a 5% pv composite slug injected in three steps can be thought of as (5/3)% pv oil-rich slug followed by (5/3)% pv water-rich slug followed again by (5/3)% pv of the oil-rich slug. The choice of the component slugs is based on the equilibrium micellar phases determined from the phase diagram. Such a combination enhances the stability, and therefore, the performance of the micellar slugs in recovering the tertiary oil. Another approach to prolong the integrity of the micellar slug is to use a 'graded composite slug'. Here, the component slugs are injected such that a gradation is formed with respect to the oil and/or the surfactant concentration of the individual slugs, i.e. the grading starts with oil-rich slug and ends with water-rich slug. Compositions that fall on the same dilution path in the phase diagram are in equilibrium with each other and hence, have favourable phase behaviour. This helps to delay the slug breakdown and thus, improve the displacement efficiency.

Objectives

The primary objectives of this research were :

1. Formulate efficient micellar slugs for the tertiary recovery of three light oils viz. Bradford crude, Bonnie Glen crude, and Provost crude;
2. Improve the efficiency of the micellar flooding process through the use of multiple micellar slugs;
3. Devise methods to reduce the economic disadvantages inherent in the process by suitable selection of slugtype, size and combination, such as substituting a single slug with a graded composite slug of equivalent size.

Experimental Procedure and Apparatus

Apparatus. A constant rate displacement pump charged with mercury was used to displace the fluid of interest from steel cylinders to the core. A pressure transducer connected to the chart recorder provided the pressure history of each core flood. An automatic sampler with

timer was used to collect the effluent. Schematic of the experimental set up is shown in Figure 1.

Procedure. Core floods were carried out in horizontally mounted Berea sandstone cores of length 61 cm and diameter 5 cm. Porosity varied from 18 to 25% and brine permeability from 100 to 800 μm^2 . The cores were coated with a thin layer of epoxy and cast in stainless steel core holders using molten Cerrobend alloy (melting point 70°C). The ends of the cores were machined flush with the core holder and flanges were bolted on. Pore volume was determined by vacuum followed by imbibition of brine. Absolute permeability and porosity were determined. The cores were initially saturated with brine (2% NaCl). An oil flood was then started at a rate of 10m/day until an irreducible water saturation (26-38%) was established. The cores were then waterflooded with brine (2% NaCl) to obtain residual oil saturation.

A micellar flood was then started with the injection of the micellar slug, polymer buffer, and the drive water in succession, at a rate of 1.3 m/day. Two types of polymers - polyacrylamide polymer (Dow Pusher 700) and Xanthan Gum polymer (Kelzan XC) - were used as the polymer buffers. Sodium chloride brine (1%) was used as the drive water. Effluent was collected and analyzed for surfactant content using the IR and UV techniques. All experiments were conducted at room temperature (22-24°C).

Analysis of the Produced Fluids

The oil phase of the effluent was analyzed using the IR method for sulfonate content. Petrostep B100 and Petrostep B110 absorb IR radiation at 1008 cm^{-1} and 1176 cm^{-1} respectively. In the case of slug L1, it is assumed that the proportion of sulfonates (a blend of Petrostep B100 and Petrostep B110) is identical in the injected and the produced fluids.) The surfactant content of each sample and the total amount of sulfonate produced were then calculated. Sulfonate produced in the aqueous phase was determined using the UV method. Absorbance was measured at 206 nm using 10 mm cuvettes. It was found that the bulk of the sulfonate recovered was in the oleic phase of the effluent. Five to ten percent of the total sulfonate injected went into the aqueous phase. The loss of surfactant is calculated as milliequivalents per 100 gram rock.

Accuracy. All fluids properties measured were within $\pm 1\%$. The volumes injected and produced were in agreement within $\pm 0.1\%$. The reproducibility of the core floods was between 0.002-8%.

Crude Oils and Connate Water. The multiple micellar slug process was developed for the tertiary recovery of three light oils viz. Bradford crude, Bonnie Glen crude and Provost crude. The viscosities and densities of the three crude oils used are listed in Table I.

Table I. Viscosities and Densities of Crude Oils

Crude Oil	Viscosity, mPa.s	Density, g/ml
Bonnie Glen	5	0.836
Bradford	5	0.817
Provost	11	0.866

A 2% (w/v) sodium chloride solution was used as the connate water in all corefloods. It should be mentioned that it is desirable to incorporate divalent cations, such as Ca^{++} and Mg^{++} , in the slug formulations as well as in the connate water to simulate an actual reservoir.

Micellar Solutions

Micellar slug B4 was formulated for the tertiary recovery of Bonnie Glen crude. Figure 2 shows the ternary diagram for this crude oil, distilled water, and surfactant system. Solutions a, b, c, and d separated into oil-rich and water-rich microemulsions in equilibrium with each other. For example, solution a equilibrated into a water-rich microemulsion a' and an oil-rich microemulsion a''. Similarly, solutions b, c, and d equilibrated to form b', b''; c', c''; and d', d'' respectively. The tie lines shown connect the solutions in equilibrium. Point P refers to the plait point, where the oil-rich and water-rich solutions become miscible and hence, a single phase. Micellar solution B4 lies in the single phase region, just outside the binodal curve. Solution B4 was diluted with distilled water once to form solution B4W and, twice to form solution B4X. Solutions B4, B4W, and B4X were used in combination to form the composite slug for the recovery of Bonnie Glen crude.

Micellar slug L1 was formulated for the recovery of the Provost crude. Figure 3 shows the ternary phase behaviour diagram for this crude, distilled water and surfactant system. Petroleum sulfonates Petrostep B100 and Petrostep B110 were the surfactants used in these micellar solutions. Solutions A, B, C, and D separated into water-rich microemulsions in equilibrium with excess oil. Micellar solution L1 lies in the single phase region. Solutions L1W1 and L1W2 were formed by diluting solution L1 with distilled water. When solutions L1W1 and L1W2 were allowed to equilibrate, they separated into two phases, the compositions of which are given by the

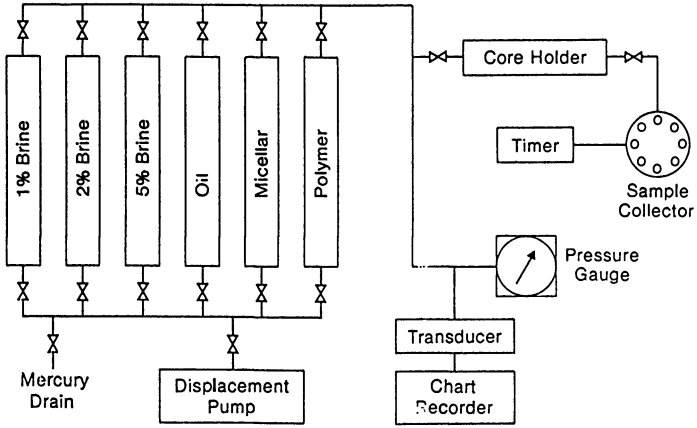


Figure 1. Schematic of Core Flooding Apparatus

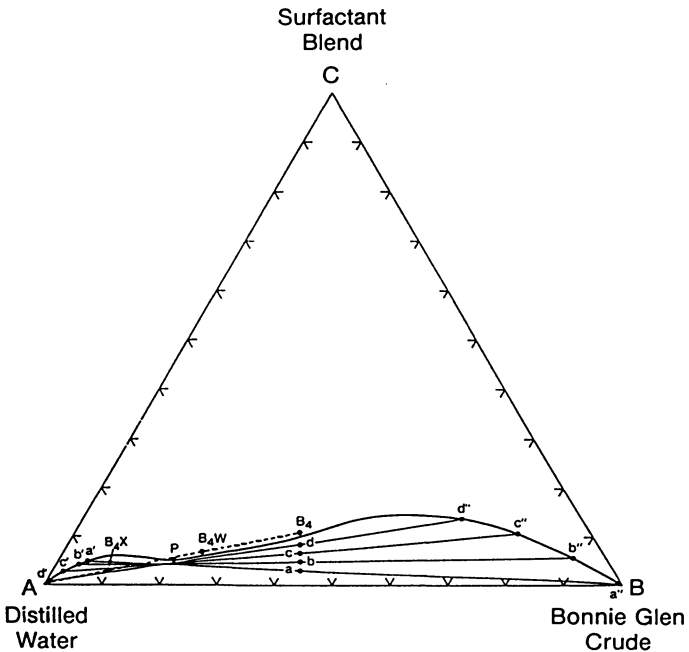


Figure 2. Phase Behaviour of Bonnie Glen Crude, Distilled Water, and Surfactant System

ends of the tie lines passing through the overall composition points.

Micellar slugs for the recovery of Bradford crude were formulated using a different approach. Upon the completion of the phase diagram, equilibrium micellar phases lying along the binodal curve were chosen as the oil-rich and water-rich solutions. These solutions have similar surfactant/cosurfactant concentration, but differ in oil/brine ratios. Figures 4 and 5 show the ternary phase behaviour diagrams for these systems. Since the solutions lie along the same tie line, they are in equilibrium with each other, but have opposing affinities for oil and brine. Two oil-rich slugs were formulated, using two different surfactants, for the tertiary recovery of Bradford crude were P1 and T1. The corresponding water-rich slugs were P2 and T2. Penn State surfactants PRL-5A and TRS-10B were used in these slugs. Table II shows the composition and viscosities of the various micellar slugs.

Polymers

The success of the micellar flooding process for recovering tertiary oil is largely dependent on the mobility buffer which serves to delay viscous fingering of the drive water into the slug and hence, its dilution. Solutions of polyacrylamide polymer and Xanthan gum polymer were used as mobility controlling agents in these experiments. Choice of the type and concentration of the polymer is made depending on the extent to which it is degraded by brine and the rock minerals, resistance factor of the polymer solution, micellar-polymer interaction and the thermal stability of the polymer solution. It was found that polymer degradation by the slug is directly dependent on the surfactant concentration of the slug. The presence of alcohol in the slug improves the micellar-polymer compatibility. Polymer degradation by brine is determined by the ionic strength of the brine. Divalent cations have grater effect in reducing the polymer viscosity than monovalent cations.

Discussion of Results

Single Slugs. Minimum slug size required for the efficient recovery of the tertiary crude was determined by carrying out a series of single slug runs. The slug sizes varied from 2-15% pv. Table III shows the results for a single micellar slug driven by 500 ppm polymer solution for three crude oils.

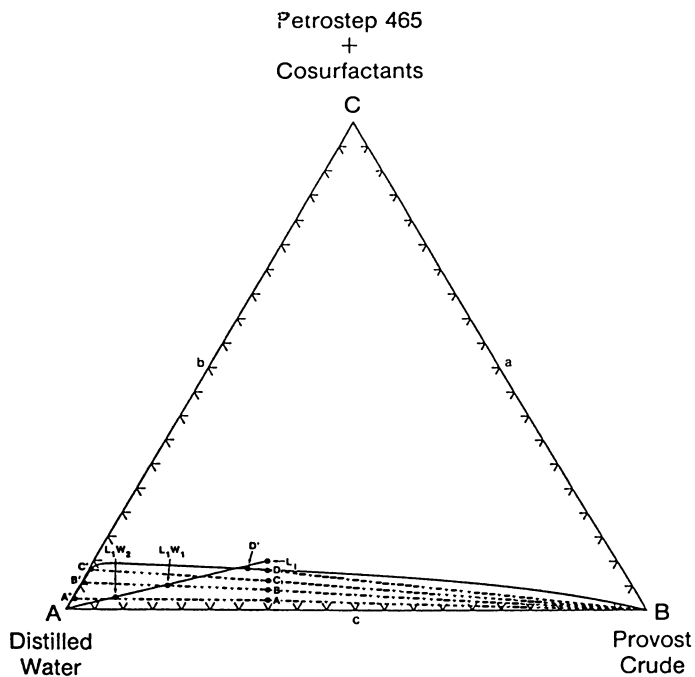


Figure 3. Phase Behaviour of Provost Crude, Distilled Water and Surfactant System

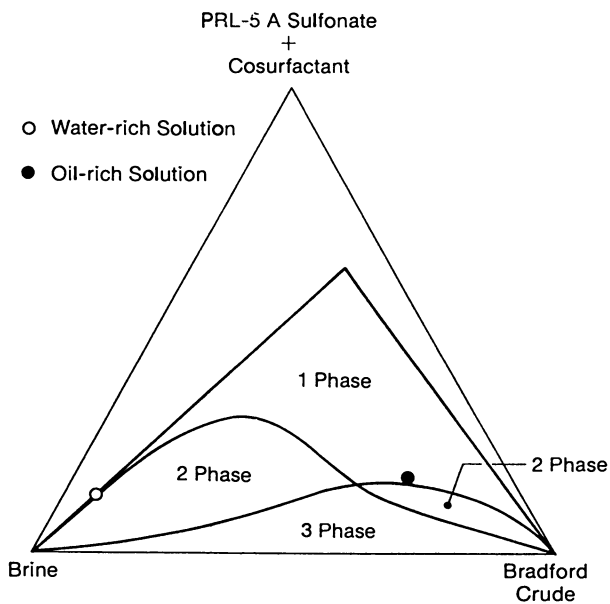


Figure 4. Phase Behaviour of Bradford Crude, Brine, and Surfactant (PRL-5A) System

Table II. Composition and Viscosities of Micellar Slugs

Components	Composition, % vol.										Composition, % w		
	B4	B4W	B4X	L1	L1W1	L1W2	P1	P2	T1	T2			
Crude oil*	39.00	19.50	9.75	30.05	15.00	7.50	63.50	5.50	85.00	2.00			
Distilled water	50.00	75.00	87.50	60.09	80.00	90.00							
Brine (2% w/v NaCl)							20.10	84.00	5.00	92.50			
Petrostep 465	9.00	4.50	2.25										
Petrostep B110				5.54	2.81	1.40							
Petrostep B100				3.07	1.56	0.78							
PRI-5							11.99	7.63	8.01	4.00			
TRS-10													
IPA	1.50	0.75	0.38	1.25	0.63	0.32							
NBA	0.50	0.25	0.13										
Isoamyl Alcohol							4.51	2.87					
Cyclohexanol									1.49	1.00			
Viscosity, m.Pa.s	45.50	2.50	1.50	17.74	2.40	1.60	10.00	8.70	1.50	21.20			

* B4, B4W, B4X : Bonnie Glen crude
L1, L1W1, L1W2 : Provost crude
P1, P2, T1, T2 :Bradford crude

Table III. Tertiary Recovery with Single Micellar Slugs

Crude Oil	Slug Type	Slug Size	Tertiary Recovery
		% pv	% oil in place
Bonnie Glen	B4 (oil-rich)	2.0	16.9
		5.0	61.4
		6.0	73.6
		10.0	79.0
		15.0	82.4
Provost Crude	L1 (oil-rich)	2.0	64.0
		5.0	73.4
Bradford Crude	P1 (oil-rich)	2.5	24.4
		5.0	27.3
		10.0	36.7,
			41.2
	P2 (water-rich)	2.5	3.7
		5.0	16.5
		10.0	44.3
	T1 (oil-rich)	2.5	19.9
		5.0	23.6
		10.0	47.5
T2 (water-rich)	2.5	7.1	
	5.0	15.7	
	10.0	30.9	

The results show that the largest increment in tertiary recovery occurs around a micellar slug size 5% pv for all the slugs used. Figure 6 shows the results for Bonnie Glen crude oil, indicating that the relative increase in tertiary recovery reaches a maximum at slug sizes between 4 and 8% pv. Further increase in slug size gives only minimal increment in tertiary recovery and, greatly reduces the cost-effectiveness of the slug. Process efficiency peaked at 5% pv slug size for micellar slug B4 in the case of Bonnie Glen crude oil. This is shown in Figure 7. Tertiary recovery of Bradford crude using single and composite slugs of various sizes is shown in Figure 8.

Composite Slugs. A single micellar slug was replaced by an equivalent volume of composite slugs to examine the effect of composite slugs on tertiary recovery. An oil-rich slug was followed by a water-rich slug in a 50:50 volume ratio. Selected results are shown in Table IV. Slug compositions T1, T2 and B4 and B4W are given in Table II and shown in Figures 2, 3, 4 and 5, respectively.

The results show that for a given slug size, a composite slug recovered more crude than a single slug of equivalent size.

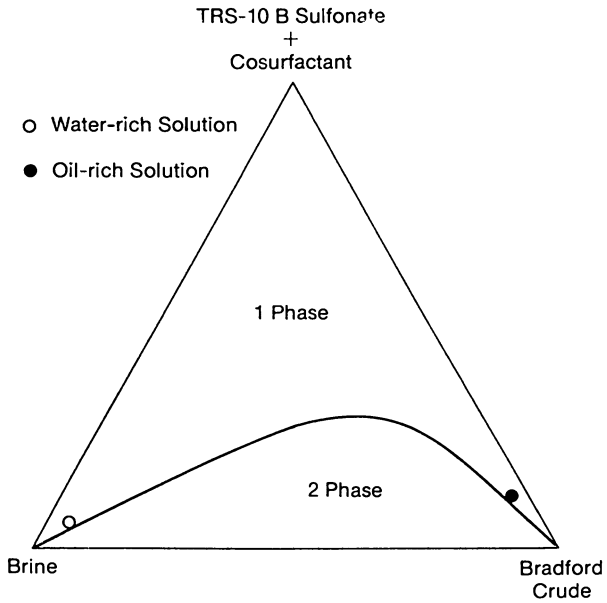


Figure 5. Phase Behaviour of Bradford Crude, Brine, and Surfactant (TRS-10B) System

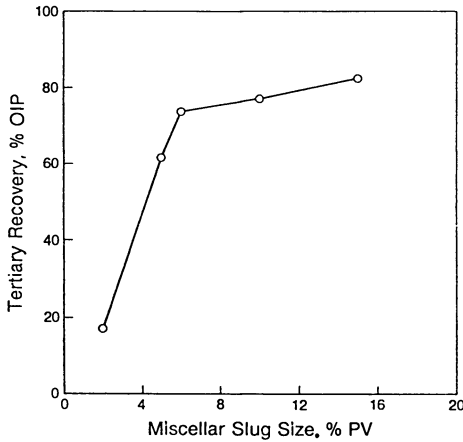


Figure 6. Effect of Micellar Slug Size on Tertiary Recovery

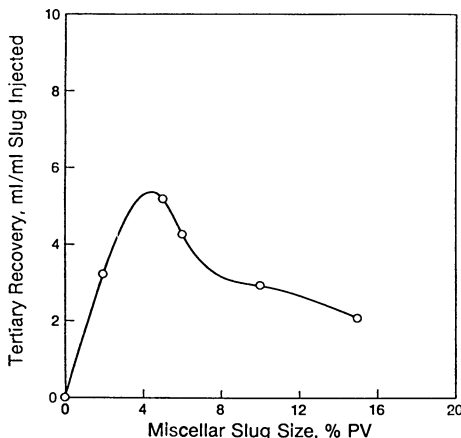


Figure 7. Effect of Micellar Slug Size on the Oil Recovery Efficiency of Micellar Slug B4

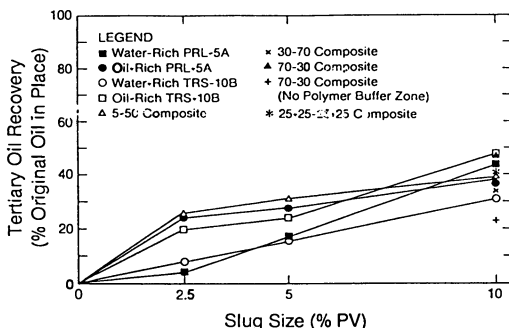


Figure 8. Tertiary Recovery of Bradford Crude Using Oil-Rich, Water-Rich and Composite Slugs

Table IV. Tertiary Recovery Using Paired (Oil-Rich and Water-Rich) Micellar Slugs

Micellar Slug	Total Slug Size, % pv	Tertiary Recovery, % oil in place		
		Single Slug		Composite Slug
		oil-rich	water-rich	
T1/T2	2.5	19.9	7.1	25.0
	5.0	23.6	15.7	31.6
B4/B4W	5.0	62.92	-	80.9
	10.0	77.02	-	94.7

Next, the proportions of oil-rich and water-rich slugs were varied for a given slug size (10% pv) and the tertiary recoveries were compared. As seen in Table V, oil-rich slugs were more effective

Table V. Effect of Oil-Rich/Water-Rich Slug Volume Ratio on Tertiary Recovery

Micellar Slug	oil-rich : water-rich ratio (vol.)	Tertiary Recovery % oil in place
T1/T2	100 : 00	47.5
	70 : 30	42.2
	50 : 50	39.9
	30 : 70	34.5
	00 : 100	30.9

than water-rich slugs in recovering tertiary oil. The efficiency of the process can be improved by following the oil-rich slug with water-rich slug. For example, a 70:30 composite slug recovered as much crude as a single slug of equivalent size.

Multiplicity of Slugs. The effect of multiplicity of slug on recovery efficiency was examined by alternating the oil-rich and water-rich slugs in 2, 3 and 4 steps, for a given slug size (5% pv). In each case, tertiary recovery was higher for 3 and 4 steps than for 2 steps. (Slug size "5/3" stands for a total slug size of 5% pv split into 3 equal parts.) The order of injection o/w/o represents oil-rich slug followed by water-rich slug followed by oil-rich slug. Table VI shows selected results for a 5% slug in several steps. It is clear that the three slug configuration gave higher oil recovery than a single slug.

Table VI. Comparison of Tertiary Recovery Using Single and Composite Micellar Slugs

Slug Type	Slug Size % pv	Order of Injection	Tertiary Recovery % oil in place
B4	5	o	62.93
B4	5/2*	o/w	80.85
B4	5/3	o/w/o	87.02
L1	5	o	73.35
L1	5/3	o/w/o	81.91

* denotes a 5% pv slug, consisting of two equal parts, being oil-rich, water-rich, respectively.

Graded Composite Slugs. In graded micellar slugs, two or more slugs are injected so that a gradation starts with

oil-rich slug and ends with a water-rich slug. Micellar compositions formed along the dilution path of an oil-rich slug are excellent in forming a gradation and are efficient in mobilizing the tertiary oil. Table VII shows the results of single, composite, and graded composite slugs of B4 and L1, in recovering Bonnie Glen crude and Provost crude, respectively.

Table VII. Comparison of Tertiary Recovery with Single, Composite, and Graded Composite Micellar Slugs

Slug Type	Slug Size % pv	Order of Injection	Tertiary Recovery, % oil in place
B4	5	o	62.93
	5/3*	o/w/o	87.02
	5/3	o/w/+w	97.94
L1	5	o	73.35
	5/3	o/w/o	81.91
	5/3	o/w/+w	96.87

o : oil-rich w : water-rich, +w : more water-rich
* denotes a 5% pv slug, consisting of three equal parts, being oil-rich, water-rich and oil-rich, respectively.

Smaller Slug Size. Efficiency of graded composite slugs over a single slug was high enough to reduce the slug volume requirement to less than one-half and still obtain the same tertiary recovery. This is shown in Table VIII.

Each volume of a composite slug injected recovered 3 to 15 times its volume in tertiary oil. Sulfonate loss in graded composite slug runs was considerably lower than in single slug runs. This shows that slug dissipation due to sulfonate loss is lower in graded composite slug runs, and hence the residual oil was mobilized and recovered more efficiently. Typical oil recovery curves for 5% pv single slug runs and multiple slug runs using micellar slug B4 are shown in Figures 9 and 10. Similar curves for micellar slug L1 are shown in Figures 11 and 12, respectively.

Conclusions

Based upon over 50 micellar floods carried out on sandstone cores, the following conclusions are reached:

1. Oil-rich slugs recovered more crude oil than water-rich slugs.
2. Small micellar slugs (2-5% pv) can recover 3 to 15 times their volume of waterflood residual oil. Final oil saturation was reduced to 0.02% pv for 2% pv slug size and, 0.01% pv for 5% pv slug size.
3. Oil displacement efficiency can be improved considerably when a composite slug is used in place

Table VIII. Tertiary Recovery with Smaller Slug Size

Slug Type	Slug Size % pv	Tertiary Recovery % oil in place	Sulf. Recovery meq/100g rock	Process Efficiency*
B4 (s)	5	62.93	0.085	5.02
B4 (g)	5	97.94	0.028	6.26
B4 (s)	2	16.86	0.040	3.01
B4 (g)	2	92.36	0.017	15.39
L1 (s)	5	73.35	0.037	5.51
L1 (g)	5	96.87	0.018	6.65
L1 (s)	2	63.99	0.022	11.34
L1 (g)	2	70.26	0.006	12.27

s : single slug g : graded composite slug

* vol. of oil recovered/Total slug volume

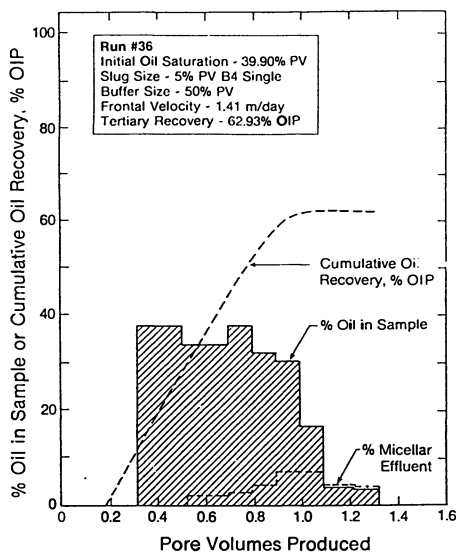


Figure 9. Production History of 5% PV Micellar Slug B4 and 50% PV Buffer Injected at 1.41 m/day

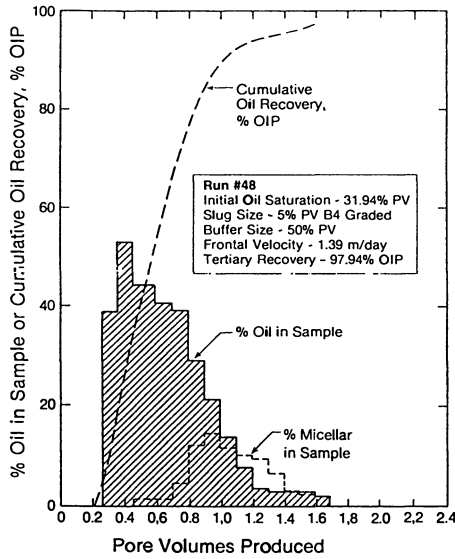


Figure 10. Production History of 5% PV Graded Composite Slug of B4 and 50% PV Buffer Injected at 1.35 m/day

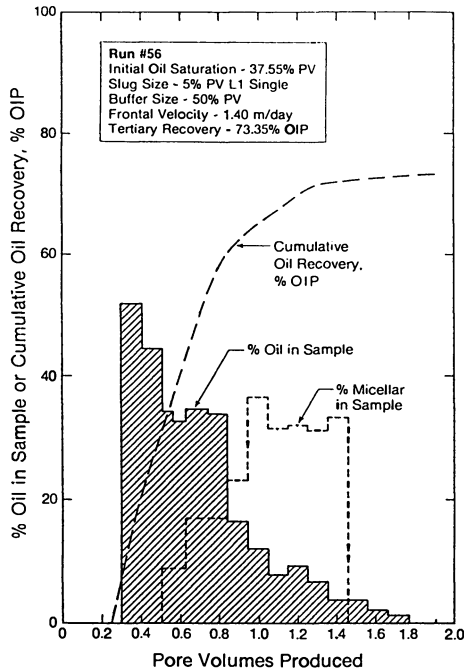


Figure 11. Production History of 5% PV Micellar Slug L1 and 50% PV Buffer Injected at 1.40 m/day

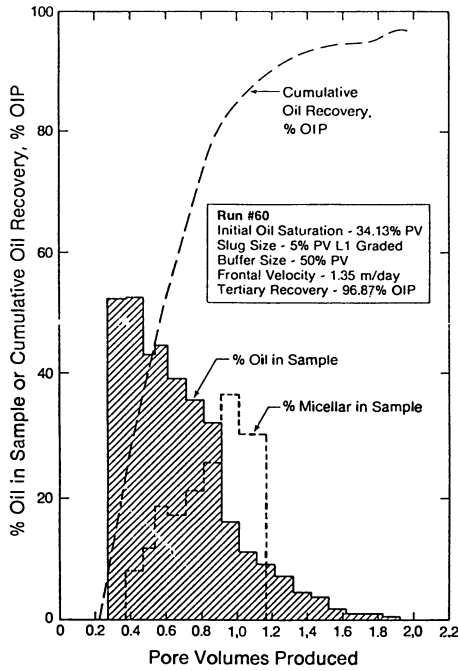


Figure 12. Production History of 5% PV Graded Composite Slug of L1 Injected at 1.35 m/day

- of a single slug. Process efficiency increased substantially (12-15%) for a 2% pv slug size when a graded composite slug was used instead of a single slug of equivalent size.
4. Oil recovery increases with an increase in micellar slug size. But the process efficiency drops and the surfactant loss increases.
 5. The slug requirement, and therefore, the cost of production, can be reduced by using a graded composite slug in place of a conventional single slug. For example, a 5% pv of a graded composite slug B4 recovered 97.74% oil in place, whereas a 2% pv of the same slug recovered 92.36% oil in place, increasing the process efficiency from 6 to 15.

Literature Cited

1. Gogarty, W.B. and Tosch, W.C.: "Miscible-Type Waterflooding : Oil Recovery with Micellar Solutions", J. Pet. Tech. (Dec. 1968) 1407-1415.
2. Healy, R.H. and Reed R.L.: "Physicochemical Aspects of Microemulsion Flooding", Soc. Pet. Eng. J. (Oct.1974) 14, 491-501.
3. Davis, J.A. and Jones, S.C.: "Displacement Mechanisms of Micellar Solution", J. Pet. Tech. (Dec. 1968), 1415-1428.
4. Holm, L.W.: "Mobilization of Waterflood Residual Oil by Miscible Fluids", SPE Res. Eng. (July 1986) 354-362.
5. Pope, G.A, Tsaur, K., Schechter, R.S. and Wang, B.: "The Effect of Several Polymers on the Phase Behaviour of Micellar Fluids", Soc. Pet. Eng. J. (Dec. 1982) 816-830.
6. Sayyoub, M.H.M., Farouq Ali, S.M. and Stahl, C.D.: "Rate Effects in Tertiary Micellar Flooding of Bradford Crude Oil", Soc. Pet. Eng. J. (Aug. 1981) 469-479.
7. Eney, S.L., Farouq Ali, S.M. and Stahl, C.D.: "Competing Roles of Interfacial Tension and Surfactant Equivalent Weight in the Development of a Chemical Flood", Soc. Pet. Eng. J. (Aug. 1982) 472-480.

RECEIVED February 7, 1989

Chapter 19

Effect of Demulsifiers on Interfacial Properties Governing Crude Oil Demulsification

Surajit Mukherjee¹ and Arnold P. Kushnick

Exxon Chemical Company (ECTD), Houston, TX 77029

Effectiveness of a crude oil demulsifier is correlated with the lowering of shear viscosity and dynamic tension gradient of the oil-water interface. Using the pulsed drop technique, the interfacial dilational moduli with different demulsifiers have been measured. The interfacial tension relaxation occurs faster with an effective demulsifier. Electron spin resonance with labeled demulsifiers indicate that the demulsifiers form 'reverse micelle' like clusters in bulk oil. The slow unclustering of the demulsifier at the interface appears to be the rate determining step in the tension relaxation process.

Crude oil is almost always produced as persistent water-in-oil emulsions which must be resolved into two separate phases before the crude oil can be accepted for transportation. The water droplets are sterically stabilized by the asphaltene and resin fractions of the crude oil. These are condensed aromatic rings containing saturated carbon chains and naphthenic rings as substituents, along with a distribution of heteroatoms (S, O and N) and metals (Ni, V). It has been suggested (1) that a stabilizing film protecting the water drops from coalescence is created by hydrogen bonding of the N-, O-, and S- containing groups at the water drop--oil interface.

Although, many other methods (e.g. electrostatic separation, heating, centrifugation, etc.) may be used to separate the oil and water phases, chemical demulsification is the most inexpensive and widely used technique to resolve crude oil emulsions. The demulsifiers are oil-soluble water-dispersible non-ionic polymeric

¹Current address: Lever Research, Inc., Edgewater, NJ 07020

(molecular weight 2,000-100,000) surfactants. They are added to the crude oil in very small (10-400 ppm) amounts. One of the most commonly used demulsifier is the oxyalkylated alkyl phenol formaldehyde resin, the alkyl group may be butyl, amyl or nonyl group. The interfacial activity is controlled by the amounts of ethylene and propylene oxides attached to the resin.

The major problem in demulsifying crude oil emulsions is the extreme sensitivity to demulsifier composition. There have been attempts (2, 3) to correlate demulsifier effectiveness with some of the physical properties governing emulsion stability. However, our understanding in this area is still limited. Consequently, demulsifier selection has been traditionally based on a 'trial and error' method with hundreds of chemicals in the field.

Our goal is to develop a property-performance relationship for different types of demulsifiers. The important interfacial properties governing water-in-oil emulsion stability are shear viscosity, dynamic tension and dilational elasticity. We have studied the relative importance of these parameters in demulsification. In this paper, some of the results of our study are presented. In particular, we have found that to be effective, a demulsifier must lower the dynamic interfacial tension gradient and its ability to do so depends on the rate of unclustering of the ethylene oxide groups at the oil-water interface.

Experimental Techniques

The oil-water dynamic interfacial tensions are measured by the pulsed drop (4) technique. The experimental equipment consists of a syringe pump to pump oil, with the demulsifier dissolved in it, through a capillary tip in a thermostated glass cell containing brine or water. The interfacial tension is calculated by measuring the pressure inside a small oil drop formed at the tip of the capillary. In this technique, the syringe pump is stopped at the maximum bubble pressure and the oil-water interface is allowed to expand rapidly till the oil comes out to form a small drop at the capillary tip. Because of the sudden expansion, the interface is initially at a nonequilibrium state. As it approaches equilibrium, the pressure, $\Delta P(t)$, inside the drop decays. The excess pressure is continuously measured by a sensitive pressure transducer. The dynamic tension at time t , is calculated from the 'Young-Laplace' equation

$$\Delta P(t) = \frac{2\sigma(t)}{R_d} \quad (1)$$

where R_d is the radius of the drop. The interfacial dilational modulus is then calculated by a Fourier Transformation of the transient interfacial tension data (see later).

The interfacial shear viscosities are measured by the deep channel viscous traction surface viscometer (5) at the Illinois Institute of Technology. The oil-water equilibrium tensions are measured by either the spinning drop or the du Nouy ring (6) method.

Electron Spin Resonances are measured at 9.5 GHz at room temperature. Demulsifiers are labeled by reacting the terminal OH groups with the spin-label 3-chloroformyl 2,2,5,5 tetramethyl pyrroline 1-oxy] (Figure 5a). This is done by the Schotten-Baumann reaction (7). The carboxylic form of the spin-label (obtained from Eastman Kodak Company) is dissolved in a benzene/pyridine mixture and is reacted, in situ, with thionyl chloride (also from Eastman Kodak Company). After 15 minutes, vacuum-dried demulsifier is added to the mixture. The solution is mixed and left overnight. All the reactions are carried under a nitrogen blanket. Excess benzene is then added and the insoluble part is eliminated. The tagged demulsifier is separated from the free label either by precipitating it with methanol or by size exclusion chromatography.

Results and Discussion

Interfacial Shear Viscosity

The demulsification process involves coalescence of smaller water droplets into larger ones. During this process, the oil in the liquid film between the droplets drains out, thereby thinning the film and finally rupturing it. The faster the film thins, the greater is the demulsification effectiveness. The liquid drainage rate depends, among other factors, on the interfacial shear viscosity. A high (>1 surface poise) interfacial shear viscosity significantly slows down the liquid drainage. Consequently, the emulsion is stable. But the reverse is not true. Emulsions have been found to be stable (8) even with a low interfacial viscosity.

Our results suggest that the lowering of interfacial shear viscosity, although necessary, is not a sufficient criterion for effective demulsification. In addition, a demulsifier must also rapidly dampen any fluctuations in the oil-water interfacial tension.

The demulsification data with four different demulsifiers for a crude oil-water system (Table I) support this conclusion. Structurally, the demulsifier P1 and R0 are of moderate (MW = 2,000-5,000) molecular weights, whereas P1 and P2 are large (MW >50,000) three dimensional structures.

The results show that although all the demulsifiers lower the shear viscosity, they differ widely in their demulsification effectiveness, as measured by the residual bottom sediment and water content (Figure 1) (BS and W%) of the dehydrated oil. For example, the demulsifier OPl, although it lowers both the equilibrium interfacial tension (Figure 2) and the shear viscosity (Table I), nevertheless is ineffective. This is because it takes a much longer time for the oil-water interfacial tension to reach equilibrium with OPl than with P1 or P2 (see later).

In general, there is no correlation between the tension and the shear viscosity of an oil-water interface. However, for systems containing demulsifiers, a low interfacial tension (IFT) often leads to a lowering of the shear viscosity. Demulsifiers, in general, are large disordered molecules and when they are present at the interface they create a mobile, low viscosity zone. However, a low IFT is not a necessary condition for a low viscosity interface. A large demulsifier such as P1, although not very surface active, can still lower the shear viscosity to a very low value (Table I).

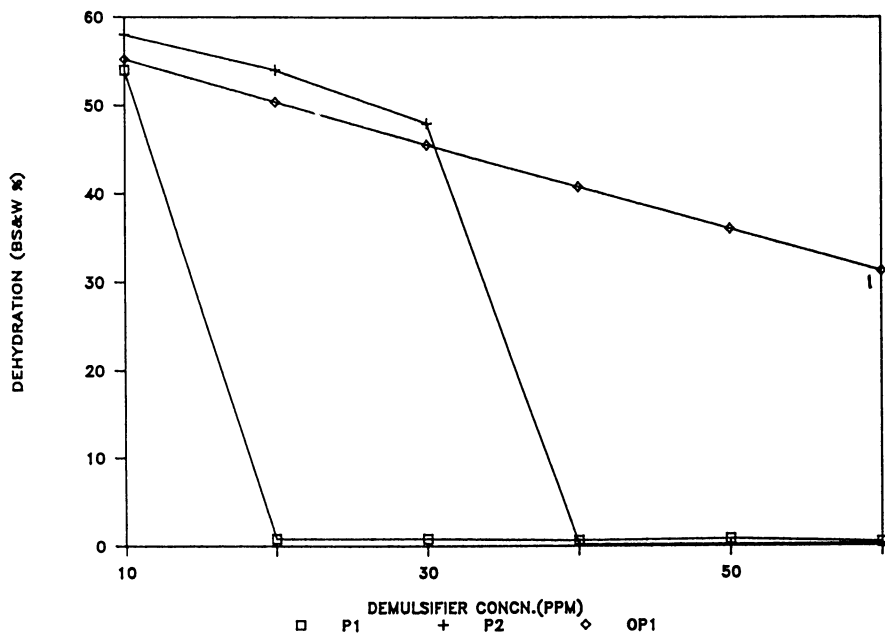


Figure 1: Residual water content of a brine-in-crude oil emulsion with the demulsifiers P1, P2 and OP1.

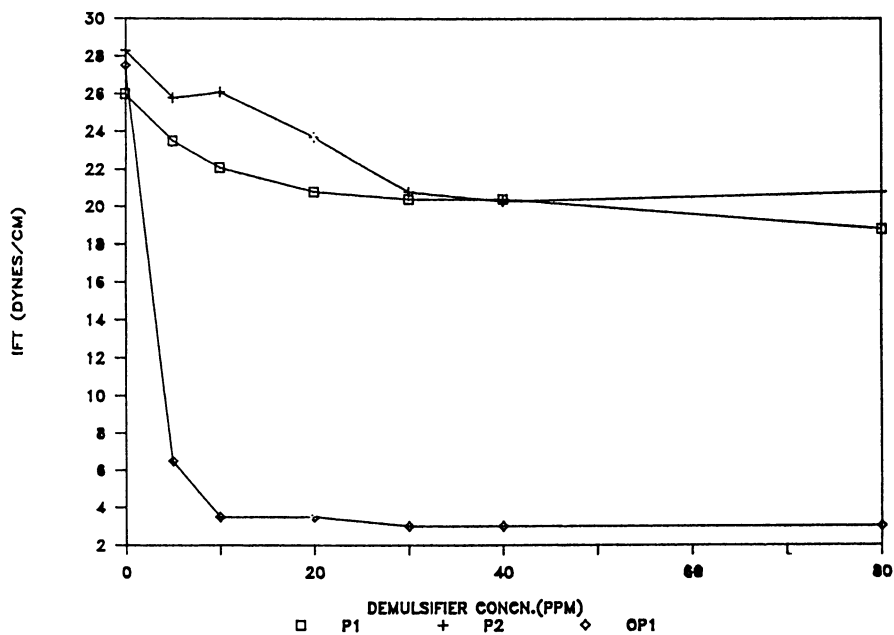


Figure 2: Interfacial tension of brine vs the crude oil with P1, P2 and OP1.

Table I. Comparison of Effectiveness and Interfacial Properties of Different Demulsifiers in a Crude Oil-Water System

Demulsifier	Concn. (ppm)	BS&W (vol%)	IFT (Dynes/cm)	Shear Viscosity (Surface Poise)
NONE	-	50	28	2.0×10^{-1}
R0	200	16	9	8×10^{-2}
P1	60	0.2	21	1×10^{-4}
P2	60	0.6	20	1×10^{-2}
OP1	40	50	4	1×10^{-2}

R0: Oxyalkylated nonyl phenol resin

P1: Oxyalkylated cross-linked polypropylene glycol

P2: Cross-linked polypropylene glycol

OP1: Oxyalkylated trimethylol propane

Dynamic Interfacial Tension Gradient

When the interfacial film between two droplets thins, the liquid in the film flows out towards the plateau border region. Such a flow removes some of the surfactants from the interface thus creating an uneven concentration of the surfactant along the interface (9, 10). Furthermore, the interfacial film often thins unevenly thus creating locally thin and thick regions (11). A local thinning implies an increase in the interfacial area and hence a decrease in the surfactant concentration. On the other hand, the surfactant concentration increases in the thick region. This nonuniform surfactant concentration at the interface leads to local variations in the interfacial tensions which produces a flow of liquid from the high to the low tension regions. This is known as the 'Gibbs-Marangoni' effect. This interfacial tension induced flow opposes the outward drainage in the film. It also helps to 'heal' the film to its original uniform thickness. The net result is a reduced rate of film thinning and consequently a more stable emulsion.

In order to be effective, a demulsifier has to reduce the 'Gibbs-Marangoni' resistive liquid flow. It does so by migrating from the interior to the interface, equalizing the interfacial surfactant concentration and bringing the interfacial tension of the film to its equilibrium value. As pointed out by Ross and Haak (12), if this process is faster than the surfactant migration induced flow along the interface, the local thin spots in the film are not 'healed' and the liquid drainage in the film continues unabated. Consequently, the drop coalescence rate is enhanced and the emulsion is rapidly destabilized.

The importance of rapid relaxation in demulsification effectiveness can be seen with the crude oil-water dynamic tension results with P2 (Figure 3) and OP1 (Figure 4). As can be seen, it takes only about 60 seconds for the interface to reach its equilibrium state with the effective demulsifier P2, whereas with less effective demulsifier OP1, the equilibrium is reached only after 800 seconds.

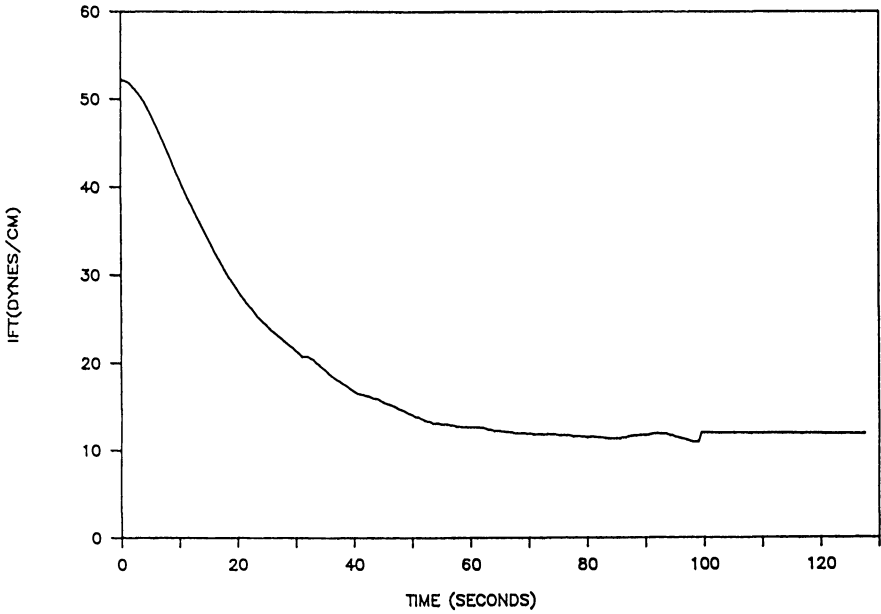


Figure 3: Dynamic interfacial tension of the crude oil-brine interface as a function of time, with 40 ppm P2.

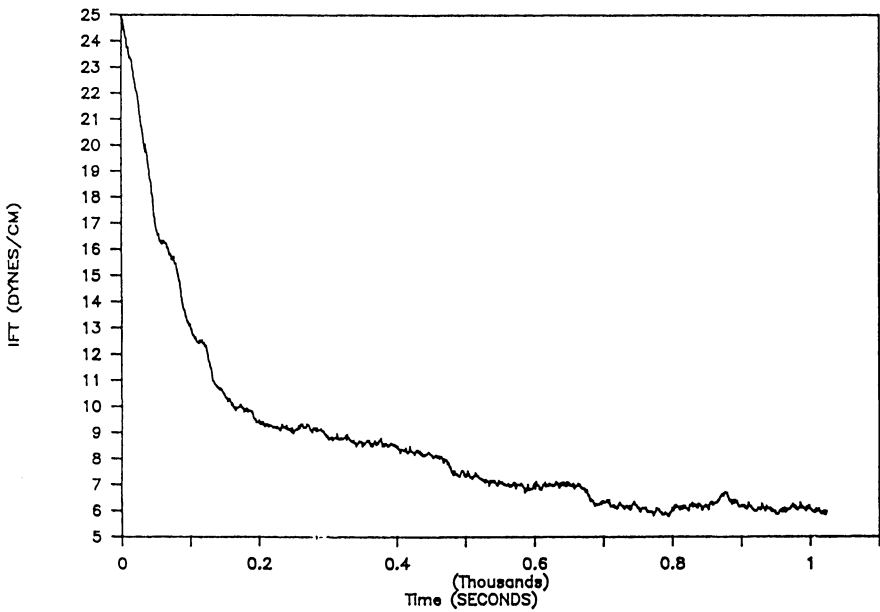


Figure 4: Dynamic interfacial tension of the crude oil-brine interface as a function of time, with 40 ppm OP1.

The time it takes for an oil-water interface to reach equilibrium depends strongly on the ethylene oxide content of the demulsifier molecule. The interfacial tension decay process can often be an order of magnitude longer than what is observed in systems where the surfactant diffusion from bulk to interface is the rate determining step. Demulsifiers form 'reverse-micelle' like structures in the bulk oil with the ethylene oxide groups clustering together to minimize their interactions with the oil phase. We believe, the unclustering of the ethylene oxide groups as well as rearrangement of the demulsifier molecules at the interface are the rate determining steps in the tension relaxation process. Similar interfacial tension behavior has been observed (13) with large oil-soluble water-insoluble surfactant such as Cholesterol.

Electron Spin Resonance

We have studied demulsifier association by the electron spin resonance (ESR) technique. The spin label is covalently attached (Figure 5a) to the demulsifier. Normally, the ESR spectrum of a freely tumbling nitroxyl radical consists of three sharp peaks (Figure 5b). However, the spectrum for a tagged ethoxylated nonyl phenol resin (Figure 6a or 6b) shows only a single broad peak.

The results may be explained in the following manner. The spin labels are attached next to the ethylene oxide groups. Clustering of the ethylene oxide groups brings the nitroxide radicals in close proximity with other. As the orbitals containing unpaired electron from different labels overlap, there is a spin exchange which leads to a single resonance peak. Similar exchange broadening has been observed (14) in lipid films in which spin probes are excluded to form aggregates. With stronger interaction, the single resonance peak narrows.

The ethylene oxide clustering depends on the polarity of the medium. The peak-to-trough separation gives an indication of the clustering strength. A smaller separation implies stronger clustering. We have found that in toluene (Figure 6a) the separation is 15 gauss whereas in isopropyl alcohol (Figure 6b) it increases to 25 gauss. This suggests a weaker clustering of the ethylene oxide groups with increasing polarity of the medium.

Interfacial Dilation Modulus

The complex interfacial dilational modulus (ϵ^*) is a key fundamental property governing foam and emulsion stability. It is defined as the interfacial tension increment ($d\sigma$) per unit fractional interfacial area change (dA/A) i.e.,

$$\epsilon^*(f) = \epsilon'(f) + i \epsilon''(f) = \frac{d\sigma}{(dA/A)} = \frac{d\sigma}{d \ln A} \quad (2)$$

where $\epsilon'(f)$ and $\epsilon''(f)$ are the real and the imaginary components at a frequency f . We have used a procedure (4), where the complete frequency spectrum is obtained by a Fourier Transform of the dynamic interfacial tension data. The relevant relationships are:

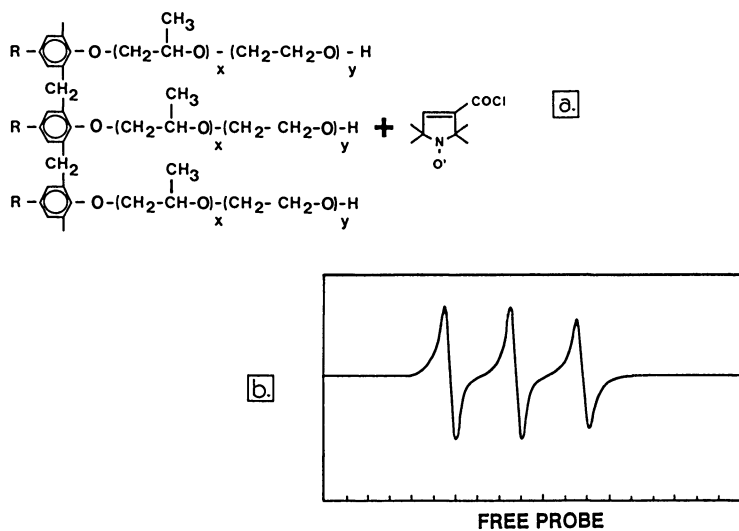


Figure 5: a) Chemical structure of a nonyl phenol resin and the spin label 3-chloroformyl 2,2,5,5 tetramethyl pyrroline 1-oxyl; b) ESR of a free label in toluene.

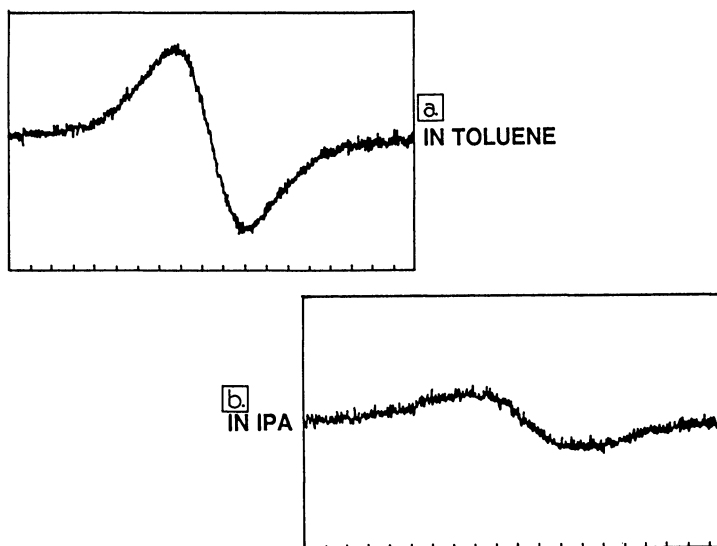


Figure 6: ESR of the labeled nonyl phenol resin in a) toluene and in b) isopropyl alcohol.

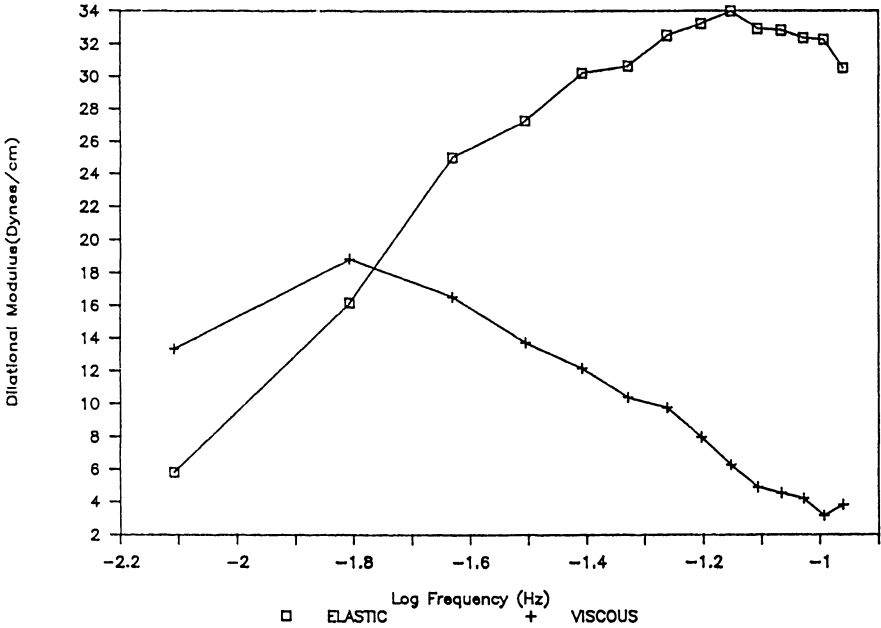


Figure 7: Elastic (in-phase) and viscous (out-of-phase) components of crude oil-brine interfacial dilational modulus with 40 ppm P2.

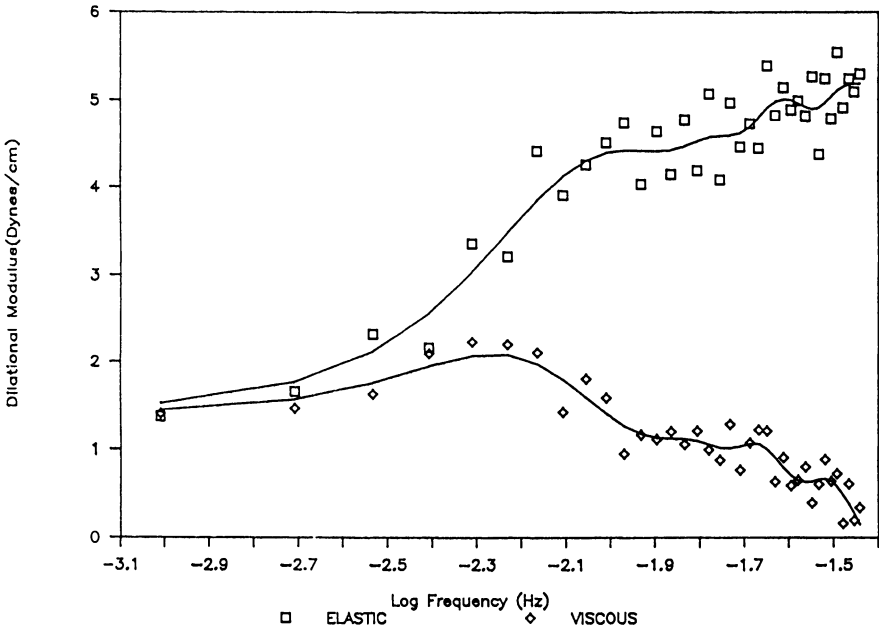


Figure 8: Elastic (in-phase) and viscous (out-of-phase) components of crude oil-brine interfacial dilational modulus with 40 ppm OP1.

$$\epsilon^*(f) = \frac{\int_0^{\infty} \Delta\sigma(t)e^{-2\pi ift} dt}{\int_0^{\infty} \Delta \ln A(t)e^{-2\pi ift} dt} \quad (3)$$

$$\epsilon'(f) = \frac{2\pi f}{\Delta \ln A} \text{ Im FT } (\Delta\sigma) \quad (4)$$

$$\epsilon''(f) = \frac{2\pi f}{\Delta \ln A} \text{ Real FT } (\Delta\sigma) \quad (5)$$

The real component, $\epsilon'(f)$, is the dilational elastic modulus (Figure 7). It is the interfacial tension gradient that is in phase with the area change. At a low frequency, the interfacial film behaves as a soluble monolayer. Interfacial concentration and the tension are then governed by the bulk concentration and so remain invariant to a change in area. On the other hand, at a very high frequency the interfacial film behave as a completely insoluble monolayer and the variation in interfacial tension resulting from a local change in area is virtually instantaneous.

The imaginary component, $\epsilon''(f)$, is the dilational viscosity modulus. This arises when the demulsifier in the monolayer is sufficiently soluble in the bulk liquid, so that the tension gradient created by an area compression/expansion can be short circuited by a transfer of demulsifiers to and from the surface. It is 90° out of phase with the area change.

The shape of the curves for the dilational modulus (Figures 7 and 8) suggests a single relaxation mechanism, probably the unfolding of the demulsifier molecules at the interface. The frequency peak in the $\epsilon''(f)$ plot is a measure of the characteristic relaxation time. A shorter relaxation time, by inducing faster film drainage, increases demulsification efficiency.

The dynamic response data for P1 and P2 (Figure 7) are similar. They are, however, quite different from that of OP1 (Figure 8). The characteristic relaxation times for P1 and P2 are 50 and 69 seconds respectively, whereas with OP1 it is 158 seconds. This indicates that with P1 and P2, the oil-water interface will have much shorter response time leading to an improved demulsification effectiveness.

Summary

For effective demulsification of a water-in-oil emulsion, both shear viscosity as well as dynamic tension gradient of the water-oil interface have to be lowered. The interfacial dilational modulus data indicate that the interfacial relaxation process occurs faster with an effective demulsifier. The electron spin resonance with labeled demulsifiers suggests that demulsifiers form clusters in the bulk oil. The unclustering and rearrangement of the demulsifier at the interface may affect the interfacial relaxation process.

Acknowledgment

The authors wish to thank the Exxon Chemical Company for permission to publish this paper. We thank Dr. Darsh T. Wasan and Mr. Chandrashekar Shetty at IIT, Chicago for measuring some of the interfacial shear viscosities. A special thanks to Ms. Layce Gebhard of Exxon Research and Engineering for measuring the ESR spectra. Finally, a special thanks to Ms. Rose Mary Rangel of Energy Chemicals (Exxon Chemical Company) for the preparation of the manuscript.

Literature Cited

1. Oren, J. J.; Mackay, D. M. Fuel. 1977, 56, 382.
2. Burger, P. D.; Hsu, C.; Arendele, J. P. SPE 16285, SPE International Symposium on Oilfield Chemistry. San Antonio, Texas. February 4-6, 1987; p 457.
3. Blair, C. M. Chem. Ind. 1960, 538.
4. Clint, J. H.; Neustadter, E. L.; Jones, T. J. Proc. 3rd. Eur. Symp. on Enhanced Oil Recovery, Bournemouth, U.K., 1981, p 135.
5. Wasan, D. T.; Gupta, L.; Vora, M. K. AIChE J. 1971, 17(6), 1287.
6. Adamson, A. W. Physical Chemistry of Surfaces, 3rd Ed.; J. Wiley and Sons.: New York, 1976; Chapter 1.
7. Tormala, P.; Lattila, H.; Lindberg, J. J. Polymer. 1973, 14, 481.
8. Neustadter, E. L.; Whittingham, K. P.; Graham, D. E. In Surface Phenomena in Enhanced Oil Recovery; Shah, D. O., Ed.; Plenum Press: New York, 1981; p 307.
9. Zapryanov, Z.; Malhotra, A. K.; Adrengi, N.; Wasan, D. T. Int. J. Multiphase Flow. 1983, 9, 105.
10. Ivanov, I. B.; Jain, R. K. In Dynamics and Instability of Fluid Interfaces; Sorensen, T. S. Ed.; Lecture Notes in Physics Series No. 105; Springer Verlag: Berlin, W. Germany, 1979; p 120.
11. Jain, R. K.; Ivanov, I. B.; Maldarelli, C.; Ruckenstein, E. Ibid; p 140.
12. Ross, S.; Haak, R. M. J. Phys. Chem. 1969, 73, 2828.
13. Van Hunsel, J.; Bleys, G.; Joos, P. J. Colloid Interface Sci. 1986, 114, 432.
14. Smith, I. C. P.; Butler, K. W. In Spin Labeling: Theory and Practice, Berliner, L. J., Ed.; Academic Press: New York, 1976; Vol. 1, p 423.

RECEIVED December 21, 1988

Chapter 20

Useful Surfactants from Polar Fractions of Petroleum and Shale Oil

Kazem M. Sadeghi, Mohammad-Ali Sadeghi, Dawood Momeni,
Wen Hui Wu,¹ and Teh Fu Yen

School of Engineering, University of Southern California, Los Angeles,
CA 90089-0231

Fossil fuel derived liquids from two different origins, shale oil and petroleum crude oil, were subjected to solvent fractionation through a silica gel column. The solvent system for fractions consisted of n-hexane, toluene, and toluene/methanol (for polar fractions). The polar fraction of the samples were subfractionated by ion exchange chromatography. The columns used were anion exchange resin, cation exchange resin, and clay-FeCl₃ to obtain the acid, base, and neutral fractions, respectively. The polarity increased for each column as more polar solvents were used. In order to compare surface activity of subfractions derived from shale oil and crude oil, the interfacial tension (IFT) of each subfraction was measured against aqueous solutions with different amounts of sodium silicate concentrations. It was proven that representative samples obtained from shale oil fractionation led to much lower interfacial tensions compared to the ones obtained with crude oil fractionation samples. It was also shown that the most polar fraction of the anion exchange column was from shale oil.

Surface active agents, more commonly known as “surfactants,” are the groups of chemical compounds that in the most common form constitute an ionic or polar portion (hydrophilic head) and a hydrocarbon portion (hydrophobic tail). The ionic or polar portion interacts strongly with the water via dipole-dipole or ion-dipole interactions and

¹Current address: Research Institute of Petroleum Processing, P.O. Box 914, Beijing, Peoples Republic of China

is solvated. On the other hand, the strong interactions between the water molecules arising from dispersion forces and hydrogen bonding of the chain act cooperatively to squeeze the hydrocarbon out of water. Furthermore, the hydrophobic moiety is a single or double hydrocarbon chain and the hydrophilic moiety is either an anionic, cationic, non-ionic or zwitterionic polar group (1). The unique property of surface active materials makes them able to react strongly at various interfaces (e.g., air-water, oil-water, water-solid, oil-solid, etc.) and to lower the interfacial surface energy. Surfactants in solution tend to accumulate and adsorb at interfaces between their solution and adjacent phases. The orientation of these molecules as well as molecular interaction and molecular packing result in an interfacial behavior different from that in bulk phases. The present state-of-the-art enhanced oil recovery processes reveals that of the potential oil reserves, about 60 percent are estimated to be compatible to chemical flooding with surfactants (2). The surfactant selection for a tertiary oil recovery process is made on the basis of ultralow interfacial tension between the oil and the aqueous phase. Melrose and Brander (3) and Taber (4) have shown that successful immiscible oil displacement depends on the existence of a very low interfacial tension, between the oil and water phases. A value of about 10^{-3} dyne/cm or less is required to mobilize the oil. It is shown that the recovery of residual oil from laboratory test cases is greatly improved for systems with ultra low interfacial tension (3). The achievement and maintenance of low interfacial tensions during chemical flooding therefore seems essential.

Numerous methodologies have been developed for separation of polar compounds from crude oils (5-7). Among these, the most well-known is the scheme developed by the Bureau of Mines in American Petroleum Institute Research Project 60 (5,6) which involves ion-exchange chromatographic and ferric chloride complexation techniques for removal of acids, bases, and neutral nitrogen compounds. However, this procedure is rather complex and tedious. The definition of acids or bases by ion-exchange methods is in terms of the hydrogen donating or accepting tendency of the molecule. Since many polar compounds are amphoteric, their definitions as acids or bases depend on the analytical sequence employed. Seifert et al. (8-10) have extracted acids from crude oil and showed that carboxylic acids are primarily responsible for the observed surface activity. Some long-chain acids in the crude oil, however, exist as natural esters, amides, and other acid-base complexes. The presence of these compounds in crude oil has been identified by many investigators including Snyder (11,12) and McKay et al. (13).

The current research objective is to evaluate the surface activity of the subfractions obtained from the solvent fractionated crude oil and shale oil samples as they are passed through the separation process developed for this work. The columns used are anion exchange resin,

cation exchange resin, and clay- FeCl_3 to obtain the acid, base, and neutral fractions, respectively. The clay- FeCl_3 complexation technique alone could specifically concentrate nitrogen and oxygen-containing compounds in shale oil. Although petroleum sulfonates (i.e., sodium salts of sulfonated crude oil) are known as main candidates in practical surfactant flood systems (14) they are usually very hard to structurally characterize and need to be combined with co-surfactants and blocking agents to enhance or protect the main surfactant. Besides having a broad range of molecular weights which make them more complex, their production is often cumbersome and very costly. The surface active compounds obtained from crude oil and especially from shale oil samples in this work, are shown to be very stable and produce very low interfacial tension in an alkaline system. Structural characterization studies of these compounds are also discussed.

Experimental

Sample. Petroleum crude oil sample from Long Beach Field (TUMS Well C-331, API° 20), California, and shale oil obtained by retorting at 500°C the Green River Oil Shale (Anvil Point Mine) were studied. About 20 g of shale oil was dissolved in 200 ml of THF and then filtered. The sample was recovered by a rotary evaporator. Although the same procedure was done on the other samples, the percent ash was different for each sample. All the samples were evaporated to a constant weight in a vacuum oven at 50°C.

Silica Gel Chromatography. The ratio of sample to absorbent was about 1:35. The columns were exhaustively eluted with n-hexane, toluene, 4:1 toluene/methanol, and 2:1 toluene/methanol volume ratios, to get Fractions I, II, III, and IV, respectively (Figure 1). Fraction III was then sub-fractionated further by ion exchange chromatography. In order to separate polar fractions from the samples, as discussed in detail in one of our works (Sadeghi, K.M.; Sadeghi, M.-A.; Wu, W.H.; Yen, T.F. *Fuel*, in press.), a column was slurry packed with the Baker analyzed reagent grade silica gel (60-200 mesh) in n-hexane and topped with a layer of sand before each experiment. Silica gel had neutral activity and was thermally activated before use.

Ion Exchange Chromatography. The polar oil (Fraction III) obtained from silica gel chromatography was mixed with cyclohexane. The slurry was then passed through an anion exchange resin column packed with Amberlyst A-27 (Aldrich Chemical Co.), a strongly basic, macroreticular resin. In order to obtain the acidic fractions from the anion exchange resin column, an eluting scheme based on the increasing polarity of the solvent system was employed. This scheme included the use of cyclohexane, toluene, a mixture of 3:2 toluene/methanol, and

a mixture of 3:2 toluene/methanol saturated with CO₂, for extraction into the four fractions. The one obtained from elution with cyclohexane was further fractionated by passing it through a cation exchange resin column packed with an Amberlyst 15 (Aldrich Chemical Co.), which is a macroreticular resin and strongly acidic in its nature. The solution obtained was exposed to the same elution scheme in the first stage with the exception of substituting the toluene methanol/CO₂ mixture with a mixture of 5.4:3.6:1.0 toluene/methanol/isopropylamine in the last phase. Three basic fractions resulted from these fractionations. A column packed with clay-FeCl₃ (Engelhard Minerals and Chemicals) was employed to further subfractionate the extracted sample obtained from cyclohexane eluting in the second stage. The solvent system used was cyclohexane and dichloromethane. The ratio of sample to absorbent was about 1:10 for the three absorbents used. Two neutral fractions were obtained at this last stage of separation process for each sample tested. The detailed flowchart of the separation procedure is shown in Figure 2.

Interfacial Tension (IFT) Measurements. All IFT measurements were done using a University of Texas Model 300 Spinning Drop Interfacial Tensiometer. The basic principle is to introduce a drop (about 2 $\mu\ell$) of an oil sample into a glass capillary tube (1.5 mm I.D., 78 mm long) filled with the aqueous medium. The tube is then spun about its main axis. The oil drop will elongate to a length determined by the IFT value of the system. Details of the theory and application can be found elsewhere (15,16). According to the equipment manufacturer, the formula used to calculate IFT value is:

$$\text{IFT (dyne/cm)} = [1.234(\Delta d)^3 \Delta \rho] / p^2$$

where

Δd = the thickness of the elongated oil drop in cm;

$\Delta \rho$ = density difference between the oil and the aqueous phase in gm/ml;

p = period of spinning in seconds.

RESULTS AND DISCUSSION

The weight percentage breakdown of fractions and subfractions obtained from fractionation of both the crude oil and shale oil samples are shown in Figure 3 and 4, respectively. The percentage recoveries of Fraction III from the crude oil and shale oil samples were 16.5% and 24.1%, respectively. To investigate the interfacial activity of these subfractions upon reaction with alkali, IFT measurements were carried out with a 1% solution of each fraction in toluene against aqueous

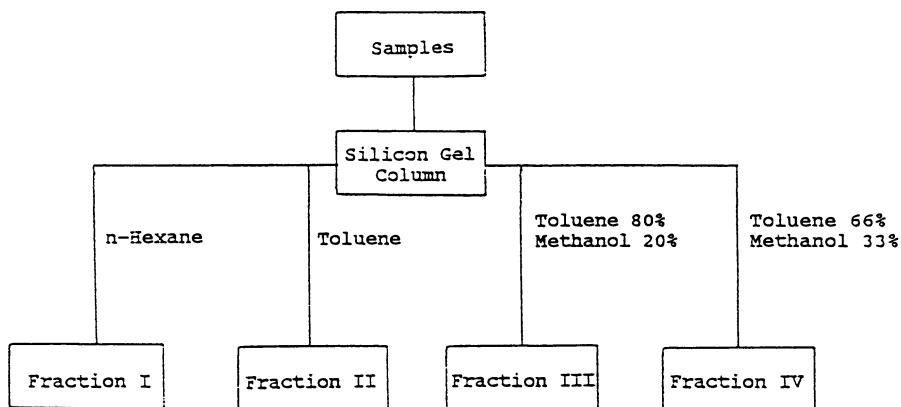


Figure 1. Solvent Fractionation Scheme Using Silicon Gel Column for Crude Oil and Shale Oil.

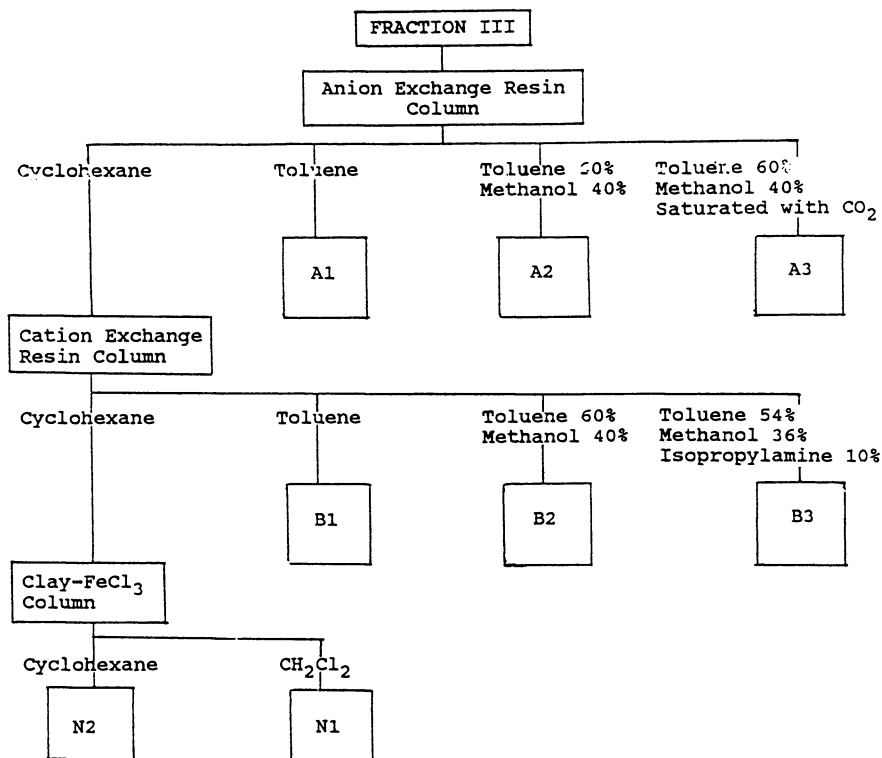


Figure 2. Separation of Fraction III (see Figure 1) to Subfractions by Ion Exchange Chromatography (A = Acid, B = Base, and N = Neutral Fractions).

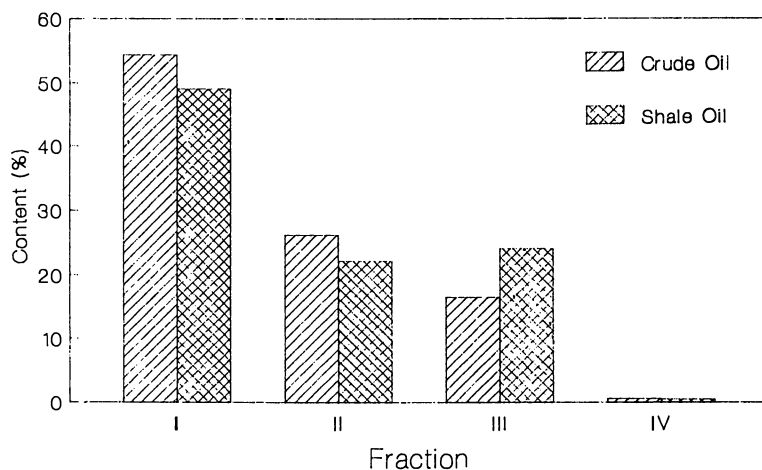


Figure 3. Content of Fractions of Crude Oil and Shale Oil by Silicon Gel Column.

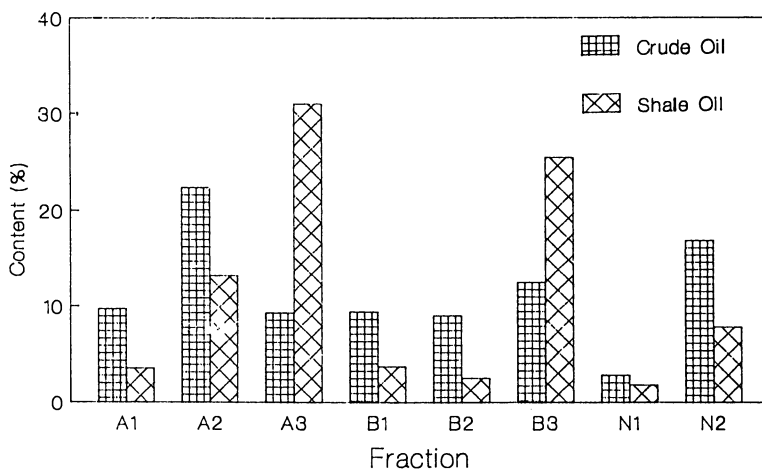


Figure 4. Content of Subfractions of Crude Oil and Shale Oil by Ion Exchange Chromatography (A = Acid, B = Base, and N = Neutral Fractions).

solutions of different sodium silicate contents. The results of these investigations are shown in Figures 5 through 7. As these results clearly indicate, the fractions show considerable interfacial activity under alkaline conditions. The separated shale oil fractions result in lower IFT values compared to the ones obtained from crude oil fractions. The lowest IFT and therefore highest surface activity is achieved for fraction A3 separated from shale oil with the lowest concentration of sodium silicate in the aqueous solution. This is very significant when considering that this fraction (A3) has the highest yield of recovery (31% of Fraction III, equal to 7.4% of the original shale oil sample) among the others separated from both the crude oil and shale oil samples. It is interesting to note that the same conditions were applied to crude oil; and the fraction A3 obtained from this sample exhibits a low value of IFT but it is more than 40 times higher than the one separated from the shale oil. The highest yield in this category, however, belongs to the fraction eluted from the anion exchange resin column with the toluene/methanol solvent system. Although many studies have been done in the past (17-20) to explain the interaction of alkali and acids in the oil for the lowering of IFT, the results of this study do not imply a direct relationship between acidity of the fraction and its surface activity. Jang et al. (21) reported that non-reactive, naturally occurring esters, amides and acid-base complexes were present in sufficient quantities when fractions of crude oil were isolated and characterized.

The results of experiments with crude oil fractions in this study also suggest that several species were present in reaction interface. There are mainly long chain carboxylic acids. The difference in size and structure is expected to give them different pka values. As a result, different surface activity (i.e., IFT value) is obtained with different levels of alkali concentration. Crude oil fractions with lower surface activity only yield surface inactive salts that may appear as precipitates at the interface.

The highest surface activity of fraction A3 extracted from shale oil needs to be explored in detail in order to understand this very unique phenomena. The benchmark experiments performed by Lee et al. (22) in studies of dissociation phenomena of Stuart oil shale in an alkaline environment proved the formation of carboxylic acids as it was verified from GC results. In another study by Lee et al. (23), it was shown that the hydroxyl ions from an alkaline solution could decompose the silicate and aluminasilicate structures in oil shale samples, provided that ultrasonic radiation and electrolytic current were simultaneously applied.

A hypothetical structural model developed by Yen (24) represented the organic components of Green River oil shale. The major components were isoprenoids, steroids, terpenoids and cartenoids. The common bridges consisted of disulfide, ether, ester, heterocyclic and alkadiene. Elemental analysis of typical oil shale samples has shown

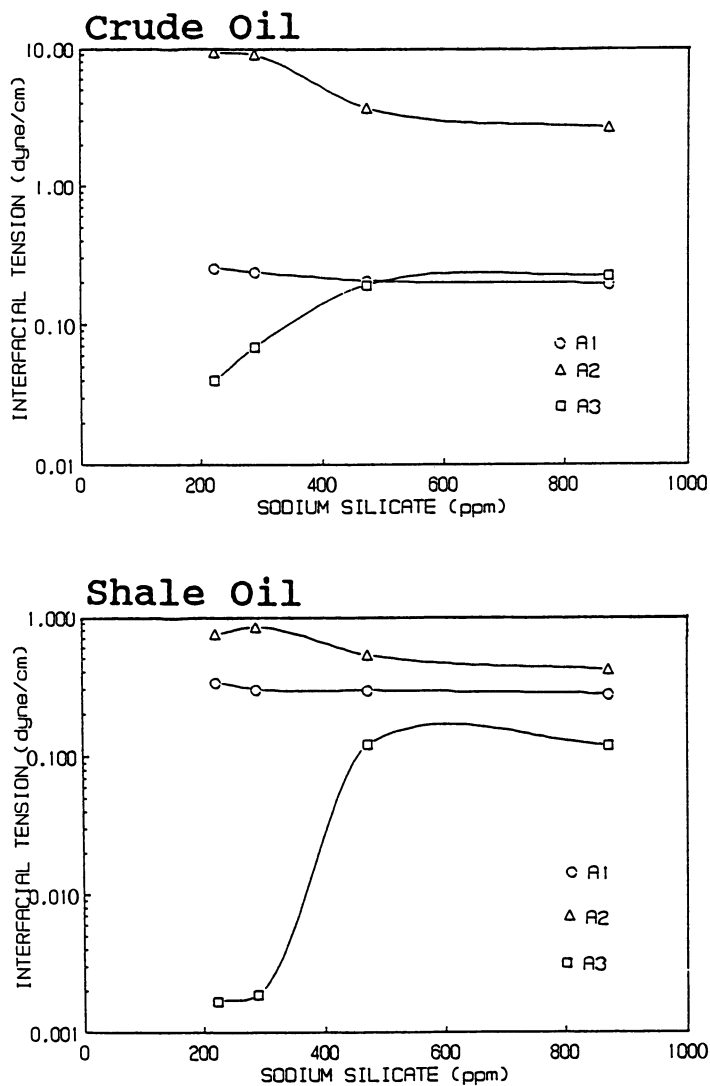


Figure 5. Interfacial Tension versus Alkali Concentrations for the Acid (A1 to A3) Fractions of Crude Oil and Shale Oil.

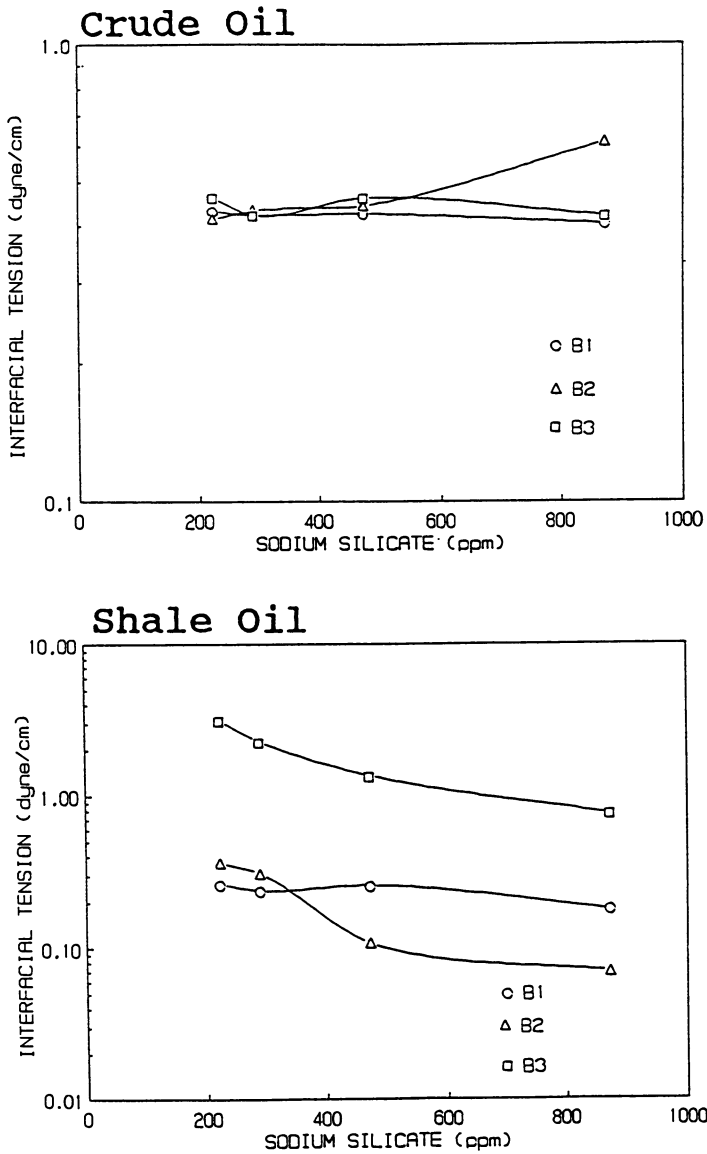


Figure 6. Interfacial Tension versus Alkali Concentrations for the Base (B1 to B3) Fractions of Crude Oil and Shale Oil.

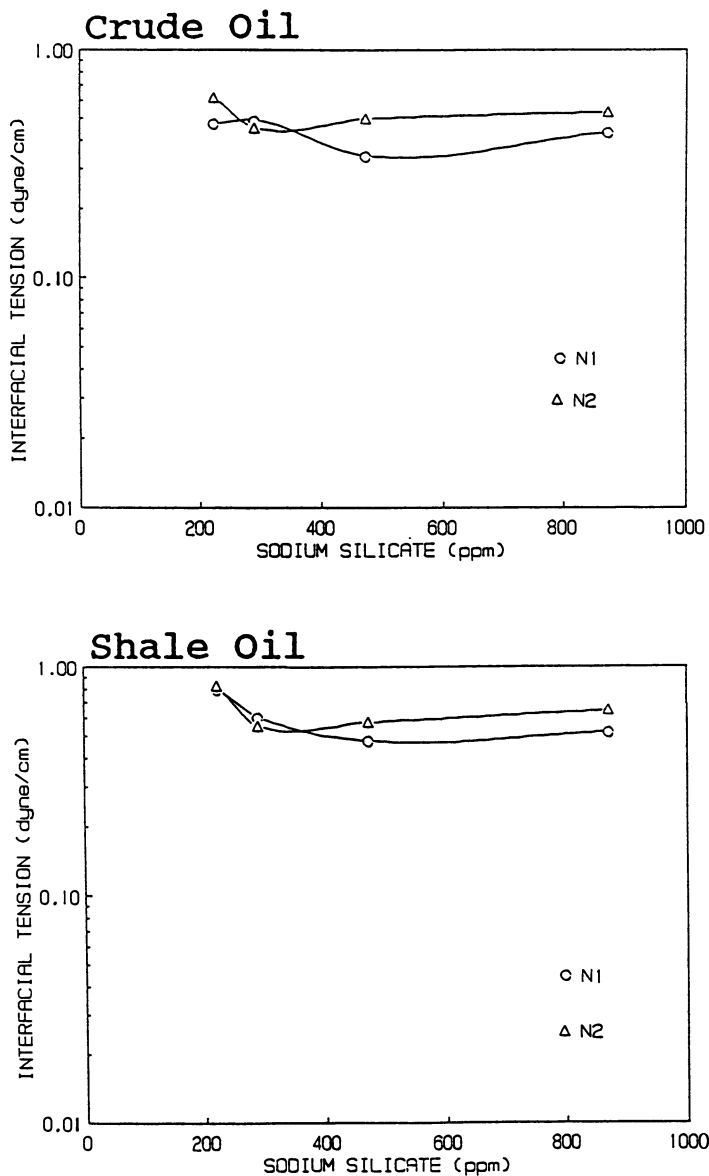


Figure 7. Interfacial Tension versus Alkali Concentrations for the Neutral (N1 and N2) Fractions of Crude Oil and Shale Oil.

that they are very rich in nitrogen compounds (30-84%). Poulson and co-workers (25) reported that pyridines and pyrroles were the two major types of nitrogen compounds in shale oil. Cyclic amides and anilides were proposed as possible additional types of nitrogen compounds in shale oil (26). The concentrating of the nitrogen-containing compounds in shale oil and related fossil fuels by clay- FeCl_3 complexation chromatography techniques was reported previously by Yen et al. (27,28). Based on these studies and our research in progress, we expect that enriched nitrogen compounds in oil shale could facilitate the acid extraction, mainly carboxylic acids, and subsequently increase the surface activity of the acid fraction (A3) extracted from the shale oil sample. A hypothetical model is proposed (Figure 8) to show the association of molecules at the oil-water interface. It is postulated that the surfactant molecules will be oriented in such a way that each molecule lies on the oil side of the interface and each nitrogen compound lies on the aqueous side. When the interfacial tension falls in the alkaline environment the surface pressure increases and the hydrocarbon chains of the surfactant molecules are prevented from moving close together because of the width of the nitrogen compounds. More research work is essential to structurally characterize this surfactant, but these results would clearly indicate that methods are to be developed to aid in the in-situ generation of bio-surfactants in oil shale processing which could significantly reduce the interfacial tension and lead to the ultimate recovery of shale oil.

CONCLUSION

Surface active compounds were extracted from both the crude oil and shale oil samples through a separation scheme developed for this work. These substances could effectively decrease interfacial tension between them and aqueous alkaline phase one hundred thousand fold (Figure 5). The surface activity of fractions derived from shale oil samples were much higher than the ones obtained from crude oil. The abundance of nitrogen compounds in shale oil samples was considered to be the main reason for reducing the interfacial tension to its lowest value. A hypothetical model was developed to describe the interfacial activity of the acidic fraction derived from shale oil. Experiments with this fraction led to the lowest IFT value compared to the other fractions. Since the lowering of interfacial tension is the first major step in enhancement of heavy oil recovery from both the shale oil and petroleum reservoir, it is strongly believed that application of those such surfactants, with their low cost and high stability, could lead to optimum recovery of residue oils from these reservoirs in an alkaline environment. Employment of such new methods as proposed by Lee et al. (22) ultrasonic radiation and electrolytic dissociation processes,

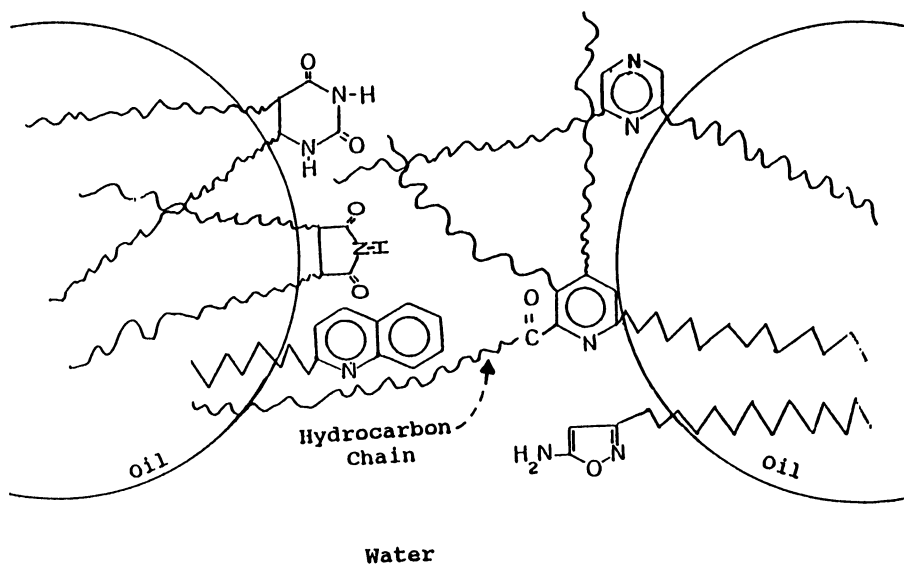


Figure 8. A Hypothetical Model of Shale Oil at the Oil-Water Interface.

could further enhance the generation of these surfactants and lead to the ultimate reserves recovery.

ACKNOWLEDGMENTS

The authors thank Western Extraction Technology, Inc. and EER Labs, Inc. for their partial financial support. We also would like to thank Dr. H. L. Wong and Mr. Leon Lemons for the preparation of this manuscript.

LITERATURE CITED

1. Schwartz, A.M.; Perry, J.W. *Surface Active Agents, Their Chemistry and Technology*; Inter-Science Publishers, Inc.: New York, 1949.
2. Geffen, T.M. "Here's What's Needed to Get Tertiary Recovery Going," *World Oil* 1975, March, 53.
3. Melrose, J.C.; Brandner, C.F. "Role of Capillary Forces in Determining Microscopic Displacement Efficiency for Oil-Recovery by Water Flooding," *J. Canadian Petrol. Tech.* 1974, 13(1), 13.
4. Taber, J.J. "Dynamic and Static Forces Required to Remove a Discontinuous Oil Phase from Porous Media Containing Both Oil and Water," *Soc. Petrol. Eng. J.* 1969, 9(1), 3.
5. Jewell, D.M.; Weber, J.H.; Bunger, J.W.; Plancher, H.; Latham, D.R. "Ion-Exchange, Coordination and Adsorption Chromatographic Separation of Heavy-End Petroleum Distillates," *Anal. Chem.* 1972, 44, 1391.
6. Hirsch, D.E.; Hopkins, R.C.; Coleman, H.J.; Cotton, F.O.; Thompson, C.J. "Separation of High-Boiling Petroleum Distillates Using Gradient Elution Through Dual-Packed (Silica Gel-Alumina Gel) Adsorption Columns," *Anal. Chem.* 1972, 44, 915.
7. Suatoni, J.C.; Swab, R.E. "Preparative Hydrocarbon Compound Type Analysis by High Performance Liquid Chromatography," *J. Chromatogr. Sci.* 1976, 14, 535.
8. Seifert, W.K.; Howells, W.G. "Interfacially Active Acids in a California Crude Oil," *Anal. Chem.* 1969, 41, 554.
9. Seifert, W.K. "Effect of Phenols on the Interfacial Activity of Crude Oil (California) Carboxylic Acids and the Identification of Carbazoles and Indoles," *Anal. Chem.* 1969, 41, 562.
10. Seifert, W.K.; Teeter, R.M. "Preparative Thin-layer Chromatography and High Resolution Mass Spectrometry of Crude Oil Carboxylic Acids," *Anal. Chem.* 1969, 41, 786.
11. Snyder, L.R. "Nitrogen and Oxygen Compound Types in Petroleum. Total Analysis of a 400-700°F Distillate from a California Crude Oil," *Anal. Chem.* 1969, 41, 314.

12. Snyder, L.R. "Nitrogen and Oxygen Compound Types in Petroleum. Total Analysis of an 850-1000°F Distillate from a California Crude Oil," *Anal. Chem.* 1969, **41**, 1084.
13. McKay, J.F.; Cogswell, T.E.; Latham, D.R. "Analytical Methods for the Analysis of Acids in High-Boiling Petroleum Distillates," *Prepr., Am. Chem. Soc., Div. Pet. Chem.*, 1974, **19**, 25.
14. Shah, D.O.; Schechter, R.S., Eds. *Improved Oil Recovery by Surfactant and Polymer Flooding*; Academic Press, Inc.: New York 1977.
15. Cayias, J.L.; Schechter, R.S.; Wade, N.H. *Adsorption at Interfaces*, ACS Symp. Series No. 8, 1975, 234.
16. Chan, M. "Interfacial Activity in Alkaline Flooding Enhanced Oil Recovery," Ph.D. Thesis, USC, Los Angeles, 1980.
17. Dunning, H.N.; Moore, J.W.; Denekas, M.O. "Interfacial Activities and Porphyrin Contents of Petroleum Extracts," *Ind. Eng. Chem.* 1953, **45**, 1759.
18. Bansal, V.K.; Chan, K.S.; McCallough, R.; Shah, D.O. "The Effect of Caustic Concentration on Interfacial Charge, Interfacial Tension and Droplet Size: A Simple Test for Optimum Caustic Concentration for Crude Oils," *J. Canadian Petrol. Tech.* 1978, **17(1)**, 69.
19. Chan, M.; Sharma, M.M.; Yen, T.F. "Generation of Surface Active Acids in Crude Oil for Caustic Flooding Enhanced Oil Recovery," *I & EC Process Des. Dev.* 1982, **21**, 580.
20. Chan, M.; Yen, T.F. "A Chemical Equilibrium Model for Interfacial Activity of Crude Oil in Aqueous Alkaline Solution: The Effects of pH, Alkali and Salt," *Canadian J. Chem. Eng.* 1982, **60**, 305.
21. Jang, L.K.; Sharma, M.M.; Chang, Y.I.; Chan, M.; Yen, T.F. "Correlation of Petroleum Component Properties for Caustic Flooding," In *Interfacial Phenomena in Enhanced Oil Recovery*; Wasan, D., Payatakes, A., Eds.; AIChE Symposium Series No. 212, 1982, **78**, 97.
22. Lee, A.S.; Sadeghi, M.-A.; Yen, T.F. "Characterization of the Stuart Oil Shale System. 1. New Method of Releasing Organic Matter," *Energy & Fuels* 1988, **2**, 88.
23. Lee, A.S.; Lian, H.J.; Yen, T.F. "Dissociation of Organic and Mineral Matrix of Maoming Oil Shale at Low-Temperature and Ambient-Atmosphere," *Proc. Int. Conf. on Oil Shale and Shale Oil*, May 16-19, 1988, Chemical Industry Press, Beijing, China, 112.
24. Yen, T.F. "Structural Investigations on Green River Oil Shale Kero-gen," In *Science and Technology of Oil Shale*; Yen, T.F., Ed.; Ann Arbor Science, Michigan, 1976, 193.
25. Poulson, R.E.; Frost, C.M.; Jensen, H.B. "Characteristics of Synthetic Crude from Crude Shale Oil Produced by In-situ Combustion Retorting," In *Shale Oil, Tar Sands, and Related Fuel Sources*; Yen, T.F., Ed; ACS Adv. Chem. Ser. No. 151, 1976, 1.

26. Poulson, R.E.; Jensen, H.B.; Cook, G.L. "Nitrogen Bases in a Shale-Oil Light Distillate," *Prepr., Am. Chem. Soc. Div. Pet. Chem.*, 1971, *16(1)*, A49.
27. Yen, T.F.; Shue, F.F.; Wu, W.H.; Tzeng, D. "Ferric Chloride-Clay Complexation Method. Removal of Nitrogen-Containing Components from Shale Oil and Related Fossil Fuels," In *Geochemistry and Chemistry of Oil Shales*; Miknis, F.P., McKay, J.F., Eds.; ACS Adv. Sym. Ser. No. 230; 1983, 457.
28. Shue, F.F.; Yen, T.F. "Concentration and Selective Identification of Nitrogen- and Oxygen-Containing Compounds in Shale Oil," *Anal. Chem.* 1981, *53*, 2081.

RECEIVED January 26, 1989

Chapter 21

Microscopic Studies of Surfactant Vesicles Formed During Tar Sand Recovery

Mohammad-Ali Sadeghi, Kazem M. Sadeghi, Dawood Momeni,
and Teh Fu Yen

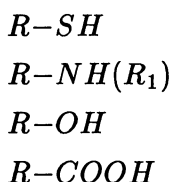
School of Engineering, University of Southern California, Los Angeles,
CA 90089-0231

By applying ultrasonic energy and using an alkaline solution, self-propagating surfactants are formed. The principle of membrane-mimetic chemistry via the process mechanism is being explored in this work by the thorough examination of the photomicrographs. Giant-sized multilamellar surfactant vesicles are analyzed under both transmittance and reflectance light during their initial formation and, after a few hours, four months, and three years following the completion of the process. From these studies, the optimum time period needed for the vesicles to stabilize is determined. The vesicles are proven to be very stable under the slow reaction condition of six-hour process time. With free radical initiator added (e.g., H_2O_2), the reaction takes minutes to complete. Based on the surfactant vesicles characterization derived from current investigations, it is suggested that these surfactants could retain their effectiveness necessary for bitumen recovery in the reservoir environment for a number of years.

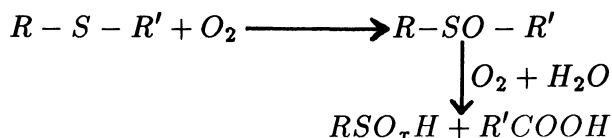
Tar sands, also called bituminous sands or oil sands, are essentially siliceous materials such as sands, sandstones or diatomaceous earth deposits impregnated with 5 to 20 percent by weight of a dense, viscous, low gravity bitumen. Deposits of tar sands exist and are widely distributed throughout the world. Wen et al. (1) pointed out that bitumens, increasing in the order of the size and complexities, consist of the following fractions: (1) gas oil, (2) resin, (3) asphaltene, (4) carbene, and (5) carboid. The chemical and physical properties of tar sands depend significantly on the relative amounts of each fraction and their properties. The values of molecular weight, number of condensed aromatic rings, number of heteroatoms (N, O, S) and concentration of

metals (V, Ni, Ti, etc.) all generally increase from the gas oil fraction to the preasphaltene fraction (carbene and carboid). Generally, there are three types of hydrocarbons present in bitumens; paraffinic, naphthenic, and aromatic, although many of the molecules are combinations of the three types, especially the heavier fractions.

Self-generated surfactants (produced from fossil fuels by a chemical/physical process) or natural surfactants (existing in fossil fuels) are derived from the inherent organic acids and replaceable acidic protons which are present in crude oils or bitumens (e.g., mercaptans). Yen and Farmanian (2) isolated native petroleum fractions that form surfactants and contain hydrogen displacable components including one, two, three, or four of the following types:



in which R is a hydrocarbon of 3 to 20 carbon atoms, R_1 is hydrogen or a hydrocarbon of 3 to 20 carbon atoms, and R and R_1 are either separate or cyclically combined. These acids, when coming into contact with alkaline solutions, yield in-situ surface active materials or self-generated surfactants of various forms of liquid crystals (e.g., giant micelles, large vesicles, etc.). These self-generated surfactants reduce the interfacial tension between the crude oil hydrocarbon and water. In the tar sand production processes in operation in Alberta, Canada, caustic additives (e.g., NaOH) are used to improve recovery rates by about 15%. Bowman (3) isolated some of the dissolved organics by foam fractionation techniques and showed that the materials were surfactants. A similar discovery was found by Ali (4), where a tentative mechanism was given as the following:



($x = 2$ or 3 ; sulphenic or sulphonic acids). He concluded from infrared studies that the two functional groups of carboxylic acids and sulphonic acids were on the same molecule, in other words, that the parent sulphide was a cyclic one. The study on the reactions initiated by ultrasonic energy in the U.S.A. dates back to 1927, which is about the same period for the research on the reaction initiated by

ionizing radiation (5). The mechanisms, responsible for the observed increases in rates in transport and unit operation processes utilizing ultrasonic energy, can be divided into two categories; (1) First-order effects of fluid particles (acceleration, displacement, and velocity) and (2) Second-order phenomena (cavitation, radiation pressure, acoustic streaming, and interfacial instabilities). Mostly, it is one or more of the second-order effects which are responsible for the enhancements in the transport process (6). The use of ultrasonic energy in conjunction with self-generated surfactants to recover bitumen from tar sand is a new extraction technique having a 95% recovery and reaction times that are in minutes (7,8). Chan et al. (9,10) proposed a simple equilibrium chemical model for the surface reaction at heavy crude oil-caustic interfaces. Each acid species dissociates at certain pH value, referred to as the onset pH or pK_a value, and yields the surface active anion. The dissociation constant of each species depends on its molecular size and structure. For crude oil, being such a complex mixture of organic acids, the pK_a values range from 8 to 11 (11). Some other components in crude oil besides fatty acids have been reported as being interfacially active (12,13). It was reported that compounds of zinc, copper, nickel, titanium, calcium, and magnesium were found to be adsorbed selectively to crude oil-water interfaces. All these metals occur in petroleum as porphyrin-metal chelates, or other types of complexes or even possibly form non-nitrogen binding complexes. The interfacial films were thought to consist of waxes and resins with stabilizing porphyrin-metal complexes, free porphyrins, porphyrin oxidation products and protein-metal salts or complexes.

The concept of differing pK_a values for the different acidic species has been used to suggest a method of enhancement for generation of self-propagating surfactants formed during the bitumen extraction process (Yen, T.F., USC, Unpublished data). By the application of ultrasonic energy and using an alkaline solution, self-propagating surfactant vesicles are formed from the natural surfactant vesicles which have onion-like multicompartiment structures. Prolonged ultrasonication of these results in the formation of submicroscopic spheroidal vesicles consisting usually of a fairly uniformed single-compartment bilayer surfactant vesicle surrounding a solvent core (14). The reaction can be reversible. Many unilamellar vesicles can coalesce together and form a giant multilamellar vesicle in which the liquid-crystal feature can be observed in microscopic range using a polarized light source and analyzer. To verify the existence of self-generated surfactants during tar sand recovery process and to analyze their structural behavior, the vesicles are studied in this work under transmittance and reflectance light of the microscope. The principles of membranemimetic chemistry are employed to describe the process phenomena. The vesicles' stability for a prolonged period of time is carefully studied and the duration for these surfactants which can withstand the severity of the

reservoir environmental conditions to effectively enhance the bitumen recovery efficiency from tar sand deposits is evaluated.

EXPERIMENTAL

Tar sand samples mined from Athabasca, in Alberta, Canada, were High Grade Athabasca Tar Sand, Sample No. 1981HG. The bitumen present in the tar sand was 14.5% by weight as determined by Soxhlet extraction (15). A quantity of 100 grams of tar sands was added to a 800 ml of alkaline solution (20:1 by volume distilled water to sodium silicate) and sonicated for several hours until all the bitumen had dissipated in the solution (sand was bitumen-free). The sodium silicate reagent (Na_2SiO_3) was BJ-120 (wt. ratio $SiO_2/Na_2O = 1.80$) from the PQ Corporation, Huntington Beach, CA. A 10-gallon transducerized tank (Branson Model ATH610-6) and a companion generator (Branson Model EMA 0-6) having six piezo-electric transducers with a 40 kHz frequency was used. We have reported the detailed experimental procedures in previous publications (7,8,15,16). As reported before (8), the reaction takes minutes to recover bitumen with the aid of radicals (e.g., hydrogen peroxide, benzoyl peroxide). The slow reaction kinetics (no radicals added) were used to isolate the micelles formed during the process, for analysis under the microscope.

The surfactants formed in the tar sand recovery were examined using light microscopic techniques. A representative sample was pipeted during sonication and immediately taken for observation under a Leitz SM-Lux-Pol Cross Polarizing Microscope. One drop of each sample to be examined was placed over a clean glass slide and restrained with a cover lid. Photomicrographs were then taken (equipped with a high speed camera and color film using WILD MP515 Semiphomat) of both reflection polarized light and transmittance of the incident light upon the sample. Air tight amber vials were used to store the processed solution for the given durations of twelve hours, four months and three years, before examining the surfactants under the microscope.

RESULTS AND DISCUSSION

The heavy-end portions (usually called heavy fractions) of bitumen (e.g. asphaltenes, preasphaltenes) can exist both in a random oriented particle aggregate form or in an ordered micelle form, peptized with resin molecules (16,17). In their natural state, asphaltenes exists in an oil-external (Winsor's terminology) or reversed micelle. The polar groups are oriented toward the center, which can be water, silica (or clay), or metals (V, Ni, Fe, etc.). The driving force of the polar groups

assembled toward the center originates from either hydrogen-bonding, or charge transfer, or even acid-base salt formation.

In crude oil, asphaltene micelles are present as a discrete or colloiddally dispersed particles in the oily phase. As the various intermediate and low boiling fractions are removed during the distilling or evaporation process, the particles of asphaltene micelles are massed together to form the larger colloidal sizes (Yen, T. F., "Asphaltic Materials," *Encyclopedia of Polymer Science & Engineering*, 2nd Ed., John Wiley, in press). The so-called precipitation or aggregation processes are colloidal in nature (Figure 1). Single sheet, usually the pi-system with saturated substitutes, is associated into stacks or piles of 4-5 layers. These "stacks" are commonly referred to as "asphaltenes", which are precursors of micelles (18,19) (either reverse, random-oriented or normal) and the supermicelle. The accompanied transformation of liquid crystal-gel stage or the floc stage is widely observed in industrial practices. Actually, investigators have isolated supermicelles, particles, flocs, etc. and performed many experimental determinations, including molecular weights which range from a few thousand up to hundreds of millions. They all attribute this discrepancy to "asphaltene", which may be misleading for other investigators. One knows for certain that the single sheet of asphaltene is under 1000 in molecular weight. Often people believe this is the controversy of Yen's model (20) of asphaltene, yet clearly all findings, including the most recent ones (21,22), can always be interpreted by that simple model.

It is essential to state that the heavy fractions such as asphaltene and preasphaltene do contain large numbers of polar molecules (23,24). These polar molecules behave exactly as surfactants or amphiphiles (asphaltene usually contains a long-chain substituent (25)). We again have to emphasize that it is almost not possible to create a colloidal micelle from pure hydrocarbon and water without any surfactant. Hence, we conclude to say that asphaltene or asphaltene-like molecules (asphatics) will participate in a manner according to membrane-mimetic chemistry.

Surfactant molecules can be considered as building blocks for certain forms of geometry in colloidal chemistry. Various forms of association molecules can be obtained as the concentration of surfactant in water is increased and/or physicochemical conditions are changed (e.g. CMC, Craft-point, etc.). Figure 2 schematically shows the most likely structural configurations and assemblages of surfactants association in an aqueous system (26). Upon addition of oil and a short-chain alcohol, for example, one can convert the oil-in-water micelles into water-in-oil microemulsions. It is therefore possible to induce a transition from one structure to another by changing the physicochemical conditions such as temperature, pH and addition of mono or di-valent cations to the surfactant solution. It should be also noted that the sur-

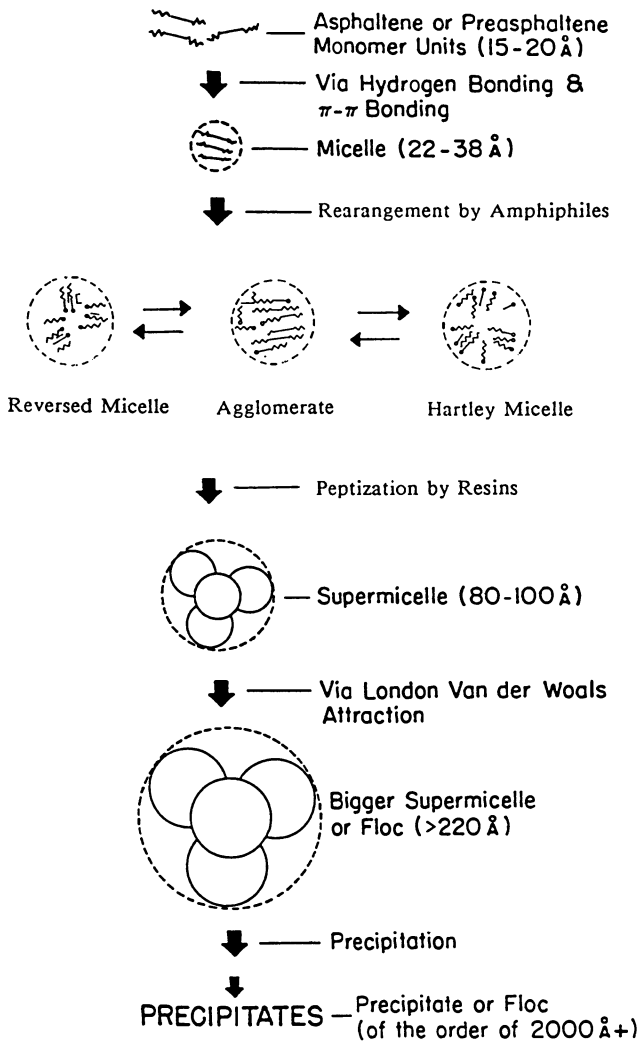


Figure 1. Asphaltic substances in different stages of a process. The size and weight depend on the environment [modified from Ref. 27 and others].

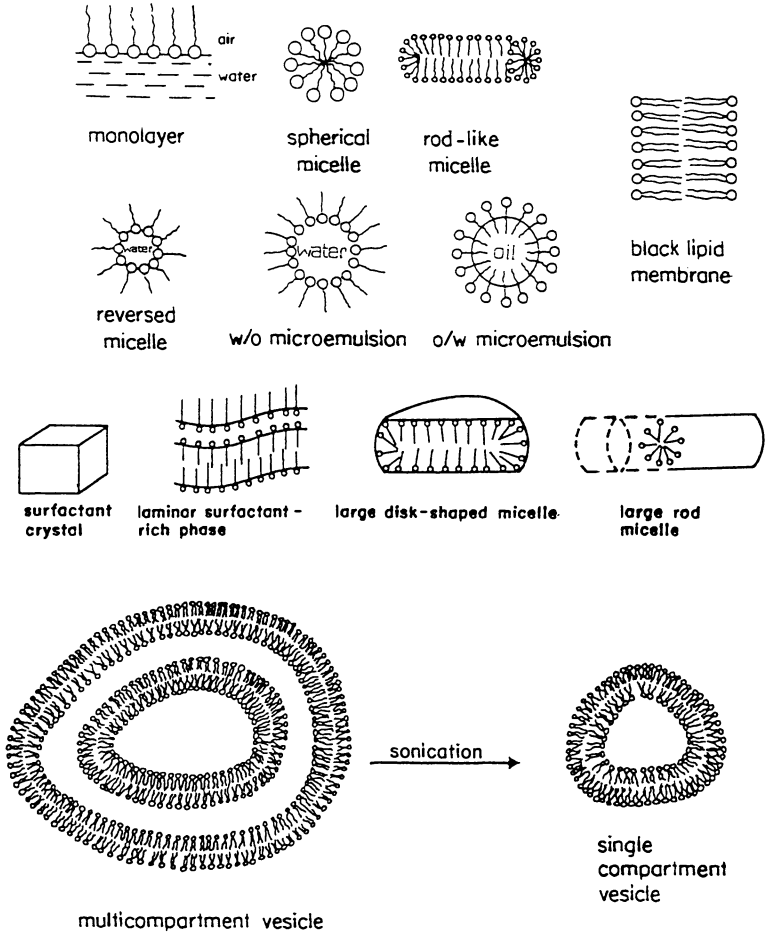


Figure 2. Some organized structures of surfactants in different media and the effect of sonication to vesicles [modified from Ref. 26 and others].

factant may skip several phase transitions depending upon its structure and the physicochemical conditions.

In an alkaline environment (pH greater than 10), for a membrane-mimetic system, the interaction of cations (e.g., sodium, potassium) with the peptized resin molecules acts in a membrane mimetic fashion. The cation reacts with the acid-bearing functional group to develop a host-guest cavity in a cylindrical shape. The counter anion (e.g., hydroxide, silicate) is activated and dissolves in the oil phase. In this manner, the resin molecule containing the heterocycle center is dissociated and any ionizable proton such as in $-\text{COOH}$, $-\text{SH}$, or $-\text{NH}$ is replaced with the cation. The self-generated surfactant molecules are produced. When this self-generated surfactant migrates into the naturally reversed micelles (oil external-water internal) of asphaltene, it disrupts the polar structure to form a Hartley micelle (polar-external) as shown in Figure 3. This is termed as the "micellar inversion process." The counter anions emulsify the oil and the micellar structure becomes a microemulsion stabilized by the self-generated surfactant molecules (7,15).

In the micellar inversion process, the heavy fractions (asphaltenes and preasphaltenes) are separated from the bitumen. This separation results, as the micelles containing the less polar or lighter hydrocarbon components and the individual molecules breaking away from the micelle, moving to the surface of the aqueous phase and coalescing to form an oil layer. After the separation of lighter components, the higher polar molecules form asphaltenes and preasphaltenes micelles strongly reassociated and complexed with metals to form colloidal-size flocs and precipitates. As Briggs et al. (27) indicated that the preasphaltene fraction contains an aliphatic to aromatic hydrogen ratio of 3.6, and the presence of alkyl side chains and the larger molecules by weight would attribute to the large size of colloidal particles. These particles are formed by inter-molecular association of 3 to 5 polyaromatic molecules (single sheet) of asphaltene and/or preasphaltene. Most of these colloidal particles are spherical with diameters in the range of 22-38 angstroms. The ultrasonic vibration energy effect is expected to accelerate the aggregation of these colloidal particles through the orthokinetic flocculation mechanism. Four of the 22-38 angstroms particles could agglomerate to form a supermicelle or floc with a diameter in excess of 220 angstroms (see Figure 1). According to many indications, such as x-ray small-angle scattering data (27-29), supermicelle structures with dimensions in excess of 1000 angstroms would precipitate from the solution.

The purpose of employing various light incidents when using a microscope was to distinguish between different crystals such as mineral crystals (e.g., clays, silicons, NaOH, etc.) from surfactant crystals (30-33). It was found that under transmittant light only bituminous hydrocarbons were non-transparent (absorb light) and appeared either

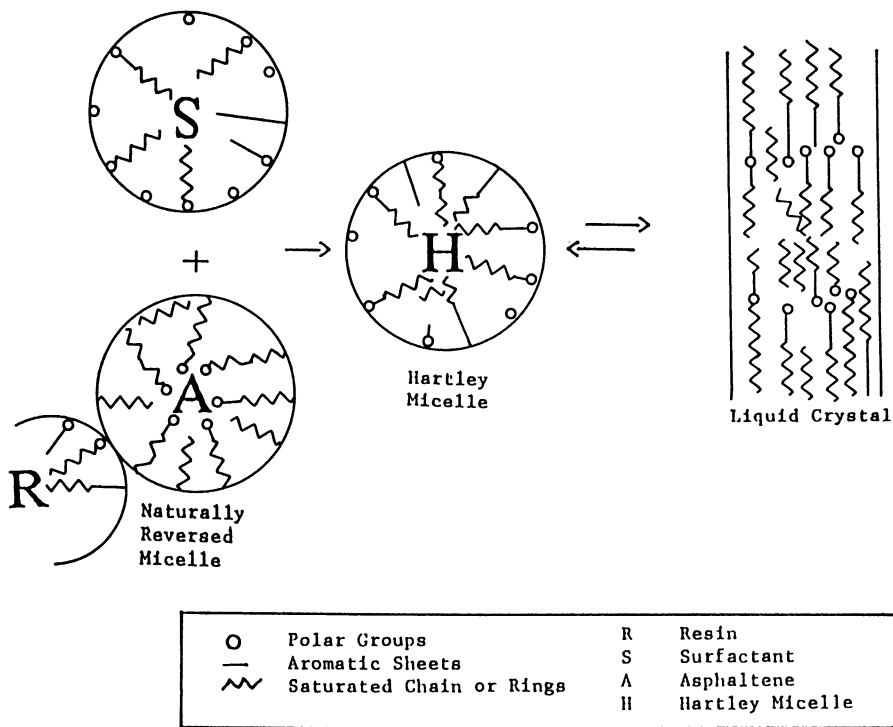


Figure 3. Dynamic equilibrium of asphaltene micelle inversion process.

black, orange and/or yellow in photomicrographs. This is the stage of reaction in which the removal of hydrocarbon contaminants is suspected to take place. As shown in Figures 4a (transmittance) and 4b (reflectance), asphaltic micelles (isotropic black circles) are going through the micellar inversion process (34).

At the completion of above reaction (after the 6th hour of sonication) another batch of solution was withdrawn for observation. Figure 4c shows the emulsions that have formed during the reaction. These emulsions were all optically active under polarized light (reflectant) as shown in Figure 4d. This was interpreted as a sign for surfactant activity. Also there were no asphaltic micelles observed in the solution, which meant total removal of contaminants had taken place and the contaminants had precipitated as solid asphaltic agglomerates. The emulsions formed during the reaction started to coalesce a few minutes after the processing had stopped (Figures 5a and 5b). At the time of emulsion coalescence, many surfactant molecules rearranged in an orderly fashion and formed a thick layer surrounding some oil emulsions (Figures 5c and 5d). The trapped oil emulsions within the surfactant layer continuously burst and their surfactant molecules moved outwards adding another surfactant layer to the outer boundary. This is the suspected mechanistic sequence that forms the large multi-compartment surfactant vesicles from single-compartment vesicles during the sonication process. The optical activity of these layers shows the true nature of the surfactant molecules being highly organized.

These membrane-mimetic agents are also osmotically active as shown in Figure 6 (4 months later). Notice the centers of the vesicles are completely covered with the upgraded bitumen without any air or water gaps present as compared to Figures 5c and 5d. Also, these vesicles are quite stable even after three years of storage in an air tight amber vial (Figures 7a and 7b). Amber vials were used to avoid any photolysis of the samples which might initiate unsuspected radical reactions.

In order to determine whether these surfactant vesicles were of polymerized vesicle forms, a 25% V/V ethanol (standard grade) was added to the three year old sample solution. Alcohols are known (34) to destroy surfactant vesicles derived from natural phospholipids, however, synthetically prepared polymerized vesicles are stable in as much as 25% (V/V) alcohol addition. Photomicrographs shown in Figures 7c and 7d indicate that these vesicles partially retain their stability (being mesomorphic) and therefore are suspected to be polymerized surfactants. Whether surfactant molecules of these vesicles are single or multipla bonds in tail, or in head groups remains to be seen.

As indicated by Puig et al. (35), surfactant retention and attendant pressure buildup in the rock can be greatly reduced if the surfactant dispersion is converted into the liquid crystalline state. Unilamellar vesicles are preferred in the field work rather than the multilamellar

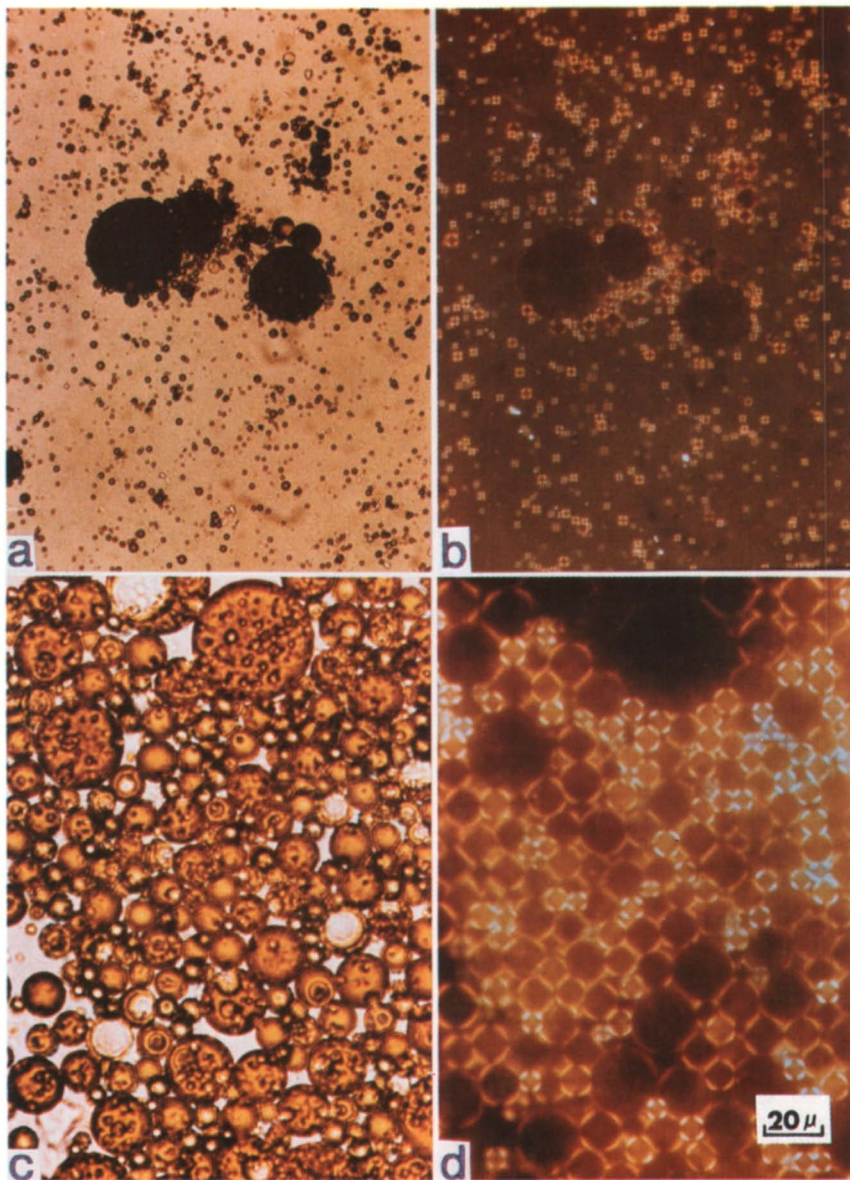


Figure 4. Bitumen removal during 3rd/4th hour of the processing [(a) transmittance and (b) reflectance]. Emulsification phenomena after completion (6th hour) of the processing [(c) transmittance and (d) reflectance].

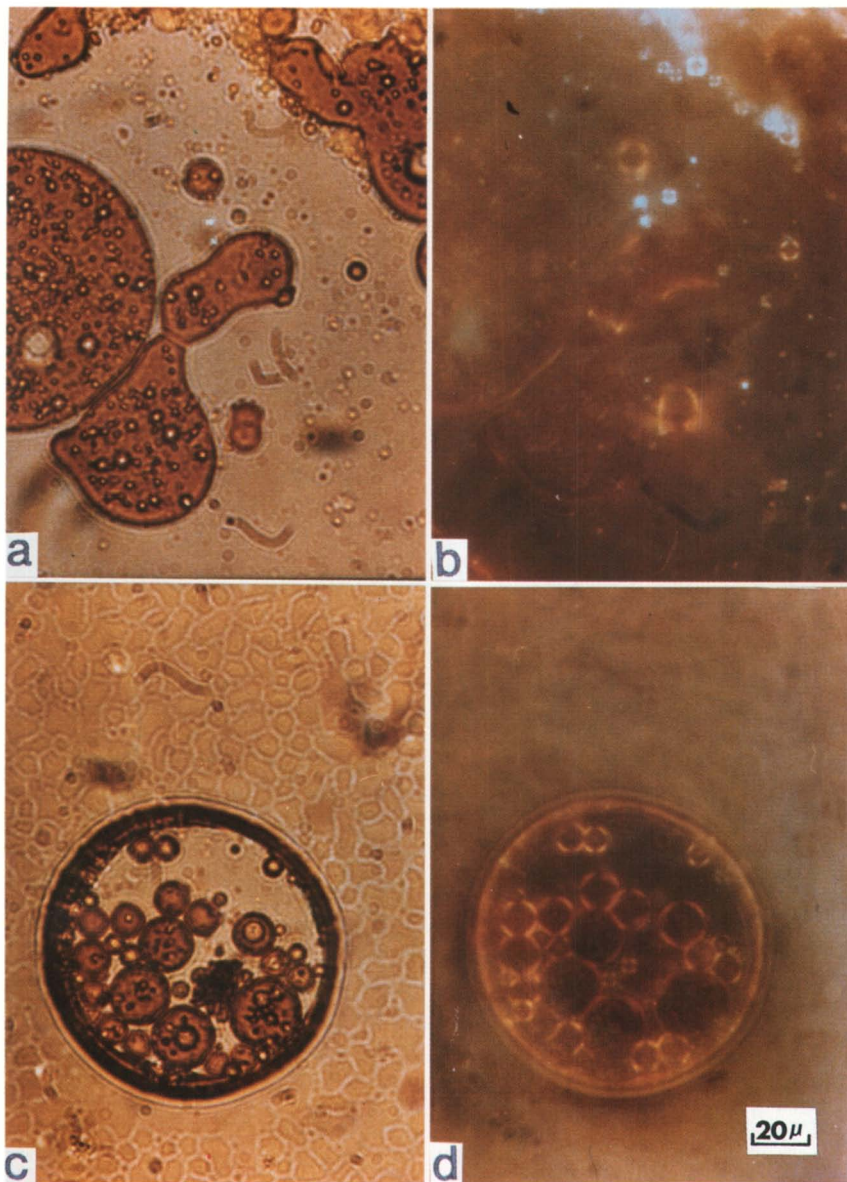


Figure 5. Coalescence phenomena a few hours after completion of the processing [(a) transmittance and (b) reflectance]. Multilamellar surfactant vesicle development phenomena twelve hours after the completion of the processing [(c) transmittance and (d) reflectance].

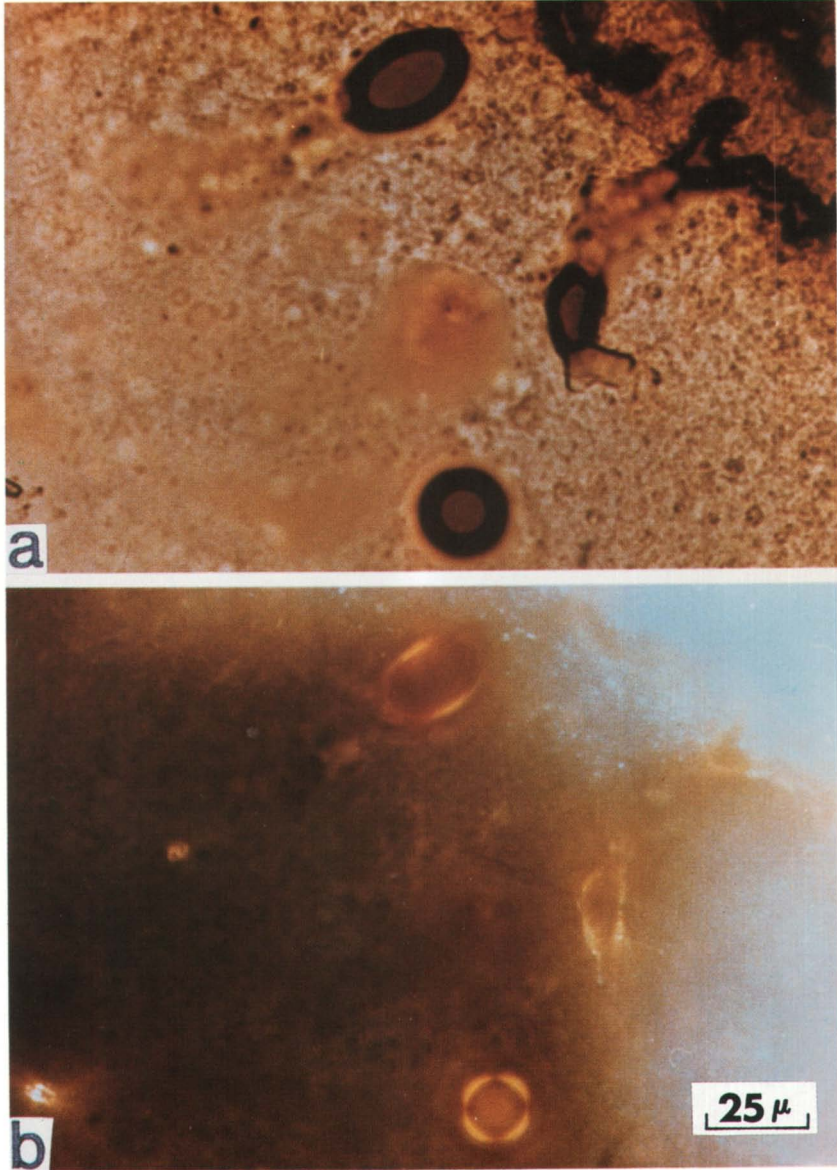


Figure 6. Multilamellar surfactant vesicles four months following the processing [(a) transmittance and (b) reflectance].

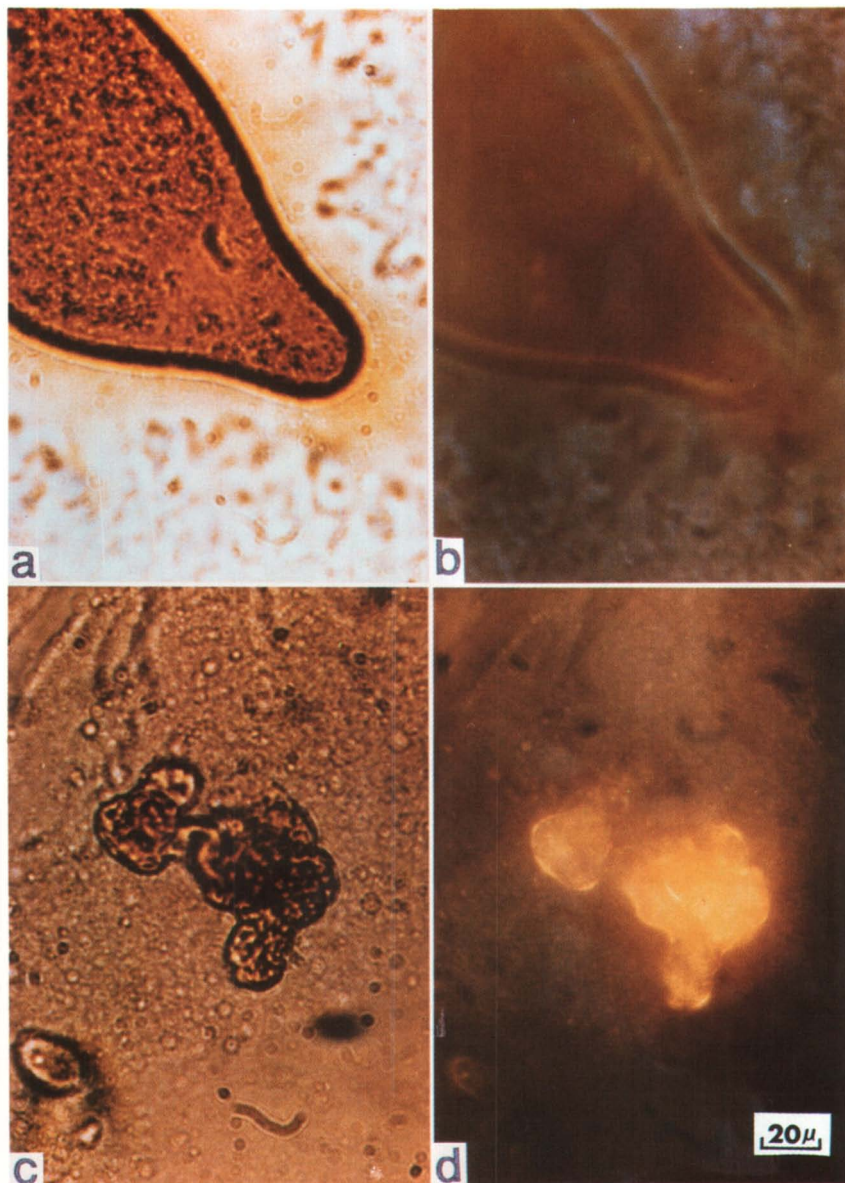


Figure 7. Multilamellar surfactant vesicle three years following the processing [(a) transmittance and (b) reflectance]. Partial disruption of vesicle in 7a and 7b, upon addition of 25% V/V of ethanol [(c) transmittance and (d) reflectance].

vesicles. Other than the use of sonication, different chemical additives can be equally efficient in the application of vesicles as surfactant delivery agents for enhanced oil recovery or decontamination in soil.

CONCLUSION

Benchmark studies demonstrated that the application of ultrasonic energy in an alkaline solution media (i.e. $\text{pH} > 10$) will induce generation of self-propagating surfactants which could effectively extract bitumen from tar sand deposits. The photomicrographs taken by the application of both the transmittance and reflection of polarized light were carefully analyzed and it was concluded that the surfactant vesicles generated during and after the process completion were quite stable even after three years of storage. This indicates that these surfactant vesicles were polymerized during the processing due to the presence of free radicals, whether generated by sonication or added as initiators (7,8). The membrane-mimetic chemistry (34) concepts were applied to thoroughly examine the reaction pathways of the process by the microscopic studies. The overall studies did indicate clearly that the development of such a process in a tar sand reservoir environment could similarly lead to generation of multiple-layered or multi-compartment surfactant vesicles and subsequently to the ultimate in-situ bitumen recovery. In a similar manner, emulsification, transportation, upgrading, production, recovery, etc., of tar sand and related heavy oil industries can be benefited.

ACKNOWLEDGMENTS

The authors thank Energy and Environment Research Laboratories, Inc. for partial financial support. We want to acknowledge Dr. Jih-Fen Kuo of Groundwater Technology, Inc. and Dr. John G. Reynolds of Lawrence Livermore National Lab for technical discussions. We also thank Dr. H.L. Wong and Mr. Leon Lemons for the preparation of this manuscript.

LITERATURE CITED

1. Wen, C. S.; Chilingarian, G. V.; Yen, T. F. "Properties and Structure of Bitumens," *Bitumens, Asphalts, and Tar Sands*; Chilingarian, G. V.; Yen, T. F., Eds.; Elsevier Publishing Company: New York, 1978, 7, p 155.
2. Yen, T. F.; Farmanian, P. A. "Native Petroleum Surfactants," U.S. Patent 4 411 816, 1983.

3. Bowman, C. W. "Molecular and Interfacial Properties of Athabasca Tar Sands," *Proceedings of the Seventh World Petroleum Congress*; Elsevier Publishing Company: New York, 1967, 3, p 583.
4. Ali, L. H. "Surface-Active Agents in the Aqueous Phase of the Hot-Water Flotation Process for Oil Sands," *Fuel*, 1978, 57, 357.
5. Chendke, P. K.; Fogler, H. S. "Second-Order Sonochemical Phenomena. Extensions of Previous Work and Applications in Industrial Process," *Chem. Eng. J.* 1974, 8, 165.
6. Frederick, J. R. *Ultrasonic Engineering*; John Wiley and Sons: New York, 1965.
7. Sadeghi, M.-A.; Sadeghi, K. M.; Kuo, J. F.; Jang, L. K.; Yen, T. F. "Treatment of Carbonaceous Materials," U.S. Patent 4 765 885, 1988.
8. Kuo, J. F.; Sadeghi, K. M.; Jang, L. K.; Sadeghi, M.-A.; Yen, T. F. "Enhancement of Bitumen Separation From Tar Sand by Radicals in Ultrasonic Irradiation," *Appl. Phys. Comm.* 1986, 6(2), 205.
9. Chan, M.; Sharma, M. M.; Yen, T.F. "Generation of Surface Active Acids in Crude Oil for Caustic Flooding Enhanced Oil Recovery," *Ind. Eng. Chem. Process Des. Dev.* 1982, 21, 580.
10. Chan, M. "Interfacial Activity in Alkaline Flooding Enhanced Oil Recovery," Ph.D. Dissertation, USC, Los Angeles, 1980.
11. Chan, M.; Yen, T.F. "Role of Sodium Chloride in the Lowering of Interfacial Tension Between Crude Oil and Alkaline Aqueous Solution," *Fuel*, 1981, 60, 552.
12. Dunning, H. N.; Moore, J. W.; Denekas, M. O. "Interfacial Activities and Porphyrin Contents of Petroleum Extracts," *Ind. Eng. Chem.* 1953, 45, 1759.
13. Dodd, C. G.; Moore, J. W.; Denekas, M. O. "Metalliferous Substances Adsorbed at Crude Petroleum-Water Interfaces," *Ind. Eng. Chem.*, 1952, 44, 2585.
14. Huang, C. "Studies of Phosphatidylcholine Vesicles. Formation and Physical Characteristics," *Biochemistry*, 1969, 8, 344.
15. Sadeghi, K. M.; Sadeghi, M.-A.; Kuo, J. F.; Jang, L. K.; Yen, T. F. "Self-Propogated Surfactants Formed During Separation of Bitumen From Tar Sands Using an Alkaline Solution and Sonication," Presented at ACS, 1987 Pacific Conference on Chemistry and Spectroscopy, October 28-30, 1987.
16. Sadeghi, M.-A.; Jang, L. K.; Kuo, J. F.; Sadeghi, K. M.; Palmer, R. B.; Yen, T. F. "A New Extraction Technology for Tar Sand Production," *The 3rd UNITAR/UNDP International Conference on Heavy Crude and Tar Sand*; AOSTRA: Alberta, 1988, p 739.
17. Yen, T. F. "The Role of Asphaltene in Heavy Crude and Tar Sands," *The Future of Heavy Crude and Tar Sands*; McGraw Hill: New York, 1981, p 174.
18. Dickie, J. P.; Haller, M. N.; Yen, T. F. "Electron Microscopic Investigations on the Nature of Petroleum Asphaltics," *J. Colloid Interface Sci.*, 1969, 29(3), 475.

19. Yen, T. F. "Structural Differences Between Asphaltenes Isolated from Petroleum and from Coal Liquid," *Chemistry of Asphaltenes*; Bunger, J. W.; Li, N. C., Eds.; Advances in Chemistry Series No. 195; American Chemical Society: Washington, D.C., 1981, p 39.
20. Yen, T. F. "Present States of the Structure of Petroleum Heavy Ends and Its Significance to Various Technical Applications," *ACS, Div. Petrol. Chem., Prepr.* 1972, *17*(4), F102.
21. Ravey, J. C.; Duconret, G.; Espinat, D. "Asphaltene Macrostructure by Small Angle Neutron Scattering," *Fuel*, 1988, *67*, 1560.
22. Kotlyar, L. S.; Ripmerster, J. A.; Sparks, B. D.; Woods, J. "Comparative Study of Organic Matter Derived from Utah and Althabasca Oil Sands," *Fuel*, 1988, *67*, 1529.
23. Tissot, B. P.; Welte, O. H. *Petroleum Formation and Occurrence*; Springer Verlag: New York, 1984, 2nd Ed.
24. Yen, T. F. "Chemical Aspects of Interfuel Conversion," *Energy Sources*, 1973, *1*, 117.
25. Yen, T. F. "Long-Chain Alkyl Substituents in Native Asphaltic Molecules," *Nature, Phys. Sci.*, 1971, *233*, 36.
26. Fendler, J. H., "Microemulsions, Micelles, and Vesicles for Membrane Mimetic Photochemistry," *J. Phys. Chem.*, 1980, *84*, 1485.
27. Briggs, D. E.; Addington, D. V.; Mckeen, J. A. *Coal IV*, CEP Technical Manual, 1978.
28. Pollack, S. S.; Yen, T. F. "Structural Studies of Asphaltics by X-Ray Small Angle Scattering," *Anal. Chem.*, 1970, *42*, 623.
29. Dwiggin, C. W., Jr. "A Small Angle X-Ray Scattering Study of the Colloidal Nature of Petroleum," *J. Phys. Chem.*, 1965, *69*, 3500.
30. Hartshorne, N. H.; Stewart, A. *Crystals and the Polarizing Microscope*; Arnold: London, 1970.
31. Hartshorne, N. H. *The Microscopy of Liquid Crystal*; Microscope Publications Ltd: London, 1974.
32. Tiddy, G. J. T. "Surfactant-Water Liquid Crystal Phases," *Physics Reports (Review Section of Physics Letters)* 1980, *57*(1), 1.
33. Franses, E. I.; Talmon, Y.; Scriven, L. E.; Davis, H. T.; Miller, W. G. "Vesicle Formation and Stability in the Surfactant Sodium 4-(1'-Heptylnonyl) benzenesulfonate," *J. Colloid Interface Sci.*, 1982, *86*(2), 449.
34. Fendler, J. H. *Membrane Mimetic Chemistry*; Johy Wiley & Sons: New York, 1982.
35. Puig, J. E.; Franses, E. I.; Yeshayahu, T.; Davis, H. T.; Miller, W. G.; Scriven, L. E. "Vesicular Dispersion Delivery Systems and Surfactant Waterflooding," *Soc. Petrol. Eng. J.*, 1982, February, 37.

Chapter 22

Modifications in the Composition of Crude Oils During In Situ Combustion

A. Audibert and J. Roucaché

Institut Français du Pétrole, B.P. 311, 92506 Rueil-Malmaison, Cedex, France

During enhanced oil recovery by in-situ combustion, crude oil undergoes chemical and physical changes. In in-situ combustion laboratory tests, air injection was stopped to interrupt the reactions. The organic matter sampled ahead of the burnt zone was analyzed using an analytical procedure specifically designed to characterize the evolution of the composition of the crude oil. The coke deposit was characterized by Infrared Spectroscopy and Oil Show Analyzer. The residual oil and the produced oil samples were characterized by SARA Analysis. The interpretation of tests involving crude oils with different geochemical compositions shows the possible influence of the crude oil composition on the amount of coke deposit and on its ability to undergo in-situ combustion. The results which provide valuable information for numerical simulation of in-situ combustion, concern not only the coke deposit (amount, composition, oxygen reactivity) but also the organic matter sampled ahead of the combustion zone (composition, coke precursors) and the produced oil.

During enhanced oil recovery by in-situ combustion, a crude oil undergoes chemical changes (pyrolysis reactions) and physical changes (dilution by the cracking products, vaporization and condensation of some fractions). Both phenomena are important for oil production :

- easier and higher recovery due to the change in oil viscosity,
- influence of the amount of coke deposit on the propagation of the combustion process.

The cracking and the low-temperature oxidation of crude oils have been studied previously in order to simulate the thermal transformations of oil to gas and coke during enhanced oil recovery (1-6). Other authors characterize the thermal modifications of oil in the presence of a vapor phase (7).

The objective of this work is to study the possible influence of the crude oil composition on the amount of coke deposit and on its ability to undergo in-situ combustion. Thus, the results would provide valuable information not only for numerical simulation of in-situ combustion but also to define better its field of application. With this aim, five crude oils with different compositions were used in specific laboratory tests that were carried out to characterize the evolution of the crude oil composition. During tests carried out in a porous medium representative of a reservoir rock, air injection was stopped to interrupt the reactions. A preliminary investigation has been described previously (8).

EXPERIMENTAL

Oils properties.

Five crude oils with different geochemical compositions have been studied. The different properties of the oils are listed in Table I. These oils can be classified under different categories :

- . Oil A (Paris Basin) - from a marine origin which is already altered and will not be further transformed.
- . Oil B (Rumania) - from the class of naphthenic-aromatic crude oils. This oil will need only a small quantity of energy to be chemically modified to form lighter hydrocarbons.
- . Oils C (Boscan), D (Cerro Negro), E (Athabasca) - from the class of asphaltenic-aromatic crude oils, have a high sulfur content. The first two oils coming from carbonate source rocks contain polar compounds consisting of very stable polycyclic aromatics. On the other hand, the last oil contains aromatics which are less condensed and more reactive.

Procedure.

The combustion cell, which is 2.1 m long and 20 cm in diameter and the procedure have been described previously (9).

The fluids produced are regularly sampled during the propagation of the combustion front. The oil samples are separated and analyzed according to the analytical procedure detailed in the next paragraph. The air injection is generally stopped when the combustion front has propagated along the first half of the length of the porous medium. After a complete cooling of the combustion cell under rotation, samples are taken at different points of the porous medium, generally at each thermocouple and at half distance between two successive thermocouples. All the coke zone which is observed downstream from the combustion front is sampled.

TABLE I - OIL PROPERTIES

Oil	ρ kg/m ³	μ mPa.s	Saturates %	Aromatics %	Resins %	Asphaltenes %	Sulfur % wt
A	890 (15°C)	40 (30°C)	55.2	34	10.7	0.1	0.3
B	960 (20°C)	2000 (18°C)	47.4	23.6	28.8	0.3	0.2
C	1005 (15°C)	1300 (60°C)	15.5 (210°)	43.0	29.5	12.0	5.3
D	1007 (15°C)	7092 (60°C)	17.3	32.1	36.8	13.8	4
E	1000 (20°C)	2150 (50°C)	21.5	36.5	30.8	8.1	4.3

Analytical procedure.

An analytical procedure (Fig. 1) has been improved to characterize both the residual organic matter in the sands and the oil recovered during the tests. For example, the analysis of samples by the Oil Show Analyzer (OSA, IFP Fina process, commercialized by Delsi Instruments-France) gives the organic content of rocks (10) and permits the study of the evolution in the oil composition. This analysis (Fig. 2) is based on a two-step procedure involving successively (a) pyrolysis from ambient temperature up to 600°C, and (b) combustion in air at 600°C. The first peak corresponds to the detection of the gaseous hydrocarbons up to C₇, volatilized at about 90°C during 2 minutes (gas amount S0 in g/100 g of rock), the following to the liquid hydrocarbons, volatilized at 300°C during 3 minutes (oil amount S1); the hydrocarbons released during the cracking of the residual organic matter from 300°C to 600°C form the peak S2. The detection of the CO₂ produced by combustion in air at 600°C during 5 minutes of the previously pyrolyzed sample leads to the peak S4 and allows the residual organic carbon content to be determined. The different product contents are generally given in g per 100 g of rock. Here, the different product contents are also given versus the total carbon content (for example S0/S0+S1+S2+S4) to eliminate the effect of oil saturation.

The oil extracted from the sand samples or the produced oil is studied by thin layer chromatography, which gives the distribution of the different structural groups : saturates, aromatics, resins, asphaltenes (SARA). If changes are observed in the oil composition, the different fractions are further analyzed by gas chromatography on capillary columns with a specific detector for each group (Flame ionisation detector for aromatics, flame photometry detector for thiophenic compounds and thermoionic specific detector for nitrogen compounds). After extraction of the liquid oil phase, the residual organic matter is isolated from the mineral phase by acid attack (HCl/HF), in a nitrogen atmosphere at 70°C (11). The residual organic matter is then characterized by elemental analysis and infrared spectroscopy.

RESULTS

The porous medium properties for the different tests are presented in Table II. The tests are carried out in a porous medium constituted of silica sand, kaolinite (4%), mixed with heavy crude oil and water.

Analysis of the residual organic matter by Oil Show Analyzer.

The evolution in the composition of the residual organic matter is studied by OSA in the coke zone and in all the zone ahead of the combustion front. Whatever the oil, in each sand sample, the amount of gaseous hydrocarbons (S0) is low because all the light hydrocarbons have been stripped by the gas flow.

For oil A, ahead of the coke zone, the amount of organic carbon in S0+S1+S2 has decreased from 6 g/100 g of rock (initial amount in the porous medium) to 3 g/100 g. The higher decrease can

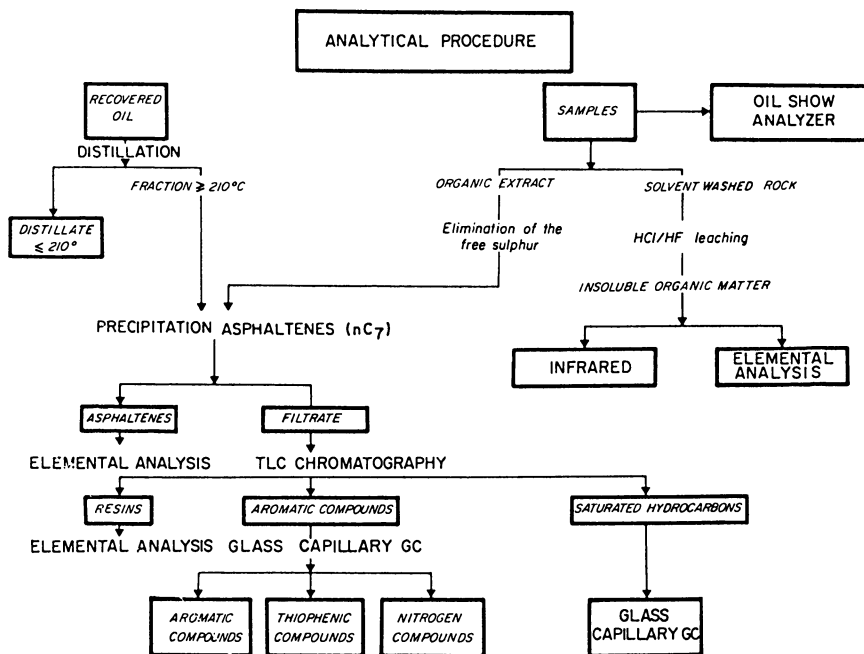


Figure 1. Analytical procedure. (Reproduced with permission from ref. 8. Copyright 1984 Institut Français du Pétrole.)

TABLE II - POROUS MEDIUM PROPERTIES

Oil	A	B	C	D	E
So %	57.1	50.5	57.8	54.4	58.4
Sw %	35.4	20.1	26.5	25.1	26.7
Oil content kg/cm ³	167.4	172.7	207.3	203.4	209.5
Air requirement Nm ³ /m ³	212	298	393	427	376
Front temperature °C	450-470	450-500	510-750	635-750	660-750
% burned	10.2	11.8	19.5	19.3	16.7

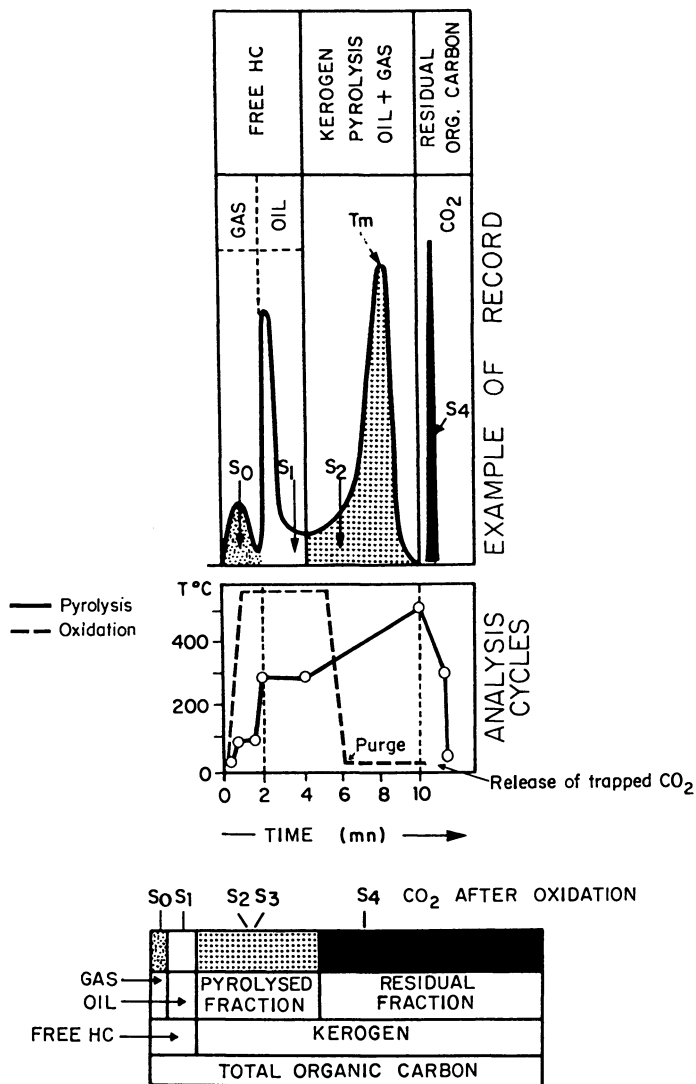


Figure 2. OSA diagram. (Reproduced with permission from ref. 8. Copyright 1984 Institut Français du Pétrole.)

be observed for S2 which corresponds to the content of heavy components released from 300 to 600°C. Just ahead of the coke zone, there is an increase in the ratio S1/S2 with respect to the initial oil. This is due to the presence of liquid hydrocarbons which have been formed by cracking of heavier hydrocarbons or have been swept by the combustion gases. The same cracking effect is observed for the other oils B to E but on the contrary, the amount of organic carbon in S0+S1+S2 is equal or even higher than the original one. Thus, all the zone ahead of the coke zone has been enriched by the cracking products but the heavy product content (S2) remains also high. An example of the progressive changes of the organic matter properties due to the combustion can be observed on Fig. 3 for OIL E. The coke zone and the zone ahead of the coke where the changes are noticeable have been specially studied.

Analysis of the coke zone

The amount of the residual organic matter is given in Table III for different samples studied.

The material balance is consistent with the results obtained by OSA (S2+S4 in g/100 g). For oil A, the coke zone is very narrow and the coke content is very low (Table III). On the contrary, for all the other oils, the coke content reaches higher values such as 4.3 g/100 g (oil B), 2.3 g/100 g (oil C), 2.5 g/100 g (oil D), 2.4/100 g (oil E). These organic residues have been studied by infrared spectroscopy and elemental analysis to compare their compositions. The areas of the bands characteristic of C-H bands ($3000-2720\text{ cm}^{-1}$), C=C bands ($1820-1500\text{ cm}^{-1}$) have been measured. Examples of results are given in Fig. 4 and 5 for oils A and B. An increase of the temperature in the porous medium induces a decrease in the atomic H/C ratio, which is always lower than 1.1, whatever the oil (Table III). Similar values have been obtained in pyrolysis studies (4). Simultaneously to the H/C ratio decrease, the bands characteristics of CH₂ and CH₃ groups progressively disappear. The absorbance of the aromatic C-H bands also decreases. This reflects the transformation by pyrolysis of the heavy residue into an aromatic product which becomes more and more condensed. Depending on the oxygen consumption at the combustion front, the atomic O/C ratio may be comprised between 0.1 and 0.3.

Analysis of the zone ahead of the coke zone.

In this zone, the quantity of extracted oil is generally sufficient to obtain the distribution of the different structural groups (SARA analysis) except for oil A (Fig. 6 to 9). For oil B (Fig. 6), for the first two samples, the amount of extracted products is too low and the analysis is uncertain. It can only be noticed that the asphaltene content is null. On the contrary, just beyond the coke zone (samples III-IV), the asphaltene content respectively reaches 12.9 and 5.4% whereas the asphaltene content of the initial oil is only 0.3%. This effect is also observed for oil C (10% versus 6.3%) (Fig. 7), D (24% versus 13.8%) (Fig. 8), E (24.4% versus 8.1%) (Fig. 9). For all the oils, the amount of resins+asphaltenes generally remains constant and the amount of saturates increases

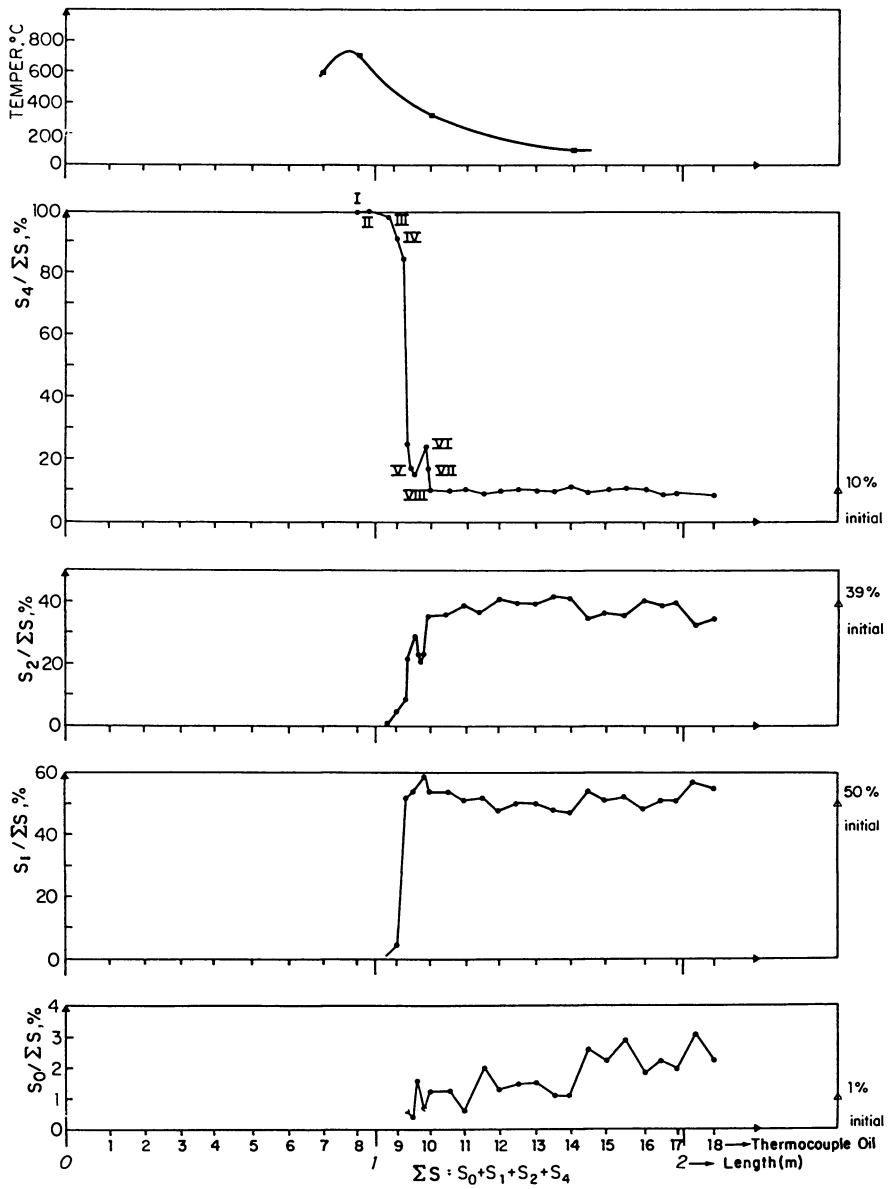


Figure 3. Analysis by OSA of samples taken in the porous medium for Oil E.

Publication Date: July 10, 1989 | doi: 10.1021/bk-1989-0396.ch022

TABLE III - COKE PROPERTIES

Sample nb	A		B		C		D		E	
	(1)	(2)	(1)	(2)	(1)	(2)	(1)	(2)	(1)	(2)
I	1.02	0.75	0.103	-	2.1	0.34	2.51	0.31	1.96	0.32
II	0.79	0.55	3.52	0.5	2.27	0.35	2.37	0.4	1.9	0.42
III	0.7	0.7	4.27	0.65	1.59	0.4	2.17	0.58	2.39	0.5
IV	0.4	1.15	2.06	0.92	0.15	1	1.49	0.6	1.48	0.63
V	0.35	0.95	0.134	-	0.22	1.1	0.048	-	-	-
VI	-	-	0.096	-	0.194	0.8	0.094	-	-	-
VII	-	-	-	-	0.082	1.05	-	-	-	-

(1) amount of residual organic matter in g/100 g of rock.

(2) H/C ratio determined by elemental analysis.

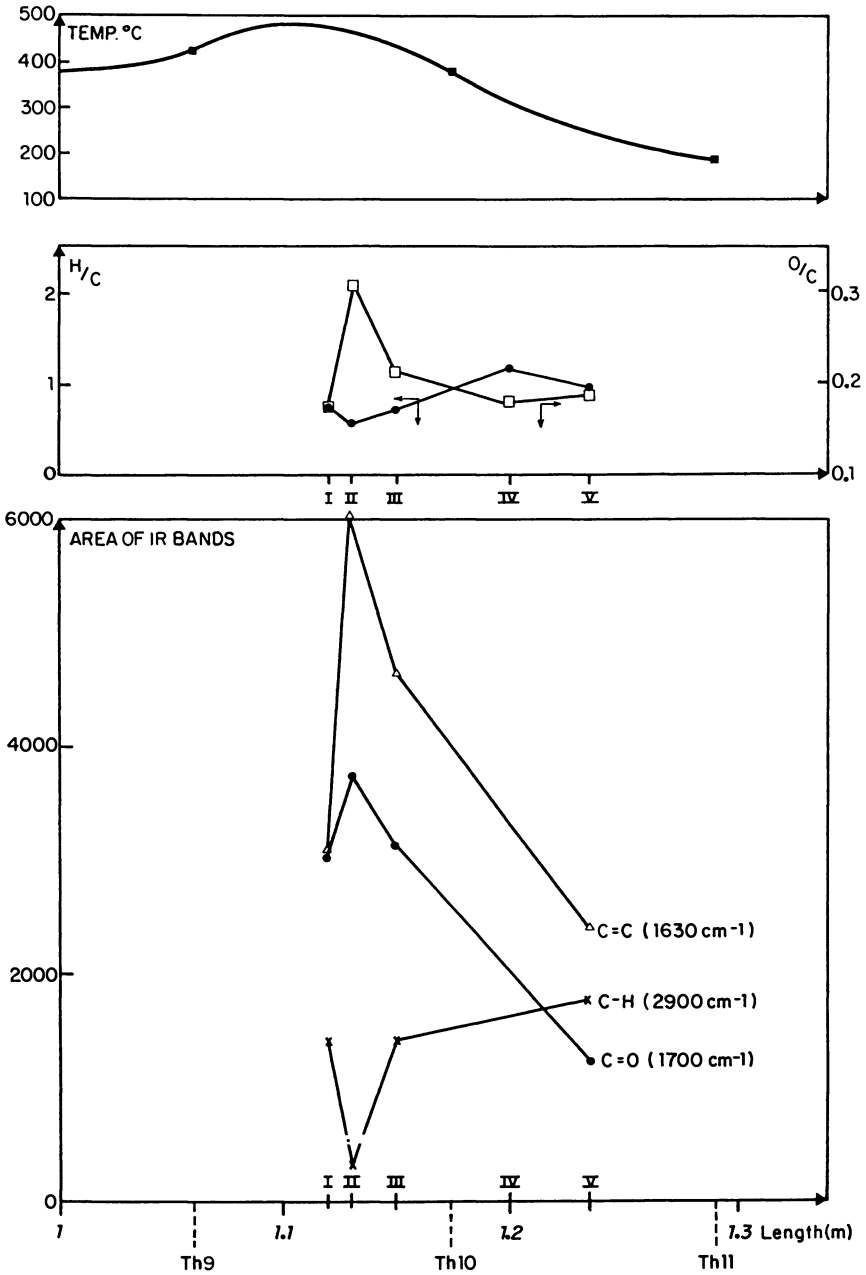


Figure 4. Analysis of the coke zone for Oil A.

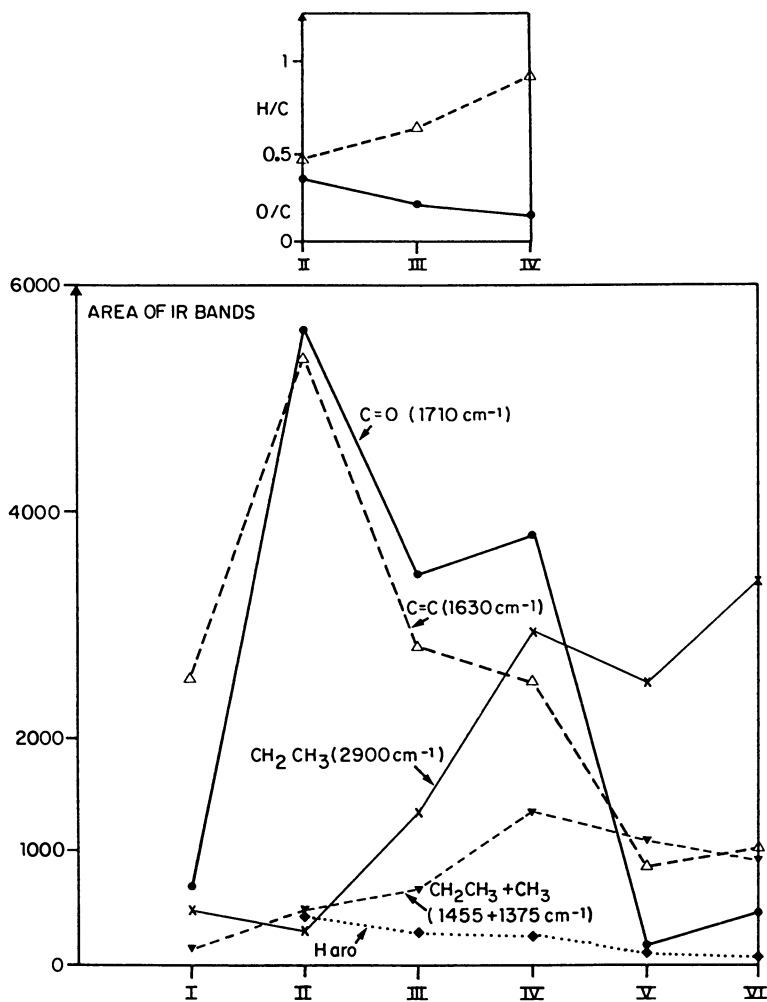


Figure 5. Analysis of the coke zone for Oil B.

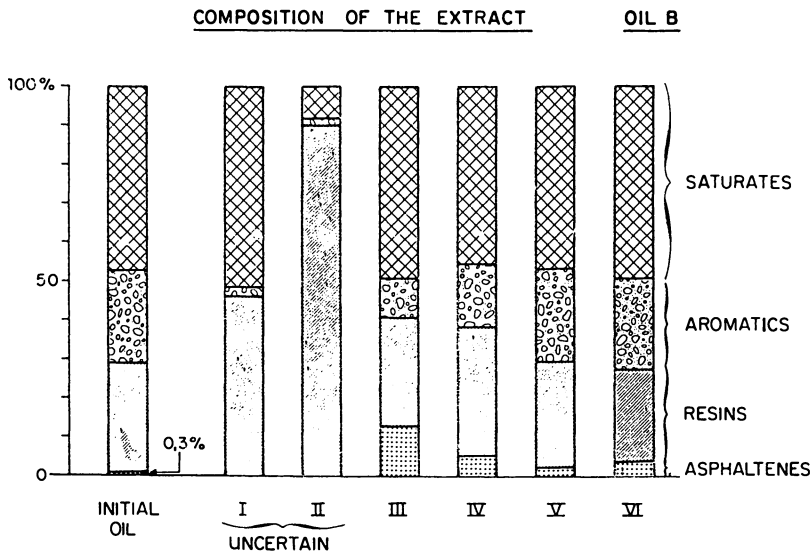


Figure 6. SARA analysis of extracted oil for Oil B.

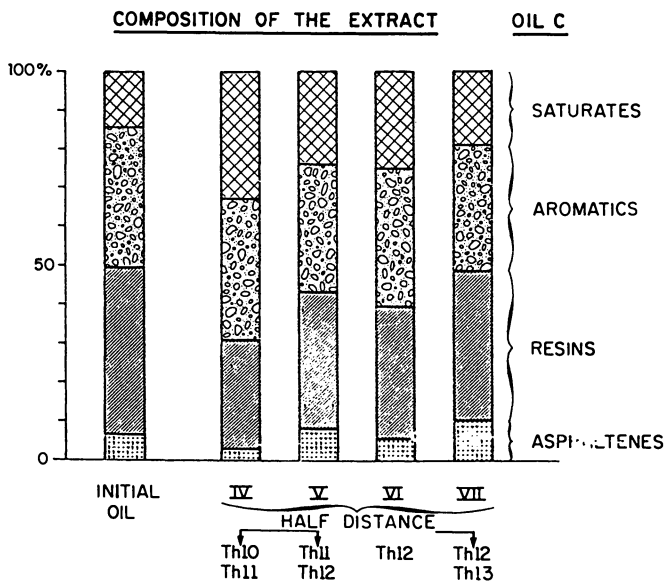


Figure 7. SARA analysis of extracted oil for Oil C.

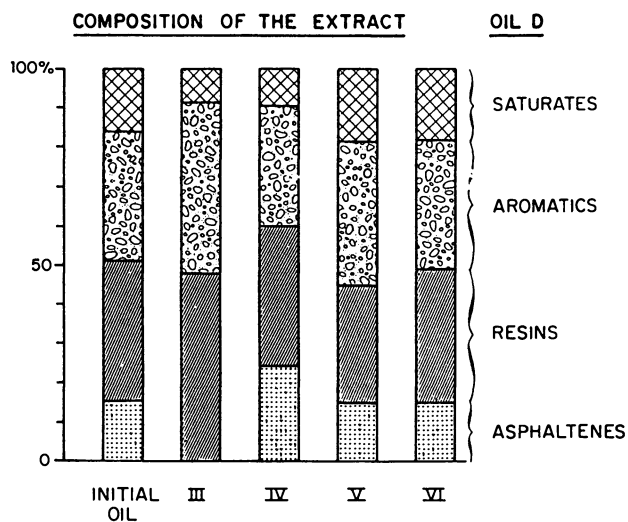


Figure 8. SARA analysis of extracted oil for Oil D.

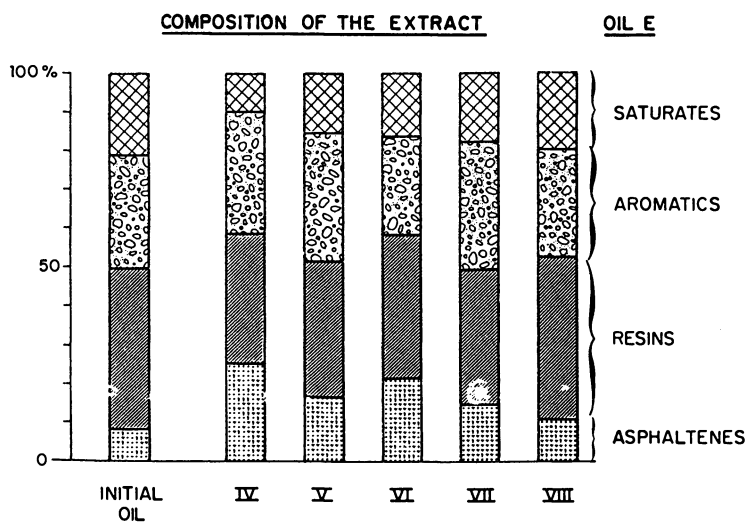


Figure 9. SARA analysis of extracted oil for Oil E. (Reproduced with permission from ref. 8. Copyright 1984 Institut Français du Pétrole.)

whereas there is a slight decrease in the aromatic content. For example, for oil C, the $C_{15}-C_{20}$ saturate content increases from 37.9% (initial value) to 58.7% (sample IV). Ahead of this zone, the oil extracted from the porous medium progressively recovers its initial properties.

Analysis of the recovered oil.

The oil recovered is first distilled. For oil A, the fraction having a boiling point lower than 210°C at atmospheric pressure (210^- or C_{12}^- fraction) represents 2.6 to 11% of the recovered oil, whereas the initial oil contains 2.5% of this fraction. The chemical changes affecting the produced oil are consistent with the evolution of its physical properties (Fig. 10). The same effect can be observed for a heavier crude. For example, for oil E, the 210^- fraction represents 10 to 15% of the recovered oil even though this fraction doesn't exist in the initial crude oil.

The variations in the composition of the fraction having a boiling point higher than 210°C (210^+) depend strongly on the initial composition of the oil.

For oil A, slight differences in composition exist; the aromatic and resin fractions hardly decrease to form lighter saturate compounds. The effects are quite similar to those on oil B whose global composition does not change. But in the saturate fraction, the amount of *n* and iso alkanes is three times higher in the recovered samples than in the initial one (Fig. 11).

For crude oils C and D, some lighter hydrocarbons are formed during the cracking reactions but the composition of the 210^+ fraction is hardly modified. In particular, it can be noticed that the asphaltene contents of both of the recovered oils remain high.

On the contrary, for oil E the quantity of asphaltenes decreases from 8.1% for the initial crude oil to 4.1% for the sample produced at the end of the test (Fig. 12). Moreover, the amounts of resins + asphaltenes decreases whereas the amounts of saturates and aromatics increase (51.4% in the initial oil, 72.4% for a sample recovered at $t = 24$ h). The analysis by GC shows that each oil fraction is enriched in components with molecular chains ranging from 15 to 30 carbons which don't exist in the initial oil (*n*-alkanes, aromatics $C_{20}-C_{30}$ which are less complex than the initial ones, thiophenic $C_{15}-C_{25}$ compounds). The elemental composition of the asphaltene fraction of the samples recovered during the test are shown in Table IV. There is an high increase in the oxygen/carbon ratio compared to the slight decrease in the hydrogen/carbon ratio. The results of the analysis of the resin fraction are quite similar. The thermal cracking of the oil induces the formation of lighter molecular weight compounds and of a polar denser residue. Those results are consistent with the observations of a field study (12).

CONCLUSIONS

Elemental analysis and infrared spectroscopy give a good characterization of the coke deposit. From one crude oil to

PHYSICAL PROPERTIES OF THE RECOVERED OIL

- OIL A -

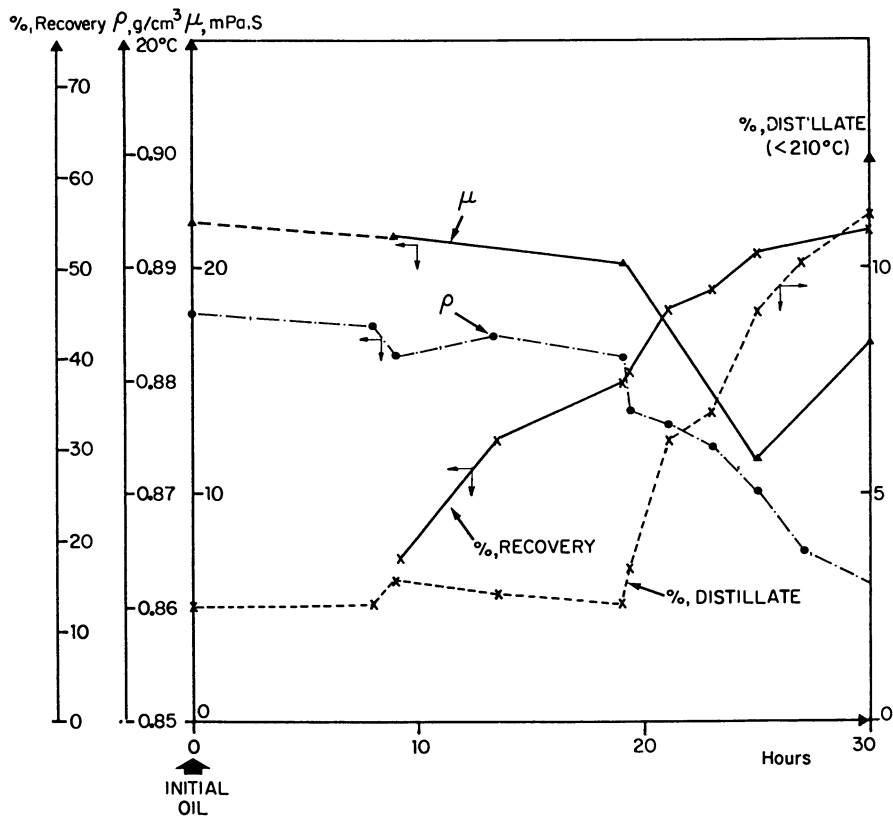


Figure 10. Characterization of the recovered oil for Oil A.

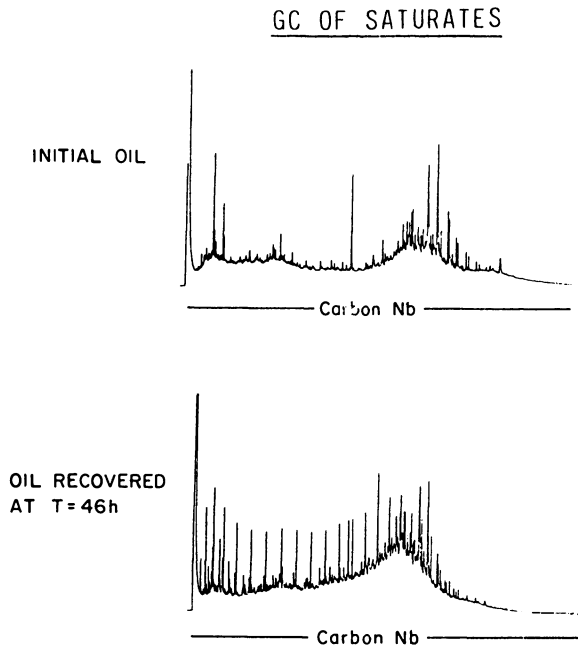


Figure 11. Saturates chromatography for a sample recovered at 46 h of test, compared to the initial one for Oil B.

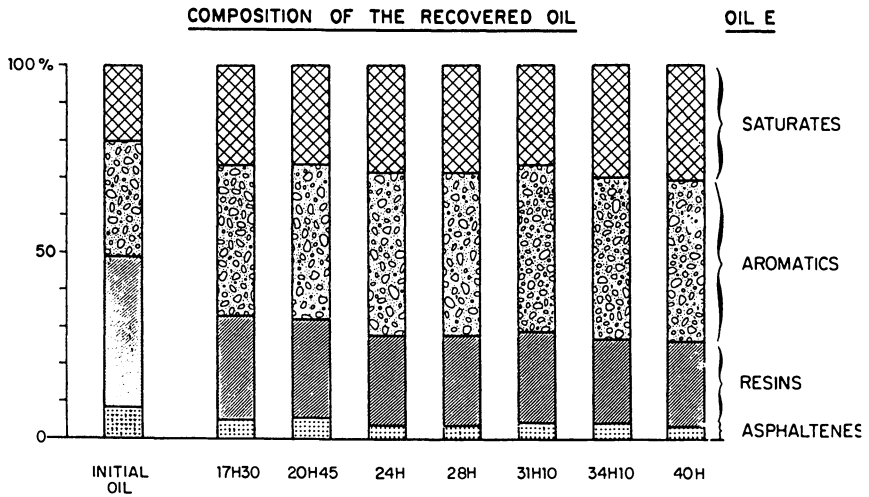


Figure 12. SARA analysis of the recovered oil for Oil E.

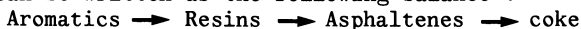
TABLE IV - ELEMENTAL ANALYSIS OF ASPHALTENES
IN THE RECOVERED SAMPLES - OIL E -

	H/C	O/C
Initial	1.21	0.028
Sample recovered at t=		
17h30	1.12	0.144
20h45	1.15	0.137
24h	1.16	0.054
28h	1.16	0.133
31h10	1.17	0.053
34h10	1.16	0.052
40h	1.12	0.048

another, the amount of coke is quite different, the highest amounts of coke being obtained from the heaviest crude oils, and especially those which contain more reactive compounds. For all the oils, the evolution of the coke composition versus the temperature evolution is similar; for example, the H/C ratio is generally comprised between 0.5 and 0.6 for a temperature equal to 400°C. The lowest H/C values (i.e. lower than 0.4) are observed for the highest temperatures of the combustion front (i.e. higher than 500°C). It means that the coke composition can be related to the temperature reached in the porous medium and its amount to the oil thermal reactivity which is influenced by the oil geochemical composition.

As the sampling moves downstream from the coke zone, it may be noticed that whatever the oil composition,

- the first samples contain the highest amount of residual carbon and no asphaltenes in the extracted fraction of the sample,
- in the following samples having a lower residual carbon content, the extracted oil contains a higher asphaltene content than the initial oil. This effect is observed even if the initial asphaltene content of the oil is quite null. It seems that the coke formation can be written as the following balance :



where the resin + asphaltene content remains constant and asphaltenes are the main precursors of coke. The same observations have been made in low-temperature oxidation experiments (6).

Whatever the oil composition, the cracking reactions enhance the amount of the 210^- fraction in the recovered oil. The composition of the 210^+ fraction depends on the initial oil composition : it is not modified if the oil is already altered or if the oil contains very stable compounds.

This experimental work gives data that help us to understand the mechanisms of coke formation during in-situ combustion. Moreover, in case of a field application, a study of the oil produced and the organic matter from cores taken behind the combustion front, related to the analysis of the initial oil could provide information on the propagation of the combustion front.

REFERENCES

1. Fassihi, M.R., Meyers, K.O., Weisbrod, K.R., "Thermal Alteration of Viscous Crude Oils", Annu. Fall Meeting of Soc. Petroleum Engrs, SPE paper No 14225 (Sept. 1985).
2. Ungerer, P., Béhar, F., Villalba, M., Heum, O.R., Audibert, A., "Kinetic Modelling of Oil Cracking". 13th Internation. Meeting on Organic Geochem., Venice (Sept. 1987).
3. Béhar, F., Audibert, A., Villalba, M., "Secondary Cracking of Crude oils : Experimental Study" - Submitted to Energy and Fuel (1988).
4. Abu Khamsin, S.A., Brigham, W.E., Ramey, H.J., "Reaction Kinetics of fuel formation for in-situ combustion", Fith Soc Petroleum Engrs Middle East Show, SPE paper No 15736, (March 1987).
5. Millour, J.P., Moore, R.G., Bennion, D.W., Ursenbach, M.G., Gie, D.N., "A simple Implicit Model for Thermal Cracking of Crude Oils", Annu. Fall Meeting of Soc. Petroleum Engrs, SPE Paper No 14226 (Sept. 1985).
6. Millour, J.P., Moore, R.G., Bennion, D.W., Ursenbach, M.G., Gie, D.N., "An Expanded Compositional Model for Low Temperature Oxidation of Athabasca Bitumen". J. Canad. Petroleum Technol., (May-June 1987), p. 24-32.
7. Monin, J.C., Audibert, A., "Thermal Cracking of Heavy Oil/Mineral Matrix Systems", Soc. Petroleum Engrs, Internation. Symp. on Oilfield Chemistry, SPE paper No 16269, (Feb. 1987).
8. Audibert, A., Roucaché, J., "Evolution of the Composition of a Crude Oil During In-situ Combustion", Characterization of Heavy Crude Oils and Petroleum Residues. Ed. Technip, Paris, p 135-139, (1984).
9. Burger, J., Sourieau, P., Combarous, M., "Thermal Methods of Oil Recovery", Ed. Technip, Paris and Gulf Publishing Company, Houston (1985).
10. Espitalié, J., Marquis, F., Barsony, J., "Geochemical Logging by the Oil Show Analyzer" Analytical Pyrolysis - Techniques et Applications - Voorhees, Ed. Butterworth, Londres, (1984).
11. Durand, B., "Kerogen", Ed. Technip, Paris (1980).
12. Bojes, J.M., Wright, G.B., "Application of Fluid Analyses to the Operation of an in-situ Combustion Pilot". Annu. Technical Meeting of Petroleum Soc. of CIM, Paper No 86-37-61, (June 1986).

RECEIVED November 28, 1988

Chapter 23

Kinetics and Energetics of Oxidation of Bitumen in Relation to In Situ Combustion Processes

Leslie Barta, Andrew W. Hakin, and Loren G. Hepler

Department of Chemistry, University of Alberta, Edmonton, Alberta T6G 2G2, Canada

Using a "home made" aneroid calorimeter, we have measured rates of production of heat and thence rates of oxidation of Athabasca bitumen under nearly isothermal conditions in the temperature range 155-320°C. Results of these kinetic measurements, supported by chemical analyses, mass balances, and fuel-energy relationships, indicate that there are two principal classes of oxidation reactions in the specified temperature region. At temperatures much lower than 285°C, the principal reactions of oxygen with Athabasca bitumen lead to deposition of "fuel" or coke. At temperatures much higher than 285°C, the principal oxidation reactions lead to formation of carbon oxides and water. We have fitted an overall mathematical model (related to the factorial design of the experiments) to the kinetic results, and have also developed a "two reaction chemical model". Subsequent measurements in which water vapor has been introduced along with oxygen have led to modified kinetics and also a modified chemical model for wet oxidation of Athabasca bitumen.

In situ combustion processes involve injection of air or oxygen into the formation to burn part of the bitumen, thereby producing heat that raises the temperature of the reservoir. At low temperatures oxidation is incomplete and leads to formation of "fuel" or partly oxidized bitumen that has higher viscosity and lower heating value than the original bitumen. These incomplete oxidation reactions, collectively called "low temperature oxidation" or "LTO", predominate during the ignition delay period of in situ combustion and also occur ahead of the combustion front when oxygen is available. It is therefore important to have knowledge of the kinetics and energetics of oxidation of bitumen in the temperature range in which LTO occurs.

In this paper we summarize some of the results of our measurements of rates of dry oxidation. Results of chemical analyses of residues produced by heating in flowing nitrogen atmosphere (distillation) are also reported and combined with our kinetic data to obtain values of kinetic parameters. Preliminary results of measurements of rates of wet oxidation are presented.

Experimental

The focus of our investigations of the kinetics of oxidation of Athabasca bitumen has been on the use of an aneroid calorimeter (1) for measuring rates of heat production under nearly isothermal ($\Delta T < 1.2^\circ\text{C}$ in each experiment) conditions. Initial attention was given to just two of the variables that affect the kinetics of oxidation: (i) temperature and (ii) pressure of oxygen. Preliminary studies into a third variable, the partial pressure of water vapor in the system, are discussed in Part 3 of the Results and Calculations section. Each calorimetric sample (≈ 1 g, 13.47 mass % bitumen) came from a large sample of "reconstructed" oil sand consisting of Athabasca bitumen loaded onto a chemically inert solid support material (60/80 mesh acid washed Chromosorb W) of well-defined particle size.

We represent the overall oxidation reaction by



and express the rate of reaction in terms of the rate of production of heat as in

$$\text{Rate} = dQ/dt = k [p(\text{O}_2)]^r \quad (2)$$

where Q is the instantaneous heat produced per gram of bitumen, t is time, $p(\text{O}_2)$ is the pressure of oxygen, k is a specific rate constant, and r is the reaction order with respect to pressure of oxygen. Because the stoichiometry of the process represented by Equation 1 is not known and because fuel quality changes with extent of reaction, we have used the method of initial rates for evaluation of r and k .

Elemental compositions and masses of organic residues produced by distillation and by oxidation were determined as described previously (2).

Results and Calculations

Part 1. Kinetics and Energetics of Dry Oxidation. The simplest approach to data analysis is to assume that only a single class of oxidation reactions is important and to make the related assumption that the temperature dependence of the single rate constant k can be represented by an Arrhenius equation. In this way we obtain

$$\ln W_1 = \ln A - E_a/RT + r \ln [p(\text{O}_2)_1] \quad (3)$$

in which W_1 is the initial rate of heat production, A is the Arrhenius pre-exponential factor, and E_a is the average activation

energy. According to this simple model, both E_a and r are independent of temperature. Consideration of a factorial design model showed that we require the results of five experiments (different temperatures and pressures of oxygen) to test Equation 3. Results of such experiments and related mathematical analysis (2) have shown that the "first order mathematical model" or "one class of reaction chemical model" represented by Equation 3 is inadequate.

Because earlier experimental results and data analyses (3-10) had led us to anticipate the inadequacy of the simple approach considered above, we also planned and carried out (2) a second order factorial design of experiments and related data analysis. Mathematical analysis (of the results of 11 experiments) based on the second order model showed that all of these results could be represented satisfactorily by an equation of the form

$$\ln W_i = b_0 + (b_1 + b_3/T)(1/T) + (b_2 + b_4/T) \ln [p(O_2)_i] \quad (4)$$

Comparison of Equation 4 with Equation 3 shows that

$$\ln k = b_0 + (b_1 + b_3/T)(1/T) \quad (5)$$

and

$$r = b_2 + b_4/T \quad (6)$$

Because the dependence of kinetic parameters k and r on temperature as described by Equations 5 and 6 is constrained by the factorial design, it is possible that these equations and therefore Equation 4 may not give the best overall representation of the kinetic data. We have therefore carried out four more experiments and analyzed these results along with those mentioned earlier to obtain (2) the best overall mathematical representation that is summarized by the following equations:

$$\ln k = a_0 + a_1 T + a_2 / (595 - T)^2 \quad (7)$$

$$r = a_3 + a_4 / (600 - T) \quad (8)$$

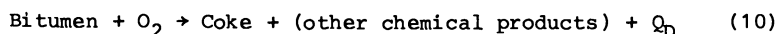
$$\ln W_i = a_0 + a_1 T + a_2 / (595 - T)^2 + a_3 \ln [p(O_2)_i] + a_4 \ln [p(O_2)_i] / (600 - T) \quad (9)$$

The composite rate constant k summarized by Equation 7 has a maximum near 302°C. The reaction order r is nearly constant at low temperatures and increases dramatically at higher temperatures.

The kinetic results and related analysis (2) summarized above indicate that there is a change in the predominant class of oxidation reaction with increasing temperature, which led to the expectation that the total heat developed in the overall oxidation also depends on temperature. Because the measurements that led to kinetic data based on initial rates were continued nearly isothermally until oxidation was complete, it has also been possible to establish (2) that the total heat developed increased by nearly ten-fold over the range 155 to 320°C.

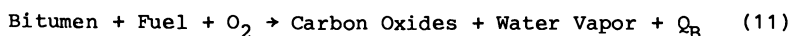
On the basis of our kinetic results, our heats of oxidation mentioned above, independent heats of total combustion (Yan, H-k.; Hepler, L.G. to be published), our chemical analyses, and the results of earlier investigations by others (11-15), we have developed a chemical model or picture of the dry oxidation process as follows.

We propose that the complicated dry oxidation of bitumen can be represented as the sum of contributions from two classes of oxidation reaction. One class of reactions is the partial oxidation that leads to deposition of coke and formation of "oxygenated bitumen", with very little production of carbon oxides and water. This class of reactions is concisely summarized by



in which Q_D represents the heat production associated with deposition of fuel.

The second class of reactions is similar to conventional combustion or burning reactions that yield mostly carbon oxides and water vapor, as summarized by



in which Q_B represents the heat produced by the "burning reactions".

The "two classes of chemical reactions model" represented by Equations 10 and 11 can be represented mathematically by the following:

$$\ln W_D = \ln A_D - E_{a(D)}/RT + r_D \ln [p(\text{O}_2)] \quad (12)$$

$$\ln W_B = \ln A_B - E_{a(B)}/RT + r_B \ln [p(\text{O}_2)] \quad (13)$$

Not all of the bitumen initially present in the calorimetric sample is available for oxidation, due to distillation during heating to the temperature of the experiment. As a preliminary to evaluating the kinetic parameters appearing in Equations 12 and 13, we have performed distillation experiments as described in Part 2 to identify the mass fraction of the original bitumen that is available for oxidation at each temperature. Kinetic parameters based on the initial rate of heat production per gram of bitumen available are listed in Table I. The temperature at which deposition and burning contribute equally to the total rate of heat production is $\sim 270^\circ\text{C}$. Deposition continues to be important to a little over 300°C . The ratio of the rate of heat production by burning to that by deposition is < 0.001 at 155°C , indicating that deposition is the sole process of interest at temperatures $< 155^\circ\text{C}$.

Table I. Values of Kinetic Parameters for Low Temperature Oxidation of Athabasca Bitumen

Equation (a)	ln A	E _a (kJ/mol)	r
$\ln W_D = \ln A_D - E_{a(D)}/RT + r_D \ln p(O_2)$	17.3	51	0.55
$\ln W_B = \ln A_B - E_{a(B)}/RT + r_B \ln p(O_2)$	34.5	143	1.15

^aCorrelation coefficients are -0.995 for deposition (subscript D) and -0.996 for burning (subscript B).

The enthalpy of the depositional process described by Equation 10 is obtained by dividing the measured heat produced at 155°C by the mass of bitumen converted to coke, yielding $\Delta H_D = -2 \text{ kJ g}^{-1}$.

By combining the total heat produced, the available mass of organic material (see Part 2), and the fraction of the available carbon that is converted to CO₂, ΔH_B can be calculated from the relationship

$$Q \text{ (kJ/g bit avail)} = f_D \Delta H_D + f_B \Delta H_B \quad (14)$$

where f_D and f_B are the mass fractions of the available bitumen involved in each of the two processes. In a new experiment on dry oxidation at 285°C and 210 kPa O₂, 870 kJ was produced by 0.053 g of available bitumen and 36% of the available carbon was recovered as CO₂. Since the fraction of available carbon is a reliable estimate of the fraction of available bitumen (Part 2), $f_B = 0.36$ and therefore $f_D = 0.64$. Combining these values of the appropriate mass fractions with the value of ΔH_D cited above leads to $\Delta H_B = -42 \text{ kJ g}^{-1}$. Results of a similar experiment at 317°C lead to $\Delta H_B = -45 \text{ kJ g}^{-1}$. The combined values of ΔH_D and ΔH_B yield an average value of $\sim -45 \text{ kJ g}^{-1}$ for the heat of combustion of bitumen, within 6% of the value obtained by bomb calorimetry (Yan, H-k.; Hepler, L.G. to be published). In view of the much higher precision of heat measurement with the bomb calorimeter as compared with our aneroid calorimeter, the value $\Delta H_B = -41 \text{ kJ g}^{-1}$ that may be derived from the measured heat of combustion is preferable to that obtained from Equation 14, although the example given here serves as an independent check on our value of ΔH_B .

In principle both ΔH_D and ΔH_B can be obtained from Equation 14, using data for the conversion of available carbon to CO₂ at two different temperatures. In practice, however, this calculation does not yield reliable values because of the very small range of carbon conversion available under our experimental conditions and because of the very large difference in magnitude of the two enthalpies.

Part 2. Distillation Experiments. Distillation experiments were performed to determine the fraction of the original mass of bitumen in a calorimetric sample that is available for oxidation at each temperature in the range 155-320°C, to determine the quality of this "fuel" as expressed by the molar ratio of hydrogen to carbon,

and to provide some of the information needed to obtain a mass balance for carbon in the oxidation process.

Samples of bitumen on Chromosorb W (loading factor = 12.20 ± 0.05 mass %) were heated in flowing nitrogen at a pressure of 210 kPa absolute (flow rate = 13 mL min⁻¹) to 155, 180, 230, 275, or 330°C and allowed to equilibrate overnight. A cold trap was placed in the gas train at the outlet of the calorimeter to collect the volatile fractions that distilled at each temperature. The heated samples were cooled to room temperature under flowing nitrogen, removed from the calorimeter, analyzed for carbon, hydrogen, nitrogen, and sulfur, and ashed to determine the total mass of organic residue.

Table II. Mass % of Total Bitumen Remaining After Heating and Elemental Composition of the Residue Produced

Temperature (°C)	L.F. (a)	Mass %				
		Bitumen Remaining	C	H	S	N
25	12.20	100.00	82.49	9.64	5.45	0.41
155	11.30	83.90	83.75	9.32	6.60	0.71
182	8.77	71.90	82.45	9.29	7.80	0.46
229	7.74	63.40	80.78	8.58	8.71	0.13
275	6.16	50.50	81.69	7.67	7.52	0.16
330	5.18	42.50	80.34	7.58	10.28	0.10

^aLoading factor (%).

Table II lists the elemental compositions of the organic residues produced at the various temperatures. The molar H/C ratio of the residue produced by heating decreases slightly with increasing temperature, from 1.3 at 155°C to 1.1 at 330°C. Carbon content of the organic residue produced by heating is approximately independent of temperature in the range 155-330°C. Table III lists the mass fractions, expressed as %, of original bitumen and of original C, H, and S remaining as residue. The mass % of whole bitumen and mass % of original carbon remaining at each temperature are approximately the same. Sulfur is not lost by heating until the temperature exceeds 230°C, and appreciable S (more than half the original mass present) remains even at 330°C.

Table III. Mass % of Total Bitumen and of C, H, and S Remaining as Residue After Heating

Temperature (°C)	Bitumen	C	H	S
25	100.0	100.0	100.0	100.0
155	83.9	85.2	81.1	101
182	71.9	76.2	69.3	103
187	71.9	74.9	-	-
229	63.4	62.1	56.4	101
275	50.5	50.0	40.2	69.7
330	42.5	41.4	33.4	80.2

No condensate was found in the cold trap (ice or dry ice/acetone) after any of the experiments, nor was any material recovered from the gas train by flushing with toluene and ethanol. However, the quantity of condensate expected on the basis of ashing of the heated samples is gravimetrically significant in all cases (15 mg expected at 155°C, 56 mg expected at 330°C).

Table IV. Mass Balance of Carbon in Dry Oxidation, Expressed as Mass % Relative to Original Mass of Carbon (Distillation) and Available Mass of Carbon (Final Products)

Temperature (°C)	Distillation		Final Products of Oxidation		
	C _{Δ(s)}	C _{Δ(v)}	C _{ox(s)}	C _{ox(v)}	Heat (kJ/g bit avail)
155	82.4	17.6	77.3	22.7	1.9
174	75.0	25.0	(69.7)	(30.3)	4.0
225	59.5	40.5	49.7	50.3	12.5
285	48.7	51.3	29.8	70.2	16.4
317	44.6	55.4	0.0	100.0	18.1

The mass balance for carbon during dry oxidation of bitumen in our calorimeter can be calculated from the above results in combination with some of our chemical results for oxidized samples reported elsewhere (2). This mass balance is summarized in Table IV, where the following relationships have been used:

$$C_{\text{total}} = C_{\Delta(s)} + C_{\Delta(v)} \quad (15)$$

$$C_{\Delta(s)} = C_{\text{ox}(s)} + C_{\text{ox}(v)} \quad (16)$$

Here "Δ" indicates products produced by thermostating the calorimeter and its contents prior to oxidation and "ox" indicates products produced from the thermostatted samples by dry oxidation. The subscripts s and v refer to the phase (solid or vapor) in which the product remains or to which the product is transferred. Thus C_{Δ(s)} represents the amount of carbon actually available as fuel at each temperature, C_{ox(s)} represents the amount of carbon remaining as oxygenated bitumen, C_{Δ(v)} represents the amount of carbon distilled during heating, and C_{ox(v)} represents the amount of additional carbon converted by oxidation to volatile hydrocarbons and CO₂. The values listed in columns 1 through 4 of Table IV were obtained using Equations 15 and 16 rewritten (for convenient interpretation of the results) as Equations 17 through 20:

$$C_{\Delta(s)} = b_r c_r / b_o \quad (17)$$

$$C_{\Delta(v)} = 100 - C_{\Delta(s)} \quad (18)$$

$$C_{\text{ox}(s)} = c_c b_c / b_r \quad (19)$$

$$C_{\text{ox}(v)} = 100 - C_{\text{ox}(s)} \quad (20)$$

where b_r = mass of bitumen remaining in the heated sample, g
 c_r = carbon content of bitumen remaining, %
 b_o = original mass of bitumen, g
 c_c = carbon content of residual coke, %
 b_c = mass of residual coke, g

Values of $C_{Ox(s)}$ at 155, 225, and 317°C were calculated from the results of the distillation experiments described above, using data (2) for residual cokes. The value of $C_{Ox(s)}$ at 285°C was calculated from data from a new dry oxidation at 285°C. An estimate of the value of $C_{Ox(s)}$ at 174°C was obtained by fitting a line to the values for $C_{Ox(s)}$ at 155, 225, and 285°C (correlation coefficient = -0.999):

$$C_{Ox(s)} = 133.4 - 0.336 t \quad (21)$$

where t is temperature in °C. Smoothed values of $C_{\Delta(s)}$ at each temperature were calculated from the fitted equation

$$\text{mass \% bitumen remaining} = 8.11 + 1.1817 \times 10^4/t \quad (22)$$

Values of $C_{Ox(s)}$, and thence $C_{Ox(v)}$, for 174°C calculated as described here are shown in parentheses in Table IV.

The values in the first two columns of Table IV show the distribution of original carbon in products of distillation; values in the next two columns show the distribution of available carbon in products of oxidation. The large difference between the value of $C_{Ox(s)}$ at 317°C predicted by Equation 21, 17.4%, and the observed value of 0% underscores the validity of our proposed change in mechanism near 285°C. Additional evidence for this change is provided by the carbon contents of the residual cokes: 82% at room temperature, 72% at 155°C, 56% at 225°C, and 55% at 285°C. The levelling-off of carbon content of residual cokes between 225 and 285°C suggests that the depositional reaction begins to compete with a second type of reaction. That this second type of reaction involves burning of coke and other hydrocarbons is apparent in the much lower yield of residual coke at 285°C and higher yield of CO_2 (see discussion of Table IV below) at 285°C as compared to the yield at 225°C. The last column lists the total heat produced per gram of bitumen available and shows that the total heat relative to the mass of material from which it is produced increases an order of magnitude over the temperature range 155-320°C.

On the basis of the analysis presented in Tables II, III, and IV and measurements of the mass of CO_2 evolved during oxidation, Figure 1 was constructed to display the fraction of original carbon mobilized by heating, the fraction of the remaining (available) carbon mobilized as incompletely oxidized hydrocarbon by oxidation, and the fraction of available carbon deposited as coke by oxidation. The distribution of available carbon between the mobile and non-mobile products of oxidation lends additional support to our proposed "two-reactions" mechanism.

Part 3. Effect of Water Vapor on Kinetics and Energetics of Oxidation. A saturator containing distilled water at a known and controlled temperature (and hence a known vapor pressure of water) was inserted in the gas train between the oxygen cylinder and the inlet to the calorimeter. The saturator can be thoroughly flushed with oxygen and brought to the desired pressure of the oxidation experiment prior to injection of oxygen to the calorimeter. To prevent condensation of water vapor, the gas train between the oven and the saturator was wrapped with resistance tape which could be heated to a temperature above the temperature of the saturator. Pressure of oxygen was obtained as the difference between the measured total pressure and the vapor pressure of water at the measured temperature of water in the saturator. To avert complications due to corrosion, the aluminum combustion tube was replaced with a 316 stainless steel tube of the same outside diameter but having slightly thinner walls to aid in heat transfer. The dry oxidation experiments described in Part 2 were used to verify that neither the values of the calibration constants nor the values of initial rates of heat production and total heats produced were affected by the change in properties of the combustion tube.

Preliminary experiments to refine the operation of the calorimeter during wet oxidation have been performed at 225°C. Vapor pressure of water was approximately 13 kPa, corresponding to a saturator temperature of about 55°C. Pressures of oxygen were varied from 117 kPa to 368 kPa, with three experiments at $p(\text{O}_2) = 210$ kPa to determine reproducibility of the results.

Initial rates of oxidation were determined as described in Reference 1. Mass of residual coke was determined by ashing, and carbon and hydrogen content of the residual coke was determined by microanalysis. Because the relative error in the total heat produced by oxidation of the bitumen exceeded 50%, the heats were considered unreliable and are not reported here.

Experimental conditions and initial rates of oxidation are summarized in Table V. For comparison, initial rates of dry oxidation at the same temperature and pressure of oxygen predicted by Equation 9 are included in parentheses. The predicted dry rate, measured dry rate, and measured wet rates are compared in Figure 2. The logarithms of the initial rates of heat production during wet oxidation increase approximately linearly (correlation coefficient = 0.92) with the logarithm of the partial pressure of oxygen and lead to values of $\ln k = 2.5$ and $r = 0.9$, as compared with values of $\ln k = 4.8$ and $r = 0.6$ for dry oxidation at this temperature.

The results of the chemical analyses are summarized and compared in Table VI with similar results from dry oxidation. In comparison with dry oxidation at 225°C, wet oxidation at this same temperature leads to less residual coke. As shown by the molar H/C ratio, this residual coke is enriched in carbon. Less of the available carbon is converted to residual coke.

The conclusions that may be drawn from these exploratory kinetic and chemical data for wet oxidation are "sketchy" at best. Nevertheless, some observations and suggestions relevant to our continuing investigation are presented here.

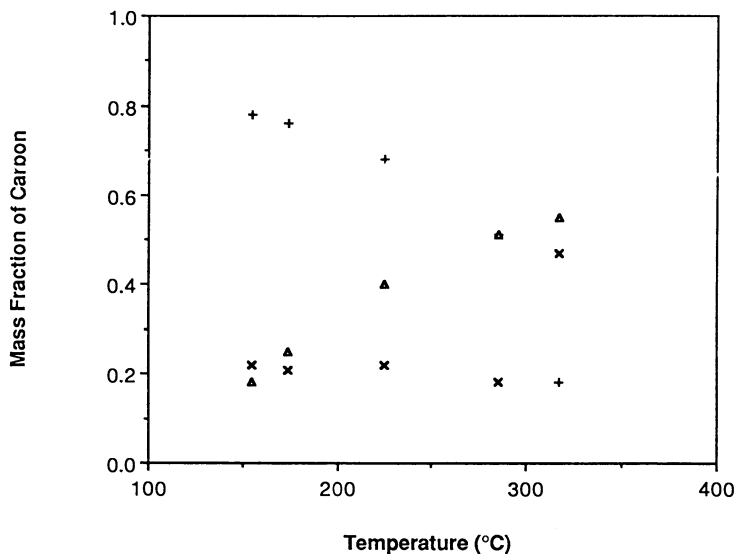


Figure 1. Distribution of available carbon. Symbols are: +, carbon deposited as coke by oxidation, g/g available; x, mobile carbon (minus carbon dioxide) produced by oxidation, g/g available; Δ , mobile carbon produced by heating in inert atmosphere, g/g original.

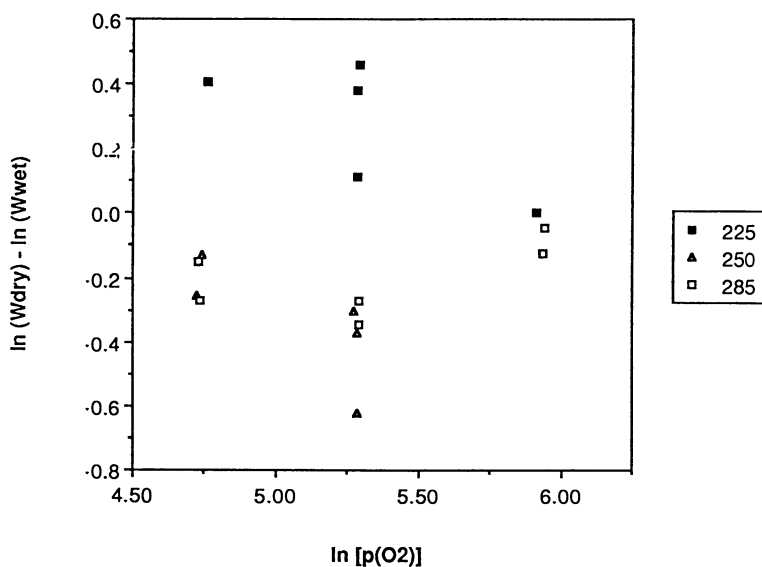


Figure 2. Rate of heat production by wet oxidation relative to dry oxidation at the same temperature and pressure of oxygen.

Table V. Initial Rates of Wet Oxidation at 225°C and 13 kPa H₂O^(a)

p(O ₂) (kPa)	p(H ₂ O) (kPa)	Initial Rate (W/g Bitumen)
198.2	12.3	1.2 (1.9)
197.4	13.1	1.3 (1.9)
197.4	13.1	1.7 (1.9)
368.4	13.6	2.8 (2.8)
117.0	13.6	1.0 (1.5)

^aLoading factor of calorimetric samples was 12.20%. Numbers in parentheses are the predicted dry rates.

Table VI. Residual Coke and Conversion of Available Carbon During Wet Oxidation of Athabasca Bitumen at 225°C^(a)

LF After Heating (%)	LF After Oxidation (%)	p(O ₂) (kPa)	p(H ₂ O) (kPa)	Residual Coke (g/g Bit Avail)	Molar H/C of Coke	C _{ox(s)} (%) ^(b)
8.62	6.18	210.7	-	0.70	0.77	49.7
8.42	5.11	198.1	12.3	0.64	0.37	42.2
8.42	5.21	197.4	13.1	0.65	0.32	42.2
8.42	5.30	197.4	13.1	0.66	0.33	42.7
8.42	5.53	386.4	13.6	0.69	0.68	44.6

^aData for dry oxidation are included for comparison. Loading factor (LF) of the original sample used in the dry oxidation experiments is 13.47 mass % bitumen. Loading factor of the original sample used in the wet oxidation experiments is 12.20 mass % bitumen. Molar H/C of unoxidized residue produced by heating to 225°C = 1.27.

^b(Mass of carbon converted to coke/mass of carbon available) x 100.

First, the rate of heat production is again related to the sum of the rates of depositional and burning processes, and if the predominant factor affecting the overall rate is temperature, then it does not seem likely that the specific effect of water vapor on the oxidation reported here is chemical catalysis, since a lowering of activation energy for either process would result in an increase in the overall rate relative to dry oxidation.

Second, the difference between the rates of wet and dry oxidation is dependent on p(O₂), being largest at low p(O₂) and essentially negligible at high p(O₂). Since p(H₂O) was held

constant in these experiments, this suggests a "concentration" effect; i.e., it appears that water vapor may interfere with some of the pathways by which the various components of bitumen react with oxygen. Millour et al. (16) and others (3-10, 11-15) have proposed that deposition of coke by low temperature oxidation of bitumen can be represented in terms of pseudocomponent reactions that involve conversion of original maltenes to new asphaltenes and resins and conversion of original asphaltenes to new resins. The results reported in Table VI suggest that water vapor induces selective removal of saturates, possibly by steam distillation of some of the polar intermediate compounds produced by oxidation of the original saturate fraction. Thus we observe a lower yield of coke, a lower molar H/C ratio of the residual coke, and a lower extent of conversion of total available carbon to coke. Such selective removal of saturates would be greatest at low $p(\text{O}_2)$ for a given $p(\text{H}_2\text{O})$. Finally, the amount of residual coke and the extent of conversion of carbon to coke would decrease with increasing $p(\text{H}_2\text{O})$ for a given $p(\text{O}_2)$.

What would be the corresponding effect of water vapor on the overall rate of heat production? The rate of heat production must now be considered as the sum of the rates of heat evolution by deposition and burning plus the rate of heat absorption by distillation; i.e., the overall rate of heat production must be smaller than the dry rate:

$$W_{\text{wet}} = W_{\text{dry}} - W_{\text{d}} \quad (23)$$

where $W_{\text{dry}} = W_{\text{D}} + W_{\text{B}}$ and the subscript d refers to water-enhanced distillation.

Tentative values of a reaction order, x , and rate constant, k_{d} , for the proposed distillation reaction can be calculated from the data in Table V using Equation 23 and the relationship

$$\ln W_{\text{d}} = \ln k_{\text{d}} + x \ln [p(\text{H}_2\text{O})/p_{\text{total}}] \quad (24)$$

The result is $\ln k_{\text{d}} = 9.2 \pm 0.2$ and $x = 1.4 \pm 0.1$. Representing the rate constant k_{d} with an Arrhenius equation and approximating the activation energy, $E_{\text{a(d)}}$, with an average heat of vaporization equal to $\sim 80 \text{ kJ mol}^{-1}$, a value of $\ln A_{\text{d}} = 28.7 \pm 0.2$ is obtained.

Further to our preliminary studies at 225°C subsequent wet oxidation experiments have been carried out at temperatures of 250 and 285°C. Partial pressures of oxygen were varied from 19 to 289 kPa whilst the partial pressure of water vapor in the calorimetric system was maintained at approximately 15 kPa.

As for the distillation experiments (Part 2) no condensate was found in the cold trap (dry ice/acetone) at the end of each wet oxidation experiment. On exiting the cold trap the flowing gases were directed through a drying tube containing phosphorus pentoxide supported on glass wool. It was on this boundary that most distillate was recovered. Apparently the distillate is too volatile to be condensed by dry ice/acetone and is only recovered when it undergoes a chemical reaction with the P_2O_5 . The oily liquid produced at this boundary, which is found to be soluble in ethanol and water, is under investigation. In an attempt to

simplify this process it is planned to collect a sample of the volatile distillate and subject it to a mass spectrophotometric investigation. The results of these studies will be discussed in a future publication.

Table VII. Initial Rates of Wet Oxidation at 285°C and 250°C^(a)

p(O ₂) (kPa)	p(H ₂ O) (kPa)	Temperature (°C)	Initial Rate (W/g bitumen)
113.00	15.15	284.98	12.84 (11.06)
113.92	15.00	284.33	14.19 (10.80)
198.81	15.00	283.03	19.12 (14.62)
197.95	17.14	283.82	21.31 (15.11)
381.17	14.72	284.82	25.42 (24.30)
377.51	15.87	283.92	26.17 (23.09)
114.37	15.58	249.93	3.59 (3.15)
112.82	16.50	248.55	3.86 (3.00)
194.57	17.14	248.44	5.47 (4.05)
197.47	15.00	249.78	7.95 (4.26)
197.76	16.66	250.05	6.24 (4.30)

^aLoading factor of calorimetric samples was 12.20%. Numbers in parentheses are the predicted dry rates calculated from Equation 9.

Initial rates of heat production are recorded together with the experimental conditions in Table VII. Comparison with the initial rates of heat production for dry oxidation, estimated from Equation 9, shows that at both 250 and 285°C the rate of heat production for the wet oxidation process is faster than that for the dry oxidation process at the same temperature. For experiments conducted at 285°C the relationship between the logarithms of the initial rates of heat production for wet oxidation and the logarithm of the partial pressure of oxygen in the system are found to be linear. A linear least squares fit to these data gave estimates of the kinetic parameters $\ln k$ and r which are contained in Table VIII together with estimates of the same parameters for the dry oxidation process, calculated from Equation 9. The reaction order with respect to oxygen is decreased for the wet oxidation process relative to the dry process at the same temperature. However, this is over-compensated by increases in the rate constant for the wet oxidation process, leading to an overall increase in the initial rate of heat production compared to the dry oxidation process at the same temperature. There are not yet enough data points for the wet oxidation process at 250°C to justify a fit to the data, but initial trends in the plot of the logarithm of the initial rate of heat production against the logarithm of the partial pressure of oxygen suggest a similar situation as discussed for the wet oxidation process at 285°C. On comparison with our wet oxidation results at 225°C it appears that by raising the temperature only 25°C we have gone from the situation in which the initial rate of heat production for the wet oxidation process is slower than the rate of the dry oxidation to a situation in which the rate of heat production for the wet oxidation process is faster than that of the corresponding dry

process. Figure 2 clearly identifies the situation described above by showing a plot of the logarithm of the ratio of the dry to the wet initial rates of heat production against the logarithm of the partial pressure of oxygen in the system.

Table VIII. Values of Kinetic Parameters for the Wet Oxidation of Athabasca Bitumen at 285°C

Equation (a)	ln k	r
$\ln W_{w285} = \ln k + r \ln p(O_2)$	7.03±0.35	0.53±0.07
$\ln W_{d285} = \ln k + r \ln p(O_2)$	6.22	0.65

^aThe correlation coefficient for wet oxidation at 285°C (subscript w285) is -0.97. Subscript d285 refers to the dry oxidation process at 285°C. Kinetic parameters for the dry oxidation process were calculated with the aid of Equation 9.

Equation 23 can no longer be used to describe the initial rate of heat production for the wet oxidation process at these elevated temperatures. However, it was expected that an equation of the form shown below would suffice:

$$W_{wet} = W_{dry} + W_x \quad (25)$$

Here W_x represents the initial rate of heat production for some process (or processes) that is dependent on the partial pressure of the water vapor in the calorimetric system and gives a positive contribution to the initial rate of heat production by wet oxidation (unlike the steam distillation process envisaged for wet oxidation at 225°C, which aids in the retardation of the initial rate of heat production). If this relationship were valid, then a plot of the logarithm of the initial rate W_x against the logarithm of the ratio of the partial pressure of water vapor in the system to the total pressure in the system would be linear. However, as demonstrated by Figure 3, no such simple relationship is found. This procedure illustrates the difficulties involved in interpreting experimental results when there are three variables, instead of two variables as in dry oxidation.

Table IX. Mass % Composition of Cokes Produced by the Wet Oxidation Process at 285°C

Average Oxygen Pressure in System (kPa)	Mass %						Molar H/C ^(c)
	C	H	S	N	O ^(a)		
113.46	35.0	0.3	-	-	64.7	0.10	
198.38	51.5	2.0	-	-	46.3	0.46	
379.34	40.0	1.5	-	-	58.5	0.45	
Unoxidized ^(b)	81.4	8.9	6.0	trace	3.8	1.31	

^aMass composition of oxygen calculated by difference.

^bMass % composition of oil sand prior to oxidation experiment.

^cThe molar H/C ratio for the dry oxidation process at 285°C is estimated at 0.62.

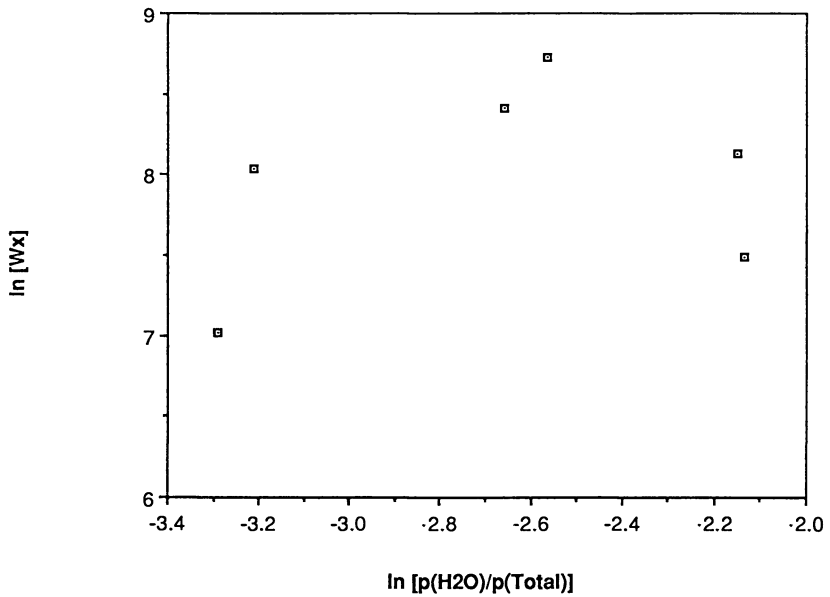


Figure 3. Variation of the difference between the wet and the dry initial rates of heat production as a function of the partial pressure of water vapor in the system at 285°C.

The elemental compositions of the oxidized oil sands produced from our calorimetric experiments at 285°C have been determined. The results, corrected for the elemental composition of the support material, are reported in Table IX. The elemental composition of the unoxidized bitumen is included for comparison. As predicted from our dry oxidation experiments, all of the sulfur present in the bitumen at the start of the wet oxidation experiments has been oxidized to volatile products and subsequently removed. The mass percents of carbon and hydrogen present in the analyzed cokes follow the pattern described by the initial rate of heat production for the process described by W_x , i.e., the mass percents of carbon and hydrogen in the cokes initially increase with an increase in oxygen pressure, reach a maximum value at some intermediate oxygen pressure, and then decrease with increasing oxygen pressure. The molar H/C ratio is very small at low oxygen pressures; however, it can be seen to increase with an increase of the oxygen pressure.

The results of ashing experiments on the samples from wet oxidation experiments conducted at 285°C are contained in Table X. The loading factors of the oxidized oil samples are dramatically reduced compared to those for samples oxidized at 225°C (see Table VI). The amount of residual coke per gram of bitumen available in each sample can also be seen to have undergone a dramatic reduction as have the estimates of $C_{Ox(s)}$, the amount of available carbon converted to coke, compared to the lower temperature wet oxidation study.

Table X. Residual Coke and Conversion of Available Carbon During Wet Oxidation of Athabasca Bitumen at 285°C

LF After Heating ^(b) (%)	LF After Oxidation (%)	$p(O_2)$ (kPa)	$p(H_2O)$ (kPa)	Residual Coke (g/g Bit Avail)	$C_{Ox(s)}$ ^(a) (%)
6.05	1.16	113.00	15.15	0.14	5.5
6.05	1.23	113.92	15.00	0.14	6.9
6.05	1.62	198.81	15.00	0.20	14.1
6.05	1.52	197.95	17.14	0.20	11.3
6.05	1.00	381.17	14.72	0.14	7.1
6.05	1.52	377.51	15.87	0.18	8.2

^a(Mass of carbon converted to coke/mass of carbon available) x 100.

For dry oxidation at 285°C $C_{Ox(s)}$ is estimated at 29.8%.

^bEstimated from Equation 22.

Both of the above chemical studies point towards the increased importance of the burning process at 285°C in determining the initial rate of heat production. The role of water as yet remains undefined other than at the higher temperature of 285°C it appears to have the opposite effect on the bitumen sample compared to the process at 225°C; i.e., it appears that water vapor encourages pathways by which the various components of bitumen react with oxygen. Preliminary calculations of the total heats evolved during the wet oxidation of bitumen sands indicate that they are independent of the partial pressure of oxygen in the system at

285°C, a conclusion that is supported by the loading factors of the residual cokes shown in Table X.

Our earlier (2) and present results pertaining to the dry oxidation of Athabasca bitumen have provided a clear picture of the dependence of rate and energetics on temperature and on pressure of oxygen. These results have led to an overall mathematical model and also to a "two reaction chemical model" that can be represented by two relatively simple equations. Introducing the additional variable of partial pressure of water vapor that is pertinent to wet oxidation processes also introduces many complications and ambiguities so that the present results have led to specific information but no clear overall picture. Continuing measurements of rates of wet oxidation, supplemented with chemical investigations, are providing more specific information from which we hope to develop an overall mathematical model and also a chemical model, as already done for dry oxidation.

LITERATURE CITED

1. Zhang, Z.-l.; Barta, L.; Hepler, L. G. AOSTRA J. Research 1987, 3, 249.
2. Barta, L.; Hepler, L. G. Energy and Fuels 1988, 2, 309.
3. Dabbous, M. K.; Fulton, B. F. Soc. Petrol. Eng. J. 1974, 14, 253.
4. Fassihi, R. Z.; Brigham, W. E.; Ramey, H.J., Jr. Soc. Petrol. Eng. J. 1984, 24, 399 and 408.
5. Phillips, C. R.; Hsieh, I. C. Fuel 1985, 64, 985.
6. Yoshiki, K. S.; Phillips, C. R. Fuel 1985, 64, 1591.
7. Verkoczy, B.; Jha, K. N. J. Can. Petrol. Techn. 1986, 25, 47.
8. Vossoughi, S.; Bartlett, G. W.; Willhite, G. P. Soc. Petrol. Eng. J. 1985, 25, 656.
9. Kharrat, R.; Vossoughi, S. J. Petrol. Techn. 1985, 37, 1441.
10. Burger, J.; Sahuquet, B. Rev. Inst. Fr. Petrol. 1977, 32, 141.
11. Ciajolo, A.; Barbella, R. Fuel 1984, 63, 657.
12. Moschopedis, S. E.; Speight, J. G. J. Mat. Sci. 1977, 12, 990.
13. Moschopedis, S. E.; Speight, J. G. Fuel 1975, 54, 210.
14. Moschopedis, S. E.; Speight, J. G. Fuel 1973, 52, 83.
15. Nouredin, N. A.; Lee, D. G.; Mourits, F. M.; Jha, K. N. AOSTRA J. Research 1987, 3, 155.
16. Millour, J. P.; Moore, R. G.; Bennion, D. W.; Ursenback, M. G.; Gie, D. N. An Expanded Compositional Model for Low Temperature Oxidation of Athabasca Bitumen, paper no. 86-32-41, Petroleum Society of CIM. June 8-11, 1986.

RECEIVED February 7, 1989

Chapter 24

Thermodynamic and Colloidal Models of Asphaltene Flocculation

S. Kawanaka, K. J. Leontaritis, S. J. Park, and G. A. Mansoori

Department of Chemical Engineering (M/C 110), University of Illinois,
Chicago, IL 60680

This paper reviews the experiences of the oil industry in regard to asphaltene flocculation and presents justifications and a descriptive account for the development of two different models for this phenomenon. In one of the models we consider the asphaltenes to be dissolved in the oil in a true liquid state and dwell upon statistical thermodynamic techniques of multicomponent mixtures to predict their phase behavior. In the other model we consider asphaltenes to exist in oil in a colloidal state, as minute suspended particles, and utilize colloidal science techniques to predict their phase behavior. Experimental work over the last 40 years suggests that asphaltenes possess a wide molecular weight distribution and they may exist in both colloidal and dissolved states in the crude oil.

The key to solving many of the technical problems that face the fossil fuel industries in our modern technological society today lies heavily in understanding the thermodynamic and transport aspects of these problems. Most of the irreplaceable energy resources available are mainly mixtures of gases, liquids and solids of varying physical and chemical properties contained in the crust of the earth in a variety of geological formations. Knowledge of the fluid phase equilibrium thermodynamic and transport characteristics of these mixtures is a primary requirement for the design and operation of the systems which recover, produce and process such mixtures.

There has been extensive progress made in the past several years in the formulation of statistical thermodynamics of mixtures and transport phenomena modeling of multiphase flow in composite media. This knowledge may now be applied to the understanding and prediction of the phase and transport behavior of reservoir fluids and other

hydrocarbon mixtures. The present report is designed with the purpose of describing the role of modern theoretical and experimental techniques of statistical thermodynamics and transport and electrokinetic phenomena to develop methods that will predict asphaltene and asphalt flocculation during the production, transportation, and processing of petroleum.

The mechanisms of gas injection and oil recovery involved with miscible gas flooding are basically of three kinds [1,2]: (i) The first-contact miscible gas drive, (ii) The condensing gas drive (or the enriched gas drive), and (iii) The vaporizing gas drive (or the high pressure gas drive) processes. The first and second processes are based on the injection of hydrocarbons that are soluble in the residual oil, while the third process involves injection of a high density gas, such as high-pressure nitrogen or carbon dioxide. In the case of the first-contact miscible process, a typical injection fluid is propane, which is soluble in oil. For the condensing gas drive process the injection fluid could be natural gas containing relatively high concentration of intermediate hydrocarbons, such as ethane, propane, and butane.

Miscible flooding of petroleum reservoirs by carbon dioxide, natural gas, and other injection fluids has become an economically viable technique for petroleum production (1,2). The most common problem in petroleum recovery is poor reservoir volumetric sweep efficiency, which is due to channeling and viscous fingering because of the large difference between mobilities of the displacing and displaced fluids. Introduction of a miscible fluid in the petroleum reservoirs in general will produce a number of alterations in the flow behavior, phase equilibrium properties, and the reservoir rock characteristics. One such alteration is asphaltene and wax precipitation, which is expected to affect productivity of a reservoir in the course of oil recovery from the reservoir. (3,4,5). In most of the instances observed asphaltene and wax precipitation may result in plugging of or wettability reversal in the reservoir. Effect of asphaltene deposition could be positive (like prevention of viscous fingering) or negative (complete plugging of the porous media) depending on whether it could be controlled and predicted before it occurs.

The parameters that govern precipitation of asphaltene and wax appear to be composition of crude and injection fluid, pressure, and temperature of the reservoir. With alterations in these parameters the nature of asphaltene and wax substances which precipitate will vary. Also, precipitation of asphaltene is generally followed with polymerization or flocculation of the resulting precipitate, which produces an insoluble material in the original reservoir fluid (6,7,8). Because of the complexity of the nature of asphaltic and wax substances the phenomena of precipitation and flocculation of these substances are not well understood. Also in view of the complexity of the petroleum reservoirs, study and understanding of the in situ precipitation of asphaltene and wax seems to be a challenging and timely task. Such an understanding will help to design a more profitable route for miscible gas flooding projects.

In part II of the present report the nature and molecular characteristics of asphaltene and wax deposits from petroleum crudes are discussed. The field experiences with asphaltene and wax deposition and their related problems are discussed in part III. In order to predict the phenomena of asphaltene deposition one has to consider the use of the molecular thermodynamics of fluid phase equilibria and the theory of colloidal suspensions. In part IV of this report predictive approaches of the behavior of reservoir fluids and asphaltene depositions are reviewed from a fundamental point of view. This includes correlation and prediction of the effects of temperature, pressure, composition and flow characteristics of the miscible gas and crude on: (i) Onset of asphaltene deposition; (ii) Mechanism of asphaltene flocculation. The in situ precipitation and flocculation of asphaltene is expected to be quite different from the controlled laboratory experiments. This is primarily due to the multiphase flow through the reservoir porous media, streaming potential effects in pipes and conduits, and the interactions of the precipitates and the other in situ material present. In part V of the present report the conclusions are stated and the requirements for the development of successful predictive models for the asphaltene deposition and flocculation are discussed.

Nature and Properties of Asphaltenes

The classic definition of asphaltenes is based on the solution properties of petroleum residua in various solvents. The word asphaltene was coined in France by J.B. Boussingault in 1837. Boussingault described the constituents of some bitumens (asphalts) found at that time in eastern France and in Peru. He named the alcohol insoluble, essence of turpentine soluble solid obtained from the distillation residue "asphaltene", since it resembled the original asphalt.

In modern terms, asphaltene is conceptually defined as the normal-pentane-insoluble and benzene-soluble fraction whether it is derived from coal or from petroleum. The generalized concept has been extended to fractions derived from other carbonaceous sources, such as coal and oil shale (8,9). With this extension there has been much effort to define asphaltenes in terms of chemical structure and elemental analysis as well as by the carbonaceous source. It was demonstrated that the elemental compositions of asphaltene fractions precipitated by different solvents from various sources of petroleum vary considerably (see Table I). Figure 1 presents hypothetical structures for asphaltenes derived from oils produced in different regions of the world. Other investigators (10,11) based on a number of analytical methods, such as NMR, GPC, etc., have suggested the hypothetical structure shown in Figure 2.

It has been shown (9) that asphaltenes contain a broad distribution of polarities and molecular weights. According to these studies, the concept of asphaltenes is based on the solubility behavior of high-boiling hydrocarbonaceous materials in benzene and low-molecular weight n-paraffin hydrocarbons. This solubility behavior is a result of physical effects that are caused by a spectrum of chemical properties. Long also

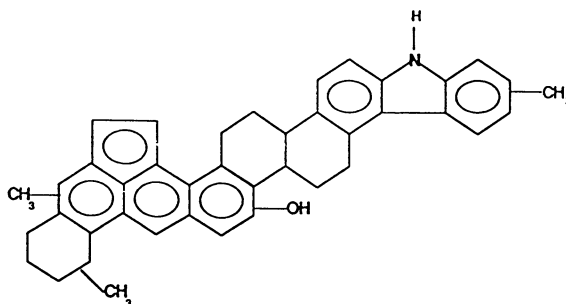


Figure 1. An example of a hypothetical structure of asphaltene, among the many suggested, showing their aromatic character.

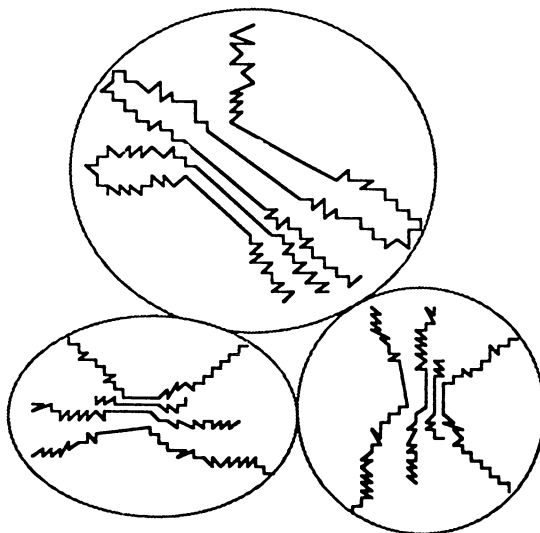


Figure 2. Asphaltene structure deduced from microscopic and macroscopic analysis, showing their micro- and macro-molecular bonding. T. F. Yen, 1972, first suggested this type of structure.

explained that by considering molecular weight and molecular polarity as separate properties of molecules, the solvent-precipitation behavior of materials derived from various carbonaceous sources can be understood. Future quantification of Long's approach probably can be achieved by developing a polarity scale based on solubility parameter.

According to Marcusson (11) there is a close relation between asphaltenes, resins, and high molecular weight polycyclic aromatic hydrocarbons which may exist in petroleum. The heavy polycyclic aromatics of petroleum, on oxidation gradually form neutral resins (and probably asphaltogenic acids,); asphaltenes are made as a result of further oxidation of neutral resins. On the contrary, the hydrogenation of asphaltic products containing neutral resins and asphaltenes produces heavy hydrocarbon oils, i.e., neutral resins and asphaltenes are hydrogenated into high molecular weight polycyclic aromatic structures. Asphaltenes are very similar to neutral resins in the ultimate analysis. The process of transformation of neutral resins into asphaltenes is very simple even at low temperatures. Specially neutral resins can easily be converted to asphaltenes in the presence of air or oxygen at elevated temperatures. Thus neutral resins and asphaltenes are similar in their chemical structure.

The physical and physico-chemical properties of asphaltenes are different with those of neutral resins. The molecular weight of asphaltenes is very high. Published data (9,12,13,14,15,16) for the molecular weight of petroleum asphaltenes range from approximately 1,000 to 2,000,000. The reported molecular weight of asphaltene varies considerably depending upon the method of measurement. A major concern in reporting molecular weights is the association of asphaltenes which can exist at the conditions of the method of measurement. Vapor pressure osmometry (VPO) has become the most prevalent method for determining asphaltene molecular weights. However, the value of the molecular weight from VPO must be weighed carefully since, in general, the measured value of the molecular weight is a function of the solvent and its dielectric constant. Reported molecular weights from ultracentrifuge and electron microscope studies are high. To the contrary, those from solution viscosity and cryoscopic methods are low. Asphaltenes are lyophilic with respect to aromatics, in which they form highly scattered colloidal solutions. Specifically, asphaltenes of low molecular weight are lyophobic with respect to paraffins like pentanes and petroleum oils.

Thus the degree of dispersion of asphaltenes in petroleum oils depends upon the chemical composition of the oil. In heavy highly aromatic oils the asphaltenes are colloiddally dispersed; but in the presence of an excess of petroleum ether and similar paraffinic hydrocarbons they are coagulated and precipitated. The coagulated and precipitated asphaltenes can be re-peptized (colloiddally dispersed) by the addition of aromatics. Neutral resins are particularly effective as peptizers. Such components as resins or high molecular weight aromatics are readily adsorbed by asphaltenes and act as protective layers, isolating the colloidal particles from the coagulative action of

lyophobic constituents of petroleum oils. If the proportion of the peptizing constituents in a petroleum oil is sufficient, the asphaltenes form stable suspensions.

Sachanen (11) explained that the solution of asphaltenes in an aromatic solvent is preceded by swelling of the powdered asphaltenes accompanied by evolution of heat. Nellensteyn discovered that the peptizing or precipitating properties of different liquids with respect to asphaltenes are closely related to the surface tension. Flocculation occurs when the solvent has a surface tension below 24 dynes/cm at 25°C. Total peptization takes place when the surface tension exceeds 26 dynes/cm. In the intermediate zone between 24 and 26 dynes/cm, either flocculation or peptization may occur, depending on the properties of the asphaltenes. Asphaltenes in solution are generally recognized as colloidal systems. Several investigators have observed that colloidal solutions can be precipitated by flow through capillaries and porous media (4,7). The precipitation is believed to result from the electrical interactions with the walls which disturb the stabilizing electrical forces around the colloidal particles and the particles agglomerate to a precipitate. The asphaltene particles are electrically charged and thus can be precipitated by application of an electrical potential or by flow of the asphaltene-containing product through the sand, due apparently to electrical effects resulting from the flow. On the contrary, application of a counter-potential may prevent precipitation of asphaltenes from the crude oil flowing through a porous material.

Asphaltenes are not crystallized and cannot be separated into individual components or narrow fractions. Thus, the ultimate analysis is not very significant, particularly taking into consideration that the neutral resins are strongly adsorbed by asphaltenes and probably cannot be effectively separated from them. Not enough is known of the chemical properties of asphaltenes. On heating, they are not melted, but decompose, forming carbon and volatile products above 300-400 °C. They react with sulfuric acid forming sulfonic acids, as might be expected on the basis of the polyaromatic structure of these components. The color of dissolved asphaltenes is deep red at very low concentration in benzene as 0.0003 per cent makes the solution distinctly yellowish. The color of crude oils and residues is due to the combined effect of neutral resins and asphaltenes. The black color of some crude oils and residues is related to the presence of asphaltenes which are not properly peptized.

Field Experiences

Asphaltene deposition during oil production and processing is a very serious problem in many areas throughout the world. In certain oil fields (12,13,14) there have been wells that, especially at the start of production, would completely cease flowing in a matter of a few days after an initial production rate of up to 3,000 BPD. The economic implications of this problem are tremendous considering the fact that a problem well workover cost could get as high as a quarter of a million

dollars. In another field the formation of asphaltic sludges after shutting in a well temporarily and/or after stimulation treatment by acid has resulted in partial or complete plugging of the well (7). Still in another field, deposit of asphaltenes in the tubing was a very serious production problem and necessitated frequent tubing washings or scrapings to maintain production (17). Asphaltenes have played a significant role in the production history and economics of the deep horizons of some oil reservoirs (18). For example in one case asphaltene problems have ranged from asphaltene deposition during early oil production to asphaltene flocculation and deposition resulting from well acidizing and carbon dioxide injection for enhanced oil recovery.

Table I. Elemental compositions of asphaltenes precipitated by different flocculants from various sources (16)

Source	Flocculant	Elemental Composition(wt%)					Atomic Ratios			
		C	H	N	O	S	H/C	N/C	O/C	S/C
Canada	n-pentane	79.5	8.0	1.2	3.8	7.5	1.21	.013	.036	.035
	n-heptane	78.4	7.6	1.4	4.6	8.0	1.16	.015	.044	.038
Iran	n-pentane	83.8	7.5	1.4	2.3	5.0	1.07	.014	.021	.022
	n-heptane	84.2	7.0	1.6	1.4	5.8	1.00	.016	.012	.026
Iraq	n-pentane	81.7	7.9	0.8	1.1	8.5	1.16	.008	.010	.039
	n-heptane	80.7	7.1	0.9	1.5	9.8	1.06	.010	.014	.046
Kuwait	n-pentane	82.4	7.9	0.9	1.4	7.4	1.14	.009	.014	.034
	n-heptane	82.0	7.3	1.0	1.9	7.8	1.07	.010	.017	.036

Even for reservoirs in which asphaltene deposition was not reported previously during the primary and secondary recovery, it was reported that asphaltene deposits were found in the production tubing during carbon dioxide injection enhanced oil recovery projects (18).

Asphaltene precipitation, in many instances, carries from the well tubing to the flow lines, production separators, and other downstream equipment. It has also been reported (19) that asphaltic bitumen granules occurred in the oil and gas separator with oil being produced from certain oil fields.

The downtime, cleaning, and maintenance costs are a sizable factor in the economics of producing a field prone to asphaltene deposition. Considering the trend of the oil industry towards deeper reservoirs, heavier and as a result asphaltic crudes, and the increased utilization of miscible gas injection techniques for recovering oil, the role of asphaltene deposition in the economic development of asphaltene containing oil discoveries will be important and crucial.

Modeling of Asphaltene Flocculation, and its Interaction with Oil

Solution of the asphaltene problem calls for detailed analyses of asphaltene containing systems from the statistical mechanical standpoint and development of molecular models which could describe the behavior of asphaltenes in hydrocarbon mixtures. From the available laboratory and field data it is proven that the asphaltene which exists in oil consists of very many particles having molecular weights ranging from one thousand to several hundred thousands. As a result distribution-function curves are used to report their molecular weights. The wide range of asphaltene size distribution suggests that asphaltenes may be partly dissolved and partly in colloidal state (in suspension) peptized (or stabilized) primarily by resin molecules that are adsorbed on asphaltene surface (12,13,14,19,20). As a result, a realistic model for the interaction of asphaltene and oil should take into account both the solubility in oil of one segment and suspension characteristic (due to resins) of another segment of the molecular weight distribution curve of asphaltene. We have proposed two different models (12,13,21,22) which are based on statistical mechanics of particles (monomers and polymers) dissolved or suspended in oil. A combination of the two models is general enough to predict the asphaltene-oil interaction problems (phase behavior or flocculation) wherever it may occur during oil production and processing.

Such a model may be constructed by joining the concepts of continuous thermodynamic theory of liquid-solid phase transition, fractal aggregation theory of colloidal growth, and steric colloidal collapse and deposition models.

Solubility Model of Interaction of Asphaltene and Oil : It is generally assumed that two factors are responsible for maintaining the mutual solubility of the compounds in a complex mixture such as the petroleum crude: These are the ratio of polar to nonpolar molecules and the ratio of the high molecular weight to low molecular weight molecules in the mixture. Of course, polar and nonpolar compounds are basically immiscible, and light and heavy molecules of the same kind are partially miscible depending on the differences between their molecular weights. However, in the complex mixture of petroleum crude or coal liquids and the like all these compounds are probably mutually soluble so long as a certain ratio of each kind of molecule is maintained in the mixture. By introduction of a solvent into the mixture this ratio is altered. Then the heavy and/or polar molecules separate from the mixture either in the form of another liquid phase or to a solid precipitate. Hydrogen bonding and the sulfur and/or the nitrogen containing segments of the separated molecules could start to aggregate (or polymerize) and as a result produce the irreversible asphaltene deposits which are insoluble in solvents. In order to formulate the necessary model for prediction of the "onset of deposition" of asphaltene we have taken advantage of the theories of polymer solutions (22,23,24). Both asphaltenes and asphaltene-free crude consist of mixtures of molecules with a virtually

continuous molecular weight distributions in order to formulate the theory of interaction of oil and asphaltene systems we can utilize the concept of continuous mixture (16,21) joined with the thermodynamic theory of heterogeneous polymer solutions (22,24). We have already formulated the necessary continuous mixture model for the prediction of the "onset of deposition" of asphaltene due to injection of a miscible solvent. In the course of our ongoing research we intend to extend our model to varieties of crude oils and miscible solvents of practical interest (Figure 3).

Suspension Model of Interaction of Asphaltene and Oil : This model is based upon the concept that asphaltenes exist as particles suspended in oil. Their suspension is assisted by resins (heavy and mostly aromatic molecules) adsorbed to the surface of asphaltenes and keeping them afloat because of the repulsive forces between resin molecules in the solution and the adsorbed resins on the asphaltene surface (see Figure 4). Stability of such a suspension is considered to be a function of the concentration of resins in solution, the fraction of asphaltene surface sites occupied by resin molecules, and the equilibrium conditions between the resins in solution and on the asphaltene surface. Utilization of this model requires the following (12): 1. Resin chemical potential calculation based on the statistical mechanical theory of polymer solutions. 2. Studies regarding resin adsorption on asphaltene particle surface and measurement of the related Langmuir constants. 3. Calculation of streaming potentials generated during flow of charged asphaltene particles. 4. Development and use of asphaltene colloidal and aggregation models for estimating the amount of asphalt which may be irreversibly aggregated and flocculated out. The amount of resins adsorbed is primarily a function of their concentration in the liquid state (the oil). So, for a given system (i.e., fixing the type and amount of oil and asphaltenes) changing the concentration of resins in the oil will cause the amount of resins adsorbed on the surface to change accordingly. This means that we may drop the concentration of resins in the oil to a point at which the amount of resins adsorbed is not high enough to cover the entire surface of asphaltenes. This may then permit the asphaltene particles to come together (irreversible aggregation), grow in size, and flocculate.

One major question of interest is how much asphaltene will flocculate out under certain conditions. Since the system under study consist generally of a mixture of oil, aromatics, resins, and asphaltenes it may be possible to consider each of the constituents of this system as a continuous or discrete mixture (depending on the number of its components) interacting with each other as pseudo-pure-components. The theory of continuous mixtures (24), and the statistical mechanical theory of monomer/polymer solutions, and the theory of colloidal aggregations and solutions are utilized in our laboratories to analyze and predict the phase behavior and other properties of this system.

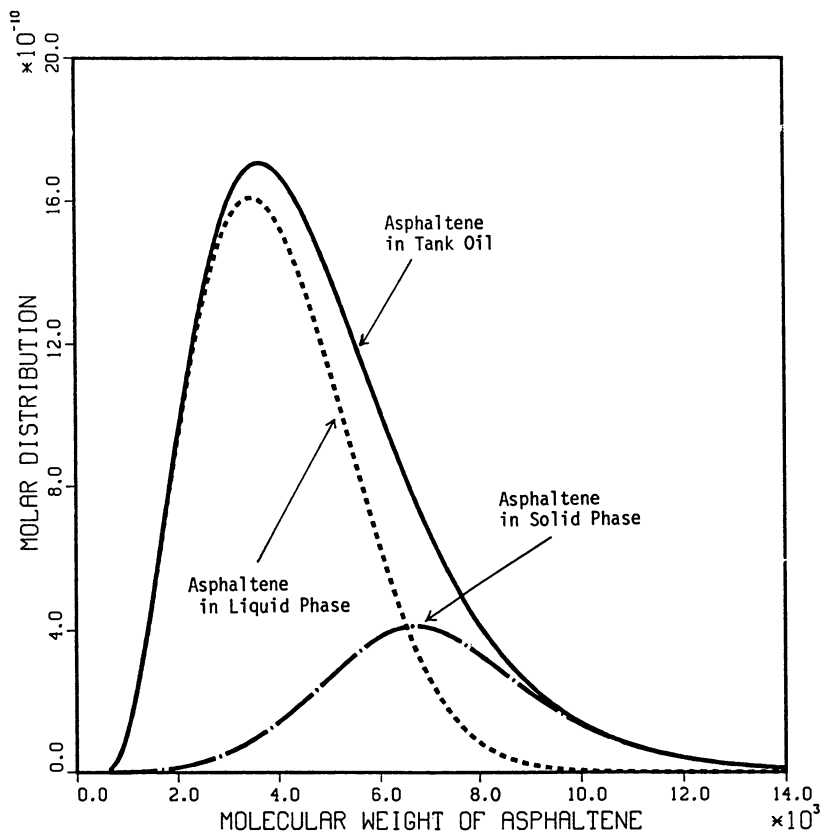
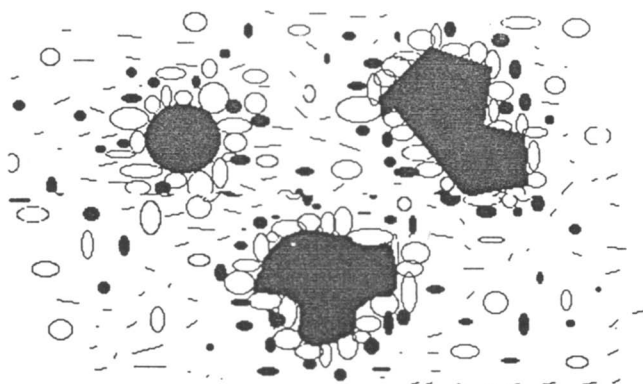


Figure 3. Molecular weight distributions of asphaltenes before and after flocculation predicted by our continuous mixture model.

**NOTES**


- 1.0 ○ represents resin molecules
- 2.0 ● represents aromatic molecules
- 3.0 — represents oil molecules of different size and paraffinic nature
- 4.0  represents asphaltene particles of different sizes and shapes

Figure 4. Asphaltene particle peptization effected by adsorbed resin molecules. This physical model is the basis of our asphaltene Thermodynamic-Colloidal Model.

Discussions

It has been shown experimentally (4,7,12,13,14) beyond any reasonable doubt that the electrical charge of colloidal asphaltenes is a very important property and, regardless of the charge sign, it seems possible to devise colloidal asphaltene deposition preventive measures by controlling the electrical effects attributed to the charge of asphaltenes. The primary electrokinetic phenomenon in effect is the "streaming potential" generated by the movement of the electrically charged colloidal asphaltene particles due to the flow of oil. This streaming potential seems to neutralize the similar charge of the colloidal asphaltene particles and cause them to flocculate. The electric charge of colloidal asphaltenes has not been explained yet, primarily because of the complexity of the composition of asphaltic materials. The difference in charge (+or-) displayed by asphaltene particles derived from different crudes has not been explained either. One suggestion has been that the large quantities of nickel and vanadium found in asphaltene deposits may hold the key to these charges (7). This idea may be investigated by analyzing metal contents of asphaltene deposits that contain colloidal asphaltene particles with different electric charge.

One thing that appears to be universally accepted is that resins in the petroleum act as peptizing agents of the colloidal asphaltene particles. A number of experiments have been performed that point out the peptizing role of resins (4,7,12,19,25). However, because of the significance of the resins as peptizing agents of the colloidal asphaltene particles and the fact that based on current experimental information they appear to be the main hope for combating the colloidal asphaltene problem in the field, more experiments must be performed to establish clearly and beyond any doubt the resin role in the asphaltene deposition problem and generate enough thermodynamic properties of the resins to be utilized in modeling efforts to the problem.

Experimental evidence (4,25) suggests that for an oil mixture there is a critical concentration of resins below which the colloidal asphaltene particles may flocculate and above which they cannot flocculate regardless of how much the oil mixture is agitated, heated, or pressurized sort of changing its composition. The authors believe that there should be certain unique geological conditions which favor the formation of an oil whose actual resin concentration is less than its critical resin concentration. Such conditions are responsible for the transformations the hydrocarbon deposits undergo. These geological conditions could conceivably be identified and established after sufficient experimental data on actual resin concentration and critical resin concentration are generated for different crude oils around the world. As a result, geological conditions alone could provide clues for predicting potential asphaltene problems for oils that have not yet been produced.

The postulated and sufficiently proven notion that asphaltenes are oxidation products of resins and that resins are oxidation products of oil (11) sort of makes the probability of finding oils whose actual resin concentration is less than their critical resin concentration small. In other

words, an oil deposit must have a substantial amount of resins before starting to form asphaltenes during the natural geological transformation process. Table II seems to corroborate this statement. Thus, it would be interesting to find out what kind of geological conditions are suitable for generating oils whose actual resin concentration is less than their critical resin concentration. A model which is based on the notion of the resin critical concentration described above and predicts the phase behavior of asphaltenes in oil mixtures was published recently by the authors (12). Since asphaltene deposition takes place during primary, secondary and tertiary oil recovery, and in the refinery, injection of peptizing agents (i.e.: resins) in proper amounts and places could prevent or at least control the colloidal asphaltene deposition problem. Furthermore, experiments could be performed (i.e.: of the coreflood type) where peptizing agents are injected to study their effect on inhibition of asphaltene deposition or permeability reductions.

Table II. Resin and Asphaltene Content of Crude Oils (11)

Crude Oil	Sp.gr. (60°/60°F)	Resins (% by wt)	Asphaltenes (% by wt)
Pennsylvania	0.805	1.5	0.0
Oklahoma, Tonkawa	0.821	2.5	0.2
Oklahoma, Okla. City	0.835	5.0	0.1
Oklahoma, Davenport	0.796	1.3	0.0
Texas, Hould	0.936	12.0	0.5
Texas, Mexia	0.845	5.0	1.3
Louisiana, Rodessa	0.807	3.5	0.0
Calif., Huntington Beach	0.897	19.0	4.0
Mexico, Panuco	0.988	26.0	12.5
Russia, Surachany	0.850	4.0	0.0
Russia, Balachany	0.867	6.0	0.5
Russia, Bibi-Eibat	0.865	9.0	0.3
Russia, Dossor	0.862	2.5	0.0
Russia, Kaluga	0.955	20.0	0.5
Asia, Iraq (Kirkuk)	0.844	15.5	1.3
Mississippi, Baxterville ¹⁸	0.959	8.9	17.2

One interesting question posed by previous researchers (14,19) is why there was asphaltic bitumen deposited at the bottom of the well considering that no phase change or any substantial temperature or pressure changes had taken place. The conclusion was that the question

could only be answered after considerable light was thrown upon the nature of the asphaltic bitumen prior to its separation from the crude oil in the well. There were a few efforts to try to determine the size and nature of asphaltene particles while they still are in the original oil (15,19). Katz and Beu (19) did not see any asphaltene particles in the original oil of size 65 Å or larger, but they did see these particles after mixing the crude with solvents. They concluded that the particles, if they do exist, must be smaller than 65 Å. Witherspoon et al. (15), using ultracentrifuge techniques, found that the particles that eluded Katz and Beu do exist and are of the 35-40 Å range. By careful work of electron micrography with rapid lyophilization, the size of asphaltene is found to be 20-30 Å (27). In native oil or solutions, the asphaltene particle size can be doubled (28,29).

Conclusions

Because the asphaltene problem is so elusive, it seems that, before one can formulate a comprehensive model describing the problem, the true asphaltene deposition mechanism(s) must be clearly understood and backed by field and experimental data; then an accurate and representative model can be formulated. In this report we have tried to address this basic question. The mere fact that there are several basic schools of thought with regards to the asphaltene deposition problem points out that we are still far from formulating a universally accepted model for describing the behavior of asphaltenes in crude oil. Establishing the state of the asphaltene particles in the original crude oil seems to be a basic building block in the scientific quest to find a solution to the asphaltene deposition problem. More experiments must be done to duplicate Witherspoon et al.'s ultracentrifuge work for different oils and possibly utilize other contemporary experimental techniques to establish the state of asphaltenes in crude oils. Meanwhile, a model that describes the phase behavior of asphaltenes in oil must take into account the lack of positive information on the structure of asphaltenes in the original oil and rely as little as possible on the concept of an asphaltene molecule or of specific properties of asphaltenes. This was the philosophy that we followed in our models, mentioned earlier, predicting the behavior of asphaltenes in petroleum.

Acknowledgments

This research is supported in part by the National Science Foundation Grant CBT-8706655 and in part by the Shell Oil Company.

Literature Cited

1. Mansoori, G.A.; Jiang, T.S. Proc. of the 3rd European Conference on Enhanced Oil Recovery, Rome, Italy, April, 1985.
2. Stalkup, F.I. Miscible Displacement; Society of Petroleum Engineers Monograph, June 1983; Chapters 1,2,3

3. David, A., Asphaltenes Flocculation During Solvent Simulation of Heavy Oils. American Institute of Chemical Engineers. Symposium Series 1973, 69 (no. 127), 56-8.
4. Preckshot, C.W.; Dehisle, N.G.; Cottrell, C.E.; Katz, D.L., Asphaltic Substances in Crude Oil Trans. AIME 1943, 151, 188.
5. Shelton, D.A.; Yarborough, L. J. of Petroleum Technology 1977, 1171.
6. Cole, R.J.; Jessen, F.W. Oil and Gas Journal 1960, 58, 87.
7. Lichaa, P.M. and Herrera, L. Society of Petroleum Engineers Journal, paper no. 5304, 1975, 107.
8. Speight, J.G.; Long, R.G.; Trawbridge, T.D. Fuel 1984, 63, no. 5, 616.
9. Long, R.B. In Chemistry of Asphaltenes; Bunger, J.W.; Li, N.C., Eds.; Advances in Chemistry Series No. 195; Washington, DC, 1981; p 17.
10. Yen, T.F., Present Status of the Structure of Petroleum Heavy Ends and its Significance to Various Technical Applications. Preprints ACS Div. Pet. Chem. 1972, 17, No. 4, 102.
11. Sachanen, A.N. The chemical constituents of petroleum; Reinhold Publishing Corp., 1945.
12. Leontaritis, K.J.; Mansoori, G.A. SPE Paper#16258; Proceedings of the 1987 SPE Symposium on Oil Field Chemistry, Society of Petroleum Engineers, Richardson, TX, 1987.
13. Leontaritis, K.J.; Mansoori, G.A.; Jiang, T.S., Asphaltene Deposition in Oil Recovery: a Survey of Field Experiences and Research Approaches J. of Petr. Sci. and Eng., 1988 (to appear).
14. Adalialis, S. M.Sc. thesis, Petroleum Engineering Department, Imperial College of the University of London, London, 1982.
15. Ray, B.R.; Witherspoon, P.A.; Grim, R.E. J. Phys. Chem. 1957, 61, 1296.
16. Speight, J.G.; Moschopedis, B.C. In Chemistry of Asphaltenes; Bunger, J.W.; Li, N.C., Eds.; Advances in Chemistry Series No. 195; Washington, DC, 1981; p 115.
17. Haskett, C.E.; Tartera, M. Journal of Petroleum Technology 1965, 387-91.
18. Tuttle, R.N. Journal of Petroleum Technology 1983, 1192.
19. Katz, D.L.; Beu, K.E. Ind. and Eng. Chem. 1945, 37, 195.
20. Koots, J.A.; Speight, J.C., Fuel, 54, 1975, p179.
21. Mansoori, G.A.; Jiang, T.S.; Kawanaka, S. Arabian J. of Sci. & Eng. 1988, 13, No. 1, 17.
22. Du, P.C.; Mansoori, G.A. SPE Paper #15082, Proc. of the 1986 California Regional Meeting of SPE, Society of Petroleum Engineers, Richardson, TX, 1986.
23. Hirschberg, A. ; de Jong, L.N.J. ; Schipper, B.A.; Meijers, J.G., Society of Petroleum Engineers Journal 1984, 24, No 3, 283-293.
24. Scott, R.L.; Magat, M. J. Chem. Phys., 1945, 13, 172; Scott, R.L. J. Chem. Phys. 1945, 13, 178.
25. Swanson, J. Phys. Chem. 1942, 46, 141.

26. Kawanaka, S.; Park, S.J.; and Mansoori, G.A. SPE/DOE Paper #17376; Proc. 1988 SPE/DOE Symposium on Enhanced Oil Recovery, p 617, Society of Petroleum Engineer, Tulsa, OK, 1988.
27. Dickie, J.P.; Haller, M.N.; Yen, T.F. J. Coll. Interface Sci. 1969, 29, 475.
28. Dwiggens, C.W. J. Phys. Chem. 1965, 69, 3500.
29. Pollack, S.S.; Yen, T.F. Anal. Chem. 1970, 42, 623.

RECEIVED March 8, 1989

Chapter 25

Dynamic Stability of Foam Lamellae Flowing Through a Periodically Constricted Pore

A. I. Jiménez and C. J. Radke

Department of Chemical Engineering, University of California, Berkeley,
CA 94720

The stability threshold or critical capillary pressure of foam flowing in porous media depends on the flow rate, with higher velocities breaking the foam. We present a hydrodynamic theory, based on a single lamella flowing through a periodically constricted cylindrical pore, to predict how the critical capillary pressure varies with velocity. As the lamella is stretched and squeezed by the pore wall, wetting liquid from surrounding pores fills or drains the moving film depending on the difference between the conjoining/disjoining pressure and the porous-medium capillary pressure. The interplay between stretching/squeezing and draining/filling ascertains the critical velocity at which the film breaks in a given porous medium of fixed wetting-liquid saturation.

Comparison of the proposed dynamic stability theory for the critical capillary pressure shows acceptable agreement to experimental data on $100\text{-}\mu\text{m}^2$ permeability sandpacks at reservoir rates and with a commercial α -olefin sulfonate surfactant. The importance of the conjoining/disjoining pressure isotherm and its implications on surfactant formulation (i.e., chemical structure, concentration, and physical properties) is discussed in terms of the Derjaguin-Landau-Verwey-Overbeek (DLVO) theory of classic colloid science.

Foam generated in porous media consists of a gas (or a liquid) dispersed in a second interconnected wetting liquid phase, usually an aqueous surfactant solution (1). Figure 1 shows a micrograph of foam flowing in a two-dimensional etched-glass porous medium micromodel (replicated from a Kuparuk sandstone, Prudhoe Bay, Alaska (2)). Observe that the dispersion microstructure is not that of bulk foam. Rather discontinuous

gas bubbles essentially fill the pore space. They are separated from each other by thin surfactant-stabilized lamellae and from the pore walls by liquid channels and films. Each lamella joins the pore wall through curved regions known as Plateau borders (3). The lamellae can either block flow paths or flow as connected bubble trains (4). Not all of the gas need be discontinuous (1). Some can transport as a continuous phase.

The primary factor controlling how much gas is in the form of discontinuous bubbles is the lamellae stability. As lamellae rupture, the bubble size or texture increases. Indeed, if bubble coalescence is very rapid, then most all of the gas phase will be continuous and the effectiveness of foam as a mobility-control fluid will be lost. This paper addresses the fundamental mechanisms underlying foam stability in oil-free porous media.

Lamellae longevity in porous media is dominated by the mean capillary pressure difference between the nonwetting foam phase and the continuous wetting aqueous phase. Consider Figure 2 which reports the transient pressure drop across the 7-cm long etched-glass micromodel of Figure 1 upon injection of an 80% quality foam stabilized by a 0.5 wt % active commercial α -olefin sulfonate surfactant of carbon number between 14 and 16 (ENORDET AOS 1416). The foam is steadily generated in an identical upstream micromodel and flows into the second downstream micromodel where the pressure behavior is recorded. The two pressure histories labelled wet and dry refer, respectively, to the downstream micromodel being completely aqueous surfactant saturated or being completely dry. For the wet case, the foam enters and achieves steady state after several pore volumes. A mobility reduction compared to water of about 90% ensues. However, for the dry case, there is about a one pore-volume time lag before the pressure responds. During this time, visual observations into the micromodel indicate a catastrophic collapse of the foam at the inlet face. The liquid surfactant solution released upon collapse imbibes into the smaller pores of the medium. Once the water saturation rises to slightly above connate (ca 30%), foam enters and eventually achieves the same mobility as that injected into the wet medium.

These observations are consistent with the concept of a critical capillary pressure for foam to exist in porous media. The dry micromodel porous medium exerted essentially an infinite capillary suction pressure and the foam lamellae drained to breakage at the inlet. After enough wetting liquid filled the smaller pores to decrease the capillary pressure below a critical value, P_c^* , foam could enter. Recently Khatib, Hirasaki and Falls (5) directly measured the critical capillary pressure of foam coalescence for bead packs of permeabilities ranging from 72 to 8970 μm^2 and for various surfactant formulations. These authors found that with all other variables held constant, P_c^* decreases with increasing flow velocity (see Figure 8 of (5)).^c That is, for a porous medium with a given permeability and wetting-phase saturation (and corresponding capillary pressure) there is a critical gas velocity above which lamellae rupture. Similarly, if the capillary pressure is increased at a given velocity of flow, the foam will break. These findings suggest that for higher velocities the wetting-liquid content of the medium must increase

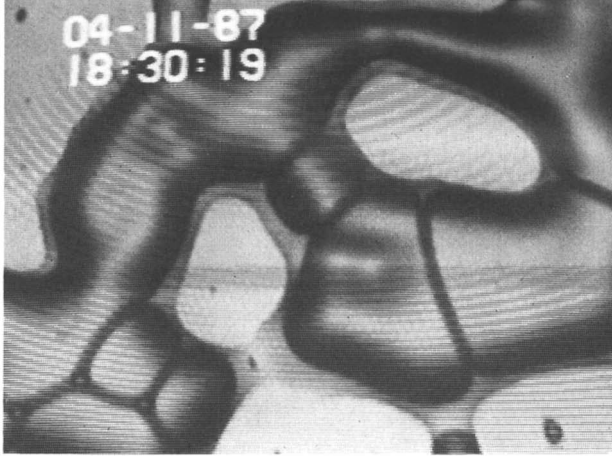


Figure 1. Micrograph of foam in a $1.1 \mu\text{m}^2$, two dimensional etched-glass micromodel of a Kuparuk sandstone. Bright areas reflect the solid matrix while grey areas correspond to wetting aqueous surfactant solution next to the pore walls. Pore throats are about 30 to 70 μm in size. Gas bubbles separated by lamellae (dark lines) are seen as the nonwetting "foam" phase.

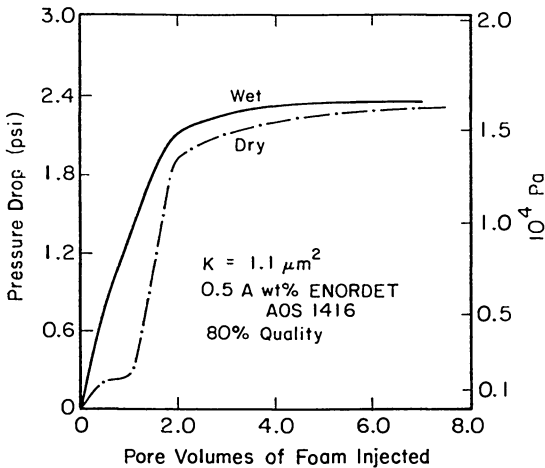


Figure 2. Transient pressure drop across the porous-medium micromodel of Figure 1 for foam pregenerated in an identical upstream medium. The foam frontal advance rate is 186 m/d. In the wet case, foam advanced into the downstream micromodel which was completely saturated with aqueous surfactant solution. In the dry case, the downstream micromodel contained only air.

proportionately in order to reduce P_c^* enough for foam to remain stable.

The purpose of this paper is to explain quantitatively the origin of a critical capillary pressure for foam existence in porous media. We first address the value of P_c^* for static foam that is not flowing and show that it depends on the medium wetting-liquid saturation and absolute permeability in addition to surfactant formulation. We then focus on dynamic or flowing foam stability. A hydrodynamic theory is introduced to explain how P_c^* depends on velocity by analyzing the stability of foam lamellae moving through a periodically constricted sinusoidal pore.

Stability of Static Foam in Porous Media

To explain the role of the medium capillary pressure upon foam coalescence, consider a flat, cylindrical, stationary foam lamella of thickness, $2h$, circa 1000 \AA , and radius, R (i.e., 50 to $100 \mu\text{m}$), subject to a capillary pressure, P_c , at the film meniscus or Plateau border, as shown in Figure 3. The liquid pressure at the film meniscus is $(P_g - P_c)$, where P_g is the gas pressure.

Inside the lamella, there is an excess force or conjoining/disjoining pressure, Π , as introduced and tested experimentally by Derjaguin et al. (6,7). The conjoining/disjoining pressure is a function of the film thickness, $2h$. A typical isotherm for $\Pi(h)$ is shown in dimensionless form in Figure 4. In this case the very short range molecular contributions (8), thought to be of structural origin, are not shown because such ultrathin films seem unlikely for foam application in porous media. The particular

form of $\hat{\Pi}(h)$ in Figure 4 is calculated from the constant potential and weak overlap subcase of the DLVO theory (9):

$$\hat{\Pi} = -\frac{1}{\theta \hat{h}^3} + \exp(-\hat{h}), \quad (1)$$

where $\hat{\Pi} = \Pi/B$, $\hat{h} = 2\kappa h$, and $\theta = B/\kappa^3 A_H$. The first term on the right side of this expression reflects attractive dispersion forces while the second term corresponds to repulsive electrostatic double-layer forces. B is a known function of the surface potential, ionic strength, surfactant concentration, and temperature (9), A_H is a Hamaker constant, and $1/\kappa$ is the Debye length. θ is a measure of the ratio of repulsive to attractive forces whose value in Figure 4 is set at 5. Later we shall also employ the constant and low surface charge density (i.e., q) form of the DLVO theory (9):

$$\hat{\Pi} = -\frac{1}{\theta \hat{h}^3} + \text{csch}(\hat{h}/2), \quad (2)$$

where $\hat{\Pi} = \epsilon \Pi / 2\pi q^2$, $\theta = 2\pi q^2 / \epsilon \kappa^3 A_H$, and ϵ is the bulk permittivity of the surfactant solution.

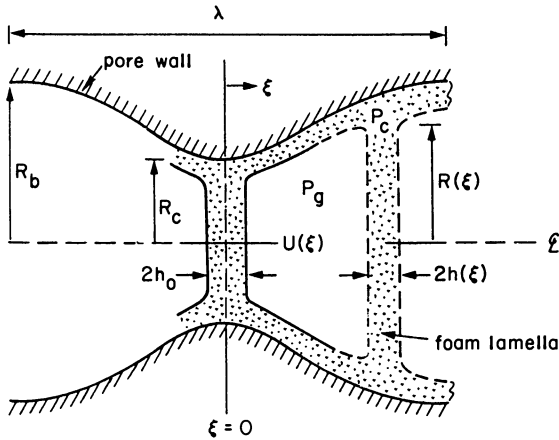


Figure 3. Schematic of flowing lamellae in a periodic constricted pore. The porous medium imposes a capillary pressure, P_c , at each Plateau border.

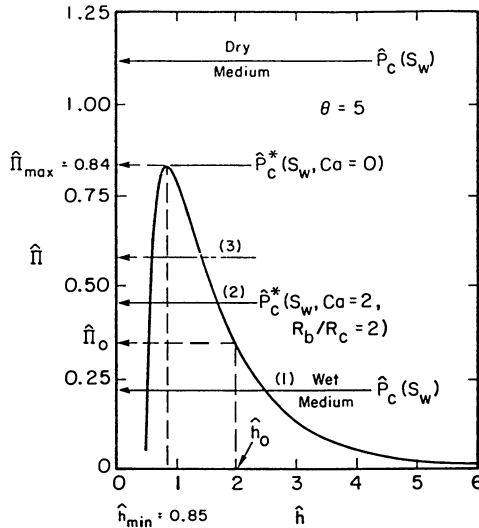


Figure 4. A conjoining/disjoining pressure isotherm for the constant-potential and weak overlap electrostatic model.

The driving force for exchange of fluid into and out of the film is $(P_c - \Pi)$. When P_c is greater than Π the pressure difference $(P_c - \Pi)$, drives liquid out of the lamella and vice versa. If it happens that $P_c = \Pi$, then an equilibrium metastable film is possible. Whether a particular intersection of P_c and Π yields a metastable or an unstable foam film depends on the specific shape of the conjoining/disjoining curve (10-12).

For a nonthinning, unbounded film, Vrij (10) showed via a thermodynamic analysis (i.e., a surface energy minimization) that when $\partial\Pi/\partial h$ is greater than zero the film is unstable. Thus, in Figure 4 the critical thickness limit for metastable films, \hat{h}_{\min} , is given by the maximum of the conjoining/disjoining curve, $\hat{\Pi}_{\max}$, or equivalently when $\partial\Pi/\partial h = 0$ for any value of θ . Unbounded films thinner than \hat{h}_{\min} are unstable to infinitesimal perturbations; films thicker than \hat{h}_{\min} are stable to such perturbations.

It is now possible to explain the origin of a critical capillary pressure for the existence of foam in a porous medium. For strongly water-wet permeable media, the aqueous phase is everywhere contiguous via liquid films and channels (see Figure 1). Hence, the local capillary pressure exerted at the Plateau borders of the foam lamellae is approximately equal to the mean capillary pressure of the medium. Consider now a relatively dry medium for which the corresponding capillary pressure in a dimensionless sense is greater than $\hat{\Pi}_{\max}$, as shown in Figure 4. Given sufficient time any foam lamella present in such a medium will thin down to a thickness less than \hat{h}_{\min} and rupture. Hence, the entire foam breaks. This explains why foam cannot enter a completely dry porous medium. Conversely, for a relatively wet medium with $P_c < \hat{\Pi}_{\max}$ the lamellae will establish a metastable equilibrium state with $\hat{\Pi} = P_c$ and $\hat{h} > \hat{h}_{\min}$. In this case, unless subjected to large disturbances (i.e., those with amplitude of order h), the foam lamellae remain intact and the foam is metastable. Clearly for a static foam, a critical capillary pressure at $\hat{P}_c^* = \hat{\Pi}_{\max}$ demarks the boundary between metastable and unstable foam lamellae.

In a given porous medium at a fixed water saturation (i.e., with $P_c(S_w)$ set), static foam stability depends solely on the value of $\hat{\Pi}_{\max}$. If $P_c(S_w)$ is greater than $\hat{\Pi}_{\max}$, the foam must break. $\hat{\Pi}_{\max}$ in turn is determined by the surfactant formulation, since the shape of the conjoining/disjoining pressure isotherm reflects the surfactant charge, size, structure, and concentration as well as the ionic strength and hardness of the aqueous solvent.

A given surfactant package characterized by a very high value of Π_{\max} will produce a highly stable foam. Since, in general, lower permeability media exhibit higher capillary-pressure suction, we argue that it is more difficult to stabilize foam when the permeability is low. Indeed the concept of a critical capillary pressure for foam longevity can be translated into a critical permeability through use of the universal Leverett capillary-pressure J-function (13) and, by way of example, the constant-charge model in Equation 2 for Π :

$$K^* = \phi \left(\frac{J\sigma\epsilon}{2\pi q^2 \hat{\Pi}_{\max}} \right)^2, \quad (3)$$

where ϕ is the porosity, σ is the surfactant solution equilibrium surface tension, and J is a known function of the wetting-phase saturation, S_w (13). For absolute permeabilities below K^* the foam is unstable, while above K^* , it is metastable. Figure 5 shows some typical curves generated from Equation 3 for K^* as a function of the liquid saturation, S_w , for two indifferent ionic concentrations. As expected, lower water saturations require a more permeable medium for foam stability. With the simple constant-charge electrostatic model, there is also a strikingly strong dependence of the critical permeability on the ionic concentration. At low salt concentrations foam can survive in low permeability media. According to DLVO theory, increasing significantly the ionic concentration for a given absolute permeability and water saturation is detrimental to stability. We can conclude that the stability of static foam in porous media depends on the medium permeability and wetting-phase saturation (i.e., through the capillary pressure) in addition to the surfactant formulation. More importantly, these effects can be quantified once the conjoining/disjoining pressure isotherm is known either experimentally (8) or theoretically (9). Our focus now shifts to the velocity dependence of P_c^* (and K^*).

Stability of Dynamic Foam in Porous Media

To explain coalescence of dynamic foam in porous media consider a single lamella flowing through a periodically constricted sinusoidal pore, as shown in Figure 3. As noted above, the capillary pressure of the medium imposed on the lamella at the pore wall is assumed constant and is set by the local wetting-liquid saturation. Assuming constant volumetric flow, Q , the lamella transports from pore constriction, of radius R_c , to pore body, of radius R_p , with a local interstitial velocity $^cU(\xi)$ which varies according to the square of the pore radius given by the periodic function, $\hat{R} = R(\xi)/R_c$:

$$\hat{R}(\xi) = (1+a) + a \cos[\pi(1+2\xi/\lambda)], \quad (4)$$

where ξ is the axial distance measured from the pore constriction, and λ is the wavelength of the periodic pore. \underline{a} characterizes the pore structure and is given by $(1/2)(R_b/R_c - 1)$. Thus, for a perfectly straight pore \underline{a} is equal to zero.

Upon moving from the pore constriction ($\xi=0$) to the pore body ($\xi = \lambda/2$), the lamella is stretched as it conforms to the wall. To achieve the requisite volume rearrangement a radial pressure differential is induced which thins the film but results in no net fluid efflux into the Plateau borders. The converse occurs when the film is squeezed upon moving from a pore body to a pore constriction. If R_b/R_c , or equivalently \underline{a} , is large enough to thin the lamella at the pore body to about h_{\min} in Figure 4, then rupture is imminent. Since eventual encounter with a large pore body is virtually assured, this reasoning predicts the collapse of all foam lamellae independent of the flow velocity.

Conversely, whenever the stretched lamella of local thickness h exerts a conjoining/disjoining pressure $\Pi(h)$ which lies above the value of P_c , then fluid transports out of the pendular wetting liquid surrounding the sand grains and into the thin lamellae to prevent the thickness from falling below h_{\min} . Unfortunately, the thin lamella resists instantaneous fluid exchange. According to the simple Reynolds parallel-film model (14,15) adopted below, this hydrodynamic resistance is inversely proportional to h^3 (we ignore any resistance to liquid flow along the channels lining the pore walls and in the Plateau borders (16)). When the foam flow rate Q is low, there is sufficient time to heal the thinning of a lamella at the pore body. When Q is raised sufficiently, however, healing cannot occur quickly enough and the film thickness drops below h_{\min} initiating breakage.

Accordingly, for a given capillary pressure in a porous medium there will be a specific foam flow rate at which the lamellae rupture. This is the proposed origin of the flow-rate dependence of P_c^* measured by Khatib, Hirasaki and Falls (5).

To quantify how P_c^* varies with Q it is first necessary to compare the time scales of lamella transport, film drainage/ filling, and film collapse. The characteristic time for a lamella to transport through one constriction, $\lambda/\langle U \rangle$, is estimated to be between 0.1 and 10 s by taking a typical value of 100 μm for λ and a range for the average interstitial velocity of 10^{-5} to 10^{-3} m/s. Likewise, the characteristic time for liquid film drainage according to Reynolds theory, $3\mu R^2/4h^2 P_c$, is estimated to be between 0.1 and 1 s if the viscosity of the surfactant solution, μ , is taken as 1 mPa·s, the lamella initial thickness is 0.1 μm , the lamella radius is 100 μm , and the capillary pressure is 1 to 10 kPa. These two time constants overlap assuring that film liquid exchange by capillary pumping or suction can keep pace with the pore-wall stretching and squeezing of the film during flow through several constrictions. On the other hand, based on a linear stability analysis summarized in Appendix A for a free,

nonthinning film including both disjoining and conjoining forces (17), the time for film rupture is $1.5\mu h_{\min}^5 \sigma/A_H^2$ which for $\sigma = 30$ mN/m and $h_{\min} = 10$ nm gives values between $0.5 \mu\text{s}$ and 5 ms.

Hence, film rupture is much faster than either film transport or film drainage and filling. In this initial analysis we therefore neglect any time lag for the rupture event and assess breakage as instantaneous whenever h_{\min} is reached. This approximation also neglects any effects of drainage velocity (16,18-20) or stretching rate (17) on rupture time.

Based on the picture above, we combine the expressions for the rate of change of the film thickness due to wall conformity and capillary- pressure-driven influx or efflux into a dimensionless evolution equation (17):

$$\frac{\partial \hat{h}}{\partial \xi} = \frac{2\pi a \hat{h} \sin[\pi(1+\hat{\xi})]}{1+a+a \cos[\pi(1+\hat{\xi})]} - \frac{\hat{\theta} \hat{h}^3}{Ca} \left[\hat{P}_c - \hat{\Pi} \right] \left[1 - \alpha_s \hat{R}^2/\hat{h} \right]^{-1} \quad (5)$$

where

$$\hat{P}_c = \begin{cases} P_c/B & \text{constant potential,} \\ \epsilon P_c/2\pi q^2 & \text{constant charge,} \end{cases} \quad (6a)$$

$$Ca = \frac{3\mu Q}{4\pi\lambda\kappa A_H} \quad (6c)$$

$$\alpha_s = 6\mu\kappa R_c^2/5\mu_s \quad (6d)$$

with $\hat{\xi} = 2\xi/\lambda$ and with μ_s defining the Newtonian viscosity of the interface. $\hat{\Pi}$ follows from either Equation 1 or 2, depending whether the constant-potential or constant-charge model is invoked, and \hat{R} varies with ξ according to Equation 4.

The first term on the right side of Equation 5 corresponds to the rate of stretching/squeezing and is sensitive to pore geometry. The sharper the constriction (i.e., high R_b/R_c), the larger is the contribution of this term to the total rate of thinning of the lamella. The second term represents the rate of film drainage/filling caused by the difference between the capillary pressure and the instantaneous conjoining/disjoining pressure. Note that if \hat{P}_c is always less than $\hat{\Pi}(\xi)$ this term causes film thickening and vice versa.

Following Ivanov et al. (21-23) a factor involving the parameter α_s is included in the drainage/filling term to account for surfactant viscous dissipation at the gas/liquid interface in the limit of high surfactant concentrations. When $\alpha_s = 0$ the

lamella exhibits an infinitely viscous interface obeying the no-slip condition. For finite values of α_s the lamella exhibits less resistance to fluid influx or efflux.

The scaling factor appearing in the denominator of the draining/ filling term is a modified capillary number, defined by Equation 6c, which parameterizes how fast the lamella moves through the constriction. In the limit of $Ca \rightarrow \infty$ the second term is negligible compared to the first term indicating that the time of flow through the constriction is too short to allow liquid to move into or out of the lamella under the influence of the porous-medium capillary pressure. In the limit of $Ca \rightarrow 0$ the lamella is at rest, and, regardless of the shape of the constriction, the capillary pressure will drive liquid into or out of the lamella until a metastable equilibrium or an unstable state is reached. In this case, as stated earlier, the limiting capillary pressure above which lamellae cannot exist, P_c^* , is identical to Π_{\max} .

For a finite flow velocity both the stretching/squeezing and the drainage/filling rates play important roles. Figure 6 reports the numerical marching solution of Equation 5 for the parameters listed and with the conjoining/disjoining curve of Figure 4 (17).

In curve 1 of Figure 6 with $\hat{P}_c = 0.225$, the film thickness generally increases from $\hat{h}_o = 2$ to oscillate periodically from pore to pore about $\hat{h}_e \sim 2.4$, where the preset capillary pressure intersects the conjoining/disjoining pressure curve. The film evolution may also be traced in Figure 4 by a thickening along the $\hat{\Pi}$ curve followed by periodic swings about $\hat{P}_c = 0.225$. The maximum and minimum film thicknesses do not occur precisely at the pore-throat and pore-body locations because of time lag due to capillary pumping and suction. Without large scale disturbances, the film of curve 1 can transport indefinitely without breaking.

In curve 3 with $\hat{P}_c = 0.575$, reflecting a drier porous medium, the film thickness generally diminishes toward the periodic steady state. However, near the first pore body the lamella thickness falls below $\hat{h}_{\min} = 0.85$ corresponding to $\hat{\Pi}_{\max}$ of Figure 4. At this point the film becomes unstable and ruptures.

Curve 2 in Figure 6 shows the film evolution when the minimum film thickness just reaches \hat{h}_{\min} . This curve defines the critical capillary pressure, \hat{P}_c^* . Thus upon changing the pertinent parameters, the solution to Equation 5 traces a locus of critical capillary pressures, \hat{P}_c^* as a function of Ca , \hat{h}_o , \underline{a} , θ , and α_s . Conversely, given the wetting-liquid saturation, or equivalently P_c of the permeable medium, the locus of marginally stable states specifies a critical Ca^* , \underline{a}^* , etc. We investigate briefly the

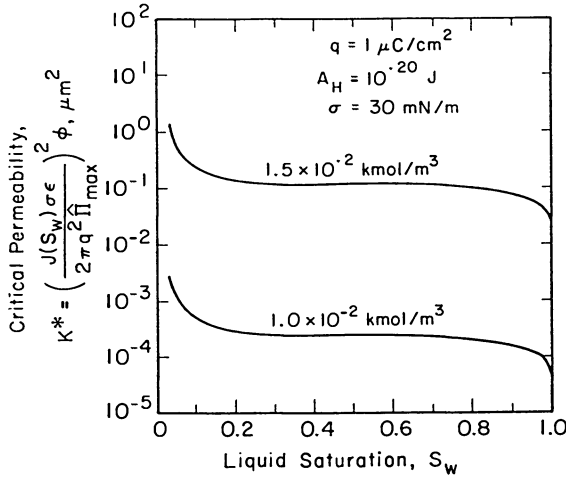


Figure 5. The critical absolute permeability necessary to sustain the stability of a static foam as a function of liquid saturation. Calculations are for the constant-charge electrostatic model.

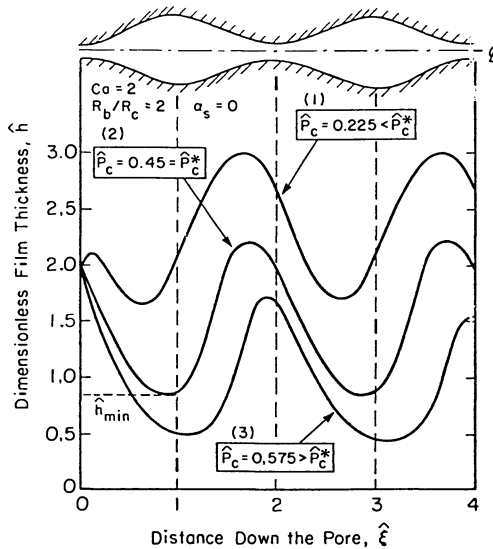


Figure 6. Evolution of the lamella thickness as it transports down the periodic pore for the conjoining/disjoining pressure isotherm of Figure 4. Three capillary pressures are considered in curves 1 through 3. These capillary-pressure values are also labelled in Figure 4. Curve 2 defines the critical or marginally stable capillary pressure, \hat{P}_c^* .

behavior of \hat{P}_c^* with Ca (flow rate), α_s (surface viscosity), and a (pore geometry).

Figure 7 reports calculations of the effect of flow velocity on the critical capillary pressure for the constant-charge electrostatic model and for different initial film thicknesses. Values of \hat{P}_c and Ca lying above the curves reflect unstable lamellae while values below the curves yield metastable foams. At capillary numbers less than 10^{-4} , \hat{P}_c^* asymptotically approaches the static stability limit of Π_{\max} , as discussed in the previous section. Higher capillary numbers demand lower critical capillary pressures for metastability, or equivalently, higher water saturations in the porous medium. The reason is that capillary pumping into the lamella is required to stabilize the film against rupture due to the pore-wall stretching. Lower capillary pressures are necessary at higher velocity because of the finite fluid resistance. At high capillary numbers all curves eventually result in a zero \hat{P}_c^* . This means that conceptually, a completely water-saturated medium would be required to support the foam lamellae. How the critical capillary pressure approaches zero depends on the initial film thickness (for R_b/R_c fixed). Thinner initial films clearly rupture more readily. For the particular parameters listed, once \hat{h}_0 is greater than about 5 all curves collapse onto a single curve. This is because at large initial thicknesses, capillary suction quickly depletes fluid from the lamellae.

For $Ca < 0.1$ in Figure 7 the critical capillary pressure is also independent of the initial film thickness. In this case, the hydrodynamic resistance to fluid filling or draining is small enough that the film reaches the periodic steady state in less than half a pore length. Figure 7 confirms the trend observed by Khatib, Hirasaki and Falls that P_c^* falls with increasing flow rate (5).

The role of surface viscosity is demonstrated in Figure 8 with the constant-potential and weak overlap electrostatic model. We note that the underlying theory is restricted to large values of the surface viscosity, μ_s (21-23). As $\alpha_s = 6\mu\kappa R_c^2/5\mu_s$ increases, the gas/liquid interface varies from a no-slip or inextensible boundary toward a stress-free boundary. Hence, there is less fluid resistance to capillary pumping or suction and the lamellae can withstand a drier porous medium. The critical capillary pressure, accordingly, first increases monotonically up to $\alpha_s \sim 0.5$. Thereafter, the critical capillary pressure decreases, indicating the need for a wetter porous medium to support the foam lamellae. For α_s approaching unity in Figure 8, the local radius factor multiplying α_s in Equation 5 dominates and forces a greater resistance for healing inflow when the lamella

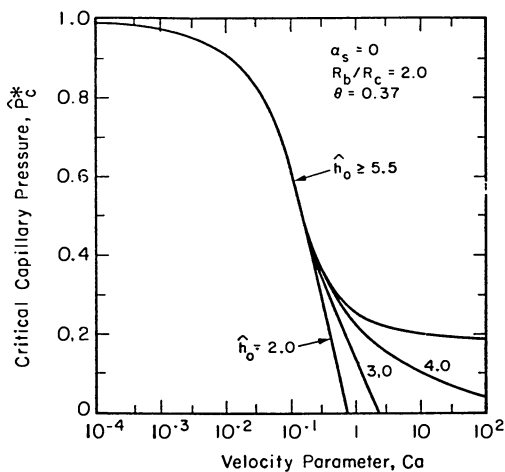


Figure 7. The effect of gas velocity on the critical capillary pressure.

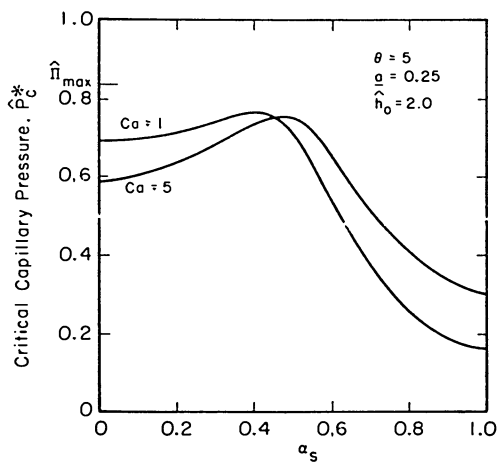


Figure 8. The effect of surface viscosity on the critical capillary pressure.

thickness is near \hat{h}_{\min} (i.e., when \hat{R} is near R_b/R_c) compared to that for $\alpha_s = 0$. The higher hydrodynamic resistance for lamella thickening permits \hat{h} to fall below \hat{h}_{\min} unless \hat{P}_c is lowered. Since the correction factor for surface viscosity in Equation 5 is not rigorous, the results in Figure 8 for α_s greater than about 0.4 should be viewed with caution.

Figure 9 reports the effect of the pore-body to pore-throat radius ratio, R_b/R_c , on the critical capillary pressure for various values of the capillary number and for the constant-potential and weak overlap electrostatic model. Given a constant value of Ca and a wetting-phase saturation (i.e., given \hat{P}_c), Figure 9 teaches that large pore-body to pore-throat radii ratios lead to a more unstable foam. The effect is more dramatic for higher capillary numbers.

In a given porous medium there will be a distribution of pore-body and pore-throat sizes. If a lamella exits a constriction into a pore body whose ratio, R_b/R_c , is less than that set by the appropriate curve in Figure 9, the lamella survives. Conversely, if it exits into a pore body whose value of R_b/R_c is greater than that in Figure 9, that lamella must break. Thus, particular combinations of pore throats and pore bodies (i.e., those with R_b/R_c greater than critical) can be classified as termination sites, in analogy with the germination sites for foam generation (1). The overall rate of foam coalescence in a porous medium then depends directly on the number density of termination sites. This number density in turn is a function, among other variables, of the wetting-phase saturation. Given the pore-throat and pore-body size distribution and their probability of interconnection, the termination site density appears calculable. Hence, our periodic-pore theory in Figure 9 bears directly on foam coalescence kinetics in porous media (24).

Comparison to Experimental Results

Huh, Cochrane and Kovarik (25) recently studied the behavior of aqueous surfactant CO_2 foams in etched-glass porous-medium micromodels. They report qualitative visual observations of lamellae stretching and breaking during transport through pore bodies of the medium. This confirms the basic tenet of the proposed dynamic foam stability theory.

Figure 10 reports as dark circles the critical-capillary-pressure measurements of Khatib, Hirasaki and Falls (5) for foam stabilized by an α -olefin sulfonate of 16 to 18 carbon number (ENORDET AOS 1618) in an 81- μm^2 permeability sandpack. Using the parameters listed and the constant-charge electrostatic model for the conjoining/disjoining pressure isotherm, the data are rescaled and plotted as \hat{P}_c^* versus Ca on a logarithmic abscissa. The

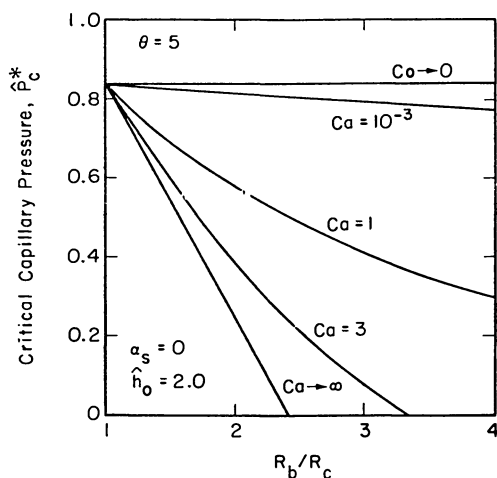


Figure 9. The effect of pore-body to pore-throat radius ratio on the critical capillary pressure.

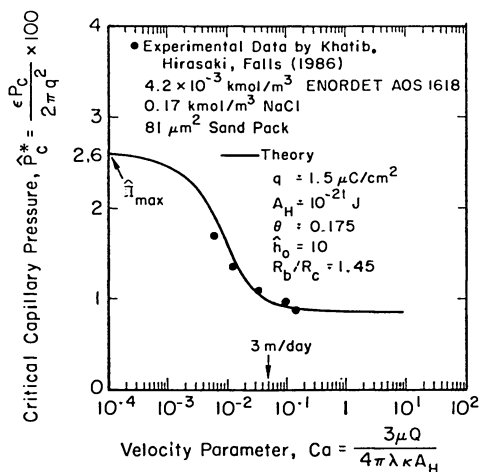


Figure 10. Comparison of the critical-capillary-pressure data of Khatib, Hirasaki and Falls (5) (darkened circles) to the proposed dynamic foam stability theory (solid line). Best fitting parameters for the constant-charge electrostatic model are listed.

experimental data clearly show the decrease of the critical capillary pressure at higher flow rates.

The solid line in Figure 10 is best eye fit using the suite of parameter values labelled on the figure. These values are not unique, but they are physically reasonable. Under this constraint the theory proves acceptable. We find about a 3-fold reduction in P_c^* for capillary numbers relevant to reservoir displacement rates. More definitive evaluation of the proposed theory must await direct measurement of the conjoining/disjoining curve for the specific surfactant formulation under investigation.

Conclusions

The stability of flowing lamellae controls the longevity of foam in porous media. By analyzing a single lamella as it percolates through a periodically constricted tube, we have developed a hydrodynamic stability theory that explains the physical phenomena governing foam coalescence in porous media. The conjoining/disjoining pressure isotherm proves to be the crucial physical property of the surfactant system. It determines the maximum capillary pressure that foam can sustain at rest in a porous medium. This static critical capillary pressure can be associated with a critical permeability or a critical wetting-liquid saturation for a given medium through the Leverett J-function.

For transporting foam, the critical capillary pressure is reduced as lamellae thin under the influence of both capillary suction and stretching by the pore walls. For a given gas superficial velocity, foam cannot exist if the capillary pressure and the pore-body to pore-throat radii ratio exceed a critical value. The dynamic foam stability theory introduced here proves to be in good agreement with direct measurements of the critical capillary pressure in high permeability sandpacks.

Acknowledgment

This work was supported by a Department of Energy Grant DE-AC-76SF00098 to the Lawrence Berkeley Laboratories of the University of California.

Legend of Symbols

- a = $1/2 (R_b/R_c - 1)$ dimensionless sinusoidal pore geometric factor
- A_H = Hamaker constant, J
- B = pre-exponential scale factor of the electrostatic disjoining pressure for constant potential and small degrees of overlap, Pa
- Ca = $3\mu Q/4\pi\lambda\kappa A_H$, capillary number
- E = dimensionless disturbance amplitude
- h = lamella half thickness, m
- \hat{h} = $2\kappa h$, dimensionless lamella thickness

- H - dimensionless deviation in film thickness
 i - $\sqrt{-1}$
 J - Leverett capillary-pressure function
 K - absolute permeability, m^2
 P_c^{\wedge} - capillary pressure, Pa
 P_c - dimensionless capillary pressure defined by Equation 6
 P_g - gas pressure, Pa
 q - lamella surface charge density, C/m^2
 Q - volumetric flow rate, m^3/s
 R - local pore radius, m
 R_b - radius of pore body, m
 R_c^{\wedge} - radius of pore constriction, m
 R - R/R_c , dimensionless local pore radius
 S_w - wetting-phase saturation
 t - time, s
 U - interstitial velocity, m/s
 x - linear distance tangential to a lamella, m
 α - dimensionless disturbance wavenumber
 α_s - $6\mu\kappa_c^2/5\mu_s$, surface-viscosity parameter
 β - dimensionless equilibrium film thickness, defined in Equation A4
 γ - $\theta/3$
 ϵ - bulk permittivity of the surfactant solution, F/m
 θ - dimensionless ratio of electrostatic repulsive to Hamaker attractive forces in the conjoining/disjoining pressure isotherm, defined under Equations 1 and 2
 κ - inverse Debye length, m^{-1}
 λ - wavelength of periodic pore, m
 μ - Newtonian viscosity of the surfactant solution, Pa·s
 μ_s - Newtonian surface viscosity, g/s
 ξ_{\wedge} - axial distance from pore constriction, m
 ξ - $2\xi/\lambda$, dimensionless axial distance from pore constriction
 Π^{\wedge} - conjoining/disjoining pressure, Pa
 Π - dimensionless conjoining/disjoining pressure, defined under Equations 1 and 2
 σ - equilibrium surface tension of surfactant solution, N/m
 ϕ - porosity
 ω - dimensionless disturbance growth rate

Subscripts

- o - initial
 e - equilibrium
 max - maximum
 min - minimum

Superscripts

- ^ - dimensionless
* - critical

Literature Cited

1. Ransohoff, T.C.; Radke, C.J. SPE Reservoir Engineering 1988, 3(2), 573-585.
2. Manlowe, D.S. M.S. Thesis, University of California, Berkeley, 1988.
3. Bikerman, J.J. Foams; Springer-Verlag: New York, 1973; Chapter 1.
4. Ginley, G.M.; Radke, C.J. this series, 1989.
5. Khatib, Z.I.; Hirasaki, G.J.; Falls, A.H. SPE Reservoir Engineering 1988, 3(3), 919-926.
6. Derjaguin, B.V. Acta Physicochim. 1939, 10(1), 25-44.
7. Derjaguin, B.V.; Titievskaja, A.S. Proc. 2nd Int. Congr. Surface Activity; Butterworths, London, 1957, Vol. 1, pp. 211-219.
8. Exerowa, D.; Kolarov, T.; Khristov, K.H.R. Colloids and Surfaces 1987, 22, 171-185.
9. Verwey, E.J.W.; Overbeek, J.T.G. The Theory of Lyophobic Colloids; Elsevier: Amsterdam, 1948.
10. Vrij, A. Disc. Faraday Soc. 1966, 42, 23-33.
11. Ivanov, I.B.; Radoev, B.; Manev, E.D.; Scheludko, A. Trans Faraday Sci. 1970, 66, 1262-1273.
12. Scheludko, A. Adv. Colloid Interface Sci. 1967, 1, 391-464.
13. Leverett, M.C. Trans. AIME. 1941, 142, 152-169.
14. Reynolds, O. Phil. Trans. Roy. Soc. (London) 1886, A177, 157-234.
15. Rao, A.A.; Wasan, D.T.; Manev, E.D. Chem. Eng. Commun. 1982, 15, 63-81.
16. Malhotra, A.K.; Wasan, D.T. Chem. Eng. Commun. 1986, 48, 35-56.
17. Jimenez, A.I. Ph.D. Thesis, University of California, Berkeley, in preparation, 1989.
18. Gumerman, R.J.; Homsy, G.M. Chem. Eng. Commun. 1975, 2, 27-36.
19. Sharma, A; Ruckenstein, E. J. Coll. Int. Sci. 1987, 119, 1-13; 14-29.
20. Sharma, A.; Ruckenstein, E. Langmuir 1987, 3, 760-768.
21. Radoev, B.P.; Dimitrov, D.S.; Ivanov, I.B. Colloid and Polymer Sci. 1974, 252, 50-55.
22. Ivanov, I.B.; Dimitrov, D.S. Colloid and Polymer Sci. 1974, 252, 982-990.
23. Ivanov, I.B.; Dimitrov, D.S.; Somasundaran, P.; Jain, R.K. Chem. Eng. Sci. 1985, 40(1), 137-150.
24. Friedmann, F.; Chen, W.H.; Gauglitz, P.A. SPE 17357, presented at the SPE/DOE Enhanced Oil Recovery Symposium, Tulsa, OK, April 17-20, 1988.

25. Huh, D.G.; Cochrane, T.D.; Kovarik, F.S. SPE 17359, presented at the SPE/DOE Enhanced Oil Recovery Symposium, Tulsa, OK, April 17-20, 1988.
26. Drazing, P.G.; Reid, W.H. Hydrodynamic Stability; Cambridge, 1981.
27. Chandrasekhar, S. Hydrodynamic and Hydromagnetic Stability; Dover, 1961.
28. Williams, M.B.; Davis, S.H. Journal of Coll. and Int. Sci., 1982, 90(1), 220-228.
29. Gallez, D.; Prevost, M. Chemical Hydrodynamics, 1985, 6(5/6), 731-745.

Appendix A - Linear Stability Analysis of a Free Lamella

To establish the characteristic time for rupture of a free (unbounded), nondraining lamella, we perform a simple, normal modes linear stability analysis(26,27) including both an attractive Hamaker conjoining force and a repulsive electrostatic disjoining force. Consider a planar film, initially of equilibrium half thickness h_e , that undergoes a gentle symmetric disturbance in thickness. Following Williams and Davis (28) and Gallez and Prevost (29), the dimensionless film thickness $\hat{h} = h/h_e$ evolves in dimensionless time, \hat{t} , and space, \hat{x} , according to

$$\hat{h}_t^{\wedge} + \left[\hat{h}^{-1} \hat{h}_x^{\wedge} + \hat{h}^3 \hat{h}_{xxx}^{\wedge} - \gamma \beta^4 \hat{h}^3 \hat{h}_x^{\wedge} \exp(-\beta \hat{h}) \right]_{\hat{x}}^{\wedge} = 0, \quad (A1)$$

where subscripts indicate differentiation. The last term on the left of Equation A1 corresponds to the constant surface-potential form of the weak overlapping double-layer disjoining force given in Equation 1. The nondimensional variables and parameters in Equation A1 are

$$\hat{t} = t / \left(\mu \sigma h_e^5 / 6 A_H^2 \right), \quad (A2)$$

$$\hat{x} = x / h_e^2 \sqrt{\sigma / 3 A_H}, \quad (A3)$$

$$\beta = 2 \kappa h_e, \quad (A4)$$

and

$$\gamma = B / 3 \kappa^3 A_H. \quad (A5)$$

For an infinitesimal disturbance with $\hat{h} = 1 + H$ and $H \ll 1$, Equation A1 may be linearized out to terms of $O(H^2)$ as

$$\frac{\partial \hat{H}}{\partial \hat{t}} + \frac{\partial^4 \hat{H}}{\partial \hat{x}^4} + \left[1 - \gamma \beta^4 \exp(-\beta) \right] \frac{\partial^2 \hat{H}}{\partial \hat{x}^2} = 0. \quad (A6)$$

According to normal modes, the infinitesimal disturbance is taken as sinusoidal:

$$H = E \exp(\omega \hat{t} + i\alpha x), \quad (\text{A7})$$

where ω is the dimensionless growth rate, α is the dimensionless wavenumber, and E ($\ll 1$) is the disturbance amplitude.

Substitution of Equation A7 into A6 gives the dispersion equation relating the disturbance growth rate and wavelength:

$$\omega = \alpha^2 [1 - \gamma\beta^4 \exp(-\beta) - \alpha^2]. \quad (\text{A8})$$

We conclude that H grows ($\omega > 0$) in time if $\alpha^2 < 1 - \gamma\beta^4 \exp(-\beta)$ but decays ($\omega < 0$) to zero if $\alpha^2 > 1 - \gamma\beta^4 \exp(-\beta)$. Thus, when $1 - \gamma\beta^4 \exp(-\beta)$ is negative corresponding to $\partial\Pi/\partial h < 0$, the film is metastable. Conversely, when $1 - \gamma\beta^4 \exp(-\beta)$ is positive corresponding to $\partial\Pi/\partial h > 0$, the lamella is unstable to the longer wavelength disturbances. In this latter case, the fastest growing mode is characterized by

$$\omega_{\max} = \frac{1}{4} [1 - \gamma\beta^4 \exp(-\beta)]^2, \quad (\text{A9})$$

with the corresponding wavenumber

$$\alpha_{\max} = \sqrt{\frac{1}{2} [1 - \gamma\beta^4 \exp(-\beta)]}. \quad (\text{10})$$

Finally, the rupture time follows from Equation A7 by setting $H = 1$ (i.e., $\hat{h} = 0$) and by using the expressions above for α_{\max} , ω_{\max} and $x = \pi/\alpha_{\max}$:

$$t = \frac{\ln E^{-4}}{[1 - \gamma\beta^4 \exp(-\beta)]} \left(\frac{\mu\sigma h_e^5}{6A_H^2} \right). \quad (\text{A11})$$

Upon setting $E = 0.1$ and $\gamma = 0$, we recover the characteristic rupture time listed in the main text.

RECEIVED April 3, 1989

Chapter 26

Influence of Soluble Surfactants on the Flow of Long Bubbles Through a Cylindrical Capillary

G. M. Ginley¹ and C. J. Radke

Department of Chemical Engineering, University of California, Berkeley,
CA 94720

Flow of trains of surfactant-laden gas bubbles through capillaries is an important ingredient of foam transport in porous media. To understand the role of surfactants in bubble flow, we present a regular perturbation expansion in large adsorption rates within the low capillary-number, singular perturbation hydrodynamic theory of Bretherton. Upon addition of soluble surfactant to the continuous liquid phase, the pressure drop across the bubble increases with the elasticity number while the deposited thin film thickness decreases slightly with the elasticity number. Both pressure drop and thin film thickness retain their $2/3$ power dependence on the capillary number found by Bretherton for surfactant-free bubbles. Comparison of the proposed theory to available and new experimental data at capillary numbers less than 10^{-2} and for anionic aqueous surfactant above the critical micelle concentration shows good agreement with the $2/3$ power prediction on capillary number and confirms the significant impact of soluble surfactants on bubble-flow resistance. Finally, scaling arguments extend the single-bubble theory to predict the effective viscosity of the flowing bubble regime in porous media. Again, comparison of the effective-viscosity prediction to available pressure-drop data in Berea sandstone demonstrates good agreement.

¹Current address: Marathon Oil Company, Littleton, CO 80160

Foam is a promising fluid for achieving mobility control in underground enhanced oil recovery (1-3). Widespread application of this technology to, for example, steam, CO₂, enriched

hydrocarbon, or surfactant flooding requires quantitative understanding of foam flow properties in porous media. Because foam in porous media is a complicated dispersion of gas (or liquid) in an aqueous surfactant phase (4), the pressure drop-flow rate relationship depends critically on the pore-level microstructure or texture (i.e., on the bubble size and/or bubble-size distribution). Foam texture in turn depends on the dynamic interaction of the generation and breakage mechanisms (5), both of which are strong functions of pore geometry, and surfactant type and concentration.

Numerous visual micromodel studies of foam generated and shaped in oil-free, water-wet porous media with robust stabilizing surfactants, show that the bubble size is variable but generally is on the order of one to several pore-body volumes (4,6-11). As shown in the schematic of Figure 1, the bubbles ride over thin-film cushions of the wetting phase adjacent to the rock surfaces. They are separated from one another by surfactant-stabilized lamellae which terminate in Plateau borders (12). The curvature in the Plateau borders is set primarily by the saturation of the continuous wetting phase which occupies the smallest pores (13,14). To a reasonable approximation the mean capillary suction pressure of the wetting phase is applied to each lamella. When flowing, the lamellae transport as a contiguous bubble train which snakes through available pores not occupied by the wetting phase.

The foam microstructure depicted in Figure 1 suggests that important aspects of the hydrodynamic resistance of flowing bubble trains in porous media can be captured in studies of bubbles in capillaries (7). This work considers the hydrodynamic behavior of a single gas bubble translating in a cylindrical capillary whose radius is smaller than that of the undeformed bubble. The continuous liquid phase contains a surfactant whose concentration is near to or above the critical micelle concentration. Specifically, we extend Bretherton's analysis for a clean gas bubble (15) to include the effects of a soluble surfactant which is kinetically hindered from attaining local equilibrium at the gas/liquid interface. The shape of the bubble and the resulting pressure drop across the bubble are obtained numerically for small deviations in surfactant adsorption from equilibrium. Given the dynamic pressure drop across a single bubble, we briefly show how foam-flow behavior in porous media may be predicted using scaling arguments similar to those adopted for non-Newtonian polymer solutions (16).

Previous Work

In 1961 Bretherton solved the problem of a long gas bubble, uncontaminated by surface-active impurities, flowing in a cylindrical tube at low capillary numbers, $Ca = \mu U / \sigma$ (μ is the

Newtonian liquid viscosity, U is the bubble velocity, and σ^0 is the equilibrium surface tension), where surface tension and viscous forces dominate the bubble shape (15). Using a lubrication analysis, Bretherton established that the bubble slides over a stationary, constant-thickness film whose thickness divided by the radius of the tube, h_0/R_T , varies as the capillary number to the 2/3 power. The dimensionless pressure drop to drive the bubble, $(-\Delta P_B)R_T/\sigma^0$, is calculated from the altered shape of the bubble at its two ends and also scales as the capillary number to the 2/3 power. Experimental measurements by Bretherton of the film thickness deposited by the bubble are in good accord with his theory for capillary numbers ranging from 10^{-5} to 10^{-2} . To our knowledge no corresponding measurements have been reported for the pressure drop of single, clean bubbles at low capillary numbers.

Lawson and Hirasaki recently analyzed the case of single bubbles immersed in a surfactant solution and flowing at low capillary numbers through a narrow capillary (7). These authors consider the rate-limiting step in the transfer of surfactant to and from the interface to be finite adsorption-desorption kinetics. Surface and bulk diffusion resistances are neglected, and surfactant depletion in the thin film region is shown to be negligible. Following Levich (17), the surfactant adsorption and the surface tension along the bubble are assumed to deviate only slightly from their equilibrium values. Lawson and Hirasaki attribute all the effects of the surfactant to the constant film thickness region of the bubble while the bubble ends are ignored. Because of this approach, these authors are unable to obtain the value of the deposited film thickness as part of their analysis. By asserting that the film thickness remains proportional to the 2/3 power of the capillary number, they establish that the dynamic pressure drop for surfactant-laden bubbles also varies with the capillary number to the 2/3 power but with an unknown constant of proportionality. New pressure-drop data for a 1 wt% commercial surfactant, sodium dodecyl benzene sulfonate (Siponate DS-10), in water, after correction for the liquid indices between the bubbles, confirmed the 2/3 power dependence on Ca and revealed significant increases over the Bretherton theory due to the soluble surfactant.

Here we also consider sorption kinetics as the mass-transfer barrier to surfactant migration to and from the interface, and we follow the Levich framework. However, our analysis does not confine all surface-tension gradients to the constant thickness film. Rather, we treat the bubble shape and the surfactant distribution along the interface in a consistent fashion.

Problem Statement

Figure 2 portrays a schematic of a long bubble flowing in zero gravity through a tube filled with a completely wetting

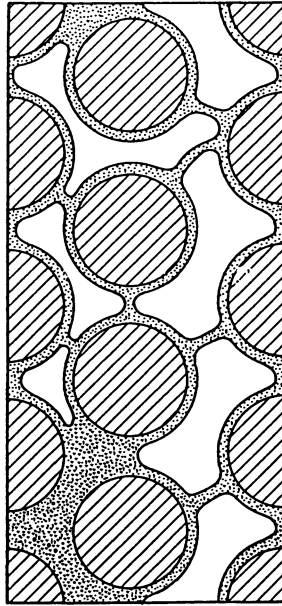


Figure 1. Schematic of the bubble-flow regime in porous media. Open space corresponds to bubbles, dotted space is the aqueous surfactant solution, and cross-hatched areas are sand grains.

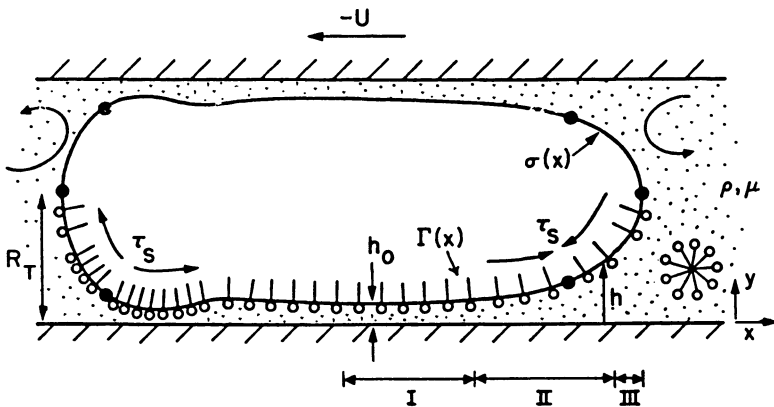


Figure 2. Flow of a single gas bubble through a liquid-filled cylindrical capillary. The liquid contains a soluble surfactant whose distribution along the bubble interface is sketched.

surfactant solution. The reference frame is such that the bubble is stationary with the walls moving past at a velocity of $-U$. The height of the bubble interface, h , is measured from the tube wall. In this analysis the undistorted bubble radius is always greater than the tube radius, and the bubble is longer than at least twice the tube radius. Consequently, there is a region of constant liquid film thickness, h_0 , in the middle of the bubble, even when surfactants are present (18). The origin of the axial coordinate, x , is placed near the constant thickness film, but its exact location is initially unspecified.

The shape of the front and rear menisci change as a result of the resistance to bubble flow. Calculation of this deviation in bubble shape establishes the dynamic pressure drop across the bubble.

The expected surfactant distribution is also portrayed qualitatively in Figure 2. At low Ca , recirculation eddies in the liquid phase lead to two stagnation rings around the bubble, as shown by the two pairs of heavy black dots on the interface (18,19). Near the bubble front, surfactant molecules are swept along the interface and away from the stagnation perimeter. They are not instantaneously replenished from the bulk solution. Accordingly, a surface stress, τ_s , develops along the interface directed from low to high surface tension (i.e., from high to low surfactant adsorption). Surface stresses at the rear stagnation perimeter also occur, only now surfactant accumulates near the ring and there is a net flux of surfactant away from the interface. Sufficiently far from the stagnation rings, the surfactant achieves sorption equilibrium, and the surface tension approaches the equilibrium value, σ_0 . Thus a stress-free, constant thickness film underlies the bubble (18). Equilibrium surface tension in the constant thickness film portion of the bubble implies that all resistance to flow occurs near the ends. Thus, the bubble can be viewed as infinite in length, and the front and back menisci may be treated separately.

If the supply of surfactant to and from the interface is very fast compared to surface convection, then adsorption equilibrium is attained along the entire bubble. In this case the bubble achieves a constant surface tension, and the formal results of Bretherton apply, only now for a bubble with an equilibrium surface excess concentration of surfactant. The net mass-transfer rate of surfactant to the interface is controlled by the slower of the adsorption-desorption kinetics and the diffusion of surfactant from the bulk solution. The characteristic time for diffusion is $\Gamma_0^2/(Dc_0^2)$ where D is the bulk surfactant diffusion coefficient, c_0 is the bulk concentration, and Γ_0 is the

equilibrium adsorption at that concentration. Conversely, the characteristic time for adsorption is $\Gamma_o / (k_1 c_o \Gamma_{max})$ where k_1 is an adsorption rate constant and Γ_{max} corresponds to monolayer coverage. Hence, low surfactant concentrations likely lead to diffusion control whereas kinetic limitations may dominate at high concentrations. Since our focus is on concentrations above the critical micelle concentration, we take sorption kinetics to be rate limiting.

In examining either end of the bubble, the interface can be divided into three distinct regions (15,20), as shown in Figure 2. Region I is characterized by a constant film thickness, h_o .

In region III near the tube center, viscous stresses scale by the tube radius and for small capillary numbers do not significantly distort the bubble shape from a spherical segment. Thus, even though surfactant collects near the front stagnation point (and depletes near the rear stagnation point), the bubble ends are treated as spherical caps at the equilibrium tension, σ_o . Region II provides a transition between the two asymptotic limits. Viscous stresses now scale by the local thickness of the film, h , and the bubble shape varies from the constant thickness film to the spherical segment. Here the surfactant distribution along the interface may be important. Fortunately, for small capillary numbers, $dh/dx < 1$ and the lubrication approximation may be used throughout. Region II is quantified below.

Problem Formulation

The axial velocity profile in region II follows from the lubrication form of the Navier-Stokes equations with the following boundary conditions. The liquid velocity at the tube wall equals $-U$, and the tangential stress at the surfactant-contaminated, gas-liquid interface is given by the negative gradient of the surface tension, $-\sigma/dx$ (17). Pressure in the liquid phase is replaced by a normal stress balance and the Young-Laplace equation, consistent with the lubrication approximation. Finally, macroscopic continuity demands that the average flow rate at any x position along the bubble must equal the flow rate in the constant thickness thin film region. Combination of the normal stress balance, the Navier-Stokes equation, and the macroscopic continuity balance results in a third-order differential equation for the position of the bubble interface as a function of x :

$$\frac{h^3}{3\mu} \sigma_{hxxx} + \frac{h^3}{3\mu} \sigma_x h_{xx} + \frac{h^2}{2\mu} \sigma_x - Uh + Uh_o = 0, \quad (1)$$

where the subscript x denotes differentiation. If $\sigma_x = 0$ (i.e., if $\sigma = \sigma_o$), this relationship reduces to that of Br etherton for a constant-tension bubble. The second term originates from the

normal stress balance, and the third term emerges from the shear-stress boundary condition.

A second equation is needed to determine the surface tension as a function of axial position. We adopt the quasistatic assumption that σ is a unique equilibrium function of the surface excess concentration, Γ , even during dynamic events (17). A surface species continuity balance dictates how Γ varies along the interface. Upon neglect of surface diffusion and for $h_x < 1$, the steady state form of this balance is

$$(\Gamma U_s)_x = k_c \Gamma_{\text{max}} \left[1 - \frac{\Gamma}{\Gamma_0} \right], \quad (2a)$$

where

$$k = k_1 / (1 + k_1 \Gamma_{\text{max}} / k_m), \quad (2b)$$

and U_s is the bubble surface velocity so that ΓU_s is the convected flux of surfactant along the bubble interface. k_1 is the adsorption rate constant, and k_m is a constant mass-transfer coefficient. At high surfactant concentrations and with slow sorption kinetics, Equation 2 reduces to the Langmuir kinetic model. For low surfactant concentrations and with slow diffusion rates, Equation 2 reflects a Nernst constant diffusion-layer-thickness model (17).

With the surface-velocity expression known from the hydrodynamics, Equation 2 can be rewritten as

$$\left[\Gamma \left\{ \frac{\sigma h^2}{2\mu} h_{xxx} + \frac{h^2}{2\mu} \sigma_x h_{xx} + \frac{h}{\mu} \sigma_x - U \right\} \right]_x = k_c \Gamma_{\text{max}} \left[1 - \frac{\Gamma}{\Gamma_0} \right]. \quad (3)$$

The above expression and the quasistatic adsorption assumption provide the additional information necessary to establish both the bubble profile, $h(x)$ from Equation 1, and the surfactant distribution, $\Gamma(x)$ from Equation 3.

To reduce Equations 1 and 3 to canonical form we adopt the scaling of Bretherton (15):

$$\eta = \frac{h}{h_0} \quad (4a)$$

and

$$\xi = \frac{x}{h_0} \left\{ \frac{3\mu U}{\sigma_0} \right\}^{1/3} \quad (4b)$$

Here, $h_0^{(0)}$ is the constant thin film thickness obtained by Bretherton for a constant-tension bubble. The value of the surface tension used in the capillary number is the equilibrium value, σ_0 . It also proves convenient to express the surface

excess concentration as a deviation from equilibrium in the following manner:

$$\theta = \left[\frac{\Gamma}{\Gamma_0} - 1 \right] (3Ca)^{-2/3}. \quad (5)$$

Finally, the surface tension is expanded about the equilibrium adsorption, Γ_0 , and only the first term in the deviation from equilibrium is retained.

These transformations, after elimination of terms that are appropriately higher order in capillary number, yield the following expressions (21):

$$\eta^3 \eta_{\xi\xi\xi} - \frac{3}{2} \alpha \eta^2 \theta_{\xi} - \eta + \eta_0 = 0, \quad (6)$$

and

$$\frac{3}{2} \eta^2 \eta_{\xi\xi\xi} + 3\eta \eta_{\xi\xi\xi} - 3\alpha \eta_{\xi} \theta_{\xi} - 3\alpha \eta \theta_{\xi\xi} + \beta \theta = 0, \quad (7)$$

where again the subscript, ξ , refers to differentiation with respect to ξ . Equations 6 and 7 quantify the interface shape and surfactant distribution, respectively, in region II.

Two important parameters, α and β , arise which depend on the equilibrium and kinetic properties of the surfactant. First, α measures the fractional change in equilibrium surface tension with a fractional change in surfactant adsorption:

$$\alpha = \left[- \frac{d\sigma_0}{d\Gamma_0} \right] \left[\frac{\Gamma_0}{\sigma_0} \right]. \quad (8)$$

It is based on equilibrium properties and is directly related to the Gibbs elasticity (17). In the present context α gauges how strongly the surface tension depends on the surfactant distribution along the bubble interface. Second, β captures the kinetics of the adsorption process and is defined by

$$\beta = 3P^{(0)} \left[\frac{k c_0 \Gamma_{\max}}{\Gamma_0} \right] \left[\frac{R_T \mu}{\sigma_0} \right]. \quad (9)$$

Observe that β is a Damköhler number since it can be interpreted as the ratio of a characteristic contact time for flow in a thin film ($R_T \mu / \sigma_0$), to a characteristic time for adsorption, ($\Gamma_0 / [k c_0 \Gamma_{\max}]$). The constant $P^{(0)} = 0.643$ reflects the curvature of the bubble front for the constant-tension Bretherton analysis.

The ratio of the two parameters, $\alpha/\beta = E$, is also important:

$$E = (-d\sigma_0/d\Gamma_0) \Gamma_0^2 / (3P^{(0)} \mu R_T k c_0 \Gamma_{\max}). \quad (10)$$

E is one of several elasticity numbers characterizing the stabilizing effect which adsorbed surfactant molecules have on an interface during mass-transfer processes (22). Note that E is inversely proportional to the capillary radius so that the effect of soluble surfactants on the bubble-flow resistance is larger for smaller capillary radii.

When β approaches infinity, Equation 7 reveals that θ equals zero, which corresponds to infinitely fast sorption kinetics and to an equilibrium surfactant distribution. In this case Equation 6 becomes that of Bretherton for a constant-tension bubble. Equation 6 also reduces to Bretherton's case when α approaches zero. However, $\alpha = 0$ means that the surface tension does not change its value with changes in surfactant adsorption, which is not highly likely. Typical values for α with aqueous surfactants near the critical micelle concentration are around unity (21).

Matching. Equations 6 and 7 demand boundary conditions. Near the constant thickness film region the interface position asymptotically approaches h_0 , and the surface excess concentration limits to Γ_0 . Likewise, Equations 6 and 7 for large values of ξ (large positive values for the bubble front and small negative values for the bubble rear) must meld into the static-cap region. However, the small-slope approximation inherent in Equations 6 and 7 does not apply in region III. Thus, the problem is singular and matching conditions are required.

We utilize the ad hoc procedure of Bretherton (15) which has been formally justified by Park and Homsy (20). Figure 3 displays the meridional circle characterizing the spherical cap of the bubble front. As shown, let \hat{x} be a shifted axial coordinate measured from the origin of that circle and let $R_T - h_*$ be its radius. h_*/R_T is considered to be small. The translated x coordinate, after scaling according to Equation 4b or $\zeta = \hat{x} (3Ca)^{1/3} / h_0^{(0)}$, is related to the ξ coordinate by $\zeta = \xi - \xi_*$. Matching between regions II and III is then stated mathematically by

$$\lim_{\xi \rightarrow \infty} \eta(\xi = \zeta + \xi_*) = \lim_{\hat{x}/R \rightarrow 0} \left\{ \frac{R_T}{h_0^{(0)}} - \sqrt{\left[\frac{R_T - h_*}{h_0^{(0)}} \right]^2 - (3Ca)^{-2/3} \zeta^2} \right\}. \quad (11)$$

From Equation 6 the outer limit of the inner solution is a parabola: $\eta(\xi \rightarrow \infty) = 1/2 P \xi^2 + Q \xi + R$. The outer solution, corresponding to the right side of Equation 11, is a circle. From a Taylor expansion about $\hat{x} = 0$, its inner limit is also a polynomial. Following the proscription of Equation 11, equating

terms of $O(\zeta^2)$ specifies the constant film thickness, h_o . Terms of $O(\zeta)$ locate the coordinate shift factor, ξ_* , and the constant terms yield h_* , all as expressions of the known constants P , Q , and R .

According to the Young-Laplace expression, the pressure difference across the bubble-front interface is $2\sigma_o/(R_T-h_*)$. Since $h_*/R_T < 1$, the dynamic pressure contribution in excess of the static value, $2\sigma_o/R_T$, is given by:

$$\frac{\Delta P R_T}{2\sigma_o} = \frac{h_*}{R_T} \tag{12}$$

This completes the analysis for the bubble front.

Matching procedures for the bubble rear follow by analogy. In this case, however, the bubble aft translates over the constant thickness film deposited by the bubble front so that h_o is already fixed.

Regular Perturbation Solution. To effect an analytical expression for the bubble-flow resistance, we consider fast sorption kinetics or equivalently, small deviations from equilibrium surfactant coverage making β large. Hence, a regular perturbation expansion is performed in $1/\beta$ about the constant-tension case. The resulting equations for θ and η are to zero and first order in $1/\beta$ (21):

$$O[1] \quad \theta^{(0)} = 0, \tag{13}$$

$$[\eta^{(0)}]_{\xi\xi\xi}^3 - \eta^{(0)} + 1 = 0, \tag{14}$$

$$O\left[\frac{1}{\beta}\right] \quad \theta^{(1)} = -\frac{3}{2} \eta_{\xi}^{(0)} \frac{1}{[\eta^{(0)}]^2}, \tag{15}$$

and

$$\begin{aligned} & [\eta^{(0)}]_{\xi\xi\xi}^3 \eta^{(1)} + 3[\eta^{(0)}]_{\xi\xi\xi}^2 \eta^{(0)} \eta^{(1)} - \eta^{(1)} \\ & = \frac{3}{2\alpha} \frac{1}{\eta^{(0)}} \left\{ 3[\eta_{\xi}^{(0)}]^2 - \frac{3}{2} \eta^{(0)} \eta_{\xi\xi}^{(0)} \right\} - \eta_o^{(1)}, \end{aligned} \tag{16}$$

where the superscripted variables refer to the order in $1/\beta$. Equations 13 and 14 represent the constant-tension equations with

an equilibrium surfactant distribution and have been solved by Bretherton. Equations 15 and 16 can be solved to obtain the first-order contribution to the surface position and surfactant surface excess concentration due to the presence of a soluble surfactant.

Once $\eta^{(0)}$ is known, the surfactant distribution $\theta^{(1)}$ is available directly from Equation 15. Thereafter, the first-order correction to the interface position $\eta^{(1)}$ may be calculated. Following Bretherton, Equations 14 and 16 are restated as initial value problems and solved by a numerical marching technique. We use a 4th-order, Runge-Kutta procedure and calculate $\eta^{(0)}$ and $\eta^{(1)}$ for the front and back of the bubble separately (21). The matching condition, Equation 11, is applied to each order in $1/\beta$. Extensive details on the mathematical and numerical procedures are available elsewhere (21).

Results

Figures 4 and 5 depict the calculated surfactant distribution, expressed as $\theta^{(1)}$, for the bubble front and rear, respectively. For perspective, the locations of the stagnation rings are indicated by arrows. As anticipated, near the front stagnation perimeter there is a deficiency of surfactant because surface convection is directed away from that point. The largest gradients in surface velocity occur just aft of the stagnation ring. Hence, in Figure 4, the surfactant adsorption attains a minimum at $\xi \sim 10$.

Again, as expected, in Figure 5 there is an excess of surfactant near the rear stagnation ring due to surface convection towards that point. Forward from that location, however, there is also a depletion relative to equilibrium adsorption. This is caused by the traveling wave in the rear bubble profile as demonstrated in Figure 2 and in Figure 7 to follow.

The total dimensionless film thickness, $\eta = \eta^{(0)} + (1/\beta)\eta^{(1)}$, is plotted on the ζ scale in Figures 6 and 7 for the bubble front and rear, respectively. A range of elasticity numbers from zero (the Bretherton equilibrium surfactant coverage case) to unity is shown for comparison. The bubble-front profile in Figure 6 is only slightly altered even for $E = 1$. The effect of surfactant on the rear profile is more interesting, as demonstrated in Figure 7. Here additional and higher amplitude oscillations appear as E is raised.

The main results of our first-order regular perturbation analysis are the expressions for the constant thin film thickness, h_0 , and for the total hydrodynamic pressure drop across the entire bubble (front and back), $-\Delta P_B$:

$$h_0/R_T = 1.34 [1 - 1.56(10^{-2})E] Ca^{2/3}, \quad (17)$$

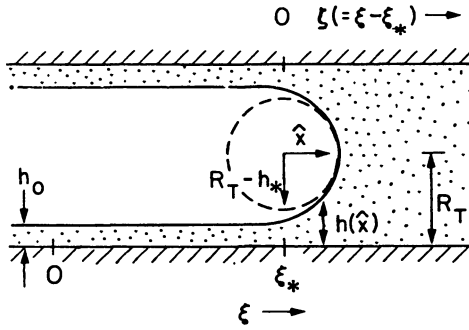


Figure 3. Schematic of matching to the spherical cap at the bubble front. The radius of the flow-altered sphere is $R_T - h_*$. For a static bubble, the bubble radius is R_T .

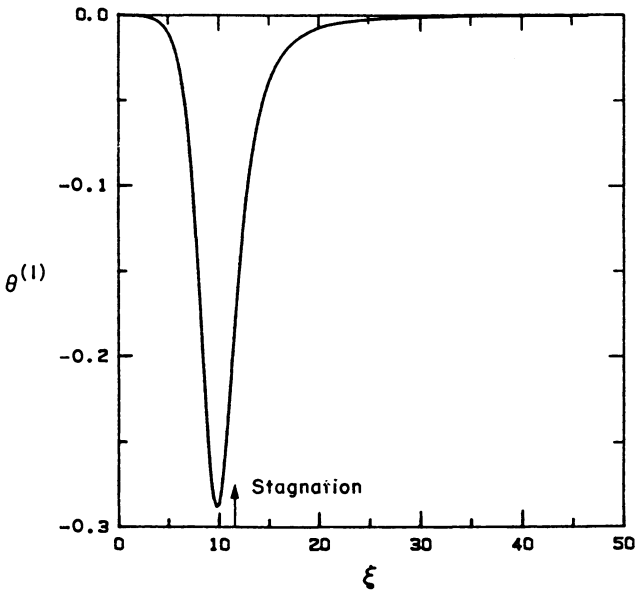


Figure 4. The surfactant distribution at the bubble front expressed as a deviation from equilibrium.

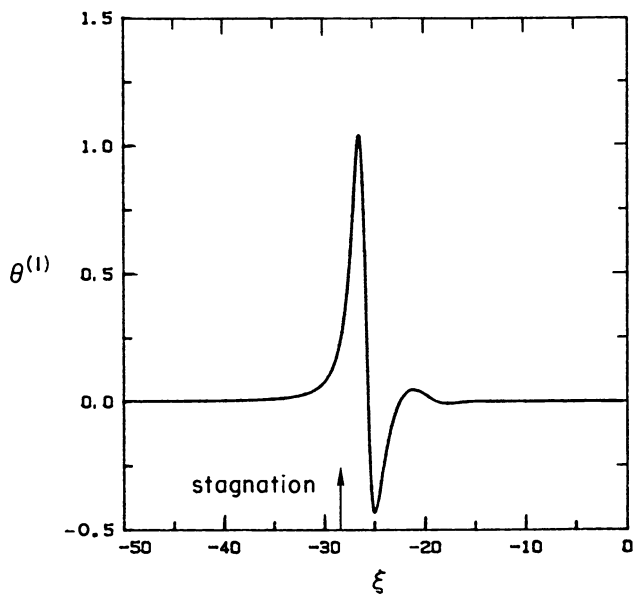


Figure 5. The surfactant distribution at the bubble rear expressed as a deviation from equilibrium.

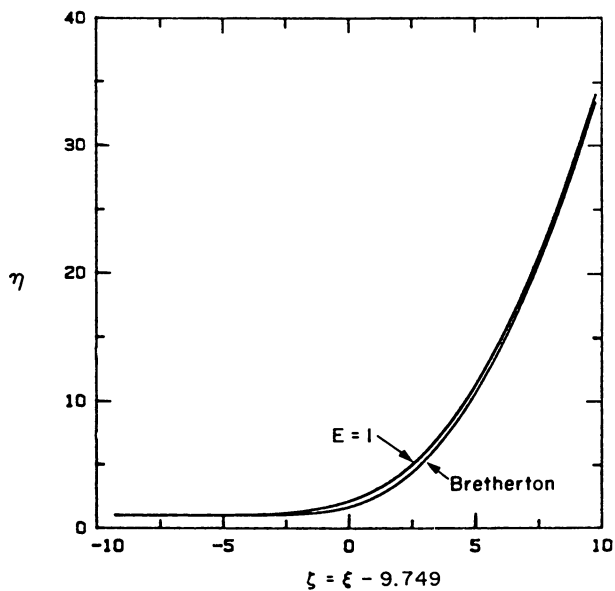


Figure 6. The bubble shape at the front for the elasticity number equal to 0 and 1.

and

$$\frac{(-\Delta P_B)R_T}{\sigma_0} = 9.40 [1 + 0.469E] Ca^{2/3} . \quad (18)$$

The first term in both Equations 17 and 18 is the constant surface-tension contribution and the second term gives the first-order contribution resulting from the presence of a soluble surfactant with finite sorption kinetics. A linear dependence on the surfactant elasticity number arises because only the first-order term in the regular perturbation expansion has been evaluated. The thin film thickness deviates negatively by only one percent from the constant-tension solution when $E = 1$, whereas the pressure drop across the bubble is significantly greater than the constant-tension value when $E = 1$.

Comparison to Experiment

Goldsmith and Mason (18) have experimentally observed the constant thickness thin film region underlying a gas bubble flowing in a tube. They report that its value does not differ significantly upon addition of surfactant to the continuous liquid phase. This is in accord with Equation 17 demonstrating a very small influence of surfactant on the film thickness.

Figure 8 gives ambient temperature pressure drop-flow rate data for trains of isolated bubbles in precision cylindrical capillaries. A dimensionless pressure drop per bubble is plotted as a function of the capillary number on logarithmic scales. Open triangles are the data of Hirasaki and Lawson (7) for a 1 wt% aqueous solution of a commercial sodium dodecyl benzene sulfonate (Siponate DS-10) in a 1 mm diameter tube. Open squares reflect preliminary data of Ginley (21) for a 1 wt% solution of sodium dodecyl sulfate in a 50 wt% mixture of glycerol and water. The capillary tube diameter is 2 mm both for these experiments and for those in pure water, shown as open circles. The lowest solid line, labelled by $E = 0$, corresponds to the constant-tension theory of Bretherton. The remaining two lines are best fit according to a $2/3$ power dependence on the capillary number.

Figure 8 reveals that the few data available for surfactant-laden bubbles do confirm the capillary-number dependence of the proposed theory in Equation 18. Careful examination of Figure 8, however, reveals that the regular perturbation analysis carried out to the linear dependence on the elasticity number is not adequate. More significant deviations are evident that cannot be predicted using only the linear term, especially for the SDBS surfactant. Clearly, more data are needed over wide ranges of capillary number and tube radius and for several more surfactant systems. Further, it will be necessary to obtain independent measurements of the surfactant properties that constitute the elasticity number before an adequate test of theory can be made. Finally, it is quite apparent that a more general solution of Equations 6 and 7 is needed, which is not restricted to small deviations of surfactant adsorption from equilibrium.

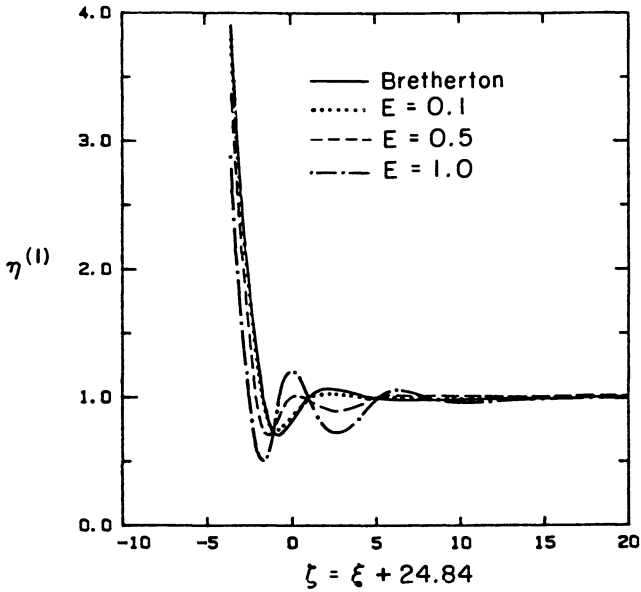


Figure 7. The bubble shape at the rear for the elasticity number equal to 0, 0.1, 0.5, and 1.0.

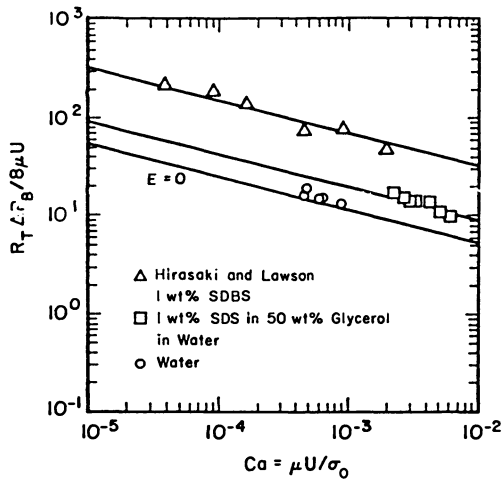


Figure 8. Experimental data of the dimensionless pressure drop per bubble as a function of capillary number for 1 and 2 mm diameter glass capillaries. The solid line denoted by $E = 0$ gives the theory of Bretherton.

Extension to Porous Media

In this section we illustrate how the proposed theory for single, surfactant-laden bubbles in a cylindrical tube can be extended to predict the hydrodynamic resistance of bubble trains flowing in porous media. Some of the basic ideas are known (7, 23), so the present discussion is brief.

Refer again to Figure 1. In strongly water-wet media, capillarity forces the aqueous surfactant phase to occupy the smaller pores in addition to residing in lamellae and in thin films coating the solid grains. Thus, flowing bubbles trains must transport in the larger pore channels, making foam a "nonwetting" phase. Accordingly, Darcy's law can be written as

$$\bar{v}_n = - \frac{k_{rn} K}{\mu_e} \nabla P_n, \quad (19)$$

where \bar{v}_n is the superficial velocity of the flowing foam, P_n is a volume-averaged pressure of the foam, K is the absolute permeability, and k_{rn} is the traditional relative permeability to the nonwetting phase evaluated at the saturation of the flowing bubble trains, S_n . Unfortunately, because the foam is neither a continuum fluid nor a bulk fluid, its effective or apparent viscosity, μ_e , is not a constant. Indeed, μ_e depends on S_n in addition to surfactant type and concentration, bubble texture, and flow rate. Equation 19 essentially serves as a definition of μ_e ; progress can be made only when μ_e is known.

Three steps are necessary to transform Equation 18 into an expression for μ_e . First, the pressure drop over a unit capillary length is taken as directly proportional to the linear bubble density, n_b , and the pressure drop per bubble. Second, the bubbles form intervening lamellae rather than liquid indices. This requires a curvature correction from that of the capillary to that of the Plateau border (7). Third, the scaling arguments of Blake and Kozeny are invoked in a manner similar to that done for non-Newtonian polymers in porous media (16). The final result is (23):

$$\mu_e = \left\{ \mu_o^{2/3} \sigma_o^{1/3} n_b \sqrt{k_{rn} K} a \left[1 + 0.25b \epsilon (r_1 + r_2) \sqrt{\phi S_n / 2k_{rn} K} / \tau_n r_1 r_2 \right] \right\}$$

$$\left[\frac{2r_2}{r_1(r_1+r_2)} \left[1 + (r_1/r_2)^2 \right] \right] \left/ 2 \sqrt{2} \tau_n^{1/3} S_n^{1/6} \phi^{1/6} v_n^{1/3} \right. , \quad (20)$$

where $a = 9.40$, $b = 0.469$, ϕ is the porosity, τ_n is the tortuosity of the nonwetting phase, and r_1 and r_2 are nondimensional radii of curvature of the Plateau border. These are known functions of the quantity, $J \tau_n \sqrt{k_{rn}/S_n}$, where J is the Leverett capillary-pressure function (24) evaluated at the saturation of the wetting phase. The role of the surfactant in controlling the foam effective viscosity is inherent in the parameter $\epsilon = R_{TE}$, whose definition is available in Equation 10. Again, smaller radii pores, or equivalently lower permeability media, exhibit more sensitivity to the surfactant properties, as confirmed in Equation 20. Note the shear-thinning behavior of the bubble flow regime and the linear dependence on the texture through n_B . Equation 20 should be compared to other empirical expressions which are currently available (5,25).

Barring direct measurement of foam texture, we adopt the following reasoning. Because of the generation of foam bubbles by the snap-off and division mechanisms (4), bubble sizes are expected to be approximately that of pore bodies. Thus, the linear bubble density should scale roughly as $n_B = \delta/D_g$ where D_g is the grain diameter of the medium (obtained from the absolute permeability) and δ is a proportionality constant not significantly larger than unity.

Figure 9 compares Equation 20 with the recent pressure drop flow rate data of Friedmann, Chen, and Gauglitz (5) for a 1 wt% commercial sodium alkyl sulfonate dimer (Chaser SD-1000) stabilized foam in a Berea sandstone. These data are particularly useful because they have been corrected for foam blockage and therefore correctly reflect the flowing bubble regime. The solid line in Figure 9 is best fit according to Equation 20. Unfortunately, neither of the parameters ϵ or δ is available. Two sets of estimates are shown in Figure 9. When $\epsilon = 0$ (i.e., no surfactant effect) the bubble size is about 30% of a grain diameter. When $\epsilon = 0.1$ mm (i.e., a value characteristic of those in Figure 8) the bubble size is about 10 grain diameters. We assert that Equation 20 not only predicts the correct velocity behavior of foam but it does so with reasonable parameter values (23).

These results are very encouraging. They do, however, emphasize the need to measure flowing bubble texture and surfactant properties independently before rigorous experimental tests of detailed theories can be made.

Conclusions

The effect of a soluble surfactant on the flow of long bubbles in a cylindrical tube has been quantified when the surfactant

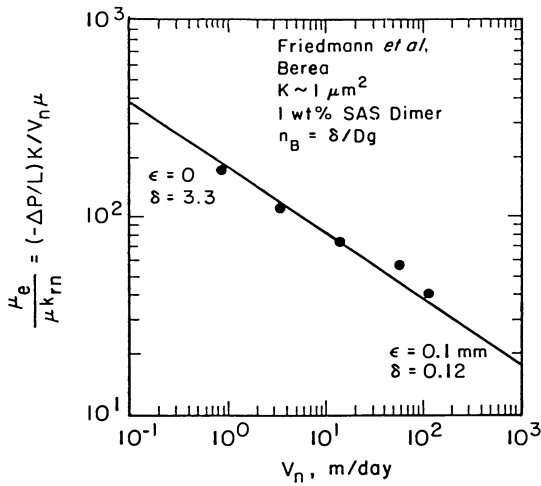


Figure 9. Experimental data for the effective viscosity of the foam bubble regime in Berea sandstone as a function of the foam superficial velocity. The solid line is drawn according to the scaling theory with values of the two sets of parameters ϵ and δ listed.

exhibits small deviations from equilibrium adsorption. A regular perturbation expansion in large adsorption rates is constructed about the low capillary-number, singular perturbation theory of Bretherton. The pressure drop across the bubble increases upon the addition of surfactant, whereas the thin film thickness decreases slightly. Both the pressure drop and the thin film thickness retain their $2/3$ power dependence on the capillary number found by Bretherton for surfactant-free bubbles. To first order, a linear dependence on the surfactant elasticity number arises. Comparison of the proposed theory to new and available pressure-drop data for single bubbles immersed in anionic surfactant solutions confirms the $Ca^{2/3}$ prediction but demonstrates that higher order terms in the elasticity number are required.

Using Kozeny scaling arguments, the proposed single-bubble theory is applied to predict the flow resistance of foam in porous media. Comparison of the predicted foam effective viscosity to experimental data at characteristic reservoir rates in Berea sandstone shows good agreement. The scaling procedure, therefore, provides a powerful tool for quantitative modeling of foam flowing in the bubble regime through porous media.

Acknowledgments

This work was supported by a Department of Energy Grant DE-AC-76 SF00098 to the Lawrence Berkeley Laboratory of the University of California. We thank John Newman for helpful discussions on several mathematical issues.

Legend of Symbols

a, b	-	known constants
Ca	-	$\mu U / \sigma_0$, capillary number, ratio of viscous to surface tension forces
c_0	-	bulk concentration of surfactant, mol/m ³
D	-	diffusion coefficient of surfactant, m ² /s
D_g	-	grain diameter, m
E	-	elasticity number, α/β
h	-	local film thickness measured from the capillary wall, m
h_0	-	constant thin film thickness, m
h_x	-	distance from wall to the minimum of the spherical cap of the bubble ends, m
J	-	Leverett capillary-pressure function
K	-	absolute permeability, m ²
k	-	effective rate constant defined in Equation 2b, m ³ /mol·s
k_r	-	relative permeability
k_m	-	mass-transfer coefficient, m/s

- k_1 - adsorption rate constant, $m^3/mol \cdot s$
 L - porous-medium length, m
 n_B - number of bubbles per unit length, m^{-1}
 P, Q, R - second, first and zero-degree constants in the constant curvature parabola of region II
 ΔP - pressure difference, Pa
 ΔP_B - negative of the pressure drop across the entire bubble, Pa
 R_T - capillary tube inner radius, m
 $r_{1,2}$ - dimensionless radii of curvature of a Plateau border
 S - saturation
 U - bubble velocity, m/s
 U_s - surface velocity of bubble, m/s
 V_n - superficial velocity of nonwetting phase, m/s
 x - axial position, m
 \hat{x} - shifted axial coordinate, m
 α - $(-d\sigma_o/d\Gamma_o)(\Gamma_o/\sigma_o)$, fractional Gibbs elasticity
 β - $1.929 (k c_o \Gamma_{max}/\Gamma_o)(R_T \mu/\sigma_o)$, Damköhler number
 Γ - surface excess concentration, mol/m^2
 Γ_o - equilibrium surface excess concentration, mol/m^2
 Γ_{max} - surface excess concentration corresponding to monolayer coverage, mol/m^2
 δ - $D n_B/g_B$, proportionality constant
 ϵ - $R_T E$, radius independent surfactant elasticity number, m
 ζ - $\xi + \xi_*$, dimensionless shifted axial coordinate
 η - $h/h_o^{(0)}$, dimensionless film thickness
 η_o - $h_o/h_o^{(0)}$, dimensionless thin film thickness

 θ - $(\Gamma/\Gamma_o - 1)(3Ca)^{-2/3}$, dimensionless relative surface excess concentration
 μ - liquid viscosity, $mPa \cdot s$
 μ_e - effective viscosity of foam in bubble-flow regime, $mPa \cdot s$
 ξ - $x/h_o^{(0)}(3Ca)^{-1/3}$, dimensionless axial coordinate
 ξ_* - origin of spherical bubble caps on the ξ scale
 ρ - liquid density, kg/m^3
 σ - surface tension, mN/m
 σ_o - equilibrium surface tension, mN/m

- τ = tortuosity
 τ_s = shear stress at gas/liquid interface of bubble, Pa
 ϕ = porosity

Subscript

- n = nonwetting

Superscripts

- (0) = zero order in $1/\beta$
 (1) = first order in $1/\beta$

Literature Cited

1. Dilgren, R.E.; Deemer, A.R.; Owens, K.B. SPE 10774, presented at the California Regional Meeting of SPE, San Francisco, CA, March 24-26, 1982.
2. Mohammadi, S.S.; Van Slyke, D.C. SPE 16736, presented at the 62nd Annual Fall Meeting of SPE, Dallas, TX, September 27-30, 1987.
3. Patzek, T.W., Konis, M.T. SPE 17380, presented at the SPE/DOE Enhanced Oil Recovery Symposium, Tulsa, OK, April 17-20, 1988.
4. Ranschoff, T.C.; Radke, C.J. SPE Reservoir Engineering 1988, 3(2), 573-585.
5. Friedmann, F.; Chen, W.H.; Gauglitz, P.A. SPE 17357, presented at the SPE/DOE Enhanced Oil Recovery Symposium, Tulsa, OK, April 17-20, 1988.
6. Mast, R.F. SPE 3997, presented at the Annual Fall Meeting of SPE, New Orleans, LA, October 4-6, 1972.
7. Hirasaki, G.J.; Lawson, J.B. SPEJ 1985, 25, 176-190.
8. Owete, O.S.; Brigham, W.E. SPE Reservoir Engineering 1987, 2(3), 315-323.
9. Kuhlman, M.I. SPE 17356, presented at the SPE/DOE Enhanced Oil Recovery Symposium, Tulsa, OK, April 17-20, 1988.
10. Huh, D.G.; Cochrane, T.D.; Kovarik, F.S. SPE 17359, presented at the SPE/DOE Enhanced Oil Recovery Symposium, Tulsa, OK, April 17-20, 1988.
11. Manlowe, D.S. M.S. Thesis, University of California, Berkeley, 1988.
12. Bikerman, J.J. Foams; Springer-Verlag: New York, 1973; Chapter 1.
13. Khatib, Z.I.; Hirasaki, G.J.; Falls, A.H. SPE Reservoir Engineering 1988, 3(3), 919-926.
14. Jimenez, A.I.; Radke, C.J., In Advances in Oil Field Chemistry; Borchardt, J.K., Yen, T.F., Eds; Chapter , in this book.
15. Bretherton, F.P. J. Fluid Mech. 1961, 10, 166-188.
16. Christopher, R.H.; Middleman, S. I&EC Fundamentals 1965, 4(4), 423-426.

17. Levich, V.G. Physicochemical Hydrodynamics; Prentice-Hall: Englewood Cliffs, 1962; Chapters VII, VIII.
18. Goldsmith, H.L.; Mason, S.G. J. Coll. Sci. 1963, 18, 237-261.
19. Shen, E.I.; Udell, K.S. J Appl. Mech. 1985, 52, 253-256.
20. Park, C.W.; Homsy, G.M. J. Fluid Mech. 1984, 139, 291-308.
21. Ginley, G.M. M.S. Thesis, University of California, Berkeley, 1987.
22. Berg, J.C. In Recent Developments in Separation Science; Li, N.N., Ed.; CRC Press: Cleveland, 1972; Vol. 2, pp. 1-31.
23. Ettinger, R.A. M.S. Thesis, University of California, Berkeley, in progress, 1989.
24. Leverett, M.C. Trans. AIME 1941, 142, 152-169.
25. Marfoe, C.H.; Kazemi, H. SPE 16709, presented at the 62nd Annual Fall Meeting of SPE, Dallas, TX, September 27-30, 1987.

RECEIVED November 28, 1988

Chapter 27

Mobility of CO₂ and Surfactant Adsorption in Porous Rocks

Hae Ok Lee and John P. Heller

New Mexico Petroleum Recovery Research Center, New Mexico Institute of Mining and Technology, Socorro, NM 87801

High pressure equipment has been designed to measure foam mobilities in porous rocks. Simultaneous flow of dense CO₂ and surfactant solution was established in core samples. The experimental condition of dense CO₂ was above critical pressure but below critical temperature. Steady-state CO₂-foam mobility measurements were carried out with three core samples. Rock Creek sandstone was initially used to measure CO₂-foam mobility. Thereafter, extensive further studies have been made with Baker dolomite and Berea sandstone to study the effect of rock permeability. Also, other dependent variables associated with CO₂-foam mobility measurements, such as surfactant concentrations and CO₂-foam fractions have been investigated as well. The surfactants incorporated in this experiment were carefully chosen from the information obtained during the surfactant screening test which was developed in the laboratory. In addition to the mobility measurements, the dynamic adsorption experiment was performed with Baker dolomite. The amount of surfactant adsorbed per gram of rock and the chromatographic time delay factor were studied as a function of surfactant concentration at different flow rates.

For a miscible displacement at the required reservoir conditions, carbon dioxide must exist as a dense fluid (in the range 0.5 to 0.8g/cc). Unfortunately, the viscosity of even dense CO₂ is in the range of 0.03 to 0.08 cp, no more than one twentieth that of crude oil. When CO₂ is used directly to displace the crude, the unfavorable viscosity ratio produces inefficient oil displacement by causing fingering of the CO₂, due to frontal instability. In addition, the unfavorable mobility ratio accentuates flow non-

uniformities due to permeability stratification or other heterogeneities.

The mobility of CO₂ in porous rock can be decreased by containing it in a foam-like dispersion. Such CO₂-foams have been proposed as a useful injection fluid in enhanced oil recovery (1,2). A critical literature review on general foam rheology is given elsewhere (3). The foam flooding method modifies the flow mechanism by changing the structure of the displacing fluid at the pore level. This method of decreasing the mobility of a low-viscosity fluid in a porous rock requires the use of a surfactant to stabilize a population of bubble films or lamellae within the porespace of the rock (4). However, the degree of thickening achieved apparently depends to a great extent on the properties of the rock itself. These properties probably include both the distance scale of the pore space and the wettability, and so can be expected to differ from reservoir to reservoir, as well as to some extent within a given field. Laboratory measurements of CO₂-foam mobility as well as studies involving mobility control of CO₂/surfactant in core flooding have been investigated by several researchers recently (5-7). Special efforts have been made to investigate the reservoir application of mobility control foams in CO₂ floods (8), and the influence of reservoir depth on enhanced oil recovery by CO₂ flooding (9). Furthermore, the economic model of mobility methods for CO₂ flooding has been taken into consideration to determine the profitability of carbon dioxide flooding in non-waterflooded fields, and of the use of thickening agents for mobility control (10). Also, an actual field test was conducted with CO₂-foam. The results of the field test of CO₂ mobility control at Rock Creek have been published (11).

In order to understand the nature and mechanisms of foam flow in the reservoir, some investigators have examined the generation of foam in glass bead packs (12). Porous micromodels have also been used to represent actual porous rock in which the flow behavior of bubble-films or lamellae have been observed (13,14). Furthermore, since foaming agents often exhibit pseudo-plastic behavior in a flow situation, the flow of non-Newtonian fluid in porous media has been examined from a mathematical standpoint. However, representation of such flow in mathematical models has been reported to be still inadequate (15). Theoretical approaches, with the goal of computing the mobility of foam in a porous medium modelled by a bead or sand pack, have been attempted as well (16,17).

The use of surfactant as a foaming agent to stabilize the CO₂-foam motivated additional subresearch areas related to foam flooding. Over the past years, continuous efforts and a great deal of time were invested to find the most suitable surfactant for CO₂ flooding (18,19). In addition to research to find the most effective surface active agents, the use of surfactant causes concern that, due to the inherent amphipatic nature of this type of molecule, adsorption on the rock surfaces would reduce their concentration to such an extent that the process would not be successful. Consequently there has been much careful analysis of adsorption, and several independent experiments have been carried out to study this question (20-22).

The purpose of this paper is to present the result of two

kinds of relevant laboratory measurement. The first kind measures the mobility of CO₂-foam at different flow rates, carrying out steady-state experiments using real rock samples as the porous media. The second experiment deals with the dynamic adsorption of surfactant on porous rock. The mobility of CO₂-foam is greatly dependent on the size of the porespace, as expressed in the single-phase permeability of the rock sample. This is shown by comparison of mobility measurements made with Baker dolomite and with Berea sandstone. This result was supported by the previous work with Rock Creek and Berea sandstones. Also the adsorption results indicate that indeed additional surfactant is required due to the permanent adsorption, and that the chromatographic delay associated during the flow of surfactant through the core sample cannot be ignored. In addition to presenting the results of these measurements, the operation of the apparatus and the conduct of both experiments are discussed.

Measurements of CO₂-Foam Mobility

In this section the laboratory measurements of CO₂-foam mobility are presented along with the description of the experimental procedure, the apparatus, and the evaluation of the mobility. The mobility results are shown in the order of the effects of surfactant concentration, CO₂-foam fraction, and rock permeability. The preparation of the surfactant solution is briefly mentioned in the Effect of Surfactant Concentrations section. A zwitterionic surfactant Varion CAS (ZS) from Sherex (23) and an anionic surfactant Enordet X2001 (AECS) from Shell were used for this experimental study.

Experimental. A simplified representation of the basic elements of the flow system is shown in Figure 1 and the schematic of the CO₂-foam mobility measurement experiment is presented in Figure 2. The CO₂ flows through the capillary tube and the pressure drop across the tube is measured by a Validyne differential pressure transducer. An Isco pump is used to pressurize the brine/surfactant solution, which also flows through the foam generator and the core. The foams are generated inside the short core used as a foam generator, where the mixing between CO₂ and surfactant solution occurs. The mixed CO₂-foam flows through the core. The pressure drop across the core is recorded by a second Validyne differential pressure transducer. Two fine tapered needle valves in series are used to regulate the output flow rate of the mixture of surfactant solution and dense CO₂. In addition to the digital readout of the values of pressure drop across the capillary and across the core, a two-pen recorder is used to record these simultaneous measurements. Both of these measurements are subject to rapid short-term variations of fairly small magnitude, that seem to be indicative of the mechanism of foam flow. All calculations were performed with steady-state values that were averaged over these short-term variations. In this experiment, the measured variables are ΔP_{cap} and ΔP_{core} . Knowing the ΔP_{cap} , the flow rate of pure CO₂ into the core is computed by using a calibration constant obtained by measuring the flow of dense CO₂ through the capillary tube. The

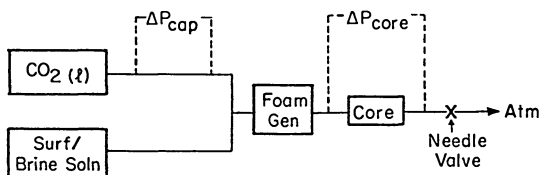


Figure 1. Basic flow system for mobility measurements.

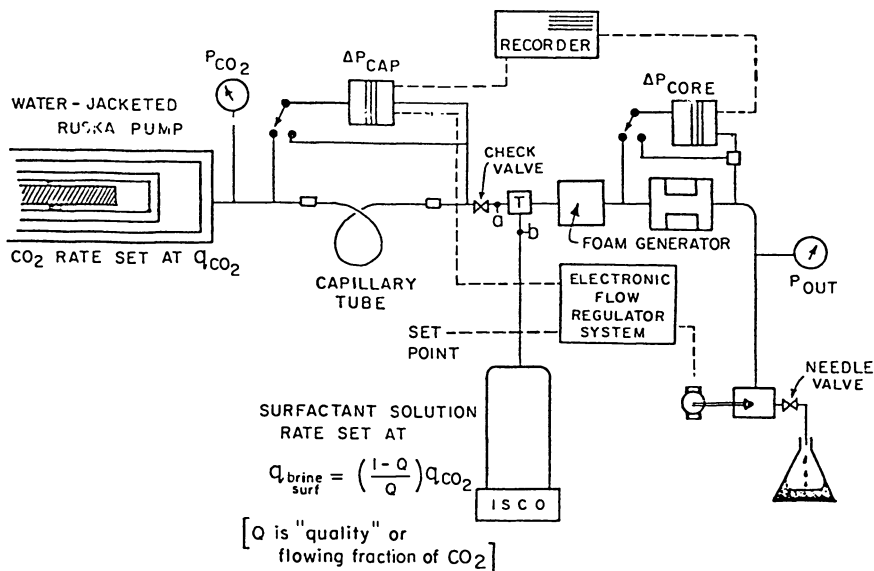


Figure 2. Schematic of the CO₂-foam mobility apparatus. (Taken from Lee, H.O. in Surfactant-Based Mobility Control; Smith, D.H., Ed.; ACS Symposium Series No. 373; American Chemical Society: Washington, DC, 1987; p. 378.)

setting of the Isco pump gives the flow rate of the aqueous surfactant solution, and the total flow rate is simply the sum of these two. From the total flow rate and the ΔP_{core} , the mobility λ can be evaluated from:

$$\lambda = \frac{Q/A}{\Delta P_{\text{core}}/L} \quad (1)$$

where Q is the total flow rate in cc/sec
 A is the cross-sectional area of the rock sample in cm^2
 L is the length of the rock sample in cm
 ΔP_{core} is the pressure drop across the rock sample in standard atmospheres
 and λ is the mobility in $\text{cm}^2/(\text{atm}\cdot\text{sec})$ or darcy/cp.

The Effect of Surfactant Concentrations. The effect of surfactant concentrations on CO_2 -foam mobility is plotted on a log-log scale in Figure 3. The presented data points are the average mobility values obtained from a superficial velocity range of 2-10 ft/day, with the CO_2 -foam fraction was kept constant around 80%. With Berea sandstone, ZS and AEGS surfactants were used. The measured average permeability of the Berea sandstone with 1% brine was 305 md. With Baker dolomite, AEGS was used to make comparison with Berea sandstone. The permeability of the Baker dolomite was 6.09 md measured with 1% brine solution.

Interfacial tension measurements were used to select the surfactant concentration for the initial experiments. The interfacial tension measurements were performed with a Rosano surface tensiometer which uses the Wilhelmy plate method. The interfacial tension was measured at atmospheric conditions against isoctane to simulate dense CO_2 . Isooctane was selected because it is a nonpolar compound and has low solvent power, like dense CO_2 . The initial concentration was chosen around the CMC (critical micelle concentration) and the subsequent concentrations were increased above CMC to well-above CMC. The mobility measurements were conducted from low to high concentrations. Each time whenever the concentration has been increased, sufficient pore volumes of new surfactant concentration was flowed through the rock to establish equilibrium condition. The results in Figure 3 indicate that in general, mobility decreases with increase of surfactant concentration. In the case of ZS, there seems to be an upper critical concentration (0.05%), beyond which the mobility reduction is quite negligible. With AEGS, such upper critical concentrations were not observed for either Baker dolomite or Berea sandstone because the measurements were not carried out beyond 0.5% AEGS. However, the slopes of the curves of AEGS measured with both rocks show similar behavior to that of ZS, and likely reach such plateaus. This graph also shows that the magnitudes of mobility reached in Baker dolomite and Berea sandstone are similar with the same surfactant at identical concentrations. It can be noted that in Berea core, about 30 times the CMC of the ZS was required to obtain the same mobility magnitude as was attained by 0.05% AEGS. This suggests that surfactant type can play indeed an important role in lowering foam mobility.

Effect of CO₂-Foam Fraction. The effect of CO₂-foam fraction, which is defined as the fractional flow of CO₂, on mobility was studied with 0.1% AEGS. Four different CO₂-foam fractions were used to study the foam fraction effect at various flow rates. The results obtained with Baker dolomite is presented in Figure 4 and with Berea sandstone in Figure 5. Both figures clearly demonstrate that the mobility decreases with increase of surfactant fraction. These experimental results indicate that the population of lamellae present in the pore spaces is responsible for decreasing the foam mobility as well as stabilizing the foam flow. The slopes of the fitted lines (that is, the derivatives of the mobility with flow velocity) in both cores suggest that more shear-thinning behavior is evident at 90% of CO₂-foam (which indicates a surfactant deficient environment) compared to 60% or 70% of CO₂. Figure 6 also presents the CO₂-foam fraction effect. The data presented are the mobility measurements as a function of foam fraction at an average velocity of 7.0 ft/day with 0.1% AEGS. These fitted curves show the same trend noted in figures 4 and 5.

Effect of Rock Permeability. The effect of rock permeability has been investigated by comparison of mobility measurements made with Baker dolomite and Berea sandstone. Mobility measurements carried out with Rock Creek sandstone (from the Big Injun formation in Roane County, W.Va) is also reported. Rock Creek sandstone has a permeability of 14.8 md. A direct comparison was made with Berea sandstone and Baker dolomite measured with 0.1% AEGS. As mentioned in an earlier section, the permeability of Baker dolomite (a quarried carbonate rock of rather uniform texture with microscopic vugs distributed throughout) was 6.09 md, and of Berea sandstone was 305 md. The single phase permeabilities were measured with 1% brine solution.

To emphasize the difference between the results in different kinds of rock, it is helpful to consider the relative mobility, λ_r , which is the ratio of the measured absolute mobility to the rock permeability. The dimension of relative mobility is reciprocal centipoise, whereas absolute mobility is measured in (md/cp). Thus, in the very approximate sense in which "foam" is considered to be a single fluid that saturates the porespace (so that single-phase permeability could be used to characterize the rock), the "effective viscosity" of the foam could be taken to be the reciprocal of the relative mobility.

Figure 7 is a semi-log plot which graphically presents the relative mobility measurements made at different total flow rates (the latter are given as Darcy velocity in the rock) in the three kinds of rock. The CO₂-foam fraction was kept constant around 80%. Four different surfactants from different manufacturers were used. Concentrations of 0.1% Chembetaine BC-50 (Z) and 0.05% Alipal CD-128 (A) were used in experiments with Rock Creek sandstone. With Berea sandstone, 0.03% ZS and 0.05% and 0.1% AEGS were used. For Baker dolomite, 0.1% AEGS was used to make an exact comparison with Berea sandstone which was also tested with 0.1% AEGS. It is evident that the effect of rock permeability overshadows that of the surfactant type, at least in these rocks. The figure indicates that the magnitude of the relative mobility for the Rock Creek

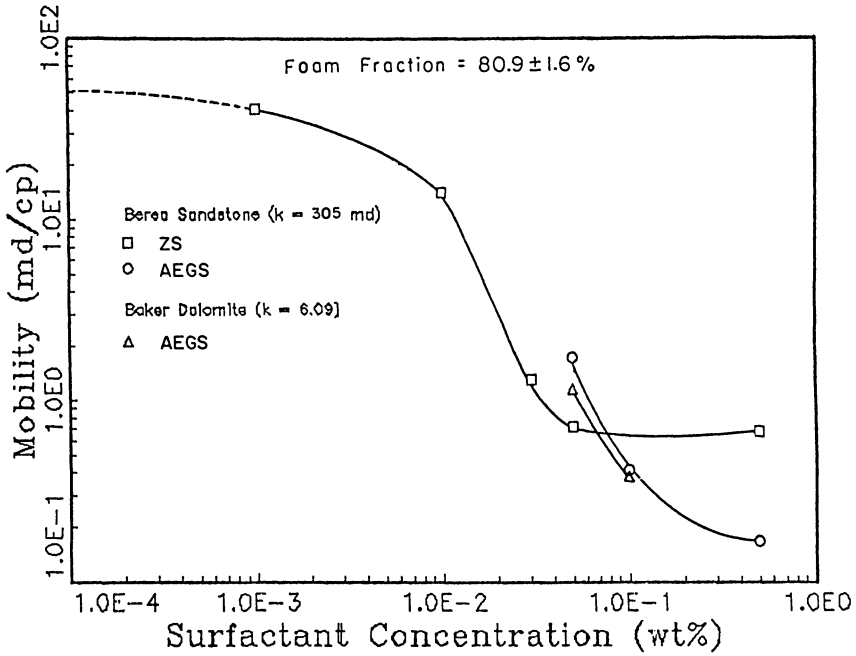


Figure 3. Effect of surfactant concentrations.

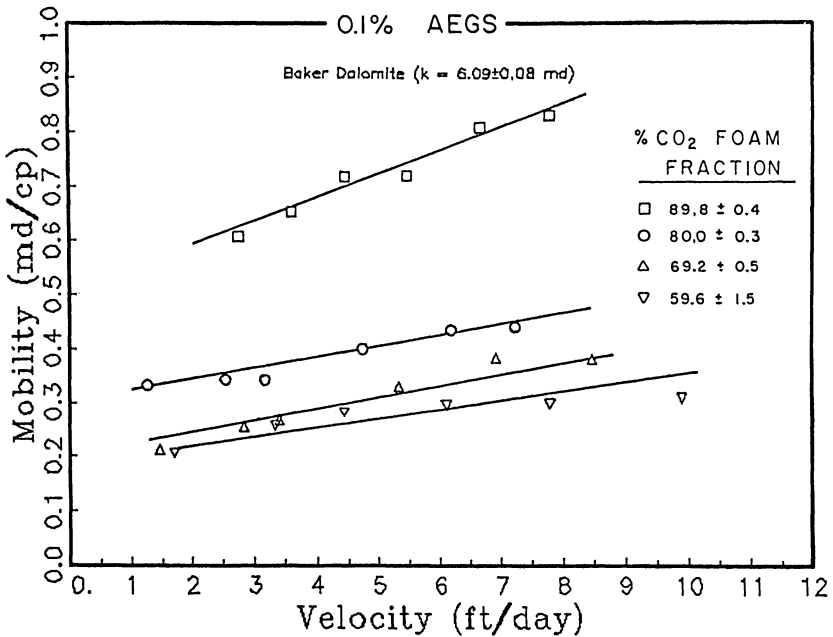


Figure 4. Effect of CO₂-foam fraction with Baker dolomite.

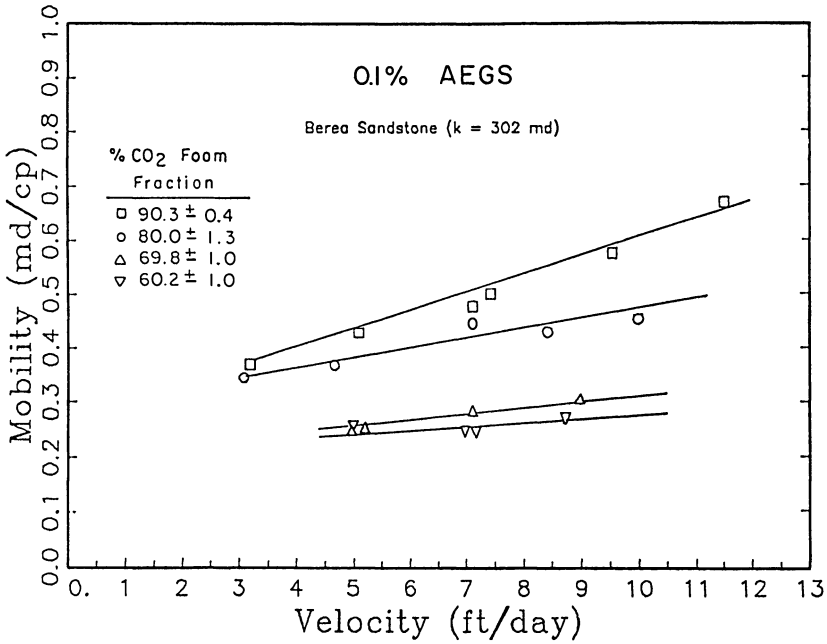


Figure 5. Effect of CO₂-foam fraction with Berea sandstone.

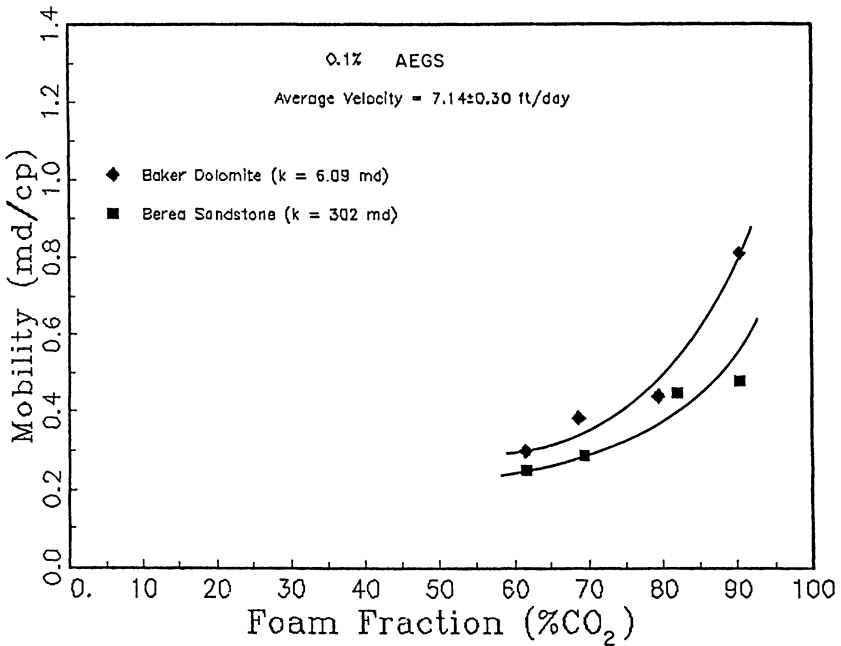


Figure 6. Effect of CO₂-foam fraction at 0.1% AEGS.

sandstone is approximately 36 times higher than that of Berea sandstone, although the inverse ratio of permeabilities is only about 21. The similar comparison made with Berea sandstone and Baker dolomite show that the relative mobility for the Baker dolomite is 46 times higher than Berea sandstone. The permeability measurements indicated that Berea was 50 times more permeable than Baker dolomite.

The effect of rock permeability is a significant result. These tests show that CO₂-foam is not equally effective in all porous media, and that the relative reduction of mobility caused by foam is much greater in the higher permeability rock. It seems that in more permeable sections of a heterogeneous rock, CO₂-foam acts like a more viscous liquid than it does in the less permeable sections. Also, we presume that the reduction of relative mobility is caused by an increased population of lamellae in the porous medium. The exact mechanism of the foam flow cannot be discussed further at this point due to the limitation of the current experimental set-up. Although the quantitative exploration of this effect cannot be considered complete on the basis of these tests alone, they are sufficient to raise two important, practical points. One is the hope that by this mechanism, displacement in heterogeneous rocks can be rendered even more uniform than could be expected by the decrease in mobility ratio alone. The second point is that because the effect is very non-linear, the magnitude of the ratio of relative mobility in different rocks cannot be expected to remain the same at all conditions. Further experiments of this type are therefore especially important in order to define the numerical bounds of the effect.

Dynamic Adsorption Experiment

The adsorption of the surfactant on porous media is an important variable in any enhanced oil recovery process that uses these chemicals. It is well understood that permanent adsorption does occur in the porous rock, which could drastically increase the cost of the process. To maintain a specific concentration to achieve the desired mobility reduction, it is necessary to calculate an additional amount of surfactant that is required to satisfy its permanent or irreversible adsorption in the flood area of the reservoir. Furthermore, the time required for a 'front' of the surfactant to flow through the core will be longer compared to the brine solution. This is an indication of chromatographic delay, a reversible adsorption of the surface active agents within the available times determined by the flow rates in the reservoir. The particular experiment described here will provide both the expected chromatographic delay factor of the surfactant front in the reservoir, and a measure of the quantity of surfactant that is (or might as well be) irreversibly adsorbed at the flow rates of the experiment. In this section, the description of the experimental apparatus and the nature of the experiment are discussed. As noted, dual results of the adsorption measurements are presented, as the amount of surfactant adsorbed per gram of rock and as the chromatographic time delay factor.

Description of the Experiment and Apparatus. The apparatus for this experiment is shown in Figure 8. At the left side of the figure, inside the dashed box, the procedure for core saturation is shown. Initially, the core tested is saturated with 1% acidified brine solution. The saturation of the core is achieved in the following manner.

The core is put into a Hassler sleeve inside a core holder where overburden pressure is applied outside of the sleeve by using water. Gas is not used, since it has the potential to diffuse through the rubber sleeve. The overburdened core holder is connected to the Isco pump, from which 1% acidified brine is pumped into the core. The needle valve that restricts flow from the output end of the core is opened slightly to allow the escape of air and air-saturated brine. The needle valve which restricts flow from the input end of the core is opened fully. Complete saturation is attained after several pore volumes of brine have been pumped through the core under pressure, and this fully saturated core is used throughout the experiment.

The first of two large circles in the figure represents the sampling valve (from Valco Instruments Corp.). This valve has six ports which are designated alphabetically. The sample loop is filled with a slug injection of the sample solution through port C at the "load" position of the valve. During this operation, flow within the valve is as shown by the solid lines. The excess of the sample solution flows out of port D during this time. Meanwhile, the 1% acidified brine solution is pumped continuously into port A and out through port F of the valve.

The sample loop, V_s , has a volume of 0.25 cc. To initiate injection at time zero of the experiment, the valve handle is rotated 60°, and the flows within the valve are redirected along the dashed lines as shown in the figure. The sample solution in the loop is then displaced through port F by the 1% acidified brine from the pump. The sample loop therefore must be long enough to contain a sufficient "slug" of sample solution. Here, the phrase "sample solution" refers to the surfactant solution prepared in 1% acidified brine solution. Teflon tubing and connections are used to minimize the uptake of any corrosion products into the 1% acidified brine solution.

The fluid leaves the sampling valve from port F and enters port 2 of a second switching valve (Rheodyne type 7010). The Rheodyne valve has six ports designated by Arabic numerals. The position of this valve determines the direction of flow from port 2; either through the core or through the capillary tube. These alternative paths are depicted in the second circle shown in the figure, by either dashed or solid lines. The capillary tube, V_c , has a volume of 0.50 cc. The core, which has been saturated with the 1% acidified brine, has a length of about 5 inches and is 1/2 inch in diameter. The solid line shows the flow inside the valve when external flow is through the core, and the dashed line represents the flow during an experiment that uses the capillary tube in place of the core.

The fluid from the tube or the core leaves the valve through port 5 and enters the inlet of the sample cell of the differential refractometer (made by Knauer of West Germany). The residue flows out of the sample cell to the waste. The reference cell contains

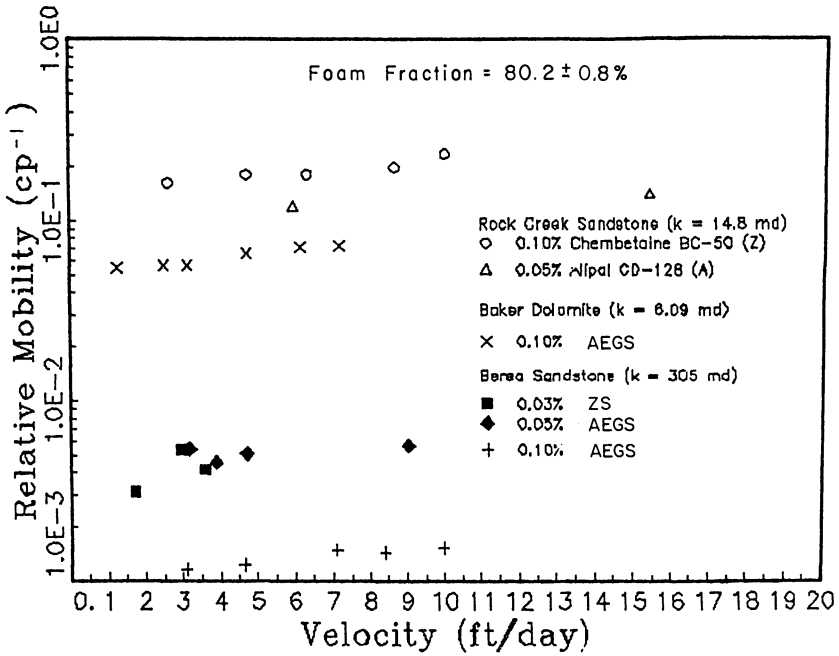


Figure 7. Effect of rock permeabilities.

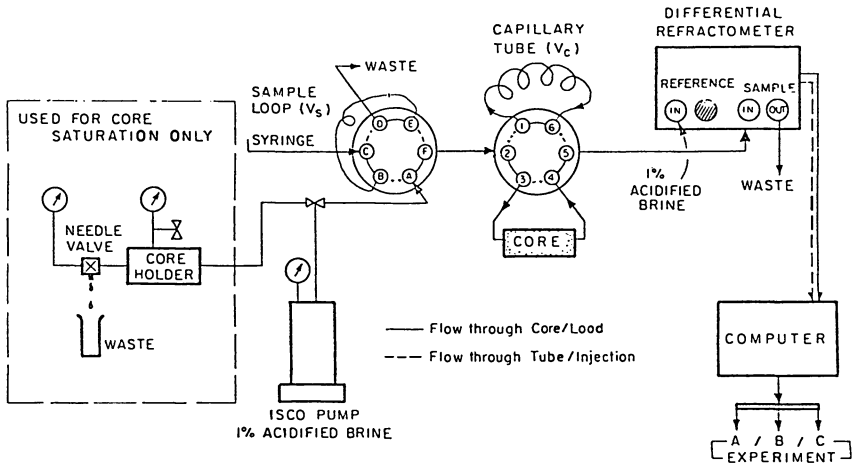


Figure 8. Dynamic adsorption apparatus.

the 1% acidified brine, and its outlet is plugged for convenience. The differential refractometer is used to achieve high sensitivity for the surfactants under test. The refractive index detector can be interfaced with the (Terak) computer for on-line data acquisition and analyses.

Basically, three types of experiments are carried out for measurement of the adsorption parameters of a given rock sample. The response of the experiment is the measured refractive index difference, which can be readily seen on the computer screen and also recorded by the chart recorder during operation. The descriptions of the experiments are as follows.

Experiment A is a non-adsorption experiment through the core, performed to measure the time for emergence of the peak. A 1.3% (concentration higher than the standard) acidified brine is loaded into the sample loop to be used as a sample medium. This particular experiment is carried out to measure the retention time by recording the time required before the peak is observed. The retention time can also be used to compute the exact porosity of the core, under the assumption of zero adsorption of salts from the brine.

Experiment B is also a non-adsorption experiment in which flow through the capillary tube is used. The sample medium used is the surfactant solution prepared in the 1% acidified brine. Results will be combined with those from Experiment C to get the information on the permanent or irreversible adsorption on the porous medium by measuring peak areas.

Experiment C is designed to yield information on the amount of the surfactant that is actually adsorbed on the rock. This experiment measures the variation of surfactant concentration at the outlet of the core, after injection of a "slug" of surfactant. The surfactant concentration in the brine depends on the position along the core and on time. The experiment is dynamic because the changing, but near equilibrium level of the adsorbed surfactant at any point along the rock sample is a function of the concentration in the solution at that point. This is described by the adsorption isotherm from a plot of M , the mass of surfactant adsorbed per gram of rock vs. Concentration.

From type B and type C experiments, the permanent adsorption can be computed from the ratio of one peak area to the other. The mass of surfactant adsorbed, in mg per gram of rock, is computed in the following manner: By knowing the volume of the sample loop which contains the surfactant solution, the initial surfactant concentration and its density, and the ratio of one peak area to the other, the amount of surfactant adsorbed can be calculated. Similarly, the mass of the rock can be computed from the volume of the rock and the density of the solid. The density of the solid can be computed by knowing the porosity of the rock and the density of the rock material. For the computational purpose, this density was taken to be 2.7 g/cc. This result will provide necessary information to compute the additional amount of surfactant that will be required in a reservoir, over and above that required to give the necessary surfactant concentration in the aqueous part of the CO₂-foam. Furthermore, combining the data from types A and C experiments makes it possible to compute the time delay factor. The chromatographic time delay factor is simply the ratio of the time required

to observe a peak of surfactant flow to the time before the peak of concentrated brine flow through the core is observed. The time for the surfactant peak is longer than that measured in Experiment A using the concentrated brine solution alone through the same core. This indicates chromatographic delay factor or reversible adsorption. Knowing the area ratio and chromatographic delay factor, the additional amount of surfactant that will be required, as well as time delay to be observed in reservoir application, can be computed.

Results and Discussion on Dynamic Adsorption Measurements. Baker dolomite was used to study the dynamic adsorption experiment. The computed porosity of the rock was 24%. One concentration below the CMC of AEGS, one at CMC, and two concentrations above CMC were chosen to measure the adsorption of this surfactant with Baker dolomite. The mass of surfactant adsorbed per gram of rock is plotted as a function of flow rate in a semi-log plot in Figure 9. The corresponding chromatographic time delay factors are presented in Table I. The results of Figure 9 apparently indicate that more adsorption of surfactant occurred at low flow rate. The shapes of the peaks from the flow through the core are also broader at low flow rate than at high flow rate. Also more anti-symmetry or deviations from the bell-shaped curve was observed with increase of concentration. Furthermore, more time was needed to reach baseline zero at high concentration. This must be due to the fact that as there is more adsorption, the time molecules spend in the mobile phase decreases which results in broad peak. Compared to the broad peak observed in core experiments, narrow and sharp peaks were observed with the tube flow. In the concentration range of this experiment, adsorption increased with increase of surfactant concentration. Data presented in Table I shows a chromatographic delay factor at the three flow rates. The results show that at high concentration strong adsorption causes a longer retention time at the rate of 10 cc/hr. However, at 0.5% with a flow rate of 20 cc/hr and similarly at 0.1% and 0.5% with 30 cc/hr did not give an expected trend similar to 10 cc/hr. Further tests are necessary to support this observation.

The slopes of the peaks in the dynamic adsorption experiment is influenced by dispersion. The 1% acidified brine and the surfactant (dissolved in that brine) are miscible. Use of a core sample that is much longer than its diameter is intended to minimize the relative length of the transition zone produced by dispersion because excessive dispersion would make it more difficult to measure peak parameters accurately. Also, the underlying assumption of a simple theory is that adsorption occurs instantly on contact with the rock. The fraction that is classified as "permanent" in the above calculation depends on the flow rate of the experiment. It is the fraction that is not desorbed in the time available. The rest of the adsorption occurs reversibly and equilibrium is effectively maintained with the surfactant in the solution which is in contact with the pore walls. The inlet flow rate is the same as the outlet rate, since the brine and the surfactant are incompressible. Therefore, it can be clearly seen that the dynamic adsorption depends on the concentration, the flow rate, and the rock. The two parameters

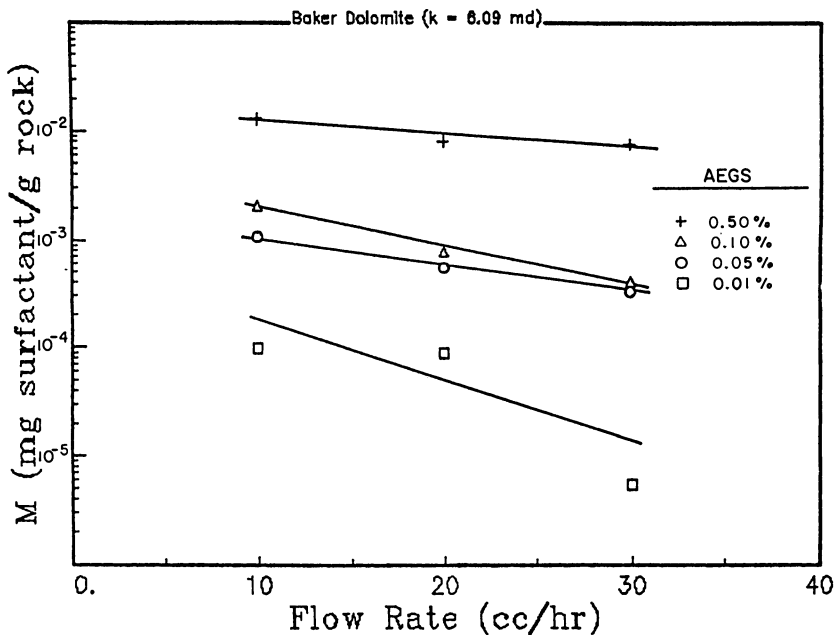


Figure 9. Mass of surfactant adsorbed per gram of rock.

Table I. Adsorption Measurements

**Effects of Concentrations and Flow Rates
on Chromatographic Time Delay Factors**

Q ($\frac{\text{cc}}{\text{hr}}$)	Conc. (wt.%)	Time Delay Factor
10	0.01	1.15
	0.05	1.16
	0.1	1.21
	0.5	1.24
20	0.01	1.04
	0.05	1.05
	0.1	1.10
	0.5	1.05
30	0.01	1.10
	0.05	1.17
	0.1	1.06
	0.5	1.06

calculated from these experiments are expected to be those that would be operative in the field.

Conclusions

The following conclusions can be made from the CO₂-foam mobility measurements and dynamic adsorption experiment. The effect of surfactant concentration shows that the mobility decreases with increasing surfactant concentration regardless of the type of surfactant or rock type. The effect of CO₂-foam fraction also demonstrates that mobility can be reduced by increasing the surfactant fraction at constant surfactant concentration. The effects of surfactant concentration and CO₂-foam fraction suggest that there has to be a sufficient quantity of surfactant available, in order to stabilize the number or population of lamellae for the foam flow through the porous rock. Also, more of the shear-thinning behavior was evident at high CO₂-fraction. The effect of rock permeability illustrates that CO₂-foam is not equally effective in all porous media. The reduction of relative mobility caused by foam is much greater in the higher permeability rock. By this mechanism, displacement in heterogeneous rocks can be rendered even more uniform than could be expected by the decrease in mobility ratio alone. Hence, this type of experiment is important to define the numerical bounds of the effect. The dynamic adsorption measurements show that additional surfactant is needed to compensate for permanent adsorption, and also that, chromatographic delay cannot be ignored.

Acknowledgment

The work reported here is a part of a larger project entitled Improvement of CO₂ Flood Performance, which has been supported by the US Department of Energy, the New Mexico Research and Development Institute, and a Consortium of oil companies. We extend them our great appreciation. Acknowledgement is also made of the efforts of Mustofa Sadeq for collecting the data for adsorption measurements and James McLemore for his assistance in the experimental parts.

Literature Cited

1. Heller, J.P.; Lien, C.L.; Kuntamukkula, M.S. Soc. Pet. Eng.J. 1985, 25, 603-13.
2. Bernard, G.G.; Holm, L.W.; Harvey, C.P., SPEJ 1980, 20, 281-92.
3. Heller, J.P.; Kuntamukkula, M.S. Ind. Eng. Chem. Res. 1987, 26, 318-25.
4. Radke, C.J.; Ransohoff, T.C., SPE 15441 presented in part at the 61st Annual Technical Conference and Exhibition of the Society of Petroleum Engineers, New Orleans, LA, Oct. 1986.
5. Lee, H.O.; Heller, J.P., SPE 17363 presented at the SPE/DOE Enhanced Oil Recovery Symposium, Tulsa, OK, April 1988.
6. Casteel, J.F.; Djabbarah, N.F., SPE 14392 presented at the 60th Annual Technical Conference and Exhibition of the Society of Petroleum Engineers, Las Vegas, NV, Sept. 1985.
7. Wellington, S.L.; Vinegar, H.J., SPE 14393 presented at the

- 60th Annual Technical Conference and Exhibition of the Society of Petroleum Engineers, Las Vegas, NV, Sept. 1985.
8. Heller, J.P., SPE/DOE 12644 presented at the SPE/DOE Fourth Symposium on Enhanced Oil Recovery, Tulsa, OK, April 1984.
 9. Heller, J.P.; Taber, J.J., SPE 15001 presented at the Permian Basin Oil & Gas Recovery Conference of the Society of Petroleum Engineers, Midland, TX, March 1986.
 10. Pande, P.K.; Heller, J.P., SPE 12753 presented at the California Regional Meeting, Long Beach, CA, April 1984.
 11. Heller, J.P.; Boone, D.A.; Watts, R.J., SPE 14395 presented at the 60th Annual Technical Conference and Exhibition of the Society of Petroleum Engineers, Las Vegas, NV, Sept. 1985.
 12. Patton, J.T.; Holbrook, S.T.; Hsu, W. Soc. Pet. Eng. J. 1983 23, 456-60.
 13. Owete, O.S.; Brigham, W.E., SPERE, 1987, 2, 315-23.
 14. Huh, D.G.; Cochrane, T.D.; Kovarik, F.S., SPE/DOE 17359 presented at the SPE/DOE Enhanced Oil Recovery Symposium, Tulsa, OK, April 1988.
 15. Abou-Kassem, J.H.; Farouq Ali, S.M., SPE 15954 presented at the SPE Eastern Regional Meeting, Columbus, Ohio, Nov. 1986.
 16. Khatib, Z.I.; Hirasaki, G.J.; Falls, S.H., SPE 15442 presented at the 61st Annual Technical Conference and Exhibition of the Society of Petroleum Engineers, New Orleans, LA, Oct. 1986.
 17. Rossen, W.R., SPE 17358 presented at the SPE/DOE Enhanced Oil Recovery Symposium, Tulsa, OK, April 1988.
 18. Borchardt, J.K., Bright, D.B.; Dickson, M.K.; Wellington, S.L., SPE 14394 presented at the 60th Annual Technical Conference and Exhibition of the Society of Petroleum Engineers, Las Vegas, NV, Sept. 1985.
 19. Borchardt, J.K., SPE 16279 presented at the SPE International Symposium on Oilfield Chemistry, San Antonio, TX, Feb. 1987.
 20. Mannhardt, K.; Novosad, J.J., presented at the European Symposium on EOR, Hamburg, West Germany, Oct. 1987.
 21. Bae, J.H.; Petrick, C.B., SPEJ 1977, 17, 353-57.
 22. Grow, D.T.; Shaeiwitz, J.A., J. Colloid Interface Sci. 1982, 86, 239-53.
 23. McCutcheon's Emulsifiers & Detergents, McCutcheon Division, MC Publishing Co., Glen Rock, NJ, 1986 North American Edition, 1986, p. 276.

RECEIVED November 28, 1988

Chapter 28

Laboratory Apparatus for Study of the Flow of Foam in Porous Media Under Reservoir Conditions

C. W. Nutt,^{1,2} R. W. Burley,^{1,2} A. J. MacKinnon,¹ and P. V. Broadhurst³

¹Heriot-Watt University, Edinburgh, United Kingdom

²IMOD Processes Ltd., Linlithgow, West Lothian, EH 49 7JU,
United Kingdom

³ICI Chemicals and Polymers Ltd., Wilton, Cleveland, Great Britain

The numerous previous studies of the flow of foam in porous media and of its application for improving the displacement of oil from such media, have almost always been conducted under ambient conditions of temperature and pressure; there have been very few reports of laboratory studies under reservoir conditions. Although many interfacial properties are known to be temperature dependant, little attention has been paid to the influence of temperature upon the properties of foam. Furthermore, the rheological properties of foams, and their effectiveness for the displacement of oil are strongly dependant upon foam quality, which is in turn strongly dependant upon the pressure to which the foam is subjected.

This paper describes an apparatus for the determination of the viscous properties of foam, and for the measurement of its ability to displace oil from porous media, under reservoir conditions, and will report and discuss some of the preliminary results obtained.

It is now well established through studies in many laboratories throughout the world that foam injection shows considerable promise as an agent for the improvement of oil recovery from watered-out porous media, and for the diversion of the flow of other oil-displacing fluids from more permeable paths into less permeable paths in the medium⁽¹⁾. Whilst the reasons for the effectiveness of foam for these purposes are not completely clear, the explanation is thought to lie in the behaviour of the foam lamellae

0097-6156/89/0396-0518\$06.00/0

© 1989 American Chemical Society

during their motion through the pore structure, and to derive from the rheological properties of the interfacial layers of the lamellae^(2,3). Comparison of the behaviour of foams formed by surfactants which are typical of the main classes of commercially available reagents has revealed that the effectiveness of a foam depends strongly on the chemical nature of the foaming agent as well as on the quality of the foam⁽¹⁾.

Now it has been the usual practice to conduct laboratory tests of the effectiveness of foam to improve oil recovery from porous media at room temperature and atmospheric pressure. Yet it is well established that the stability of foams often diminishes with increase of temperature, and indeed the ability of aqueous solutions of many surfactants to form foams disappears completely at a characteristic temperature which is less than the temperature within many deep oil fields. Moreover, since the effectiveness of a foam to displace oil, or to selectively divert flow, are functions of foam quality and since the quality of a foam is strongly dependant upon the pressure, the selection of a foaming agent for EOR applications therefor requires an understanding of the behaviour of the foam at the elevated temperature and pressure which exists in the oil field. Experimental study of these aspects is therefore required, but regrettably few such investigations have been reported⁽⁴⁻⁶⁾. This paper is concerned with a description of an apparatus designed for this purpose, and a preliminary report of some aspects of its performance together with some preliminary observations on the effect of pressure on the apparent viscosity of a foam flowing in a straight capillary tube.

APPARATUS

The central feature is a high pressure cell (1 in Figure 1), a cylindrical vessel, internally about 0.9 m in length and 0.1 m in internal diameter mounted with its axis horizontal. The cell is constructed of selected stainless steel with a wall thickness and design such that it can withstand an internal pressure of 5250 p.s.i.g. The screwed-on end caps of this test cell are capable of carrying various different test units (2 in Figure 1) within the pressure cell, and are provided with inlet and outlet lines for the test fluid. The test units which can be incorporated include straight, glass, capillary tubes up to 0.76 m long and sand pack or core sample holders up to the same length and 0.1 m in diameter. Optical glass windows, 0.1 m long and 0.01 m wide at the top and bottom of the test cell can permit visual observation of the behaviour of the fluid within glass test units.

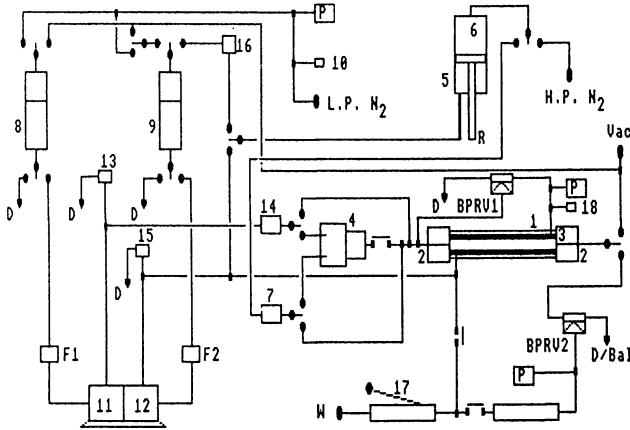


Figure 1. Schematic representation of the flow diagram of the foam rheology rig.

- | | |
|--------------------------|-----------------------------|
| 1 High pressure cell | 2 End caps of test cell |
| 3 Test unit | 4 Foam generator |
| 5 Rodded cell | 6 Gas in rodded cell |
| 7 Non-return valve | 8 Surfactant storage vessel |
| 9 Water storage vessel | 10 Pressure relief valve |
| 11 Surfactant pump | 12 Water pump |
| 13 pressure relief valve | 14 Non-return valve |
| 15 Pressure relief valve | 16 Pressure reducing valve |
| 17 Pressure pump | 18 Pressure relief valve |
| (hand operated) | |

- | | |
|--------------------|--------------------------------------|
| D | Discharge to drain |
| F1, F2 | Filters |
| P | Pressure gauge |
| BPRV1 | Back pressure relief valve |
| BPRV2 | Back pressure relief valve |
| D/Bal | Digital balance |
| L.P.N ₂ | Low pressure nitrogen blanket supply |
| H.P.N ₂ | High pressure nitrogen supply |
| Vac | Vacuum line |
| W | Water supply |

Another thick walled cylindrical, stainless steel, vessel(4 in Figure 1), inside diameter 0.03 m and inside length 0.075 m also capable of withstanding an internal pressure of 5250 p.s.i.g. is mounted close to the inlet feed of the high pressure test cell. Cores or sand packs can be installed within this vessel, which serves as a foam generator.

Gas can be supplied to the foam generator or to the test cell from a rodded cell(5 in Figure 1), a stainless steel cylinder, inside dimensions approximately 0.5 m long and 0.04 m diameter, mounted with its axis vertical, and designed for an internal working pressure of 6000 p.s.i.g.

Electrical strip heaters, wrapped around the three stainless steel vessels enable them to be operated at any desired temperature. Thermocouples strapped to the surfaces of the vessels permit measurement of their temperatures and, coupled to controllers, maintain the vessels at constant temperature or ensure that the rate of change of the temperature of the vessels is not excessive, so avoiding unnecessary thermal stress in them.

As shown in Figure 1, for investigations at pressures up to 2000 p.s.i.g. high pressure nitrogen, from a cylinder, can be introduced into the rodded cell. The gas, 6, in the rodded cell at the desired pressure can be driven by the motion of the piston, R, via a non-return valve, 7, to the foam generator or directly to the test unit. The position of the piston can be determined by a digital position indicator gauge mounted on the end of the piston rod(R in Figure 1), which thus permits determination of the volume of gas injected and the rate of injection.

Two 4 l cylindrical glass(QVF) vessels with stainless steel end plates, serve as reservoirs(Figure 1) for surfactant solution(8) and water(9). Facility is available to evacuate these vessels as required by means of a rotary vacuum pump with glass cold trap in line to minimise water vapour. Another pipeline permits supply of pure nitrogen, or other gas, at low pressure, to the vessels, to provide a blanket, as desired. Proper operation and safety from over pressure is ensured by a pressure relief valve(10 in Figure 1) and the pressure gauge(P in Figure 1).

The desired surfactant solution, prepared by dissolving the appropriate weight in a known volume of distilled water, can be introduced into the storage vessel(8) from which it may be discharged to a drain(D in Figure 1), or fed via a filter(F1 in Figure 1), to one side of a dual peristaltic pump(11 in Figure 1). From the pump outlet the surfactant solution flows through a line equipped with pressure relief valve(13 in Figure 1C), to a non-return valve(14 in Figure 1C), and thence to the foam generator, or to the test cell as desired. The rate of delivery of solution can be

controlled by suitable adjustment of the variable volume setting of the pump, previously calibrated to permit easy operation.

The other part of the dual pump(12 in Figure 1) can similarly supply water from the reservoir(9 in Figure 1), via a filter(F2 in Figure 1) past a pressure relief valve(15 in Figure 1) to the underside of the piston of the rodded cell(5 in Figure 1). This in turn drives a gas from the upper side of the piston to the other inlet of the foam generator. To refill the rodded cell with high pressure gas, the water from the underside of the piston can be returned to the reservoir(9) via a pressure reduction valve(16 in Figure 1). The filters(F1 and F2 in Figure 1), 5 micron pore size, in the feeds to the pumps, serve to protect these devices from damage and additional security is provided by pressure relief valves(13 and 15 in Figure 1) on the effluent flow lines of the pumps.

Foam created in the foam generator is fed directly to the inlet of the test unit in the test cell, and the pressure drop developed by its flow through the test unit is measured by means of a differential pressure transducer, not shown in the figure, connected between inlet and outlet, and provided with by-pass and isolation valves for protection against accidental overloading.

The water pumped to the underside of the piston of the rodded cell can also be delivered to the test cell, to fill the jacket surrounding the test unit(Figure 1). The contents of the jacket can be discharged via a back-pressure relief valve(BPRV1 in Figure 1) which is arranged to open when the water pressure exceeds that of the foam flowing to the inlet of the test unit.

Foam leaves the test unit via another back-pressure relief valve(BPRV2 in Figure 1). In most of the investigations which are planned the foam will be collected in a suitable vessel on a continuous weighing top loading digital balance(D/Bal in Figure 1). As shown in Figure 1, the setting of this back-pressure relief valve is determined by the water pressure applied to the jacket surrounding the test unit so that flow out of the test unit occurs when the internal pressure in the unit exceeds that in the water jacket surrounding the test unit.

Facility is provided to bring the equipment up to the desired absolute pressure without subjecting the test unit to excessive pressure difference between its interior and exterior. This is accomplished by first filling the test cell with water by means of a hand operated hydraulic pump(17 in Figure 1) to a suitable value as indicated on the Bourdon dial gauges(P in Figure 1). The pressure thus developed is used also to control the appropriate back-pressure relief valve

which remains closed until the internal pressure in the test unit has increased to the same value as the external pressure. Once the necessary pressure has been reached, the supply of water from the hand operated pump is discontinued and the test cell water jacket connected to the peristaltic pump used to supply water to the rodded cell. Excessive pressure difference between the interior of the test cell and exterior is avoided by feeding the inlet pressure of the test unit to the other back-pressure relief valve which opens to permit water from the exterior of the test unit to be discharged should the external pressure become too high. A pressure relief valve (18 in Figure 1) provides additional protection. Facilities are provided to fit pressure transducers at various points on the flow lines, should it be desired to monitor such pressures in the future.

Signals from the digital balance, the rodded cell rod position indicator, the gauge indicating the pressure differential over the test unit and the output of thermocouples indicating the temperature of foam entering and leaving the test unit are transmitted to a data logging facility and recorded on floppy discs on an Acorn "BEC Mode B" microcomputer, and conveyed to an Acorn "Archimedes" computer for processing as desired. Several hundred values for each of the variables could be recorded during a run lasting up to ninety minutes, in this way, for subsequent analysis.

EXPERIMENTAL

The experiments initially conducted were designed to test the performance of the apparatus by determination of the effect of pressure on the viscosity/quality spectrum of a typical foaming agent when it flows through a straight capillary tube. The method used is based on a technique recently developed in the laboratories(7) for this purpose, at atmospheric pressure.

The viscosity/foam quality spectrum at a fixed pressure is derived from a single experiment in which the foam generating vessel is first filled completely with foaming agent solution, and then the gas supply is turned on. Initially, aqueous solution is displaced from the generator, but once gas break-through commences a wet foam is discharged. As gas flow continues, the foam becomes drier and drier until ultimately only gas flows.

Determination of the rodded cell rod position, as a function of time (Figure 2 shows a typical set of results), permits computation of the volumetric gas flow rate into the foam generator.

Figure 3 shows a typical set of results for the cumulative weight of fluid discharged from the

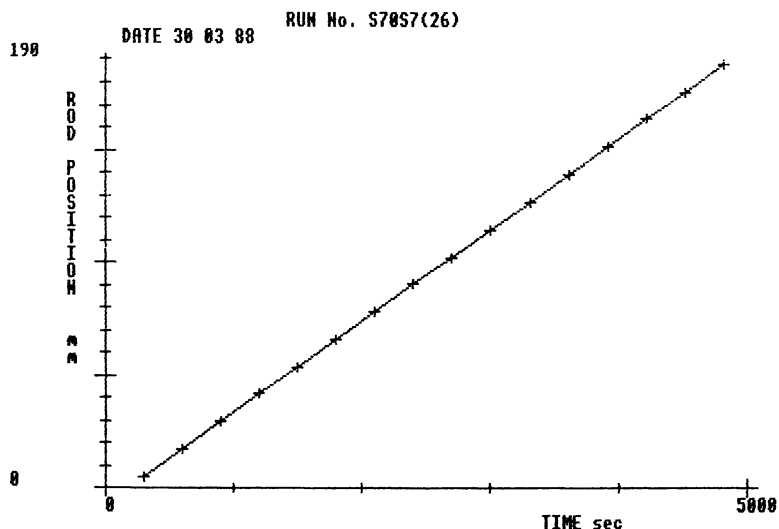


Figure 2. Typical plot of data output from the rig, showing values of the position of the rodded cell piston as a function of time, during an experiment.

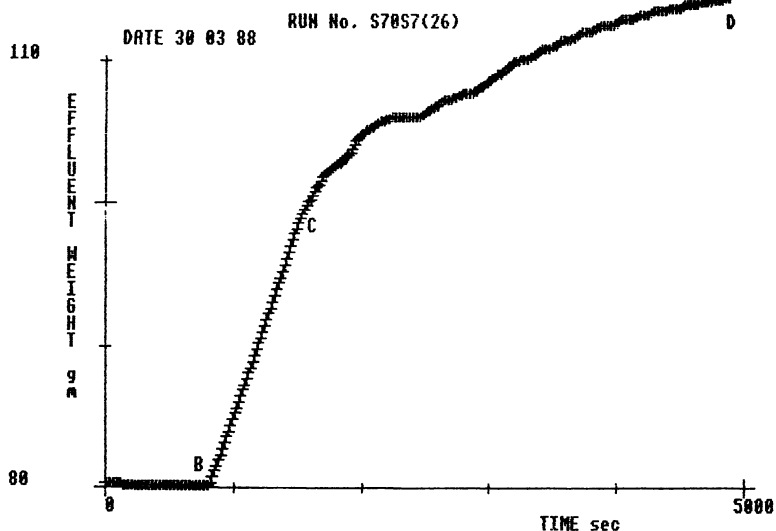


Figure 3. Typical plot of data output from the rig, showing values of the weight of effluent from the capillary test unit as a function of time, during an experiment. The portion of the curve from B - C shows the efflux of surfactant solution from the foam generator which precedes gas break-through. Portion C - D shows the efflux of foam of increasing quality. At times larger than D only "dry" gas, without liquid phase, emerges.

apparatus, during the course of an experiment. The results demonstrate clearly how in the initial stage, aqueous surfactant solution is eluted from the foam generator, followed by foam once gas break-through has commenced. The steady decline in the rate of increase of cumulative weight of foam through the course of the experiment shown by the results in Figure 3, clearly demonstrates how the foam quality steadily increases in dryness until at the end of the experiment, only gas emerges from the foam generator.

After gas break-through, the incremental rate of increase in effluent weight can be taken as a measure of the incremental weight of liquid in the foam. This, together with a knowledge of the instantaneous volumetric gas flow rate, permits calculation of the quality of the foam. Provided the pressure drop over the foam generator is sufficiently small, the volumetric flow rate for such calculations can be taken to be constant throughout an experiment and equal to that indicated by data such as that shown in Figure 2. This assumption was justified in the studies at atmospheric pressure reported previously(7), but in the present investigations correction for changes in pressure drop across the foam generator during the course of an experiment may be necessary.

By conducting a series of such measurements at a number of different gas flow rates, measurements of the pressure drop across a capillary tube having a known diameter and length, during each experiment (Figure 4 shows a typical set of values of the differential pressure gauge output as a function of time), permit evaluation of the wall shear stress and wall shear rate as functions of time(7), and thereby for the range of foam qualities created during the experiment. Previous studies(6) have shown that under such conditions, at atmospheric pressure, foam conforms closely to the simple power law relation for non-Newtonian fluids:

$$\mu_{app} = \tau_w / \dot{\gamma}_w = K \dot{\gamma}_w^{n-1} \quad (1)$$

where K is the flow consistency,
 n is the power index,
 μ_{app} is the apparent viscosity,
 τ_w is the wall shear stress, and
 $\dot{\gamma}_w$ is the wall shear rate.

The results shown in Figure 2 illustrate that a satisfactorily constant gas flow rate over a period of time in excess of one hour could be achieved readily.

Consideration of the slope of the effluent weight/time curve just after gas breakthrough, shown in Figure 3, indicates that the foam first breaking through had a quality of about 60%, whilst that emerging near the end of the run has a quality of approximately 92%. The foam quality at intermediate

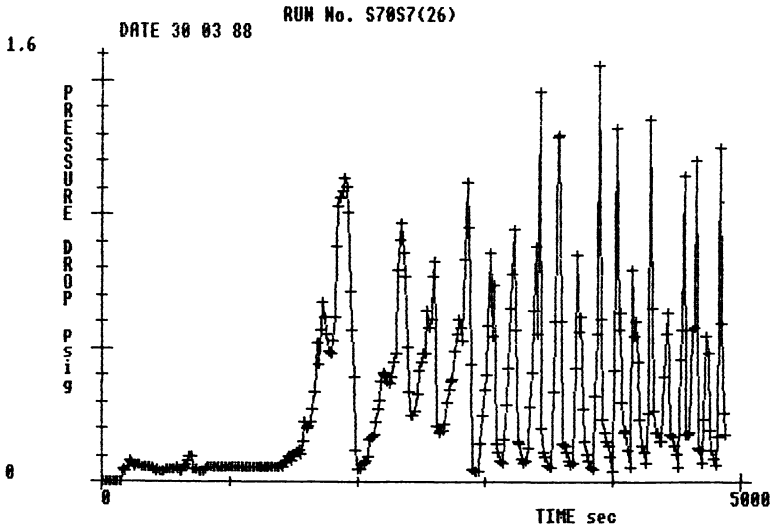


Figure 4. Differential pressure transducer output, as a function of time, during a typical experiment at atmospheric pressure.

times between these limits sometimes fluctuated irregularly, sometimes becoming drier and then showing an abrupt increase in wetness. Each such irregularity was accompanied by corresponding changes in the pressure drop observed for the flow through the capillary tube, as illustrated in Figure 4. The change in foam quality indicated by the effluent weight curve was delayed by approximately 150 secs behind that indicated by the pressure drop/time curve, at the particular gas flow rate used in that experiment. This was due to the hold-up of effluent in the back-pressure relief valve in the foam outlet line. These irregularities in foam quality were caused by the gas flow process through the sand pack in the foam generator. From time to time as the sand pack dried out, new gas flow paths developed, and associated with each such event there occurred a transient increase in foam wetness. Careful packing of the foam generator could minimise this phenomenon. Alternatively or additionally, the effect could be eliminated by inclusion of a mixing vessel of properly selected capacity, in the foam flow line between the generator and the test unit.

The rheological behaviour of a typical surfactant at atmospheric pressure, derived using this technique, has been reported and illustrated in various figures in an earlier communication(7).

FURTHER DEVELOPMENT

In the current program of investigations it is intended to study the rheological behaviour of foams formed by a range of surfactants, during flow through a capillary tube, over the quality range 50-60% to 95%, at temperatures up to 100°C and pressures up to 2000 psig. After the addition of a pressure intensifier the studies of certain selected foams will be extended to pressures up to 5,000 psig.

By the addition of other liquid reservoirs, e.g. for water and crude oils, and replacement of the capillary test unit by a sand pack, the effectiveness of the same foams for enhanced oil recovery at reservoir temperatures and pressures will be investigated.

ACKNOWLEDGMENTS

The authors wish to record their thanks and appreciation to ICI Chemicals and Polymers Ltd. and to Offshore Supplies Office for financial support and for permission to publish this paper, and to Alval Engineering Ltd for equipment manufacture and high pressure design input.

REFERENCES

- (1) Ali J., Burley R.W. and Nutt C.W. "Foam Enhanced Oil Recovery from Sand Packs" Chem. Eng. Res. Des. 1985 63 101.
- (2) Giordano R.M and Slattery J.C.
A.I.Chem.E. Symp. Series 1982 78 58.
- (3) Nutt C.W., Burley R.W., Stavenam A. and Naismith S.M. "Mechanism of the Displacement of Oil from a Porous Medium by Foam" (*in press*)
- (4) Heller J.P. and Kuntamukkula M.S. "Critical Review of Foam Rheology Literature" Ind. Eng. Chem. 1987 26 318.
- (5) Farouq Ali S.M. and Selby R.J. "Function, Characteristics of EOR Foam Behaviour Covered in Laboratory Investigations" Technology, Oil & Gas J. Feb 3 1986 57-63
- (6) McPhee C.A., Tehrani A.D.H. and Jolly R.P.S.
S.P.E. 1988 Paper No.17360
- (7) Assar G.R., Nutt C.W. and Burley R.W.
"The Viscosity-Quality Spectrum of Foam Flowing in Straight Capillary Tubes" (*in press*)
Int. J. of Eng. Fluid Mech. 1988.

RECEIVED November 28, 1988

Chapter 29

Associative Organotin Polymers

Triorganotin Fluorides in Miscible Gas Enhanced Oil Recovery

D. K. Dandge, P. K. Singh, and John P. Heller

New Mexico Petroleum Recovery Research Center, New Mexico Institute of Mining and Technology, Socorro, NM 87801

Preparation, characterization, and properties of silicon-containing triorganotin fluorides, both symmetrical and unsymmetrical, were investigated. It was observed that introduction of a trimethylsilyl group in the alkyl chain results in a considerable enhancement of solubility in various nonpolar solvents including dense carbon dioxide.

Enhanced oil recovery processes involving displacing fluids such as dense CO₂ and liquified petroleum gases (LPG) are currently being applied in different parts of the world. At moderately high pressure and reasonable temperatures common in many reservoirs, CO₂ is capable of extracting the light ends of the oil in the region of contact with the oil.

The effectiveness of CO₂ in displacing oil from reservoirs is marred, however, by its extremely low viscosity. The viscosity of dense CO₂ remains low (in the range from 0.03 to 0.08 cp or 0.03 to 0.08 mpa) despite its relatively high density (above 0.45 g/cm³) under reservoir conditions. This low viscosity of CO₂ as compared to that of crude oil (1-10 cp) results in a high mobility ratio which degrades the macroscopic efficiency of the displacement process. Therefore, some method of mobility control is required for efficient use of CO₂, to increase greatly the quantity of producible oil.

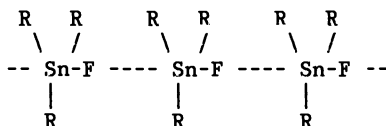
The desired low mobility ratio (approaching 1) could be achieved by the viscosification of CO₂. This prompted the search for compounds which can dissolve in and viscosify dense CO₂ and nonpolar hydrocarbons.

Certain triorganotin fluorides are known to be effective viscosifiers for nonpolar solvents. Dunn and Oldfield (1) have studied the solution properties of tri-*n*-butyltin fluoride (BUF) in various organic solvents. They reported that, among *n*-alkanes, BUF dissolves only in *n*-hexane and not in *n*-heptane. This

0097-6156/89/0396-0529\$06.00/0

© 1989 American Chemical Society

intriguing solubility behavior was attributed to the matching size of solvent molecules with those of the solute. Dandge et al. (2,3), however, found that increasing the alkyl chain beyond C₄ in alkyltin fluorides (R₃SnF) substantially increases their solubility in most organic solvents. Furthermore, viscosification of nonpolar solvents by these trialkyltin fluorides (which ranged from triamyl to tridecyltin fluoride) was as effective as that by BUF or even better (2,3). Due to the large difference in the electronegativity of Sn and F atoms, R₃SnF-type compounds form polymeric chains (1) by association wherein Sn assumes a penta-coordinate structure:



These transient polymeric chains resulting from dipole-dipole interactions are responsible for the increase in solvent viscosity which is asymptotic above a certain concentration. The structure dependence of both solubility and viscosity in triorganotin compounds is known (1,2,3). For example, trimethyl and tripropyltin fluorides are insoluble in most organic solvents while the bulky trineophyltin fluoride (4) dissolves in many solvents but does not increase their viscosity.

Our previous work (2,3) showed that while increasing the alkyl chain in R₃SnF increases both their solubility and viscosity in hydrocarbons such as propane (d = 0.5 g/cc) and butane (d = 0.5 g/cc) (5), the solubility in CO₂ did not show a considerable increase. Also, in a separate study (6), it was observed that silicon-containing polymers are more soluble in dense CO₂ than any other polymer of similar molecular weight. Taking these observations into consideration, we decided to synthesize silicon substituted trialkyltin fluorides in order to increase the solubility of these associative compounds in CO₂. The field applicability of such viscosifiers, it is found, would depend on the price of oil. R₃SnF compounds with long chain R groups are nontoxic and offer little risk to the environment. This paper describes the synthesis, characterization, and solution properties of three silicon containing organotin fluorides.

Experimental

Materials. The chemicals used in the synthesis were purchased from Aldrich Chemical Co. and Petrach Systems.

Methods. FTIR spectra were obtained in nujol mull on a Perkin Elmer model No. 1700GC-IR spectrophotometer. ¹H NMR spectra were obtained at 363 MHz. ¹³C NMR spectra were obtained at 91 MHz. All NMR spectra were run by Spectral Data Services. No external standard such as TMS was added to the sample as the compounds had (CH₃)₃Si groups. X-ray diffraction patterns were obtained on Rigaku-Geiger flex x-ray diffraction machine. Melting points and

boiling points are uncorrected. Elemental analysis was carried out by Galbraith Laboratories, Knoxville, Tennessee.

Viscosity measurements were carried out using Cannon-Fenske viscometers of appropriate capillary diameter so as to keep the efflux time between 200-300 seconds. Approximate shear rate at the wall was calculated using the equation

$$\gamma_w = 4V/(\pi R^3 t)$$

where	γ_w	=	Shear rate at the wall
	V	=	Volume of the viscometer bulb
	R	=	Capillary radius
	t	=	Efflux time

Shear rate and viscosity curves were obtained at 25°C using Contraves low shear viscometer (Model LS-30).

General Synthesis Procedures

Tetraorganotin. A Grignard reagent was prepared in THF from equimolar amounts of bromoalkane and metallic magnesium. A few drops of bromoethane were used to initiate the reaction. To the reagent was added benzene solution of stannic chloride (1/18 mole bromo-alkane used), so as to keep the reaction mixture under gentle reflux. Unreacted magnesium was filtered, and the filtrate was treated with saturated ammonium chloride. The organic layer was separated and dried. Removal of solvent and fractional distillation yielded the corresponding tetraorganotin which was characterized by boiling point and refractive index.

Triorganotin Bromide. Tetraorganotin compounds were brominated with stoichiometric quantities of bromine (2 moles of bromine for each mole of tetraorganotin). Bromination was carried out after cooling the tetraorganotin compound in a dry ice-acetone bath. The contents then were slowly brought to room temperature. In most cases, the crude bromides were used as such for fluorination.

Triorganotin Fluoride. Fluorination of triorganotin bromide was carried out by an excess of ammonium fluoride at 120°C for one hour.

Results and Discussion

Synthesis and Characterization. Tris(trimethylsilylpropyl)tin fluoride (PTF) and tris(trimethylsilylmethyl)tin fluoride (MTF) were synthesized according to scheme A (Figure 1) while scheme B (Figure 1) was followed in the synthesis of dibutyl-(trimethylsilylpropyl)tin fluoride (BTF). MTF has been reported in the literature (6); however, it was synthesized to compare its solution properties with the other two novel compounds. The steps involved in these syntheses were straight-forward and thus need no elaboration. In the synthesis of BTF, the unsymmetrical triorganotin fluoride, bromination of tetraorganotin compound resulted

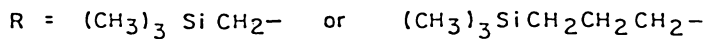
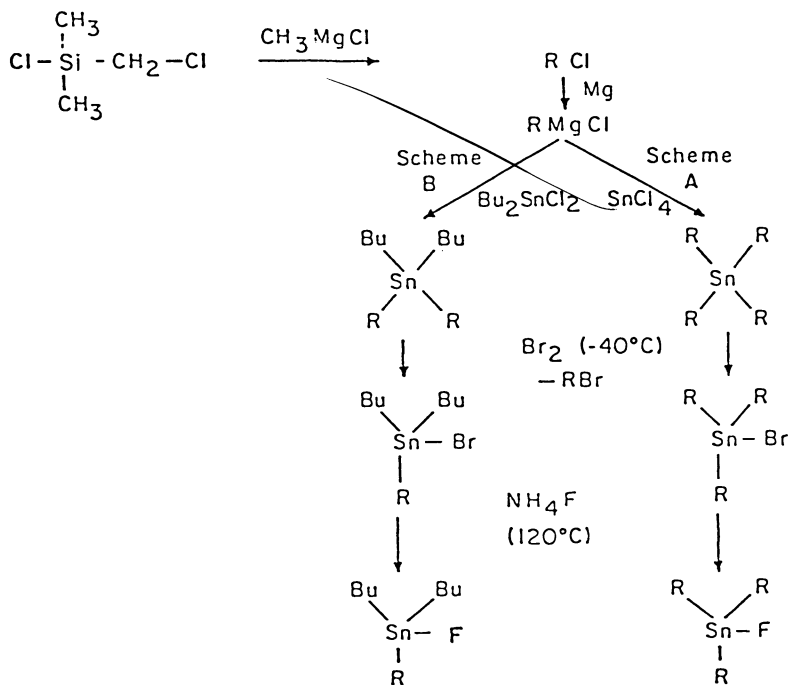


Figure 1. Schemes for the synthesis of silicon containing triorganotin fluorides.

in the preferential displacement of the trimethylsilylpropyl group. Similar observations were reported by Seyferth (8).

Measured and calculated percentages of the elements in the compounds are shown in Table I. It is apparent that these values are separated by no more than the probable experimental error. Also shown in the same table are boiling points and the refractive indices of the tetraorganotin compounds, which are the precursors of MTF, PTF, and BTF.

The x-ray diffraction patterns for MTF, PTF, and BTF are given in Figure 2. The unsymmetrical BTF shows broad dispersed peaks indicating an increase in amorphousness compared to MTF, its symmetrical analogue. The peaks in the pattern for PTF, on the other hand, are broader and less sharp than those for MTF, which may be the result of an increase in the alkyl chain length by two carbon atoms.

FTIR spectra of the three fluorides are given in Figure 3. Typical frequencies of the peaks found in the region of 450 cm^{-1} to 1300 cm^{-1} region and their assignments are as follows:

525 cm^{-1}	Sn-C Stretch
615 cm^{-1}	Sn-C Stretch
690 cm^{-1}	-CH ₂ Stretch
712 cm^{-1}	-CH ₂ Stretch
755 cm^{-1}	Nujol
840 cm^{-1}	Si-C Stretch
860 cm^{-1}	(CH ₃) ₃ Si Stretch
1250 cm^{-1}	Si - CH ₃

Due to the unavailability of appropriate cells, the Sn-F absorptions in the far infrared region cannot be observed.

The ¹H and ¹³C NMR spectra of the three fluorides are given in Figures 4 and 5 respectively. The peak assignments for various groups in each compound are given in Tables II and III, while calculated and observed peak ratio values are given in Tables IV and V.

Solution Properties

Solubility Behavior - The solubilities of MTF, PTF and BTF in various organic solvents including CO₂ are given in Table VI. The solvents are arranged in the order of increasing solubility parameter. It has been observed, after a comparative study with tri-n-alkyltin fluorides, that replacement of a methyl group by a trimethylsilyl group enhanced the solubility in nonpolar solvents, and is well reflected in the markedly higher solubility of MTF, PTF, and BTF in CO₂. For example, tri-n-alkyltin fluorides dissolve to an extent of 1.26 gm/liter whereas compounds having trimethylsilyl group with appropriate number of CH₂- groups dissolved to an extent of 4.5 gm/liter (see Table VI).

The rate of dissolution of PTF and BTF in nonpolar solvents is considerably higher than in tri-n-alkyltin fluorides. The former dissolve instantly while the latter dissolve only by a slow swelling process. This indicated that the presence of the trimethylsilyl group, at the end of the chain and somewhat away from

Table I
Silicon Containing Triorganotin Fluorides

Compound	m.p. °C	Elemental Analysis								
		Calc. for %			Found %					
		25nD	C	H	Si	F	C	H	Si	F
MTF	102	--	36.09	8.27	21.13	4.74	36.35	8.42	20.51	4.89
PTF	180	--	44.72	9.32	17.45	3.94	44.74	9.65	15.74	3.15
BTF	82	1.4765	45.81	8.99	7.66	5.18	46.15	8.50	7.20	4.26

MTF Tris(trimethylsilylmethyl)tin fluoride
 PTF Tris(trimethylsilylpropyl)tin fluoride
 BTF Dibutyl(trimethylsilylpropyl)tin fluoride

Intermediates for the synthesis of the above compounds were:

<u>Tetraorganotin Compound</u>	<u>b.p</u>	<u>25nD</u>
Tetra(trimethylsilylmethyl)tin	140°C	1.4825
Tetra(trimethylsilylpropyl)tin	205°C	1.4694
Dibutyl-di(trimethylsilylpropyl)tin	160°C	1.4674

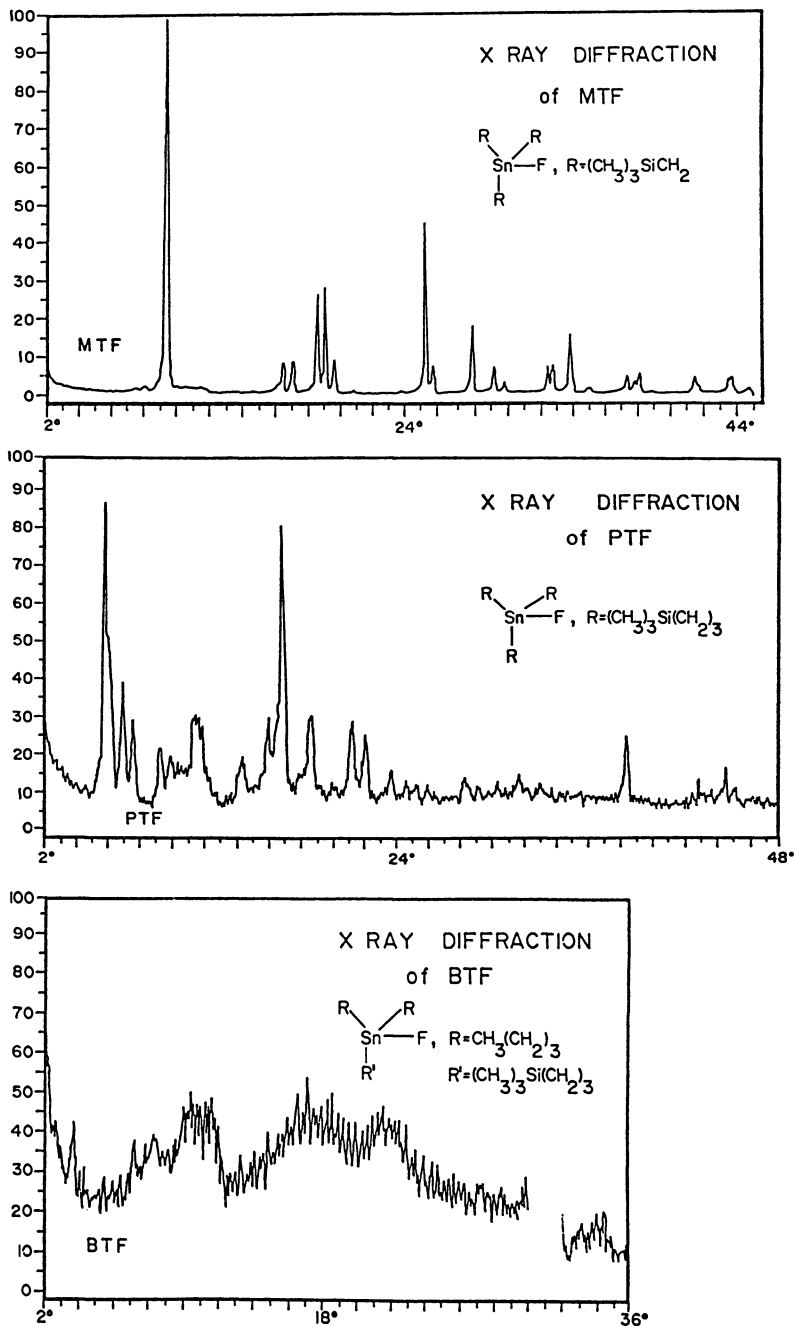


Figure 2. X-ray diffraction of silicon-containing triorganotin fluorides.

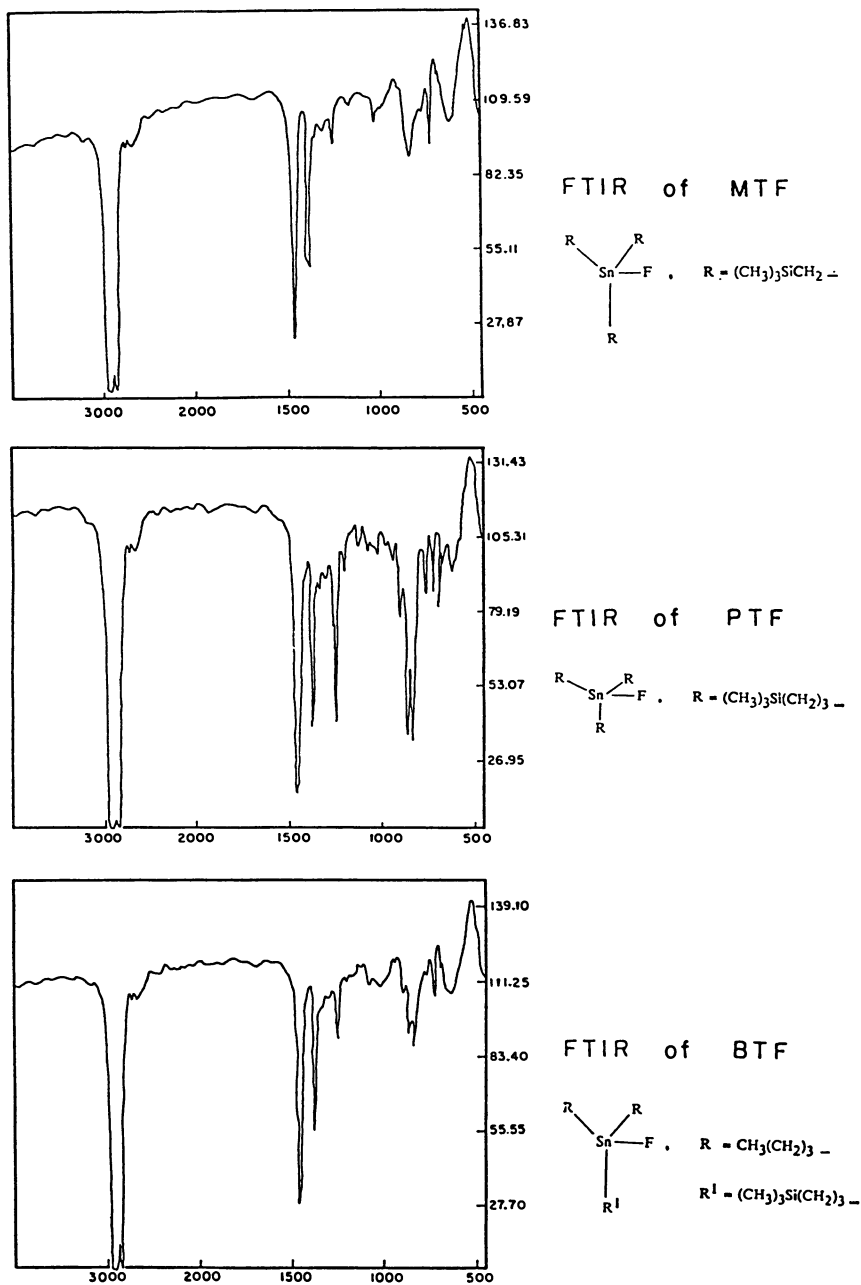


Figure 3. FTIR of silicon-containing triorganotin fluorides.

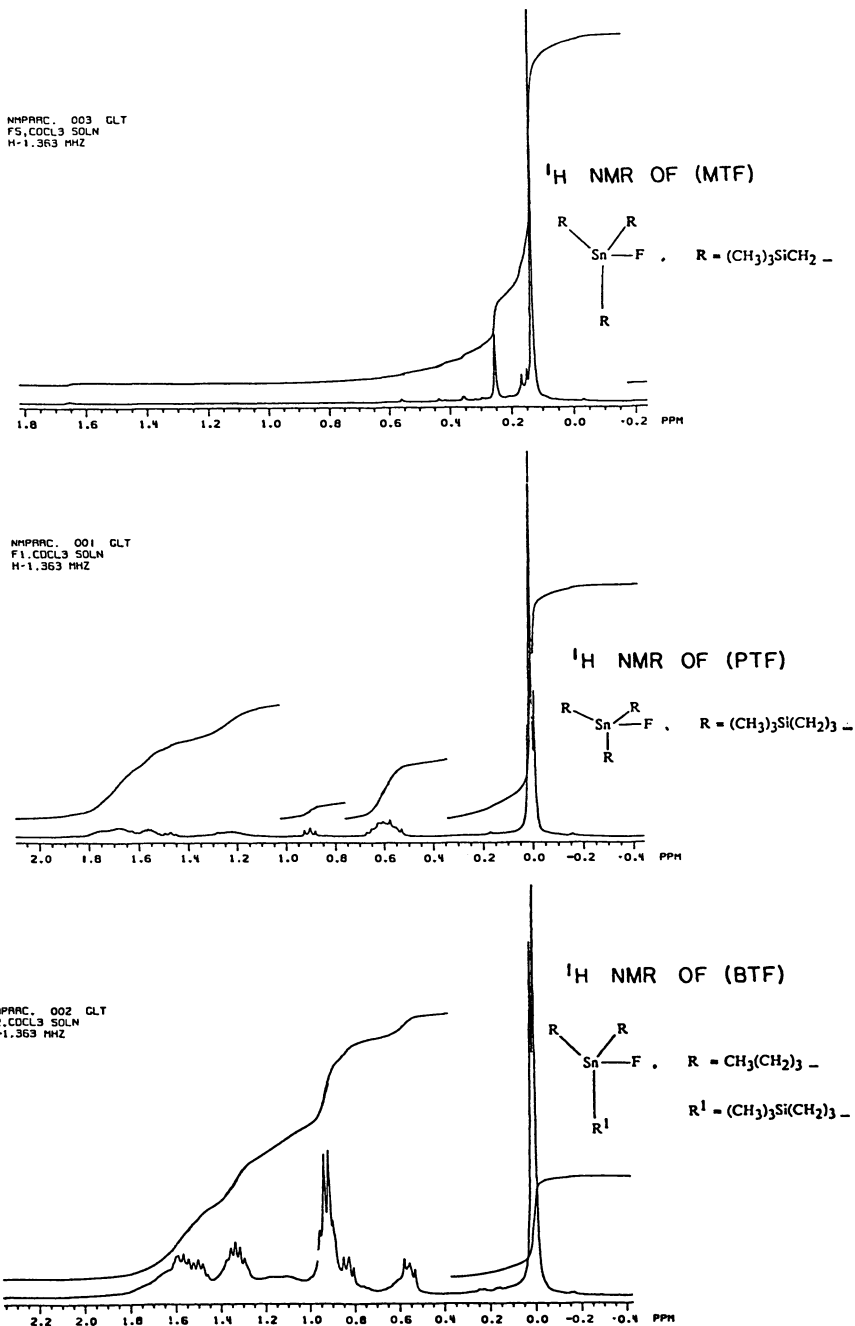


Figure 4. ¹H NMR of silicon-containing triorganotin fluorides.

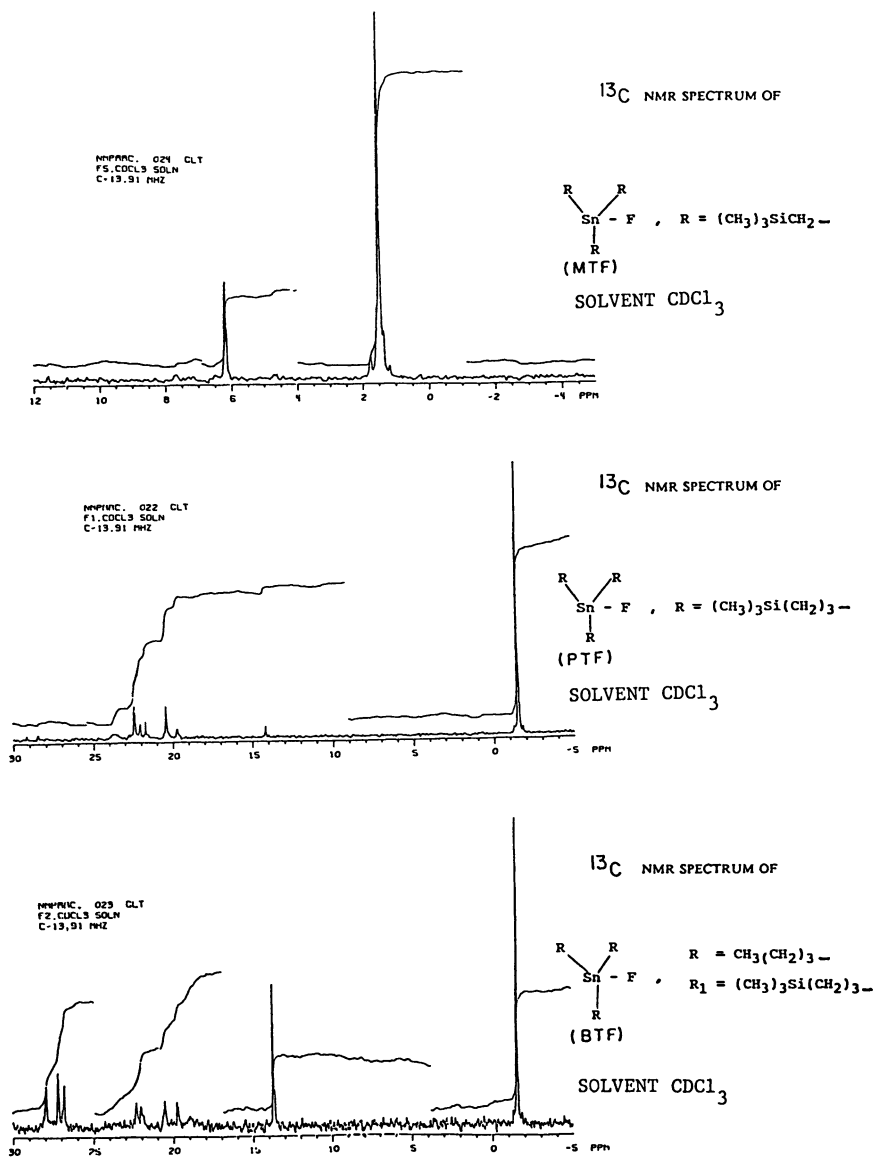


Figure 5. ¹³C NMR of silicon-containing triorganotin fluorides.

Table II. Proton NMR, Chemical Shifts in CDCl_3 , δppm

MTF	.190 (CH_3) ₃ Si		.25 -CH ₂ (Near Sn)		
PTF	.013 (CH_3) ₃ SiCH ₂ -		.6 -CH ₂ (Near Sn)		1.6 -CH ₂
BTF	.504 (CH_3) ₃ SiCH ₂ -	.549/.822 CH ₃ -	.909 (CH ₂ -Sn)	1.329 -CH ₂ -	1.514 -CH ₂ -

Table III. ^{13}C NMR, Chemical Shifts, δppm

MTF	1.441 (CH_3) ₃ Si-		6.159 -CH ₂ (Near Sn)		
PTF	-1.559 (CH_3) ₃ Si-		20.00 -CH ₂ (Near Sn)		22.205 -CH ₂ -
BTF	-1.809 (CH_3) ₃ Si	13.880 -CH ₃	19.80 (-CH ₂ -) (Near Sn)	22.00 C ₂ -H ₅	27.157 -CH ₂ -

Table IV. Calculated and Observed Ratios of Protons
MTF, PTF, and BTF

	$(\text{CH}_3)_3\text{Si CH}_2/\text{CH}_2$		$(\text{CH}_3)_3\text{Si CH}_2/\text{CH}_3$	
	<u>Observed</u>	<u>Calculated</u>	<u>Observed</u>	<u>Calculated</u>
MTF	5.71	5.501		
PTF	4.7 4.7	5.5 5.5		
BTF	5.5, 2.85 2.85	5.5, 3.3	4.46	4.00

the Sn-F bond, imparts higher solubility as well as higher dissolution rates to triorganotin fluorides.

Viscosity Behavior. The polymeric nature of triorganotin fluorides dissolved in nonpolar solvents is outlined in the introduction. As a result of the transient polymer formation, these solutions exhibit nonlinear concentration vs. viscosity curves. The concentration at which a steep rise in this curve begins has been termed as the critical or threshold concentration (2,3). Figure 6 shows such typical curves for PTF and BTF in n-hexane. Despite the fact that different shear rates are involved in capillary viscometry, it can be qualitatively said that at a given concentration, PTF viscosified n-hexane better than BTF. It is clear from Figure 6 that the critical concentration for these two compounds is above 0.7%, while analogous tri-n-alkyltin fluorides showed a critical concentration of less than 0.4% (3). This may be due to the presence of bulky Me_3Si -groups nearer to the Sn-F bond, which causes some steric hindrance to auto-association.

These results suggest that the solubility of trialkyltin fluoride in nonpolar solvents is considerably increased by the introduction of a trimethylsilyl group at the end of the chain but very much so at the expense of decreasing their ability to viscosify these solvents.

Figure 7 shows the viscosity vs. concentration curves for PTF in various organic solvents. As would be expected, in toluene, the most polar among the four solvents, the viscosity was the lowest at any given concentration. Figure 8 shows the effect of concentration on the viscosity of CO_2 at 25°C. The observed 50% increase in viscosity is not sufficient for enhanced oil recovery operations.

The viscosity vs. shear rate data for PTF and BTF (Figure 9) were obtained in n-heptane solution at 25°C using a Contraves low shear rate instrument. n-Heptane was used as a nonpolar solvent, as it has a high enough boiling point to avoid losses due to evaporation during the measurement period. The curves presented here are reproducible in both directions of shear and are thus time-independent.

In conclusion, synthesis of novel silicon-containing triorganotin fluorides was accomplished. It was shown that the introduction of a trimethylsilyl group on the alkyl chain considerably enhances the solubility of trialkyltin fluorides. However, if the bulky trimethylsilyl group is closer to the Sn-F bond, the effectiveness of such compounds in enhancing solvent viscosity is adversely affected. Higher solubilities in CO_2 were achieved but the viscosification of CO_2 at the highest solubility (0.4%) was only 50%. Additional viscosity measurements are to be made of the other two compounds described above. Further modifications in the molecular structure of these compounds might also increase both their solubility and the viscosity of their CO_2 solutions.

Table V. Calculated and Observed Ratios of Carbon Atoms in MTF, PTF, and BTF

	$(\text{CH}_3)_3\text{Si CH}_2/\text{CH}_2$		$(\text{CH}_3)_3\text{Si CH}_2/\text{CH}_3$	
	<u>Observed</u>	<u>Calculated</u>	<u>Observed</u>	<u>Calculated</u>
MTF	4.4	4.5		
PTF	4.6 4.00	4.00 5.5		
BTF	1.11 2.85	1.00	2.05	2.00

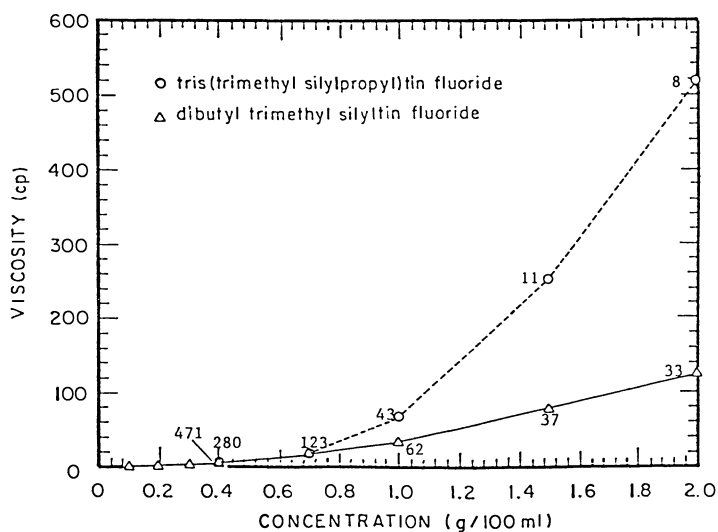


Figure 6. Viscosity as a function of concentration for PTF and BTF. Solvent n-hexane temperature 25°C. Number near each point indicates approximate shear rate at the wall.

Table VI

Solubilities of Silicon Containing Triorganotin Fluorides at 25°C

Solvent	Solvent Solubility Parameter (cal/cm ³)	Dipole Moment D [†]	Dielectric Constant (ε) [†]	Solvent ^{††} Viscosity CP	MTF*	PTF*	BTF*
carbon dioxide**	6.0	0	1.60	0.07		4.46 [■]	4.14 [■]
ethane**	6.0	0		0.16			
propane**	6.4	0.084	1.61	0.22 (25°C)			
butane	6.8	0.05		0.27	0	X [†]	X [†]
pentane	7.0	0	1.84	0.4	0	X [†]	X [†]
hexane	7.3	0.08	1.89 (25°C)	0.4	X	X [†]	X [†]
heptane	7.4	0	1.92 (20°C)	0.6	0	X [†]	X [†]
decane	8.0	0	1.99	1.26			
cyclohexane	8.2	0	2.02	1.3 (17°C)	X		
carbon tetra-chloride	8.6	0	2.24	0.5	X	X [†]	X [†]
toluene	8.9	0.36	2.38	0.6 (30°C)	X [†]	X [†]	X [†]
benzene	9.2	0	2.275	0.7	X	X [†]	X [†]
chloroform	9.3	1.0	4.80	0.3	X	X [†]	X [†]

†Reference 3

††Reference 4

■ In g/l

0 - insoluble

X - solubility at least 0.2 g/dl

X[†] - solubility >> 0.4%

* As in Table I

**Conditions used for solubility determinations

Pressure PSI

Temp. °C

CO₂: 2500

ethane: 1200

propane: 1200

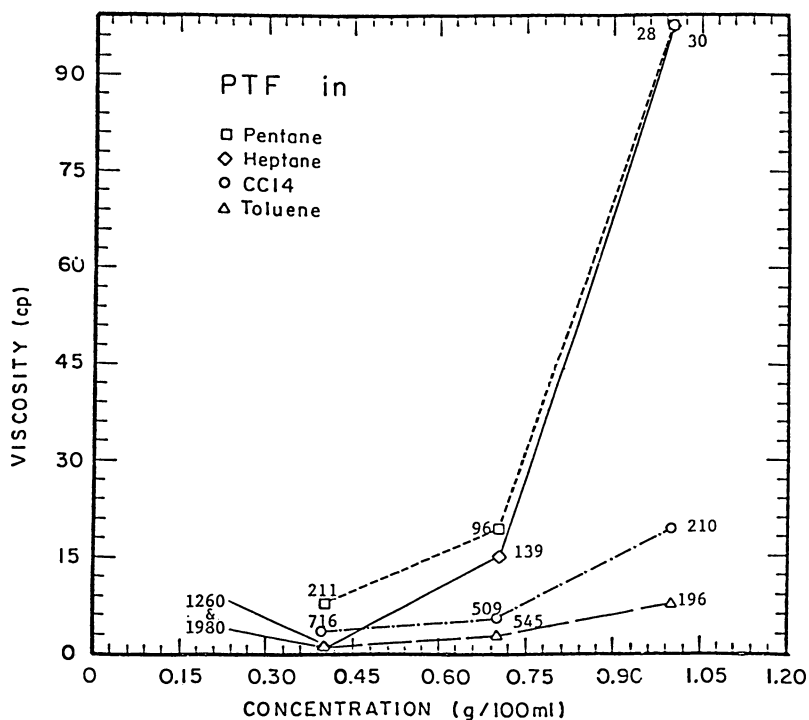


Figure 7. Viscosity vs. concentration curves for PTF in various solvents at 25°C. The number near each point indicates approximate shear rate at the wall.

Publication Date: July 10, 1989 | doi: 10.1021/bk-1989-0396.ch029

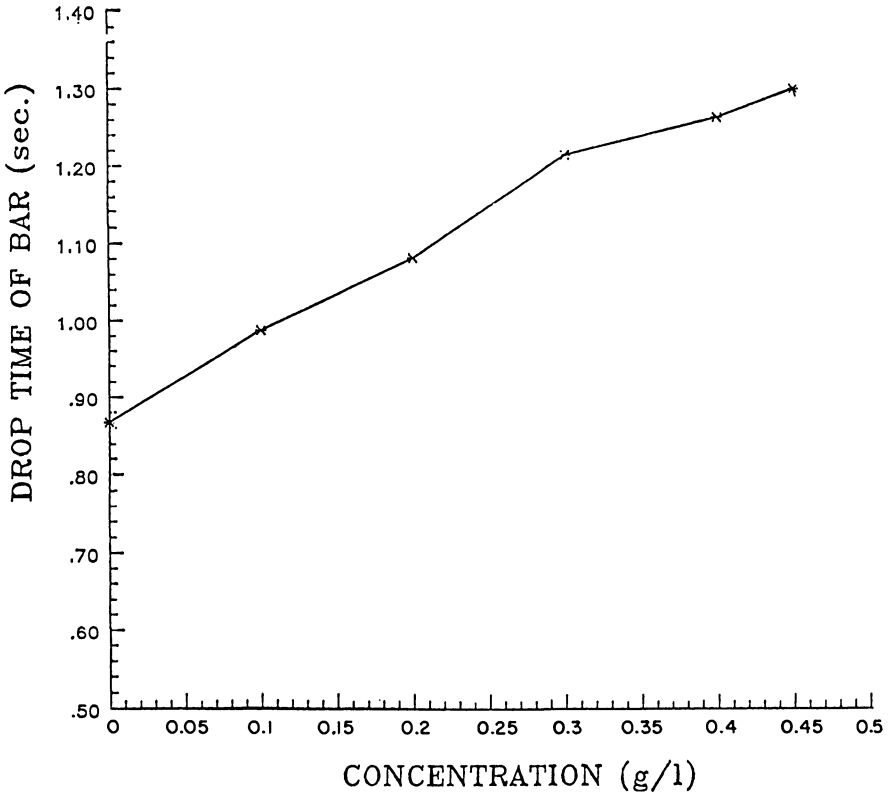


Figure 8. Viscosity of PTF in carbon dioxide.

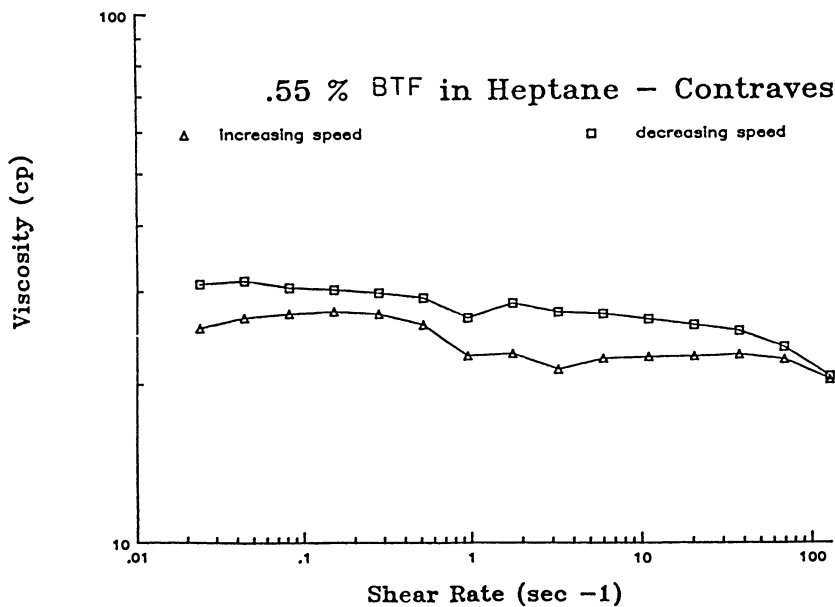
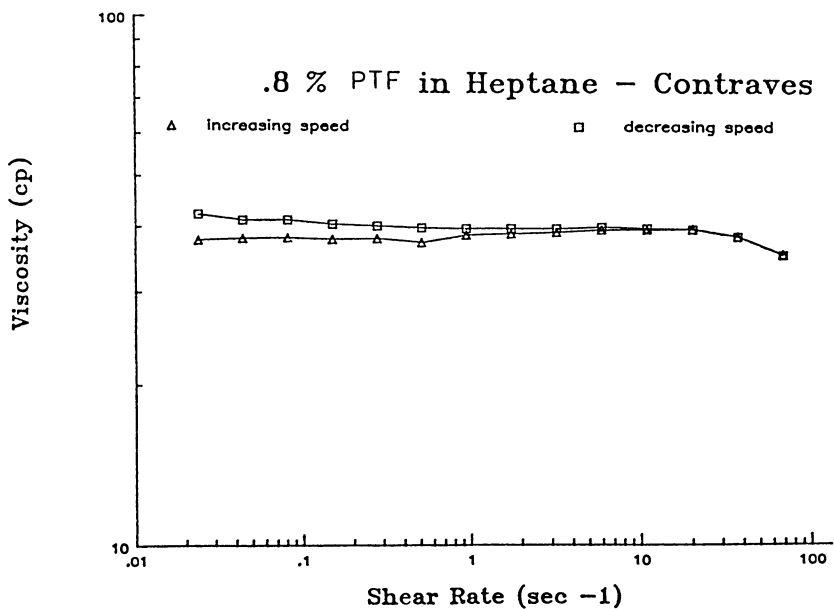


Figure 9. Shear rate vs. viscosity curve for PTF and BTF.

References

1. Dunn, P. and Oldfield, D.J.; Macromol. Sci. Chem., A4, 1157 (1970).
2. Dandge, D.K., Taylor, C. and Heller, J.P., Wilson, K.V., and Brumley, N.: Submitted to J. Polym. Sci.-Chem. (1987).
3. Taylor C., M.S. Thesis, Dept. of Chem., New Mexico Institute of Mining and Technology, Socorro, NM 87801.
4. Reichle, W.T.; J. Inorg. Chem., 5(1), 88 (1966.)
5. Heller, J.P. and Dandge, D.K., U.S. Patent 4,607,696.
6. Heller, J.P., Dandge, D.K., Card, R. and Donamura, L.G, Soc. Petr. Engr. J., 679 (1985).
7. Kruglaya, O.A., Kalima, G.S., Petrov, B.I., and Vyazankin, N.S.; J. Organomet. Chem.,46, 51 (1972).
8. Seyferth, D.J.; J. Am. Chem. Soc., 5881 (1957).

RECEIVED November 28, 1988

Chapter 30

Hydrodynamic Forces Necessary To Release Non-Brownian Particles Attached to a Surface

Habib Chamoun, Robert S. Schechter, and Mukul M. Sharma

Department of Chemical and Petroleum Engineering, The University of Texas at Austin, Austin, TX 78712

The release of non-Brownian particles (diameter $\geq 5 \mu\text{m}$) from surfaces has been studied. The influence of several variables such as flow rate, particle size and material, surface roughness, electrolyte composition, and particle surface charge has been considered. Experiments have been performed in a physically and chemically well-characterized system in which it has been observed that for certain particle sizes there exists a critical flow rate at which the particles are released from surfaces. This critical flow rate has been found to be a function of the particle size and composition. In addition, it has been determined that the solution pH and ionic strength has an effect on the release velocity. These observations imply that both fluid-mechanical effects and surface-force effects control the particle release.

A number of important processes depend on the permanence of particle attachment to surfaces by Van der Waal forces in the presence of flowing fluids. These include enzyme fixation, particle filtration, oil production, nuclear reaction excursions, migration of surface contaminants, etc. The release of particles attached to a surface plays an important role in these processes.

For the purpose of this study, particles are classified as Brownian or non-Brownian, where Brownian particles are defined as those for which the diameter is less than five microns and non-Brownian are those with diameter greater than five microns. The major focus of this work is on the second category. The particle release process has been studied both theoretically and experimentally, and it is found that for non-Brownian particles the surface charge and the electrolyte composition of the flowing phase are less significant factors than the hydrodynamic effects. However, Van der Waals forces are found to be important and the distortion of particles by these forces is shown to be crucial.

In this investigation we experimentally determine the factors controlling the release of non-Brownian particles. Also, we discover the initial particle release mechanism. (i.e., rolling-vs-sliding).

Literature Survey

The problem of detachment of particles under the action of a water stream has also been considered by Visser (1). He mentioned that a tangential force, F_t , due to the fluid drag, contributes to the dislodging force acting on the particle; however, he remarked that the lift force contributes negligibly to the dislodging force. The tangential force on a spherical particle of radius R in contact with a plane wall in a slow linear shear flow has been calculated theoretically by Goldman, Cox, and Brenner (2) and O'Neill (3). The tangential force that they obtained is given by the following equation:

$$F_H = 1.7005(6\pi)\eta R V_{X=R} \quad (1)$$

where R is the particle radius, η is the fluid viscosity, and $V_{X=R}$ is the fluid velocity at $r = R$.

Visser uses the preceding equation for the tangential force, and makes the additional assumption of laminar flow near the wall to arrive at the following equation:

$$F_H = 32 R^2 \tau_0 \quad (2)$$

where R is the particle radius.

That is, the removal of spherical particles from a flat surface is determined by the magnitude of the wall shear stress, τ_0 . Visser (1) also claims that since the removal mechanism is unknown, it is not possible to relate the F_H (tangential force) to the F_a (adhesive force) on theoretical grounds. Therefore, he assumes that the tangential force required for particle release is proportional to the adhesive force.

$$F_H = \alpha F_a \quad (3)$$

where F_a is the force of adhesion and α is the proportionality constant. This constant of proportionality has been determined experimentally for different systems. For example, Visser (1) found a value of 1 for α on the removal of 0.21 μ carbon-black colloidal particles from a cellophane surface. Zimon (4) experimentally found a value for α of 0.65 on the removal of submicron glass particles from a flat surface by a water stream.

For non-Brownian particles it is believed that the particle may come off by a rolling, rather than by a lifting, mechanism. Polke (5) and St. John (6) compared the normal and parallel direction forces necessary to remove gold particles from a gold surface in vacuo. They found that removing a particle by rolling requires a tangential force 10 to 50 times smaller than removal caused by a normal acting force. A general overview of the non-Brownian particle release is given by Hubb (7). He

developed a theoretical model for the detachment of colloidal particles from surfaces. The final product of his analysis gives a relationship between particle radius, R , and shear stress at the wall, τ_0 . This is done for different modes of incipient motion, in particular, sliding, rolling, and lifting. The case of rolling motion is presented in this paper. In order to analyze this case, a torque balance is performed between the hydrodynamic torque and the product LF_A , where L is a characteristic length and F_A is the net force of attraction acting through the particle center (see Figure 1). The characteristic length is a function of the particle material and particle size. Hubb considered the two cases: (1) surfaces with a high elastic modulus and (2) surfaces with a low elastic modulus. In this chapter we discuss only the latter one for which the characteristic length, L , is related to the contact area of deformation strictly due to attractive forces [Krupp (8), Muller et al. (9), and Johnson et al. (10)]. From the torque balance, considering that L is proportional to $R^{2/3}$ from the elasticity theory (see Hubb (7)), the following equation is found:

$$\tau_0(\text{rolling}) = \alpha R^{-2/3} \quad (4)$$

The above presentation due to Hubb (7) is a good initial approach which gives one physical insight into the problem, but a more detailed presentation for the release of elastic particles from rigid surfaces (specifically, cylindrical particles) may be found in Chamoun (11). In addition, extensive experimental data on the release of particles from various surfaces is reported by this author. An analysis of this experimental data is presented in Shirzadi et al. (12).

A summary of the most important experimental findings of Chamoun (11), along with a description of the experimental apparatus and procedure, is presented in this chapter. In particular, the experiments have shown which factors (such as pH, ionic strength, etc.) control the release of non-Brownian particles and also have proven that the initial particle release mechanism is rolling rather than sliding.

Experimental Methods

Two different types of studies have been carried out: flow experiments and centrifuge experiments.

Apparatus

Flow Experiments. The main components of the experimental apparatus are illustrated in Figure 2. The most important component is the glass flow cell, shown in detail in Figure 3.

The glass cell consists of a microscope slide overlying a flat glass plate, being held together with epoxy and separated by a paper gasket. The cell dimensions are 1-1/2 inches in width and 3 inches in length, with a spacing of $200 \pm 10 \mu\text{m}$ between the microscope slide and the glass surface.

A flow system has been designed to pump fluid through the flow cell. A piston-cylinder arrangement is used as a "pump-like" device by

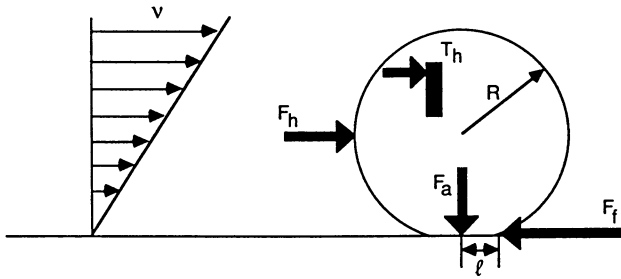
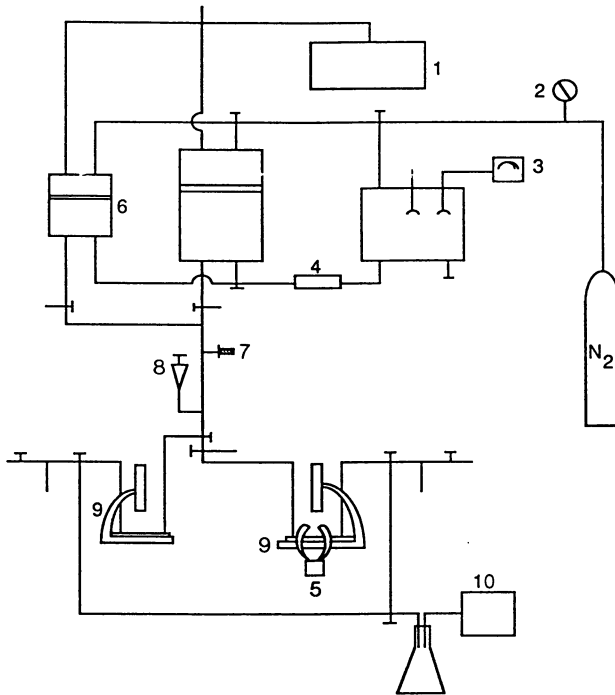


Figure 1. Torque balance.



- | | |
|----------------------------|-----------------------------|
| 1. Fluid Reservoir | 6. Cylinder Pump N2/H2O |
| 2. Pressure Gauge | 7. Flow Rate Vernier |
| 3. PH Meter | 8. Particle Syringe |
| 4. Pump | 9. Microscopes / Flow Cells |
| 5. Fiber Optic Illuminator | 10. Vacuum pump |

Figure 2. Experimental apparatus.

the application of pressurized nitrogen on one side of the piston; and the flow rate of fluid is controlled by a vernier located on the other side of the piston. Other elements of the apparatus are two microscopes and a fiber-optic illuminator. These are integrated within the flow system as illustrated in Figure 2. (Note that one microscope uses transmitted light while the other uses reflected light.)

Centrifuge Experiments. The design of the centrifuge cell is virtually identical to that of the flow cell. However, the experimental procedures are different and will be explained in the procedure section of this paper.

Materials

The effect of particle size was investigated by using different sizes of microspheres. Two types of particles and several different fluid media were used on the glass surface. The particles examined were charged polystyrene spheres and glass microspheres. (All the particles used are available from Duke Scientific.) Three different sizes of polystyrene particles were used: 10, 20, and 40 μm with a standard deviation of ± 1 to 2% and a specific density of 1.05 g/cc. The glass microsphere sizes were 10, 15, and 30 μm with a $\pm 15\%$ standard deviation and a specific density of 2.5 g/cc. The surface charge on the particle was determined experimentally for different particles through the measurement of zeta potential as a function of pH.

Procedure

Flow Experiments. The flow cell was evacuated for two hours prior to each test. Then, after having filled the cylinder with fluid from the reservoir, the cylinder was pressurized with nitrogen to 40 psia., the flow rate vernier was opened, and the entire flow system was circulated with the desired solution. After the flow system had been completely flushed, particles of the desired size were injected with a syringe. The particles were allowed to settle for a specified length of time, typically 24 hours. At each flow rate, surface concentrations of particles were measured by point counting. The point counting of particles on the surface was accomplished with the help of a grid in the microscope eyepiece. The flow was increased incrementally until the maximum allowable flow rate of the flow cell was reached. This maximum flow rate was approximately 0.6 cc/sec which corresponds to an average velocity of 8 cm/sec or a Reynolds number of about 0.8 (based on particle diameter).

Centrifuge Experiments. The particles to be studied were deposited in the cell by syringe injection. The cell was then sealed by capping the fittings and the particles were allowed to settle for the same length of time attained in the flow cell. A specific area of the cell to be studied was chosen and marked. The number of particles in this area was counted using a microscope. The cell was then placed in the centrifuge rotor perpendicular to the rotational axis (Figure 4) and spun at a constant RPM for a specified length of time, usually two to three minutes. The cell was

then carefully removed from the centrifuge and the particles in the selected area were again counted. The same procedure was repeated once more at a higher RPM.

Experimental Results

Flow Experiments. A "critical velocity," v_c , is defined as that velocity at which a "measurable" release of particles is observed; above this critical velocity, release of particles is continuous. Specifically, it is taken to be the velocity at which 10% of the particles have been released. Based on this definition, v_c is a function of particle size--the larger the particle, the smaller is v_c (Figure 5).

As mentioned in the introduction, the particle composition has an effect on the release velocity. In particular, from Figure 6 it is clear that 10 μm glass particles release more easily than 10 μm polystyrene particles.

Solution pH and ionic strength also have an effect on the release velocity. Figure 7 demonstrates the moderate effect of solution pH on release velocity, with an increasing pH lowering the release velocity. Figure 8, on the other hand, shows that the effect of ionic strength is quite small, with a decreasing ionic strength causing only a marginal decrease in release velocity.

Centrifuge Experiments

For the same experimental conditions as described in the flow experiments, (i.e., 10 μm glass particles, pure water flowing solution) centrifuge tests yield a higher force to release particles. The torque required for particle release is the same in both experiments; hence, particle release in the flow cell is initiated by a rolling rather than sliding motion (Figure 9).

Discussion of Results

The DLVO theory, with the addition of hydration forces, may be used as a first approximation to explain the preceding experimental results. The potential energy of interaction between spherical particles and a plane surface may be plotted as a function of particle-surface separation distance. The total potential energy, V_t , includes contributions from Van der Waals energy of interaction, the Born repulsion, the electrostatic potential, and the hydration force potential. [Israelachvili (13)].

The Hamaker constants used in these calculations were obtained from values reported in the literature [Gregory (14)]. Zeta potentials were obtained both experimentally and from the literature [Huang and Stumm (15) and Sharma (16)].

Experimentally derived potential energy curves are shown in Figures 10 and 11. (Note that only one particle size is illustrated, namely, 10 μm .) The shape of these potential energy curves as a function of ionic strength, solution pH, particle and surface composition, etc. may be used to explain the effect of some of these variables on particle capture and

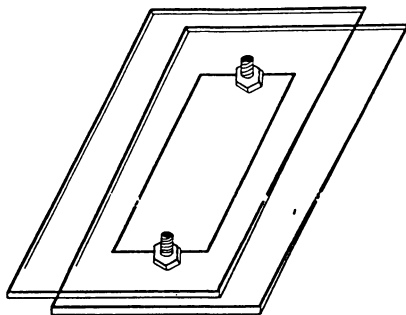


Figure 3. Glass flow cell.

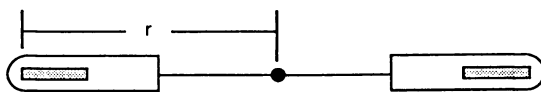


Figure 4. Centrifuge illustration.

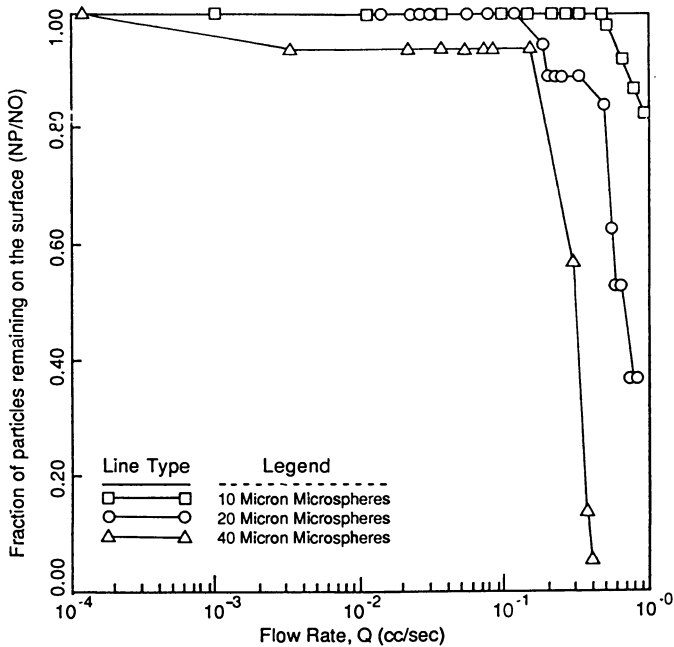


Figure 5. Effect of particle size on the release of polystyrene particles from a glass surface.

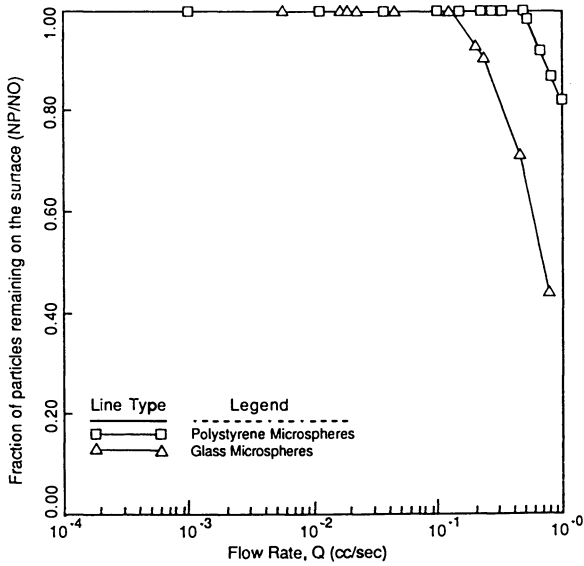


Figure 6. Effect of particle composition on the release phenomena.

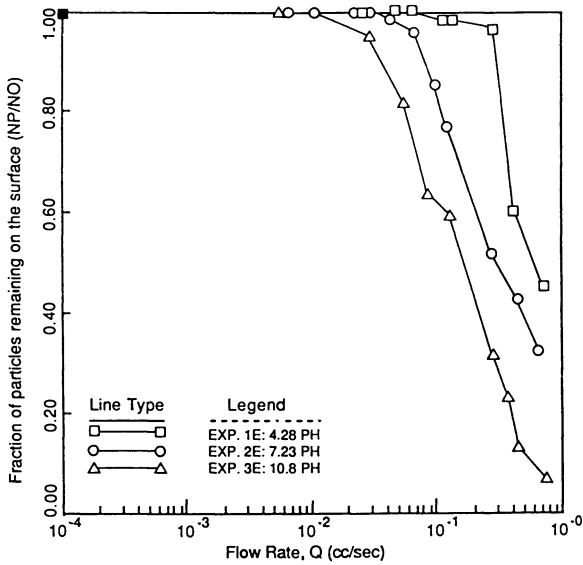


Figure 7. Effect of solution pH on the release of 10 μm glass microspheres from a glass surface.

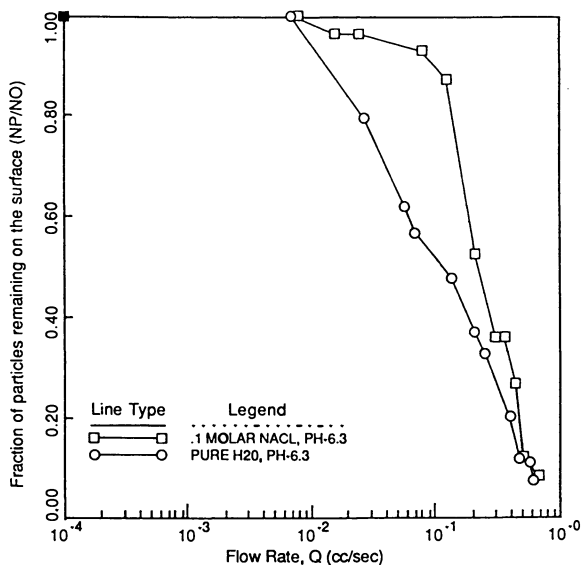


Figure 8. Effect of ionic strength on the release of 10 μm glass particles from a glass surface.

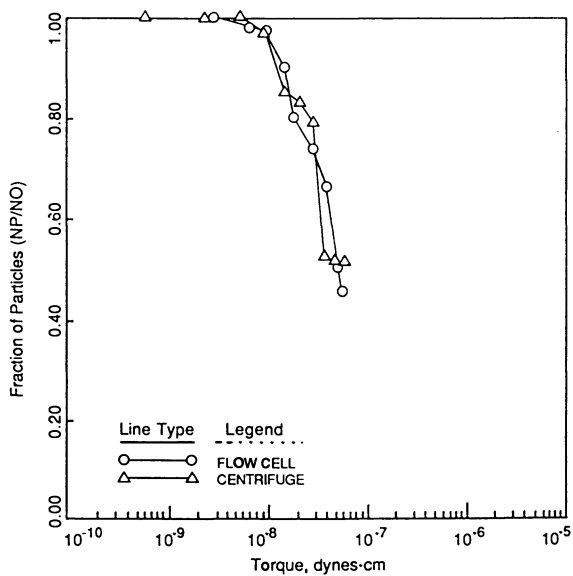


Figure 9. Comparison of the release of 10 μm glass microspheres from a glass surface between a flow cell experiment and a centrifuge experiment.

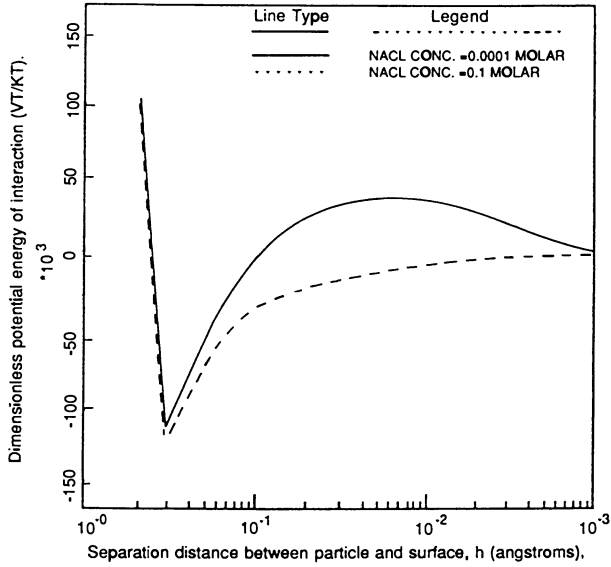


Figure 10. Potential energy of 10 μm glass particles as a function of ionic concentration, solution pH = 6.

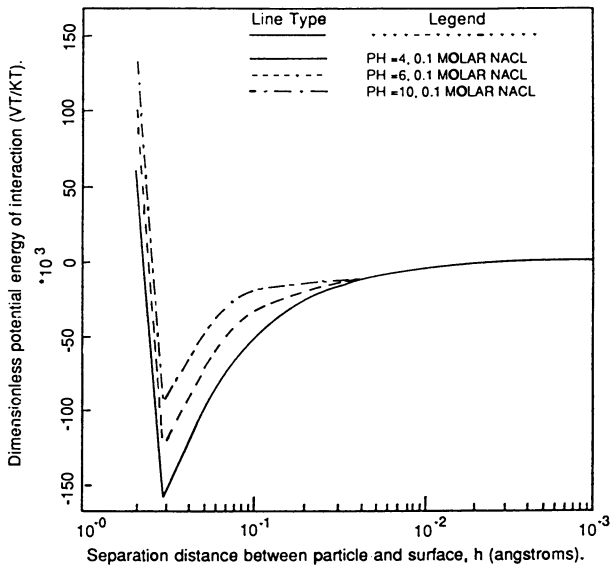


Figure 11. Effect of the solution pH on the potential energy of 10 μm glass particles interacting with glass surfaces.

release. For example, it is clear that both decreasing ionic strength and increasing pH decrease the depth of the attractive energy trough at about 3 Å. Also, a repulsive energy barrier is created at 50 Å by decreasing the solution salinity. The height of this barrier is about 24×10^3 kT. In order to see how the DLVO theory can explain these experimental results, consider the effect of pH. In the experiments an increasing pH results in the release of more particles at a given velocity. From the DLVO theory the attractive trough depth becomes smaller in this situation. This is because both the particle and the surface become more negatively charged as pH increases. As a result, a smaller hydrodynamic force is required for particle release. The relationship between potential energy and release velocity is similar for the other important variable, ionic strength, and for this variable the experiments are also consistent with the theory. On the other hand, the effects of particle composition and size are not consistent with the above theoretical predictions but can be explained using the aforementioned torque balance model [Chamoun (11)].

Conclusions

- (1) A critical flow rate or velocity for release of particles has been observed.
- (2) The critical velocity depends on particle radius, particle composition fluid medium, and fluid conditions such as solution pH and ionic strength.
- (3) Increasing the particle radius decreases the critical velocity required to remove it from any surface studied.
- (4) Increasing solution pH and decreasing the ionic strength decreases the critical velocity for all cases examined.
- (5) The effect of surface roughness has not yet been studied, but in all experiments the surface roughness was small on the scale of particle sizes used.
- (6) Centrifuge experiments show that the particle release mode is rolling rather than sliding.
- (7) The DLVO theory provides a qualitative explanation of the ionic strength and solution pH effects on particle release.
- (8) The effect of particle size and composition on the release problem is explained by the use of a torque-balance [Chamoun (11)].

Literature Cited

1. Visser, J. Surface and Colloid Science; Matijeric, E., Ed.; John Wiley: New York, 1976; Vol. 8.
2. Goldman, A. J.; Cox, R. G.; Brenner, H. Chem. Eng. Sci. 1968, 23, 1293.
3. O'Neill, M. E. Chem. Eng. Sci. 1968, 23, 1293.
4. Zimon, A. D. Adhesion of Dust and Powders; Consultants Bureau: New York, 2nd Edition, 1982.
5. Polke, R. Bull. Soc. Chim. Fr. 1970, 3241.
6. St. John, D. F.; Montgomery, D. J. J. Appl. Phys. 1971, 663.
7. Hubb, M. A. Colloid Surfaces 1984, 12, 151.

8. Krupp, H. Adv. Colloid Interface Sci. 1967, 1, 111.
9. Muller, V. M.; Yushchenko, V. S.; Deryagin, B. V. J. Colloid Interface Sci. 1983, 92, 92.
10. Johnson, K. L.; Kendall, K.; Roberts, A. D. Proc. R. Soc. Lond. 1971, A324, 301.
11. Chamoun, H. Ph.D. Dissertation (in progress), The University of Texas at Austin, Texas, 1988.
12. Shirzadi, S.; Sarkar, A.; Sharma, M. M. AIChE J. 1988.
13. Israelachvili, J. N. Adv. Colloid Interface Sci. 1982, 16, 31.
14. Gregory, J. Adv. Colloid Interface Sci. 1969, 2, 396.
15. Huang, C. P.; Stumm, W. J. J. Colloid Interface Sci. 1973, 43, 409.
16. Sharma, M. M. Ph.D. Dissertation, University of Southern California, Los Angeles, 1985.

RECEIVED September 26, 1988

Chapter 31

Formation Wettability Studies that Incorporate the Dynamic Wilhelmy Plate Technique

Dale Teeters,¹ Mark A. Andersen,² and David C. Thomas²

¹Chemistry Department, University of Tulsa, Tulsa, OK 74104

²Amoco Production Company, Tulsa, OK 74102

The dynamic Wilhelmy plate technique, a new method for characterizing oil reservoir wettability, gave quantitative values of wetting preference and comparisons of surface energy values related to wetting properties. Water-wetting and oil-wetting systems were distinguished readily, as were hybrid-wetting systems which have both types of wetting behaviors, and interfacial properties were quantified. Oxygen contamination caused inconsistent wetting behavior for some crude oil/brine/solid systems, but operating in a newly developed anaerobic vessel gave reproducible wetting behavior. The contact angle hysteresis of dolomite, marble, glass and polytetrafluoroethylene in a series of solvents gave a qualitative evaluation of surface energies. Dolomite and marble had similar surface energies which correlated to the wetting behavior for these solids obtained with the dynamic Wilhelmy plate technique. Other advantages of the Wilhelmy technique in studying reservoir wettability are discussed.

The preferential wetting characteristics of crude oil/water/rock systems play an important role in characterizing oil reservoirs. Formation wetting preference affects the success of most conventional and enhanced recovery methods. Waterflood performance depends on the amount of imbibition which can be expected of a reservoir and the selection of enhanced oil recovery methods are affected by the formation wettability. Matching and predicting performance successfully depends on the ability to determine the degree of wetting preference of the formation. The relative permeability, capillary pressure, electrical response, and occasionally the rock mechanical response all depend on the position of the fluids in the pores. The importance of these aspects of formation wettability has been covered in a series of thorough review papers by Anderson (1-6).

Contact angle measurement is one method of obtaining quantitative wettability values and is usually done in the petroleum industry by the sessile drop method (7-10) or a modification of this technique (11, 12). The contact angle is measured at the edge of a drop of crude oil placed between parallel crystals in a brine bath. One crystal is displaced, creating a new contact angle when the water advances over a portion of the crystal formerly covered by oil, and another new angle on the other side of the drop when the oil advances over a portion of the crystal formerly covered by water. The displacement is repeated until the equilibrium contact angle has been reached.

The sessile drop method has several drawbacks. Several days elapse between each displacement, and total test times exceeding one month are not uncommon. It can be difficult to determine that the interface has actually advanced across the face of the crystal. Displacement frequency and distance are variable and dependent upon the operator. Tests are conducted on pure mineral surfaces, usually quartz, which does not adequately model the heterogeneous rock surfaces in reservoirs. There is a need for a simple technique that gives reproducible data and can be used to characterize various mineral surfaces. The dynamic Wilhelmy plate technique has such a potential. This paper discusses the dynamic Wilhelmy plate apparatus used to study wetting properties of liquid/liquid/solid systems important to the oil industry.

The Dynamic Wilhelmy Plate Method

The Wilhelmy hanging plate method (13) has been used for many years to measure interfacial and surface tensions, but with the advent of computer data collection and computer control of dynamic test conditions, its utility has been greatly increased. The dynamic version of the Wilhelmy plate device, in which the liquid phases are in motion relative to a solid phase, has been used in several surface chemistry studies not directly related to the oil industry (14-16). Fleureau and Dupeyrat (17) have used this technique to study the effects of an electric field on the formation of surfactants at oil/water/rock interfaces. The work presented here is concerned with reservoir wettability.

Figure 1 is a schematic of the apparatus used in our studies. A Cahn Model 29 microbalance and a stepper motor were interfaced to an IBM PC/XT through an RS-232 interface and an IEEE488 general purpose interface bus (GPIB), respectively. The microbalance rested on top of a housing containing a flat platform on a vertical stage moved by the stepper motor. The vessel holding the liquids rested on the platform. The plate hanging from the balance was immersed in and removed from the liquids in a continuous motion so that immersion-emersion cycles or "wetting cycles" could be obtained. Clean surfaces on the plates were of the utmost importance for reproducible wetting cycles. The cleaning procedures for the plates used in this work and the preparation of the mineral plates from bulk samples have been described elsewhere (18). The initial plate position was typically 4 mm above the liquid/vapor interface. A wetting cycle run consisted of moving the liquid interface a certain distance up onto the plate and then the same distance down at a standard speed of 0.127 mm/sec. During this movement, 720 data values

were recorded by the microcomputer for total cycle distances of 50.4 mm and 360 values for cycles of 25.4 mm.

Figure 2 is a representation of the force balance on a Wilhelmy plate that has gone through one phase and has been wetted by a second phase. The three interfacial tensions are related to the contact angle (measured through phase 2) by the familiar Young equation

$$\gamma_{12} \cos \theta = \gamma_{S1} - \gamma_{S2} \quad (1)$$

where the subscripts 12, S1 and S2 represent the phase 1/phase 2, solid/phase 1 and solid/phase 2 interfaces, respectively.

In the experiment described above the force, F , on a plate in an air/liquid system which is partially submersed in the liquid is

$$F = p \gamma \cos \theta - B \quad (2)$$

where p is the perimeter of the plate, γ is the surface tension, θ is the contact angle and B the buoyant force on the portion of the plate below the general surface. When two liquids such as oil and water are involved, the force on a plate which has passed through the oil layer into the water layer is given by

$$F = p \gamma_{AO} \cos \theta_{AO} - B_O + p \gamma_{OW} \cos \theta_{OW} - B_W \quad (3)$$

where AO and OW indicate the air/oil and oil/water interface respectively, B_O is the buoyant force caused by the oil and B_W that caused by the water layer.

The hexadecane/water/glass system was used as an initial model for crude oil/brine systems. Characterization of wetting behavior of this system from the dynamic Wilhelmy plate data shown in Figure 3 is interpreted by using Equation 3. The mass read by the balance was converted to a tension by multiplying by the gravitational acceleration, g , and dividing by the plate perimeter, p . As the plate was immersed, the tension increased when the solid surface was wetted by the hexadecane ($\gamma_{AO} \cos \theta_{AO} < 90^\circ$ in Equation 3). Further immersion of the plate into the hexadecane resulted in a slight decrease in the tension because of the buoyant force. Another increase in tension was observed at the hexadecane/water interface since the water wetted the glass surface in preference to hexadecane and the advancing contact angle as measured through the aqueous layer was again less than 90° . The buoyant force of the water caused the measured tension to slightly decrease as the slide went further into the water layer. The direction of motion was reversed for the emersion half of the cycle and the contact angles in Equation 3 changed from advancing to receding angles. The difference between these two angles caused the hysteresis observed in the wetting cycle shown in Figure 3. The hexadecane/water/glass system is a typical example of water-wetting behavior.

Oil-wetting systems can be modeled by replacing the glass plate with a plate of polytetrafluoroethylene (PTFE), as shown in the hexadecane/water/PTFE system in Figure 4. At the hexadecane/water interface the water phase did not wet the PTFE surface, the contact angle was thus greater than 90° and the tension decreased. The peak

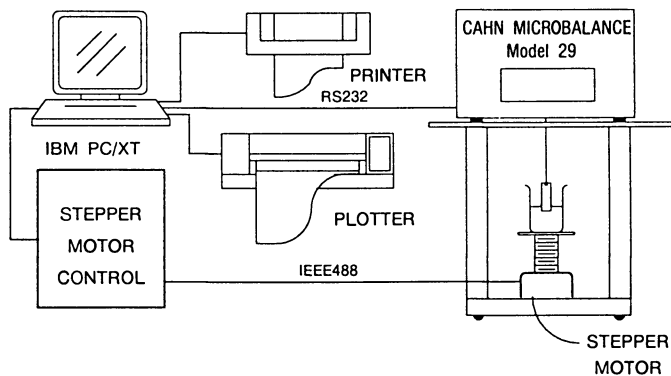


Figure 1. Schematic diagram of the dynamic Wilhelmy Plate Apparatus.

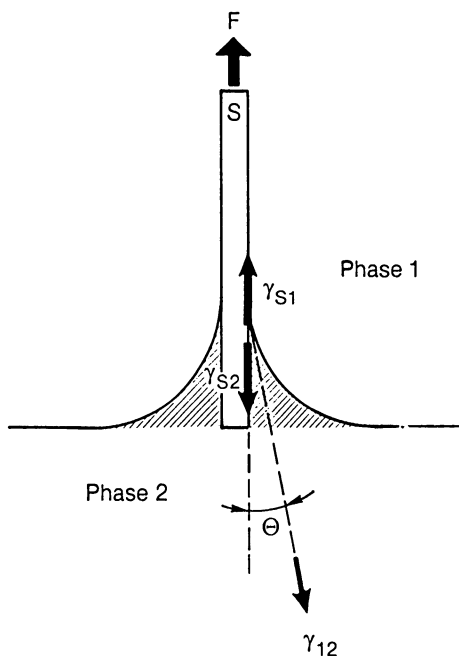


Figure 2. Forces on a thin plate with a meniscus. The surface tensions are γ_{S1} and γ_{S2} for the solid against fluids 1 and 2, respectively, and γ_{12} for the interfacial tension between the liquids at contact angle θ . The force on the plate F is measured by a microbalance.

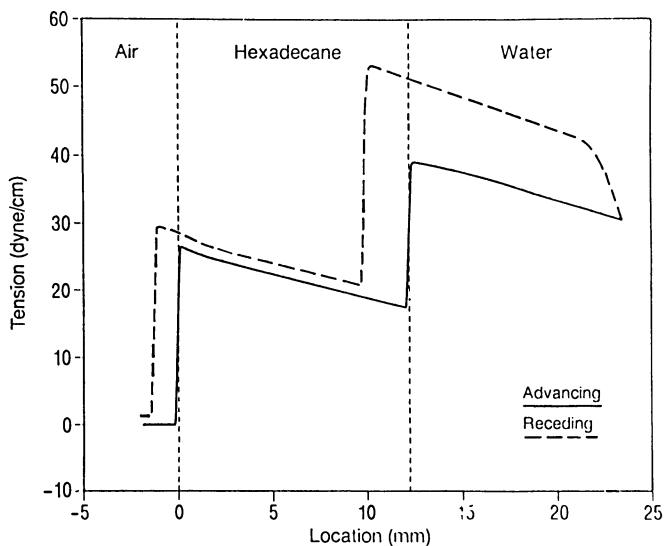


Figure 3. Hexadecane/water/glass wetting cycle exhibiting water-wetting behavior. (Reproduced with permission from Teeters, D.; Wilson, J. F.; Andersen, M. A.; Thomas, D. C. *J. Colloid Interface Sci.*, 1988, 126 in press. Copyright 1988 Academic Press.)

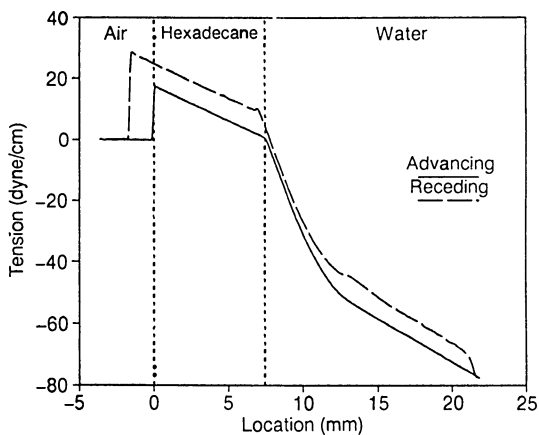


Figure 4. Hexadecane/water/PTFE wetting cycle showing oil-wetting behavior.

observed at the hexadecane/water interface on emersion was typical of other oil-wetting systems and is believed to be caused by edge effects at the bottom of the plates.

Crude/brine systems have been known to have large amounts of hysteresis with advancing contact angles greater than 90° and receding angles less than 90° (8). This type of wetting behavior is shown in Figure 5 which is a hexadecane/water/glass system in which the hexadecane phase contains oleic acid (0.8 molar). When the plate was immersed, the water did not displace the hexadecane-oleic acid phase and the advancing contact angle was greater than 90° . When the direction of motion was reversed, the line of hexadecane/water contact on the plate was pinned and the magnitude of the tension increased until a stable meniscus with receding contact angle less than 90° was formed. This wetting cycle demonstrated oil-wetting behavior on immersion and water-wetting on emersion and has been termed a hybrid-wetting cycle. The large hysteresis is most likely due to adsorption of oleic acid onto the glass surface during the immersion part of the cycle since Langmuir (19) has observed a marked difference between contact angles of an advancing and a receding water surface on glass covered by an oleic acid monolayer.

The computer interface system lends itself well to the determination of interfacial tension and contact angles using Equation 3 and the technique described by Pike and Thakkar for Wilhelmy plate type experiments (20). Contact angles for crude oil/brine systems using the dynamic Wilhelmy plate technique have been determined by this technique and all three of the wetting cycles described above have been observed in various crude oil/brine systems (21) (Teeters, D.; Wilson, J. F.; Andersen, M. A.; Thomas, D. C.; *J. Colloid Interface Sci.*, 1988, 126, in press). The dynamic Wilhelmy plate device also addresses other aspects of wetting behavior pertinent to petroleum reservoirs.

Advantages of Dynamic Crude Oil Wetting Measurements

The dynamic Wilhelmy plate technique directly measures the adhesion tension, which is the product of the interfacial tension (IFT) and the cosine of the contact angle, as illustrated in Equation 3. The degree of wetting of a system depends on the adhesion tension rather than the contact angle alone. As an example, consider the systems listed in Table I. Using Craig's criteria (22) the contact angles indicate that system A has intermediate wettability while system B is oil-wetting. The IFT of system A is higher than the IFT of system B, leading to a greater adhesion tension for the "intermediate" system than for the "oil-wetting" system. That is, the oil in the "intermediate" system A adheres more strongly to the solid surface than the "oil-wetting" system B.

The Leverett J-function is used in reservoir engineering (22) to relate the permeability k , porosity ϕ , and wetting characteristics to water saturation S_w

$$J(S_w) = \frac{P_c}{\gamma_{OW} \cos(\theta)} \sqrt{\frac{k}{\phi}} \quad (4)$$

TABLE I. EXAMPLE OF TWO WETTING SYSTEMS

	Interfacial Tension	Contact Angle	Adhesion Tension	Wetting Character
System A	39 dyne/cm	105°	-10.1 dyne/cm	"Intermediate"
System B	12 dyne/cm	130°	- 7.7 dyne/cm	"Oil-wetting"

where P is the capillary pressure. Other wetting effects, such as the pressure drop across a curved interface (Young-Laplace equation) and the height of capillary rise also depend on both the IFT and the contact angle (23). The adhesion tension should be used whenever wetting forces are being compared with any other forces - it is not sufficient to determine the contact angle alone. Since a dynamic Wilhelmy plate measurement yields the adhesion tension it is remarkably well suited to petroleum industry wettability studies.

Far from a wellbore, the velocity of reservoir fluids is about one linear foot per day. Near a wellbore, the velocity can increase one-hundred fold. A static or quasi-static test such as the sessile drop (contact angle) test may not represent the dynamic behavior of the fluids in the field. The dynamic Wilhelmy device gives results which are comparable in interface velocity to the field displacement rate. The interface in the Wilhelmy test described here moved at a steady rate of 0.127 mm/sec or 36 ft/day. The wetting cycle for a hybrid-wetting crude oil system was not affected by moving at a rate less than 1 ft/day.

Another measure of wetting character in the field is the dimensionless capillary number N_c , which is the ratio of viscous to capillary forces. One expression for this number is (24)

$$N_c = \frac{V \mu}{\gamma} \quad (5)$$

where V is the macroscopic velocity of the fluid and μ is the viscosity. Residual oil saturation, which is the oil left behind after a waterflood, is approximately constant for capillary numbers up to 1.0×10^{-3} , then begins to decrease (24). For a 2 centipoise oil with an interfacial tension of 31 dyne/cm flowing at 1 ft/day, $N_c = 2.27 \times 10^{-5}$, and at 100 ft/day, $N_c = 2.27 \times 10^{-3}$. For such an oil/brine system, the dynamic Wilhelmy device had an equivalent capillary number of 8.21×10^{-4} - in contrast, the sessile drop test is quasi-static.

Wetting preference affects the location of fluids flowing in porous media, influencing the behavior of waterfloods and other methods of improved oil recovery. In a waterflood, water displaces oil from the pore space. At the leading edge of the water bank, the capillary forces given by the water-advancing adhesion tension influence the displacement process. An oil bank can build in front of the water bank, so there can also be a water-receding zone ahead of the oil bank. Both the water-advancing and the water-receding wetting information needed to model this displacement behavior is provided by the dynamic Wilhelmy technique. Specifically, a water-

wetting system shows hysteresis in the oil relative permeability curve, but not in the water relative permeability curve. An oil-wetting system is the opposite.

All crude oil/brine/solid systems examined for this study exhibited wetting hysteresis. In some cases the difference between advancing and receding adhesion tensions was small. These cases correspond to the water-wetting or oil-wetting cases generally studied in the laboratory which display relative permeability hysteresis only in the non-wetting phase. In several cases studied with the dynamic Wilhelmy device, the wetting hysteresis was very large and the system was characterized as hybrid, similar in form to the hexadecane/water system with oleic acid. In such a system, the solid tends to hold whichever fluid is in contact with it in preference to the displacing fluid, regardless of which fluid is in contact with the solid. Although a systematic relative permeability study has not been conducted of such systems, it is likely a rock saturated with a crude oil/brine system which displays hybrid behavior would have a relative permeability hysteresis for both phases. These systems have been observed in relative permeability tests, but a connection with hybrid wettability has not been hypothesized before.

Crude Oil Wettability Results

Dynamic Wilhelmy wettability tests on single component systems, such as hexadecane/water/glass, can be done quickly in open beakers. Some crude oils contain components which can oxidize and change wettability (12, 25) so tests on reservoir oil samples must be performed in an oxygen-free environment. Exposure to air had a marked effect on the wetting cycle of one crude oil discussed below.

The apparatus shown in Figure 6 was assembled with a cover containing oil, brine and argon/vacuum lines. Three vacuum/argon cycles purged oxygen from the vessel. These cycles also purged the lines to the brine and oil supplies. Argon bubbled through the brine storage vessel for about fifteen minutes. Brine was drained from a glass storage tank into the vessel to cover the glass plates. The vacuum pump pulled gas from the brine in the vessel for forty-five minutes. A positive pressure of argon on the brine assisted a gravity drain from the vessel until the brine level dropped below the bottom of the glass plates. The oil inlet valve was opened and the pressure in the cylinder forced oil into the vessel until the glass slides were covered with oil.

Six glass slides hung from a PTFE and glass support around the periphery of the vessel (Figure 6). The hooks holding the slides were not wetted by brine or oil. As noted above, brine contacted the plates first followed by oil to replicate the order of exposure of fluids to the rocks in an oil field. A plate could be suspended from the microbalance through the central port of the vessel for the dynamic Wilhelmy test. A beaker centered in the vessel kept the brine level under the central port higher than the general oil/brine interface. Thus, for the dynamic Wilhelmy test the plate passed through a central thin layer of oil into the brine while the suspended plates aged in a thick layer of oil around the periphery of the vessel.

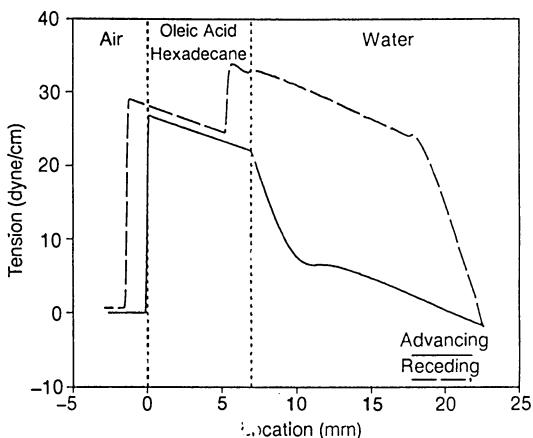


Figure 5. Hexadecane-oleic acid /water/glass wetting cycle with hybrid-wetting behavior.

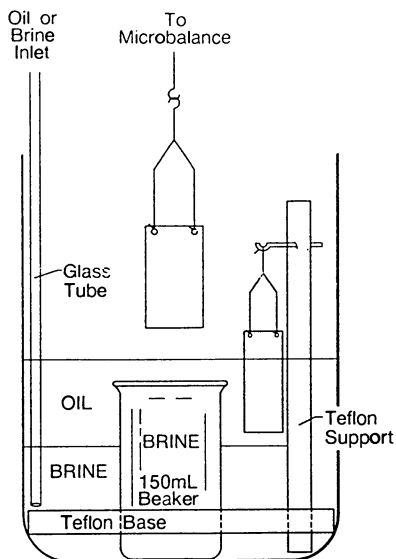


Figure 6. Schematic of interior configuration of anaerobic vessel, covering lid omitted. (Reproduced with permission from ref. 21. Copyright 1988 Society of Petroleum Engineers.)

Argon flowed through a relief valve to keep a slight positive pressure in the anaerobic vessel. To perform the test, the central stopper was removed and the plate to be tested was "fished" from its hanger and suspended from the microbalance. A small flow of argon out of the port prevented air from diffusing into the vessel during the ten minute period of the test. By testing each of the plates after extended times, the influence of the interface age was determined.

Several crude oils have been examined in both aerobic and anaerobic systems (21). Oil-wetting, water-wetting and hybrid-wetting systems have all been observed in these systems. The wetting cycles generally were performed on glass slides, although some studies using marble have been done. Quartz, limestone (or marble) and dolomite can be used to model reservoir rocks.

The behavior of each crude oil was examined quickly by testing the oil/brine system in an open beaker. Air contacted the oil; only glass covers protected the fluids from contamination by dust between tests. The brine had 50 kppm NaCl and 5 kppm CaCl₂ in distilled water. Most of the crude oils examined when exposed to air came to equilibrium in about one day (21). One West Texas crude oil (SS1473) tested in an open beaker (Figure 7) displayed a wetting behavior which changed in a way which was not systematic. Each wetting cycle used a new, clean glass plate but the same beaker of oil and brine. A second sample of oil from the same oil field behaved in a qualitatively similar way.

Figure 8 shows the results of the tests on SS1473 in the anaerobic vessel. The interface age noted on Figure 8 was also the aging time of the plate prior to performing the dynamic Wilhelmy test. The first plate tested immediately after preparing the vessel displayed hybrid wetting behavior in two wetting cycles. The water-advancing adhesion tension was somewhat less oil-wetting during the first cycle. Both cycles displayed strong water-wetting behavior during the water-receding portion of the cycle. After one day of soaking in crude oil and on subsequent days up to six days the behavior was oil-wetting with a small hysteresis. The water-advancing adhesion tension for all of these tests (listed in Table II) was almost constant. The water-receding adhesion tension values were generally less consistent for most tests involving crude oils. The thinning of the oil layer in the latter cycles was due to loss of volatile components from the oil.

TABLE II. ANAEROBIC CRUDE OIL ADHESION TENSION MEASUREMENTS AND CONTACT ANGLES USING IFT = 36.4 DYNE/CM

Interface Age	Measured Adhesion Tension		Calculated Contact Angle	
	Water-Advancing	Water-Receding	Advancing	Receding
15 min.	-21.72 dyne/cm	25.04 dyne/cm	127°	47°
30 min.	-30.65 dyne/cm	23.03 dyne/cm	147°	51°
22 hours	-29.76 dyne/cm	-26.54 dyne/cm	145°	137°
3 days	-32.45 dyne/cm	-25.92 dyne/cm	153°	135°
6 days	-30.80 dyne/cm	-19.53 dyne/cm	148°	122°

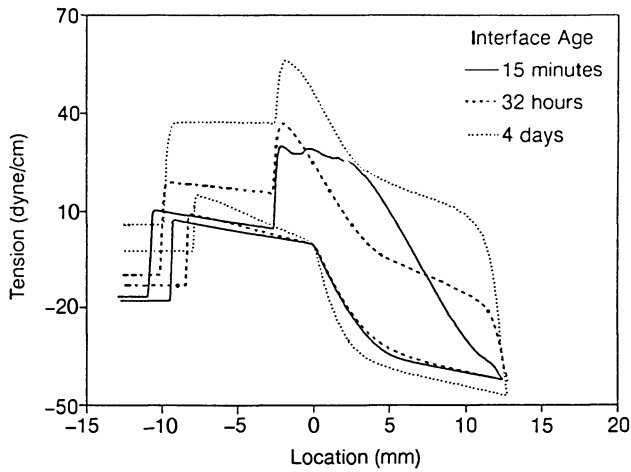


Figure 7. Wetting cycles of crude oil SS1473 tested in an open beaker. (Reproduced with permission from ref. 21. Copyright 1988 Society of Petroleum Engineers.)

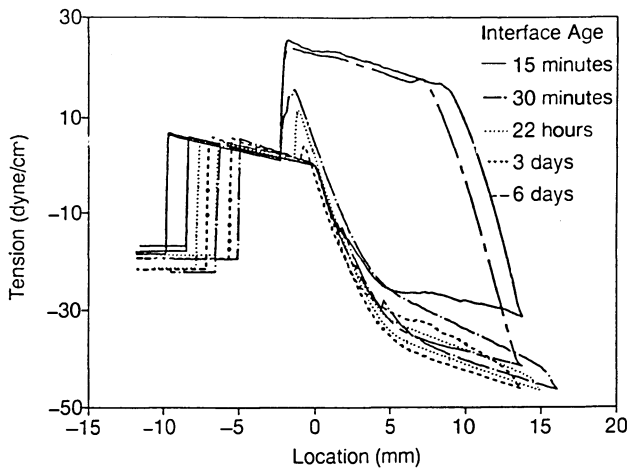


Figure 8. Wetting cycles of crude oil SS1473/brine/glass tested in an anaerobic vessel. (Reproduced with permission from ref. 21. Copyright 1988 Society of Petroleum Engineers.)

The IFT of this crude oil and brine was 36.4 (+/- 0.5) dyne/cm, measured using the maximum bubble pressure method. This value was used to calculate the contact angles shown in Table II. The equilibrium value of the water-advancing contact angle was 149°, and the water-receding contact angle was 131°. The value for sessile drop water-advancing contact angle measurements on six other samples of oil from the same reservoir ranges from 112° to 145°, with an average of 131° (12).

In many oil-wetting systems a film of oil adhered to the plate below the oil/brine meniscus. In some cases, the film was not persistent; during the minute or so the bottom of the plate was submerged in brine, it was swept clear of the oil film and the receding cycle switched from oil-wetting to water-wetting as the cycle progressed. After about one day of equilibration between the oil and the brine, this short-time behavior was no longer seen.

For water-wetting oil/brine systems, the receding portion of the wetting cycle was more consistent (smoother) than the advancing portion, which is opposite to the effect noted with the oil-wetting crude oils discussed above. This has been seen with other water-wetting materials in our laboratory. In both the oil-wetting and water-wetting cases, the smoother curves were noted when the relative motion of the plate pulled the wetting fluid into the non-wetting fluid. The more ragged features were seen when the non-wetting fluid advanced over the thin edge of the wetting fluid. This raggedness appeared to be a result of irregular detachment of the wetting fluid along the contact line, a localized "stick-slip" behavior.

This study demonstrated two aspects of measurement of wettability of crude oils. Exposure to air can cause changes in the wetting cycle. This was not true of normal paraffins such as hexadecane, which yielded stable wetting cycles for days and weeks when exposed to air. Equilibration of the crude oil/brine/solid system also caused changes in the wetting behavior. From this study it is not clear whether the changes were due to equilibration of the oil and brine phases or the aging of the solid in the oil phase. It is likely that both affect the measurement.

The four-to-six day duration of the dynamic Wilhelmy tests (wherein equilibrium actually occurred after one day) were much shorter than the times generally required for the sessile drop test. The conventional contact angle measurements on oil from the fields mentioned above required up to 48 days (12).

Surface Energy Study Related to Wettability

The wetting behavior of liquid/liquid/solid systems is not only dependent on the two liquid phases, but upon the interaction of the solid surface with these liquids (see Equation 1). An example is in the wetting cycles for glass and PTFE in a hexadecane/water system. A wetting cycle for a glass slide in a hexadecane/water system has the typical water-wetting cycle shown previously in Figure 3. Figure 4 shows the data for PTFE used as the solid phase with the same liquid/liquid system where an oil-wetting cycle is observed. When wetting cycles for plates of the minerals dolomite and marble were obtained for the hexadecane/water system, hybrid wetting cycles such as those shown in Figure 5 were seen.

The surface free energy of the solid is important in understanding the interaction of a solid with liquids. Solids with low surface energies, such as PTFE, tend to be wetted by only those liquids that have low surface tensions; in an oil/water system such solids tend to have oil-wetting behavior as shown in Figure 4 for hexadecane/water/PTFE. Solids with higher surface energies, such as glass, are wetted by water with its high surface tension in preference to hydrocarbons of low surface tension such as hexadecane. Surface energy values can thus be very important in understanding the wetting phenomenon. Unfortunately, surface energies of single crystalline solids are inaccessible to direct measurement and postulating values for heterogeneous reservoir rock complicates matters even more. However, approximate values of surface energies can be deduced by contact angle studies with probe liquids (26).

Surface free energies calculated by this technique use only advancing contact angles or "equilibrium" angles which are somewhere between the advancing and receding angles; the surface energy is represented with a single value. This practice is probably not adequate for samples with heterogeneous surfaces. In light of these difficulties, Penn and Bowler (27) used both the advancing and receding contact angles for a series of liquids to compare the surface energies of solids. They suggested that advancing and receding contact angle data for a series of probe liquids against a solid be presented in bar graph form, describing a "fingerprint" for that solid. The bar graphs for one solid are compared to those for another solid; if the graphs are similar, the solids have similar surface energies and good adhesive performance (27).

This same technique should be helpful in understanding wetting properties important in the oil industry since wetting is very dependent on mineral surface energies. The use of contact angle hysteresis information may allow a better understanding of the effects of surface heterogeneities of natural mineral samples. The dynamic Wilhelmy plate technique is ideally suited for such experiments.

Plates of glass, PTFE, dolomite and marble were used. Dolomite and marble were chosen because they represent minerals found in oil reservoirs. Glass and PTFE were investigated because they represent high and low surface energy solids respectively and are good model systems for data comparisons. Liquid/solid wetting cycles were obtained for each of the solids in the liquids listed in Table III.

The contact angles were calculated by using Equation 2 and the surface tension values listed in Table III for the respective liquids (determined with the Wilhelmy maximum pull method). All liquids used were of the highest purity and these surface tension values and accepted literature values are in close agreement. Figure 9 shows the bar graph presentation of these data. The abscissa of the graph is an ordered listing of the surface tensions of the probe liquids. Several runs of each liquid/solid system were averaged. The bottom of each bar is the cosine of the advancing contact angle and the top is the cosine of the receding angle of the liquid/solid system. The data for those liquid/solid systems having little or no hysteresis between advancing and receding contact angles were very reproducible. The data for the PTFE, dolomite and marble for the liquids showing the largest hysteresis had scatter of 0.06 cosine units or

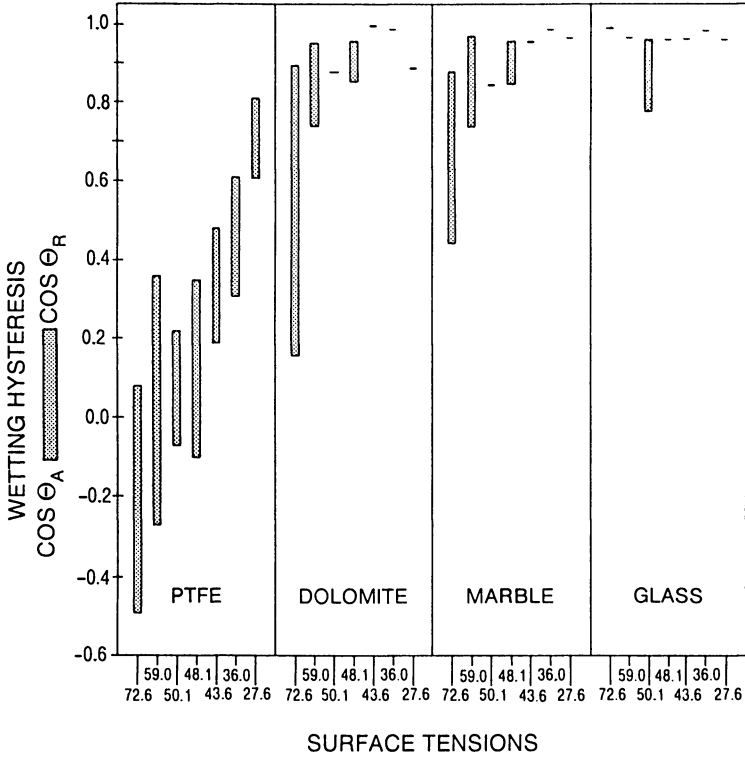


Figure 9. Bar graphs giving contact angle information for a series of probe liquids on PTFE, dolomite, marble, and glass.

TABLE III. SURFACE TENSIONS OF LIQUIDS USED FOR SOLID SURFACE CHARACTERIZATION

Liquid	Surface Tension (dyne/cm)
Water	72.6
Formamide	59.0
Methylene iodide	50.1
Ethylene glycol	48.1
1-Bromonaphthalene	43.6
N,N-Dimethylacetamide	36.0
Hexadecane	27.6

less. Advancing contact angles calculated in this study for water/PTFE and methylene iodide/PTFE of 119° and 93° , respectively, compare well with reported values of 112° (28) and 88° (29).

Figure 9 shows that the dolomite and marble had very similar hysteresis response while the glass and PTFE were much different. This corresponds with the hybrid wetting seen for dolomite and marble in a hexadecane/water system as compared with the water-wetting behavior of glass and the oil-wetting nature of PTFE in the same liquid/liquid system. Calculated values for the surface energy of glass, marble and PTFE are approximately 300 (30), 200 (31) and 19 ergs/cm² (32) respectively. No literature values for dolomite were found. Glass and marble have surface energies that are very similar; however the Wilhelmy technique is still able to distinguish between the wetting behavior of the two systems. The importance of this type of surface characterization has been shown in wetting studies using glass and marble in a crude oil/brine system under anaerobic conditions (Andersen, M. A.; Thomas, D. C.; Teeters, D. C. The Log Analyst, Society of Core Analysts paper 8801, to be published). The two solids exhibited different wetting cycles as would be predicted from the work presented here. From the similarity of the bar graphs for marble and dolomite, we believe that dolomite must have a surface energy near that of marble. The very oil-wetting PTFE surface is easily distinguished from the hybrid-wetting marble and dolomite and the water-wetting glass. Studies such as these make it possible to more fully characterize the wetting behavior of reservoir rock.

Other Applications of the Dynamic Wilhelmy Plate Technique

In addition to the work described in this paper, the dynamic Wilhelmy plate technique lends itself to other surface studies important to the oil industry. This technique has been used to investigate drilling fluid emulsions by characterizing the liquid/liquid/solid interactions of weighing agents such as barite and hematite with drilling fluid oils containing emulsifiers (Cline, J. T.; Teeters, D.; Andersen, M. A., SPE Preprint 18476, Society of Petroleum Engineers, in press). Because tensions as low as 1 dyne/cm can be observed, it can be used to study the change in adhesion tension and contact angles with the adsorption of surfac-

tants on rock surfaces (17) and used to study micellar properties (33).

Conclusions

The dynamic Wilhelmy plate technique provides a novel way to study wetting behavior. It can be used to easily and quickly distinguish water-wetting, oil-wetting and hybrid-wetting systems, under anaerobic conditions if necessary. Quantitative values of contact angles can also be obtained. This technique can be used to compare surface energies of natural mineral systems making the prediction of reservoir rock wettability more reliable. The dynamic Wilhelmy plate technique has much potential for future studies of importance to the oil industry.

Acknowledgments

We would like to thank Amoco Production Company for funding this work and for allowing its publication. We would also would like to acknowledge Dr. Jeffrey T. Cline of Amoco for providing the marble samples.

Legend of Symbols

B	- buoyant force
F	- force on Wilhelmy plate
g	- gravitational acceleration
h	- capillary rise
k	- permeability
N _c	- capillary number
p _c	- perimeter of plate in Wilhelmy test
ΔP	- pressure drop across a curved interface
P _c	- capillary pressure (P _o - P _w)
r	- radius of a narrow capillary
S _w	- water or brine saturation
V ^w	- fluid velocity
γ	- surface tension or interfacial tension
μ	- viscosity
θ	- contact angle
φ	- porosity
Δρ	- density difference between two fluid phases

Subscripts

A	- air	S	- solid
O	- oil	1	- Phase 1
W	- water or brine	2	- Phase 2

Literature Cited

1. Anderson, W. G., J. Pet. Technol. 1986, 38(10), 1125.
2. Anderson, W. G., J. Pet. Technol. 1986, 38(11), 1246.
3. Anderson, W. G., J. Pet. Technol. 1986, 38(12), 1371.
4. Anderson, W. G., J. Pet. Technol. 1987, 39(10), 1283.
5. Anderson, W. G., J. Pet. Technol. 1987, 39(11), 1453.

6. Anderson, W. G., J. Pet. Technol. 1987, 39(12), 1605.
7. Neumann, A. W.; Good, R. J. In Surface and Colloid Science; Good, R. J.; Stronberg, R. R., Eds.; Plenum Press: New York, 1977; Vol. 11, pp 31-91.
8. Hjelmeland, O. S.; Larrondo, L. E. SPE Reservoir Eng., 1986, 1(4), 321.
9. McCaffery, F. G.; Mungan, N. J. Can. Petrol. Technol. 1970, 9, 185.
10. McCaffery, F. G. J. Can. Petrol. Technol. 1972, 11, 26.
11. Leach, R. O.; Wagner, O. R.; Wood, H. W.; Harpke, C. F. J. Petrol. Technol. 1962, 14, 206.
12. Treiber, L. E.; Archer, D. L.; Owens, W. W. Soc. Petrol. Engrs. J. 1972, 12, 531.
13. Wilhelmy, L. Ann. Physik. 1863, 119, 117.
14. Dognon, A.; Atribat, M. Bull. Soc. Chim. Biol. 1941, 23, 62.
15. Bendure, R. L. J. Colloid Interface Sci. 1973, 42, 137.
16. Johnson, R. E.; Detter, R. H.; Brandreth, D. A. J. Colloid Interface Sci. 1977, 62, 205.
17. Fleureau, J.-M.; Dupeyrat, M. J. Colloid Interface Sci., 1988, 123, 249.
18. Teeters, D.; Smith, B.; Andersen, M. A.; Thomas, D. C. In Symposium on Advances in Oil Field Chemistry, Toronto 1988; American Chemical Society Preprints, Division of Petroleum Chemistry, Inc.; Washington, DC, 1988, p 146.
19. Langmuir, I. Science 1938, 87, 493.
20. Pike, F. P.; Thakkar, C. R. In Colloid and Interface Science; Kerker, M., Ed.; Academic Press: New York, 1976, Vol. 3, p. 375.
21. Andersen, M. A.; Thomas, D. C.; Teeters, D. 1988 SPE/DOE Symposium on Enhanced Oil Recovery; SPE Preprint 17368; Society of Petroleum Engineers: Richardson, Texas, 1988, pp 529-537.
22. Craig, F. F. The Reservoir Engineering Aspects of Waterflooding; Monograph Series 3, Society of Petroleum Engineers: Richardson, TX 1971.
23. Adamson, A. W. Physical Chemistry of Surfaces; 4th ed.; Wiley: New York 1982.
24. Stalkup Jr., F. I. Miscible Displacement; Monograph Series 8, Society of Petroleum Engineers: New York 1983.
25. Bartell, F. E., Niederhauser, D. O. Fundamental Research on Occurrence and Recovery of Petroleum, American Petroleum Institute: New York 1946-1947, pp 57-80.
26. Kaelble, D. H. J. Adhes. 1970, 2, 66.
27. Penn, L. S.; Bowler, E. R. Surf. Interface Anal. 1981, 3, 161.
28. Damm, J. R. J. Colloid Interface Sci. 1970, 32, 302.
29. Fowkes, F. M.; McCarthy, D. C.; Mostafa, M. A. J. Colloid Interface Sci. 1980, 78, 200.
30. Shartsis, L.; Smock, A. W. J. Amer. Ceram. Soc. 1947, 30, 130.
31. Janczuk, B.; Chibowski, E.; Staszczuk, P. J. Colloid Interface Sci. 1983, 96, 1.
32. Zisman, W. A. In Contact Angle, Wettability, and Adhesion; Fowkes, F. M., Ed.; Advances in Chemistry No. 43; American Chemical Society: Washington, DC, 1964.
33. Thomas, D. C.; Christian, S. D. J. Colloid Interface Sci. 1980, 78, 466.

RECEIVED November 28, 1988

Chapter 32

Enhanced Oil Recovery by Wettability Alteration

Laboratory and Field Pilot Waterflood Studies

H. H. Downs¹ and P. D. Hoover^{2,3}

¹Baker Performance Chemicals, Inc., Houston, TX 77227-7714

²Santa Fe Energy Company, Torrance, CA 90503

Thin Film Spreading Agents are alkoxyated nonylphenol resins which displace asphaltene molecules from oil-water interfaces and mineral surfaces. Laboratory studies on demulsification, wettability alteration and oil recovery efficiency indicate that TFSA molecules recover incremental oil by coalescing near wellbore emulsions, making reservoir rock surfaces water-wet, and improving areal sweep efficiency. In a 36 acre waterflood pilot study, a 0.1 pore volume bank containing 239 mg/kg of TFSA was injected into an irregular pattern of 1 injector surrounded by 9 producing wells. An interwell chemical tracer study established fluid flow patterns within the pilot. Decline curve analysis showed that TFSA injection recovered more than 8150 ± 850 bbl of incremental oil, and provided a 54 % DCF rate of return for the 18 month pilot project.

Clean mineral surfaces are strongly water-wet and when in contact with an aqueous phase are positively, neutrally or negatively charged depending on the zeta potential of the surface. When crude oil is added to the system, surface active species in the crude oil (eg., asphaltenes) diffuse through the intervening water film and adsorb on the charged mineral surfaces(1). Polar portions of the asphaltene molecules are oriented towards the charged surface, while nonpolar portions are directed away from the interface and thereby render the surface oil-wet. The chemical identity of the mineral surface, physiochemical properties of the asphaltenes, salinity, temperature, pressure and history of the system all influence asphaltene adsorption and desorption, and thereby determine the wetting state of the surface. Thus, water-wet sedimentary rocks can become oil-wet in the presence of crude oil. Authoritative studies(2,3) have indicated that as many as 50 % of all silicate reservoirs and 80 % of all carbonate reservoirs are oil-wet.

³Current address: Petroleum Underground Pump Specialists, Inc., Torrance, CA 90501

0097-6156/89/0396-0577\$06.00/0

© 1989 American Chemical Society

It is very difficult to determine the wetting state of reservoirs. Whenever the composition or distribution of fluids in reservoir rock changes, the equilibrium between surface-adsorbed and solubilized surfactants is disturbed. As a result, the wettability of the rock surface can also change. During core sampling and testing, the wettability of native state rock can be significantly altered by the flushing action of drilling fluids, the presence of surfactants in drilling fluids, and changes in pH, pressure and temperature(1).

Wetting conditions control the location, distribution and flow properties of oil and brine through porous media(4). Due to differences in capillary forces and pore pressures for wetting and non-wetting fluids, only the wetting fluid is located in small pores while both the wetting and non-wetting fluids occupy the larger pores. When a uniformly oil-wet medium is waterflooded, the non-wetting water phase channels through the larger pores and bypasses much of the oil located in the smaller pores(5,6). Water breakthrough occurs early in the flood(7) and most of the economically produced oil is recovered after water breakthrough(6). Compared to a waterflood in a water-wet medium, the flowing fraction of oil in a waterflood of the corresponding oil-wet medium is lower(4,5), substantially more water must be injected into and produced from the oil-wet medium in order to recover a given amount of oil(6,8-10), and the oil saturation at the economic limit of the waterflood is higher than it would have been had the flood been conducted in a water-wet medium(5,7,9-12). Furthermore, because the relative brine permeability is higher and the relative oil permeability is lower in an oil-wet medium than in the corresponding water-wet medium, the water-oil mobility ratio for a waterflood in an oil-wet medium is higher and the areal sweep efficiency is lower than in a waterflood of a water-wet medium(5). Thus, it is widely recognized that the efficiency of a waterflood increases as the wettability of the uniformly wetted porous medium is varied from oil-wet to water-wet(4,6-8,10,11,13-15).

In general, reservoir rock surfaces are not wetted uniformly. Different mineral types and crystalline faces having different surface properties are exposed to the reservoir fluids of regionally varying chemical composition. Surface active components in the crude oil can be strongly adsorbed at certain locations within the porous media and the wettability of the rock surface can vary throughout the reservoir(1). In a fractionally wetted medium(16), the oil-wet and water-wet regions have sizes on the order of a single pore. In a mixed wettability medium(17), the oil-wet regions form continuous paths for oil to flow through several of the larger pores. It is likely that all petroleum reservoirs, even those which have been waterflooded, contain regions of oil-, water-, intermediate-, fractional-, and mixed-wettability over various length scales. Furthermore, during the lifetime of a waterflood, these regions of wettability can change from water-wet to oil-wet as well as from oil-wet to water-wet. Oil is displaced from fractionally wetted porous media in a similar manner to its displacement from uniformly wetted media(4). As the fractional water-wet surface area increases, the flowing fraction of oil

increases and substantially less water must be injected into and produced from the reservoir in order to recover a given amount of oil. In addition, the oil saturation at the economic limit of the waterflood decreases, and oil recovery efficiency increases as the reservoir becomes more widely water-wet(4,18).

Increasing the water-wet surface area of a petroleum reservoir is one mechanism by which alkaline floods recover incremental oil(19). Under basic pH conditions, organic acids in acidic crudes produce natural surfactants which can alter the wettability of pore surfaces. Recovery of incremental oil by alkaline flooding is dependent on the pH and salinity of the brine(20), the acidity of the crude and the wettability of the porous medium(1,19,21,22). Thus, alkaline flooding is an oil and reservoir specific recovery process which can not be used in all reservoirs. The usefulness of alkaline flooding is also limited by the large volumes of caustic required to satisfy rock reactions(23).

It appears that many of the limitations of alkaline flooding can be overcome by injecting a synthetic surfactant into the oil-bearing formation instead of generating the surfactant in situ with caustic. Thin Film Spreading Agents (designated TFSA) are a class of surface active, alkoxyated resins which are designed to generate high spreading pressures and displace asphaltene molecules from rock surfaces(24). As a result of TFSA treatment, the wettability of reservoir rock is changed from oil-wet and fractionally-wet to strongly water-wet. Recovery of incremental oil by wettability alteration with TFSA molecules depends on the wettability of the rock surface, the efficacy of the TFSA in making the rock surface more strongly water-wet, and the oil saturation at the beginning of the TFSA flood(25). In addition, members of this class of resin may function as demulsifiers. Thus, TFSA molecules can also promote the recovery of oil by coalescing emulsions in the near-wellbore region of production wells(26).

TFSA molecules have been extensively and successfully used as steam additives in cyclic steam operations(27-32). Recently, results of a TFSA-waterflood which was conducted in West Texas were reported(33). The purpose of the work described in this paper was to further evaluate the feasibility of recovering incremental oil in a mature waterflood by injection of surfactants which change the wettability of reservoir rock surfaces. In this paper, we present the results of laboratory studies with Thin Film Spreading Agents and the results of a carefully conducted TFSA-waterflood pilot in the Torrance Field located in the Los Angeles Basin of California.

EXPERIMENTAL SECTION

THIN FILM SPREADING AGENTS. The Thin Film Spreading Agent used in this study was an alkoxyated substituted phenol formaldehyde resin of relatively high molecular weight. The surfactant was prepared by a previously described procedure(34). Magnaflood 907 is a commercial product of Baker Performance Chemicals, Inc. and contains the Thin Film Spreading Agent formulated with anionic surfactants.

SAND DEOILING. Sand deoiling tests provide information about the relative performance of TFSA's in recovering crude oil from oil-wet sand and formation brine. To conduct the tests, sand/oil mixtures were prepared by saturating clean, dry sand (99.8% silica, 60-120 mesh) with crude oil in an 8/1 weight ratio. 9.0 g samples of the oil-sand mixture were then transferred to citrate bottles, blanketed with nitrogen, capped and aged overnight in a 85 °C oven. After cooling to room temperature, the oil-sand samples were contacted with 0.030 dm³ of the formation brine containing the specified concentrations of TFSA and placed in a 60 °C water bath for a total of 20 minutes. After 10 min in the water bath, all tubes (including the blank) were gently inverted to insure that the TFSA contacted the entire oil-sand mixture. At the end of 20 minutes, the samples were removed from the bath and cooled to room temperature. Ten milliliters (0.010 dm³) of xylene were then slowly added and gently mixed with the oil phase at the top of the citrate bottles. The amount of oil recovered from the sand was determined spectrophotometrically from a calibration curve of the crude oil in xylene using a Bausch and Lomb Spectronic 88 set at a wavelength of 430 nm. Each TFSA was tested in duplicate to obtain an average oil recovery and the percent deviation from the mean.

CONTACT ANGLE MEASUREMENTS. Asphaltene molecules were precipitated from crude oil onto borosilicate glass surfaces so that the effect of TFSA molecules on the wettability of asphaltene-modified surfaces could be quantified. Initially, the optically smooth glass surfaces were cleaned with chromic acid, then thoroughly rinsed with deionized water and dried in a vacuum oven. When the borosilicate surface was rigorously cleaned by this procedure, water droplets spread on the uniformly water-wet surface. A number of procedures for depositing a film of asphaltene molecules on the borosilicate surface were investigated; one procedure was particularly convenient and gave reproducible results. The clean, dry borosilicate glass was aged for 3 days in crude oil. During the aging process, successively larger volumes of pentane were gradually added to the crude oil. At the end of the aging-precipitation process, the borosilicate surface was coated with a heterogeneous asphaltene layer. The contact angles of water droplets on the asphaltene-modified surface were measured with a Rame-Hart contact angle goniometer. While the magnitude of the contact angle varied with the details of the surface treatment, all contact angles for surfaces prepared by the above procedure were consistently between 85° and 95°.

DEMULSIFICATION TESTS. Demulsification tests were conducted using standard bottle test procedures to evaluate the relative performance of Thin Film Spreading Agents in coalescing emulsions of formation brine in crude oil under reservoir conditions. Specified concentrations of TFSA were injected into sample bottles containing 0.1 dm³ of the untreated crude oil emulsion. The sample bottles were then capped, vigorously shaken and heated to the appropriate reservoir temperature. The volume percentage of the total water phase which separates from the oil, the clarity of

the separated oil phase, oil-water interface characteristics and the residual level of water remaining in the crude oil phase were measured as functions of time and TFSA concentration.

RESERVOIR DESCRIPTION. The TFSA-waterflood pilot study was conducted in Santa Fe Energy Company's Torrance Field. The field was discovered in 1922 and produces from Miocene and Pliocene sands located at depths of 3100 ft to 4400 ft (945 m to 1340 m) subsea. Within the pilot area, the net pay thickness of the Main Zone averages 96 ft (29 m) and varies from less than 90 ft (27 m) in the center of the pattern to more than 110 ft (34 m) in the northwest and southeast sections of the pilot.

Wells which are completed to the Main Zone inject brine and produce fluids from four sands, termed the C-, D-, E- and F-sands. The C-sand is well isolated from the D-, E-, and F-sands which were not discrete. Spinner surveys obtained before and after injection of TFSA indicate that the TFSA did not adversely alter the injectivity of the formation and that the formation was not damaged by TFSA injection.

Low salinity brine is produced from and injected into the Main Zone of the Torrance Field. Brine produced from Well TU-101, located within the pilot pattern, contains 16,000 mg/kg of total dissolved solids (TDS) while brine injected into the pilot injector, Well TU-120, contains 15010 mg/kg of TDS. The brine contains approximately 560 mg/kg of Ca^{2+} and 250 mg/kg of Mg^{2+} .

The crude oil produced from the Main Zone of the Torrance Field has an API gravity of 18° and contains 5.3 weight percent asphaltenes. The solubility of the asphaltene molecules in Main Zone oil was measured by the Oliensis Test(35). In this test, the solubility parameter of the oil was lowered by adding to the oil successively larger volumes of hexadecane, a poor solvent for asphaltene molecules. The minimum volume (in milliliters) of hexadecane, which when added to 5 g of crude oil, will cause the chromatographic separation of the asphaltene fraction is termed the Oliensis Number. The Oliensis Number for the Main Zone crude oil is 3, indicating that the asphaltene molecules are not well-solubilized in the oil. Small changes in the solubility parameter of the Main Zone oil can cause the asphaltenes to precipitate. Such changes can occur during production.

PILOT DESCRIPTION. The site of the TFSA-waterflood pilot was chosen on the basis of four criteria: the site was representative of reservoir conditions and production operations in the Main Zone, extensive historical production data was available for each of the production wells in the pattern, production wells completely surrounded the injection well, and the pattern appeared to be well isolated from adjacent patterns and injection wells. The production wells surrounding Well TU-120, an injection well, appeared to meet most of the site selection criteria.

The pilot, shown in Figure 1, was an irregular pattern with nine production wells surrounding a single injector, Well TU-120. Based on results of the tracer study, all nine producing wells are in communication with the injector. With the exception of Well TU-127 which came on production on February 12, 1986, all produc-

Publication Date: July 10, 1989 | doi: 10.1021/bk-1989-0396.ch032

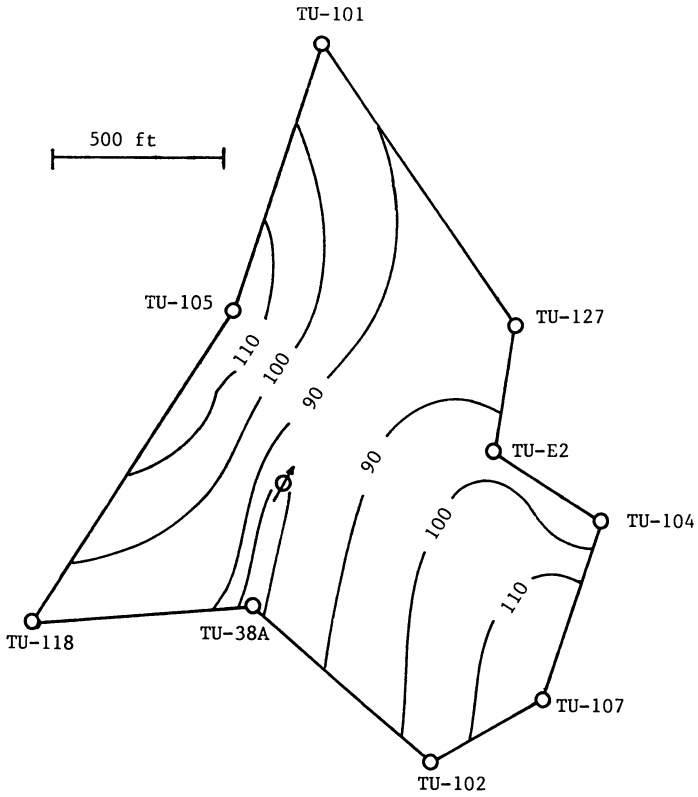


Figure 1. 36 acre TFSA-waterflood pilot showing bottom-hole well locations and net pay thickness in feet.

tion wells have extensive well-documented production histories. The pilot appears to be bounded on the southeastern flank by a fault and on the northeast by the water-oil contact. The pilot area was estimated to encompass 35.6 acres ($1.44 \times 10^5 \text{ m}^2$) with a net pay thickness of 3450 acre-ft ($4.26 \times 10^6 \text{ m}^3$). At the start of the TFSA-waterflood, the oil saturation was estimated to be 36 % and the oil cut in fluids produced from the pilot was 3.1 %.

To establish the well drainage boundaries and fluid flow patterns within the TFSA-waterflood pilot, an interwell chemical tracer study was conducted. Sodium thiocyanate was selected as the tracer on the basis of its low adsorption characteristics on reservoir rocks(36-38), its low and constant background concentration (0.9 mg/kg) in produced fluids and its ease and accuracy of analysis(39). On July 8, 1986, 500 lb (227 kg) of sodium thiocyanate dissolved in 500 gal (1.89 m^3) of injection brine (76700 mg/kg of thiocyanate ion) were injected into Well TU-120. For the next five months, samples of produced fluids were obtained three times per week from each production well. The thiocyanate concentration in the produced brine samples were analyzed in duplicate by the standard ferric nitrate method(39) and in all cases, the precision of the thiocyanate determinations were within 0.3 mg/kg. The concentration of the ion in the produced brine returned to background levels when the sampling and analysis was concluded.

RESULTS AND DISCUSSION

RECOVERY MECHANISMS. Being surface active, TFSA's lower oil-water interfacial tension, but not by the three orders of magnitude needed to increase the capillary number sufficiently to recover a substantial amount of incremental oil. Instead, TFSA's enhance the recovery of oil by changing the wettability of reservoir rock surfaces from oil-wet and intermediate wettability to strongly water-wet, and by coalescing emulsions in the near-wellbore region of the production wells.

A number of screening tests were conducted to select the best TFSA surfactant for use in the Main Zone of the Torrance Field and results of these screening tests illustrate the recovery mechanisms. Sand deoiling tests were conducted to evaluate the relative performance of TFSA molecules in recovering oil from the surface of oil-wet sand grains. Results of the sand deoiling experiments are shown for three different crude oils in Table I. For each crude oil studied, oil recovery increased as the concentration of TFSA increased from 0 to 500 mg/kg. The biggest percentage increase was observed for the California crude; oil recovery from oil-wet sand increased from 2.7 % to 33.5 % of the oil in place as the concentration of TFSA in the formation brine was increased from 0 mg/kg to 500 mg/kg. Compared to microemulsion floods which typically require surfactant concentrations in excess of 2 % to generate ultralow interfacial tensions, a substantial amount of incremental oil can be recovered by the wettability alteration mechanism using very low concentrations of TFSA surfactant. That high oil recoveries can be achieved with low concentrations of surfactants may be due to the low reservoir rock adsorption

Table I. Recovery of Oil from Oil-Wet Sand Increases As Concentration of Thin Film Spreading Agent Increases

	Percent Oil Recovery ⁽¹⁾ With Increasing TFSA Concentrations			
	0 mg/kg	100 mg/kg	250 mg/kg	500 mg/kg
Crude A West Texas	5.6	7.4	11.7	18.6
Crude B Alberta	4.8	--	7.5	20.3
Crude C California	2.7	--	13.2	33.5

⁽¹⁾ Oil recoveries after the oil-wet sand was contacted with equal volumes of brine containing the reported concentrations of Thin Film Spreading Agents.

characteristics reported for anionic-nonionic surfactant mixtures of certain members of the TFSA family(36).

Contact angle measurements for a water droplet on an asphaltene modified borosilicate surface confirmed that low concentrations of TFSA molecules change the wettability of the surface from fractionally-wet to water-wet. Table II shows the results of the contact angle measurements; all reported results are the average of 10 separate measurements, none of which varied from the mean by more than 5°. As the concentration of the TFSA

Table II. Thin Film Spreading Agents Make Asphaltene-Modified Surfaces More Strongly Water-Wet

	Contact Angle, θ , At Time T		
	Initial	5 min	10 min
Brine Alone	91	90	90
200 mg/kg TFSA	88	74	43
400 mg/kg TFSA	80	66	45
TFSA Alone	15	0	0

in the brine droplet increased, the contact angle of the brine droplet on the asphaltene modified surface decreased from approximately 90° to 0° . Although the numerical values of the contact angles reported in Table II are dependent on the details of the surface treatment, the data show that surfaces become more strongly water-wet in the presence of TFSA. Recovery efficiency by the wettability alteration mechanism depends on the wetting state of the reservoir rock, the efficacy of the TFSA in making the rock surface more strongly water-wet, and the oil saturation at the beginning of the TFSA flood(25).

In addition to adsorbing at mineral-oil interfaces, asphaltene molecules also adsorb at oil-water interfaces. Strong intermolecular dipole-dipole, hydrogen bonding, electron donor-acceptor and acid-base interactions cause the surface-adsorbed asphaltene molecules to form rigid "skins" at oil-water interfaces(41-43). When water droplets are dispersed in an oil which contains asphaltene molecules, molecularly thick, viscous asphaltene films form around the water droplets, inhibit the drainage of intervening oil and sterically stabilize the water-in-oil emulsion.

Flow properties of macroemulsions are different from those of non-emulsified phases(19,44). When water droplets are dispersed in a non-wetting oil phase, the relative permeability of the formation to the non-wetting phase decreases. Viscous energy must be expended to deform the emulsified water droplets so that they will pass through pore throats. If viscous forces are insufficient to overcome the capillary forces which hold the water droplet within the pore body, flow channels will become blocked with persistent, non-draining water droplets. As a result, the flow of oil to the wellbore will also be blocked.

Alkoxyated phenol formaldehyde resins are a well-known class of demulsifier, and the emulsion coalescence data in Table III confirm that Thin Film Spreading Agents, which belong to this class, can also function as chemical demulsifiers. When water in

Table III. Thin Film Spreading Agents Are a Well-Known Class of Chemical Demulsifier

	Percent Coalescence with 60 mg/kg of TFSA			
	15 min	30 min	60 min	120 min
Crude A West Texas	43	68	73	77
Crude B Alberta	--	18	54	72
Crude C California	16	80	89	90

crude oil emulsions are treated with low concentrations of TFSA molecules, a clear water phase separates from the oil and the volume percent of dispersed water in the crude oil decreases to very low levels. While the mechanisms by which demulsifiers coalesce water-in-oil emulsions are poorly understood, it is clear that TFSA molecules generate high spreading pressures(31,41) and displace asphaltene molecules from oil-water interfaces(41). When adsorbed at oil-water interfaces, the TFSA molecules present an energy barrier to coalescence of water droplets which is significantly lower than the energy barrier presented by thick, viscous asphaltene films. Thus, Thin Film Spreading Agents can promote recovery of oil from porous media by coalescing "emulsion blocks"(26) and perhaps by lowering oil-water interfacial viscosity(45).

TFSA-WATERFLOOD PILOT. A 36 acre ($1.14 \times 10^5 \text{ m}^2$) TFSA-waterflood pilot was recently conducted in the Torrance Field in the Los Angeles Basin of Southern California. To characterize the fluid flow patterns within the pilot, an interwell chemical tracer study was conducted with sodium thiocyanate. Results of the tracer study are shown in Table IV. Only 61.6 % of the injected tracer was recovered in the produced fluids, indicating that as much as 38.4 % of the injected fluids were flowing out of the pattern. Furthermore, since only 1604 bbl/d ($255 \text{ m}^3/\text{d}$) of brine was injected into the pattern, as much as 75.9 % of the total fluids produced by pilot wells were from outside the pattern.

Starting on May 19, 1986, Magnaflood 907 was continuously metered into the injection brine. The TFSA concentration averaged 239 mg/kg and the total TFSA bank size was 0.09 pore volumes. During the TFSA injection stage, the brine injection rate averaged 1604 bbl/d ($255 \text{ m}^3/\text{d}$) and varied from 1226 bbl/d ($195 \text{ m}^3/\text{d}$) in February 1987 to 1838 bbl/d ($292 \text{ m}^3/\text{d}$) during the first week in November 1987. The injection pressure which averaged 1380 psig (9.51 MPa) was maintained between 1250 psig (8.62 MPa) in February 1987 and 1450 psig (10.0 MPa) during the third week in October 1986. Therefore, the injectivity during the TFSA-waterflood varied by less than 16 % from the average of 1.16 bbl/d/psig ($26.8 \text{ m}^3/\text{d}/\text{MPa}$). These results, along with results of spinner surveys obtained before and after TFSA injection, clearly indicate that injection of TFSA did not adversely affect the injectivity of the formation.

The effects of injecting TFSA into the pilot are shown for Well TU-E2 in graphs of water cut versus cumulative oil (Figure 2) and oil cut versus date (Figure 3). After TFSA injection began, the oil cut in the fluids produced from Well TU-E2 increased by 96 %, from an oil cut of 2.9 % to an oil cut of approximately 5.7 %. This increase in oil cut upon injection of TFSA represented a significant 180 % increase in oil production rate from 15 bbl/d ($2.4 \text{ m}^3/\text{d}$) just prior to TFSA injection to 42 bbl/d ($6.7 \text{ m}^3/\text{d}$) after TFSA injection. The tracer study indicated that 40.5 % of Well TU-E2's gross production is from the pilot pattern (see Table IV). Other wells in the pilot have lower percentages of their gross production from the pilot. Consequently, the response in oil production rate due to TFSA injection was proportionate to the

Table IV. Tracer Study Established Fluid Flow Patterns Within the Pilot Area

Well Number	Production Rate, Bbl/d		NaSCN Tracer Recovered		Predicted Tracer Recovery(1) % of Produced
	Total Fluids	Pilot Fluids	Weight, lb.	% of Injected	
TU-38A	1075	423	84.7	16.9	25.1
TU-107	1096	248	49.6	9.9	15.7
TU-104	1240	218	39.4	7.9	13.8
TU-E2	727	290	34.5	6.9	18.4
TU-127	797	168	29.4	5.9	10.6
TU-102	608	111	21.9	4.4	7.0
TU-118	424	37	20.4	4.1	2.3
TU-101	483	43	16.9	3.4	2.7
TU-105	210	66	11.0	2.2	4.2
	====	====	====	====	=====
TOTALS	6660	1604	307.8	61.6	100.0
					cc = 0.91

(1) Results of simulation model.

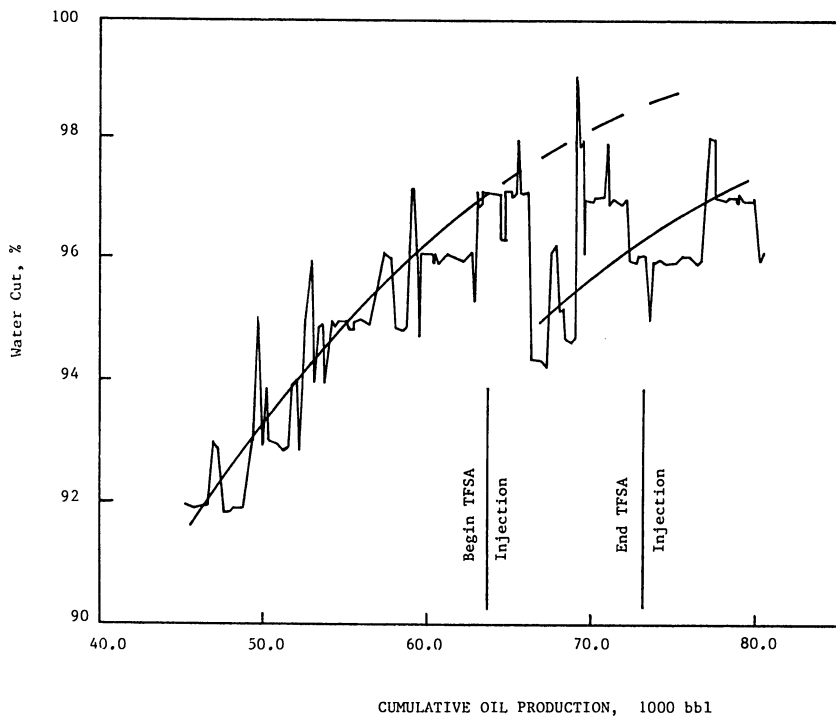


Figure 2. The efficiency of the waterflood increased upon injection of TFSA.

Publication Date: July 10, 1989 | doi: 10.1021/bk-1989-0396.ch032

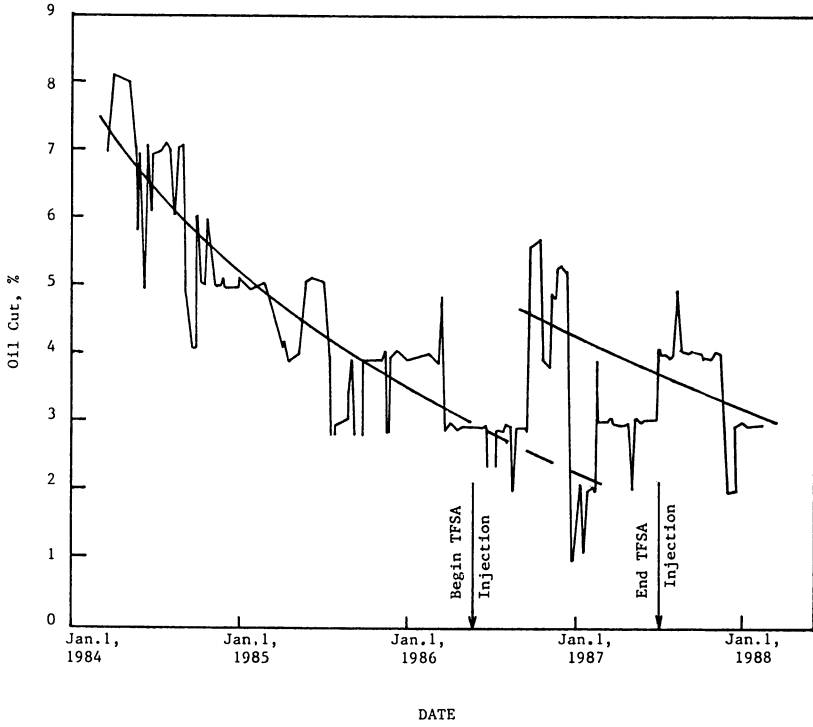


Figure 3. Injection of TFSA significantly increased oil cut in fluids produced from pilot wells.

percentage of each well's gross production which was from the pilot pattern.

To establish the amount of incremental oil which was produced by TFSA injection, the historical production decline rate for wells in the pattern was determined from the three years of production history prior to TFSA injection. The site of the TFSA-waterflood was specifically chosen because all wells in the pilot had extensive, well-documented production histories. Semilogarithmic graphs of oil production rate versus date, shown in Figure 4 for one representative well (TU-E2), are not linear; the production decline rate prior to TFSA injection was best fit by a hyperbolic decline model. Hyperbolic decline models are widely used to fit the oil production decline observed in water-drive reservoirs having good pressure maintenance. The use of a hyperbolic decline curve to model the production decline rate in this pilot is supported by the fact that Santa Fe Energy Company produces oil from the Main Zone with good pressure maintenance. Compared to an exponential decline model, the hyperbolic model gives a conservative estimate of the incremental oil produced by TFSA.

Incremental oil production for each of the pilot wells was calculated by subtracting the extrapolated production decline curve which was established prior to TFSA injection from the actual production after TFSA injection. Results of this analysis indicate that a total of 8150 ± 850 bbl (1295 ± 135 m³) of incremental oil were obtained due to injection of TFSA. Incremental oil production was assumed to have ceased by October 10, 1987 when the two high brine producing Wells TU-107 and TU-104 were shut in.

The economics of the TFSA-waterflood project were evaluated for three cases - each case was based on different assumptions. In the first case, the minimum values for the economic yardsticks were evaluated assuming that a conservative 7300 bbl (= 8150 bbl - 850 bbl; 1160 m³ = 1295 m³ - 135 m³) of incremental oil had been produced by the end of the project. Maximum values for the economic data were calculated by assuming that 9000 bbl (= 8150 bbl + 850 bbl; 1430 m³ = 1295 m³ + 135 m³) of incremental oil were produced by only 61.6 % of the TFSA which had been injected into Well TU-120; this assumption is based on the results of the tracer study which showed that as much as 38.4 % of the injected fluids flowed out of the pilot pattern. In the final case, the most probable values for the economic yardsticks were calculated assuming the 8150 bbl (1295 m³) of incremental oil were produced by 90 % of the TFSA.

Results of the economic analysis are summarized in Table V. At a sales price of \$13.00 per barrel, the value of the incremental oil produced by the TFSA was between \$94,900.00 and \$117,000.00. This revenue was generated at a chemical cost of between \$1.93 and \$3.87 per incremental barrel. Cumulative incremental oil production, shown in Figure 5, indicates that the volume of incremental oil produced reached a constant and maximum value 18 months after the pilot was started. Of the total incremental oil recovered, 37.5 % was produced in the first six months of the pilot and 81.25 % was produced by the end of the

Publication Date: July 10, 1989 | doi: 10.1021/bk-1989-0396.ch032

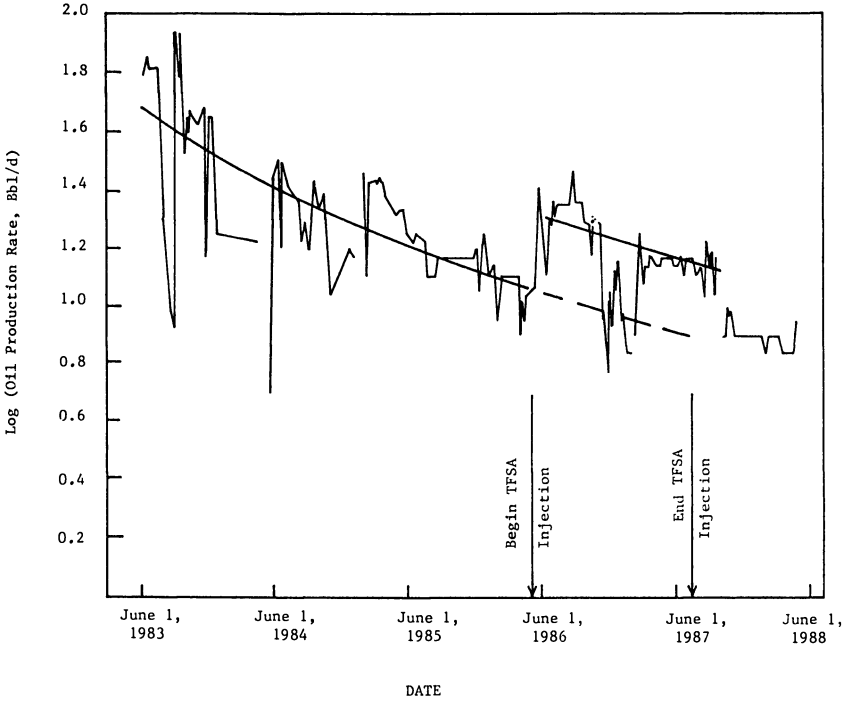


Figure 4. Production decline rate for wells in the pilot was best fit by a hyperbolic decline model.

Table V. Economic Analysis of TFSA-Waterflood Production Results

	Minimum Value (1)	Most Probable Value (2)	Maximum Value (3)
Incremental Oil Produced, bbl	7300	8150	9000
Value of Incremental Oil at \$13.00/bbl	\$94,900.00	\$105,950.00	\$117,000.00
Cost of TFSA Utilized	\$28,253.40	\$25,428.06	\$17,404.09
Chemical Cost per Bbl Incremental Oil	\$3.87	\$3.12	\$1.93
Discounted-Cash-Flow Rate of Return(4)	35 %	54 %	108 %

- (1) Assumes minimum amount of incremental oil production and that none of the TFSA flowed out of the pilot.
- (2) Assumes mean value for incremental oil production and that 10% of the TFSA flowed out of the pilot.
- (3) Assumes maximum amount of incremental oil production and that 38.4% of the TFSA flowed out of the pilot.
- (4) Assumes the project life is 18 months, semi-annual compounding, chemical cost is the only expense, and cost is paid in full before the start of the project.

Publication Date: July 10, 1989 | doi: 10.1021/bk-1989-0396.ch032

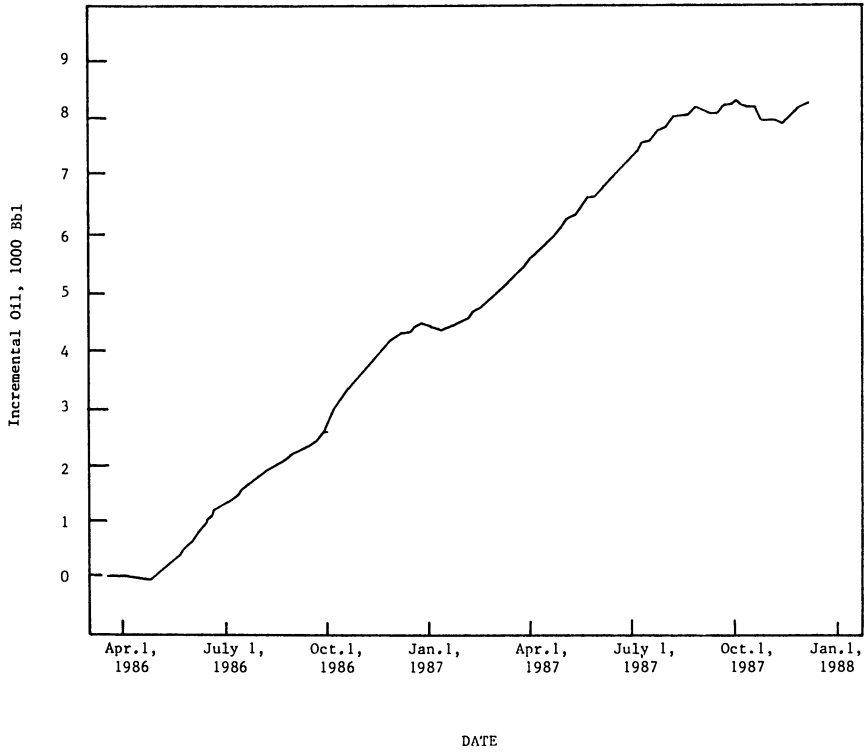


Figure 5. Cumulative incremental oil production indicates that 8150 bbl of incremental oil were recovered by TFSA.

first year. Based on semi-annual compounding, the discounted cash flow rate of return for the project was approximately 54 %.

SUMMARY AND CONCLUSIONS

1) Changing the wettability of reservoir rock surfaces from oil-wet to water-wet, increases the permeability of the formation to oil, decreases the permeability to water, decreases mobility ratio, increases sweep efficiency, increases the flowing fraction of oil at every saturation, and increases oil recovery at the economic limit of the waterflood.

2) Thin Film Spreading Agents are synthetic surfactants which change the wettability of reservoir rock surfaces from oil-wet and intermediate wettability to water-wet.

3) A 36 acre TFSA-waterflood pilot study was conducted in the Main Zone of Santa Fe Energy Company's Torrance Field.

4) Fluid flow patterns within the pilot pattern were characterized by an interwell chemical tracer study which showed that as much as 38.4 % of the fluids injected into the pilot flowed out of the unconfined pattern and 75.9 % of the produced fluids are from outside the pattern.

5) Beginning on May 19, 1986, a 0.09 pore volume bank containing an average TFSA concentration of 239 mg/kg was injected into the reservoir.

6) Analysis of the hyperbolic decline curves indicated that 8150 ± 850 bbl (1295 ± 135 m³) of incremental 18° API oil were recovered during the 18 month pilot project.

7) The discounted cash flow rate of return for the pilot TFSA-waterflood project was 54 %.

ACKNOWLEDGMENT

The authors gratefully acknowledge the helpful discussions, guidance and technical support given by Dr. Charles M. Blair, Mr. Richard E. Scribner and Mr. John E. Frederiksen.

LITERATURE CITED

1. Anderson, W. G. J. Petrol. Techn., **38**, 1125 (1986).
2. Treiber, L. E.; Archer, D. L.; Owens, W. W. Soc. Petrol. Eng. J., 531 (1972).
3. Chilinger, G. V.; Yen, T. F. Energy Sources, **7**, 67 (1983).
4. Anderson, W. G. J. Petrol. Techn., **39**, 1453, 1605 (1987).
5. Craig, F. F. The Reservoir Engineering Aspects of Waterflooding; Society of Petroleum Engineers of AIME: Dallas, 1971.
6. Raza, S. H.; Treiber, L. E.; Archer, D. L. Producers Monthly, **32**, 2 (1968).
7. Owens, W. W.; Archer, D. L. J. Petrol. Techn., 873 (1971).
8. Kyte, J. R.; Naumann, V. O.; Mattax, C. C. J. Petrol. Techn., 579 (1961).
9. Donaldson E. C.; Thomas, R. D. SPE 3555 (1971).
10. Mungan, N. Soc. Petrol. Eng. J., 247 (1966).
11. Mungan, N. World Oil, **192**, 149 (1981).

12. Jennings, H. Y. *J. Petrol. Techn.*, 116 (1966).
13. Kinney, P. T.; Nielsen, R. F. *Producers Monthly*, 14, 29 (1950).
14. Kinney, P. T.; Nielsen, R. F. *World Oil*, 132, 145 (1951).
15. Bobek, J. E.; Bail, P. T. *J. Petrol. Techn.*, 950 (1961).
16. Brown, R. J. S.; Fatt, I. *Trans. AIME*, 207, 262 (1956).
17. Salathiel, R. A. *J. Petrol. Techn.*, 1216 (1973).
18. Fatt, I.; Klikoff, W. A. *Trans. AIME*, 216, 426 (1959).
19. Johnson, C. E. *J. Petrol. Techn.*, 85 (1976).
20. Cooke, C. E.; Williams, R. E.; Kolodzie, P. A. *J. Petrol. Techn.*, 1365 (1974).
21. Wagner, O. R.; Leach, R. O. *Trans. AIME*, 216, 65 (1959).
22. Castor, T. P.; Somerton, W. H.; Kelly, J. F. In *Surface Phenomena in Enhanced Oil Recovery*; Shah, D. O., Ed.; Plenum Press: New York, 1981.
23. Breit, V. S.; Mayer, E. H.; Carmichael, J. D. In *Enhanced Oil Recovery: Proceedings of the Third European Symposium on Enhanced Oil Recovery*; Fayers, J. F., Ed.; Elsevier: New York, 1981; Chapter 13.
24. Blair, C. M. U.S. Patent 4 341 265, 1982.
25. Since Thin Film Spreading Agents do not produce ultralow interfacial tensions, capillary forces can trap oil in pore bodies even though the oil has been displaced from the surface of the porous medium. Therefore, recovery of incremental oil is dependent on the formation of an oil bank.
26. Muggee, F. D. U.S. Patent 3 396 792, 1968.
27. Blair, C. M. SPE 14906 (1986).
28. Stout, C. A.; Blair, C. M.; Scribner, R. E. *J. Can. Petrol. Techn.*, 24, 37 (1984).
29. Adkins, J. D. SPE 12007 (1983).
30. Blair, C. M.; Scribner, R. E.; Stout, C. A. SPE 11739 (1983).
31. Blair, C. M.; Scribner, R. E.; Stout, C. A. *J. Petrol. Techn.*, 34, 2757 (1982).
32. Blair, C. M.; Scribner, R. E.; Stout, C. A. SPE 10700 (1982).
33. Blair, C. M.; Stout, C. A. *Oil and Gas J.*, 83, 55 (1985).
34. Blair, C. M. U.S. Patent 4 337 828, 1982.
35. ASTM D 1370-58.
36. Scamehorn, J. F.; Schechter, R. S.; Wade, W. H. *J. Colloid Interface Sci.*, 85, 494 (1982).
37. Greenkorn, R. A. *J. Petrol. Techn.*, 97 (1962).
38. Wagner, O. R. *J. Petrol. Techn.*, 1410 (1977).
39. Brigham, W. E.; Smith, D. H. SPE 1130 (1965).
40. *Standard Methods for the Examination of Water and Waste Water*; Rand, M. C.; Greenberg, A. E.; Taras, M. J.; Franson, M. A., Eds.; American Public Health Association: Washington, DC, 1976; p 383.
41. Blair, C. M. *Chem. and Ind.*, 538 (1960).
42. Neumann, H. J. *Erdol V. Kohle, Erdgas Petrochenue*, 18, 776 (1965).
43. Strassner, J. E. *J. Petrol. Techn.*, 303 (1968).
44. McAuliffe, C. D. *J. Petrol. Techn.*, 727 (1973).
45. Kimbler, O. K.; Reed, R. L.; Silberberg, I. H. *Soc. Petrol. Eng. J.*, 153 (1966).

RECEIVED November 28, 1988

Chapter 33

Bound Water in Shaly Sand

Its Determination and Mobility

Ying-Chech Chiu

Department of Chemistry, Chung Yuan Christian University, Chung-Li,
Taiwan 32023, Republic of China

Specific ion electrodes were used for anion-free water determination of clay minerals at equilibrium with electrolyte solutions. A new equation was developed for determining anion-free water. Mobility of the anion-free water was determined by compaction experiments with pressure up to 10,000 psi. At NaCl concentrations of 0.2 M or higher, the anion-free water is immobile. At lower concentrations, it is movable under high pressure. Under ordinary flowing conditions, the anion-free water gives a good indication of the immobile water. At high pressure, the amount of the immobile water seems to be related to the porosity of the rock. The actual amount of the immobile water can be found by the method described in this paper. Through compaction of the clay-water slurry, bound water can be concentrated in the sample to facilitate NMR measurements and other studies.

Recent interest in clay hydration water and its effect on various petrophysical properties of shaly sand (1-13) has prompted the author to reinvestigate the subject of "bound water". It has long been suggested that water associated with the clay mineral surfaces causes deviations from the normal petrophysical measurements (14-16). Since bound water exists in the interfacial region between liquid and solid, it is quite difficult to obtain accurate and meaningful results concerning the nature and amount of water in this region. In the past, information concerning bound water has mainly been extracted from vapor phase adsorption of water (8,9,17,18). In recent years, NMR studies have provided much insight into the problem. It is generally recognized now by NMR study that some water molecules are preferentially oriented at the clay surfaces (10,13,19-21). The mobility of water in the interfacial region depends on the type of clay and the amount of sorbed water (22-24). Many authors believe that the tightly bound water occupies only a small fraction of a monolayer (25-27).

Little direct, quantitative measurement has been done on bound water existing in equilibrium with clay mineral substances in

0097-6156/89/0396-0596\$06.00/0

© 1989 American Chemical Society

aqueous solution. Dmitrenko (28) was the first to devise a method for determining bound water in natural sediments. The method is based on the determination of "nonsolvent water". By assuming the bound water a nonsolvent and assuming chloride ion adsorption negligible, Dmitrenko (28) calculated the amount of bound water after chemical analysis and material balance of water and chloride in the sample. Hill et al. (2), using the Dmitrenko method in conjunction with the "anion exclusion (29-31) technique" based on electrical double layer theory, determined the amount of bound water in twenty-eight samples from six fields. They called the water determined by this method "anion-free water" and assumed this water to be the clay hydration water (2). By using the amount of anion-free water and assuming that the anion-free water is immobile for normal flow processes, Hill et al. (2) developed procedures for (1) obtaining an estimate of brine permeability, (2) correcting mercury injection curves to estimate oil-water or gas-water capillary curves, (3) obtaining a more realistic estimate of formation water salinity from core water salinity and (4) calculating oil or water saturations for predicting whether oil or water will be produced.

This paper discusses the use of specific ion electrodes for determining the anion-free water. This method is simpler and more accurate at low electrolyte concentration than ordinary chemical methods. It is potentially useful for oilfield application and laboratory automation. The mobility of this water is also examined under forced conditions with pressure gradients. It is expected that by using the methods developed in this paper, one may obtain a better understanding of the clay properties.

Experimental

Bound Water Determination. A modified method of Hill et al. (2) was used in determining the bound water (anion-free water). No separation of solid and liquid was made during this determination. The ion concentrations were measured by specific ion electrodes. The major equipment consisted of an Orion Model 801 digital pH/mv meter, a Beckman 39278 sodium electrode, an Orion 94-17 chloride electrode and an Orion 90-01 reference electrode. Glen Rose Shale (Baroid Division of NL Industries supplied this sample in a fine powder) was used as the sample. Samples in bottles were weighed and dried at 110°C overnight. A known quantity of distilled water or NaCl solution was added to the bottle. After shaking with a floor shaker for 2 hours, the clay and sand were allowed to settle overnight. The ion potential was measured by placing the electrode in the clear liquid on top. All experiments were carried out at 24±1°C. The electrodes were calibrated with NaCl solutions of known concentration. The concentration of the unknown solution was determined from the calibration curves.

The amount of anion-free water was calculated by a material balance of chloride and water in the system. The calculation can be simplified by using volume concentrations. Details of the calculation are illustrated in Appendix I.

Compaction Experiments and Other Related Measurements. After the

anion-free water was determined, the shale-electrolyte slurry was poured into a filtration or a compaction cell. Gas or hydraulic pressure was applied to force the water out of the system. A Millipore filter (No. 4004700) or a Fann Filter press was used when the gas pressure was below 100 psi. Hydraulic pressure of 400 to 10,000 psi was applied through a compaction cell having a configuration as described by Darley (32). The solution forced out of the cell was collected, weighed, and its chloride concentration was determined. When no more liquid could be forced out, the mineral cake was weighed and dried at 110°C to constant weight. The amount of water in the cake is taken as the residual water in clay. The volume of the cake was also measured.

The pore size distribution of the dried sample was measured by a Aminco 60,000 psi Mercury-Intrusion Porosimeter.

The NMR measurement on water retained in the compacted sample was performed by using a Bruker CXP-200 NMR Spectrometer.

Some properties of the rock used in this study were measured: The cation exchange capacity (cec) was determined by the barium sulfate method as described by Mortland and Mellor (33). Surface area was measured by using a Digisorb Meter (Micromeritics Instrument Corporation) through nitrogen adsorption. Estimation of mineral composition and identification of the rock were performed by X-ray diffraction.

Results and Discussion

Bound Water Determination at Low Electrolyte Concentration. From the theoretical and experimental investigation of the anion-free water in the literature, it is most reasonable to conclude that the anion-free water is the water inside the electrical double layer. This concept has been discussed in more details using the "dual water model" (1) in which the anion-free water is referred to as the "clay water". Figure 1 compares the experimentally determined anion-free water contents. The three circles in Figure 1 are data taken from Ref. 2 determined in the NaCl concentration region 0.228 -5.41 M. The other data are taken from this investigation in the low concentration region. W_s is the anion-free water in g/100 g rock. The cec value and other properties of the sample, Glen Rose Shale, are given in Table I. In order to check the agreement between the values obtained in Ref. 2 and in this study, four points have been gathered around 0.2 M NaCl ($C_0^{-2}=2.4$). All the points coincide well and are shown as one point in Figure 1. The agreement between the two studies is good. A straight line passing through the origin correlates all the points in Figure 1. At extremely high electrolyte concentrations, flocculation of clay should occur. Therefore, when $C_0^{-2}=0$, $W_s=0$.

Figure 2 compares data from this investigation with those from the literature. Most literature data in Figure 2 are from Figure 3 of Ref. 2. The equations mentioned in Figure 2 have the following forms: Equation 1 comes from Schofield (29) and Bolt et al. (30-31),

$$\frac{\bar{\lambda}}{SC_0} = \frac{2}{(BC_0)^{\frac{1}{2}}} - \frac{4S}{Bcec} \quad (1)$$

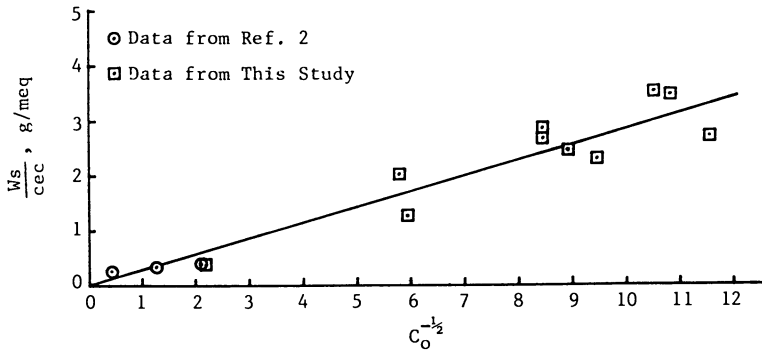


Figure 1. Anion-free Water As A Function of NaCl Concentration.

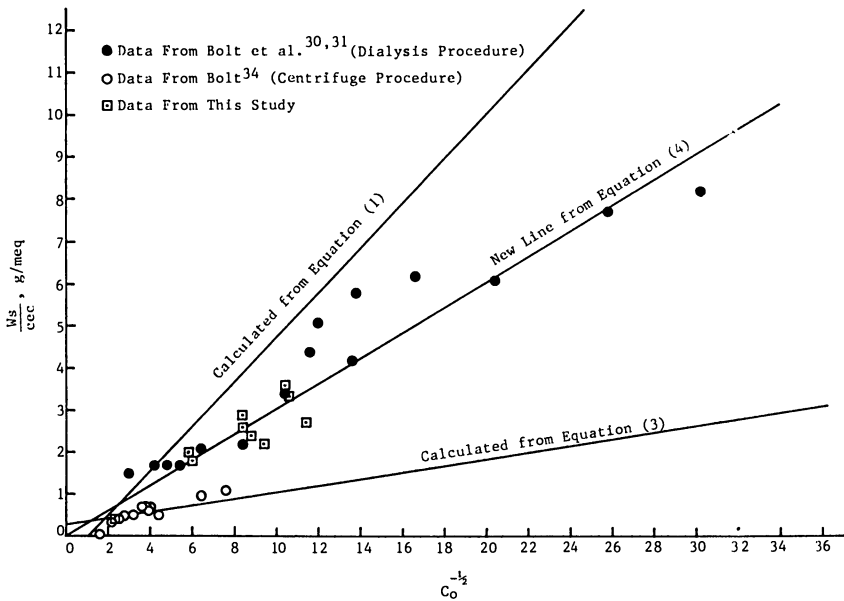


Figure 2. Hydration Water As A Function of Concentration and Method of Determination.

Table I. Properties of the Rock Sample

Sample	Surface Area m ² /g	cec meq/ 100g	Surface Charge Density (meq/m ²) x 10 ³	Composition, % from X-Ray Diffraction									
				Quartz	Calcite	Dolomite	Pyrite	Feldspar	Clay	Illite Chlorite Kaolinite Mixed layer Illite			
Grundite													
Illite (Magco- bar)	42.7	13.33	3.11	48			2	50	30				70
Glen Rose Shale	16.8	10.83	6.45	45	25	3	2	5	20	40			
Berea Sand- stone	0.97	0.45	4.65	80				5	15	10		90	
Fithian Illite (Ward's)	51.5	13.73	2.66	40	5	2	3	50		20			80
Rochester Illite (Ward's)	19.0	5.0	2.63	45		5		50		10			

where λ^- is the negative anion adsorption, C_0 has the same meaning as the equilibrium solution concentration, S is the area of the charged surface, and B is a constant. By assuming cec/S to be constant and λ^-/C_0 to be equivalent to W_s , Hill et al. (2) defined equation 2,

$$\frac{W_s}{\text{cec}} = AC_0^{-1/2} - B \quad (2)$$

where A and B are coefficients affected by the ratio, cec/S . By fitting their data into equation 2, Hill et al. (2) obtained equation 3 in this form :

$$\frac{W_s}{\text{cec}} = 0.084 C_0^{-1/2} + 0.22 \quad (3)$$

Data from this study seem to coincide better with the data of Bolt et al.. A straight line passing through the origin best fits all the points in Figure 2. This line has the following form :

$$\frac{W_s}{\text{cec}} = 0.31 C_0^{-1/2} \quad (4)$$

Surface Charge Density. In the previous section, it was assumed that the surface charge density, cec/S , is a constant. Table I gives the surface charge density for five samples. It varies from 2.63×10^{-3} to 6.45×10^{-3} meq/m^2 . Figure 3 shows a plot of these points. Four of the points can be fitted closely by a straight line with a slope of 2.9×10^{-3} meq/m^2 . One point deviates from the line. Patchett (35) has plotted some cec vs. S for nine API standard clays on a log-log paper. The best line representing the 9 points has a slope of 2.4×10^{-3} meq/m^2 . When the data in Figure 3 were plotted in Patchett's diagram, the five points lie around his line with about the same degree of scattering as his own data. It appears that the assumption of cec/S being a constant is a reasonable assumption for many rocks.

Mobility of The Anion-Free Water. It is well known that water in the electrical double layer is under a field strength of 10^6 - 10^7 V/cm and that the water has low dielectric constants (36). Since anion-free water is thought to be the water in the electrical double layer between the clay and the bulk solution, at high electrolyte concentrations, the double layer is compressed; therefore, the water inside is likely quite immobile. At low electrolyte concentrations, the electrical double layer is more diffuse, the anion-free water is expected to be less immobile. Since the evaluation of the shaly formation properties requires the knowledge of the immobile water, experiments were conducted to find out the conditions for the anion-free water to become mobile.

By definition, the anion-free water is free of salt. When pressure is applied to a clay-brine slurry to force out water (as that described in the experimental section), the solution that flows out of the cell should maintain the same chloride concentration as the brine's if the anion-free water is immobile. Otherwise, the concentration of the chloride decreases. Pressure forces water to flow through the pores with a certain velocity; meanwhile, the pore size

is reduced. By accounting material balances during the experiment, useful information was deduced.

Table II shows the result of compaction experiments with Glen Rose Shale. Column 2 gives the equilibrium NaCl concentration of the solution before the compaction experiment. Column 3 gives the anion-free water calculated as shown in Appendix I. Column 4 gives the amount of the bulk solution which has the NaCl concentration given in Column 2. Column 5 gives the total amount of fluid flowing out of the cell. Column 6 indicates the pressure applied and Column 7, the initial flow rate. The flow rate decreased with time and could be measured or estimated from equations (37). Column 8 gives the water retained in the clay sample after compaction by determining the weight loss after heating at 110°C. Porosity of the dried clay sample was determined by comparing the volume of residual water and total volume of the sample and is given in Column 9. Water density was assumed to be 1g/cm^3 . Column 10 gives the average pore diameter of the dried clay sample.

Experiments No. 1, 2 and 3 were performed at gas pressure beginning at 15 psi and stepping up to 77 psi. The total fluid collected was less than the bulk solution in the system. The concentration of chloride in the fluid collected in these three runs was about the same as the values given in Column 2. It was concluded that under these conditions, the anion-free water was immobile. It was observed that under the same applied pressure, the higher the NaCl concentration, the faster the flow rate -- consistent with observations reported by Engelhardt and Gaida (38).

In order to increase the flow rate without too much pressure, Experiment 4 was performed with a Fann filter press which has a wider cross sectional area. A constant air pressure of 100 psi was applied, the flow rate was 26 times that of Experiment 1 while the NaCl concentration was only slightly higher than that of Experiment 1. Although the flow rate was much increased in Experiment 4, the result was similar to Experiment 1. The water retained in the clay (Column 8) determined by drying was found to be close to the amount of anion-free water. The porosity of the sediment was 0.4 and the average pore diameter was 4466 Å. It was concluded from this experiment, that the anion-free water was immobile even at 100 psi and 7.4 ft/day. The pore size distribution of the sample showed 90% of the pores to have a diameter above 350 Å and less than 3% of the pores to have a diameter below 100 Å (Figure 4).

It was decided to increase the pressure in subsequent experiments to push the anion-free water out. Experiments 5 and 6 were performed at 400 psi at a NaCl concentration around 0.01 M. Experiments 5-10 were performed in the compaction cell as described in the experimental section. This apparatus was rated for 10,000 psi. The pressure regulation at 400 psi region was about ± 100 psi. Some evaporation occurred that made the total fluid collection less than expected from total material balance. NaCl concentration of the collected fluid could not be measured accurately. However, the amount of fluid collected and the amount of water retained in the sediments in Experiments 5 and 6 clearly indicated some anion-free water was mobilized.

Experiment 7 was the first run under 400 psi hydraulic pressure followed by 10,000 psi. Most of the fluid was collected at the low

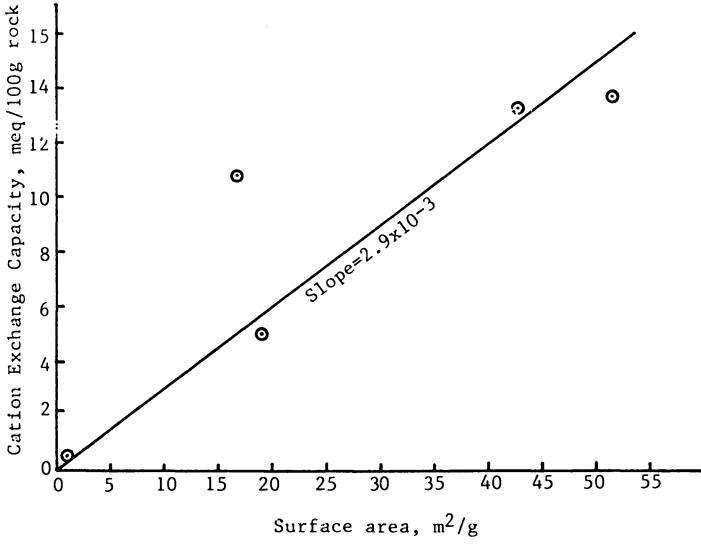


Figure 3. Cation Exchange Capacity As A Function of Surface Area.

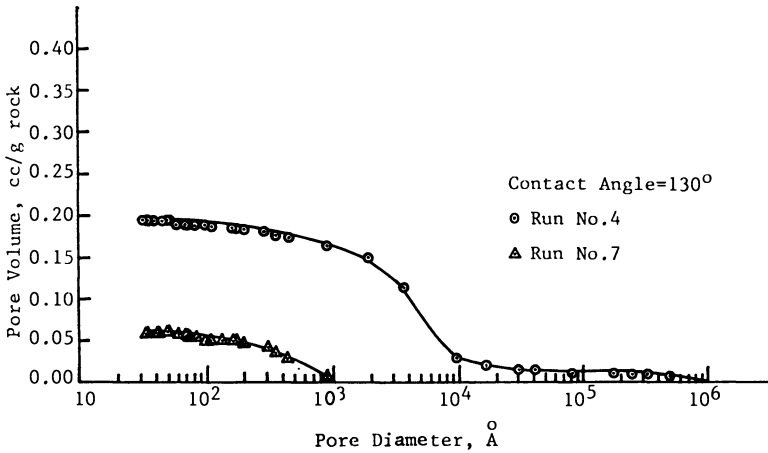


Figure 4. Pore Size Distribution By Mercury Intrusion.

Table II. Compaction Experiments of Glen Rose Shale

Run No.	NaCl Conc'n, M	Anion-free H ₂ O, g	Bulk Soln. Collected, g	Fluid Collected, g	Pressure, psi	Initial Flow Rate, cm/sec	Residual H ₂ O in clay, g	Porosity	Av. Pore Dia., Å
1	0.0086	18.5	31.3	29.6	15-77 (N ₂ or air)	0.00010			
2	0.0300	10.9	38.9	32.2	same as above	0.00013			
3	0.212	2.0	48.2	32.9	same as above	0.00026			
4	0.0126	12.7	35.7	34.8	100 (air)	0.0026	12.0	0.40	4466
5	0.0091	18.8	53.2	54.8	400 (hydraulic)	0.0015	9.8	0.42	2728
6	0.0140	15.6	37.8	39.1	same as above	0.00067	9.6	0.34	3337
7	0.216	1.8	46.2	32.8	400 (hydraulic)	0.0024			
8	0.0096	16.6	27.4	29.0	10,000 (hydraulic)		3.2	0.15	440
9	0.033	9.1	32.5	15.6	10,000 (hydraulic)		3.6		
10	0.235	1.5	37.0	13.6	10,000 (hydraulic)		3.1	0.16	491
					same as above		3.1	0.17	487

pressure. NaCl concentration of the collected fluid was the same as the bulk concentration, 0.216 M. The high pressure of 10,000 psi was applied for three days. Only 0.1 g liquid was collected during the last two days because of evaporation. NaCl concentration of the fluid was not measured. In this experiment, the amount of water retained in the sediment was less than that of anion-free water.

Experiments 8,9 and 10 were all performed up to 10,000 psi hydraulic pressure. Evaporation occurred during Experiments 9 and 10, although high flow rate was attained. It appears that At this high pressure, the porosities of the dried sediment decreased to 0.15-0.17 and the residual water contents in the clay decreased to 3.1-3.6 g, regardless the original NaCl concentration. At 0.2M NaCl concentration, the residual water content was higher than that of anion-free water; whereas at lower NaCl concentrations, the residual water content is lower. Even at such a high pressure (10,000 psi), the anion-free water was not mobile at the NaCl concentrations above 0.2 M. The porosity was decreased by pressure close to those of some Berea rocks. Figure 4 shows the pore size distribution curve for the dried sediment of Run No. 7. The curve is quite typical for samples compressed at 10,000 psi such as Run No. 8 and 9. The average pore diameter of the dried sediments for these three runs was in the range Of 440-491 Å.

The experiments listed in Table II suggested that the anion-free water was not pressed out until the bulk water had been squeezed and sufficient pressure was applied. Data obtained by Von Engelhardt and Gaida (38) also follow the same trend. They measured the change in NaCl concentrations for pore solutions in compressed montmorillonite clay under the pressure range of 440 psi to 470,000 psi. The concentration of NaCl in the solution decreased very slowly until the porosity of the clay was decreased to 0.5. Then the concentration decreased very quickly with further decrease of the porosity. At extremely high pressure, the NaCl concentration showed a slight tendency of reversing the trend. When kaolinitic clays were compressed, the concentration change in pore solution was not observed. Von Engelhardt and Gaida (38) did not measure the anion-free water. The decrease of pore solution concentration would be expected, only if the bulk solution was pressed out first, followed by the anion-free water. Since the cec value of kaolinitic clay is low, the amount of anion-free water should also be low; thus the concentration change is not expected.

NMR Measurement of The Residual Water. The residual water obtained in Experiments No. 5 and No. 6 was measured with a broadline NMR spectrometer, in which, proton signal of the water gives a very broad line. The full width at half height of the NMR signal is 15750 Hz and 18000 Hz for samples obtained in Experiments No. 5 and No. 6, respectively. The line width for liquid water is normally less than 5 Hz while the line width for polycrystalline ice is 56000 Hz (39). Therefore, the residual water is expected to have a mobility closer to ice than to liquid water. The wider line given by sample obtained in Experiment No. 6 seems to agree with the expectation that the water is more immobile at higher electrolyte concentration.

This study suggests a method for sample preparation to increase the concentration of bound water. By compressing the clay-water

slurry, most of the mobile water can be removed. The resulting sample should show more of the bound water characteristics. The use of NMR in studying this kind of sample could provide much insight into the subject.

Conclusions

Under the experimental conditions of this study, several conclusions can be drawn :

(1) Anion-free water determined by using a chloride ion electrode agrees well with data given in the literature. (2) A new equation has been proposed for the bound water calculation. (3) The mobility of the anion-free water was found to be affected by pressure, porosity and electrolyte concentration. (4) Compaction experiments indicated that the anion-free water will not move until all the bulk water has been removed. (5) It is possible to increase the ratio of bound water to bulk water in a sample through compaction experiment.

Acknowledgment

The author wishes to thank J.F. Huang and L.J. Chen for their assistance in this work. This research was supported by the National Science Council, R.O.C., grant number NSC 77-0402-E033-01. Special thanks are due to Mrs. Yuh-Shing Chang Wu for typing the manuscript.

Appendix I. Calculation of Anion-Free Water

	Bottle A	Bottle B
wt. of Glen Rose Shale, g.	33.1	42.6
wt. of added 0.200 M NaCl, g.	0	50.0
wt. of added distilled water, g.	49.8	0
Volume of added NaCl solution, ml	0	49.9
Volume of added distilled water, ml	49.9	0
Final concentration, Na ⁺ , M	0.0158	0.208
Cl ⁻ , M	0.0023	0.210

Let V_f = final volume of the solution, ml

material balance of Cl⁻ gives

$$0.210 V_f = 0.200 \times 49.9 + 0.0023 \times 49.9 \times \frac{42.6}{33.1}$$

$$V_f = 48.2 \text{ ml.}$$

$$\text{volume of anion-free water} = 49.9 - 48.2 = 1.7 \text{ ml.}$$

$$\text{wt. of anion-free water} = 1.7 \times 0.998 \times \frac{100}{42.6}$$

$$= 4.0 \text{ g/100 g rock.}$$

Carrying out the six step calculation listed in Ref. 2 gives the same answer.

Literature Cited

1. Clavier, C.; Coates, G.; Dumanoir, J. 52nd Annual Fall Tech. Conf. Soc. Pet. Eng. AIME, 1977, SPE paper No. 6859.
2. Hill, H.J.; Shirley, O.J.; Klein, G.E. The Log Analyst 1979, 3.
3. Juhasz, I. SPWLA 20th Annual Logging Sym., 1979.
4. Holditch, S.A. J. Pet. Tech. 1979, 1515.
5. Jones, F.O.; Owens, W.W. J. Pet. Tech. 1980, 1631.

6. Fertl, W.H.; Frost, E. Jr. J. Pet. Tech. 1980, 1641.
7. Low, P.E. Soil Sci. Soc. Am. J. 1980, 44, 667.
8. Branson, K.; Newman, A.C.D. Clay Minerals 1983, 18, 277.
9. Odom, J.W.; Low, P.F. Soil Sci. Soc. Am. J. 1983, 47, 1039.
10. Fripiat, J.; Cases, J.; Francois, M.; Letellier, M. J. Coll. Interface Sci. 1982, 89, 378.
11. Fripiat, J.; Letellier, M.; Levitz, P. Philos. Trans. R. Soc. London 1984, Ser. A., 311 (1517), 287.
12. Lipsicas, M.; Straley, C; Costanzo, P.M.; Giese, R.F. Jr. J. Coll. Interface Sci. 1985, 107, 221.
13. Giese, R.F. Jr.; Costanzo, P.M. ACS Sym. Ser. 1986, 323, 37.
14. Klinkenberg, L.J. in Drilling and Production Practice; Am.Pet. Inst., 1951, P.200.
15. Baptist, O.C.; Sweeney, S.A. Bur. Mines Report Inv. 5180, 1955.
16. Von Engelhardt, W.; Tunn, W.L.M. State Geological Survey Circular 194, 1955, Urbana, Illinois.
17. Grim, R.E. Clay Mineralogy; McGraw-Hill Co., 1953; pp. 161-183.
18. Martin, R.T. 9th National Conf. on Clays and Clay Minerals, 1962, p.28.
19. Woessner, D.E.; Snowden, B.S. Jr. J. Coll. Interface Sci. 1969, 30, 54.
20. Woessner, D.E. Proc. NMR Spectrosc. Pestic. Chem. Symposium, 1974, 279.
21. Woessner, D.E. Mol. Phys. 1977, 34, 899.
22. Slonimskaya, M.V.; Raitburd, Ts. M. Dokl. Akad. Nauk SSSR 1965, 162, 176.
23. Kitagawa, Y. Am. Mineral 1972, 57, 751.
24. Laughlin, L.J. U.S. Gov. Report Announce. Index 1979, 79, 111.
25. Matyash, I.V.; Litovchenko, A.S.; Vasilev, N.G. Kolloid Zhurnal 1974, 36, 531.
26. Kvlivdze, V.I.; Krasnushkin, A.V. Dokl. Phys. Chem. 1975, 222, 480.
27. Ananyan, A.A.; Golovanova, G.F.; Volkova, E.V. Merzlotnye Issled. 1976, 15, 182.
28. Dmitrenko, O.I. Kolloid Zhurnal 1957, 20, 157.
29. Schofield, R.K. Nature, 1947, 160, 408.
30. Bolt, G.H.; Warkentin, B.P. Kolloid Z. 1958, 156, 41.
31. Bolt, G.H. VI^e Congres International De La Science Du Sol 1956, Paris.
32. Darley, H.C.H. J. Pet.Tech. 1969, 883.
33. Mortland, M.M.; Mellor, J.L. Proc. Soil Sci. Soc. Am. 1954, 18, 363.
34. Bolt, G.H. Ph.D. Thesis, Cornell University, 1954.
35. Patchett, J.G. Trans. SPWLA 16th Annual Logging Symposium 1975, Paper V.
36. Kavanau, J.L. Water and Solute-Water Interactions; Holden-Day Inc., 1964, pp. 28-78.
37. Von Engelhardt, W.; Schindewolf, E. Kolloid Z. 1952, 127, 150.
38. Von Engelhardt, W.; Gaida, K.H. J. Sed. Petrology 1963, 33, 919.
39. Barnall, D.E.; Lowe, I.J. J. Chem. Phys. 1967, 46, 4808.

RECEIVED December 12, 1988

Chapter 34

Acid Wormholing in Carbonate Reservoirs

Validation of Experimental Growth Laws Through Field Data Interpretation

Olivier Liétard and Gérard Daccord

Dowell Schlumberger, BP 90, 42003 Saint-Etienne Cedex, France

Actual responses of two carbonate petroleum reservoirs to matrix injection of hydrochloric acid are compared with a recently proposed experimental model for wormholing. This model is shown to be applicable in undamaged primary porosity reservoirs, and should be useable in damaged double porosity ones. Formations of no primary porosity are shown to respond very differently.

The dissolution channels (wormholes), obtained under certain conditions of attack of carbonate rocks by hydrochloric acid, have been recently proven to have a fractal geometry. An equation was proposed, relating the increase of the equivalent wellbore radius (i.e. the decrease of the skin) to the amount of acid injected, in wellbore geometry and in undamaged primary porosity rocks. This equation is herein extended to damaged double porosity formations through minor modifications.

Two cases of initially undamaged reservoirs have been selected for proper validation of modeling equations. From pressure and rate data recorded all along their treatment, the skin variations during acid attack are derived according to a recently published methodology. Their analysis validates the proposed model. This would mean that wormholes in reservoirs do scale up with laboratory ones according to the proposed law.

One third of the world production of hydrocarbons originates from carbonate reservoirs, which, in addition, are supposed to contain half of the reserves of these compounds (1). The economical importance of such reservoirs is therefore large enough to justify the research of new methods aiming at better producing oil from these rocks.

Most of these reservoirs have natural permeabilities below 10 mD, and the stimulation of their production is achieved through acid fracturing operations. Viscosified hydrochloric acid is pumped into wells at pressures larger than formation parting pressure. Irregular etching of the fracture walls by the acid is expected to create highly

conductive channels which remain open to oil flow when the injection pressure is released and the fracture heals up.

Some carbonate reservoirs are naturally fairly permeable (more than 10 mD) and are not candidates for acid fracturing. Such a treatment would neither be technically feasible (large fluid loss rates would prevent fracture propagation) nor boost originally large productivities. However, wells drilled through such rocks usually demonstrate productions lower than one could expect according to their permeability. This is the consequence of the presence, around the wellbore, of a zone of reduced conductivity, referred to as damage. Many causes of damage have been recognized (2). In carbonate reservoirs, the most common ones are invasion by drilling muds and precipitation of scales or petroleum heavy ends due to the production pressure drop at wellbore.

The damaged zone has variable extension and severity, the latter being defined as the ratio of undamaged to damaged permeabilities, k_u and k_d respectively. This zone is responsible for an additional, large resistance to oil flow, dramatically impairing production. When initiating production by imposing a given pressure drawdown ΔP , part of the latter is lost through the damaged zone. This results in lower production rate Q and productivity index $Q/\Delta P$. The differential pressure through the damaged zone is given by:

$$\Delta P_d = \frac{\mu Q}{2\pi k_u h} S \tag{1}$$

where μ is the viscosity of the flowing fluid and h the height of the producing interval. The skin S is a coefficient representative of the characteristics of the damaged zone:

$$S = \int_{r_w}^{r_d} \left[\frac{k_u}{k(r)} - 1 \right] \frac{dr}{r} \tag{2}$$

where r_w is the wellbore radius, r_d the radial extension of the damaged zone, and $k(r)$ the permeability profile throughout it. When the severity is constant from r_w to r_d , Equation 2 reduces to (3):

$$S = \left(\frac{k_u}{k_d} - 1 \right) \log \left(\frac{r_d}{r_w} \right) \tag{3}$$

The aim of a matrix acidizing job, which, in carbonate reservoirs, generally consists in injecting plain hydrochloric acid at pressures below the formation parting pressure, is to decrease S down to zero. This operation is more often referred to as damage removal. It is not, strictly speaking, a reservoir stimulation, since it merely recovers the natural productivity index of the formation. In addition, the wording "damage removal", originating from similar operations in sandstone reservoirs, is not fitted to carbonate ones. It would be better to talk about "damage by-pass", since in carbonates the damaging materials are seldom soluble in hydrochloric acid, whereas the rock is.

Matrix acidizing jobs are inexpensive treatments, but their effect on well productivity is often spectacular, with common 5 to 20-fold increases of the productivity index. This one fact would justify devoting lots of effort in the understanding and the modeling of phenomena occurring while acidizing a carbonate reservoir. However, the particularly puzzling behavior of the acid in such rocks prevented progress to be made in this area despite numerous efforts and studies.

Acid Wormholing in Carbonate Rocks

When submitting a carbonate rock to the flow of an acidic solution, the attack, most of the time, leads to the preferential growth of large pores. The dissolution of the rock is not uniform, and the final pore size distribution is much broader than the original one. This fact has been recognized and described in detail more than fifteen years ago (4-5). Macroscopic pores, which are the end result of such an unstable attack, have received the name of wormholes.

It has been shown that the development of wormholes in carbonate rocks is a consequence of diffusion-limited (mass-transfer-limited) kinetics of attack (6). Such kinetics prevail in most of these rocks, i.e. limestones and dolomites, providing that, for the latter, the temperature is larger than about 200°F (90°C) (7-8).

The determination of the evolution of the permeability of these rocks during acidizing is necessary when attempting to predict the evolution of the skin (Equation 2). Previous studies (6) have tried to model the shift of the pore size distribution due to acid attack. Then, permeability profiles were computed by integrating the contributions to the overall flow of each of the rock pores, all over the considered volume of rock. The main limitation of this method lies in the disregarding of the spatial correlation between rock pores.

Another approach of the problem has been proposed recently (9). Based on a comprehensive experimental study, it considers that wormholes have an almost infinite conductivity in comparison with the original pores of the rock. Consequently, a fair approximation of the permeability profile of an acidized piece of rock of length L is a step function. From its inlet up to almost the tip of the wormholes, the permeability is infinite. In the rest of the rock, it is equal to the original one, i.e. k_0 , and the overall permeability of this core becomes:

$$k = k_0 \left[\frac{L}{L - L_e} \right] \quad (4)$$

where L_e , strictly speaking, is not the length of the largest wormhole, but an equivalent distance over which the permeability can reasonably be assumed to be infinite as compared to k_0 (10).

Similarly, in 3D-radial geometries of interest for petroleum engineers, an equivalent wellbore radius r_e is defined. The near-wellbore region, including radially distributed wormholes from r_w up to r_e , is infinitely permeable and therefore becomes a mere radial extension of the wellbore itself. Equation 2 can be used to calculate the pseudo-decrease of the skin when an undamaged primary porosity formation of permeability k_0 includes wormholes as described hereabove:

$$S = \int_{r_w}^{r_e} \left[\frac{k_0}{k(r)} - 1 \right] \frac{dr}{r} = -\log \left(\frac{r_e}{r_w} \right) \quad (5)$$

since $k(r) \rightarrow \infty \quad \forall r$ with $r_w \leq r \leq r_e$, and $k(r) = k_0 \quad \forall r > r_e$.

Therefore, the problem reduces to the definition of the relation linking r_e with the volume V of injected acid. In (9), the following equation was proposed for 3D-radial acid injection into an undamaged primary porosity reservoir:

$$\frac{r_e}{r_w} = \left[1 + A(N_{ac}, D, Q \dots) \times \left(\frac{V}{h}\right) \right]^{1/df}, \quad A(\dots) = \frac{bN_{ac}}{\pi\phi r_w^{df}} \left(\frac{Q}{Dh}\right)^{-1/3} \quad (6)$$

where A is a slowly varying function. Q , h , r_w , r_e and V are defined as before, ϕ is the initial rock porosity, and D is the diffusivity constant. df is the fractal dimension of the wormholing structure, experimentally determined as being equal to 1.6 ± 0.1 (11).

b is a constant that reflects the relative conductivity of wormholes compared with the rock permeability. It is equivalent to the constant B in (10), and was given a value of 1.7×10^4 S.I. units in (9). N_{ac} , the acid capacity number, is defined as in (12):

$$N_{ac} = \frac{\phi CM}{\beta(1 - \phi)\rho} \quad (7)$$

where C is the acid concentration, M the molar weight of the chemical species constituting the rock, ρ the density of the latter, and β the stoichiometric coefficient of the reaction (2 in the case of carbonate and hydrochloric acid).

One difficulty in Equation 6 lies in the determination of the diffusivity constant for highly concentrated acids over a broad range of temperature. However, available data (13), combined with viscosity values of hydrochloric acid, lead to estimates shown in Tables I and II for the field cases that will be described later on.

This wormholing model was shown to agree with previously published experimental data (14).

Extension to Damaged Double Porosity Reservoirs

Most of the carbonate reservoirs consist in thick layers of double porosity rocks. There are few limestones, such as chalks, that show primary porosity only (voids being intergranular spaces). On the other hand, there are also some deep dolomites of secondary porosity only: intergranular spaces have disappeared due to large overburden pressures and diagenetic recrystallization. Their secondary porosity consists in cracks, fissures, fractures, faults and vugs. The vast majority of carbonate reservoirs lie in between these two extremes. The main part of their permeability (50-500 mD) originates from a pattern of diagenetic and/or tectonic fissures (secondary porosity), whereas the permeability of a piece of rock containing no cracks is much lower, in the order of several milliDarcies.

In double porosity carbonate reservoirs, whatever the nature of the damaging materials, the damage is preferentially located in the secondary porosity, and its distribution seems fairly regular. Considering a thin slice of reservoir at a given depth, a good approximation of its permeability profile along any direction perpendicular to the wellbore axis is the following (Figure 1):

- from r_w to r_d , a crown of damaged rock wherein the original double-porosity-related permeability k_{DP} has been reduced to its sole primary porosity contribution k_{PP} , natural fissures being almost completely filled with and sealed by damaging materials (such as drilling mud cakes, for instance);

- from r_d up to the reservoir boundary, the permeability is constant and equal to k_{DP} .

It is likely that, in natural reservoirs, the extension r_d of

the damaged zone is not even all over the height of the producing interval. This is a consequence of variable conditions of hydrostatic head during drilling, or of variable pressure drawdown during production. For the sake of simplicity, however, we will here consider that r_d is constant.

Injecting acid in such an interval produces wormholes in the near-wellbore region, which is damaged, so that the acid flow only takes place in the clean primary porosity of the rock. This superposes to the original step function of the permeability profile a second, similar function, stating that the acidized profile now includes in the vicinity of the wellbore, from r_w up to r_e , a zone of infinite conductivity (Figure 1). Using Equation 2 again, it comes :

$$S = -\log\left(\frac{r_e}{r_w}\right) + \left(\frac{k_{DP}}{k_{PP}} - 1\right) \log\left(\frac{r_d}{r_e}\right) \quad \forall r_e \leq r_d \quad (8)$$

The initial skin S_0 of this reservoir was (Equation 3) :

$$S_0 = \left(\frac{k_{DP}}{k_{PP}} - 1\right) \log\left(\frac{r_d}{r_w}\right) \quad (9)$$

so that Equation 8 becomes :

$$S = S_0 - \frac{k_{DP}}{k_{PP}} \log\left(\frac{r_e}{r_w}\right) \quad \forall r_e \leq r_d \quad (10)$$

On the other hand, Equation 6 can be written :

$$\log\left(\frac{r_e}{r_w}\right) = \frac{1}{df} \log(1 + A'V) \quad , \quad A' = \frac{A}{h} \quad (11)$$

so that the skin value of this reservoir is related to the cumulative volume of acid V . It comes :

$$S(V) = S_0 - \frac{1}{df} \frac{k_{DP}}{k_{PP}} \log(1 + A'V) \quad \forall r_e \leq r_d \quad (12)$$

keeping in mind that the proportionality factor A' includes a porosity term which is the one related to the sole primary porosity (corresponding to k_{PP}).

When r_e becomes larger than r_d , a complete modification of the flow and attack conditions happens. Etching of the secondary-porosity fissures walls becomes the predominant phenomenon. Modeling equations established for wormholing propagation in primary porosity rocks most likely do not hold true anymore. However, at the time the wormholes tips reach the undamaged part of the reservoir, the treatment is virtually finished, its objective being already fulfilled. There is no need, consequently, to develop modeling equations for the rest of the treatment: a correct job design methodology would just aim at allowing the volume of acid necessary to achieve breakthrough, i.e. damage by-pass.

For undamaged primary porosity reservoirs, Equation 12 reduces to :

$$S(V) = -\frac{1}{df} \log(1 + A'V) \quad \forall V \quad (13)$$

Comparison with Actual Skin Histories during Acid Jobs

In damaged double porosity reservoirs, the influence of the fractal dimension df is masked by the severity ratio k_{DP}/k_{PP} (Equation 12).

Therefore, it has been chosen here to study very particular and rare treatments performed in undamaged reservoirs. Equation 13 is then applicable, and a direct access to the values of both parameters df and A' becomes possible. Two cases have been considered. First, a clean reservoir of secondary porosity only, where Equation 13 should not fit with actual data. Second, an undamaged, primary porosity formation, where it should.

Matrix acidizing treatments are more often performed, nowadays, with sensors and data acquisition systems continuously recording the surface pressure and rate histories. According to a recently proposed methodology (15), these records can be used to compute downhole rate and pressure evolutions. The bottomhole pressure history is then compared to the theoretical response of an equivalent reservoir wherein a non-reactive fluid would have been injected according to an identical rate schedule. Following this method, the difference between both theoretical and actual pressure responses originates from the evolution of the skin of the true reservoir under the influence of the acid attack. Equation 1 is then used to derive the skin decrease from this pressure difference.

Well A. This oil producer was to be converted into a water injector. Though its production period had been relatively smooth, with no sign of production damage build-up, the operator wanted to be sure to obtain a maximum injectivity index before initiating water injection. The well data and acid job main parameters are summarized in Table I.

Analyses of three rock samples from the pay zone show almost pure calcium carbonate (no magnesium) associated with traces of quartz, kaolinite and pyrite. Solubilities in hydrochloric acid range in between 94.6 and 97.5 %. Nitrogen permeabilities are below 1 mD, except for one sample containing a visible crack for which a permeability of about 10 mD was measured when submitting the sample to a minimum confining pressure. These laboratory data were obtained after the acid job was performed on this well. They show a formation having secondary porosity only, with an overall permeability that should amount several milliDarcies. Consequently, the skin history should not be interpretable according to the hereabove proposed modeling equations.

An injection/fall-off test was performed in this well, one hour and a half prior to the acid treatment. Two cubic meters (12.6 barrels) of water were injected during 14 minutes at an average rate of 1300 bpd. Then the pressure was recorded during 45 minutes. The fall-off data were interpreted on the basis of an homogeneous primary porosity reservoir, in the absence of suitable interpretation tools for naturally fissured formations. The derived values of the permeability, skin and wellbore storage coefficient are given in Table I. The negative pseudo-skin value, together with the large wellbore storage coefficient, are indicators of an undamaged fissured reservoir. The overall permeability is in line with laboratory data.

Then, 11 m³ (70 barrels) of 15 % HCl were pumped downhole through a coil tubing. The bottomhole pressure history is in this case precisely derived from surface data, since the latter are collected in the open annular space between the coil tubing and the casing. No computation of friction pressure drops all along the injection string is needed, which removes a major source of errors in the derivation of bottomhole data. The bottomhole pressure is just equal to the sum of the surface

Table I. Characteristics of Well A

Nature :	oil producer, to be converted to water injector
Deviated depth, mid-perforations :	6534 feet (1992 m)
Completion :	cased hole, perforation density 4 shots/foot
Wellbore radius :	3 inches (0.0762 m)
Formation height :	88.6 feet (27 m)
Bottom Hole Static Temperature (BHST) :	ca. 150°F (65°C)
Bottom Hole Static Pressure (BHSP) :	3000 psi
Formation fluid :	oil (viscosity not communicated)
Formation nature :	secondary porosity limestone
Reservoir porosity :	not communicated
Reservoir permeability :	14.1 mD
Initial skin value :	-2.6
Wellbore storage coefficient :	3.05×10^{-3} bbl/psi
Bottom Hole Injection Temperature :	ca. 115°F (45°C)
Average injection rate :	1400 bpd (2.57×10^{-3} m ³ .s ⁻¹)
Acid capacity number :	0.0121
Acid diffusivity :	2.3×10^{-9} m ² .s ⁻¹

one and of the hydrostatic head. Surface rate and bottomhole pressure histories are depicted in Figure 2.

The relative skin ($S - S_0$) evolution with respect to the cumulative acid volume is given in Figure 3 (solid line). Peaks at about 0.5 and 3.5 m³ are artifacts due to hammering effects following rapid variations of the injection rate. According to Equations 6 and 13, the skin evolution, if the formation were a primary porosity one, should be :

$$\Delta S = -0.625 \log(1 + 3.17 \times V) \quad (14)$$

with V expressed in cubic meters (dashed curve in Figure 3). We used $\phi = 0.13$, as if the permeability of this formation originated from primary porosity, and according to common relations between these two characteristics in carbonate rocks (16). Actually, the best fit to the skin curve of Well A is :

$$\Delta S_{AC} = -0.165 \log(1 + 21.1 \times V) \quad (15)$$

(dotted curve in Figure 3). There is a large discrepancy between these two equations, as evident in Figure 3. Not only the curvatures are different; the amplitudes are visibly not comparable.

The actual response of Well A to the injection of acid cannot fit with any kind of theoretical equation for undamaged primary porosity or damaged double porosity reservoir. Therefore, the acid attack in secondary porosity formations proceeds very differently, as expected.

Well B. Well B is an exploratory well in an oil bearing formation. Its characteristics are summarized in Table II. As common for exploratory wells, whose purpose is not economical, its perforation density is low. Only 163 perforations had been opened, the perforated intervals being regularly spaced all over the entire formation height. Most of the initial skin value originates from this low density.

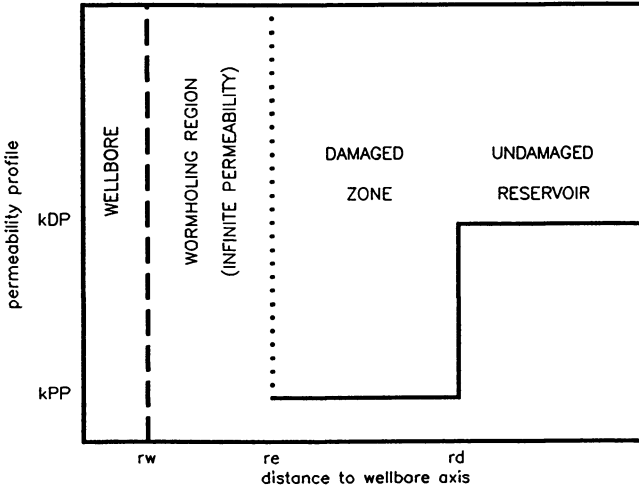


Figure 1 : Permeability profile in a damaged double porosity reservoir during acidizing. r_w : wellbore radius, r_e : wormholes penetration, r_d : damage radius, k_{DP} : undamaged reservoir permeability (total contribution of both primary and secondary porosities), k_{PP} : damaged permeability (primary porosity contribution only).

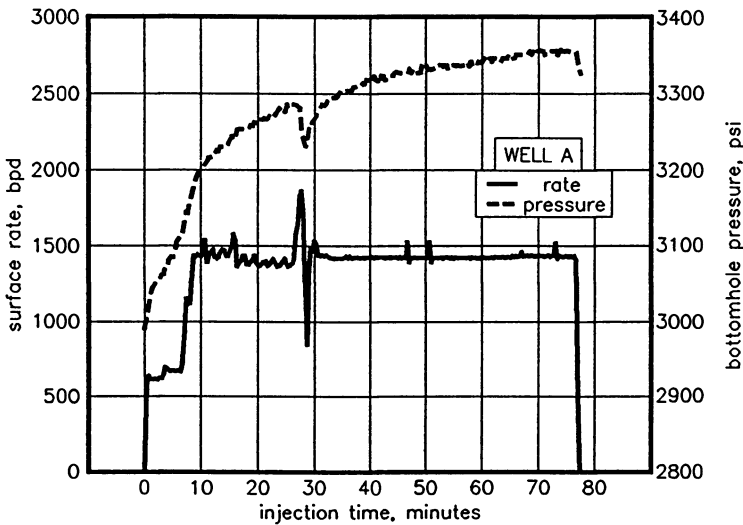


Figure 2 : Surface rate and bottomhole pressure evolutions during treatment of Well A.

Table II. Characteristics of Well B

Nature :	exploratory well
Deviated depth, mid-perforations :	13130 feet (4002 m)
Completion :	cased hole, perforation density 1 shot/foot
Wellbore radius :	3 inches (0.0762 m)
Formation height :	561 feet (171 m)
Bottom Hole Static Temperature (BHST) :	240°F (115°C)
Bottom Hole Static Pressure (BHSP) :	6100 psi
Formation fluid :	oil, viscosity 6.85 cps. at BHST
Formation nature :	mainly primary porosity, faulted
Reservoir porosity :	0.13 (estimate, according to (16))
Reservoir permeability :	16.4 mD
Initial skin value :	+3.3
Wellbore storage coefficient :	2.5×10^{-4} bbl/psi
Bottom Hole Injection Temperature :	ca. 170°F (75°C)
Average injection rate :	5200 bpd (9.56×10^{-3} m ³ .s ⁻¹)
Acid capacity number :	0.0121
Acid diffusivity :	3.2×10^{-9} m ² .s ⁻¹

Other wells in the same field had shown a limestone reservoir of fair permeability, with major tectonic faults and some associated fissures. Well data were provided by the operator. The low value of the wellbore storage demonstrates no coupling of the well with secondary porosity. However, the operator suspected the presence of some kind of fault not far from Well B, whose production test was unusual. He decided to acidize in an attempt to establish communication.

The original wellbore fluid was a sodium chloride brine. A 3500 meter-long coil tubing was lowered into the well, then most of the brine was displaced by 9.7 m³ (61 bbl) of 15 % HCl, in circulating while pulling out the coil. There remained 3.7 m³ (23 bbl) of brine at the bottom of the well. Then the wellbore fluids were squeezed into the formation by directly pumping 5.7 m³ of water then 12 m³ of 22 % HCl through the tubing. The surface rate and bottomhole pressure histories corresponding to this squeeze are given in Figure 4. The rest of the job is not provided, since ball sealers were then dropped into the well to divert the acid flow to low intake intervals. From this moment the skin curve is not interpretable anymore.

The skin history, given in Figure 5, shows six steps :

- Brine injection (negative values of the volume): the relative skin is constant (no attack) and nil, which confirms the formation data provided by the operator.
- 15 % HCl injection (0 - 5 m³): the arrival of the acid is clearly visible and the onset of the attack fairly rapid.
- The rest of the 15 % HCl injection (5 - 9.7 m³) shows a much more rapid skin decrease; this is interpreted as being the sign of the establishment of communication between the wellbore and some adjacent fissures by propagating wormholes.
- Water injection (9.7 - 15.4 m³), demonstrating a very erratic response at a more or less constant relative skin of -2.2.
- 22 % HCl stage (15.4 - 27.4 m³), resuming a very sharp decrease of the skin, whose absolute final value is equal to -3.2,

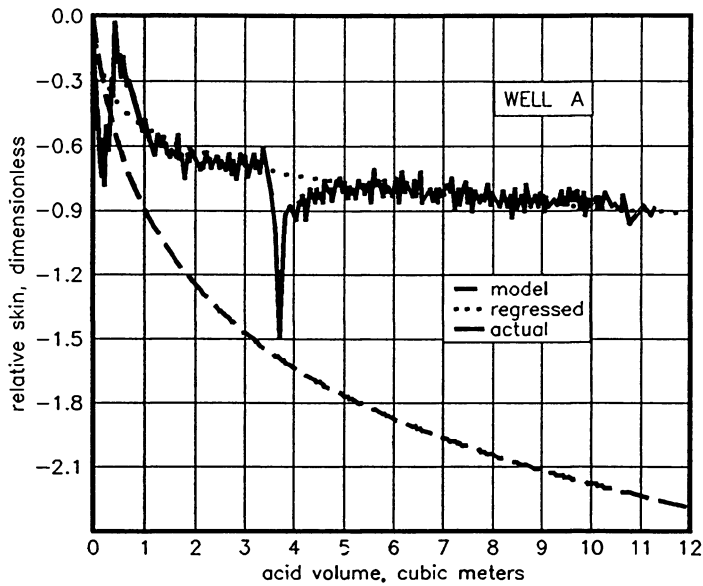


Figure 3 : Comparison of actual, regressed and model skin curves during treatment of Well A.

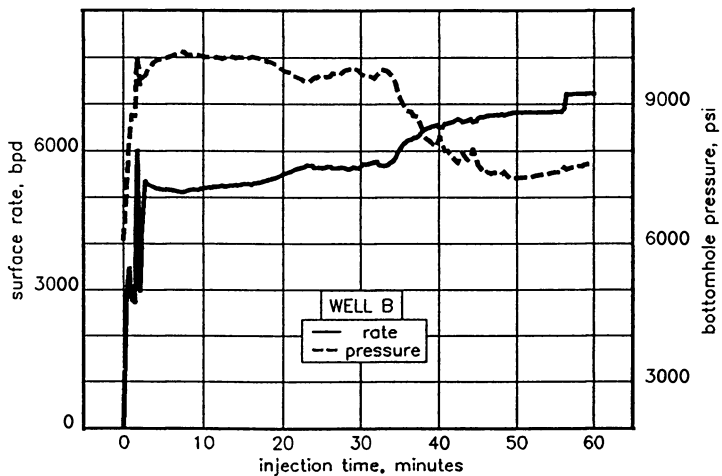


Figure 4 : Surface rate and bottomhole pressure evolutions during treatment of Well B.

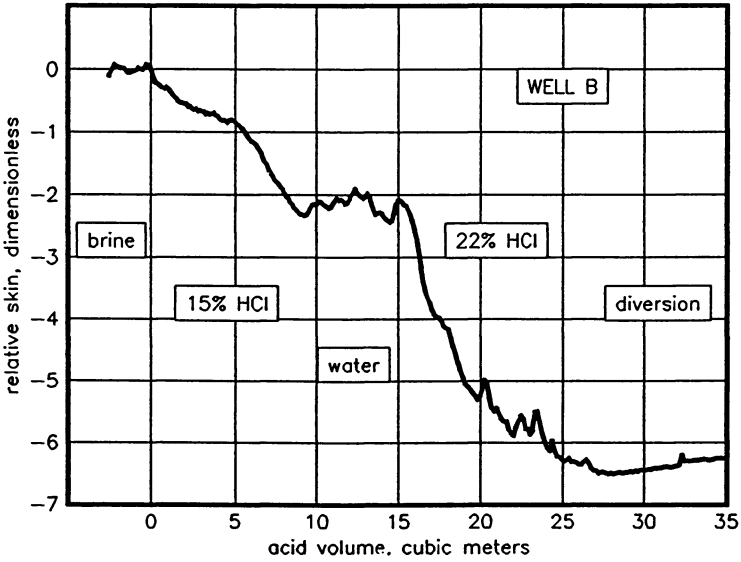


Figure 5 : Actual skin evolution during treatment of Well B.

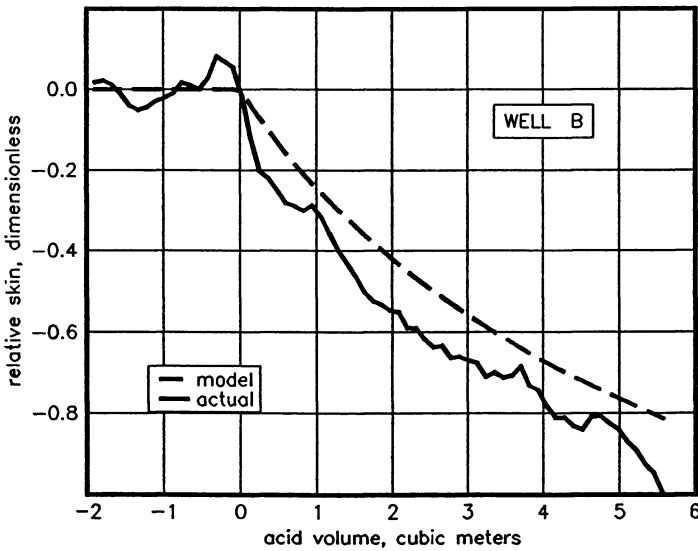


Figure 6 : Comparison of actual and model skin curves during wormholing of 15 % HCl (first acid stage of Well B treatment).

showing that the objective of the treatment was already apparently fulfilled. However, the flow equation used to derive these data are merely adapted to primary porosity reservoirs. Because communication has been established with some kind of secondary porosity, they are not applicable anymore, so that such negative values of the absolute skin have to be considered with extreme care.

- Onset of the diversion stage (27.4 m^3), with the skin now increasing due to the closure of some perforations by ball sealers (the rest of the curve would have shown that the relative skin value reached -2.5 at the end of the diversion stage).

Figure 6 is a scale-up of the first two steps of this skin history (solid curve), relevant to the present study. It corresponds to the injection of brine and 15 % HCl in the primary porosity zone surrounding the wellbore, before communication was established with adjacent fissures and/or faults.

Again, according to Equations 6 and 13, the theoretical response during the acid stage, if wormholing were to take place, would be :

$$\Delta S_{TH} = -0.625 \log(1 + 0.48 \times V) \quad (16)$$

The curve corresponding to this expression is given in Figure 6 (dashed). Though not perfect, the agreement between the two curves validates Equation 6. The best fit with actual data, when fixing $1/df$ equal to 0.625, would give $A' \simeq 0.65$. Such a discrepancy is acceptable, keeping in mind the imprecisions attached, on one hand, to flow equations in heterogeneous reservoirs, computations of friction pressure drops in tubings and, on the other hand, to the determination of treatment and reservoir data (mainly ϕ and D).

Conclusion

Because of the highly unstable nature of the acid attack in most of the carbonate reservoirs (propagation of wormholes), the development of a descriptive model of the skin evolution was not possible until the recent advent of the theory of fractals. In addition, the characteristics of the damaged zone greatly affect the behavior of the skin during acid injection in any type of reservoir, but particularly in carbonate ones. A correct validation of descriptive models stems from either the perfect description of the damage, or from its absence : hence the choice of the two described cases.

Two examples are certainly not sufficient for validating a model. However, some preliminary conclusions can already be drawn :

- the orders of magnitude are respected in the case of primary porosity reservoirs ; therefore the model could be used to describe unstable acid attacks in damaged primary and double porosity formations ;
- the fractal nature of wormholes, assessed by laboratory studies, seems to scale up at formation size according to the present model ;
- secondary porosity formations do not obey the proposed modeling equations, as was expected.

Literature Cited

1. Pettijohn F.J. Sedimentary Rocks; Harper and Row Publishers; 3rd Edition, 1975; chapter 10, 317.

2. Piot B.M.; Liétard O.M. In Reservoir Stimulation; Economides M.J. and Nolte K.G. Ed.; Schlumberger Educational Services, Houston, 1987; chapter 12, 'Nature of Formation Damage'.
3. Dake L.P. Fundamentals of Reservoir Engineering; Elsevier, 1978; chapter 5, 149.
4. Horton H.L.; Hendrickson A.R.; Crowe C.W. API Division of Production 1965, paper number 906-10-F.
5. Nierode D.E.; Williams B.B. SPE 1973, paper number 3101.
6. Schechter R.S.; Gidley J.L. AIChE J. 1969, 15, 3, 339-50.
7. Daccord G.; Lemaczyck R.Z. In Reservoir Stimulation; Economides M.J. and Nolte K.G. Ed.; Schlumberger Educational Services, Houston, 1987; chapter 13, 'Acidizing Physics'.
8. Lund K.; Fogler H.S. Chem. Eng. Sci. 1973, 28, 691-700.
9. Daccord G.; Touboul E.; Lenormand R. SPE 1987, paper number 16887, to appear in SPE Prod. Eng., February 1989.
10. Daccord G. Phys. Rev. Lett. 1987, 58, 479-82.
11. Daccord G.; Lenormand R. Nature 1987, 325, 41-3.
12. Lund K.; Fogler H.S. Chem. Eng. Sci. 1976, 31, 381-92.
13. Lund K.; Fogler H.S. Chem. Eng. Sci. 1975, 30, 825-35.
14. Hoefner M.L.; Fogler H.S. AIChE J. 1988, 34, 45-54.
15. Prouvost L.; Economides M.J. Pet. Sci. Eng. 1987, 1, 145-54.
16. Timmerman E.H. Practical Reservoir Engineering; PennWell Books, 1982; Vol. 1, 85.

RECEIVED December 12, 1988

Chapter 35

A Unique Source of Potassium for Drilling and Other Well Fluids

John T. Patton¹ and W. T. Corley²

¹Department of Chemical Engineering, New Mexico State University, Las Cruces, NM 88003

²Mayco Wellchem, Inc., 1525 North Post Oak Road, Houston, TX 77055

Laboratory and field tests of a clear well fluid, formulated with tetrapotassium pyrophosphate, TKPP, indicate increased productivity from inhibition of clay swelling, sloughing and dispersion. Adding small amounts of multivalent cations to TKPP fluids further suppresses clay-water interactions. TKPP completion fluids can be converted to superior drilling fluids by viscosifying with xanthan gum. Handling characteristics of TKPP solutions are superior to most other well fluids. They are not acidic, nontoxic and non-corrosive, a definite benefit for both rig personnel and the environment. They are compatible with most formation fluids, but will precipitate when mixed with spent acid. Unlike well fluids containing zinc and calcium, pH can be adjusted. TKPP is available to petroleum operators worldwide as free-flowing powder or a 60% wt. solution.

Since the invention of rotary rigs, used for drilling oil and gas wells, scientists have been searching for fluids that will both facilitate the drilling process and provide maximum productivity once the well is completed. There are two prime requisites for all well fluids. These are:

- (1) They must perform their required functions in a superior manner; e.g., completion fluids must balance the formation pressure and, thus, avoid the possible loss of the well due to blow-out. Drilling fluids should minimize the cost of making hole.
- (2) Filtrate lost to the formation or particulates deposited in oil flow passages must not impair a well's flow potential when the well is returned to operation.

The most sensitive test for identifying damage characteristic of a well fluid involves flowing the well fluid through a reservoir core. For fluids containing particulates, it is necessary to test both the whole fluid and the filtrate

in order to assess the total damage potential and identify the mechanisms responsible.

Clay minerals, inevitably present in a petroleum formation, are sensitive to the type and concentration of ions contained in the well fluid filtrate lost to the reservoir. This sensitivity is demonstrated by a reduction in the permeability caused by the well fluid filtrate flowing through the core under investigation.

Clays have the capacity to exchange ions with well fluids. When calcium ions, incorporated in the clay matrix, are exchanged for sodium or even potassium ions, clays can swell and/or become dispersed in the fluid. This mechanism significantly reduces permeability, i.e., causes large productivity damage^[1,2]. The equilibrium concentration of the various ions strongly favors the adsorption of multivalent ions by the clay minerals. For this reason, it is possible to counteract the swelling effect of well fluids on clays by the addition of small amounts of polyvalent ions. Calcium is by far the most effective, but the least soluble in the presence of other salts. Magnesium has been found to be advantageous and also synergistic when used in conjunction with calcium ions. Fluids containing divalent ions usually cause less permeability damage in petroleum reservoir cores.

A second cause of reduced productivity is mechanical blockage. When the well fluid contains particulates, damage occurs when the solids become tightly wedged in the tiny interstices through which oil flows. This damage, which can be so severe as to render a well uneconomic, has prompted many investigators to regard particulate blocking as the prime cause of productivity impairment^[3,4]. The now popular "clear" well fluids were introduced to avoid particulate damage. These fluids are often viscosified to minimize leak-off^[5].

Both field and laboratory results indicate that formation damage can only be minimized through the selection of well fluids whose chemical composition is formulated to avoid both fluid and particulate damage. This objective has been difficult if not impossible to achieve with current well fluid additives. Recognition of the chemistry required to formulate such a nondamaging well fluid is not in itself sufficient to prevent damage. Kruger has observed that strict quality control of a fluid's physical and chemical properties, especially during the completion process, is essential. In addition, damage can be further minimized through the use of clean pipe and continuous circulation and filtration of the fluid being used in the well operation^[6].

What has long been sought and badly needed is a soluble weighting agent less corrosive than, and equally non-damaging as, the popular calcium and zinc halides. Preliminary laboratory and field data indicate TKPP may be the solution.

Work by Jones identified the desirability of incorporating TKPP as a scale inhibitor for packer fluids^[7]. Subsequent work by Siskorski identified TKPP's superior properties in a blend for preparing high density, clear well fluids^[8]. TKPP has long been recognized as a builder for liquid detergents. The fact that detergency is not a requisite property of a superior well fluid probably obscured excellent petroleum applications until now. This paper

addresses the opportunities that exist for preparing improved well fluids, especially for wide application in drilling, based on TKPP.

GENERAL:

TKPP ($K_4P_2O_7$) is a merchant chemical produced by many major companies throughout the world. It is available commercially as a free flowing, white, granular solid or as a 60% wt. solution. In addition to its widespread use in the liquid detergent formulations, TKPP is also utilized in the food industry. It has been certified by the U. S. Department of Transportation as nontoxic. The solubility of TKPP in water at 60°F is shown in Table I. It is possible to achieve increased density at temperatures above 60°F because of increased solubility.

Table I. Concentration - Density of TKPP Solutions

Density lb/gal @ 16°C	TKPP Wt %	Concentration lb/bbl
9.0	8.7	33
9.6	16	64
10.7	28	126
12.0	41	206
14.0	57	335
15.2 (Solubility limit)	66	422

DAMAGE ASSESSMENT; CORE TESTS:

Tests were run to compare conventional completion fluids, i.e., those containing calcium, zinc, and potassium salts. Each well fluid was passed through a five micron filter and then flowed through a fresh Berea sandstone core having a brine permeability of approximately 800 md. Prior to testing a well fluid, the core's initial permeability had been established by flowing a filtered reservoir brine through the core. The damage imparted by a filtered well fluid was determined by noting the decrease effected in the core's permeability compared to its initial permeability.

The results, shown in Table II, quantify the adverse effect of common well fluid ions on permeability. Especially relevant are the data indicating that even calcium chloride/calcium bromide fluids cause some permeability reduction, although the cause of the adverse interaction is obscure.

With the exception of saturated zinc bromide, all of the fluids tested minimized permeability damage relative to fresh water which reduced permeability an average of 54% for three cores.

Table II. Formation Damage Effected by Clear Well Fluids

Fluid Type	Ion Conc., wt. %				Core Perm., md Damage		
	K	Ca	Mg	Zn	Init.	Final	%
TKPP +	3.8	.04	.41	—	874	844	3
TKPP	3.8	—	—	—	837	718	14
TKPP+	11.3	.04	.41	—	874	738	16
CaCl ₂ /CaBr ₂	—	.16	—	—	711	583	18
KCl	1.6	—	—	—	794	625	22
TKPP	11.3	—	—	—	837	580	32
CaCl ₂ /CaBr ₂	—	.10	—	—	855	581	32
KCl	5.2	—	—	—	794	531	33
KCl	11.3	—	—	—	794	381	52
ZnBr ₂	—	—	—	.22	673	34	95

Although potassium chloride fluids performed better than the calcium and zinc halides, damage was still measurable. These results, confirmed in triplicate, were unexpected since it is well accepted that even 0.5 weight % KCl should protect Berea cores against permeability damage. The most plausible explanation lies in variation between the test procedures.

The formation brine used to establish the core's initial permeability contained 2.7% total dissolved solids, TDS, with a monovalent-divalent (calcium) ratio of 30. Once a core is equilibrated with this brine, any increase in the ratio or drastic decrease in TDS has the potential for decreasing permeability. Obviously fresh water represents a significant decrease in TDS and, hence, the 54% permeability damage. Adding KCl helps overcome the decreased salinity but, in so doing, increases the ionic ratio resulting in still measurable but usually reduced permeability damage.

Even very small amounts of calcium provide a desirable decrease in the Na/Ca ratio. Prior studies indicating potassium chloride totally negates permeability reduction may have utilized water that contained some small amount of calcium ion to measure KCl solution permeability. A second factor, which might explain the lack of KCl damage reported in prior studies is a low ionic concentration, especially calcium, in the water used to equilibrate the cores prior to the KCl tests.

Increasing KCl concentration lowers inhibition as shown in Table II. The fact that damage increased with KCl concentration is consistent with the ionic ratio hypothesis and suggests a base exchange mechanism whereby calcium ions are more easily extracted from the clay and replaced by potassium ions as the potassium concentration increases.

Similar tests were performed with 10% and 20% by weight aqueous solutions of TKPP having approximately the same potassium ion concentration

as the KCl tests. Damage, although measurable, was reduced, indicating for the first time that an anion, in this case pyrophosphate, can contribute to reducing permeability damage.

The damage potential of TKPP fluids was further reduced by the addition of multivalent cations. When these salts were added at approximately their solubility limit in TKPP solutions, damage decreased, lending additional credence to the observation that the addition potassium ions alone is not sufficient to completely eliminate formation damage.

The severe interaction of the zinc bromide fluid, 19.2 ppg (2.32 g/cc), was unexpected. Severe plugging of the core occurred, caused by precipitation of zinc hydroxide, as the injected solution mixed with and was neutralized by formation brine. Tests in which the zinc bromide fluid was simply titrated with distilled water also produced a precipitate, 0.0036 g/cc. Titration in the presence of the common reservoir clay, montmorillonite, increased both the rate of precipitation, and total quantity to 0.03 g/cc.

At the conclusion of a few selected damage tests, an additional experiment was performed in which solutions containing 10% TKPP, 0.1% calcium chloride, and 0.4% magnesium chloride were pumped through the damaged cores. In each instance, the permeability of the core recovered dramatically, as shown in Figure 1.

DAMAGE ASSESSMENT; CLAY SWELLING:

Tests were conducted to determine the effect of TKPP solutions on the hydration and dispersion tendencies of clay particles. The test involved immersing a standard bentonite Volclay pellet in the solutions of TKPP and observing the degree of disintegration as a function of time. Comparable tests were also conducted using fresh water, halide completion fluids, and diesel oil for comparative purposes. TKPP solutions having densities ranging from ten to fifteen pounds per gallon, ppg, were tested to define the effect of TKPP concentration on clay inhibition. These tests indicate that TKPP, when used at higher solution densities, can inhibit the hydration and disintegration of water-sensitive clays almost completely. When used in conjunction with polyvalent cations, inhibition is evident at concentrations as low as 75 ppb (0.21 g/cc). Even at this low concentration the inhibitive character of the fluid is much superior to that of the calcium bromide and zinc bromide clear completion fluids. This can be seen from the data shown in Table III.

Publication Date: July 10, 1989 | doi: 10.1021/bk-1989-0396.ch035

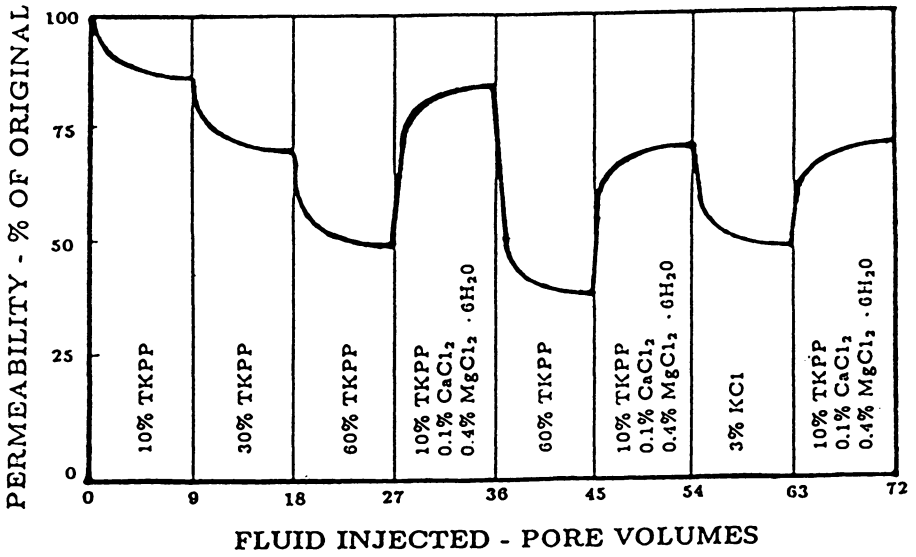


Figure 1. Composition and Concentration Effects of Potassium Based Clear Well Fluids on Core Permeabilities.

Table III. Clay Disintegration Due to Fluid Interaction

Time, Minutes	Well Fluid Properties	Disintegration State of Volclay Tablet					
		Conventional			Tetrapotassium Pyrophosphate		
	Salt Type K ⁺ , ppm. Density, ppg.	CaBr ₂ 0 14.2	ZnBr ₂ 0 19.2	KCl 127,000 9.7	TKPP* 81,000 9.7	TKPP* 128,400 10.6	TKPP* 176,000 11.6
0.5		2	2	2	1	1	1
1.0		3	2	2	1	1	1
5.0		3	3	3	2	2	1
10.0		3	3	3	2	2	1
14.0		3	3	3	3	2	1
18.0		3	3	3	3	3	1
30.0		3	3	3	3	3	2

1 - No Visible Effect 2 - Cracks/Sloughing 3 - Complete Disintegration

*TKPP solutions contain 0.21% CaCl₂ and 0.65% MgCl₂

At solution densities of 13 ppg and above, the TKPP virtually eliminates any hydration and disintegration effects an aqueous fluid might have on water-sensitive clays. In this concentration range, the results of TKPP plus polyvalent cations are comparable to those obtained with a non-aqueous fluid such as diesel oil. However, as evidenced by the permeability regain effects noted in damaged sandstone cores, TKPP solutions invading the producing formation adjacent to the well bore might have the capacity to actually remove damage whereas the diesel oil has no ability to restore permeability in a similar manner. If so, the responsible mechanism would be the dehydration and subsequent shrinking of clays by the highly structured, concentrated TKPP solution.

TKPP IN DRILLING FLUIDS:

The long-recognized ability of potassium ions to minimize the swelling and disintegration of water-sensitive clays would infer that TKPP should be a desirable additive for drilling fluids^[9]. Current practice is to formulate drilling fluids with KCl or KOH to supply the required potassium ion concentration. However, both chemicals generate problems that are often expensive to overcome. Potassium hydroxide is little used because of the high pH (above 12.0) and loss of desirable mud properties when enough is added to supply the requisite amount of potassium ion. It is good practice to avoid pH's above 11.5

because of danger to rig crews, increased problems in controlling shale sloughing or clay swelling and difficulty in maintaining acceptable mud rheology. Therefore, the use of KOH is generally limited to pH control for KCl muds.

There are two major problems associated with adding KCl to a drilling fluid. First, the corrosivity of the fluid is increased, often several fold^[10]. The increased corrosion of drill pipe, drill collars, bits, and pumps can be a significant expense.

Of even more economic importance is the rheological impact of the addition of KCl to conventional water-base drilling fluids. KCl causes undesirable increases in both yield point and gel strength that can only be eliminated by chemical disperants or by dilution with fresh water. Dilution in turn requires more KCl for clay inhibition, and the cycle continues with mud costs escalating exponentially.

Tests were conducted to compare the effect of KCl and TKPP on the rheology of an unweighted (nondispersed) and a weighted (dispersed) drilling fluid. All fluids were mixed in an industry standard Hamilton Beach mixer. The rheology of each fluid was then measured in a Fann viscometer at 120°F at 300 rpm and 600 rpm.

The results of these tests and the fluid formulations are shown in Table IV. The adverse effect on fluid rheology of adding potassium, KCl, Test B, and TKPP, Test C, is evident. Both salts cause increases in yield point, YP, and initial gel strength. TKPP produced only about half as much increase as did KCl and can be added in much higher concentrations before the rheological properties of the drilling mud become unacceptable.

Similar results were obtained with a barite-weighted, dispersed drilling mud. The base fluid, Test D, has acceptable rheology; however, the addition of only 10 ppb of KCl, Test E, elevated the yield point and initial gel to unacceptable levels. Although the addition of TKPP, Test F, caused increases in both YP and gel, they were only about 75% as great, as increases caused by KCl. This reduced adverse effect translates into a significant reduction in mud costs, as detailed in the results of actual drilling in experimental wells. The decrease in plastic viscosity for the weighted system, Test F, is beneficial. It indicates an increased pseudoplasticity that, in practice, will provide better hole cleaning and more horsepower available at the bit during drilling operations.

When suitably viscosified, TKPP solutions become superior low solids drilling fluids. Many water-soluble polymers were tested to identify satisfactory viscosifiers. Most commercially available polymers were found to be insoluble in TKPP solutions at densities above 11 ppg. Only xanthan gum

Table IV. Effect of Potassium Salts on Conventional Drilling Muds

<u>Composition/Property</u>	<u>A</u>	<u>B</u>	<u>C</u>	<u>D</u>	<u>E</u>	<u>F</u>
Concentration, ppb						
Gel	15	15	15	15	15	15
Drill Solids	30	30	30	30	30	30
Chrome lignosulfonates	0	0	0	6	6	6
K Lignite	0	0	0	3	3	3
Barite	0	0	0	216	216	216
KCl	0	11	0	0	10	0
TKPP	0	0	11	0	0	10
Weight, ppb	9.0	9.0	9.0	12.0	12.0	12.0
Plastic Vis., cp	7	4	5	17	17	15
YP, lbs/100 ft ²	6	23	11	4	54	39
Initial Gel lbs/100 ft ²	2	10	6	2	42	30

exhibited enough solubility to be useful in viscosifying TKPP solutions up to 14.5 ppb. This common drilling polymer is available in both powder and liquid form in the oil field. Its use is well known and does not require any special techniques or mixing equipment.

A series of TKPP solutions were prepared; varying in weight from 10 to 12 ppb, these were viscosified with 2 ppb of Kelzan XC, a commercial xanthan drilling product. The rheological properties were measured at 120°F using a standard Fann Viscometer. Table V summarizes the rheological properties of the solutions so prepared. It was found that hydration of xanthan is retarded by high concentrations of TKPP. When preparing solutions having a density above 12 ppb, it is advisable to hydrate the xanthan in relatively fresh water first. After the xanthan is completely hydrated, granular TKPP can be added to achieve the desired solution density. The presence of the xanthan does not retard the rapid dissolution of the TKPP.

Table V. Rheology of TKPP - Xanthan Drilling Muds

TKPP Conc. ppb	Wt%	Density		Apparent Visc., cp	Plastic Visc., cp	Yield Point lb/100 Ft. ²
		ppb	g/cc			
0	0	8.33	1.00	15.5	6	19
86	20	10	1.20	26.5	7	23
145	31	11	1.32	31	10	26
206	41	12	1.44	42.5	19	33

There may be instances where a high concentration of TKPP is required to inhibit clay hydration, but a lower density or higher lubricity is desired. This can be achieved by emulsifying diesel or mineral oil in a TKPP solution viscosified with xanthan. Emulsion of oil in TKPP solutions can be achieved with a viscosifier such as xanthan alone although it is usually desirable to add a surfactant to improve stability. Many different surfactant structures were tested for suitability as an emulsifying agent for oil in TKPP solutions. The best additive identified is a phosphate ester surfactant, Pluradyne OF-90, manufactured by BASF Wyandotte. This material has been tested in the past for improving producing well productivity by reversing clay swelling and mitigating paraffin deposition problems.

A TKPP solution having a density of 12 ppg was formulated by dissolving 1.5g of Kelco's KOD-85, a finely ground commercial xanthan gum product, in 299 cc tap water by mixing at high speed for 5 minutes in a standard Hamilton Beach mud mixer. 206 g of TKPP, followed by 18 ml of diesel oil, was then added and the viscosified solution blended for an additional 5 minutes with a Hamilton Beach mixer. A smooth, water-continuous emulsion formed immediately that contained a small amount of entrained air. One percent of BASF Pluradyne OF-90 was added to the emulsion and blended for an additional 5 minutes. The resulting fluid was a smooth, creamy, drilling fluid containing finely dispersed air bubbles which broke out slowly. After standing overnight, the fluid was a homogeneous, water-containing emulsion containing no entrained air. Fluid rheology measured at room temperature in a Fann Viscometer. produced the following results:

Apparent vis.=18.5 cp, Plastic vis.=13.0 cp, Yield point=11 lb/100 ft.²
These values are characteristic of a superior, low-solids, drilling fluid that promotes a high drilling rate and good solids removal. In addition, maximum inhibition of hydrating clays is provided.

DRILLING FIELD TEST

Two wells were drilled in Frio County, Texas, using TKPP for clay/shale inhibition. They were compared to three wells that had just been finished in the same field, to the same depths, using the same rig and crews; all three using a KCl/polymer drilling fluid. The KCl polymer wells experienced numerous hole problems including balling, stuck pipe, poor hole cleaning (gel sweeps were necessary), high torque, drag, and washout. The average mud cost for these KCl polymer wells was \$45,276. Two wells, drilled using TKPP and polymer, experienced no hole problems. The average mud cost for the two wells was \$13,952, a 69% cost reduction in mud alone. Dollar savings on rig time were even more significant. The new additive was used on six wells in

Lavaca County, Texas. Once again, the wells were free of the hole problems experienced in preceding offset wells.

COMPATIBILITY OF TKPP SOLUTIONS:

Solutions of TKPP were mixed with aqueous fluids commonly encountered in drilling or completion of wells. Unlike saturated zinc bromide, concentrated TKPP solutions can be mixed in any proportion with fresh water with the only result being a decrease in solution density. Similar results were obtained with conventional oil field brines containing as much as 400 parts per million polyvalent cations, mostly calcium. Saturated solutions of calcium hydroxide also can be added to TKPP in any proportion without promoting precipitation as can concentrated hydrochloric acid solutions, conventionally used for well stimulation. The acid tends to generate a slight haze as the pH is reduced from 11.5 to approximately 8; however, this haze rapidly disappears as the pH is lowered by further addition of acid.

The only fluid, common to oil field operations, that has a significant interaction with TKPP solutions was concentrated calcium chloride. Solutions of calcium chloride, spent acid, are generated during the acidization of a limestone or a dolomite formation. When solutions containing 10% calcium chloride were mixed in equal proportions with 14.5 ppg TKPP solutions, massive precipitation occurred. Similar precipitation was observed with oil field brines having calcium concentrations above 400 ppm.

In normal operations, there is little chance for spent acid to contact the completion fluid as the well will usually be produced after perforation, effecting the removal of completion fluid prior to acidization. The fact that a calcium precipitation reaction can occur should be recognized by those using TKPP solutions as a clear completion fluid in well operations. A KCl spacer is recommended to avoid completion problems in formations having high calcium brines.

Not only should well fluids be compatible with reservoir fluids and minerals, but they must also be stable at surface conditions. One disadvantage of conventional halide fluids is their tendency to crystallize at ambient temperatures. Solutions containing varying amounts of TKPP were exposed to constant temperatures as low as -76°F (-60°C) for a period of 30 hours. No crystallization was observed at any temperature above 36°F (2°C) even at concentrations as high as 60% by weight. At low fluid densities, less than 11.7 ppg, there is no evidence of TKPP crystallization even at temperatures as low as 30°F (-1°C), the freezing point of most fresh water drilling fluids.

The addition of TKPP lowers the freezing point of the fluid significantly. This offers the opportunity of using a subfreezing TKPP mud to drill through strata, i.e., the permafrost in Alaska and Canada, without thawing of the

formation. Problems in stability of the drilled hole as well as the rig foundation could thus be minimized.

WELL LOGGING:

Another advantage, unique to using TKPP in drilling fluids, would be its contribution to more accurate log interpretation. The popular neutron lifetime logs respond to the presence of chloride ions in the formation pore space. The addition of TKPP does not add any chloride ions, and the drilling fluid reacts to neutron logs much like conventional fresh water muds. The contrast in log response between TKPP and chloride fluids is also useful in the potential log-inject log procedure for determining porosity and oil saturations. As experience is gained in logging wells drilled with TKPP drilling fluids, additional benefits may become apparent.

CORROSION:

One property of drilling fluids that has received only minimal attention in the past is corrosiveness imparted by various additives. Additives improve the requisite properties of well fluid substantially; and, hence, increase in corrosiveness is usually ignored.

This is particularly true with respect to drilling fluids containing potassium chloride to inhibit shale hydration. In 1974 Bodine, et al., recognized the potential of the phosphate ion to combat the increased corrosion rate produced by potassium chloride^[11]. Accelerated corrosion is especially severe at the elevated temperatures now being encountered in deep wells and geothermal reservoirs. In most systems, phosphate corrosion inhibition is enhanced in solutions containing oxygen^[12]. All drilling fluids are constantly aerated; and, hence, it should be no surprise to find TKPP-based fluids with reduced corrosion rates one or more orders of magnitude lower than fluids containing the same amount of potassium ion introduced by the addition of potassium chloride.

Radenti et al. reported the corrosion rate of a typical potassium chloride fluid of 247 mils/year at 212°F. In contrast, they found by substituting potassium carbonate for potassium chloride, the corrosion rate was reduced to 3 mils/year^[10]. Unfortunately, potassium carbonate is not optimum as a drilling fluid additive because it can produce massive amounts of calcium precipitation, may elevate the pH to undesirable levels, and in all cases reduces the calcium ion concentration to such a low level as to promote destabilizing cation exchange with clay minerals.

Corrosion rates for TKPP solutions measured at 194°F were low, 2 mils/year. Data at 400°F are equally impressive, 14 mils/year for 1020 steel

coupons exposed to 14.5 ppg TKPP solutions for 60 days. Of special significance is the fact that TKPP reacts with steel to form a protective coating of potassium iron pyrophosphate. This coating protects the steel surface, and corrosion rates after 60 days were less than 2 mils/year even at 400°F.

Although the importance of considering corrosion in the formulation of a drilling fluid is of secondary importance for shallow wells, the effect is still unmistakable. As drilling continues to deeper, hotter horizons, the more expensive rigs and tubular goods, such as those utilized in offshore operations, magnify the importance of considering corrosion in formulating an optimum drilling mud.

Paralleling the corrosion problem is one involving compatibility of any well fluid with nonmetallic materials used in well completion apparatus. All injection wells and many producing wells are equipped with packers to isolate the casing annulus from the high temperature, pressure, and salinity characteristic of the petroleum reservoir environment. Conventional packers, as well as other well tools, utilize elastomeric materials to mechanically seal appropriate locations.

At the request of an international petroleum company, a major manufacturer and supplier of down-hole equipment performed tests of the various elastomers commonly used in the construction of packers and other oil field tools. Seven of the nine most commonly used thermoplastic materials were found to be completely inert to TKPP solutions. The test included continual immersion in saturated TKPP for 21 days at 280°F. Only two elastomers, Viton and Fluorel, showed any adverse reaction. O-rings made from these two elastomers showed minor cracking at the termination of the test. A listing of the elastomers that tested inert to TKPP solutions include nitrile, saturated nitrile (HNBR), Aflas, Kalrez, PEEK, Glass-filled Teflon, and Ryton. Several of these elastomers are attacked or degraded by conventional clear completion fluids containing calcium and zinc halides. The inertness of commonly employed elastomers to TKPP is an important advantage for TKPP fluids in normal operations.

ENVIRONMENTAL CONSIDERATIONS:

Governmental regulations relative to acceptable environmental practices have multiplied many fold in recent years. The impetus for these new regulations comes from an increased awareness and public concern for the value of maintaining the existing quality of our environment. There are many additives for well fluids, now being phased out, which were adopted without adequate regard for the effect accidental spills and disposal operations might have on fish and other forms of wildlife.

An example of some of the newer regulations is the restriction against the use of the popular mud dispersant, chrome lignosulfonate. It is expected that this regulation is merely the initial step toward ruling out the use of all heavy metal salts commonly employed in the formulation of well fluids because of their toxicity to aquatic life and humans. This means that the use of zinc and lead, in addition to chromium, may not be allowed in the future. At least one major oil company has already taken steps in this direction by ruling out the use of heavy metal salts in any well fluid in their worldwide operations.

Although at high concentration, TKPP is toxic to fish and shrimp. When diluted, 500-1000 PPM, it is non-toxic and expected to be both environmentally acceptable and of low risk to humans. The widespread use of TKPP in detergent formulations supports this expectation. It is listed by the U. S. Department of Transportation as a nontoxic substance relative to shipping regulations.

CONCLUSIONS:

Solutions of TKPP have been shown to have unique and advantageous properties for use in formulating a wide variety of well fluids. Its reasonable cost, worldwide availability, and nontoxic properties make it a preferred additive for use in many petroleum applications. It has been shown to be a most effective salt with respect to inhibiting hydration and swelling of clay minerals commonly encountered in drilling operations and/or reservoirs. Avoiding clay problems is the major impetus for the incorporation of potassium ions in well fluids, and the use of TKPP provides advantages over and above those available from other potassium salts.

The use of TKPP solutions as drilling fluids for clay inhibition and increased density appears to be the prime application, at least initially. Excellent rheology and fluid loss is obtained by viscosifying with xanthan. Higher density, above 15 ppg, can be achieved by incorporating finely ground weighting agents, such as barite or hematite, in the drilling fluid. As a source of potassium ions, the addition of TKPP to a conventional drilling fluid for clay control has been shown to produce less of an adverse effect on rheology than the addition of a comparable amount of potassium chloride.

Perforating fluids are conventionally prepared with soluble salts for weighting and usually filtered to avoid formation damage. Many operators perforate with the hydrostatic pressure slightly below the expected formation pressure (under balanced) to eliminate fluid loss and subsequent formation damage after the well is perforated. The nondamaging character of TKPP perforating fluids reduces the need for under balance and provides a higher degree of safety in perforation operations.

Gravel pack completions involve placing an annular layer of gravel between the liner and the producing formation. The gravel is carried into the annular space, suspended in a clear fluid, usually viscosified with hydroxyethylcellulose (HEC). Much of the carrying fluid is lost, often purposely, to the formation and, hence, should be formulated to be nondamaging. Solutions of TKPP viscosified with xanthan are outstanding in this respect. HEC cannot be used with high concentrations of TKPP.

Packer fluids are used to provide hydrostatic balance to partially offset the reservoir pressure and eliminate a large pressure differential across the packer element. TKPP solutions more than meet the requirements of being noncorrosive, nondestructive to elastomers, variable in density, and stable for many years. It is desirable to perforate with a well bore filled with packer fluid so that the packer can be set and the well produced as soon as the perforation operation is complete. Since TKPP solutions make superior perforation fluids, their dual use as a packer fluid is further enhanced.

Work-over fluids are used routinely to kill wells for remedial operations, wash-out fill, or provide a safe environment for special logging or other well diagnostic procedures. In such operations it is often necessary to store the work-over fluid in tanks at the well site. TKPP solutions are stable even at sub-freezing temperatures, which provides a distinct advantage over solutions of halide salts that sometimes crystallize at ambient conditions encountered in rig operation. The avoidance of a crystallization problem coupled with the noncorrosive nature of TKPP work-over fluids makes them attractive with respect to other clear work-over fluids now popular in the industry.

LITERATURE CITED:

1. Jones, F.O., Jr. *J. Pet. Tech.* April 1964, 441-446.
2. Mungan, N. "Permeability Reduction through Changes in pH and Salinity," *J. Pet. Tech.* Dec. 1965, 1449-1453.
3. Glenn, E.E.; Slusser, M.L. *J. Pet. Tech.* May 1957, 132-39.
4. Tuttle, R.N.; Barkman, J.H. *J. Pet. Tech.* Nov. 1974, 1221-1226.
5. Chatterji, J.; Borhardt, J.K. *J. Pet. Tech.* Nov. 1981, 2042-2056.
6. Krueger, R.F. *J. Pet. Tech.*, Feb. 1986, 131-152.
7. Jones, L. W. U. S. Patent 3 481 869, 1969.
8. Sikorski, C. F. U. S. Patent 4 521 316, 1985.
9. Steiger, Ronald P. *J. Pet. Tech.* Aug. 1982, 1661-1670.
10. Radenti, G., Palumbo, S.; Zucca, G. *Pet. Eng. Intr.* Sept. 1987, 32-40.
11. Boding, O. K.; Sauber, C. A. U. S. Patent 4 000 076, 1976.
12. Uhlig, H. H. *I & E Chem.*, 44, 1952.

RECEIVED January 27, 1989

Chapter 36

Impedance Spectroscopy

A Dynamic Tool for the Design of Corrosion Inhibitors

F. B. Growcock¹ and R. J. Jasinski

Dowell Schlumberger, P.O. Box 2710, Tulsa, OK 74101

The corrosion of steel in HCl, with and without inhibitors, shows relatively straightforward impedance spectroscopy (IS) phenomenology and can be represented by simple equivalent circuits of primarily passive electrical elements. Inductive effects are, apparently, a consequence of the measurement altering the surface being measured. IS reveals that during steel corrosion in hot concentrated HCl, the heterogeneity of the surface is established rapidly and can be simulated with a single type of equivalent electrical circuit. Chemisorbing and electrostatic inhibitors in all cases reduce surface heterogeneity. At the same time, all of the inhibitors increase the charge-transfer resistance without producing a concomitant decrease in the interfacial capacitance. Time constant analysis suggests this arises from specific adsorption of the inhibitor to form insulating "islands", rather than uniform adsorption to give an electronically conductive monolayer. In some cases, polymerization of the inhibitor occurs subsequent to adsorption; this can lead to formation of a protective multilayer film atop the adsorbed monolayer, but, at the same time, result in significant loss of inhibitor in the solution.

Corrosion of steel during oil well acidizing or acid pickling treatments can be controlled effectively and economically with organic corrosion inhibitors. These additives interact with the steel surface to form an adherent barrier, the nature of which depends on the additives' physicochemical properties. Work to date has established that acetylenic alcohols chemisorb and subsequently polymerize on steel surfaces (1-5). α,β -Unsaturated aldehydes and α -alkenylphenones appear to behave in a similar manner (6,7). The nature of

¹Current address: Amoco Production Company, Tulsa, OK

the chemisorption process is, however, not very well understood. In addition, although the polymer films appear to contribute to the long-term protection of the underlying steel, it is not at all clear how important polymerization is initially.

Electrochemical techniques have been utilized for many years to study metal corrosion. Two of these techniques, linear polarization (LP) and cyclic voltammetry (CV), complement each other, LP providing corrosion rates under conditions where the surface is minimally altered and CV furnishing information about the corrosion mechanism. With the advent of impedance spectroscopy (IS), both kinds of information can be gleaned simultaneously and more rapidly, while leaving the surface almost intact. In this paper, we discuss the application of IS to the study of rapid steel corrosion and describe a study we undertook to elucidate the roles played by adsorption and film formation in the inhibition mechanisms of the above-named compounds. For comparison, we also investigated two quaternary nitrogen salts, which appear to adsorb electrostatically and presumably do not form macroscopic films (8).

Experimental Approach

Materials. 1-Octyn-3-ol (98%, from Aldrich), trans-cinnamaldehyde (TCA - 99%, from Cofinil, Milan, Italy) and benzoyl allyl alcohol (BAA - 80% solution in isopropanol, prepared by D. G. Hill) were chosen to represent acetylenic alcohols, α,β -unsaturated aldehydes and α -alkenylphenones, respectively. A quinoline quat (QQ - 97%) and n-dodecylpyridinium bromide (DDPB - 80% solution in isopropanol), which were prepared as described in Reference (8), served as model quaternary nitrogen salts. The HCl solutions were prepared by dilution of reagent-grade 37% HCl (Mallinckrodt). API N80 steel, obtained from U.S.X. Corp., had a mixed structure of ferrite (α -Fe, grain size ASTM No. 12) and a fine aggregate of ferrite and cementite (Fe_3C); impurity levels were 0.34% C, 0.015% S, 0.010% P, 1.31% Mn, 0.02% Mo and 0.06% Si, with Cr, Ni and Cu below detectable levels.

Procedure. All IS experiments were conducted under a blanket of N_2 in a thermostatted IBM Instruments cell, using 20 mL of deaerated solution and a 3-electrode configuration. The Pt foil counter electrode measured 4.0 cm^2 . The potential between the N80 steel rotating disk working electrode (WE - 0.20 cm^2 , 1000 rpm) and the Ag/AgCl reference electrode (with Luggin capillary) was maintained at the open-circuit value with a Solartron 1286 ECI. The AC frequency was varied from 60 kHz to 0.01 Hz (10 mV peak to peak) with a 1250 FRA, 5 or 10 steps/decade using a 1-cycle minimum integration time (6 min total time). Some experiments were run only to 0.1 or 1.0 Hz (1 min total time) in order to minimize the scan period. The WE was ground to a 600-grit finish before most tests and wiped with a methanol-saturated soft cloth. Prior to immersion in the test solution, the WE was exposed to a stream of N_2 maintained at the solution temperature, so that the test temperature was reached and deaeration was complete within seconds after immersion.

Equivalent Circuit Analysis. IS measurements yield values of Z' and Z'' , the real and imaginary components of the impedance, as a function of f , the AC frequency. The data are usually displayed as Nyquist plots (Z'' vs. Z') or Bode plots (impedance modulus, $|Z| = \sqrt{(Z'')^2 + (Z')^2}$, and phase angle shift, ϕ , vs. f). The electrochemical system is then simulated with an electrical circuit that gives the same impedance response. Ideally this electrical circuit is composed of linear passive elements, e.g. resistors and capacitors, each of which represents individual physicochemical steps in the electrochemical reaction.

The impedance data were fitted to candidate electrical circuits using the non-linear weighted least-squares fitting program "EQIVCT" developed by Boukamp (9). Graphical analysis was utilized to furnish reasonable first guesses of the circuit parameters for input to EQIVCT.

Characterization of the Corroding Surface. Mechanistic studies of steel corrosion in aggressive environments, such as hot concentrated HCl, have to deal with a rapidly changing and, hence, poorly characterized surface. For example, exposure of a mild steel to uninhibited 15% (4.4 N) HCl at 65°C gives a typical corrosion rate of 1 g/cm²/day, which corresponds to a surface removal rate of 150 Å/sec. Exacerbating this problem is surface area development, which proceeds in a manner dictated by physical and chemical heterogeneities of the surface. Characterization of an inhibited steel surface also has some fundamental complications. Although the steel surface is changing less rapidly, the chemical and physical nature of the film, as well as the rate of film formation, depends on acid concentration, temperature and exposure time (6). Thus, the film itself is often a poorly characterized complex mixture of polymeric materials.

Nevertheless, we will show that all of the systems studied exhibited relatively straightforward electrochemical phenomenology and could be represented by simple equivalent circuits involving primarily passive electrical elements.

Corrosion of Steel in Uninhibited HCl

Consider first the corrosion of low alloy steel in HCl per se, i.e. before the addition of organic inhibitors. As shown in Figures 1 and 2 for N80 steel in 15% and 28% HCl at 65°C, Nyquist plots for steel in concentrated HCl typically have only one distinct feature: a single capacitance loop (a loop above the Z' axis) with a hint of a second capacitance loop at lower frequencies. The low-frequency loop is more fully developed in 28% HCl than in 15% HCl. Mass transport limitations are not evident except under extreme conditions, e.g. above 28% HCl and 65°C.

This impedance response, in general, is similar to that elicited from an Armstrong electrical circuit, shown in Figure 3, which we represent by $R_0 + C_d / (R_t + C_a / R_a)$. R_0 is identified with the ohmic resistance of the solution, leads, etc.; C_d with the double-layer capacitance of the solution/metal interface; R_t with its resistance to charge transfer; and C_a and R_a with the capacitance and resistance

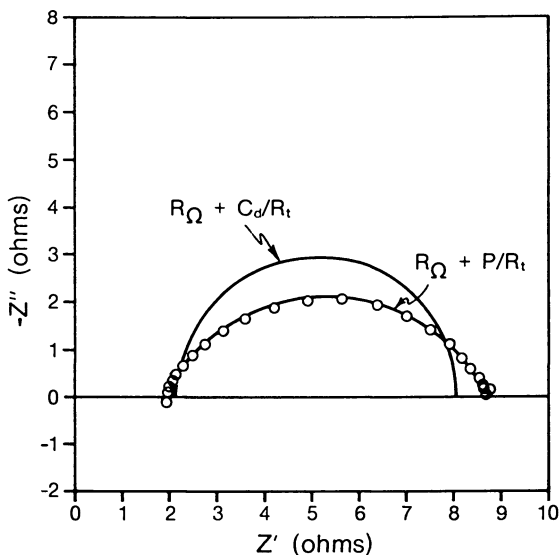


Figure 1. Nyquist plot of N80 steel in 15% HCl at 65°C.

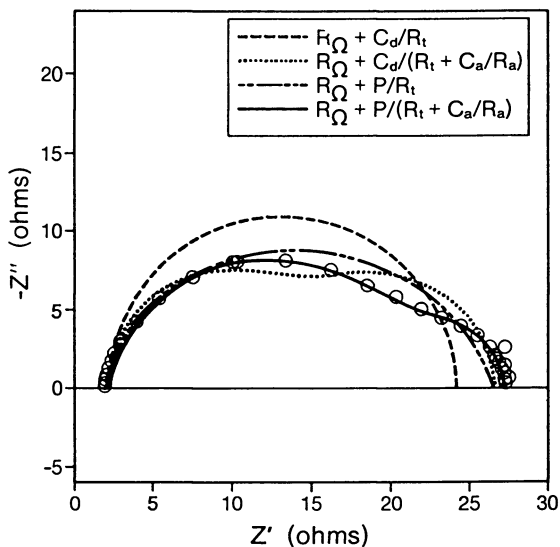


Figure 2. Nyquist plot of N80 steel in 28% HCl at 65°C.

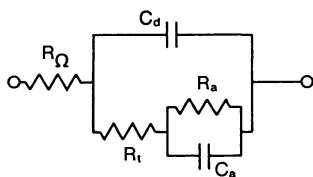


Figure 3. Armstrong electrical circuit.

associated with a slow (low frequency) intermediate process (10,11). The total resistance at the limit of $f \rightarrow 0$, $R_t + R_a$, is equivalent to the corrosion resistance measured in a DC experiment and is inversely proportional to the net corrosion rate.

Harrington and Conway (12) point out that in the case of the H_2 evolution reaction, C_a is equivalent to the H^+ adsorption pseudocapacitance only when H^+ adsorption and electron transfer (the Volmer reaction) occur in an almost reversible fashion and electrochemical desorption or recombination is the rate-determining step. Although we believe such is the case for steel in concentrated HCl, the low-frequency loop is usually so poorly developed that neglect of the R_a/C_a sub-circuit generally changes the data fits very little. This is especially true for the 15% HCl data. The calculated value of C_a is usually 1 to 2 orders of magnitude higher than that of C_d , in agreement with studies in weaker HCl and consistent with an adsorption pseudocapacitance. But R_a is considerably smaller than R_t , opposite of that found in the other work (10), and so contributes little to the total corrosion resistance. Thus, the data in many cases can be represented equally well by $R_{\Omega} + C_d/R_t$ and by the Armstrong circuit. Fits of the data in Figure 2 to these two circuits are shown in that figure for comparison.

The C_d -values (per unit surface area) are, in most cases, considerably higher than C_d -values expected for a perfectly smooth surface; for example, on mercury, $C_d \sim 20-30 \mu F/cm^2$ (13), whereas our values range from 30 to 500 $\mu F/cm^2$. C_d is high because the steel surface is rough on a microscale, even with a 600-grit finish, so that the "true" surface area is actually greater than the geometric surface area used here. Corrosion develops surface roughness to an even greater extent; in fact, the true surface area increases continuously with exposure time. This is apparent from visual inspection of the surface. Thus, it is not uncommon to be working with a steel surface whose true surface area is several-fold greater than its apparent surface area (14,15).

Surface roughness is also expected to result in depression of the capacitance semi-circle. This phenomenon, which is indeed apparent in both Figures 1 and 2, is, however, unrelated to surface area. Rather, it is attributable to surface heterogeneity, i.e. the surface is characterized by a distribution of properties. Macdonald (16) recently reviewed techniques for representing distributed processes. A transmission line model containing an array of parallel R/C units with a distribution of values is physically attractive, but not practical. An alternative solution is introduction of an element which by its very nature is distributed. The Constant Phase Element (CPE) meets such a requirement. It has the form

$$P = Y_0 \cdot \omega^{-n}$$

where Y_0 is a combination of properties related to both the surface and the electroactive species, and $n=1$ for a pure capacitance. In our case, we can substitute P for C_d and the value of n can be used as a gauge of the heterogeneity of the surface (17). Thus, fitting the data in Figure 1 via EQIVCT to the CPE-containing circuit $R_{\Omega} + P/R$ generates a well-matched calculated curve (see Figure 1) with $n = 0.84$. Rammelt and Reinhard (18) have treated the case of roughened

polycrystalline iron in H_2SO_4 using a CPE in parallel with C_d and R_t ; however, fits of our data to that circuit are very poor and generate n -values less than 0.5, which is not theoretically possible.

Although the true surface area increases with increasing exposure time, Figure 4 shows that the impact of heterogeneity on electrochemical measurements is established quickly and remains constant with time.

Utilizing the $R_{\Omega}+P/R_t$ circuit, we find that n reaches a relatively constant value almost immediately and changes very little over the next two hours. The n -values for different steels range from 0.76 to 0.92 at 1-min exposure, depending on the metal and the environment. The relative surface areas displayed in Figure 4 for comparison with n were determined from capacitance measurements of the steel in 4M LiCl at pH=1, immediately after the corrosion experiments. These results are consistent with Mulder and Sluyters' argument that the CPE is related to the fractal surface properties of the roughened steel (17). Furthermore, the near-constancy of the n -values implies that, at least in the case of steel in HCl, the fractal properties of the surface are relatively constant throughout the exposure period.

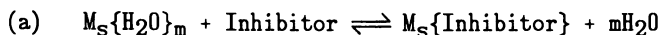
The CPE appears to arise solely from roughening of the surface by the corrosion process. This was verified with IS experiments on iron and several steels in 15% HCl at 25°C. The electrodes were polished with alumina and maintained at 150 mV cathodic of the rest potential. Complex plane plots of the impedance responses were near-perfect semi-circles centered on the Z' axis. Analyses via EQIVCT using the $R_{\Omega}+P/R_t$ circuit, gave rise to n -values of the CPE in excess of 0.93 in all cases and remained constant throughout the tests.

Thus, it appears that in most cases we can treat steel corrosion in concentrated HCl adequately with the circuit $R_{\Omega}+P/R_t$. In cases where the two capacitance loops are sufficiently distinguishable, we must resort to the full circuit $R_{\Omega}+P/(R_t+R_a/P_a)$, where P_a is the CPE counterpart of C_a ; when the full circuit is prescribed, the fitted n -value of P_a is always less than the n -value of P .

Consider next the effect of adding corrosion inhibitors.

Effect of Corrosion Inhibitors

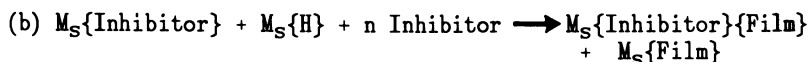
Adsorption and Film Formation. Inhibition of HCl corrosion by organic compounds is a complicated multi-step process. Nevertheless, the effect of an inhibitor on corrosion of a metal is often treated mathematically with an equilibrium adsorption model for displacement of water (19,20):



where M_S represents an active surface site(s) and the brackets denote sorbed species. Equilibrium (a) competes with adsorption of the corrosive species on M_S and is assumed to be fast, so that the corrosion rate rapidly reaches a "steady state" value. However, chemical analyses of products on the steel surface have revealed that in many

cases a macroscopic film is formed via polymerization reactions and that the film thickens with increasing time (3).

To account for the effect of polymerization on the corrosion rate, it has been proposed (4) that film formation be considered as a series of iterative elementary steps, the sum of which may be expressed as



where the polymer film is draped over uncovered active surface sites, i.e. $M_S\{\text{Film}\}$, and anchored by sorbed inhibitor, i.e. $M_S\{\text{Inhibitor}\}\{\text{Film}\}$. Coverage of inactive surface sites also occurs, but at a slower rate (21).

Equivalent Electrical Circuit. In spite of the complex nature of the inhibition process, the inhibited systems actually display simple impedance responses.

Tests were run with N80 steel in 15% and 28% HCl at 25°C with and without octynol for periods extending up to 2 hours. Immediately after injection of octynol into the acid, two phenomena were observed. First, near the low-frequency limit of the tests, a prominent inductive loop (below the Z' axis) appeared which then vanished within a few minutes. Secondly, fits of the data above 1 Hz to the $R_{\Omega}+P/R_t$ circuit, i.e. ignoring the inductive loop, gave rise to a higher CPE n-value, which then remained relatively constant for the duration of each experiment. This result is shown in Figure 5.

Other inhibitors, namely TCA and BAA, gave a similar response to octynol. Furthermore, the octynol and BAA systems were tested with and without rotation at 1000 rpm of the steel disk, giving virtually the same result, which indicates that the sorbed inhibitor and polymer film are strongly adherent. In all cases, the standard deviations of the fitted parameters, σ_i , fell considerably on addition of inhibitor, e.g. in the case of 15% HCl with octynol, σ_n fell from 1 to 3% (no inhibitor) down to 0.2 to 0.6% (with inhibitor). Generally, the inhibited systems gave less scatter in the data, a result we attribute to slower evolution of H_2 and lower variability in the size of attached bubbles, i.e. lower variability in instant average contact area of specimen with solution.

Inductive loops, such as that described above, are sometimes associated with adsorption of an oxidizable or reducible intermediate. Indeed, the polymer film and perhaps the adsorbed form of octynol are created by surface-mediated reductions. However, when we re-ran the octynol tests above using a peak-to-peak voltage of 4 mV instead of 10 mV, the size of the inductive loop fell by an order of magnitude, which suggests it is an artifact of the IS technique whereby the measurement alters the surface being measured. More detailed investigation of this inductive behavior may yield clues about the nature of the polymerization process. For our purposes, it suffices to know that its effect is small at the rest potential (open-circuit potential) and we shall ignore it in the discussion that follows.

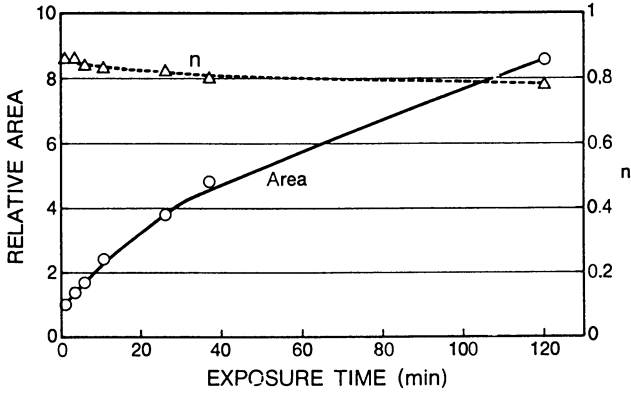


Figure 4. Effect of exposure time on CPE n-value and relative surface area.

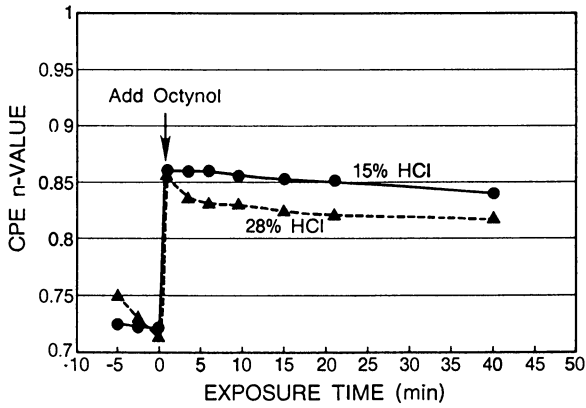


Figure 5. Effect of octynol on CPE n-value.

An interesting incidental effect observed when an inhibitor is present in such a great excess that it forms a separate phase is the appearance of a large low-frequency capacitance loop which we attribute to precipitation (physical adsorption). This effect, however, plays no role in the experiments discussed above, since they all deal with aqueous single-phase solutions.

In conclusion, though the inhibitor chemistry is complex, IS sees only a slightly roughened surface covered with an adsorbed film. Since this is representable by a single type of equivalent circuit, analysis of the inhibition process per se is relatively straightforward, as will be discussed below.

Adsorption versus Polymerization. It is instructive to examine further the time dependence of the corrosion inhibition. In acid corrosion inhibition tests, steady state is customarily assumed to be reached within 10 to 20 min after initial exposure of the metal specimen. Since the inhibitors function by reducing the available active surface area, we expect an increase in R_t and a corresponding decrease in P . The degree of corrosion protection the inhibitor provides is given by

$$\psi = \frac{R_{t0}^{-1} - R_t^{-1}}{R_{t0}^{-1}} \quad (1)$$

where R_{t0} and R_t are the resistances in the $R_{\Omega}+P/R_t$ circuit without and with inhibitor, respectively. If the sorbed inhibitor is impermeable (blocking), we can approximate the fractional surface coverage by the parallel-plate two-capacitor model (22):

$$\theta = \frac{P_0 - P}{P_0 - P_{\infty}} \quad (2)$$

where P_0 , P and P_{∞} are the CPE's without the inhibitor (coverage = 0), with the inhibitor and with excess inhibitor (coverage = 1), respectively, and are evaluated at $\omega_z''_{\max}$ (the frequency at which Z'' is a maximum). Using C_d instead of P , we obtain identical results. Thus, θ may be considered the fraction of the total surface area covered by the inhibitor, while ψ is the fraction of the active surface that is covered.

When step (a) reaches equilibrium, both ψ and θ should have steady state values. To test this hypothesis, we determined the effect of exposure time on ψ and θ for N80 steel in 15% HCl at 25°C and in 28% HCl at 65°C, as shown in Figures 6 and 7, respectively. Here [octynol] = $3.5 \times 10^{-3}M$ in 15% HCl and $2.1 \times 10^{-2}M$ in 28% HCl. It is immediately apparent from these plots that neither ψ nor θ reaches a steady state value during the course of the experiments. Although ψ appears to be relatively constant throughout the 15% HCl test and during the first stage of the 28% HCl test, it is continually increasing in both cases.

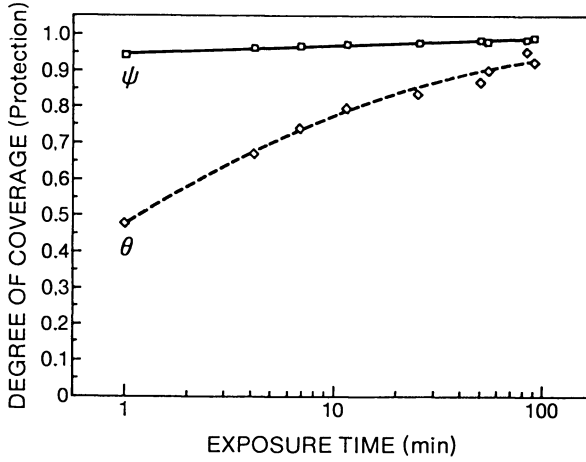


Figure 6. Effect of exposure time on θ and ψ : 15% HCl with 3.5×10^{-3} M octynol, 25°C.

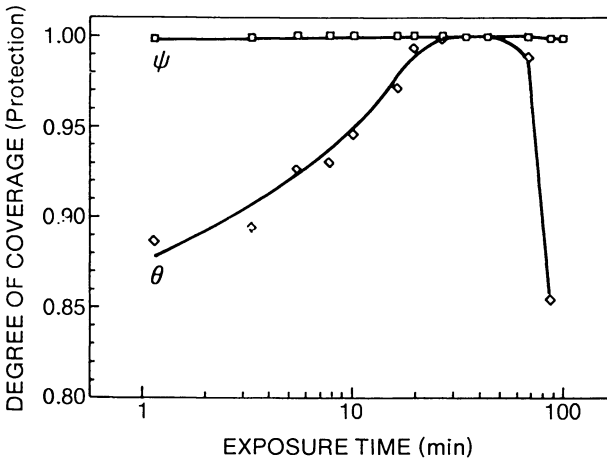


Figure 7. Effect of exposure time on θ and ψ : 28% HCl with 2.1×10^{-2} M octynol, 65°C.

Adsorption reactions on nonporous surfaces are generally quite rapid (unless there is a large activation energy barrier). By contrast, surface polymerization reactions are usually much slower. Thus it is likely that the initial high level of Ψ arises from adsorption, while the subsequent small, but continuous, increase in Ψ is caused by the thickening polymer film.

The precipitous drop in Ψ observed in Figure 7 for 28% HCl is also attributable to film formation. Previous work has shown that octynol itself is stable under these conditions in the absence of a steel surface (3). In the presence of the steel, however, polymerization occurs, which consumes octynol. These reactions slow with increasing exposure time, but they do not stop. We surmise, therefore, that the sudden decrease in inhibition after 50 min arises from the concentration of octynol in the solution reaching too low a level to maintain the sorbed monolayer; the inhibitor adsorption equilibrium shifts so that octynol desorbs and the corrosion rate returns to the level attained in uninhibited acid. This result was verified by spectrophotometric measurements of [octynol], which showed a large decrease in [octynol] with exposure time. The decrease in inhibition was also corroborated with companion weight-loss tests, which showed that catastrophic failure generally occurred at sufficiently long exposure times. In the long run, then, although the polymer film contributes to the protection of the steel, the polymerization reactions prove to be deleterious.

Adsorption Mechanism. If P_{∞} is negligibly small and the surface is homogeneous (all surface sites are equally active), the surface coverage, θ , and the degree of protection, Ψ , will be identical. It is clear, however, from Figures 6 and 7 that, although the two parameters track the same way, θ does not go hand-in-hand with Ψ . Significantly, the discrepancy between θ and Ψ is greatest at short exposure times. Ψ reaches a very high value — near its "steady state" value — almost immediately, whereas θ initially is quite low and increases slowly with increasing exposure time. If adsorption of octynol were entirely responsible for the inhibition, the initial difference between θ and Ψ would imply that sorbed octynol can provide a high degree of protection to the steel while only covering a small fraction of the surface. This arises from the assumption that the P_{∞} value corresponds to a surface covered with a monolayer of sorbed octynol when, in fact, it actually corresponds to the film-covered surface. Indeed, the initial discrepancy between θ and Ψ is consistent with the following limiting adsorption mechanisms: (I) octynol forms an insulating barrier but adsorbs non-uniformly (a permeable, or porous, barrier), covering active sites to a greater extent than inactive — or less active — sites; and (II) octynol adsorbs uniformly (an impermeable barrier), covering the entire surface with a monolayer that is electronically and ionically conductive. While the monolayer may or may not be a good electrical insulator, the aged polymer film, by virtue of being a saturated hydrocarbon, is a good electrical insulator. The slow but large rise of θ with exposure time results from the decrease in P as the interface becomes more non-polar.

In the end, analysis of Ψ vs θ (the "classical" approach) is not quantitative, a problem we associate with surface area variability and ambiguity arising from the interpretation of P_{ω} . To help determine which adsorption mechanism is operative, we turn to an alternative parameter, the IS impedance "time constant", τ , which does not suffer from these drawbacks.

Time Constant Analysis. τ is the relaxation time of the corrosion process and is dependent on the dielectric properties of the interface. τ is given by $\tau = R_t P$, but can be measured independently: $\tau = \omega_z^{\text{max}}^{-1}$. Since R_t and P vary with surface area in exactly opposite fashion, τ (or ω_z^{max}) should be independent of surface area. To verify that this is indeed the case, we examined the corrosion of N80 steel in uninhibited 15% HCl at 65°C. With increasing exposure time, we observed a continuous decrease in R_t (hence an increase in corrosion rate) and a concomitant increase in P . And, as expected, ω_z^{max} did not vary at all (see Figure 8).

All of the inhibitors we examined reduce ω_z^{max} substantially, although they vary considerably in mode of inhibition, e.g. QQ and DDPB are electrostatic adsorbers, whereas TCA forms a thick film with carbonyl character and octynol forms a thin hydrocarbon film. Figures 8 and 9 show this effect in plots of ω_z^{max} versus exposure time and inhibitor concentration, respectively, for several inhibitors and inhibitor mixtures. Because of variability in reactivity among the specimens of N80, the ω_z^{max} values were normalized to the same initial value. Initial inhibitor concentrations ranged from 0.005 to 0.01 M. Figure 8 shows that all of the inhibitors produce a large, almost instantaneous, initial drop in ω_z^{max} . Thus, all of the inhibitors increase τ , i.e. they slow the kinetics of the corrosion charge-transfer reaction.

According to Figure 8, QQ and DDPB give a relatively constant value of ω_z^{max} within a few minutes; interestingly, though, the response with QQ is considerably slower than with DDPB, suggesting that QQ undergoes a secondary reaction at the surface, e.g. reorientation or electrochemical reduction. Octynol, BAA and the mixtures of DDPB with BAA or TCA do not give a constant value of ω_z^{max} ; rather, ω_z^{max} continues to fall, albeit slowly, even after 30 min exposure. Considering that octynol, BAA and TCA are all film-forming inhibitors, we conclude that the large magnitude of the initial decrease in ω_z^{max} corresponds to adsorption and the slow fall-off in ω_z^{max} to film-forming reactions. Furthermore, the large magnitude of the initial decrease in ω_z^{max} indicates that adsorption is the dominant mode of inhibition.

The experiments on which Figure 9 (ω_z^{max} vs [Inhibitor]) is based were all run with repolished electrodes pre-exposed for 5 minutes; this is sufficient time to achieve a constant temperature, yet too short a period for extensive polymerization. It is evident from Figure 9 that, at a high enough concentration, every one of the inhibitors reduces ω_z^{max} by at least an order of magnitude.

Indeed, the relative values of ω_z^{max} for all of the inhibitors are almost the same, falling in the range 10 to 20, e.g. ω_z^{max} decreases by factors of 16-22 for DDPB, 12-26 for TCA, and 17 for

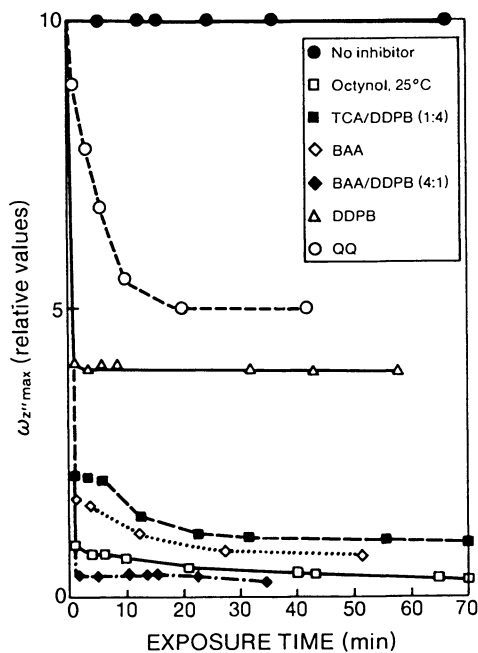


Figure 8. Effect of exposure time on $w_{z''\max}$ for various inhibitors in 15% HCl at 65°C.

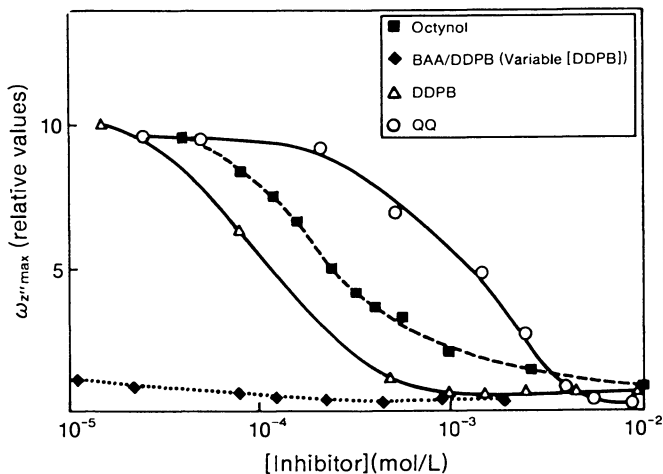


Figure 9. Effect of inhibitor concentration on $w_{z''\max}$ for various inhibitors in 15% HCl at 65°C.

BAA. That ω_z^{max} is so nearly independent of the nature of the inhibitor lends additional credence to mechanism (I). By contrast, if mechanism (II) were operative, we would expect ω_z^{max} to vary greatly with the electronic conductivity (and polarity) of the inhibitor barrier.

Conclusions

The impedance spectroscopy of steel corrosion in concentrated HCl, with and without inhibitors, exhibit relatively straightforward electrochemical phenomenology and can be represented by simple equivalent circuits involving primarily passive electrical elements. Analysis of these circuits for steel corroding in HCl per se reveals that the heterogeneity of the surface is established rapidly and can be simulated with a simple electrical circuit model.

Classical IS measurements indicate that corrosion inhibitors reduce surface heterogeneity and function primarily by adsorption. Furthermore, the sorbed monolayer is either (I) permeable and insulating or (II) impermeable and conductive. Analysis of the time-constant, τ , for the corrosion process, suggests that mechanism (I) is operative.

Non-steady state corrosion rate behavior appears to be a general phenomenon and is associated with polymerization reactions. The latter, which results in formation of a film on the sorbed monolayer, provides a smaller increment of protection than does adsorption and occurs at the expense of inhibitor loss from the solution. In some cases, however, the increased protection provided by the film is substantial and merits further investigation.

Acknowledgments

We thank Dowell Schlumberger for permission to publish this work.

Literature Cited

1. Poling, G. W. *J. Electrochem. Soc.*, 1967, 114, 2109.
2. Duwell, E. J.; Todd, J. W.; Butzke, H. C. *Corros. Sci.*, 1964, 4, 435.
3. Growcock, F. B.; Lopp, V. R.; Jasinski, R. J. *J. Electrochem. Soc.*, 1988, 135, 823.
4. Growcock, F. B.; Lopp, V. R. *Corros. Sci.*, 1988, 28, 397.
5. Growcock, F. B. *Corrosion '88*, 1988, Paper No. 338.
6. Growcock, F. B.; Lopp, V. R. *Corrosion*, 1988, 44, 248.
7. Frenier, W. W.; Lopp, V. R.; Growcock, F. B. *Corrosion*, in press.
8. Growcock, F. B.; Frenier, W. W. *Corrosion '84*, 1984, Paper No. 121.
9. Boukamp, B. A. *Solid State Ionics*, 1986, 20, 31.
10. Armstrong, R. D.; Race, W. P.; Thirsk, H. R. *J. Electroanal. Chem.*, 1968, 16, 517.
11. Mansfeld, F. *Corrosion*, 1981, 36, 301.

12. Harrington, D. A.; Conway, B. E. Electrochim. Acta, 1987, 32, 1703.
13. Hurt, R. L.; Macdonald, J. R. Solid State Ionics, 1986, 20, 111.
14. de Levie, R. Electrochim. Acta, 1965, 10, 113.
15. Armstrong, R. D.; Burnham, R. A. J. Electroanal. Chem., 1976, 72, 257.
16. Macdonald, J. R. J. Electroanal. Chem., 1987, 223, 25.
17. Mulder, W. H.; Sluyters, J. H. Electrochim. Acta, 1988, 33, 303.
18. Rammelt, U.; Reinhard, G. Corrosion Sci., 1987, 27, 373.
19. Uhlig, H. K. Corrosion and Corrosion Control, 2nd Ed.; John Wiley: New York, 1971; pp. 265-271.
20. Ateya, B. G. J. Electroanal. Chem., 1977, 76, 191.
21. Growcock, F. B.; Frenier, W. W.; Lopp, V. R. Proc. 6th European Conf. on Corrosion Inhibition, 1985.
22. Schuhmann, D. Electrochimica Acta, 1987, 32, 1331.

RECEIVED December 7, 1988

Chapter 37

Use of Starved Bacteria To Increase Oil Recovery

Hilary M. Lappin-Scott, Francene Cusack, F. Alex MacLeod,
and J. William Costerton

Department of Biological Sciences, University of Calgary, Calgary, Alberta
T2N 1N4, Canada

Limitations in present oil recovery methods leave the majority of oil as unobtainable in the reservoir. Therefore, any technique that increases or enhances the recovery rate of this resource would have great potential for field applications. Our interest lies in utilizing microorganisms to assist in enhanced recovery by virtue of their growth properties. We report on our recent laboratory data in model rock strata. Our laboratory data demonstrate a new method of blocking the high permeability formations using starved forms of bacteria. It also has applications to control oilwell coning.

Estimates suggest that a maximum range of between 8-30% of the total oil is presently recovered from petroleum reservoirs leaving vast quantities underground as the focus for developing new techniques to increase recovery rates. One recovery method now in use is the waterflooding of differing permeability rock strata (Fig. 1). As the waterflood commences the high and low permeability zones are oil saturated (Fig. 1A). The waterflood follows the routes of least resistance, that is the high permeability channels, and acts as an energy force to push out any oil along its path. However, once the oil has been displaced from these zones the water continues to follow the same course leaving the lower permeability zones unswept and therefore full of oil (Fig. 1B). The process of blocking off the higher permeability strata and diverting the waterflood to other unswept zones is called selective plugging. In order to be effective, the plug must penetrate throughout the high permeability zone or the water will return preferentially from the lower back to the higher permeability strata. If a shallow plug is established (Fig. 1C) the waterflood is initially blocked from the higher permeability strata and pushes out some oil. However, beyond the plug the waterflood returns to the high permeability zone leaving much oil in the low permeability strata. With a deeper plug in the high permeability strata the waterflooding is forced to stay in the lower permeability zone and push the oil out (Fig. 1D) until most of the oil is drained (Fig. 1E).

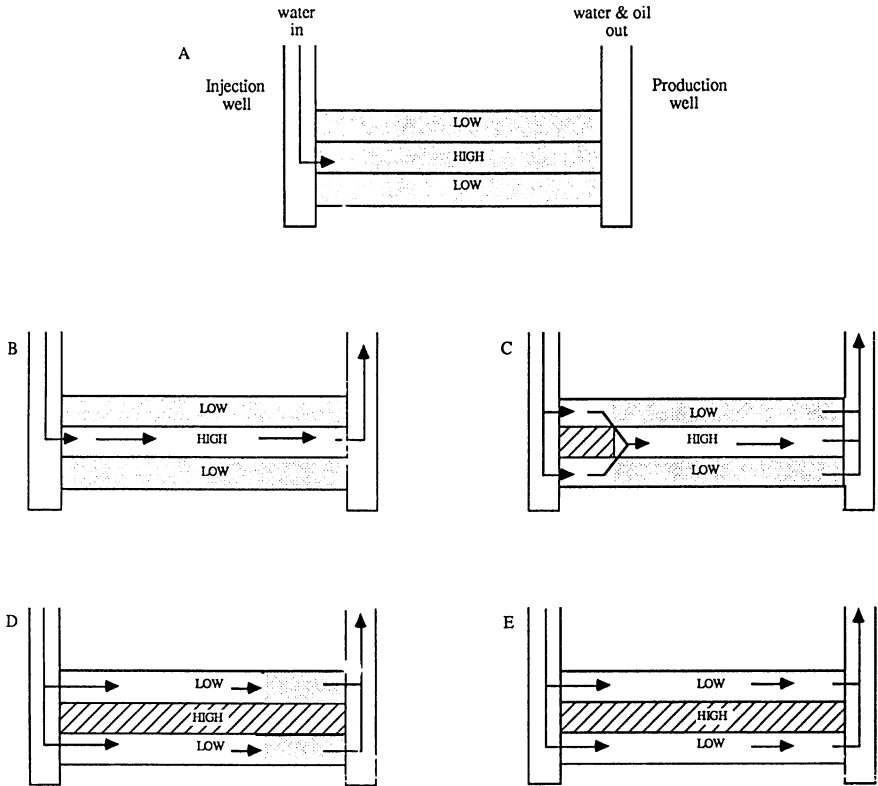


Figure 1. Schematic diagram of the effects of shallow and deep plugs on enhanced oil recovery.

Several agents are currently used for plugging high permeability strata. These include small fibers that are carried in the waterflood and deposited in the high permeability zones and chemical reactions forming insoluble precipitations². Some of the current methods available, for example polymers or foams, are subject to deterioration and are costly. This gives them limited application as they are not able to penetrate deep into the strata.

In some reservoirs another problem develops that reduces oil recovery, called coning. This occurs most commonly when water lies below heavy oil in the reservoir. During primary recovery instead of the oil being pumped out, water, being of lower viscosity, is preferentially pulled to the surface. Continued pumping only succeeds in pulling up more water, thus reducing or halting further oil recovery³.

Crawford^{4,5} reported that bacteria could be used as selective plugging agents and have the ability to penetrate the high permeability areas. Another advantage is that bacteria can grow in the rock and produce plugging both by their growth and their growth products. Research at the University of Oklahoma^{7,8} demonstrated that when bacteria were injected into two sandstone cores of differing permeabilities the bacteria preferentially grew and plugged up the higher permeability core first. However, when full-sized bacteria, 2.0 μm or more in length, are injected into solid matrices the bacteria collect at the inlet in a sticky mass⁶ containing microbial growth and growth products, called biofilms^{9,10} and the plug is referred to as a skinplug. Reducing the concentration of bacteria to approximately $10^6/\text{ml}$ reduced the opportunity for skinplug formation¹¹ and this could be further reduced by using dormant, smaller forms of bacteria. The smaller size of dormant bacteria, that is spores or starved bacteria, together with their absence of sticky growth products may allow them to travel further into rock strata.

Microorganisms have been reported to decrease substantially in size as a response to low nutrient conditions¹². Then, after a period of starvation when the organisms exist in a dormant state, they commence growth again and return to full size when given nutrients¹³. Our work at the University of Calgary attempted to harness these changes in cell size during starvation-resuscitation as a method for enhanced oil recovery. We considered that the smaller cell size may enable them to penetrate deeper into rock strata than full-sized bacteria. By injecting organisms in a starved state into rock then giving them growth nutrients would allow them to grow and plug the rock. Further waterflooding would bypass these plugged regions and sweep the areas containing oil. Starved bacteria may also be used to control coning. They may be injected at the oil-water interface then resuscitated with nutrients. Bacterial growth will form a deep pancake of sticky slime to physically separate the water from the oil and prevent any more water being sucked to the surface.

Klebsiella pneumoniae was isolated as a representative microorganism from produced water¹⁴. The bacterium was starved in phosphate buffer salts solutions at concentrations of either $10^4/\text{ml}$ or $10^8/\text{ml}$. During starvation periods of up to 24 days the bacterial cells changed in size and shape from rod-shaped, up to 2.2 μm long,

producing sticky slimes of polysaccharide-containing biofilms to spherical or small rods $0.5 \mu\text{m}$ by $0.25 \mu\text{m}$ with little or no biofilm (Fig. 2). Such microorganisms are termed ultramicrobacteria¹³ (UMB). We investigated the ability of the UMB to grow and resuscitate using different nutrients. One contained a rich mixture of growth substances, called Brain Heart Infusion or BHI. The BHI was added at half of the manufacturers recommended concentration as this was sufficient to support rapid growth. Another nutrient contained only one carbon source, called sodium citrate medium or SCM. The SCM was added at concentrations of 7.36 g/l . BHI was a fast acting nutrient and supported rapid resuscitation in 4 hours, SCM was a slow acting nutrient and supported resuscitation in 8 hours¹⁴.

After establishing that microorganisms from oilwells could decrease in size and form UMB then return to full size when given nutrients in laboratory growth cultures, we investigated whether the UMB were able to penetrate deeper when injected into porous matrices than their full sized counterparts. The experimental core flood apparatus consisted of a constant pressure, variable flow rate injection system. The pressure was maintained at 3.5 psi. In a comparative study using sintered glass bead cores with permeabilities of between 6 and 7 Darcys, one set of cores were injected with $10^8/\text{ml}$ *K. pneumoniae* starved for 4 weeks, the other with $10^9/\text{ml}$ of the full sized bacteria grown on SCM¹⁰. The full sized cultures blocked the cores quickly and reduced the permeability to less than 1% of the original value with the addition of 500 pore volumes. The starved bacteria only reduced the permeability to 82% despite the addition of in excess of 800 pore volumes¹⁰. After the injections were completed the glass bead cores were cut up into equal size sections and examined by electron microscopy to establish the position of the bacteria within the cores. The electron microscopy of different sections of cores treated with full sized cells showed that a mass of large rod-shaped bacteria was located at the core inlet. The bacteria had produced polysaccharides and the biofilm which plugged the core inlet. With the starved cultures the UMB were evenly distributed throughout each of the core sections with little or no biofilm apparent. From this work, we were able to conclude that starved *K. pneumoniae* was able to penetrate deeper into solid matrices than full sized cells as a result of their smaller size, less sticky glycocalyx and reduced biofilm production.

Another series of experiments used sandstone cores previously injected with starved bacteria to investigate the ability of the bacteria to grow within rock cores when given a suitable nutrient¹⁵. Berea sandstone cores of 200 and 400 millidarcy (md) permeabilities were used as they were considered to be more representative of reservoir conditions than the glass bead cores. The sandstone cores were injected with 300 to 450 pore volumes of $10^5/\text{ml}$ starved bacteria until the cores contained an even distribution of bacteria (Fig. 3A & B) and the core permeabilities were between 13% and 18%. SCM nutrient was injected through the cores (Fig. 3C) until the core permeability fell to 0.1%, this required 360 pore volumes of SCM. The starved bacteria resuscitated by utilizing the SCM and grew within the sandstone forming a deep bacterial plug composed of cells

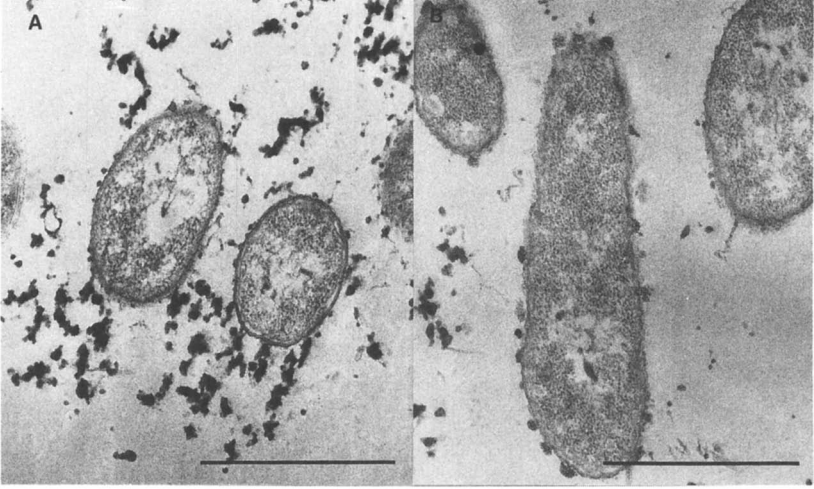


Figure 2. Starved (A) and full-sized (B) *Klebsiella pneumoniae* in laboratory cultures viewed through an electron microscope. The sizes and shapes of the cells differ markedly. The bar represents 1 μ m.

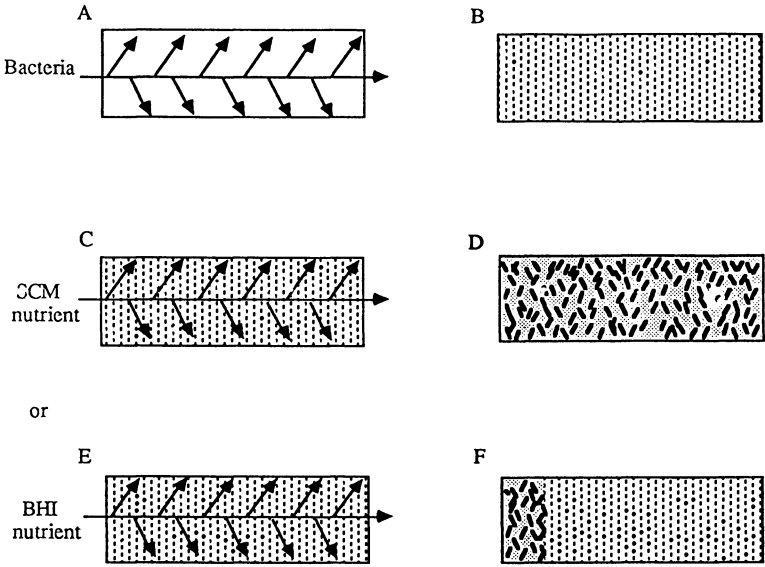


Figure 3. Diagrammatic representation of the plugging of rock cores with resuscitated starved bacteria. See text for details.

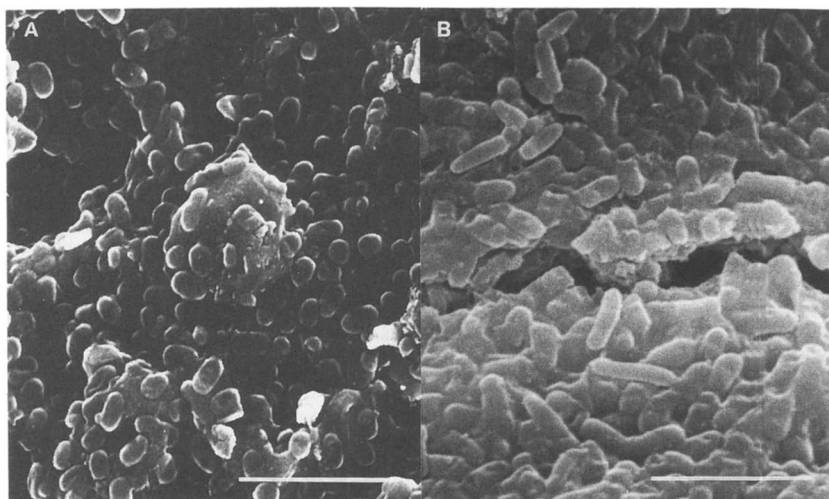


Figure 4. Scanning electron microscopy of starved (A) and nutrient stimulated (B) Klebsiella pneumoniae in sandstone rock cores. The bar represents 5 μm .

and glycocalyx (Fig. 3D). The resuscitation followed a similar pattern to that reported in laboratory batch growth systems¹⁵, that is, a difference in resuscitation rates was observed with SCM and BHI. With SCM the slower resuscitation permitted a nutrient flow to all of the starved bacteria in the sandstone and the subsequent growth produced a deep plug throughout the entire core (Fig. 3C & 3D). With BHI, a 95 pore volume injection resulted in a drop in permeability to 0.5%. Resuscitation was so rapid that the growth of bacteria by the core inlet blocked off the supply of nutrients to lower down the core resulting in a shallow bacterial plug only at the top of the core (Fig. 3E & 3F). Sectioning and examination of the sandstone cores using scanning electron microscopy showed large differences in the bacteria before and after nutrient additions (Fig. 4A & B). The nutrient fed bacteria were observed to have increased noticeably in size and a mass of biofilm was produced. The starved bacteria were still tiny and singular with little or no biofilm.

We also investigated several cost reduction exercises, such as, a) giving the starved bacteria short bursts of nutrient (less than 50 pore volumes) instead of a continuous flow and b) injecting fewer starved bacteria into the core (150 pore volumes) before nutrient injection. Both still resulted in deep bacterial plugs when SCM was used as a nutrient.

Other experiments are planned to study the location, distribution and resuscitation of ultramicrobacteria in large three-dimensional sandpacks. Such studies will allow a more realistic approximation of reservoir conditions than the unidirectional core studies. We do not consider that the ultramicrobacteria will reach or grow in areas where residual oil is located. Selective plugging involves blocking the high permeability zones already drained of oil. We consider that the injection of ultramicrobacteria will be carried, like waterflood operations, to the areas of the strata already drained of oil and permit them to disperse through pore spaces and resuscitate in these areas.

Conditions differ in each reservoir with respect to temperature, pressure and salinity. No one microorganism will be expected to survive, grow and plug all these different reservoirs. We suggest that a bacterium is chosen from laboratory collections that cover a range of environmental conditions best suited to the particular well.

In summary, care must be taken to inject nutrients that do not encourage rapid growth as undesirable shallow bacterial plugs form (Fig. 3F). With the correct nutrient package, such as SCM in this instance, a deep plug will form throughout the strata (Fig. 3D). In conclusion, our laboratory based studies demonstrate that starved bacteria may be used to physically block rock strata already drained of oil. Further recovery operations can then deal with strata still containing oil and thus enhance recovery rates.

Literature Cited

1. Moses, V. Microbiol. Sci. 1987, 4, 306-309.
2. Breston, J. N. J. Petrol. Technol. March 1957, 26-31.

3. Hower, W. F.; Ramos, J. J. Petrol. Technol. January 1957, 137-140.
4. Crawford, P. B. Producers Monthly 1961, 25, 10-11.
5. Crawford, P. B. Producers Monthly 1962, 26, 12.
6. Jenneman, G. E.; Knapp, R. M.; McInerney, M. J.; Menzie, D. E.; Revus, D. E. Soc. Petrol. Eng. J. Feb. 1984, 33-37.
7. Raiders, R. A.; Freeman, D. C.; Jenneman, G. E.; Knapp, R. M.; McInerney, M. J.; Menzie, D. E. Paper SPE 14336 presented at 60th Annual Technical Conf. & Exhibition of Soc. Petrol. Eng., Las Vegas, NV, 1985.
8. Raiders, R. A.; McInerney, M. J.; Revus, D. E.; Torbati, H. M.; Knapp, R. M.; Jenneman, G.E. J. Industr. Microb., 1986, 1, 195-203.
9. Shaw, J. C.; Bramhill, B.; Wardlaw, N. C.; Costerton, J. W. Appl. & Envir. Microbiol., 1985, 50, 693-701.
10. MacLeod, F. A.; Lappin-Scott, H. M.; Costerton, J. W. Appl. & Envir. Microbiol., 1988, 54, 1365-1372.
11. Jang, L.-K.; Chang, P. W.; Findley, J. E.; Yen, T. F. Appl. & Envir. Microbiol., 1983, 46, 1066-1072.
12. Novitsky, J. A.; Morita, R. Y. Appl. & Envir. Microbiol., 1976, 33, 635-641.
13. Torella, F.; Morita, R. Y. Appl. & Envir. Microbiol., 1981, 41, 518-527.
14. Lappin-Scott, H. M.; Cusack, F.; MacLeod, F. A.; Costerton, J. W. J. Appl. Bacteriol., 1988, 64, 541-549.
15. Lappin-Scott, H. M.; Cusack, F.; Costerton, J. W. Appl. & Envir. Microbiol., 1988, 54, 1373-1382.

RECEIVED January 13, 1989

Appendix

Weldon M. Harms

Halliburton Services, P.O. Drawer 1431, Duncan, OK 73536-0426

Reviews of Oil & Gas Fracturing(Ref. 1)

- Clark, J.B., Fast, C.R., and Howard, G.C.: "A Multiple Fracturing Process for Increasing the Productivity of Wells," 1952 Spring Meeting of the Midcontinent District API, Wichita, KS, March 19-21.
- Prusick, J.H. and Morgan, Z.V.: "The Use of Emulsions and Related Techniques in the Treatment of Oil and Gas Wells," Pet. Eng. (May 1954) B54-B56.
- Hurst, R.E., Moore, J.M., Ramsey, D.E.: "Development and Application of 'Frac' Treatments in the Permian Basin," T.P. 4032, Soc. Pet. Eng. J. (1955) Trans., AIME, 204.
- Alderman, E.N., Mack, D.J., and Ousterhout, R.S.: "Evaluation of Fracturing Materials for Optimum Well Stimulation," API paper 801-37J, 1961 Spring Meeting of Pacific Coast District, Los Angeles, May 11-12.
- Hassebroek, W.E. and Saunders, C.D.: "Hydraulic Fracturing," Modern Well Completion Series, Part 13, Pet. Eng. (July, 1961), B55,B63,B69,B72,B74,B75,B77,B78,B81.
- Grubb, W.E.; Martin, F.G. "A Guide to Chemical Well Treatments," Part 1, Pet. Eng., May 1963, 94-110; Part 2, *ibid* June 1963, 100-104; Part 3, *ibid*, July 1963; Part 4, *ibid* August 1963, 100-110; Part 5, *ibid* September 1963, 94-108; Part 6, *ibid* October 1963, 122-126; Part 6, *ibid* October 1963, 118-128; and Part 7, *ibid*, November 1963, 122,126.
- Hassebroek, W.E. and Waters, A.B.: "Advancements Through 15 Years of Fracturing," J. Pet. Technol. (July 1964) 760-764,787.
- Hill, K.E. and Coqueron, F.G.: "The Petroleum Industry A Look Backward...and Forward," SPE paper 1622, 1966 SPE Annual Meeting, Dallas, October 2-56
- Howard, G.C. and Fast, C.R.: Hydraulic Fracturing, Monograph Series, SPE(1970)2.
- Alderman, E.N.: "Super Thick Fluids Provide New Answers to Old Fracturing Problems," SPE paper 2852, 1970 Spring Symposium SPE, Fort Worth, March 8-10.
- Dysart, G.R., Richardson, D.W., and Kannenberg, B.G.: "Second Generation Fracturing Fluids," API paper 906-15-H, 1970 Spring Meeting of the Southwestern District Division of Production, Odessa, March 18-20.
- Coulter, G.R. and Wells, R.D.: "The Advantages of High Proppant Concentration in Fracture Stimulation," SPE paper 3298, 1971 SPE Annual Meeting, New Orleans, October 3-6.
- Rosene, R.B. and Shumaker, E.F.: "Viscous Fluids Provide Improved Results from Hydraulic Fracturing Treatments," SPE paper 3347, 1971 SPE Rocky Mountain Regional Meeting, Billings, June 2-4.
- Weiland, D.R., "Recent Trends in Hydraulic Fracturing," SPE paper 3659, 1971 SPE Eastern Regional Meeting, Charleston, November 4-5.
- Coulter, G.R.: "Hydraulic Fracturing - New Developments," Transactions Gulf Coast Association of Geological Societies, XXIII(1973), 47-53.
- White, J.L., Rosene, R.B., and Hendrickson, A.R.: "New Generation of Frac Fluids," 1973 SPE Annual Meeting, Edmonton, May 8-12.
- Buechley, T.C. and Lord, D.L.: "Hydraulic Fracturing Fluid Mechanics - State of the Art," Fluid Mechanics of Oil and Gas Production Symposium, 1973 National Meeting, A.I.Ch.E., New Orleans, March 11-15.
- Krueger, R.F.: "Advances in Well Completion and Stimulation During JPT's First Quarter Century," J. Pet. Technol., December, 1973, 1447-1462.
- Anderson, R.W. and Baker, J.R.: "Use of Guar Gum and Synthetic Cellulose in Oilfield Stimulation Fluids," SPE paper 5005, 1974 SPE Annual Meeting, Houston, October 6-9.
- White, J.L. and Free, D.L.: "Properties of Various Frac Fluids as Compared to the Ideal Fluid," Proc. Symp. Stimul. Low Perm. Reserv. Colo. School Mines.(1976), 1-14.
- Kohlhaas, C.A.: "Fracturing," Subsurf. Geology (4th Ed), edited by LeRoy, et al. (1977) 400-406.
- Waters, A.B.: "Stimulation of Hydrocarbon Reservoirs," 1980 Industrial Mineral Meeting, Houston, September 11-12.
- Waters, A.B.: "Hydraulic Fracturing Deep Gas Wells," 1981 International Gas Research Conference.
- Holman, G.B.: "State-of-the-Art Well Stimulation," J. Pet. Technol., February 1982, 239-241.
- Waters, A.B.: "History of Hydraulic Fracturing," 1982 SPE Hydraulic Fracturing Symposium, Lubbock, 1-20.

0097-6156/89/0396-0659\$06.00/0

© 1989 American Chemical Society

- Veatch, R.W., Jr.: "Current Hydraulic Fracturing Treatment and Design Technology," SPE paper 10039, 1982 SPE International Petroleum Exhibition and Technical Symposium, Beijing, China, March 28-26.
- Pai, V.J. and Garbis, S.J.: "Review of the Completion Practices in the Morrow Formation in Eddy, Chaves, and Lea Counties of Southeast New Mexico," SPE paper 11335, 1982 SPE Production Technology Symposium, Hobbs, Nov.
- Veatch, R.W., Jr.: "Overview of Current Hydraulic Fracturing Design and Treatment Technology - Part 1," J. Pet. Technol., April 1983, 677-864.; *ibid.* Part 2, J. Pet. Technol., May 1983, 853-864.
- Matson, B.G. and Baker, J.R.: "Advanced Stimulation Technology," Drilling-DCW April 20, 1977, 64-65.
- Menjivar, J.A.: "The Use of Water-Soluble Polymers in Oil Field Applications: Hydraulic Fracturing," 1984 Proc. Annu. M.I.T. Seagrants Colloq. Program Lecture Seminar (3rd), Cambridge, Mass.
- Ely, J.: "Fracturing Fluid Systems State of the Art," 1981 Proc. Annu. Southwest Pet. Short Course, Lubbock, April 23-24, 1981.
- Almond, S.W. and Garvin, T.R.: "High Efficiency Fracturing Fluids for Low Temperature Reservoirs," 1984 Proc. Annu. Southwest Pet. Short Course, Lubbock, May 1984, 76-88.
- Krueger, R.F.: "An Overview of Formation Damage and Well Productivity in Oilfield Operations," J. Pet. Technol., February 1986, 131-152.
- Ely, J.W.: "Stimulation Treatment Handbook," Penwell Publications: Tulsa, OK, 1985.
- Veatch, R.W., Jr. and Moschovidis, Z.A.: "An Overview of Recent Advances in Hydraulic Fracturing Technology," SPE paper 14085, 1986 International Meeting on Petroleum Engineering, Beijing, China, March 17-20.
- Allen, T.O. and Roberts, A.P. "Production Operations," Vol. 2, Penwell Publications, 2nd ed.:Tulsa,OK, 1982.
- Bleakely, W.B.: "How Chemicals Improve Ultimate Recovery," PET. ENG. Internat., May 1986, pages 53-58.
- Gray, G.R., Darley, H.C.H., Rogers, W.F.: "Compositions and Properties of Oil Well Drilling Fluids" 4th Ed, Gulf Publishing:Houston, TX 1980.
- Economides, M.J.; Nolte, K.G.: "Reservoir Stimulation," Schlumberger Educational Services:Houston,TX. 1987.
- Harris, P.C.: "Fracturing-Fluid Additives," J. Pet. Technol., Oct. 1988, 1277-79.
- Gidley, J. and Holditch, S.A., eds, "Recent Advances in Hydraulic Fracturing," Ely, J.W., in Chapter 7, "Fracturing Fluids and Additives," Society of Petroleum Engineers, Dallas, TX, 1989.

Fracturing Fluid Leakoff(Ref. 4.)

- Settari, A.: "A New General Model of Fluid Loss in Hydraulic Fracturing," SPE/DOE paper 11625, 1983 SPE/DOE Symposium on Low Permeability, Denver, March 14-16.
- Pye, D.S. and Smith, W.A.: "Fluid Loss Additive Seriously Reduces Fracture Proppant Conductivity and Formation Permeability," 1973 SPE Annual Meeting, Las Vegas, Sept. 30-Oct. 3.
- Zweigle, M.L. and Lamphere, J.C.: "Crosslinked, Water-Swellable Polymer Microgels," US Patent 4,172,066(1979).
- Ely, J.W.: "Methods of Using Aqueous Gels," US Patent 4,321,968(1982).
- McDaniel, R.R., Deysarkar, A.K., Callanan, M.J., and Kohlhaas, C.A.: "An Improved Method for Measuring Fluid Loss at Simulated Fracture Conditions," Soc. Pet. Eng. J., August 1985, 482-490.
- Block, J.: "Viscosifier and Fluid Loss Control System," US Patent 4,349,443(1982).
- Penny, G.S., Conway, M.W., and Lee, W.S.: "The Control and Modelling of Fluid Leak-Off During Hydraulic Fracturing," SPE paper 12486, 1984 Formation Damage Symposium, Bakersfield, January.
- Green, P.C. and Black, J.C.: "High Temperature Stable Viscosifier and Fluid Loss Control System," US Patent 4,486,318(1984).
- Bellis, H.E and McBride, E.F.: "Composition and Method for Temporarily Reducing Permeability of Subterranean Formations," US Patent 4,715,967(1987).
- McGowen, J.M. and McDaniel, B.W.: "The Effects of Fluid Preconditioning and Test Cell Design on the Measurement of Dynamic Fluid Loss Data," SPE paper 18212, 1988 SPE Annual Technical Conference and Exhibition, Houston, October 2-5.
- Woo, G.T. and Cramer, D.D.: "Laboratory and Field Evaluation of Fluid-Loss Additive Systems Used in the Williston Basin," SPE paper 12899, 1984 Rocky Mountain Regional Meeting, Casper, May 21-23.
- Hall, B.E. and Houk, S.G.: "Fluid-Loss Control in the Naturally Fractured Buda Formation," SPE paper 12152, 1983 SPE Annual Technical Conference and Exhibition, San Francisco, October 5-8.
- Gulbis, J.: "Dynamic Fluid Loss of Fracturing Fluids," SPE paper 12154, 1983 SPE Annual Technical Conference and Exhibition, San Francisco, October 5-8.
- Penny, G.S.: "Nondamaging Fluid Loss Additives for Use in Hydraulic Fracturing of Gas Wells," SPE paper 10659, 1982 SPE Formation Damage Control Symposium, Lafayette, March 24-25.

- Harris, P.C. and Penny, G.S.: "Influence of Temperature and Shear History on Fracturing Fluid Efficiency," SPE paper 14258, 1985 SPE Annual Technical Conference and Exhibition, Las Vegas, September 22-25.
- Cantu, L.A. and Boyd, P.A.: "Laboratory and Field Evaluation of a Combined Fluid-Loss Control Additive and Gel Breaker for Fracturing Fluids," SPE paper 18211, 1988 SPE Annual Technical Conference and Exhibition, Houston, October 2-5.
- Ford, W.G.F. and Penny, G.S.: "Influence of Downhole Conditions on the Leakoff Properties of Fracturing Fluids," SPE Prod. Eng., 1988, 3(1), 43-51.
- Harris, P.C.: "Dynamic Fluid-Loss Characteristics of CO₂-Foam Fracturing Fluids," SPE Prod. Eng., 1987, 2(2), 89
- Roodhart, L.P.: "Fracturing Fluids: Fluid-Loss Measurements Under Dynamic Conditions," Soc. Pet. Eng. J., 1985, 25(5), 629-36.
- Zigrye, J.L., Whitfill, D.L., and Sievert, J.A.: "Fluid-Loss Control Differences of Crosslinked and Linear Fracturing Fluids," J. Pet. Technol., 1985, 37(2), 315-20.
- Crowell, R.F.: "Formation Fracturing Method," US Patent 4,442,897(1984).
- Pachelke, G., Rettig, D., Eins, I., Shul'ts, G., Foerster, M., Ballschuh, D., Rusche, J., Ohme, R., and Markert, H.: "Stimulation of Reservoir Rocks," German Patent DD 159,657(1983).
- Ely, J.W.: "Water Flooding and Fracturing Using Clean, Nondamaging Fracturing Fluids," US Patent 4,265,311(1981).
- King, G.E.: "Low Fluid Loss Foam," US Patent 4,217,231(1980).
- Pachelke, G., Rettig, D., Foerster, M., Stark, H.J., and Tide, R.: "Solution for Hydrofracturing an Oil- and Gas-Saturated Stratum," SU Patent 683,640(1979).
- Dill, W.R. and Elphinstone, E.A.: "Preparing and Using Acidizing and Fracturing Compositions, and Fluid Loss Additives for Use Therein," US Patent 4,107,057(1978).
- Hill, O.F., Ward, A.J., and Clement, C.C.: "Austin Chalk Fracturing Design Using a Crosslinked Natural Polymer as a Diverting Agent," J. Pet. Technol., 1978, 30(12), 1795-804.
- Fisher, H.B.: "Sealing a Permeable Stratum with Resin," US Patent 3,525,398(1970).
- McClafflin, G.G. and Jacocks, C.L.: "Polyolefin-Encapsulated Silica: Low-Fluid-Loss Additive for Fracturing Fluids," US Patent 3,466,242(1969).
- Harper, B.G. and Smith, C.F.: "Fluid-Loss Control in Oil Well Treatment," US Patent 3,409,548(1968).
- Kuhn, D.A. and Brown, J.L.: "Loss Control Additive for Subterranean Fracturing Fluids," US Patent 3,408,296(1968).
- Kuhn, D.A.: "Low Liquid Loss Composition," US Patent 3,405,062(1968).
- Gibson, D.L.: "Low-Fluid-Loss Additive," US Patent 3,351,079(1967).

Modelling of Fracture Behavior(Ref. 12)

- Barby, G.B. and Barbee, W.C.: "Ultra-High Conductivity Fracture Stimulations: A Case History," SPE paper 16222, 1987 SPE Production Operations Symposium, Oklahoma City, March 8-10.
- Odeh, A.S. and Yang, H.T.: "Flow of Non-Newtonian Power Law Fluids Through Porous Media," SPE paper 7150, 1977 SPE of AIME Annual Fall Technical Conference and Exhibition, Denver, October 9-12.
- Warpinski, N.R., Clark, J.A., Schmidt, R.A., and Huddle, C.W.: "Laboratory Investigation on the Effect of In-Situ Stresses on Hydraulic Fracture Containment," Soc. Pet. Eng. J., June 1982, 333-339.
- Hanson, M.E., Anderson, G.D., Shaffer, R.J., and Thorson, L.D.: "Some Effects of Stress, Friction, and Fluid Flow on Hydraulic Fracturing," Soc. Pet. Eng. J., June 1982, 321-332.
- Settari, A.: "A New General Model of Fluid Loss in Hydraulic Fracturing," SPE/DOE paper 11625, 1983 SPE/DOE Symposium on Low Permeability, Denver, March 14-16.
- Dickey, P.A. and Andresen, K.H.: "The Behavior of Water-Input Wells," API, Secondary Recovery of Oil in the United States, Second Edition, 1950, 332-40.
- Scott, P.P., Jr., Bearden, W.G., and Howard, G.C.: "Rock Rupture as Affected by Fluid Properties," Soc. Pet. Eng. J.(1953) 111-124; Trans., AIME, 198.
- Hubbert, M.K. and Willis, D.G.: "Mechanics of Hydraulic Fracturing," Soc. Pet. Eng. J.(1957) 153,166,167; Trans., AIME, 210.
- Khristianovic, S.A. and Zheltov, Y.P.: "Formation of Vertical Fractures by Means of Highly Viscous Liquid," Proc., Fourth World Pet. Cong. (1954) Section 11/T.O.P., 579-586.
- Perkins, T.K. and Kern, L.R.: "Widths of Hydraulic Fractures," J. Pet. Technol.(September 1961) 937-949.
- Geertsma, J. and de Klerk, F.: "A Rapid Method of Predicting Width and Extent of Hydraulically Induced Fractures," J. Pet. Technol.(1969) 1571-1581.
- Whitsitt, N.F. and Dysart, G.R.: "The Effect of Temperature on Stimulation Design," J. Pet. Technol.(April 1970) 493,495-502.
- Daneshy, A.A.: "Opening of a Pressurized Fracture in an Elastic Medium," SPE paper 7616, 1971 Annual Technical Meeting of SPE of CIM, Banff, June 2-4.
- Nordgren, R.P.: "Propagation of a Vertical Hydraulic Fracture," Soc. Pet. Eng. J.(August 1972), 306-314.

- Harrington, L.J., Hannah, R.R., and Williams, D.: "Dynamic Experiments on Proppant Settling in Crosslinked Fracturing Fluids," SPE paper 8342, 1979 SPE Annual Technical Conference and Exhibition, Las Vegas, September 23-26.
- Hannah, R.R., Harrington, L.J. and Potter, J.S. Jr.: "Post Fracturing Behavior of Fracturing Gels and Its Influence on Fracture Closure and Proppant Distribution," SPE paper 9331, 1980 Annual Fall Technical Conference and Exhibition of SPE of AIME, Dallas, September 21-24.
- Cloud, J.E. and Clark, P.E.: "Stimulation Fluid Rheology III. Alternatives to the Power Law Fluid Model for Crosslinked Fluids," SPE paper 9332, 1980 SPE Annual Technical Conference and Exhibition, Dallas, September 21-24.
- Rogers, R.E., Veatch, R.W., Jr. and Nolte, K.G.: "Pipe Viscometer Study of Fracturing Fluid Rheology," SPE paper 10258, 1981 SPE Annual Technical Conference and Exhibition, San Antonio, October 5-7.
- White, J.L. and Daniel, E.F.: "Key Factors in MHF Design," J. Pet. Technol., August 1981, 1501-1512.
- Clark, P.E. and Quadir, J.A.: "Prop Transport in Hydraulic Fractures: A Critical Review of Particle Settling Velocity Equations," SPE/DOE paper 9866, 1981 SPE/DOE Low Permeability Symposium, Denver, May 27-29.
- Clark, P.E. and Guler, N.: "Prop Transport in Vertical Fractures: Settling Velocity Correlations," 1983 SPE/DOE paper 11636, SPE/DOE Symposium on Low Permeability, Denver, March 14-16.
- Torr, R.S.: "Particle Settling in Viscous Non-Newtonian Hydroxyethyl Cellulose Polymer Solutions," AIChE Journal (Vol. 29, No. 3) May, 1983, pages 506-508.
- Meyer, B.R.: "Generalized Drag Coefficient Applicable for All Flow Regimes," Oil Gas J., May 26, 1986, 71-77.
- Lord, D.L.: "Turbulent Flow of Stimulation Fluids: An Evaluation of Friction Loss Scale-Up Methods," SPE paper 16889, 1987 SPE Annual Technical Conference and Exhibition, Dallas, September 27-30.
- Lee, W.S. and Daneshy, A.A.: "Fracture Geometry and Proppant Transport Computation for Multiple-Fracture Treatment," SPE Prod. Eng. J., (November 1987) 257-266.
- McDaniel, B.W. and Hoch, O.F.: "Realistic Proppant Conductivity Data Improve Hydraulic Fracturing Treatment Design," paper No. 87-38-73, 1987 Annual Technical Meeting of the Petroleum Society of CIM, Calgary, June 7-10.
- Daneshy, A.A.: "Numerical Solution of Sand Transport in Hydraulic Fracturing," J. Pet. Technol., January, 1978, 132-140.
- Clark, P.E., Harkin, M.W., Wahl, H.A., and Sievert, J.A.: "Design of a Large Vertical Prop Transport Model," SPE paper 6814, 1977 Annual Fall Technical Conference and Exhibition of the SPE Engineers of AIME, Denver, October 9-12.
- Shah, S.N.: "Proppant Settling Correlations for Non-Newtonian Fluids Under Static and Dynamic Conditions," SPE paper 9330, 1980 Annual Fall Technical Conference and Exhibition of the SPE of AIME, Dallas, September 21-24.
- Torrest, R.S.: "Aspects of Slurry and Particle Settling and Placement for Viscous Gravel Packing (AQUAPAC)," SPE paper 11009, 1982 Annual Fall Technical Conference and Exhibition of the SPE of AIME, New Orleans, September 26-29.
- Torrest, R.S.: "The Flow of Viscous Polymer Solutions for Gravel Packing Through Porous Media," SPE paper 11010, 1982 Annual Fall Technical Conference and Exhibition of the SPE of AIME, New Orleans, September 26-29.
- Roodhart, L.P.: "Proppant Settling in Non-Newtonian Fracturing Fluid," SPE paper/DOE 13905, 1985 Low Permeability Gas Reservoirs, Denver, May 19-22.
- Kirkby, L.L.: "Proppant Settling Velocities in Nonflowing Slurries," SPE paper/DOE 13906, 1985 Low Permeability Gas Reservoirs, Denver, May 19-22.
- Acharya, A.: "Particle Transport in Viscous and Viscoelastic Fracturing Fluids," SPE Prod. Eng., March 1986, 104-110.
- Peden, J.M. and Luo, Y.: "Settling Velocity of Various Shaped Particles in Drilling and Fracturing Fluids," SPE Drilling Engineering, December 1987, 337-343.
- Wahlmeier, M.A. and Andrews, P.W.: "Mechanics of Gravel Placement and Packing: A Design and Evaluation Approach," SPE Prod. Eng., February 1988, pages 69-82.
- Baumgartner, S.A. and Mack, D.J.: "On-Site Computer Monitoring of Foamed Stimulation Fluids," SPE paper 17531, 1988 SPE Rocky Mountain Regional Meeting, Casper, May 11-13.
- Novotny, E.J.: "Proppant Transport," SPE paper 6813, 1977 Annual Fall Technical Conference and Exhibition of the SPE of AIME, Denver, October 9-12.
- Misak, M.D., Atteberry, R.D., Venditto, J.J. and Fredrickson, S.E.: "A Fracturing Technique to Minimize Water Production," SPE paper 7563, 1978 Annual Fall Technical Conference and Exhibition of the SPE of AIME, Houston, October 1-3.
- Teesum, D. and Hesselink, F.T.: "Power-Law Flow and Hydrodynamic Behavior of Biopolymer Solutions In Porous Media," SPE paper 8982, 1980 SPE Fifth International Symposium on Oilfield and Geothermal Chemistry, Stanford, May 28-30.
- Babcock, R.E., Prokop, C.L. and Kehle, R.O.: "Distribution of Propping Agents in Vertical Fractures," paper No. 851-41-A, 1967 API Spring Meeting of the Mid-Continent District Division of Production, Oklahoma City, March 29-31.

- **Bedeaux, D.:** "The Effective Viscosity for a Suspension of Spheres," *J. Coll. Interface Sci.*, 1987, 118(1), 80-86.
- **Morita, N., Whitfill, D.L., and Wahl, H.A.:** "Stress-Intensity Factor and Fracture Cross-Sectional Shape Predictions From a 3-D Model for Hydraulically Induced Fractures," SPE paper 14262, 1985 SPE Annual Technical Conference and Exhibition, Las Vegas, September 22-25.
- **Cunningham, R.D. and Nelson, R.G.:** "A New Method for Determining a Well's In-Place Hydrocarbons From a Pressure Buildup Test," *J. Pet. Technol.* (July 1967) 859-866.
- **Acharya, A. and Deysarkar, A.K.:** "Rheology of Fracturing Fluids at Low-Shear Conditions," SPE paper 16917, 1987 Annual Technical Conference and Exhibition, Dallas, September 27-30.
- **Wilson, Ed, B. and Hsu, T.R.:** "A Technique for the Measurement of Fracture Toughness of Oil Sands," *Proc. Tar Sands Symp.* 1986, 150-5.
- **Jeffri, M.A., Nichols, K.L., and Jayaraman, K.:** "Sedimentation of Two Contacting Spheres in Dilute Polymer Solutions," *Proc. Symp. Recent Dev. Struct. Continua.*, 1985, 21-5.
- **Al-Atter, H.H.:** "The Combined Effect of Oil Viscosity, Initial Water Saturation and Water Injection Rate on the Performance of Fractured Oil Reservoirs," *J. Pet. Res.*, 1984, 3(2), 1-16.
- **Daneshy, A.A.:** "On the Design of Vertical Hydraulic Fractures," *J. Pet. Technol.*, (1973) 83-97.
- **van Domselaar, H.R. and Visser, W.:** "Proppant Concentration In and Final Shape of Fractures Generated by Viscous Gels," *Soc. Pet. Eng. J.*, (1974) 531-536.
- **Harrington, L. and Hannah, R.R.:** "Fracturing Design Using Perfect Support Fluids for Selected Fracture Proppant Concentrations in Vertical Fractures," 1975 SPE Annual Meeting, Dallas, September 28-October 1.
- **Smith, J.E.:** "Effect of Incomplete Fracture Fill-Up at the Wellbore on Productivity Ratio," 1975 Proc. Annu. Southwest Pet. Short Course, 135-144.
- **Nolte, K.G. and Smith, M.B.:** "Interpretation of Fracturing Pressures," SPE paper 8297, 1979 SPE Annual Technical Conference and Exhibition, Las Vegas, September 23-26.
- **Dobkins, T.A.:** "Methods to Better Determine Hydraulic Fracture Height," SPE paper 8403, 1979 SPE Annual Fall Technical Conference and Exhibition, Las Vegas, September 23-26.
- **Cleary, M.P.:** "Comprehensive Design Formulae for Hydraulic Fracturing," SPE paper 9259, 1980 SPE Annual Technical Conference and Exhibition, Dallas, September 21-24.
- **Cleary, M.P.:** "Mechanisms and Procedures for the Production of Desirable Fracture Shapes in Representative Reservoir Formations," SPE paper 9260, 1980 SPE Annual Technical Conference, Dallas, September 21-24.
- **van Eekelen, H.A.M.:** "Hydraulic Fracture Geometry: Fracture Containment in Layered Formations," *Soc. Pet. Eng. J.*, June 1982, 341-349.
- **Nolte, K.G.:** "Fracture Design Considerations Based on Pressure Analysis," SPE paper 10911, 1982 SPE Cotton Valley Symposium, Tyler, May 20. See also Nolte, K.G.: "Principles for Fracture Design Based on Pressure Analysis," *SPE Prod. Eng.*, February 1988, 22-30; Nolte, K.G.: "Application of Fracture Design Based on Pressure Analysis," *SPE Prod. Eng.*, February 1988, 31-42.
- **McLennan, J.D. and Roegiers, J.C.:** "How Instantaneous are Instantaneous Shut-In Pressures?," SPE paper 11064, 1982 SPE Annual Technical Conference and Exhibition, New Orleans, September 26-29.
- **Smith, M.B., Rosenberg, R.J., and Bowen, J.F.:** "Fracture Width-Design vs. Measurement," SPE paper 10965, 1982 SPE Annual Technical Conference and Exhibition, New Orleans, September 26-29.
- **Soliman, M.Y.:** "Modifications to Production Increase Calculations for a Hydraulically Fractured Well," *J. Pet. Technol.* (1983) 170-172.
- **McLeod, H.O., Jr.:** "A Simplified Approach to Design of Fracturing Treatments Using High Viscosity Crosslinked Fluids," SPE/DOE paper 11614, 1983 SPE/DOE Symposium on Low Permeability, Denver, March 14-16.
- **Ahmed, U., et al.:** "Effect of Stress Distribution on Hydraulic Fracture Geometry: A Laboratory Simulation Study in One Meter Cubic Blocks," SPE/DOE paper 11637, 1983 SPE/DOE Symposium on Low Permeability, Denver, March 14-16.
- **Nierode, D.E.:** "Comparison of Hydraulic Fracture Design Methods to Observed Field Results," SPE paper 12059, 1983 SPE Annual Technical Conference and Exhibition, San Francisco, October 5-8.
- **Lee, W.S.:** "Pressure Decline Analysis with the Christianovich and Zheltov and Penny-Shaped Geometry Model of Fracturing," SPE/DOE paper 13872, 1985 SPE Low Permeability Gas Reservoirs, Denver, May 19-22.
- **Soliman, M.:** "Fracture Conductivity Distribution Studied," *Oil Gas J.*, February 10, 1986, 89-93.
- **Medlin, W.L. and Masse, L.:** "Plasticity Effects in Hydraulic Fracturing," *J. Pet. Technol.*, (1986) 995-1006.
- **Conway, M.W., McGowen, J.M., Gunderson, D.W., and King, D.G.:** "Prediction of Formation Response from Fracture Pressure Behavior," SPE paper 14263, 1985 SPE Annual Technical Conference and Exhibition, Las Vegas, September 22-25.

- Settari, A. and Cleary, M.P.: "Development and Testing of a Pseudo-Three-Dimensional Model of Hydraulic Fracture Geometry," SPE Prod. Eng., July 1986, 449-466.
- Biot, M.A., Masse, L., and Medlin, W.L.: "A Two-Dimensional Theory of Fracture Propagation," SPE Prod. Eng., January 1986, 17-30.
- Thiercelin, M.J. and Lemanczyk, Z.R.: "Stress Gradient Affects the Height of Vertical Hydraulic Fractures," SPE Prod. Eng., July 1986, 245-254.
- Molte, K.G.: "Determination of Proppant and Fluid Schedules from Fracturing-Pressure Decline," SPE Prod. Eng., July 1986, 255-265.
- Shelley, R.F. and McGowen, J.M.: "Pump-In Test Correlation Predicts Proppant Placement," SPE paper 15151, 1986 SPE Rocky Mountain Regional Meeting, Billings, May 19-21.
- Sookprasong, P.A.: "Plot Procedure Finds Closure Pressure," Oil Gas J., September 8, 1986, 110-112.
- Lord, D.L. and McGowen, J.M.: "Real-Time Treating Pressure Analysis Aided by New Correlation," SPE paper 15367, 1986 SPE Annual Technical Conference and Exhibition, New Orleans, October 5-8.
- Poulsen, D.K. and Soliman, M.Y.: "A Procedure for Optimal Hydraulic Fracturing Treatment Design," SPE paper 15940, 1986 SPE Eastern Regional Meeting, Columbus, November 12-14.
- Acharya, A. and Kim, C.M.: "Hydraulic Fracture Treatment Design Simulation for the Rotliegendes Formation," SPE/DOE paper 16414, 1987 SPE/DOE Low Permeability Reservoirs Symposium, Denver, May 18-19.
- Branagan, P., Cipolla, C., and Lee, S.J.: "Designing and Evaluating Hydraulic Fracture Treatments in Naturally Fractured Reservoirs," SPE/DOE paper 16434, 1987 SPE/DOE Low Permeability Reservoirs Symposium, Denver, May 18-19.
- Lee, W.S.: "Fracture Propagation Theory and Pressure Decline Analysis with Langrangian Formulation for Penny-Shaped and Perkins-Kern Geometry Models," SPE paper 17151, SPE Formation Damage Control Symposium, Bakersfield, February 8-9.
- Cooper, G.D., Nelson, S.G., and Schopper, M.D.: "Improving Fracturing Design Through the Use of an On-Site Computer System," SPE paper 12063, 1983 SPE Annual Technical Conference and Exhibition, San Francisco, October 5-8.
- Roegiers, J.-C. and Ishijima, Y.: "A Coupled Fracturing Model and Its Application to Hydraulic Fracturing," SPE paper 12311, Eastern Regional Meeting, Champion, November 9-11.
- Branagan, P.T., et al.: "Comprehensive Well Testing and Modeling of Pre- and Post-Fracture Well Performance of the MXL Lenticular Tight Gas Sands," SPE paper/DOE 13867, 1985 SPE/DOE Low Permeability Gas Reservoirs, Denver, May 19-22.
- Read, D.A. and Wells, G.L.: "Measurement While Fracturing for Comparing and Optimizing the Performance of Well Stimulation Treatments," 1985 Proc. Annu. Southwest Pet. Short Course, 171-176.
- Warpinski, N.R., et al.: "Fracturing and Testing Case Study of Paludal, Tight, Lenticular Gas Sands," SPE/DOE paper 13876, 1985 SPE/DOE Low Permeability Gas Reservoirs, Denver, May 19-22.
- Warembourg, P.A., et al.: "Fracture Stimulation Design and Evaluation," SPE paper 14379, 1986 SPE Proc. Rocky Mountain Regional Meeting, Billings, May 18-21, 359-370.
- Meyer, B.R.: "Design Formulae for 2-D and 3-D Vertical Hydraulic Fractures: Model Comparison and Parametric Studies," SPE paper 15240, 1986 SPE Unconventional Gas Technology Symposium, Louisville, May 18-21.
- Lam, K.Y., Cleary, M.P., and Barr, D.T.: "A Complete Three-Dimensional Simulator for Analysis and Design of Hydraulic Fracturing," 1986 spe Unconventional Gas Technology Symposium, Louisville, May 18-21.
- Crockett, A.R., Willis, R.M. Jr., and Cleary, M.P.: "Improvement of Hydraulic Fracture Predictions by Real-Time History Matching on Observed Pressures," SPE paper 15264, 1986 SPE Unconventional Gas Technology Symposium, Louisville, May 18-21.
- Vandamme, L., Jeffrey, R.G., and Curran, J.H.: "Pressure Distribution in Three-Dimensional Hydraulic Fractures," SPE paper 15265, 1986 SPE Unconventional Gas Technology Symposium, Louisville, May 18-21.
- Elbel, J.L.: "Designing Hydraulic Fractures for Efficient Reserve Recovery," SPE paper 15231, 1986 SPE Unconventional Gas Technology Symposium, Louisville, May 18-21.
- Molte, K.G.: "Fluid Flow Considerations in Hydraulic Fracturing," SPE Paper 18537, 1988 SPE Eastern Regional Meeting, Charleston, November 1-4.
- McLeod, H.O., Jr.: "The Effect of Perforating Conditions on Well Performance," SPE paper 10649, 1982 SPE Formation Damage Control Symposium, Lafayette, March 24-25.
- Jopliff, M.W. and Ketcher, N.W.: "Real Time Decision-Making Through Use of a Log/Log Plot During a Frac Job," SPE paper 16223, 1987 SPE Production Operations Symposium, Oklahoma City, March 8-10.
- Cipolla, C.L. and Lee, S.J.: "The Effect of Excess Propped Fracture Height on Well Productivity," SPE paper 16219, 1987 SPE Production Operations Symposium, Oklahoma City, March 8-10.
- Lee, W.S.: "Study of the Effects of Fluid Rheology on Minifrac Analysis," SPE paper 16916, 1987 SPE Annual Technical Conference and Exhibition, Dallas, September 27-30.

- Ben Maceur, K., Touband, E., and Roegiers, J.-C.: "Numerical Investigation of the Effects of Fluid Rheological Properties on 3-D Fracture Propagation," CIM paper 87-37-26, 1986 Annual Technical Meeting of CIM, 8620268, Calgary, June 8-11.
- Vandamme, L., Jeffrey, R.G. and Curran, J.H.: "Effects of Three-Dimensionalization on a Hydraulic Fracture Pressure Profile," 1986 Proc. U.S. Symposium on Rock Mechanics; Key to Energy Production: 580-590, Tuscaloosa, Alabama, June 23-25.
- Ehlig-Economides, C.: "Use of the Pressure Derivative for Diagnosing Pressure-Transient Behavior," *J. Petr. Technol.*, October 1988, 1280-1282.
- McDaniel, B.W.: "Realistic Fracture Conductivities of Proppants as a Function of Reservoir Temperature," SPE/DOE paper 16453, 1987 SPE/DOE Low Permeability Reservoirs Symposium, Denver, May 18-19.
- McDaniel, B.W.: "Use of Wet Gas Flow for Long-Term Fracture Conductivity Measurements in the Presence of Gel Filter Cakes," SPE paper 17543, 1988 SPE Rocky Mountain Regional Meeting, Casper, May 11-13.
- McDaniel, B.W. and Parker, M.A.: "Accurate Design of Fracturing Treatment Requires Conductivity Measurements at Simulated Reservoir Conditions," SPE paper 17541, 1988 SPE Rocky Mountain Regional Meeting, Casper, May 11-13.
- Cunningham, R.D. and Nelson, R.G.: "A New Method for Determining a Well's In-Place Hydrocarbons From a Pressure Buildup Test," *J. Petr. Technol.*, July 1967, 859-866.
- Parker, M.A. and McDaniel, B.W.: "Fracturing Treatment Design Improved by Conductivity Measurements Under In-Situ Conditions," SPE paper 16901, 1987 SPE Annual Technical Conference and Exhibition, Dallas, September 27-30.
- Cunningham, R.D. and Nelson, R.G.: "A New Method for Determining a Well's In-Place Hydrocarbons From a Pressure Buildup Test," *J. Petr. Technol.* (July 1967), 859-866.
- Wapinski, N.R.: "In Situ Measurements of Hydraulic Fracture Behavior," *Sandia Report* SAND83-1826, July 1985.
- Aguilera, R.: "Detection and Evaluation of Naturally Fractured Reservoirs from Logs," SPE paper 4398, 1973 SPE Rocky Mountain Regional Meeting, Casper, May 15-16.
- Nelson, R.A.: "An Approach to Evaluating Fractured Reservoirs," *J. Petr. Technol.*, September 1982, 2167-2170.
- Kiel, O.M.: "The Kiel Process - Reservoir Stimulation by Dendritic Fracturing," SPE paper 6984.
- Celik, M.S., Ananthapadmanabhan, K.P., and Somasundaran, P.: "Precipitation/Redissolution Phenomena in Sulfonate/ALCl₃ Solutions," SPE paper 11796, 1983 SPE International Symposium on Oilfield and Geothermal Chemistry, Denver, June 1-3.
- Settari, A. and Price H.S.: "Simulation of Hydraulic Fracturing in Low Permeability Reservoirs," SPE/DOE paper 8939, *Soc. Pet. Eng. J.*, April 1984, 141-52.

Chemistry of Gelled Oils (Ref. 42)

- Minich, A. and Nowak, M.: "Oil Soluble Gelling Agent," US Patent 2,618,596, 1952.
- Lundberg, R.D., Peiffer, D.G., Sedillo, L.P. and Newlove, J.C.: "Hydrocarbon Soluble Polymer Complexes Useful as Viscosifiers in Fracturing Operations," US Patent 4,579,671, 1986.
- Hochwalt, C.A., Lum, J.H., Malowan, J.E., and Dyer, C.P.: "Alkyl Esters of Phosphoric Acid," *Ind. Eng. Chem.*, 1942, 34(1), 20-25.
- Self, E.S.: "Oil Base Drilling Fluid," US Patent 2,461,483(1949).
- Pellegrini, J.P. Jr. and Strange, H.O.: "Mineral Oil Containing A Rare Earth Metal Diester Phosphate," US Patent 2,983,679(1961).
- Revukas, A.J.: "Hydrocarbon Fuel Composition," US Patent 3,334,978(1967).
- Kerschner, P.M. and Hess, F.G.: "Amine Salts of Metal Organo Orthophosphates," US Patent 3,338,935(1967).
- Kiel, O.M.: "A New Hydraulic Fracturing Process," *J. Petr. Technol.* (January 1970), 89-96.
- Poklacki, E.S.: "Polyamine Salts of Aluminum Alkyl Orthophosphates," US Patent 4,007,128(1977).
- Griffin, T.J. Jr.: "Phosphate Ester-Type Reaction Product and Method of Preparing Same," US Patent 4,153,649(1979).
- Griffin, T.J. Jr.: "Gelling of organic Liquids," US Patent 4,152,289(1979).
- Griffin, T.J. Jr.: "Method of Fracturing with Gelled Organic Liquids," US Patent 4,174,283(1979).
- Burnham, J.W. and Tiner, R.L.: "Fracturing Compositions and Method of Preparing and Using the Same," US Patent 4,200,539(1980).
- Burnham, J.W.: "Method for Fracturing Subterranean Formations," US Patent 4,200,540(1980).
- Burnham, J.W.: "Gelled Oil Base Compositions and Methods of Preparation and Use of Same," US Patent 4,316,810(1982).
- Daccord, G., Lemanczyk, R., and Vercaemer, C.: "Method for Obtaining Gelled Hydrocarbon Compositions, the Compositions According to Said Method and Their Application in the Hydraulic Fracturing of Underground Formations," US Patent 4,507,213(1985).
- Harris, L.E., Holtmyer, M.D. and Pauls, R.W.: "Method for Fracturing Subterranean Formations," US Patent 4,622,155(1986).

- Hassen, B.R., Porter, K.E., and McCriston, L.L.: "Improving Oilwell Stimulations with Compatible Oils," J. Can. Pet. Technol., (November-December, 1986) Montreal, 32-38.
- Gross, J.M.: "Gelling Organic Liquids," European Patent Application 0,225,661(1986).
- Gordon, D.A.: "Gels Increase Well Fracturing Efficiency," Drilling Contractor(November 1985) 54-55.
- Kucera, C.H., Smith, C.F. and Braunlich, F.H.: "New Oil Gelling Systems Prevent Damage in Water-Sensitive Sands," SPE paper 3503, 1971 SPE Annual Meeting, New Orleans, October 3-6.
- Chatterji, J., Holtmyer, M.D. and Tiner, R.L.: "Gelling Liquid Hydrocarbons," US Patent 3,900,070(1975).
- Clark, H.B.: "Use of Fluorochemical Surfactants in Nonaqueous Stimulation Fluids," J. Pet. Technol.(October 1980) 1695-1697.
- Swanson, B.L.: "Oil Displacement Method Using Shear-Thickening Compositions," US Patent 4,289,203(1981).
- Gregorczyk, W, Pauls, R., Venditto, J., Chisholm, P., and Holtmyer, M.: "Successful Stimulation of the Olmos Formation Using Oil-Base Fluids and High Proppant Concentrations in the A.W.P. Field of McMullen County, Texas," SPE 1984 Spring Symposium, Corpus Christi, March.
- Rutinton, R.J., Jr.: "Organic Gels," US Patent 4,537,700(1985).
- Pellegrini, J.P., Jr. and Strange, H.O.: "Synthetic Oil Containing a Rare Earth Metal Diester Phosphate," US Patent 2,983,678(1961).
- Copes, J.P., Mayhew, R.L., and Williams, E.P.: "Petroleum Hydrocarbon Compositions," US Patent 3,012,966(1961).
- Matt, J.W.: "Conductivity Additive for Liquid Hydrocarbons," US Patent 3,758,283(1973).
- Jaggard, W. and Scales, A.A.: "Gel-Like Composition for Use as a Pig in a Pipeline," US Patent 4,003,393(1977).
- Horn, J.M., Johnston, B.E., Napier, R.P. and Williams, T.N.: "Process for the Preparation of Dialkyl Phosphoric Acids," US Patent 4,288,392(1981).
- Rueggeberg, W.H.C. and Chernack, J.: "Alcoholysis of Ethyl Phosphate. The Preparation of Mixed Ethyl Butyl Phosphates," J. Amer. Chem. Soc., 1948, 70, 1802-1804.
- Gay, R.L., Schlott, R.J., and Burroughs, J.E.: "Gelling Agents for Hydrocarbon Compounds," US Patent 4,104,173(1978).
- Turner, S.R., Walker, T.O. and Thaler, W.A.: "Sodium Styrene Sulfonate-Co-Sodium-N-(4-Sulfo-Phenyl)-Maleimide- An Improved Viscosity Control Additive," US Patent 4,478,727(1984).
- Agarwal, P.K. and Lundberg, R.D.: "Viscoelastic Behavior of Concentrated Oil Solutions of Sulfo Polymers. 2. EPDM and Zinc Sulfo-EPDMs" Macromolecules 1984, 17, 1918-1928.
- Thaler, W.A., Brois, S.J. and Ferrara, F.W.: "Sulfomaleation of EPDM Polymers," Macromolecules, 1987, 20, 254-258.
- Duvdevani, I., Wagensommer, J., and Agarwal, P.K.: "Novel Interpolymer Complexes of Sulfonated octene-1 Copolymer," US Patent 4,634,542(1987).
- Zulauf, M and Eicke, H.F.: "Inverted Micelles and Microemulsions in the Ternary System H₂O/Aerosol-OT/Isooctane as Studied by Photon Correlation Spectroscopy," J. Phys. Chem., 1979, 82(4), 480-486.
- Patel, A.D. and Salandanan, C.S.: "Thermally Stable Polymeric Gellant for Oil-Base Drilling Fluids," SPE paper 13560, 1985 International Symposium on Oilfield and Geothermal Chemistry, Phoenix, April 9-11.
- Deguchi, K. and Mino, J.: "Solution Properties of Long-Chain Dialkyldimethylammonium Salts," J. Coll. Interfac. Sci., 1978, 65(1), 155-161.
- Kunitake, T.: "Chemistry of Synthetic Bilayer Membranes," J. Macromol. Sci. - Chem., 1979, A13(5), 587-602.
- McNeil, R. and Thomas, J.K.: "On the Nature of Surfactant Vesicle and Micelle Systems," J. Coll. Interfac. Sci., 1980, 73(2), 522-529.
- Grantham, C.K. and McLaurine, H.C.: "Thixotropy Without Viscosity: A New Approach to Rheology Control of Oil Muds," SPE paper 15415, 1986 SPE Annual Technical Conference and Exhibition of AIME, New Orleans, October 5-8.
- MacDonald, R.G. and Frank, J.: "Sand Fracturing the Slave Point Carbonate," J. Can. Pet. Technol., November-December 1986, Montreal, 39-47.
- Portnoy, R.C., Lundberg, R.D., and Werlein, E.R.: "Novel Polymeric Oil Mud Viscosifier for High-Temperature Drilling," IADC/SPE paper 14795, 1986 IADC/SPE Drilling Conference, Dallas, February 10-12.
- Culter, J.D. and McClafin, G.G.: "Method of Friction Loss Reduction in Oleaginous Fluids Flowing Through Conduits," US Patent 3,692,676(1972).
- Driscoll, P.L., Bowen, J.G., and Roberts, M.A.: "Oil Base Foam Fracturing Applied to the Niobrara Shale Formation," 1980 SPE Annual Fall Technical Conference and Exhibition of AIME, Dallas, September 21-24.
- Sedilo, L.P., Newlove, J.C., Peiffer, D.G., and Lundberg, R.D.: "Hydrocarbon Soluble Polymer Complexes Useful as Viscosifiers in Fracturing Operations," US Patent 4,615,393(1986).
- Morgenthaler, L.N. and Mikols, W.J.: "Oil-Base Well-Treating Fluids Thickened by Block Copolymers," US Patent 4,595,513(1986).

- **Goncalves, A.A. and Saiago, C.A.:** "Composition for Use in Fracturing Petroleum-Containing Formations," Brazil Patent 84/214(1985), Chemical Abstracts 104(10):71519c(1986).
- **Daccord, G., Lemancyk, R., and Vercaemer, C.:** "Gelled Hydrocarbon Mixtures and Their Use in Hydraulic Crack Formation in Underground Formations," German Patent 3,247,758(1983), Chemical Abstracts 99(12):90859h(1983).
- **Burnham, J.W.:** "Fracturing Underground Formations," German Patent 2,915,455(1979), Chemical Abstracts 92(16):131842y(1980).
- **Griffin, T.J., Jr.:** "Fracturing with Gelled Organic Liquids," US Patent 4,174,283(1979).
- **Hill, D.G.:** "Reducing the Viscosity of an Organic Liquid, and Fracturing an Underground Formation," Brazil Patent 74/10408(1975), Chemical Abstracts 87(12):87655k(1977).
- **Gay, R.L., Schlott, R.J. and Burroughs, J.E.:** "Gelling Agents for Hydrocarbon Compounds," CA Patent 974,539(1975), Chemical Abstracts 90(10):74182f(1979).
- **Crawford, D.L., Earl, R.B., and Monroe, R.F.:** "Oil Well Fracturing Fluid Additive," GB Patent 1,355,080(1974), Chemical Abstracts 81(18):108337b(1974).
- **Ely, J.W. and Tiner, R.L.:** "Hydraulic Fracturing Method Using Benzoic Acid to Further Increase the Viscosity of Liquid Hydrocarbon," US Patent 3,799,267(1974).
- **Slagel, R.C. and Bloomquist, A.E.:** "Friction Reduction in Flowing Hydrocarbon Fluids," US Patent 3,779,969(1973).
- **Shearn, G.P. and Kiel, O.M.:** "Compositions for Use in Hydraulic Fracturing Operations Involving Wells Penetrating Subterranean Formations," US Patent 3,501,198(1971).
- **Malone, W.T., Holtmyer, M.D., Tinsley, J.M., and Chattopadhyay, J.:** "Additive for Reducing Friction Pressure Loss of Liquid Hydrocarbons Flowing Through Pipes," German Patent 2,056,700(1971), Chemical Abstracts 75(12):78860y(1971).
- **Weltmann, R.N. and Green, H.:** "Rheological Properties of Colloidal Solutions, Pigment Suspensions, and Oil Mixtures," J. Applied Physics, 1943, 14, 569-576.
- **Lundberg, R.D. and Peiffer, D.G.:** "Viscosification of Hydrocarbon Fluid," US Patent 4,448,926(1984).

Acidizing, Fracture Acidizing(Ref. 54)

- **Hessert, J.E. and Bertus, B.J.:** "Method for Acidizing Subterranean Formations," US Patent 4,068,714(1978).
- **Tate, J.F.:** "Secondary Recovery Process," US Patent 4,200,151(1980).
- **Dill, W.R. and Elphinstone, E.A.:** "Method of Preparing and Using Acidizing and Fracturing Compositions, and Fluid Loss Additives for Use Therein," US Patent 4,107,057(1978).
- **Peiffer, D.G., Lundberg, R.D., and Turner, S.R.:** "Intramolecular Polymeric Complex-Viscosifiers for Acid, Base and Salt (Aqueous) Solutions," US Patent 4,461,884(1984).
- **Abrams, A., Schuerman, R.F., Templeton, C.C., and Richardson, E.A.:** "Higher-pH Acid Stimulation Systems," J. Pet. Technol., December 1983, 2175-2184.
- **Crowe, C.W.:** "Guidelines for Selecting Iron Stabilizers for Use in Acidizing Treatments," 1980 Proc. Annu. Southwest. Pet. Short Course, Lubbock, April 17-18, 39-45.
- **Pabley, A.S.:** "Method for Stimulating Siliceous Subterranean Formations," US Patent 4,428,432(1985).
- **Pabley, A.S. and Holcomb, D.L.:** "A New Method of Acidizing or Acid Fracturing: Crosslinked Acid Gels," 1980 Proc. Annu. Southwest. Pet. Short Course, Lubbock, April 17-18, 31-38.
- **Engelhardt, F., Kuhlein, K., Riegel, U., von Halasz, S., Dawson, J.C., and Reed, A.R.:** "Water Soluble Copolymers for Use in Fracture-Acidizing of Wells," US Patent 4,500,437(1985).
- **Holcomb, D.L., Jr.:** "A New Concept in Hydrochloric-Hydrofluoric Acid Mixtures for Acidizing Low Permeability Sandstone Formations," 1974 Proc. Annu. Southwest. Pet. Short Course, Lubbock, 41-8.
- **Clampitt, R.L.:** "Gelled Prod® Fluid for High Temperature Fracturing," 1975 Proc. Annu. Southwest. Pet. Short Course, Lubbock.
- **Hall, B.E.:** "A New Technique for Generating In-Situ Hydrofluoric Acid for Deep Clay Damage Removal," SPE paper 6512, 1977 SPE Annual California Regional Meeting of AIME, Bakersfield, April 13-15.
- **Watkins, D.R. and Roberts, G.E.:** "On-Site Acidizing Fluid Analysis Shows HCl and HF Contents Often Varied Substantially From Specified Amounts," J. Pet. Technol., May 1983, 865-871.
- **Hartley, R. and Bosma, M.G.R.:** "Fracturing in Chalk Completions," J. Pet. Technol., January 1985, 73-79.
- **Crowe, C.W.:** "New Treating Technique to Remove Bacterial Residues from Water-Injection Wells," J. Pet. Technol., May 1968, 475-478.
- **McLeod, H.O., Jr., Ledlow, L.B., and Till, M.V.:** "The Planning, Execution, and Evaluation of Acid Treatments in Sandstone Formations," SPE paper 11931, 1983 SPE Annual Technical Conference and Exhibition, San Francisco, October 5-8.
- **Clementz, D.M., Patterson, D.E., Aseltine, R.J., and Young, R.E.:** "Stimulation of Water Injection Wells in the Los Angeles Basin Using Sodium Hypochlorite and Mineral Acids," SPE paper 10624, 1982 SPE International Symposium on Oilfield and Geothermal Chemistry, Dallas, January 25-27.

- Harris, L.E.: "High Viscosity Acidic Treating Fluids and Methods of Forming and Using the Same," US Patent 4,324,668(1982).
- Crowe, C.W.: "Status Report: Acid Fracturing," PET. ENG., International, June 1988, 39,41.
- Sutton, G.D. and Lasater, R.M.: "Aspects of Acid Additive Selection in Sandstone Acidizing," SPE paper 4114, 1972 SPE Annual Fall Meeting of AIME, San Antonio, October 8-11.
- Norman, L.R., Conway, M.W. and Wilson J.M.: "Temperature Stable Acid Gelling Polymers. Laboratory Evaluation and Field Results," SPE paper 10260, 1981 SPE Annual Fall Technical Conference and Exhibition of AIME, San Antonio, October 5-7.
- Broadbuss, G.C.: "Preflush Concepts in Fracture Acidizing," 1975 Proc. Annu. Southwest Pet. Short Course, 91-97.
- van Domselaar, H.R., Schols, R.S. and Visser, W.: "An Analysis of the Acidizing Process in Acid Fracturing," Soc. Pet. Eng. J., August, 1973, 239-250.
- Staudt, J.G.: "Acidizing," Pet. Eng.(July 1954) 855-858.
- Knox, J.A.: "Acidizing .. Past, Present, and Future," 1973 Annual Technical Meeting of the Petroleum Society of CIM, Edmonton, May 8-12.
- Goins, W.C., Jr. and McGlothlin, B.B.: "Two-Stage Injection of Acid-Producing Chemicals for Stimulating Wells," US Patent 3,707,192(1972).
- Burns, L.D.: Europ. Pat. App. 0 281 131 A2(1988).
- Snow, S.W.; Hough, E.V. "Field and Laboratory Experience in Stimulating Ekofisk Area North Sea Chalk Reservoirs," SPE paper 18225; 1988 SPE Annual Technical Conference and Exhibition, Houston.
- Coulter, A.W., Alderman, E.N., Cloud, J.E., and Crowe, C.W. "Mathematical Model Simulates Actual Well Conditions in Fracture Acidizing Treatment Design," SPE paper 5004, 1974 SPE Annual Fall Meeting of AIME, Houston.
- Anderson, M.S.; Fredrickson, S.E. "Dynamic Etching Tests Aid Fracture Acidizing Treatment Design," SPE/DOE paper 16452, 1987 SPE/DOE Low Permeability Reservoirs Symposium, Denver.
- Swanson, B.L. and Roper, L.E.: "Well Treating Compositions," US Patent 4,205,724(1980).
- Walker, M.L., Fredrickson, S., Norman, L., and Hoch, O.: "Heated Acids for Improved Stimulation," J. Can. Pet. Technol., 1987, 26(5), 57-9.
- Mazarov, S.N.: "Hydrochemical Fracture of Low-Permeability Materials," Neft. Khoz., 1987, (5), 59-63.
- Baumgartner, S.A. and Harrington, L.J.: "A Novel Approach to Acid Fracturing Treatment Design," 1987 Proc. Annu. Southwest. Pet. Short Course, Lubbock, 50-8.
- Dawson, J.C., McDaniel, R.R., Sedillo, L.P.: "Aqueous Acid Gels and Their Use," US Patent 4,624,795(1986).
- Gdanski, R.D. and Norman, L.R.: "Using the Hollow-Core Test to Determine Acid Reaction Rates," SPE Prod. Eng., 1986, 1(2), 111-16.
- Dawson, J.C.: "Aqueous Acid Gels and Their Use," US Patent 4,604,218(1986).
- Katona, J., Udovecz, G. and Vas, A.: "Acidic Fracturing Fluid for Geological Strata," Chemical Abstracts, 105(18):155989q(1986).
- Perlman, W.: "Fracturing Coal Formations," Chemical Abstracts, 103(24):198382n(1985).
- Graham, J.W. and Sinclair, A.R.: "Acidizing Propped Fractures," US Patent 4,527,627(1985).
- Hitzman, D.O.: "Gelled Acid Composition," US Patent 4,515,700(1985).
- Khalil, C.N. and Dacier, C.S.D.: "Gelled Liquid Acid Composition," Chemical Abstracts, 102(18):151945n(1985).
- Ford, W.G.F. and Roberts, L.D.: "The Effect of Foam on Surface Kinetics in Fracture Acidizing," J. Pet. Technol., 1985, 37(1), 89-97.
- Conway, M.W. and Norman, L.R.: "Treating Subterranean Formations Utilizing Foamed Viscous Fluids," US Patent 4,453,596(1984).
- Katona, J., Udovecz, G., and Vas, A.: "Acidic Fracturing Liquid," Chemical Abstracts, 101(8):57519j(1984).
- Josephson, C.B.: "Method and Compositions for Acidizing and Fracturing Wells," Chemical Abstracts, 101(6):40812b(1984).
- Deysarkar, A.K., Dawson, J.C., Sedillo, L.P. and Knoll-Davis, S.: "Crosslinked Acid Gel," J. Can. Pet. Technol., 1984, 23(1), 26-32.
- Smith, M.A., Dawson, J., and Scoggins, D.: "High Temperature, Crosslinked High-Strength Acid System," 1983 Proc. Annu. Southwest Pet. Short Course, Lubbock, 163-73.
- Mazarov, S.N. and Kholbaev, T.Kh.: "Hydraulic-Acid Fracturing of Formations," SU Patent 953,190(1982).
- Chauhan, K.J., Malhotra, B.D., and Goyal, K.L.: "Development of Acid Gels as Fracture Fluids," ONGC, Bull. 1981, 18(1), 53-76.
- Church, D.C., Quisenberry, J.L., and Fox, K.B.: "Field Evaluation of Gelled Acid for Carbonate Formations," J. Pet. Technol., 1981, 33(12), 2471-4.
- Crowe, C.W., Martin, R.C., and Michaelis, A.M.: "Evaluation of Acid-Gelling Agents for Use in Well Stimulation," Soc. Pet. Eng. J., 1981, 21(4), 415-24.
- Pabley, A.S. and Holcomb, D.L.: "Crosslinked Acid Gels Offer Advantages," Oil Gas J., 1981, 79(39), 286, 288, 291-2.

- Petryk, R.P. and Goruk, B.W.: "Fracture Acidizing with Foamed Acid: Success in the Crossfield D-1 Carbonate," J. Can. Pet. Technol., 1980, 19(3), 57-74.
- Needham, R.B., Thomas, C.P. and Wier, D.R.: "Well Treatment Method," US Patent 4,231,428(1980).
- Roper, L.E. and Swanson, B.L.: "Well Treating Compositions," US Patent 4,205,724(1980).
- Pabley, A.S. and Holcomb, D.L.: "A New Method of Acidizing or Acid Fracturing: Crosslinked Acid Gels," 1980 Proc. Annu. Southwest Pet. Short Course, Lubbock, 31-8.
- Knox, J.A. and Ripley, H.E.: "Fracture Acidizing in Carbonate Rock," J. Can. Pet. Technol., 1979, 18(4), 77-90.
- Jahnke, R.W.: "Thickened Aqueous Compositions for Well Treatment," US Patent 4,061,580(1977).
- Aldrich, R.G.: "Spontaneous Fracture of Coal," Fuel, 1977, 56(3), 345.
- Swanson, B.L.: "Composition for Acidifying Underground Formations," German Patent 2,657,443(1977).
- Ugolev, V.S. and Konyushenko, N.V.: "Reaction of Acid Foams with a Carbonaceous Porous Media under Dynamic Conditions," Chemical Abstracts, 86(2):6940d(1977).
- Broadus, G.C. and Fredrickson, S.E.: "Fracture Acidizing Method," US Patent 3,918,524(1975).
- Williams, B.B., Gidley, J.L., Schechter, R.S.: "Acidizing Fundamentals," Monograph Series SPE, Dallas(1979).
- Wieland, D.R. and Vinson, M.E.: "Engineered HCl-HF Treatments Provide Successful Stimulation in Cook Inlet," SPE paper 4120, 1972 SPE Annual Fall Meeting of AIME, San Antonio, October 8-11.
- Bailey, D.E. and Wickham, J.F.: "Sand Fracturing vs Fracture Acidizing," SPE paper 12898, 1984 Rocky Mountain Regional Meeting, Casper, May 21-23.
- Misak, M.D., et al.: "Edwards Limestone Completions Improved by New Stimulation Technique," SPE paper 7115, 1978 Southwest Texas Regional SPE Meeting, Corpus Christi, April 14.
- Fredrickson, S.E. and Broadus, G.C.: "Selective Placement of Fluids in a Fracture by Controlling Density and Viscosity," J. Pet. Technol.(May 1976) 597-602.
- Sutton, G.D. and Lasater, R.M.: "Aspects of Acid Additive Selection in Sandstone Acidizing," SPE paper 4114, 1972 SPE Annual Fall Meeting of AIME, Dallas, October 2-5.
- Holcomb, D.L.: "Low Concentration Hydrochloric-Hydrofluoric Acid Mixtures for Stimulation in Low Porosity, Low Permeability Sandstone Formations," Proc. Symp. Stimul. Low Permeability Reservoirs, 1976, 72-86, Colo. Sch. Mines, Golden.
- Elphinston, E.A. and Norman, L.R.: "Treating Subterranean Well Formations," US Patent 4,231,882(1980).
- Williams, B.B. and Nierode, D.E.: "Design of Acid Fracturing Treatments," J. Pet. Technol., 1972, 24(July), 849-59.

Friction and Drag Reducers(Ref. 110)

- Zakin, et al.: "Variables Affecting Drag Reduction by Nonionic Surfactant Additives," Chem. Eng. Commun., 1983, 23, 77-88.
- Ousterhout, R.S.: "Reduction of Friction Loss in Fracturing Operations," J. Pet. Technol.(March, 1961) 217-222.
- Root, R.L.: "Method for Decreasing Friction Loss in a Well Fracturing Process," US patent No. 3,254,719(1966).
- Sarem, A.M.: "Method of Decreasing Friction Loss in a Well Fracturing Process," US Patent 3,357,525(1970).
- Phillips, K.G.: "Method for Reducing Friction Loss in a Well Fracturing Process," US Patent 4,152,274(1979).
- Sylvester, N.D. and Tyler, J.S.: "Dilute Solution Properties of Drag-Reducing Polymers," Ind. Eng. Chem. Prod. Res. Develop., 1970, 9(4), 548-553.
- Kim, O.K., Little, R.C., and Ting, R.Y.: "The Correlation of Drag-Reduction Effects with Polymer Intrinsic Viscosity," J. Colloid Interface Sci., 1974, 47(2).
- Savins, J.G.: "A Stress-Controlled Drag-Reduction Phenomenon," SPE paper 1724, 1966 SPE Symposium on Mechanics of Rheologically Complex Fluids, Houston, December 15-16.
- McCormick, C.L., et al.: "Development of Laboratory Screening Tests to Predict Polymer Performance in Enhanced Oil Recovery (I). Shear Degradation, Viscosity, and Electrolyte Studies," prepared for DOE under contract No. EF-77-S-05-5603, 1977.
- Thorn, D.J. and Burnham, J.W.: "Dissolving Polymeric Materials in Hydrocarbon Liquids," US Patent 4,068,676(1978).
- Culter, J.D. and McClafflin, G.G.: "Method of Friction Loss Reduction in Oleaginous Fluids Flowing Through Conduits," US Patent 3,692,676(1972).
- Chang, H.D., Darby, R.: "Effect of Shear Degradation on the Rheological Properties of Dilute Drag-Reducing Polymer Solutions," J. Rheol., 1983, 27(1), 77-88.

Xanthan Gum(Ref. 138)

- Abdo, M.K., et al.: "Field Experience with Floodwater Diversion by Complexed Biopolymers," SPE/DOE paper 12642, 1984 SPE/DOE Symposium on Enhanced Oil Recovery, Tulsa, April 15-18.

- Crowe, "Method of Inhibiting Crosslinking of Aqueous Xanthan Gums in the Presence of Ferric Acid Ions," US Patent 4,317,735(1982).
- Shu and Szolek, W.: "Zirconium Crosslinked Gel Compositioning Methods of Preparation and Application In Enhanced Oil Recovery," US Patent 4,676,930(1987).
- Hannah, R.R.: "New Fracturing Technique Leads to Improved Performance in the Mississippian Trend," J. Pet. Technol.(August 1976) 859-864.
- Hill, O.F., Ward, A.J., and Clement, C.C.: "Austin Chalk Fracturing Design Using a Crosslinked Natural Polymer as a Diverting Agent," J. Pet. Technol.(December 1978) 1795-1804.
- Morton, C.J., Falk, D.O., and Luetzelschwab, W.E.: "Xanthan Biopolymer Semi-Pilot Fermentation," SPE paper 8420, 1979 SPE Annual Technical Conference and Exhibition, Las Vegas, September 23-26.
- Chauveteau, G. and Kohler, N., "Influence of Microgels in Xanthan Polysaccharide Solutions on Their Flow Through Various Porous Media," SPE paper 9295, 1980 SPE Annual Fall Technical Conference and Exhibition of AIME, Dallas, September 21-24.
- Bragg, J.R.: "Injectivities of Biopolymer Solutions," Chemical Abstracts, 99:P197764a(1983).
- Jamieson, A.M., et al.: "Dynamical Behavior of Xanthan Polysaccharide in Solution," Polymer Physics(1982) Edt., 20, 1513-1524.
- Southwick, J.G., et al.: "Self Association of Xanthan in Aqueous Solvent Systems," Carbohydrate Research(1980) 84, 287-295.
- Narayan, K.S. and Ramasubramanian, V.: "Rheological Properties of Polysaccharide Gums," Indian J. Technol., 1982, 20(9), 333-338.
- Patton, J.T.: "Modified Heteropolysaccharides," US Patent 3,729,460(1970).
- Kohler, N. and Chauveteau, G.: "Xanthan Polysaccharide Plugging Behavior in Porous Media - Preferential Use of Fermentation Broth," J. Pet. Technol. 1981, 33(9), 349-357.
- Salamone, J.C., Clough, S.B., Salamone, A.B., Reid, K.I.G., and Jamison, D.E.: "Xanthan Gum - A Lyotropic, Liquid Crystalline Polymer and its Properties as a Suspending Agent," Soc. Pet. Eng. J. August 1982, 555,556.
- Sato, T., Norisuye, T., and Fujita, H.: "Double-Stranded Helix of Xanthan: Dimensional and Hydrodynamic Properties in 0.1 M Aqueous Sodium Chloride," Macromolecules 1984, 17, 2696-2700.
- Burkholder, L.: "Xanthan Gel System Effective for Profile Modification," Oil Gas J. 1985, 68, 69.
- Chow, A.W. and Fuller, G.G.: "Response of Moderately Concentrated Xanthan Gum Solutions to Time-Dependant Flows Using Two-Color Flow Birefringence," J. Rheol. 1984, 28(1), 23-43.
- McNeely, W.H.: "Process for Producing a Polysaccharide," Canadian Patent 821 534(1969).
- Hartfiel, A.H.: "Clay-Free, Thixotropic Wellbore Fluid," US Patent 4,247,402(1981).
- Schuppner, H.R., Jr.: "Heat Reversible Gel and Method for Preparing Same," US Patent 3,557,016(1971).
- Jordan, W.A.: "Thickening Compositions Containing Xanthomonas Gum and Hydroxyalkyl Ether of Guar Gum," US Patent 3,748,201(1973).
- Jordan, W.A. and Carter, W.H.: "Blends of Xanthomonas and Guar Gum," US Patent 3,765,918(1973).
- Norton, C.J. and Falk, D.D.: "Polyalkeneoxide and Polysaccharide Gum Derivatives Mobility Control Agent and Process," US Patent 3,919,092(1975).
- Karl, C.L.: "Hydroxyalkyl Locust Bean/Xanthomonas Hydrophilic Colloid Blends," US Patent 4,038,206(1977).
- Patton, J. T.: "Chemical Treatment Enhances Xanflood Polymer," SPE paper 4670, 1973 SPE Annual Meeting, Las Vegas, Sept. 30-Oct. 3.
- Abdo, M.K.: "Waterflood Oil Recovery Process Employing Stabilized Biopolymers," US Patent 4,141,842(1979).
- Clark, P.E., Halvaci, M., and Ghaeli, H.: "Proppant Transport by Xanthan and Xanthan-Hydroxypropyl Guar Solutions: Alternatives to Crosslinked Fluids," SPE/DOE 13907, 1985 Low Permeability Gas Reservoirs, Denver, May 19-22.
- Clifford, P.J. and Sorbie, K.S.: "The Effects of Chemical Degradation on Polymer Flooding," SPE paper 13586, 1985 SPE International Symposium on Oilfield and Geothermal Chemistry, Phoenix, April 9-11.

Frac Gel Residue and Formation Damage(Ref. 142)

- van Poolen, H.K., Tinsley, J.M. and Saunders, C.D.: "Hydraulic Fracturing: Fracture Flow Capacity vs. Well Productivity," SPE paper 890-G, 1957 SPE Annual Fall Meeting of AIME, Dallas, October 6-9.
- Methven, N.E.: "Effects of Drilling Fluids on Gas Well Productivity," SPE paper 3504, 1971 SPE Annual Meeting, New Orleans, October 3-6.
- Carney, M.J. and Wieland, D.R.: "Stimulation of Low Permeability Gas Wells in the Rocky Mountain Area," SPE paper 4396, 1973 Rocky Mountain Regional Meeting of AIME, Casper, May 15-16.
- Smith, C.F.: "Gas Well Fracturing Using Gelled Non-Aqueous Fluids," SPE paper 4678, 1973 SPE Annual Meeting of AIME, Las Vegas, September 30-October 3.

- **Pye, D.S. and Smith, W.A.:** "Fluid Loss Additive Seriously Reduces Fracture Proppant Conductivity and Formation Permeability," 1973 SPE Annual Meeting, Las Vegas, Sept. 30-Oct. 3.
- **Tindell, W.A., Misak, M.D., and Gras, E.H.:** "The Use of Alcohol-Water Mixtures in Fracture Stimulation of Gas Wells," 1974 Proc. Annu. Southwest. Pet. Short Course, Lubbock, 61-65.
- **Tiner, R.L., Stahl, E.J. Jr., and Malone, W.T.:** "Developments in Fluids to Reduce Potential Damage from Fracturing Treatments," SPE paper 4790, 1974 SPE Symposium on Formation Damage Control, New Orleans, February 7-8.
- **Tuttle, R.N. and Barkman, J.H.:** "The Need for Nondamaging Drilling and Completion Fluids," SPE paper 4791, 1974 SPE Symposium on Formation Damage Control, New Orleans, February 7-8.
- **Christian, W.W. and Ayres, H.J.:** "Formation Damage Control in Sand Control and Stimulation Work," SPE paper 4775, 1974 SPE Symposium on Formation Damage Control, New Orleans, February 7-8.
- **Tannich, J.D.:** "Liquid Removal From Hydraulically Fractured Gas Wells," *J. Pet. Technol.*, November, 1975, 1309-1317.
- **Cooke, C.E., Jr.:** "Effect of Fracturing Fluids on Fracture Conductivity," *J. Pet. Technol.*, October 1975, 1273.
- **Pence, S.A.:** "Evaluating Formation Damage in Low Permeability Sandstone," 1975 SPE Annual Meeting, Dallas, September 28-October 1.
- **Barth, H.G. and Smith, D.A.:** "High-Performance Size-Exclusion Chromatography of Guar Gum," *J. Chromatog.*, (1981) 206, 410-415.
- **Gall, B.L. and Raible, C.J.:** "The Use of Size Exclusion Chromatography to Study the Degradation of Water-Soluble Polymers Used in Hydraulic Fracturing Fluids," *Polym. Mater. Sci. Eng.* 1986, 55, 572-75, Anaheim.
- **Southwick, J.G. and Manke, C.W.:** "Molecular Degradation, Injectivity, and Elastic Properties of Polymer Solutions," SPE paper 15652, 1986 SPE Annual Technical Conference and Exhibition, New Orleans, October 5-8.
- **Clifford, P.J. and Sorbie, K.S.:** "The Effects of Chemical Degradation on Polymer Flooding," SPE paper 13586, 1985 International Symposium on Oilfield and Geothermal Chemistry, Phoenix, April 9-11.
- **Barth, H.G. and Regnier, F.E.:** "High-Performance Gel Permeation Chromatography of Water-Soluble Cellulosics," *J. Chromatog.* (1980) 192, 275-293.
- **Raible, C.J.:** "Formation Damage Due to Hydraulic Fracturing Fluids," National Institute for Petroleum and Energy Research, Cooperative Agreement DE-FC01-83FE60149, October 1, 1983-September 30, 1988.
- **Volk, L.J., et al.:** "A Method for Evaluation of Formation Damage Due to Fracturing Fluids," SPE paper/DOE 11638, 1983 SPE/DOE Symposium on Low Permeability, Denver, March 14-16.
- **Gall, B.L. and Raible, C.J.:** "A Method to Study Fracture Fluid Polymer Degradation Using Size Exclusion Chromatography," United States Department of Energy, DOE/BETC/RI-83/10(DE84008316), February 1984.
- **Sattler, A.R., Raible, C.J., and Gall, B.R.:** "Integration of Laboratory and Field Data for Insight on the Multiwell Experiment Paludal Stimulation," SPE paper/DOE 13891, 1985 SPE/DOE Low Permeability Gas Reservoirs, Denver, May 19-22.
- **Raible, C.J. and Gall, B.L.:** "Laboratory Formation Damage Studies of Wester Tight Gas Sands," SPE paper/DOE 13903, 1985 SPE/DOE Low Permeability Gas Reservoirs, Denver, May 19-22.
- **Sattler, A.R., et al.:** "Laboratory Studies for the Design and Analysis of Hydraulic Fractured Stimulations in Lenticular, Tight Gas Reservoirs," SPE paper 15245, 1986 SPE Unconventional Gas Technology Symposium, Louisville, May 18-21.
- **Gall, B.L., et al.:** "Permeability Damage to Natural Fractures Caused by Fracturing Fluid Polymers," SPE paper 17542, 1988 SPE Rocky Mountain Regional Meeting, Casper, May 11-13.
- **Sattler, et al.:** "Stimulation-Fluid Systems for Naturally Fractured Tight Gas Sandstones: A General Case Study from Multiwell Experiment Stimulations," SPE paper 17717, 1988 SPE Gas Technology Symposium, Dallas, June 13-15.
- **Tuttle, R.N. and Barkman, J.H.:** "The Need for Nondamaging Drilling and Completion Fluids," paper 4791, 1974 SPE Symposium on Formation Damage Control, New Orleans, February 7-8.
- **van Poolen, H.K.:** "Do Fracture Fluids Damage Productivity?," *Oil Gas J.* (1957) May 27, 120-124.
- **Leon, L.:** "The Role of the Service Company in Minimizing and Reducing Formation Contamination," SPE paper 4660, 1973 SPE Annual Meeting, Las Vegas, September 30-October 3.
- **Roodhart, L., Kuiper, T.O. and Davies, D.R.:** "Proppant Rock Impairment During Hydraulic Fracturing," SPE paper 15629, 1986 SPE Annual Technical Conference and Exhibition, New Orleans, October 5-8.
- **Cooke, C.E. Jr.:** "Effect of Fracturing Fluids on Fracture Conductivity," *J. Pet. Technol.* (October 1975) 1273-1282.
- **Almond, S.W.:** "Factors Affecting Gelling Agent Residue Under Low Temperature Conditions," SPE paper 10658, 1982 SPE Formation Damage Control Symposium, Lafayette, March 24-25.

- Almond, S.W. and Bland, W.E.: "The Effect of Break Mechanism on Gelling Agent Residue and Flow Impairment in 20/40 Mesh Sand," SPE paper 12485, 1984 Formation Damage Control Symposium, Bakersfield, February 13-14.
- Kim, C.M. and Losacano, J.A.: "Fracture Conductivity Damage Due to Crosslinked Gel Residue and Closure Stress on Propped 20/40 Mesh Sand," 1985 SPE Annual Technical Conference and Exhibition, Las Vegas, September 22-25.
- Abrams, A. and Vinegar, H.J.: "Impairment Mechanisms in Vicksburg Tight Gas Sands," SPE paper/DOE 13883, 1985 SPE Low Permeability Gas Reservoirs, Denver, May 19-22.
- Tinsley, J.M. and Williams, J.R. Jr.: "A New Method of Providing Increased Fracture Conductivity and Improving Stimulation Results," SPE paper 4676, 1973 SPE Annual Meeting, Las Vegas, September 30-October 3.
- Hough, E.W. and Allen T.O.: "Laboratory Techniques and Results of Tests to Determine Formation Damage from Fracturing Fluids," 1957 Spring Meeting of the Southern District Division of Production, Shreveport, March 20-22.
- Kottb, A.K. and Kasraie, B.: "Laboratory Investigation of Damage from Guar Gum Base Gels," SPE paper 3660, 1971 SPE Appalachian Section, Charleston, November 4-5.
- Pober, K.W., Hoff, M.H., and Darlington, R.K.: "Water-Insoluble Residue Following Acid Hydrolysis of Water-Soluble Polysaccharides," *J. Pet. Technol.*, (December 1983) 2185-2191.
- Ely, J.W.: "Methods of Water Flooding and Fracturing Using clean, Non-Damaging Fracturing Fluids," US Patent 4,265,311(1981).
- Gall, B.L. and Raible, C.J.: "Formation Damage from Exposure to Hydraulic Fracturing Fluids," NIPER-63, 1985 National Institute for Petroleum and Energy Research Topical Report, March 7.
- Gall, B.: "Degradation of Fracturing Fluid Polymers," NIPER-132, 1986 National Institute for Petroleum and Energy Research Final Report, February.
- Gall, B.L. and Raible, C.J.: "Characterization of Degraded Polymer Fracturing Fluids," NIPER-48, National Institute for Petroleum and Energy Research Topical Report, February, 1985.
- Raibel, C.J.: "Formation Damage Studies of Low-Permeability Sands," NIPER-130, National Institute for Petroleum and Energy Research Final Report, February 1986.
- Woodroof, R.A. Jr. and Anderson, R.W.: "Synthetic Polymer Friction Reducers Can Cause Formation Damage," SPE paper 6812, 1977 SPE Annual Technical Conference and Exhibition, Denver, October 9-12.
- Hawkins, G.W.: "Molecular Weight Reduction and Physical Consequences of Chemical Degradation of Hydroxypropylguar in Aqueous Brine Solutions," *Polym. Mat. Sci. Eng.* (1986) 55, 588-93.
- Hawkins, G.W.: "Laboratory Study of Proppant-Pack Permeability Reduction Caused by Fracturing Fluids Concentrated During Closure," SPE paper 18261, 1988 Annual Technical Conference and Exhibition, Houston, Oct. 2-5.
- Branagan, P.T., et al: "Case History of Hydraulic Fracture Performance in the Naturally Fractured Paludal Zone: The Transitory Effects of Damage," SPE paper/DOE 16397, 1987 SPE Low Permeability Reservoirs Symposium, Denver, May 18-19.
- Harris, J.F.: "Acid Hydrolysis and Dehydration Reactions for Utilizing Plant Carbohydrates," *Applied Polymer Symposium*, 1975, 28, 131-144.
- Barth, H.G. and Smith D.A.: "High-Performance Size-Exclusion Chromatography of Guar Gum," *J. Chromatog.* (1981) 206, 410-415.
- Gall, B.L. and Raible, C.J.: "A Method to Study Fracture Fluid Polymer Degradation Using Size Exclusion Chromatography," United States Department of Energy, No. DOE/BETC/RI-83/10 (DE84008316), February 1984.
- Gall, B.L. and Raible, C.J.: "Molecular Size Studies of Degraded Fracturing Fluid Polymers," SPE paper 13566, 1985 International Symposium on Oilfield and Geothermal Chemistry, Phoenix, April 9-11.
- Wojtanowicz, A.K., Krilov, Z., Langlais, J.P.: "Study on the Effect of Pore Blocking Mechanisms on Formation Damage," SPE paper 16233, SPE Production Operations Symposium, Oklahoma City, OK, March 8-10, 1987.
- Gall, B.L.: "Permeability Damage to Cracked Core by Fracturing Fluids," National Institute for Petroleum and Energy Research, proposal No. NIPER 85-688, (ECR) M-Report, January 23, 1986.
- Gall, B.L., Maloney, D.R., and Raible, C.J.: "Permeability Damage to Artificially Fractured Cores," Final Report, National Institute for Petroleum and Energy Research, May 1988.
- McDaniel, B.W.: "Use of Wet Gas Flow for Long-Term Fracture Conductivity Measurements in the Presence of Gel Filter Cakes," SPE paper 17543, 1988 SPE Rocky Mountain Regional Meeting, Casper, May 11-13.
- McDaniel, B.W. and Parker, M.A.: "Accurate Design of Fracturing Treatment Requires Conductivity Measurements at Simulated Reservoir Conditions," SPE paper 17541, 1988 SPE Rocky Mountain Regional Meeting, Casper, May 11-13.
- McLeod, H.O. Jr.: "The Effect of Perforating Conditions on Well Performance," SPE paper 10649, 1982 SPE Formation Damage Control Symposium, Lafayette, March 24-25.
- McDaniel, B.W.: "Use of Wet Gas Flow for Long Term Fracture Conductivity Measurements in the Presence of Gel Filter Cakes," SPE paper 17543, 1988 Rocky Mountain Regional SPE Meeting, May 11-13.

- Gray, D.H. and Rex, R.W.: "Formation Damage in Sandstones Caused by Clay Dispersion and Migration," 1966 Fourteenth National Conference on Clays and Clay Minerals," 355-366.
- Parker, M.A. and McDaniel, B.W.: "Fracturing Treatment Design Improved by Conductivity Measurements Under In-Situ Conditions," SPE paper 16901, 1987 SPE Annual Technical Conference and Exhibition, Dallas, September 27-30.

Crosslinked Gels from Other Industries(Ref. 204)

- Lagally, P. and Lagally H.: "Atomistic Approach to the Crosslinking of Cellulose Fibers and Their Reaction with Fillers," TAPPI, Vol. 39, No. 11, November 1956, 747-754.
- Corben, L.D.: "Micro-Inclusions and Method of Making Same," US Patent 3,201,353(1965).
- Roy, G.L., Laferriere, A.L. and Edwards, J.O.: "A Comparative Study of Polyol Complexes of Arsenite, Borate, and Tellurate Ions," J. Inorg. Nucl. Chem.(1957) Vol. 4, 106-114.
- Schultz, R.K. and Myers, R.R.: "The Chemorheology of Poly(vinyl Alcohol)-Borate Gels," Macromolecules(1969) Vol. 2.
- Gorin, P.A.J. and Mazurek, M.: "Carbon-13 Resonance Spectroscopic Studies on the Formation of Borate and Diphenylborinate Complexes of Polyhydroxy Compounds," Can. J. Chem. Vol. 51, 1973, pages 3277-3286.
- Gorin, P.A.J. and Mazurek, M.: "C Magnetic Resonance Spectroscopic Evidence for Formation of Borate Complexes of Polyhydroxy Compounds," Carbohydrate Research, 27(1973), 325-339.
- Haug, A.J.: "Guar Mannogalactan Studies: II. Effect of Certain Variables, Including Borax, on the Rate of Oxidation of the Purified Mucilage," TAPPI, Vol. 36, No. 1, January 1953, 53-62.
- Lagally, P.: "Preparation and Stabilization of Water Soluble Reactive Titanium Derivatives," US Patent 2,950,174(1960).
- Gash, V.W.: "Metal Chelates and Process of Preparing Same," US Patent 2,976,285(1961).
- Nossal, R.: "Network Formation in Polyacrylamide Gels," Macromolecules, (1985) 18, 49-54.
- Rondstedt, C.S., Jr.: "Titanium Compounds, Organic" in Kirk Othmer Encyclopedia of Chemical Technology, 3rd Ed, V.23, 176-244, Wiley, New York, 1983.
- Barnhart, R.E. and Sawyer, F.C.: "Gelled Ammonium Nitrate Blasting Explosive and Process," US Patent 3,072,509(1963).
- Moe, W.A., Miller, S.E. and Iwen, M.H.: "Investigation of the Reserve Carbohydrates of Leguminous Seeds. I. Periodate Oxidation," J. Amer. Chem. Soc., 1947, 69, 2621-2625.
- McIrvine, J.D.: "TNT-Tetraborate Gelled Aqueous Explosive Slurry," US Patent 3,108,917(1963).
- Kiefer, J.E. and Touey, G.P.: "Cellulose Acetate Spinning Solutions and Process of Spinning Fine Denier Filaments," US Patent 3,033,698(1962).
- Crisp, J.D.: "Method for Gelling Water-Bearing Explosive Compositions Containing Galactomannan Gums," US Patent 3,202,556(1965).
- Jordan, W.A.: "Organo-Metallic Gel-Producing Compositions and Processes for Preparing Organo-Metallic Gels," US Patent 3,251,781(1966).
- Crisp, J.D.: "Gelled Compositions Containing Galactomannan Gums," US Patent 3,301,723(1967).
- Revukas, A.J.: "Hydrocarbon Fuel Composition," US Patent 3,334,978(1967).
- Needles, H.L. and Whitfield, R.E.: "Crosslinking of Collagens Employing a Redox System Comprising Persulphate and a Reducing Agent," US Patent 3,427,301(1969).
- Angstadt, R.L. and Tyeer, S.Y.: "The Nature of Zirconyl Chloride in Strong Hydrochloric Acid: Light Scattering," J. Inorganic Chem., 1962, 24, 913-917.
- Kraitzer, I., McTaggart, K., and Winter, G.: "Esters of Titanium," J. Oil Colour Chem. Assoc., 1948, 405-417.
- Balthis, J.: "Polymeric Hydroxyl-Containing Titanium Carboxylates and Methods for Preparing Same," US Patent 2,621,194(1950).
- Davidson, D.: "Explosive Compositions," US Patent 2,768,073(1956).
- Hock, A.L.: "Zirconium Compounds: The Industrial Importance of Their Aqueous Chemistry," Chemistry and Industry, November 2, 1974.
- Vladimirova, Z.A., Prozorovskaya, A.N., and Komissarova, L.N.: "Investigation of Complex Formation by Zirconium and Hafnium with Formic Acid by a Kinetic Method," Russian Journal of Organic Chemistry, 1975, 20(10), 1477-1480.
- Konunova, Ts.B., Popov, M.S., and Venichenko, A.S.: "Study of the Interaction of Zirconium with Certain Monocarboxylic Acids by the Metal-Indicator Method," Russian Journal of Inorganic Chemistry, 1975, 20(6), 861-865.
- Russell, C.A.: "Process for the Preparation of Stabilized Organotitanium Compounds," US Patent 2,894,966(1959).
- Shokal, E.C.: "Sulfur-Containing Resinous Products from Polyepoxides," US Patent 2,633,458(1953).
- Mills, J.A.: "Association of Polyhydroxy Compounds with Cations in Solution," Biochem. Biophys. Res. Commun., 1961/62, 6(6), 418-21.

Quality Control of Fracturing Fluids(Ref. 335)

- Huebinger, T., Webster, D., Chisholm, P., Venditto, J., and Hunt, J.: "Optimizing Program Increases Field's Profits," Oil Gas J., Aug 29, 1988, 35-39.
- Osborne, M.W., McLeod, H.O., Jr. and Schroeder, H.D.: "The Analysis and Control of Hydraulic Fracturing Problems," SPE/DOE paper 9868, 1981 SPE/DOE Low Permeability Symposium, Denver, May 27-29.
- Schlottman, B.W., Miller, W.K., II and Lueders, R.K.: "Massive Hydraulic Fracture Design for the East Texas Cotton Valley Sands," SPE paper 10133, 1981 SPE Annual Technical Conference and Exhibition of AIME, San Antonio, October 5-7.
- Pai, V.J.: "Predicting, Preventing and Remediating Hydraulic Fracturing Screen Outs," 1984 Proc. Annu. Southwest. Pet. Short Course, Lubbock, 122-135.
- Conway, M.W. and Harris, L.E.: "A Laboratory and Field Evaluation of a Technique for Hydraulic Fracturing Stimulation of Deep Wells," SPE paper 10964, 1982 SPE Annual Technical Conference and Exhibition of AIME, New Orleans, September 26-29.
- Payne, K.L., and Harms, S.D.: "Recent Developments in Polymer Fracture Fluid Technology," 1984 AIChE National Meeting, Anaheim, May 20-24.
- Freck, J. and Gottschling, J.: "A Field and Laboratory Study of Polysaccharides in Fracturing Treatments," 1984 Proc. Annu. Southwest. Pet. Short Course, Lubbock, 141-156.
- Evans, D.W. and Willis, K.: "Fracture Execution - An Essential Part of Every Fracture Design," paper No. 86-37-70, 1986 Annual Technical Meeting of the Petroleum Society of CIM, Calgary, June 8-11.
- Zigray, J.L., Osborne, M.W., and Westbrook, G.H.: "Field Analysis and Flow Loop Tests Diagnose Problems with Delayed Action Crosslinked Fracturing Fluid Systems," SPE paper 15633, 1986 Annual Technical Conference and Exhibition of the SPE, New Orleans, October 5-8.
- Hodge, R. M. and Baranet, S.E.: "Evaluation of Field Methods to Determine Crosslink Times of Fracturing Fluids," SPE paper 16249, 1987 International Symposium on Oilfield Chemistry, San Antonio, February 4-6.
- Tyssee, D.A. and Vetter, O.J.: "Chemical Characterization Problems of Water-Soluble Polymers," Soc. Pet. Eng. J., December 1981, 721-730.
- Lescarbourea, J.A., Sifferman, T.R. and Wahl, H.A.: "Evaluation of Frac Fluid Stability Using a Heated, Pressurized Flow Loop," SPE paper 10962, 1982 SPE Annual Technical Conference and Exhibition, New Orleans, September 26-29.
- Gardner, D.C. and Eikerts, J.V.: "Effects of Shear and Proppant on the Viscosity of Crosslinked Fracturing Fluids," SPE paper 11066, 1982 SPE Annual Fall Technical Conference and Exhibition, New Orleans, September 26-29.
- McLeod, H.O., Jr.: "A Simplified Approach to Design of Fracturing Treatments Using High Viscosity Crosslinked Fluids," SPE/DOE paper 11614, 1983 SPE/DOE Symposium on Low Permeability, Denver, March 14-16.
- Gardner, D.C. and Eikerts, J.V.: "Rheological Characterization of Crosslinked and Delayed Crosslinked Fracturing Fluids Using a Closed-Loop Pipe Viscometer," SPE paper 12028, 1983 SPE Annual Technical Conference and Exhibition, San Francisco, October 5-8.
- Shah, S.N. and Watters, L.T.: "Time and Shear Effects on Rheological Properties of Crosslinked Fluids - Evaluation Method," SPE Prod. Eng.(January 1986) 55-61.
- Constien, V.G., et al.: "Automated Rheology Laboratory. 1," American Chemical Society Symposium Series 313 (1986): 105-113.
- Graves, G. and Fellin, E.: "Automated Rheology Equipment Facilitates Acid Fracturing Fluid Characterization," Presented at the SPE Computer Technology Symposium, Texas Tech University, Lubbock, March 6, 1986.
- King, M.T., Constien, V.G., and Fellin, E.L.: "Automated Rheology Laboratory. 2," American Chemical Society Symposium Series, 313 (1986): 114-122.
- Saucier, R.J.: "A Field Development Program in Hydraulic Fracture Stimulation," SPE paper 18257, 1988 SPE Annual Technical Conference and Exhibition, Houston, October 2-5.
- Shah, S.N., Lee, Y.N., and Jensen, D.G.: "Frac Treatment Quality Improved with Field Rheology Unit," Oil Gas J. (February 4, 1985), 47-51.
- Ely, J.W., Haskett, S.E., Holditch, S.A.: "Field Measurement of Fracturing Fluid Viscosity at In-Situ Conditions of Temperature and Shear," SPE paper 16915, 1987 SPE Annual Technical Conference and Exhibition, Dallas, September 27-30.
- England, A.A. and Davis, N., II: "The Characterization of a Drilling Fluid Additive," IADC/SPE paper 17199, 1988 IADC/SPE Drilling Conference, Dallas, February 28-March 2.
- Craigie, L.J.: "A New Method for Determining the Rheology of Crosslinked Fracturing Fluids using Shear History Simulation," SPE/DOE paper 11635, 1983 SPE/DOE Symposium on Low Permeability, Denver, March 14-16.

Emulsion Frac Fluids(Ref. 342)

- Matthews, T.M.: "Field Use of 'Superfrac' - A New Hydraulic Fracturing Technique," SPE paper 2625, 1969 SPE Annual Meeting, Denver, September 28-October 1.
- Sinclair, A.R.: "Rheology of Viscous Fracturing Fluids," J. Pet. Technol.(June 1970) 711-719.

- Kiel, O.M. and Weaver, R.H.: "Emulsion Fracturing System," *Oil Gas J.*(February 21, 1972) 72-73.
- Dauben, D.L. and Froning, H.R.: "Micellar Solutions Stimulate Wells," *Oil Gas J.*(September 18, 1972) 83, 72-78.
- Kiel, O.M.: "Method of Fracturing Subterranean Formations Using Oil-In-Water Emulsions," US Patent 3,710,865(1973).
- Gogarty, W.B. and Olson, R.W.: "Use of Microemulsions in Miscible-Type Oil Recovery Procedure," US Patent 3,254,714(1966).
- Kremesec, V.J. and Treiber, L.E.: "Effect of System Wettability on Oil Displacement by Micellar Flooding," SPE paper 6001, 1976 SPE Annual Technical Conference and Exhibition, New Orleans, October 3-6.
- Sinclair, A.R., Terry, W.M. and Kiel, O.M.: "Polymer Emulsion Fracturing," *J. Pet. Technol.*(July 1974), 731-738.
- Fast, C.R., Holman, G.B. and Covlin, R.J.: "The Application of Massive Hydraulic Fracturing to the Tight Muddy "J" Formation, Wattenberg Field, Colorado," *J. Pet. Technol.*(January 1977), 10-16.
- Graham, J.W., Gruesbeck, C., and Salathiel, W.M.: "Method of Fracturing Subterranean Formations Using Oil-in-Water Emulsions," US Patent 3,977,472(1976).
- Gidley, J.L., et al.: "Stimulation of Low-Permeability Gas Formations by Massive Hydraulic Fracturing - A Study of Well Performance," *J. Pet. Technol.*(April 1979), 525-531.
- McClafflin, G.G.: "Method of Transporting Viscous Hydrocarbons," US Patent 4,249,554(1981).
- Sifferman, T.R.: "Method of Transporting Viscous Hydrocarbons," US Patent 4,265,264(1981).
- Kiel, O.M.: "A New Hydraulic Fracturing Process," *J. Pet. Technol.*(January 1970), 89-96.
- Salathiel, W.M.; Muecke, T.W.; Cooke, C.E.; Li, N.N.: "Well Treatment with Emulsion Dispersions," US Patent 4,233,165(1980).
- Blauer, R.E., Phillips, A.M., and Craig, D.P.: "Rheological and Physical Differences Between Foam and Emulsion Fracturing Fluids," SPE paper 18214, 1988 SPE Annual Technical Conference and Exhibition, Houston, October 2-5.
- Miller, K.A.: "Pumping and Loading Emulsion Slurry Blasting Composition," European Patent Appl. 182,661A2(1986), *Chemical Abstracts* 105(16):136821n(1986).
- Krishan, K., Kapoor, S., and Goyal, K.L.: "Development of Polymer Emulsion as Fracturing Fluid," *Chemical Abstracts* 103(20):162915z(1985).
- Matveev, D.F.: "Hydrophobic Thermally Stable Emulsions for Treatment of Productive Strata," *Chemical Abstracts* 102(14):116185t(1985).
- Matveev, D.F., Starikova, T.V., Fuki, B.I., Makarenko, P.P., Stetsenko, G.I., Sergeev, V.P.: "Hydrophobic Emulsion Composition for Hydraulic Fracturing of a Formation," *Chemical Abstracts* 98(22):182419x(1983).
- Salathiel, W.M., Muecke, T.W., Cooke, C.F., Jr., and Li, N.N.: "Well Treatment with Emulsion Dispersions," US Patent 4,359,391(1982).
- Matveev, D.F., Reznikov, I.G., Kulikova, A.V., Belolaptnikov, G.G., Zhadanova, K.M., Grebennikova, A.I., and Perel, Z.P.: "Composition for Hydraulic Fracturing of Oil-Producing Formation," SU Patent 729,334(1980), *Chemical Abstracts* 93(14):134836f(1980).
- Matveev, D.F., Reznikov, I.G., Fuki, B., Kulikova, A.V., Belolaptnikov, G.G., Zhadanova, K.M., Grebennikova, A.I., and Starikova, T.V.: "Hydrophobic Emulsion for Hydraulic Breakage of a Formation," SU Patent 731,998(1980), *Chemical Abstracts* 93(14):134835e(1980).
- Kuvandykov, I.Sh.: "Use of an Emulsion in the Repair of Wells," *Neftepromysl. Delo.* (9), 36-9, *Chemical Abstracts* 92(12):96410g(1980).
- Thorn, D.J. and Burnham, J.W.: "Dissolving Polymeric Materials in Hydrocarbon Liquids," US Patent 4,068,676(1978).
- Perkins, L.F.: "Propping Subterranean Formation Fractures," US Patent 4,029,149(1977).
- Graham, J.W., Gruesbeck, C., and Salathiel, W.M.: "Fracturing Subterranean Formations Using Oil-in-Water Emulsions," US Patent 3,977,472(1976).
- Gogarty, W.B.: "Fracturing Fluids," GB Patent 1,388,909(1975), *Chemical Abstracts* 83(22):181880u(1975).
- Christopher, C.A. and Allen, J.C.: "Hydraulic Fracturing," US Patent 3,865,190(1975).
- Sinclair, A.R., Terry, W.M., and Kiel, O.M.: "Polymer Emulsion Fracturing," *J. Pet. Technol.*, 1974, 26(July), 731-8.
- Kiel, O.M.: "Hydraulic Fracturing," CA Patent 943,860(1974), *Chemical Abstracts* 81(18):108342z(1974).
- Crawford, D.L., Earl, R.B., and Monroe, R.F.: "Oil Well Fracturing Fluid Additive," GB Patent 1,355,808(1974).
- Kiel, O.M.: "Fracturing Using Acid External Emulsions," US Patent 3,799,266(1974).
- Kiel, O.M.: "Treating a Well Using a Volatile Hydrocarbon Liquid," US Patent 3,766,986(1973).
- Kiel, O.M.: "Treatment of Wells with Fluids Containing Complexes," US Patent 3,760,881(1973).
- Hummel, J.L. and Svaldi, M.A.: "Use of Micellar Solutions to Improve the Perforation of Oil-Bearing Subterranean Formations," US Patent 3,754,599(1973).

- Gogarty, W.B.: "Hydraulic Fracturing Subterranean Formations Using a Temperature-Inverted Fracturing Fluid," US Patent 3,734,189(1973).
- Bernard, P.J.: "Neutral Cationic Emulsion Containing a Slow-Fracturing Hydrocarbon Binder," Chemical Abstracts, 78(12):74596f (1973).
- Son, M.O., Jr.: "Micellar Dispersion for Use in Multiple Fracturing of Subterranean Formations," US Patent 3,613,789(1971).
- Son, M.O., Jr.: "Hydraulic Fracturing of Subterranean Formations Using Hydrocarbon Micellar Dispersions," US Patent 3,603,400(1971).
- Kiel, O.M.: "Hydraulic Fracturing of a Subterranean Formation with a Viscous Oil-In-Water Emulsion," US Patent 3,552,494(1971).
- Kiel, O.M.: "New Hydraulic Fracturing Process," J. Pet. Technol., 22(Jan), 89-96.
- Siegele, F.H.: "Oil Well Fracturing Wax Emulsion Fluid Loss Additive," US Patent 3,477,512(1969).
- Watkins, D.R. and O'Donnell, E.J.: US Patent 4,614,236(1986).

Non-Emulsifiers, Water Blockage Additives(Ref. 361)

- Cross, B., Scher, H.B., Eds.: "Pesticide Formulations" Chapter 13. Berger, P., et al.: "Dynamic Surface Tensions of Spray Tank Adjuvants," ACS 1988, Washington, DC.
- Berger, P.D., Hsu, C., and Arendell, J.P.: "Designing and Selecting Demulsifiers for Optimum Field Performance on the Basis of Production Fluid Characteristics," SPE Prod. Eng., November 1988, 522-526.
- Robb, D.J.M. and Alexander, A.E.: "Adsorption and Wetting of a Polymer Latex by Cationic Surfactants," Soc. Chem. Ind. Monograph No. 25, 1967, 292-299.
- Hsu, C. and Berger, P.D.: "Surface Chemistry of Surfactants Used to Prevent Surface Coatings Defects," 1988 Symposium on Coatings Defects; Federation of Soc. for Coatings Technol., Orlando, May 17-18.
- Mungan, N.: "Permeability Reduction Through Changes in pH and Salinity," J. Pet. Technol., December 1965, 1449-53.
- Hurst, R.E.: "Using Chemicals in Well Completion and Stimulation: What Kind and How Much," Oil Gas J., April 13, 1970, 80-85.
- Kellerhals, G.E. and Chiou, C.S.: "Use of Perspective Plots to Aid in Determining Factors Affecting Interfacial Tensions Between Surfactant Solutions and Crude Oil," Soc. Pet. Eng. J., June 1982, 350-352.
- Shaughnessy, C.M. and Kline, W.E.: "EDTA Removes Formation Damage at Prudhoe Bay," SPE paper 11188, 1982 SPE Annual Fall Technical Conference and Exhibition of AIME, New Orleans, September 26-29.
- Meyers, K.O., Skillman, H.L., and Herring, G.D.: "Control of Formation Damage at Prudhoe Bay, Alaska, by Inhibitor Squeeze Treatment," J. Pet. Technol., June 1985, 1019-1034.
- Schulman, J.H. and Cockrain, E.G.: "Molecular Interactions at Oil/Water Interfaces. Part I. Molecular Complex Formation and the Stability of Oil in Water Emulsions," Trans. Faraday Soc., 1940, 36, 24.
- Bonnet, C.F.: "Treatment of Oil Sands with Surface-Active Chemicals," 1941 Mid-Year Meeting of the American Petro-Institute, Division of Production, Tulsa, May 22. See also: Division of Production Transactions, Vol. 22M(IV) (1941).
- Clason, C.E. and Hower, W.F.: "Removal of Flow Restrictions in Well Completions," API paper 851-27-C, 1953 API Spring Meeting of the Mid-Continent District, Division of Production, Tulsa, March 18-20.
- Ribe, K.H.: "Production Behavior of a Water-Blocked Oil Well," SPE paper 1295-G, 1959 SPE Annual Fall Meeting of AIME, Dallas, October 4-7.
- Kusakov, M.M. and Nekrasov, D.N.: "Hysteresis in Capillary Rise," Russian Journal of Physical Chemistry, 1960, 37(7),764-767.
- Jarvis, N.L. and Zisman, W.A.: "Surface Activity of Fluorinated Organic Compounds at Organic-Liquid/Air Interfaces: Part II. Surface Tension vs Concentration Curves, Adsorption Isotherms, and Force-Area Isotherms for Partially Fluorinated Carboxylic Esters," Naval Research Labs Report 5364, Surface Chemistry Branch, Chemistry Division, October 8, 1959.
- Shafrin, E.G. and Zisman, W.A.: "Constitutive Relations in the Wetting of Low-Energy Surfaces and the Theory of the Retraction Method of Preparing Monolayers," Naval Research Labs Report 5394, Surface Chemistry Branch, Chemistry Division, October 21, 1959.
- Jarvis, N.L. and Zisman, W.A.: "Surface Activity of Fluorinated Organic Compounds at Organic-Liquid/Air Interfaces: Part III. Equation of State of Adsorbed Monolayers and Work of Adsorption of a Fluorocarbon Group," Naval Research Labs Report 5401, Surface Chemistry Branch, Chemistry Division, November 17, 1959.
- Baker, H.R., Leach, P.B., Singletary, C.R., and Zisman, W.A.: "Surface Chemical Methods of Displacing Water and/or Oils and Salvaging Flooded Equipment: Part I. Practical Applications," Naval Research Labs Report 5606, Surface Chemistry Branch, Chemistry Division, February 23, 1961.

- Bascom, W.D. and Singleterry, C.R.: "The Adsorption of Oil-Soluble Sulfonates at the Metal/Oil Interface," Naval Research Labs Report 5623, Surface Chemistry Branch, Chemistry Division, July 14, 1961.
- Bascom, W.D. and Singleterry, C.R.: "The Adsorption of Oil-Soluble Sulfonates at the Metal/Oil Interface," Naval Research Labs Report 5623, Surface Chemistry Branch, Chemistry Division, July 14, 1961.
- Zisman, W.A.: "Adhesion," Ind. Eng. Chem., 1963, 55(10), 19-37.
- Atwood, D.K.: "Restoration of Permeability to Water-Damaged Cores," SPE paper 905, 1964 SPE Annual Fall Meeting, Houston, October 11-14.
- Schmolka, I.R. and Raymond, A.J.: "Micelle Formation of Polyoxyethylene-Polyoxypropylene Surfactants," 1965 Annual Spring Meeting American Oil Chemists' Society, Houston, April 26.
- Kelly, W.R.: "Relationship Among 'Emulsion' Type, Detergency and Foam," J. Amer. Oil Chem. Soc., 1966, 43, 358-363.
- Wade, W.H.: "Spontaneous Imbibition of fluids in Porous Vycor," Soc. Pet. Eng. J., 1974, 139-144.
- Schechter, R.S., Wade, W.H., and Wingrave, J.A.: "Sorption Isotherm Hysteresis and Turbidity Phenomena in Mesoporous Media," J. Colloid Sci., Manuscript # 4880-2.
- Doe, P.H., El-Emary, M.M., Wade, W.H., Schechter, R.S.: "The Influence of Surfactant Structure on Low Interfacial Tensions," ACS Symp. Ser., 1979, 21, 17-34.
- Koukounis, C., Wade, W.H., and Schechter, R.S.: "Phase Partitioning of Anionic and Nonionic Surfactant Mixtures," SPE paper 8261, 1979 SPE Annual Fall Technical Conference and Exhibition of AIME, Las Vegas, September 23-26.
- Ziegler, V.M. and Handy, L.L.: "The Effect of Temperature on Surfactant Adsorption in Porous Media," SPE paper 8264, 1979 SPE Annual Fall Technical Conference and Exhibition of AIME, Las Vegas, September 23-26.
- Eakin, J.L., Johansen, R.T., Hopkins, A.D., and Taleferro, R.W.: "How Chemical Treatment Gets Rid of Gas-Well Water Blocks," Oil Gas J.(November 26, 1962), 85-89.
- Carney, M.J. and Wieland, D. R.: "Stimulation of Low Permeability Gas Wells in the Rocky Mountain Area," SPE paper 4396, 1973 SPE Rocky Mountain Regional Meeting, Casper, May 15-16.
- Smith, C.F.: "Gas Well Fracturing Using Gelled Non-Aqueous Fluids," SPE paper 4678, 1973 SPE Annual Meeting, Las Vegas, Sept. 30-Oct. 3.
- Gras, E.H.: "Alcohol Comes on Strong as a Fracturing Fluid," Drilling-DCW(May, 1973).
- Tindell, W.A., Misak, M.D. and Gras, E.H.: "The Use of Alcohol-Water Mixtures in Fracture Stimulation of Gas Wells," Proc. Annu. Southwest. Pet. Short Course, 1974, 61-65.
- Tannich, J.D.: "Liquid Removal From Hydraulically Fractured Gas Wells," J. Pet. Technol.(November 1975) 1309-1317.
- Holditch, S.A.: "Factors Affecting Water Blocking and Gas Flow from Hydraulically Fractured Gas Wells," J. Pet. Technol.(December 1979) 1515-1524.
- Agarwal, R.G., Carter, R.D., and Pollock, C.B.: "Evaluation and Performance Prediction of Low-Permeability Gas Wells Stimulated by Massive Hydraulic Fracturing," J. Pet. Technol.(March 1979) 362-372.
- Bostic, J.N., Agarwal, R.G., and Carter, R.D.: "Combined Analysis of Postfracturing Performance and Pressure Buildup Data for Evaluating an MHF Gas Well," J. Pet. Technol.(October 1980) 1711-1719.
- Craighead, M.S and Hossaini, M.: "Foamed Anhydrous Methanol Stimulation," SPE paper 12315, 1983 Eastern Regional Meeting, Champion, PA, November 9-11.
- Penny, G.S.: "Method of Increasing Hydrocarbon Production from Subterranean Formations," US Patent 4,702,849(1987).
- Denekas, M.O., Mattax, C.C. and Davis, G.T.: "Effects of Crude Oil Components on Rock Wettability," paper No. T.P. 8095, Pet. Transactions, AIME, Vol. 216, 1959, 330-333.
- Graham, J.W., Monaghan, P.H., and Osoba, J.S.: "Influence of Propping Sand Wettability on Productivity of Hydraulically Fractured Oil Wells," T.P. 8094, Pet. Transactions, AIME, Vol. 216, 1959, 324-329.
- Wade, W.H., et al.: "Low Interfacial Tensions Involving Mixtures of Surfactants," SPE paper 6002, 1976 SPE Annual Technical Conference and Exhibition, New Orleans, October 3-6.
- Trogus, F., Sophany, T., Schechter, R.S., Wade, W.H.: "Static and Dynamic Adsorption of Anionic and Nonionic Surfactants," SPE paper 6004, 1976 SPE Annual Technical Conference and Exhibition, New Orleans, October 3-6.
- Wade, W.H., Schechter, R.S. and Jacobson, J.K.: "Low Interfacial Tensions Involving Mixtures of Surfactants," SPE paper 6002, 1976 SPE Annual Technical Conference and Exhibition, New Orleans, October 3-6.
- Newlove, J.C., McDougall, L.A., Walker, J.R., and Stockwell, J.R.: "Polymer Article of Manufacture," CA 1230219 A1(1987).
- Saliba, C.A.M. and Gonzalez, G.: "Capillary Pressure, Wettability, and Corrosiveness of Stimulation Fluids Containing Alcohols," Bol. Tec. PETROBRAS, 1987, 30(1), 25-32, Chemical Abstracts 106(26):216585z(1987).

- Crema, S.C.: "Liquid Foaming Additives Used in the Stimulation of Oil and Gas Wells, US Patent 4,609,477(1986).
- Dunning, J.: "Surfactants Revisited," CHEMTECH, 1984, 14(1), 46-50.
- Schechter, R.S. et al.: "Modeling Crude Oils for Low Interfacial Tension," Soc. Pet. Eng. J., Dec. 1976, 351-357.
- Schechter, R.S. et al.: "Low Interfacial Tension Involving Mixtures of Surfactants," Soc. Pet. Eng. J., April 1977, 122-128.
- Schechter, R.S. et al.: "Static and Dynamic Adsorption of Anionic and Nonionic Surfactants," Soc. Pet. Eng. J., Oct. 1977, 337-344.
- Schechter, R.S. et al.: "Interfacial Tension and Phase Behavior of Surfactant Systems," Soc. Pet. Eng. J., Aug. 1978, 242-252.
- Wade, W.H. et al.: "Interfacial Tension and Behavior of Nonionic Surfactants," Soc. Pet. Eng. J., Dec. 1979, 349-356.
- Wasan, D.T. et al.: "Observations on the Coalescence Behavior of Oil Droplets and Emulsion Stability in Enhanced Oil Recovery," Soc. Pet. Eng. J., Dec. 1978, 409-417.
- Saidi, A.M. and Hesselink, F.T.: "Method for Recovering Oil from an Underground Formation," UK Patent GB 2062063(1981), Chemical Abstracts 95(26):222643n(1981).
- Redford, D.A.: "Solvent Process for Developing Interwell Communication Path in a Viscous Petroleum Containing Formation Such as a Tar Sand Deposit," CA Patent 1015656(1977).
- Johnson, F.S., Jones, R.A., and Miller, J.S.: "Laboratory Investigation Using Solvent to Recover Heavy Oil from a Fractured Reservoir," Chemical Abstracts, 87(24):186798r(1977).
- Thompson, J.L.: "Composition and Method for Reducing the Surface Tension of Aqueous Fluids," US Patent 4,018,689(1977).
- Davis, J.A., Jr. and Rhudy, J.S.: "Hydraulic Fracturing of Subterranean Reservoirs Using Polyethylene Oxide-Based Fracturing Fluid," US Patent 3,747,681(1973).
- Redford, D.A.: "Developing Interwell Communication in a Tar Sand," US Patent 3,706,341(1972).
- Formation Damage at Prudhoe Bay, Alaska, by Inhibitor Squeeze Treatment," J. Pet. Technol., June 1985, 1019-1034.

RECEIVED February 21, 1989

Author Index

- Ali, S. M. Farouq, 347
Andersen, Mark A., 560
Audibert, A., 410
Barta, Leslie, 428
Borchardt, John K., 2,204
Broadhurst, P. V., 520
Burley, R. W., 520
Chamoun, Habib, 550
Chauveteau, G., 224
Chiu, Ying-Chech, 596
Clarke-Sturman, Anthony J., 157
Corley, W. T., 622
Costerton, J. William, 652
Covatch, G. L., 294
Cusack, Francene , 652
Daccord, Gérard, 608
Dandge, D. K., 531
Dexter, R. W., 102
Downs, H. H., 577
Dunn, R. O., 294
Elgsaeter, Arnljot, 145
Foulser, Robert W. S., 261
François, Jeanne, 111,124
Ginley, G. M., 482
Goodyear, Stephen G., 261
Growcock, F. B., 637
Hakin, Andrew W., 428
Harms, Weldon M., 55,660
Heller, John P., 504,531
Hepler, Loren G., 428
Hoover, P. D., 577
Isaacs, E. Eddy, 327
Jasinski, R. J., 637
Jian, Li, 327
Jiménez, A. I., 462
Kawanaka, S., 445
Kheradmand, Houchang, 111
Kikani, Jitendra, 241
Kushnick, Arnold P., 366
Lappin-Scott, Hilary M., 652
Lawless, Thomas A., 309
Lecourtier, J., 224
Lee, Hae Ok, 504
Lee, L. T., 224
Lee-Snape, John R., 309
Leontaritis, K. J., 445
Li, Chin Tia, 169
Liétard, Olivier, 608
MacKinnon, A. J., 520
MacLeod, F. Alex, 652
Mansoori, G. A., 445
Maunder, J. Darol, 327
Meister, John J., 169
Minssieux, L., 276
Momeni, Dawood, 378,393
Mukherjee, Surajit, 366
Nutt, C. W., 520
Ottelander, Dirk den, 157
Park, S. J., 445
Patton, John T., 622
Radke, C. J., 462,482
Rahbari, Ramine, 124
Roucaché, J., 410
Ryles, R. G., 102
Sadeghi, Kazem M., 378,393
Sadeghi, Mohammad-Ali, 378,393
Sarazin, Dominique, 124
Schechter, Robert S., 550
Sharma, Mukul M., 550
Shu, Paul, 137
Sims, Russell J., 261
Singh, P. K., 531
Smidsrød, Olav, 145
Smith, Duane H., 294
Somerton, W. H., 241
Stokke, Bjørn T., 145
Sturla, Phillip L., 157
Supon, S. B., 347
Teeters, Dale, 560
Thomas, David C., 347,560
Thomas, S.
Wu, Wen Hui, 378
Yen, Teh Fu, 378,393

Affiliation Index

- Alberta Research Council, 327
 American Cyanamid Company, 102
 Amoco Production Company, 560
 Baker Performance Chemicals, 577
 Chung Yuan Christian University, 596
 Dowell Schlumberger, 608,637
 Exxon Chemical Company (ECTD), 366
 Halliburton Services, 55,660
 Heriot-Watt University, 520
 ICI Chemicals and Polymers Ltd., 520
 IMOD Processes Ltd., 520
 Institut Charles Sadron, CRM-EAHP,
 CNRS-ULP, 111,124
 Institut Français du Pétrole, 224,276,410
 Mayco Wellchem, 622
 Mobile Research and Development
 Corporation, 137
 New Mexico Institute of Mining and
 Technology, 504,531
 New Mexico State University, 622
 Norwegian Institute of Technology, 145
 Pennsylvania State University, 347
 Santa Fe Energy Company, 577
 Shell Development Company, 2,204
 Shell Research Ltd., 157
 Stanford University, 241
 University of Alberta, 347,428
 University of Calgary, 652
 University of California, Berkeley, 241,462,482
 University of Detroit, 169
 University of Illinois, 445
 University of Southern California, 378,393
 University of Texas, Austin, 550
 University of Tulsa, 560
 U.S. Department of Energy, 292
 Winfrith AEE, 261,309

Subject Index

A

- Acid attack, propagation of wormholes, 619
 Acid corrosion inhibition, time
 dependence, 644
 Acid fracturing, friction reducers, 15
 Acid hydrolysis, lignin, 173
 Acid injection into carbonate
 reservoir, 610–611
 Acid–rock reactions, rate, 15,16
 Acid wormholing
 in carbonate reservoirs, 608–620
 in carbonate rocks, 610–611
 Acidity-controlled redox reactions, 141–142
 Acidization
 hydrocarbon production, 66
 methodology and treatment chemistry, 63
 Acidizing chemicals, 13–18
 fracture acidizing, 14
 matrix acidizing, 13–14
 Acrylamide–acrylic acid copolymers
 interactions with aluminum ions, 124–126
 viscosity of solutions, 111–123
 Acrylamide-based polymers, 102–110
 Acrylamide copolymers, 31
 Acrylamide terpolymers, heterocyclic ring in
 the polymer backbone, 31
 Additive solutions, in porous media, 279–282
 Adherent barrier, physicochemical
 properties, 636
 Adhesion tension
 dynamic Wilhelmy plate technique, 565
 measurements and contact angles, 569†
 water-advancing, 569
 water-receding, 569
 Adhesive force, non-Brownian particles, 549
 Admicelle formation, 277
 Adsorption
 flow rate, 514
 mechanism, 646–647
 on reservoir rocks, 224
 patterns, on kaolinite, 231
 process, kinetics, 487
 reactions, nonporous surfaces, 646
 surface area of sand, 251
 surfactant on porous media, 510
 Adsorption–desorption equilibria,
 dynamic, 279–239
 Adsorption plateau, calcium
 concentration, 229
 Adsorption vs. polymerization, corrosion
 inhibition, 644–646
²⁷Al NMR, 127–129
 Alcohols, structure, 172f

Affiliation Index

- Alberta Research Council, 327
 American Cyanamid Company, 102
 Amoco Production Company, 560
 Baker Performance Chemicals, 577
 Chung Yuan Christian University, 596
 Dowell Schlumberger, 608,637
 Exxon Chemical Company (ECTD), 366
 Halliburton Services, 55,660
 Heriot-Watt University, 520
 ICI Chemicals and Polymers Ltd., 520
 IMOD Processes Ltd., 520
 Institut Charles Sadron, CRM-EAHP,
 CNRS-ULP, 111,124
 Institut Français du Pétrole, 224,276,410
 Mayco Wellchem, 622
 Mobile Research and Development
 Corporation, 137
 New Mexico Institute of Mining and
 Technology, 504,531
 New Mexico State University, 622
 Norwegian Institute of Technology, 145
 Pennsylvania State University, 347
 Santa Fe Energy Company, 577
 Shell Development Company, 2,204
 Shell Research Ltd., 157
 Stanford University, 241
 University of Alberta, 347,428
 University of Calgary, 652
 University of California, Berkeley, 241,462,482
 University of Detroit, 169
 University of Illinois, 445
 University of Southern California, 378,393
 University of Texas, Austin, 550
 University of Tulsa, 560
 U.S. Department of Energy, 292
 Winfrith AEE, 261,309

Subject Index

A

- Acid attack, propagation of wormholes, 619
 Acid corrosion inhibition, time
 dependence, 644
 Acid fracturing, friction reducers, 15
 Acid hydrolysis, lignin, 173
 Acid injection into carbonate
 reservoir, 610–611
 Acid–rock reactions, rate, 15,16
 Acid wormholing
 in carbonate reservoirs, 608–620
 in carbonate rocks, 610–611
 Acidity-controlled redox reactions, 141–142
 Acidization
 hydrocarbon production, 66
 methodology and treatment chemistry, 63
 Acidizing chemicals, 13–18
 fracture acidizing, 14
 matrix acidizing, 13–14
 Acrylamide–acrylic acid copolymers
 interactions with aluminum ions, 124–126
 viscosity of solutions, 111–123
 Acrylamide-based polymers, 102–110
 Acrylamide copolymers, 31
 Acrylamide terpolymers, heterocyclic ring in
 the polymer backbone, 31
 Additive solutions, in porous media, 279–282
 Adherent barrier, physicochemical
 properties, 636
 Adhesion tension
 dynamic Wilhelmy plate technique, 565
 measurements and contact angles, 569†
 water-advancing, 569
 water-receding, 569
 Adhesive force, non-Brownian particles, 549
 Admicelle formation, 277
 Adsorption
 flow rate, 514
 mechanism, 646–647
 on reservoir rocks, 224
 patterns, on kaolinite, 231
 process, kinetics, 487
 reactions, nonporous surfaces, 646
 surface area of sand, 251
 surfactant on porous media, 510
 Adsorption–desorption equilibria,
 dynamic, 279–239
 Adsorption plateau, calcium
 concentration, 229
 Adsorption vs. polymerization, corrosion
 inhibition, 644–646
²⁷Al NMR, 127–129
 Alcohols, structure, 172f

- Alkaline flooding, oil- and reservoir-specific recovery process, 579
- Alkaline refining, insoluble materials, 11
- Alkane-aqueous NaCl systems, interfacial tension behavior, 326
- Alkane carbon number, phase-inversion temperature, 311f
- Alkanes
conductivity-temperature profiles, 309f
conductivity-titration profiles, 317f
optimal salinity variation, 317f
phase-inversion temperature, 310f,316f
- Alkyl chain length, solubility in organic solvents, 530
- Alkylaromatic sulfonates, 36-37
- Alternate slugs, polymer and cross-link solutions, 25
- Aluminum, fraction bound on polymer, 127
- Aluminum chloride solutions, pH dependence of composition, 125
- Aluminum cross-link moiety, 62f
- Aluminum salts of acid orthophosphate esters, 60
- Aluminum(III), fracturing fluids, 79
- Amide group hydrolysis
rate, 108
to carboxylate, 102-110
- Amphiphile-water systems, miscibility gaps, 300,302
- Amphiphiles, enhanced oil recovery, 290
- Amphiphiles at oil-water interface, microstructure, 327f
- Amphiphilic petroleum recovery systems, calorimetric phase studies, 290-304
- Amylopectin, molecular structure, 172
- Amylose, molecular structure, 171-172
- Anion-free water
at low electrolyte concentration, 598-601
determination, 597
function of NaCl concentration, 599f
in the electrical double layer between clay and bulk solution, 601
mobility, 601-605
- Anionic acrylamide copolymers, triad distributions, 109t
- Anionic comonomers, 102-110
- Anionic surfactant concentrations, quantitative determination, 257-271
- Antimony cross-linked gels, 75
- Armstrong electrical circuit, 639f
- Arsenic compounds, corrosion inhibitors, 17
- Ashing experiments, samples from wet oxidation, 441
- Asphaltene
classic definition, 445
colloidal
electrical charge, 454
resins as peptizing agents, 454
color, 448
- Asphaltene-Continued
deposition during oil production, 448
electrical potential, 448
elemental compositions, 449t
flocculation
critical concentration of resins, 454
interaction with oil, 449
modeling, 449
thermodynamic and colloidal models, 443-457
hypothetical structure, 446f
in recovered samples, elemental analysis, 424t
irreversible aggregation, 451
membrane-mimetic chemistry, 395
modern definition, 445
molecular weight distributions, 452f
nature and properties, 445-448
onset of deposition, 450-451
particle peptization, 453f
particles in the oily phase, 395
physical and physicochemical properties, 447
precipitation, 449
floculation of precipitate, 444
governing parameters, 444
plugging or wettability reversal, 444
quantity in recovered oil, 421
size distribution, 450
solution in aromatic solvent, 448
- Asphaltene and oil
solubility model, 450-451
suspension model, 451
- Asphaltene-modified borosilicate surface, wettability change, 584
- Asphaltene molecules, stabilize water-in-oil emulsion, 585
- Asphaltic bitumen, deposition in well, 455
- Asphaltic substances, 396f
- Associative organotin polymers, 529-546
- Athabasca bitumen
kinetics of oxidation, 426-442
values of kinetic parameters for low-temperature oxidation, 430t
- Autotitrator
detection of chloroform emulsification, 266
effect of oil, 268
error analysis, 268
principle of operation, 258-260
surfactant concentrations, 257-271
- Axial velocity profile, 485
- B**
- Backbone scission, 182
- Bacteria
biofilms, 653

- Bacteria—Continued**
 dormant, 653
 selective plugging agents, 653
 starved forms, 651–658
- Bacterial slime, injectivity, 20**
- Bactericides, 6,29**
- Base-catalyzed hydrolysis, mechanism, 108**
- Berea core flood test, 215**
- Biocides, 12**
- Bitumen**
 burning reactions, 429
 dry oxidation, 429
 heavy fractions, 394
 kinetics and energetics of oxidation, 426–44
 mass percent and elemental composition, 431*t*
 partial oxidation, 429
 recovery from tar sand, 393
- Bitumen removal, emulsification phenomena, 401*f***
- Borate complexation, 76**
- Borate cross-linked fluids, 78**
- Boron cross-linking moiety, 77*f***
- Boron gels, properties, 76**
- Bottomhole pressure**
 evolution, 615*f*
 history, 613
- Bound water**
 at low electrolyte concentration, 598–601
 in shaly sand, determination and mobility, 596–607
 interfacial region between liquid and solid, 596
- Boundary conditions, 488**
- Breakers**
 controlled depolymerization, 9
 oil gel, 60–61
 thermal initiation, 78
 viscosity, 12
- Brine completion fluids**
 corrosion inhibitors, 17
 fluid loss, 5
 wetting agents, 5
- Brine-in-crude-oil emulsion, residual water content, 367*f***
- Brine vs. crude oil, interfacial tension, 367*f***
- Bubble**
 immersed in a surfactant solution, 482
 pressure drop at low capillary numbers, 48
 surfactant-laden, 493
 trains of surfactant-laden gas, 480
- Bubble flow**
 in porous media, 483*f*
 liquid-filled cylindrical capillary, 483*f*
 shear-thinning behavior, 496
- Bubble front**
 matching to the spherical cap, 491*f*
 surfactant distribution, 492*f*
- Bubble rear**
 bubble shape, 494*f*
 surfactant distribution, 492*f*
- Bubble shape, deviation, 484**
- Bubble-size distribution, 481**
- Bubble trains in porous media, hydrodynamic resistance, 493–496**
- Buffering agents, 83**
- n*-Butanol–water, excess enthalpies, 297*f***
- n*-Butoxyethanol–water**
 excess enthalpies, 295*f*
 temperature-composition phase diagrams, 292*f*
- C**
- Calcic environment, CMC values of surfactants, 275**
- Calcite fines, stabilization, 215**
- Calcium**
 adsorption
 effect on PAM and HPAM, 230*f*,232*f*
 of anionic polyacrylamides, 237
 of xanthan, 234–237,239
 on Na–kaolinite vs. ionicity, 236*f*
 on sand vs. ionicity, 235*f*
 on SiC vs. ionicity, 235*f*
 concentration effect on adsorption, 229
 effect on intrinsic viscosity and Huggins constant, 228*f*
 effect on zero shear rate-reduced specific viscosity, 227*f*,228*f*
 influence on adsorption properties, 224–240,236*f*,238*f*
 intrinsic viscosity vs. ionicity, 233*f*
- Calcium sulfate precipitation, 20**
- Calorimetry**
 CO₂–hydrocarbon systems, 293
 miscibility gaps, 302
- Capillary number, residual oil saturation, 249**
- Capillary-pressure suction, lower permeability media, 466**
- Carbon, distribution, 435*f***
- Carbonate reservoirs**
 acid fracturing, 609
 damage, 609
 matrix acidizing job, 609
 permeability, 611
 secondary porosity, 611
 stimulation of production, 608
 wormholing, 608–620
- Carboxymethyl cellulose, structure and characteristics, 71**
- Cation exchange capacity, function of surface area, 603*f***
- Cationic lignin–graft copolymer, synthesis data, 198*t***

- Cationic polymers, permanent clay protective chemicals, 66
- Caustic flooding, 37–38
- Caustic formulation, surfactant, 38
- Cellulose
characteristics, 170
derivatives, 71
structure and characteristics, 71
- Cement slurry
additives, 8,209
cement set time, 8
foamed, 8
- Cementing fluids, 7–8
- Centralizers, 7
- Chain expansion, overestimation, 116–117
- Chemical reactions model, dry oxidation, 429
- Chemical stabilizers, 12
- Chemicals, used in oil-field operations, 3–54
- Chitin, 174
- Chloroform
droplet size, interfacial tension, 263
layers, visible spectra, 262*f*
- Chromatographic delay, 510
- Chromium redox reaction, acidity influence, 142
- Chromium(III)
common cross-linker, 137
gelation mechanism, 137–144
hydrolysis, 137–139
- Circulation test conditions, 279–282
- Clay
aqueous solutions of acids, 63
capacity to exchange ions with well fluid, 622
clay–FeCl₃ complexation technique, 378
disintegration due to fluid interaction, 627
organophylic, 74
sloughing and swelling in fresh waters, 63
treatment chemicals, 66
water-swelling, 204
- Clay and mineral fines stabilizers, chemical structures, 207*f*
- Clay hydration, high concentration of TKPP, 630
- Clay hydration water
anion-free, 597
effect on petrophysical properties, 596
- Clay minerals
equilibrium with electrolyte solutions, 596
ions in well fluid filtrate, 622
scanning electron microscope photos, 64–65*f*
- Clay particles
flocculation, 231
hydration and dispersion tendencies, 625
swelling, 18–19
- Clay-size sand particles, 249
- Clay stabilization, surfactant adsorption, 37
- Clay stabilizers
dissolved KCl, 74
history, 63–66
quaternary ammonium salt polymers, 217,219
- Clay suspension, solid–liquid ratio, 229
- Clay swelling, 19
- Cloud point
definition, 302
nonionic surfactants, 308
phase transition, 318
salinity, 309*f*
- CO₂-foam mobility
apparatus, schematic, 505*f*
in porous rocks, 502–517
measurements, 504–506
- CO₂-hydrocarbon systems, phase behavior, 291
- CO₂ oil recovery processes, viscosity, 529
- Coke
evolution of composition, 424
mass percent composition produced by wet oxidation, 439*t*
- Coke deposit, influence of the crude oil composition, 408–425
- Coke zone, analysis, 414
- Colloidal chemistry, geometry, 395
- Colloidal particles, detachment from surfaces, 549–550
- Commercial sulfonate formulations, salinity, 323
- Comonomer sequence distributions, 217
- Completion fluids
and operations, 8–10
prime requisites, 621
- Composite slugs
effect on tertiary recovery, 355–358
oil recovery efficiency, 346
size, 359
- Concentration loss
coarse sand, 253*f*
effect of rehydration pH, 252*f*
static test, 252*f*
- Concentrations and flow rates,
chromatographic time-delay factors, 515*t*
- Condensation polymers, 209
- Condensing gas drive, 444
- Conformational change, temperature- or salt-driven, 145–146
- Coning
control by bacteria, 653
definition, 653
- Conjoining–disjoining pressure, inside the lamella, 463
- Constant-charge electrostatic model
critical absolute permeability, 470*f*
critical capillary pressure, 471
ionic concentration, 466
- Constant-phase element
effect of exposure time, 643*f*
effect of octynol, 643*f*
- Constant-potential and weak-overlap electrostatic model, 464*f*
- Constant-thickness thin-film region,
bubble flowing in a tube, 493
- Contact angle
bar graphs, 573*f*

- Contact angle—*Continued*
 crude oil–brine systems, 565
 measurement
 sessile drop method, 561
 water droplets on asphaltene-modified surface, 580
 water-advancing, 571
 water-receding, 571
 Contact angle hysteresis, surface
 heterogeneities of natural mineral samples, 572
 Contaminant precipitation, asphaltic agglomerates, 400
 Contour length distribution, xanthan, 148
 Copolymer mineral fines stabilizers, permeability damage characteristics, 216f
 Copolymers, effectiveness as mineral fines stabilizers, 212,213f
 Core flooding apparatus, schematic, 245f,351f
 Core permeability, 208
 Corrosion
 deep wells and geothermal reservoirs, 632
 drilling-fluid additives, 632
 Corrosion inhibition
 acidizing, 17
 time dependence, 644
 Corrosion inhibitors
 acid concentration, 14
 design, 636–650
 typical, 6
 Corrosion of steel
 effect of corrosion inhibitors
 adsorption and film formation, 641–642
 adsorption mechanism, 646–647
 adsorption vs. polymerization, 644–646
 equivalent electrical circuit, 642–644
 time constant analysis, 647–649
 in uninhibited HCl, 638–641
 oil well acidizing or acid pickling treatments, 636
 Corrosion-resistant cements, supercritical carbon dioxide, 8
 Cr(III) olates, gelation mechanism and rate, 139–140
 Cr(VI) reduction, pH dependence, 141
 Cracking effect, zone ahead of the coke zone, 414
 Cracking products, by dilution, 408
 Critical capillary pressure
 effect of flow velocity, 471
 foam in porous media, 461–466
 gas velocity, 472f
 initial film thickness, 471
 pore-body-to-pore-throat radius ratio, 472f,473
 surface viscosity, 472f
 Critical flow rate, release of non-Brownian particles, 548–557
 Critical gas velocity, lamellae rupture, 461
 Critical micellar concentration
 anionic–nonionic surfactant mixtures, 287
 definition, 273–277
 Critical velocity
 definition, 553
 particle composition, 553
 solution pH and ionic strength, 553
 Cross-linked gelled fluid, types and use, 75
 Cross-linked gels, frictional resistance, 79
 Cross-linked polymers, thief zones, 24
 Cross-linkers
 high temperatures, 81
 stress, 82
 Cross-linking agents
 delayed cross-linking, 12,79–80
 development, 78–79
 titanium(IV), 81–83
 zirconium(IV), 80–81
 Cross-linking reactivities, olates, 139
 Cross-linking system, 25
 Crude–brine systems, hysteresis, 565
 Crude oil
 acid number, 37
 conditions, alkane equivalences, 323
 content of fractions, 381f
 demulsifiers, 364–374
 evolution of the composition, 408
 fractions
 interfacial tension, 382
 long-chain carboxylic acids, 382
 modification during in situ combustion, 408–425
 persistent water-in-oil emulsions, 364
 resin and asphaltene content, 455f
 viscosities and densities, 350f
 wettability, 567–571
 Crude oil–brine interface
 dilatational modulus, 372f
 dynamic interfacial tension, 369f
- D
- Damage assessment
 clay swelling, 625–627
 core tests, 623–625
 Damaged double porosity reservoir during acidizing, permeability profile, 615f
 Decane–cyclohexane blends, optimal salinity variation, 319f
 Decane–Gulfaks crude blends,
 phase-inversion temperature, 314f
 Decane–toluene blends, phase-inversion temperature, 316f
 Decomposition, autocatalytic, 34
 Defoamers, 5

- Degradation**
 succinoglycan, 163–166
 xanthan, 163
- Degradation kinetics**
 chemical stability, 113–116, 115*f*
 decomposition of chain hydroperoxides, 116
 oxygen and salts of transition metals, 113–116
- Degradation of polymers, 118–120**
- Delayed-onset cross-linking agent**
 titanium, 81–83
 zirconium, 80–81
- Demulsification**
 interfacial shear viscosity, 366
 relative performance of TFSAs, 580
 water-in-oil emulsion, 373
- Demulsifier selection, property–performance relationship, 365**
- Demulsifiers**
 effect on interfacial properties, 364–374
 electron spin resonance, 370
 ethylene oxide content, 368
 description, 364
- Depolymerization, fluid viscosity, 9**
- Depositional process, enthalpy, 430**
- Deprotonation, critical step of olation, 140**
- Desorbent breakthrough, ethylene oxide distribution of cosurfactant, 284*f***
- Desorbents increasing ethoxylation, retention properties, 285**
- Deuterium, with heavy oil samples, 341**
- Deviated wells, 7**
- Differential pressure transducer output, 526*f***
- Dilational elastic modulus, interfacial tension, 370–373**
- Dilute polymer solutions, retention behavior in oil sands, 241–260**
- Dimensionless pressure drop per bubble, 494*f***
- Dispersion, slopes of adsorption peaks, 514**
- Displacing fluid**
 channeling, 241
 mobility reduction, 241
 polymer flooding, 27
- Dissolution channels, fractal geometry, 608**
- Distillation experiments, 430–433**
- Distillation reaction, 437**
- Diversion stage, 619**
- Diverting agents, 17**
- Dolomite, wetting studies, 574**
- Double porosity reservoirs, damaged, 611–612**
- Drag reduction, starch graft copolymer, 177*t***
- Drilling field test, clay–shale inhibition, 630**
- Drilling fluids**
 additives, 4–7
 corrosiveness imparted by additives, 632
 oil-based muds, 4
 prime requisites, 621
 use, 3–7
 viscosity, 4
- Drilling muds**
 appearance, 3
 cost, 628, 630
 displacement, 7
 effect of potassium salts, 629
 properties before and after hot rolling, 196*t*
 rheological properties, 628
 rheology of TKPP–xanthan, 629*t*
 turbulent flow, 7
 water-soluble polymers, 195–199
- Droplet size distribution, titration cup, 266**
- Dry oxidation**
 chemical model, 429–430
 dependence on temperature and oxygen pressure, 442
 kinetics and energetics, 427–430
 mass balance of carbon, 432–433
- Dynamic adsorption apparatus, 512*f***
- Dynamic adsorption experiment, 510–516**
- Dynamic crude oil wetting measurements, advantages, 565–567**
- Dynamic flow tests, adsorption–desorption data, 281*t***
- Dynamic foam, coalescence, 466**
- Dynamic foam stability theory**
 confirmation, 473
 critical capillary pressure data, 474*f*
- Dynamic interfacial tension gradient, local variations, 366–370**
- Dynamic pressure drop, across the bubble, 484**
- Dynamic Wilhelmy plate apparatus, 563*f***
- Dynamic Wilhelmy plate technique**
 adhesion tension and contact angles, 574
 distinguish among wetting systems, 575
 formation wettability studies, 560–576
 liquid–liquid–solid interactions of weighing agents, 574
 liquid phases in motion relative to a solid phase, 561
 reservoir wettability, 561
- E**
- Elastic modulus, surfaces, 550**
- Electrochemical techniques**
 cyclic voltammetry, 637
 linear polarization, 637
- Electrolyte effect, on polymer solution rheology, 181**
- Electrostatic effects, polymer adsorption and flocculation, 135–136**
- Electrostatic interaction, model, 125–127**
- Electrostatic repulsion, polymer chain, 30, 135**
- Electrostatic term, 117**
- Emulsifiers, 7**
- Emulsion**
 history, 83–84
 interfacial dilation modulus, 370

Emulsion—*Continued*
 interfacial shear viscosity, 366
 oil–water interfaces, 585–586
 Emulsion blocks, 20
 Emulsion coalescence, surfactant molecules, 400
 Emulsion mechanism, 263–268
 Enhanced oil recovery, 23
 Enhanced oil recovery polymers adsorption properties, 224–240
 calcium, 224–240
 Enzyme digestion, lignin, 173
 Equilibrium metastable film, 465
 Equilibrium micellar phases, composite slugs, 345
 Equivalent electrical circuit, corrosion inhibition, 642–644
 Etching
 fracture acidizing, 14
 secondary-porosity fissure walls, 612
 Ethoxylation, 273–275
 Ethylene oxide
 demulsifier, 370
 distribution, nonionic surfactants, 287
 electron spin resonance, 370
 Excess enthalpies, 299*r*
 Experimental growth laws, field data interpretation, 608–620
 Exploratory wells, 614

F

Fermentation, production of succinoglycan, 158
 Fermentation broths, flash drying, 29
 Film formation
 decrease in corrosion inhibition, 646
 effect on corrosion rate, 641–642
 Fines migration
 Berea sandstone, 19
 critical flow velocity, 20
 First-contact miscible gas drive, 444
 Fish eyes, 72
 Flocculants, 6
 Flocculation, asphaltene, 443–457
 Flooding strategies, optimal structure of surfactants, 305
 Flow channels, plugged with solid xanthan residues, 29
 Flow experiments
 experimental apparatus, 554*f*
 glass flow cell, 554*f*
 Flow tests, polymer adsorption, 247
 Fluid banks, mobility ratio, 241
 Fluid communication between formations, 8
 Fluid flow patterns, pilot study, 594
 Fluid injection wells, sodium hypochlorite, 17
 Fluid leakoff, 56
 Fluid loss additives, 4–5,11

Fluid loss control agents, 56
 Fluid-phase equilibrium, thermodynamic and transport characteristics, 443
 Fluorinated surfactants, 87
 Fluorochemicals, epoxy resin fluidity, 10
 Foam
 aqueous fracture, 84
 behavior at elevated temperature and pressure, 519
 behavior in porous media, 32–33,466–473
 calculation of quality, 525
 effectiveness, 519
 flow in porous media under reservoir conditions, 518–528
 formation damage, 13
 interfacial dilation modulus, 370
 irregularities in quality, 527
 microstructure, 481
 mobility-control fluid, 461
 oil and alcohol, 84
 stability, 519
 static, stability in porous media, 463–466
 viscosity, 85*f*
 Foam bubble regime, effective viscosity, 497*f*
 Foam coalescence, medium capillary pressure, 463
 Foam flooding method, mobility of a low-viscosity fluid, 503
 Foam-flow behavior, in porous media, 481
 Foam generation, mechanisms, 33
 Foam injection, oil recovery from watered-out porous media, 518
 Foam lamellae flowing through a periodically constricted pore, 460–479
 Foam mobilities, in porous rocks, 502–517
 Foam processes, enhancement of oil recovery, 326
 Foam-rheology rig
 schematic representation, 520*f*
 typical plot of data output, 524*f*
 Foam stability, surfactants, 33
 Foam texture, 481
 Foam transport, in porous media, 480
 Foamed fracturing fluids, 84–87
 Foaming agents
 drilling fluids, 5
 performance, 86*f*
 Foamlike dispersion, mobility of CO₂, 503
 Formation brine, initial core permeability, 624
 Formation damage
 by water, 63
 causes, 205
 clear well fluids, 624*r*
 definition, 18
 fluid and particulate damage, 622
 productivity decline, 204
 solid particles in wellbore fluids, 18
 Formation damage control additives, clay swelling, 13

Formation damage control chemicals
 cationic organic polymer, 204–221
 permeability damage, 7
 various types, 18–22

Formation permeability damage, treatment
 design, 16

Formation wettability studies, 560–576

Frac fluids, *see* Fracturing fluids

Fracture conductivity, proppant, 57–59

Fracture dimensions, 58*f*

Fracturing
 oil and gas well, 55–100
 physical and engineering aspects, 56
 rate of production, 56

Fracturing fluids
 additives available, 55
 bacterial degradation, 12
 cross-linked, 74–80
 history, 59–61
 humidity, 61
 micelles, 61
 water-based, 66

Fracturing gel, 82

Fracturing process and equipment, 58*f*

Free radical copolymerization, 212

Friction reducers, 6,60

Frictional resistance, cross-linked gels, 79

G

Gas-injection mechanisms, 444

Gas production, 219

Gel balls, 72

Gel network model, 62*f*

Gel structure, ionic strength effects, 83

Gel viscosity, cross-linking, 73*f*

Gelation
 favorable conditions, 133–135
 intramolecular bridgings, 129

Gelation rate, function of disulfite
 concentration, 143*r*

Gelation reactions, 141–142

Gelation time
 rapid cross-linking, 25
 variation, 139*r*

Gelled oils, 59–60

Gelling agents
 dispersion, 72–74
 history, 66–67
 selection, 72

Gibbs–Marangoni effect, demulsifier, 368

Glass, wetting studies, 574

Glass microspheres
 comparison of flow cell and centrifuge
 experiments, 556*f*
 effect of ionic strength on release, 556*f*
 effect of solution on pH on release, 555*f*

Glen rose shale, compaction experiments, 604

Graded composite slug, delay of slug
 breakdown, 348

Graded composite slugs, 358

Graft copolymers
 hydrolysis, 179
 synthesis data, 195*r*

Grafting reaction, lignin models, 194

Gravel pack treatments, formation damage, 10

Gravel packing
 mixtures of polymers, 9
 particle size, 9

Gravity override
 low steam density, 33
 surfactants, 33–34

Guar, hydraulic fracturing, 11

Guar gum
 derivatives, 67
 preparation, 67
 structure, 174

Gypsum scaling, 20

H

Heat production
 definition of rate, 437
 function of partial pressure of water
 vapor, 440*f*
 rate, 434,438
 wet and dry oxidation, 435*f*

Heavy crude oil, transition metal ions, 35

Heavy oil–aqueous systems, interfacial
 tension, 325–344

Heavy oil desaturation, interfacial tension, 326

Heavy oils, physical and chemical
 properties, 329*r*

Hematite fines, stabilization, 215

Hexadecane–oleic acid–water–glass wetting
 cycle, hybrid-wetting behavior, 568*f*

Hexadecane–water–glass system, model for
 crude oil–brine systems, 562

Hexadecane–water–glass wetting cycle,
 water-wetting behavior, 564*f*

Hexadecane–water–PTFE wetting cycle,
 oil-wetting behavior, 568*f*

High-temperature steam, enhanced oil
 recovery, 33

Hyamine
 increase in transmittance, 266
 phase separation, 263

Hybrid wetting, 574

Hydration water, function of concentration
 and method of determination, 599*f*

Hydraulic fractures, growth patterns, 57

Hydraulic fracturing
 definition, 10
 discussion, 10–13
 history, 59

Hydraulic pressure stimulation, 55
 Hydrocarbon gellants, 59–60
 Hydrocarbon mixtures, behavior of
 asphaltenes, 450
 Hydrodynamic behavior, single gas bubble, 481
 Hydrodynamic forces, release of non-Brownian
 particles, 548–557
 Hydrodynamic stability theory, foam
 coalescence in porous media, 475
 Hydrodynamic theory, lamella flowing through
 a cylindrical pore, 460
 Hydrogen bonds, adsorption, 136
 Hydrogen sulfide, corrosion inhibitors, 17
 Hydrolysis
 acrylamide in copolymers, rate, 105
 amide group, 108
 amide in AMPS copolymers, 106*f*
 amide in sodium acrylate copolymers, 106*f*
 Cr(III), 137–139
 graft copolymers to anionic terpolymers, 180*r*
 initial rate constants, 107*f*
 kinetics, 112–113, 114*f*
 Monte Carlo simulation method, 111
 polyacrylamide and acrylamide–sodium
 acrylate copolymers, 103
 polyacrylamide decomposition, 30
 pseudo-unimolecular rate constants, 105
 rate, acidity, and salt concentration, 120
 Hydrolysis experiments, to simulate harsh
 reservoir environments, 104
 Hydrophilic head, 376
 Hydrophilic nonionic surfactant, 285
 Hydrophobic tail, 376
 Hydrotrope, increased oil recovery, 34
 Hydroxyaluminum, polymerization, 19
 Hydroxyethyl cellulose, hydraulic
 fracturing, 11
 Hysteresis
 definition, 79
 water-wetting system, 567

I

Immiscible oil displacement, low interfacial
 tension, 377
 Impedance spectroscopy, 636–650
 In situ combustion
 air injection, 39
 description of processes, 426
 enhanced oil recovery, 408–425
 ignition delay period, 426
 oxidation of bitumen, 426–442
 In situ emulsion formation, pressure drops
 across the core, 249

Incremental oil production
 cumulative, 593*f*
 pilot wells, 590
 Induced fractures
 fluid viscosity and injection rates, 59
 mathematical models, 57
 shape and dimensions, 57
 temperatures inside, 59
 Inductive loops, surface-mediated
 reductions, 642
 Industrial anionic–nonionic surfactants, 277
 Industrial surfactant mixtures, in calcic
 saline media, 272
 Inhibition of steel corrosion, by organic
 compounds, 641–642
 Initiation mechanisms, starch and
 cellulose, 178*f*
 Injectivity index, 613
 Inorganic salts, formation damage, 19
 Instantaneous fluid exchange, 467
 Interfacial film, local thinning, 368
 Interfacial properties, governing crude oil
 demulsification, 364–374
 Interfacial shear viscosity,
 demulsification, 366
 Interfacial surfactant curvature, electric
 double layer effects, 323
 Interfacial tension
 Ca²⁺, 338
 determination by computer interface
 system, 565
 effect of CaCl₂ concentration and
 temperature, 339*f*, 340*f*
 effect of NaCl concentration and
 temperature, 335*r*, 336*r*, 337*f*
 effect of temperature, 332*f*, 340*f*
 effect on spinning rate, 332*f*
 NaCl concentration, 331–333
 oil–water, 325–344
 pH, 334
 pH and temperature, 337*f*
 presence of surfactant in brine, 331–333
 surfactant concentration, 506
 temperature, 328, 333–334
 Interfacial tension–temperature relation-
 ships, CaCl₂ concentrations, 338
 Interfacial tension vs. alkali concentrations,
 383*f*, 384*f*, 385*f*
 Intermolecular bridges, 135
 Intramolecular bonds of polymers, high
 shear, 56
 Intrinsic viscosity, hydrolyzed
 polyacrylamides, 117
 Inversion process, salinity effects, 321
 Ionic ratio hypothesis, 624
 Iron metal fines
 disposal problem, 205
 fracture flow capacity, 205

K

Kaolinite

- adsorption of xanthan, 237
- polymer adsorption density, 229
- reduction in adsorption with ionicity, 234

Kaolinitic clay, amount of anion-free water, 605

Klebsiella pneumoniae

- in sandstone rock cores, 656f
- starved and full-sized, 655f
- use in oil recovery, 653–657

Kraft lignin, 173,187

L

Laboratory apparatus, flow of foam, 518–528

Ladder backbone copolymer, 175f

Lamella

- flowing in a periodically constricted pore, 464f
- in porous media, relative mobility, 510
- longevity, in porous media, 461
- stretching and breaking during transport, 473
- thickness, evolution, 470f
- volume rearrangement, 467

Light source and probe, schematic diagram, 259f

Lignin

- cationic graft copolymer, 197
- composition, 173
- recovery methods, 173
- structure, 172
- woody plants, 172–174

Lignin copolymers, elemental assay, percent hydrolysis, and limiting viscosity number, 195r

Lignin graft copolymers

- composition of reaction mixture, 199r
- description, 187
- drilling mud additives, 196
- synthesis, 191–195

Lignin polymer, structure, 191f

Lignin reactions, viscosity number, 193r

Lignosulfonates

- cement set time retarders, 8
- cross-linked, 26
- gelation technology, 26
- oil recovery from unconsolidated sands, 36
- resource recovery, 173

Limestone reservoir, 616

Limiting viscosity number

- complex copolymers, 181r
- copolymer molecular weight, 180
- hydrolyzed graft copolymers, 182
- hydrolyzed sample, 190f

Limiting viscosity number—*Continued*
molecular weight and hydrolysis, 199

Long bubbles, flow through a cylindrical capillary, 480–501

Lost circulation chemical treatments, 5

Low-temperature oxidation, ignition delay period, 426

Lubricants, 6

M

Macroemulsions, flow properties, 585

Macroscopic continuity, flow rate, 485

Marble, wetting studies, 574

Matching, 488–489

Matrix acidizing job, effect on well productivity, 609

Mechanical blockage, reduced productivity, 622

Membrane-mimetic agents, osmotically active, 400

Membrane-mimetic system

alkaline environment, 398

reaction pathways, 405

Metal ion complexing agents, 72

Metallic soaps

friction reduction, 61

performance, 59

Methacrylamide backbone, 212

Micellar flooding process

economics, 346

process description, 346

sandstone cores, 359–363

watered-out light oil reservoirs, 345

Micellar hydrophobe expansion, oil molar volume, 323

Micellar inversion process

asphaltic micelles, 400

description, 398

Micellar slug

components, 346

composition and viscosities, 354r

multiple, 345–363

single, composite, and graded composite, 359r

size, 360r

oil recovery efficiency, 357f

tertiary recovery, 356f

volume ratio, 358r

Micellar solutions

complex behavior, 347

formulation, 350–352

monomer vs. overall surfactant

concentrations, 278f

Micellar systems, characteristic interaction parameter, 273

Micelle inversion process, asphaltene, 399f

Micelles, sonication energy, 61

- Micellization and adsorption phenomena, simultaneous, 277
- Micellization and desorption effects, 272–288
- Micellization phenomenon, recovery mechanism of surfactants, 285
- Microbial polysaccharides, enhanced oil recovery, 30
- Microspheres
effect of solution pH on potential energy, 557f
potential energy as function of ionic concentration, 557f
- Migrating clay stabilizers, nonionic polymers, 217
- Milled wood lignin, 173
- Mineral acids, hydrochloric and hydrofluoric acid, 14
- Mineral fine particle properties and stabilization, 208,208t
- Mineral fines production
NVP copolymers, 215t
unconsolidated test columns, 212t
- Mineral fines stabilizers
cationic organic polymer, 219
field test results, 217–220
laboratory test results, 211–217
- Mineral surfaces, 577
- Miscible displacement, CO₂ viscosity ratio, 502
- Miscible-flood mobility control, 301
- Miscible flooding, surfactant-based mobility control, 291
- Miscible gas flooding
mechanisms, 444
oil-displacement efficiency, 38
- Mist or foam drilling, 5
- Mixed acid systems, fluid injection rates, 15
- Mixed surfactant adsorption, 277–279
- Mixed wettability medium, petroleum reservoirs, 578
- Mobile fines
creation, 205
formation damage, 205
- Mobility
CO₂-foam fraction, 508f,509f,516
rock permeabilities, 512f
surfactant concentration, 508f,516
- Mobility buffer
micellar flooding process, 352
micellar slug, 346
- Mobility control
adsorption losses of polymers, 255
complex copolymers, 169–203
displacing fluid, 241
efficient use of CO₂, 529
flow channels, 242
foam, 480
surfactants, 32
- Mobility control agents, 28–30
- Mobility measurements, basic flow system, 505f
- Mobility ratio
definition, 27
gas:oil, 32
rock permeability, 27
- Monomer, difunctional, 26
- Monomer–micelle equilibrium, 273
- Monomers in solution, limit concentration, 275
- Monovalent to divalent ratio, effect on adsorption, 231
- Montmorillonite clay, NaCl concentration and porosity, 605
- Mud, *See* Drilling muds
- Multilamellar surfactant vesicle development phenomena, 402f
four months after processing, 403f
three years after processing, 404f
- Multiple micellar slug
choice of components, 348
efficiency of displacement process, 348
- Multiplicity of slugs, 358
- Multivalent cations, damage potential of TKPP, 625
- Mutual solvents, surfactant adsorption, 16
- N**
- NaCl, effect on adsorption of HPAM, 232f
- Napalm
refinements in chemistry, 59
use in gasoline, 59
- Natural polymers, 170–174
- Navier–Stokes equations, 485
- Neighboring group inhibition, 108–109
- Non-Brownian particles
attached to a surface, 548–557
definition, 548
removal mechanisms
rolling motion, 549–550
torque balance, 550
- Nonionic surfactants, 318
- Nonvertical wells, 7
- North Sea oil reservoirs, 305
- Nyquist plot of N80 steel, 639f
- O**
- Octynol, corrosion of steel, 646
- Oil and brine, location and distribution through porous media, 578
- Oil and water volume ratio, phase inversion temperature, 314f
- Oil bank, waterflood, 566
- Oil-based muds, types, 4
- Oil-containing rock, inadvertent overtreatment, 26

- Oil displacement efficiency
 definition, 24
 large concentrations of surfactants, 35
- Oil field, discovery rate, 3
- Oil-field gelling agents, general properties, 70*f*
- Oil ganglia
 breaking up, 249
 plugging of core, 247
- Oil gel, associative, 63
- Oil gel breakers, 60–61
- Oil gelation, by orthophosphate esters, 61–63
- Oil inclusion, oil molar volume, 323
- Oil prices, effect on oil-recovery processes, 39
- Oil production decline, water-drive
 reservoirs having good pressure
 maintenance, 590
- Oil recovery
 gas drive, 21–22
 natural water drive, 21–22
 on pump, 22
 primary, 21–22
 scaling, 22
 waterflooding, 22
- Oil-recovery mechanisms, 24
- Oil-recovery methods, limitations at
 present, 651
- Oil reserves, cost of discovery, 23
- Oil reservoir wettability, 560–576
- Oil sands
 oxidized, elemental compositions, 441
 retention behavior of dilute
 polymers, 241–260
- Oil shale, organic components, 382–386
- Oil-wet rock, 21
- Oil-wetting systems, models, 562
- Olated Cr(III), UV–VIS spectral data, 138*r*
- Olates
 chromium, 142*r*
 reactive cross-linking species, 137
- α -Olefin sulfonates, 36
- Optimal salinities
 anionic surfactants, 313–318, 322
 nonionic surfactants, 313
- Order–disorder transition
 structural, 157
 temperature, 163
 xanthan, 145–156
- Organic acids, 15
- Organic polymer structures, field use, 206
- Organophylic clays, 74
- Orthokinetic flocculation mechanism, 398
- Orthophosphate gellants, 61–63
- Oxidation
 asphaltenes, resins, and oil, 454
 athabasca bitumen, 426–442
 reaction change with increasing
 temperature, 428
- Oxygen scavengers, 29
- P
- Paired micellar slugs, tertiary recovery, 357*t*
- Paraffin deposits, productivity, 20
- Particle composition, release phenomena, 555*f*
- Particulate damage, tightly wedged solids, 622
- Peptizing agents
 colloidal asphaltene deposition problem, 455
 neutral resins, 447
- Perforating gun, 8–9
- Perforation density, 614
- Permeability
 evolution during acidizing, 610
 initial and damaged, 623
 secondary-porosity well, 613
- Permeability damage
 adjacent formations, 13
 clay swelling, 211
 effect of anion, 625
 fines migration, 208
 nonswelling clays, 205
 silica fines, 205
- Permeability tests, relative permeability
 hysteresis, 567
- Petroleum crude oil, surfactants, 376–390
- pH buffers
 cross-linking reactions, 13
 polymer particle dispersion, 12
- pH control aids, 6
- Phase behavior
 calorimetry, 291
 discussion of results, 299–302
 experimental data, 294–298
 experimental difficulties, 291
 three-phase problem, 291
- Phase-inversion conditions, surfactant blends
 in contact with alkanes, 323
- Phase-inversion temperatures
 anionic surfactants, 313, 321
 nonionic surfactants, 308
- Phase separation
 critical concentration, 120
 pH dependence, 131–133
- Phase titration, 129
- Phase transition, clouding phenomena, 318
- Photometric titration
 basic principles, 260
 choice of filter, 261
 experimental procedures, 261
 SDBS against hyamine, 264*f*
- Pilot description, TFSA–waterflood
 pilot study, 581
- Pipe-freeing agents, 6
- Plateau borders
 lamella and pore wall, 461
 surfactant-stabilized lamellae, 481
- Plugging
 current methods, 653

Plugging—*Continued*
 high-permeability zone, 651
 resuscitated starved bacteria, diagram, 655f
 Polar compounds, separation from crude oils, 377
 Polar molecules, heavy fractions, 395
 Polyacrylamide
 adsorption on kaolinite, 229–231
 adsorption on siliceous minerals, 226–229
 emulsion polymers, 30
 hydrolysis, 112
 hydrolytic stability, 102–110
 properties, 28
 unhydrolyzed, 131
 Polyacrylamide decomposition, hydrolysis, 30
 Polyacrylamide solution viscosity, saline waters, 31
 Polycyclic aromatic hydrocarbons, 447
 Polyelectrolyte adsorption behavior, 229
 Polyelectrolyte effects, 127,179
 Polymer association complexes, water viscosity, 31
 Polymer clay stabilizers, permeability damage, 20
 Polymer concentrations, injected-water viscosity, 28
 Polymer cross-linking, Cr(III) species, 143
 Polymer degradation, 251
 Polymer dependence on solid–liquid ratio, 229–231
 Polymer film, electrical insulator, 646
 Polymer flooding, 27–32
 adsorption, 224
 brines or sea water, 102
 Polymer hydration
 techniques to promote, 12–13
 treatments to delay, 13
 Polymer ionicity
 effect on adsorption, 231–234
 intrinsic viscosities of polyacrylamides, 231
 Polymer loss, static and dynamic tests, 254
 Polymer molecules
 adsorption and trapping, 242
 retention mechanisms, 242
 Polymer stability, different species of aluminum, 129–133
 Polymeric chains, transient, 530
 Polymeric viscosifiers, dispersion, 72–74
 Polymerization, effect on corrosion rate, 641–642
 Polynuclear aluminum ions
 interaction with polymers, 129
 NMR study, 127–129
 Polysaccharide base gels, cross-linkers, 82
 Polysaccharide fluids, formation damage characteristics, 10
 Polysaccharide gelling agents
 relative viscosities, 70f
 structures, 68–69f

Polysaccharide thickeners, cost and performance effectiveness, 67
 Polystyrene particles, effect of particle size on release, 554f
 Pore size distribution, mercury intrusion, 603f
 Porous media, retention behavior, 242
 Porous medium micromodel, kupa-ruk sandstone, 460
 Porphyrin–metal chelates, in petroleum, 393
 Potassium, for drilling, 621–635
 Potassium-based clear well fluids,
 composition and concentration effects on core permeabilities, 626f
 Potassium chloride
 clay inhibition, 628
 conventional water-base drilling fluids,
 rheological impact, 628
 corrosivity, 628
 Potassium salts, effect on conventional drilling muds, 629
 Precipitation, intramolecular fixation, 129
 Preferred curvature state, surfactant molecules, 322
 Pressure buildup, surfactant retention, 400
 Pressure responses, theoretical and actual, 613
 Pressurized fluid, high-shear forces, 56
 Profile control gels, 137
 Propagation, enhanced oil-recovery chemicals through rock, 31
 Proppants, 11–12,57
 Pseudoplasticity, 185
 Pulsed-drop technique, interfacial tension, 365
 Pyrolysis reactions, 408

Q

Quaternary ammonium salt groups, 204–221
 Quaternary ammonium salt polymers, 19

R

Radius of gyration, 185r
 Rate of drilling, drilling fluids, 4
 Reactive monomers, 26
 Recovered oil, analysis, 421
 Recovery mechanisms
 changing the wettability of reservoir rock surfaces, 583
 coalescing emulsions in near-wellbore region, 583,585–586
 sand deoiling tests, 583
 Redox-generated Cr(III), gelation reaction, 140–141
 Redox reactions, control of acidity, 141–142
 Reduced injectivity
 production at offset wells, 18
 water-expandable clays, 18–19

- Regular perturbation solution, 489–490
 Regular solution theory, 273,285
 Relative skin evolution, cumulative acid volume, 614
 Relaxation time, 181
 Reservoir conditions, flow of foam in porous media, 518–528
 Reservoir description, TFSA–waterflood pilot study, 581
 Reservoir fluids
 location in porous media, 566
 velocity, 566
 Reservoir oils, physicochemical problems, 30†
 Reservoir volumetric sweep efficiency, miscible gas flooding, 444
 Reservoirs, wetting state, 578
 Residual coke, wet oxidation, 434
 Residual organic matter
 analytical procedure, 411,412f
 evolution in composition, 411,413f
 Residual resistance effects, water permeability reductions, 28
 Residual water, NMR measurement, 605
 Resin
 adsorption on asphaltene, 451
 asphaltene suspension, 451
 physical and physicochemical properties, 447
 repulsive molecular forces, 451
 role in asphaltene formation, 454
 Resource recovery
 complex polymers, 176–180
 graft copolymers, 176
 rheology, 174
 solubility, 174
 stability, 175
 starch graft copolymers, 176
 surface behavior, 175–176
 Retarded acids
 diffusion rates, 16
 sandstone acidizing, 15
 Reynolds parallel-film model, 467
 Rheology modifiers, 5
 Rock dissolution, oil-wetting surfactant, 16
 Rock permeability
 effect on mobility, 507–510
 polymerization, 26
 Rock–polymer interactions, random chain scission, 247
 Rock sample, properties, 600†
 Rock structure, 56
 Rock surface, altered wettability, 578
 Rock wettability, 21

S
 Sacrificial adsorption agents, 32
 Sacrificial agents, surfactant propagation rate, 37
 Salinity, cross-linker effectiveness, 25–26
 Salinity–alkane sensitivity, surfactant hydrophile, 321
 Salinity tolerance, carboxymethylate surfactant, 321
 Salt content, cross-linked gel network, 83
 Salt loadings, commercial grade anionic surfactants, 323
 Sand control
 gravel packing, 10
 resins, 10
 Sand deoiling, relative performance of TFSA's, 580
 Sand packs, preparation, 246
 Sand production, 9–10
 Sandstone acidizing, retarded acids, 15
 Sandstone formation permeability, corrosion inhibitors, 20
 Scale inhibitors, 7,18
 Scaling behavior, xanthan, 153
 Scaling factor, 469
 Scission of polymer chains, viscosity, 247
 Scratchers, 7
 Screen factor, 181,183f
 Secondary oil recovery, injection rate, 22
 Selective plugging, definition, 651
 Self-propagating surfactant vesicles, ultrasonic energy and alkaline solution, 393
 Sessile drop method, 561
 Shale oil
 content of fractions, 381f
 oil–water interface, 387f
 surfactants, 376–390
 Shale oil fractions
 dissociation phenomena, 382
 interfacial tension, 382
 Shallow and deep plugs, effects, 652f
 Shaly sand, determination and mobility of bound water, 596
 Shear rate vs. viscosity curve, 545f
 Shear-thinning behavior, CO₂-foam fraction, 516
 Silica dissolution, gravel pack stability, 10
 Silica fines stabilization, 215,217
 Silica–kaolinite fines, stabilization, 215
 Silicate mineral fines, rapid production declines, 217
 Siliceous minerals, adsorption of polyacrylamides, 226–229
 Silicon halide, sand control, 10
 Single and composite micellar slugs, comparison of tertiary recovery, 358†
 Single micellar slugs, tertiary recovery, 355†
 Single slugs, 352–355
 Skin curves
 actual and model, during wormholing, 618f
 treatment of well A, 617f
 Skin evolution
 theory of fractals, 619

- Skin evolution—*Continued*
 treatment of well B, 618f
- Skin histories, during acid jobs, 612–619
- Skinplug, definition, 653
- Slug breakdown, oil displacement, 347
- Slug formulation
 micellar slug, 346
 multiphase region, 347
- Slug injection runs, profiles of additive produced, 286f
- Solid–liquid ratios, monomer concentration vs. initial sulfonate fraction, 280f
- Solubility in nonpolar solvents
 rate of dissolution, 533
 trimethylsilyl group, 533
 triorganotin fluorides, 529
- Solubility in petroleum crude, asphaltene and oil, 450
- Solubility limit, 119f
- Soluble surfactants, influence, 480–501
- Solvent fractionation scheme, 380f
- Sorption kinetics, mass-transfer barrier to surfactant migration, 482
- Spacer fluid, use and composition, 7
- Spacing agent, 57
- Spent acid, completion problems, 631
- Spinning drop technique
 interfacial tension, 325–344
 surfactant precipitation, 338
 use of deuterium, 328
- Squeeze cementing, gaps in the cement sheath, 8
- Stability
 foam flowing in porous media, 460–479
 potassium formate, 166
 to polymer chain scission, 175
 xanthan and succinoglycan, 166
- Stabilizing agents, 6
- Stagnation rings
 around the bubble, 484
 excess of surfactant, 490
 gradients in surface velocity, 490
- Starch, 170–172
- Starch graft copolymers, 176–187
- Starved bacteria
 ability to grow within rock cores, 654–657
 changes in cell size, 653
 cost-reduction exercises, 657
 nutrients, 654
 penetration into porous media, 654
 resuscitation pattern, 657
 size changes, 654
 to increase oil recovery, 651–658
 use in plugging, 653
- Static batch tests, 246–247, 251
- Steam-based processes, foam-forming surfactants, 341
- Steam flooding, high-viscosity crude oils, 38
- Steam foaming, interfacial tension reduction, 39
- Steam foaming agents, screening agents, 34
- Steam injection temperature, 33
- Steel corrosion
 low alloy, 638–649
 electrical circuit model, 649
- Succinoglycan, 157–168
 chemical analysis, 158–159
 comparison with xanthan, 160
 composition and structure, 159–160, 161t, 161f
 degradation, 163–166
 effect of temperature, 160
 order–disorder transition, 160
 production, 158
 rheology, 160
 salt effects, 163
 transition temperature, 163, 165f
 viscosity, 158, 161f
- Sulfonates, surfactant flood systems, 378
- Supermicelle, 398
- Surface-active species, asphaltenes, 577
- Surface activity, complex copolymers, 169–203
- Surface behavior, between phases, 175–176
- Surface charge density, 601
- Surface energy study, related to wettability, 571–574
- Surface free energy
 contact angle studies with probe liquids, 572
 interaction of a solid with liquids, 572
- Surface rate, 615f
- Surface stress, along the interface, 484
- Surface tension
 equilibrium, 487
 function of axial position, 485–488
 liquids used for solid surface characterization, 574t
 surfactant adsorption, 488
- Surface tension gradients, 482
- Surfactant adsorption, in porous rocks, 502–517
- Surfactant concentrations
 effect on CO₂-foam mobility, 506
 quantitative determination, 257–271
- Surfactant distribution, calculated, 490
- Surfactant elasticity number, 490–493
- Surfactant losses, in reservoirs, 285
- Surfactant mixtures, CMC determination, 276f
- Surfactant molecule
 hydrophilic sheath, 318
 palisade layer, 318
- Surfactant performance, critical parameters, 34
- Surfactant–polymer interactions, interfacial behavior and oil displacement efficiency, 37
- Surfactant precipitation, 27, 338
- Surfactant propagation, 34, 37

- Surfactant remobilization, by means of desorbent, 282
- Surfactant retention tests, 279–282
- Surfactant slug
elution in presence of a desorbent, 282
oil recovery, 247
suitable desorbent, 285
- Surfactant solutions
in equilibrium with an adsorbent solid, 277–279
micellar properties, 273–275
- Surfactant structures, tertiary flooding strategies, 305–324
- Surfactant synthesis, 37
- Surfactant transport, in porous media, 279–285
- Surfactant vesicles
mimic of biological membranes, 61
stability, 391
- Surfactants
activity at interfaces, 377
advantages as gas mobility control agents, 33
anionic, 36
characteristics, 274*t*
cost and effectiveness, 35
elution, 283*f*
from polar fractions of petroleum and shale oil, 376–390
in contact with alkanes, alkyl benzenes, and stock tank oils, 386*f*
interfacial tension, 386*f*
low-mobility oil emulsions, 16
mass adsorbed per gram of rock, 515*f*
mobility control characteristics, 33
nonionic, 308
optimal characteristics, 35–37
optimum recovery of residue oils, 386*f*
organized structures, 397*f*
propagation in porous media, 272–288
properties, 329*t*
self-generated, 392
stable foam or emulsion, 84
sulfonate performance characteristics, 322–323
surfactant vesicles formed during tar sand recovery, 391–407
water-soluble fluorochemicals, 13
- Suspension additives, 74
- Synthetic brine, composition, 274*t*
- Synthetic polymers, 169
- T**
- Tangential force
release of non-Brownian particles, 549
removal mechanism, 549–550
- Tar sand
definition, 391
production processes, 392
- Termination site density, 473
- Tertiary oil recovery process, surfactant selection, 377
- Tetrapotassium pyrophosphate, 621–635
advantages, 634–635
concentration–density of solutions, 623*t*
in drilling fluids, 627–630
interaction with calcium chloride, 631
reacts with steel to form protective coating, 633
reduced corrosion rates, 632
solution compatibility, 631–632
subfreezing mud, 631
toxicity, 634
well logging, 632
- Thermal cracking, 421
- Thief zones
chemical treatments, 5
cross-linking polymers, 24–27
permeability, 25–27
volumetric sweep efficiency, 24–27
- Thin-film spreading agent
asphaltene-modified surfaces, 584*t*
chemical demulsifier, 585*t*
coalescing emulsions in the near-wellbore region, 579
displace asphaltene molecules, 577,579
high spreading pressures, 579
laboratory studies, 579–594
recovery of oil from oil-wet sand, 584*t*
steam additives in cyclic steam operations, 579
- Thin-film spreading agent–waterflood pilot
economics, 590,592*t*
efficiency, 588*f*
fluid flow patterns, 587*t*
production decline rate, 590,591*f*
site diagram, 582*f*
water cut vs. cumulative oil, 589*f*
- Thinners and dispersants, 6
- Time constant analysis, relaxation time of the corrosion process, 647
- Titanium
cross-linkers, 81–83
gel characteristics, 82–83
- Titration
comparison of methods, 261,263
photometric and turbidimetric, 263
physicochemical mechanism, 263
- Toluene–decane blends
conductivity–temperature profiles, 309*f*
phase-inversion temperature, 310*f*
- Torque balance, 551*f*
- Transesterification, 81

Transient pressure drop, porous-medium micromodel, 462*f*
 Transport process, second-order effects, 393
 Triad distribution, 109
 Triorganotin fluorides
¹³C NMR, chemical shifts, δ ppm, 539*t*
 miscible gas enhanced oil recovery, 529–546
 NMR, 537*f*, 538*f*
 proton NMR, chemical shifts in CDCl₃, δ ppm, 539*t*
 ratios of protons, 539*t*
 silicon-containing, 529, 534*t*
 solubilities, 529, 542*t*
 synthesis, 532*f*
 viscosity behavior, 540
 X-ray diffraction, 535*f*
 Turbidimetric titration
 basic principles, 260–261
 experimental procedures, 261
 SDBS against hyamine, 264*f*, 269*f*
 Turbidimetry, 131, 263
 Turbidity measurements, effect of pH and time, 245*f*
 Two-phase compositions, 298*t*

U

Ultra-low-tension flooding, 301
 Ultramicrobacteria
 definition, 654
 planned studies, 657
 selective plugging, 657
 survival in a particular well, 657
 Ultrasonic energy, alkaline solution media, 405
 Ultrasonic vibration energy effect, 398

V

Van der Waals forces, non-Brownian particles, 548
 Vaporizing gas drive, 445
 Vesicle forms, polymerized, 400
 Vesicles, giant-sized multilamellar surfactant, 391–407
 Viscosification, xanthan gum, 621
 Viscosifiers
 cellulose, 71–72
 for nonpolar solvents, triorganotin fluorides, 529
 guar gum, 67
 history, 66–67
 hydraulic fracturing, 11
 rheology modifiers, 5–6
 Viscosimetry, 131
 Viscosity
 before and after heating, 164*f*
 bridged associational model, 61

Viscosity—*Continued*
 change with time, 186*f*
 copolymer solutions, 199
 effect of sodium chloride concentration, 184*f*
 evolution, in presence of Ca²⁺, 120
 evolution with time, 111–123
 function of concentration, 162*f*, 186*f*, 188*f*, 189*f*, 541*f*
 function of shear rate, 190*f*
 function of temperature, 162*f*
 intrinsic, 116
 loss with time, 185–187
 molecular weight and charge density, 116–120
 neutralization, 60
 nonionic copolymers, 182
 polymer concentration, 116
 PTF in carbon dioxide, 544*f*
 transition temperature, 166
 treatment methods, 75
 vs. concentration curves, 543*f*
 Viscosity collapse, partially reversible, 157
 Viscosity evolution, 121*f*, 122*f*
 Viscosity–foam quality spectrum, 523
 Viscous stresses
 local thickness of film, 485
 tube radius, 485
 Volumetric sweep efficiency, improvement, 24–27

W

WAG process, supercritical CO₂ injection, 32
 Water bank, waterflood, 566
 Water gelling agents, fracturing effectiveness, 63
 Water–oil mobility ratio, waterflood, 578
 Water purification, complex copolymers, 169–203
 Water-swelling clay stabilization, 208, 209, 210*t*, 211*t*
 Water-swelling clays, 204
 Water vapor
 concentration effect, 437
 effect on kinetics and energetics of oxidation, 433–442
 rate of heat production, 437
 selective removal of saturates, 437
 Water-wet rock, 21
 Water-wetting nonemulsifier, 219
 Waterflood
 cross-linked polymers, 22
 description, 566
 economics, 22
 high permeability channels, 651
 oil saturation at the economic limit, 579
 Waterflood performance, amount of imbibition, 560

- Waterflood pilot studies, laboratory and field, 577–595
- Wax precipitation, governing parameters, 444
- Weighting materials, adjust fluid density, 4
- Well characteristics, 614*t*, 616*t*
- Well completion, 166
- Well fluids
clear, 622
compatible with nonmetallic materials, 633
environmental considerations, 633
prime requisites, 621
stability at surface conditions, 631
test for identifying damage, 621
- Well production
economics of asphaltene deposition, 449
plugging, 448–449
- Well productivity, fluid flow capacity of rock, 18
- Well stimulation
field test results, 217–220
hydrochloric acid, 63
- Wellbore fluid, sodium chloride brine, 616
- Wet oxidation
initial rates, 436*t*, 438*t*
kinetic parameters, 439*t*
partial pressure of water vapor, 442
residual coke and conversion of available carbon, 436*t*, 441*t*
- Wettability, 560–576
crude oils, 571
definition, 21
measurement, 571
reservoir rock, 594
- Wettability alteration
enhanced oil recovery, 577–595
inadvertent, 21
mechanism, recovery efficiency, 585
TFSA molecules, 579
- Wetting behavior, liquid–liquid–solid systems, 571
- Wetting cycle
anaerobic vessel, 568*f*, 570*f*
exposure to air, 567–569
open beaker, 570*f*
- Wetting systems, examples, 566*t*
- Wilhelmy hanging plate method, interfacial and surface tensions, 561
- Wilmington oil sand
brine-saturated, 248*f*
- Wilmington oil sand—*Continued*
coarse-grained fraction, 250*f*
core and fluid properties, 246*t*
mineralogy, 243*t*
oil–water–surfactant-saturated, 250*f*
residual oil–brine-saturated, 248*f*
surface area measurements, 244*t*
- Wormholes
conductivity, 610
fractal geometry, 608
largest diameter flow channels, 14
near-wellbore region, 612
- X
- Xanthan
adsorption in presence of calcium, 234–237
adsorption on kaolinite, 237
adsorption on siliceous minerals, 234–237
contour length distributions, 149*f*
disordered conformation, 153–154
double-stranded chains, 151
electron micrographs, 147*f*, 150*f*, 152*f*
molecular weights, contour lengths, and linear mass densities, 148*t*, 151*t*
ordered and disordered conformation, 145–156
properties, 72
similarities and differences, 154
strandedness and topology, 145–146
structure and characteristics, 71
transition temperature–salinity profile, 164*f*
use in polymer flooding, 145
- Xanthan gum
cost, 29
cross-linked, 25–26
dissolved in saline waters, 29
problems, 29
properties, 28*t*, 29
solution injectivity, 29
viscosifiers, 629
viscosity, 29
- Xanthan polymer, gelation, 139, 141
- Z
- Zirconium(IV), cross-linkers, 80–81